

Multicarrier Communications

LIE-LIANG YANG

Amplitude

0

$$x_3 \cos\left(\frac{2\pi 3t}{T}\right)$$

$$x_4 \cos\left(\frac{2\pi 4t}{T}\right)$$

$$x_5 \cos\left(\frac{2\pi 5t}{T}\right)$$

$$x_6 \cos\left(\frac{2\pi 6t}{T}\right)$$

$$x_7 \cos\left(\frac{2\pi 7t}{T}\right)$$

 WILEY

Multicarrier Communications

Multicarrier Communications

Lie-Liang Yang

University of Southampton, UK



A John Wiley and Sons, Ltd, Publication

This edition first published 2009
© 2009 John Wiley & Sons Ltd

Registered office
John Wiley & Sons Ltd, The Atrium, Southern Gate, Chichester, West Sussex, PO19 8SQ, United Kingdom

For details of our global editorial offices, for customer services and for information about how to apply for permission to reuse the copyright material in this book please see our website at www.wiley.com.

The right of the author to be identified as the author of this work has been asserted in accordance with the Copyright, Designs and Patents Act 1988.

All rights reserved. No part of this publication may be reproduced, stored in a retrieval system, or transmitted, in any form or by any means, electronic, mechanical, photocopying, recording or otherwise, except as permitted by the UK Copyright, Designs and Patents Act 1988, without the prior permission of the publisher.

Wiley also publishes its books in a variety of electronic formats. Some content that appears in print may not be available in electronic books.

Designations used by companies to distinguish their products are often claimed as trademarks. All brand names and product names used in this book are trade names, service marks, trademarks or registered trademarks of their respective owners. The publisher is not associated with any product or vendor mentioned in this book. This publication is designed to provide accurate and authoritative information in regard to the subject matter covered. It is sold on the understanding that the publisher is not engaged in rendering professional services. If professional advice or other expert assistance is required, the services of a competent professional should be sought.

Library of Congress Cataloging-in-Publication Data

Yang, Lie-Liang.

Multicarrier communications / Lie-Liang Yang.

p. cm.

Includes bibliographical references and index.

ISBN 978-0-470-72200-8 (cloth)

1. Spread spectrum communications. 2. Code division multiple access. 3. Mobile communication systems. I. Title.

TK5103.45.Y35 2009

621.3845–dc22

2008028059

A catalogue record for this book is available from the British Library.

ISBN 9780470722008 (H/B)

Set in 10/12pt Times by Sunrise Setting Ltd, Torquay, UK.
Printed in Singapore by Markono Pte Ltd.

Dedicated to:

My wife Xiang Ling and our son Linghent Yang

Contents

Preface	xv
1 Introduction	1
1.1 Spread Spectrum	1
1.2 Orthogonal Frequency-Division Multiplexing	6
1.3 Multiple Access	8
1.4 Duplex	11
1.4.1 Time-Division Duplex (TDD)	11
1.4.2 Frequency-Division Duplex (FDD)	12
1.4.3 Multicarrier-Division Duplex (MDD)	13
1.4.4 Code-Division Duplex (CDD)	14
1.5 Diversity in Wireless Communications	14
1.6 Organization of the Book	18
2 Principles of Code-Division Multiple-Access Communications	21
2.1 Direct-Sequence Spread Spectrum	22
2.1.1 Transmitted Signals	23
2.1.2 Detection of DS-SS Signals	25
2.1.2.1 Correlation Receiver	25
2.1.2.2 Matched-Filter Receiver	27
2.1.3 Anti-Jamming Property of DS-SS Systems	30
2.1.4 Direct-Sequence Code-Division Multiple Access	33
2.2 Multicarrier Spread-Spectrum Communications	34
2.2.1 Transmitted Signals	34
2.2.2 Detection of MC Spread-Spectrum Signals	36
2.2.3 Multicarrier Code-Division Multiple Access	38
2.3 Frequency-Hopped Spread-Spectrum Communications	40
2.3.1 M -ary Frequency-Shift Keying	40
2.3.2 M -ary Frequency-Shift Keying Aided Slow Frequency-Hopping . . .	42
2.3.3 M -ary Frequency-Shift Keying Aided Fast Frequency-Hopping . . .	44
2.3.4 Detection of FH/MFSK Signals	47

2.3.5	Frequency-Hopping Multiple-Access	51
2.3.5.1	Slow Frequency-Hopping Multiple-Access	51
2.3.5.2	Fast Frequency-Hopping Multiple-Access	53
2.4	Time-Hopping Spread-Spectrum Communications	54
2.4.1	Slow Time-Hopping M -ary Pulse-Position Modulation	56
2.4.2	Fast Time-Hopping M -ary Pulse-Position Modulation	60
2.4.3	Detection of Slow Time-Hopping Signals	61
2.4.4	Detection of Fast Time-Hopping Signals	64
2.4.5	Time-Hopping Multiple-Access	67
2.4.5.1	Slow Time-Hopping Multiple-Access	68
2.4.5.2	Fast Time-Hopping Multiple-Access	70
2.5	Hybrid Direct-Sequence/Frequency-Hopping Multiple-Access	73
2.5.1	Hybrid DS/SFH Signals	74
2.5.1.1	DS/SFH Using BPSK Modulation	74
2.5.1.2	Detection of BPSK Modulated DS/SFH Signals	75
2.5.2	Hybrid DS/FFH Signals	78
2.5.2.1	DS/FFH Using MFSK Modulation	79
2.5.2.2	Detection of DS/FFH Signals Using MFSK	80
2.5.2.3	DS/FFH Using M -ary Orthogonal Modulation	82
2.5.2.4	Detection of DS/FFH Signals Using M -ary Orthogonal Modulation	83
2.6	Hybrid Direct-Sequence/Time-Hopping Multiple-Access	86
2.6.1	Hybrid DS/STH Signals	87
2.6.1.1	DS/STH Using MPPM	87
2.6.1.2	Detection of DS/STH Signals Using MPPM	87
2.6.2	Hybrid DS/FTH Signals	90
2.6.2.1	DS/FTH Using MPPM	90
2.6.2.2	Detection of DS/FTH Signal Using MPPM	90
2.6.2.3	DS/FTH Using M -ary Orthogonal Modulation	92
2.6.2.4	Detection of DS/FTH Signals Using M -ary Orthogonal Modulation	93
2.7	Summary and Discussion	96
3	Principles of Multicarrier Communications	97
3.1	Introduction	97
3.2	Orthogonal Frequency-Division Multiplexing	99
3.2.1	Modulator	99
3.2.2	Modulation Parameters	100
3.2.3	Demodulator	101
3.2.4	Implementation of Multicarrier Modulation/Demodulation	103
3.3	Frequency-Domain Spread Multicarrier CDMA	108
3.3.1	Transmitted Signal	108
3.3.2	Modulation Parameters	109
3.3.3	Correlation Receiver	111
3.4	Single-Carrier Frequency-Division Multiple Access	115

3.5	Orthogonal Multicarrier DS-CDMA	122
3.5.1	Transmitted Signal	122
3.5.2	Modulation Parameters	123
3.5.3	Correlation Receiver	125
3.6	Multitone DS-CDMA	128
3.6.1	Transmitted Signal	128
3.6.2	Modulation Parameters	130
3.6.3	Correlation Receiver	131
3.7	Generalized Multicarrier DS-CDMA	134
3.7.1	Transmitted Signal	136
3.7.2	Modulation Parameters	137
3.7.3	Correlation Receiver	138
3.8	Time-Hopping Multicarrier CDMA	140
3.8.1	Transmitted Signal	140
3.8.2	Modulation Parameters	141
3.8.3	Receiver Model	143
3.9	Time-Frequency-Domain Spread Multicarrier DS-CDMA	145
3.9.1	Transmitted Signal	146
3.9.2	Receiver Model	146
3.10	Summary and Discussion	150
4	Performance of Multicarrier Systems over Gaussian Channels	153
4.1	Introduction	153
4.2	Performance of Orthogonal Frequency-Division Multiplexing	154
4.3	Performance of Single-User Frequency-Domain Spread Multicarrier CDMA	158
4.4	Performance of Single-User Multicarrier DS-CDMA	159
4.5	Performance of Single-User Time-Hopping Multicarrier CDMA	169
4.5.1	Power Spectral Density of TH/MC-CDMA Signals	169
4.5.2	Error Probability of TH/MC-CDMA Systems	173
4.6	Performance of Time-Frequency-Domain Spread Multicarrier DS-CDMA Supporting Multiusers	177
4.6.1	Transmitted signal	178
4.6.2	Power Spectral Density	179
4.6.3	Representation of the Received Signal	181
4.6.4	Single-User Detection and Analysis	185
4.6.5	Bit-Error Rate (BER) Performance Analysis	190
4.6.6	Bit-Error Rate (BER) Performance Results	192
4.7	Equivalence Between Single-Carrier DS-CDMA and Multicarrier CDMA	195
4.8	Summary and Discussion	198
	Appendix 4.A Standard Gaussian Approximation	199
5	Performance of Multicarrier Systems over Frequency-Selective Fading Channels	203
5.1	Introduction	203
5.2	Frequency-Selective Fading in Multicarrier Systems	205
5.3	Intersymbol Interference Suppression: Cyclic-Prefixing and Zero-Padding	211

5.4	Generation of Fading Statistics for Multicarrier Signals	215
5.5	Performance of Orthogonal Frequency-Division Multiplexing	216
5.6	Performance of Single-User Frequency-Domain Spread Multicarrier CDMA	218
5.6.1	Representation of the Received Signals	218
5.6.2	MRC-Assisted Detection and Performance Analysis	219
5.6.3	Performance Results	222
5.7	Performance of Single-Carrier Frequency-Division Multiple Access	225
5.8	Frequency-Domain Equalization in Single-Carrier DS-CDMA	228
5.9	Performance of Single-User Multicarrier DS-CDMA	234
5.9.1	Representation of the Received Signals	234
5.9.2	MRC-Assisted Detection and Performance Analysis	238
5.9.3	Interbit and Intercarrier Interference in MC DS-CDMA: An Example	241
5.10	Performance of Single-User Time-Hopping Multicarrier CDMA	245
5.10.1	Decision Variables and Their Statistics	245
5.10.2	Error Probability Analysis	248
5.10.3	Performance Results	250
5.11	Performance of Time-Frequency-Domain Spread Multicarrier DS-CDMA Supporting Multiusers	251
5.11.1	Representation of the Received Signal	253
5.11.2	Single-User Detection and Analysis	255
5.11.3	Statistics Analysis	257
5.11.4	Bit-Error Rate (BER) Analysis	260
5.11.4.1	Standard Gaussian Approximation	260
5.11.4.2	Simplified Improved Gaussian Approximation	262
5.11.5	Performance Results	264
5.12	Summary and Discussion	266
Appendix 5.A	$\int_0^{\infty} Q(\sqrt{2\gamma}) f(\gamma) d\gamma$	269
Appendix 5.B	$E[\exp(-\sum_{j=1}^N (\gamma_j / \sin^2 \theta))]$ in Correlated Nakagami- m Fading	270
Appendix 5.C	Derivation of the Variance of Ψ	272
6	Coherent Multiuser Detection	275
6.1	Introduction	275
6.2	Multiuser Detection in Frequency-Domain Spread Multicarrier CDMA	277
6.2.1	Decorrelating	280
6.2.2	Minimum Variance Distortionless Response (MVDR)	285
6.2.3	Minimum Mean-Square Error (MMSE)	287
6.2.4	Maximum Signal-to-Interference-plus-Noise Ratio (MSINR)	292
6.2.5	Minimum Power Distortionless Response (MPDR)	294
6.2.6	Multiuser Detection in Subspaces	296
6.2.6.1	Signal Subspace	298
6.2.6.2	Principal Components (PCs)	300
6.2.6.3	Cross-Spectral Metric (CSM)	301
6.2.6.4	Taylor Polynomial Approximation (TPA)	303
6.2.7	Decision Feedback Multiuser Detection	306
6.2.7.1	Matched-Filtering Decision-Feedback	308

6.2.7.2	Zero-Forcing Decision-Feedback	314
6.2.7.3	Minimum Mean-Square Error Decision-Feedback	317
6.2.8	Maximum <i>A Posteriori</i> Probability Multiuser Detection	318
6.2.9	Maximum Likelihood Decision Multiuser Detection	329
6.2.10	Minimum Error-Probability Linear Multiuser Detection	331
6.3	Multiuser Detection in Multicarrier DS-CDMA	343
6.3.1	Zero-Forcing Multiuser Detection	346
6.3.2	Minimum Mean-Square Error Multiuser Detection	353
6.3.3	Maximum Likelihood Decision Multiuser Detection	358
6.4	Multiuser Detection in Time-Frequency-Domain Spread Multicarrier DS-CDMA	362
6.4.1	Time-Frequency-Domain Zero-Forcing Multiuser Detection	365
6.4.2	Time-Frequency-Domain MMSE Multiuser Detection	371
6.4.3	Hybrid Time-Frequency-Domain ZF-MMSE Multiuser Detection	377
6.4.4	Maximum-Likelihood Decision Multiuser Detection	380
6.5	Summary and Discussion	381
Appendix 6.A	Derivatives with Respect to Complex Vector/Matrix	383
Appendix 6.B	Matrix Inversion	386
Appendix 6.C	Suboptimal Algorithms for Maximum Likelihood Decision Multiuser Detection	388
6.C.1	Search Algorithms	388
6.C.1.1	QRD-M Tree-Search Algorithm	389
6.C.1.2	Greedy Search Algorithm	390
6.C.1.3	Sphere-Decoding-Based Search	391
6.C.1.4	Coordinate Descent Search Algorithm	392
6.C.1.5	Evolutionary Programming Algorithm	393
6.C.1.6	Genetic Algorithm	394
6.C.1.7	Ant-Colony-Inspired Search	396
6.C.2	Non-Search Algorithms	398
6.C.2.1	Expectation Maximization	398
6.C.2.2	Probabilistic Data Associated Algorithm	400
6.C.2.3	Semidefinite Programming Relaxation	403
7	Noncoherent Multiuser Detection	405
7.1	Representation of Discrete Time-Hopping Multicarrier CDMA Signals	406
7.2	Noncoherent Single-User Detection	411
7.3	Optimum Prior Noncoherent Multiuser Detection	415
7.4	Prior Noncoherent Decorrelating Multiuser Detection	418
7.5	Prior Noncoherent MMSE Multiuser Detection	423
7.6	Optimum Posterior Noncoherent Multiuser Detection	429
7.6.1	Optimum Posterior Noncoherent Multiuser Detection in Noiseless Rayleigh Fading Channels	433
7.6.2	Optimum Posterior Noncoherent Multiuser Detection in Noisy Rayleigh Fading Channels	436
7.7	Suboptimum Posterior Noncoherent Multiuser Detection in Rayleigh Fading Channels	439

7.8	Posterior Noncoherent Interference Cancellation	443
7.8.1	Conventional Single-User Posterior Noncoherent Detection	443
7.8.2	Minimum-Distance Decoding Based Interference Cancellation	450
7.8.3	Iterative Posterior Interference Cancellation	455
7.8.4	Posterior Multistage Interference Cancellation	461
7.9	Summary and Discussion	467
Appendix 7.A Noncoherent Diversity Combining Schemes for M -ary Orthogonal Signalling		469
Appendix 7.B Derivation of $P_{NC}(i)$		472
8	Multiuser Transmitter Preprocessing	475
8.1	Principles of Transmitter Preprocessing: An Example	476
8.2	Transmitter Preprocessing in Frequency-Domain Spread MC-CDMA	479
8.2.1	Transmitted Signal	479
8.2.2	Representation of the Received Signal	481
8.2.3	Transmitter Matched-Filtering Single-User Preprocessor	483
8.2.4	Zero-Forcing Multiuser Transmitter Preprocessor	488
8.2.5	Minimum Mean-Square Error (MMSE) Multiuser Transmitter Preprocessing	495
8.2.6	Maximum Signal-to-Interference-Plus-Noise Ratio (MSINR) Multiuser Transmitter Preprocessing	499
8.2.7	Minimum Variance Distortionless Response (MVDR) Multiuser Transmitter Preprocessing	501
8.2.8	Minimum Power Distortionless Response (MPDR) Multiuser Transmitter Preprocessing	504
8.2.9	Eigenspace-Based Multiuser Transmitter Preprocessing	506
8.2.10	Minimum Bit-Error Rate (MBER) Multiuser Transmitter Preprocessing	510
8.2.11	Maximum Mutual Information (MMI) Multiuser Transmitter Preprocessing	515
8.2.12	Transmitter Multiuser Interference Cancellation	523
8.3	Transmitter Preprocessing in Frequency-Domain Spread MC DS-CDMA Systems	530
8.3.1	Transmitted Signal	531
8.3.2	Representation of the Received Signal	535
8.3.3	Minimum Mean-Square Error Multiuser Transmitter Preprocessing	540
8.3.3.1	Matched Filtering	542
8.3.3.2	Zero-Forcing	545
8.3.3.3	Minimum Mean-Square Error	546
8.3.4	Maximum Mutual Information Multiuser Transmitter Preprocessing	551
8.3.5	Transmission Power Allocation	555
8.3.5.1	Joint Power Normalization	555
8.3.5.2	Individual Power Normalization	556
8.3.5.3	Maximal SNR Assisted Normalization for ZF-MUTP	556
8.4	Relationship Between Linear Multiuser Transmission and Linear Multiuser Detection	557

8.5 Extraction of Channel Knowledge for Transmitter Preprocessing in Multicarrier CDMA Systems	561
8.5.1 Time-Division Duplex (TDD)	562
8.5.2 Frequency-Division Duplex (FDD)	563
8.5.3 Multicarrier-Division Duplex (MDD)	564
8.5.3.1 Principles of MDD: Gaussian Channels	565
8.5.3.2 MDD Systems in Frequency-Selective Fading Channels	568
8.5.3.3 Channel Estimation/Prediction in MDD Systems	572
8.6 Summary and Discussion	578
9 Multiantenna Multicarrier CDMA	581
9.1 Multiple-Input Multiple-Output Communications	582
9.1.1 Multiple-Input Multiple-Output System Model	582
9.1.2 Capacity of Multiple-Input Multiple-Output Channels	583
9.2 Spatial Diversity	597
9.2.1 Receive Diversity	597
9.2.2 Transmit Diversity	598
9.2.2.1 Switched Transmit Diversity	598
9.2.2.2 TMRC-Assisted Transmit Diversity	599
9.2.2.3 Orthogonal Transmit Diversity	599
9.2.2.4 Transmit Diversity Based on Space-Time Coding	600
9.2.2.5 Transmit Diversity Based on Space-Time Spreading	610
9.2.3 MIMO Diversity	613
9.3 Spatial-Division Multiple Access	614
9.4 Performance of Multicarrier CDMA Using Space-Time Coding	616
9.4.1 Transmission Scheme	616
9.4.2 Receiver Scheme	618
9.4.3 Analysis of Probability of Error	621
9.4.4 Performance Results	625
9.5 Time-Frequency-Domain Space-Time Spread Multicarrier DS-CDMA	627
9.5.1 Transmission Scheme	628
9.5.2 Receiver Scheme	630
9.5.3 Analysis of Probability of Error	633
9.6 Space-Time MC DS-CDMA over Fast Time-Varying Fading Channels	635
9.6.1 System Model	637
9.6.1.1 Transmitter Model	637
9.6.1.2 Receiver Model	639
9.6.2 Detection Schemes	643
9.6.3 Analysis of Single-User Bit-Error-Rate	646
9.6.4 Performance Results	649
9.6.5 Conclusions	653
9.7 Summary and Discussion	655
Bibliography	657
Index	675

Preface

The purpose of this book is to provide a comprehensive and unified introduction to the principles and applications of the wireless communications invoking multicarriers for transmission and/or detection. The multicarrier schemes covered include orthogonal frequency-division multiplexing (OFDM), single-carrier frequency-division multiple-access (SC-FDMA) and a variety of multicarrier code-division multiple-access (CDMA) schemes using frequency-domain spreading, time-domain spreading, or both frequency-domain and time-domain spreading. After a background introduction in the first chapter, Chapter 2 of the book addresses the principles of various spread-spectrum schemes with an emphasis on the principles of CDMA based on these spread-spectrum schemes; four basic spread-spectrum schemes and two hybrid spread-spectrum schemes are highlighted. The remaining chapters of the book are intended to provide a comprehensive coverage of the many issues related to the theory, design and implementation of multicarrier communications.

Typical characteristics of the book include the following. The book presents the reader with a broad introduction to the principles of spread-spectrum and multicarrier communications. It describes the approach for in-depth analysis of the performance of various multicarrier communications systems, when communicating over Gaussian or multipath fading channels. It analyses in detail the implementation issues of multicarrier modulation/demodulation in the context of various multicarrier schemes, in addition to OFDM. In this book the theory of multiuser detection and multiuser transmitter preprocessing is established in a parallel way, in order to illustrate the strong coupling between transmitter optimization and receiver optimization, and to show the duality of optimizations in linear multiuser detection and linear multiuser transmitter preprocessing. In this book the theory of noncoherent multiuser detection is developed in great detail and also in a unified manner, and a range of noncoherent multiuser detection and noncoherent interference suppression techniques are established. This book also deals with the theory of multiple-input multiple-output (MIMO) and space–time processing as well as their applications in multicarrier communications, when considering the communications environments experiencing frequency-selective fading and possibly time-selective fading. Furthermore, this book presents discussions of the equivalency between single-carrier direct-sequence CDMA (DS-CDMA) and multicarrier CDMA, as well as of the unification of the transmit diversity schemes based on space–time coding and space–time spreading.

This book has been derived partly from the lectures that I gave in a senior undergraduate-level course and a graduate-level course on wireless communications at the University of Southampton. It has been designed for senior undergraduate students (Chapters 1–3 and a few sections at the start of the other chapters), graduate students, researchers and engineers with some prior exposure to digital communications and signal processing. The book is in general structured from the fundamental principles to the more advanced topics. In the chapters dealing with the advanced topics, the materials are organized to progress from the straightforward concepts to the more involved analysis.

I wish to express my thanks to the many people who have contributed to the development of this book. First of all, I would like to thank my colleague Professor L. Hanzo for his continued support in many different ways throughout my professional career. I am indebted to him for co-authoring with me the second chapter as well as for providing corrections and suggestions for some sections in the third chapter. I am grateful to my colleagues Professor S. Chen, Dr S. X. Ng and Dr R. G. Maunder for their help, collaborations and stimulating discussions. A debt of gratitude is owed to all my current and former Ph.D. students as well as to all my former M.Sc. project students, who have made many contributions, either directly or indirectly, during the preparation of the manuscript. I owe thanks to the reviewers for their constructive comments, suggestions and criticisms. I would like to thank Mark Hammond, Katharine Unwin and Sarah Tilley at Wiley for their help in the production of the book. Finally, my sincere gratitude is due to the many researchers whose significant contributions in wireless communications, especially in the fields of multicarrier communications, multiuser communications, space–time processing, etc., have made it possible to write this book.

Lie-Liang Yang

Chapter 1

Introduction

With the continued dramatic increase in demand for various types of high-speed wireless service, future generations of wireless communications will be aiming at wideband, broadband and ultrawide bandwidth (UWB) systems, which are capable of achieving the highest possible spectral efficiency by using the most advanced wireless communications techniques possible. However, in the design of wireless communications systems, particularly, for commercial applications, a well-balanced trade-off between complexity, flexibility, performance (which may include data rate, quality-of-service (QoS), etc.), and cost is often an important consideration. In light of the great progress made in the fields of microelectronics, signal processing, computing, etc., in modern wireless communications complexity has often been one of the efficient routes for improving flexibility and performance. In this book we present the principles and applications of a wide range of techniques that have been or may be applied for achieving high spectral efficiency wireless communications with high flexibility. Below, we provide an overview of the issues widely concerned in wireless communications that are also related to this book.

1.1 Spread Spectrum

The phrase '*spread spectrum*' has been a well-known terminology in the field of wireless communications for several decades. The research and application of spread-spectrum techniques have evolved from the desire to support covert communications in the 1950s and have now reached a state of maturity, finding applications in nearly every corner of wireless communications. Spread-spectrum techniques have been widely applied in providing anti-jamming and anti-detection communications. Simultaneously, these techniques have been invoked to support multiuser communications and efficiently to exploit wireless resources in military and civilian wireless communications, rendering the term '*spread spectrum*' truly ubiquitous.

Spread spectrum is a type of modulation technique that spreads the energy of a signal many times the particular bandwidth generated by the signal, under the control of a spreading sequence referred to as a 'pseudo-random' or 'pseudo-noise' (PN) sequence. Typically, there

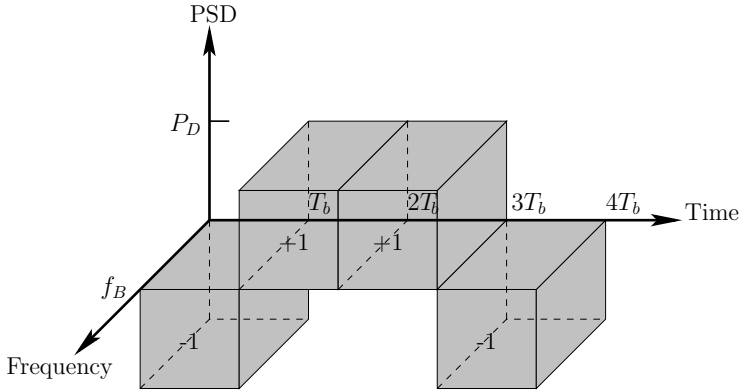


Figure 1.1: Conceptual illustration of the PSD–time–frequency relationship of conventional narrow-band signals.

are four types of basic spread-spectrum technique: the time (T)-domain direct-sequence spread spectrum (DS-SS), which is the DS-SS that we usually imply; the frequency (F)-domain direct-sequence spread spectrum which has been referred to as multicarrier spread spectrum (MC-SS); the frequency-hopping spread spectrum (FH-SS); and the time-hopping spread spectrum (TH-SS). Although the spread-spectrum operations embedded in these basic spread-spectrum schemes are different, one of their common characteristics is that the power spectral density (PSD) of the transmitted signals by these spread-spectrum schemes is usually very low, spans a very wide bandwidth and is akin to the PSD of Gaussian noise.

In more detail, we describe below the principles of the above-mentioned four types of basic spread-spectrum scheme. Let us assume that a binary sequence, say four bits expressed as $\{-1, +1, +1, -1\}$, is transmitted. Without spreading, the PSD-time-frequency (PTF) relationship of the transmitted signals in a conventional narrow-band communications system is illustrated in Fig. 1.1. Here, T_b represents the bit duration, f_B represents the bandwidth conveying the signal and P_D represents the corresponding transmission PSD. Note that in Fig. 1.1, the thickness of a block represents the transmission PSD, the blocks above the horizontal plane denote the $+1$'s transmitted, while those below the horizontal plane denote the -1 's transmitted. In (binary) digital modulations the transmission bandwidth required is usually the reciprocal of the time duration conveying a binary bit. Hence, in Fig. 1.1 we have $f_B = 1/T_b$. Furthermore, the total energy spent for transmitting the four bits is determined by the volume of the four blocks.

The DS-SS signal is formed by the spreading operation, which multiplies each of the binary data bits of $\{-1, +1, +1, -1\}$ with a PN sequence, say $\{+1, -1, -1, +1, -1\}$, yielding a binary sequence

$$\underbrace{-1, +1, +1, -1, +1}_{\text{Bit 1 } (-1)}; \underbrace{+1, -1, -1, +1, -1}_{\text{Bit 2 } (+1)}; \underbrace{+1, -1, -1, +1, -1}_{\text{Bit 3 } (+1)}; \underbrace{-1, +1, +1, -1, +1}_{\text{Bit 4 } (-1)} \quad (1.1)$$

where every binary is referred to as a *chip*. This chip sequence of $\{+1, -1\}$ is then transmitted within a time duration of $4T_b$. Since after the spreading operation, as shown in (1.1), there

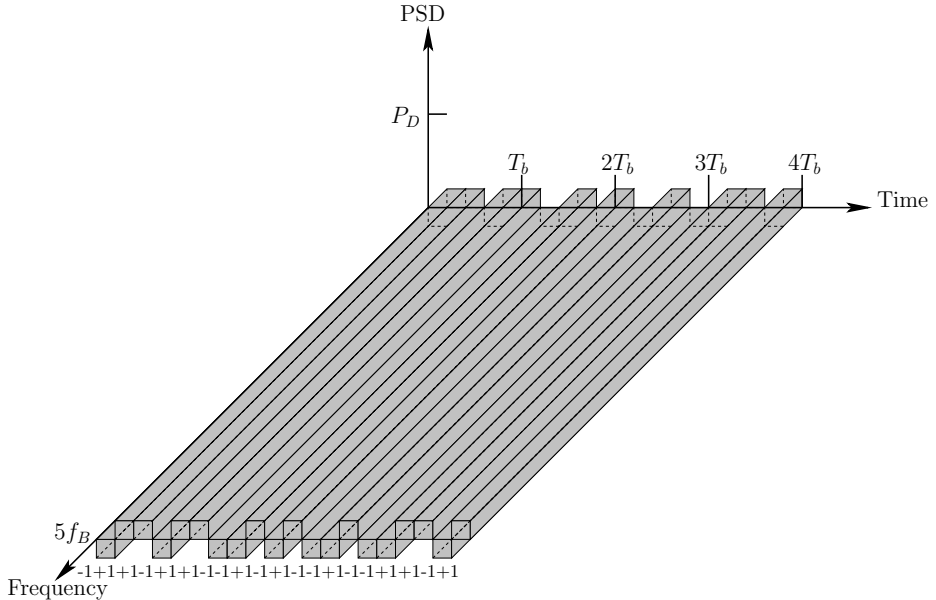


Figure 1.2: Conceptual illustration of the PSD-time-frequency relationship of DS-SS signals.

are now 20 chips that need to be transmitted within $4T_b$, the time duration for transmitting a chip is hence given by

$$T_c = \frac{4T_b}{20} = \frac{T_b}{5} \quad (1.2)$$

where T_c denotes the chip duration, which is only 1/5 of the bit duration T_b . Therefore, the bandwidth of the DS-SS signals is $f_s = 1/T_c = 5/T_b = 5f_B$, which is five times the bandwidth of the conventional narrow-band signals without spreading, as shown in Fig. 1.1. In a DS-SS system, the bandwidth expansion is measured by the *spreading factor*, which is defined as the ratio of the bandwidth after and before spreading. In this example, the spreading factor is $N = 5f_B/f_B = T_b/T_c = 5$.

The PTF-relationship of the DS-SS signals is conceptually illustrated in Fig. 1.2. When comparing Fig. 1.2 with Fig. 1.1, we can see that the bandwidth of the DS-SS signals is five times the bandwidth of the conventional narrow-band signals. In return, the transmission PSD of the DS-SS signals is only one-fifth of that of the conventional narrow-band signals as seen in Fig. 1.1. Note that, when given the transmission energy per bit, the volume of the 20 blocks in Fig. 1.2 should be the same as that of the four blocks seen in Fig. 1.1.

The MC-SS signal is also formed by the spreading operation, which multiplies each of the binary data bits, say, $\{-1, +1, +1, -1\}$, with a PN sequence of, say $\{+1, -1, -1, +1, -1\}$, yielding a binary sequence as shown in (1.1). Then, each chip is conveyed using a bandwidth of f_B within one bit duration. The PTF relationship of the MC-SS signals is conceptually illustrated in Fig. 1.3.

As shown in Fig. 1.2, in the DS-SS scheme each bit duration is divided into five chip durations and each chip is transmitted within one chip duration using the bandwidth, $5f_B$.

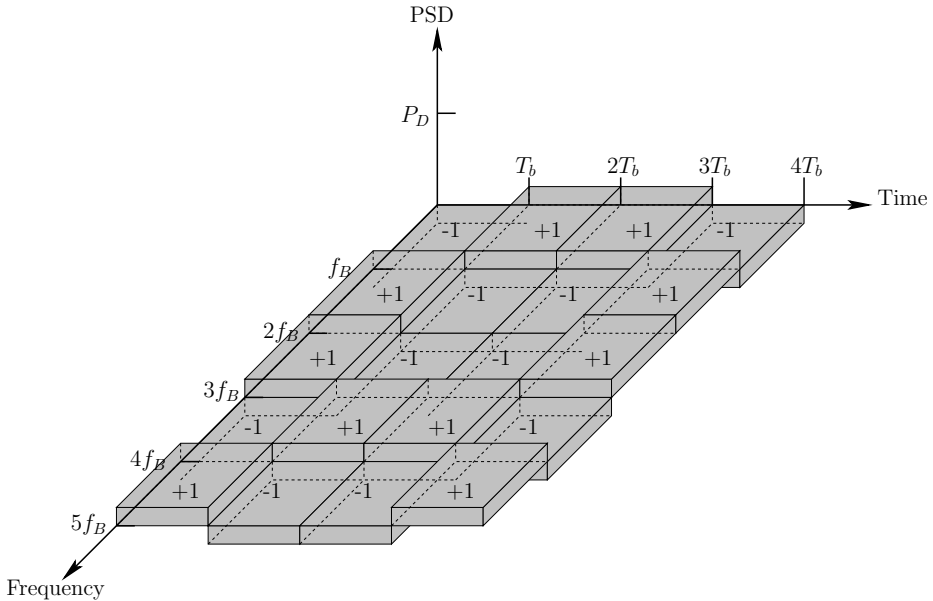


Figure 1.3: Conceptual illustration of the power–time–frequency relationship of MC-SS signals.

By contrast, in the MC-SS scheme, as shown in Fig. 1.3, the frequency band is divided into five sub-bands each with bandwidth f_B and each chip is transmitted on one sub-band within a bit duration T_b . Furthermore, for given transmission energy per bit, it can be shown that the transmission PSD in Fig. 1.3 is the same as that in Fig. 1.2 and it is one-fifth of the transmission PSD P_D seen in Fig. 1.1.

The principles behind the FH-SS can be well understood with the aid of Fig. 1.4. In the FH-SS scheme the frequency band is also divided into a number of sub-bands. In contrast to the MC-SS scheme as shown in Fig. 1.3, where the transmitted signal always occupies the whole frequency band, in the FH-SS scheme the signal is transmitted only on a sub-band at any time. The transmission sub-band is activated under the control of a so-called *FH pattern*, which may be generated randomly or pseudo-randomly. In Fig. 1.4 the FH pattern was assumed to be $\{5, 1, 3, 2\}$. Therefore, the fifth, first, third and second sub-bands are activated within the first, second, third and fourth bit durations, respectively.

In comparison with Fig. 1.1, we can see that in the FH-SS scheme the transmitted signal within each bit duration is a narrow-band signal that is the same as that in Fig. 1.1. In the FH-SS scheme the spectrum-spreading is obtained by the FH operation.

In the FH-SS shown in Fig. 1.4 the FH rate is the same as the bit (symbol) rate. The FH rate can be lower than the bit (symbol) rate, implying that several bits (symbols) are transmitted after one hop. This type of FH is referred to as slow FH (SFH). The FH rate can also be designed to be higher than the bit (symbol) rate, implying that one bit (symbol) is transmitted by invoking several frequency sub-bands. Correspondingly, this type of FH is called the fast FH (FFH).

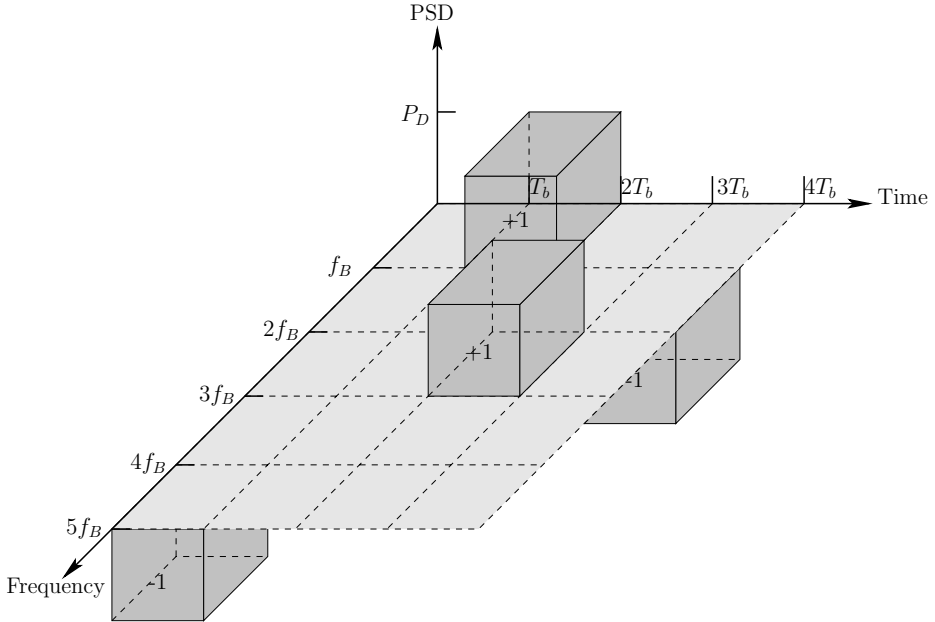


Figure 1.4: Conceptual illustration of the PSD–time–frequency relationship of FH-SS signals.

Finally, in the TH-SS scheme the time axis is divided into chips or *time slots* and the transmission is only activated at certain time slots. For example, as shown in Fig. 1.5, each bit duration is divided into five time-slots and only one-fifth of the time slots are activated for transmission. In principle, if we consider that the FH-SS scheme transmits F-domain pulses under the control of an FH pattern, then the TH-SS scheme can be viewed as a spread-spectrum scheme, which transmits T-domain pulses under the control of a TH pattern. In Fig. 1.5 the TH pattern was assumed to be $\{5, 1, 3, 2\}$. Hence, the four T-domain pulses are activated within the fifth, first, third and second time slots within the first, second, third and fourth bit durations, respectively. As shown in Fig. 1.5 the width of each T-domain pulse is only one-fifth of the bit duration T_b , hence each pulse spans a bandwidth $5f_B$.

Furthermore, in parallel with the SFH or FFH in the FH-SS scheme, the TH in the TH-SS scheme may also be implemented using slow TH (STH) or fast TH (FTH).

In addition to the above-presented four types of basic spread-spectrum scheme, as shown in Chapter 2, hybrid spread-spectrum schemes may be designed by combining two or more basic spread-spectrum schemes, in order to make use of their advantages while, simultaneously, overcoming their disadvantages.

Spread-spectrum communications have many advantages in comparison to the conventional narrow-band communications, and they have found a wide range of applications in the context of both secure military as well as civilian mobile wireless communications. It can be said that many advantages of the spread-spectrum communications schemes are inherent in their wideband noise-like signals. First, because spread-spectrum signals are noise-like, they are usually hard to detect and have a low probability of interception, except by the intended receivers which employ the knowledge of the spreading sequences used by the

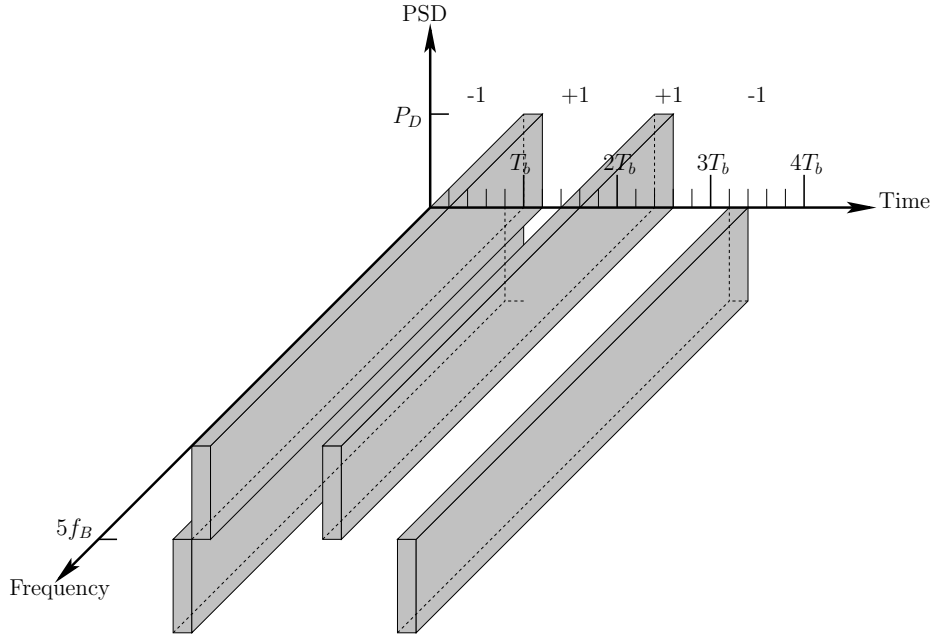


Figure 1.5: Conceptual illustration of the PSD–time–frequency relationship of TH-SS signals.

transmitter(s). Second, because spread-spectrum signals are wideband and noise-like, spread-spectrum signals are usually difficult to be interfered or jammed, even though the knowledge about the frequency band being used by the spread-spectrum systems is available. Third, their wideband, low PSD nature makes the spread-spectrum signals less likely to interfere with the other types of wideband or narrow-band wireless signal. Hence, spread-spectrum techniques may provide wireless communications design alternative approaches to overlay (fully or partially) with the existing wireless systems, in order to maximize the overall spectral-efficiency of wireless communications. Fourth, spread spectrum is a feasible technique for the implementation of multiple-access communications, yielding spread-spectrum multiple-access (SSMA) or code-division multiple-access (CDMA). In SSMA/CDMA systems different users (or terminals) can be readily distinguished by their unique spreading (or so-called signature) codes. Furthermore, wideband noise-like spread-spectrum signals have the property of high time-resolution. Spread-spectrum signals can be applied for accurate timing and location, such as in the global position system (GPS). Additionally, wideband spread-spectrum signals usually experience frequency-selective fading, which may be used to obtain the frequency diversity in order to enhance the reliability of wireless communications.

1.2 Orthogonal Frequency-Division Multiplexing

Orthogonal frequency-division multiplexing (OFDM) is a type of multicarrier modulation scheme that transmits data symbols in parallel on multiple subcarriers that share the system bandwidth using some form of frequency-division multiplexing (FDM). The idea behind

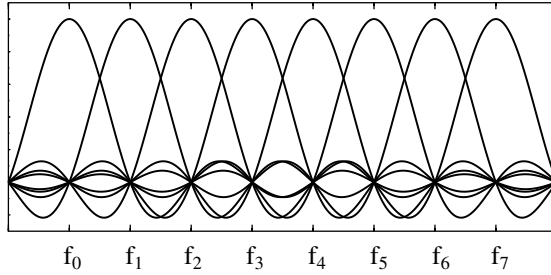


Figure 1.6: Illustration of OFDM signal's spectrum.

OFDM is to divide the system transmission bandwidth into a large number of small orthogonal sub-bands that are supported by subcarriers. The frequency spectrum of OFDM signals may be illustrated by Fig. 1.6, where the transmission bandwidth is divided into eight small orthogonal sub-bands supported by eight subcarriers. OFDM is a nature parallel data transmission scheme that transmits OFDM symbols consisting of parallel data symbols with the aid of serial-to-parallel (S/P) conversion, instead of transmitting data streams serially. For example, let the OFDM system consist of M number of subcarriers. Let

$$\mathbf{x} = [x(0), x(1), \dots, x(M-1)]^T \quad (1.3)$$

denote a block of data symbols to be transmitted. Then, in OFDM the transmitted signal can be formed as

$$s(t) = \sum_{m=0}^{M-1} \Re\{A_m x(m) \exp(j2\pi f_m t)\} \quad (1.4)$$

where $\Re\{\cdot\}$ denotes the real part of the argument, A_m denotes the amplitude of the m th subcarrier signal and f_m is the m th carrier frequency.

OFDM has been proposed for both broadband and ultrawide bandwidth (UWB) wireless communications. OFDM is beneficial to high data rate transmission in broadband or UWB wireless communications systems. A central feature of OFDM is that it can take advantage of the fast Fourier transform (FFT) to implement efficiently the multicarrier modulation/demodulation. Due to employment of the FFT-assisted multicarrier modulation/demodulation, in OFDM no band-pass filters matching the subcarrier frequencies are necessary, provided that the orthogonality of the subcarrier signals can be maintained. Consequently, the transceiver's complexity in OFDM systems can be significantly reduced.

In OFDM each sub-band can be made much smaller than the coherence bandwidth of the wireless channel. Hence, the subcarrier signals expose only frequency-nonselective (flat) fading, which is beneficial for employing low-complexity equalization techniques. In OFDM systems intersymbol interference (ISI) may be efficiently mitigated by the insertion of guard intervals.

It is well recognized that one of the main implementation disadvantages at the transmitter side of OFDM systems is the high peak-to-average power ratio of the transmitted signal, which may yield nonlinear distortions. The nonlinear distortion results in out-of-band

emission and co-channel interference, potentially causing degradation in the system's performance. The performance of OFDM systems is very sensitive to frequency offsets, and also to time offsets in multiuser OFDM systems. In order to take advantage of the FFT-based multicarrier modulation/demodulation, in multiuser OFDM systems accurate synchronization among the multiuser signals is essential.

OFDM was originally proposed for point-to-point communications, and is itself unsuitable for supporting multiple-access communications. In wireless communications OFDM can be combined with some other techniques, such as CDMA, spatial division multiple-access (SDMA), etc. for implementation of multiple-access communications.

1.3 Multiple Access

Multiple access is a technique allowing several (or even many) users (terminals) to communicate in the same physical medium and to share the available resources, such as capacity, spectrum, etc., among the users (terminals). In wireless communications typical multiple-access schemes include:

- frequency division multiple access (FDMA);
- time division multiple access (TDMA);
- code division multiple access (CDMA);
- spatial division multiple access (SDMA).

In FDMA systems the frequency band available is divided into a number of sub-bands and each sub-band constitutes a physical channel, for example, as shown in Fig. 1.7. In FDMA systems, whenever a user requests to communicate, a corresponding channel is assigned, provided that there is a channel available. In principle, in FDMA systems the channels may be divided evenly or unevenly, in order to support the services with different data rate requirements. A high data rate service in FDMA systems may also be supported by assigning to the service a corresponding number of channels. In FDMA each channel is associated with a (sub)carrier frequency.

In TDMA systems the time axis is first divided into frames of a certain frame length. Then, each of the frames is divided into a number of time slots of a certain duration, and each time slot is defined as a physical channel for supporting a user's communications. In TDMA systems the channels are conceptually illustrated in Fig. 1.8, where each frame is divided into five time slots for simultaneously supporting the communications of up to five users. A corresponding channel is assigned, whenever a user requests to communicate, provided that there is a channel available. In TDMA systems a high data-rate service can be supported by assigning the service more than one channel. In TDMA all the channels use the same carrier frequency.

One common feature of FDMA and TDMA is that the maximum number of channels is a constant and hence the maximum number of users supportable is fixed. In FDMA and TDMA the channels (capacity) are 'hard'; a channel cannot be assigned (even partially) to the other users once it is occupied, no matter how good the channel is. In FDMA and TDMA systems the channels are physically separated and they are orthogonal either in the frequency

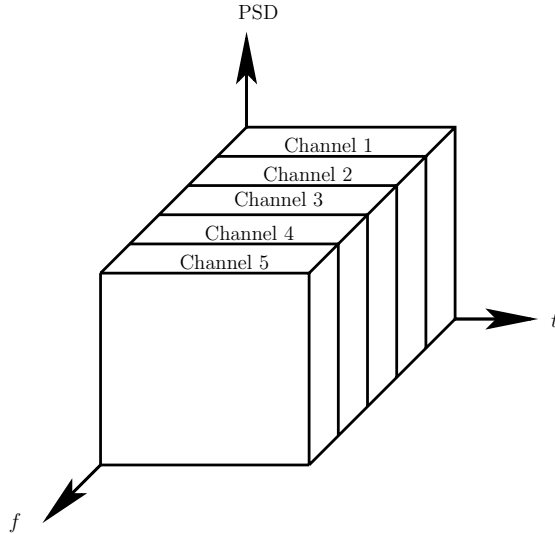


Figure 1.7: Illustration of channel configuration in FDMA systems. Different users transmit signals on different frequencies at the same time.

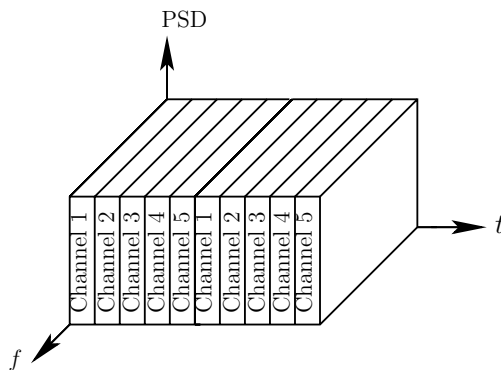


Figure 1.8: Illustration of channel configuration in TDMA systems. Different users transmit signals at different time slots using the whole frequency band available.

domain (FDMA) or in the time domain (TDMA). Hence, there is general no interchannel interference, when communicating in the same cell, unless the communications environment is deficient, thus destroying the orthogonality among the channels.

The concept of CDMA is illustrated in Fig. 1.9. All the users in CDMA communicate within the same frequency band at the same time. CDMA supports multiple users with the aid of spread-spectrum techniques as discussed in Section 1.1. In CDMA systems each user is assigned a unique spreading code, which is often referred to as the user signature code. Different users in CDMA systems can be distinguished by their unique spreading codes, provided that the cross-correlation among the spreading codes is sufficiently low, allowing the detector thereby with sufficient information to identify different users. In CDMA the

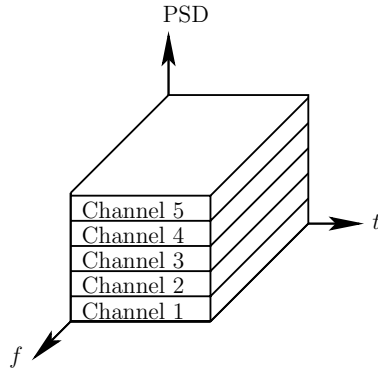


Figure 1.9: Illustration of channel configuration in CDMA systems. Different users are distinguished by their unique codes. All user signals are transmitted on the same frequency band at the same time.

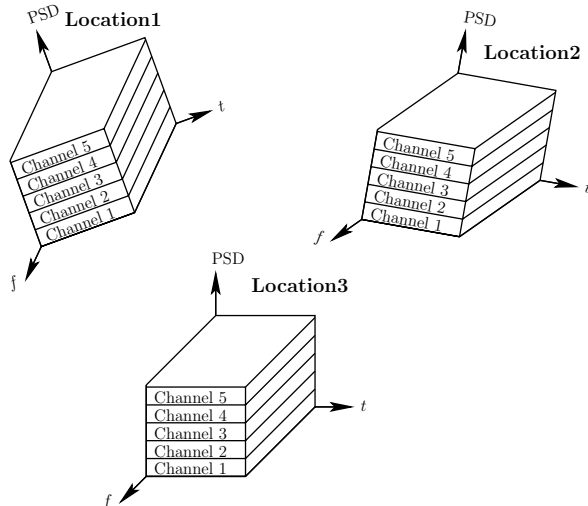


Figure 1.10: Illustration of channel configuration in SDMA systems. Different users or user sets can also be distinguished by their locations.

maximum number of channels is determined by the maximum number of spreading codes available, which is usually very high. Hence, the maximum number of users supportable by a CDMA system is generally not determined by the maximum number of spreading codes available, but mainly by the communications environment. Therefore, the maximum number of users supportable or the capacity of a CDMA system is ‘soft’: more users may be supported in good communications environments having high signal-to-interference-plus-noise ratio (SINR), while fewer users are allowed in worse communications environments resulting in low SINR. CDMA techniques are suitable for wideband, broadband and UWB communications.

Finally, the idea of SDMA is illustrated in Fig. 1.10, where three sets of CDMA users are geographically separated into three locations, and at each location five CDMA users share the same spectrum at the same time. Hence, we can view Fig. 1.10 as a spatial-code-division multiple-access (SCDMA) scheme. In SDMA systems different users (which use the same spreading code) may be distinguished by making use of the characteristics of wireless communications channels. Specifically, the wireless channels of different users separated geographically with sufficient distance will experience uncorrelated fading, yielding different channel impulse responses (CIRs) observed by a receiver. Once the receiver obtains the CIR information of the users, these CIRs can be viewed as the signature codes of the users as in the CDMA systems. Consequently, the receiver is capable of distinguishing the users with the aid of their unique CIRs.

In SDMA systems the CIRs are determined by the wireless communications channels, which are random, time-varying and cannot be regulated during system design. Hence, in SDMA systems powerful detectors are usually required.

1.4 Duplex

Duplex considers the techniques (or strategies) of communications against two directions, generally, incoming and outgoing, or uplink and downlink in cellular wireless systems. Below we provide a brief overview of the duplex techniques, including the well-known time-division duplex (TDD) and frequency-division duplex (FDD), the less known code-division duplex (CDD) as well as the multicarrier-division duplex (MDD) proposed in Chapter 8. Let us first consider the TDD scheme.

1.4.1 Time-Division Duplex (TDD)

In the context of the wireless communications systems based on TDD, the uplink (incoming) and downlink (outgoing) communications are separated (orthogonal) in the time domain, while communicating within the same frequency band. Specifically, as shown in Fig. 1.11, in the TDD-based wireless systems the time axis is divided into a number of time slots. A time slot can be assigned either for the uplink (U) transmission or for the downlink (D) transmission. Due to the fact that wireless channels experience delay-spread, which results in ISI, a certain amount of guard-time is usually inserted between two adjacent time slots, as shown in Fig. 1.11. TDD has a typical advantage in the case where the uplink and downlink data rates are asymmetric and variable. In this case, as the amount of downlink data increases and that of the uplink data decreases, more time slots (bandwidth) can be dynamically allocated to the downlink, while fewer time slots (bandwidth) are correspondingly allocated to the uplink. Another advantage of using TDD is that the uplink (incoming) and downlink (outgoing) channels in TDD-based systems are reciprocal. In this case, the broadcast downlink channels from base-station (BS) to mobile terminals (MTs) can be estimated or predicted using its reciprocity with the uplink channels from MTs to BS.

While the TDD-based wireless communications employ the above-mentioned advantages, especially the advantage of facilitating the downlink channel estimation at the BS, the TDD-based systems have some common disadvantages, especially when cellular communications are considered. First, the TDD-based systems place a high demand on

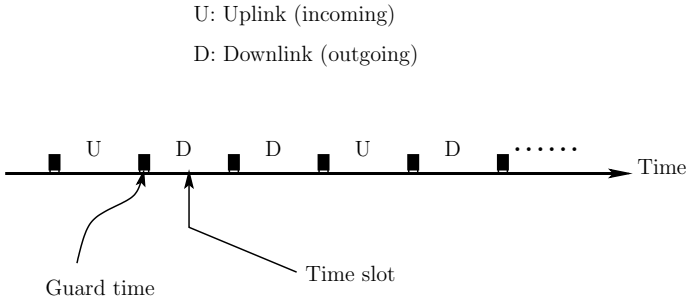


Figure 1.11: Illustrate of the time-division duplex (TDD).

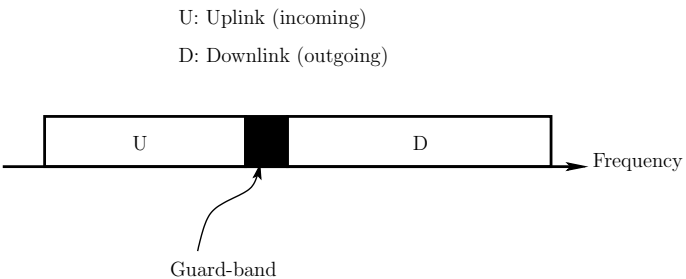


Figure 1.12: Illustrate of the frequency-division duplex (FDD).

system synchronization. Second, the TDD mode is not efficient when the uplink and downlink transmissions are symmetric. In this case, the TDD mode tends to waste bandwidth during switching frequently between transmitting and receiving. Furthermore, the fast switching between transmitting and receiving requires complex and power-hungry circuitry. Additionally, since in the TDD-based systems the uplink and downlink are operated within the same frequency band, the TDD mode tends to experience severe intra-cell and inter-cell interference. In a multicell TDD-based wireless system, an uplink (downlink) signal experiences interference not only from the other uplink (downlink) signals of its own cell but also from both the uplink and downlink signals of the other cells.

1.4.2 Frequency-Division Duplex (FDD)

For wireless communications systems based on FDD, the uplink (incoming) and downlink (outgoing) are separated (orthogonal) in the frequency domain. The principles of FDD can be well-understood with the aid of Fig. 1.12. In FDD-assisted wireless communications, the available frequency bandwidth is divided into two sub-bands – one is for the uplink transmission and the other is for the downlink transmission – which are supported by two carrier frequencies. The uplink and downlink sub-bands are separated by a so-called guard-band.

The FDD mode is efficient for the transmission of symmetric traffic of the uplink and downlink. Another advantage of the FDD is that it makes radio planning easier and

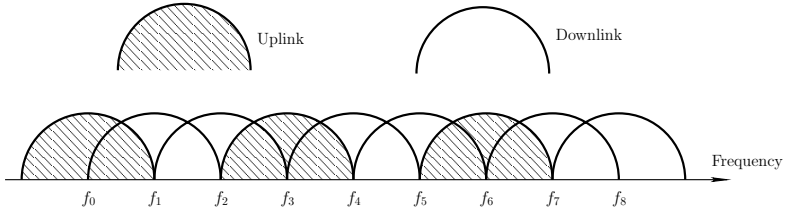


Figure 1.13: Illustration of the multicarrier-division duplex (MDD), where one-third of the sub-bands are allocated for uplink transmission and two-thirds of the sub-bands are allocated for downlink transmission.

more efficient. In FDD-based wireless systems, in principle, there is no interference between uplink and downlink signals. An uplink signal suffers interference only from the uplink signals of the intracell and intercells, while a downlink signal conflicts interference only from the downlink signals of the intracell and intercells.

Since in FDD-based systems the uplink and downlink are operated on two separate frequency bands, the uplink and downlink channels are not reciprocal. Therefore, applying transmitter preprocessing techniques, such as those studied in Chapter 8, at BS in FDD-based systems is much more difficult than applying them in TDD-based systems. In FDD-based systems the channel knowledge required for carrying out the transmitter preprocessing might have to be fed back from the receiver(s) to the transmitter(s). However, the feedback process introduces delay, which results in the transmitter preprocessing generally operating on inaccurate or even outdated channel information. Furthermore, feeding back the channel knowledge requires extra bandwidth – more bandwidth for feedback is required when the channel fading becomes faster – which may substantially reduce the communications efficiency.

1.4.3 Multicarrier-Division Duplex (MDD)

When multicarrier communications are considered, MDD may be employed for the uplink (incoming) and downlink (outgoing) transmissions. The MDD essentially belongs to the family of FDD. The principles of MDD mode can be understood by referring to Fig. 1.13, where one-third of the subcarriers are allocated to support the uplink transmission, while the remaining two-thirds are allocated to support the downlink transmission. Generally, in MDD-mode, both the uplink and downlink channels are operated within the same frequency band. A fraction of the sub-bands (subcarriers) can be allocated to support the uplink transmission, the others to the downlink transmission. Usually, the subcarrier signals are chosen to be orthogonal with each other. In MDD-mode, according to the practical requirements, the number of sub-bands allocated to the uplink or downlink of a user can be fixed or dynamic. The number of sub-bands allocated to a user can also be different from that allocated to another user.

In short, the MDD mode employs all the advantages of the TDD-mode. First, the MDD mode is capable of supporting asymmetric and variable traffics for the uplink and downlink. This can be readily achieved by dynamically allocating the corresponding number of sub-bands for the uplink and downlink. Second, in MDD mode the channel knowledge required for carrying out transmitter preprocessing can be readily obtained with the aid of

frequency-domain channel estimation or prediction. The MDD mode also inherits some of the merits of the FDD mode. For example, in FDD mode there is no switch-over between transmission and receiving. In MDD mode there is no, or only very little, chance of switch-over between transmission and receiving. Furthermore, the MDD mode may employ some merits that the TDD and FDD modes are incapable of providing. The MDD mode has the greatest flexibility for design or online reconfiguration, as, in comparison with the TDD and FDD modes, the MDD mode uses a higher number of parameters that can be adjusted according to the requirements in practice. Furthermore, it appears that the MDD mode is suitable for many types of communications environment, including short-distance and long-distance communications, different types of cellular wireless communication, indoor and outdoor, etc.

One typical problem with the MDD mode is the added intercarrier interference, which may degrade significantly the achievable performance when the channel fading becomes time-selective or when there are frequency offsets. Hence, in MDD mode the intercarrier interference should be taken care of, which may be mitigated with the aid of some advanced signal-processing techniques.

1.4.4 Code-Division Duplex (CDD)

In addition to the above-reviewed three types of duplex technique, the uplink (incoming) and downlink (outgoing) transmissions can also be operated in a scheme called as CDD [1]. As the name CDD indicates, in CDD-based systems the uplink and downlink transmissions are supported by different codes. Specifically, let \mathcal{C}_U and \mathcal{C}_D be two sets of codes defined for the uplink and downlink transmissions, respectively. Then, for each active user in a CDD-based wireless system, its uplink transmission is supported by a code chosen from set \mathcal{C}_U , while its downlink transmission is by a code chosen from set \mathcal{C}_D .

The CDD mode may have many advantages, including flexibility and spectral efficiency. In CDD mode, in order to reduce the interference between the uplink and downlink, the cross-correlation between any two codes, one of which is from \mathcal{C}_U and the other from \mathcal{C}_D , should be sufficiently low. However, wireless channels are typically dynamic and experience delay-spread yielding frequency-selective fading. Hence, even though every code from \mathcal{C}_U is orthogonal to any code from \mathcal{C}_D , it is generally hard to maintain the orthogonality in practice. In [1] a set of codes referred to as *large area synchronous* (LAS) codes has been suggested for the CDD mode. The LAS codes are capable of maintaining the orthogonality among the codes, provided that the delay-spread of wireless channels does not exceed a certain value known as the correlation window. However, the maximum number of LAS codes is inversely proportional to the width of the correlation window.

1.5 Diversity in Wireless Communications

It is well known that signals transmitted over wireless channels experience fading, which, when not being taken care of or made use of, may greatly degrade the performance of communications. In modern wireless communications, fading can be efficiently mitigated by exploiting various types of diversity, which may be extracted from the time domain, frequency domain, space domain, etc. Here, by diversity we mean that the receiver can observe the transmitted signal through different angles, yielding multiple (possibly uncorrelated) observation copies of the same transmitted signal. Let us use a simple example to show the advantages of using diversity, by considering two communications cases.

Case 1: The receiver can only obtain one observation of the transmitted signal, which is expressed as

$$r_A = \alpha s + n \quad (1.5)$$

where s represents the transmitted data symbol, α denotes the fading channel amplitude, while n denotes the additive white Gaussian noise (AWGN), which obeys the Gaussian distribution with zero mean and a variance of σ^2 .

From (1.5), we know that the instantaneous signal-to-noise ratio (SNR) is $\gamma = \alpha^2 E[s^2]/(2\sigma^2)$, while the average SNR is $\gamma_c = E[\alpha^2]E[s^2]/(2\sigma^2) = \Omega E[s^2]/(2\sigma^2)$, where $E[\alpha^2] = \Omega$.

Case 2: The receiver can obtain two independent observations of the same transmitted signal, expressed as

$$r_{B1} = \alpha_1 s + n_1 \quad \text{and} \quad r_{B2} = \alpha_2 s + n_2 \quad (1.6)$$

respectively, where α_1 and α_2 are fading amplitudes, and n_1 and n_2 are AWGN samples with a common variance of σ^2 .

From (1.6), the total instantaneous SNR is given by $\gamma_B = (\alpha_1^2 + \alpha_2^2)E[s^2]/(2\sigma^2)$, while the average SNR of each observation is given by $\gamma_{c1} = \gamma_{c2} = E[\alpha_1^2]E[s^2]/(2\sigma^2) = 0.5\Omega E[s^2]/(2\sigma^2)$, implying that $E[\alpha_1^2] = E[\alpha_2^2] = 0.5\Omega$.

From the above two cases, we can observe that first, the total average SNR for both cases is the same, which is $\gamma_c = \Omega E[s^2]/(2\sigma^2)$. Hence, when communicating over Gaussian channels corresponding to $\alpha = 1$, $\alpha_1 = \alpha_2 = 0.5$, both cases achieve the same bit error rate (BER) performance. Second, the instantaneously received SNR values for Cases 1 and 2 can be expressed as

$$\gamma = \frac{\alpha^2}{\Omega} \gamma_c \quad (1.7)$$

$$\gamma_B = \frac{(\alpha_1^2 + \alpha_2^2)}{\Omega} \gamma_c \quad (1.8)$$

Now let us consider the communications over Rayleigh fading channels. Then, α , α_1 and α_2 obey the Rayleigh distributions associated with the PDFs given by

$$p_\alpha(y) = \frac{2y}{\Omega} \exp\left(-\frac{y^2}{\Omega}\right), \quad y \geq 0 \quad (1.9)$$

$$p_{\alpha_1}(y) = p_{\alpha_2}(y) = \frac{2y}{0.5\Omega} \exp\left(-\frac{y^2}{0.5\Omega}\right), \quad y \geq 0 \quad (1.10)$$

With the aid of (1.9) and (1.10), it can be shown that γ in (1.7) and γ_B in (1.8) obey the central χ^2 -distributions with two and four degrees-of-freedom, with their PDFs given by

$$f(\gamma) = \frac{1}{\gamma_c} \exp\left(-\frac{\gamma}{\gamma_c}\right), \quad \gamma \geq 0 \quad (1.11)$$

$$f(\gamma_B) = \frac{\gamma_B}{(0.5\gamma_c)^2} \exp\left(-\frac{\gamma_B}{0.5\gamma_c}\right), \quad \gamma_B \geq 0 \quad (1.12)$$

respectively.

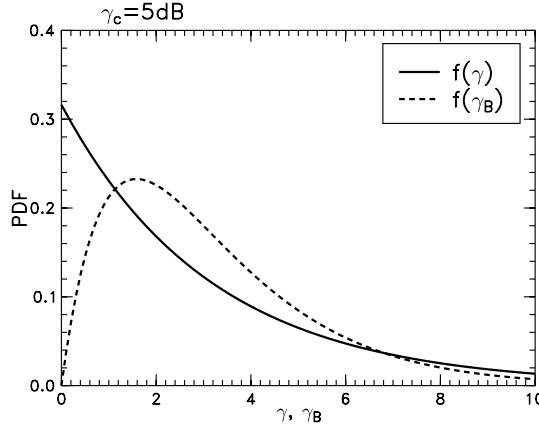


Figure 1.14: Illustration of the PDFs of γ and γ_B , shown in (1.11) and (1.12).

The PDFs of (1.11) and (1.12) are depicted in Fig. 1.14, where the total average SNR was assumed to be $\gamma_c = 5$ dB. According to Fig. 1.14, we can observe explicitly that γ_B has a relatively higher chance than γ to yield relatively high instantaneous SNR for detection, even though both cases have the same total average received power or SNR. Therefore, when, e.g., BPSK baseband modulation is assumed, the average BER of Case 1 should be higher than that of Case 2. In other words, when the receiver can obtain two independent observations (Case 2) instead of one (Case 1) of the transmitted signal, the detection performance of the communications scheme can then be improved. Correspondingly, we say that (Case 2) is capable of achieving a diversity order of two.

In the context of the general case, where the receiver can obtain L number of independent observations having the same average power of Ω/L for the same transmitted signal, the PDF of the instantaneously received SNR can be expressed as

$$f(\gamma) = \frac{\gamma^{L-1}}{(L-1)! \bar{\gamma}^L} \exp\left(-\frac{\gamma}{\bar{\gamma}}\right), \quad \gamma \geq 0 \quad (1.13)$$

which is a central χ^2 -distribution with ($n = 2L$) degrees-of-freedom. In (1.13) $\bar{\gamma}_l = \Omega E[s^2]/(L \times 2\sigma^2) = \gamma_c/L$, implying that the total average received SNR is the same, regardless of the diversity order of L .

The PDFs of (1.13) associated with various values of L are depicted in Fig. 1.15. As shown, when the diversity order L increases, the shape of the PDF becomes more similar to the Gaussian PDF. When the diversity order L increases, the range that the PDF spans becomes smaller and converges to a value of $\gamma_c = 5$ dB ($= \sqrt{10} \approx 3.2$). Therefore, it can be implied that when the diversity order L tends to infinity, the PDF will converge to a Dirac delta function located at $\gamma = \gamma_c = \sqrt{10}$. Correspondingly, the BER performance of a communications scheme will converge to that achieved in Gaussian channels.

In order to illustrate this, let us assume that the BPSK baseband digital modulation scheme is used. Then, given the instantaneous SNR value of γ , it can be shown (see, e.g., [2]) that the conditional BER can be expressed as $Q(\sqrt{2}\gamma)$, where $Q(x)$ is the Gaussian Q -function,

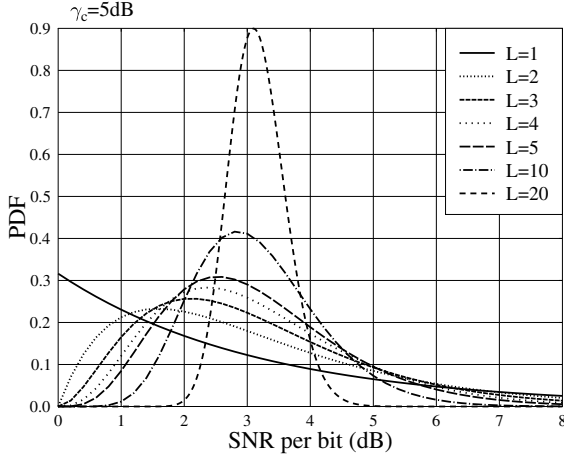


Figure 1.15: Illustration of the PDF of (1.13), when various diversity orders are assumed.

which is defined as $Q(x) = (\sqrt{2\pi})^{-1} \int_x^\infty \exp(-t^2/2) dt$. Furthermore, the average BER can be evaluated as [2]

$$P_e = \int_0^\infty Q(\sqrt{2\gamma}) f(\gamma) d\gamma \quad (1.14)$$

On substituting $Q(\sqrt{2\gamma})$ and (1.13) into the above equation and simplifying it, the average BER of the L th-order diversity BPSK scheme can be found as [2]

$$P_e = \left[\frac{1-\mu}{2} \right] \sum_{k=0}^{L-1} \binom{L-1+k}{k} \left[\frac{1+\mu}{2} \right]^k \quad (1.15)$$

where $\bar{\gamma}$ has been defined under (1.13) and $\mu = \sqrt{\bar{\gamma}}/(1 + \bar{\gamma})$.

The average BER of (1.15) is depicted in Fig. 1.16 against the SNR per bit, when various diversity order L is assumed. Figure 1.16 also shows the BER of the BPSK communicating over AWGN channels. As predicted, when the diversity order L increases, the BER performance in multipath Rayleigh fading channels becomes closer to that achieved in the AWGN channels.

The above analysis shows us that, in order for the receiver to achieve diversity, the receiver should be able to generate a number of, preferably independent, observations for the same transmitted signal. In wireless communications, diversity may be achieved in the frequency domain, time domain, space domain or jointly, through a wealth of techniques. Correspondingly, the diversity is called *frequency-diversity*, *time-diversity*, *spatial-diversity*, etc. The principles behind these types of diversity-achieving schemes are described as follows.

- **Frequency-diversity:** Wireless channels are frequency-selective, resulting in signals that are transmitted on different frequency bands sufficiently separated in frequency experiencing uncorrelated fading. Hence, when a signal is transmitted on two frequency bands sufficiently separated in frequency, e.g., higher than the *coherence bandwidth* of

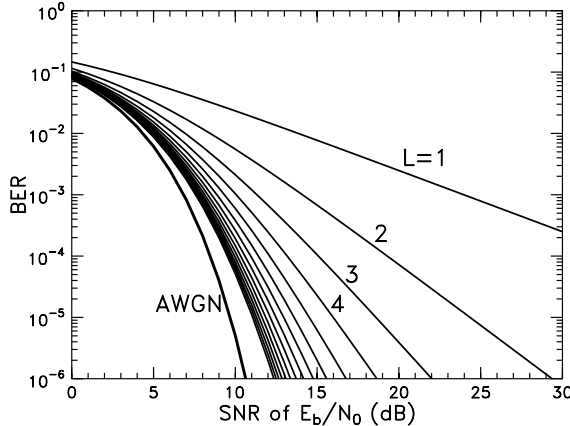


Figure 1.16: BER versus SNR per bit of E_b/N_0 performance of the BPSK system, when communicating over AWGN and multipath Rayleigh fading channels.

the channel, two uncorrelated observations of the transmitted signal may be obtained by the receiver from these two frequency bands, and a diversity order of two can then be achieved.

- **Time-diversity:** Wireless channels are typically time-variant and time-selective, resulting in signals that are transmitted on different time slots that are sufficiently separated in time experiencing uncorrelated fading. Therefore, when a signal is transmitted within two time slots sufficiently separated in time, e.g. higher than the *coherence time* of the channel, two uncorrelated observations of the transmitted signal may be obtained by the receiver from these two time slots, and a diversity order of two can then be achieved.
- **Spatial-diversity:** Wireless channels are also spatial-selective, resulting in signals that are transmitted at different locations that are sufficiently separated (usually higher than 10 wavelengths between any two locations) experiencing uncorrelated fading. Hence, when a transmitted signal is received by two receive antennas separated by a sufficient distance in space, the received signals of these two receive antennas are uncorrelated, and a diversity order of two can be achieved. Instead of using two receive antennas, when two copies of a same signal are transmitted through two transmit antennas sufficiently separated in space, two uncorrelated observations of the transmitted signal may also be obtained by a receiver and, correspondingly, a diversity order of two can be achieved.

1.6 Organization of the Book

This book is divided into nine chapters. The remaining chapters can be summarized as follows.

Chapter 2 presents the principles of various spread-spectrum schemes, including both the basic spread-spectrum schemes as well as the hybrid spread-spectrum schemes. The main objective of this chapter is to explore the principles of spread-spectrum communications in a unified treatment and to design novel hybrid spread-spectrum schemes based on attractive combinations of various spread-spectrum schemes.

Chapter 3 first considers the communications principles of OFDM. Then, the communications principles of seven types of multicarrier scheme are investigated. These seven multicarrier schemes include frequency-domain spread multicarrier CDMA (MC-CDMA), orthogonal multicarrier direct-sequence CDMA (MC DS-CDMA), single-carrier frequency-division multiple access (SC-FDMA), multitone DS-CDMA, generalized MC DS-CDMA, time-hopping multicarrier CDMA (TH/MC-CDMA) and time-frequency-domain spread MC DS-CDMA. The advantages and disadvantages of the above-listed multicarrier schemes are discussed in this chapter.

In Chapters 4 and 5 the BER performance of a variety of multicarrier systems is investigated, when communicating over AWGN channels (Chapter 4) or over frequency-selective fading channels (Chapter 5). The detectors considered in these two chapters are the single-user detectors, which are either the single-user correlation detectors or the single-user matched-filter (MF) detectors. In these two chapters we focus mainly on the analysis of the single-user BER-bound performance for various multicarrier systems. We also investigate the BER performance of the generalized time-frequency-domain spread MC DS-CDMA systems supporting multiple users.

Chapter 6 covers the multiuser detection (MUD) principles and applications in multicarrier CDMA systems. A wide range of MUD schemes are treated under various optimization principles. Many BER performance examples obtained by simulations are provided in this chapter, in order to characterize the achievable BER performance of the MUD schemes considered.

In contrast to Chapter 6, where the MUDs are derived by assuming that the corresponding receivers are capable of tracking the carrier phases, resulting in coherent MUD, in Chapter 7 noncoherent MUD is investigated in the context of the TH/MC-CDMA, since in the TH/MC-CDMA the carrier phases of the received signals are difficult to estimate owing to its time-hopping characteristics. In Chapter 7 a wide range of noncoherent MUDs are derived and the performance of the TH/MC-CDMA using these noncoherent MUDs is investigated. Note that, the noncoherent MUDs considered in Chapter 7 are general and their extension to the other noncoherent multiuser systems, such as to the FFH multiuser systems, is straightforward.

Chapter 8 investigates the multiuser transmitter preprocessing in association with three types of representative multicarrier CDMA scheme, namely the frequency-domain spread MC-CDMA, the MC DS-CDMA and the time-frequency-domain spread MC DS-CDMA. In this chapter a wide range of transmitter preprocessing schemes are derived. It can be shown that, in downlink multiuser communications, the downlink multiuser interference can be efficiently mitigated with the aid of the transmitter preprocessing carried out at the BS. In this chapter, furthermore, the acquisition of the channel knowledge for transmitter preprocessing is discussed in the context of the TDD-, FDD-, and MDD-based systems.

Finally, in Chapter 9 we explore the space-time processing in multiple-antenna (multi-antenna) multicarrier CDMA systems. Capacity of multiple-input multiple-output (MIMO) channels is first considered, followed by the principles of a range of spatial diversity techniques, including receive diversity, closed-loop and open-loop transmit diversity, etc.

Then, the applications of space–time processing in the context of different multicarrier CDMA schemes are analysed. Furthermore, in this chapter design of multiantenna MC DS-CDMA is considered for wireless environments experiencing simultaneously both frequency-selective and time-selective fading.

Chapter 2

Principles of Code-Division Multiple-Access Communications

L.-L. Yang and L. Hanzo

The phrase ‘*spread-spectrum transmission*’ has been a well-known terminology in the field of wireless communications for several decades [3–5]. The research and application of spread-spectrum techniques have evolved from the desire to support covert communications in the 1950s and by now have reached a state of maturity, finding its application in nearly every corner of wireless communications. Spread-spectrum techniques have been widely applied for providing anti-jamming and anti-detection communications [3–6]. Simultaneously, these techniques have been invoked for supporting multiuser communications and for efficiently exploiting wireless resources, in military and civilian wireless communications, rendering the terminology ‘*spread spectrum*’ truly ubiquitous.

This chapter is devoted to the review and analysis of the principles of various spread-spectrum systems with an emphasis on the principles of code-division multiple-access (CDMA) communications [3–8]. Specifically, four basic spread-spectrum schemes and two hybrid spread-spectrum schemes will be highlighted. These basic spread-spectrum schemes include:

- direct-sequence spread spectrum (DS-SS), which is also referred to as time-domain DS-SS;
- multicarrier spread spectrum (MC-SS), which is also referred to as frequency (F)-domain DS-SS;
- frequency-hopping spread spectrum (FH-SS);
- time-hopping spread-spectrum (TH-SS).

The hybrid spread-spectrum schemes considered include:

- hybrid direct-sequence frequency-hopping (DS/FH) spread spectrum [9, 10];
- hybrid direct-sequence time-hopping (DS/TH) spread spectrum [11, 12].

In the above-mentioned set of spread-spectrum schemes, the most widely known techniques are constituted by the family of DS-SS and FH schemes. Both of them have found wide-ranging application in the context of both secure military wireless communications [3–6, 13] as well as in the second [7, 8] and third [14] generations of civilian mobile wireless communications systems. The spread-spectrum scheme using hybrid DS/FH [9, 10] was widely studied during the end of 1980s and the beginning of 1990s. Despite the intensive research efforts, to date, no hybrid DS/FH spread-spectrum schemes have found use in civilian wireless communications. By contrast, the suite of MC- [15, 16] and TH- [17, 18] based spread-spectrum techniques has attracted attention in more recent years, in particular in the context of broadband [19] and ultrawide bandwidth (UWB) [20–22] wireless communications systems, respectively. The multicarrier broadband wireless systems and the DS-, TH- as well as DS/TH-based UWB systems are becoming more and more attractive in wireless communications. Our prime objective in this chapter is to explore the principles of spread-spectrum communications in a unified treatment and to show the design of novel hybrid spread-spectrum schemes based on attractive combinations of various spread-spectrum schemes.

The material found in this chapter draws on an amalgam of the following references by [2–6, 9, 10, 13, 15–18, 20–25].

2.1 Direct-Sequence Spread Spectrum

In order to introduce the basic concepts of direct-sequence spread-spectrum (DS-SS) communications, let us commence by considering conventional binary phase shift keying (BPSK). The BPSK modulated signal can be expressed as

$$s_k(t) = \sqrt{2P} b_k(t) \cos(2\pi f_c t + \varphi_k) \quad (2.1)$$

where the subscript k represents the index of the k th user, P is the user's transmitted power, f_c is the carrier frequency, while φ_k denotes the initial phase angle associated with the carrier modulation. Furthermore, in (2.1) $b_k(t) = \sum_{n=-\infty}^{\infty} b_k[n] P_{T_b}(t - nT_b)$ represents the infinite-duration transmitted waveform generated by the binary data stream, which consists of a sequence of rectangular signalling pulses $P_{T_b}(t)$ of duration T_b , weighted by the bit-related values of amplitude +1 or -1. Here, T_b is usually referred to as the bit duration, while the signalling pulse $P_\tau(t)$ of duration τ is defined as

$$P_\tau(t) = \begin{cases} 1, & 0 \leq t \leq \tau \\ 0, & \text{otherwise} \end{cases} \quad (2.2)$$

The signal waveforms involved in (2.1) are shown in Fig. 2.1, demonstrating the process of BPSK modulation. As shown in Fig. 2.1, the phase of the carrier changes by 180° , whenever the data waveform toggles from +1 to -1 or from -1 to +1. Hence, the BPSK modulated signal of (2.1) can also be written as

$$s_k(t) = \sqrt{2P} \cos\left(2\pi f_c t + b_k(t)\frac{\pi}{2} + \varphi_k\right) \quad (2.3)$$

Therefore, BPSK modulation can be viewed either as amplitude modulation, as shown in (2.1) or as phase modulation as shown in (2.3).

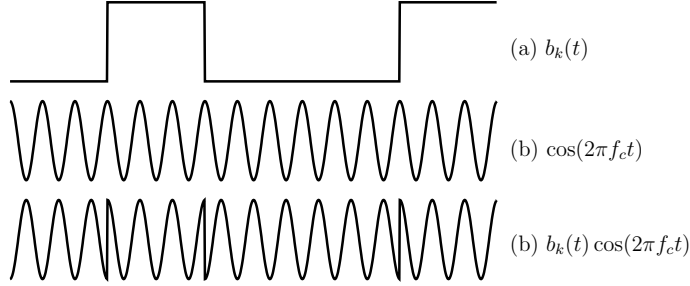


Figure 2.1: Illustration of BPSK related waveforms.

Assume that $b_k[n]$ in $b_k(t)$ is an independent identically distributed (iid) random variable, which assumes values of $+1$ or -1 with equal probability of 0.5. Then, the baseband equivalent power spectral density (PSD) of a BPSK modulated signal can be derived as [6]

$$S_{\text{BPSK}}(f) = \frac{2P}{T_b} |P(f)|^2 \quad (2.4)$$

where $P(f)$ represents the Fourier transform of the pulse shape $P_{T_b}(t)$, which is derived as

$$\begin{aligned} P(f) &= \int_{-\infty}^{\infty} P_{T_b}(t) \exp(-j2\pi ft) dt \\ &= \int_0^{T_b} \exp(-j2\pi ft) dt \\ &= \frac{1}{j2\pi f} [1 - \exp(-j2\pi f T_b)] \end{aligned} \quad (2.5)$$

The magnitude or modulus of $P(f)$ can be derived using the above equation, which is given by $|P(f)| = T_b \text{sinc}(\pi f T_b)$, where $\text{sinc}(x) = \sin(x)/x$. Upon substituting $|P(f)|$ into (2.4), it can be shown that

$$S_{\text{BPSK}}(f) = 2PT_b |\text{sinc}(\pi f T_b)|^2 \quad (2.6)$$

Figure 2.2 shows the baseband equivalent PSD of the BPSK modulated signal of (2.1), indicating that the one-sided bandwidth of a BPSK signal measured up to its first zero-crossing is equal to $1/T_b$, while its peak value is $2PT_b$, which is located at the position, $f = 0$ Hz. For the sake of simplicity it is often assumed that the energy outside this bandwidth may be neglected, although strictly speaking, owing to the employment of rectangular signalling pulses, the sinc-shaped PSD expands over an infinite frequency band.

Having reviewed some basic characteristics of BPSK modulated signals, let us now consider the philosophy of DS-SS systems using BPSK modulation.

2.1.1 Transmitted Signals

A DS-SS scheme transmits DS-spread signals using a single carrier. The k th user's transmitter schematic that employs a DS-SS scheme and BPSK modulation is shown in Fig. 2.3. In

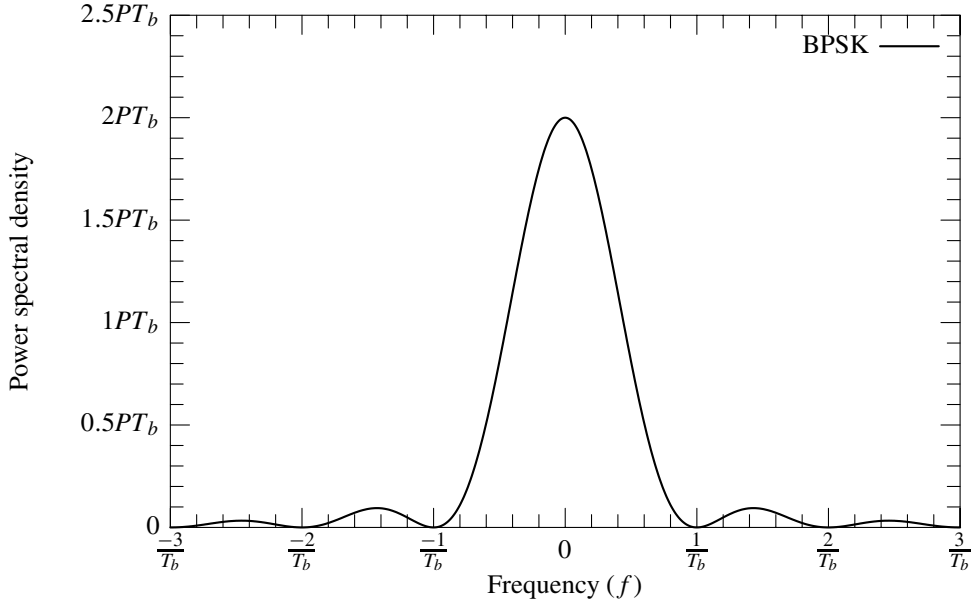


Figure 2.2: Baseband equivalent PSD of the transmitted signal in (2.1) using BPSK modulation.

the DS-SS scheme of Fig. 2.3 the original data stream $b_k(t)$ of bit duration T_b is spread with the aid of the k th user's spreading code $c_k(t)$, which is also often referred to as a unique user signature sequence. The spreading code $c_k(t)$ is constituted by short pulses of duration T_c , where the time duration T_c is referred to as *chip*. The spreading sequence $c_k(t)$ can be generated by a so-called pseudo-noise (PN) sequence generator.¹ Usually, the chip duration T_c is significantly lower than the bit duration T_b , and $N = T_b/T_c$ is defined as the *spreading gain* or *spreading factor*. After the DS spreading operation of Fig. 2.3, the DS-spread waveform modulates the carrier frequency f_c using BPSK modulation, in order to form the transmitted signal $s_k(t)$. Hence, the transmitted signal of the DS-SS scheme using BPSK modulation can be expressed as

$$s_k(t) = \sqrt{2P} b_k(t) c_k(t) \cos(2\pi f_c t + \varphi_k) \quad (2.7)$$

where P , f_c and φ_k represent the transmitted power, carrier frequency and initial phase, respectively, $b_k(t) = \sum_{n=-\infty}^{\infty} b_k[n] P_{T_b}(t-nT_b)$ is the infinite-duration transmission waveform as in (2.1). In (2.7) the infinite-duration spreading sequence $c_k(t) = \sum_{n=-\infty}^{\infty} c_k[n] \psi_{T_c}(t-nT_c)$ denotes the unique, user-specific signature sequence waveform of the k th user, where $c_k[n]$ assumes values of $+1$ or -1 , while $\psi_{T_c}(t)$ is the chip waveform, which is defined over the interval $[0, T_c]$ and is normalized so that we have

$$\int_0^{T_c} \psi_{T_c}^2(t) dt = T_c \quad (2.8)$$

¹The terminology PN is used, since PN spreading codes have a frequency-domain representation, which is reminiscent of the flat spectrum of white noise.

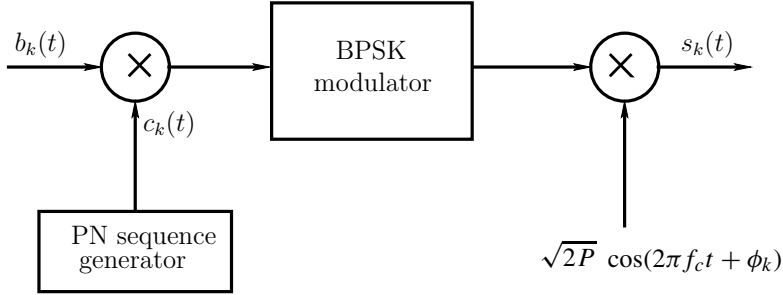


Figure 2.3: The k th user's transmitter schematic, when employing a DS-SS scheme and BPSK modulation.

By comparing (2.7) to (2.1) we can infer that the only difference between these two equations is that the binary waveform $b_k(t)$ in (2.1) is now replaced by the waveform $b_k(t)c_k(t)$ in (2.7), which is also binary, if we assume the employment of rectangular chip waveforms, i.e. we assume that $\psi_{T_c}(t) = P_{T_c}(t)$. However, since the chip-duration T_c is significantly lower than the bit-duration T_b , the bandwidth W_{DS} of the transmitted DS-SS signal of (2.7) is determined by the chip waveforms. As an example, if we assume that $c_k[n]$ in $c_k(t)$ is an iid random variable taking values of $+1$ or -1 with an equal probability of 0.5, and that a rectangular chip waveform of $P_{T_c}(t)$ is employed, then, the baseband equivalent PSD of the DS-SS signal of (2.7) can be expressed as

$$S_{\text{DS-SS}}(f) = 2PT_c|\text{sinc}(\pi f T_c)|^2 \quad (2.9)$$

The baseband equivalent PSD of the DS-SS signal of (2.7) and that of the conventional BPSK signal of (2.1) are shown in Fig. 2.4 in conjunction with a spreading gain of $N = T_b/T_c = 15$. It can be seen that the effect of convolving the modulated signal with the DS spreading sequence is that the bandwidth of the transmitted signal measured up to its first zero-crossing was expanded by a factor of 15, and that this spreading operation reduces the peak of the PSD by the spreading factor, namely by a factor of 15.

2.1.2 Detection of DS-SS Signals

2.1.2.1 Correlation Receiver

In order to introduce the basic detection principles of DS-SS signals, the k th user's signal of (2.7) is assumed to be transmitted via a distortionless and noiseless channel, which is assumed to have a transmission delay of τ seconds. Hence, the received signal can be expressed as

$$r(t) = \sqrt{2P}b_k(t - \tau)c_k(t - \tau)\cos(2\pi f_c t + \phi_k) \quad (2.10)$$

where we have $\phi_k = \varphi_k - 2\pi f_c \tau$. Assuming that the receiver has achieved perfect carrier synchronization, then, upon multiplying both sides of (2.10) by $\cos(2\pi f_c t + \phi_k)$, we obtain

$$r(t)\cos(2\pi f_c t + \phi_k) = \sqrt{2P}b_k(t - \tau)c_k(t - \tau)\left[\frac{1}{2} + \frac{1}{2}\cos(4\pi f_c t + 2\phi_k)\right] \quad (2.11)$$

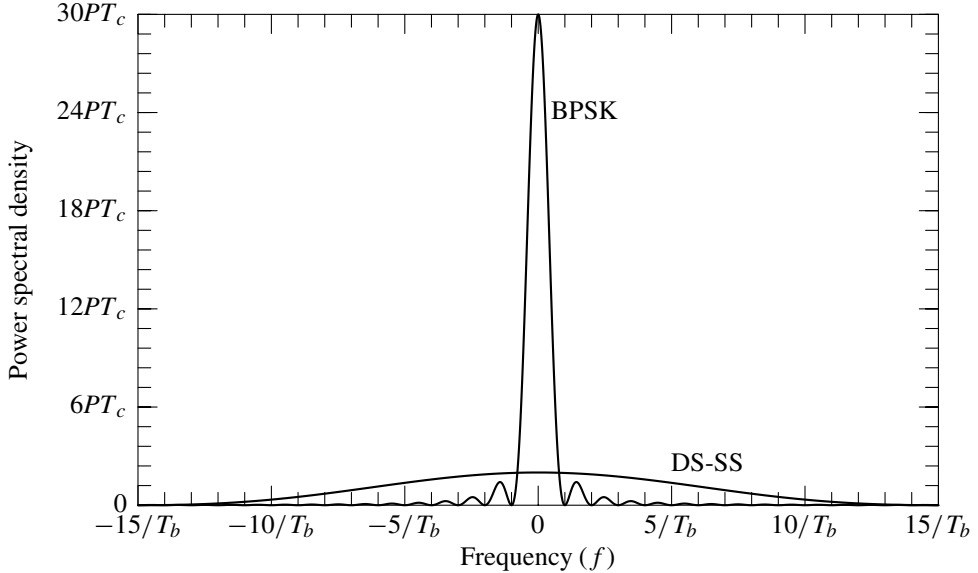


Figure 2.4: Baseband equivalent PSD of the DS-SS signal using BPSK modulation and rectangular chip waveforms for $T_b = 15T_c$.

Let us now assume that we have a perfect low-pass filter,² which is capable of perfectly removing the second additive term in the square bracket of the above equation. This can be readily achieved, since this term is associated with a frequency of $2f_c$, which is far from the baseband signal contribution of $\sqrt{P/2}b_k(t)c_k(t)$ and hence does not require a high-order filter. Then, the low-pass filtered output can be expressed as

$$r_L(t) = \sqrt{\frac{P}{2}}b_k(t - \tau)c_k(t - \tau) \quad (2.12)$$

We assume that the receiver has a perfect estimate of the transmission delay τ and that the receiver is capable of generating a replica of the DS spreading sequence waveform $c_k(t - \tau)$. Then, the despreading of the DS-SS signal can be achieved by multiplying $r_L(t)$ with the despreading sequence waveform $c_k(t - \tau)$, which is expressed as

$$\begin{aligned} r_d(t) &= \sqrt{\frac{P}{2}}b_k(t - \tau)c_k(t - \tau)c_k(t - \tau) \\ &= \sqrt{\frac{P}{2}}b_k(t - \tau) \end{aligned} \quad (2.13)$$

since at any time instant we have $c_k(t - \tau)c_k(t - \tau) = 1$. Finally, let us focus our attention on the detection of the n th bit, which is located within the time interval of

²In the forthcoming discourse of this book, unless specifically indicated, we assume that there is a low-pass filter following the carrier demodulation, which is capable of ideally removing the high-frequency components of the received signals.

$[nT_b + \tau, (n + 1)T_b + \tau]$. The decision variable corresponding to the n th transmitted bit is obtained by integrating (2.13) from $nT_b + \tau$ to $(n + 1)T_b + \tau$, which is expressed as

$$\begin{aligned} Z_k[n] &= \int_{nT_b + \tau}^{(n+1)T_b + \tau} r_d(t) dt \\ &= \int_{nT_b + \tau}^{(n+1)T_b + \tau} \sqrt{\frac{P}{2}} b_k(t - \tau) dt \\ &= \sqrt{\frac{P}{2}} T_b b_k[n] \end{aligned} \quad (2.14)$$

For binary data we have $b_k[n] \in \{+1, -1\}$ and in (2.14) $Z_k[n]$ has the same sign as $b_k[n]$. Hence, the n th transmitted data bit $b_k[n]$ can be determined as either +1 or -1, depending on whether $Z_k[n]$ is positive or negative.

The above demodulation process represented by equations (2.11) to (2.14) can be expressed in a more compact form as

$$Z_k[n] = \int_{nT_b + \tau}^{(n+1)T_b + \tau} r(t) c_k(t - \tau) \cos(2\pi f_c t + \phi_k) dt \quad (2.15)$$

According to equations (2.11) to (2.14) we observe that the despreading of DS-SS signals is based on the autocorrelation properties of the DS-spreading sequences. In fact, (2.15) represents the correlation operation between the received signal $r(t)$ and the local spreading sequence waveform $c_k(t - \tau)$. Therefore, the detector based on (2.15) is referred to as a correlation receiver, a correlation-based detector or simply a correlator.

The correlation receiver described above can be characterized using the schematic diagram of Fig. 2.5, where $\hat{\tau}$ and $\hat{\phi}_k$ represent the estimates of the transmission delay τ and that of the carrier phase ϕ_k . Furthermore, the spreading and despreading principle of the BPSK-modulated DS-SS signals can be augmented with the aid of Fig. 2.6. From Fig. 2.6 we observe that after multiplying the received signal $r(t)$ by $\cos(2\pi f_c t)$, the resultant signal $r(t) \cos(2\pi f_c t)$ seen at Fig. 2.6(f) contains a direct-current component and a superimposed sine-wave component having a frequency of $2f_c$. The presence of the direct-current component becomes more explicit after multiplying the signal $r(t) \cos(2\pi f_c t)$ with the locally generated PN sequence waveform $c_k(t)$, as shown in Fig. 2.6(g). Finally, the transmitted data waveform $b_k(t)$ can be recovered as $r_d(t)$ of Fig. 2.6(h), when removing the superimposed high-frequency sine-wave component from the despread signal $r(t)c_k(t) \cos(2\pi f_c t)$.

2.1.2.2 Matched-Filter Receiver

Instead of using the above-mentioned correlation detection for DS-SS signals, they may be detected also with the aid of a matched filter. This terminology is justified, since a filter is matched to the signal $s(t)$, where $s(t)$ is assumed to be confined to the time interval $0 \leq t \leq T$, and the filter's impulse response $h(t)$ has to satisfy the relationship of $h(t) = s(T - t)$. The response of the matched filter having an impulse response of $h(t) = s(T - t)$ to the

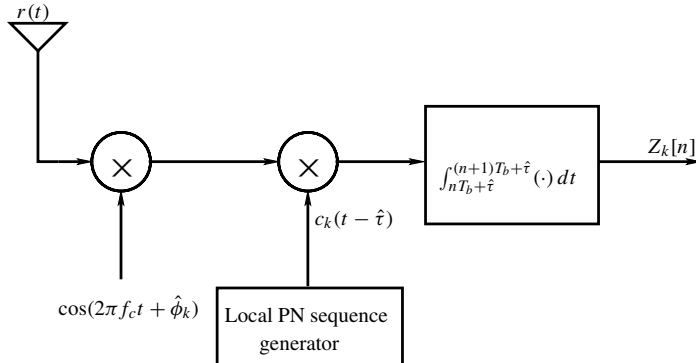


Figure 2.5: Correlation receiver of BPSK-modulated DS-SS signals.

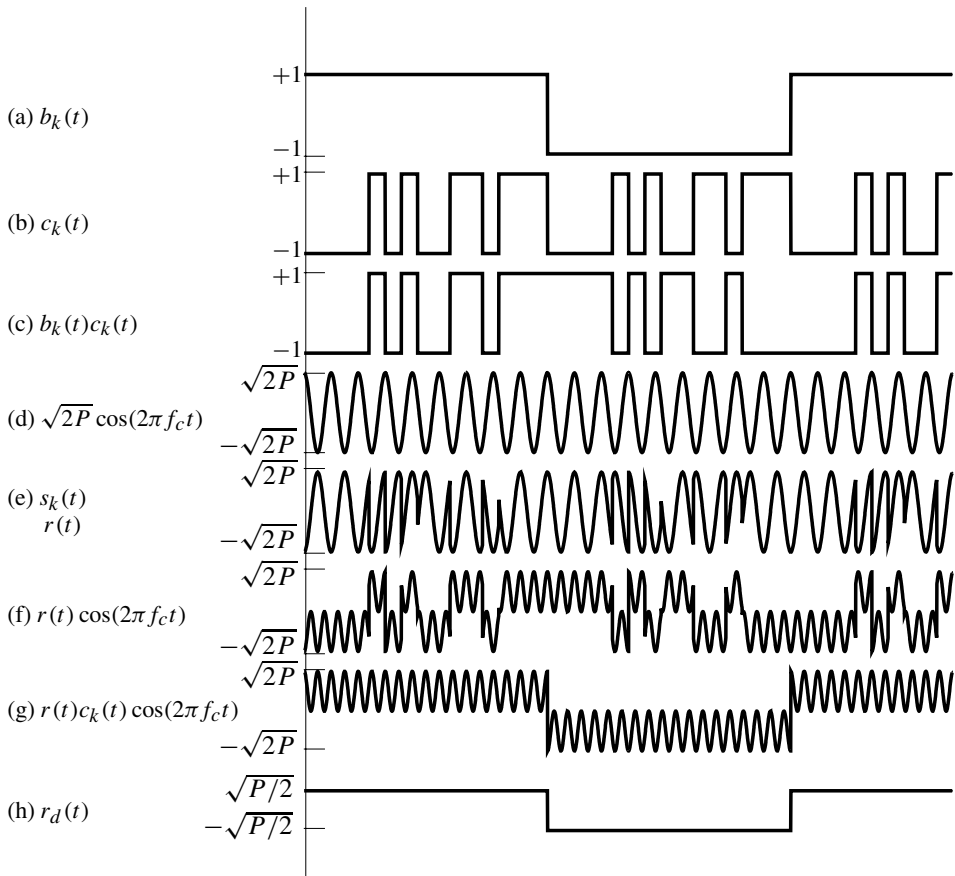


Figure 2.6: Spreading and despreading of DS-SS signals using BPSK modulation, when assuming that $\varphi_k = 0$ and $\tau = 0$.

signal $s(t)$ is expressed as

$$\begin{aligned} y(t) &= \int_0^t s(\lambda)h(t - \lambda) d\lambda \\ &= \int_0^t s(\lambda)s(T - t + \lambda) d\lambda \end{aligned} \quad (2.16)$$

which is physically the autocorrelation function of the signal $s(t)$ within the time duration of $[0, t]$. The autocorrelation function $y(t)$ is an even function of t , which achieves its maximum value at $t = T$.

Hence, in addition to correlation receivers, DS-SS signals can be detected using the principle of matched filtering. To be more specific, let us assume that the carrier frequency f_c as well as the carrier phase ϕ_k of the received DS-SS signal $r(t)$ have been removed by multiplying $r(t)$ with $\cos(2\pi f_c t + \phi_k)$, i.e. yielding the signal $r_L(t)$, as shown in (2.12). Let the n th bit $b_k[n]$, which is confined to the time interval $nT_b + \tau \leq t \leq (n+1)T_b + \tau$ be detected. Then $r_L(t)$ can be expressed as

$$r_L(t) = \sqrt{\frac{P}{2}} b_k[n] c_k(t - \tau), \quad nT_b + \tau \leq t \leq (n+1)T_b + \tau \quad (2.17)$$

Let us assume that we have a matched filter with an impulse response of $h(t) = c_k((n+1)T_b - t)$, which is matched to the PN sequence waveform $c_k(t - \tau)$ over the time interval of $nT_b + \tau \leq t \leq (n+1)T_b + \tau$. Furthermore, we assume that the matched filter's output is set to zero at the time instant $t = nT_b + \tau$. Then, for the time interval of $nT_b + \tau \leq t \leq (n+1)T_b + \tau$ the matched filter's output is given by

$$\begin{aligned} y(t) &= \int_{nT_b + \tau}^t r_L(\lambda)h(t - \lambda) d\lambda \\ &= \int_{nT_b + \tau}^t \sqrt{\frac{P}{2}} b_k[n] c_k(\lambda - \tau) c_k((n+1)T_b - t + \lambda) d\lambda \\ &= \sqrt{\frac{P}{2}} b_k[n] \int_{nT_b + \tau}^t c_k(\lambda - \tau) c_k((n+1)T_b - t + \lambda) d\lambda \end{aligned} \quad (2.18)$$

Specifically, at the time instant of $t = (n+1)T_b + \tau$, the matched filter reaches its maximum output value given by

$$\begin{aligned} y((n+1)T_b + \tau) &= \sqrt{\frac{P}{2}} b_k[n] \int_{nT_b + \tau}^{(n+1)T_b + \tau} c_k(\lambda - \tau) c_k(\lambda - \tau) d\lambda \\ &= \sqrt{\frac{P}{2}} T_b b_k[n] \end{aligned} \quad (2.19)$$

which is in fact the decision variable $Z_k[n]$ given in (2.14) that was previously derived in the context of the correlation receiver. Therefore, (2.19) implies that DS-SS signals can be detected with the aid of a filter, provided that its impulse response is matched to the transmitted PN sequence waveform.

If the PN sequence waveform $c_k(t)$ is periodic and has a period of T_b , then we have a matched-filter impulse response $h(t) = c_k((n+1)T_b - t) = c_k(T_b - t)$. In this case,

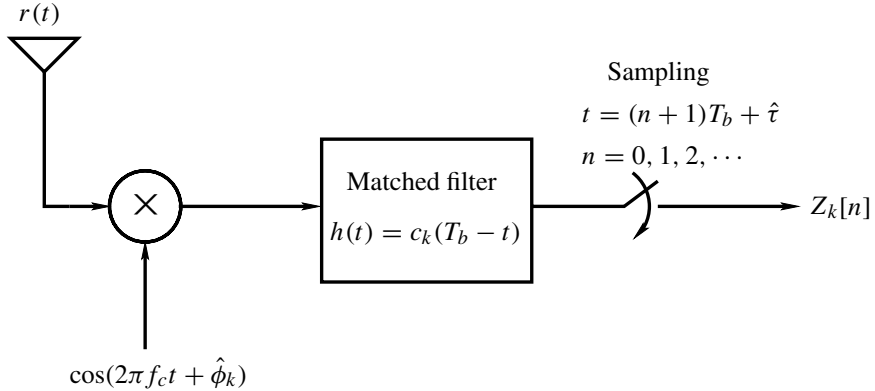


Figure 2.7: Matched filter-based receiver for BPSK modulated DS-SS signals.

the impulse responses of the matched filter are the same for detecting different bits. As an example, a matched filter-based receiver designed for DS-SS systems using periodic PN sequences is shown in Fig. 2.7. Note that for the correlation receiver of Fig. 2.5 the decision variable $Z_k[n]$ corresponding to the n th bit is the output of the integrator. By contrast, for the matched filter-based receiver the decision variable $Z_k[n]$ is the sampling output of the matched filter at the time instant of $t = (n + 1)T_b + \hat{\tau}$, $n = 0, 1, 2, \dots, \infty$.

2.1.3 Anti-Jamming Property of DS-SS Systems

DS-SS signals are typically transmitted using a high bandwidth of W_{DS} Hz, which is significantly higher than the bit rate R_b expressed in terms of bits/second (bits/s). As shown in Fig. 2.4, the DS-SS signals' PSD is typically fairly flat. When the spreading gain of $N = T_b/T_c$ assumes a high value, the PSD of DS-SS signals will become similar to that of the white Gaussian noise. The property of possessing low white Gaussian noise-like PSD makes DS-SS signals hard to be detected when without the *a priori* knowledge of the spreading sequence used, since there exists an extremely high number of possible sequences that have to be correlated with the received signal. Therefore, the DS-SS scheme and also virtually all other types of spread-spectrum scheme that will be discussed in the forthcoming sections constitute inherently secure transmission schemes. Furthermore, spread-spectrum signals exhibit resilience against certain types of intentional or unintentional interference. Below, as an example, we briefly demonstrate the antijamming capability of DS-SS systems against partial-band jamming.

A *partial-band jammer* transmits pulses of band-limited white Gaussian noise having a total average power of J . As shown in Fig. 2.8, when using partial-band jamming, the total jamming power J is evenly spread over a given frequency range of bandwidth W_J , which is a fraction of the total system bandwidth W_S , where we have $W_S = W_{DS}$ when using a DS-SS scheme. The ratio of W_J to W_S is expressed as

$$\rho = \frac{W_J}{W_S} \leq 1 \quad (2.20)$$

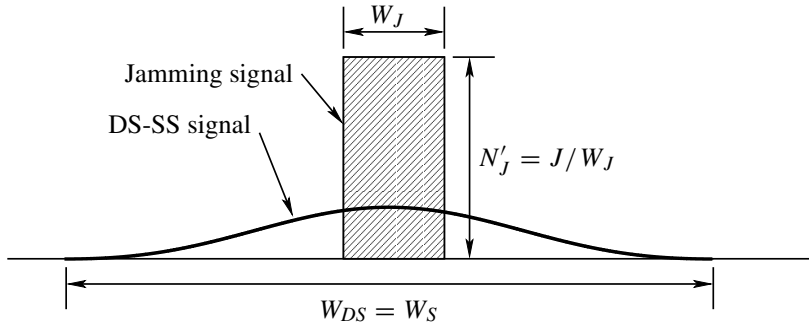


Figure 2.8: Stylized baseband equivalent PSD of the received DS-SS signal plus partial-band jamming signal.

which is defined as the *duty factor* of the jammer. Consequently, within the bandwidth exposed to jamming, the PSD is given by

$$\begin{aligned} N'_J &= \frac{J}{W_J} = \frac{J}{W_S} \cdot \frac{W_S}{W_J} \\ &= N_J / \rho \end{aligned} \quad (2.21)$$

where $N_J = J / W_S$ represents the PSD, when the jamming power J is evenly spread over the whole system bandwidth W_S .

Without considering the effects of background noise, the sum of the received DS-SS signal plus partial-band interference signal can be expressed as

$$r(t) = \sqrt{2P}b_k(t)c_k(t) \cos(2\pi f_c t + \varphi_k) + n_J(t) \quad (2.22)$$

where $n_J(t)$ represents the partial-band jamming signal having a bandwidth of $W_J = \rho W_S$ and a total jamming power of J . The corresponding stylized baseband equivalent PSDs of the received DS-SS signal and that of the partial-band jamming signal are shown in Fig. 2.8, which demonstrates that the jamming power spreads only over a bandwidth of $W_J < W_S$. By contrast, the received DS-SS signal's power spreads over the entire system bandwidth of $W_S = W_{DS}$.

When we despread the received signal of (2.22) using the k th user's spreading sequence $c_k(t)$, we obtain

$$y(t) = \sqrt{2P}b_k(t) \cos(2\pi f_c t + \varphi_k) + n_J(t)c_k(t) \quad (2.23)$$

where the first additive term at the right-hand side of the equation is a conventional BPSK modulated signal, which has a baseband equivalent PSD mainly distributed over the bandwidth of $[-1/T_b, 1/T_b]$, as shown in Fig. 2.9. By contrast, the second additive term at the right-hand side of (2.23) is due to the jamming signal, which is now spread by the k th user spreading sequence $c_k(t)$. Consequently, the jamming power is now spread over the entire system bandwidth of $W_S = W_{DS}$ essentially distributed in the range $[-1/T_c, 1/T_c]$. The corresponding PSD is hence given by $N_J = J / W_S = \rho N'_J$, which may be significantly lower than the PSD of N'_J seen in Fig. 2.8 before the despreading operation, provided that ρ is small.

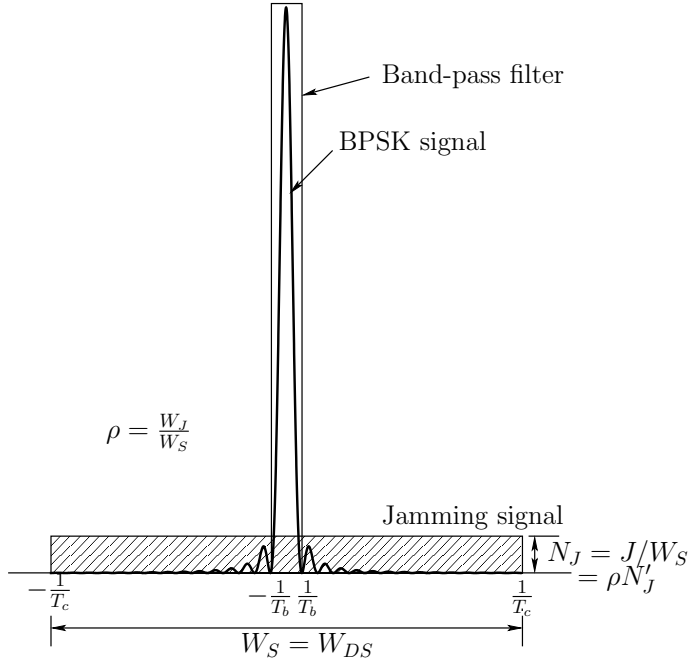


Figure 2.9: Baseband equivalent PSD of the despread received DS-SS signal plus partial-band jamming signal.

Suppose that we have an ideal band-pass filter exhibiting a pass-band of $[-1/T_b, 1/T_b]$, as shown in Fig. 2.9 that is the bandwidth of the desired part of the despread signal in (2.23). Then, the jamming power after the band-pass filtering operation is given by

$$\begin{aligned} J' &= N_J \times \frac{2}{T_b} = \frac{J}{W_s} \times \frac{2}{T_b} \\ &= \frac{J}{2/T_c} \times \frac{2}{T_b} = J/N \end{aligned} \quad (2.24)$$

where $N = T_b/T_c$ represents the spreading gain of the DS-SS scheme considered. Equation (2.24) implies that the jamming power after despreading is decreased by a factor of N . Therefore, the DS-SS scheme is capable of efficiently mitigating the detrimental effects of partial-band jamming. Furthermore, the DS-SS scheme can be employed for reducing the effects of various other types of jamming signal, including multitone jamming, pulse jamming, etc. [3–5].

We note furthermore that other types of spread-spectrum signal also have the capability of mitigating the effects of some intentional and/or unintentional jamming [3–5]. This antijamming capability is achieved because spread-spectrum signals have a transmission bandwidth expressed in Hz, which is significantly higher than the data transmission rate expressed in bits/s. As this book is concerned with multiple-access communications, the detailed principles of antijamming communications relevant in the context of spread-

spectrum schemes other than DS-SS are not considered in our forthcoming discourse. Readers interested in antijamming spread-spectrum communications are referred to references [3–6].

2.1.4 Direct-Sequence Code-Division Multiple Access

In addition to its antijamming capability, DS-SS also has the ability to support multiple users within the same frequency band at the same time. In direct-sequence code-division multiple-access (DS-CDMA) systems different users can be identified with the help of their unique, user-specific signatures or spreading sequences. As an example, let us consider a DS-CDMA system supporting $K = 2$ users. Let the composite received BPSK modulated DS-CDMA signal of the two users be given by

$$\begin{aligned} r(t) = & \sqrt{2P}b_1(t - \tau_1)c_1(t - \tau_1)\cos(2\pi f_c t + \phi_1) \\ & + \sqrt{2P}b_2(t - \tau_2)c_2(t - \tau_2)\cos(2\pi f_c t + \phi_2) \end{aligned} \quad (2.25)$$

where $c_1(t)$ and $c_2(t)$ represent the signature waveforms of user 1 and user 2, respectively, while τ_1 and τ_2 represent their transmission delays. We refer to a DS-CDMA system having $\tau_1 = \tau_2 = \dots = \tau_k = \dots$ as a synchronous DS-CDMA system. Otherwise, if we cannot assume that $\tau_1 = \tau_2 = \dots = \tau_k = \dots$, we refer to it as an asynchronous DS-CDMA system. Explicitly, the assumption of synchronous DS-CDMA constitutes a special case of asynchronous DS-CDMA systems. In the context of our example we assume encountering an asynchronous DS-CDMA system corresponding to $\tau_1 \neq \tau_2$.

Without loss of generality, let us assume that user 1 is the desired user and we are detecting its first transmitted bit of $b_1[0]$. Let us also assume that the receiver has been perfectly synchronized with the desired user's signal. Therefore, we can set $\tau_1 = 0$ and $\phi_1 = 0$. Consequently, with the aid of the correlation receiver of Fig. 2.5 and equation (2.15), the decision variable corresponding to the first transmitted bit of user 1 can be expressed as

$$\begin{aligned} Z_1[0] &= \int_0^{T_b} r(t)c_1(t)\cos(2\pi f_c t) dt \\ &= \sqrt{\frac{P}{2}}T_bb_1[0] + \sqrt{\frac{P}{2}}\cos(\phi_2)\int_0^{T_b} b_2(t - \tau_2)c_2(t - \tau_2)c_1(t) dt \end{aligned} \quad (2.26)$$

where the quantity of $\sqrt{P/2}T_bb_1[0]$ is the desired output, which is the same as the expression in (2.14) derived for the single-user case. By contrast, the quantity of

$$I_2 = \sqrt{\frac{P}{2}}\cos(\phi_2)\int_0^{T_b} b_2(t - \tau_2)c_2(t - \tau_2)c_1(t) dt \quad (2.27)$$

constitutes the interference imposed by the second user's signal on the first user's signal. As shown in (2.27), the interference term of I_2 is the result of the cross-correlation between $b_2(t - \tau_2)$, $c_2(t - \tau_2)$ and $c_1(t)$ within the interval of $[0, T_b]$. When PN signature sequences are employed, this cross-correlation value is usually low. Hence the interference term I_2 is usually significantly lower than the desired output of $\sqrt{P/2}T_bb_1[0]$. Consequently, the desired bit $b_1[0]$ can be decided to be either +1 or -1 simply depending on, whether $Z_1[0]$ is higher or lower than zero, i.e. positive or negative.

The second user's transmitted data can be detected using the same procedure described above, when the second user is assumed to be the desired user, while the first user is the interfering user.

Generally, in a DS-CDMA system, if there are K number of users sharing the same frequency band at the same time, then the received signal can be expressed as

$$r(t) = \sum_{k=1}^K \sqrt{2P} b_k(t - \tau_k) c_k(t - \tau_k) \cos(2\pi f_c t + \phi_k) \quad (2.28)$$

We also assume that the first user is the desired user and that we have perfect estimates of τ_1 and ϕ_1 . Then, the decision variable associated with the first user's n th bit can be expressed as

$$Z_1[n] = \sqrt{\frac{P}{2}} T_b b_1[n] + \sum_{k=2}^K I_k, \quad n = 0, 1, 2, \dots \quad (2.29)$$

where I_k for $k = 2, 3, \dots, K$ represents the multiuser interference imposed by the k th user on the desired user of $k = 1$. The multiuser interference term I_k is given by

$$I_k = \sqrt{\frac{P}{2}} \cos(\phi'_k) \int_{nT_b + \tau_1}^{(n+1)T_b + \tau_1} b_k(t - \tau_k) c_k(t - \tau_k) c_1(t - \tau_1) dt \quad (2.30)$$

where $\phi'_k = \phi_k - \phi_1$. Note that if the multiuser interference of $\sum_{k=2}^K I_k$ is high due to supporting a large number of users, the desired user's information will be detected with a high probability of errors even without background noise. In this case advanced detection techniques having a significantly higher detection efficiency than the correlation detector of Fig. 2.5 or the matched-filter detector of Fig. 2.7 will be employed. These advanced detection techniques will be discussed in the context of multicarrier CDMA schemes in the following chapters.

2.2 Multicarrier Spread-Spectrum Communications

2.2.1 Transmitted Signals

In contrast to DS spread-spectrum schemes, which spread the original data stream in the time (T)-domain with the aid of spreading sequences, multicarrier spread-spectrum (MC-SS) schemes constitute a class of direct-sequence spread-spectrum schemes that spread the original data stream in the frequency (F)-domain with the aid of a number of N subcarriers. Therefore, MC-SS schemes can also be interpreted as frequency (F)-domain DS-SS arrangements. However, as a consequence of using multiple subcarriers, the terminology of multicarrier spread spectrum has established itself.

Figure 2.10 shows the transmitter block diagram of the MC-SS scheme. In MC-SS arrangements the transmitter spreads the original data stream over N subcarriers using a given spreading code of $\{c_k[0], c_k[1], \dots, c_k[N-1]\}$. Observe in Fig. 2.10 that after multiplication with the corresponding chips of $n = 0, 1, \dots, N-1$ of the N -chip spreading sequence \mathbf{c}_k of the k th user, the original data bits are mapped to N number of subcarriers. In the MC-SS scheme, the data rate of each of the N subcarriers is the same as the input data rate. With reference to Fig. 2.10, the k th user's transmitted signal can be expressed as:

$$s_k(t) = \sqrt{\frac{2P}{N}} \sum_{n=0}^{N-1} b_k(t) c_k[n] \cos(2\pi f_n t + \varphi_n^{(k)}) \quad (2.31)$$

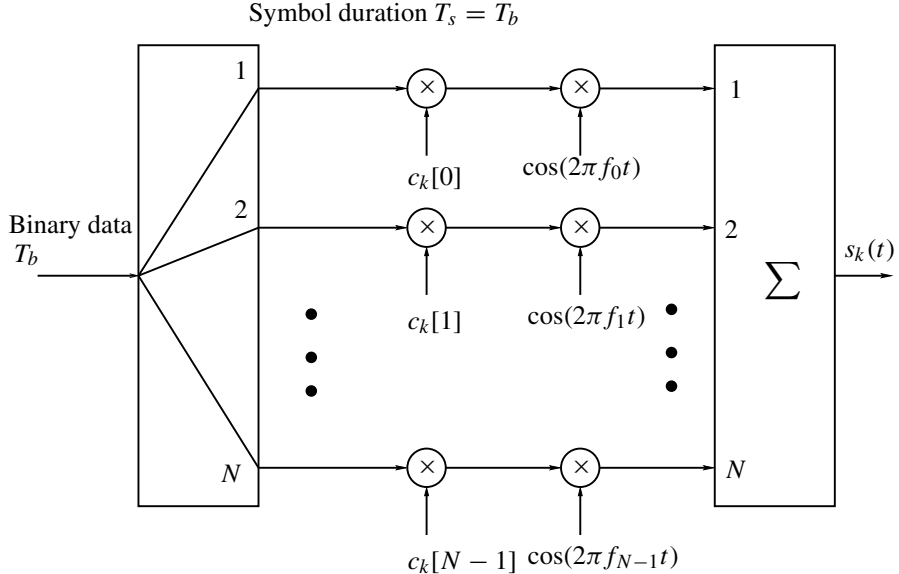


Figure 2.10: Transmitter schematic of the MC-SS system.

where P represents the transmitted power of the MC-SS signal, $\varphi_n^{(k)}$ represents the initial phase angle with respect to the k th user and the n th subcarrier, N is the number of subcarriers as well as the spreading gain, $\{c_k[0], c_k[1], \dots, c_k[N - 1]\}$ is the k th user's spreading code, $\{f_n, n = 0, 1, \dots, N - 1\}$ are the subcarrier frequencies, and finally, $b_k(t)$ represents the binary data sequence transmitted by the k th user.

The baseband equivalent spectrum of the transmitted MC-SS signal is shown in Fig. 2.11, where we assumed that the MC-SS system had eight subcarriers and the spacing between two adjacent subcarriers was $1/T_b$, where T_b represents the bit duration. Since each subcarrier signal in (2.31) constitutes a conventional BPSK signal obeying (2.1), the baseband equivalent PSD of the MC-SS signal of (2.31) in fact is given by the sum of N number of BPSK PSDs. In the MC-SS system the subcarrier waveforms are chosen to be orthogonal to each other, i.e. the subcarrier waveforms satisfy the following condition:

$$\int_0^{T_b} \cos(2\pi f_i t + \phi_i) \cdot \cos(2\pi f_j t + \phi_j) dt = 0, \quad \text{for } i \neq j \quad (2.32)$$

Therefore, the spacing Δ between two adjacent subcarriers can take the value of $\Delta = n/T_b$, where n is an integer assuming values of $n = 1, 2, \dots$. Usually, n assumes values of one or two, so that the available frequency bandwidth can be efficiently exploited. In MC-SS, if $\Delta = 2/T_b$ is assumed, which is associated with allowing no spectral overlap amongst the F-domain main-lobes of the subcarrier signals' spectra, then the bandwidth required by the MC-SS system for achieving a spreading gain of N becomes $2N/T_b$. It is worth noting, furthermore, that if each subcarrier's spectrum obeys the shape of (2.6) and Fig. 2.2, then the corresponding

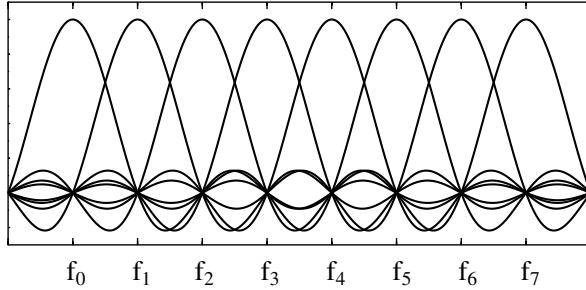


Figure 2.11: Stylized baseband equivalent spectrum of the transmitted MC-SS signal.

side-lobes have a zero at all legitimate subcarrier frequencies. This is advantageous in terms of minimizing the interference of the adjacent subcarrier signals.

2.2.2 Detection of MC Spread-Spectrum Signals

Assuming that the k th user's MC-SS signal obeying (2.31) is transmitted over a distortionless and noiseless channel, which is assumed to have a transmission delay of τ_k seconds, the received signal can be expressed as

$$r(t) = \sqrt{\frac{2P}{N}} \sum_{n=0}^{N-1} b_k(t - \tau_k) c_k[n] \cos(2\pi f_n t + \phi_n^{(k)}) \quad (2.33)$$

where $\phi_n^{(k)} = \phi_n^{(k)} - 2\pi f_n \tau_k$, $n = 1, 2, \dots, N - 1$, represents the carrier phase associated with the n th subcarrier of the k th user.

The information conveyed by the k th user's MC-SS signal can be detected using correlation detectors that exploit the correlation properties of the PN-spreading codes employed by the MC-SS scheme. The receiver structure of the MC-SS scheme is shown in Fig. 2.12, where we assumed that the receiver has perfect estimates of the transmission delay τ_k and the carrier phases $\phi_n^{(k)}$. In Fig. 2.12 the transmission delay τ_k is assumed to be zero, since only a single user is considered. In this MC-SS receiver the received bit is recovered by detecting the N chips conveyed by the N subcarriers, where each chip is demodulated using the approach invoked for the BPSK demodulator of Section 2.1. As shown in Fig. 2.12, for the i th branch, the effects of the carrier are first removed by multiplying the received signal $r(t)$ with the carrier $\cos(2\pi f_i t + \phi_i^{(k)})$. After BPSK demodulation the decision variable corresponding to the n th bit is obtained by despreading the N number of subcarrier signals with the help of the k th user's signature sequence $\{c_k[0], c_k[1], \dots, c_k[N - 1]\}$. The demodulation process of MC-SS signals can be summarized as follows. First, BPSK

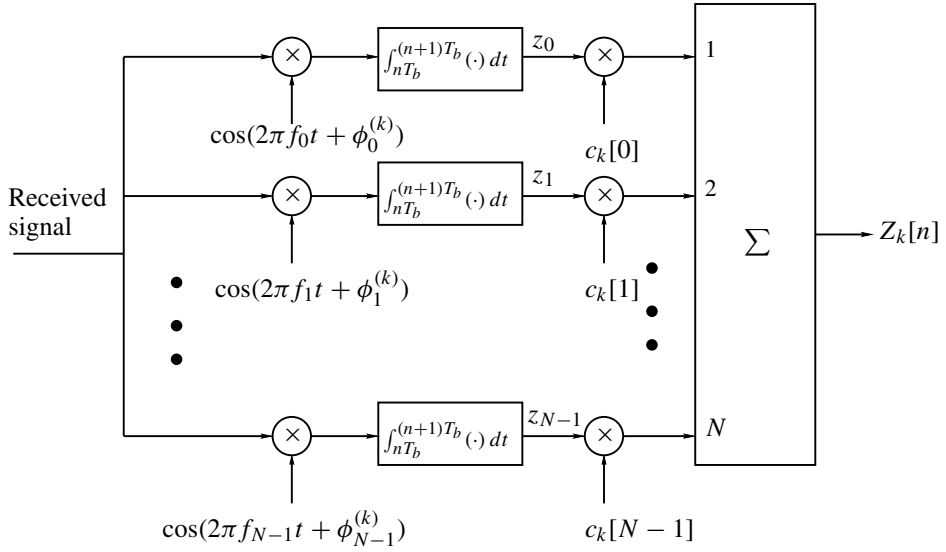


Figure 2.12: Receiver block diagram of a MC-SS scheme.

demodulation is carried out for each of the N branches and is expressed as

$$\begin{aligned} z_i &= \int_{nT_b}^{(n+1)T_b} r(t) \cos(2\pi f_i t + \phi_i^{(k)}) dt \\ &= \sqrt{\frac{2P}{N}} \sum_{j=0}^{N-1} \int_{nT_b}^{(n+1)T_b} b_k(t) c_k[j] \cos(2\pi f_j t + \phi_j^{(k)}) \cos(2\pi f_i t + \phi_i^{(k)}) dt \\ &= \sqrt{\frac{2P}{N}} \sum_{j=0}^{N-1} b_k[n] c_k[j] \int_{nT_b}^{(n+1)T_b} \cos(2\pi f_j t + \phi_j^{(k)}) \cos(2\pi f_i t + \phi_i^{(k)}) dt \end{aligned} \quad (2.34)$$

Owing to the orthogonality of the subcarriers for $i \neq j$ we have

$$\int_0^{T_b} \cos(2\pi f_i t + \phi_i) \cdot \cos(2\pi f_j t + \phi_j) dt = 0 \quad (2.35)$$

(2.34) can be simplified to

$$z_i = \sqrt{\frac{P}{2N}} T_b b_k[n] c_k[i] \quad (2.36)$$

for $i = 0, 1, \dots, N - 1$.

Following BPSK demodulation of each of the N branches, the decision variable $Z_k[n]$ corresponding to the n th transmitted bit is given by

$$Z_k[n] = \sum_{i=0}^{N-1} z_i c_k[i] \quad (2.37)$$

On substituting (2.36) into the above equation, we arrive at

$$Z_k[n] = \sum_{i=0}^{N-1} \sqrt{\frac{P}{2N}} T_b b_k[n] c_k[i] c_k[i] = \sqrt{\frac{NP}{2}} T_b b_k[n] \quad (2.38)$$

Equation (2.38) shows that the decision variable $Z_k[n]$ has the same polarity as $b_k[n]$ in the presence of a perfect noiseless channel. Therefore, the n th transmitted bit $b_k[n]$ can be determined as either +1 or -1 according to the sign of $Z_k[n]$.

Note that the decision variable of $Z_k[n]$ can be written in a compact form as

$$Z_k[n] = \sum_{i=0}^{N-1} c_k[i] \int_{nT_b}^{(n+1)T_b} r(t) \cos(2\pi f_i t + \phi_i^{(k)}) dt \quad (2.39)$$

where $n = -\infty, \dots, 0, 1, \dots, \infty$.

2.2.3 Multicarrier Code-Division Multiple Access

In the previous section we considered MC-SS transmission, while supporting a single user. In this section we extend this concept to multiuser communications. The principle of multicarrier code-division multiple access (MC-CDMA) may be understood using the following example in the context of a two-user system. Let $\mathbf{c}_1 = \{c_1[0], c_1[1], \dots, c_1[N-1]\}$ and $\mathbf{c}_2 = \{c_2[0], c_2[1], \dots, c_2[N-1]\}$ be two PN sequences assigned to user 1 and user 2, respectively. Based on Fig. 2.10 and equation (2.31), the composite received MC-CDMA signal corresponding to two users can be expressed as

$$\begin{aligned} r(t) = & \sqrt{\frac{2P}{N}} \sum_{n=0}^{N-1} b_1(t - \tau_1) c_1[n] \cos(2\pi f_n t + \phi_n^{(1)}) \\ & + \sqrt{\frac{2P}{N}} \sum_{n=0}^{N-1} b_2(t - \tau_2) c_2[n] \cos(2\pi f_n t + \phi_n^{(2)}) \end{aligned} \quad (2.40)$$

Let us use the receiver of Fig. 2.12 to detect the first user's transmitted information. Assuming that the receiver has perfect estimates of the first user's transmission delay τ_1 and carrier phases $\{\phi_n^{(1)}\}$, the decision variable corresponding to the n th bit of the first user can be written as

$$Z_1[n] = \sum_{i=0}^{N-1} c_1[i] \int_{nT_b + \tau_1}^{(n+1)T_b + \tau_1} r(t) \cos(2\pi f_i t + \phi_i^{(1)}) dt \quad (2.41)$$

On substituting (2.40) into (2.41), we arrive at

$$Z_1[n] = \sqrt{\frac{NP}{2}} T_b b_1[n] + I_2 \quad (2.42)$$

where the interference I_2 imposed by user 2 on user 1 can be expressed as

$$\begin{aligned} I_2 &= \sum_{i=0}^{N-1} c_1[i] \int_{nT_b+\tau_1}^{(n+1)T_b+\tau_1} \sqrt{\frac{2P}{N}} \sum_{j=0}^{N-1} b_2(t - \tau_2) c_2[j] \\ &\quad \times \cos(2\pi f_j t + \phi_j^{(2)}) \cdot \cos(2\pi f_i t + \phi_i^{(1)}) dt \\ &= \sqrt{\frac{P}{2N}} \sum_{i=0}^{N-1} c_1[i] \sum_{j=0}^{N-1} c_2[j] \int_{nT_b+\tau_1}^{(n+1)T_b+\tau_1} b_2(t - \tau_2) \cos(2\pi [f_j - f_i]t + \phi_{ji}^{(21)}) dt \end{aligned} \quad (2.43)$$

where $\phi_{ji}^{(21)} = \phi_j^{(2)} - \phi_i^{(1)}$. If we ignore the interference imposed by the subcarriers having a different frequency; i.e. for a given subcarrier i we assume that interference is only imposed by subcarrier i of the second user's signal, then the above equation can be simplified to

$$I_2 = \sqrt{\frac{P}{2N}} \sum_{i=0}^{N-1} c_1[i] c_2[i] \cos(\phi_{ji}^{(21)}) \int_{nT_b+\tau_1}^{(n+1)T_b+\tau_1} b_2(t - \tau_2) dt \quad (2.44)$$

Equation (2.44) shows that the interference I_2 imposed by the second user on the first user is dependent on the cross-correlation value between the spreading codes \mathbf{c}_1 and \mathbf{c}_2 which is usually significantly lower than the amplitude $\sqrt{NP/2}T_b$ of the desired user's contribution in (2.42). Hence, the desired bit $b_1[n]$ can be determined as either +1 or -1, depending simply on whether $Z_1[n]$ is higher or lower than zero.

The second user's transmitted data can also be detected using the procedure described above, when the second user is assumed to be the user-of-interest, while treating the first user as the interfering user.

Furthermore, in general if the MC-CDMA system supports K number of users, then the received signal can be expressed as

$$r(t) = \sum_{k=1}^K \sqrt{\frac{2P}{N}} \sum_{n=0}^{N-1} b_k(t - \tau_k) c_k[n] \cos(2\pi f_n t + \phi_n^{(k)}) \quad (2.45)$$

Similarly to the two-user case, for the reference user of $k = 1$ and assuming that the receiver has perfect estimates of the transmission delay of τ_1 and of the initial phases $\phi_i^{(1)}$ for $i = 0, 1, \dots, N-1$, the decision variable corresponding to the n th bit can be written as

$$Z_1[n] = \sqrt{\frac{NP}{2}} T_b b_1[n] + \sum_{k=2}^K I_k \quad (2.46)$$

where I_k represents the interference imposed by the k th interfering user that can be expressed as

$$I_k = \sqrt{\frac{P}{2N}} \sum_{i=0}^{N-1} c_1[i] \sum_{j=0}^{N-1} c_k[j] \int_{nT_b+\tau_1}^{(n+1)T_b+\tau_1} b_k(t - \tau_k) \cos(2\pi [f_j - f_i]t + \phi_{ji}^{(k1)}) dt \quad (2.47)$$

where $\phi_{ji}^{(k1)} = \phi_j^{(k)} - \phi_i^{(1)}$. In the absence of background noise, it can be observed based on (2.46) that the reference user's information can be reliably detected, provided that the absolute

value of $\sum_{k=2}^K I_k$, i.e. $|\sum_{k=2}^K I_k|$ is lower than $\sqrt{NP/2}T_b$. Otherwise, when $|\sum_{k=2}^K I_k|$ is higher than $\sqrt{NP/2}T_b$, erroneous detection occurs even without transmission impairment such as background noise, fading, dispersion, etc.

2.3 Frequency-Hopped Spread-Spectrum Communications

In Sections 2.1 and 2.2 both DS-SS and MC-SS have been discussed. One of the common characteristics of these two spread-spectrum schemes is that the PN spreading codes invoked directly modulate the data-bearing carriers. Hence, both of them belong to the family of direct-sequence (DS) spread-spectrum schemes. In this section a third method devised for widening the spectrum of the modulated carrier is discussed. This spread spectrum method changes the carrier frequency periodically under the control of a PN-spreading code. Therefore, this spread-spectrum scheme is referred to as a frequency-hopping (FH) spread-spectrum arrangement. In FH systems the carrier frequency is chosen from a set of Q frequencies and the carrier frequency hops from one frequency to the next. Since each given spreading sequence of a FH system corresponds to a specific order of activating the legitimate set of carrier frequencies, the spreading sequence of FH systems is also often termed *FH patterns*. In FH systems, typically noncoherent data modulation schemes are used, because the carrier phases are difficult to estimate within a small fraction of the hopping duration. The most common noncoherent data modulation scheme used in conjunction with FH systems is M -ary frequency-shift keying (MFSK). Hence, let us first briefly review the philosophy of MFSK-based modulation.

2.3.1 M -ary Frequency-Shift Keying

The legitimate signal set of noncoherent MFSK modulation consists of M sinusoids at distinct frequencies, expressed as

$$s_m(t) = \sqrt{2P} \cos[2\pi(f_c + f_m)t + \varphi_m], \quad 0 \leq t \leq T_s, \quad 0 \leq m \leq M - 1 \quad (2.48)$$

where f_c is the carrier frequency and P is the power of the transmitted signal, f_m denotes the frequency of the m th signalling tone and φ_m is the unknown random phase associated with the m th signalling tone. The correlation coefficient between two signalling tones expressed in the form of (2.48) is defined as

$$\rho_{ij} = \frac{1}{E_s} \int_0^{T_s} s_i(t)s_j(t) dt = \frac{1}{T_s} \int_0^{T_s} \cos[2\pi(f_i - f_j)t + \varphi_i - \varphi_j] dt \quad (2.49)$$

where $E_s = PT_s$ represents the energy per MFSK symbol, $f_i - f_j$ is the frequency separation between tone i and tone j , and φ_i , φ_j are the random carrier phases associated with the i th and j th signalling tones, when signals $s_i(t)$ and $s_j(t)$ are transmitted. An orthogonal MFSK signal set is generated, if for any value of $0 \leq i \neq j \leq M - 1$ we have $\rho_{ij} = 0$. Because of the random nature of the phase $\varphi_i - \varphi_j$, the only way of satisfying the orthogonality condition is to assume that the frequency separation of the signalling tones assumes values of

$$f_i - f_j = \frac{n}{T_s}, \quad n = 1, 2, \dots \quad (2.50)$$

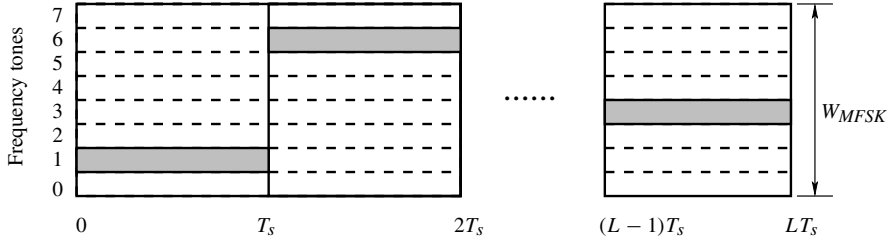


Figure 2.13: Stylized representation of an MFSK modulation scheme.

Given a minimum frequency separation of $1/T_s$ between two adjacent signalling tones, the frequency set of

$$\left\{ \frac{0}{T_s}, \frac{1}{T_s}, \dots, \frac{M-1}{T_s} \right\} \quad (2.51)$$

is capable of guaranteeing an orthogonal MFSK scheme, which requires a bandwidth of $W_{MFSK} = (M+1)/T_s$ Hz.

Figure 2.13 shows the stylized representation of an MFSK system. A signal tone associated with one of the legitimate signalling frequencies is transmitted within each MFSK symbol interval. The frequency tone transmitted in a given MFSK symbol interval is chosen according to the value of the corresponding $b = (\log_2 M)$ -bit information symbol transmitted. Assuming that the m th tone is transmitted within the first symbol interval, then the received noiseless signal can be expressed as

$$r(t) = \sqrt{2P} \cos[2\pi(f_c + f_m)t + \varphi_m], \quad 0 \leq t \leq T_s \quad (2.52)$$

The maximum likelihood (ML) receiver designed for the noncoherent reception of MFSK signals is shown in Fig. 2.14. The receiver computes M number of decision variables on the basis of calculating the energy at the correlator outputs according to $Z_i = Z_{c,i}^2 + Z_{s,i}^2$ for $i = 0, 1, \dots, M-1$, where $Z_{c,i}$ and $Z_{s,i}$ are given by

$$Z_{c,i} = \int_0^{T_s} r(t) \cos[2\pi(f_c + f_i)t] dt \quad (2.53)$$

$$Z_{s,i} = \int_0^{T_s} r(t) \sin[2\pi(f_c + f_i)t] dt \quad (2.54)$$

where we have $i = 0, 1, \dots, M-1$. Upon substituting the received signal $r(t)$ obeying (2.52) into (2.53) and (2.54), it can be shown that

$$\begin{aligned} Z_m &= Z_{c,m}^2 + Z_{s,m}^2 \\ &= \left(\sqrt{\frac{P}{2}} T_s \cos \varphi_m \right)^2 + \left(\sqrt{\frac{P}{2}} T_s \sin \varphi_m \right)^2 = \frac{E_s T_s}{2}, \quad \text{when } i = m \end{aligned} \quad (2.55)$$

$$Z_i = Z_{c,i}^2 + Z_{s,i}^2 = 0, \quad \text{when } i \neq m \quad (2.56)$$

where $E_s = PT_s$ represents the energy per MFSK symbol. After the receiver obtained the M number of decision variables Z_0, Z_1, \dots, Z_{M-1} , the largest one of them is selected as the

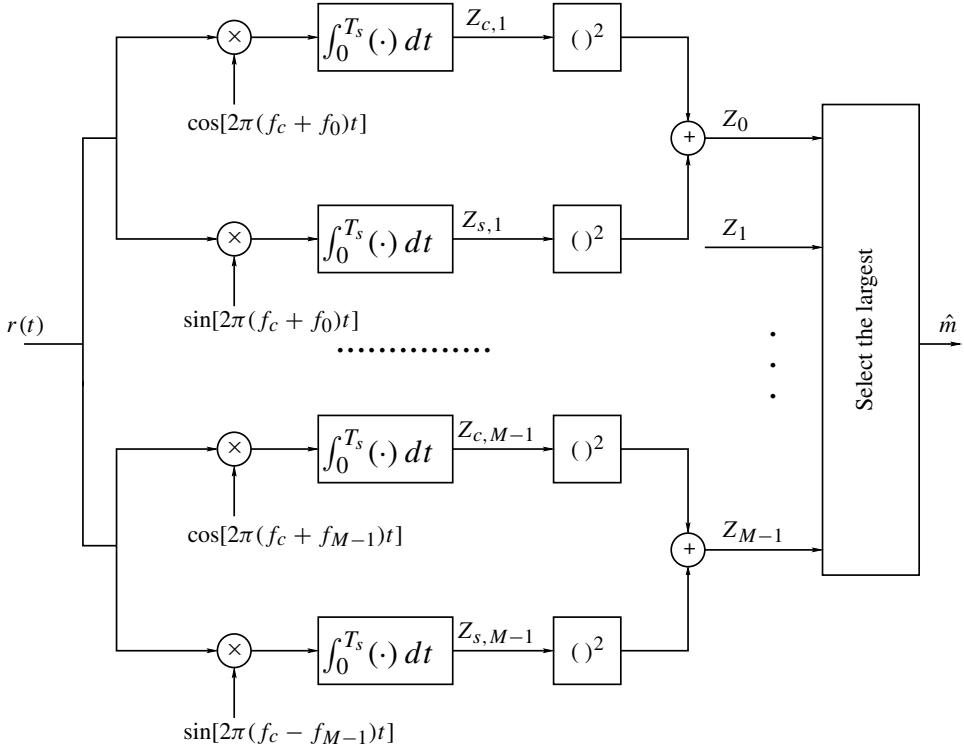


Figure 2.14: Maximum likelihood (ML) detection based noncoherent MFSK demodulator. Observe in the figure that the knowledge of the carrier frequencies is necessary, but that of the carrier phase is not. Hence no phase-coherent carrier recovery is required for the noncoherent receiver.

most likely one and it is mapped to an M -ary symbol representing the ML estimate of the transmitted symbol. Naturally, when the channel imposes impairment, the estimated symbol might be erroneous.

2.3.2 M -ary Frequency-Shift Keying Aided Slow Frequency-Hopping

The operation of a FH spread-spectrum system using noncoherent MFSK data modulation may be understood by referring to Fig. 2.15 and Fig. 2.16. As shown in Fig. 2.15, following MFSK data modulation, the MFSK signal $s_m(t)$ modulates a carrier $\cos(2\pi f_k(t)t)$ having a frequency $f_k(t)$, which is generated by a so-called frequency synthesizer generating the FH patterns required under the control of a PN sequence. The transmitted signal can be expressed as

$$s_k(t) = \sqrt{2P} \cos\{2\pi[f_c + f_m + f_k(t)]t + \varphi_m + \alpha_k(t)\} \quad (2.57)$$

where $f_k(t)$ represents the frequency-hopping pattern of user k , which is derived from a sequence $(f_j^{(k)})$ of frequencies, where we have $f_k(t) = f_j^{(k)}$ for $jT_h \leq t < (j+1)T_h$ and

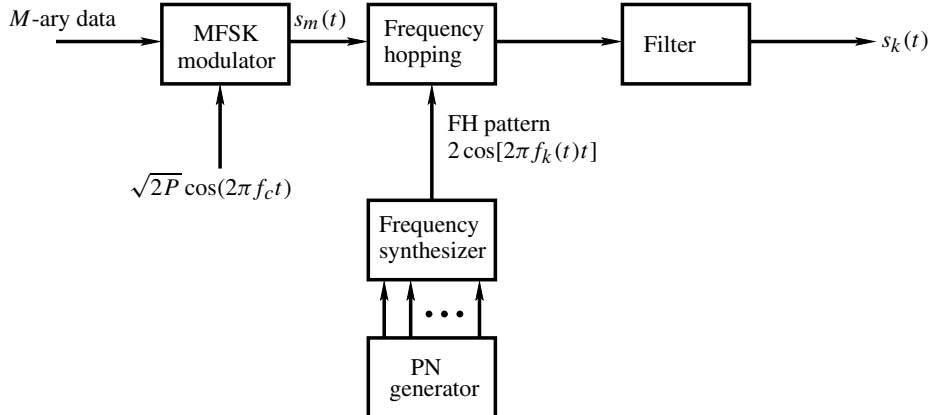


Figure 2.15: Transmitter schematic of FH spread-spectrum systems using MFSK data modulation.

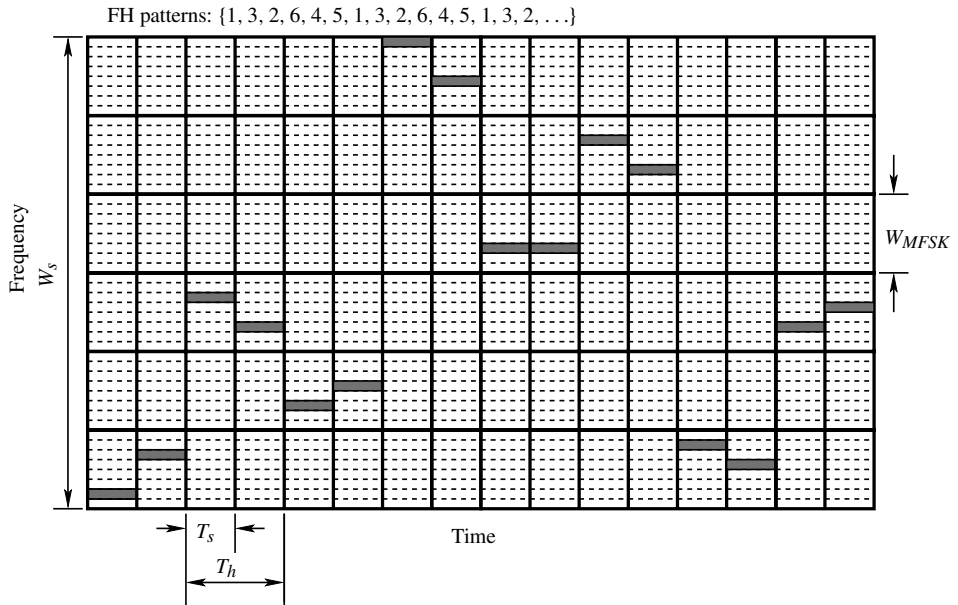


Figure 2.16: Graphical representation of slow FH spread-spectrum signals using six frequency slots and 8FSK data modulation, where two 8FSK symbols are transmitted within one FH slot, i.e. $T_h = 2T_s$.

T_h represents the FH dwell time quantifying the amount of time the synthesizer camps at a given frequency. In (2.57) $\alpha_k(t)$ represents the phase waveform of user k introduced by the k th frequency hopper, which takes on the constant value of $\alpha_j^{(k)}$ during the j th frequency hopping dwell time having a duration of T_h seconds. The other parameters in Eq. (2.57) are the same as in (2.48).

In Fig. 2.16 the operating principle of a FH spread-spectrum system using MFSK modulation is shown in a graphical form, where we assumed that the FH system employed six frequency slots for hopping and 8FSK data modulation. Furthermore, we assumed that the FH dwell time T_h was twice the MFSK symbol duration, i.e. we had $T_h = 2T_s$, which implied that two MFSK symbols were transmitted within each FH dwell time. The FH pattern used in Fig. 2.16 was $\{1, 3, 2, 6, 4, 5; 1, 3, 2, \dots\}$, which is a periodic sequence. As shown in Fig. 2.16, the FH signal transmitted within an MFSK symbol duration constitutes a narrow-band signal, whose frequency band is determined by the current FH frequency controlled by the FH pattern, while the frequency of the current MFSK tone is determined by the transmitted data.

Let W_s be the system bandwidth and W_{MFSK} the bandwidth required by the MFSK modulation scheme. As shown in Fig. 2.16, W_s and W_{MFSK} obey the relationship of $W_s = QW_{MFSK}$, where Q represents the number of FH frequencies. As discussed above in the context of MFSK signals, a noncoherent MFSK scheme requires a minimum bandwidth of $(M + 1)/T_s$ Hz. Hence, a noncoherent MFSK assisted FH spread-spectrum system using Q number of FH frequencies requires a minimum bandwidth of $Q(M + 1)/T_s$ Hz.

2.3.3 *M*-ary Frequency-Shift Keying Aided Fast Frequency-Hopping

In the above FH spread-spectrum system we have assumed that the FH dwell time T_h is higher than the MFSK symbol duration T_s , i.e. that we have $L = T_s/T_h < 1$, where $1/L = T_h/T_s$ is usually an integer. In this type of FH system, several MFSK symbols are transmitted within a FH interval. The family of FH spread-spectrum systems exhibiting the above characteristics is referred to as the class of *slow frequency-hopping* (SFH) spread-spectrum systems. Alternatively, in a FH spread-spectrum system a single MFSK symbol can be transmitted with the aid of several FH frequencies, implying that only a fraction of the MFSK symbol is transmitted within a FH dwell time. In this type of FH spread-spectrum systems we have $L = T_s/T_h > 1$, where L is an integer, and this type of FH systems are referred to as *fast frequency-hopping* (FFH) spread-spectrum systems.

The graphical representation of a FFH scheme using six FH slots and 8FSK data modulation is shown in Fig. 2.17, where we assume that one 8FSK symbol is transmitted using two FH slots, i.e. we assume that $T_s = 2T_h$. The FH pattern used in Fig. 2.17 is the same as that used in Fig. 2.16, namely $\{1, 3, 2, 6, 4, 5; 1, 3, 2, \dots\}$. In FFH systems an MFSK signal having a symbol-duration of T_s is usually detected by first detecting its fractional constituent signals during the hopping interval T_h . The decision variable generated for detecting an MFSK signal is obtained by combining the decision variables corresponding to its constituent signals, with the aid of specific combining schemes [26]. Assuming that $L = T_s/T_h$ is an integer, in FFH systems the frequencies are designed to satisfy the orthogonality condition of

$$\begin{aligned} \rho_{ij} &= \frac{L}{E_s} \int_0^{T_h} s_i(t)s_j(t) dt \\ &= \frac{1}{T_h} \int_0^{T_h} \cos[2\pi(f_i - f_j)t + \varphi_i - \varphi_j] dt \\ &= 0, \quad i \neq j \end{aligned} \tag{2.58}$$

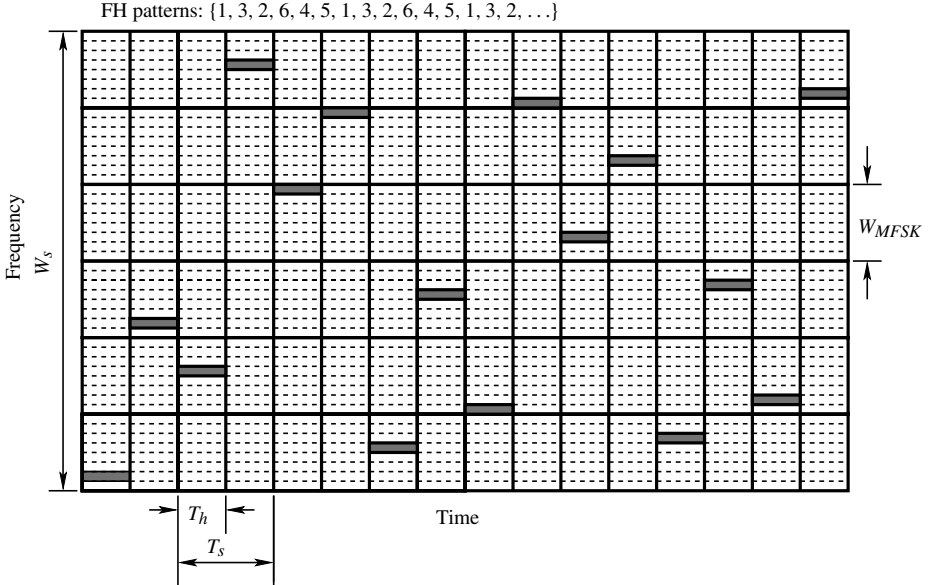


Figure 2.17: Graphical representation of fast FH (FFH) spread-spectrum signals using six frequency slots and 8FSK data modulation, where one 8FSK symbol is transmitted within two FH slots, i.e. $T_s = 2T_h$.

Therefore, the frequency spacing between two frequencies must obey

$$f_i - f_j = \frac{n}{T_h}, \quad n = 1, 2, \dots \quad (2.59)$$

Given a minimum frequency spacing of $1/T_h$, the frequency set of

$$\mathbf{F} = \left\{ \frac{0}{T_h}, \frac{1}{T_h}, \dots, \frac{M-1}{T_h} \right\} \quad (2.60)$$

is capable of guaranteeing an orthogonal MFSK scheme, requiring a minimum bandwidth of $W_{MFSK} = (M+1)/T_h$ Hz. Hence, a FH system employing Q number of FH frequencies and noncoherent MFSK data modulation requires a total system bandwidth given by $W_s = QW_{MFSK}$ and a minimum system bandwidth of $W_s = Q(M+1)/T_h$.

The above-mentioned FFH system has the same transmitter schematic as the SFH system of Fig. 2.15. One of the typical characteristics of this type of FH system is that the bandwidth W_{MFSK} used for MFSK modulation spans only a fraction of the total system bandwidth W_s . In the context of FFH systems, the above arrangement cannot efficiently exploit the frequency resources available. Figure 2.18 shows a more efficient FFH arrangement, where the FH and MFSK modulation schemes are designed jointly in order to share efficiently the total available frequency bandwidth.

The operation of the transmitter associated with the FFH system of Fig. 2.18 is as follows. During an MFSK signalling interval of T_s seconds, b message bits of the k th user having a bit rate of R_b are loaded into a b -bit buffer. We denote this b -bit symbol as X_k , where $X_k \in [0, M = 2^b]$. Hence, the b -bit output symbol rate is $R_s = R_b/b$. Let $R_h = 1/T_h$ be

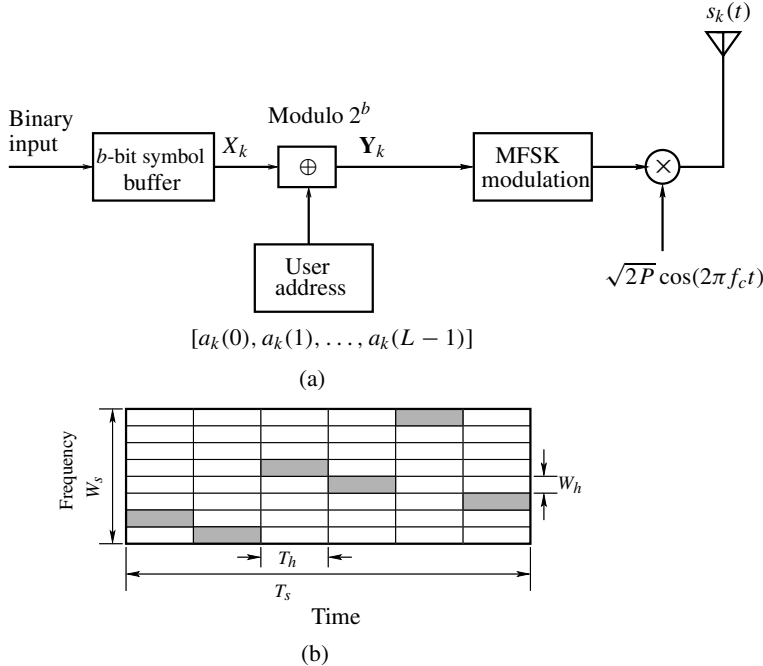


Figure 2.18: (a) Transmitter schematic and (b) graphical representation of a bandwidth-efficient fast FH (FFH) spread-spectrum scheme. In the graphical representation the number of FH frequencies and the number of frequencies used for MFSK modulation are of the same value, which is assumed to be $Q = M = 2^b = 8$. Furthermore, we assume that $L = T_s/T_h = 6$, the k th user's address code is $\mathbf{a}_k = [4, 3, 7, 6, 2, 5]$ and the transmitted 8-ary symbol value is $X_k = 5$.

the FH rate, where T_h , as noted previously, represents the duration of the FH dwell time, also referred to as chips in the FFH systems. In FFH systems $L = T_s/T_h > 1$. Hence, an $M = 2^b$ -ary symbol activates a particular MFSK tone only for the duration of $T_h = T_s/L$ seconds and then hops to a further $(L - 1)$ other legitimate FH frequencies of the MFSK scheme used.

In the FFH systems considered, in order to distinguish between different users, each user is assigned a unique user-specific signature FH pattern also referred to as an address code. The FH patterns of the different users can be designed such that the interference among the users is as low as possible. Let the address code of the k th user, $1 \leq k \leq K$, be expressed as $\mathbf{a}_k = [a_k(0), a_k(1), \dots, a_k(L-1)]$, where $a_k(l) \in GF(M)$, $l = 0, 1, \dots, L-1$ and $GF(M)$ denotes a Galois field having a finite number of elements of $M = 2^b$ [13]. Then, the transmitted symbol X_k is signalled by invoking the k th user's address code, which can be expressed as

$$\mathbf{Y}_k = [y_k(0), y_k(1), \dots, y_k(L-1)] = X_k \cdot \mathbf{1} \oplus \mathbf{a}_k \quad (2.61)$$

where $\mathbf{1}$ is an all-one vector of length L , while $y_k(l)$ for $1 \leq l < L$ are elements of $GF(M)$. Furthermore, in (2.61) \oplus denotes the addition operation in $GF(M)$. However, in this chapter it simply represents the modulo- M or modulo- 2^b addition, as seen in Fig. 2.18(a). Obeying the user address codes, the components of \mathbf{Y}_k are passed serially to an MFSK modulator,

where they are converted to the MFSK tones $\mathbf{F}_m^{(k)} = [f_0^{(k)}, f_1^{(k)}, \dots, f_{L-1}^{(k)}]$, where $f_l^{(k)} \in \mathbf{F}$, also often referred to as chips having a duration of T_h . Finally, the MFSK modulated signal is transmitted after modulating a carrier of frequency f_c . The k th user's transmitted signal for the M -ary symbol of X_k during $iT_s \leq t < (i+1)T_s$ can be expressed as

$$s_k(t) = \sum_{l=0}^{L-1} \sqrt{2P} P_{T_h}(t - iT_s - lT_h) \cos(2\pi[f_c + f_l^{(k)}]t + \varphi_l^{(k)}) \quad (2.62)$$

where P is the transmitted power, $P_{T_h}(t)$ is the rectangular pulse-shaped signalling waveform associated with a chip defined over the interval $[0, T_h]$, while $\varphi_l^{(k)}$ represents the phase angle introduced by the MFSK and carrier modulation stages.

In the context of the example of Fig. 2.18(b), we used the user address of $\mathbf{a}_k = [4, 3, 7, 6, 2, 5]$ and assumed that the transmitted 8-ary data symbol was $X_k = 5$. Hence, \mathbf{Y}_k in Fig. 2.18 (a) is given by

$$\begin{aligned} \mathbf{Y}_k &= X_k \cdot \mathbf{1} \oplus \mathbf{a}_k \\ &= [5, 5, 5, 5, 5] \oplus [4, 3, 7, 6, 2, 5] \\ &= [1, 0, 4, 3, 7, 2] \end{aligned} \quad (2.63)$$

After mapping the sequence $\mathbf{Y}_k = [1, 0, 4, 3, 7, 2]$ to the corresponding frequencies, the MFSK tones transmitted are shown in Fig. 2.18 (b), which are $\{f_1, f_0, f_4, f_3, f_7, f_2\}$.

Above, the transmitters of three types of FH scheme – an SFH scheme and two FFH schemes – have been discussed. Let us now consider their corresponding receivers.

2.3.4 Detection of FH/MFSK Signals

Assuming that the k th FH signal of (2.57) is transmitted over a noiseless channel, the received FH signal can be expressed in the form

$$r(t) = \sqrt{2P} \cos[2\pi[f_c + f_m + f_k(t - \tau_k)]t + \phi_m^{(k)}] \quad (2.64)$$

where τ_k represents the transmission delay, while $\phi_m^{(k)}$ represents the total resultant phase angle.

The receiver schematic of the FH spread-spectrum system is shown in Fig. 2.19. This receiver is suitable for both the SFH scheme corresponding to the transmitter schematic of Fig. 2.15 characterized with the aid of the graphical representation of Fig. 2.16, and for the FFH scheme corresponding to the transmitter schematic of Fig. 2.17. By comparing Fig. 2.19 and Fig. 2.15 we observe that the receiver essentially follows the inverse structure of the transmitter. At the receiver, the received signal is first frequency dehopped using the FH pattern $\{f_k\}$ of the k th user. Following the frequency dehopping stage, the dehopped signal is filtered by a BPF in order to remove the high-frequency components having the frequency of twice the carrier frequency of f_c . The BPF output signal of Fig. 2.19 can be expressed as

$$\begin{aligned} s_m(t) &= \sqrt{2P} \cos[2\pi[f_c + f_m + f_k(t - \tau_k)]t + \phi_m^{(k)}] \\ &\times 2 \cos[2\pi[f_k(t - \tau_k)]t] \\ &= \sqrt{2P} \cos[2\pi(f_c + f_m)t + \phi_m^{(k)}] \end{aligned} \quad (2.65)$$

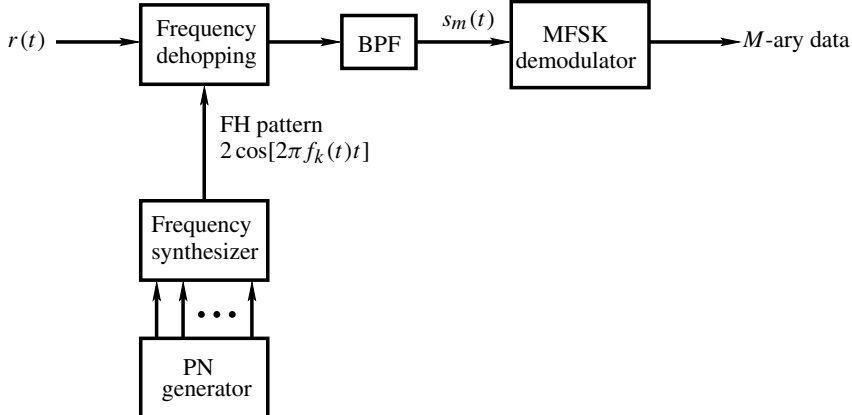


Figure 2.19: Receiver block diagram of the FH spread-spectrum system corresponding to the transmitter of Fig. 2.15 using noncoherent MFSK demodulation.

which, in fact, is the conventional MFSK modulated signal previously formulated in (2.52). Consequently, the transmitted M -ary data can now be detected using the MFSK detection scheme shown in Fig. 2.14.

The concept of frequency dehopping can be further augmented with the aid of Fig. 2.16 and Fig. 2.20(a) corresponding to an SFH scheme, as well as using Fig. 2.17 and Fig. 2.20(b) corresponding to a FFH scheme. Specifically, in the context of the SFH signals represented by Fig. 2.16, if we dehop these signals using the corresponding FH patterns $\{1, 3, 2, 6, 4, 5; 1, 3, \dots\}$ based on the FH dwell time of $T_h = 2T_s$, we will obtain the group of MFSK signals shown in Fig. 2.20(a). Explicitly, from Fig. 2.20(a) we can infer that the transmitted M -ary symbols are $\{1, 5, 5, 2, 2, 4, 7, 3, 2, 2, 5, 2, 6, 4, 2, 4\}$. By contrast, for the transmitted FFH signals represented by Fig. 2.17, if we dehop these FFH signals using the corresponding FH patterns of $\{1, 3, 2, 6, 4, 5; 1, 3, \dots\}$ based on the FH dwell time of $T_h = 0.5T_s$, the corresponding MFSK signals are shown in Fig. 2.20(b). When we make decisions on the basis of the total symbol duration, we can infer that the transmitted M -ary symbols are $\{1, 4, 7, 4, 0, 2, 5, 1\}$.

Considering the FFH transmitter of Fig. 2.18 and the transmitted signal $s_k(t)$ in the form of (2.62), the received signal can be expressed as

$$r(t) = \sum_{l=0}^{L-1} \sqrt{2P} P_{T_h}(t - iT_s - lT_h - \tau_k) \cos(2\pi[f_c + f_l^{(k)}]t + \phi_l^{(k)}) \quad (2.66)$$

The corresponding receiver schematic designed for demodulating the FFH signal of (2.66) is shown in Fig. 2.21(a), which essentially follows the inverse structure of the transmitter of Fig. 2.18. At the receiver the received signal is first down-converted from the carrier frequency band to the FH band corresponding to the FH pattern used. Then, the down-converted signal is input to a bank of M energy detectors matched to the M frequency tones of the MFSK stage. Note that the energy detector is the same as the corresponding detector of Fig. 2.14 invoked for generating the decision variables. The detection interval is of a duration of T_h seconds, which is synchronized with the chips or FH intervals of the desired user.

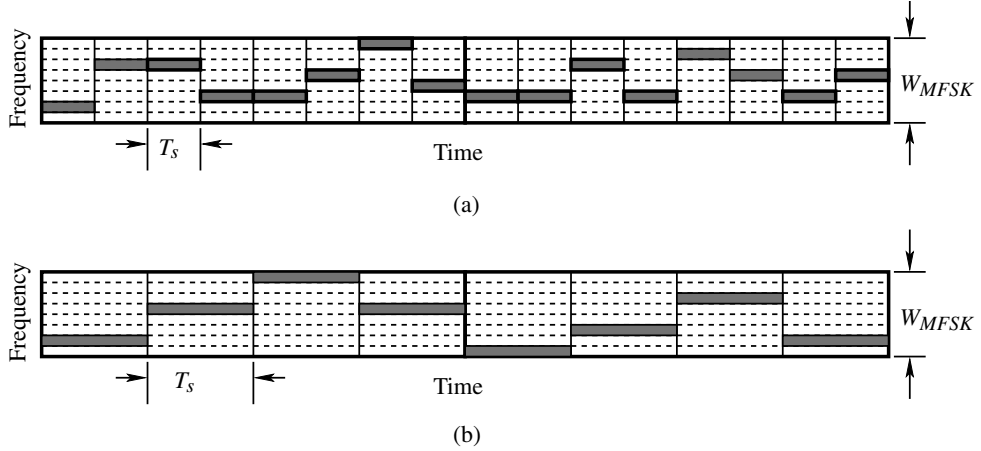


Figure 2.20: (a) Graphical representation of the demodulation of SFH and (b) FFH spread-spectrum signals for the transmitted SFH signals represented by Fig. 2.16 and for the transmitted FFH signals represented by Fig. 2.17. These figures show that after frequency dehopping, the M -ary data can be detected using the conventional noncoherent detector designed for MFSK signals. Explicitly, for the SFH scheme the detected symbols are $\{1, 5, 5, 2, 2, 4, 7, 3, 2, 2, 5, 2, 6, 4, 2, 4\}$. By contrast, for the FFH scheme the detected symbols are $\{1, 4, 7, 4, 0, 2, 5, 1\}$.

Since there are L FH chips within an M -ary symbol interval duration of T_s seconds, the M energy detectors provide ML outputs during a symbol period of T_s seconds. As shown in Fig. 2.21(a), the spectrum of each T_s -duration transmission is analysed in order to determine, which frequency tone and hence which b -bit symbol X_k was transmitted by invoking the FH address code of the desired user.

In FFH spread-spectrum systems, as described previously in the context of the transmitter of Fig. 2.18, a user address is employed as a unique user-specific signature sequence, in order to signal the MFSK tones conveying a b -bit symbol of the user considered, as shown in (2.61). Following energy detection in each frequency band during all of the L chips, the sequence \mathbf{Y}_k of (2.61) is recovered by the receiver. By performing modulo- $(M = 2^b)$ subtraction³ of the unique user address \mathbf{a}_k of the k th user (desired user) from \mathbf{Y}_k on a chip-by-chip basis, we arrive at

$$\mathbf{X}_k \cdot \mathbf{1} = \mathbf{Y}_k \ominus \mathbf{a}_k \quad (2.67)$$

which allows us to recover the transmitted symbol X_k of user k . More specifically, since $\mathbf{Y}_k = \mathbf{X}_k \cdot \mathbf{1} \oplus \mathbf{a}_k$, we have that

$$\begin{aligned} \mathbf{Y}_k \ominus \mathbf{a}_k &= \mathbf{X}_k \cdot \mathbf{1} \oplus \mathbf{a}_k \ominus \mathbf{a}_k \\ &= \mathbf{X}_k \cdot \mathbf{1} \oplus \mathbf{0} \\ &= \mathbf{X}_k \cdot \mathbf{1} \end{aligned} \quad (2.68)$$

where $\mathbf{0}$ represents an all-0 vector of length L .

³Note that the subtraction operation is usually defined in $GF(M)$. For the sake of simplicity, we use modulo- M subtraction in this chapter.

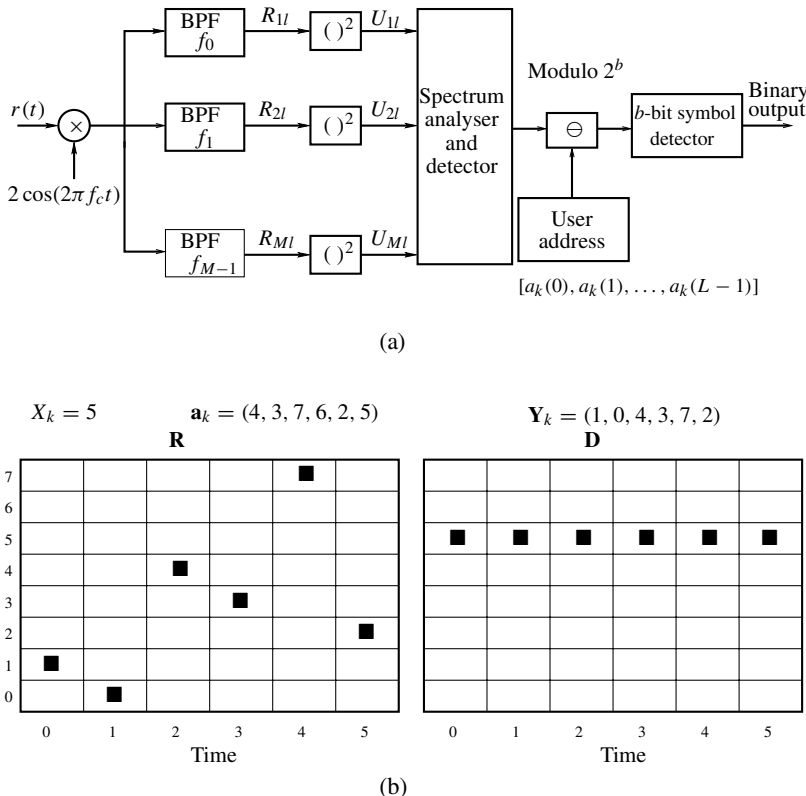


Figure 2.21: (a) Receiver block diagram and (b) detection example for FFH systems corresponding to Fig. 2.18. The eight rows indicate the 8-ary FSK tones, while the six columns correspond to the six FH intervals or chips of a symbol duration. For example, for $\mathbf{Y}_k = (1, 0, 4, 3, 7, 2)$ shown in the received time-frequency matrix \mathbf{R} and for $\mathbf{a}_k = (4, 3, 7, 6, 2, 5)$, according to (2.67) we have $X_k \cdot \mathbf{1} = (-3, -3, -3, -3, 5, -3) = (5, 5, 5, 5, 5, 5)$ as shown in the time-frequency matrix \mathbf{D} . Observe that \mathbf{D} has a unique complete row, yielding a unanimous symbol decision of 5.

The detection operations associated with the user address of the FFH system can be illustrated by means of time-frequency matrices having M rows and L columns, where the M rows correspond to the M distinct frequency values, while the L columns represent the L number of chips corresponding to one MFSK symbol duration. The elements of the time-frequency matrices are referred to as time-frequency elements. In Fig. 2.21(b) \mathbf{R} represents the received time-frequency matrix of a FFH system using 8-ary FSK. Provided that no channel impairments are imposed, all elements of the time-frequency matrix are received correctly. Specifically, if a particular chip corresponding to a particular time-frequency element is present at the receiver, the corresponding time-frequency element output is flagged by a marker (or logical 1), otherwise by a space (or logical 0).

As seen in the matrix \mathbf{R} of Fig. 2.21(b) representing the received time-frequency matrix of the k th user, the signals marked as *black-squares* are present at the time-frequency elements, which correspond to the time-frequency elements activated by user k . Specifically, the tones $(1, 0, 4, 3, 7, 2)$ are activated, which convey the 8FSK symbol 5, as will be shown below. We have assigned the unique user-specific signature address $(4, 3, 7, 6, 2, 5)$ to user k . The time-frequency matrix obtained by modulo-8 subtraction of the unique addresses \mathbf{a}_k from \mathbf{Y}_k according to (2.67) is denoted by \mathbf{D} in Fig. 2.21(b). Let us, for example, employ the majority logic decision-based decoder, which opts for deciding in favour of the particular 8-ary symbol corresponding to the specific row having the highest number of non-zero entries, to provide an estimate of the transmitted symbol of user k . Hence, based on the time-frequency matrix of \mathbf{D} in Fig. 2.21, we find that the transmitted symbol was symbol 5, which is correctly decoded with the help of unambiguous majority logic decision.

2.3.5 Frequency-Hopping Multiple-Access

The principle of multiple-access communications based on FH-assisted systems may be readily understood with the help of the graphical representation of the FH spread-spectrum signals. Below, we give two examples for illustrating how multiple users share the same frequency band using FH, in order to implement FH multiple-access (FHMA)-aided communications. The first example considers FHMA communications using SFH in the context of the transmitter of Fig. 2.15, using the receiver of Fig. 2.19 and the graphical representations of Figs 2.16 and 2.20(a). The second example considers FHMA communications using FFH corresponding to the transmitter of Fig. 2.18(a), using the receiver of Fig. 2.21(a) and the graphical representation of Figs 2.18(b) and 2.21(b).

2.3.5.1 Slow Frequency-Hopping Multiple-Access

Fig. 2.22 shows the graphical representation of two SFH signals over a FH period duration of $6T_h$ seconds, where $T_h = 2T_s$ indicating that two MFSK symbols are transmitted within one FH slot. In SFH systems the various users are distinguished by their unique user-specific FH patterns or FH addresses. In the context of the example shown in Fig. 2.22, the first user's FH pattern is $\{1, 3, 2, 6, 4, 5\}$, while the second user's FH pattern is $\{2, 6, 4, 3, 1, 5\}$. The FH frequencies are activated correspondingly according to the FH patterns of both users 1 and 2. In Fig. 2.22 we assumed that the 8-ary symbols transmitted in the FH period considered are $(1, 5, 5, 2, 2, 4, 7, 5, 0, 2, 3, 4)$ for user 1 and $(3, 5, 1, 7, 4, 0, 3, 1, 6, 7, 5, 4)$ for user 2. Therefore, within each symbol interval of T_s seconds an MFSK tone is activated according to the corresponding value of the 8-ary symbol. As shown in the first five FH slots of Fig. 2.22, since the FH frequencies of user 1 and user 2 are different within a given FH slot, only one active MFSK tone is received within an MFSK band having a total bandwidth of W_{MFSK} . By contrast, in the sixth FH slot both user 1 and user 2 transmit their signal at the same FH frequency of f_5 , hence the two user signals interfere with each other within this FH slot. Furthermore, since the first 8-ary symbol transmitted within the last FH slot is 3 for user 1 and 5 for user 2, we observe two different active MFSK tones. By contrast, the second symbols transmitted by both users within the last FH slot have the same value of 4, consequently, only one active MFSK tone is observed.

User 1. FH patterns: {1, 3, 2, 6, 4, 5}; Transmitted 8-ary symbol: 1, 5, 5, 2, 2, 4, 7, 5, 0, 2, 3, 4
User 2. FH patterns: {2, 6, 4, 3, 1, 5}; Transmitted 8-ary symbol: 3, 5, 1, 7, 4, 0, 3, 1, 6, 7, 5, 4

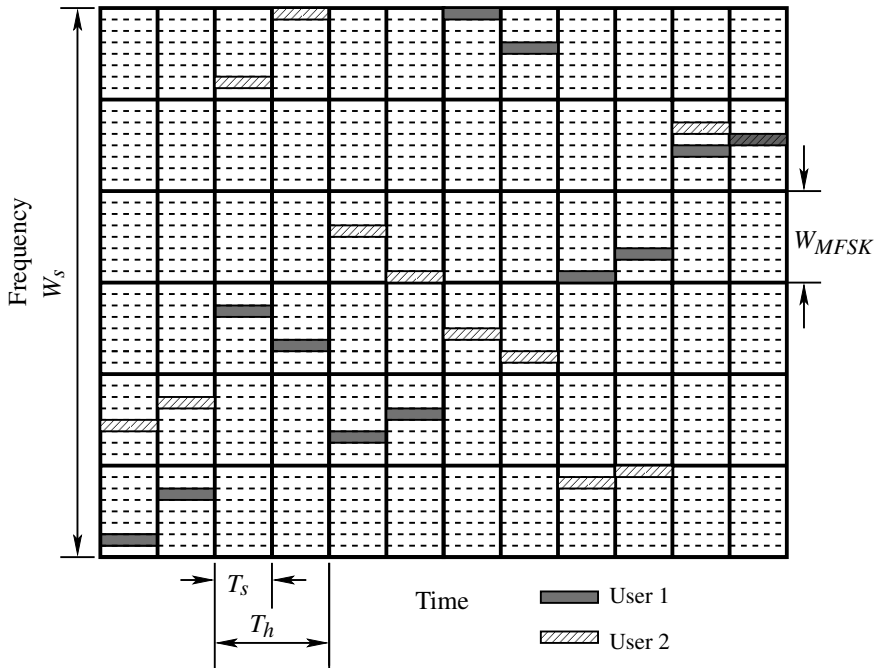


Figure 2.22: Graphical representation of two-user-based FHMA signals over one FH period. The first user's FH address is {1, 3, 2, 6, 4, 5} and his transmitted 8-ary symbols are (1, 5, 5, 2, 2, 4, 7, 5, 0, 2, 3, 4), while the second user's FH address is {2, 6, 4, 3, 1, 5} and his transmitted 8-ary symbols are (3, 5, 1, 7, 4, 0, 3, 1, 6, 7, 5, 4). Observe that the two user signals interfere with each other within the final FH slot.

As argued in Section 2.3.4, the frequency dehopping operation in SFH systems is carried out to remove the FH frequencies with the help of a given user's FH pattern. Fig. 2.23(a) represents the dehopped MFSK signals after removing the FH frequencies by multiplying the received signal of Fig. 2.22 with the frequency tones $\{f_1, f_3, f_2, f_6, f_4, f_5\}$ derived from the FH pattern {1, 3, 2, 6, 4, 5} of user 1. By contrast, Fig. 2.23(b) represents the dehopped signals after removing the FH frequencies by multiplying the received signal of Fig. 2.22 with the frequency tones $\{f_2, f_6, f_4, f_3, f_1, f_5\}$ derived from the FH pattern {2, 6, 4, 3, 1, 5} of user 2. Explicitly, for both users the first ten symbols corresponding to the first five FH slots can be correctly detected, provided that no channel impairments are imposed. By contrast, the 11th symbol of both users transmitted in the last FH slot may be detected erroneously, since two active MFSK tones interfere with each other. However, in the absence of channel impairment, the last symbol of both users may be correctly detected, since at this moment both users transmit the 8-ary symbol value of 4.

The above example demonstrated that in SFH spread-spectrum systems multiple-access communications can be achieved by assigning different FH patterns to different users sharing

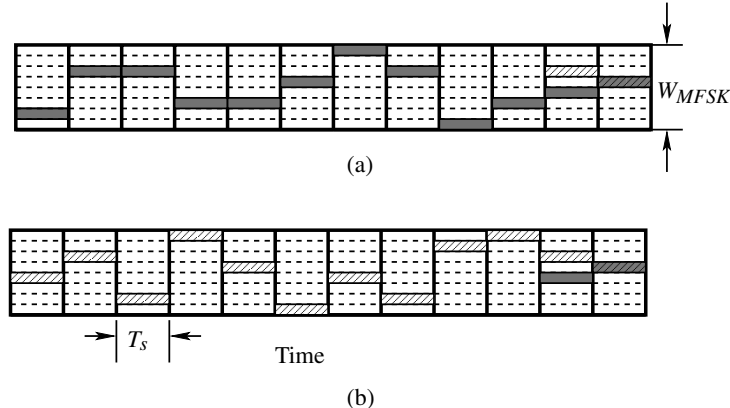


Figure 2.23: Graphical representations of 8-ary FSK signals of users 1 and 2 after dehopping operations using their FH address codes {1, 3, 2, 6, 4, 5} for user 1 and {2, 6, 4, 3, 1, 5} for user 2. Since two users' transmitted FH signals hit with each other within the sixth FH slot, it can be observed that within this FH slot they interfere with each other, resulting in possible erroneous decisions.

the same FH band. Different users can be successfully distinguished by their unique FH patterns or FH addresses. Furthermore, the performance of SFH systems is dependent on the FH patterns employed. A FH system employing a set of FH patterns having a low probability of interfering frequency slots referred to as a hit is usually capable of achieving a better performance than a system employing a set of FH patterns having a high probability of hit. Hence, an important task associated with the design of FH patterns is to ensure that the probability of hits is as low as possible.

2.3.5.2 Fast Frequency-Hopping Multiple-Access

Let us now consider the FHMA systems using FFH. Fig. 2.24 shows an example corresponding to the transmitter block diagram of Fig. 2.18, where two users share the same FH band. In Fig. 2.24 the FH addresses of the two users are $\mathbf{a}_1 = [4, 3, 7, 6, 2, 5]$ for user 1 and $\mathbf{a}_2 = [2, 4, 6, 3, 1, 7]$ for user 2. We assumed that the transmitted 8-ary symbols are $X_1 = 5$ and $X_2 = 3$, respectively. Consequently, according to (2.61) we have $\mathbf{Y}_1 = [5, 5, 5, 5, 5] \oplus [4, 3, 7, 6, 2, 5] = [1, 0, 4, 3, 7, 2]$ and $\mathbf{Y}_2 = [3, 3, 3, 3, 3, 3] \oplus [2, 4, 6, 3, 1, 7] = [5, 7, 1, 6, 4, 2]$. In response to \mathbf{Y}_1 and \mathbf{Y}_2 , the time-frequency matrix of the transmitter seen in Fig. 2.24 has the elements of $\{f_1, f_0, f_4, f_3, f_7, f_2\}$ for user 1 and $\{f_5, f_7, f_1, f_6, f_4, f_2\}$ for user 2.

Assuming that the FHMA signals represented by Fig. 2.24 are transmitted over a perfect channel, the time-frequency matrix recorded by the receiver after the energy detectors of Fig. 2.21 is the same as that seen in Fig. 2.24. However, we note that, before the detection procedure, the receiver has no knowledge about which of the time-frequency elements were activated by the first user and which of them by the second user. The detection procedure of FFH schemes has been described by (2.67), where modulo- M subtracts a given user's FH address from the time-frequency matrix recorded by the receiver for detecting its transmitted

$$X_1 = 5, \quad \mathbf{a}_1 = (4, 3, 7, 6, 2, 5), \quad \mathbf{Y}_1 = (1, 0, 4, 3, 7, 2)$$

$$X_2 = 3, \quad \mathbf{a}_2 = (2, 4, 6, 3, 1, 7), \quad \mathbf{Y}_2 = (5, 7, 1, 6, 4, 2)$$

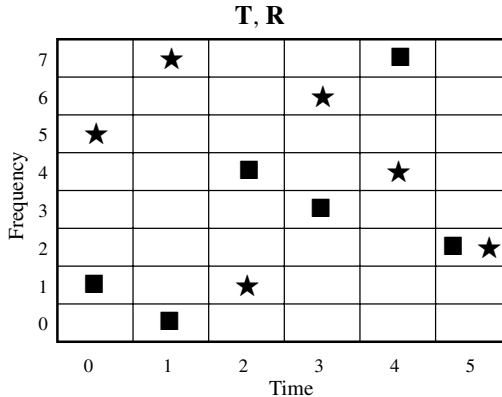


Figure 2.24: Graphical representation of the fast FH (FFH) spread-spectrum signals of two users within a symbol duration. In this figure, both the number of FH frequencies and MFSK modulation frequencies is eight. The number of hops per modulated symbol is $L = T_s/T_h = 6$.

data. The individual users' time-frequency matrices are obtained after subtracting the FH addresses of user 1 and user 2, respectively, from the time-frequency matrix of the receiver, as seen in Fig. 2.24. The corresponding results are shown in Fig. 2.25, where \mathbf{D}_1 corresponds to user 1, while \mathbf{D}_2 to user 2. As shown in Fig. 2.25, in \mathbf{D}_1 there is a full row representing the transmitted symbol $X_1 = 5$, while in \mathbf{D}_2 we observe a full row corresponding to the transmitted symbol of $X_2 = 3$. Note that the remaining marked elements of \mathbf{D}_1 and \mathbf{D}_2 represent interference imposed by the interfering user 2 or user 1, respectively.

The time-frequency matrices \mathbf{D}_1 and \mathbf{D}_2 in Fig. 2.25 show that, in the absence of channel impairment, the transmitted symbol can be correctly detected, provided that there exists no more than a single complete row that is marked in all entries. However, if there are many users and/or their FH addresses result in a high probability of hits, there may exist more than one row that is marked in all entries. In this case, erroneous decisions may occur. Therefore, in FHMA systems using FFH, the design of FH addresses resulting in a low probability of hits is important for achieving a good performance.

2.4 Time-Hopping Spread-Spectrum Communications

In Section 2.3 the philosophy of FH spread-spectrum communications has been discussed, where the carrier frequency changes were controlled by a PN sequence. Alternatively, the FH schemes concerned may also be viewed as a F-domain on–off modulation scheme, whose legitimate carrier frequencies are switched on or off, i.e. activated or deactivated according to a PN sequence. In a manner analogous to using F-domain on–off keying, time-domain on–off keying may also be employed for spread-spectrum communications. The spectrum spreading is achieved by carrying out the on–off keying in the time-domain, referred to as

$$\mathbf{Y}_1 = (1, 0, 4, 3, 7, 2), \quad \mathbf{a}_1 = (4, 3, 7, 6, 2, 5), \quad X_1 = 5$$

$$\mathbf{Y}_2 = (5, 7, 1, 6, 4, 2), \quad \mathbf{a}_2 = (2, 4, 6, 3, 1, 7), \quad X_2 = 3$$

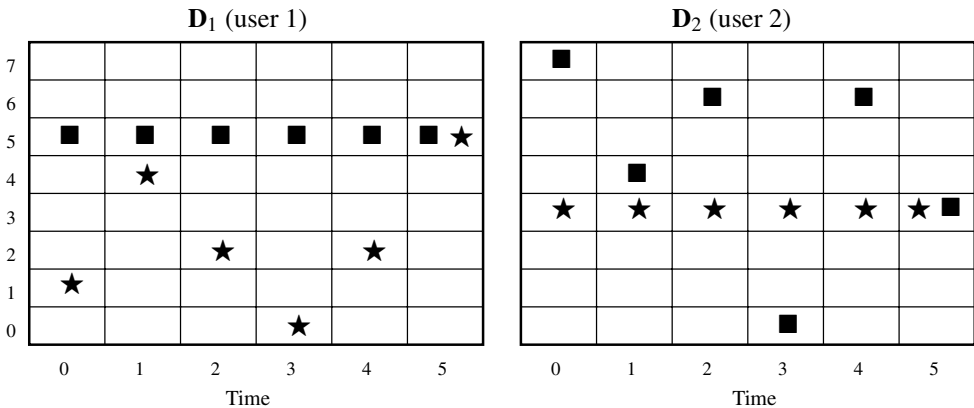


Figure 2.25: Graphical representations of detections of FFH signals, where \mathbf{D}_1 represents user 1's time-frequency matrix after subtracting user 1's address of $\mathbf{a}_1 = (4, 3, 7, 6, 2, 5)$ from the received matrix \mathbf{R} , while \mathbf{D}_2 represents user 2's time-frequency matrix after subtracting user 2's address of $\mathbf{a}_2 = (2, 4, 6, 3, 1, 7)$ from the received matrix \mathbf{R} . Observing that \mathbf{D}_1 contains only one full row corresponding to the first user's transmitted 8-ary symbol of $X_1 = 5$, and that \mathbf{D}_2 also contains only one row corresponding to the second user's transmitted 8-ary symbol of $X_2 = 3$.

time-hopping (TH). Explicitly, assume that in TH spread-spectrum systems the time axis is segmented into T_f duration intervals representing the frames, and each frame is further segmented into a number of, say M , intervals referred to as time-slots. Then, in TH spread-spectrum communications a user signal is transmitted employing a number of frames with each frame transmitting a single pulse, which is positioned in one of the M possible time-slots of the frame based on the M -ary symbol transmitted. In TH systems, each spreading sequence corresponds to a specific arrangement of the time-slot locations, hence the spreading sequence appears in the form of time-slot locations, referred to as *TH patterns*.

Figure 2.26 shows the transmitter block diagram of a general TH spread-spectrum system. In the transmitter of Fig. 2.26 the binary data are first temporarily stored in a buffer, awaiting their assignment to the appropriate time-slots for transmission. As shown in Fig. 2.26, time-hopping is carried out by a gating circuit, which is switched on/off under the control of the TH pattern generated from a PN sequence and the data symbol transmitted. When the 'gate' is on, then a data symbol is passed to the modulator of Fig. 2.26, where various baseband modulation schemes may be employed for the data modulation. Finally, as shown in Fig. 2.26, the baseband modulated signal modulates the carrier f_c , in order to translate the signal to the appropriate frequency band for transmission using the power P .

In TH systems the demodulation time-duration is of the order of a time-slot, which is usually very short. Due to the fact that attaining accurate carrier phase estimation within a time-slot interval is impractical, typically noncoherent data modulation schemes requiring no carrier phase knowledge are preferred in TH spread-spectrum systems. Hence, in our

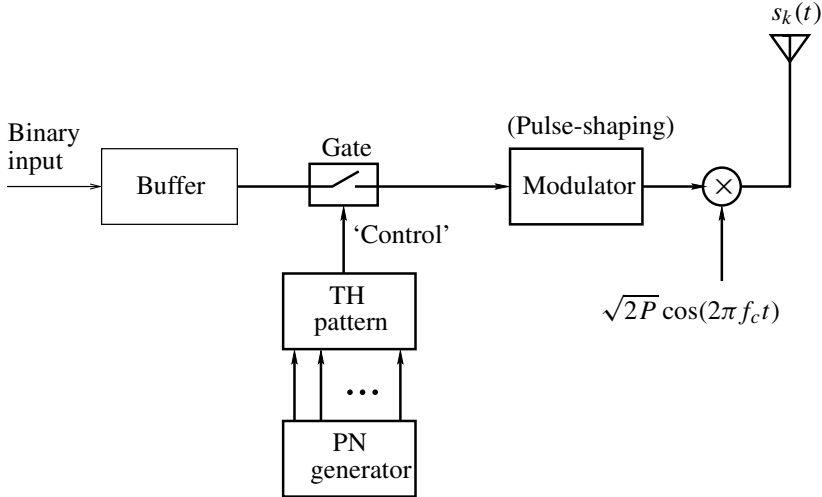


Figure 2.26: Transmitter schematic of a general TH spread-spectrum system.

discussions associated with the family of TH spread-spectrum systems, only noncoherent modulation schemes are considered. Specifically, as an example, M -ary pulse-position modulation (MPPM) is employed, in order to highlight the rudimentary principles of TH spread-spectrum communications.

In the class of MPPM modulation schemes the transmitted information is extracted from one of the M possible time-slot positions. In an effort to link the less widely known to the classic, the well-established family of M -ary frequency-shift keying (MFSK) schemes belongs to a class of F-domain MPPM arrangements, where a transmitted symbol is mapped to one of the M possible frequency positions (frequency tones, or F-domain pulses). Again, analogously, the MPPM schemes considered belong to a class of position modulation arrangements, where a transmitted symbol is mapped to one of the M possible time-domain positions or slots with the aid of a time-domain pulse. Interestingly, in contrast to the established terminology of M -ary pulse-position modulation, MFSK has been widely used instead of adopting the terminology of ' M -ary F-domain pulse-position modulation'. We note furthermore that analogously to the classic MFSK modulation scheme, M -ary time-domain pulse-position modulation could also have justifiably inherited the terminology of M -ary time-shift keying (MTSK) modulation. In fact, by using the terminology of MTSK in analogy to MFSK, we are capable of augmenting one with the help of the other.

2.4.1 Slow Time-Hopping M -ary Pulse-Position Modulation

In FH-aided spread-spectrum communications two fundamental types of FH scheme have been discussed, namely slow FH (SFH) and fast FH (FFH) arrangements. In the context of the SFH systems, several M -ary symbols are transmitted at a given FH frequency, i.e. in a FH dwell-time interval. By contrast, in FFH systems an M -ary symbol is transmitted using a set of, say L , FH frequencies; hence the dwell time at each frequency is a fraction of the symbol

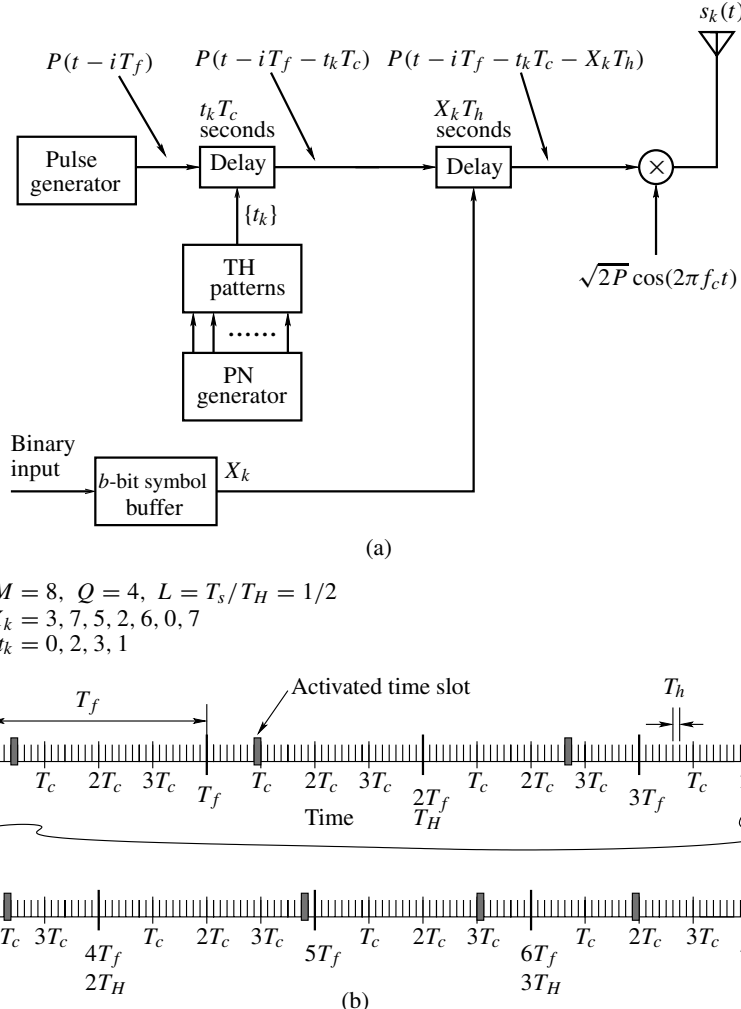


Figure 2.27: (a) Transmitter schematic and (b) graphical representation of a slow TH (STH) spread-spectrum scheme using MPPM. In the graphical example, T_s represents the symbol interval, T_f the frame (average pulse repetition) duration, T_c denotes the chip duration, T_H the TH interval, $L = T_s/T_H$ the number of $M = 2^b = 8$ -ary symbols transmitted per TH interval, T_h is the time-slot duration, Q is the number of chips per frame, X_k represents the transmitted symbol value, and finally $\{t_k\}$ the TH pattern set of user k .

duration. In parallel to FH systems, TH systems can also be implemented using either slow TH (STH) (Fig. 2.27) or fast TH (FTH) (Fig. 2.28). Let us first discuss the STH scheme of Fig. 2.27.

Analogously to the philosophy of the SFH scheme in Section 2.3.2, in STH systems several M -ary symbols are transmitted within a TH interval. Specifically, let T_s represent the symbol-duration, T_H denote the TH interval and $R_H = 1/T_H$ quantify the TH rate.

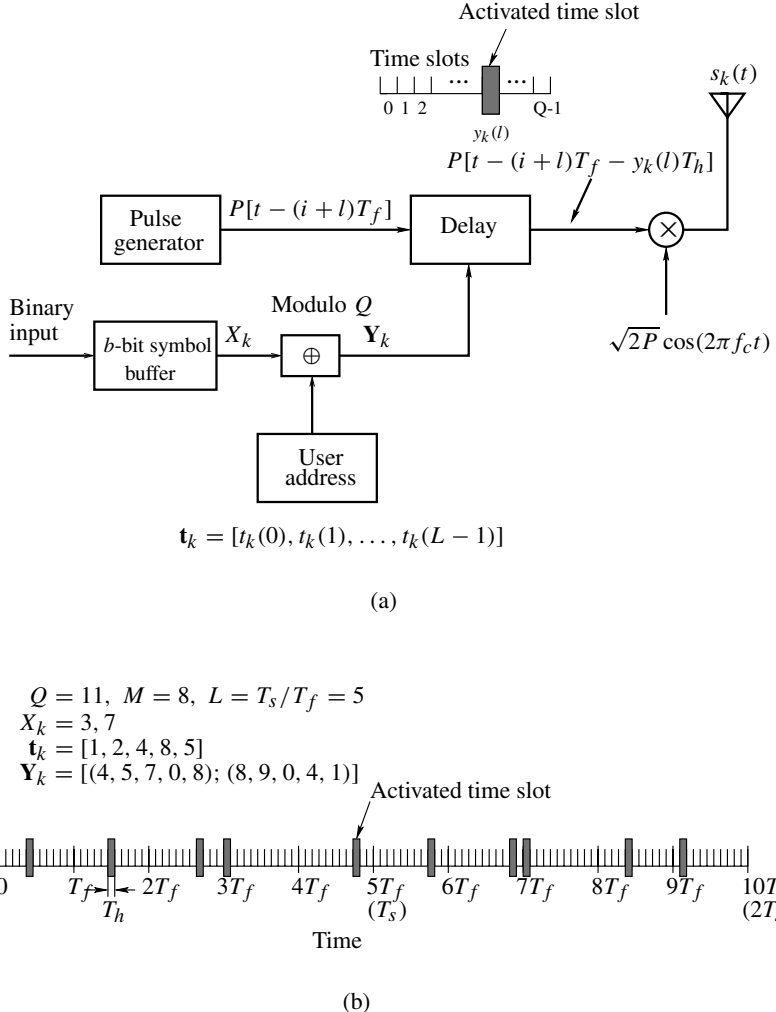


Figure 2.28: (a) Transmitter schematic and (b) graphical representation of a fast TH (FTH) spread-spectrum scheme using MPPM. In the graphical example T_f represents the frame duration (time-hopping duration or average pulse repetition time), Q is the number of time slots per frame, $\mathbf{t}_k = [t_k(0), t_k(1), \dots, t_k(L-1)]$ denotes the k th user's TH address, where the modulating signal X_k is combined with the user's TH address code \mathbf{t}_k according to $\mathbf{Y}_k = X_k \cdot \mathbf{1} \oplus \mathbf{t}_k$ and \oplus denotes modulo- Q addition. The other variables have the same meaning as in Fig. 2.27.

Note that here the TH interval is defined as the average time duration that a given TH pattern value lasts. Consequently, a TH scheme is referred to as an STH scheme, when we have $L = T_s/T_H < 1$. By contrast, when we have $L = T_s/T_H > 1$, which implies that a given M -ary symbol is transmitted using several time hops, the corresponding TH scheme is referred

to as a FTH scheme. The operation of the transmitter associated with STH spread-spectrum systems may be further augmented by referring to Fig. 2.27(a) helped by the specific STH example of Fig. 2.27(b). As shown in Fig. 2.27(a), during a signalling interval duration of T_s seconds, b message bits of the k th user are loaded into a b -bit buffer. We denote this b -bit symbol as X_k , where we have $M = 2^b$ and $X_k \in \{0, 1, \dots, M - 1\}$. The M -ary symbol X_k is temporarily stored in the buffer, where it awaits its time slot, in which it is transmitted. Let T_f be the frame duration, which corresponds to the average time duration between two activated time-domain pulses. Notice that in STH systems each transmitted time-domain pulse conveys an M -ary symbol; therefore $T_s = T_f$. As shown in Fig. 2.27(a) in the context of each M -ary symbol, the transmitter generates a time-domain pulse expressed as $P(t - iT_f)$, where i represents the frame index, $P(t)$ is defined within the interval of $[0, T_h]$ and is normalized such that we have $\int_0^{T_h} P^2(t) dt = T_h$. In Fig. 2.27(a) $\{t_k\}$ represents the PN-code-based time-hopping pattern assigned to user k , where $\{t_k\}$ are integers assuming values in the range $0 \leq t_k \leq Q - 1$. The PN time-hopping pattern is governed by the PN sequence generated by the PN generator of Fig. 2.27(a). As shown in Fig. 2.27(a), each frame is divided into Q chips, each having a duration of T_c seconds. The TH pattern imposes a PN-code-dependent time shift on the pulse during every frame. Each PN-code-dependent time shift is a discrete-time value given by $t_k T_c$ obeying $0 \leq t_k T_c \leq (Q - 1)T_c$. As shown in Fig. 2.27(a), following this time shift obeying the TH pattern, the signalling pulse is now located at the instant of $P(t - iT_f - t_k T_c)$.

In STH systems each chip duration is further divided into M number of time slots, each having a duration of T_h seconds. In the context of MPPM used for baseband modulation, one of the M possible time slots within the TH chip determined by the TH pattern is activated for transmission, signalling the presence of a pulse. As seen in Fig. 2.27(a) the $M = 2^b$ -ary symbol X_k assuming a value from the range of $0 \leq X_k \leq M - 1$ imposes a further $X_k T_h$ seconds of information symbol-dependent time shift on the time-domain pulse position locating it at the instant of $P(t - iT_f - t_k T_c - X_k T_h)$. Finally, the time-domain pulse modulates the carrier having a frequency of f_c , and then the signal is transmitted at a power of P . In summary, the transmitted STH signal of the i th frame can be expressed as

$$s_k(t) = \sqrt{2P} P(t - iT_f - t_k T_c - X_k T_h) \cos(2\pi f_c t + \varphi_i^{(k)}) \quad (2.69)$$

where $\varphi_i^{(k)}$ represents the initial phase angle due to carrier modulation.

The operating principles of the STH transmitter may be further augmented by an example, as shown in Fig. 2.27(b). In the context of this example, we assumed that the number of time slots per chip-duration of T_c was $M = 2^3 = 8$, the number of STH chips per frame was $Q = 4$ and we had $L = T_s/T_H = 1/2$, implying that two 8-ary symbols were transmitted within a TH interval. Furthermore, we assumed that seven $b = 3$ -bit symbols corresponding to seven frames or seven symbol intervals were transmitted, which assumed the symbol values of $X_k = \{3, 7, 5, 2, 6, 0, 7\}$ and the TH pattern corresponding to the seven symbol intervals or four TH intervals was $t_k = \{0, 2, 3, 1\}$. Consequently, according to (2.69) we can derive the set of activated time slots, located at positions

$$\begin{aligned} &0T_f + 0T_c + 3T_h, 1T_f + 0T_c + 7T_h, 2T_f + 2T_c + 5T_h, 3T_f + 2T_c + 2T_h \\ &4T_f + 3T_c + 6T_h, 5T_f + 3T_c + 0T_h, 6T_f + 1T_c + 7T_h \end{aligned}$$

As seen in Fig. 2.27(b), the corresponding activated time slots are marked by shaded bars.

Note, furthermore, that the schematic of the STH arrangement of Fig. 2.27(a) is also suitable for fast TH (FTH), provided that the corresponding parameters in Fig. 2.27(a) are appropriately set. Specifically, for FTH the TH interval of T_H is usually set to the value of the frame duration of T_f , i.e. to $T_H = T_f$, and hence a given M -ary symbol is transmitted using several frames, implying that we have $L = T_s/T_H = T_s/T_f > 1$, where L is a positive integer. The other parameters of the FTH scheme of Fig. 2.27(a) have the same meaning, as those of the STH arrangement. The transmitted FTH signal based on the transmitter of Fig. 2.27(a) also obeys (2.69), except that a given M -ary symbol X_k is now transmitted using $L > 1$ number of frames, which implies that $X_k T_h$ in (2.69) remains constant over L number of frames. Below, we consider another type of FTH scheme.

2.4.2 Fast Time-Hopping M -ary Pulse-Position Modulation

In this section we consider a type of FTH scheme for the sake of analogy with the FFH scheme characterized by Fig. 2.18. This type of FTH scheme has the advantage of exploiting the set of time slots with high efficiency. The transmitter schematic of the FTH system considered is shown in Fig. 2.28(a), which is similar to the transmitter schematic of the FFH scheme seen in Fig. 2.18, except that the MFSK modulator of Fig. 2.18 is now replaced by a pulse generator in Fig. 2.28(a), which generates time-domain pulses when the time slots are activated for transmissions. Specifically, the operation of the transmitter associated with the FTH system can be described by referring to Fig. 2.28(a), which is further augmented by the specific example seen in Fig. 2.28(b). Similarly to the FFH scheme discussed in Section 2.3.2, each user is assigned a unique user signature TH pattern also referred to as an address code, in order to distinguish among different users. Let the TH address code of user k be expressed as $\mathbf{t}_k = [t_k(0), t_k(1), \dots, t_k(L-1)]$, where L represents the number of frames used for transmitting an M -ary symbol. Furthermore, each element of the TH address code is an element of the finite Galois field having Q elements, which is expressed as $t_k(l) \in GF(Q)$ for $l = 0, 1, \dots, L-1$ and Q represents the number of time slots per frame. As shown in Fig. 2.28(a) for a given M -ary transmitted symbol X_k of user k , X_k is first combined with the k th user's TH address code, which can be expressed as

$$\mathbf{Y}_k = [y_k(0), y_k(1), \dots, y_k(L-1)] = X_k \cdot \mathbf{1} \oplus \mathbf{t}_k \quad (2.70)$$

where $\mathbf{1}$ is an all-one vector of length L , $y_k(l)$ for $1 \leq l < L$ represents element of $GF(Q)$, and \oplus denotes modulo- Q addition. Note that both Q and M may assume the same value, as in the FFH scheme of Fig. 2.18.

Let the symbol X_k be transmitted by L number of frames started at the i th frame. As shown in Fig. 2.28(a) for the $(i+l)$ th frame, the pulse generator generates a time-domain pulse, which is expressed as $P[t - (i+l)T_f]$, $l = 0, 1, \dots, L-1$. The L number of components of \mathbf{Y}_k used for conveying the symbol X_k uniquely identify L specific time-shifts for the transmission of the corresponding pulses in L successive frames, commencing at the i th frame. The time shift corresponding to the component $y(l)$, $l = 0, 1, \dots, L-1$ is $y(l)T_h$ within the $(i+l)$ th frame, which is a discrete time shift value obeying $0 \leq y(l)T_h \leq (Q-1)T_h$. Finally, as shown in Fig. 2.28(a), in each frame a carrier modulated pulse is transmitted within the activated time-slot by using the transmission power of P . Hence, the transmitted FTH signals conveying the $M = 2^b$ -ary symbol X_k within the interval of $iT_f \leq t < (i+l)T_f$

can be expressed as

$$s_k(t) = \sqrt{2P} \sum_{l=0}^{L-1} P[t - (i+l)T_f - y_k(l)T_h] \cos(2\pi f_c t + \varphi_i^{(k)}) \quad (2.71)$$

where $\varphi_i^{(k)}$ represents the initial phase angle due to carrier modulation.

The operating principle of the FTH transmitter can be further augmented by referring to Fig. 2.28(b) for a specific example characterizing FTH. In the context of this example, we assumed that the number of T_f -duration time slots per frame was $Q = 11$, the number of bits per MPPM symbol was $b = 3$ corresponding to $M = 2^b = 8$ and we had $L = T_s/T_f = 5$, implying that a symbol is transmitted using five frames. Furthermore, two information symbols transmitted using ten frames were $X_k = \{3, 7\}$ and the user-specific TH address code of user k was assumed to be $\mathbf{t}_k = \{1, 2, 4, 8, 5\}$. Consequently, according to (2.70) we know that

$$\begin{aligned} \mathbf{Y}_k &= X_k \cdot \mathbf{1} \oplus \mathbf{t}_k \\ &= \{3 \oplus 1, 3 \oplus 2, 3 \oplus 4, 3 \oplus 8, 3 \oplus 5\}; \{7 \oplus 1, 7 \oplus 2, 7 \oplus 4, 7 \oplus 8, 7 \oplus 5\} \\ &= \underbrace{\{4, 5, 7, 0, 8\}}_{\text{Symbol 3}}; \underbrace{\{8, 9, 0, 4, 1\}}_{\text{Symbol 7}} \end{aligned} \quad (2.72)$$

The above ten elements in \mathbf{Y}_k provide specific time shifts for the corresponding signalling pulses. These specific time shifts are

$$\underbrace{\{4T_h, 5T_h, 7T_h, 0T_h, 8T_h\}}_{\text{Symbol 3}}; \underbrace{\{8T_h, 9T_h, 0T_h, 4T_h, 1T_h\}}_{\text{Symbol 7}} \quad (2.73)$$

As shown in Fig. 2.28(b), the activated time slots corresponding to the above specific time-shift values are marked by the shaded bars.

2.4.3 Detection of Slow Time-Hopping Signals

In this section we consider the detection of the STH signals having the form of (2.69). Assuming that the STH signal of (2.69) is transmitted over a noiseless channel, the received signal corresponding to the transmitted signal X_k can be expressed as

$$r(t) = \sqrt{2P} P(t - iT_f - t_k T_c - X_k T_h - \tau_k) \cos(2\pi f_c t + \phi_i^{(k)}) \quad (2.74)$$

where τ_k represents the transmission delay, while $\phi_i^{(k)} = \varphi_i^{(k)} - 2\pi f_c \tau_k$.

The block diagram of a correlation receiver designed for detecting the STH signal of (2.74) is shown in Fig. 2.29, which employs noncoherent detection, hence requiring no knowledge of the carrier phases $\{\phi_i^{(k)}\}$. Assuming that the receiver has achieved synchronization for the received signal of (2.74), the receiver has the perfect knowledge of the transmission delay of τ_k . Furthermore, we assume that the receiver employs a TH pattern replica, which is generated by a local PN generator. Based on the knowledge of τ_k , the pulse-generator generates a time-domain pulse $P(t - iT_f - \tau_k)$ for the i th frame and the TH pattern generator outputs the corresponding TH pattern value or synonymously, the address code $\{t_k\}$,

as shown in Fig. 2.29. The TH pattern t_k provides a time shift of $t_k T_c$ seconds for the time-domain pulse $P(t - iT_f - \tau_k)$, which yields $P(t - iT_f - t_k T_c - \tau_k)$. As shown in Fig. 2.29, this time-domain pulse is input to M number of noncoherent correlators, after appropriately time-shifting or delaying them according to the M delay values of $0T_h$, $1T_h$, \dots , $(M-1)T_h$. In each of the M noncoherent correlators the appropriately delayed time-domain pulse is correlated with the down-converted receive signal, in order to obtain a decision variable. Specifically, for the m th correlator, where $m = 0, 1, \dots, M-1$, the appropriately delayed time-domain pulse input to the m th correlator of Fig. 2.29 is $P(t - iT_f - t_k T_c - mT_h - \tau_k)$. Hence, according to Fig. 2.29, the corresponding decision variable can be expressed as

$$\begin{aligned} Z_{km} = & \left[\int_{iT_f+t_k T_c+mT_h+\tau_k}^{iT_f+t_k T_c+(m+1)T_h+\tau_k} r(t) P(t - iT_f - t_k T_c - mT_h - \tau_k) \cos(2\pi f_c t) \right]^2 \\ & + \left[\int_{iT_f+t_k T_c+mT_h+\tau_k}^{iT_f+t_k T_c+(m+1)T_h+\tau_k} r(t) P(t - iT_f - t_k T_c - mT_h - \tau_k) \sin(2\pi f_c t) \right]^2 \end{aligned} \quad (2.75)$$

From Fig. 2.29, we can see that the M correlators are operated within different time-durations. Hence, it may be implemented in a way as shown in Fig. 2.30, where the two filters on the in-phase and quadrature branches match the transmitted time-domain pulse $P(t)$. The matched filter's outputs are sampled at a rate of $1/T_h$, which provide M decision variables $\{Z_{k0}, Z_{k1}, \dots, Z_{k(M-1)}\}$ per symbol for detection.

On substituting (2.74) into (2.75), it can be shown that, if $m \neq X_k$, which implies that there is no pulse with respect to the m th time slot, the t_k th chip and the i th frame, the noncoherent correlator outputs no energy, which can be expressed as

$$Z_{km} = 0, \quad \text{if } m \neq X_k \quad (2.76)$$

By contrast, if $m = X_k$, we have that

$$\begin{aligned} Z_{kX_k} = & \left[\int_{iT_f+t_k T_c+X_k T_h+\tau_k}^{iT_f+t_k T_c+(X_k+1)T_h+\tau_k} \sqrt{2P} P(t - iT_f - t_k T_c - X_k T_h - \tau_k) \right. \\ & \times \cos(2\pi f_c t + \phi_i^{(k)}) P(t - iT_f - t_k T_c - X_k T_h - \tau_k) \cos(2\pi f_c t) \Big]^2 \\ & + \left[\int_{iT_f+t_k T_c+X_k T_h+\tau_k}^{iT_f+t_k T_c+(X_k+1)T_h+\tau_k} \sqrt{2P} P(t - iT_f - t_k T_c - X_k T_h - \tau_k) \right. \\ & \times \cos(2\pi f_c t + \phi_i^{(k)}) P(t - iT_f - t_k T_c - X_k T_h - \tau_k) \sin(2\pi f_c t) \Big]^2 \\ = & \left[\sqrt{\frac{P}{2}} T_h \cos(\phi_i^{(k)}) \right]^2 + \left[-\sqrt{\frac{P}{2}} T_h \sin(\phi_i^{(k)}) \right]^2 \\ = & \frac{E_s}{2} T_h \end{aligned} \quad (2.77)$$

where $E_s = PT_h$ represents the transmitted energy per M -ary TH symbol.

According to (2.76) and (2.77) we know that the noncoherent correlator outputs zero, when it is not matched to the transmitted M -ary symbol X_k , while its output is $E_s T_h/2$, when

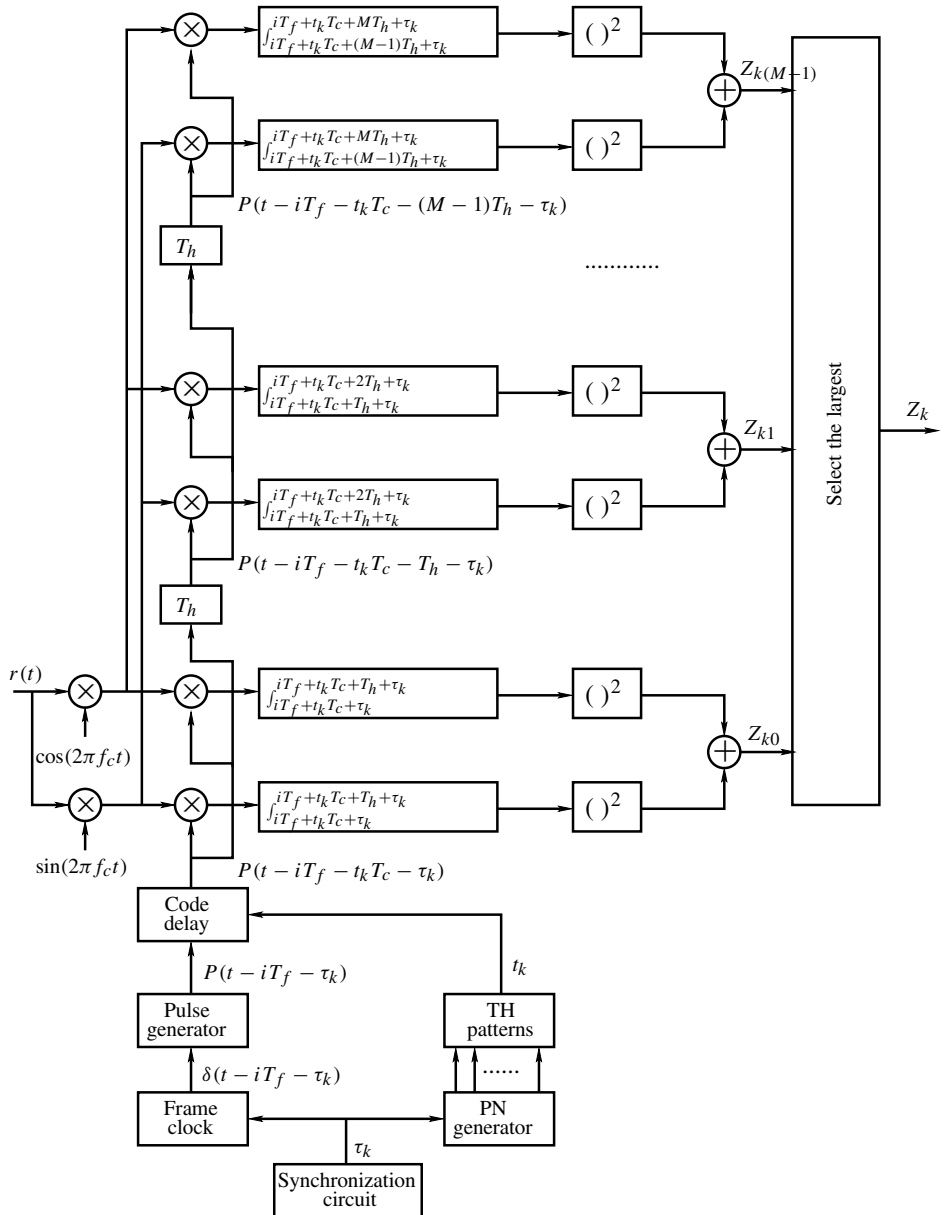


Figure 2.29: Receiver schematic block diagram for the slow time-hopping systems implemented by M number of correlators. The corresponding transmitter schematic was shown in Fig. 2.27.

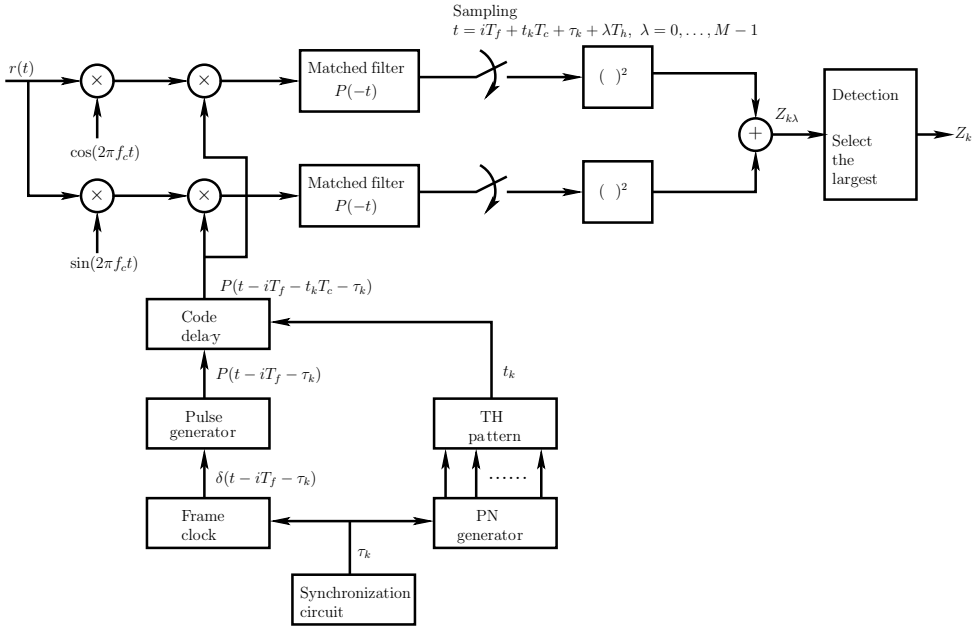


Figure 2.30: Alternative receiver schematic for the slow time-hopping systems implemented with matched filters.

it is matched to the transmitted M -ary symbol X_k . Therefore, as shown in Fig. 2.29, when the receiver obtains M number of decision variables $\{Z_{k0}, Z_{k1}, \dots, Z_{k(M-1)}\}$ in the context of a frame, the largest of the set $\{Z_{k0}, Z_{k1}, \dots, Z_{k(M-1)}\}$ is selected and mapped to an M -ary symbol representing the estimate to the transmitted symbol X_k .

According to the detection principle described above, the graphical example of Fig. 2.27(b) can now be extended further. The decision variables associated with the seven 8-ary symbols $\{3, 7, 5, 2, 6, 0, 7\}$ transmitted are expressed in the form of Fig. 2.31. Without the contaminating effects of noise, as shown in Fig. 2.31, for each symbol interval, we have only one non-zero decision variable corresponding to the transmitted 8-ary symbol. In the more realistic noise-contaminated scenario we select the largest one as the most likely transmitted symbol from the set of eight decision variables $\{Z_{k0}, Z_{k1}, \dots, Z_{k7}\}$. Hence, all the seven transmitted symbols are correctly detected.

2.4.4 Detection of Fast Time-Hopping Signals

For the FTH scheme of Fig. 2.28 we have the transmitted signal expression of (2.71), while the corresponding received signal can be expressed as

$$r(t) = \sqrt{2P} \sum_{l=0}^{L-1} P[t - (i+l)T_f - y_k(l)T_h - \tau_k] \cos(2\pi f_c t + \phi_i^{(k)}) \quad (2.78)$$

when communicating over a noiseless channel, where τ_k represents the transmission delay, while $\phi_i^{(k)} = \varphi_i^{(k)} - 2\pi f_c \tau_k$.

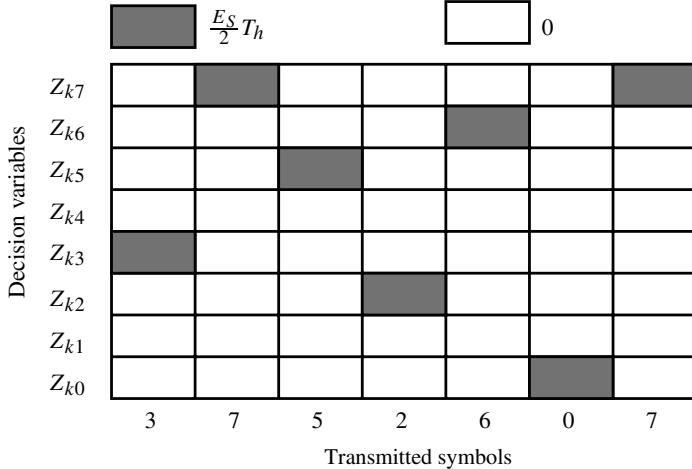


Figure 2.31: Graphical representation of the decision variables corresponding to the detection of the transmitted STH signals portrayed in Fig. 2.27(b).

The corresponding receiver schematic designed for the demodulation of the FTH signals of (2.78) is shown in Fig. 2.32(a), which essentially follows the inverse structure of the transmitter of Fig. 2.28(a). Note that in Fig. 2.32(a) the noncoherent correlators are the same as those seen in Fig. 2.29, which detect the energy associated with each of the Q time slots. As shown in the receiver block diagram, for each frame of l , $l = 0, 1, 2, \dots, L - 1$ with respect to the L number of frames of the transmitted symbol, the received signal is input to a bank of Q number of energy detectors matched to the Q time slots of a frame. The detection interval duration is the same as the time-slot interval of T_h seconds, which is synchronized with the time slot. Since there are L frames within a symbol interval duration of T_s seconds, the Q number of energy detectors provide a total of QL outputs during a symbol period of T_s seconds. As shown in Fig. 2.32(a), the QL number of time slots corresponding to each symbol-duration of T_s seconds are analysed in order to determine which of the time slots are activated for the transmission of the b -bit symbol X_k by invoking the unique TH address of the desired user.

As for the type of FFH spread-spectrum system described in Section 2.3.4, after the energy detection stage of Fig. 2.32 carried out during the L consecutive frames, the signalling sequence \mathbf{Y}_k of (2.70) conveying the symbol X_k can be recovered by the receiver. By performing modulo- Q subtraction of the unique user address code \mathbf{t}_k of the k th user (desired user) from \mathbf{Y}_k on a frame-by-frame basis, we arrive at

$$X_k \cdot \mathbf{1} = \mathbf{Y}_k \ominus \mathbf{t}_k \quad (2.79)$$

which allows us to recover the transmitted symbol X_k of user k .

The detection operations associated with the unique user address code of the FTH system can be illustrated by means of time-time matrices having Q rows and L columns of the type seen in Fig. 2.32(b). These time-time matrices can be viewed as analogous to the time-frequency matrices used in Section 2.3.4 for FFH systems. In the time-time matrices exemplified in Fig. 2.32(b) the Q rows correspond to the Q distinct time slots of

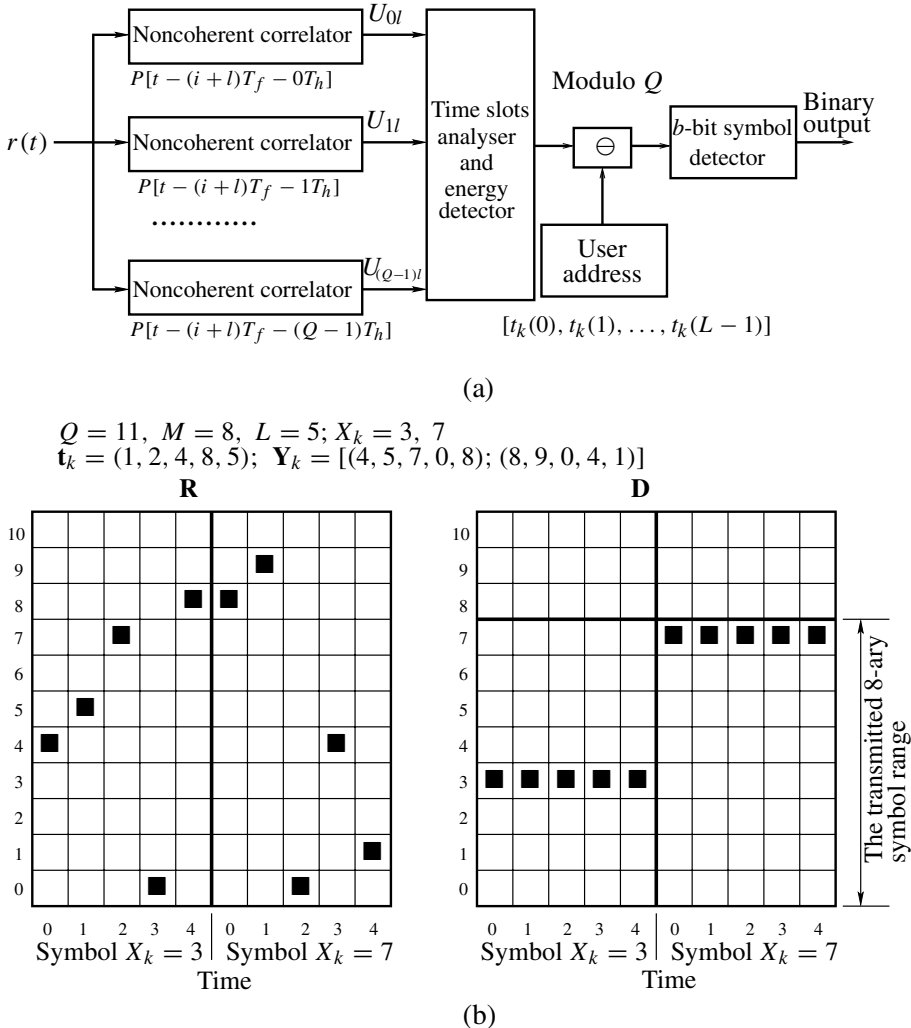


Figure 2.32: (a) Receiver block diagram designed for detecting the FTH spread-spectrum signals expressed in the form of (2.71); (b) detection example for FTH signals. The $Q = 11$ rows indicate the $Q = 11$ time-slots per frame, and the first $L = 5$ columns in \mathbf{R} and \mathbf{D} correspond to the five frames of the transmitted symbol $X_k = 3$, while the remaining $L = 5$ five columns of \mathbf{R} and \mathbf{D} correspond to the five frames used for signalling the transmitted symbol $X_k = 7$. For example, for $\mathbf{Y}_k = [4, 5, 7, 0, 8]$ corresponding to the transmitted symbol of $X_k = 3$ and to the TH address code of $\mathbf{t}_k = (1, 2, 4, 8, 5)$, from (2.79) we have that $X_k \cdot \mathbf{1} = (3, 3, 3, -8, 3) = (3, 3, 3, -8 + 11, 3) = (3, 3, 3, 3, 3)$ as shown in the matrix \mathbf{D} . Observe that \mathbf{D} has a unique complete row having the row-index value in the 8-ary symbol range of $[0, 7]$, which yields a unanimous symbol decision of 3. Therefore, $X_k = 3$. The transmitted symbol $X_k = 7$ can be detected similarly.

a frame used for conveying a fraction of an M -ary symbol X_k of the k th user, while the L columns represent the L number of frames within a symbol duration. The elements of the time-time matrices exemplified in Fig. 2.32(b) can be referred to as time-time elements. In Fig. 2.32(b) \mathbf{R} represents the received time-time matrix of a FTH system employing 8-ary pulse position modulation (PPM) and using $Q = 11$ time slots per frame. Provided that neither noise nor fading is present, all elements of the received time-time matrix can be correctly detected, with the aid of a threshold-based scheme. Specifically, if a decision variable of $\{Z_{k0}, Z_{k1}, \dots, Z_{k(Q-1)}\}$, which corresponds to a particular time-time element of the time-time matrix, exceeds the threshold of $h > 0$, the corresponding time-time element of the received time-time matrix is flagged by a marker (or logical 1), otherwise by a space (or logical 0).

According to the transmitted FTH signals represented by Fig. 2.28(b), the time-time matrices corresponding to the two transmitted 8-ary symbols of $X_k = 3, 7$ are shown in Fig. 2.32(b). As seen in the matrix \mathbf{R} of Fig. 2.32(b), the signals marked as *black-squares* are present at the time-time elements corresponding to user k . Specifically, the time slots $(4, 5, 7, 0, 8)$ and $(8, 9, 0, 4, 1)$ are activated, which convey the 8-ary PPM symbols $X_k = 3$ and $X_k = 7$, as will be shown. Since the unique TH address assigned to user k is $t_k = (1, 2, 4, 8, 5)$, for the matrix \mathbf{R} associated with the activated time slots $(4, 5, 7, 0, 8)$, the resultant time-time matrix \mathbf{D} obtained by modulo-11 subtraction of the unique user code address \mathbf{t}_k from \mathbf{Y}_k according to (2.79) is shown in Fig. 2.32(b). Let us employ a simple majority logic decision-based decoder, which opts for deciding in favour of the particular 8-ary symbol corresponding to the specific row having the highest number of non-zero entries, for the sake of providing an estimate of the transmitted symbol X_k of user k . Hence, based on the time-time matrix \mathbf{D} of Fig. 2.32(b), we infer that the transmitted symbol $X_k = 3$ has been correctly decoded with the aid of the majority logic decision. This is because according to $\mathbf{Y}_k = (4, 5, 7, 0, 8)$ and $t_k = (1, 2, 4, 8, 5)$ we have that

$$\begin{aligned} X_k \cdot \mathbf{1} &= \mathbf{Y}_k \ominus \mathbf{t}_k \\ &= (4, 5, 7, 0, 8) \ominus (1, 2, 4, 8, 5) \\ &= (3, 3, 3, -8, 3) \\ &= (3, 3, 3, -8 + 11, 3) \\ &= (3, 3, 3, 3, 3) \end{aligned} \tag{2.80}$$

Therefore, we confirm that the transmitted symbol was $X_k = 3$. By using a similar approach to that invoked for detecting the symbol $X_k = 3$, it is readily seen that the second symbol of $X_k = 7$ can also be correctly detected.

2.4.5 Time-Hopping Multiple-Access

Having introduced the rudimentary principles of TH spread-spectrum communications, let us now demonstrate how multiple users may access a common channel using a TH scheme.

In TH-aided spread-spectrum communications each user's time-hopping operation is controlled using a PN sequence. This operation is analogous to the frequency-hopping procedure controlled by a PN sequence in FH communications. Hence, supporting multiple users in TH multiple-access systems can be achieved by assigning each of the users sharing the same physical channel a unique PN sequence, resulting in a unique TH pattern. Similarly

to the multiple-access principles discussed in this chapter in the context of DS-CDMA, MC-CDMA and FHMA, where users are distinguished by their unique user-specific signature PN sequences, in TH multiple-access (THMA) users can also be distinguished at the receiver with the aid of their unique TH patterns, provided that the correlation between any two of them is sufficiently low. Below, a simple illustrative example associated with supporting two TH users is considered, in order to introduce the principles of THMA communications.

2.4.5.1 Slow Time-Hopping Multiple-Access

First, let us consider the STH multiple-access (STHMA) scheme using the transmitter block diagram of Fig. 2.27 and the receiver block diagram of Fig. 2.29. Assuming that the two users transmit their STH signals in the form of (2.69) synchronously over a perfect noiseless channel, the received signal can be expressed as

$$\begin{aligned} r(t) = & \sqrt{2P} \sum_{i=-\infty}^{\infty} P(t - iT_f - t_1(i)T_c - X_1(i)T_h) \cos(2\pi f_c t + \phi_i^{(1)}) \\ & + \sqrt{2P} \sum_{j=-\infty}^{\infty} P(t - jT_f - t_2(j)T_c - X_2(j)T_h) \cos(2\pi f_c t + \phi_j^{(2)}) \end{aligned} \quad (2.81)$$

where we assumed that the transmission delays $\tau_1 = \tau_2 = 0$, as a consequence of using synchronous transmission. Furthermore, $\phi_i^{(1)}$ and $\phi_j^{(2)}$ represent the carrier phase angles associated with the received signals of the two users, respectively. Furthermore, in (2.81) $t_1(i)$ and $X_1(i)$ represent the TH pattern and the M -ary symbol transmitted, associated with the i th frame of user 1, respectively, while $t_2(j)$ and $X_2(j)$ represent the TH pattern and the M -ary symbol, associated with the j th frame of user 2, respectively.

Let us assume that the receiver's objective is to demodulate the first user's signal. The receiver has to exploit the knowledge of the TH pattern $\{t_1\}$ and the corresponding frame timing iT_f of the first user. Then, according to the STH demodulation principle described by Fig. 2.29, we arrive at the decision variable

$$\begin{aligned} Z_{1m} = & \left[\int_{iT_f+t_1(i)T_c+mT_h}^{iT_f+t_1(i)T_c+(m+1)T_h} r(t) P(t - iT_f - t_1 T_c - m T_h) \cos(2\pi f_c t) dt \right]^2 \\ & + \left[\int_{iT_f+t_1(i)T_c+mT_h}^{iT_f+t_1(i)T_c+(m+1)T_h} r(t) P(t - iT_f - t_1 T_c - m T_h) \sin(2\pi f_c t) dt \right]^2 \end{aligned} \quad (2.82)$$

where $m = 0, 1, \dots, M - 1$ corresponding to the M number of decision variables related to the MPPM scheme. Notice that in equation (2.82) the correlation window's width is the same as the time-slot interval duration, namely T_h second, and for the m th decision variable of user 1 the correlation window falls in the range $[iT_f + t_1(i)T_c + mT_h, iT_f + t_1(i)T_c + (m + 1)T_h]$. Then, according to (2.82), (2.76) and (2.77), we can see that the m th noncoherent correlator outputs non-zero energy, if and only if there is a pulse in the form of $P(t)$, which appears in the correlation window of $[iT_f + t_1(i)T_c + mT_h, iT_f + t_1(i)T_c + (m + 1)T_h]$. Therefore, upon substituting (2.81) into (2.82) and following the derivation of (2.76) and (2.77), the value of the m th noncoherent correlator output corresponds to one of the following three cases.

Case 1: Both the first and second users' transmitted signals reside outside the correlation window. In this case the m th noncoherent correlator outputs zero, i.e. we have that

$$Z_{1m} = 0, \quad m \in \{0, 1, \dots, M - 1\} \quad (2.83)$$

Case 2: Either the first user's signal or the second user's signal is within the correlation window. In this case, as seen in (2.77), the m th noncoherent correlator output can be expressed as

$$Z_{1m} = \frac{E_s}{2} T_h, \quad m \in \{0, 1, \dots, M - 1\} \quad (2.84)$$

Case 3: Both the first and second users' transmitted signals are within the correlation window. In this case, following the derivation of (2.77), the m th noncoherent correlator output may be expressed as

$$\begin{aligned} Z_{1m} = & \left[\sqrt{\frac{P}{2}} T_h \cos(\phi_i^{(1)}) + \sqrt{\frac{P}{2}} T_h \cos(\phi_j^{(2)}) \right]^2 \\ & + \left[-\sqrt{\frac{P}{2}} T_h \sin(\phi_i^{(1)}) - \sqrt{\frac{P}{2}} T_h \sin(\phi_j^{(2)}) \right]^2 \end{aligned} \quad (2.85)$$

If both $\phi_i^{(1)}$ and $\phi_j^{(2)}$ are assumed to be random variables uniformly distributed in the range $[0, 2\pi]$, the average output of the m th noncoherent correlator can be expressed as

$$Z_{1m} = E_s T_h, \quad m \in \{0, 1, \dots, M - 1\} \quad (2.86)$$

According to the above three cases, in the context of the M number of decision variables evaluated for detecting the first user's transmitted symbol, we find that the decision corresponds to one of the following two cases.

Case 1: There is a single noncoherent correlator that outputs non-zero energy, while the other $(M - 1)$ noncoherent correlators output zero energy. This is encountered, when only the first user's signal appears in one of the M time slots, or when both users' signals appear in the same one from the set of the M time slots. Explicitly, this case results in a correct decision for the symbols transmitted by the first user.

Case 2: There exist two noncoherent correlators that output non-zero energy, while the remaining $(M - 2)$ noncoherent correlators output zero energy. This is the case, when two user signals appear in two different time slots of the M time slots considered. In this case, the first user's transmitted symbol may be detected in error by incorrectly selecting the decision variable as a consequence of the presence of the second user.

When two users transmit during the same chip interval of T_c seconds, as shown in Fig. 2.33, we refer to this phenomenon as a *hit*. As discussed above, not all occurrences of a hit result in erroneous detection. Specifically, a hit occurring as a consequence of two users' signals appearing in the same time slot in fact results in a correct decision. By contrast, the second type of hit encountered due to two user signals appearing in two different time slots of a chip duration, when only a single energized time slot is expected, may result in an incorrect detection.

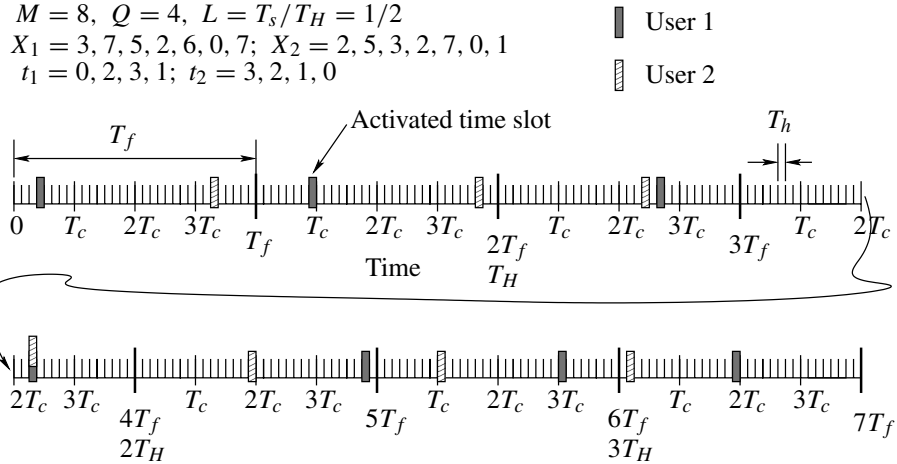


Figure 2.33: Graphical representation of two users' STH signals in the form of (2.69). The corresponding single-user example was displayed in Fig. 2.27, where user 1 transmitted the same information using the same TH sequence.

The above THMA principle can be further understood with the aid of the following example, where the two users' transmitted STH signals generated during seven consecutive frames are represented in Fig. 2.33. In addition to the common parameters of $M = 8$, $Q = 11$, $L = 1/2$, the TH pattern of user 1 is $t_1 \in \{0, 2, 3, 1\}$, while that of user 2 is $t_2 \in \{3, 2, 1, 0\}$. The 8-ary transmitted symbol is $X_1 = 3, 7, 5, 2, 6, 0, 7$ for user 1 and $X_2 = 2, 5, 3, 2, 7, 0, 1$ for user 2. Observe in Fig. 2.33 that within the third and the fourth frames the two user signals' activated chips coincide with each other; i.e. they encounter a hit, since in these frames both of their TH patterns have $t_1 = t_2 = 2$. The difference between the third and the fourth frames, however, is that, by coincidence, in the third frame the transmitted symbols of the two users are $X_1 = 5$ and $X_2 = 3$, which appear in the same chip but occupy different time slots. By contrast, in the fourth frame the transmitted symbols of both users are $X_1 = 2$ and $X_2 = 2$, which appear in the same chip and active the same time slot.

After time dehopping using the two users' TH addresses, the noncoherent correlator's output decision variables associated with user 1 and user 2 are shown in Fig. 2.34. Explicitly, except for the third symbol, the symbols of both users can be correctly detected, since in the context of each symbol there is only one noncoherent correlator having a non-zero output. However, as for the third symbol, since we have a non-zero output for both users, making a decision based on selecting the largest of the correlator outputs may result in an erroneous decision.

2.4.5.2 Fast Time-Hopping Multiple-Access

We have discussed the principle of THMA, when using slow time-hopping (STH). We now turn our attention to the THMA principle using fast time-hopping (FTH) and invoking the transmitter of Fig. 2.28. The FTH signals can be detected in a fashion analogous to the detection of FFH signals, as discussed in Section 2.3.4. Specifically, in the FFH scheme of

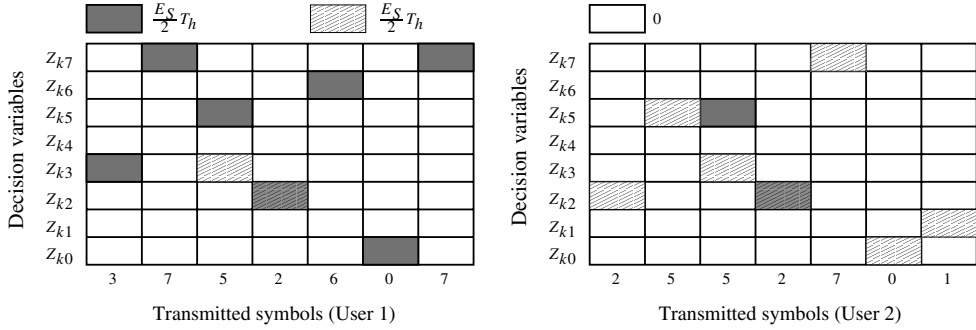


Figure 2.34: Graphical representation of the decision variables of users 1 and 2 corresponding to the detection of the transmitted STH signals graphically shown in Fig. 2.33.

Section 2.3.4 the detection process is based on time-frequency matrices, while in the FTH arrangement the detection procedure relies on time-time matrices. These two types of matrix have the same structure. Furthermore, the detection philosophy of FFH and FTH is identical, when ignoring their time-frequency and time-time dependence. The principle of THMA using fast time-hopping is also analogous to that used in fast frequency-hopping assisted FHMA, which was outlined in Section 2.3.5.2. Below, we use an example for addressing the philosophy of fast time-hopping assisted THMA.

We will extend the single-user FTH example of Fig. 2.28 to a multiuser scenario. Explicitly, Fig. 2.35 represents the received time-time matrix, when there are two users who communicate employing the FTH scheme. The TH address code of user 1 is $\mathbf{t}_1 = [1, 2, 4, 8, 5]$, while that of user 2 is $\mathbf{t}_2 = [5, 10, 9, 7, 3]$. The transmitted 8-ary symbols of user 1 are $X_1 = 3, 7$, while those of user 2 are $X_2 = 5, 3$, where each symbol is transmitted by five consecutive frames, i.e. $L = 5$. Furthermore, the number of time slots per frame is $Q = 11$. Consequently, according to (2.70), $\mathbf{Y}_1 = [3, 3, 3, 3, 3] \oplus [1, 2, 4, 8, 5] = [4, 5, 7, 0, 8]$ for symbol $X_1 = 3$ and $\mathbf{Y}_1 = [7, 7, 7, 7, 7] \oplus [1, 2, 4, 8, 5] = [8, 9, 0, 4, 1]$ for $X_1 = 7$. Similarly, $\mathbf{Y}_2 = [10, 4, 3, 1, 8]$ for $X_2 = 5$ and $\mathbf{Y}_2 = [8, 2, 1, 10, 6]$ for $X_2 = 3$, respectively. In response to \mathbf{Y}_1 and \mathbf{Y}_2 having the above values, in the received time-time matrix of Fig. 2.35 the corresponding elements are marked as \blacksquare for user 1 and \star for user 2 for illustration purposes only. In fact, the receiver does not know whether a marker is due to user 1 or to user 2, or furthermore, to the background noise.

Following the detection principles of THMA using FTH, described previously in Section 2.4.3, the resultant time-time matrix \mathbf{D}_1 of user 1 is obtained after subtracting its TH address \mathbf{t}_1 from the received time-time matrix of \mathbf{R} . Similarly, \mathbf{D}_2 of user 2 is generated after subtracting its TH address \mathbf{t}_2 from the received time-time matrix of \mathbf{R} . As shown in Fig. 2.35(b), in the matrix \mathbf{D}_1 there are full rows, representing the transmitted symbols of $X_1 = 3$ and 7, while in \mathbf{D}_2 there are complete rows corresponding to the transmitted symbols of $X_2 = 5$ and 3. The other marked elements in \mathbf{D}_1 and \mathbf{D}_2 represent the interference inflicted by the interfering user 2 or user 1, respectively. However, there are no extra full rows, which would result in erroneous decisions, in addition to the above-mentioned complete rows.

$$Q = 11, M = 8, L = 5; X_1 = 3, 7; X_2 = 5, 3$$

$$\mathbf{t}_1 = (1, 2, 4, 8, 5); \mathbf{Y}_1 = [(4, 5, 7, 0, 8); (8, 9, 0, 4, 1)]$$

$$\mathbf{t}_2 = (5, 10, 9, 7, 3); \mathbf{Y}_2 = [(10, 4, 3, 1, 8); (8, 2, 1, 10, 6)]$$

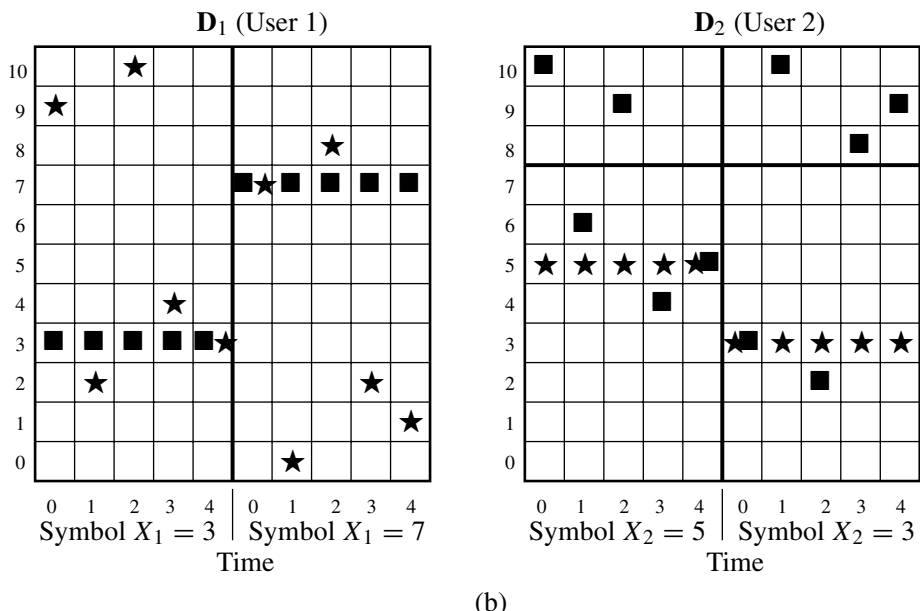
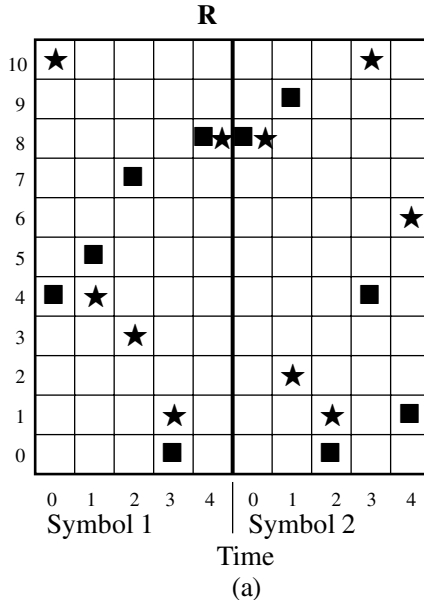


Figure 2.35: Detection example of FTH signals, where $\mathbf{D}_1 = \mathbf{R} \ominus \mathbf{t}_1$, while $\mathbf{D}_2 = \mathbf{R} \ominus \mathbf{t}_2$. (a) Graphical representation of the received FTH spread-spectrum multiple-access signals of two users; (b) the detection of FTH spread-spectrum signals. The corresponding single user FTH example was shown in Fig. 2.28.

In summary, in FTH-assisted THMA systems multiple-access communications can be supported by assigning unique user-specific TH address codes to different users.

In the last four sections of this chapter, four basic spread-spectrum communication schemes, namely DS-, multicarrier- (MC), FH- and TH-arrangements, have been discussed. One of the common characteristics of these spread-spectrum schemes is that the transmitted data rate is usually significantly lower than the system bandwidth, which justifies the terminology, *spread-spectrum communications*. Specifically, in DS spread-spectrum communications spectral spreading is achieved by using high-chip-rate DS spreading sequences. In MC spread-spectrum communications spectral spreading is carried out with the aid of a high number of narrow-band subcarriers. In FH spread-spectrum communications the system bandwidth available is divided into a number of sub-bands, which carry the transmitted signals. The transmitted signals occupy the entire system bandwidth by hopping to different sub-bands under the control of PN sequences. Analogously to the philosophy of TH schemes, FH spread-spectrum systems using frequency-shift keying (FSK) may also be referred to as FH schemes using ‘frequency-domain pulse-position modulation’. Finally, in TH spread-spectrum communications spectral spreading is achieved by transmitting narrow time-domain pulses. Analogously to the approach of FH schemes, TH spread-spectrum systems using PPM may be termed as TH schemes using *time-shift keying* (TSK) modulation.

Each of the above-mentioned four spread-spectrum schemes achieves spectral spreading using a different signalling model, or in other words, the transmitted spread-spectrum signal of each scheme exhibits different characteristics. Hence, as expected, each spread-spectrum scheme has different advantages and disadvantages, depending on the application environments concerned. However, in practice we may expect a spread-spectrum communication system that employs advantages of several spread-spectrum schemes and, simultaneously, overcomes their disadvantages, in order that the spread-spectrum system exhibits a high versatility. This type of high-versatility spread-spectrum system can be implemented by using hybrid spread-spectrum schemes that combine two or more of the four basic spread-spectrum schemes. Therefore, in the remaining sections of this chapter, hybrid spread-spectrum schemes will be discussed. Note that, as shown in Fig. 2.36, based on basic spread-spectrum schemes, such as the *direct-sequence (DS)*, *frequency-hopping (FH)* and *time-hopping (TH)* arrangements, various hybrid spread-spectrum schemes may be designed depended on the practical applications. Specifically, in the following two sections two hybrid spread-spectrum schemes, namely hybrid DS/FH and hybrid DS/TH, will be discussed, which are formed by combining the DS scheme with the FH and TH schemes, respectively. Let us first consider the DS/FH spread-spectrum scheme in more detail.

2.5 Hybrid Direct-Sequence/Frequency-Hopping Multiple-Access

In Section 2.3 we argued that there exist two fundamental types of FH scheme, namely slow FH (SFH) and fast FH (FFH). Correspondingly, we can design hybrid DS/SFH and hybrid DS/FFH spread-spectrum schemes. Let us first consider the hybrid DS/SFH spread-spectrum scheme.

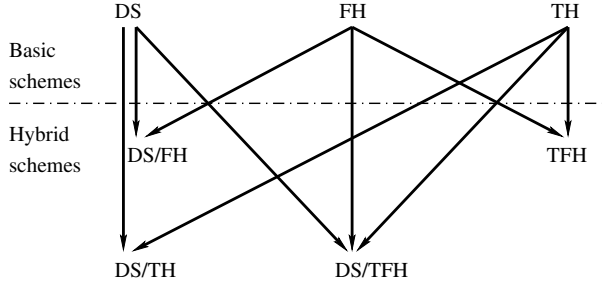


Figure 2.36: Illustration of the family of hybrid spread-spectrum schemes derived from the basic spread-spectrum schemes of direct-sequence (DS), frequency-hopping (FH) and time-hopping (TH).

2.5.1 Hybrid DS/SFH Signals

2.5.1.1 DS/SFH Using BPSK Modulation

In SFH a number of symbols are transmitted within an FH interval and accurate carrier phase estimation is possible at the receiver, in order to achieve coherent demodulation. Hence, below, a DS/SFH scheme using BPSK data modulation is addressed, in order to demonstrate the principles of DS/SFH spread-spectrum communications.

The k th user's transmitter schematic applicable to DS/SFH communication systems is shown in Fig. 2.37. Explicitly, the transmitter of DS/SFH is constituted by two main components: a DS spreader and a frequency hopper, where the DS spreader is similar to that seen in Fig. 2.3 of Section 2.1.1, while the frequency hopper is similar to that portrayed in Fig. 2.15 of Section 2.3.2.

In Fig. 2.37 the data signal $b_k(t)$ of the k th user is constituted by a sequence of rectangular pulses of duration T_b . The data signal $b_k(t)$ can be expressed as $b_k(t) = \sum_{n=-\infty}^{\infty} b_k[n]P_{T_b}(t - nT_b)$, where $b_k[n] \in \{+1, -1\}$ and $P_{T_b}(t)$ represents the rectangular pulse of duration T_b . This data signal is spread by a PN sequence waveform given by $c_k(t) = \sum_{n=-\infty}^{\infty} c_k[n]\psi_{T_c}(t - nT_c)$, which is assigned to the k th user, where $c_k[n]$ assumes values of +1 or -1, while $\psi_{T_c}(t)$ is the chip waveform defined by (2.8). We assume that there are N chips within each data bit duration, i.e. we assume that $T_b = NT_c$. The output of the DS-spreader is given by

$$d_k(t) = b_k(t)c_k(t) \quad (2.87)$$

As shown in Fig. 2.37, in DS/SFH systems the DS spread-spectrum signal $d_k(t)$ is further frequency-hopped to a set of legitimate carriers according to the k th user's hopping pattern $f_k(t)$, which is derived from a sequence $(f_j^{(k)})$ of frequencies originating from a set $\mathbf{F} = \{f_1, f_2, \dots, f_q\}$ of $q \geq 1$ frequencies. It is usually assumed that $f_1 < f_2 < \dots < f_q$. The FH pattern follows the sequence of $f_k(t) = f_j^{(k)}$ for $jT_h \leq t < (j+1)T_h$, where T_h represents the FH dwell time at a given carrier frequency. Hence, $N_b = T_h/T_b > 1$ represents the number of data bits transmitted per hop. As shown in Fig. 2.37, the transmitted DS/SFH signal can be expressed as

$$s_k(t) = \sqrt{2P}b_k(t)c_k(t)\cos\{2\pi[f_c + f_k(t)]t + \varphi_k + \alpha_k(t)\} \quad (2.88)$$

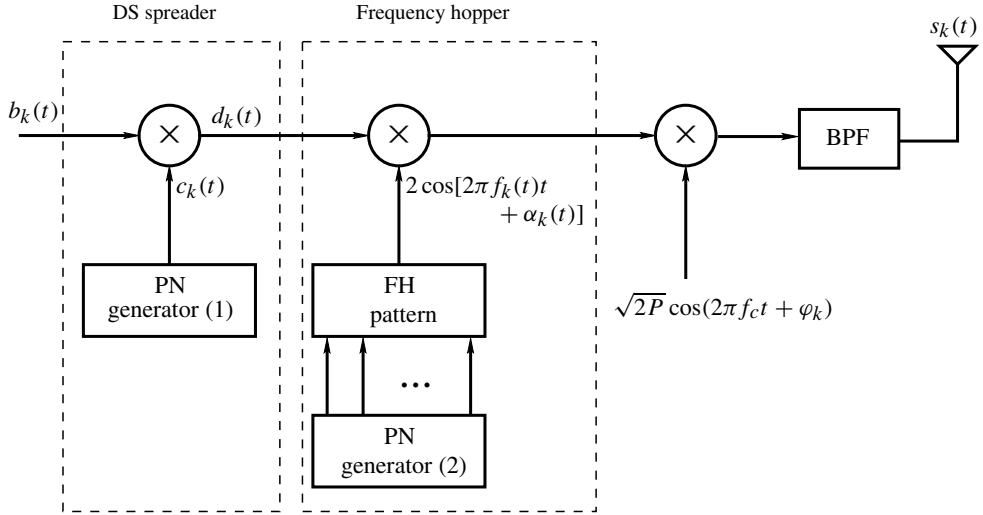


Figure 2.37: The k th user's transmitter schematic in DS/SFH using BPSK modulation.

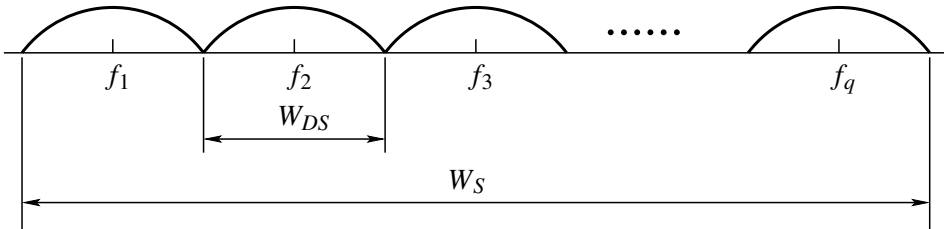


Figure 2.38: Stylized illustration of the PSD of DS/SFH spread-spectrum signals expressed in the form of (2.88).

where P represents the transmitted power, f_c is the carrier frequency and φ_k is the phase angle introduced by the carrier modulation. Furthermore, in (2.88) $\alpha_k(t)$ represents the phase waveform introduced by the frequency hopper of user k , which assumes the constant value $\alpha_j^{(k)}$ during the j th frequency hopping dwell time of $jT_h \leq t < (j+1)T_h$.

The stylized power spectral density of the DS/SFH signal of (2.88) is shown in Fig. 2.38, where we assumed that the spectra of the DS signal associated with different FH frequencies do not overlap. Fig. 2.38 shows that the bandwidth W_s of the DS/SFH signal is divided into q number of sub-bands, each having a bandwidth of W_{DS} , and each DS spread signal has a bandwidth of W_{DS} Hz.

2.5.1.2 Detection of BPSK Modulated DS/SFH Signals

For the sake of outlining the corresponding detection principle, we consider a synchronous DS/SFH system, where perfect synchronization is assumed at both the FH stage concerning

the perfect alignment of the FH patterns and at the chip level of the DS spreading sequences. Assuming that $K \geq 1$ synchronous DS/SFH signals obeying (2.88) are transmitted over a nonfading and noiseless perfect channel, the received signal can be expressed as

$$r(t) = \sum_{k=1}^K s_k(t) = \sum_{k=1}^K \sqrt{2P} b_k(t) c_k(t) \cos\{2\pi[f_c + f_k(t)]t + \beta_k(t)\} \quad (2.89)$$

where we assumed that the carrier phase angle φ_k in (2.88) has been absorbed by the phase angle $\beta_k(t)$, and hence $\beta_k(t)$ includes both $\alpha_k(t)$ and φ_k of (2.88).

Let us assume that the first user's signal is the desired signal that has to be detected. The receiver schematic of the first user is shown in Fig. 2.39. The effect of the carrier f_c involved in the received signal $r(t)$ is first removed, in order to translate the received signal spectrum to the intermediate frequency (IF) band corresponding to the FH pattern used. As shown in Fig. 2.39, the carrier-frequency down-converter stage is followed by a frequency-dehopper controlled by the FH pattern of the desired signal. This stage establishes perfect FH pattern synchronization and introduces a phase waveform $\beta_1(t)$ analogous to that in (2.89) for the sake of achieving coherent demodulation. The phase waveform $\beta_1(t)$ assumes a constant value of $\beta_j^{(1)}$ for $jT_h \leq t < (j+1)T_h$. The frequency-dehopper is followed by a low-pass filter (LPF), which only allows the baseband DS spread-spectrum signals to pass, and thus it removes the unwanted upper-harmonic demodulation products. The output of the LPF can be expressed as

$$\begin{aligned} r_d(t) &= r(t) \cos\{2\pi[f_c + f_1(t)]t + \beta_1(t)\} \\ &= \sqrt{\frac{P}{2}} b_1(t) c_1(t) + \sum_{k=2}^K \sqrt{\frac{P}{2}} b_k(t) c_k(t) \delta[f_k(t), f_1(t)] \cos[\phi_k(t)] \end{aligned} \quad (2.90)$$

where we have $\phi_k(t) = \beta_k(t) - \beta_1(t)$ and the function $\delta[x, y]$ is defined by $\delta[x, y] = 0$ for $x \neq y$ and $\delta[x, x] = 1$. The function $\delta[f_k(t), f_1(t)]$ in (2.90) implies that user k imposes interference on the desired user, when user k uses the same FH frequency as the desired user, i.e. when $\delta[f_k(t), f_1(t)] = 1$. Explicitly, interference imposed by the interfering users, namely the multiuser interference, is inflicted only by those users who activate the same FH frequency as the desired user. Hence, at different time instants the number of interfering users may be different. The number of interfering users within a given FH dwell-time interval is a random variable distributed over the interval of $[0, K - 1]$. Whenever $\delta[f_i(t), f_j(t)] = 1$ during a FH dwell-time interval, i.e. whenever user i and user j activate the same FH frequency, this event is referred to as a *hit*.

Let us consider the detection of the first bit transmitted by the desired user within $[0, T_b]$. As shown in Fig. 2.39, the frequency-dehopper is followed by a DS-despreader. We assume that the DS-despreader is capable of acquiring⁴ the DS spreading sequence of the desired user, which is expressed as $c_1(t)$ in Fig. 2.39. Then, the decision variable required for detecting $b_1[0]$ can be expressed as

$$Z_1 = \int_0^{T_b} r_d(t) c_1(t) dt \quad (2.91)$$

⁴The acquisition of a PN sequence is defined as the process of aligning the locally generated PN sequence of a user with the received PN sequence with a certain tolerance. Once this initial PN sequence acquisition has been achieved, a PN code-tracking process is then used for maintaining accurate PN sequence synchronization.

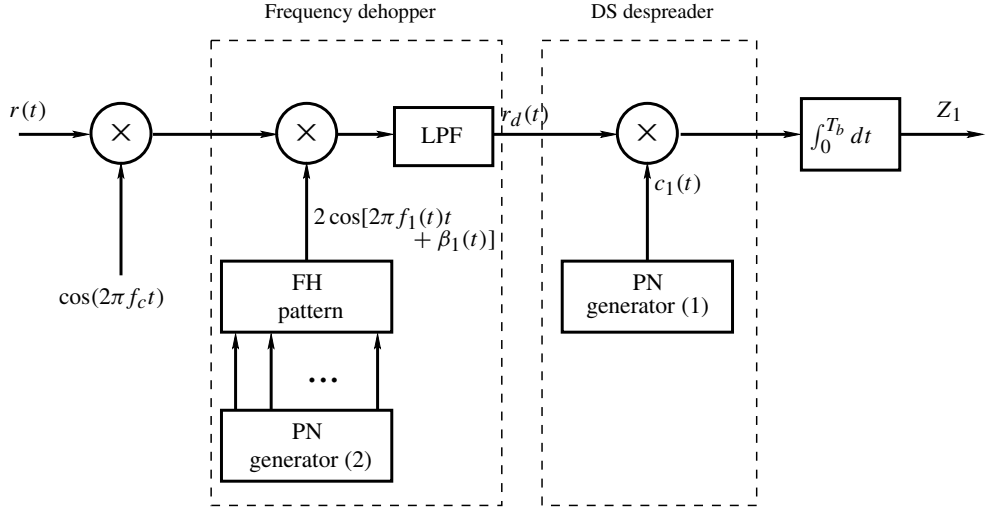


Figure 2.39: Receiver block diagram for an DS/SFH spread-spectrum system.

On substituting (2.90) into (2.91), it can be shown that the decision variable Z_1 of user 1 can be expressed as

$$Z_1 = \sqrt{\frac{P}{2}} T_b b_1[0] + \sum_{k=2}^K \sqrt{\frac{P}{2}} b_k[0] \delta[f_k(t), f_1(t)] \cos(\phi_k) \int_0^{T_b} c_k(t) c_1(t) dt \quad (2.92)$$

where ϕ_k replaces $\phi_k(t)$ of (2.90), indicating that $\phi_k(t)$ is independent of time, since both $\beta_k(t)$ and $\beta_1(t)$ in $\phi_k(t) = \beta_k(t) - \beta_1(t)$ are constants within the data bit detection interval of $[0, T_b]$. Let

$$\rho_{k1} = \frac{1}{T_b} \int_0^{T_b} c_k(t) c_1(t) dt \quad (2.93)$$

represent the cross-correlation between the k th user's and the first user's spreading sequence waveforms. Then, (2.92) can be written as

$$Z_1 = \sqrt{\frac{P}{2}} T_b b_1[0] + \sum_{k=2}^K \sqrt{\frac{P}{2}} T_b b_k[0] \delta[f_k(t), f_1(t)] \cos(\phi_k) \rho_{k1} \quad (2.94)$$

where equation (2.94) shows that when the absolute value of the multiuser interference is lower than $\sqrt{P/2}T_b$, i.e. when

$$\sqrt{\frac{P}{2}} T_b > \left| \sum_{k=2}^K \sqrt{\frac{P}{2}} T_b b_k[0] \delta[f_k(t), f_1(t)] \cos(\phi_k) \rho_{k1} \right| \quad (2.95)$$

or when

$$\left| \sum_{k=2}^K b_k[0] \delta[f_k(t), f_1(t)] \cos(\phi_k) \rho_{k1} \right| < 1 \quad (2.96)$$

then the decision variable Z_1 will always have the same sign as that of $b_1[0]$. Hence, the estimate of the transmitted bit can be decided upon taking the sign of Z_1 , which is expressed as $\hat{b}_1[0] = \text{sgn}(Z_1)$, where $\text{sgn}(x)$ represents a sign function defined by $\text{sgn}(x) = +1$ for $x > 0$ and $\text{sgn}(x) = -1$ for $x \leq 0$.

It may be readily shown that when the condition of (2.95) or (2.96) cannot be guaranteed, which implies encountering a high multiuser interference, then by using the above decision rule the transmitted bit may be decided in error. Therefore, in multiuser communications systems using the DS/SFH spread-spectrum scheme an erroneous detection may happen, even when the DS/SFH signals are transmitted over nonfading, noiseless channels as a consequence of multiuser interference. This is one of the common characteristics of all the multiple-access schemes considered in this chapter.

2.5.2 Hybrid DS/FFH Signals

In FFH a given symbol is transmitted by mapping it to several FH frequencies during several time slots (also known as chips in FFH systems) each associated with a different frequency. Since each time-slot interval is relatively short and is on the order of fraction of the transmitted signal's symbol duration, accurate carrier phase estimation is often impractical, in particular, when the symbol rate is high. Hence, in this section DS/FFH schemes dispensing with the requirement of phase estimation are discussed, which use M -ary orthogonal signalling for data modulation. Let us first review the basic principles of M -ary orthogonal signalling.

An M -ary orthogonal signalling set is constituted by M number of signals, which are expressed as

$$\{s_0(t), s_1(t), \dots, s_{M-1}(t)\} \quad (2.97)$$

The elements of the M -ary signalling set defined in (2.97) are defined over the interval of $[0, T_s)$ and satisfy the following orthogonality property:

$$\begin{aligned} \rho_{ij} &= \frac{1}{T_s} \int_0^{T_s} s_i(t)s_j(t) dt \\ &= \begin{cases} 1 & \text{if } i = j \\ 0 & \text{otherwise} \end{cases} \end{aligned} \quad (2.98)$$

With the aid of the above M -ary orthogonal signalling set, $b = \log_2 M$ number of bits can be transmitted per symbol by correspondingly transmitting one of the M possible orthogonal signals of (2.97).

The normalized orthogonal MFSK signals expressed in (2.48) having a frequency spacing obeying (2.51) constitute the elements of an M -ary orthogonal signalling set. In addition to the orthogonal MFSK signalling set, in this section another M -ary orthogonal signalling set derived from the spreading sequences will also be used. Specifically, this set of M -ary orthogonal signalling waveforms is represented as

$$\{W_0(t), W_1(t), \dots, W_{M-1}(t)\} \quad (2.99)$$

and the modulation scheme based on this set of orthogonal signals is referred to as M -ary orthogonal modulation.

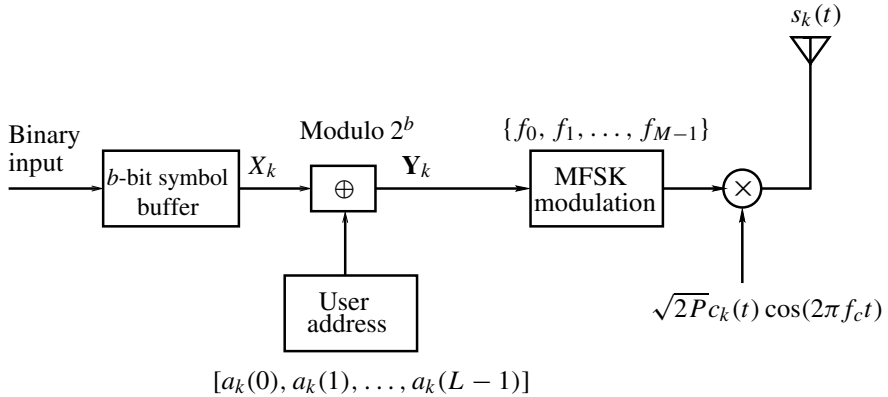


Figure 2.40: Transmitter block diagram for a DS/FFH scheme using MFSK modulation. The corresponding FFH system dispensing with DS spreading was shown in Fig. 2.18.

The reason for us to consider two different types of orthogonal signal for the data modulation in the context of the DS/FFH system considered is as follows. The stylized PSD of the DS/FFH signals can also be represented with the aid of Fig. 2.38, which consists of q number of DS bands. As discussed in the context of the FFH scheme of Section 2.3.2, ($b = \log_2 M$)-bit information can be carried by transmitting a single frequency from the set of M number of frequencies by using MFSK modulation. Since in DS/FFH systems DS spreading-based modulation is employed, ($b = \log_2 M$)-bit information can also be carried by using M -ary orthogonal modulation associated with M number of orthogonal spreading codes. This issue will become more clear during our later analysis.

2.5.2.1 DS/FFH Using MFSK Modulation

We assume that the DS/FFH system considered employs M number of frequencies for FH. The transmitter block diagram of DS/FFH using MFSK modulation is shown in Fig. 2.40, which is similar to Fig. 2.18 invoked for the transmitter of a FFH system, except that Fig. 2.40 includes the DS spreading operation invoked for multiplying the DS chip waveform $c_k(t)$. Except for the DS spreading operation carried out with the aid of multiplication by $c_k(t)$, in Fig. 2.40 the parameters as well as the operations are the same as those in Fig. 2.18. The transmitted signals corresponding to the i th symbol are given by

$$s_k(t) = \sum_{l=0}^{L-1} \sqrt{2P} P_{T_h}(t - iT_s - lT_h) c_k(t) \cos(2\pi[f_c + f_l^{(k)}]t + \varphi_l^{(k)}) \quad (2.100)$$

where $f_l^{(k)} \in \{f_0, f_1, \dots, f_{M-1}\}$ for $l = 0, 1, \dots, L-1$ are the FH frequencies determined by the k th user's address code $\mathbf{a}_k = [a_k(0), a_k(1), \dots, a_k(L-1)]$ and by the current M -ary transmitted symbol X_k , according to the equation $\mathbf{Y}_k = X_k \cdot \mathbf{1} \oplus \mathbf{a}_k$.

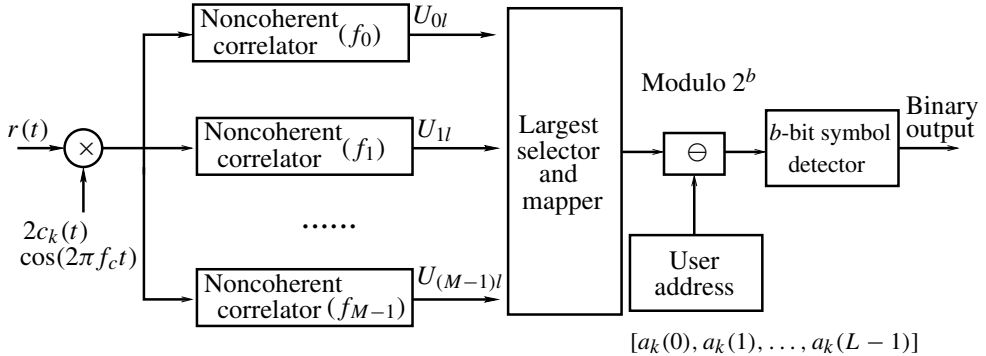


Figure 2.41: Receiver block diagram of a DS/FFH system using MFSK modulation. The corresponding FFH system dispensing with DS spreading was illustrated in Fig. 2.21(a).

2.5.2.2 Detection of DS/FFH Signals Using MFSK

Assuming the presence of K number of DS/FFH signals expressed in the form of (2.100), which are synchronously transmitted over a perfect nonfading and noiseless channel, the received signal can be expressed as

$$r(t) = \sum_{k=1}^K \sum_{l=0}^{L-1} \sqrt{2P} P_{T_h}(t - iT_s - lT_h) c_k(t) \cos(2\pi[f_c + f_l^{(k)}]t + \phi_l^{(k)}) \quad (2.101)$$

The receiver schematic of DS/FFH using MFSK modulation is shown in Fig. 2.41, which is similar to Fig. 2.21(a) contrived for the FFH scheme using no DS spreading, except for the difference that the term $2 \cos(2\pi f_c t)$ corresponding to carrier demodulation and the spectrum-analyser block seen in Fig. 2.21(a) are now represented by $2c_k(t) \cos(2\pi f_c t)$ and the *Largest-Selector and Mapper* block. However, owing to the employment of DS spreading in the DS/FFH systems, the detection of DS/FFH signals is substantially different from that of the FFH signals described in Section 2.3.2. Let us therefore discuss the detection of DS/FFH signals in more detail.

Let the first user corresponding to $k = 1$ be the desired user. We assume that the receiver aims to demodulate the first symbol ($i = 0$) transmitted by the desired user. Furthermore, we assume that the receiver is capable of acquiring perfect synchronizations of both the FH pattern and the DS spreading sequence of the desired user. Consequently, by referring to Fig. 2.41 and Fig. 2.14, the decision variables corresponding to the L number of time slots during the first symbol's transmission interval can be written as

$$\begin{aligned} U_{ml} &= \left[\int_{lT_h}^{(l+1)T_h} r(t)c_1(t) \cos(2\pi[f_c + f_m]t) dt \right]^2 \\ &\quad + \left[\int_{lT_h}^{(l+1)T_h} r(t)c_1(t) \sin(2\pi[f_c + f_m]t) dt \right]^2 \\ m &= 0, 1, \dots, M-1; l = 0, 1, \dots, L-1 \end{aligned} \quad (2.102)$$

On substituting (2.101) into the above equation, we obtain

$$\begin{aligned} U_{ml} = & \left[\sum_{k=1}^K \sqrt{\frac{P}{2}} \delta[f_l^{(k)}, f_m] \cos(\phi_l^{(k)}) \int_{lT_h}^{(l+1)T_h} c_k(t) c_1(t) dt \right]^2 \\ & + \left[- \sum_{k=1}^K \sqrt{\frac{P}{2}} \delta[f_l^{(k)}, f_m] \sin(\phi_l^{(k)}) \int_{lT_h}^{(l+1)T_h} c_k(t) c_1(t) dt \right]^2 \end{aligned} \quad (2.103)$$

By defining the cross-correlation factor between the DS spreading sequences of user k and user 1 over $[lT_h, (l+1)T_h]$ as

$$\rho_{1k}^l = \frac{1}{T_h} \int_{lT_h}^{(l+1)T_h} c_k(t) c_1(t) dt \quad (2.104)$$

(2.103) can be written as

$$U_{ml} = \left[\sum_{k=1}^K \sqrt{\frac{P}{2}} T_h \delta[f_l^{(k)}, f_m] \rho_{1k}^l \cos(\phi_l^{(k)}) \right]^2 + \left[- \sum_{k=1}^K \sqrt{\frac{P}{2}} T_h \delta[f_l^{(k)}, f_m] \rho_{1k}^l \sin(\phi_l^{(k)}) \right]^2 \quad (2.105)$$

In the context of the desired user's signal, $\rho_{11}^l = 1$ for $l = 0, 1, \dots, L-1$. Hence, when $f_m = f_l^{(1)}$,

$$\begin{aligned} U_{ml} = & \underbrace{\left[\sqrt{\frac{P}{2}} T_h \cos(\phi_l^{(1)}) + \sum_{k=2}^K \sqrt{\frac{P}{2}} T_h \delta[f_l^{(k)}, f_m] \rho_{1k}^l \cos(\phi_l^{(k)}) \right]^2}_{\text{Multiuser interference}} \\ & + \underbrace{\left[-\sqrt{\frac{P}{2}} T_h \sin(\phi_l^{(1)}) - \sum_{k=2}^K \sqrt{\frac{P}{2}} T_h \delta[f_l^{(k)}, f_m] \rho_{1k}^l \sin(\phi_l^{(k)}) \right]^2}_{\text{Multiuser interference}} \\ l = & 0, 1, \dots, L-1 \end{aligned} \quad (2.106)$$

By contrast, when $f_m \neq f_l^{(1)}$, (2.105) can be simplified to

$$\begin{aligned} U_{ml} = & \underbrace{\left[\sum_{k=2}^K \sqrt{\frac{P}{2}} T_h \delta[f_l^{(k)}, f_m] \rho_{1k}^l \cos(\phi_l^{(k)}) \right]^2}_{\text{Multiuser interference}} \\ & + \underbrace{\left[- \sum_{k=2}^K \sqrt{\frac{P}{2}} T_h \delta[f_l^{(k)}, f_m] \rho_{1k}^l \sin(\phi_l^{(k)}) \right]^2}_{\text{Multiuser interference}} \\ l = & 0, 1, \dots, L-1 \end{aligned} \quad (2.107)$$

Based on (2.106) and (2.107) we observe that when the multiuser interference is sufficiently low, the noncoherent correlator's output U_{ml} matched to the transmitted frequency

of $f_l^{(1)}$, as formulated in (2.106), is higher than any one of the other noncoherent correlators' outputs, denoted by U_{ml} which are mismatched to the transmitted frequency of $f_l^{(1)}$, as expressed in (2.107). Therefore, the transmitted frequencies $\{f_0^{(1)}, f_1^{(1)}, \dots, f_{L-1}^{(1)}\}$ can be determined by selecting the highest value from the set $\{U_{0l}, U_{1l}, \dots, U_{(M-1)l}\}$ for each given value of l , where $l = 0, 1, \dots, L - 1$. Having obtained $\{f_0^{(1)}, f_1^{(1)}, \dots, f_{L-1}^{(1)}\}$, we can map the set acquired to the sequence $\mathbf{Y}_1 = [y_1(0), y_1(1), \dots, y_1(L - 1)]$ by letting $y_1(l) = m$, if $f_l^{(1)} = f_m$ for $l = 0, 1, \dots, L - 1$. Finally, according to (2.67), by performing modulo- $(M = 2^b)$ subtraction of the unique user address \mathbf{a}_1 of the desired user from \mathbf{Y}_1 on a chip-by-chip basis, we arrive at the sequence

$$\begin{aligned} \mathbf{X}_1 &= \mathbf{Y}_1 \ominus \mathbf{a}_1 \\ &= [y_1(0) \ominus a_1(0), y_1(1) \ominus a_1(1), \dots, y_1(L - 1) \ominus a_1(L - 1)] \end{aligned} \quad (2.108)$$

In the absence of multiuser interference, i.e. when supporting $K = 1$ user, and when communicating over a noiseless channel, it can be easily seen that when transmitting a specific symbol X_1 with the aid of a specific address code \mathbf{a}_1 , all the elements in \mathbf{X}_1 will be the same, having a value of X_1 corresponding to the transmitted M -ary symbol. In the presence of noise and/or multiuser interference, some elements of \mathbf{X}_1 might be erroneously detected, resulting in having different elements in \mathbf{X}_1 . In this case the transmitted symbol X_1 can be decided on the basis of the symbol that appeared most frequently in \mathbf{X}_1 .

2.5.2.3 DS/FFH Using M -ary Orthogonal Modulation

The transmitter block diagram of the DS/FFH system using M -ary orthogonal modulation is shown in Fig. 2.42. Let

$$\{W_0(t), W_1(t), \dots, W_{M-1}(t)\} \quad (2.109)$$

represent an M -ary orthogonal sequence or code set defined over the time interval of $[0, T_h]$, which satisfies

$$\frac{1}{T_h} \int_0^{T_h} W_i(t) W_j(t) dt = \begin{cases} 1 & \text{if } i = j \\ 0 & \text{otherwise} \end{cases} \quad (2.110)$$

The M -ary orthogonal sequence set is used for signalling M -ary data symbols at a rate of one symbol every T_s seconds. Let the transmitted M -ary symbol be λ . Then, the specific value of λ used for signalling $b = \log_2 M$ bits is mapped to the orthogonal signalling waveform of $W_\lambda(t)$. As shown in Fig. 2.42, following this mapping operation the frequency-hopping operation obeying the k th user's FH pattern is invoked. Specifically, for a given time slot l , $0 \leq l \leq L - 1$, of the L -chip FFH sequence residing within a given symbol interval of T_s , a frequency $f_l^{(k)}$ determined by the FH pattern is invoked for transmitting the orthogonal signalling waveform $W_\lambda(t)$. Following the FH operation, the signal is further spread by the signature sequence $c_k(t)$ of user k . Referring to Fig. 2.42, the signal transmitted by the k th user in order to signal the M -ary symbol of λ during the time interval $[iT_s, (i + 1)T_s)$ can be expressed as

$$\begin{aligned} s_k(t) &= \sum_{l=0}^{L-1} \sqrt{2P} P_{T_h}(t - iT_s - lT_h) W_\lambda(t - iT_s - lT_h) c_k(t) \\ &\quad \times \cos(2\pi[f_c + f_l^{(k)}]t + \varphi_l^{(k)}) \end{aligned} \quad (2.111)$$

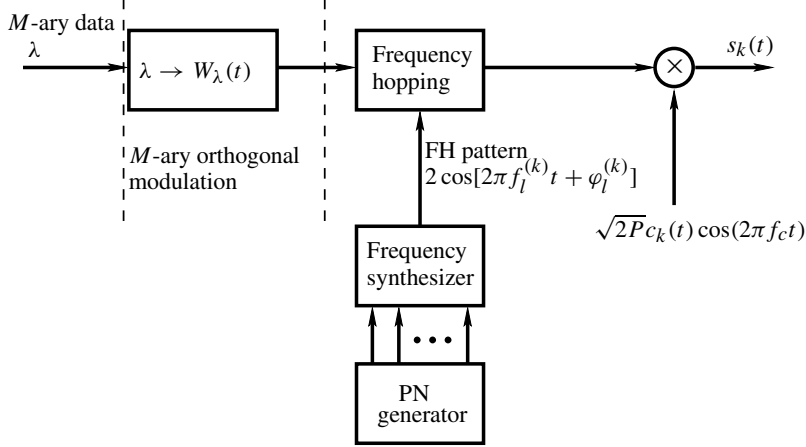


Figure 2.42: Transmitter block diagram of an DS/FFH system using M -ary orthogonal modulation.

2.5.2.4 Detection of DS/FFH Signals Using M -ary Orthogonal Modulation

Assuming that $K \geq 1$ number of users synchronously transmit their signals in the form of (2.111) over a perfect nonfading and noiseless channel, the received signal arriving during the first symbol interval of $[0, T_s)$ can be expressed as

$$\begin{aligned} r(t) = & \sum_{k=1}^K \sum_{l=0}^{L-1} \sqrt{2P} P_{T_h}(t - lT_h) W_\lambda(t - lT_h) c_k(t) \\ & \times \cos(2\pi[f_c + f_l^{(k)}]t + \phi_l^{(k)}) \end{aligned} \quad (2.112)$$

The receiver block diagram designed for detecting the DS/FFH signals conveyed using M -ary orthogonal modulation is shown in Fig. 2.43. Specifically, the receiver block diagram is constituted by three parts. The first part removes the effects of the carrier f_c and those of DS based spreading imposed by the desired user's signature sequence. Note that in Fig. 2.43 we assumed that the first user employing the signature sequence of $c_1(t)$ was the desired user. The second part of the schematic seen in Fig. 2.43 implements the frequency dehopping operation by invoking the desired user's unique FH pattern $\{f_l^{(k)}\}$. The final part of the schematic seen in Fig. 2.43 represents an M -ary orthogonal demodulator, where the dehopped signal is noncoherently correlated with each of the M possible orthogonal signalling sequences expressed in (2.109), in order to generate M number of decision variables. Finally, the maximum of the M number of decision variables is selected and mapped to a M -ary symbol represented as $\hat{\lambda}_l$. This operation is repeated for each of the time slots l , $0 \leq l \leq L - 1$.

Let us assume that the receiver is capable of achieving perfect FH pattern and DS code acquisition as well as tracking in the context of the reference user. Then, referring to Fig. 2.43, for the l th time-slot, the corresponding decision variable U_{ml} , $m = 0, 1, \dots, M - 1$;

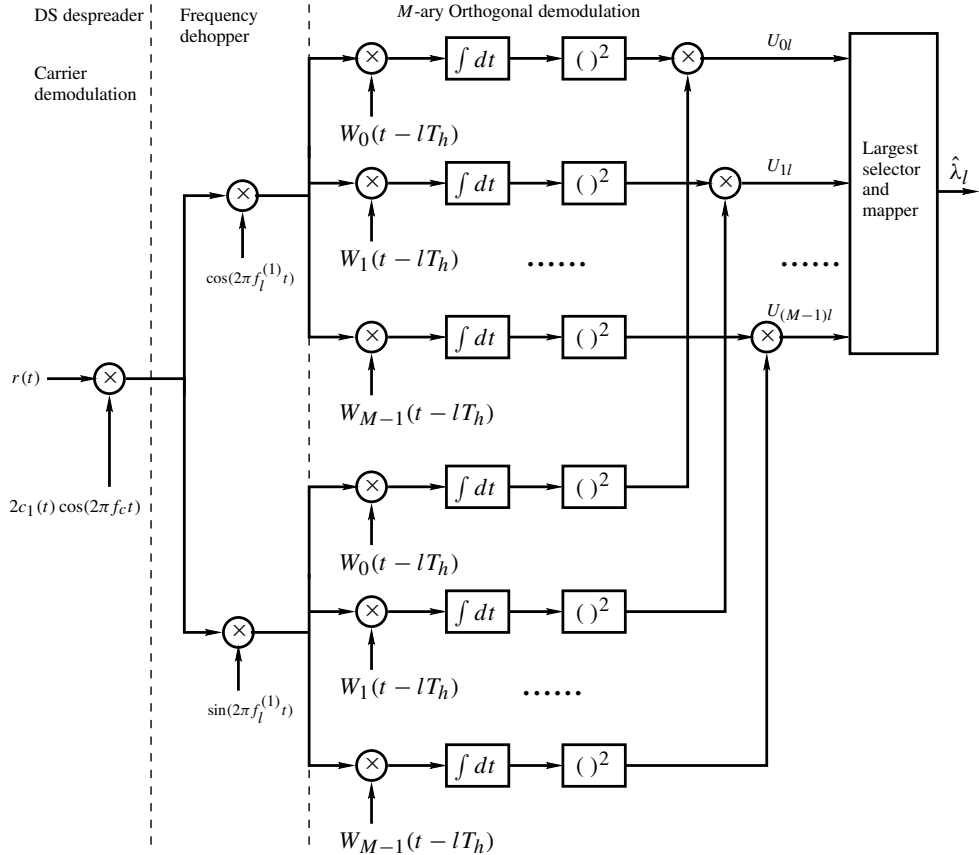


Figure 2.43: Receiver block diagram of DS/FFH using M -ary orthogonal demodulation.

$l = 0, 1, \dots, L - 1$ corresponding to the first user can be written as

$$U_{ml} = \left[\int_{lT_h}^{(l+1)T_h} r(t)c_1(t)W_m(t - lT_h)\cos(2\pi[f_c + f_l^{(1)}]t)]^2 + \left[\int_{lT_h}^{(l+1)T_h} r(t)c_1(t)W_m(t - lT_h)\sin(2\pi[f_c + f_l^{(1)}]t) \right]^2 \right]^{1/2} \quad (2.113)$$

Substituting (2.112) into (2.113), we obtain

$$U_{ml} = \left[\sum_{k=1}^K \sqrt{\frac{P}{2}} \delta[f_l^{(k)}, f_l^{(1)}] \cos(\phi_l^{(k)}) \times \int_{lT_h}^{(l+1)T_h} c_k(t)c_1(t)W_\lambda(t - lT_h)W_m(t - lT_h)dt \right]^2$$

$$\begin{aligned}
& + \left[- \sum_{k=1}^K \sqrt{\frac{P}{2}} \delta[f_l^{(k)}, f_l^{(1)}] \sin(\phi_l^{(k)}) \right. \\
& \times \left. \int_{lT_h}^{(l+1)T_h} c_k(t) c_1(t) W_\lambda(t - lT_h) W_m(t - lT_h) dt \right]^2
\end{aligned} \quad (2.114)$$

By defining the cross-correlation factor between user k and user 1 over the interval $[lT_h, (l+1)T_h]$ as

$$\rho_{1k}^l = \frac{1}{T_h} \int_{lT_h}^{(l+1)T_h} c_k(t) c_1(t) W_\lambda(t - lT_h) W_m(t - lT_h) dt \quad (2.115)$$

(2.114) can be expressed as

$$\begin{aligned}
U_{ml} = & \left[\sum_{k=1}^K \sqrt{\frac{P}{2}} T_h \delta[f_l^{(k)}, f_l^{(1)}] \rho_{1k}^l \cos(\phi_l^{(k)}) \right]^2 \\
& + \left[- \sum_{k=1}^K \sqrt{\frac{P}{2}} T_h \delta[f_l^{(k)}, f_l^{(1)}] \rho_{1k}^l \sin(\phi_l^{(k)}) \right]^2
\end{aligned} \quad (2.116)$$

Since for $k = 1$ we have $c_1(t)c_1(t) = 1$, the corresponding correlation factor of (2.114) can be expressed as

$$\rho_{11}^l = \frac{1}{T_h} \int_{lT_h}^{(l+1)T_h} W_\lambda(t - lT_h) W_m(t - lT_h) dt \quad (2.117)$$

Furthermore, since $W_\lambda(t - lT_h)$ and $W_m(t - lT_h)$ are orthogonal sequences obeying (2.109), we have

$$\rho_{11}^l = \begin{cases} 1 & \text{if } m = \lambda \\ 0 & \text{otherwise} \end{cases} \quad (2.118)$$

Consequently, for $m = \lambda$ the decision variable of (2.116) can be expressed as

$$\begin{aligned}
U_{\lambda l} = & \underbrace{\left[\sqrt{\frac{P}{2}} T_h \cos(\phi_l^{(1)}) + \sum_{k=2}^K \sqrt{\frac{P}{2}} T_h \delta[f_l^{(k)}, f_l^{(1)}] \rho_{1k}^l \cos(\phi_l^{(k)}) \right]^2}_{\text{Multiuser interference}} \\
& + \underbrace{\left[- \sqrt{\frac{P}{2}} T_h \sin(\phi_l^{(1)}) - \sum_{k=2}^K \sqrt{\frac{P}{2}} T_h \delta[f_l^{(k)}, f_l^{(1)}] \rho_{1k}^l \sin(\phi_l^{(k)}) \right]^2}_{\text{Multiuser interference}}
\end{aligned} \quad (2.119)$$

for $l = 0, 1, \dots, L - 1$. By contrast, when $m \neq \lambda$, the corresponding decision variable can be expressed as

$$U_{itml} = \underbrace{\left[\sum_{k=2}^K \sqrt{\frac{P}{2}} T_h \delta[f_l^{(k)}, f_l^{(1)}] \rho_{1k}^l \cos(\phi_l^{(k)}) \right]^2}_{\text{Multiuser interference}} + \underbrace{\left[- \sum_{k=2}^K \sqrt{\frac{P}{2}} T_h \delta[f_l^{(k)}, f_l^{(1)}] \rho_{1k}^l \sin(\phi_l^{(k)}) \right]^2}_{\text{Multiuser interference}} \quad (2.120)$$

where $l = 0, 1, \dots, L - 1$.

Based on the set of decision variables $\{U_{0l}, U_{1l}, \dots, U_{(M-1)l}\}$, the maximum of the set can be selected and mapped to an M -ary symbol of $\hat{\lambda}_l$. It can be shown that when the values of the multiuser interference terms in (2.119) and (2.120) are sufficiently low, the maximum of the set $\{U_{0l}, U_{1l}, \dots, U_{(M-1)l}\}$ found for each given value of l , $l = 0, 1, \dots, L - 1$, will match the transmitted symbol of λ . More specifically, $U_{\lambda l}$ represented by (2.119) will be the maximum of the set $\{U_{0l}, U_{1l}, \dots, U_{(M-1)l}\}$. Consequently, $\hat{\lambda}_l = \lambda$ for $l = 0, 1, \dots, L - 1$ and the transmitted M -ary symbol is detected correctly. However, when the multiuser interference is high, or when the channel imposes impairment, some $\hat{\lambda}_l$ values in $\{\hat{\lambda}_0, \hat{\lambda}_1, \dots, \hat{\lambda}_{L-1}\}$ might be in error, hence not all of them are equal to the transmitted value of λ . In this case λ can be detected as the symbol, which appeared in the set $\{\hat{\lambda}_0, \hat{\lambda}_1, \dots, \hat{\lambda}_{L-1}\}$ that is most frequent. Provided that the multiuser interference and/or the channel noise is not excessive, so that correct detection was achieved for most of the values in the set $\{\hat{\lambda}_0, \hat{\lambda}_1, \dots, \hat{\lambda}_{L-1}\}$, then we can see that the transmitted symbol λ can still be correctly detected with a high probability.

Above we have discussed two classes of DS/FFH communication scheme. In the first class the transmitted M -ary information is embedded in the M number of legitimized MFSK frequencies. By contrast, in the second class of DS/FFH schemes the transmitted M -ary information is conveyed by one of the M number of time-domain orthogonal sequences. We note furthermore that the above-mentioned two classes of DS/FFH scheme can be combined, where an M -ary symbol can be signalled simultaneously by one of the M number of orthogonal time-domain sequences mapped to one of the M legitimate MFSK frequencies. Furthermore, when a DS/FFH system uses more than M_1 number of FH frequencies plus more than M_2 number of orthogonal sequences, it can be shown that we can transmit $(\log_2 M_1 + \log_2 M_2)$ number of bits in every symbol interval. This is achieved by conveying $\log_2 M_1$ bits with the aid of the M_1 number of FH frequencies and $\log_2 M_2$ bits using the M_2 number of orthogonal signalling sequences. Motivated readers might like to construct the corresponding detectors for these extended DS/FFH schemes, which are not further discussed in this book.

2.6 Hybrid Direct-Sequence/Time-Hopping Multiple-Access

In Section 2.4 we have shown that both FH and TH belong to the family of pulse-position modulation schemes with FH being a ‘F-domain pulse-position modulation’ arrangement,

while TH was a time-domain pulse-position modulation scheme. As discussed in the context of the FH and TH systems in the previous Sections 2.3 and 2.4, for a given FH scheme, usually there exists a corresponding TH scheme. For example, SFH using MFSK modulation corresponds to STH using MPPM, while MFSK-assisted FFH corresponds to MPPM-assisted FTH, etc. Furthermore, we have shown that the detection schemes invoked in these FH and TH systems can be discussed in parallel. Similarly, the hybrid DS/TH scheme considered in this section may be discussed in parallel with the hybrid DS/FH spread-spectrum scheme considered in Section 2.5. Therefore, in this section the hybrid DS/TH spread-spectrum arrangement is discussed following similar arguments to those outlined in Section 2.5. Let us first consider the DS/STH scheme in the next section.

2.6.1 Hybrid DS/STH Signals

2.6.1.1 DS/STH Using MPPM

The transmitter block diagram of the hybrid DS/STH scheme is similar to that seen in Fig. 2.27(a), except that the signal hosted by the activated time slots is now multiplied by the DS spreading waveform $c_k(t)$ of user k , in order to achieve DS spreading. This multiplication-based operation can be readily implemented by replacing the term $\sqrt{2P} \cos(2\pi f_{ct})$ in Fig. 2.27(a) with $\sqrt{2P}c_k(t) \cos(2\pi f_{ct})$. Consequently, the transmitted MPPM-based DS/STH signal can be obtained by appropriately modifying the transmitted STH signal of (2.69), which can now be expressed as

$$s_k(t) = \sqrt{2P}c_k(t)P(t - iT_f - t_kT_c - X_kT_h) \cos(2\pi f_{ct} + \phi_i^{(k)}) \quad (2.121)$$

where i represents the frame index, $\{t_k\}$ denotes the TH pattern of the k th user and X_k represents the k th user's M -ary transmitted symbol. The details of the other parameters used in (2.121) can be found in the context of Fig. 2.27 and of (2.69). Note that since the parameter T_c in (2.121) represents the chip-duration of the TH scheme, the chip-duration of the DS spreading sequence $c_k(t)$, which was also represented by T_c , is now denoted by T'_c , when it would conflict with the chip duration T_c of the TH arrangement. Furthermore, we assume that the time-slot interval of T_h is higher than the chip duration T'_c of the DS spreading sequence, i.e. we assume that $N = T_h/T'_c > 1$. Since we have $T'_c < T_h$, we can argue that in DS/STH systems the system's bandwidth is essentially determined by the chip duration of T'_c , while it is determined by T_h in STH systems dispensing with DS spreading.

2.6.1.2 Detection of DS/STH Signals Using MPPM

Similarly to the DS/SFH system considered in Section 2.5.1, in DS/STH systems we also assume that K number of synchronous users are supported by the DS/STH system. Furthermore, we assume that the DS/STH signals expressed in the form of (2.121) are transmitted over a perfect nonfading and noiseless channel. Then, the received signal arriving during the i th frame or the i th symbol duration $[iT_f, (i+1)T_f)$ can be expressed as

$$r(t) = \sum_{k=1}^K \sqrt{2P}c_k(t)P(t - iT_f - t_kT_c - X_kT_h) \cos(2\pi f_{ct} + \phi_i^{(k)}) \quad (2.122)$$

The noncoherent receiver designed for DS/FTH is also similar to that contrived for the FTH scheme, which was shown in Fig. 2.29, except that the terms $\cos(2\pi f_c t)$ and $\sin(2\pi f_c t)$ in Fig. 2.29 are now replaced by $c_k(t) \cos(2\pi f_c t)$ and $c_k(t) \sin(2\pi f_c t)$, in order to remove the DS spreading imposed by the transmitter by multiplying the transmitted signal of (2.121) by $c_k(t)$.

Let the first user corresponding to $k = 1$ be the desired user to be detected. We assume that the receiver has acquired the TH pattern of $\{t_1\}$. We also assume that the receiver has achieved frame synchronization corresponding to the frame duration of T_f as well as PN sequence acquisition for the DS spreading code $c_1(t)$. Then, based on the above assumptions and by referring to Fig. 2.29, the M number of decision variables associated with the M number of time slots can be expressed as

$$\begin{aligned} Z_{1m} = & \left[\int_{iT_f+t_1T_c+mT_h}^{iT_f+t_1T_c+(m+1)T_h} r(t)c_1(t)P(t - iT_f - t_1T_c - mT_h) \cos(2\pi f_c t) dt \right]^2 \\ & + \left[\int_{iT_f+t_1T_c+mT_h}^{iT_f+t_1T_c+(m+1)T_h} r(t)c_1(t)P(t - iT_f - t_1T_c - mT_h) \sin(2\pi f_c t) dt \right]^2 \end{aligned} \quad (2.123)$$

Substituting (2.122) into (2.123), it can be shown that (2.123) can be simplified to

$$\begin{aligned} Z_{1m} = & \left[\sum_{k=1}^K \sqrt{\frac{P}{2}} \delta[t_k, t_1] \delta[X_k, m] \cos(\phi_i^{(k)}) \int_{iT_f+t_1T_c+mT_h}^{iT_f+t_1T_c+(m+1)T_h} c_k(t)c_1(t) dt \right]^2 \\ & + \left[- \sum_{k=1}^K \sqrt{\frac{P}{2}} \delta[t_k, t_1] \delta[X_k, m] \sin(\phi_i^{(k)}) \int_{iT_f+t_1T_c+mT_h}^{iT_f+t_1T_c+(m+1)T_h} c_k(t)c_1(t) dt \right]^2 \\ = & \left[\sum_{k=1}^K \sqrt{\frac{P}{2}} T_h \delta[t_k, t_1] \delta[X_k, m] \rho_{1k}^m \cos(\phi_i^{(k)}) \right]^2 \\ & + \left[- \sum_{k=1}^K \sqrt{\frac{P}{2}} T_h \delta[t_k, t_1] \delta[X_k, m] \rho_{1k}^m \sin(\phi_i^{(k)}) \right]^2 \end{aligned} \quad (2.124)$$

where ρ_{1k}^m represents the cross-correlation factor between the DS spreading sequences $c_k(t)$ and $c_1(t)$ within the interval $[iT_f + t_1T_c + mT_h, iT_f + t_1T_c + (m + 1)T_h]$. In (2.124) $\delta[t_k, t_1] = 1$, provided that we have $t_k = t_1$, implying that a hit was encountered between user k and the desired user. By contrast, $\delta[X_k, m] = 1$, provided that $X_k = m$, implying that the m th noncoherent correlator is matched to the transmitted symbol X_k of user k . Substituting $\delta[t_1, t_1] = 1$ and $\rho_{11}^m = 1$ into the above equation, we find that for the noncoherent correlator matched to the transmitted symbol X_1 of the desired user, i.e. for $\delta[X_1, m] = 1$, the decision

variable can be expressed as

$$\begin{aligned}
 Z_{1m} = & \left[\underbrace{\sqrt{\frac{P}{2}} T_h \cos(\phi_i^{(1)}) + \sum_{k=2}^K \sqrt{\frac{P}{2}} T_h \delta[t_k, t_1] \delta[X_k, m] \rho_{1k}^m \cos(\phi_i^{(k)})}_{\text{Multiuser interference}} \right]^2 \\
 & + \left[\underbrace{-\sqrt{\frac{P}{2}} T_h \sin(\phi_i^{(1)}) - \sum_{k=2}^K \sqrt{\frac{P}{2}} T_h \delta[t_k, t_1] \delta[X_k, m] \rho_{1k}^m \sin(\phi_i^{(k)})}_{\text{Multiuser interference}} \right]^2 \\
 m = X_1
 \end{aligned} \tag{2.125}$$

By contrast, for the noncoherent correlators that are mismatched with respect to the transmitted symbol X_1 of the desired user, i.e. for $\delta[X_1, m] = 0$, we have the following decision variables

$$\begin{aligned}
 Z_{1m} = & \left[\underbrace{\sum_{k=2}^K \sqrt{\frac{P}{2}} T_h \delta[t_k, t_1] \delta[X_k, m] \rho_{1k}^m \cos(\phi_i^{(k)})}_{\text{Multiuser interference}} \right]^2 \\
 & + \left[\underbrace{-\sum_{k=2}^K \sqrt{\frac{P}{2}} T_h \delta[t_k, t_1] \delta[X_k, m] \rho_{1k}^m \sin(\phi_i^{(k)})}_{\text{Multiuser interference}} \right]^2 \\
 m = 0, 1, \dots, M-1; m \neq X_1
 \end{aligned} \tag{2.126}$$

Based on (2.125) and (2.126) we find that from the set of M number of decision variables $\{Z_{10}, Z_{11}, \dots, Z_{1(M-1)}\}$, the maximum one is matched to the desired user's transmitted symbol X_1 , provided that the multiuser interference quantified in (2.125) and (2.126) is sufficiently low. Specifically, if we assume that the TH patterns of the K number of users are orthogonal, i.e. if we assume that $\delta[t_k, t_1] = 0$ for any $k \neq 1$, then (2.125) and (2.126) can be correspondingly simplified to

$$\begin{aligned}
 Z_{1m} = & \left[\sqrt{\frac{P}{2}} T_h \cos(\phi_i^{(1)}) \right]^2 + \left[-\sqrt{\frac{P}{2}} T_h \sin(\phi_i^{(1)}) \right]^2 \\
 = & \frac{P}{2} T_h^2 = \frac{E_s T_h}{2}, \quad m = X_1
 \end{aligned} \tag{2.127}$$

$$Z_{1m} = 0, \quad m = 0, 1, \dots, M-1; \quad m \neq X_1 \tag{2.128}$$

where $E_s = P T_h$ represents the transmitted energy per M -ary symbol. Specifically, only that particular noncoherent correlator, which is matched to the transmitted symbol of X_1 will output non-zero energy, while all the others output zero. As expected, in this case the transmitted symbol can be correctly detected. However, sometimes when the multiuser interference is excessive, or when the other noise or jamming power is excessive, the output of the noncoherent correlator matched to the transmitted symbol may not be the largest one of the decision variables. Consequently, this scenario will result in an erroneous decision.

2.6.2 Hybrid DS/FTH Signals

It has been shown in Section 2.4.1 that in FTH the M -ary symbols are transmitted by mapping them to L consecutive frames, and in each frame one of the M number of time slots is activated according to the ($b = \log_2 M$)-bit transmitted symbol and the user's unique TH address. Specifically, in DS/FTH systems an M -ary symbol can also be transmitted using the similar scenario of the FTH scheme and the ($b = \log_2 M$)-bit symbols are transmitted using the M number of time slots. Furthermore, since DS spreading is employed in the family of DS/FTH systems, M -ary orthogonal modulation can also be employed for transmitting the ($b = \log_2 M$)-bit symbols by M number of orthogonal time-domain sequences. This approach is in fact analogous to the philosophy of DS/FFH schemes using M -ary orthogonal modulation, which was investigated in Section 2.5.2.3. In this section DS/FTH using both MPPM and M -ary orthogonal modulation will be analysed. Let us first consider the operating principles of the MPPM-assisted DS/FTH scheme.

2.6.2.1 DS/FTH Using MPPM

The transmitter block diagram of the MPPM-assisted DS/FTH system can be constructed with the aid of Fig. 2.28 by replacing the carrier-frequency term of $\sqrt{2P} \cos(2\pi f_c t)$ with $\sqrt{2P} c_k(t) \cos(2\pi f_c t)$, where $c_k(t)$ represents the DS spreading sequence waveform of the k th user. Consequently, by referring to (2.71), the transmitted DS/FTH signal associated with symbol X_k of user k can be expressed as

$$s_k(t) = \sqrt{2P} \sum_{l=0}^{L-1} P[t - (i + l)T_f - y_k(l)T_h] c_k(t) \cos(2\pi f_c t + \varphi_i^{(k)}) \quad (2.129)$$

where we assumed that X_k was transmitted by mapping it to L consecutive frames commencing at the i th frame. The parameters used in (2.129) were defined in the context of the FTH scheme dispensing with DS spreading in (2.71).

2.6.2.2 Detection of DS/FTH Signal Using MPPM

In synchronous DS/FTH systems, when we assume that K number of user signals expressed in the form of (2.129) are transmitted over a perfect nonfading and noiseless channel, the received multiple-access signal arriving within the interval $[iT_f, (i + L)T_f]$ can be expressed as

$$r(t) = \sum_{k=1}^K \sqrt{2P} \sum_{l=0}^{L-1} P[t - (i + l)T_f - y_k(l)T_h] c_k(t) \cos(2\pi f_c t + \phi_{il}^{(k)}) \quad (2.130)$$

Let us assume that the first user associated with $k = 1$ is the desired user, whose transmitted symbol X_1 is detected by the receiver. We also assume that the receiver is capable of acquiring perfect synchronization both in the context of the FTH frame and the DS spreading sequence. The receiver schematic of the MPPM assisted DS/FTH system is shown in Fig. 2.44, which is similar to Fig. 2.32, except that in Fig. 2.44 additional DS despreading is invoked for removing the effect of DS spreading from the received signal of (2.130). Furthermore, the 'time-slot analyser and detector' in Fig. 2.32 is now

replaced by the block marked as *Largest selector and mapper*. According to Fig. 2.44, within the $(i + l)$ th frame earmarked for detecting the element $y_1(l)$, where $y_1(l) \in \{0, 1, \dots, Q - 1\}$ and $l = 0, 1, \dots, L - 1$, the Q number of decision variables can be expressed as

$$U_{ql} = \left[\int_{(i+l)T_f+qT_h}^{(i+l)T_f+(q+1)T_h} r(t) P[t - (i + l)T_f - qT_h] c_1(t) \cos(2\pi f_c t) dt \right]^2 + \left[\int_{(i+l)T_f+qT_h}^{(i+l)T_f+(q+1)T_h} r(t) P[t - (i + l)T_f - qT_h] c_1(t) \sin(2\pi f_c t) dt \right]^2 \quad (2.131)$$

Substituting (2.130) into (2.131) and following the approach used in (2.124) and (2.126), it can be shown that for $q = y_1(l)$,

$$U_{ql} = \left[\underbrace{\sqrt{\frac{P}{2}} T_h \cos(\phi_{il}^{(1)}) + \sum_{k=2}^K \sqrt{\frac{P}{2}} T_h \delta[y_k(l), q] \rho_{1k}^l \cos(\phi_{il}^{(k)})}_{\text{Multiuser interference}} \right]^2 + \left[\underbrace{-\sqrt{\frac{P}{2}} T_h \sin(\phi_{il}^{(1)}) - \sum_{k=2}^K \sqrt{\frac{P}{2}} T_h \delta[y_k(l), q] \rho_{1k}^l \sin(\phi_{il}^{(k)})}_{\text{Multiuser interference}} \right]^2, \quad q = y_1(l) \quad (2.132)$$

By contrast, the noncoherent correlators associated with $q \neq y_1(l)$ only output interference, which can be expressed as

$$U_{ql} = \left[\underbrace{\sum_{k=2}^K \sqrt{\frac{P}{2}} T_h \delta[y_k(l), q] \rho_{1k}^l \cos(\phi_{il}^{(k)})}_{\text{Multiuser interference}} \right]^2 + \left[\underbrace{-\sum_{k=2}^K \sqrt{\frac{P}{2}} T_h \delta[y_k(l), q] \rho_{1k}^l \sin(\phi_{il}^{(k)})}_{\text{Multiuser interference}} \right]^2, \quad q \neq y_1(l) \quad (2.133)$$

By selecting the largest one from the set of decision variables $\{U_{0l}, U_{1l}, \dots, U_{(Q-1)l}\}$ for $0 \leq l \leq L - 1$, we obtain the estimated sequence $\hat{\mathbf{Y}}_1 = [\hat{y}_1(0), \hat{y}_1(1), \dots, \hat{y}_1(L - 1)]$ associated with the transmitted sequence $\mathbf{Y}_1 = [y_1(0), y_1(1), \dots, y_1(L - 1)]$. Processing $\hat{\mathbf{Y}}_1$ using the desired user's TH address \mathbf{t}_1 according to $\hat{\mathbf{Y}}_1 \ominus \mathbf{t}_1$, where \ominus represents modulo- Q subtraction, we then obtain a sequence

$$\begin{aligned} \mathbf{X}_1 &= [X_1(0), X_1(1), \dots, X_1(L - 1)] \\ &= [\hat{y}_1(0) \ominus t_1(0), \hat{y}_1(1) \ominus t_1(1), \dots, \hat{y}_1(L - 1) \ominus t_1(L - 1)] \end{aligned} \quad (2.134)$$

Finally, the transmitted symbol X_1 is decided to be the particular symbol that appears most frequently in \mathbf{X}_1 .

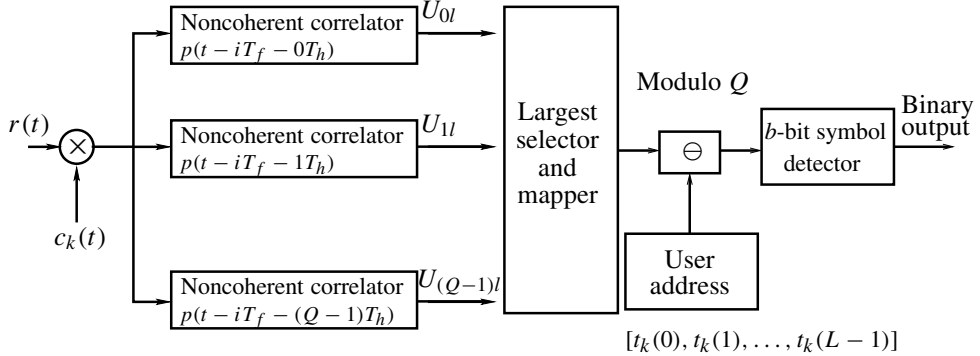


Figure 2.44: Receiver block diagram of MPPM assisted DS/FTH systems. The corresponding system using no DS spreading was shown in Fig. 2.32.

Specifically, if we assume that $K = 1$, there is no multiuser interference. Hence, (2.132) and (2.133) can be reduced to

$$\begin{aligned} U_{ql} &= \left[\sqrt{\frac{P}{2}} T_h \cos(\phi_{il}^{(1)}) \right]^2 + \left[-\sqrt{\frac{P}{2}} T_h \sin(\phi_{il}^{(1)}) \right]^2 \\ &= \frac{P}{2} T_h^2 = \frac{E_s T_h}{2L}, \quad q = y_1(l) \end{aligned} \quad (2.135)$$

$$U_{ql} = 0, \quad q = 0, 1, \dots, Q-1; \quad q \neq y_1(l) \quad (2.136)$$

In this case $y_1(l)$ for $l = 0, 1, \dots, L-1$ can be detected without errors, and all elements in \mathbf{X}_1 will be the same, which equal the transmitted symbol X_1 .

2.6.2.3 DS/FTH Using M -ary Orthogonal Modulation

In the context of DS/FTH using M -ary orthogonal modulation, the transmitter block diagram is shown in Fig. 2.45, which is similar to Fig. 2.42 contrived for DS/FFH using M -ary orthogonal modulation. As shown in Fig. 2.45, when the value of the M -ary transmitted symbol is λ , it is first mapped to the orthogonal signalling waveform $W_\lambda(t)$ with the aid of M -ary orthogonal modulation. Following the M -ary orthogonal modulation stage of Fig. 2.45 time-hopping is carried out, where L number of time slots – with each being located in one of the L consecutive frames – are activated according to the k th user's unique TH pattern, in order to transmit the orthogonal signalling waveform $W_\lambda(t)$. Following the TH stage, the time-hopped signal is DS spread using the k th user's unique signature sequence $c_k(t)$. Finally, the signal modulates a carrier having a frequency of f_c . The signal transmitted by the k th user in order to convey the λ th data symbol during the time interval $[iT_f, (i+L)T_f)$ can be represented as

$$\begin{aligned} s_k(t) &= \sum_{l=0}^{L-1} \sqrt{2P} W_\lambda[t - (i+l)T_f - t_k(l)T_h] c_k(t) \\ &\times P[t - (i+l)T_f - t_k(l)T_h] \cos(2\pi f_c t + \varphi_{il}^{(k)}) \end{aligned} \quad (2.137)$$

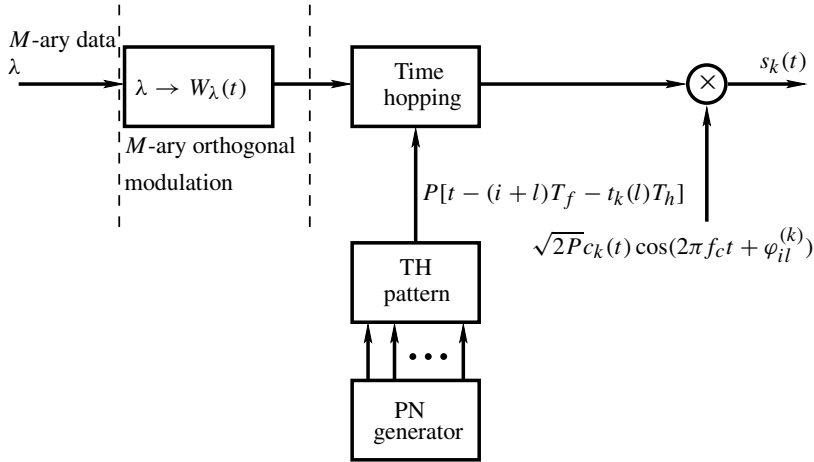


Figure 2.45: Transmitter block diagram of DS/FTH systems using M -ary orthogonal modulation. The schematic of the corresponding DS/FFH system using M -ary orthogonal modulation was shown in Fig. 2.42.

where $t_k(l) \in \{0, 1, \dots, Q - 1\}$.

2.6.2.4 Detection of DS/FTH Signals Using M -ary Orthogonal Modulation

Assuming that $K \geq 1$ number of users synchronously transmit their signals in the form of (2.137) over a perfect nonfading and noiseless channel, the received signal arriving during the interval $[iT_f, (i+L)T_f)$ can be expressed as

$$r(t) = \sum_{k=1}^K \sum_{l=0}^{L-1} \sqrt{2P} W_\lambda[t - (i+l)T_f - t_k(l)T_h] c_k(t) \\ \times P[t - (i+l)T_f - t_k(l)T_h] \cos(2\pi f_c t + \phi_{il}^{(k)}) \quad (2.138)$$

The receiver schematic contrived for detecting the desired signal – which is assumed to correspond to the user of $k = 1$ – is shown in Fig. 2.46, which can be divided into three parts similarly to the schematic of DS/FFH seen in Fig. 2.43. In fact, the third and right most part of Fig. 2.46 representing M -ary orthogonal demodulation is the same as that in Fig. 2.43. By contrast, the first and left-most part of Fig. 2.46 was designed for DS despreading and time-dehopping, while the second part in the middle was incorporated for down-converting the received signal to the base-band, where orthogonal demodulation can be carried out. Referring to Fig. 2.46, the decision variables corresponding to the l th time slot can be written as

$$U_{ml} = \left[\int_{(i+l)T_f + t_1(l)T_h}^{(i+l)T_f + (t_1(l)+1)T_h} r(t) W_m[t - (i+l)T_f - t_1(l)T_h] c_1(t) \right. \\ \left. \times P[t - (i+l)T_f - t_1(l)T_h] \cos(2\pi f_c t) dt \right]^2$$

$$\begin{aligned}
& + \left[\int_{(i+l)T_f+t_1(l)T_h}^{(i+l)T_f+(t_1(l)+1)T_h} r(t) W_m[t - (i + l)T_f - t_1(l)T_h] c_1(t) \right. \\
& \times P[t - (i + l)T_f - t_1(l)T_h] \sin(2\pi f_c t) dt \left. \right]^2
\end{aligned} \tag{2.139}$$

where $m = 0, 1, \dots, M - 1$. Substituting (2.138) into (2.139), it can be shown that (2.139) can be simplified to

$$\begin{aligned}
U_{ml} = & \left[\sum_{k=1}^K \sqrt{\frac{P}{2}} T_h \delta[t_k(l), t_1(l)] \rho_{1k}^l \cos(\phi_{il}^{(k)}) \right]^2 \\
& + \left[- \sum_{k=1}^K \sqrt{\frac{P}{2}} T_h \delta[t_k(l), t_1(l)] \rho_{1k}^l \sin(\phi_{il}^{(k)}) \right]^2 \\
l = & 0, 1, \dots, L - 1
\end{aligned} \tag{2.140}$$

where

$$\begin{aligned}
\rho_{1k}^l = & \frac{1}{T_h} \int_{(i+l)T_f+t_1(l)T_h}^{(i+l)T_f+(t_1(l)+1)T_h} c_k(t) c_1(t) W_\lambda[t - (i + l)T_f - t_k(l)T_h] \\
& \times W_m[t - (i + l)T_f - t_1(l)T_h] dt
\end{aligned} \tag{2.141}$$

Since for the desired user associated with $k = 1$ we have $\delta[t_1(l), t_1(l)] = 1$, $\rho_{11}^l = 1$ for $m = \lambda$ and $\rho_{11}^l = 0$ for $m \neq \lambda$, hence for the case of $m = \lambda$ (2.140) can be rewritten as

$$\begin{aligned}
U_{ml} = & \left[\underbrace{\sqrt{\frac{P}{2}} T_h \cos(\phi_{il}^{(1)}) + \sum_{k=2}^K \sqrt{\frac{P}{2}} T_h \delta[t_k(l), t_1(l)] \rho_{1k}^l \cos(\phi_{il}^{(k)})}_{\text{Multiuser interference}} \right]^2 \\
& + \left[- \underbrace{\sqrt{\frac{P}{2}} T_h \sin(\phi_{il}^{(1)}) - \sum_{k=2}^K \sqrt{\frac{P}{2}} T_h \delta[t_k(l), t_1(l)] \rho_{1k}^l \sin(\phi_{il}^{(k)})}_{\text{Multiuser interference}} \right]^2
\end{aligned} \tag{2.142}$$

where $l = 0, 1, \dots, L - 1$. By contrast, for the cases $m \neq \lambda$ (2.140) can be rewritten as

$$\begin{aligned}
U_{ml} = & \left[\underbrace{\sum_{k=2}^K \sqrt{\frac{P}{2}} T_h \delta[t_k(l), t_1(l)] \rho_{1k}^l \cos(\phi_{il}^{(k)})}_{\text{Multiuser interference}} \right]^2 \\
& + \left[- \underbrace{\sum_{k=2}^K \sqrt{\frac{P}{2}} T_h \delta[t_k(l), t_1(l)] \rho_{1k}^l \sin(\phi_{il}^{(k)})}_{\text{Multiuser interference}} \right]^2
\end{aligned} \tag{2.143}$$

where $l = 0, 1, \dots, L - 1$.

As shown in Fig. 2.46, for each value of l in the range $0 \leq l \leq L - 1$, the largest of the set $\{U_{0l}, U_{1l}, \dots, U_{(M-1)l}\}$ is selected and mapped to $\hat{\lambda}_l$, which assumes integer values in

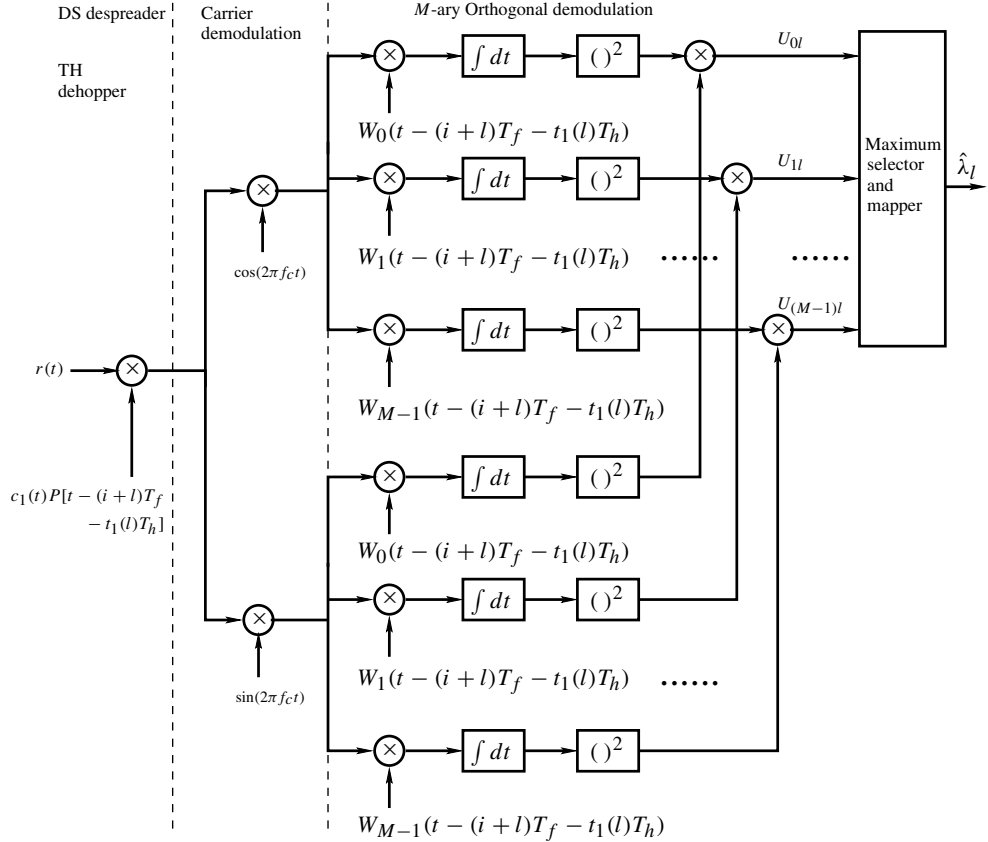


Figure 2.46: Receiver block diagram of DS/FTH using M -ary orthogonal demodulation. The related receiver schematic of DS/FFH using M -ary orthogonal modulation was shown in Fig. 2.43, where the right-most M -ary orthogonal demodulator is seen to be identical to that in this schematic.

the range $[0, M - 1]$. Hence, for the L number of consecutive time slots we have a sequence given by $\{\hat{\lambda}_0, \hat{\lambda}_1, \dots, \hat{\lambda}_{L-1}\}$, which jointly represent an estimate of the transmitted M -ary symbol λ . Therefore, λ can be detected as the symbol that appears most frequently in the set $\{\hat{\lambda}_0, \hat{\lambda}_1, \dots, \hat{\lambda}_{L-1}\}$.

Following the above-mentioned detection principles, readers might like to verify that when the TH patterns of the K number of multiple-access users are orthogonal, i.e. when $\delta[t_k(l), t_1(l)] = 0$, data symbols transmitted by these users can always be detected correctly, provided that no channel impairment, such as noise or interference, contaminate the received signal.

Recall from Section 2.5.2 that in DS/FFH systems the frequencies and the orthogonal time-domain sequences can be either jointly or separately used for carrying the information symbols of a user. Similarly, in DS/FTH systems the time slots used for TH and the orthogonal time-domain sequences can also be either jointly or separately used for conveying a user's

information symbols. Specifically, for a DS/FTH system using M number of time slots per frame and M -number of orthogonal signalling sequences, $(2 \times \log_2 M)$ bits per symbol information can be transmitted by this DS/FTH scheme, where $(\log_2 M)$ bits are signalled by the M number of time slots per frame, while the remaining $(\log_2 M)$ bits are conveyed by the M number of orthogonal signalling sequences with the aid of M -ary orthogonal modulation.

2.7 Summary and Discussion

In this chapter the principles of four basic spread-spectrum schemes and two hybrid spread-spectrum schemes have been explored. The basic spread-spectrum schemes considered include the DS, MC, FH and TH spread-spectrum schemes. Following the basic spread-spectrum schemes, the principles of hybrid DS/FH and hybrid DS/TH have been analysed in detail.

The multiple-access principles have been established in the context of all the spread-spectrum schemes considered. It has been shown that in spread-spectrum communications different users can be distinguished by assigning the users different spreading sequences or hopping patterns, yielding the so-called CDMA. When supporting multiple users, the spread-spectrum-based CDMA systems usually conflict multiuser interference, as a result of the cross-correlation existing among the spreading sequences and hopping patterns. Hence, spread-spectrum-based CDMA systems are usually interference-limited wireless systems, where the number of users supportable is mainly determined by the interference level engendered by the communications users. As will be illustrated in Chapters 6, 7 and 8, in spread-spectrum-based CDMA systems the spectral-efficiency and error performance can usually be significantly enhanced by the use of advanced transmitter preprocessing and/or advanced receiver processing techniques.

In this chapter, two representative hybrid spread-spectrum schemes have been established. In principle, other types of hybrid spread-spectrum scheme can also be designed by combining two or more basic spread-spectrum schemes in similar ways as shown in this chapter.

Chapter 3

Principles of Multicarrier Communications

3.1 Introduction

Orthogonal frequency division multiplexing (OFDM) [27–29] is an efficient parallel data transmission scheme, in which high data rates can be achieved by transmitting a number of orthogonal subcarriers. The *intersymbol interference* (ISI) and *inter-channel interference* in OFDM systems are mitigated by the insertion of guard intervals. Furthermore, code synchronization is made easier by extending symbol periods of conventional serial modems by a factor corresponding to the number of subcarriers. OFDM is a nature parallel data transmission scheme, which transmits OFDM symbols consisting of parallel data symbols with the aid of *serial-to-parallel* (S/P) conversion, instead of transmitting data streams serially. Recently, *code-division multiple-access* (CDMA) systems based on the combination of CDMA schemes and OFDM signalling, which are referred to as multicarrier CDMA systems, have attracted wide attention in the field of wireless communications. This is mainly due to the demand to support high data-rate services in wireless environments characterized by hostile radio channels. These signals can be efficiently modulated and demodulated using *fast Fourier transform* (FFT) devices. These systems also exhibit the attractive feature of high spectral efficiency, since they can operate using a low Nyquist roll-off factor of approximately zero. Hence, OFDM systems can approach the 2 baud/Hz maximum bandwidth efficiency associated with Nyquist sampling [30]. The combination of code division and OFDM can combat the effects of fading channels by spreading signals over several carriers, in order to achieve frequency diversity.

Depending on whether all the subcarriers are activated continuously, *multicarrier CDMA* (MC-CDMA) arrangements can be classified as the non-frequency hopping MC-CDMA and the FH assisted MC-CDMA schemes. The family of non-FH MC-CDMA schemes includes frequency(F)-domain spread MC-CDMA [31–34], subchannel bandlimited multicarrier direct-sequence CDMA (MC DS-CDMA) [35–37], orthogonal multicarrier DS-CDMA [38–42] and multitone DS-CDMA [43–45]. The class of FH assisted multicarrier

CDMA schemes belongs to the extended family of the above multicarrier schemes, which include MC-CDMA using adaptive FH [46], as well as multicarrier DS-CDMA using adaptive subchannel allocation [47, 48] and the subclass of constant-weight code assisted multicarrier DS-CDMA using slow FH [49–52]. The features of the representative members of these system families will be highlighted during our further discourse.

Multicarrier schemes can also be categorized based on their signal-spreading models. Specifically, they can be divided into two main categories. In the first class of schemes, the serial data stream is spread using, say, an N_p -chip, spreading code and then converting into N_p parallel chip sequences with each chip modulating one of N_p different subcarriers. More explicitly, the number of subcarriers is N_p , which equals the number of chips per data symbol. In other words, the rate of the original information bits is first increased by a factor of N_p . This rate increase is then compensated by mapping the N_p chips to N_p subcarriers. Hence, the subcarriers convey the same rate as that of the original information bit sequence, but in the form of chips. Furthermore, although a spreading factor of N_p was applied, the required processing speed is the same as that of the original serial modem, but these are N_p parallel modulators. Since, instead of one carrier, there are now N_p parallel OFDM subcarriers, the spreading operation in this type of MC-CDMA arrangement occurs in the F-domain. This type of system combines the robustness of orthogonal modulation with the flexibility of CDMA schemes [15, 23].

In the second type of MC-CDMA system, the original data stream is first S/P converted into, say U , number of substreams. Then, each substream is spread using a given spreading code in the time (T)-domain, and finally, modulates a different subcarrier with each of the data streams. In this type of MC-CDMA system each subcarrier's signal is similar to that of a conventional single carrier DS-CDMA scheme [41, 53]. For the above reason, the second type of MC-CDMA is usually referred to as *multicarrier DS-CDMA* (MC DS-CDMA). In contrast to the first type of MC-CDMA scheme of [35–37], where the symbol rate is first increased by a factor of N_p , before it is mapped to N_p subcarriers, in the MC DS-CDMA schemes the symbol rate is first reduced by a factor of U after splitting the original bitstream into U substreams. The symbol rate of these U -fold reduced-rate substreams is then increased again by invoking subcarrier-based DS spreading. The first type of MC-CDMA system includes one particular scheme, namely F-domain spread MC-CDMA. Other known multicarrier CDMA schemes belong to the second type.

It can be implied from the first chapter that, in parallel with the FH schemes, *time-hopping* (TH) schemes may also be combined with the OFDM principles, in order to implement so-called TH multicarrier CDMA schemes. Specifically, the TH assisted MC-CDMA does not belong to either of the above-mentioned multicarrier schemes, since it uses neither F-domain nor T-domain spreading. Hence, it should be classified into a third type of multicarrier scheme. Furthermore, in MC DS-CDMA schemes, transmitted information can be spread in the F-domain, in addition to in the T-domain. This type of multicarrier DS-CDMA schemes can be referred to as the time-frequency domain spread MC DS-CDMA [54–56].

It is well-recognized that one of the main implementation disadvantages at the transmitter side of OFDM based multicarrier CDMA systems is the high peak-to-average power ratio (PAPR) [27, 57, 58] of the transmitted signal. Whenever the peak transmitted power is limited by regulatory or implementation constraints – such as the minimum required transmit power or the power efficiency of the amplifier – this has the effect of reducing the average power of the transmitter and limiting the distance range of transmissions. Moreover,

since the multicarrier signal exhibits a high amplitude variation, it is subject to nonlinear distortions inflicted by the power amplifier. This distortion inevitably results in out-of-band emissions and co-channel interference, potentially causing a significant degradation in the system's performance. It can be realized that the high PAPR has more harmful effect on the uplink communications than on the downlink communications, due to the constraint on the transmission power of mobile terminals. Hence, in recent years an alternative multicarrier scheme referred to as single-carrier frequency-division multiple-access (SC-FDMA) [59–64] has been proposed for supporting the uplink transmission.

In this chapter we first establish the principles of OFDM in detail. Then, the communication principles of a range of other multicarrier schemes are analysed. The other multicarrier schemes considered in this chapter include the F-domain spread MC-CDMA in Section 3.3, the SC-FDMA in Section 3.4, the orthogonal MC DS-CDMA in Section 3.5, the multitone DS-CDMA in Section 3.6, the generalized MC DS-CDMA in Section 3.7, the TH/MC-CDMA in Section 3.8 and the time-frequency (TF)-domain spread MC DS-CDMA in Section 3.9. Let us now provide an overview of the OFDM principles.

3.2 Orthogonal Frequency-Division Multiplexing

3.2.1 Modulator

OFDM is a type of multicarrier communications scheme that transmits data symbols in parallel on multiple subcarriers that share the system bandwidth using some form of *frequency-division multiplexing* (FDM). The transmitter block diagram of OFDM systems is in principle represented by Fig. 3.1. Here, the serial data input into the OFDM transmitter is first S/P converted and allocated to M parallel sub-branches, where a_m and b_m represent the data symbols that are allocated to the inphase (I) and quadrature-phase (Q) of the m sub-branch. Following the S/P conversion, each of the M sub-branches is carrier modulated in conjunction with one of the M subcarriers. Finally, these sub-branch signals are added, in order to form a composite transmitted signal. Based on Fig. 3.1 the OFDM signal $s(t)$ can be expressed as

$$\begin{aligned} s(t) &= \sum_{m=0}^{M-1} \Re\{(a_m + jb_m) \exp(j2\pi f_m t)\} \\ &= \sum_{m=0}^{M-1} [a_m \cos(2\pi f_m t) - b_m \sin(2\pi f_m t)] \end{aligned} \quad (3.1)$$

Note that, in Fig. 3.1 the data symbols associated with different sub-branches may be based on different symbol dynamic ranges and do not have to be in the same range. Furthermore, the modulation scheme on each sub-branch may be chosen independent of that used on other sub-branches. The advantages of using independently chosen modulation scheme associated with each sub-branch are explicit. For example, in a frequency selective fading communication environment, some subcarrier signals may yield severer degradation than other subcarrier signals due to the frequency-selective fading. Consequently, the sub-branches with high output *signal-to-noise ratio* (SNR) values may use high-rate modulations,

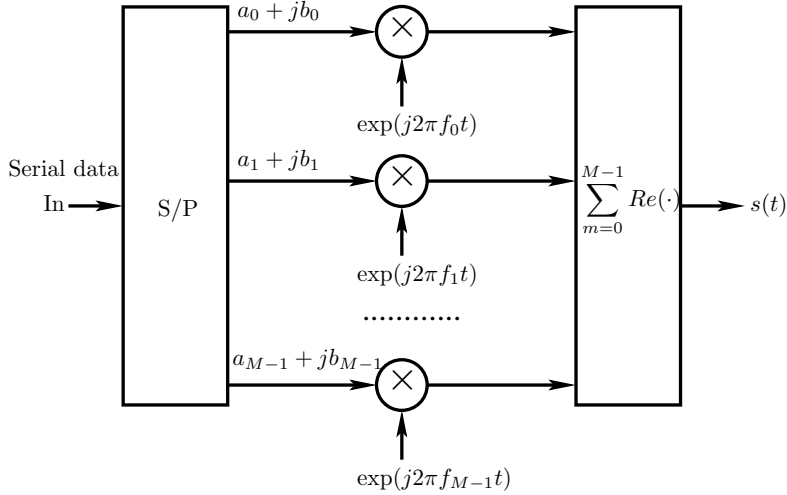


Figure 3.1: Transmitter block diagram in principle for an OFDM system using M number of subcarriers, where $\{a_m, b_m\}$ represent the data symbols that are not, of necessity, the same value.

while those with degraded output SNR values use low-rate modulations or simply cease to transmit data.

As an example, the T-domain subcarrier signals as well as the output OFDM signal are shown in Fig. 3.2, where we assumed that the data input into the in-phase sub-branches are $(a_0, a_1, a_2, a_3, a_4, a_5, a_6, a_7) = (+1 -1 -1 +1 -1 +1 +1 -1)$, while the quadrature-phase sub-branches are switched off, i.e. $(b_0, b_1, b_2, b_3, b_4, b_5, b_6, b_7) = (0, 0, 0, 0, 0, 0, 0, 0)$. Furthermore, in Fig. 3.2 $R_s = 1/T_s$ represents the symbol rate and T_s represents the symbol duration. Figure 3.2 shows that, at any given time instant, the OFDM signal represents the composite signal of $s(t)$, which is constituted by the sum of the $M = 8$ number of subcarrier signals with different frequencies. One of the typical characteristics of the output OFDM signal is that the signal amplitude has a high dynamic range and the peak amplitude value may be significantly higher than the average amplitude value. This high peak-to-average amplitude value in practice requires that the OFDM transmitter is capable of providing a high linear range for signal amplification. Otherwise, the transmitted signal conflicts non-linear distortion, which may substantially degrade the achievable performance.

3.2.2 Modulation Parameters

In Fig. 3.1 we see that an OFDM signal is constituted by M number of subcarriers in conjunction with M number of frequencies. In OFDM systems the M number of subcarrier signals are chosen to be orthogonal to each other, i.e. the subcarrier signals obey the relationship

$$\int_0^{T_s} (a_m + jb_m) \exp(j2\pi f_m t) \times (a_n + jb_n)^* \exp(-j2\pi f_n t) dt = 0 \quad (3.2)$$

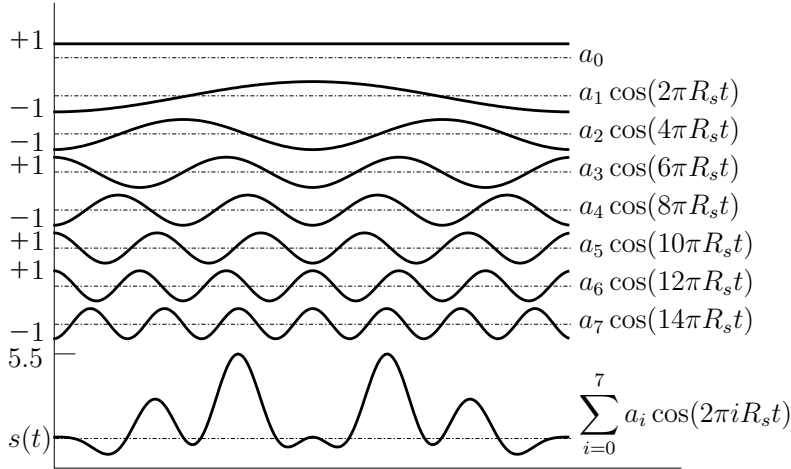


Figure 3.2: Typical appearance of the subcarrier signals and the transmitted signal in an OFDM system, where we assumed that the number of bits per symbol is eight, $R_s = 1/T_s = 1$ and the eight bits transmitted are $(a_0, a_1, a_2, a_3, a_4, a_5, a_6, a_7) = (+1, -1, -1, +1, -1, +1, +1, -1)$.

whenever $m \neq n$, where ‘*’ represents the complex conjugation. Hence, it can be readily worked out that the M number of frequencies should be chosen to satisfy

$$f_m - f_n = \frac{i}{T_s} \quad (3.3)$$

where $i \geq 1$ is an integer. In OFDM systems the common method of obtaining orthogonality of subcarrier signals is to choose their frequency spacing equal to the inverse of the OFDM symbol duration. Hence, the frequency set

$$\left\{ 0, \frac{1}{T_s}, \frac{2}{T_s}, \dots, \frac{M-1}{T_s} \right\} \quad (3.4)$$

can be used for generating an orthogonal subcarrier signal set, resulting in half the spectral main-lobe of two adjacent subcarrier signals overlapping.

Let m_i , where $i = 0, 1, \dots, M-1$, be the number of bits transmitted by the i th subcarrier within a symbol duration. Hence, the total number of bits per OFDM symbol represented is $\sum_{i=0}^{M-1} m_i$. Let T_b be the bit duration of the serial data input to the S/P converter of Fig. 3.1. Hence, the OFDM symbol duration is given by

$$T_s = \left(\sum_{i=0}^{M-1} m_i \right) \times T_b \quad (3.5)$$

3.2.3 Demodulator

The principle of the OFDM demodulator can be understood using Fig. 3.3, which includes $2M$ number of correlators and a parallel-to-serial (P/S) converter. Let us show how we extract

the information symbols a_0 and b_0 from the OFDM signal $s(t)$. Referring to Fig. 3.3 we see that a_0 is obtained by first multiplying the OFDM signal $s(t)$ with $2 \cos(2\pi f_0 t)$ related to the first subcarrier and then integrating the product signal over a symbol time interval. The above process can be expressed as

$$\begin{aligned} & \frac{1}{T_s} \int_0^{T_s} s(t) 2 \cos(2\pi f_0 t) dt \\ &= \frac{1}{T_s} \int_0^{T_s} \sum_{m=0}^{M-1} [a_m \cos(2\pi f_m t) - b_m \sin(2\pi f_m t)] 2 \cos(2\pi f_0 t) dt \\ &= \sum_{m=0}^{M-1} a_m \frac{1}{T_s} \int_0^{T_s} (\cos[2\pi(f_m + f_0)t] + \cos[2\pi(f_m - f_0)t]) dt \\ &\quad - \sum_{m=0}^{M-1} b_m \frac{1}{T_s} \int_0^{T_s} (\sin[2\pi(f_m + f_0)t] + \sin[2\pi(f_m - f_0)t]) dt \end{aligned} \quad (3.6)$$

Since in OFDM systems the subcarrier frequencies are in the form i/T_s , as shown in (3.4), it can be easily shown that in (3.6)

$$\begin{aligned} & \frac{1}{T_s} \int_0^{T_s} \cos[2\pi(f_m + f_0)t] dt = 0 \\ & \frac{1}{T_s} \int_0^{T_s} \cos[2\pi(f_m - f_0)t] dt = \begin{cases} 1 & \text{if } f_m = f_0 \\ 0 & \text{if } f_m \neq f_0 \end{cases} \\ & \frac{1}{T_s} \int_0^{T_s} \sin[2\pi(f_m + f_0)t] dt = 0 \\ & \frac{1}{T_s} \int_0^{T_s} \sin[2\pi(f_m - f_0)t] dt = 0 \end{aligned}$$

Using the above results into (3.6), it can be shown that

$$\frac{1}{T_s} \int_0^{T_s} s(t) 2 \cos(2\pi f_0 t) dt = a_0 \quad (3.7)$$

By referring to Fig. 3.3, the quadrature-phase symbol b_0 carried by the first subcarrier f_0 can be demodulated following the same procedure as described above. Specifically,

$$\frac{1}{T_s} \int_0^{T_s} s(t) \times [-2 \sin(2\pi f_0 t)] dt = b_0 \quad (3.8)$$

Similarly, the data symbols carried by the other subcarriers can be demodulated by following the approaches for demodulating a_0 and b_0 . Finally, all the demodulated symbols associated with the M number of subcarriers are input into the P/S converter, where they are P/S converted to form the serial output data.

The above demodulation process shows that in the OFDM demodulator, no band-pass filters matching the subcarrier frequencies are necessary, provided that the orthogonality of the subcarrier signals can be maintained. This property constitutes one of the advantages of

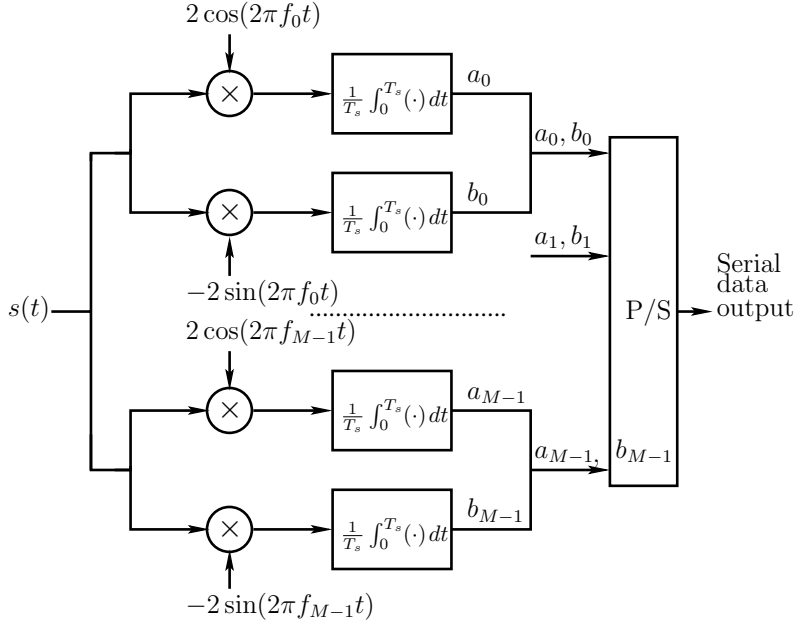


Figure 3.3: Demodulator block diagram in principle for an OFDM system using M number of subcarriers.

using OFDM, since, when the demodulation is free from using subcarrier associated filters, the demodulator's complexity can be significantly reduced. Furthermore, as will be discussed below, in OFDM systems the multicarrier modulation and demodulation can be implemented using *inverse discrete Fourier transform* (IDFT) and *discrete Fourier transform* (DFT) with the aid of the low-complexity *fast Fourier transform* (FFT) techniques. Hence, the complexity of the OFDM transceiver can be further simplified. This constitutes another of the advantages of using OFDM.

3.2.4 Implementation of Multicarrier Modulation/Demodulation

In OFDM-based systems the multicarrier modulation and demodulation can be implemented using IDFT and DFT, respectively, with the aid of the FFT techniques. In this section we demonstrate the relationship between the multicarrier modulation/demodulation and the DFT/IDFT.

The OFDM signal of (3.1) can be rewritten as

$$s(t) = \sum_{m=0}^{M-1} \Re \left\{ (a_m + jb_m) \exp \left(j \frac{2\pi mt}{T_s} \right) \right\} \quad (3.9)$$

$$= \sum_{m=0}^{M-1} \left[a_m \cos \left(\frac{2\pi mt}{T_s} \right) - b_m \sin \left(\frac{2\pi mt}{T_s} \right) \right] \quad (3.10)$$

When we sample the OFDM signal of (3.9) at the time instant of $0, \Delta t, 2\Delta t, \dots, (M-1)\Delta t$, where $\Delta t = T_s/M$, then we obtain a vector $s = [s_0, s_1, \dots, s_{M-1}]^T$, where the superscript of T represents the vector transpose and the n th element of s can be expressed as

$$\begin{aligned} s_n &= s(n\Delta t) \\ &= \sum_{m=0}^{M-1} \Re \left\{ (a_m + jb_m) \exp \left(j \frac{2\pi mn}{M} \right) \right\} \end{aligned} \quad (3.11)$$

$$= \sum_{m=0}^{M-1} \left[a_m \cos \left(\frac{2\pi mn}{M} \right) - b_m \sin \left(\frac{2\pi mn}{M} \right) \right] \quad (3.12)$$

for $n = 0, 1, \dots, M-1$. Observing (3.11) and (3.12) we can see that the vector s represents the real part of the IDFT¹ on the M number of transmitted symbols expressed as $\{S_k = a_k + jb_k\}_{k=0}^{M-1}$, except for a constant of $1/\sqrt{M}$ difference. Hence, when ignoring the constant coefficient, which is related to the transmission power, the elements in the vector s can be expressed as

$$\begin{aligned} s_n &= \Re \{ \text{IDFT}\{a_0 + jb_0, a_1 + jb_1, \dots, a_{M-1} + jb_{M-1}\} \} \\ &= \frac{1}{\sqrt{M}} \sum_{m=0}^{M-1} \left[a_m \cos \left(\frac{2\pi mn}{M} \right) - b_m \sin \left(\frac{2\pi mn}{M} \right) \right], \quad n = 0, 1, \dots, M-1 \end{aligned} \quad (3.15)$$

Since, as indicated in reference [29], the transmitted OFDM signal $s(t)$ can be obtained by applying the elements of s to a low-pass filter at time intervals Δt , we can see that the multicarrier modulation invoked in the OFDM transmitter can be implemented using the IDFT technique. The transmitted signal corresponding to (3.15) can be expressed as

$$s(t) = \frac{1}{\sqrt{M}} \sum_{m=0}^{M-1} \left[a_m \cos \left(\frac{2\pi mt}{T_s} \right) - b_m \sin \left(\frac{2\pi mt}{T_s} \right) \right] \quad (3.16)$$

Let us now turn to consider the multicarrier demodulation in OFDM systems.

When a distortionless channel is considered, the OFDM signal appearing at the demodulator's input is the same as (3.16). Because only the real part of the IDFT has been transmitted, it is necessary [29] to sample at intervals $\Delta t/2 = T_s/2M$. The samples can be expressed as the received signal twice the rate of $1/\Delta t$, implying

$$\begin{aligned} s_n &= s \left(\frac{n\Delta t}{2} \right) \\ &= \frac{1}{\sqrt{M}} \sum_{m=0}^{M-1} \left[a_m \cos \left(\frac{2\pi mn}{2M} \right) - b_m \sin \left(\frac{2\pi mn}{2M} \right) \right], \quad n = 0, 1, \dots, 2M-1 \end{aligned} \quad (3.17)$$

¹Let $\{x(0), x(1), \dots, x(M-1)\}$ be an M -length sequence. Then, the DFT and IDFT can be defined as

$$\text{DFT: } X(k) = \frac{1}{\sqrt{M}} \sum_{m=0}^{M-1} x(m) \exp \left(-j \frac{2\pi km}{M} \right), \quad k = 0, 1, \dots, M-1 \quad (3.13)$$

$$\text{IDFT: } x(m) = \frac{1}{\sqrt{M}} \sum_{k=0}^{M-1} X(k) \exp \left(j \frac{2\pi km}{M} \right), \quad m = 0, 1, \dots, M-1 \quad (3.14)$$

Considering $\cos \alpha = (e^{j\alpha} + e^{-j\alpha})/2$ and $\sin \alpha = (e^{j\alpha} - e^{-j\alpha})/2j$, (3.17) can be expressed as

$$s_n = \frac{1}{\sqrt{M}} \sum_{m=0}^{M-1} \left[\left(\frac{a_m}{2} - \frac{b_m}{2j} \right) \exp\left(j \frac{2\pi mn}{2M}\right) + \left(\frac{a_m}{2} + \frac{b_m}{2j} \right) \exp\left(-j \frac{2\pi mn}{2M}\right) \right]$$

$$n = 0, 1, \dots, 2M - 1 \quad (3.18)$$

The DFT in the context of the above sequence $\{s_n\}_{n=0}^{2M-1}$ can be expressed as

$$S_k = \frac{1}{\sqrt{2M}} \sum_{n=0}^{2M-1} s_n \exp\left(-j \frac{2\pi nk}{2M}\right)$$

$$= \frac{1}{\sqrt{2}} \frac{1}{M} \sum_{n=0}^{2M-1} \sum_{m=0}^{M-1} \left[\left(\frac{a_m}{2} - \frac{b_m}{2j} \right) \exp\left(j \frac{2\pi mn}{2M}\right) + \left(\frac{a_m}{2} + \frac{b_m}{2j} \right) \exp\left(-j \frac{2\pi mn}{2M}\right) \right] \exp\left(-j \frac{2\pi nk}{2M}\right)$$

$$= \frac{1}{\sqrt{2}} \frac{1}{M} \sum_{n=0}^{2M-1} \sum_{m=0}^{M-1} \left[\left(\frac{a_m}{2} - \frac{b_m}{2j} \right) \exp\left(j \frac{2\pi n(m-k)}{2M}\right) + \left(\frac{a_m}{2} + \frac{b_m}{2j} \right) \exp\left(-j \frac{2\pi n(m+k)}{2M}\right) \right]$$

$$k = 0, 1, 2, \dots, 2M - 1 \quad (3.19)$$

Using the equality

$$\frac{1}{2M} \sum_{n=0}^{2M-1} \exp\left(j \frac{2\pi mn}{2M}\right) = \begin{cases} 1, & \text{if } m = 0, \pm 2M, \pm 4M, \dots \\ 0, & \text{otherwise} \end{cases} \quad (3.20)$$

we obtain that

$$S_k = \sum_{n=0}^{2M-1} s_n \exp\left(-j \frac{2\pi nk}{2M}\right)$$

$$= \begin{cases} \sqrt{2}a_0, & k = 0 \\ \frac{1}{\sqrt{2}}(a_k - jb_k), & k = 1, 2, \dots, M - 1 \\ \text{irrelevant}, & k \geq M \end{cases} \quad (3.21)$$

which shows that, except for the case corresponding to $k = 0$, the real part and the image part of the DFT's outputs at $k = 1, 2, \dots, M - 1$ represent the transmitted symbols on the in-phase and the quadrature-phase branches after ignoring the constant $1/\sqrt{2}$. Therefore, when we assume that $a_0 = b_0$ at the transmitter, the transmitted symbols in OFDM systems can be recovered with the aid of the DFT operation at the receiver. Hence, the OFDM signals can be demodulated by using the DFT techniques.

It is well known that [65] the DFT and IDFT can be implemented using the computationally efficient algorithms, known collectively as FFT algorithms, which result in that the OFDM transceivers being implemented with relatively low complexity.

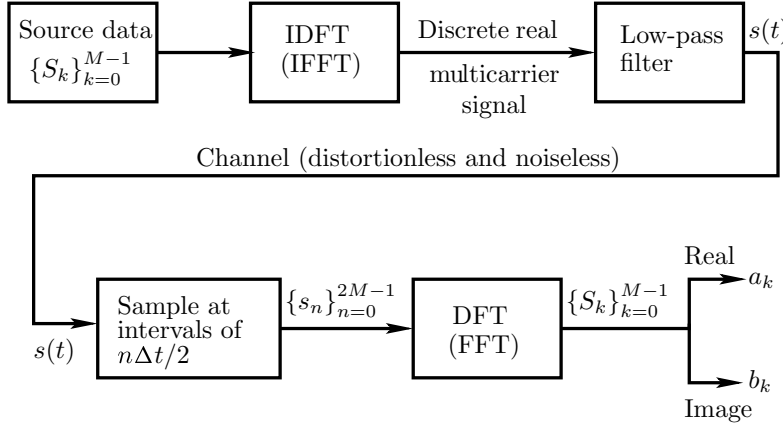


Figure 3.4: Modulation and demodulation block diagram in OFDM systems, where the multicarrier modulation is implemented by IDFT, while the multicarrier demodulation is implemented by DFT.

These principles have been analysed in detail in [29]. The block diagram of Fig. 3.4 summarizes the modulation and demodulation procedures in OFDM systems, as described above. In Fig. 3.4 the multicarrier modulation and demodulation are completed with the aid of IDFT (IFFT) and DFT (FFT), respectively.

The multicarrier modulation/demodulation scheme described above has the properties that (a) at the transmitter side only the real part of the IDFT output is transmitted, and (b) at the receiver the received signal is sampled twice as quickly as the expected interval of Δt and $2M$ samples are used for recovering the transmitted M symbols. In [66] another multicarrier modulation/demodulation scheme is provided, which uses M subcarriers to transmit $M/2$ symbols per DFT symbol and the receiver uses M samples to recover the transmitted symbols.

The proposed modulation/demodulation scheme in [66] makes use of the property of the DFT [65] that if the T-domain sequence $\{s(n)\}$ is real, then the DFT on $\{s(n)\}$ yields an F-domain sequence $\{x(k)\}$, which satisfies $x(M-k) = x(k)$. Now let us assume that M is even and let the $M/2$ symbols to be transmitted in the F-domain be arranged as

$$x(k): a_0, (a_1 + jb_1), \dots, (a_{(M/2)-1} + jb_{(M/2)-1}), b_0, a_{(M/2)-1} - jb_{(M/2)-1}, \dots, (a_1 - jb_1) \quad (3.22)$$

where the 0th and the $(M/2)$ th symbols are real symbols, taken from the real and image parts of the complex symbol $(a_0 + jb_0)$, while the other $(M/2 - 1)$ are complex symbols. Then, the IDFT on the sequence of (3.22) can be expressed as

$$s(n) = \frac{1}{\sqrt{M}} \sum_{k=0}^{M-1} x(k) \exp\left(j \frac{2\pi nk}{M}\right), \quad n = 0, 1, \dots, M-1 \quad (3.23)$$

Substituting (3.22) into (3.23), we have that

$$\begin{aligned} s(n) = & \frac{1}{\sqrt{M}} \left\{ a_0 + (a_1 + jb_1) \exp\left(j \frac{2\pi n}{M}\right) + (a_2 + jb_2) \exp\left(j \frac{2\pi n 2}{M}\right) \right. \\ & + \cdots + (a_{(M/2)-1} + jb_{(M/2)-1}) \exp\left(j \frac{2\pi n ((M/2) - 1)}{M}\right) \\ & + b_0 \exp\left(j \frac{2\pi n M/2}{M}\right) + \cdots + (a_{(M/2)-1} - jb_{(M/2)-1}) \exp\left(j \frac{2\pi n ((M/2) + 1)}{M}\right) \\ & \left. + (a_2 - jb_2) \exp\left(j \frac{2\pi n (M - 2)}{M}\right) + (a_1 - jb_1) \exp\left(j \frac{2\pi n (M - 1)}{M}\right) \right\} \end{aligned} \quad (3.24)$$

After the simplification, it gives

$$\begin{aligned} s(n) = & \frac{2}{\sqrt{M}} \left\{ a_0 + b_0 \cos(\pi n) + \sum_{k=1}^{M/2-1} \left[a_k \cos\left(\frac{2\pi nk}{M}\right) - b_k \sin\left(\frac{2\pi nk}{M}\right) \right] \right\} \\ n = & 0, 1, \dots, M - 1 \end{aligned} \quad (3.25)$$

Explicitly, $\{s(n)\}$ of (3.25) is a real sequence, which can be transmitted directly over a real channel without requiring the real part of an IDFT output to be taken.

At the receiver, DFT can be carried out on the M -length sampled sequence, in order to recover the transmitted sequence $\{x(k)\}$ of (3.22). When without fading and/or background noise, the transmitted information can be recovered by computing the first $M/2 + 1$ items of $\{x(k)\}$. When the communications channel is non-ideal, the whole M items related to $\{x(k)\}$ can be computed. In this case, except for the 0th and the $(M/2)$ th symbols, any of the other symbols can be decided based on two observations that can thus provide a two-order diversity for making the decisions. Furthermore, we can let $a_0 = b_0$, and then the 0th symbol can also be decided based on two observations and a diversity order of two can also be achieved.

Note that for the sake of convenience of mathematical description, the complex baseband equivalent processing and transmission can be applied. In this case, let

$$\mathbf{x} = [x(0), x(1), \dots, x(M - 1)]^T \quad (3.26)$$

represent a block of data symbols to be transmitted. When carrying out the IDFT on \mathbf{x} , the IDFT outputs can be expressed in matrix form as

$$\mathbf{s} = \mathcal{F}^H \mathbf{x} \quad (3.27)$$

where

$$\mathbf{s} = [s(0), s(1), \dots, s(M - 1)]^T \quad (3.28)$$

and \mathcal{F} is the DFT matrix given by

$$\mathcal{F} = \frac{1}{\sqrt{M}} \begin{bmatrix} 1 & 1 & \dots & 1 \\ 1 & \exp\left(-j \frac{2\pi}{M}\right) & \dots & \exp\left(-j \frac{2\pi(M-1)}{M}\right) \\ \vdots & \vdots & \ddots & \vdots \\ 1 & \exp\left(-j \frac{2\pi(M-1)}{M}\right) & \dots & \exp\left(-j \frac{2\pi(M-1)(M-1)}{M}\right) \end{bmatrix} \quad (3.29)$$

The DFT matrix has the property

$$\mathcal{F}\mathcal{F}^H = \mathcal{F}^H\mathcal{F} = \mathbf{I}_M \quad (3.30)$$

Hence, the DFT on \mathbf{s} of (3.27) can be readily obtained, which is

$$\mathcal{F}\mathbf{s} = \mathcal{F}\mathcal{F}^H\mathbf{x} = \mathbf{x} \quad (3.31)$$

which recovers \mathbf{x} .

Let us now consider various multicarrier CDMA arrangements.

3.3 Frequency-Domain Spread Multicarrier CDMA

3.3.1 Transmitted Signal

The F-domain spread MC-CDMA is also referred to as the spreading-assisted OFDM. Figure 3.5 shows the transmitter diagram of the multicarrier CDMA (MC-CDMA) scheme associated with using F-domain spreading [31, 33, 34, 67]. As shown in Fig. 3.5, at the transmitter of the MC-CDMA the input serial data is first S/P converted into q substreams indicated in the figure as $\{b_i^{(k)}\}_{i=1}^q$. Hence the symbol duration of the transmitted MC-CDMA signal is given by $T_s = qT_b$, where T_b represents the bit duration of the original serial data stream before the S/P conversion. After the S/P conversion, the MC-CDMA transmitter spreads each of the data substreams over N_p subcarriers using the k th user's spreading code of $\{c_k[0], c_k[1], \dots, c_k[N_p - 1]\}$ in the F-domain. Following the usually physical interpretation associated with OFDM systems the modulation process is viewed as mapping the original information bits to the individual subcarriers in the F-domain, before IFFT-based modulation is used for transforming the F-domain signal to the T-domain. Hence this class of MC-CDMA systems are said to employ spreading. According to Fig. 3.5 the MC-CDMA system transmits N_p chips of a data symbol in parallel on N_p different subcarriers, one chip per subcarrier, where N_p is the total number of chips per data bit or the processing gain. Hence, the chip duration in the concerned MC-CDMA scheme is the same as the symbol duration T_s of the transmitted MC-CDMA signal. With reference to Fig. 3.5 the k th MC-CDMA user's transmitted signal can be expressed as:

$$s_k(t) = \sqrt{\frac{2P}{N_p}} \sum_{i=1}^q \sum_{j=1}^{N_p} b_i^{(k)}(t) c_k[j-1] \cos(2\pi f_{ij} t + \phi_{ij}^{(k)}) \quad (3.32)$$

where P represents the transmitted power per bit, N_p is the number of subcarriers invoked for spreading one of the q bits. Therefore, the total number of subcarriers required by the MC-CDMA scheme is qN_p . In (3.32) $\{c_k[0], c_k[1], \dots, c_k[N_p - 1]\}$ is the spreading code assigned to the k th user, and $\{f_{ij}, j = 1, 2, \dots, N_p; i = 1, 2, \dots, q\}$ are the subcarrier frequencies. Furthermore, in (3.32) $b_i^{(k)}(t)$ represents the i th binary data substream of user k , $b_i^{(k)}(t) = \sum_{n=-\infty}^{\infty} b_i^{(k)}[n] P_{T_s}(t - nT_s)$, where $b_i^{(k)}[n]$ is usually assumed to be a random variable taking the value of $+1$ or -1 with equal probability, while $P_{T_s}(t)$ represents the rectangular waveform defined as $P_{T_s}(t) = 1$, if $0 \leq t \leq \tau$, and zero otherwise. Finally, $\{\phi_{ij}^{(k)}\}$ in (3.32) is the random phase introduced by the carrier modulation, which is assumed to be uniformly distributed in $[0, 2\pi]$.

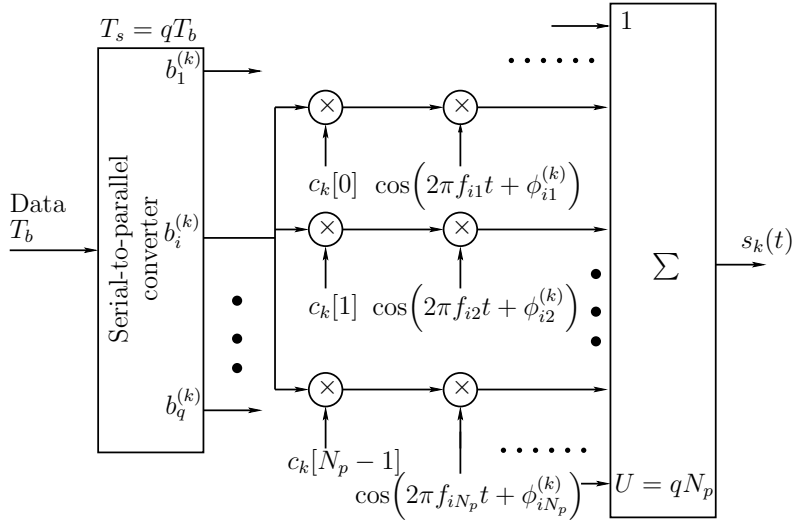


Figure 3.5: The transmitter schematic of the MC-CDMA system using F-domain spreading and serial-to-parallel data conversion.

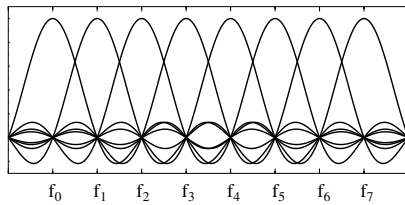


Figure 3.6: Spectrum of the frequency-domain spread MC-CDMA signal.

3.3.2 Modulation Parameters

The spectrum of the transmitted MC-CDMA signal in the F-domain spread MC-CDMA system is shown in Fig. 3.6, where we assume that the MC-CDMA system has eight subcarriers and that all the chip values of the spreading code of $\{c_k[0], c_k[1], \dots, c_k[N_p - 1]\}$ are $+1$. In this MC-CDMA system the subcarrier frequencies are chosen so that the subcarrier signals are orthogonal to each other. Hence, the subcarrier frequencies satisfy the following condition

$$\int_0^{T_s} \cos(2\pi f_i t + \phi_i) \cdot \cos(2\pi f_j t + \phi_j) dt = 0, \quad \text{for } i \neq j \quad (3.33)$$

where T_s is the symbol duration. Therefore, the minimum spacing Δ between two adjacent subcarriers satisfies $\Delta = 1/T_s$, which is a widely used assumption [31, 33, 34, 67] and it is also the case in Fig. 3.6, where $f_n = f_0 + n/T_s$ for $n = 0, 1, \dots, 7$.

Let

$$\{f_{ij}\} = \begin{pmatrix} f_{11} & f_{12} & \dots & f_{1N_p} \\ f_{21} & f_{22} & \dots & f_{2N_p} \\ \vdots & \vdots & \ddots & \vdots \\ f_{q1} & f_{q2} & \dots & f_{qN_p} \end{pmatrix} \quad (3.34)$$

be the subcarrier frequency set in the F-domain spread MC-CDMA system, where the frequencies arranged according to

$$f_{ij} = f_0 + \frac{1}{T_s}[(i-1) + (j-1)q], \quad i = 1, 2, \dots, q; \quad j = 1, 2, \dots, N_p \quad (3.35)$$

Hence, according to (3.35) each column of (3.34) represents q number of successive subcarriers, while the minimum spacing between two subcarriers from the same row is q/T_s . According to Fig. 3.5, the subcarrier frequencies modulating the same data bit are from the same row of the matrix in equation (3.34), and these subcarriers are sufficiently separated in the F-domain in order to avoid correlated fading.

According to Fig. 3.6 and the characteristics of the MC-CDMA signals of (3.32), if we assume that the frequency spacing, Δ , between two adjacent subcarriers is set to be $\Delta = 1/T_s$ associated with 50% spectral overlap, then we can find that the bandwidth required by the MC-CDMA system is $(qN_p + 1) \cdot 1/T_s$. However, when the MC-CDMA systems having qN_p non-overlapping subcarriers are considered, a total bandwidth of $qN_p \cdot 2/T_s$ is then required. The spectral gain of a multicarrier system is defined as the ratio between the bandwidth required by the multicarrier system using non-overlapping subcarriers and the actual bandwidth required by the corresponding multicarrier system. Hence, the spectral gain of the F-domain spread MC-CDMA system using the subcarrier frequency spacing of $\Delta = 1/T_s$ is given by

$$SG = \frac{qN_p(2/T_s)}{(qN_p + 1)(1/T_s)} \quad (3.36)$$

which approaches two, as the product qN_p increases. Thus, this MC-CDMA system exhibits an increased processing gain given by $N_p \approx 2N$, as explained by the 50% overlap of the main lobes of adjacent MC-CDMA subcarrier spectra, where $N = T_b/T_{c1}$ is the spreading gain of the single-carrier DS-CDMA benchmarker, which occupies the same amount of bandwidth as the F-domain spread MC-CDMA system using $q = 1$.

In F-domain spread MC-CDMA systems, we usually assume that frequency non-selective fading is encountered by each subcarrier signal. Hence, the following condition is satisfied

$$1/T_s \ll (\Delta B)_c \quad (3.37)$$

where $(\Delta B)_c$ represents the coherence bandwidth of the wireless channel [2]. The reciprocal of $(\Delta B)_c$ is a measure of the multipath delay spread of the channel, which is denoted by T_m , $T_m \approx 1/(\Delta B)_c$. In order to guarantee independent fading of the subcarrier signals carrying chips of the same data bit, the fading coherence bandwidth in the F-domain should not span more than q number of successive subcarriers, i.e. the following condition is required to be satisfied by the subcarrier signals.

$$(\Delta B)_c \ll q/T_s \quad (3.38)$$

The conditions of equation (3.37) and equation (3.38), i.e. $1/T_s \ll (\Delta B)_c \ll q/T_s$ imply that the modulated subcarriers having transmission bandwidth of $1/T_s$ do not experience significant dispersion.

However, if the conditions of $1/T_s \ll (\Delta B)_c \ll q/T_s$ cannot be satisfied, the system model of Fig. 3.5 can be modified, in order to satisfy this condition. Specifically, if $1/T_s \ll (\Delta B)_c$ cannot be satisfied, we can decrease the term $1/T_s$ by transmitting more bits per symbol, i.e. by increasing the value of q in Fig. 3.5. By contrast, if the condition of $(\Delta B)_c \ll q/T_s$ cannot be satisfied, the independence between the adjacent subcarriers conveying the same data bit can be further guaranteed by incorporating sufficient interleaving at the cost of an increased delay. For example, assuming that the first N_p symbols, i.e. $= N_p q$ bits, emitted by the source modulate the $N_p q$ subcarriers in the first time interval, where each symbol is modulated by the subcarrier frequencies from the same column of equation (3.34), in the second time interval, the same N_p symbols modulate the $N_p q$ subcarriers, but cyclically shift by one symbol. Similarly, in the i th interval, $1 \leq i \leq N_p$, the N_p symbols after the $(i - 1)$ th cyclic shift modulate the $N_p q$ subcarriers. At the receiver, a de-interleaver is employed to recover the original ordering of the symbols. However, interleaving techniques can only be used for the transmission of delay-insensitive data.

3.3.3 Correlation Receiver

Assume that there are K asynchronous CDMA users in the system communicating with the base station using the MC-CDMA scheme. We assume that all the users use the same q and N_p values. The average power received from each user at the base station is also assumed to be the same, i.e. perfect power control is assumed. Consequently, the received signal at the base station can be expressed as

$$r(t) = \sum_{k=1}^K \sum_{i=1}^q \sum_{j=1}^{N_p} \sqrt{\frac{2P}{N_p}} \alpha_{ij}^{(k)} b_i^{(k)} (t - \tau_k) c_k[j - 1] \cos(2\pi f_{ij} t + \varphi_{ij}^{(k)}) + n(t) \quad (3.39)$$

where $\varphi_{ij}^{(k)} = \phi_{ij}^{(k)} + \psi_{ij}^{(k)} - 2\pi f_{ij} \tau_k$ and the random phase $\psi_{ij}^{(k)}$ corresponds to the subcarrier frequency f_{ij} of user k , which was introduced by the channel. The phase $\varphi_{ij}^{(k)}$ is usually assumed to be a random variable uniformly distributed in $[0, 2\pi]$. In (3.39), τ_k is the misalignment of user k with respect to the reference user – we assumed that for, $k = 1$, $\tau_1 = 0$ – at the receiver, which is assumed to be i.i.d for different k values and uniformly distributed in $[0, T_s]$. Furthermore, $\alpha_{ij}^{(k)}$ represents the amplitude attenuation due to the channel, which is also a random variable. Finally, in (3.39) $n(t)$ is the *additive white Gaussian noise* (AWGN) with zero mean and double-sided power spectral density (PSD) of $N_0/2$.

The receiver structure for the F-domain spread MC-CDMA scheme in the context of the first user ($k = 1$) is shown in Fig. 3.7, where the superscripts or subscripts denoting the reference user are omitted. In this MC-CDMA receiver each of the q received bits is recovered by detecting the N_p chips of the corresponding spreading code, in a sense, in the F-domain. Therefore the receiver can always make use of all the received signal energy of an N_p -chip code scattered in the F-domain. This is the main advantage of the F-domain spread MC-CDMA scheme of Figures 3.5 and 3.7 over other multicarrier CDMA

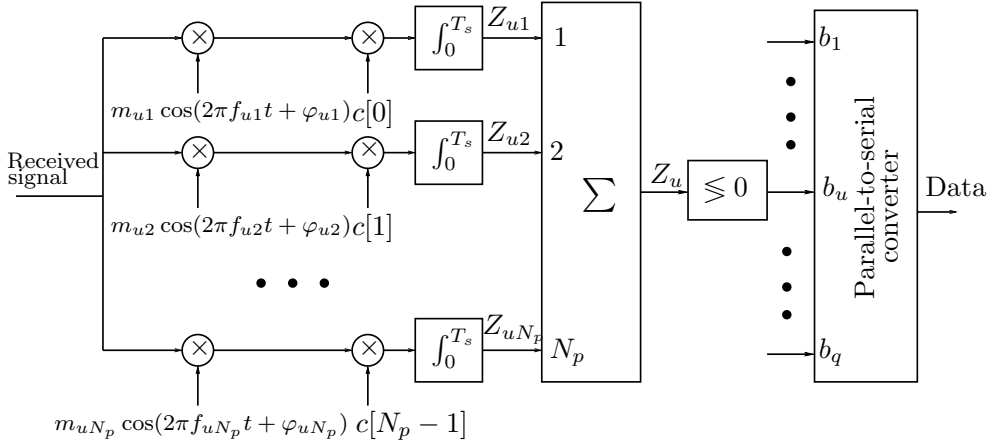


Figure 3.7: The correlation receiver block diagram of the MC-CDMA system using frequency-domain spreading for the reference user.

schemes [23]. However, in a frequency selective fading channel different subcarriers may encounter different amplitude attenuations and phase shifts, which can consequently result in destroying the orthogonality of the subcarriers and leading to interchannel interference. There are many combining and detection techniques that can be employed by the F-domain spread MC-CDMA receiver, in order efficiently to exploit the received signal energy [23]. One of the most common approaches is *maximal ratio combining* (MRC), where the subcarrier signals' weighting factors, m_{ui} , $i = 1, 2, \dots, N_p$ in Fig. 3.7, are computed as the complex conjugate of the specific received subcarrier signal's envelope. This approach minimizes the bit-error rate (BER), as long as a single-user system is considered.

For the coherent correlator detector shown in Fig. 3.7, the decision variable Z_u of the 0th data bit in the u th data substream for the reference user can be expressed as

$$Z_u = \sum_{v=1}^{N_p} Z_{uv} \quad (3.40)$$

$$Z_{uv} = \int_0^{T_s} r(t)c[v-1]m_{uv} \cos(2\pi f_{uv}t + \varphi_{uv}) dt \quad (3.41)$$

where m_{uv} is a parameter determining which type of combining model of the chips belonging to the same data bit is used. Depending on the choice of $\{m_{uv}, v = 1, 2, \dots, N_p\}$, there are two ways of combining the chips of the same data bit; namely MRC, which corresponds to setting $m_{uv} = \alpha_{uv}$, $v = 1, 2, \dots, N_p$, and *equal gain combining* (EGC), which, by contrast, sets $m_{uv} = 1$ for $v = 1, 2, \dots, N_p$.

Substituting equation (3.39) into equation (3.41), the variable Z_{uv} can be simplified to

$$Z_{uv} = \sqrt{\frac{P}{2N_p}} T_s \left[D_{uv} + \sum_{k=2}^K I_1^{(k)} + \sum_{k=2}^K \underbrace{\sum_{i=1}^q \sum_{j=1}^{N_p} I_2^{(k)}}_{j \neq v \text{ for } i=u} + \eta_{uv} \right] \quad (3.42)$$

where D_{uv} is the desired term given by

$$D_{uv} = \alpha_{uv} m_{uv} b_u \quad (3.43)$$

and b_u is the 0th data bit in the u th substream of the reference user, which is transmitted by the (uv) th subcarrier associated with $v = 1, 2, \dots, N_p$. Due to the orthogonality of the subcarrier signals associated with the same user, no self-interference is inflicted by the reference signal to the v th subcarrier of the u th data stream. The multiuser interference imposed by user k can be divided into two terms. The first term is constituted by the subcarrier signal having the same subcarrier frequency, f_{uv} , as the branch considered. This term is $I_1^{(k)}$ in equation (3.42), which can be expressed as

$$\begin{aligned} I_1^{(k)} &= \left(\sqrt{\frac{P}{2N_p}} T_s \right)^{-1} \int_0^{T_s} \sqrt{\frac{2P}{N_p}} \alpha_{uv}^{(k)} b_u^{(k)}(t - \tau_k) c_k[v-1] \cos(2\pi f_{uv} t + \varphi_{uv}^{(k)}) \\ &\quad \times c[v-1] m_{uv} \cos(2\pi f_{uv} t + \varphi_{uv}) dt \\ &= \frac{\alpha_{uv}^{(k)} m_{uv} \cos \theta_{uv}^{(k)}}{T_s} [b_u^{(k)}[-1] c_k[v-1] c[v-1] \tau_k + b_u^{(k)}[0] c_k[v-1] c[v-1] (T_s - \tau_k)] \end{aligned} \quad (3.44)$$

where $\theta_{uv}^{(k)} = \varphi_{uv}^{(k)} - \varphi_{uv}$, while $b_u^{(k)}[-1]$ and $b_u^{(k)}[0]$ represents the previous and current transmitted binary bits, respectively, by user k . The second term of the multiuser interference imposed by user k is the result of the other subcarrier signals associated with $\{f_{ij}, i = 1, 2, \dots, q; j = 1, 2, \dots, N_p; j \neq v \text{ for } i = u\}$. The interference, $I_2^{(k)}$, arising from the subcarrier signal associated with the frequency f_{ij} of user k can be expressed as

$$\begin{aligned} I_2^{(k)} &= \left(\sqrt{\frac{P}{2N_p}} T_s \right)^{-1} \int_0^{T_s} \sqrt{\frac{2P}{N_p}} \alpha_{ij}^{(k)} b_i^{(k)}(t) c_k[j-1] \cos(2\pi f_{ij} t + \varphi_{ij}^{(k)}) \\ &\quad \times c[v-1] m_{uv} \cos(2\pi f_{uv} t + \varphi_{uv}) dt \\ &= \frac{\alpha_{uv}^{(k)} m_{uv}}{T_s} [b_i^{(k)}[-1] R_{ij}^{(k)}(\tau_k, \theta_{ij}^{(k)}) + b_i^{(k)}[0] \hat{R}_{ij}^{(k)}(\tau_k, \theta_{ij}^{(k)})] \end{aligned} \quad (3.45)$$

where, again, $b_i^{(k)}[-1]$ and $b_i^{(k)}[0]$ represents the previous and current binary bits transmitted by the (ij) th subcarrier of user k , $R_{ij}^{(k)}(\tau_k, \theta_{ij}^{(k)})$ and $\hat{R}_{ij}^{(k)}(\tau_k, \theta_{ij}^{(k)})$ are chip-partial cross-correlation functions defined as

$$R_{ij}^{(k)}(\tau_k, \theta_{ij}^{(k)}) = \int_0^{\tau_k} c_k[j-1] c[v-1] \cos[2\pi(f_{ij} - f_{uv})t + \theta_{ij}^{(k)}] dt, \quad (3.46)$$

$$\hat{R}_{ij}^{(k)}(\tau_k, \theta_{ij}^{(k)}) = \int_{\tau_k}^{T_s} c_k[j-1] c[v-1] \cos[2\pi(f_{ij} - f_{uv})t + \theta_{ij}^{(k)}] dt \quad (3.47)$$

and $\theta_{ij}^{(k)} = \varphi_{ij}^{(k)} - \varphi_{uv}$. Considering equation (3.35), equation (3.46) and equation (3.47) can be written as

$$\begin{aligned} R_{ij}^{(k)}(\tau_k, \theta_{ij}^{(k)}) &= \int_0^{\tau_k} c_k[j-1]c[v-1] \cos\left[\frac{2\pi[(i-u)+(j-v)q]t}{T_s} + \theta_{ij}^{(k)}\right] dt \\ &= \frac{T_s c_k[j-1]c[v-1]}{2\pi[(i-u)+(j-v)q]} \left\{ \sin\left[\frac{2\pi[(i-u)+(j-v)q]\tau_k}{T_s} + \theta_{ij}^{(k)}\right] - \sin\theta_{ij}^{(k)} \right\} \\ &= c_k[j-1]c[v-1] \text{sinc}\left[\frac{\pi[(i-u)+(j-v)q]\tau_k}{T_s}\right] \\ &\quad \times \cos\left[\frac{\pi[(i-u)+(j-v)q]\tau_k}{T_s} + \theta_{ij}^{(k)}\right] \tau_k \end{aligned} \quad (3.48)$$

$$\begin{aligned} \hat{R}_{ij}^{(k)}(\tau_k, \theta_{ij}^{(k)}) &= \int_{\tau_k}^{T_s} c_k[j-1]c[v-1] \cos\left[\frac{2\pi[(i-u)+(j-v)q]t}{T_s} + \theta_{ij}^{(k)}\right] dt \\ &= \frac{T_s c_k[j-1]c[v-1]}{2\pi[(i-u)+(j-v)q]} \left\{ \sin\theta_{ij}^{(k)} - \sin\left[\frac{2\pi[(i-u)+(j-v)q]\tau_k}{T_s} + \theta_{ij}^{(k)}\right] \right\} \\ &= -R_{ij}^{(k)}(\tau_k, \theta_{ij}^{(k)}) \end{aligned} \quad (3.49)$$

where $(i-u)+(j-v)q \neq 0$. Finally, η_{uv} in (3.42) is the noise term engendered by the AWGN $n(t)$, which can be expressed as

$$\eta_{uv} = \left(\sqrt{\frac{P}{2N_p}} T_s \right)^{-1} \int_0^{T_s} n(t) c[v-1] m_{uv} \cos(2\pi f_{uv} t + \varphi_{uv}) dt \quad (3.50)$$

which is a Gaussian random variable distributed with zero mean and a variance of $N_p m_{uv}^2 N_0 / 2E_b$ for a given value of m_{uv} , where $E_b = P T_s$ represents the transmitted energy per bit.

Finally, based on the decision variable of Z_u of (3.40), where $u = 1, 2, \dots, q$, the data bit b_u transmitted by the u th substream can be decided as the sign of the decision variable of Z_u , i.e. $b_u = \text{sign}(Z_u)$. It can be shown that the transmitted data bits can be detected correctly, provided that the multiuser interference and the background noise terms in (3.42) are sufficiently low. Furthermore, if $\{\alpha_{uv}\}_{v=1}^{N_p}$ in (3.43) can be modelled as independent variables, i.e. if the subcarrier signals conveying the same data bit experience independent fading, a diversity order of N_p can then be achieved, which is indicated by the N_p -order of sum in (3.40).

In this section a MC-CDMA scheme using F-domain spreading has been considered, which uses no T-domain spreading. The F-domain spread MC-CDMA is sometimes also interpreted as the F-domain direct-sequence (DS) CDMA scheme, since, at the transmitter, the PN sequences are directly multiplied with the transmitted data. In the following sections, except Section 3.4 and Section 3.8, all the multicarrier schemes concerned will include the T-domain DS spreading. Hence, these types of multicarrier CDMA scheme are sometimes broadly referred to as the *multicarrier DS-CDMA* (MC DS-CDMA) [38, 39, 41, 68]. Let us now consider the SC-FDMA scheme.

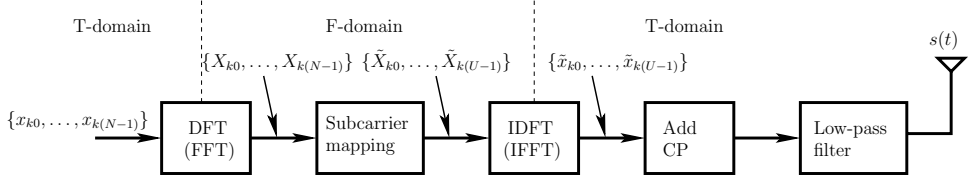


Figure 3.8: Transmitter schematic for the k th user supported by the SC-FDMA uplink.

3.4 Single-Carrier Frequency-Division Multiple Access

As shown in Fig. 3.2, one of the typical characteristics of the OFDM/MC signals is that the amplitude of the transmitted signal may have a high dynamic range, or, in other words, the peak amplitude value of the transmitted signals may be significantly higher than its average amplitude value, resulting in the high peak-to-average power ratio (PAPR) [27, 57, 58] of the transmitted signal. The high PAPR requires that the OFDM/MC transmitters have a high linear range for signal amplification, otherwise, the transmitted OFDM/MC signals may conflict non-linear distortion, which results in out-of-band emissions and co-channel interference, causing significant degradation of the system's performance. Moreover, it can be understood that the high PAPR has a more harmful effect on the uplink communications than on the downlink communications, owing to the power limit of mobile terminals.

In order to take advantage of multicarrier communications while simultaneously circumventing the high PAPR problem, the SC-FDMA scheme [59–64] has been proposed for supporting high-speed uplink communications. In principle, the SC-FDMA can be viewed as a DFT-spread multicarrier CDMA scheme, where T-domain data symbols are transformed to the F-domain by a DFT before carrying out the multicarrier modulation. Figure 3.8 depicts the transmitter schematic of the SC-FDMA uplink, while Fig. 3.11 shows the corresponding receiver schematic. Let us analyse the principles in detail.

Assume a multicarrier, OFDM or MC-CDMA, system employing $U = MN$ subcarriers and supporting $K \leq M$ uplink users; each user transmits N data symbols within a time-duration of T_s seconds. As shown in Fig. 3.8, let the N symbols transmitted by the k th user be expressed as

$$\mathbf{x}_k = [x_{k0}, x_{k1}, \dots, x_{k(N-1)}]^T, \quad k = 0, 1, \dots, K - 1 \quad (3.51)$$

Note that the symbols in \mathbf{x}_k may represent N independent source data symbols of user k . Alternatively, they may denote N symbols obtained from one or several source data symbols through the T-domain spreading operation. For example, \mathbf{x}_k may contain the N chips of a symbol after it is spread using an N -length spreading sequence. As shown in Fig. 3.8, the source symbols in \mathbf{x}_k are first transformed to the F-domain with the aid of N -point DFT, yielding N F-domain symbols

$$\mathbf{X}_k = [X_{k0}, X_{k1}, \dots, X_{k(N-1)}]^T = \mathcal{F}_N \mathbf{x}_k \quad (3.52)$$

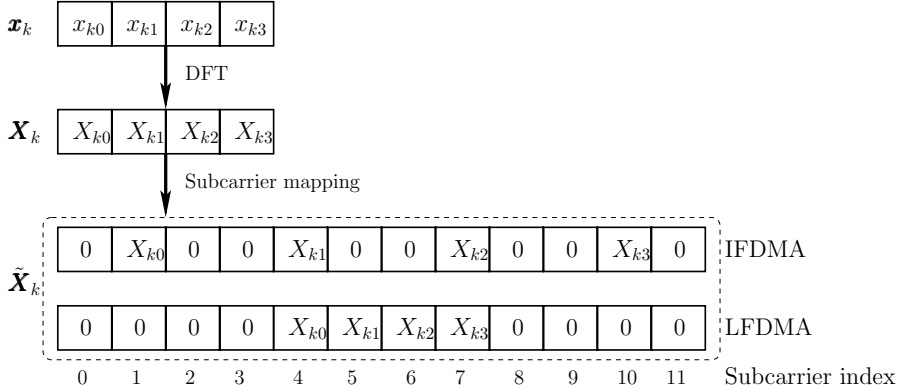


Figure 3.9: An example to illustrate the F-domain transmitted symbols by user \$k = 1\$ in the SC-FDMA using a total of \$U = 12\$ subcarriers for \$N = 4\$ subcarriers per user. The SC-FDMA can support \$K \leq M = 3\$ users.

where \$\mathcal{F}_N\$ denotes an \$N\$-point FFT matrix in the form of (3.29). More specifically, the \$N\$ F-domain symbols in \$\mathbf{X}_k\$ are given by

$$X_{kl} = \frac{1}{\sqrt{N}} \sum_{n=0}^{N-1} x_{kn} \exp\left(-j \frac{2\pi ln}{N}\right), \quad l = 0, 1, \dots, N-1 \quad (3.53)$$

As shown in Fig. 3.8, following the DFT operation, the \$N\$ F-domain symbols in \$\mathbf{X}_k\$ are mapped to \$N\$ of the \$U = MN\$ subcarriers. According to the literature [59–64], there are two strategies for mapping \$\mathbf{X}_k\$ to \$N\$ out of the \$U = MN\$ subcarriers, yielding the so-called interleaved FDMA (IFDMA) and localized FDMA (LFDMA).

In the context of the IFDMA, the \$N\$ F-domain symbols are evenly distributed across the \$U = MN\$ subcarriers. After the subcarrier mapping, as shown in Fig. 3.8, the transmitter forms an extended \$U\$-length F-domain symbol vector, which can be expressed as

$$\tilde{\mathbf{X}}_k = [\tilde{X}_{k0}, \tilde{X}_{k1}, \dots, \tilde{X}_{k(U-1)}]^T \quad (3.54)$$

where the value of \$\tilde{X}_{ku}\$ is set according to

$$\tilde{X}_{ku} = \begin{cases} X_{kn}, & \text{if } u = nM + k \\ 0, & \text{otherwise} \end{cases} \quad (3.55)$$

As shown in Fig. 3.9 for the IFDMA associated with \$k = 1\$, \$U = 12\$, \$M = 3\$ and \$N = 4\$, the locations 1, 4, 7, 10 of \$\tilde{X}_1\$ are filled by \$X_{10}\$, \$X_{11}\$, \$X_{12}\$, \$X_{13}\$, respectively, whereas the other entries of \$\tilde{X}_1\$ are set to zero.

In the context of the LFDMA, \$N\$ consecutive subcarriers of the \$U\$ are assigned to convey the \$N\$ F-domain symbols of user \$k\$. Specifically, for the LFDMA, the value of \$\tilde{X}_{ku}\$ in \$\tilde{\mathbf{X}}_k\$ are set as

$$\tilde{X}_{ku} = \begin{cases} X_{kn}, & \text{if } u = kN + n \\ 0, & \text{otherwise} \end{cases} \quad (3.56)$$

As shown in Fig. 3.9 for the LFDMA associated with $k = 1$, $U = 12$, $M = 3$ and $N = 4$, the locations 4, 5, 6, 7 of \tilde{X}_1 are filled by X_{10} , X_{11} , X_{12} , X_{13} , respectively, whereas the other entries of \tilde{X}_1 are set to zero.

As shown in Fig. 3.8, after the subcarrier mapping to extend an N -length symbol vector X_k to a $U = MN$ -length symbol vector \tilde{X}_k , multicarrier modulation is carried out by the IDFT operation, which generates a U -length T-domain symbol vector as

$$\tilde{\mathbf{x}}_k = \mathcal{F}_U^H \tilde{\mathbf{X}}_k \quad (3.57)$$

where \mathcal{F}_U denotes an U -point FFT matrix as shown in (3.29). The v th element of $\tilde{\mathbf{x}}_k$ is given by

$$\tilde{x}_{kv} = \frac{1}{\sqrt{U}} \sum_{u=0}^{U-1} \tilde{X}_{ku} \exp\left(j \frac{2\pi vu}{U}\right), \quad v = 0, 1, \dots, U-1 \quad (3.58)$$

In the context of the IFDMA, as shown in (3.55), \tilde{X}_{ku} is zero except for $u = nM + k$. Hence, for the IFDMA (3.58) can be simplified to

$$\begin{aligned} \tilde{x}_{kv} &= \frac{1}{\sqrt{U}} \sum_{n=0}^{N-1} \tilde{X}_{k(nM+k)} \exp\left(j \frac{2\pi v(nM+k)}{U}\right) \\ &= \frac{1}{\sqrt{M}} \exp\left(j \frac{2\pi vk}{U}\right) \times \frac{1}{\sqrt{N}} \sum_{n=0}^{N-1} X_{kn} \exp\left(j \frac{2\pi vn}{N}\right) \\ &\quad v = 0, 1, \dots, U-1 \end{aligned} \quad (3.59)$$

where $U = MN$ was used. In the above equation, let $v = qN + i$, $q = 0, 1, \dots, (M-1)$; $i = 0, 1, \dots, N-1$. Then, we have

$$\begin{aligned} \tilde{x}_{k(v=qN+i)} &= \frac{1}{\sqrt{M}} \exp\left(j \frac{2\pi(qN+i)k}{U}\right) \times \frac{1}{\sqrt{N}} \sum_{n=0}^{N-1} X_{kn} \exp\left(j \frac{2\pi(qN+i)n}{N}\right) \\ &= \frac{1}{\sqrt{M}} \exp\left(j \frac{2\pi(qN+i)k}{U}\right) \times \frac{1}{\sqrt{N}} \sum_{n=0}^{N-1} X_{kn} \exp\left(j \frac{2\pi in}{N}\right) \\ &= \frac{1}{\sqrt{M}} \exp\left(j \frac{2\pi(qN+i)k}{U}\right) x_{ki} \\ &\quad q = 0, 1, \dots, M-1; \quad i = 0, 1, \dots, N-1 \end{aligned} \quad (3.60)$$

According to (3.60), for the IFDMA, the N symbols in \mathbf{x}_k of user k are repeatedly transmitted on one subcarrier with a frequency of k/T_s , each symbol is transmitted M times within one symbol duration of T_s seconds. Specifically, for the example considered in Fig. 3.9, the corresponding T-domain transmitted signals within one symbol duration are shown in Fig. 3.10. Since in the IFDMA system there is only one subcarrier activated for transmission at any time, the IFDMA signals conflict no PAPR problem.

As shown in Fig. 3.8, after the IDFT, a cyclic prefix (CP) may be added in order to mitigate ISI, as will be studied in detail in Chapter 5. However, for the AWGN channels considered in the current section, no CP is necessary. Finally, based on Fig. 3.8 and

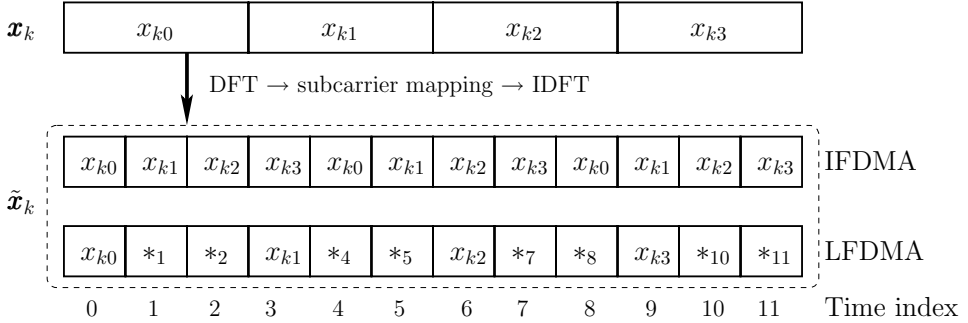


Figure 3.10: An example to illustrate the T-domain transmitted symbols by user $k = 1$ in the SC-FDMA using a total of $U = 12$ subcarriers for $N = 4$ subcarriers per user.

(3.60), the complex baseband equivalent signal transmitted by the IFDMA system can be expressed as

$$s_k(t) = \sum_{v=0}^{U-1} \sqrt{\frac{2P}{M}} \exp\left(j \frac{2\pi kv}{U}\right) x_{k[v/N]} \psi(t - vT_c) \quad (3.61)$$

where P represents the transmission power per dimension, $[v/N]$ denotes the N -modulo operation on v and $\psi(t)$ is a chip-waveform impulse defined in $(0, T_c]$, where T_c is the chip duration and $T_s = UT_c$.

For the LFDMA system, as shown in (3.56), \tilde{X}_{ku} is zero except for $u = kN + n$. In this case, (3.58) can be simplified to

$$\begin{aligned} \tilde{x}_{kv} &= \frac{1}{\sqrt{U}} \sum_{n=0}^{N-1} \tilde{X}_{k(kN+n)} \exp\left(j \frac{2\pi v(kN+n)}{U}\right) \\ &= \frac{1}{\sqrt{M}} \exp\left(j \frac{2\pi vk}{M}\right) \tilde{x}'_{kv}, \quad v = 0, 1, \dots, U-1 \end{aligned} \quad (3.62)$$

where, by definition,

$$\tilde{x}'_{kv} = \frac{1}{\sqrt{N}} \sum_{n=0}^{N-1} X_{kn} \exp\left(j \frac{2\pi vn}{U}\right) \quad (3.63)$$

Upon substituting (3.53) into the above equation, it can be shown that

$$\begin{aligned} \tilde{x}'_{kv} &= \frac{1}{N} \sum_{m=0}^{N-1} x_{km} \sum_{n=0}^{N-1} \exp\left(j \frac{2\pi(v-mM)n}{U}\right) \\ &= \begin{cases} x_{kl}, & \text{if } v = lM \\ \left[1 - \exp\left(j \frac{2\pi v}{M}\right)\right] \frac{1}{N} \sum_{m=0}^{N-1} \frac{1}{1 - \exp(j2\pi v/U) \exp(-j2\pi m/N)}, & \text{otherwise} \end{cases} \end{aligned} \quad (3.64)$$

where $l = 0, 1, \dots, N-1$.

According to (3.62) and (3.64), for the LFDMA, the U signals conveyed within the U chips are as follows: $x_{k0}, x_{k1}, \dots, x_{k(N-1)}$ are transmitted within the chip durations (time slots) of $0, M, \dots, (N-1)M$, respectively, using the same subcarrier with the frequency kN/T_s corresponding to kv/M in (3.62); within the other chip durations, the transmitted signal is in the form of (3.62) associated with \tilde{x}'_{kv} given by the second part of (3.64). Specifically, for the example corresponding to $M = 3, N = 4$ and $k = 1$, the T-domain transmitted signals within one symbol duration is shown in Fig. 3.10.

Finally, based on Fig. 3.8, (3.62) and (3.64), the complex baseband equivalent signal transmitted by the LFDMA system can be expressed as

$$s_k(t) = \sqrt{\frac{2P}{M}} \exp\left(j\frac{2\pi kv}{M}\right) x_{kl} \psi(t - lMT_c) \quad (3.65)$$

for $v = lM, lMT_c < t \leq (lM + 1)T_c, l = 0, 1, \dots, N - 1$, and

$$\begin{aligned} s_k(t) = & \sqrt{\frac{2P}{M}} \exp\left(j\frac{2\pi kv}{M}\right) \left[1 - \exp\left(j\frac{2\pi v}{M}\right) \right] \\ & \times \left(\frac{1}{N} \sum_{m=0}^{N-1} \frac{1}{1 - \exp(j2\pi v/U) \exp(-j2\pi m/N)} \right) \psi(t - vT_c) \end{aligned} \quad (3.66)$$

for $v \neq lM$ and $vT_c < t \leq (v + 1)T_c$.

It can be seen from (3.65) that, within the chip durations of $lMT_c < t \leq (lM + 1)T_c$ for $l = 0, 1, \dots, N - 1$, only one subcarrier is invoked for transmission in the LFDMA systems. By contrast, within the other chip durations, as shown in (3.66), three subcarriers having the frequencies $kN/T_s, N/T_s$ and $1/T_s$, which are respectively corresponding to the terms $kv/M, v/M$ and v/U in (3.66), are invoked for transmission, regardless of the total number of subcarriers employed by the LFDMA systems. Hence, the PAPR problem in LFDMA systems is significantly less severe than that in the conventional multicarrier systems, such as in OFDM systems. In the conventional multicarrier schemes the PAPR is usually a function of the total number of subcarriers employed. The PAPR problem is a common drawback of the conventional multicarrier schemes, and needs to be taken care of with the aid of various PAPR reduction techniques [30, 57, 58, 69–81].

The receiver schematic block diagram for the SC-FDMA is shown in Fig. 3.11, which carries out generally the inverse operations of the functions seen in the transmitter schematic of Fig. 3.8. Let us consider the IFDMA scheme specifically, in order to explain the demodulation principles of the SC-FDMA scheme. The demodulation principles for the LFDMA scheme can be similarly analysed.

Let us assume that the IFDMA system supports $K \leq M$ users. Then, when the K uplink user signals in the form of (3.61) are transmitted over AWGN channels, the received complex baseband equivalent signal at the BS receiver can be expressed as

$$R(t) = \sum_{k=0}^{K-1} \sum_{v=0}^{U-1} \sqrt{\frac{2P}{M}} \exp(j\phi_k) \exp\left(j\frac{2\pi kv}{U}\right) x_{k[v/N]} \psi(t - vT_c) + n(t) \quad (3.67)$$

where ϕ_k is the phase introduced by the k uplink channel.

As shown in Fig. 3.11, the received signal $R(t)$ is first filtered by a filter matched to the chip waveform $\psi(t)$ transmitted. The MF's output is sampled at the chip rate of $1/T_c$

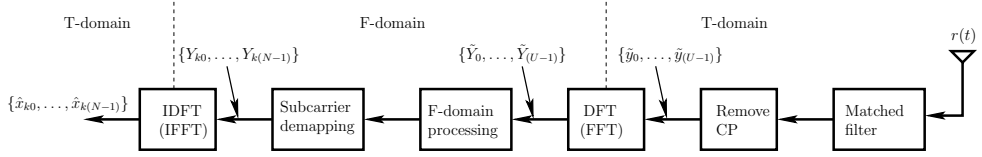


Figure 3.11: Receiver schematic for the k th user supported by the SC-FDMA uplink.

(which is not shown in Fig. 3.11). It can be shown that, after normalization using $1/\sqrt{2P}T_c$, the u th sample of the MF's output can be expressed as

$$\tilde{y}_u = \frac{1}{\sqrt{2P}T_c} \int_{uT_c}^{(u+1)T_c} R(t)\psi(t-uT_c) dt, \quad u = 0, 1, \dots, U-1 \quad (3.68)$$

Substituting (3.67) into the above equation, it can be shown that

$$\tilde{y}_u = \sum_{k=0}^{K-1} \frac{\exp(j\phi_k)}{\sqrt{M}} \exp\left(j \frac{2\pi k u}{U}\right) x_{k[u/N]} + n_u, \quad u = 0, 1, \dots, U-1 \quad (3.69)$$

where the Gaussian noise sample n_u is given by

$$\tilde{n}_u = \frac{1}{\sqrt{2P}T_c} \int_{uT_c}^{(u+1)T_c} n(t)\psi(t-uT_c) dt, \quad u = 0, 1, \dots, U-1 \quad (3.70)$$

As shown in Fig. 3.11, following the matched filtering, the CPs added at the transmitter are removed. Then, the DFT operation is carried out to transform the T-domain observation samples $\tilde{y}_0, \tilde{y}_1, \dots, \tilde{y}_{U-1}$ to the F-domain; the v th sample in the F-domain can be expressed as

$$\begin{aligned} \tilde{Y}_v &= \frac{1}{\sqrt{U}} \sum_{u=0}^{U-1} \tilde{y}_u \exp\left(-j \frac{2\pi v u}{U}\right) \\ &= \sum_{k=0}^{K-1} \frac{\exp(j\phi_k)}{\sqrt{M^2 N}} \sum_{u=0}^{U-1} x_{k[u/N]} \exp\left(j \frac{2\pi(k-v)u}{U}\right) + \tilde{N}_v, \quad v = 0, 1, \dots, U-1 \end{aligned} \quad (3.71)$$

where we used $U = MN$ and \tilde{N}_v is the noise sample after the DFT operation. In the above equation let $v = pM + l$ and $u = qN + i$. Then, we can arrange it in a form as

$$\begin{aligned} \tilde{Y}_{pM+l} &= \sum_{k=0}^{K-1} \exp(j\phi_k) \frac{1}{M} \sum_{q=0}^{M-1} \exp\left(j \frac{2\pi(k-pM-l)q}{M}\right) \\ &\quad \times \frac{1}{\sqrt{N}} \sum_{i=0}^{N-1} x_{ki} \exp\left(j \frac{2\pi(k-pM-l)i}{U}\right) + \tilde{N}_{pM+l} \\ p &= 0, 1, \dots, N-1; \quad l = 0, 1, \dots, M-1 \end{aligned} \quad (3.72)$$

Since, in the above equation, the second part

$$\frac{1}{M} \sum_{q=0}^{M-1} \exp\left(j \frac{2\pi(k-pM-l)q}{M}\right) = \begin{cases} 1, & \text{if } k = l \\ 0, & \text{otherwise} \end{cases} \quad (3.73)$$

hence $\tilde{Y}_{pM+l} = \tilde{N}_{pM+l}$ if $K \leq l \leq M - 1$. When $l < K$, \tilde{Y}_{pM+l} can be expressed as

$$\begin{aligned} \tilde{Y}_{pM+l} &= \exp(j\phi_l) \frac{1}{\sqrt{N}} \sum_{i=0}^{N-1} x_{li} \exp\left(-j \frac{2\pi i p}{N}\right) + \tilde{N}_{pM+l} \\ &= \tilde{X}_{pM+l} \exp(j\phi_l) + \tilde{N}_{pM+l}, \quad p = 0, 1, \dots, N-1; \quad l = 0, 1, \dots, K-1 \end{aligned} \quad (3.74)$$

Assuming that the BS receiver employs the ideal knowledge about $\{\phi_0, \phi_1, \dots, \phi_{K-1}\}$, then, after processing \tilde{Y}_{pM+l} using $\exp(-j\phi_l)$, the output can be expressed as

$$\tilde{Y}'_{pM+l} = \tilde{X}_{pM+l} + \tilde{N}'_{pM+l}, \quad p = 0, 1, \dots, N-1; \quad l = 0, 1, \dots, K-1 \quad (3.75)$$

where $\tilde{N}'_{pM+l} = \tilde{N}_{pM+l} \exp(-j\phi_l)$.

As shown in Fig. 3.11, after the F-domain processing, subcarrier de-mapping follows. According to the subcarrier mapping rule of (3.55) used by the transmitter, after the subcarrier de-mapping, the corresponding outputs can be expressed as

$$Y_{lp} = X_{lp} + \tilde{N}'_{lp}, \quad l = 0, 1, \dots, K-1; \quad p = 0, 1, \dots, N-1 \quad (3.76)$$

Explicitly, the symbols transmitted by the K users are successfully separated without interfering with each other. Let us define

$$\begin{aligned} \mathbf{Y}_l &= [Y_{l0}, Y_{l1}, \dots, Y_{l(N-1)}]^T \\ \mathbf{N}_l &= [N'_{l0}, N'_{l1}, \dots, N'_{l(N-1)}]^T \end{aligned} \quad (3.77)$$

Then, we have

$$\mathbf{Y}_l = \mathbf{X}_l + \mathbf{N}_l, \quad l = 0, 1, \dots, K-1 \quad (3.78)$$

where \mathbf{X}_l is given by (3.52).

Finally, as shown in Fig. 3.11, for each of the K users, an N -point IDFT is applied on \mathbf{Y}_l , generating the decision variables for the N transmitted symbols in \mathbf{x}_l , which can be expressed as

$$\mathbf{z}_l = \mathcal{F}_N^H \mathbf{Y}_l, \quad l = 0, 1, \dots, K-1 \quad (3.79)$$

Substituting (3.78) and \mathbf{X}_l from (3.52) into the above equation, we obtain

$$\mathbf{z}_l = \mathbf{x}_l + \mathcal{F}_N^H \mathbf{N}_l, \quad l = 0, 1, \dots, K-1 \quad (3.80)$$

based on which, the estimate $\hat{\mathbf{x}}_l$ to \mathbf{x}_l can be obtained, as shown in Fig. 3.11.

Above, the principles of the SC-FDMA have been studied in great detail. Note that, in addition to the merit of low PAPR, the SC-FDMA also enjoys a range of other advantages. In addition to the common advantages of the OFDM, it also employs some advantages of the single-carrier CDMA: it is a multiple-access scheme combining the advantages of both. The IFDMA is capable of achieving the frequency diversity, since each symbol of a user is conveyed by N subcarriers distributed evenly across the transmission frequency band, as shown in Fig. 3.9. By contrast, in LFDMA systems, as seen in Fig. 3.9, the N subcarriers of a given user are constituted by N consecutive subcarriers, which may experience highly correlated fading. Hence, in the LFDMA scheme, it is hard to achieve the frequency diversity without help from the base station (BS). The LFDMA is capable achieving the frequency diversity (or so-called multiuser diversity), if the BS can schedule the uplink users, so that each of them is assigned the portion of subcarriers having favourable transmission characteristics. The error performance of the SC-FDMA scheme will be studied in Section 5.7 of Chapter 5, when communicating over frequency-selective fading channels.

3.5 Orthogonal Multicarrier DS-CDMA

3.5.1 Transmitted Signal

Orthogonal MC DS-CDMA systems have been studied in references [38, 39, 41, 68]. The orthogonal MC DS-CDMA transmitter spreads the S/P converted data streams using a given spreading code in the T-domain so that the resulting spectrum of each subcarrier can satisfy the orthogonality condition with the minimum frequency separation [38, 41]. This scheme was originally proposed for an uplink communication system, because the characteristics of the orthogonal MC DS-CDMA are effective for establishing a quasi-synchronous channel. The transmitter diagram shown in Fig. 3.12 for the orthogonal MC DS-CDMA system is the same as that used in reference [41]. In this scheme the initial data stream having the bit duration of T_b is S/P converted to q number of lower-rate substreams. Hence, the new bit duration after the S/P conversion or the symbol duration is $T_s = qT_b$. Each of the q lower-rate substreams is spread by the T-domain spreading code $c_k(t)$. As shown in Fig. 3.12, each of the q substreams is transmitted by p number of subcarriers, in order to achieve a frequency diversity order of p at the receiver by combining these subcarrier signals with the aid of certain types of combining scheme. Hence, the total number of subcarriers required by the orthogonal MC DS-CDMA system is $U = pq$. Based on Fig. 3.12, the transmitted signal of user k can be expressed as

$$s_k(t) = \sum_{i=1}^q \sum_{j=1}^p \sqrt{\frac{2P}{p}} b_i^{(k)}(t) c_k(t) \cos(2\pi f_{ij} t + \phi_{ij}^{(k)}), \quad k = 1, 2, \dots, K \quad (3.81)$$

where P is the transmitted power of each substream, $b_i^{(k)}(t) = \sum_{n=-\infty}^{\infty} b_i^{(k)}[n] P_{T_s}(t - nT_s)$, $i = 1, 2, \dots, q$ represents the binary data of the i th substream, where $b_i^{(k)}[n]$ is assumed to be a random variable taking value of $+1$ or -1 with equal probability, while $P_{T_s}(t)$ represents the rectangular waveform. In (3.81) $c_k(t)$ represents the T-domain spreading code assigned to the k th user, which is the same for all the $U = pq$ number of subcarriers. The spreading

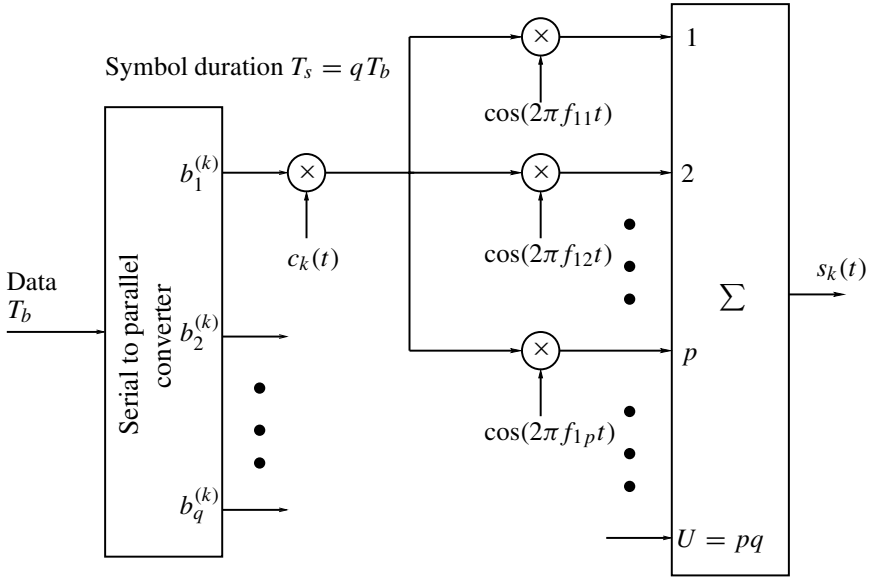


Figure 3.12: The transmitter diagram of the orthogonal MC DS-CDMA system.

sequence $c_k(t)$ can be expressed as

$$c_k(t) = \sum_{j=-\infty}^{\infty} c_j^{(k)} \psi(t - jT_c) \quad (3.82)$$

where $c_j^{(k)}$ assumes values of $+1$ or -1 , while $\psi(t)$ is the chip waveform of the T-domain spreading sequence, which is defined over the interval $[0, T_c]$ and normalized to $\int_0^{T_c} \psi^2(t) dt = T_c$. Finally, in (3.81) $\phi_{ij}^{(k)}$ represents the initial phase associated with the carrier modulation in the context of the subcarrier determined by (i, j) in (3.81).

3.5.2 Modulation Parameters

In orthogonal MC DS-CDMA systems subcarrier signals are chosen to be orthogonal to each other with the minimum frequency separation after the DS spreading. Hence, the orthogonality can be formulated as

$$\int_0^{T_c} \cos(2\pi f_{ij}t + \phi_{ij}) \cdot \cos(2\pi f_{i'j'}t + \phi_{i'j'}) dt = 0, \quad \text{for } i \neq i' \text{ or } j \neq j' \quad (3.83)$$

According to (3.83), it can be shown that the minimum spacing Δ between two adjacent subcarriers satisfies $\Delta = 1/T_c$, which results in a successively half-overlapping spectrum, as shown, for example, in Fig. 3.13, in which W_s represents the available bandwidth for the orthogonal MC DS-CDMA system, while W_{DS} represents the null-to-null bandwidth of each

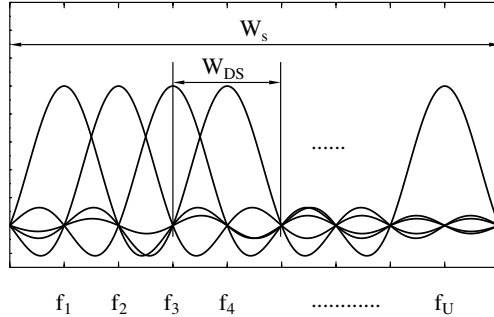


Figure 3.13: Spectrum of the orthogonal MC DS-CDMA signal of (3.81), when rectangular direct-sequence chip waveforms were assumed.

DS spread subcarrier signal. It can be shown that, for binary spreading sequences having a chip duration of T_c , W_{DS} can be expressed as

$$W_{DS} = \frac{2}{T_c} \quad (3.84)$$

Let us assume that T_{c1} represents the chip duration of a corresponding single-carrier DS-CDMA signal, having a null-to-null bandwidth of W_s . Then, we have

$$W_s = \frac{2}{T_{c1}} \quad (3.85)$$

According to Fig. 3.13, the number of subcarriers, U , the chip-duration, T_c , in the orthogonal MC DS-CDMA system and the chip-duration, T_{c1} , in the corresponding single-carrier DS-CDMA satisfy the relationship of

$$\frac{2}{T_{c1}} = \frac{U + 1}{T_c} = \frac{pq + 1}{T_c} \quad (3.86)$$

Let $N_e = T_s/T_c$ be the spreading gain or the spreading factor of the subcarrier signals in the orthogonal MC DS-CDMA system and $N_1 = T_b/T_{c1}$ be the spreading gain of a corresponding single-carrier DS-CDMA system. Then, multiplying both sides of (3.86) by the symbol duration, T_s , and taking into account that $T_s = N_e T_c$ as well as $T_s = q T_b = q N_1 T_{c1}$, the processing gain, N_e , the number of subcarriers, U , and the processing gain, N_1 , then obey the relationship expressed as

$$N_e = \frac{2qN_1}{U + 1} = \frac{2qN_1}{pq + 1} \approx \frac{2N_1}{p} \quad (3.87)$$

The spectral gain of the orthogonal MC DS-CDMA system is given by

$$SG = \frac{pq(2/T_c)}{(pq + 1)(1/T_c)} = \frac{2U}{U + 1} \quad (3.88)$$

which approaches a factor of two as $U = pq$ increases. Thus, the orthogonal MC DS-CDMA system exhibits an increased spectral gain, which amounts to approximately a factor of two, as explained by the 50 per cent overlap of the main lobes of the adjacent subcarrier spectra.

Finally, in orthogonal MC DS-CDMA systems, the subcarrier frequencies conveying the same data bit are designed to be spaced as far as possible, in order to achieve the highest possible frequency diversity order over frequency-selective fading channels. Specifically, let $\{f_{11}, f_{12}, \dots, f_{U=pq}\}$ be the subcarrier frequencies. These subcarrier frequencies can be written in the form of a matrix as

$$\{f_{ij}\} = \begin{pmatrix} f_{11} & f_{12} & \dots & f_{1p} \\ f_{21} & f_{22} & \dots & f_{2p} \\ \vdots & \vdots & \ddots & \vdots \\ f_{q1} & f_{q2} & \dots & f_{qp} \end{pmatrix} \quad (3.89)$$

As shown in Fig. 3.12, the subcarrier frequencies conveying the i th, $i = 1, 2, \dots, q$, bit are the frequencies from the i th row of the matrix of (3.89). In order to maximize the spacing among these frequencies, they can be set to be the frequencies as

$$f_{ij} = f_0 + \frac{1}{T_c}[(i-1) + (j-1)q], \quad j = 1, 2, \dots, p \quad (3.90)$$

for $i = 1, 2, \dots, q$.

3.5.3 Correlation Receiver

Assuming that there are K asynchronous CDMA users in the orthogonal MC DS-CDMA system, where all of them use the same $U = pq$ and N_e values, the average power received from each user at the base station is also assumed to be the same, implying perfect power control. Furthermore, we assume that each subcarrier signal experiences frequency non-selective fading. Consequently, when the transmitted signal is in the form of (3.81), the received signal at the base station can be expressed as

$$r(t) = \sum_{k=1}^K \sum_{i=1}^q \sum_{j=1}^p \sqrt{\frac{2P}{p}} \alpha_{ij}^{(k)} b_i^{(k)} (t - \tau_k) c_k(t - \tau_k) \cos(2\pi f_{ij} t + \varphi_{ij}^{(k)}) + n(t) \quad (3.91)$$

where τ_k represents the channel delay in the context of the k th user, $\alpha_{ij}^{(k)}$ is due to the channel fading, which is set to be $\alpha_{ij}^{(k)} = 1$ for the AWGN channel. Furthermore, in (3.91) $\varphi_{ij}^{(k)} = \phi_{ij}^{(k)} - \psi_{ij}^{(k)} - 2\pi f_{ij} \tau_k$, which is assumed to be an i.i.d random variable having a uniform distribution in $[0, 2\pi]$, $\psi_{ij}^{(k)}$ is due to the transmission channel, while $n(t)$ represents the AWGN with zero mean and double-sided PSD of $N_0/2$.

Let us assume that the first user of $k = 1$ is the reference user. The correlation receiver block diagram of the reference user is shown in Fig. 3.14, where the superscripts and subscripts concerning the reference user have been omitted for the sake of simplicity. The receiver provides a correlator for each subcarrier and the correlator outputs associated with the same data bit are combined to form a decision variable. Finally, a P/S converter is employed to recover the serial data stream. In Fig. 3.14 $\{g_{i1}, g_{i2}, \dots, g_{ip}\}$ for $i = 1, 2, \dots, q$

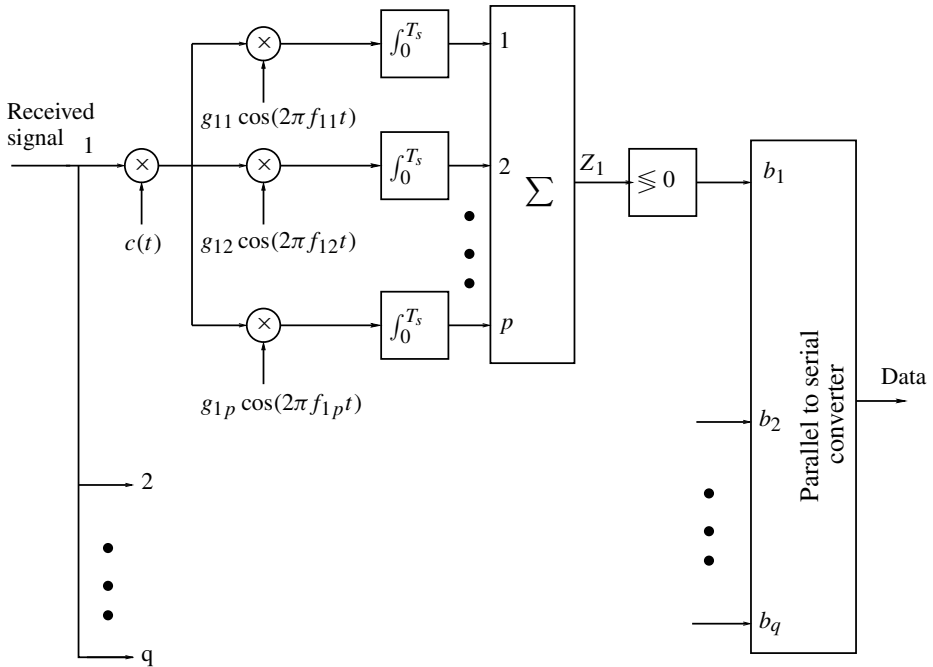


Figure 3.14: The receiver block diagram of the orthogonal MC DS-CDMA systems for the reference user.

represent the weight factors of the subcarrier signals. The weight factors can be set as the corresponding values, in order to take into account various combining schemes for the subcarrier signals conveying the same data bit.

Let us consider the detection of the u th bit, b_u , transmitted by the first user during the time duration $[0, T_s]$. We assume that the receiver has achieved the synchronization with the first user's transmitted signal at the chip level. Hence, we assume $\tau_1 = 0$ for convenience. We also assume that the receiver is capable of tracking the carrier phases of the subcarrier signals of the reference user. Therefore, we can set $\varphi_{uv} = 0$, when we consider demodulating the subcarrier signal using the frequency of f_{uv} . Consequently, the decision variable for detecting b_u can be written as

$$Z_u = \sum_{v=1}^p Z_{uv} \quad (3.92)$$

$$Z_{uv} = \int_0^{T_s} r(t) g_{uv} c(t) \cos(2\pi f_{uv} t) dt \quad (3.93)$$

Substituting (3.91) into (3.93), we can show that Z_{uv} can be expressed as

$$Z_{uv} = \sqrt{\frac{P}{2p} T_s} \left[D_{uv} + N_{uv} + \sum_{k=2}^K I_{M1}^{(k)} + \underbrace{\sum_{k=2}^K \sum_{i=1}^q \sum_{j=1}^p I_{M2}^{(k)}(i, j)}_{j \neq v \text{ if } i=u} \right] \quad (3.94)$$

where N_{uv} is contributed by $n(t)$ of (3.91), which can be expressed as

$$N_{uv} = \left(\sqrt{\frac{P}{2p}} T_s \right)^{-1} \int_0^{T_s} n(t) g_{uv} c(t) \cos(2\pi f_{uv} t) dt \quad (3.95)$$

where N_{uv} is a Gaussian random variable with zero mean and a variance of $p g_{uv}^2 N_0 / 2E_b$, and $E_b = P T_s$ represents the energy per bit. Furthermore, in (3.94) D_{uv} is the desired output derived by substituting (3.91) into (3.93) and setting $k = 1$, $i = u$ and $j = v$, which can be shown to be

$$D_{uv} = g_{uv} \alpha_{uv} b_u \quad (3.96)$$

In (3.94) the multiuser interference term $I_{M1}^{(k)}$ is due to the subcarrier signal of the k th user signal, which uses the same frequency as the considered subcarrier of the reference user, i.e. the subcarrier determined by (u, v) . $I_{M1}^{(k)}$ can be expressed as

$$\begin{aligned} I_{M1}^{(k)} &= \frac{g_{uv} \alpha_{uv}^{(k)} \cos(\varphi_{uv}^{(k)})}{T_s} \int_0^{T_s} b_u^{(k)}(t - \tau_k) c_k(t - \tau_k) c(t) dt \\ &= \frac{g_{uv} \alpha_{uv}^{(k)} \cos(\varphi_{uv}^{(k)})}{T_s} [b_u^{(k)}[-1] R_{k1}(\tau_k) + b_u^{(k)}[0] \hat{R}_{k1}(\tau_k)] \end{aligned} \quad (3.97)$$

where $b_u^{(k)}[-1]$ and $b_u^{(k)}[0]$ represent the previous and the current transmitted bits by the uv th subcarrier of user k , with respect to bit b_u transmitted by the reference user. Furthermore, in (3.97) $R_{k1}(\tau_k)$ and $\hat{R}_{k1}(\tau_k)$ are partial cross-correlation functions between the k th user's spreading sequence waveform $c_k(t - \tau_k)$ and the reference user's spreading sequence waveform $c(t)$, which are defined as [82]

$$R_{k1}(\tau_k) = \int_0^{\tau_k} c_k(t - \tau_k) c(t) dt \quad (3.98)$$

$$\hat{R}_{k1}(\tau_k) = \int_{\tau_k}^{T_s} c_k(t - \tau_k) c(t) dt \quad (3.99)$$

Finally, in (3.94) the multiuser interference term $I_{M2}^{(k)}(i, j)$ is due to the k th user signal's ij th subcarrier, which uses the frequency, f_{ij} , that is different from f_{uv} of the considered subcarrier for the reference user. $I_{M2}^{(k)}(i, j)$ can be expressed as

$$\begin{aligned} I_{M2}^{(k)}(i, j) &= \frac{g_{uv} \alpha_{ij}^{(k)}}{T_s} \int_0^{T_s} b_i^{(k)}(t - \tau_k) c_k(t - \tau_k) c(t) \cos[2\pi(f_{ij} - f_{uv})t + \varphi_{ij}^{(k)}] dt \\ &= \frac{g_{uv} \alpha_{uv}^{(k)}}{T_s} [b_i^{(k)}[-1] R_{k1}(\tau_k, \varphi_{ij}^{(k)}, i, j) + b_i^{(k)}[0] \hat{R}_{k1}(\tau_k, \varphi_{ij}^{(k)}, i, j)] \end{aligned} \quad (3.100)$$

where, again, $b_i^{(k)}[-1]$ and $b_i^{(k)}[0]$ represent the previous and the current bits transmitted on the ij th subcarrier of user k , with respect to bit b_u transmitted by the reference user. Due to the difference of the frequencies f_{ij} and f_{uv} , in (3.100) the corresponding partial cross-correlation functions between the k th user's spreading sequence waveform $c_k(t - \tau_k)$ and the reference user's spreading sequence waveform $c(t)$ are expressed as $R_{k1}(\tau_k, \varphi_{ij}^{(k)}, i, j)$ and

$\hat{R}_{k1}(\tau_k, \varphi_{ij}^{(k)}, i, j)$. Taking into account (3.90), these cross-correlation functions are defined as [53]

$$R_{k1}(\tau_k, \varphi_{ij}^{(k)}, i, j) = \int_0^{\tau_k} c_k(t - \tau_k) c(t) \cos\left(\frac{2\pi[(i-u)+(j-v)q]t}{T_c} + \varphi_{ij}^{(k)}\right) dt \quad (3.101)$$

$$\hat{R}_{k1}(\tau_k, \varphi_{ij}^{(k)}, i, j) = \int_{\tau_k}^{T_s} c_k(t - \tau_k) c(t) \cos\left(\frac{2\pi[(i-u)+(j-v)q]t}{T_c} + \varphi_{ij}^{(k)}\right) dt \quad (3.102)$$

Equation (3.94) shows that all the subcarrier signals of user k impose interference on the reference signal. However, the study in reference [83] has shown that the main contributing to multiuser interference (MUI) is by the specific subcarrier signals having overlapping main lobes with the relevant subcarrier of the reference user.

Finally, based on the above analysis, the transmitted bit b_u by the reference user can be detected as the sign of the decision variable Z_u of (3.92), i.e. $b_u = \text{sign}(Z_u)$. Furthermore, it can be shown that, when α_{uv} for different values of v are independent random variables, a diversity order of p can be achieved by combining the p number of subcarrier signals, as indicated by (3.92), which convey the same data bit.

The orthogonal MC DS-CDMA scheme can provide a range of advantages [41, 53, 83]. First, the spectral gain is increased compared to the corresponding single-carrier DS-CDMA scheme. Second, the effect of multiuser interference is mitigated because of DS spreading. Third, frequency diversity can be achieved by transmitting the same data bit on several subcarriers. Finally, a longer chip duration may lead to more relaxed synchronization schemes. However, in comparison to the F-domain spread MC-CDMA discussed in Section 3.3, a high complexity receiver has to be implemented. Furthermore, *forward error control* (FEC) techniques may also be required, in order to enhance its associated performance.

3.6 Multitone DS-CDMA

3.6.1 Transmitted Signal

The multitone DS-CDMA scheme was proposed by Vandendorpe in reference [43]. The multitone DS-CDMA transmitter spreads the S/P converted data streams using a given spreading code in the T-domain, so that the spectrum of each subcarrier prior to the spreading operation can satisfy the orthogonality condition with the minimum frequency separation [43]. Since in multitone DS-CDMA the spacing between two subcarrier frequencies is on the order of the transmitted symbol rate, therefore there exists strong spectral overlap among the different subcarrier signals after DS spreading. The transmitter schematic diagram for the multitone DS-CDMA system is shown in Fig. 3.15. At the transmitter side of Fig. 3.15, the binary data stream having a bit duration of T_b is first S/P converted to U parallel substreams. The new bit duration on each subcarrier, which defines the modulated symbol duration is $T_s = UT_b$. After the S/P conversion, the u th substream modulates the subcarrier frequency f_u , $u = 1, 2, \dots, U$. The multitone signal is obtained by the addition of the different subcarriers' signals. Then, spectrum spreading is imposed on the multitone signal by multiplying it with a spreading code, $c_k(t)$, as shown in Fig. 3.15. The transmitted signal

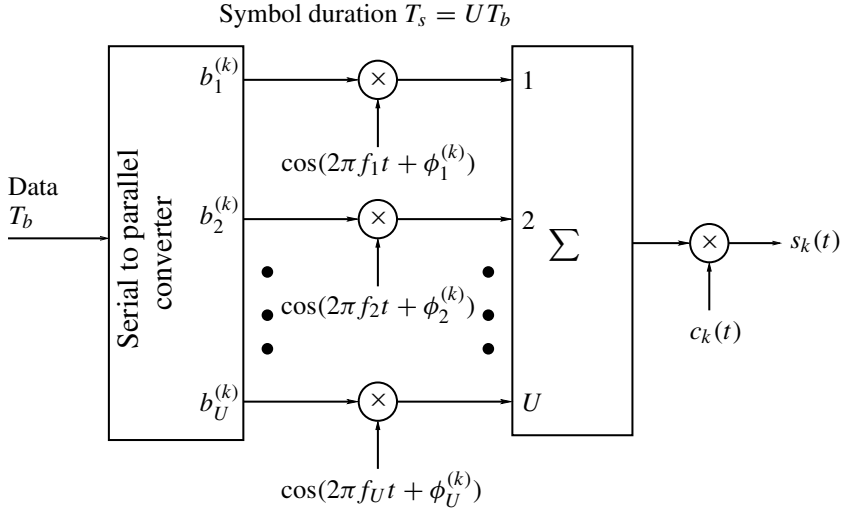


Figure 3.15: The transmitter schematic diagram of the multitone DS-CDMA system.

of user k can be expressed as

$$s_k(t) = \sum_{u=1}^U \sqrt{2P} b_u^{(k)}(t) c_k(t) \cos(2\pi f_u t + \phi_u^{(k)}) \quad (3.103)$$

where P represents the transmitted power of each subcarrier, $b_u^{(k)}(t) = \sum_{n=-\infty}^{\infty} b_u^{(k)}[n] P_{T_s}(t - nT_s)$, where $b_u^{(k)}[n] \in \{+1, -1\}$, represents the binary data sequence modulating the u th subcarrier, $c_k(t) = \sum_{n=-\infty}^{\infty} c_n^{(k)} \psi(t - nT_c)$ is the spreading code waveform of user k , where $c_n^{(k)}$ assumes a value of $+1$ or -1 , while $\psi(t)$ is the chip waveform of the T-domain spreading sequence, which is defined over the interval $[0, T_c]$ and normalized so that $\int_0^{T_c} \psi^2(t) dt = T_c$. Finally, in (3.103) f_u and $\phi_u^{(k)}$ are the u th subcarrier frequency and modulation phase, respectively.

In comparison to Fig. 3.5 in Section 3.3 for the F-domain spread MC-CDMA and Fig. 3.12 in Section 3.5 for the orthogonal MC DS-CDMA, at the transmitter of the multitone DS-CDMA system, there is no bit repetition over the F-domain and each data bit is only transmitted by one subcarrier. This is because in multitone DS-CDMA the subcarrier signals strongly overlap with each other. Hence, all the subcarrier signals experience similar fading, when communicating over frequency selective fading channels. Therefore, the frequency diversity cannot be achieved by combining the subcarrier signals conveying the same data bit. Instead of combining the subcarrier signals for achieving frequency diversity, in multitone DS-CDMA, a receiver, usually a RAKE receiver [2] with a number of fingers, must be used by each of the U subcarriers in order to achieve the frequency selective diversity [43].

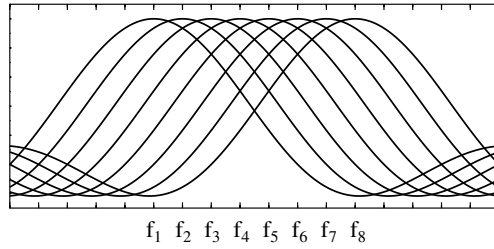


Figure 3.16: Spectrum of the multitone DS-CDMA signal.

3.6.2 Modulation Parameters

The spectrum associated with eight subcarriers for the multitone DS-CDMA signal is shown in Fig. 3.16. In the multitone DS-CDMA system the subcarrier signals are chosen to be orthogonal to each other with the minimum frequency separation before the DS spreading. Hence, the subcarrier frequencies obey the orthogonality condition

$$\int_0^{T_s} \cos(2\pi f_i t + \phi_i) \cdot \cos(2\pi f_j t + \phi_j) dt = 0, \quad \text{for } i \neq j \quad (3.104)$$

The minimum spacing, Δ , of the subcarrier frequencies is shown to be $\Delta = 1/T_s = 1/UT_b$. Hence, in multitone DS-CDMA systems, the set of subcarrier frequencies takes the form

$$\left\{ f_0 + \frac{0}{T_s}, f_0 + \frac{1}{T_s}, \dots, f_0 + \frac{U-1}{T_s} \right\}$$

Let T_{c1} and $N_1 = T_b/T_{c1}$ represent the chip duration and the spreading factor of a corresponding single-carrier DS-CDMA system, respectively. Referring to Fig. 3.16 and bearing in mind that $W_s = 2/T_{c1}$ and $W_{DS} = 2/T_c$,

$$\frac{2}{T_{c1}} = \frac{U-1}{T_s} + \frac{2}{T_c} \quad (3.105)$$

Let $T_s = UT_b = UN_1T_{c1}$; then, it can be shown that the chip duration of the spreading code for the multitone DS-CDMA system is given by

$$T_c = \frac{2UN_1}{2UN_1 - U + 1} T_{c1} \quad (3.106)$$

Observe that T_c approaches T_{c1} as N_1 increases. Furthermore, on multiplying both sides of (3.105) by T_s and letting $N_1 = T_b/T_{c1}$ and $N_e = T_s/T_c$, the spreading gain, N_e , of the subcarrier signal in the multitone DS-CDMA is given by

$$\begin{aligned} N_e &= T_s/T_c \\ &= UT_b/\frac{2UN_1}{2UN_1 - U + 1} T_{c1} \\ &= \frac{2UN_1 - U + 1}{2} \end{aligned} \quad (3.107)$$

which can be approximated by UN_1 , when N_1 is sufficiently high. Since in a multitone DS-CDMA system different data bits are transmitted on different subcarriers, the overall system's processing gain is also given by equation (3.107) [71].

The spectral gain of the multitone DS-CDMA system is given by

$$\begin{aligned} SG &= \frac{U(2/T_c)}{2/T_c + (U-1)/T_s} \\ &= \frac{2N_e U}{2N_e + U - 1} \end{aligned} \quad (3.108)$$

it approaches U , when N_e is sufficiently high, which is the highest spectral gain among the multicarrier schemes considered in this chapter.

3.6.3 Correlation Receiver

As mentioned previously in Section 3.6.1, when communicating over frequency selective fading channels, a RAKE receiver must usually be invoked by the multitone DS-CDMA systems, in order to achieve the frequency selective diversity. However, for the sake of simplicity, we analyse the detection principles of the multitone DS-CDMA systems without concerning the RAKE receiver.

Let us assume that there are K asynchronous CDMA users in the multitone DS-CDMA system, where all of them use the same values of U and N_e . We also assume that the average power received from each user at the base station is the same, which implies perfect power control. Consequently, when K number of multitone DS-CDMA signals in the form of (3.103) are transmitted over a single path channel, the received signal can be expressed as

$$r(t) = \sum_{k=1}^K \sum_{u=1}^U \sqrt{2P} \alpha_u^{(k)} b_u^{(k)} (t - \tau_k) c_k(t - \tau_k) \cos(2\pi f_u t + \varphi_u^{(k)}) + n(t) \quad (3.109)$$

where τ_k represents the channel delay in the context of the k th user, and $\alpha_u^{(k)}$ encompasses the channel fading, which takes a value of $\alpha_{ij}^{(k)} = 1$ for the AWGN channel. Furthermore, in (3.109) $\varphi_u^{(k)} = \phi_u^{(k)} - \psi_u^{(k)} - 2\pi f_u \tau_k$, which is assumed to be an i.i.d random variable having a uniform distribution in $[0, 2\pi]$, while $\psi_u^{(k)}$ is due to the transmission channel. Finally, in (3.109) $n(t)$ represents the zero-mean AWGN having a double-sided PSD of $N_0/2$.

The correlation receiver block diagram of the multitone DS-CDMA system is shown in Fig. 3.17. Associated with each subcarrier, a simple correlation detector is employed for detecting the corresponding bit transmitted on that subcarrier. Let us assume that the first user of $k = 1$ is the user-of-interest and that the receiver has achieved the perfect synchronization with the reference user's signal, i.e. that $\tau_1 = 0$. Then, for detecting the data bit b_u , $u = 1, 2, \dots, U$, which is assumed to be the first symbol transmitted by the desired user, the corresponding decision variable can be written as

$$Z_u = \int_0^{T_s} r(t) g_u c(t) \cos(2\pi f_u t) dt, \quad u = 1, 2, \dots, U \quad (3.110)$$

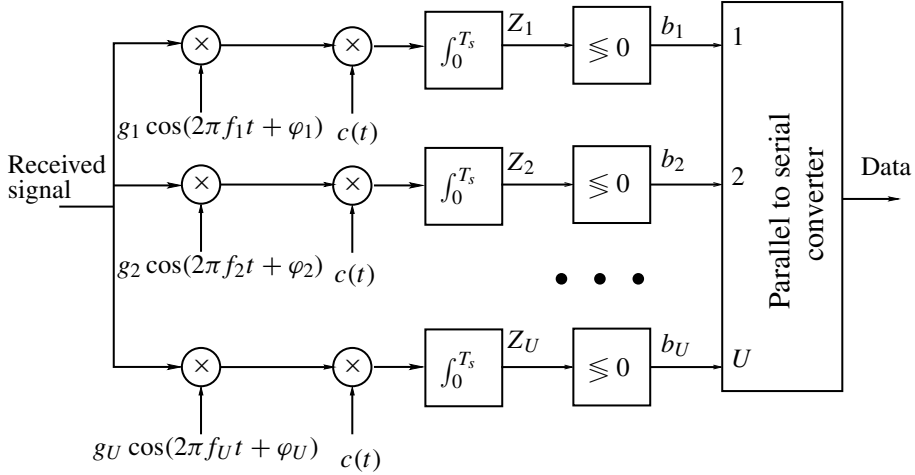


Figure 3.17: The correlation receiver block diagram for detection of multitone DS-CDMA signals transmitted by the user-of-interest.

where, for convenience, we assumed that $\varphi_u = 0$. Substituting (3.109) into the above equation, it can be shown that the decision variable, Z_u , can be expressed as

$$Z_u = \sqrt{\frac{P}{2}T_s} \left[D_u + N_u + \sum_{v=1, v \neq u}^U I_s(v) + \sum_{k=2}^K I_{M1}^{(k)} + \sum_{k=2}^K \sum_{v=1, v \neq u}^U I_{M2}^{(k)}(v) \right] \quad (3.111)$$

where N_u is the Gaussian noise contributed by $n(t)$ of (3.109), which can be expressed as

$$N_u = \left(\sqrt{\frac{P}{2}T_s} \right)^{-1} \int_0^{T_s} n(t) g_u c(t) \cos(2\pi f_u t) dt \quad (3.112)$$

which has zero mean and a variance of $g_u^2 N_0 / 2E_b$, with $E_b = PT_s$ representing the energy per bit. In (3.111) D_u is the desired output, which can be expressed as

$$D_u = g_u \alpha_u b_u \quad (3.113)$$

The self-interference term of $I_s(v)$ in (3.111) is contributed by the v th subcarrier of the reference user, which can be expressed as

$$I_s(v) = \frac{g_u \alpha_v b_v}{T_s} \int_0^{T_s} \cos[2\pi(f_v - f_u)t + \varphi_v] dt \quad (3.114)$$

Since in multitone DS-CDMA the spacing, Δ , between two adjacent subcarriers is $\Delta = 1/T_s$, $(f_v - f_u)$ has the form of n/T_s . Therefore,

$$\int_0^{T_s} \cos[2\pi(f_v - f_u)t + \varphi_v] dt = 0 \quad (3.115)$$

and, consequently,

$$I_s(v) = 0 \quad (3.116)$$

which shows that in multitone DS-CDMA there is no intercarrier interference inflicted by the same user's subcarrier signals, provided that all the subcarrier signals experience flat fading.

In (3.111) the multiuser interference has been divided into two terms, $I_{M1}^{(k)}$ and $I_{M2}^{(k)}(v)$, where $I_{M1}^{(k)}$ is due to the u th subcarrier of the k th user, which can be expressed as

$$\begin{aligned} I_{M1}^{(k)} &= \frac{g_u \alpha_u^{(k)} \cos(\varphi_u^{(k)})}{T_s} \int_0^{T_s} b_u^{(k)}(t - \tau_k) c_k(t - \tau_k) c(t) dt \\ &= \frac{g_u \alpha_u^{(k)} \cos(\varphi_u^{(k)})}{T_s} [b_u^{(k)}[-1] R_{k1}(\tau_k) + b_u^{(k)}[0] \hat{R}_{k1}(\tau_k)] \end{aligned} \quad (3.117)$$

where $R_{k1}(\tau_k)$ and $\hat{R}_{k1}(\tau_k)$ represent the partial cross-correlation functions defined as

$$R_{k1}(\tau_k) = \int_0^{\tau_k} c_k(t - \tau_k) c(t) dt \quad (3.118)$$

$$\hat{R}_{k1}(\tau_k) = \int_{\tau_k}^{T_s} c_k(t - \tau_k) c(t) dt \quad (3.119)$$

respectively.

By contrast, in (3.111) $I_{M2}^{(k)}(v)$ represents the multiuser interference from the v th, where $v \neq u$, subcarrier of the k th user, which can be expressed as

$$\begin{aligned} I_{M2}^{(k)}(v) &= \frac{g_u \alpha_v^{(k)}}{T_s} \int_0^{T_s} b_v^{(k)}(t - \tau_k) c_k(t - \tau_k) c(t) \cos[2\pi(f_v - f_u)t + \varphi_v^{(k)}] dt \\ &= \frac{g_u \alpha_v^{(k)}}{T_s} [b_v^{(k)}[-1] R_{k1}(\tau_k, \varphi_v^{(k)}, u, v) + b_v^{(k)}[0] \hat{R}_{k1}(\tau_k, \varphi_v^{(k)}, u, v)] \end{aligned} \quad (3.120)$$

where $R_{k1}(\tau_k, \varphi_v^{(k)}, u, v)$ and $\hat{R}_{k1}(\tau_k, \varphi_v^{(k)}, u, v)$ represent the partial cross-correlation functions. Considering that $(f_v - f_u) = (v - u)/T_s$, it can be shown that the partial cross-correlation functions can be expressed as

$$R_{k1}(\tau_k, \varphi_v^{(k)}, u, v) = \int_0^{\tau_k} c_k(t - \tau_k) c(t) \cos\left(\frac{2\pi(v - u)t}{T_s} + \varphi_v^{(k)}\right) dt \quad (3.121)$$

$$\hat{R}_{k1}(\tau_k, \varphi_v^{(k)}, u, v) = \int_{\tau_k}^{T_s} c_k(t - \tau_k) c(t) \cos\left(\frac{2\pi(v - u)t}{T_s} + \varphi_v^{(k)}\right) dt \quad (3.122)$$

Having obtained the decision variable Z_u as shown in (3.111), the u th bit transmitted by the user-of-interest can be detected as the sign of the decision variable Z_u , i.e. $b_u = \text{sign}(Z_u)$ for $u = 1, 2, \dots, U$.

The receiver of Fig. 3.17 for the multitone DS-CDMA system is composed of U correlators, each of which has the same structure as the corrector in single-carrier DS-CDMA. This is an optimum receiver for an AWGN channel [43], when the single-user case is considered. Unfortunately, when communicating over frequency selective fading channels the multitone DS-CDMA suffers from intercarrier interference and requires a high-complexity

RAKE-based receiver. However, in multitone DS-CDMA, the capability of achieving higher spreading gain results in the reduction of self-interference and multiple-access interference, as compared to a corresponding single-carrier DS-CDMA scheme. The multitone DS-CDMA scheme has a higher spreading factor than the corresponding single-carrier DS-CDMA scheme [23], where the relative spreading-factor extension is in proportion to the number of subcarriers. Therefore, the multitone DS-CDMA system may accommodate more users.

3.7 Generalized Multicarrier DS-CDMA

In Sections 3.5 and 3.6 we have shown the communications principles of the orthogonal MC DS-CDMA and that of the multitone DS-CDMA. In the multitone DS-CDMA system of Section 3.6, the subcarrier signals are chosen to be orthogonal to each other with minimum frequency separation before the associated DS spreading, as shown in (3.104), i.e.

$$\int_0^{T_s} \cos(2\pi f_i t + \phi_i) \cdot \cos(2\pi f_j t + \phi_j) dt = 0, \quad \text{for } i \neq j \quad (3.123)$$

Hence, the spacing Δ between two adjacent subcarrier frequencies is $\Delta = 1/T_s$, as shown in Fig. 3.16, where T_s is the multitone DS-CDMA signal's symbol duration. The subcarrier frequencies, therefore, take the values of $f_0 + i/T_s$ for $i = 0, 1, \dots, U - 1$, where f_0 represents the main carrier frequency. In contrast to the multitone DS-CDMA system of Section 3.6, in the orthogonal MC DS-CDMA system of Section 3.5, the subcarrier frequencies are chosen to be orthogonal to each other with the minimum frequency separation after the DS spreading, as shown in (3.83), which can be re-formulated as

$$\int_0^{T_c} \cos(2\pi f_i t + \phi_i) \cdot \cos(2\pi f_j t + \phi_j) dt = 0, \quad \text{for } i \neq j \quad (3.124)$$

when ignoring the data repetition on different subcarriers. Equation (3.124) implies that the spacing Δ between two adjacent subcarrier frequencies is $\Delta = 1/T_c$, as shown in Fig. 3.13, where T_c is the chip duration of the DS spreading codes and the subcarriers assume the frequency values of $f_0 + i/T_c$ for $i = 0, 1, \dots, U - 1$.

Let $N_e = T_s/T_c$ be the spreading factor of the DS spread subcarrier signals and we assume that each subcarrier signal has the same ‘null-to-null’ bandwidth of $2/T_c$. Then, it can be shown that the orthogonality condition of equation (3.123) of the multitone DS-CDMA system analysed in Section 3.6, in fact, includes the orthogonality condition of equation (3.124) stated in the context of the orthogonal MC DS-CDMA systems in Section 3.5. This observation can be proved by assuming that the frequency spacing between any two subcarriers is in the form, $f_i - f_j = mN_e/T_s$, where m is an integer. In this case, equation (3.123) can be expressed as

$$\int_0^{T_s} \cos(2\pi f_i t + \phi_i) \cdot \cos(2\pi f_j t + \phi_j) dt = \int_0^{T_s} \cos\left(\frac{2m\pi}{T_c}t + \psi_i\right) dt = 0 \quad (3.125)$$

where $\psi = \phi_i - \phi_j$. Note that, in equation (3.125) we used $N_e/T_s = 1/T_c$. To proceed further, equation (3.125) can be extended to

$$\sum_{l=0}^{N_e-1} \int_{lT_c}^{(l+1)T_c} \cos\left(\frac{2m\pi}{T_c}t + \psi_i\right) dt = 0 \quad (3.126)$$

where it can be shown that each term of the sum is zero. Hence

$$\int_0^{T_c} \cos\left(\frac{2m\pi}{T_c}t + \psi_i\right) dt = 0 \quad (3.127)$$

Furthermore, for two adjacent subcarriers associated with $m = 1$,

$$\int_0^{T_c} \cos\left(\frac{2\pi}{T_c}t + \psi_i\right) dt = 0 \quad (3.128)$$

which reflects the orthogonality between the subcarrier frequencies having the minimum frequency separation after DS spreading. In other words, (3.123) contains the orthogonality condition of the subcarrier frequencies in the orthogonal MC DS-CDMA system discussed in Section 3.5.

Furthermore, it can be readily shown that the orthogonality condition of (3.123) is obeyed, whenever the spacing Δ takes the form, $\Delta = \lambda/T_s$, $\lambda = 1, 2, \dots$, where λ is referred to as the normalized spacing between two adjacent subcarriers. The MC DS-CDMA scheme belongs to the family of multitone DS-CDMA arrangements having a spectrum of Fig. 3.16, if $\lambda = 1$, while to the class of orthogonal MC DS-CDMA systems with a spectrum shown in Fig. 3.13, if $\lambda = N_e$. Furthermore, there exists no overlap between the main lobes of the modulated subcarrier signals after DS spreading, when $\lambda = 2N_e$, which is the bandwidth requirement of the MC DS-CDMA system proposed in references [36, 37], when the time-limited chip waveform is used.

Based on the above observations, both the orthogonal MC DS-CDMA system and the multitone DS-CDMA system can be viewed as members of the class of generalized MC DS-CDMA systems having arbitrary subcarrier spacing of $\lambda \in \{1, 2, \dots\}$. Hence, the above generalized MC DS-CDMA system model includes a number of specific MC DS-CDMA schemes. Furthermore, based on the analysis of this general model, the results generated can be extended to different MC DS-CDMA systems simply by varying a single parameter, namely λ . Finally, the subcarrier spacing λ can be optimized according to specific design requirements tailored to the communication environments encountered, in order to achieve the optimum performance in terms of λ . For example, for a given total system bandwidth, λ can be optimized, in order to minimize the multiuser interference, since λ has an influence on both the overlap of the modulated signals of the subcarriers and on the processing gain. In this context a clear trade-off exists between the overlap and the processing gain. On the one hand, if λ is low – for example, $\lambda = 1$ – in the context of multitone DS-CDMA, then a subcarrier signal will overlap with a high number of subcarrier signals of both the same user and those of the interfering users. On the other hand, given a total bandwidth and a low value of λ , a high spreading gain can be maintained, which leads to the reduction of the multiuser interference. By contrast, if λ is high – for example $\lambda = 2N_e$ – which means that there exists no spectral overlap between the main lobes of the subcarrier signals, then the modulated subcarrier signals benefit from a low interference inflicted by the other subcarrier signals of both the reference and the interfering users. However, in this case the spreading gain of each subcarrier signal is low, leading to the increase of the multiuser interference. The influence of the subcarrier spacing λ on both the spreading gain and the spectral overlap of the subcarrier signals highlights that there exists an optimum spacing λ_{opt} , that may minimize the multiuser interference inflicted on each of the subcarrier signals. Another example in the context of

optimizing λ is that the subcarrier spacing λ can be set appropriately, in order to match the receiver requirements. For example, assuming that the receiver employs a three-finger RAKE receiver, then a specific spacing λ can be selected such that the number of resolvable paths associated with each subcarrier becomes three in the propagation environment typically encountered, since in this case, in addition to achieving the diversity gain, the receiver can combine all the energy scattered over the multipath components.

Below, we investigate the principles of the generalized MC DS-CDMA system having an arbitrary spacing of Δ , when assuming that each subcarrier signal experiences single-path fading. We begin by first considering the transmitter model.

3.7.1 Transmitted Signal

In references [53, 83–85], a generalized MC DS-CDMA system has been investigated, when it was assumed that each data stream is transmitted by single subcarrier, i.e. no data repetition on different subcarriers is assumed. In this section we further generalize the MC DS-CDMA scheme considered in references [53, 83–85] and consider the F-domain repetition of the transmitted data. In this case, the transmitter schematic diagram of the generalized MC DS-CDMA system is the same as that of the orthogonal MC DS-CDMA seen in Fig. 3.12. Hence, the transmitted signal can be expressed as

$$s_k(t) = \sum_{i=1}^q \sum_{j=1}^p \sqrt{\frac{2P}{p}} b_i^{(k)}(t) c_k(t) \cos(2\pi f_{ij} t + \phi_{ij}^{(k)}), \quad k = 1, 2, \dots, K \quad (3.129)$$

where q represents the number of bits transmitted per symbol, p represents the depth of repetition per bit, P is the transmitted power of each bit, $b_i^{(k)}(t) = \sum_{n=-\infty}^{\infty} b_i^{(k)}[n] P_{T_s}(t - nT_s)$, $i = 1, 2, \dots, q$ represents the binary data of the i th substream, where $b_i^{(k)}[n]$ is usually assumed to be a random variable taking the value of $+1$ or -1 with equal probability, while $P_{T_s}(t)$ represents the rectangular waveform. Furthermore, in (3.129) the spreading waveform $c_k(t)$ is formed by the T-domain spreading code assigned to the k th user, while $\phi_{ij}^{(k)}$ represents the initial phase associated with the carrier modulation in the context of subcarrier f_{ij} .

The total number of subcarriers of the generalized MC DS-CDMA system is $U = pq$. As the orthogonal MC DS-CDMA system considered in Section 3.6, we assume that the subcarriers conveying the same data substream have the frequencies chosen as far as possible, in order that a maximum possible frequency diversity gain can be achieved at the receiver. Hence, the subcarrier frequencies can be arranged according to (3.89) and (3.90). For the sake of convenience, the subcarriers below are sometimes indexed as $u = 1, 2, \dots, U = pq$. Whenever we consider the subcarriers without relating to the specific transmitted data substream, we simply use the subcarrier index of u . Note that, according to (3.90), (i, j) can be mapped to u according to the relationship of

$$u = (i - 1) + (j - 1)q + 1 \quad (3.130)$$

Based on the above assumptions, in the generalized MC DS-CDMA system, the subcarrier frequencies, $\{f_u, u = 1, 2, \dots, U\}$, can be arranged in the form

$$f_u = f_0 + \frac{\lambda(u - 1)}{T_s}, \quad u = 1, 2, \dots, U \quad (3.131)$$

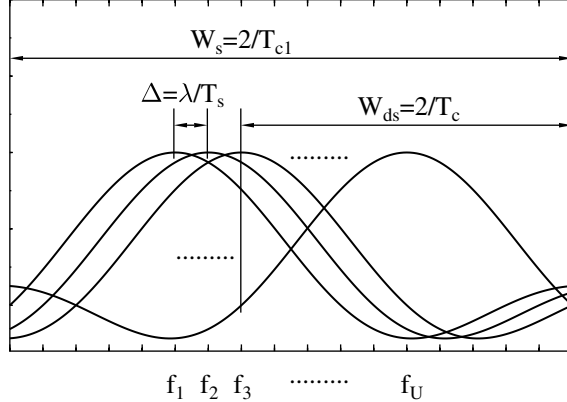


Figure 3.18: Spectrum of the generalized MC DS-CDMA signals.

where, again, λ represents the normalized spacing between two adjacent subcarriers, which may take a value of $\lambda = 1, 2, \dots, 2N_e$ corresponding to $\Delta = 1/T_s, 2/T_s, \dots, 2N_e/T_s$, if we assume that the maximum spacing between two adjacent subcarriers is $2N_e$. Note that, in the case of $\lambda = 2N_e$, there exists no spectral overlap between the main lobes of two adjacent subcarriers.

3.7.2 Modulation Parameters

The spectrum of the generalized MC DS-CDMA signal is shown in Fig. 3.18, where $W_s = 2/T_{c1}$ is the available bandwidth of the system considered, T_{c1} is the chip duration of a corresponding single-carrier DS-CDMA system, while $W_{ds} = 2/T_c$ represents the null-to-null bandwidth of the subcarrier signals. According to Fig. 3.18 the system's total transmission bandwidth, W_s , the subcarrier spacing, Δ , and the bandwidth, W_{ds} , of the subcarrier signal obey the relationship

$$W_s = (U - 1)\Delta + W_{ds} \quad (3.132)$$

This in turn means that

$$\frac{2}{T_{c1}} = (U - 1)\frac{\lambda}{T_s} + \frac{2}{T_c} \quad (3.133)$$

Since $T_s = qT_b = qN_1 T_{c1}$ and $T_s = N_e T_c$, after substituting these relationships into equation (3.133), the spreading gain associated with each subcarrier signal in the generalized MC DS-CDMA can be expressed as

$$N_e = qN_1 - \frac{(U - 1)\lambda}{2} \quad (3.134)$$

Specifically, for the orthogonal MC DS-CDMA of Section 3.5 associated with $\lambda = N_e$ in (3.134), we find that

$$N_e = \frac{2qN_1}{U + 1} \quad (3.135)$$

which is the subcarrier-related spreading factor of (3.87) for the orthogonal MC DS-CDMA. By contrast, if we substitute $\lambda = 1$ in (3.134), we obtain

$$N_e = \frac{2qN_1 - U + 1}{2} \quad (3.136)$$

which, in fact, is the subcarrier related spreading factor of (3.107) in the multitone DS-CDMA discussed in Section 3.6, when assuming that $q = U$, i.e. assuming that no F-domain repetition is employed by the data substreams.

The spectral gain of the generalized MC DS-CDMA scheme can be computed as

$$\begin{aligned} SG &= \frac{U(2/T_c)}{(U-1)(\lambda/T_s) + 2/T_c} \\ &= \frac{2N_e U}{2N_e + (U-1)\lambda} \end{aligned} \quad (3.137)$$

It can be shown that (3.137) is reduced to (3.88) of the spectral gain of the orthogonal MC DS-CDMA, when setting $\lambda = N_e$. However, (3.137) is reduced to (3.108) of the spectral gain of the multitone DS-CDMA, when we assume that $\lambda = 1$.

3.7.3 Correlation Receiver

Let us assume that the generalized MC DS-CDMA system supports K asynchronous CDMA users and all of the users use the same parameters $U = pq$ and N_e . The average power received from each user at the base station is also assumed to be the same, according to the perfect power control assumption. Furthermore, we assume that each subcarrier signal conflicts frequency non-selective fading. Consequently, when K signals described by equation (3.129) are transmitted over the above-mentioned channels, the received signal at the base station can be expressed as

$$r(t) = \sum_{k=1}^K \sum_{i=1}^q \sum_{j=1}^p \sqrt{\frac{2P}{p}} \alpha_{ij}^{(k)} b_i^{(k)} (t - \tau_k) c_k(t - \tau_k) \cos(2\pi f_{ij} t + \varphi_{ij}^{(k)}) + n(t) \quad (3.138)$$

where $\alpha_{ij}^{(k)}$ represents the channel-fading amplitude associated with the i th subcarrier, $\varphi_{ij}^{(k)} = \phi_{ij}^{(k)} + \psi_{ij}^{(k)} - 2\pi f_{ij} \tau_k$, where $\psi_{ij}^{(k)}$ is generated by the channel.

The correlation receiver diagram for the reference user of $k = 1$ is also the same, as the orthogonal MC DS-CDMA of Fig. 3.14. Therefore, the detection of the reference user can be analysed following the same procedure as that of the orthogonal MC DS-CDMA in Section 3.5.3.

Similar to the analysis for the orthogonal MC DS-CDMA in Section 3.5.3, let us consider the detection of the u th bit, b_u , transmitted by the first user (reference user) during the time-duration $[0, T_s]$. The corresponding decision variable for detecting b_u can be expressed as

$$Z_u = \sum_{v=1}^p Z_{uv} \quad (3.139)$$

$$Z_{uv} = \int_0^{T_s} r(t) g_{uv} c(t) \cos(2\pi f_{uv} t) dt \quad (3.140)$$

where g_{uv} is a parameter controlling which type of combining scheme is used, such as MRC or EGC, respectively. Moreover, in equation (3.140) the subscripts and superscripts associated with the reference user are omitted for notational simplicity. Furthermore, without loss of any generality, we let $\tau_1 = 0$, $\varphi_{uv} = 0$ in the following analysis, which represents the perfect synchronization and carrier tracking of the first user's transmitted signal. Substituting (3.138) into (3.140), Z_{uv} can be expressed as

$$Z_{uv} = \sqrt{\frac{P}{2p} T_s} \left[D_{uv} + N_{uv} + \sum_{k=2}^K I_{M1}^{(k)} + \sum_{k=2}^K \underbrace{\sum_{i=1}^q \sum_{\substack{j=1 \\ j \neq v \text{ if } i=u}}^p}_{I_{M2}^{(k)}(i, j)} I_{M2}^{(k)}(i, j) \right] \quad (3.141)$$

where N_{uv} is contributed by $n(t)$ of (3.138), which is a Gaussian random variable with zero mean and a variance of $p g_{uv}^2 N_0 / 2E_b$, where $E_b = P T_s$ represents the energy per bit. The variable D_{uv} in (3.141) represents the desired output given by combining (3.138) and (3.140) on setting $k = 1$, $i = u$ and $j = v$, which yields

$$D_{uv} = g_{uv} \alpha_{uv} b_u \quad (3.142)$$

The multiuser interference term $I_{M1}^{(k)}$ in equation (3.141) is due to the same subcarrier v inflicted by the interfering user for which we have $k \neq 1$. Then, $I_{M1}^{(k)}$ in equation (3.141) can be expressed as

$$I_{M1}^{(k)} = \frac{g_{uv} \alpha_{uv}^{(k)} \cos \varphi_{uv}^{(k)}}{T_s} [b_u^{(k)}[-1] R_{k1}(\tau_k) + b_u^{(k)}[0] \hat{R}_{k1}(\tau_k)] \quad (3.143)$$

where $R_{k1}(\tau_k)$ and $\hat{R}_{k1}(\tau_k)$ are the partial cross-correlation functions defined as

$$R_{k1}(\tau_k) = \int_0^{\tau_k} c_k(t - \tau_k) c(t) dt \quad (3.144)$$

$$\hat{R}_{k1}(\tau_k) = \int_{\tau_k}^{T_s} c_k(t - \tau_k) c(t) dt \quad (3.145)$$

Finally, the multiuser interference term $I_{M2}^{(k)}$ in equation (3.141) is due to the ij th subcarrier imposed by the interfering users associated with $k \neq 1$. Hence, $I_{M2}^{(k)}$ in equation (3.141) can be expressed as

$$I_{M2}^{(k)} = \frac{g_{uv} \alpha_{ij}^{(k)}}{T_s} [b_i^{(k)}[-1] R_{k1}(\tau_k, \varphi_{ij}^{(k)}, i, j) + b_i^{(k)}[0] \hat{R}_{k1}(\tau_k, \varphi_{ij}^{(k)}, i, j)] \quad (3.146)$$

where the associated partial cross-correlation functions are defined as

$$\begin{aligned} R_{k1}(\tau_k, \varphi_{ij}^{(k)}, i, j) &= \int_0^{\tau_k} c_k(t - \tau_k) c(t) \cos \left(\frac{2\pi\lambda[(i-u)+(j-v)q]t}{T_s} + \varphi_{ij}^{(k)} \right) dt \\ \hat{R}_{k1}(\tau_k, \varphi_{ij}^{(k)}, i, j) &= \int_{\tau_k}^{T_s} c_k(t - \tau_k) c(t) \cos \left(\frac{2\pi\lambda[(i-u)+(j-v)q]t}{T_s} + \varphi_{ij}^{(k)} \right) dt \end{aligned} \quad (3.147)$$

Finally, with the aid of (3.139), the transmitted bit $b_u, u = 1, 2, \dots, q$ by the reference user during $(0, T_s]$ can be detected as the sign of the decision variable $Z_u, u = 1, 2, \dots, q$, i.e. we have $b_u = \text{sign}(Z_u)$ for $u = 1, 2, \dots, q$.

Note that, in the context of the analysis of the orthogonal MC DS-CDMA in Section 3.5.3, we state that, when α_{uv} for different values of v are independent random variables, a diversity order of p can be achieved by combining the p number of subcarrier signals. However, in the context of the generalized MC DS-CDMA, the spacing λ between two adjacent subcarriers may take one value from $\{1, 2, \dots, 2N_e\}$. Hence, when λ has a relative high value, such as $\lambda \geq N_e$, the independently fading condition with respect to $\alpha_{uv}, v = 1, 2, \dots, p$ associated with the same data bit may be easily satisfied. However, when λ has a relative low value, the above independently fading condition might not be guaranteed. Therefore, for the generalized MC DS-CDMA system, a feasible analysis model may include a correlation function, which concerns about the correlations among the subcarriers.

Note also that both the analysis carried out in Section 3.5.3 for the orthogonal MC DS-CDMA and that in Section 3.6.3 constitute special examples of the analysis for the generalized MC DS-CDMA discussed in this section. It can be readily shown that, when the spacing $\lambda = N_e$, equations (3.143) to (3.147) reduce to the corresponding equations of the orthogonal MC DS-CDMA in Section 3.5.3. In the context of the multitone DS-CDMA corresponding to $\lambda = 1$, since F-domain repetition has not been invoked for the transmission of a data substream, the reduction from the generalized MC DS-CDMA to the multitone DS-CDMA can be achieved by letting $q = U$ and $p = 1$ and $\lambda = 1$ in the corresponding equations (3.129) and (3.147).

3.8 Time-Hopping Multicarrier CDMA

In this section the communication principles of a TH multicarrier CDMA (TH/MC-CDMA) scheme is analysed. In the TH/MC-CDMA system considered, data is transmitted using T-domain pulses with the aid of M -ary pulse-position modulation (MPPM), where information is extracted from one of the M possible time-slot positions, as shown in Section 2.4. This class of TH/MC-CDMA schemes may provide some advantages for multicarrier CDMA systems. For example, in TH/MC-CDMA the transmitter does not conflict the problem of nonlinear fluctuation resulting from the high PAPR, since, as will be seen in the forthcoming discourse, in the TH/MC-CDMA transmitter only one of the subcarrier signals is usually activated at any time instant. However, the FFT-assisted multicarrier demodulation technique can still be invoked for demodulating multiuser TH/MC-CDMA signals. Furthermore, in TH/MC-CDMA single-user or multiuser detection can be carried out after a single FFT multicarrier demodulation device.

3.8.1 Transmitted Signal

The transmitter schematic of the k th user is shown in Fig. 3.19 for the TH/MC-CDMA system. At the transmitter side, the input binary data having a period T_b and a rate R_b is S/P converted to U parallel substreams. During a frame interval of T_f seconds, each substream transmits $b = \log_2 M$ number of bits referred to as a symbol. Hence, each frame transmits U symbols in parallel and both the symbol duration and the frame duration are

$T_s = T_f = UbT_b$ seconds. Let the total number of subcarriers invoked in the TH/MC-CDMA system is UL and, hence, each substream is transmitted on L number of subcarriers. Let the TH address code of user k , $1 \leq k \leq K$, be expressed as $\mathbf{a}_k = [a_0^{(k)}, a_1^{(k)}, \dots, a_{L-1}^{(k)}]$, where $a_l^{(k)} \in GF(M)$, $l = 0, 1, \dots, L - 1$, and $GF(M)$ denotes a Galois field obeying $M = 2^b$. Furthermore, let $x_k \in GF(M)$ be a b -bit symbol of one of the U substreams, say u , which will be transmitted by the L number of subcarriers corresponding to the u th substream. Then, x_k is signatured by the k th user's TH address code, which can be expressed as

$$\mathbf{Y}_k = [y_k(0), y_k(1), \dots, y_k(L - 1)] = x_k \cdot \mathbf{1} \oplus \mathbf{a}_k \quad (3.148)$$

where $\mathbf{1}$ represents an all-one vector of length L , $y_k(l), 0 \leq l \leq L - 1$ are elements of $GF(M)$, and \oplus denotes the addition operation in $GF(M)$. As shown in Fig. 3.19, for each subcarrier branch, there are $M = 2^b$ time slots within a frame duration of T_f seconds. After the signaturing operation of (3.148), one of the M time slots corresponding to each subcarrier branch is then activated by one of the elements of \mathbf{Y}_k according to MPPM principles, as shown in Chapter 2. Specifically, for the u th substream transmitted by L number of subcarriers, the $y_k(l)$ th time slot of the l th subcarrier will be activated for transmission, while the other $(L - 1)$ time slots of the l th subcarrier cease transmission. After the above described TH operation, the l th subcarrier branch modulates a subcarrier frequency f_l for $l = 0, 1, \dots, L - 1$ within the active time slot. Finally, as shown in Fig. 3.19, the UL subcarrier-modulated signals are added in order to form the transmitted signal. For the u th substream, the transmitted signal can be expressed as

$$s_k(t) = \Re \left\{ \sqrt{\frac{2PM}{L}} \sum_{l=0}^{L-1} \psi_{T_h}(t - y_k(l)T_h) \exp(2\pi(f_c + f_l)t + \varphi_l^{(k)}) \right\} \quad (3.149)$$

where $\Re\{\cdot\}$ denotes the real-part, P represents the transmitted power of the u th substream, f_c represents the main carrier frequency, $\psi_{T_h}(t)$ represents a pulse-waveform defined within $[0, T_h]$ and it is normalized so that $\int_0^{T_h} \psi_{T_h}^2(t) dt = T_h$. Note that equation (3.149) considers only one of the U parallel substreams. The other parallel substreams can be considered in a similar way and have the same transmitted signal form as (3.149), except that the transmitted b -bit symbols and the subcarrier frequencies need to be changed accordingly.

3.8.2 Modulation Parameters

Let us assume a total W_s Hz of bandwidth that the TH/MC-CDMA system can exploit. Let us also assume that the input binary data rate be $R_b = 1/T_b$. Below, we investigate the constraints associated with the parameter M of the number of time slots per TH/MC-CDMA frame, the parameter L of the number of subcarriers per parallel substream used for transmission and the parameter W_{th} of the TH bandwidth, which is also the null-to-null bandwidth per subcarrier signal. The pictorial representation of the transmitted signal in a three-user TH/MC-CDMA system using $M = 8$ time slots per frame and $L = 4$ subcarriers is shown in Fig. 3.20, where we assumed that x_k in (3.148) are $x_1 = 3, x_2 = 5$ and $x_3 = 7$ and the TH address codes are $[1, 2, 4, 3]$ for user 1, $[4, 3, 6, 7]$ for user 2 and $[7, 5, 1, 2]$ for user 3.

First, when the TH duration is assumed to be T_h seconds, then the frequency spacing between two adjacent TH tones should not be less than $R_h = 1/T_h$ Hz, which is the constraint

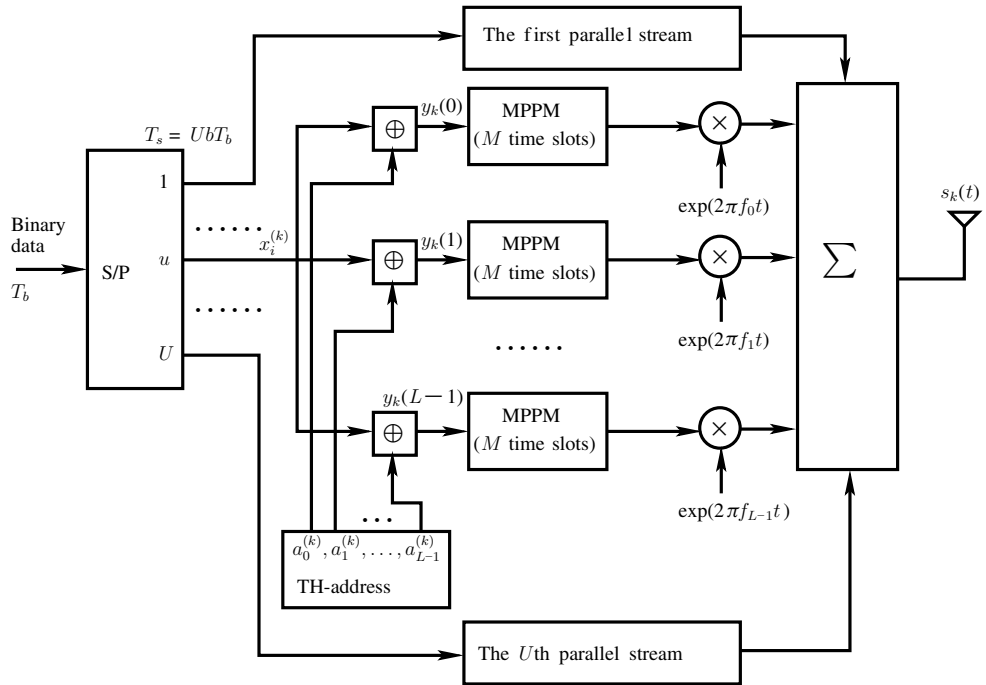


Figure 3.19: The k th user's transmitter schematic for the time-hopping multicarrier CDMA.

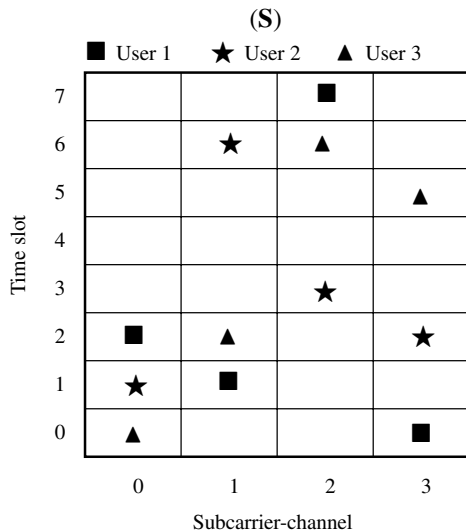


Figure 3.20: Pictorial representation of transmitted signals for a three-user TH/MC-CDMA system using $M = 8$ time slots per symbol and $L = 4$ multicarriers. The TH address codes are $[1, 2, 4, 3]$ for user 1, $[4, 3, 6, 7]$ for user 2 and $[7, 5, 1, 2]$ for user 3, while the 3-bit symbols transmitted are $x_1 = 3$ for user 1, $x_2 = 5$ for user 2 and $x_3 = 7$ for user 3.

assumed in this section. Consequently, for a TH/MC-CDMA system using UL number of subcarriers, we have the relationship among the parameters W_s , U and L expressed as

$$W_s \approx ULR_h = \frac{UL}{T_h} \quad (3.150)$$

Second, we know that the frame duration is $T_f = UbT_b$. Hence, the number of TH slots M obeys

$$M = 2^b = \frac{T_f = UbT_b}{T_h} \quad (3.151)$$

Solving for T_h from (3.150) and substituting it into (3.151), we obtain

$$\frac{M = 2^b}{b} = \frac{T_b W_s}{L} = \frac{W_s}{R_b L} \quad (3.152)$$

As an example, let us assume that $W_s = 4.096$ MHz, $R_b = 32$ K bits/second, $L = 4$. Then, using (3.152) we have $2^b/b = 32$, which can be satisfied, when we select the number of bits per symbol to be $b = 8$ implying $M = 2^b = 256$. Furthermore, if the number of parallel substreams or the number of symbols per frame is assumed to be $U = 16$, then the TH rate can be derived from (3.150), which is $R_h = 64$ K hops/second.

3.8.3 Receiver Model

When K number of TH/MC-CDMA signals obeying the form of (3.149) are transmitted synchronously over wireless channels, and if we assume that each subcarrier channel experiences flat-fading, the received complex low-pass equivalent signal can be expressed as

$$R(t) = \sum_{k=1}^K \sqrt{\frac{2PM}{L}} \sum_{l=0}^{L-1} \alpha_l^{(k)} \psi_{T_h}(t - y_k(l)T_h) \exp(j[2\pi f_l t + \varphi_l^{(k)}]) + N(t) \quad (3.153)$$

where $N(t)$ represents the complex valued low-pass equivalent AWGN with zero mean and single-sided PSD of $2N_0$, while $\alpha_l^{(k)}$ represents the fading amplitude.

Due to the TH characteristic, we assume that the receiver is unable to estimate the fading amplitudes $\{\alpha_l^{(k)}\}$ and the phases $\{\varphi_l^{(k)}\}$, except the synchronization with the received signal. The receiver schematic of the TH/MC-CDMA system considered is shown in Fig. 3.21, which essentially represents an energy assisted detector without requiring the knowledge of both the fading amplitudes and phases. The receiver constitutes a symbol-by-symbol or frame-by-frame detector. Specifically, at the receiver of Fig. 3.21, the received signal is first multicarrier demodulated with respect to each of the L subcarriers used for the transmission of the $M = 2^b$ -ary symbol x_k . Then, for each subcarrier branch, the output signal after subcarrier demodulation is input to a matched filter, which matches to the T-domain pulse $\psi_{T_h}(t)$ transmitted within a time slot. As shown in Fig. 3.21, the matched filter's output is sampled and then squared associated with each of the M number of time slots in a frame, in order to generate a decision variable for detecting the corresponding energy level. As shown in Fig. 3.21 the output variable matched to the subcarrier f_l and the m th time slot can be expressed as

$$R_{lm} = \left| \int_{mT_h}^{(m+1)T_h} R(t) \psi_{T_h}(t) \exp(-j2\pi f_l t) dt \right|^2 \quad (3.154)$$

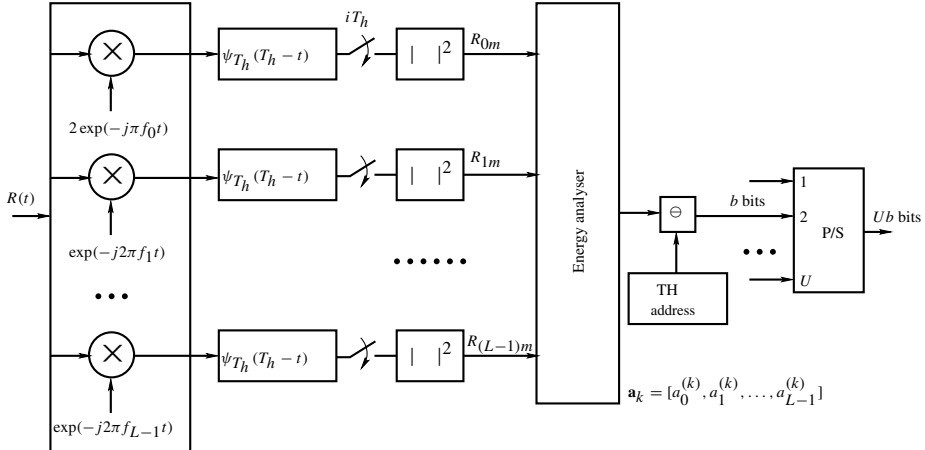


Figure 3.21: Receiver block diagram of the TH/MC-CDMA scheme.

for $m = 0, 1, \dots, M - 1; l = 0, 1, \dots, L - 1$. When orthogonal subcarriers are employed, then, on substituting the received signal of (3.153) into the above equation, the decision variable can be expressed as

$$R_{lm} = \left| \sum_{k=1}^K \sqrt{\frac{2E_s T_h}{L}} \alpha_l^{(k)} \exp(j\varphi_l^{(k)}) \delta[y_k(l), m] + N_{noise} \right|^2$$

$$m = 0, 1, \dots, M - 1; l = 0, 1, \dots, L - 1 \quad (3.155)$$

where $E_s = PT_s = PMT_h$ represents the transmitted energy per M -ary symbol and the function $\delta[x, y]$ is defined by $\delta[x, y] = 0$ for $x \neq y$ and $\delta[x, x] = 1$. Furthermore, in (3.155) N_{noise} contributed by $N(t)$ in (3.153) is a complex AWGN; both the real and image parts have zero mean and a common variance of $N_0 T_h$.

Since there are L subcarriers and each subcarrier conveys M number of time slots, we are provided with a total of ML number of outputs during a frame duration of $T_f = UbT_b$ seconds. As shown in Fig. 3.21, the time slots of L subcarriers in the context of each frame are analysed in order to determine which time slots and, hence, which b -bit symbol x_k was transmitted by invoking the detection scheme described below.

In TH/MC-CDMA systems, as described previously in the context of the transmitter of Fig. 3.19, a user address is employed as a unique signature sequence, in order to signal the time slots conveying a b -bit symbol of the user considered, as shown in (3.148). Following energy detection in terms of each time slot of the L subcarriers, the sequence \mathbf{Y}_k of (3.148) can be recovered by the receiver, provided that the channel is sufficiently good. By performing the subtraction operation of the unique user address \mathbf{a}_k of the k th user from \mathbf{Y}_k on a subcarrier-by-subcarrier basis, we arrive at

$$x_k \cdot \mathbf{1} = \mathbf{Y}_k \ominus \mathbf{a}_k \quad (3.156)$$

which allows us to recover the transmitted symbol x_k of user k . Note again that the subtraction operation in (3.156) as well as the addition operation in (3.148) should follow the rules defined in $GF(M)$.

The detection of TH/MC-CDMA signals follows the principles of the detections based on the time-frequency and time-time matrices discussed in Sections 2.3 and 2.4 in the context of FFH and FTH schemes. The detection operation can be understood by means of frequency-time matrices having M rows and L columns, where the M rows correspond to the M distinct time-slots of a frame, while the L columns represent the L number of subcarriers. We refer to the elements of the frequency-time matrices as frequency-time elements. The frequency-time matrix has the same feature as those shown in Fig. 3.20, where we assumed that a range of the frequency-time elements were activated by the transmitters of users 1, 2 and 3. In order to make use of the frequency-time matrices for facilitating the detection at the receiver, the first step is to form a received frequency-time matrix \mathbf{R} based on the decision variables. Specifically, let us assume that h is a decision threshold. Then, whenever the energy-related decision variable, say R_{lm} in (3.155), exceeds the threshold h , the corresponding frequency-time element at row m column l is flagged by a logical 1 (such as the markers shown in Fig. 3.20), otherwise, by a logical 0 (null).

Explicitly, the received frequency-time matrix \mathbf{R} considered in this section has the same characteristics as that in Sections 2.3 and 2.4. Hence, various detection schemes investigated in the above-mentioned sections can also be used in a similar way in this section for detecting the TH/MC-CDMA signals. Furthermore, with the aid of the frequency-time matrices, various single-user- or multiuser-based detection schemes [22, 86, 87] may also be employed for detecting the TH/MC-CDMA signals. The performance of the TH/MC-CDMA using the single-user and noncoherent multiuser detection will be explored in Chapters 4, 5 and 7, respectively.

TH/MC-CDMA is a multiple-access scheme that is designed based on the TH/MC modulation and CDMA techniques. The TH/MC-CDMA system is capable of providing a range of advantages. First, in TH/MC-CDMA, due to the TH characteristic, each subcarrier is only activated for a fraction of the frame time duration. Hence, the nonlinear fluctuation due to the high PAPR appearing in the conventional multicarrier systems can be significantly mitigated. However, the receiver of the TH/MC-CDMA systems can still benefit from the FFT-assisted demodulation, for detecting the multiuser signals with the aid of the frequency-time matrix-based detection schemes. Second, in the TH/MC-CDMA receiver the processing rate is on the order of the TH rate R_h . For a given system bandwidth, the TH rate R_h is inversely related to both the number of parallel data streams U and the number of subcarriers L conveying the same data symbol, i.e. $R_h \propto 1/UL$. Hence, the detection is significantly less demanding than the demodulation during each chip interval that would be necessitated in DS-CDMA. In the TH/MC-CDMA systems supporting broadband or UWB communications, relatively low-rate parallel digital signal processing techniques may be used for implementing the transceivers. Furthermore, the TH/MC-CDMA systems are in general less susceptible to the near-far problem than DS-CDMA systems, owing to the TH characteristics.

3.9 Time-Frequency-Domain Spread Multicarrier DS-CDMA

We know that in the context of the DS-CDMA communications there are two types of spread-spectrum scheme. The first of these spread-spectrum schemes, as shown in Section 2.1 spreads the original data stream using a signature code in the T-domain and the spread-

spectrum signal is transmitted using a single-carrier. By contrast, the second of these DS spread-spectrum schemes, as analysed in Sections 2.2 and 3.3, spreads the original data stream to a number of subcarriers using a signature code in the F-domain and each chip of the resultant spread-spectrum signal is transmitted by a different subcarrier. Hence, this scheme is also referred to as MC-CDMA. In this section we consider a spread-spectrum scheme that constitutes an amalgam of the above spread-spectrum schemes. More explicitly, this extended spread-spectrum arrangement spreads the transmitted data stream using two signature codes, where one of the signature codes corresponds to the T-domain spreading, while the other corresponds to the F-domain spreading. Since the proposed multicarrier DS-CDMA scheme employs both the above-mentioned T-domain spreading and F-domain spreading, it is referred to as TF-domain spread MC DS-CDMA.

3.9.1 Transmitted Signal

The transmitter schematic of MC DS-CDMA using both T-domain and F-domain, i.e. TF-domain spreading, is shown in Fig. 3.22 in the context of the k th user. At the transmitter side, the binary data stream $b_k(t)$ is first DS spread using the T-domain signature sequence $a_k(t)$. Following T-domain DS spreading, the spread-spectrum signal is divided into M parallel branches, where each branch of the signal is multiplied by the corresponding chip value of the F-domain spreading sequence $\mathbf{c}_k = [c_k[1], c_k[2], \dots, c_k[M]]^T$ of length M . Following F-domain spreading, each of the M branch signals modulates one of the M subcarrier frequencies using binary phase shift keying (BPSK). Then, the M number of subcarrier-modulated substreams are combined to form the transmitted signal $s_k(t)$. Hence, the transmitted signal of user k can be expressed as

$$s_k(t) = \sqrt{\frac{2P}{M}} \sum_{m=1}^M b_k(t)a_k(t)c_k[m] \cos(2\pi f_m t + \phi_{km}), \quad k = 1, 2, \dots, K \quad (3.157)$$

where P represents the identical transmitted power of each user, $\{f_m\}_{m=1}^M$ represents the subcarrier frequency set. The binary data stream's waveform $b_k(t) = \sum_{i=0}^{\infty} b_k[i]P_{T_b}(t - iT_b)$ consists of a sequence of mutually independent rectangular pulses of duration T_b and of amplitude $+1$ or -1 . In the T-domain spreading sequence $a_k(t) = \sum_{j=0}^{\infty} a_{kj}\psi_{T_c}(t - jT_c)$ of the k th user, $\psi_{T_c}(t)$ represents the T-domain chip waveform, which is defined over the interval $[0, T_c]$. We assume that the T-domain spreading factor is $N = T_b/T_c$, which represents the number of chips per bit duration. Furthermore, for the sake of simplicity, we assume that the subcarrier signals are orthogonal and that the spectral main lobes of the subcarrier signals do not overlap with each other.

3.9.2 Receiver Model

We assume that there are K number of asynchronous TF-domain spread MC DS-CDMA signals obeying the form of (3.157), that are transmitted over wireless channels. We assume that each subcarrier signal experiences flat-fading and also assume that the power received from each user is identical, implying perfect power control. Consequently, the received signal

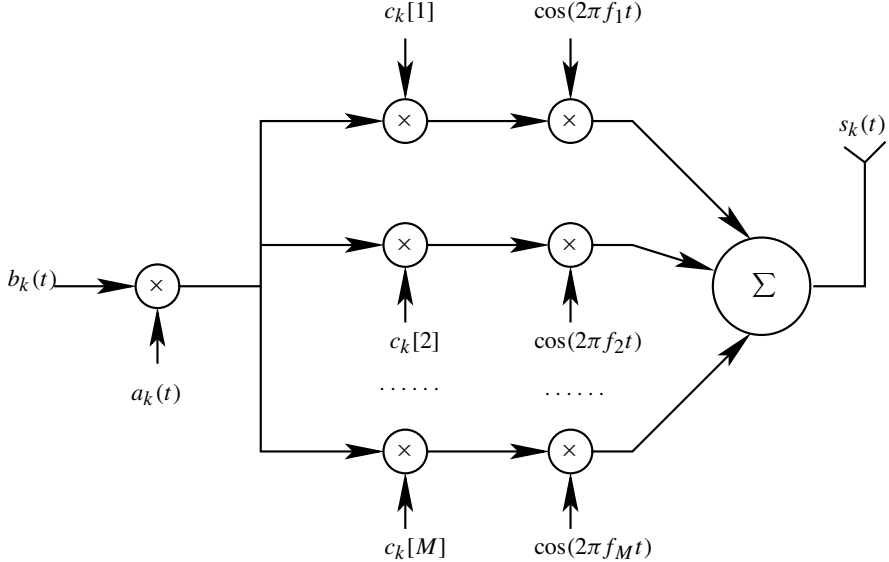


Figure 3.22: Transmitter model of MC DS-CDMA using both time-domain and frequency-domain spreading.

can be expressed as

$$r(t) = \sum_{k=1}^K \sqrt{\frac{2P}{M}} \sum_{m=1}^M \alpha_{km} b_k(t - \tau_k) a_k(t - \tau_k) c_k[m] \cos(2\pi f_m t + \varphi_{km}) + n(t) \quad (3.158)$$

where $n(t)$ represents the AWGN having zero mean and double-sided PSD of $N_0/2$, τ_k takes into account both the channel delay and the asynchronous transmission, while $\varphi_{km} = \phi_{km} - 2\pi f_m \tau_k$.

Let the first user be the user-of-interest and consider the correlator-based receiver of Fig. 3.23. It is explicit that Fig. 3.23 carries out the inverse operations of the functions seen in Fig. 3.22. We assume that the receiver has achieved perfect synchronization with the desired user's signals. Hence, we can set $\tau_1 = 0$ for convenience. Then, as shown in Fig. 3.23, the output variable related to the first data bit corresponding to the m th subcarrier of the first user can be expressed as

$$Z_{1m} = \int_0^{T_b} r(t) a_1(t) \cos(2\pi f_m t) dt, \quad m = 1, 2, \dots, M \quad (3.159)$$

where, for convenience, we assume that $\varphi_{1m} = 0$. Substituting (3.158) into (3.159) and considering the orthogonality between different subcarriers, it can be shown that the output variable Z_{1m} of Fig. 3.23 can be expressed as

$$Z_{1m} = \sqrt{\frac{P}{2M}} T_b \left\{ D_{1m} + \sum_{k=2}^K c_k[m] I_{k,m} + N_{1m} \right\} \quad (3.160)$$

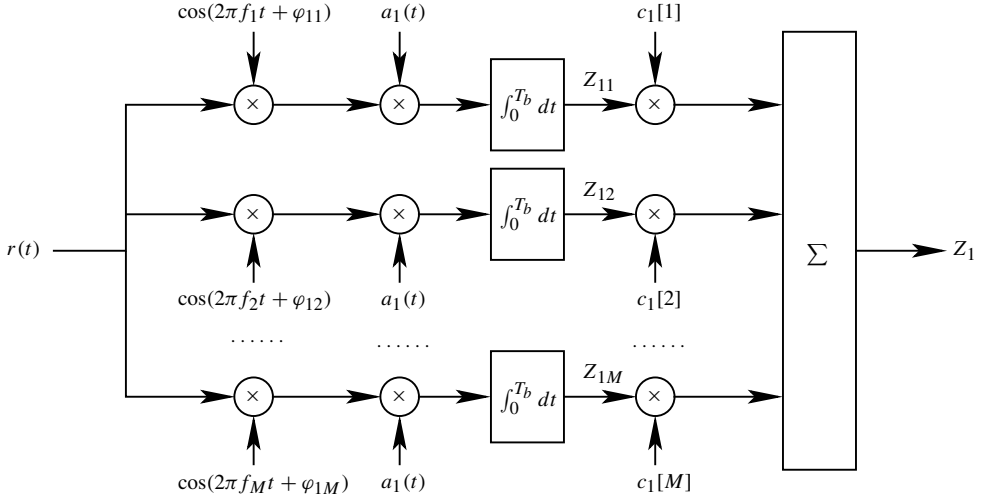


Figure 3.23: Receiver model of MC DS-CDMA using both time-domain and frequency-domain spreading.

where N_{1m} is contributed by $n(t)$ of (3.158), which is given by

$$N_{1m} = \left(\sqrt{\frac{P}{2M}} T_b \right)^{-1} \int_0^{T_b} n(t) a_1(t) \cos(2\pi f_m t) dt \quad (3.161)$$

which is a Gaussian random variable having zero mean and a variance of $MN_0/2E_b$, where $E_b = PT_b$ represents the energy per bit. In (3.160) D_{um} is the desired output derived by substituting (3.158) into (3.159) and setting $k = 1$. Hence, D_{um} can be written as

$$D_m = \alpha_{1m} b_1[0] c_1[m] \quad (3.162)$$

Finally, in (3.160) $I_{k,m}$ represents the MUI imposed by the k th user, which can be expressed as

$$\begin{aligned} I_{k,m} &= \frac{\alpha_{km} \cos(\varphi_{km})}{T_b} \int_0^{T_b} b_k(t - \tau_k) a_k(t - \tau_k) a_1(t) dt \\ &= \frac{\alpha_{km} \cos(\varphi_{km})}{T_b} [b_k[-1] R_{k1}(\tau_k) + b_k[0] \hat{R}_{k1}(\tau_k)] \end{aligned} \quad (3.163)$$

where $R_{k1}(\tau_k)$ and $\hat{R}_{k1}(\tau_k)$ represent the partial cross-correlation functions between $a_k(t - \tau_k)$ and $a_1(t)$, which can be expressed as

$$R_{k1}(\tau_k) = \int_0^{\tau_k} a_k(t - \tau_k) a_1(t) dt \quad (3.164)$$

$$\hat{R}_{k1}(\tau_k) = \int_{\tau_k}^{T_b} a_k(t - \tau_k) a_1(t) dt \quad (3.165)$$

More explicitly, the output variable corresponding to the first transmitted data bit, the m th subcarrier and the first user can be expressed as

$$Z_{1m} = \sqrt{\frac{P}{2M}} T_b \left\{ \alpha_{1m} b_1[0] c_1[m] + \sum_{k=2}^K c_k[m] I_{k,m} + N_{1m} \right\}, \quad m = 1, 2, \dots, M \quad (3.166)$$

The decision variable Z_u of Fig. 3.23, which corresponds to the first transmitted data bit of the reference user $k = 1$, is obtained by despreading each of the M branch outputs $\{Z_{11}, Z_{12}, \dots, Z_{1M}\}$ using the first user's F-domain spreading sequence \mathbf{c}_1 , which can be expressed as

$$\begin{aligned} Z_1 &= \sum_{m=1}^M c_1[m] Z_{1m} \\ &= \sqrt{\frac{P}{2M}} T_b \left\{ \sum_{m=1}^M c_1[m] D_{1m} + \sum_{k=2}^K \sum_{m=1}^M c_1[m] c_k[m] I_{k,m} + \sum_{m=1}^M c_1[m] N_{1m} \right\} \\ &= \sqrt{\frac{PM}{2}} T_b \left\{ b_1[0] \sum_{m=1}^M \alpha_{1m} + \sum_{k=2}^K I_{k,m} \sum_{m=1}^M c_u[m] c_k[m] + \sum_{m=1}^M c_1[m] N_{1m} \right\} \end{aligned} \quad (3.167)$$

It can be shown that, when the TF-domain spread MC DS-CDMA signals are transmitted over an AWGN channel, then $\alpha_{km} = \alpha_k$ is constant. Hence, (3.167) can be rewritten as

$$Z_1 = \sqrt{\frac{PM}{2}} T_b \left\{ \alpha_1 b_1[0] + \sum_{k=2}^K I_{k,m} \frac{1}{M} \sum_{m=1}^M c_1[m] c_k[m] + N_1 \right\} \quad (3.168)$$

where $N_1 = (1/M) \sum_{m=1}^M c_1[m] N_{1m}$, which is a Gaussian random variable having zero mean and a variance of $N_0/2E_b$. Let in (3.168), we define $\beta_{1k} = (1/M) \sum_{m=1}^M c_1[m] c_k[m]$, which is the cross-correlation factor between the F-domain spreading sequences \mathbf{c}_1 and \mathbf{c}_k assigned to users 1 and k . Then, (3.168) can be expressed in the form

$$Z_1 = \sqrt{\frac{PM}{2}} T_b \left\{ \alpha_1 b_1[0] + \sum_{k=1}^K I_{k1} + N_1 \right\} \quad (3.169)$$

where I_{k1} represents the multiuser interference imposed by the k th user, which can be expressed as

$$I_{k1} = I_{k,m} \beta_{1k} = \frac{\alpha_{km} \cos(\varphi_{km})}{T_b} [b_k[-1] R_{k1}(\tau_k) + b_k[0] \hat{R}_{k1}(\tau_k)] \times \beta_{1k} \quad (3.170)$$

Explicitly, according to (3.169), the first user's signal has been successfully despreaded. Furthermore, I_{k1} of (3.170) is a function of both the cross-correlation of the T-domain spreading sequences, $a_1(t)$ and $a_k(t)$, and that of the F-domain spreading sequences, \mathbf{c}_1

and \mathbf{c}_k . Furthermore, the effect of the MUI I_{k1} decreases, whenever the product of the T-domain and F-domain spreading factors, i.e. of N and M , increases.

When fading channels are considered, according to (3.167), although the first user's signal has been successfully despreaded, the decision variable of Z_1 for $b_1[0]$ represents the equal-gain combining (EGC) of the M number of subcarrier channels. This type of combining is suboptimum. When the receiver has the knowledge of the channel fading, a better (optimum) combining scheme is given by

$$\begin{aligned} Z_1 &= \sum_{m=1}^M \alpha_{1m} c_1[m] Z_{1m} \\ &= \sqrt{\frac{PM}{2}} T_b \left[b_1[0] \sum_{m=1}^M \alpha_{1m}^2 + \sum_{k=2}^K I_{k,m} \alpha_{1m} \sum_{m=1}^M c_u[m] c_k[m] + \sum_{m=1}^M \alpha_{1m} c_1[m] N_{1m} \right] \end{aligned} \quad (3.171)$$

which is the maximum ratio combining (MRC).

The benefits of employing both T-domain spreading and F-domain spreading in MC DS-CDMA systems are manifold. First, it is expected that in broadband multiple-access systems the system bandwidth may be of the order of tens or even hundreds of MHz. When single-carrier based DS-CDMA or MC-CDMA using solely T-domain spreading or solely F-domain spreading is utilized, the total system bandwidth is related to either the T-domain spreading factor or to the F-domain spreading factor. Consequently, these broadband systems may inevitably require a high chip rate and long spreading codes. In the TF-domain spread MC DS-CDMA scheme considered, the total system bandwidth is related to the product of the T-domain spreading factor and the F-domain spreading factor. Therefore, relatively low-chip-rate and short spreading codes can be used in the TF-domain spread MC DS-CDMA schemes. Second, the broadband multiple-access systems are expected to aim to support a wide range of services and bit rates, as well as to support a high number of simultaneous users. It is widely recognized that in CDMA-based communications multiuser detection [88] is capable of suppressing the multiuser interference and of significantly increasing the system's user capacity. When a single-carrier DS-CDMA or a MC-CDMA, which uses high spreading factors, is invoked for the sake of supporting a high number of users, the employment of advanced multiuser detection algorithms becomes impractical owing to their high complexity. By contrast, in the proposed TF-domain spread MC DS-CDMA schemes simultaneous users may be separated in both the T-domain and the F-domain directions with the aid of unique signature codes [55, 56]. The multiuser detection might be carried out separately in the T-domain and F-domain, as shown in the following chapters. Consequently, the detection complexity of the TF-domain spread MC DS-CDMA scheme may be significantly decreased in comparison to that of a conventional single-carrier DS-CDMA or MC-CDMA scheme.

3.10 Summary and Discussion

In this chapter we have established the principles of a range of multicarrier communications schemes, including the OFDM, F-domain spread MC-CDMA, SC-FDMA, orthogonal MC DS-CDMA, multitone DS-CDMA, generalized MC DS-CDMA, TH/MC-CDMA and the TF-domain spread MC DS-CDMA. The main characteristics as well as advantages

and disadvantages of the above-mentioned multicarrier schemes have been analysed. The principal characteristics of the multicarrier schemes include the following:

- In the OFDM scheme the number of subcarriers is determined by the number of symbols transmitted per OFDM block. In the F-domain spread MC-CDMA the number of subcarriers is determined by the number of symbols transmitted in a MC-CDMA symbol as well as by the spreading factor. The number of subcarriers in these two multicarrier schemes is usually high. Hence, multicarrier modulation/demodulation in these two multicarrier schemes can benefit from the FFT-based techniques. However, these two multicarrier schemes may conflict severe PAPR problem.
- The multicarrier schemes employing T-domain spreading, such as the orthogonal MC DS-CDMA, multitone DS-CDMA, generalized MC DS-CDMA and the TF-domain spread MC DS-CDMA, usually require a small number of subcarriers due to the T-domain spreading. For this reason, these multicarrier schemes have a less severe PAPR problem than the OFDM and F-domain spread MC-CDMA schemes. Since the number of subcarriers in these multicarrier schemes using T-domain spreading is usually not high, FFT-based multicarrier modulation/demodulation may not provide the advantages to these multicarrier schemes for reducing their implementation complexity.
- The TH/MC-CDMA scheme using MPPM may provide an alternative approach for implementing wireless systems employing huge bandwidths, such as in UWB communications. The TH/MC-CDMA scheme using MPPM can be implemented for noncoherent communications. It conflicts no PAPR problem and hence it is an energy-efficient multicarrier scheme.
- It seems that the SC-FDMA scheme employs the advantages of the OFDM, F-domain spread MC-CDMA and the conventional single-carrier DS-CDMA. Furthermore, the IFDMA scheme in SC-FDMA conflicts no PAPR problem, while the LFDMA scheme in SC-FDMA only conflicts slight PAPR problem. Since a user signal in the SC-FDMA is transmitted using only one subcarrier in the IFDMA or three subcarriers in the LFDMA in a way as in the conventional narrowband systems, the SC-FDMA signals might be readily interfered or jammed.
- The original OFDM scheme using no T-domain and/or F-domain spreading is for supporting point-to-point communications; it cannot support multiuser communications without deploying it with the other multiple-access techniques. Except for the OFDM scheme, all the multicarrier schemes considered in this chapter have the capability to support multiuser communications.

Performance of Multicarrier Systems over Gaussian Channels

4.1 Introduction

In this and the following chapters the bit-error rate (BER) performance of a variety of multicarrier systems is investigated, when the multicarrier signals are transmitted over additive white Gaussian noise (AWGN) channels or frequency selective fading channels. In these two chapters we consider only the representative multicarrier communications schemes considered in Chapter 3, which include the OFDM, frequency (F)-domain spread MC-CDMA, generalized MC DS-CDMA, time-hopping MC-CDMA (TH/MC-CDMA), as well as the time-frequency (TF)-domain spread MC DS-CDMA. As shown in Chapter 3, the other multicarrier schemes are either the special cases of the schemes considered in these two chapters, or their performance can be analysed using similar approaches to those in these two chapters. The detectors considered in these two chapters are single-user detectors, either the single-user correlation detectors or the single-user matched filter (MF)-based detectors. Furthermore, in this chapter the equivalency between the conventional single-carrier DS-CDMA and the F-domain spread MC-CDMA is established.

It is well recognized that the single-user bound BER performance, i.e. the BER performance achieved by a multicarrier system supporting the single-user, can provide insight into the performance limit that might be achieved by the corresponding multicarrier systems supporting multiple users, with the assistance of advanced signal processing techniques such as advanced multiuser detection techniques, etc. Hence, the BER performance analysis in the current and the following chapters is focused mainly on the multicarrier system supporting the single user. In the case of multiple users, we only provide the BER analysis in Section 4.6 and Section 5.11 in Chapter 5 in the context of the TF-domain spread MC DS-CDMA by invoking either the standard Gaussian approximation (SGA) or the simplified improved Gaussian approximation (SIGA). Explicitly, this multicarrier CDMA scheme is sufficiently general, and the corresponding analysis approaches can be readily extended to analyse the BER performance of the other types of multicarrier CDMA scheme supporting multiple

users. Note that a reader interested in using SGA for analysing the BER performance of various multicarrier CDMA systems may also be referred to [71] for more results.

In the current chapter we derive the BER expressions in detail for the multicarrier systems, when communicating over AWGN channels, where the observation samples $\{n_i\}$ obtained by sampling the unmodulated channels obey the zero-mean Gaussian PDF in the form

$$f_{n_i}(y) = \frac{1}{\sqrt{2\pi}\sigma} \exp\left(-\frac{y^2}{2\sigma^2}\right) \quad (4.1)$$

where σ^2 represents the noise variance, which is given by $\sigma^2 = N_0/2$, when a double-sided spectrum is observed and the double-sided power spectral density (PSD) is $N_0/2$ [2]. Note that, when a single-sided baseband spectrum is observed and the single-sided PSD is N_0 , then we have $\sigma^2 = N_0$.

We assume that, for systems employing coherent modulation, the baseband modulation scheme considered is BPSK or QPSK, when real-domain symbols or complex-domain symbols are transmitted. By contrast, for the TH/MC-CDMA that facilitates using noncoherent detections, the considered baseband modulation scheme is MPPM.

Note that, in our analysis, unless specifically notified, we assume that random spreading sequences and random hopping patterns are employed.

In the current chapter the PSD of both the TH/MC-CDMA and the TF-domain spread MC DS-CDMA are also derived. We show that the PSDs of most of the other multicarrier schemes, including OFDM, F-domain spread MC-CDMA, generalized MC DS-CDMA, frequency-hopping MC-CDMA, etc. constitute the special examples of the PSD of the TF-domain spread MC DS-CDMA scheme. These PSDs show the spectral advantages of using multicarrier CDMA over the single-carrier DS-CDMA, and can also provide us insight into the parameter design for a specific multicarrier scheme. We now consider the BER of the OFDM scheme.

4.2 Performance of Orthogonal Frequency-Division Multiplexing

Let us consider the complex baseband equivalent signals. Then, as shown in Section 3.2.4 of Chapter 3, after the multicarrier modulation with the aid of the IDFT, the time domain discrete signal can be expressed as

$$s_n = \frac{1}{\sqrt{M}} \sum_{k=0}^{M-1} x_k \exp\left(j \frac{2\pi nk}{M}\right), \quad n = 0, 1, \dots, M-1 \quad (4.2)$$

where

$$\mathbf{x} = [x_0, x_1, \dots, x_{M-1}]^T \quad (4.3)$$

contains the M number of symbols transmitted within one OFDM symbol duration of T_s seconds. It is assumed that x_k is normalized to $E[|x_k|^2] = 1$.

Let $\psi(t)$ be a time domain chip waveform, which is defined over the interval $[0, T_\psi]$ and normalized to satisfy $(T_\psi)^{-1} \int_0^{T_\psi} \psi^2(t) dt = 1$, where $T_\psi = T_s/M$ represents the chip

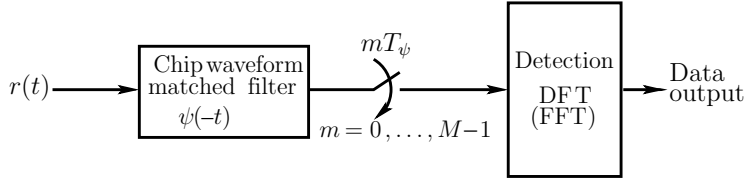


Figure 4.1: Schematic block diagram for detection of the OFDM signals.

duration. Then, after the IDFT the T-domain transmitted OFDM signal can be formulated as

$$s(t) = \sqrt{2P} \sum_{n=0}^{M-1} s_n \psi(t - nT_\psi) \quad (4.4)$$

where P represents the transmission power, and it can be seen that

$$\frac{1}{2} E[s^2(t)] = P \quad (4.5)$$

which is the total average transmission power on M number of subcarriers.

When the OFDM signal of (4.4) is transmitted over the AWGN channels, the received complex baseband equivalent signal can be expressed as

$$r(t) = \sqrt{2P} \sum_{n=0}^{M-1} s_n \psi(t - nT_\psi) + n(t) \quad (4.6)$$

where $n(t)$ represents the Gaussian process with zero mean and single-sided PSD of N_0 per dimension. Both the real and imaginary components of a sample of $n(t)$ obey the Gaussian PDF of (4.1) associated with a variance N_0 .

The schematic block diagram for detecting the OFDM signals is shown in Fig. 4.1, where the received signal $r(t)$ is first input to a filter matched to the transmitted chip waveform $\psi(t)$. The output of the MF is sampled at frequency $1/T_\psi$. Hence, corresponding to one OFDM symbol duration, a total of M samples can be obtained. Finally, the transmitted M symbols are recovered by executing the DFT on the M samples.

In more detail, after the normalization using $\sqrt{2PT_\psi}$, the i th sample can be expressed as

$$y_i = \frac{1}{\sqrt{2PT_\psi}} \int_{iT_\psi}^{(i+1)T_\psi} r(t) \psi^*(t - iT_\psi) dt \quad (4.7)$$

Substituting (4.6) into the above equation gives

$$\begin{aligned} y_i &= s_i + n_i \\ &= \frac{1}{\sqrt{M}} \sum_{k=0}^{M-1} x_k \exp\left(j \frac{2\pi i k}{M}\right) + n_i, \quad i = 0, 1, \dots, M-1 \end{aligned} \quad (4.8)$$

where

$$n_i = \frac{1}{\sqrt{2PT_\psi}} \int_{iT_\psi}^{(i+1)T_\psi} n(t) \psi^*(t - iT_\psi) dt \quad (4.9)$$

which is a Gaussian random variable having zero mean and a variance of $N_0/2E_\psi$ per dimension, where $E_\psi = PT_\psi$ represents the energy per chip.

Let

$$\begin{aligned}\mathbf{y} &= [y_0, y_1, \dots, y_{M-1}]^T \\ \mathbf{n} &= [n_0, n_1, \dots, n_{M-1}]^T\end{aligned}\quad (4.10)$$

Then, \mathbf{y} of the observations associated with the M chips per OFDM symbol can be expressed as

$$\mathbf{y} = \mathcal{F}^H \mathbf{x} + \mathbf{n} \quad (4.11)$$

where, again, \mathcal{F} is the DFT matrix given by (3.29).

Consequently, after the DFT operation on \mathbf{y} of (4.11) as seen in Fig. 4.1 and using the relationship of $\mathcal{F}\mathcal{F}^H = \mathcal{F}^H\mathcal{F} = \mathbf{I}_M$, the decision variables for \mathbf{x} can be obtained as

$$\mathbf{z} = [z_0, z_1, \dots, z_{M-1}]^T = \mathcal{F}\mathbf{y} = \mathbf{x} + \mathbf{n}' \quad (4.12)$$

where \mathbf{n}' can be expressed as

$$\mathbf{n}' = \mathcal{F}\mathbf{n} \quad (4.13)$$

which is Gaussian with mean zero and a covariance matrix given by

$$E[(\mathbf{n}')(\mathbf{n}')^H] = E[\mathcal{F}\mathbf{n}\mathbf{n}^H\mathcal{F}^H] = \mathcal{F}E[\mathbf{n}\mathbf{n}^H]\mathcal{F}^H = \frac{N_0}{E_\psi}\mathcal{F}\mathcal{F}^H = \frac{N_0}{E_\psi}\mathbf{I}_M \quad (4.14)$$

Therefore, the entries of \mathbf{n}' are independent Gaussian random variables with zero mean and a common variance of $N_0/2E_\psi$ per dimension.

Let us assume that QPSK baseband symbols are transmitted. Then, $x_m = (a_m + jb_m)/\sqrt{2}$ for $m = 0, 1, \dots, M-1$, where a_m and b_m are binary bits. Hence, a_m and b_m can be recovered, respectively, from the real and imaginary parts of z_m , which, according to (4.12), is given by

$$z_m = x_m + n'_m, \quad m = 0, 1, \dots, M-1 \quad (4.15)$$

Given E_b of the transmitted energy per bit, it can be shown that $E_\psi = PT_s/M = 2ME_b/M = 2E_b$, since M symbols are transmitted by an OFDM block and each symbol contains two bits. Hence, n'_m in (4.15) is complex Gaussian distributed with zero mean and a variance of $N_0/4E_b$. Let us assume that $a_m = -1$ is transmitted. Then, the BER can be computed as follows.

$$\begin{aligned}P_b &= P\left(\frac{-1}{\sqrt{2}} + \Re\{n_m\} > 0\right) \\ &= P\left(\Re\{n_m\} > \frac{1}{\sqrt{2}}\right) \\ &= \int_{1/\sqrt{2}}^{\infty} \frac{1}{\sqrt{2\pi N_0/4E_b}} \exp\left(-\frac{y^2}{2N_0/4E_b}\right) dy\end{aligned}\quad (4.16)$$

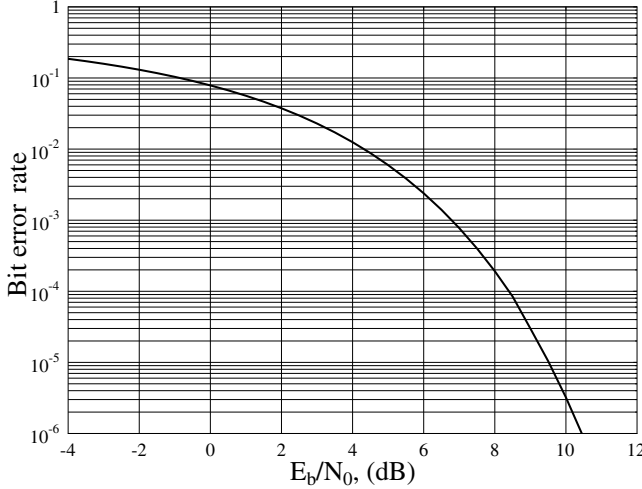


Figure 4.2: Performance of OFDM systems when communicating over AWGN channels.

Using the variable transform of $t = y/\sqrt{N_0/4E_b}$, we can modify the above equation to

$$\begin{aligned} P_b &= \frac{1}{\sqrt{2\pi}} \int_{\sqrt{2E_b/N_0}}^{\infty} \exp\left(-\frac{t^2}{2}\right) dt \\ &= Q\left(\sqrt{\frac{2E_b}{N_0}}\right) \end{aligned} \quad (4.17)$$

Equation (4.17) shows that the BER of the OFDM system is the same as the conventional well-known BPSK scheme [2], when communicating over AWGN channels. The BER performance is shown in Fig. 4.2, a BER of 10^{-6} can be achieved at an SNR of about 10.3 dB.

Above, the BER of the OFDM is analysed following the steps of the IDFT and DFT. For the sake of analysis, we can derive the decision variables following straightforwardly the multicarrier modulation/demodulation principles. Below, we demonstrate that this approach arrives at the same decision variables as the IDFT/DFT approach.

The transmitted complex baseband equivalent OFDM signal can be expressed as

$$s(t) = \sqrt{\frac{2P}{M}} \sum_{k=0}^{M-1} x_k \exp\left(j \frac{2\pi kt}{T_s}\right), \quad 0 \leq t < T_s \quad (4.18)$$

where T_s is the duration of an OFDM symbol. When this OFDM signal is transmitted over the AWGN channels, the received signal can be expressed as

$$r(t) = \sqrt{\frac{2P}{M}} \sum_{k=0}^{M-1} x_k \exp\left(j \frac{2\pi kt}{T_s}\right) + n(t), \quad 0 \leq t < T_s \quad (4.19)$$

At the receiver the decision variable z_m for x_m can be formed as

$$z_m = \frac{1}{\sqrt{2P/M T_s}} \int_0^{T_s} r(t) \exp\left(-j \frac{2\pi mt}{T_s}\right) dt, \quad m = 0, 1, \dots, M-1 \quad (4.20)$$

Substituting (4.19) into (4.20) and using the fact that the subcarrier signals are orthogonal, we obtain

$$z_m = x_m + n'_m, \quad m = 0, 1, \dots, M - 1 \quad (4.21)$$

where

$$n'_m = \frac{1}{\sqrt{2P/MT_s}} \int_0^{T_s} n(t) \exp\left(-j\frac{2\pi mt}{T_s}\right) dt \quad (4.22)$$

which is Gaussian distributed with zero mean. Furthermore, it can be shown that the single-dimensional variance of n'_m is

$$E[|n'_m|^2] = \frac{MN_0}{2PT_s} = \frac{MN_0}{2ME_\psi} = \frac{N_0}{2E_\psi} \quad (4.23)$$

Therefore, we can conclude that (4.21) is the same as (4.15). Therefore, in our forthcoming discourse, our analysis will mainly be based on the straightforward multicarrier modulation/demodulation approach, unless the IDFT/DFT-based modulation/demodulation is otherwise specified. We now analyse the BER performance of the MC-CDMA using F-domain spreading.

4.3 Performance of Single-User Frequency-Domain Spread Multicarrier CDMA

We consider the F-domain spread MC-CDMA scheme, the transmitter of which uses S/P conversion and q bits are transmitted in parallel within one MC-CDMA symbol duration of $T_s = qT_b$ seconds. The transmitted signal in the considered MC-CDMA is given in (3.32). When communicating over the AWGN channel and assuming that only one user is supported by the MC-CDMA, the received complex baseband equivalent signal can be expressed as

$$R(t) = \sqrt{\frac{2P}{N_p}} \sum_{i=1}^q \sum_{j=1}^{N_p} b_i^{(k)}(t) c_k[j-1] \exp(j2\pi f_{ij} t + \varphi_{ij}^{(k)}) + n(t) \quad (4.24)$$

where $n(t)$ represents a complex Gaussian process, which has zero mean and a single-sided PSD of N_0 per dimension. The other arguments in (4.24) have been stated associated with (3.32) and (3.39).

Consider reception of the first MC-CDMA symbol and let

$$y_\lambda = (\sqrt{2P}T_s)^{-1} \int_0^{T_s} R(t) \exp(-j2\pi f_\lambda t + \varphi_\lambda^{(k)}) dt \quad (4.25)$$

denote the normalized output of the filter matched to the λ th subcarrier. Then, it can be shown that, when $\lambda = (i-1) + (j-1)q$, the corresponding output can be expressed as

$$y_{ij} = \frac{1}{\sqrt{N_p}} b_i^{(k)}[0] c_k[j-1] + n_{ij}, \quad i = 1, 2, \dots, q; \quad j = 1, 2, \dots, N_p \quad (4.26)$$

where

$$n_{ij} = (\sqrt{2P}T_s)^{-1} \int_0^{T_s} n(t) \exp(-j2\pi f_\lambda t + \varphi_\lambda^{(k)}) dt \quad (4.27)$$

which has zero mean and both the real and imaginary components of which have a common variance of $N_0/2E_b$, where $E_b = PT_s$ represents the energy per bit.

Let

$$\begin{aligned}\mathbf{y} &= [y_{11}, \dots, y_{1N_p}, \dots, y_{q1}, \dots, y_{qN_p}]^T \\ \mathbf{n} &= [n_{11}, \dots, n_{1N_p}, \dots, n_{q1}, \dots, n_{qN_p}]^T \\ \mathbf{b}_k &= [b_1^{(k)}[0], b_2^{(k)}[0], \dots, b_q^{(k)}[0]]^T\end{aligned}\quad (4.28)$$

Then, \mathbf{y} can be expressed as

$$\mathbf{y} = \mathbf{C}_k \mathbf{b}_k + \mathbf{n} \quad (4.29)$$

where, by definition, \mathbf{C}_k is a $(qN_p \times q)$ spreading matrix, which can be expressed as

$$\mathbf{C}_k = \frac{1}{\sqrt{N_p}} \begin{bmatrix} \mathbf{c}_k & \mathbf{0} & \dots & \mathbf{0} \\ \mathbf{0} & \mathbf{c}_k & \dots & \mathbf{0} \\ \vdots & \vdots & \ddots & \vdots \\ \mathbf{0} & \mathbf{0} & \dots & \mathbf{c}_k \end{bmatrix} = \frac{1}{\sqrt{N_p}} (\mathbf{I}_q \otimes \mathbf{c}_k) \quad (4.30)$$

where \mathbf{c}_k contains the chips of the spreading code assigned to the k th user, which is expressed as $\mathbf{c}_k = [c_k[0], c_k[1], c_k[N_p - 1]]^T$, \mathbf{I}_q is a $(q \times q)$ identity matrix, while \otimes represents the *Kronecker product* operation [89].

According to (4.29), explicitly, \mathbf{b}_k can be readily recovered by a correlation detector, which generates the decision variables given by

$$\mathbf{z} = \mathbf{C}_k^T \mathbf{y} = \mathbf{b}_k + \mathbf{C}_k^T \mathbf{n} \quad (4.31)$$

where $\mathbf{C}_k^T \mathbf{C}_k = \mathbf{I}_q$ was applied. Consequently, the decision variable z_i corresponding to b_i is given by

$$z_i = b_i^{(k)}[0] + \Re\{n_i\}, \quad i = 1, 2, \dots, q \quad (4.32)$$

where n_i is the i th element of $\mathbf{C}_k^T \mathbf{n}$, which has zero mean and a variance of $N_0/2E_b$ per dimension.

Assuming that the information source constitutes independently identically distributed (i.i.d) binary bits, based on (4.32), the BER of the F-domain spread MC-CDMA system can be readily derived, which is given by

$$P_b = Q\left(\sqrt{\frac{2E_b}{N_0}}\right) \quad (4.33)$$

Hence, when supporting the single user, the F-domain spread MC-CDMA is capable of achieving the same BER of (4.17) as the OFDM scheme and the conventional BPSK communication scheme.

4.4 Performance of Single-User Multicarrier DS-CDMA

In Chapter 3 we showed that the orthogonal MC DS-CDMA [41] and the multitone DS-CDMA [43] constitute specific examples of the generalized MC DS-CDMA [53, 84]. Hence,

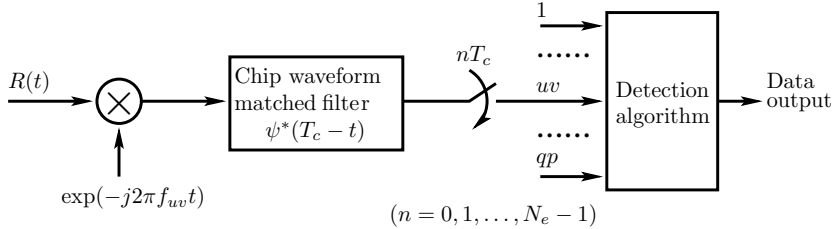


Figure 4.3: Receiver schematic for the MC DS-CDMA systems.

in this section we analyse the BER performance in detail for the generalized MC DS-CDMA. The BER for the orthogonal MC DS-CDMA and the multitone DS-CDMA can be readily obtained by appropriately modifying the spacing parameter, λ , as seen in Section 3.7. Note that, for the sake of notational convenience, we simply refer to the generalized MC DS-CDMA as the MC DS-CDMA in this section.

The transmitter schematic block diagram for the MC DS-CDMA scheme is shown in Fig. 3.12 and the transmitted MC DS-CDMA signal is given by (3.129). Consequently, when assuming that the MC DS-CDMA supports one user and that the MC DS-CDMA signal is transmitted over AWGN channels, the received complex baseband equivalent signal can be expressed as

$$R(t) = \sum_{i=1}^q \sum_{l=1}^p \sqrt{\frac{2P}{p}} b_i^{(k)}(t) c_k(t) \exp(j[2\pi f_{il} t + \varphi_{il}^{(k)}]) + n(t) \quad (4.34)$$

where $n(t)$ is the complex baseband equivalent Gaussian noise, which has zero mean and a single-sided PSD of N_0 per dimension. As shown in (4.34), in one MC DS-CDMA symbol q data bits are transmitted in parallel and each of the q bits is transmitted on p subcarriers. For the details of the other variables in (4.34), refer to (3.129).

In Chapter 3 we considered the symbol-based correlation single-user detector; the receiver schematic diagram is shown in Fig. 3.14. In this section we still consider the symbol-based correlation single-user detector. However, instead of using the symbol-based correlators as shown in Fig. 3.14, we consider the receiver schematic of Fig. 4.3, where, following the multicarrier demodulation, a chip waveform MF with the time-domain impulse response $\psi^*(T_c - t)$ is used associated with each of the subcarriers. As shown in Fig. 4.3, the MF outputs are sampled at the chip rate in order to obtain the observation samples for detecting the transmitted information.

According to Fig. 4.3, the n th observation sample with respect to the first transmitted symbol and the uv th subcarrier can be expressed as

$$y_{uv,n} = (\sqrt{2PN_e} T_c)^{-1} \int_{nT_c}^{(n+1)T_c} R(t) \exp(-j[2\pi f_{uv} t + \varphi_{uv}^{(k)}]) \psi^*(t) dt$$

$$u = 1, 2, \dots, q; v = 1, 2, \dots, p; n = 0, 1, \dots, N_e - 1 \quad (4.35)$$

where $N_e = T_s/T_c$ represents the number of chips per symbol. Substituting (4.34) into (4.35), we can express $y_{uv,n}$ as

$$y_{uv,n} = \frac{c_n^{(k)}}{\sqrt{pN_e}} [b_u^{(k)}[0](1 + \text{BI}_{uv,n}) + \text{IBI}_{uv,n}] + N_{uv,n} \quad (4.36)$$

where $N_{uv,n}$ is a complex AWGN sample,

$$N_{uv,n} = (\sqrt{2PN_e}T_c)^{-1} \int_{nT_c}^{(n+1)T_c} n(t) \exp(-j[2\pi f_{uv}t + \varphi_{uv}^{(k)}]) \psi^*(t) dt \quad (4.37)$$

which has a zero mean and a variance of $N_0/2E_b$ per dimension. In (4.36) $\text{BI}_{uv,n}$ is due to the interference imposed by the subcarriers conveying $b_u^{(k)}[0]$, which can be expressed as

$$\text{BI}_{uv,n} = \sum_{l=1, l \neq v}^p \frac{\exp(j\Delta\varphi_{u,lv}^{(k)})}{T_c} \int_{nT_c}^{(n+1)T_c} \psi^2(t) \exp(j2\pi\Delta f_{u,lv}t) dt \quad (4.38)$$

where $\Delta f_{u,lv} = f_{ul} - f_{uv}$ and $\Delta\varphi_{u,lv}^{(k)} = \varphi_{ul}^{(k)} - \varphi_{uv}^{(k)}$. In (4.36) $\text{IBI}_{uv,n}$ is due to the interference imposed by the subcarriers conveying all the other bits except $b_u^{(k)}[0]$. $\text{IBI}_{uv,n}$ can be expressed as

$$\text{IBI}_{uv,n} = \sum_{i=1, i \neq u}^q b_i^{(k)}[0] \sum_{l=1}^p \frac{\exp(j\Delta\varphi_{iu,lv}^{(k)})}{T_c} \int_{nT_c}^{(n+1)T_c} \psi^2(t) \exp(j2\pi\Delta f_{iu,lv}t) dt \quad (4.39)$$

where $\Delta f_{iu,lv} = f_{il} - f_{uv}$ and $\Delta\varphi_{iu,lv}^{(k)} = \varphi_{il}^{(k)} - \varphi_{uv}^{(k)}$.

According to (3.130) and (3.131), we then have

$$\begin{aligned} \Delta f_{u,lv} &= \frac{\lambda(l-v)q}{T_s} \\ \Delta f_{iu,lv} &= \frac{\lambda[(i-u)+(l-v)q]}{T_s} \end{aligned} \quad (4.40)$$

Furthermore, with (4.38), (4.39) and (4.40), it can be implied that, for a given λ value and a given type of chip waveform, the integrations in (4.38) and (4.39) generate constant values. Let us define

$$\begin{aligned} \text{BI}_{ul,uv,n} &= \frac{1}{T_c} \int_{nT_c}^{(n+1)T_c} \psi^2(t) \exp(j2\pi\Delta f_{u,lv}t) dt, \quad l = 1, \dots, p, \quad l \neq v \\ \text{IBI}_{il,uv,n} &= \frac{1}{T_c} \int_{nT_c}^{(n+1)T_c} \psi^2(t) \exp(j2\pi\Delta f_{iu,lv}t) dt \\ i &= 1, \dots, q, \quad i \neq u; \quad l = 1, \dots, p \end{aligned} \quad (4.41)$$

Explicitly, we have $\text{BI}_{ul,uv,n} = \text{BI}_{uv,ul,n}^*$ and $\text{IBI}_{il,uv,n} = \text{IBI}_{uv,il,n}^*$. Then, we can rewrite (4.38) and (4.39) as

$$\text{BI}_{uv,n} = \sum_{l=1, l \neq v}^p \text{BI}_{ul,uv,n} \exp(j\Delta\varphi_{u,lv}^{(k)}) \quad (4.42)$$

$$\text{IBI}_{uv,n} = \sum_{i=1, i \neq u}^q b_i^{(k)}[0] \sum_{l=1}^p \text{IBI}_{il,uv,n} \exp(j\Delta\varphi_{iu,lv}^{(k)}) \quad (4.43)$$

Let us first analyse the interference terms. Let

$$\begin{aligned} \mathbf{IBI}_{i,uv,n} &= [\text{IBI}_{i1,uv,n}, \text{IBI}_{i2,uv,n}, \dots, \text{IBI}_{ip,uv,n}]^T \\ \boldsymbol{\varphi}_{i,uv} &= [\exp(j\Delta\varphi_{iu,1v}^{(k)}), \exp(j\Delta\varphi_{iu,2v}^{(k)}), \dots, \exp(j\Delta\varphi_{iu,pv}^{(k)})]^T \end{aligned} \quad (4.44)$$

where $\boldsymbol{\varphi}_{i,uv}$ is independent of the index n . Let $\mathbf{IBI}_{i\bar{l},uv,n}$ and $\boldsymbol{\varphi}_{i\bar{l},uv}$ be the vectors formed, respectively, from $\mathbf{IBI}_{i,uv,n}$ and $\boldsymbol{\varphi}_{i,uv}$ by removing the l th elements. Then, (4.42) and (4.43) can be expressed in matrix form as

$$\text{BI}_{uv,n} = (\mathbf{IBI}_{u\bar{v},uv,n})^T \boldsymbol{\varphi}_{u\bar{v},uv} \quad (4.45)$$

$$\text{IBI}_{uv,n} = \sum_{i=1, i \neq u}^q b_i^{(k)}[0] (\mathbf{IBI}_{i,uv,n})^T \boldsymbol{\varphi}_{i,uv} \quad (4.46)$$

Let us define

$$\mathbf{IBI}_{uv,n} = [(\mathbf{IBI}_{1,uv,n})^T, (\mathbf{IBI}_{2,uv,n})^T, \dots, (\mathbf{IBI}_{q,uv,n})^T]^T \quad (4.47)$$

$$\boldsymbol{\varphi}_{uv,c} = \text{diag}\{\boldsymbol{\varphi}_{1,uv}, \boldsymbol{\varphi}_{2,uv}, \dots, \boldsymbol{\varphi}_{q,uv}\} \quad (4.48)$$

$$\mathbf{b}^{(k)} = [b_1^{(k)}[0], b_2^{(k)}[0], \dots, b_q^{(k)}[0]]^T \quad (4.49)$$

where $\mathbf{IBI}_{uv,n}$ is a pq -length vector, $\boldsymbol{\varphi}_{uv,c}$ is a $(pq \times q)$ -length matrix and $\mathbf{b}^{(k)}$ contains the q data bits transmitted within the first symbol duration. Furthermore, let $\mathbf{IBI}_{\bar{i},uv,n}$, $\boldsymbol{\varphi}_{\bar{i},uv,c}$ and $\mathbf{b}_{\bar{i}}^{(k)}$ be the matrices formed from $\mathbf{IBI}_{uv,n}$, $\boldsymbol{\varphi}_{uv,c}$ and $\mathbf{b}^{(k)}$ by removing their i th terms, respectively. Then, (4.46) can be expressed as

$$\text{IBI}_{uv,n} = (\mathbf{IBI}_{\bar{u},uv,n})^T \boldsymbol{\varphi}_{\bar{u},uv,c} \mathbf{b}_{\bar{u}}^{(k)} \quad (4.50)$$

Let us now define the vectors as follows:

$$\begin{aligned} \mathbf{y}_{uv} &= [y_{uv,0}, y_{uv,1}, \dots, y_{uv,N_e-1}]^T \\ \mathbf{N}_{uv} &= [N_{uv,0}, N_{uv,1}, \dots, N_{uv,N_e-1}]^T \\ \mathbf{BI}_{uv} &= [\text{BI}_{uv,0}, \text{BI}_{uv,1}, \dots, \text{BI}_{uv,N_e-1}]^T \\ \mathbf{IBI}_{uv} &= [\text{IBI}_{uv,0}, \text{IBI}_{uv,1}, \dots, \text{IBI}_{uv,N_e-1}]^T \end{aligned} \quad (4.51)$$

which are the N_e -length vectors.

$$\begin{aligned} \mathbf{y}_u &= [y_{u1}^T, y_{u2}^T, \dots, y_{up}^T]^T \\ \mathbf{N}_u &= [N_{u1}^T, N_{u2}^T, \dots, N_{up}^T]^T \\ \mathbf{BI}_u &= [\mathbf{BI}_{u1}^T, \mathbf{BI}_{u2}^T, \dots, \mathbf{BI}_{up}^T]^T \\ \mathbf{IBI}_u &= [\mathbf{IBI}_{u1}^T, \mathbf{IBI}_{u2}^T, \dots, \mathbf{IBI}_{up}^T]^T \end{aligned} \quad (4.52)$$

which are the $N_e p$ -length vectors.

$$\begin{aligned}\mathbf{y} &= [\mathbf{y}_1^T, \mathbf{y}_2^T, \dots, \mathbf{y}_q^T]^T \\ \mathbf{N} &= [\mathbf{N}_1^T, \mathbf{N}_2^T, \dots, \mathbf{N}_q^T]^T \\ \mathbf{IBI} &= [\mathbf{IBI}_1^T, \mathbf{IBI}_2^T, \dots, \mathbf{IBI}_q^T]^T\end{aligned}\quad (4.53)$$

which are the $N_e pq$ -length vectors. Furthermore, we define

$$\mathbf{C}_{k,uv} = \frac{1}{\sqrt{N_e}} \text{diag}\{c_0^{(k)}, c_1^{(k)}, \dots, c_{N_e-1}^{(k)}\} \quad (4.54)$$

which is a $(N_e \times N_e)$ diagonal matrix.

With the aid of the above definitions, then, when expressing in matrix form, we have

$$\mathbf{y}_{uv} = \frac{1}{\sqrt{p}} \mathbf{C}_{k,uv} [(\mathbf{1}_{N_e} + \mathbf{BI}_{uv}) \mathbf{b}_u^{(k)}[0] + \mathbf{IBI}_{uv}] + \mathbf{N}_{uv} \quad (4.55)$$

for $u = 1, 2, \dots, q$ and $v = 1, 2, \dots, p$, where $\mathbf{1}_N = [1, 1, \dots, 1]^T$ is an N -length vector with elements of 1's.

$$\mathbf{y}_u = \mathbf{C}_{k,u} [(\mathbf{1}_{N_e p} + \mathbf{BI}_u) \mathbf{b}_u^{(k)}[0] + \mathbf{IBI}_u] + \mathbf{N}_u \quad (4.56)$$

for $u = 1, 2, \dots, q$. In (4.56) $\mathbf{C}_{k,u} = \mathbf{I}_p \otimes \mathbf{C}_{k,uv}/\sqrt{p}$. Finally, we have

$$\mathbf{y} = \mathbf{C}_k [(\mathcal{I} + \mathbf{BI}) \mathbf{b}^{(k)} + \mathbf{IBI}] + \mathbf{N} \quad (4.57)$$

where

$$\begin{aligned}\mathbf{C}_k &= \text{diag}\{\mathbf{C}_{k,1}, \mathbf{C}_{k,2}, \dots, \mathbf{C}_{k,q}\} \\ \mathcal{I} &= \mathbf{I}_q \otimes \mathbf{1}_{N_e p} \\ \mathbf{BI} &= \text{diag}\{\mathbf{BI}_1, \mathbf{BI}_2, \dots, \mathbf{BI}_q\}\end{aligned}\quad (4.58)$$

It can be shown that, if all the q bits are transmitted using the same spreading code, then \mathbf{C}_k can also be expressed as

$$\mathbf{C}_k = \mathbf{I}_q \otimes \mathbf{C}_{k,u} \quad (4.59)$$

Above we have derived the observation signal vector as shown in (4.57) by treating the signals leaking to the other subcarriers as interference. However, from the above derivations, we can see that, once the phases associated with each subcarrier are estimated, except the data bits to be detected, all the other terms within the bracket of (4.57) are certain. In this case, if detection complexity can be afforded, the information provided by these terms may be utilized for achieving an enhanced BER performance. Let us consider this issue in detail.

We start by expressing (4.36) in a more convenient form. From our analysis from (4.38) to (4.49), it can be shown that the terms in the bracket of (4.36) can be expressed as

$$b_u^{(k)}[0](1 + \mathbf{BI}_{uv,n}) + \mathbf{IBI}_{uv,n} = (\mathbf{IBI}_{uv,n})^T \boldsymbol{\varphi}_{uv,c} \mathbf{b}^{(k)} \quad (4.60)$$

Hence, (4.36) can be written as

$$y_{uv,n} = \frac{c_n^{(k)}}{\sqrt{pN_e}} (\mathbf{IBI}_{uv,n})^T \boldsymbol{\varphi}_{uv,c} \mathbf{b}^{(k)} + N_{uv,n} \quad (4.61)$$

Furthermore, \mathbf{y}_{uv} can be expressed as

$$\mathbf{y}_{uv} = \frac{1}{\sqrt{p}} \mathbf{C}_{k,uv} \mathbf{F}_{uv} \boldsymbol{\varphi}_{uv} \mathbf{b}^{(k)} + \mathbf{N}_{uv} \quad (4.62)$$

where

$$\begin{aligned} \mathbf{F}_{uv} &= \text{diag}\{(\mathbf{IBI}_{uv,0})^T, (\mathbf{IBI}_{uv,1})^T, \dots, (\mathbf{IBI}_{uv,N_e-1})^T\} \\ \boldsymbol{\varphi}_{uv} &= [\boldsymbol{\varphi}_{uv,c}^T, \boldsymbol{\varphi}_{uv,c}^T, \dots, \boldsymbol{\varphi}_{uv,c}^T]^T \end{aligned} \quad (4.63)$$

\mathbf{y}_u can be expressed as

$$\mathbf{y}_u = \mathbf{C}_{k,u} \mathbf{F}_u \boldsymbol{\varphi}_u \mathbf{b}^{(k)} + \mathbf{N}_u \quad (4.64)$$

associated with

$$\begin{aligned} \mathbf{F}_u &= \text{diag}\{\mathbf{F}_{u1}, \mathbf{F}_{u2}, \dots, \mathbf{F}_{up}\} \\ \boldsymbol{\varphi}_u &= [\boldsymbol{\varphi}_{u1}^T, \boldsymbol{\varphi}_{u2}^T, \dots, \boldsymbol{\varphi}_{up}^T]^T \end{aligned} \quad (4.65)$$

Finally, \mathbf{y} can be expressed as

$$\mathbf{y} = \mathbf{C}_k \mathbf{F} \boldsymbol{\varphi} \mathbf{b}^{(k)} + \mathbf{N} \quad (4.66)$$

associated with

$$\begin{aligned} \mathbf{F} &= \text{diag}\{\mathbf{F}_1, \mathbf{F}_2, \dots, \mathbf{F}_q\} \\ \boldsymbol{\varphi} &= [\boldsymbol{\varphi}_1^T, \boldsymbol{\varphi}_2^T, \dots, \boldsymbol{\varphi}_q^T]^T \end{aligned} \quad (4.67)$$

Equation (4.66) has explicitly separated the spreading codes, frequencies, subcarrier phases and transmitted data bits.

So far, we have represented the observation samples using the matrix form, as shown in (4.57) or (4.66). Before carrying out the detection of $\mathbf{b}^{(k)}$, let us first make some notations, which may enable us to gain insight into the characteristics of the MC DS-CDMA, so as to optimize the design of the MC DS-CDMA signalling schemes.

First, let us have a close look at the equations in (4.41), which impose intercarrier interference on the desired subcarrier provided that they are nonzero. According to (4.41), we can imply that, when given the chip waveform, $\psi(t)$, and the spacing value, λ , of the adjacent subcarrier frequencies, the quantities of $\{\text{BI}_{ul,uv,n}\}$ and $\{\text{IBI}_{il,uv,n}\}$ are also given. However, as shown in (4.42) and (4.43), the total amount of intercarrier interference is also dependent on the phases associated with the $(qp - 1)$ interfering subcarriers. Since these phases are random variables, a strategy for minimizing the intercarrier interference in MC DS-CDMA is to minimize the quantity of the terms in (4.41). Hence, when the chip waveform, $\psi(t)$, is given, the subcarrier spacing value, λ , may be optimized in order to minimize the intercarrier interference. Conversely, when the subcarrier spacing value, λ , is given, an optimum chip waveform, $\psi(t)$, may be found so as to minimize the intercarrier interference.

In practice, when designing the chip waveform, $\psi(t)$, and determining the subcarrier spacing value, λ , there may be some other constraints to consider, such as the resulting spectral efficiency, multiuser interference (MUI), etc. Specifically, for the current situation when considering an MC DS-CDMA supporting only single-user, our design target is mainly to minimize the intercarrier interference. For example, if we assume that the chip

waveform, $\psi(t)$, constitutes a rectangular impulse – which is not very spectral efficient, we can choose the subcarrier spacing value to be $\lambda = N_e$, yielding an orthogonal MC DS-CDMA scheme [41]. In this case, both $\text{BI}_{ul,uv,n} = 0$ and $\text{IBI}_{il,uv,n} = 0$ for any value of n , and any $i \neq u$ or $l \neq v$. Furthermore, in this case the observation vector (4.66) is reduced to

$$\mathbf{y} = \mathbf{C}_k \mathcal{I} \mathbf{b}^{(k)} + \mathbf{N} \quad (4.68)$$

associated with $\mathcal{I} = (\mathbf{I}_q \otimes \mathbf{1}_{N_e p})$, where $\mathbf{1}_{N_e p}$ is a $N_e p$ -length vector with elements of ones.

Secondly, if there exists intercarrier interference, as analysed above, it may not greatly harm the achievable BER performance, provided that the detector is capable of taking into account the intercarrier interference. This argument will become clear in the following analysis of detection in the MC DS-CDMA.

In the context of the first detection scheme, we assume that the detector focuses only on the desired subcarriers and on the corresponding data bits conveyed by these subcarriers, while treating the intercarrier interference as noise. In this case the decision variables for the q data bits transmitted within the first symbol duration can be expressed as

$$\mathbf{z} = (\mathbf{C}_k \mathcal{I})^T \mathbf{y} \quad (4.69)$$

Substituting (4.57) into (4.69), it can be shown that

$$\mathbf{z} = \mathbf{b}^{(k)} + \frac{1}{N_e p} \mathcal{I}^T \mathbf{B} \mathbf{I} \mathbf{b}^{(k)} + \frac{1}{N_e p} \mathcal{I}^T \mathbf{B} \mathbf{I} \mathbf{B} + \bar{\mathbf{n}} \quad (4.70)$$

where $\bar{\mathbf{n}} = (\mathbf{C}_k \mathcal{I})^T \mathbf{N}$ is a q -length Gaussian vector. Where the rectangular chip waveform, $\psi(t)$, is used and the subcarrier spacing $\lambda = N_e$, i.e. the subcarrier signals are orthogonal at the chip level, (4.70) is then reduced to

$$\mathbf{z} = \mathbf{b}^{(k)} + \bar{\mathbf{n}} \quad (4.71)$$

which is capable of achieving the BER of $Q(\sqrt{2E_b/N_0})$. Let us now derive the BER of the MC DS-CDMA in the context of the general case having the decision variable given by (4.70).

Let us first analyse the term $\mathbf{I}_s = \mathcal{I}^T \mathbf{B} \mathbf{I} \mathbf{b}^{(k)}/N_e p$ in (4.70). Applying \mathcal{I} and $\mathbf{B} \mathbf{I}$, we obtain

$$\mathbf{I}_s = \frac{1}{N_e p} \mathcal{I}^T \mathbf{B} \mathbf{I} \mathbf{b}^{(k)} = \frac{1}{N_e p} \text{diag}\{\mathbf{1}_{N_e p}^T \mathbf{B} \mathbf{I}_1, \mathbf{1}_{N_e p}^T \mathbf{B} \mathbf{I}_2, \dots, \mathbf{1}_{N_e p}^T \mathbf{B} \mathbf{I}_q\} \mathbf{b}^{(k)} \quad (4.72)$$

where, when applying the results of $\mathbf{B} \mathbf{I}_u$, $\mathbf{1}_{N_e p}^T \mathbf{B} \mathbf{I}_u$ can be extended to

$$\mathbf{1}_{N_e p}^T \mathbf{B} \mathbf{I}_u = \sum_{v=1}^p \sum_{n=0}^{N_e-1} \sum_{l=1, l \neq v}^p \text{BI}_{ul,uv,n} \exp(j \Delta \varphi_{u,lv}^{(k)}), \quad u = 1, 2, \dots, q \quad (4.73)$$

Since $\Delta \varphi_{u,lv}^{(k)}$ is independent of the index of n , (4.73) can be rewritten as

$$\mathbf{1}_{N_e p}^T \mathbf{B} \mathbf{I}_u = \sum_{v=1}^p \sum_{l=1, l \neq v}^p \exp(j \Delta \varphi_{u,lv}^{(k)}) \sum_{n=0}^{N_e-1} \text{BI}_{ul,uv,n} \quad (4.74)$$

With the aid of (4.41), the above equation can be expressed as

$$\mathbf{1}_{N_e p}^T \mathbf{B} \mathbf{I}_u = \sum_{v=1}^p \sum_{l=1, l \neq v}^p \exp(j \Delta \varphi_{u,lv}^{(k)}) \sum_{n=0}^{N_e-1} \frac{1}{T_c} \int_{nT_c}^{(n+1)T_c} \psi^2(t) \exp(j 2\pi \Delta f_{u,lv} t) dt \quad (4.75)$$

Second, the term $\mathcal{I}^T \mathbf{IBI}/N_e p$ in (4.70) can be expressed as

$$\mathbf{I}_{BI} = \frac{1}{N_e p} \mathcal{I}^T \mathbf{IBI} = \frac{1}{N_e p} [\mathbf{1}_{N_e p}^T \mathbf{IBI}_1, \mathbf{1}_{N_e p}^T \mathbf{IBI}_2, \dots, \mathbf{1}_{N_e p}^T \mathbf{IBI}_q]^T \quad (4.76)$$

where, using the details about \mathbf{IBI}_u , we have

$$\mathbf{1}_{N_e p}^T \mathbf{IBI}_u = \sum_{j=1}^p \sum_{n=0}^{N_e-1} \mathbf{IBI}_{uj,n} = \sum_{i=1, i \neq u}^q b_i^{(k)}[0] \sum_{j=1}^p \sum_{l=1}^p \sum_{n=0}^{N_e-1} \mathbf{IBI}_{il,uj,n} \exp(j \Delta \varphi_{iu,lj}^{(k)}) \quad (4.77)$$

Again, since $\Delta \varphi_{iu,lj}^{(k)}$ is independent of the index n , with the aid of (4.41), (4.77) can be expressed as

$$\begin{aligned} \mathbf{1}_{N_e p}^T \mathbf{IBI}_u &= \sum_{j=1}^p \sum_{n=0}^{N_e-1} \mathbf{IBI}_{uj,n} = \sum_{i=1, i \neq u}^q b_i^{(k)}[0] \sum_{j=1}^p \sum_{l=1}^p \exp(j \Delta \varphi_{iu,lj}^{(k)}) \\ &\quad \times \sum_{n=0}^{N_e-1} \frac{1}{T_c} \int_{nT_c}^{(n+1)T_c} \psi^2(t) \exp(j 2\pi \Delta f_{iu,lj} t) dt \end{aligned} \quad (4.78)$$

Finally, with the aid of (4.72), (4.75), (4.76) and (4.78), the decision variable z_u , $u = 1, \dots, q$, for $b_u^{(k)}[0]$ in (4.70) can be expressed as

$$\begin{aligned} z_u &= b_u^{(k)}[0] + \frac{1}{N_e p} \mathbf{1}_{N_e p}^T \mathbf{B} \mathbf{I}_u b_u^{(k)}[0] + \frac{1}{N_e p} \mathbf{1}_{N_e p}^T \mathbf{IBI}_u + \bar{n}_u \\ &= b_u^{(k)}[0] + \text{ICI}_u + \bar{n}_u \end{aligned} \quad (4.79)$$

where

$$\begin{aligned} \text{ICI}_u &= \frac{1}{N_e p} b_u^{(k)}[0] \sum_{v=1}^p \sum_{l=1, l \neq v}^p \exp(j \Delta \varphi_{u,lv}^{(k)}) \\ &\quad \times \sum_{n=0}^{N_e-1} \frac{1}{T_c} \int_{nT_c}^{(n+1)T_c} \psi^2(t) \exp(j 2\pi \Delta f_{u,lv} t) dt \\ &\quad + \frac{1}{N_e p} \sum_{i=1, i \neq u}^q b_i^{(k)}[0] \sum_{j=1}^p \sum_{l=1}^p \exp(j \Delta \varphi_{iu,lj}^{(k)}) \\ &\quad \times \sum_{n=0}^{N_e-1} \frac{1}{T_c} \int_{nT_c}^{(n+1)T_c} \psi^2(t) \exp(j 2\pi \Delta f_{iu,lj} t) dt \end{aligned} \quad (4.80)$$

It can be shown that ICI_u can also be written as

$$\begin{aligned} \text{ICI}_u &= -b_u^{(k)}[0] \\ &+ \frac{1}{N_e p} \sum_{i=1}^q b_i^{(k)}[0] \sum_{j=1}^p \sum_{l=1}^p \exp(j \Delta \varphi_{iu,lj}^{(k)}) \\ &\times \sum_{n=0}^{N_e-1} \frac{1}{T_c} \int_{nT_c}^{(n+1)T_c} \psi^2(t) \exp(j 2\pi \Delta f_{iu,lj} t) dt \end{aligned} \quad (4.81)$$

Let us define

$$\beta_{iu,lj} = \sum_{n=0}^{N_e-1} \frac{1}{N_e T_c} \int_{nT_c}^{(n+1)T_c} \psi^2(t) \exp(j 2\pi \Delta f_{iu,lj} t) dt \quad (4.82)$$

where, explicitly, we have $\beta_{iu,lj} = \beta_{lj,iu}^*$. Furthermore, if we assume that the periodic chip-waveform is employed, then (4.82) can be simplified to

$$\beta_{iu,lj} = \hat{\beta}_{iu,lj} \times \frac{1}{N_e} \sum_{n=0}^{N_e-1} \exp(j 2\pi n \Delta f_{iu,lj} T_c) \quad (4.83)$$

where, by definition,

$$\hat{\beta}_{iu,lj} = \frac{1}{T_c} \int_0^{T_c} \psi^2(t) \exp(j 2\pi \Delta f_{iu,lj} t) dt \quad (4.84)$$

When $1 - \exp(j 2\pi n \Delta f_{iu,lj} T_c) \neq 0$, (4.83) can also be expressed as

$$\beta_{iu,lj} = \hat{\beta}_{iu,lj} \times \frac{1}{N_e} \frac{1 - \exp(j 2\pi \Delta f_{iu,lj} T_s)}{1 - \exp(j 2\pi \Delta f_{iu,lj} T_c)} \quad (4.85)$$

Explicitly, $\beta_{iu,lj}$ is zero, if the normalized spacing λ is chosen such that $1 - \exp(j 2\pi \Delta f_{iu,lj} T_s) = 0$, while $1 - \exp(j 2\pi \Delta f_{iu,lj} T_c) \neq 0$.

Additionally, when the periodic rectangular chip waveform is employed, it can be readily shown that $\hat{\beta}_{iu,lj} = j[1 - \exp(j 2\pi \Delta f_{iu,lj} T_c)]/2\pi \Delta f_{iu,lj} T_c$. In this case, $\beta_{iu,lj}$ is zero, provided that the normalized subcarrier spacing λ is an integer value.

With the aid of the above definition, ICI_u in (4.79) can be expressed as

$$\text{ICI}_u = -b_u^{(k)}[0] + \frac{1}{p} \sum_{i=1}^q b_i^{(k)}[0] \sum_{j=1}^p \sum_{l=1}^p \exp(j \Delta \varphi_{iu,lj}^{(k)}) \beta_{iu,lj} \quad (4.86)$$

Based on the above properties, it can be shown that, when the rectangular chip waveform is employed and when λ is an integer, or when the general periodic chip waveform is employed and when λ is an integer resulting in $1 - \exp(j 2\pi n \Delta f_{iu,lj} T_c) \neq 0$, there exists no intercarrier interference. Hence, the corresponding BER of the MC DS-CDMA can be expressed as

$$P_b = Q\left(\sqrt{\frac{2E_b}{N_0}}\right) \quad (4.87)$$

which achieves the BER performance of the BPSK system without using spreading, when communicating over AWGN channels. Furthermore, it can be implied that, when employing BPSK baseband modulation, both the orthogonal MC DS-CDMA [41] and the multitone DS-CDMA [43] are capable of achieving the BER performance as shown in (4.87), when communicating over AWGN channels.

By contrast, when the other type of chip waveform is employed, resulting in ICI_u being nonzero, the BER can be expressed as

$$P_b(\{\varphi_{ij}^{(k)}\}) = Q\left(\sqrt{\frac{2E_b}{N_0}(1 - \Re\{\text{ICI}_u\})^2}\right) \quad (4.88)$$

which is a function of the subcarrier phases, and seems very difficult from which to derive the closed-form unconditional BER expression. In this case, the BER can be obtained from (4.88) with the aid of a hybrid numerical-simulation approach, called the semi-simulation approach. With the semi-simulation approach, we first generate a number of realizations of the subcarrier phases as well as the transmitted data bits according to their corresponding PDFs. In this way, we can obtain the realizations for ICI_u seen in (4.86). These realizations are then invoked in (4.88) in order to compute their corresponding BER values. Finally, the BER values are averaged to obtain the average BER.

Thus far, the performance of the MC DS-CDMA system has been analysed, when not using the information leaking out to the other subcarrier. As noted previously, when the detector can afford the complexity, this leaked information can be utilized to achieve an enhanced BER performance, when there exists intercarrier interference. To this objective, the detection can be based on (4.66), and after the matched filtering, we obtain

$$z = (\mathbf{C}_k \mathbf{F} \boldsymbol{\varphi})^T \mathbf{C}_k \mathbf{F} \boldsymbol{\varphi} \mathbf{b}^{(k)} + (\mathbf{C}_k \mathbf{F} \boldsymbol{\varphi})^T \mathbf{N} \quad (4.89)$$

which, without any doubt, achieves the same BER performance as the detection scheme considered in (4.69). Following the matched filtering operation, the detector may further carry out a zero-forcing (ZF) operation [88], multiplying both sides of (4.89) with $[(\mathbf{C}_k \mathbf{F} \boldsymbol{\varphi})^T \mathbf{C}_k \mathbf{F} \boldsymbol{\varphi}]^{-1}$, yielding

$$\begin{aligned} z' &= [(\mathbf{C}_k \mathbf{F} \boldsymbol{\varphi})^T \mathbf{C}_k \mathbf{F} \boldsymbol{\varphi}]^{-1} z \\ &= \mathbf{b}^{(k)} + [(\mathbf{C}_k \mathbf{F} \boldsymbol{\varphi})^T \mathbf{C}_k \mathbf{F} \boldsymbol{\varphi}]^{-1} (\mathbf{C}_k \mathbf{F} \boldsymbol{\varphi})^T \mathbf{N} \end{aligned} \quad (4.90)$$

The decision variable of z' is thus Gaussian and the intercarrier interference has been successfully removed.

Note that, in addition to the ZF scheme, there are many other schemes that can be employed for suppressing the intercarrier interference [88, 90]. These interference suppression schemes will be investigated in detail in Chapter 6, when we consider multiuser detection in multicarrier CDMA systems.

Figure 4.4 depicts the BER performance of the MC DS-CDMA using a total $pq = 32$ subcarriers, when assuming rectangular chip waveform and various subcarrier spacing values. The results were evaluated from (4.88) by averaging it with the intercarrier interference shown in (4.86). Note that in Fig. 4.4 the BER curve corresponding to $\lambda = N_e$ represents the BER performance of the orthogonal MC DS-CDMA, which is the same as the conventional BPSK scheme in AWGN channels. It can be shown that, when the rectangular chip waveform is employed, the inter-carrier interference has only a slight impact on BER performance.

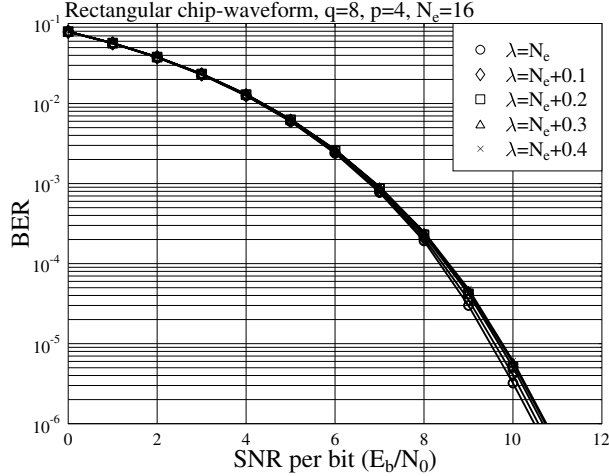


Figure 4.4: Performance of single-user MC DS-CDMA with various subcarrier spacing, when communicating over AWGN channels.

4.5 Performance of Single-User Time-Hopping Multicarrier CDMA

The transmitter and receiver principles of the time-hopping multicarrier CDMA (TH/MC-CDMA) are described in Section 3.8 of Chapter 3. The transmitted signal in TH/MC-CDMA is given in (3.149), which for the u th data stream, where $u = 1, 2, \dots, U$, can be expressed as

$$s_k(t) = \sqrt{\frac{2PM}{L}} \sum_{l=0}^{L-1} \psi_{T_h}(t - y_k(l)T_h) \cos(2\pi(f_c + f_l)t + \varphi_l^{(k)}) \quad (4.91)$$

where P represents the transmitted power of the u th stream, f_c represents the carrier frequency, $\psi_{T_h}(t)$ represents a pulse-waveform defined within $[0, T_h]$ and it is normalized so that $\int_0^{T_h} \psi_{T_h}^2(t) dt = T_h$. Note again that equation (4.91) considers only one of the U parallel streams. The other parallel streams have the same transmitted signal form as (4.91), except that the transmitted b -bit symbols and the subcarrier frequencies need to be changed accordingly.

In this section the PSD of the TH/MC-CDMA signal is first derived. Then, the error-rate performance of the TH/MC-CDMA system supporting the single-user is investigated. We now consider the PSD.

4.5.1 Power Spectral Density of TH/MC-CDMA Signals

In order to derive the PSD of TH/MC-CDMA signals, the transmitted TH/MC-CDMA signal of (4.91) needs to be written to indicate the entire time axis and the entire subcarriers,

expressed as

$$s(t) = \sqrt{\frac{2PM}{L}} \sum_{i=-\infty}^{\infty} \sum_{u=1}^U \sum_{l=0}^{L-1} \psi_{T_h}(t - iT_f - y_{iul}T_h) \cos(2\pi f_{ul}t + \varphi_{iul}) \quad (4.92)$$

where the carrier frequency f_c is absorbed in f_{ul} for convenience, $\{\varphi_{iul}\}$ is an independent random variable uniformly distributed in $[0, 2\pi]$. Furthermore, it is assumed that random TH addresses are used, yielding $\{y_{iul}\}$ in (4.92) being independent discrete random variables satisfying

$$P(y_{iul} = m) = \frac{1}{M}, \quad \text{for } m = 0, 1, \dots, M-1 \quad (4.93)$$

Based on the above-mentioned assumptions, we can infer that the TH/MC-CDMA signal of (4.92) represents a zero-mean random process.

The correlation function of $s(t)$ is given by

$$\begin{aligned} R_s(t, \tau) &= E[s(t)s(t + \tau)] \\ &= \frac{2PM}{L} E \left[\sum_{i=-\infty}^{\infty} \sum_{u=1}^U \sum_{m=0}^{L-1} \sum_{k=-\infty}^{\infty} \sum_{v=1}^U \sum_{n=0}^{L-1} \right. \\ &\quad \times \psi_{T_h}(t + \tau - kT_f - y_{kvn}T_h) \cos(2\pi f_{um}t + \varphi_{ium}) \cos(2\pi f_{vn}(t + \tau) + \varphi_{kvn}) \left. \right] \end{aligned} \quad (4.94)$$

where $E[\cdot]$ represents the ensemble average. Since $\{\varphi_{iul}\}$ for various values of i, u and l are independent random variables, (4.94) can be rewritten as

$$\begin{aligned} R_s(t, \tau) &= \frac{2PM}{L} \sum_{i=-\infty}^{\infty} \sum_{k=-\infty}^{\infty} \sum_{u=1}^U \sum_{v=1}^U \sum_{m=0}^{L-1} \sum_{n=0}^{L-1} E[\psi_{T_h}(t - iT_f - y_{iun}T_h) \\ &\quad \times \psi_{T_h}(t + \tau - kT_f - y_{kvn}T_h)] \\ &\quad \times E[\cos(2\pi f_{um}t + \varphi_{ium}) \cos(2\pi f_{vn}(t + \tau) + \varphi_{kvn})] \end{aligned} \quad (4.95)$$

Furthermore, it can be shown that

$$\begin{aligned} &E[\cos(2\pi f_{um}t + \varphi_{ium}) \cos(2\pi f_{vn}(t + \tau) + \varphi_{kvn})] \\ &= \begin{cases} \frac{1}{2} \cos(2\pi f_{um}\tau), & \text{when } i = k, u = v \text{ and } m = n \\ 0, & \text{otherwise} \end{cases} \end{aligned} \quad (4.96)$$

Applying this result to (4.95), we obtain

$$\begin{aligned} R_s(t, \tau) &= \frac{PM}{L} \sum_{i=-\infty}^{\infty} \sum_{u=1}^U \sum_{m=0}^{L-1} E[\psi_{T_h}(t - iT_f - y_{iun}T_h) \\ &\quad \times \psi_{T_h}(t + \tau - iT_f - y_{iun}T_h)] \cos(2\pi f_{um}\tau) \end{aligned} \quad (4.97)$$

Let the Fourier transform of $\psi_{T_h}(t)$ be represented by $\Psi(f)$. Then, the correlation function $R_s(t, \tau)$ can be expressed as

$$R_s(t, \tau) = \frac{PM}{L} \cos(2\pi f_{um}\tau) \sum_{i=-\infty}^{\infty} \sum_{u=1}^U \sum_{m=0}^{L-1} \int_y \int_x \Psi(x)\Psi^*(y) \\ \times E[e^{-j2\pi(x-y)iT_f} e^{-j2\pi(x-y)y_{ium}T_h} e^{-j2\pi y\tau} e^{j2\pi(x-y)t}] dx dy \quad (4.98)$$

where the integration ranges associated with x and y are $(-\infty, \infty)$.

The continuous PSD of $s(t)$ is given by [91]

$$S_T(f) = \mathcal{F}\{ < R_s(t, \tau) >_t \} \\ = \frac{PM}{L} \sum_{i=-\infty}^{\infty} \sum_{u=1}^U \sum_{m=0}^{L-1} \int_y \int_x \Psi(x)\Psi^*(y) E[e^{-j2\pi(x-y)iT_f} e^{-j2\pi(x-y)y_{ium}T_h}] \\ \times \langle e^{j2\pi(x-y)t} \rangle_t \mathcal{F}\{e^{-j2\pi y\tau} \cos(2\pi f_{um}\tau)\} dx dy \quad (4.99)$$

where $\langle \cdot \rangle_t$ denotes time average. Using

$$\mathcal{F}\{e^{-j2\pi y\tau} \cos(2\pi f_{um}\tau)\} = \frac{1}{2}[\delta(f + y - f_{um}) + \delta(f + y + f_{um})] \quad (4.100)$$

equation (4.99) can be expressed as

$$S_T(f) = \frac{PM}{2L} \left\{ \sum_{i=-\infty}^{\infty} \sum_{u=1}^U \sum_{m=0}^{L-1} \int_x \Psi(x)\Psi^*(-f + f_{um}) \right. \\ \times E[e^{-j2\pi(x+f-f_{um})iT_f} e^{-j2\pi(x+f-f_{um})y_{ium}T_h}] \langle e^{j2\pi(x+f-f_{um})t} \rangle_t dx \\ + \sum_{i=-\infty}^{\infty} \sum_{u=1}^U \sum_{m=0}^{L-1} \int_x \Psi(x)\Psi^*(-f - f_{um}) \\ \times E[e^{-j2\pi(x+f+f_{um})iT_f} e^{-j2\pi(x+f+f_{um})y_{ium}T_h}] \langle e^{j2\pi(x+f+f_{um})t} \rangle_t dx \left. \right\} \quad (4.101)$$

With the aid of (4.93), we have

$$\sum_{i=-\infty}^{\infty} E[e^{-j2\pi(x+f-f_{um})iT_f} e^{-j2\pi(x+f-f_{um})y_{ium}T_h}] \\ = \left[\frac{1}{M} \sum_{l=0}^{M-1} e^{-j2\pi(x+f-f_{um})lT_h} \right] \times \left[\sum_{i=-\infty}^{\infty} e^{-j2\pi(x+f-f_{um})iT_f} \right] \quad (4.102)$$

Using the Poisson sum formula [91]

$$\sum_{n=-\infty}^{\infty} e^{-j2\pi xnT} = \frac{1}{T} \sum_{k=-\infty}^{\infty} \delta\left(x - \frac{k}{T}\right) \quad (4.103)$$

(4.102) can be expressed as

$$\begin{aligned}
 & \sum_{i=-\infty}^{\infty} E[e^{-j2\pi(x+f-f_{um})iT_f} e^{-j2\pi(x+f-f_{um})y_{ium}T_h}] \\
 &= \sum_{k=-\infty}^{\infty} \frac{1}{T_{fM}} \sum_{l=0}^{M-1} e^{-j2\pi(x+f-f_{um})lT_h} \delta\left(x + f - f_{um} - \frac{k}{T_f}\right) \\
 &= \sum_{k=-\infty}^{\infty} \frac{1}{T_{fM}} \sum_{l=0}^{M-1} e^{-j2\pi\frac{lk}{T_f}T_h} \delta\left(x + f - f_{um} - \frac{k}{T_f}\right)
 \end{aligned} \tag{4.104}$$

By using a similar approach, we obtain

$$\begin{aligned}
 & \sum_{i=-\infty}^{\infty} E[e^{-j2\pi(x+f+f_{um})iT_f} e^{-j2\pi(x+f+f_{um})y_{ium}T_h}] \\
 &= \sum_{k=-\infty}^{\infty} \frac{1}{T_{fM}} \sum_{l=0}^{M-1} e^{-j2\pi\frac{lk}{T_f}T_h} \delta\left(x + f + f_{um} - \frac{k}{T_f}\right)
 \end{aligned} \tag{4.105}$$

Applying both (4.104) and (4.105) to (4.101), we obtain

$$\begin{aligned}
 S_T(f) = & \frac{PM}{2L} \left\{ \sum_{k=-\infty}^{\infty} \sum_{u=1}^U \sum_{m=0}^{L-1} \Psi\left(-f + f_{um} + \frac{k}{T_f}\right) \Psi^*(-f + f_{um}) \right. \\
 & \times \frac{1}{T_{fM}} \sum_{l=0}^{M-1} e^{-j2\pi\frac{lk}{T_f}T_h} \langle e^{j2\pi\frac{k}{T_f}t} \rangle_t \\
 & + \sum_{k=-\infty}^{\infty} \sum_{u=1}^U \sum_{m=0}^{L-1} \Psi\left(-f - f_{um} + \frac{k}{T_f}\right) \Psi^*(-f - f_{um}) \\
 & \left. \times \frac{1}{T_{fM}} \sum_{l=0}^{M-1} e^{-j2\pi\frac{lk}{T_f}T_h} \langle e^{j2\pi\frac{k}{T_f}t} \rangle_t \right\}
 \end{aligned} \tag{4.106}$$

The time average in (4.106) can be derived as

$$\langle e^{j2\pi\frac{k}{T_f}t} \rangle_t = \frac{1}{T_f} \int_{-T_f/2}^{T_f/2} e^{j2\pi\frac{k}{T_f}t} dt = \begin{cases} 1, & \text{if } k = 0 \\ 0, & \text{otherwise} \end{cases} \tag{4.107}$$

Hence, the PSD of (4.106) can finally be simplified to

$$S_T(f) = \frac{PM}{2LT_f} \left\{ \sum_{u=1}^U \sum_{m=0}^{L-1} \Psi^2(-f + f_{um}) + \sum_{u=1}^U \sum_{m=0}^{L-1} \Psi^2(-f - f_{um}) \right\} \tag{4.108}$$

Furthermore, when real pulse shape waveforms of $\psi_{T_h}(t)$ are considered, we have $|\Psi(f)| = |\Psi(-f)|$. In this case, the PSD of (4.108) can be expressed as

$$S_T(f) = \frac{PM}{2LT_f} \left\{ \sum_{u=1}^U \sum_{m=0}^{L-1} \Psi^2(f - f_{um}) + \sum_{u=1}^U \sum_{m=0}^{L-1} \Psi^2(f + f_{um}) \right\} \tag{4.109}$$

which shows that in TH/MC-CDMA systems the transmitted power is uniformly distributed on the subcarriers invoked.

As an example, let us consider the T_h -width pulse $\psi_{T_h}(t) = \sqrt{2} \cos(\pi t / T_h) \prod(t / T_h)$ [6], where $\prod(t / T_h)$ represents a rectangular waveform defined in $[0, T_h]$. The Fourier transform of $\psi_{T_h}(t)$ can be expressed as [6]

$$\Psi(f) = \frac{2\sqrt{2}T_h}{\pi} \times \frac{\cos(\pi T_h f)}{1 - 4T_h^2 f^2} \quad (4.110)$$

Substituting (4.110) into (4.109) and considering $T_f = MT_h$, the corresponding PSD can be expressed as

$$S_T(f) = \frac{4PT_h}{L\pi^2} \left\{ \sum_{u=1}^U \sum_{m=0}^{L-1} \frac{\cos^2[\pi T_h(f - f_{um})]}{[1 - 4T_h^2(f - f_{um})^2]^2} + \sum_{u=1}^U \sum_{m=0}^{L-1} \frac{\cos^2[\pi T_h(f + f_{um})]}{[1 - 4T_h^2(f + f_{um})^2]^2} \right\} \quad (4.111)$$

Let us assume that the centre frequency of the TH/MC-CDMA is $f_c = 0$, i.e. when the baseband signals are considered. Then, the PSD of (4.111) for the TH/MC-CDMA signals can be shown as Fig. 4.5, when $UL = 20$ subcarriers assumed. Here, the total system null-to-null bandwidth is approximately $W_s = 1.1$ GHz. We also show the PSD of the single-carrier-based TH-CDMA signals, which occupies an equivalent bandwidth of 1.1 GHz. For the considered signal pulse, the TH/MC-CDMA signals have a flat, Gaussian noise-like PSD over the available frequency band and the transmitted power is near-ideally distributed over the whole system bandwidth. This PSD characteristic is very important to broadband or UWB [18, 20–22] communications, since with the Gaussian noise-like PSD the bandwidth resource can be exploited with the greatest efficiency. Furthermore, as shown in Fig. 4.5, the PSD's sidelobes of the TH/MC-CDMA signals decrease much more rapidly, than those of the corresponding single-carrier TH-CDMA signals.

4.5.2 Error Probability of TH/MC-CDMA Systems

When considering that the TH/MC DS-CDMA supports single users and that the TH/MC-CDMA signals are transmitted over AWGN channels, the received complex low-pass equivalent signal can be expressed as

$$R(t) = \sqrt{\frac{2PM}{L}} \sum_{l=0}^{L-1} \psi_{T_h}(t - y_k(l)T_h) \exp(j[2\pi f_l t + \varphi_l^{(k)}]) + N(t) \quad (4.112)$$

where $N(t)$ represents the complex valued low-pass equivalent AWGN with zero mean and single-sided PSD of $2N_0$.

Let us consider the noncoherent detector as shown in Fig. 3.21 in Section 3.8.3. Then, the decision variables can be formed from the components as

$$R_{lm} = \left| \left(\sqrt{\frac{2PM}{L}} T_h \right)^{-1} \int_{mT_h}^{(m+1)T_h} R(t) \psi_{T_h}(t - mT_h) \exp(-j2\pi f_l t) dt \right|^2 \quad (4.113)$$

for $m = 0, 1, \dots, M - 1$; $l = 0, 1, \dots, L - 1$, where $M = 2^b$ represents the number of time slots and the number of bits per symbol is b , and L represents the number of subcarriers invoked for transmitting a given symbol.

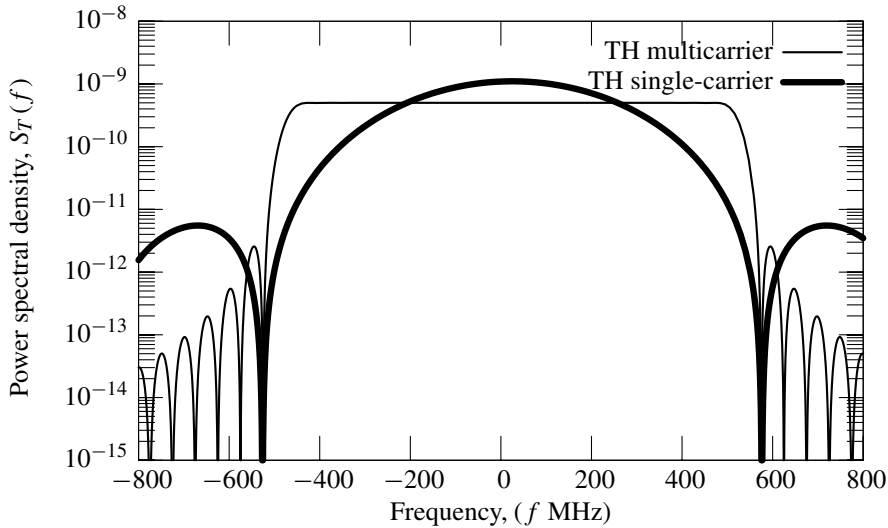


Figure 4.5: PSD centred at 3.025 GHz for both multicarrier and single-carrier-based TH signals occupying a bandwidth of approximately 1.1 GHz, when 20 subcarriers having a bandwidth of 100 MHz were assumed in the TH/MC-CDMA scheme.

We assume that

$$\frac{1}{T_h} \int_{mT_h}^{(m+1)T_h} \psi_{T_h}(t - nT_h) \psi_{T_h}(t - mT_h) \exp(j2\pi f_i t) \times \exp(-j2\pi f_j t) dt = \begin{cases} 1, & \text{if } m = n \text{ and } f_i = f_j \\ 0, & \text{otherwise} \end{cases} \quad (4.114)$$

Then, after substituting (4.112) into (4.113), it can be shown that R_{lm} can be expressed as

$$R_{lm} = |\exp(j\varphi_l^{(k)}) \delta[y_k(l), m] + n_{lm}|^2, \quad m = 0, 1, \dots, M-1; \quad l = 0, 1, \dots, L-1 \quad (4.115)$$

where n_{lm} is a complex Gaussian noise collected from the l th subcarrier and the m th time slot, which is given by

$$n_{lm} = \left(\sqrt{\frac{2PM}{L}} T_h \right)^{-1} \int_{mT_h}^{(m+1)T_h} N(t) \psi_{T_h}(t - mT_h) \exp(-j2\pi f_l t) dt \quad (4.116)$$

which has zero mean and a variance of $LN_0/E_s = L/\gamma_s$, where $E_s = PT_s = PMT_h$ represents the transmitted energy per M -ary symbol, $\gamma_s = E_s/N_0 = bE_b/N_0$ represents the SNR per symbol.

Let us assume that the transmitted symbol is $x_k = 0$ and that the TH address is \mathbf{a}_k . Then, according to Section 3.8,

$$\mathbf{Y}_k = [y_k(0), y_k(1), \dots, y_k(L-1)] = x_k \cdot \mathbf{1} \oplus \mathbf{a}_k \quad (4.117)$$

which determines the active time slots for transmission of a given symbol. At the receiver, as shown in Fig. 3.21 in Section 3.8.3, after the time de-hopping, we can imply that, when the transmitted symbol is $x_k = 0$, all the entries in the first row of the frequency-time matrix in the form of Fig. 3.20 contain both signal and noise. However, all the other $(M - 1)L$ entries of the other $(M - 1)$ rows in the frequency-time matrix contain only noise. Therefore, we can form M number of decision variables, which are

$$\begin{aligned} Z_0 &= \sum_{l=0}^{L-1} |\exp(j\varphi_l^{(k)}) + n_{l0}|^2 \\ Z_m &= \sum_{l=0}^{L-1} |n_{lm}|^2, \quad m = 1, \dots, M - 1 \end{aligned} \quad (4.118)$$

Since $\{n_{lm}\}$ are independent Gaussian variables, it can be shown that Z_0 obeys the noncentral χ^2 -distribution with $2L$ degrees-of-freedom and the PDF is given by [2]

$$f_{Z_0}(y) = \frac{\gamma_s}{L} y^{(L-1)/2} \exp\left(-\frac{\gamma_s(1+y)}{L}\right) I_{L-1}\left(\frac{2\gamma_s\sqrt{y}}{L}\right), \quad y \geq 0 \quad (4.119)$$

The decision variable Z_m , $m = 1, \dots, M - 1$ obeys the central χ^2 -distribution with $2L$ degrees-of-freedom and the PDF is given by [2]

$$f_{Z_m}(y) = \frac{1}{(L-1)!} \left(\frac{\gamma_s}{L}\right)^L y^{L-1} \exp\left(-\frac{\gamma_s y}{L}\right), \quad y \geq 0 \quad (4.120)$$

for $m = 1, 2, \dots, M - 1$.

The probability of symbol-error is given by

$$P_e = 1 - P_c \quad (4.121)$$

where P_c is the correct symbol probability, which can be expressed as

$$\begin{aligned} P_c &= P(Z_1 < Z_0, Z_2 < Z_0, \dots, Z_{M-1} < Z_0 | x_k = 0) \\ &= \int_0^\infty [P(Z_2 < y | Z_0 = y)]^{M-1} f_{Z_0}(y) dy \end{aligned} \quad (4.122)$$

where $P(Z_2 < y | Z_0 = y)$ is

$$P(Z_2 < y | Z_0 = y) = \int_0^y f_{Z_2}(x) dx \quad (4.123)$$

When substituting (4.120) into (4.123), we have

$$P(Z_2 < y | Z_0 = y) = 1 - \exp\left(-\frac{\gamma_s y}{L}\right) \sum_{n=0}^{L-1} \frac{1}{n!} \left(\frac{\gamma_s}{L}\right)^n y^n \quad (4.124)$$

Applying (4.119) and (4.124) to (4.122), we obtain

$$\begin{aligned} P_c &= \frac{\gamma_s}{L} \int_0^\infty \left[1 - \exp\left(-\frac{\gamma_s y}{L}\right) \sum_{n=0}^{L-1} \frac{1}{n!} \left(\frac{\gamma_s}{L}\right)^n y^n \right]^{M-1} \\ &\quad \times y^{(L-1)/2} \exp\left(-\frac{\gamma_s(1+y)}{L}\right) I_{L-1}\left(\frac{2\gamma_s\sqrt{y}}{L}\right) dy \end{aligned} \quad (4.125)$$

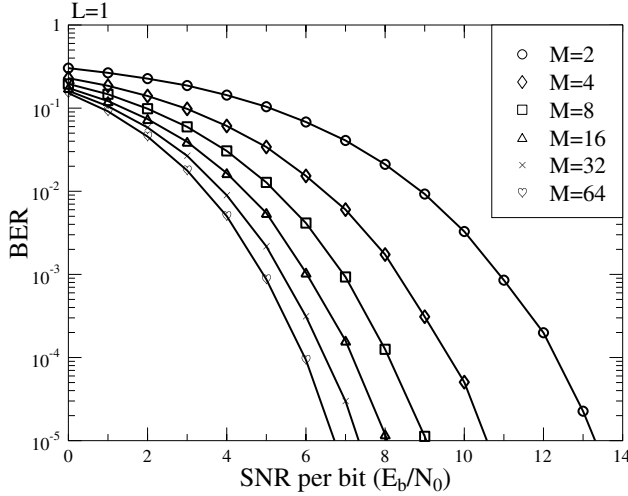


Figure 4.6: BER Performance of TH/MC-CDMA systems with $L = 1$, when communicating over AWGN channels.

Finally, when using the variable transform of $z = \gamma_s y/L$, the above equation can also be expressed as

$$P_c = \int_0^\infty \left[1 - \exp(-z) \sum_{n=0}^{L-1} \frac{z^n}{n!} \right]^{M-1} \left(\frac{Lz}{\gamma_s} \right)^{(L-1)/2} \exp\left(-\frac{\gamma_s}{L} - z\right) \times I_{L-1}\left(2\sqrt{\frac{\gamma_s z}{L}}\right) dz \quad (4.126)$$

It can be shown that, when $L = 1$, P_c can be simplified to a closed form of

$$P_c = \sum_{k=0}^{M-1} \binom{M-1}{k} \frac{(-1)^k}{k+1} \exp\left(-\frac{k\gamma_s}{k+1}\right) \quad (4.127)$$

Furthermore, when the transmitted symbols are constituted by random binary bits, it can be shown that the BER can be expressed as [2]

$$P_b = \frac{2^{b-1}}{M-1} P_e \quad (4.128)$$

Figures 4.6 and 4.7 depict the BER performance of the TH/MC-CDMA systems, when communicating over AWGN channels. Figure 4.6 corresponds to the TH/MC-CDMA systems, where each symbol is conveyed only by $L = 1$ subcarrier. It can be shown that the BER curves typically follow the behaviour of the conventional M -ary orthogonal signalling schemes [2]: the BER performance improves as the value of M increases. In Fig. 4.7 the BER performance of the TH/MC-CDMA systems having a similar bandwidth is illustrated. As seen in Fig. 4.7, $ML = 256$ is a constant, which determines that the

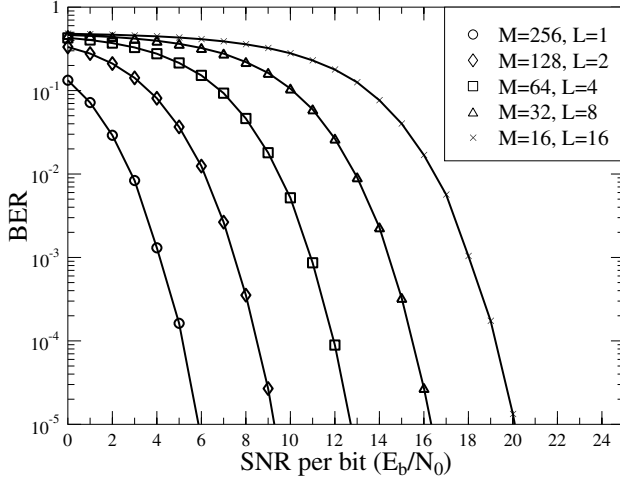


Figure 4.7: BER Performance of TH/MC-CDMA systems communicating over AWGN channels.

bandwidth required is also constant. As shown in Fig. 4.7 the BER performance degrades, as the value of L increases, implying that one symbol is conveyed by invoking more subcarriers. The implication of the results shown in Fig. 4.7 is that, when communicating over AWGN channels, it is desirable to use fewer subcarriers for conveying one symbol, so that the TH has a higher bandwidth to support higher modulation levels. As seen in Fig. 4.7, although the required system bandwidth is the same, the BER performance corresponding to $M = 256, L = 1$ is significantly better than that corresponding to $M = 16, L = 16$. Furthermore, the throughput of the case $M = 256, L = 1$ is 8 bits/symbol, which is also significantly higher than the 4 bits/symbol of case $M = 16, L = 16$.

4.6 Performance of Time-Frequency-Domain Spread Multicarrier DS-CDMA Supporting Multiusers

In this section we investigate the BER performance of the MC DS-CDMA system, which employs both time (T)- and frequency (F)-domain – i.e. TF-domain spreading. The transmitter schematic block diagram of the TF-domain spread MC DS-CDMA is shown in Fig. 4.8. In the literature, the MC DS-CDMA schemes using TF-domain spreading have received wide attention as evidenced, e.g., by the references [54–56, 92], because this type of MC DS-CDMA does not make a trade-off of the maximum number of users supportable, when requiring a relatively high frequency diversity by transmitting the same signal on more subcarriers. In the context of the TF-domain spread MC DS-CDMA, as shown in Fig. 3.22, one bit information is spread in the F-domain with the assistance of a number of subcarriers. This MC DS-CDMA scheme can be further extended to include S/P conversion, which transmits several bits within one symbol duration.

In this section, we consider the TF-domain spread MC DS-CDMA, which uses the S/P conversion for the sake of generality. However, instead of spreading each data bit on a

fraction of the total number of subcarriers, each data bit is spread and transmitted on all the subcarriers, as shown in Fig. 4.8, which will be detailed later in this section. As shown in Chapter 5 considering fading channels, for the MC DS-CDMA using this type of F-domain spreading, each transmitted data bit is capable of achieving a full frequency diversity that is available for the system.

The parameters used in this section are summarized as follows:

N_p :	length of the F-domain spreading code;
T_s , T_b , T_c :	symbol-duration, bit duration and chip duration, respectively;
U :	number of bits invoked in the S/P conversion, $T_s = UT_b$;
$N = T_b/T_c$:	number of chips per bit duration;
$N_t = T_s/T_c = UN$:	T-domain spreading factor or the number of chips per symbol duration;
$\mathbf{C}_f^{(k)}$:	F-domain spreading matrix, which is a $(N_p \times U)$ -dimensional matrix. Each column of $\mathbf{C}_f^{(k)}$ constitutes an F-domain spreading code, which is expressed as $\mathbf{c}_{fu}^{(k)} = [c_{fu,0}^{(k)}, c_{fu,1}^{(k)}, \dots, c_{fu,N_p-1}^{(k)}]^T / \sqrt{N_p}$;
$c_k(t)$:	T-domain spreading code waveform of the k th user, the corresponding T-domain spreading code is expressed as $\mathbf{c}_k = [c_{k0}, c_{k1}, \dots, c_{k(N_t-1)}]^T / \sqrt{N_t}$;
λ :	normalized spacing between two adjacent subcarriers.

4.6.1 Transmitted signal

The transmitter schematic block diagram for the TF-domain spread MC DS-CDMA is shown in Fig. 4.8, which includes the components of S/P conversion, F-domain spreading, T-domain spreading and multicarrier modulation. Specifically, as shown in Fig. 4.8 the serial binary data is first S/P converted to form the data symbols denoted in the vector as

$$\mathbf{b}_m^{(k)} = [b_m^{(k)}[0], b_m^{(k)}[1], \dots, b_m^{(k)}[U-1]]^T, \quad m = 0, 1, \dots \quad (4.129)$$

where $b_m^{(k)}[u] = +1$ or -1 with an equal probability. After the S/P conversion, the data symbol is spread in the F-domain with the aid of U F-domain spreading codes, each of the U bits is spread by an F-domain spreading code. Hence, one user is assigned U F-domain spreading codes. As shown in Fig. 4.8, the output after the F-domain spreading can be expressed as

$$\mathbf{s}_{f,m}^{(k)} = \mathbf{C}_f^{(k)} \mathbf{b}_m^{(k)}, \quad m = 0, 1, \dots \quad (4.130)$$

where $\mathbf{s}_{f,m}^{(k)}$ is an N_p -length vector, the F-domain matrix $\mathbf{C}_f^{(k)}$ can be expressed as

$$\begin{aligned} \mathbf{C}_f^{(k)} &= [\mathbf{c}_{f0}^{(k)}, \mathbf{c}_{f1}^{(k)}, \dots, \mathbf{c}_{f(U-1)}^{(k)}] \\ &= \frac{1}{\sqrt{N_p}} \begin{bmatrix} c_{f0,0}^{(k)} & c_{f1,0}^{(k)} & \cdots & c_{f(U-1),0}^{(k)} \\ c_{f0,1}^{(k)} & c_{f1,1}^{(k)} & \cdots & c_{f(U-1),1}^{(k)} \\ \vdots & \vdots & \ddots & \vdots \\ c_{f0,N_p-1}^{(k)} & c_{f1,N_p-1}^{(k)} & \cdots & c_{f(U-1),N_p-1}^{(k)} \end{bmatrix} \end{aligned} \quad (4.131)$$

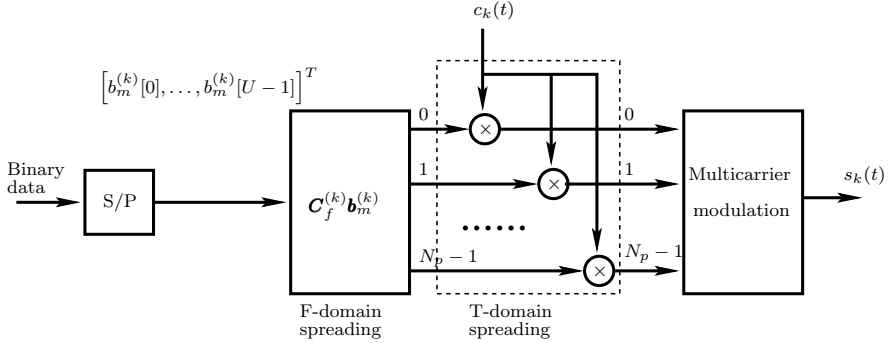


Figure 4.8: Transmitter schematic block diagram of MC DS-CDMA using both time- and frequency-domain spreading.

Following the F-domain spreading, as shown in Fig. 4.8, each of the N_p branches is spread by a common T-domain spreading code waveform $c_k(t)$ assigned to the k th user. Finally, multicarrier modulation is carried out to form the transmitted signal, which can be expressed as

$$s_k(t) = \sqrt{2P} c_k(t) [\boldsymbol{\omega}(t)]^T s_{f,m}^{(k)} = \sqrt{2P} c_k(t) [\boldsymbol{\omega}(t)]^T \mathbf{C}_f^{(k)} \mathbf{b}_m^{(k)} \quad (4.132)$$

where

$$\boldsymbol{\omega}(t) = [\exp(j[2\pi f_0 t + \phi_0^{(k)}]), \dots, \exp(j[2\pi f_{N_p-1} t + \phi_{N_p-1}^{(k)}])]^T \quad (4.133)$$

where f_{n_p} and $\phi_{n_p}^{(k)}$ are the frequency and initial phase associated with the n_p th subcarrier. Substituting (4.133) into (4.132), the transmitted real signal can be expressed in detail as

$$s_k(t) = \sqrt{\frac{2P}{N_p}} \sum_{u=0}^{U-1} \sum_{n_p=0}^{N_p-1} b_m^{(k)}[u] c_{fu,n_p}^{(k)} c_k(t) \cos(2\pi f_{n_p} t + \phi_{n_p}^{(k)}) \quad (4.134)$$

where P represents the transmitted power of one data bit. Let us first derive the PSD of the TF-domain spread MC DS-CDMA signal.

4.6.2 Power Spectral Density

When assuming random F-domain spreading codes, random T-domain spreading codes as well as random binary data, the PSD of the TF-domain spread MC DS-CDMA signals in the form of (4.134) is the same as the PSD of the signal

$$s(t) = \sqrt{\frac{2P}{N_p}} \sum_{m=-\infty}^{\infty} \sum_{u=0}^{U-1} \sum_{i=0}^{N_p-1} d_{ui}[m] \psi_{T_c}(t - mT_c) \cos(2\pi f_i t + \phi_{mi}) \quad (4.135)$$

where $d_{ui}[m] \in \{+1, -1\}$ is independent with respect to m , u and i , while ϕ_{mi} is independent with respect to i , but possibly correlated with respect to m .

The correlation function of $s(t)$ can be expressed as

$$\begin{aligned} R_s(t, \tau) &= E[s(t)s(t + \tau)] \\ &= \frac{2P}{N_p} E \left[\sum_{m=-\infty}^{\infty} \sum_{u=0}^{U-1} \sum_{i=0}^{N_p-1} \sum_{n=-\infty}^{\infty} \sum_{v=0}^{U-1} \sum_{j=0}^{N_p-1} d_{ui}[m] d_{vj}[n] \psi_{T_c}(t - mT_c) \right. \\ &\quad \times \psi_{T_c}(t + \tau - nT_c) \cos(2\pi f_i t + \phi_{mi}) \cos(2\pi f_j t + \phi_{nj}) \left. \right] \end{aligned} \quad (4.136)$$

Explicitly, the expectation in the above equation is nonzero only in the cases satisfying $m = n$, $u = v$ and $i = j$ simultaneously. Hence, after some simplification, we obtain

$$\begin{aligned} R_s(t, \tau) &= \frac{P}{N_p} \sum_{m=-\infty}^{\infty} \sum_{u=0}^{U-1} \sum_{i=0}^{N_p-1} E[\psi_{T_c}(t - mT_c) \psi_{T_c}(t + \tau - mT_c)] \cos(2\pi f_i \tau) \\ &= \frac{PU}{N_p} \sum_{m=-\infty}^{\infty} \sum_{i=0}^{N_p-1} E[\psi_{T_c}(t - mT_c) \psi_{T_c}(t + \tau - mT_c)] \cos(2\pi f_i \tau) \end{aligned} \quad (4.137)$$

Let us assume that the Fourier transform of $\psi_{T_c}(t)$ is $\Psi(f)$. Then, following the approach in Section 4.5.1 for the TH/MC-CDMA, (4.137) can be expressed as

$$\begin{aligned} R_s(t, \tau) &= \frac{PU}{N_p} \cos(2\pi f_i \tau) \sum_{m=-\infty}^{\infty} \sum_{i=0}^{N_p-1} \int_y \int_x \Psi(x) \Psi^*(y) \\ &\quad \times E[e^{-j2\pi(x-y)mT_c} e^{-j2\pi y \tau} e^{j2\pi(x-y)t}] dx dy \end{aligned} \quad (4.138)$$

where the integration ranges for both x and y are from $-\infty$ to ∞ . Consequently, the continuous PSD of the TF-domain spread MC DS-CDMA signal can be obtained by computing the Fourier transform of $R_s(t, \tau)$ with respect to τ , which can be expressed as

$$\begin{aligned} S_T(f) &= \mathcal{F}\{< R_s(t, \tau) >_t\} \\ &= \frac{PU}{N_p} \sum_{m=-\infty}^{\infty} \sum_{i=0}^{N_p-1} \int_y \int_x \Psi(x) \Psi^*(y) \times e^{-j2\pi(x-y)mT_c} \langle e^{j2\pi(x-y)t} \rangle_t \\ &\quad \times \mathcal{F}\{e^{-j2\pi y \tau} \cos(2\pi f_i \tau)\} dx dy \end{aligned} \quad (4.139)$$

where $\langle \cdot \rangle_t$ represents the time average. In (4.139)

$$\mathcal{F}\{e^{-j2\pi y \tau} \cos(2\pi f_i \tau)\} = \frac{1}{2} [\delta(f + y - f_i) + \delta(f + y + f_i)] \quad (4.140)$$

When using (4.140) in (4.139), we obtain

$$\begin{aligned} S_T(f) &= \frac{PU}{2N_p} \sum_{m=-\infty}^{\infty} \sum_{i=0}^{N_p-1} \int_x \Psi(x) \Psi^*(-f + f_i) e^{-j2\pi(x+f-f_i)mT_c} \langle e^{j2\pi(x+f-f_i)t} \rangle_t dx \\ &\quad + \frac{PU}{2N_p} \sum_{m=-\infty}^{\infty} \sum_{i=0}^{N_p-1} \int_x \Psi(x) \Psi^*(-f - f_i) e^{-j2\pi(x+f+f_i)mT_c} \langle e^{j2\pi(x+f+f_i)t} \rangle_t dx \end{aligned} \quad (4.141)$$

Then, according to the Poisson sum formula of (4.103), (4.141) can be simplified to

$$\begin{aligned} S_T(f) &= \frac{PU}{2N_p} \sum_{k=-\infty}^{\infty} \sum_{i=0}^{N_p-1} \Psi\left(-f + f_i + \frac{k}{T_c}\right) \Psi^*(-f + f_i) \langle e^{j2\pi kt/T_c} \rangle_t \\ &\quad + \frac{PU}{2N_p} \sum_{k=-\infty}^{\infty} \sum_{i=0}^{N_p-1} \Psi\left(-f - f_i + \frac{k}{T_c}\right) \Psi^*(-f + f_i) \langle e^{j2\pi kt/T_c} \rangle_t \end{aligned} \quad (4.142)$$

Finally, with the aid of the property of

$$\langle e^{j2\pi kt/T_c} \rangle_t = \frac{1}{T_c} \int_{-T_c/2}^{T_c/2} e^{j2\pi kt/T_c} dt = \begin{cases} 1, & \text{if } k = 0 \\ 0, & \text{otherwise} \end{cases} \quad (4.143)$$

we obtain the PSD for the TF-domain spread MC DS-CDMA signal, which is

$$S_T(f) = \frac{PU}{2N_p} \sum_{i=0}^{N_p-1} [\Psi^2(-f - f_i) + \Psi^2(-f + f_i)] \quad (4.144)$$

Furthermore, when the real chip waveform $\psi_{T_c}(t)$ is used, the PSD can be expressed as

$$S_T(f) = \frac{PU}{2N_p} \sum_{i=0}^{N_p-1} [\Psi^2(f - f_i) + \Psi^2(f + f_i)] \quad (4.145)$$

As an example, let us assume that the chip waveform is made up of a simple rectangular pulse. Then the corresponding PSD is given by

$$S_T(f) = \frac{PUT_c^2}{2N_p} \sum_{i=0}^{N_p-1} [\text{sinc}^2(\pi(f - f_i)T_c) + \text{sinc}^2(\pi(f + f_i)T_c)] \quad (4.146)$$

where $\text{sinc}(x) = \sin(x)/x$.

Figure 4.9 shows the baseband equivalent PSD of the transmitted signal versus the normalized spacing, λ , and the normalized frequency, fT_c for the parameters of $N_p = 8$, $N = 64$. The PSD surface shows that the transmitted signal's energy is concentrated near the centre frequency, when the normalized spacing is low. Conversely, it spreads over the whole frequency band, when the normalized spacing is high. Furthermore, it can be seen that there exist normalized spacing values, which spread the transmitted signal's energy uniformly over the valid frequency band. Since the PSD of the TF-domain spread MC DS-CDMA signals is a function of the spacing between the subcarriers, the PSD may be reshaped according to the prevalent system requirements, in order to maximize the achievable spectral efficiency by adjusting the spacing of the subcarriers.

4.6.3 Representation of the Received Signal

We assume that the TF-domain spread MC DS-CDMA system supports K number of users. The K number of MC DS-CDMA signals in the form of (4.134) are transmitted synchronously over AWGN channels. Furthermore, we assume that all users transmit at the

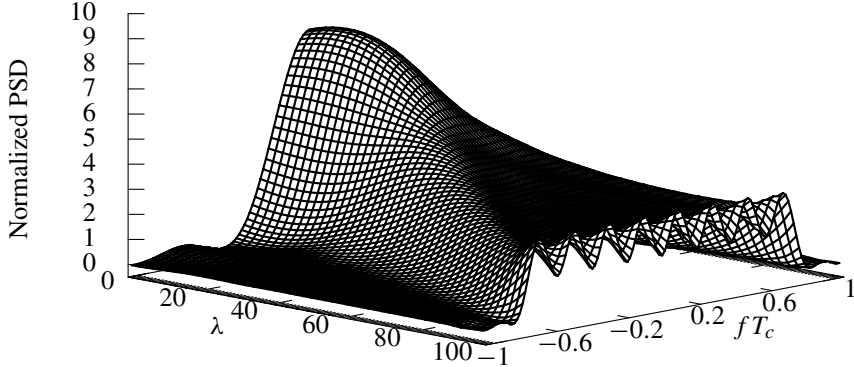


Figure 4.9: Baseband equivalent PSD of the transmitted signal in TF-domain spread MC DS-CDMA systems.

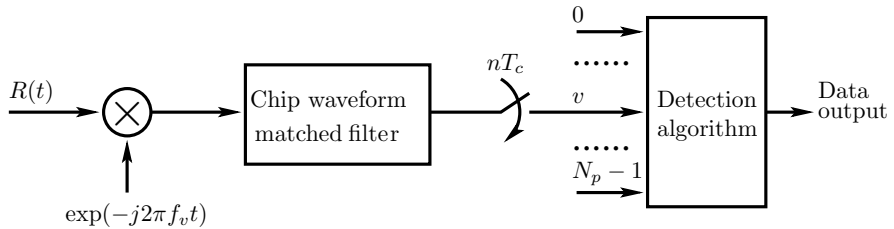


Figure 4.10: Receiver block diagram for detection of MC DS-CDMA signals that are spread in TF-domain.

same data rate implying using the same value of U . Consequently, when assuming that the average received power from any user is the same with the aid of ideal power control, the received complex low-pass equivalent signal can then be expressed as

$$R(t) = \sum_{k=1}^K \sqrt{\frac{2P}{N_p}} \sum_{u=0}^{U-1} \sum_{n_p=0}^{N_p-1} b_m^{(k)}[u] c_{fu,n_p}^{(k)} c_k(t) \exp(j[2\pi f_{n_p} t + \varphi_{n_p}^{(k)}]) + N(t) \quad (4.147)$$

where $\varphi_{n_p}^{(k)}$ contains the initial subcarrier phase and the phase engendered by the transmission channel, while $N(t)$ represents the complex low-pass equivalent Gaussian process, which has zero mean and a single-sided PSD of N_0 per dimension.

The receiver block diagram is shown in Fig. 4.10, where, for the v th, $v = 0, 1, \dots, N_p - 1$ branch, the signal is first demodulated by invoking the v th subcarrier frequency f_v . Then, the carrier demodulated signal is sent to a filter, which is matched to the transmitted chip waveform $\psi(t)$. Finally, the MF's output is sampled at a rate of $1/T_c$, and the corresponding observation samples are sent to the detector, where, when sufficient observation samples are collected, various detection algorithms may be invoked for detecting the transmitted information.

According to Fig. 4.10, the n th sample with respect to the v th subcarrier of the ($m = 0$)th symbol can be expressed as

$$y_{vn} = (\sqrt{2PN_t}T_c)^{-1} \int_{nT_c}^{(n+1)T_c} R(t) \exp(-j2\pi f_v t) \psi^*(t) dt \\ v = 0, 1, \dots, N_p - 1; \quad n = 0, 1, \dots, N_t - 1 \quad (4.148)$$

where the factor $(\sqrt{2PN_t}T_c)^{-1}$ is for the sake of normalization. Since we assume that the TF-domain spread MC DS-CDMA system employs N_p subcarriers and that there are N_t observation samples within one symbol duration of T_s seconds associated with each subcarrier, the total number of observation samples corresponding to one symbol is hence $N_p N_t$. Note that $N_p N_t$ is in fact the total spreading factor of the MC DS-CDMA system. Substituting (4.147) into (4.148), the n th observation sample with respect to the v th subcarrier and the ($m = 0$)th transmitted symbol can be expressed as

$$y_{vn} = \sum_{k=1}^K \sum_{u=0}^{U-1} \sum_{n_p=0}^{N_p-1} \frac{b_0^{(k)}[u]}{\sqrt{N_p N_t}} c_{fu,n_p}^{(k)} c_{kn} \exp(j\varphi_{n_p}^{(k)}) \\ \times \frac{1}{T_c} \int_{nT_c}^{(n+1)T_c} \psi^2(t) \exp(j2\pi[f_{n_p} - f_v]t) dt + N_{vn} \\ v = 0, 1, \dots, N_p - 1; \quad n = 0, 1, \dots, N_t - 1 \quad (4.149)$$

where N_{vn} is the Gaussian noise, which is given by

$$N_{vn} = (\sqrt{2PN_t}T_c)^{-1} \int_{nT_c}^{(n+1)T_c} N(t) \exp(-j2\pi f_v t) \psi^*(t) dt \quad (4.150)$$

for $v = 0, 1, \dots, N_p - 1; \quad n = 0, 1, \dots, N_t - 1$.

Let in (4.149)

$$\mu_{n_p v, n} = \frac{1}{T_c} \int_{nT_c}^{(n+1)T_c} \psi^2(t) \exp(j2\pi \Delta f_{n_p v} t) dt \quad (4.151)$$

where $\Delta f_{n_p v} = f_{n_p} - f_v = i\lambda/T_s$ and i is an integer determined by the spacing between f_{n_p} and f_v . In this section we assume that the chip waveform $\psi(t)$ is a periodic function. In this case

$$\sum_{n=0}^{N_t-1} \mu_{n_p v, n} = 0 \quad (4.152)$$

Furthermore, it can be shown that (4.151) can be expressed as

$$\mu_{n_p v, n} = \hat{\mu}_{n_p v} \exp(j2\pi n \Delta f_{n_p v} T_c), \quad n = 0, 1, \dots, N_t - 1 \quad (4.153)$$

where

$$\hat{\mu}_{n_p v} = \frac{1}{T_c} \int_{nT_c}^{(n+1)T_c} \psi^2(t) \exp(j2\pi \Delta f_{n_p v} t) dt \quad (4.154)$$

which is independent of the index of n . With the definition of (4.151), the Gaussian noise N_{vn} has the properties

$$E[N_{vn}] = 0, \quad E[N_{vn}N_{lm}^*] = \begin{cases} 0, & \text{if } m \neq n \\ \frac{N_0}{E_b} \mu_{lv,n}, & \text{if } m = n \end{cases} \quad (4.155)$$

where $E_b = PT_s = PN_t T_c$ represents the energy per bit. The observation of (4.149) can now be written as

$$\begin{aligned} y_{vn} &= \sum_{k=1}^K \sum_{u=0}^{U-1} \sum_{n_p=0}^{N_p-1} \frac{b_0^{(k)}[u]}{\sqrt{N_p N_t}} c_{fu,n_p}^{(k)} c_{kn} \mu_{n_p v, n} \exp(j\varphi_{n_p}^{(k)}) + N_{vn} \\ v &= 0, 1, \dots, N_p - 1; \quad n = 0, 1, \dots, N_t - 1 \end{aligned} \quad (4.156)$$

Furthermore, let

$$\begin{aligned} \boldsymbol{\mu}_{v,n}^{(k)} &= [\mu_{0v,n}, \mu_{1v,n}, \dots, \mu_{(N_p-1)v,n}]^T \\ \boldsymbol{\varphi}_k &= \text{diag}\{\exp(j\varphi_0^{(k)}), \exp(j\varphi_1^{(k)}), \dots, \exp(j\varphi_{N_p-1}^{(k)})\} \end{aligned} \quad (4.157)$$

Equation (4.156) can be expressed by invoking matrices as

$$\begin{aligned} y_{vn} &= \sum_{k=1}^K \frac{c_{kn}}{\sqrt{N_t}} (\boldsymbol{\mu}_{v,n}^{(k)})^T \boldsymbol{\varphi}_k \mathbf{C}_f^{(k)} \mathbf{b}_0^{(k)} + N_{vn}, \quad v = 0, 1, \dots, N_p - 1 \\ n &= 0, 1, \dots, N_t - 1 \end{aligned} \quad (4.158)$$

where $\mathbf{C}_f^{(k)}$ is given by (4.131) and $\mathbf{b}_0^{(k)}$ is given by (4.129) associated with $m = 0$.

Let us define

$$\begin{aligned} \mathbf{y}_v &= [y_{v0}, y_{v1}, \dots, y_{v(N_t-1)}]^T \\ \mathbf{N}_v &= [N_{v0}, N_{v1}, \dots, N_{v(N_t-1)}]^T \\ \mathbf{C}_k &= \frac{1}{\sqrt{N_t}} \text{diag}\{c_{k0}, c_{k1}, \dots, c_{k(N_t-1)}\}^T \\ \boldsymbol{\mu}_v^{(k)} &= [\boldsymbol{\mu}_{v,0}^{(k)}, \boldsymbol{\mu}_{v,1}^{(k)}, \dots, \boldsymbol{\mu}_{v,N_t-1}^{(k)}]^T \end{aligned} \quad (4.159)$$

where $\boldsymbol{\mu}_v^{(k)}$ is a $(N_t \times N_p)$ matrix. Then, we have

$$\mathbf{y}_v = \sum_{k=1}^K \mathbf{C}_k \boldsymbol{\mu}_v^{(k)} \boldsymbol{\varphi}_k \mathbf{C}_f^{(k)} \mathbf{b}_0^{(k)} + \mathbf{N}_v, \quad v = 0, 1, \dots, N_p - 1 \quad (4.160)$$

where \mathbf{N}_v is a Gaussian noise vector, which has the properties

$$E[\mathbf{N}_v] = \mathbf{0}, \quad E[\mathbf{N}_v \mathbf{N}_l^H] = \begin{cases} \frac{N_0}{E_b} \mathbf{I}_{N_t}, & \text{if } v = l \\ \frac{N_0}{E_b} \boldsymbol{\xi}_{lv}, & \text{if } v \neq l \end{cases} \quad (4.161)$$

where $\boldsymbol{\zeta}_{lv} = \text{diag}\{\mu_{lv,0}, \mu_{lv,1}, \dots, \mu_{lv,N_t-1}\}$.

Finally, let us define

$$\mathbf{y} = [\mathbf{y}_0^T, \mathbf{y}_1^T, \dots, \mathbf{y}_{N_p-1}^T]^T$$

$$\mathbf{N} = [N_0^T, N_1^T, \dots, N_{N_p-1}^T]^T$$

$$\mathcal{C}_k = \mathbf{I}_{N_p} \otimes \mathbf{C}_k$$

$$\boldsymbol{\mu}_k = [(\boldsymbol{\mu}_0^{(k)})^T, (\boldsymbol{\mu}_1^{(k)})^T, \dots, (\boldsymbol{\mu}_{N_p-1}^{(k)})^T]^T \quad (4.162)$$

Then, the total $N_p N_t$ number of observation samples can be expressed in matrix form as

$$\mathbf{y} = \sum_{k=1}^K \mathcal{C}_k \boldsymbol{\mu}_k \boldsymbol{\varphi}_k \mathbf{C}_f^{(k)} \mathbf{b}_0^{(k)} + \mathbf{N} \quad (4.163)$$

where, in summary, \mathbf{N} is a $N_p N_t$ -length Gaussian noise vector; \mathcal{C}_k is a $(N_p N_t \times N_p N_t)$ matrix structured by the T-domain spreading code of the k th user; $\boldsymbol{\mu}_k$ is a $(N_p N_t \times N_p)$ matrix containing the terms given in (4.151) with respect to the k th user and to different values of n_p, v, n ; $\boldsymbol{\varphi}_k$ is a $(N_p \times N_p)$ diagonal matrix containing the N_p subcarrier phases of the k th user; $\mathbf{C}_f^{(k)}$ is a $(N_p \times U)$ matrix containing the F-domain spreading codes of the k th user; and finally, $\mathbf{b}_0^{(k)}$ contains the U data bits of the first symbol transmitted by the k th user.

Furthermore, let

$$\mathcal{H}_k = \mathcal{C}_k \boldsymbol{\mu}_k \boldsymbol{\varphi}_k \mathbf{C}_f^{(k)}, \quad k = 1, 2, \dots, K \quad (4.164)$$

and let

$$\begin{aligned} \mathcal{H} &= [\mathcal{H}_1, \mathcal{H}_2, \dots, \mathcal{H}_K] \\ \mathbf{b}_0 &= [(\mathbf{b}_0^{(1)})^T, (\mathbf{b}_0^{(2)})^T, \dots, (\mathbf{b}_0^{(K)})^T]^T \end{aligned} \quad (4.165)$$

Then, the received vector of (4.163) can also be expressed in a compact form as

$$\mathbf{y} = \mathcal{H} \mathbf{b}_0 + \mathbf{N} \quad (4.166)$$

With the aid of (4.163) and (4.166), we now discuss the single-user assisted detection in the TF-domain spread MC DS-CDMA and analyse the corresponding detection performance.

4.6.4 Single-User Detection and Analysis

In the context of the single-user detection, we assume that the receiver is only able to exploit the signature information, which includes both the T-domain and F-domain spreading codes contained in \mathcal{C}_k and $\mathbf{C}_f^{(k)}$, respectively, as well as the channel information, which is the subcarrier phases contained in $\boldsymbol{\varphi}_k$ of the reference user. It is worth mentioning again that in this section we assume that the chip waveform is periodic. Let us assume that the first user corresponding to $k = 1$ is the reference user or the desired user. Then, the decision variable vector for $\mathbf{b}_0^{(1)}$ is given by

$$z_1 = \Re\{\tilde{z}_1\} \quad (4.167)$$

where

$$\tilde{z}_1 = \mathcal{H}_1^H \mathbf{y} = \mathcal{H}_1^H \mathcal{H}_1 \mathbf{b}_0^{(1)} + \sum_{k=2}^K \mathcal{H}_1^H \mathcal{H}_k \mathbf{b}_0^{(k)} + \tilde{\mathbf{n}}_1 \quad (4.168)$$

where $\tilde{\mathbf{n}}_1 = \mathcal{H}_1^H \mathbf{N}$. Applying $\mathcal{H}_k = \mathcal{C}_k \boldsymbol{\mu}_k \boldsymbol{\varphi}_k \mathbf{C}_f^{(k)}$ and $\mathcal{C}_k^T \mathcal{C}_k = (N_t)^{-1} \mathbf{I}_{N_p N_t}$ in (4.168), we have

$$\begin{aligned} \tilde{z}_1 &= \frac{1}{N_t} (\mathbf{C}_f^{(1)})^T \boldsymbol{\varphi}_1^H \boldsymbol{\mu}_1^H \boldsymbol{\mu}_1 \boldsymbol{\varphi}_1 \mathbf{C}_f^{(1)} \mathbf{b}_0^{(1)} \\ &\quad + \sum_{k=2}^K (\mathbf{C}_f^{(1)})^T \boldsymbol{\varphi}_1^H \boldsymbol{\mu}_1^H \mathcal{C}_k^T \mathcal{C}_k \boldsymbol{\mu}_k \boldsymbol{\varphi}_k \mathbf{C}_f^{(k)} \mathbf{b}_0^{(k)} + \tilde{\mathbf{n}}_1 \end{aligned} \quad (4.169)$$

where, at the right-hand side, the first term contains the desired information and intercarrier interference from the desired user itself, the second term represents the MUI and the last term is the Gaussian noise.

Define

$$\mathbf{G}_k = [\mathbf{G}_k(i, j)] = \boldsymbol{\mu}_k^H \boldsymbol{\mu}_k, \quad k = 1, 2, \dots, K \quad (4.170)$$

which is a $(N_p \times N_p)$ matrix. In (4.170) $\mathbf{G}_k(i, j)$ is the ij th element of \mathbf{G}_k . With the aid of (4.162), (4.159) and (4.157), $\mathbf{G}_k(i, j)$ can be expressed as

$$\mathbf{G}_k(i, j) = \sum_{v=0}^{N_p-1} \sum_{n=0}^{N_t-1} \mu_{iv, n}^* \mu_{jv, n} \quad (4.171)$$

When applying (4.151), (4.153) and (4.154), $\mathbf{G}_k(i, j)$ can be expressed as

$$\begin{aligned} \mathbf{G}_k(i, j) &= \sum_{v=0}^{N_p-1} \hat{\mu}_{iv}^* \hat{\mu}_{jv} \sum_{n=0}^{N_t-1} e^{j2\pi n \Delta f_{ji} T_c} \\ &= \sum_{v=0}^{N_p-1} \hat{\mu}_{iv}^* \hat{\mu}_{jv} \times \frac{1 - e^{j2\pi \Delta f_{ji} N_t T_c}}{1 - e^{j2\pi \Delta f_{ji} T_c}} \\ &= \sum_{v=0}^{N_p-1} \hat{\mu}_{iv}^* \hat{\mu}_{jv} \times \frac{1 - e^{j2\pi \Delta f_{ji} T_s}}{1 - e^{j2\pi \Delta f_{ji} T_c}} \end{aligned} \quad (4.172)$$

Hence, we have

$$\mathbf{G}_k(i, j) = \begin{cases} N_t \sum_{v=0}^{N_p-1} |\hat{\mu}_{iv}|^2, & \text{if } i = j \\ 0, & \text{otherwise} \end{cases} \quad (4.173)$$

Therefore, \mathbf{G}_k is a diagonal matrix.

Let us now define

$$\mathbf{Q}_k = \boldsymbol{\varphi}_k^H \boldsymbol{\mu}_k^H \boldsymbol{\mu}_k \boldsymbol{\varphi}_k = \boldsymbol{\varphi}_k^H \mathbf{G}_k \boldsymbol{\varphi}_k, \quad k = 1, 2, \dots, K \quad (4.174)$$

which is still an $N_p \times N_p$ matrix. Then, after applying (4.157) and (4.173) to (4.174), it can be shown that

$$\mathbf{Q}_k = \mathbf{G}_k \quad (4.175)$$

Finally, let us in (4.169) define

$$\begin{aligned}\mathbf{Z}_k &= \frac{1}{N_t} (\mathbf{C}_f^{(k)})^T \boldsymbol{\varphi}_k^H \boldsymbol{\mu}_k^H \boldsymbol{\mu}_k \boldsymbol{\varphi}_k \mathbf{C}_f^{(k)} \\ &= \frac{1}{N_t} (\mathbf{C}_f^{(k)})^T \mathbf{Q}_k \mathbf{C}_f^{(k)} \\ &= \frac{1}{N_t} (\mathbf{C}_f^{(k)})^T \mathbf{G}_k \mathbf{C}_f^{(k)}, \quad k = 1, 2, \dots, K\end{aligned}\quad (4.176)$$

which is a $(U \times U)$ matrix. Let $\mathbf{Z}_k(u, v)$ be the (u, v) th element of \mathbf{Z}_k . Then, according to (4.131), we have

$$\begin{aligned}\mathbf{Z}_k(u, v) &= \frac{1}{N_p N_t} \sum_{m=0}^{N_p-1} \sum_{n=0}^{N_p-1} \mathbf{Q}_k(m, n) c_{fu,m}^{(k)} c_{fv,n}^{(k)} \\ &= \frac{1}{N_p N_t} \sum_{m=0}^{N_p-1} \sum_{n=0}^{N_p-1} \mathbf{G}_k(m, n) \exp(j[\varphi_n^{(k)} - \varphi_m^{(k)}]) c_{fu,m}^{(k)} c_{fv,n}^{(k)} \\ &= \frac{1}{N_p N_t} \sum_{m=0}^{N_p-1} \mathbf{G}_k(m, m) c_{fu,m}^{(k)} c_{fv,m}^{(k)}\end{aligned}\quad (4.177)$$

Above, the first term of the right-hand side of (4.169) has been analysed, which includes the desired term and the interbit interference. Before discussing the MUI, we analyse these terms in detail. First, the desired component for the u th bit transmitted by the reference user is $\mathbf{Z}_1(u, u)$, which can be written as

$$\mathbf{Z}_1(u, u) = \frac{1}{N_p N_t} \sum_{m=0}^{N_p-1} \mathbf{G}_1(m, m) c_{fu,m}^{(k)} c_{fu,m}^{(k)} = \frac{1}{N_p N_t} \sum_{m=0}^{N_p-1} \mathbf{G}_1(m, m)\quad (4.178)$$

When the subcarrier signals are designed so that we have $\hat{\mu}_{n_p v} = 0$ for $n_p \neq v$ and $\hat{\mu}_{n_p v} = 1$ for $n_p = v$, then, we have

$$\mathbf{G}_1(m, m) = N_t \quad (4.179)$$

Correspondingly, (4.178) is reduced to

$$\mathbf{Z}_1(u, u) = 1 \quad (4.180)$$

which is the desired output for the orthogonal MC DS-CDMA [41]. Furthermore, with the aid of (4.173), the following relationship is always satisfied:

$$\mathbf{Z}_1(u, u) \geq 1 \quad (4.181)$$

Second, the u th and v th, where $u \neq v$, bits of $\mathbf{b}_0^{(1)}$ interfere with each other through $\mathbf{Z}_1(u, v)$, which is given by (4.177). It can also be shown that when the subcarrier signals are designed so that we have $\hat{\mu}_{n_p v} = 0$ for $n_p \neq v$ and $\hat{\mu}_{n_p v} = 1$ for $n_p = v$, then we have

$$\mathbf{Z}_1(u, v) = \frac{1}{N_p} \sum_{m=0}^{N_p-1} c_{fu,m}^{(1)} c_{fv,m}^{(1)} \quad (4.182)$$

which is, in fact, the cross-correlation coefficient between the F-domain spreading sequences $\mathbf{c}_{fu}^{(1)}$ and $\mathbf{c}_{fv}^{(1)}$. Explicitly, if the F-domain spreading sequences assigned to one given user are orthogonal, then we have $\mathbf{Z}_1(u, v) = 0$ for $u \neq v$, and hence there exists no interference among the bits of a given user.

Below, we discuss the MUI by first defining in (4.169)

$$\mathbf{R}_{k1} = \mathcal{C}_1^T \mathcal{C}_k, \quad k = 2, \dots, K \quad (4.183)$$

which, according to (4.162) and (4.159), can be expressed as

$$\begin{aligned} \mathbf{R}_{k1} &= (\mathbf{I}_{N_p} \otimes \mathbf{C}_1)^T (\mathbf{I}_{N_p} \otimes \mathbf{C}_k) = \mathbf{I}_{N_p} \otimes (\mathbf{C}_1^T \mathbf{C}_k) \\ &= \frac{1}{N_t} \mathbf{I}_{N_p} \otimes \text{diag}\{c_{10}c_{k0}, c_{11}c_{k1}, \dots, c_{1(N_t-1)}c_{k(N_t-1)}\} \end{aligned} \quad (4.184)$$

Let us define in (4.169)

$$\mathbf{G}_{k1} = \boldsymbol{\mu}_1^H \mathcal{C}_1^T \mathcal{C}_k \boldsymbol{\mu}_k = \boldsymbol{\mu}_1^H \mathbf{R}_{k1} \boldsymbol{\mu}_k, \quad k = 2, \dots, K \quad (4.185)$$

which is a $(N_p \times N_p)$ matrix. Then, it can be shown that

$$\mathbf{G}_{k1} = \sum_{v=0}^{N_p-1} (\boldsymbol{\mu}_v^{(1)})^H (\mathbf{C}_1^T \mathbf{C}_k) \boldsymbol{\mu}_v^{(k)} \quad (4.186)$$

Furthermore, with the aid of (4.159) and (4.157), it can be shown that the ij th element of \mathbf{G}_{k1} can be expressed as

$$\begin{aligned} \mathbf{G}_{k1}(i, j) &= \frac{1}{N_t} \sum_{v=0}^{N_p-1} \sum_{n=0}^{N_t-1} \mu_{iv,n}^* \mu_{jv,n} c_{1n} c_{kn} \\ &= \frac{1}{N_t} \sum_{n=0}^{N_t-1} (c_{1n} c_{kn}) \sum_{v=0}^{N_p-1} \mu_{iv,n}^* \mu_{jv,n} \end{aligned} \quad (4.187)$$

With the aid of (4.151), (4.153) and (4.154), (4.187) can be simplified to

$$\begin{aligned} \mathbf{G}_{k1}(i, j) &= \frac{1}{N_t} \sum_{n=0}^{N_t-1} (c_{1n} c_{kn}) e^{j2\pi n \Delta f_{ji} T_c} \sum_{v=0}^{N_p-1} \hat{\mu}_{iv}^* \hat{\mu}_{jv} \\ &= \mathbf{G}(i, j) \times \frac{1}{N_t} \sum_{n=0}^{N_t-1} (c_{1n} c_{kn}) e^{j2\pi n \Delta f_{ji} T_c} \end{aligned} \quad (4.188)$$

where we have defined

$$\mathbf{G} = [\mathbf{G}(i, j)] \quad \text{and} \quad \mathbf{G}(i, j) = \sum_{v=0}^{N_p-1} \hat{\mu}_{iv}^* \hat{\mu}_{jv} \quad (4.189)$$

Explicitly, (4.188) contains the cross-correlation between the desired user's T-domain spreading sequence and the k th user's T-domain spreading sequence. However, the subcarrier frequencies make the cross-correlation analysis complex.

It can be shown that, when the normalized spacing $\lambda = iN_e$, where i is an integer, i.e. when the subcarrier spacing between two adjacent subcarriers is i/T_c resulting in orthogonal MC DS-CDMA, (4.188) is then reduced to

$$\mathbf{G}_{k1}(i, j) = \mathbf{G}(i, j) \times \frac{1}{N_t} \sum_{n=0}^{N_t-1} c_{1n} c_{kn} \quad (4.190)$$

Define in (4.169)

$$\mathbf{Q}_{k1} = \boldsymbol{\varphi}_1^H \boldsymbol{\mu}_1^H \mathcal{C}_1^T \mathcal{C}_k \boldsymbol{\mu}_k \boldsymbol{\varphi}_k = \boldsymbol{\varphi}_1^H \mathbf{G}_{k1} \boldsymbol{\varphi}_k \quad (4.191)$$

which is a $(N_p \times N_p)$ matrix. Then, the m nth element of \mathbf{Q}_{k1} can be expressed as

$$\mathbf{Q}_{k1}(m, n) = \mathbf{G}_{k1}(m, n) \exp(j \Delta \varphi_{nm}^{(k)}) \quad (4.192)$$

where $\Delta \varphi_{nm}^{(k)} = \varphi_n^{(k)} - \varphi_m^{(1)}$.

Finally, in (4.169), let us define

$$\mathbf{Z}_{k1} = (\mathcal{C}_f^{(1)})^T \boldsymbol{\varphi}_1^H \boldsymbol{\mu}_1^H \mathcal{C}_1^T \mathcal{C}_k \boldsymbol{\mu}_k \boldsymbol{\varphi}_k \mathcal{C}_f^{(k)} = (\mathcal{C}_f^{(1)})^T \mathbf{Q}_{k1} \mathcal{C}_f^{(k)} \quad (4.193)$$

which is a $(U \times U)$ matrix, through which the k th user imposes interference on the reference user. Applying (4.131), it can be shown that the uv th element of \mathbf{Z}_{k1} can be expressed as

$$\begin{aligned} \mathbf{Z}_{k1}(u, v) &= \frac{1}{N_p} \sum_{m=0}^{N_p-1} \sum_{n=0}^{N_p-1} \mathbf{Q}_{k1}(m, n) c_{fu,m}^{(1)} c_{fv,n}^{(k)} \\ &= \frac{1}{N_p} \sum_{m=0}^{N_p-1} \sum_{n=0}^{N_p-1} \mathbf{G}_{k1}(m, n) \exp(j \Delta \varphi_{nm}^{(k)}) c_{fu,m}^{(1)} c_{fv,n}^{(k)} \end{aligned} \quad (4.194)$$

It can be shown that $\mathbf{Z}_{k1}(u, v)$ has the following properties. First, when the subcarrier signals are designed so that $\mu_{n_p v, n}$ in (4.151) is zero for $n_p \neq v$ and it is one for $n_p = v$, then, $\mathbf{G}_{k1}(i, j)$ in (4.187) can be expressed as

$$\mathbf{G}_{k1}(i, j) = \begin{cases} 0, & \text{if } i \neq j \\ \frac{1}{N_t} \sum_{n=0}^{N_t-1} c_{1n} c_{kn}, & \text{if } i = j \end{cases} \quad (4.195)$$

where, explicitly, $\mathbf{G}_{k1}(i, i)$ is the cross-correlation coefficient between the k th user's T-domain spreading sequence and the reference user's T-domain spreading sequence. When

applying this result to (4.194), we obtain

$$\begin{aligned} \mathbf{Z}_{k1}(u, v) &= \frac{1}{N_p} \sum_{m=0}^{N_p-1} \mathbf{G}_{k1}(m, m) \exp(j \Delta \varphi_{mm}^{(k)}) c_{fu,m}^{(1)} c_{fv,m}^{(k)} \\ &= \left[\frac{1}{N_t} \sum_{n=0}^{N_t-1} c_{1n} c_{kn} \right] \times \left[\frac{1}{N_p} \sum_{m=0}^{N_p-1} c_{fu,m}^{(1)} c_{fv,m}^{(k)} \exp(j \Delta \varphi_{mm}^{(k)}) \right] \end{aligned} \quad (4.196)$$

where the term within the first bracket is due to the T-domain spreading sequences, while that within the second bracket is the result of the F-domain spreading sequences of both the reference user and the k th interfering user.

According to (4.196), it can be implied that when the subcarrier signals are designed so that (4.195) can be satisfied, there will exist no MUI, when the T-domain spreading sequences assigned to different users are orthogonal. However, due to the random characteristics of the subcarrier phases associated with each user, as shown in (4.196), the MUI is unable to be removed by assigning orthogonal F-domain spreading sequences to different users.

With the aid of the definitions as specified above, (4.169) can finally be expressed as

$$\tilde{z}_1 = \mathbf{Z}_1 \mathbf{b}_0^{(1)} + \sum_{k=2}^K \mathbf{Z}_{k1} \mathbf{b}_0^{(k)} + \tilde{\mathbf{n}}_1 \quad (4.197)$$

and, furthermore, the decision variable for the u th bit of $\mathbf{b}_0^{(1)}$ can be expressed as

$$\begin{aligned} \tilde{z}_{1u} &= \mathbf{Z}_1(u, u) b_0^{(1)}[u] + \underbrace{\sum_{v=0, v \neq u}^{U-1} \mathbf{Z}_1(u, v) b_0^{(1)}[v]}_{\text{Interbit interference}} \\ &\quad + \underbrace{\sum_{k=2}^K \sum_{v=0}^{U-1} \mathbf{Z}_{k1}(u, v) b_0^{(k)}[v]}_{\text{Multiuser interference}} + \tilde{n}_{1u}, \quad u = 1, \dots, U \end{aligned} \quad (4.198)$$

which may conflicts interbit interference as well as MUI.

Let us now analyse the BER performance of the TF-domain spread MC DS-CDMA systems, when the standard Gaussian approximation on the interbit interference and MUI is assumed.

4.6.5 Bit-Error Rate (BER) Performance Analysis

In this section we analyse the BER performance of the TF-domain spread MC DS-CDMA systems, when the SGA is invoked for approximation of both the interbit interference and multiuser interference. The BER performance results obtained based on this approach are provided in Section 4.6.6. In the analysis, both T-domain and F-domain spreading sequences are assumed to be random binary sequences. The subcarrier phases for different subcarriers

and different users are assumed to be the independently distributed uniform random variables in $(0, 2\pi]$.

Following the analysis carried out in Section 4.6.4, it can be shown that the decision variable for the u th data bit of $\mathbf{b}_0^{(1)}$ of the reference user can be written as

$$z_{1u} = \Re\{\tilde{z}_{1u}\}, \quad u = 1, 2, \dots, U \quad (4.199)$$

where

$$\tilde{z}_{1u} = D_u + I_B + I_{MUI} + \tilde{n}_{1u} \quad (4.200)$$

where D_u , as shown in (4.198), represents the desired output, which is given by

$$D_u = \mathbf{Z}_1(u, u) \mathbf{b}_0^{(1)}[u] \quad (4.201)$$

where $\mathbf{Z}_1(u, u)$ is given by (4.178), which, with the aid of (4.189) and (4.173), can be expressed as

$$\mathbf{Z}_1(u, u) = \frac{1}{N_p} \sum_{m=0}^{N_p-1} \mathbf{G}(m, m) \quad (4.202)$$

I_B in (4.200) represents the interbit interference, as shown in (4.198), which is given by

$$I_B = \sum_{v=0, v \neq u}^{U-1} \mathbf{Z}_1(u, v) \mathbf{b}_0^{(1)}[v] \quad (4.203)$$

where $\mathbf{Z}_1(u, v)$ is given by (4.177). In (4.200) I_{MUI} represents the MUI, as shown in (4.198), which can be expressed as

$$I_{MUI} = \sum_{k=2}^K \sum_{v=0}^{U-1} \mathbf{Z}_{k1}(u, v) \mathbf{b}_0^{(k)}[v] \quad (4.204)$$

where $\mathbf{Z}_{k1}(u, v)$ is given by (4.194). Finally, \tilde{n}_{1u} represents the Gaussian noise, which is given by

$$\tilde{n}_{1u} = (\mathcal{H}_1^H \mathbf{N})_u = ((\mathbf{C}_f^{(1)})^T \boldsymbol{\varphi}_1^H \boldsymbol{\mu}_1^H \mathcal{C}_1^T \mathbf{N})_u \quad (4.205)$$

where $(\mathbf{x})_u$ represents the u th element of \mathbf{x} . With the aid of (4.155) and (4.161), it can be shown that the variance of \tilde{n}_{1u} can be expressed as

$$\sigma^2 = E[\tilde{n}_{1u} \tilde{n}_{1u}^*] = \frac{N_0}{E_b} \times \frac{1}{N_p} \sum_{v=0}^{N_p-1} \sum_{v'=0}^{N_p-1} \hat{\mu}_{v'v} \mathbf{G}(v', v) \quad (4.206)$$

We have assumed that both the T-domain and F-domain spreading sequences are made up of random binary sequences. Furthermore, we assume that the interbit interference as well as the MUI can be approximated as additive Gaussian noise. Consequently, the decision variable z_{1u} , $u = 1, \dots, U$ can be approximated as a Gaussian signal, which has a mean given by D_u of (4.201) and a variance given by

$$\text{Var}[z_{1u}] = \frac{1}{2}(\text{Var}[I_B] + \text{Var}[I_{MUI}] + \sigma^2) \quad (4.207)$$

where $\text{Var}[I_B]$ and $\text{Var}[I_{MUI}]$ represent the variances of the interbit interference and the MUI, which are derived in Appendix 4.A and are given, respectively, by (4.A.3) and (4.A.9). Hence, with the SGA, the BER of the general TF-domain spread MC DS-CDMA can be expressed as

$$P_b = Q\left(\left[\frac{1}{2}(\text{Var}[I_B] + \text{Var}[I_{MUI}] + \sigma^2)\mathbf{Z}_1^{-2}(u, u)\right]^{-1/2}\right) \quad (4.208)$$

Substituting (4.A.3) and (4.A.9) into (4.208), P_b can finally be expressed as

$$P_b = Q(\sqrt{2\gamma}) \quad (4.209)$$

$$\begin{aligned} \gamma = & \left[\frac{N_t(U-1) \sum_{m=0}^{N_p-1} \mathbf{G}^2(m, m) + (K-1)U \sum_{m=0}^{N_p-1} \sum_{n=0}^{N_p-1} |\mathbf{G}(m, n)|^2}{N_t(\sum_{m=0}^{N_p-1} \mathbf{G}(m, m))^2} \right. \\ & \left. + \frac{\sigma^2}{(\frac{1}{N_p} \sum_{m=0}^{N_p-1} \mathbf{G}(m, m))^2} \right]^{-1} \end{aligned} \quad (4.210)$$

Note that, when $U = 1$ and $K = 1$, the SNR of (4.210) is reduced to

$$\gamma = \frac{(\frac{1}{N_p} \sum_{m=0}^{N_p-1} \mathbf{G}(m, m))^2}{\sigma^2} \quad (4.211)$$

Furthermore, if the orthogonal MC DS-CDMA system is considered, we then have $\mathbf{G}(m, m) = 1$ and $\sigma^2 = N_0/E_b$. In this case, the BER is $P_b = Q(\sqrt{2E_b/N_0})$, which is the same as the BER of the conventional non-spreading BPSK scheme communicating over AWGN channels.

Note that the BER derived based on the SGA approach is only valid when the number of simultaneous transmission users, K , is high. In most cases, the SGA approach may seriously underestimate the BER, especially when the number of simultaneous transmission users, K , is low [93]. In order to obtain more accurate analytical results, the improved Gaussian approximation (IGA) can be invoked for dealing with the interbit interference and the multiuser interference. In the context of the single-carrier DS-CDMA, the IGA has been studied in references [93, 94]. It has been shown that the IGA approach is generally capable of providing significant accuracy improvement over the SGA approach. However, the IGA approach is very complicated and requires extreme computation time to evaluate. For this sake, a simplified version of the IGA, SIGA, may be employed for obtaining the BER performance. In Section 5.11 of Chapter 5, the SIGA approach will be invoked for analysing the BER performance of the TF-domain spread MC DS-CDMA systems, when communicating over frequency selective fading channels. Furthermore, details of SIGA in the context of the single-carrier DS-CDMA can be found in reference [95].

Let us now use some examples to show the BER performance of the TF-domain spread MC-CDMA.

4.6.6 Bit-Error Rate (BER) Performance Results

In this subsection we provide some BER performance results of the TF-domain spread MC DS-CDMA, which were obtained by evaluation of (4.209) associated with the SNR γ given

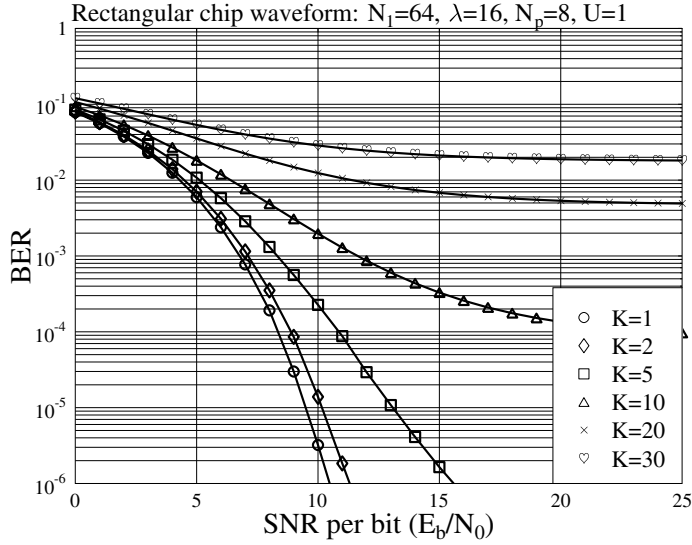


Figure 4.11: Performance of TF-domain spread MC DS-CDMA over AWGN channels.

by (4.210). In the evaluation, rectangular periodic chip waveform was assumed. Furthermore, in order to show the effect of the parameter λ of the normalized subcarrier-spacing on the BER performance, we assumed that the overall system bandwidth was $W_s = 2/T_{c1}$, where T_{c1} denotes the chip duration of a corresponding single-carrier DS-CDMA system having the zero-to-zero bandwidth of W_s . Consequently, for the TF-domain spread MC DS-CDMA having the bandwidth $W_s = 2/T_{c1}$, the relationship of $(N_p - 1)\lambda/T_s + 2/T_c = 2/T_{c1}$ is satisfied, which results in the T-domain spreading factor N_t being expressed as

$$N_t = UN_1 - \frac{(N_p - 1)\lambda}{2} \quad (4.212)$$

where $N_1 = T_b/T_{c1}$.

The BER versus SNR per bit performance for the TF-domain spread MC DS-CDMA system is shown in Fig. 4.11. The parameters used in the evaluation are shown on the top of the figure. Explicitly, the BER performance degrades as the number of users supported increases.

Figure 4.12 shows the effect of the normalized subcarrier spacing, λ , on the BER performance of the TF-domain spread MC DS-CDMA system. Based on the parameters shown on the top of the figure, it can be shown that, for the orthogonal MC DS-CDMA corresponding to $\lambda = N_t$, the T-domain spreading factor of $N_t = 14$ was assumed. As shown in Fig. 4.12, for all the SNR values considered, the lowest BER is achieved when $\lambda = 14$ or, in other words, when the TF-domain spread MC DS-CDMA is the TF-domain spread orthogonal MC DS-CDMA. Note that this observation was also obtained in reference [53] in the context of the generalized MC DS-CDMA.

Finally, in Fig. 4.13 the BER versus the number of users supported by the TF-domain spread MC DS-CDMA is depicted, when the optimum subcarrier spacing is $\lambda = 14$. Again, the BER performance degrades significantly, when the number of users supported increases.

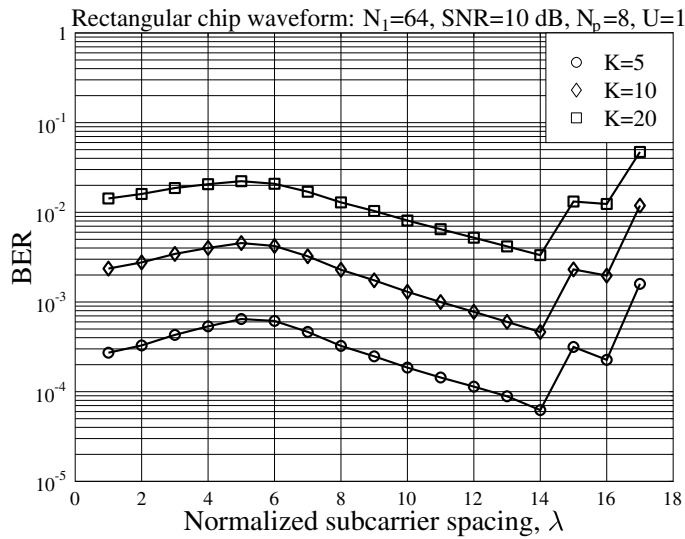


Figure 4.12: Performance of TF-domain spread MC DS-CDMA over AWGN channels.

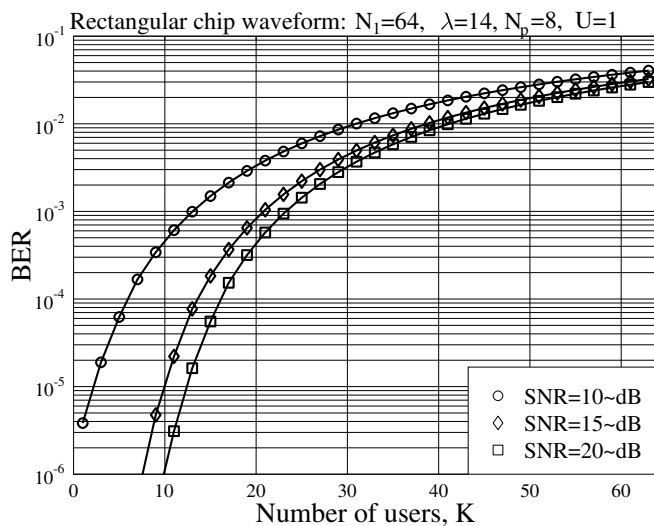


Figure 4.13: Performance of TF-domain spread MC DS-CDMA over AWGN channels.

4.7 Equivalence Between Single-Carrier DS-CDMA and Multicarrier CDMA

In this chapter we have so far illustrated the underlying principles of four types of multicarrier CDMA scheme in Sections 4.3, 4.4, 4.5 and 4.6, respectively. In this section we show that the F-domain spread MC-CDMA scheme, which carries out spreading and signal detection in the F-domain, is equivalent to the single-carrier DS-CDMA scheme, which uses T-domain spreading and carries out signal detection in the T-domain. The importance of studying the equivalence between the above-mentioned two CDMA schemes is manifold, as will become clear.

First, let us show how a single-carrier DS-CDMA scheme can be transformed into a corresponding F-domain spread MC-CDMA scheme. For brevity, we refer to the single-carrier DS-CDMA simply as the DS-CDMA and the F-domain spread MC-CDMA as the MC-CDMA. Following the discussion in Section 2.1 of Chapter 2, when a DS-CDMA system supports K synchronous users communicating over AWGN channels, the received complex baseband equivalent signal, say by a base-station (BS), can be expressed as

$$R(t) = \sum_{k=1}^K \sum_{m=0}^{M-1} \sqrt{2P} b_{km} c_k(t - mT) \exp(j\phi_k) + n(t) \quad (4.213)$$

where P denotes the one-dimension power received from each of the K users, $\{b_{km}\}$ represent the data symbols transmitted by the k th user, where we assume that M symbols are transmitted per block within MT seconds, $c_k(t)$ represents the T-domain spread-spectrum waveform assigned to the k th user, which can be expressed as

$$c_k(t) = \sum_{j=0}^{N-1} c_{kj} \psi(t - jT_c) \quad (4.214)$$

where c_{kj} may take real or complex value depending on the spreading sequences employed by the DS-CDMA system, while $\psi(t)$ is the chip waveform of the T-domain spreading sequence, which is defined over the interval $[0, T_c]$ and normalized to satisfy $\int_0^{T_c} \psi^2(t) dt = T_c$. We assume that the spreading sequence $\{c_{kj}\}$ is periodic and has a period of N , which satisfies $N = T/T_c$. We assume that c_{kj} satisfies $E[|c_{kj}|^2] = 1$. Furthermore, in (4.214) ϕ_k is the initial phase due to the carrier modulation and AWGN channel. Finally, in (4.213) $n(t)$ is a complex Gaussian noise process with zero mean and single-sided PSD of N_0 per dimension.

A typical receiver schematic for detection of the DS-CDMA signals of (4.213) is shown in Fig. 4.14. As shown in Fig. 4.14, the received signal $R(t)$ of (4.213) is first input to a matched filter (MF) having the impulse response $\psi^*(-t)$, which is matched to the transmitted chip waveform $\psi(t)$. Then, the MF's output is sampled at the chip rate of $1/T_c$, in order to provide observations for the receiver to carry out the necessary receiver processing and detection, as shown in Fig. 4.14. More specifically, let us normalize the MF's outputs by $1/\sqrt{2PNT_c}$. Then, it can be shown that the j th observation sample can be expressed as

$$y_j = \frac{1}{\sqrt{2PNT_c}} \int_{(j-1)T_c}^{jT_c} R(\tau) \psi^*(\tau) d\tau, \quad j = 1, 2, \dots, MN \quad (4.215)$$

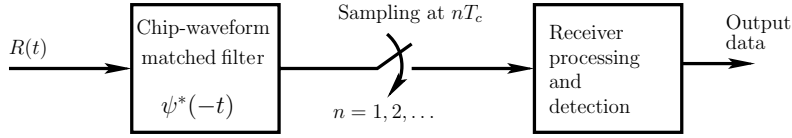


Figure 4.14: Receiver schematic for the single-carrier DS-CDMA systems.

Substituting (4.213) into the above equation yields

$$y_j = \sum_{k=1}^K \frac{1}{\sqrt{N}} c_{kN(j)} e^{j\phi_k} b_{k[(j-1)/N]} + n_j, \quad j = 1, 2, \dots, MN \quad (4.216)$$

where $N(j) = (j - 1) \bmod N$, $[(j - 1)/N]$ returns the integer part of $(j - 1)/N$, while n_j is a matched filtered Gaussian noise sample, which is Gaussian distributed with zero mean and a variance of $\sigma^2/2 = 1/2\text{SNR}$ per dimension, where $\text{SNR} = E_s/N_0$ denotes the SNR.

Let us define

$$\begin{aligned} \mathbf{y}^{(t)} &= [y_1, y_2, \dots, y_{MN}]^T \\ \mathbf{n}^{(t)} &= [n_1, n_2, \dots, n_{MN}]^T \\ \mathbf{b}_k &= [b_{k0}, b_{k1}, \dots, b_{k(M-1)}]^T \end{aligned} \quad (4.217)$$

where the superscript (t) indicates that the operations are in the T-domain. Then, it can be shown that $\mathbf{y}^{(t)}$ can be expressed as

$$\mathbf{y}^{(t)} = \sum_{k=1}^K \frac{e^{j\phi_k}}{\sqrt{N}} (\mathbf{I}_M \otimes \mathbf{c}_k) \mathbf{b}_k + \mathbf{n}^{(t)} \quad (4.218)$$

where $\mathbf{c}_k = [c_{k0}, c_{k1}, \dots, c_{k(N-1)}]^T$ is the DS spreading sequence assigned to the k th user.

The observations in $\mathbf{y}^{(t)}$ as shown in (4.218) are obtained in the T-domain. Conventionally, in DS-CDMA systems the signal processing and detection at the DS-CDMA receivers are carried out in the T-domain based on the T-domain observation equations, e.g. as shown in (4.218). In principle, the receiver has a schematic as shown in Fig. 4.14.

However, the DS-CDMA receivers can also carry out their signal processing and detection in the F-domain, as in the MC-CDMA systems studied in Section 4.3. Specifically, the DS-CDMA receivers can process the T-domain observations seen in (4.218) as follows.

Let \mathcal{F} be a $(MN \times MN)$ FFT matrix, which satisfies $\mathcal{F}^H \mathcal{F} = \mathcal{F} \mathcal{F}^H = \mathbf{I}_{MN}$. Then, applying the FFT on the T-domain observations $\mathbf{y}^{(t)}$, we obtain the F-domain observation as

$$\begin{aligned} \mathbf{y}^{(f)} &= \mathcal{F} \mathbf{y}^{(t)} = \sum_{k=1}^K \frac{\exp(j\phi_k)}{\sqrt{N}} \mathcal{F}(\mathbf{I}_M \otimes \mathbf{c}_k) \mathbf{b}_k + \mathcal{F} \mathbf{n}^{(t)} \\ &= \sum_{k=1}^K \exp(j\phi_k) \mathbf{C}_k \mathbf{b}_k + \mathbf{n}^{(f)} \end{aligned} \quad (4.219)$$

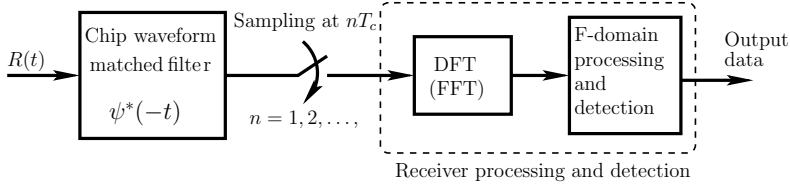


Figure 4.15: Receiver schematic for the single-carrier DS-CDMA systems using F-domain receiver processing and detection.

where the superscript (f) indicates that the corresponding operations are in the F-domain, $\mathbf{C}_k = \mathcal{F}(\mathbf{I}_M \otimes \mathbf{c}_k)/\sqrt{N}$, while $\mathbf{n}^{(f)} = \mathcal{F}\mathbf{n}^{(t)}$, each element of which is still an i.i.d. Gaussian random variable with zero mean and variance $\sigma^2/2$ per dimension.

If we compare (4.219) with (4.29) in Section 4.3, which is the F-domain observation equation for the MC-CDMA supporting $K = 1$ user and carrying out coherent detection, we can find that, after the FFT operation, the DS-CDMA scheme is equivalent to a MC-CDMA scheme having the F-domain spreading matrix \mathbf{C}_k for user k . Furthermore, the detection of $\{\mathbf{b}_k\}$ can be carried out based on (4.219) in the F-domain. For example, when correlation detection is considered, the decision variables corresponding to the k th user can be formed as

$$z_k = \exp(-j\phi_k) \mathbf{C}_k^H \mathbf{y}^{(f)} \quad (4.220)$$

The receiver schematic in the above principles can be shown as Fig. 4.15.

Alternatively, at the receiver the main signal processing may be carried out in the F-domain based on (4.219). For example, the receiver can remove the phase ϕ_k of user k by multiplying $\exp(-j\phi_k)$ with $\mathbf{y}^{(f)}$, yielding

$$\begin{aligned} \bar{\mathbf{y}}^{(f)} &= \exp(-j\phi_k) \mathbf{y}^{(f)} \\ &= \mathbf{C}_k \mathbf{b}_k + \sum_{l \neq k}^K \exp(j\phi'_l) \mathbf{C}_l \mathbf{b}_l + \bar{\mathbf{n}}^{(f)} \end{aligned} \quad (4.221)$$

where $\phi'_l = \phi_l - \phi_k$. However, following the F-domain signal processing, the receiver does not continue the detection in the F-domain, as shown in Fig. 4.15. Instead, the receiver detects the transmitted information in the T-domain by first transforming the F-domain processed observations $\bar{\mathbf{y}}^{(f)}$ into the T-domain as

$$\bar{\mathbf{y}}^{(t)} = \mathcal{F}^H \bar{\mathbf{y}}^{(f)} \quad (4.222)$$

After substituting (4.221) into (4.222) and using the fact of $\mathbf{C}_l = \mathcal{F}(\mathbf{I}_M \otimes \mathbf{c}_l)/\sqrt{N}$, we can simplify (4.222) to

$$\bar{\mathbf{y}}^{(t)} = \frac{1}{\sqrt{N}} (\mathbf{I}_M \otimes \mathbf{c}_k) \mathbf{b}_k + \sum_{l \neq k}^K \frac{\exp(j\phi'_l)}{\sqrt{N}} (\mathbf{I}_M \otimes \mathbf{c}_l) \mathbf{b}_l + \bar{\mathbf{n}}^{(t)} \quad (4.223)$$

Assuming correlation detection, based on (4.223), the decision variables for user k can now be formed as

$$z_k = \frac{1}{\sqrt{N}} (\mathbf{I}_M \otimes \mathbf{c}_k)^H \bar{\mathbf{y}}^{(t)} \quad (4.224)$$

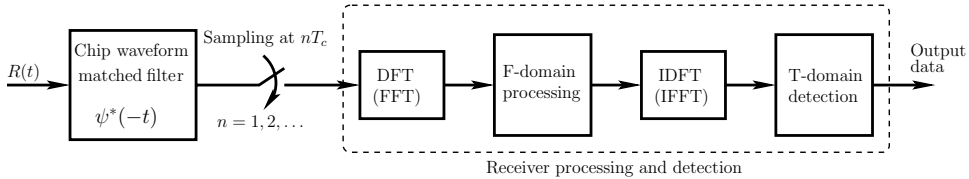


Figure 4.16: Receiver schematic for the single-carrier DS-CDMA systems, where signal processing at the receiver is mainly carried out in the F-domain, while signal detection is completed in the T-domain.

In summary, the above-described receiver operations can be illustrated by the schematic as shown in Fig. 4.16.

We have shown in principle that, at the receiver side, a DS-CDMA scheme can be modified to an equivalent MC-CDMA scheme with the aid of the Fourier transform. From the above analysis, excepting the principles, we cannot see any strong justification for the transform from T-domain to F-domain or from F-domain to T-domain, when communicating over AWGN channels. However, wireless channels are typically time variant. In this case, as our further study in Chapter 5 shows, the F-domain processing techniques may be significantly beneficial to the detection of DS-CDMA signals.

F-domain-based signal processing, such as F-domain equalization, for single-carrier communications schemes is a concept proposed a long time ago [96]. However, this technique has not drawn much attention until Sari *et.al.* showed the similarity between signal processing in OFDM and that in F-domain equalization in the conventional single-carrier communication schemes [97]. Recently, the theory and application of F-domain signal processing and F-domain equalization in single-carrier communication schemes have received wide attention in wireless communications as evidenced, e.g., by references [98–106].

Note that, similarly to the DS-CDMA systems, where the signal in the T-domain can be transformed to the F-domain to facilitate use of F-domain signal processing techniques, in the MC-CDMA systems signals in the F-domain may also be transformed to the T-domain, where T-domain signal processing can be carried out. However, the F-domain spread MC-CDMA systems have the advantages of low-complexity multicarrier modulation/demodulation, of low-complexity F-domain equalization, etc.; it seems that there is no sense in transforming signals from the F-domain to the T-domain in order to employ the T-domain signal processing techniques.

4.8 Summary and Discussion

This chapter has established the approaches for analysing the error performance of various multicarrier systems supporting single or multiple users, when communicating over AWGN channels. We have shown that, when the single-user is supported, the multicarrier systems are capable of achieving the same error performance as the conventional corresponding digital communication schemes without using spreading.

We have provided detailed analysis for the BER of the TF-domain spread MC DS-CDMA system, when multiple users are supported. In our analysis the SGA has been invoked

for approximation of both the interbit interference and the MUI as Gaussian interference. Furthermore, the effect of subcarrier spacing on the BER performance of the TF-domain spread MC DS-CDMA has been addressed. The performance results show that the BER performance of the TF-domain spread MC DS-CDMA degrades significantly when the number of users supported increases. Furthermore, for a given system bandwidth, there exists an optimum subcarrier spacing value, resulting in the lowest achievable BER. The TF-domain spread MC DS-CDMA having the optimum subcarrier spacing has been shown to correspond to the TF-domain spread orthogonal MC DS-CDMA.

We have established the equivalence between the single-carrier DS-CDMA and the F-domain spread MC-CDMA. By transforming the single-carrier DS-CDMA signals from the T-domain to the F-domain, efficient F-domain signal processing techniques may be applied to the single-carrier DS-CDMA systems. Conversely, by transforming the F-domain spread MC-CDMA signals from the F-domain to the T-domain, efficient T-domain signal processing techniques may also be employed by the F-domain spread MC-CDMA systems in order to improve their efficiency. In Section 5.8 of the next chapter, the F-domain processing (equalization) in single-carrier DS-CDMA systems will be further analysed, when frequency selective fading channels are considered.

Appendix 4.A Standard Gaussian Approximation

In this appendix we derive the variance of the interbit interference I_B of (4.203) and that of the MUI I_{MUI} shown in (4.204).

First, for the interbit interference, when assuming that the transmitted bits constitute i.i.d. random binary variables, the variance of I_B of (4.203) can be expressed as

$$\text{Var}[I_B] = \sum_{v=0, v \neq u}^{U-1} E[|\mathbf{Z}_1(u, v)|^2] = (U - 1)E[|\mathbf{Z}_1(u, v)|^2] \quad (4.A.1)$$

where $u \neq v$. Substituting (4.177) into the above equation, yields

$$\begin{aligned} \text{Var}[I_B] &= \frac{U - 1}{(N_p N_t)^2} E\left[\left|\sum_{m=0}^{N_p-1} \mathbf{G}_1(m, m) c_{fu,m}^{(1)} c_{fv,m}^{(1)}\right|^2\right] \\ &= \frac{U - 1}{(N_p N_t)^2} E\left[\sum_{m=0}^{N_p-1} \sum_{n=0}^{N_p-1} \mathbf{G}_1(m, m) \mathbf{G}_1^*(n, n) c_{fu,m}^{(1)} c_{fv,m}^{(1)} c_{fu,n}^{(1)} c_{fv,n}^{(1)}\right] \end{aligned} \quad (4.A.2)$$

In the above equation, excepting the cases corresponding to $m = n$, the expectations in the context of the other cases are zero. Hence, the variance of the interbit interference can be expressed as

$$\text{Var}[I_B] = \frac{U - 1}{(N_p N_t)^2} \sum_{m=0}^{N_p-1} |\mathbf{G}_1(m, m)|^2 = \frac{U - 1}{N_p^2} \sum_{m=0}^{N_p-1} \mathbf{G}_1^2(m, m) \quad (4.A.3)$$

where $\mathbf{G}(m, m)$ is given by (4.189).

Note that when the subcarrier signals are designed yielding $\mathbf{G}(m, m) = 1$, then (4.A.3) is reduced to

$$\text{Var}[I_B] = \frac{U - 1}{N_p} \quad (4.A.4)$$

Therefore, when random spreading sequences are employed by a given user to spread its U -bit information in the F-domain, the interbit interference may be extreme. In practice, the class of sequences having good correlation properties may be assigned to a given user to spread its information in the F-domain, or more advanced detection schemes might be employed, so that the interbit interference can be mitigated efficiently.

In the context of the MUI, we assume that the user signals are independent and, furthermore, that the data bits transmitted by the same user are also independent. Based on these assumptions, the multiuser interfering signal seen in (4.204) can be approximated as a Gaussian signal with zero mean and a variance

$$\text{Var}[I_{MUI}] = \sum_{k=2}^K \sum_{v=0}^{U-1} E[|\mathbf{Z}_{k1}(u, v)|^2] = (K - 1)U E[|\mathbf{Z}_{k1}(u, v)|^2] \quad (4.A.5)$$

Substituting (4.194) into this equation, we have

$$\begin{aligned} \text{Var}[I_{MUI}] &= \frac{(K - 1)U}{N_p^2} E \left[\sum_{m_1=0}^{N_p-1} \sum_{n_1=0}^{N_p-1} \sum_{m_2=0}^{N_p-1} \sum_{n_2=0}^{N_p-1} \mathbf{G}_{k1}(m_1, n_1) \mathbf{G}_{k1}^*(m_2, n_2) \right. \\ &\quad \times \exp(j\Delta\varphi_{n_1 m_1}^{(k)}) \exp(-j\Delta\varphi_{n_2 m_2}^{(k)}) c_{fu, m_1}^{(1)} c_{fv, n_1}^{(k)} c_{fu, m_2}^{(1)} c_{fv, n_2}^{(k)} \left. \right] \end{aligned} \quad (4.A.6)$$

When random spreading sequences are assumed, it can also be shown that, except in the case of satisfying $m_1 = m_2$ and $n_1 = n_2$ simultaneously, the expectation in (4.A.6) will be zero. Hence, (4.A.6) can be simplified to

$$\text{Var}[I_{MUI}] = \frac{(K - 1)U}{N_p^2} \sum_{m=0}^{N_p-1} \sum_{n=0}^{N_p-1} E[|\mathbf{G}_{k1}(m, n)|^2] \quad (4.A.7)$$

where $\mathbf{G}_{k1}(m, n)$ is given by (4.188), which is still a random variable determined by the T-domain spreading sequences. When substituting (4.188) into (4.A.7), we have

$$\begin{aligned} \text{Var}[I_{MUI}] &= \frac{(K - 1)U}{(N_p N_t)^2} \sum_{m=0}^{N_p-1} \sum_{n=0}^{N_p-1} |\mathbf{G}(m, n)|^2 \\ &\quad \times E \left[\sum_{i_1=0}^{N_t-1} \sum_{i_2=0}^{N_t-1} (c_{1i_1} c_{ki_1})(c_{1i_2} c_{ki_2}) e^{j2\pi i_1 \Delta f_{nm} T_c} e^{-j2\pi i_2 \Delta f_{nm} T_c} \right] \\ &= \frac{(K - 1)U}{(N_p N_t)^2} \sum_{m=0}^{N_p-1} \sum_{n=0}^{N_p-1} |\mathbf{G}(m, n)|^2 \\ &\quad \times E \left[\sum_{i_1=0}^{N_t-1} \sum_{i_2=0}^{N_t-1} (c_{1i_1} c_{ki_1})(c_{1i_2} c_{ki_2}) e^{j2\pi(i_1 - i_2) \Delta f_{nm} T_c} \right] \end{aligned} \quad (4.A.8)$$

After carrying out the expectation, we finally obtain the variance for the MUI, which is given by

$$\text{Var}[I_{MUI}] = \frac{(K-1)U}{N_p^2 N_t} \sum_{m=0}^{N_p-1} \sum_{n=0}^{N_p-1} |\mathbf{G}(m, n)|^2 \quad (4.A.9)$$

Note that when the subcarrier signals are designed so that they yield $\mathbf{G}(m, m) = 1$ and $\mathbf{G}(m, n) = 0$ for $m \neq n$, then (4.A.9) is reduced to

$$\text{Var}[I_{MUI}] = \frac{(K-1)U}{N_p N_t} \quad (4.A.10)$$

which is the desired variance value in the context of the conventional synchronous orthogonal MC DS-CDMA scheme [41, 71], when communicating over Gaussian channels.

Chapter 5

Performance of Multicarrier Systems over Frequency-Selective Fading Channels

5.1 Introduction

In this chapter the error performance of a range of multicarrier systems is investigated, when the corresponding multicarrier signals are transmitted over frequency selective fading channels. According to the previous chapters (see, e.g., Section 3.7), in multicarrier systems, the subcarriers can be configured so that the bandwidth of a subcarrier is sufficiently low for each subcarrier signal to experience flat fading. This implies that each subcarrier band belongs to the narrowband compared with the coherence bandwidth of the wireless channels investigated. Hence, even though the fading channel is frequency selective, in this chapter we assume that each subcarrier signal of a multicarrier system experiences flat fading. Specifically, we assume that each of the subcarrier signals experiences flat Nakagami- m fading, and that the fading amplitude obeys the probability density function (PDF) [53, 107–109]

$$p_{|h|}(R) = \frac{2}{\Gamma(m)} \left(\frac{m}{\Omega}\right)^m R^{2m-1} \exp\left(-\frac{m}{\Omega} R^2\right), \quad R \geq 0 \quad (5.1)$$

where $\Gamma(\cdot)$ is the gamma function [2], and m is the Nakagami- m fading parameter, which is equal to $m = E[|h|^2]/Var[|h|^2]$. Finally, in (5.1) the parameter Ω is the second moment of h , i.e. $\Omega = E[|h|^2]$.

It can easily be shown that the squared-envelope $|h|^2$ of a Nakagami- m fading channel obeys the gamma distribution with the PDF of

$$p_{|h|^2}(y) = \frac{1}{\Gamma(m)} \left(\frac{m}{\Omega}\right)^m y^{m-1} \exp\left(-\frac{my}{\Omega}\right), \quad y \geq 0 \quad (5.2)$$

The genetic Nakagami fading channel model is considered, since the Nakagami- m distribution is a generalized distribution that often gives the best fit to land-mobile and indoor-mobile multipath propagation environments, as well as to scintillating ionospheric radio links [108]. A good fit to these widely varying propagation scenarios is achieved by varying the single parameter of m in the Nakagami- m distribution. The parameter m in the fading amplitude distribution characterizes the severity of the fading [107]. Specifically, the Nakagami- m fading reduces to the Rayleigh fading when $m = 1$, $m \rightarrow \infty$ corresponds to the conventional Gaussian scenario, and $m = 1/2$ describes the so-called one-side Gaussian fading, i.e. the worst-case fading condition. The Rician and lognormal distributions can also be closely approximated by the Nakagami distribution in conjunction with values of $m > 1$. Additionally, the Nakagami- m distribution offers features of analytical convenience, as has been shown in numerous treatises [51, 53, 83–85, 107, 109–130].

Without providing the proof in detail, we summarize the correlation coefficients of the envelope and squared-envelope as functions of frequency separation, when communicating over frequency selective Nakagami- m fading channels. These results will be used in our numerical evaluations in this chapter. Specifically, when the excess delay spread obeys the exponential distribution expressed as

$$p(\tau) = \frac{1}{\bar{\tau}} \exp\left(-\frac{\tau}{\bar{\tau}}\right), \quad \tau \geq 0 \quad (5.3)$$

where $\bar{\tau}$ represents the mean value of the excess delay spread, then, the correlation coefficient of two envelopes, $|h(f)|$ and $|h(f + \Delta f)|$, which have a frequency spacing of Δf , can be given approximately by

$$\rho_E(\Delta f) \approx \frac{\Gamma^2(m + \frac{1}{2})}{4m[m\Gamma^2(m) - \Gamma^2(m + \frac{1}{2})]} \frac{1}{1 + \bar{\tau}^2(2\pi\Delta f)^2} \quad (5.4)$$

when communicating over frequency selective Nakagami- m fading channels. The correlation coefficient of two squared envelopes, $|h^2(f)|$ and $|h^2(f + \Delta f)|$, having a frequency spacing of Δf , is given by

$$\rho_{SE}(\Delta f) = \frac{1}{1 + \bar{\tau}^2(2\pi\Delta f)^2} \quad (5.5)$$

When the excess delay spread obeys the uniform distribution with the PDF given by

$$p(\tau) = \frac{1}{T_m}, \quad 0 \leq \tau \leq T_m \quad (5.6)$$

where T_m is the *maximum delay spread*, then, the correlation coefficient of two envelopes having a frequency spacing of Δf can be expressed approximately as

$$\rho_E(\Delta f) \approx \frac{\Gamma^2(m + \frac{1}{2}) \operatorname{sinc}^2(\pi\Delta f T_m)}{4m[m\Gamma^2(m) - \Gamma^2(m + \frac{1}{2})]} \quad (5.7)$$

and the correlation coefficient for two squared envelopes having a frequency spacing of Δf is given by

$$\rho_{SE}(\Delta f) = \operatorname{sinc}^2(\pi\Delta f T_m) \quad (5.8)$$

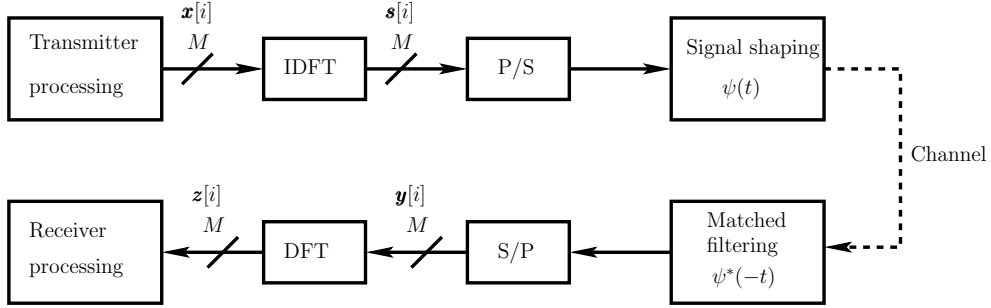


Figure 5.1: Schematic block diagram of the transmitter/receiver for multicarrier systems using IDFT/DFT assisted modulation/demodulation.

Frequency selective fading channels in time domain have been widely studied and also widely applied in investigation into the performance of various wireless communications systems [109, 131]. In this chapter the effect of frequency selective fading on various multicarrier schemes is first analysed. Then, techniques for the suppression of intersymbol interference (ISI) in OFDM and other multicarrier systems are considered. From Section 5.5, the error performance of a range of multicarrier systems when communicating over frequency-selective fading channels is investigated.

5.2 Frequency-Selective Fading in Multicarrier Systems

In this section the effect of frequency-selective fading on the multicarrier signals is analysed in detail. Assume that the multicarrier system uses M number of subcarriers. As shown in Fig. 5.1, after the transmitter processing, which may include time (T)-domain spreading, frequency (F)-domain spreading, S/P conversion, etc., the data transmitted on the M number of subcarriers within the i th discrete Fourier transform (DFT) period are given by

$$\mathbf{x}[i] = [x_0[i], x_1[i], \dots, x_{M-1}[i]]^T, \quad i = 1, 2, \dots \quad (5.9)$$

Furthermore, let T represent the duration of a DFT period, which is the time-duration that a DFT signal spans. Then, after the inverse discrete Fourier transform (IDFT) on $\mathbf{x}[i]$, it gives

$$s_n[i] = \frac{1}{\sqrt{M}} \sum_{m=0}^{M-1} x_m[i] \exp\left(j \frac{2\pi mn}{M}\right), \quad n = 0, 1, \dots, M-1; \quad i = 1, 2, \dots \quad (5.10)$$

Following the IDFT, as shown in Fig. 5.1, parallel-to-serial (P/S) conversion is carried out. Finally, the normalized transmitted multicarrier signal can be formed as

$$s(t) = \sum_{i=0}^{\infty} \sum_{n=0}^{M-1} s_n[i] \psi(t - iT - nT_\psi) \quad (5.11)$$

where $\psi(t)$ is a time-domain pulse defined in $[0, T_\psi]$, which is normalized to satisfy $\int_0^{T_\psi} \psi^2(t) dt = T_\psi$. Since each DFT period transmits M samples, $T_\psi = T/M$ is thus satisfied.

Below, we show what values of T and T_ψ might be when different multicarrier schemes are considered. Let us assume that T_s is the symbol duration transmitting a whole set of data symbols that is in fact the conventional symbol duration as defined in Chapter 3. Let W_s be the total bandwidth that the multicarrier signals occupy. Let T_c be the chip duration of the time domain DS spreading sequences used by the subcarriers, and $N = T_s/T_c$ be the spreading factor of each subcarrier signal. Furthermore, let λ be the normalized spacing between two adjacent subcarriers. Then, referring to Chapter 3, the following results for T and T_ψ can be obtained.

- OFDM: $T = T_s$, $T_\psi = T_s/M$. Since the total number of subcarriers for the OFDM system is approximately $M = W_s T_s$, when given the available system bandwidth W_s , it can be shown that $T_\psi = T_s/M = 1/W_s$;
- Generalized MC DS-CDMA: $T = T_c$, $T_\psi = T_c/M$. Since

$$\frac{(M-1)\lambda}{T_s} + \frac{2}{T_c} = W_s \quad (5.12)$$

using $T_s = NT_c$, we obtain

$$T = T_c = \frac{1}{W_s} \left(\frac{(M-1)\lambda}{N} + 2 \right) \quad (5.13)$$

Therefore

$$T_\psi = \frac{T_c}{M} = \frac{1}{MW_s} \left(\frac{(M-1)\lambda}{N} + 2 \right) \quad (5.14)$$

Sometimes, it is useful to express the above equation as

$$T_\psi = \frac{\kappa}{W_s} \quad (5.15)$$

associated with

$$\kappa = \frac{(M-1)\lambda + 2N}{MN} \quad (5.16)$$

- F-domain spread MC-CDMA: First, $T = T_c = T_s$. Second, T_ψ can be obtained from (5.14) by letting $\lambda = 1$ and $N = 1$, which yields $T_\psi \approx 1/W_s$. Furthermore, from (5.16) we have $\kappa \approx 1$;
- Orthogonal MC DS-CDMA: First, $T = T_c = T_s/N$. Second, letting in (5.14) $\lambda = N$ gives $T_\psi \approx 1/W_s$. Furthermore, according to (5.16) we have $\kappa \approx 1$ for the orthogonal MC DS-CDMA;
- Multitone DS-CDMA: $T = T_c \approx 1/W_s$ and $T_\psi = 1/MW_s$. Hence, $\kappa = 1/M < 1$.

Additionally, (5.16) shows that $\kappa \geq 1$, provided that $\lambda \geq N$.

Let the maximum delay spread of a frequency-selective fading channel be $T_m > 1/W_s$. Since the minimum resolution of the multicarrier signal in (5.11) is T_ψ , the channel impulse response (CIR) of the frequency-selective fading channel can be expressed as

$$h(\tau) = \sum_{l=0}^{L-1} h_l \delta(\tau - lT_\psi) \quad (5.17)$$

where h_l is the complex channel gain and the number of multipaths is

$$L = \left\lfloor \frac{T_m}{T_\psi} \right\rfloor + 1 = \left\lfloor \frac{T_m W_s}{\kappa} \right\rfloor + 1 \quad (5.18)$$

where the second equality is because of (5.15) and the floor function $\lfloor x \rfloor$ returns the highest integer less than or equal to x .

It is well known that, for wireless signals having a transmission bandwidth W_s , the minimum resolution for generating independent (resolvable) paths is $1/W_s$ [2]. Hence, (5.18) implies that the L number of multipath components are independent if $\kappa \geq 1$, while they may be dependent when $\kappa < 1$. Below, we show that a frequency-selective fading channel can be converted to a set of parallel flat (frequency non-selective) fading subcarrier channels, provided that $L \leq M$ is satisfied.

Without considering the background noise, when the multicarrier signal of (5.11) is transmitted over the frequency-selective fading channels having the CIR of (5.17), the received signal can be expressed as

$$r(t) = s(t) * h(t) = \sum_{i=0}^{\infty} \sum_{n=0}^{M-1} s_n[i] \psi(t - iT - nT_\psi) * h(t) \quad (5.19)$$

Applying (5.17) to this equation, we obtain

$$r(t) = \sum_{i=0}^{\infty} \sum_{n=0}^{M-1} \sum_{l=0}^{L-1} s_n[i] h_l \psi(t - iT - (n+l)T_\psi) \quad (5.20)$$

At the receiver $r(t)$ is first input into a filter having an impulse response of $\psi^*(-t)$, which is matched to the transmitted pulse $\psi(t)$. Hence, after the normalization using T_ψ , the output of the matched filter can be expressed as

$$\begin{aligned} y(t) &= \frac{1}{T_\psi} r(t) * \psi^*(-t) \\ &= \frac{1}{T_\psi} \int_{-\infty}^{\infty} \psi^*(\tau) r(t + \tau) d\tau \end{aligned} \quad (5.21)$$

Hence, when substituting (5.20) into (5.21), gives

$$y(t) = \sum_{i=0}^{\infty} \sum_{n=0}^{M-1} \sum_{l=0}^{L-1} s_n[i] h_l \frac{1}{T_\psi} \int_{-\infty}^{\infty} \psi^*(\tau) \psi(t + \tau - iT - (n+l)T_\psi) d\tau \quad (5.22)$$

Since the time-domain pulse $\psi(t)$ is defined in $[0, T_\psi]$ and we also assumed that $L \leq M$, then, when sampling $y(t)$ of (5.22) at $uT_\psi = vT + mT_\psi = vMT_\psi + mT_\psi$, we obtain

$$\begin{aligned} y_u &= y(t)|_{t=uT_\psi} = \sum_{i=0}^{\infty} \sum_{n=0}^{M-1} \sum_{l=0}^{L-1} s_n[i] h_l \\ &\quad \times \frac{1}{T_\psi} \int_{-\infty}^{\infty} \psi^*(\tau) \psi(\tau + (v-i)T + (m-n-l)T_\psi) d\tau \\ &= \sum_{i=0}^{\infty} \sum_{n=0}^{M-1} \sum_{l=0}^{L-1} s_n[i] h_l \delta((v-i)M + m - n - l) \end{aligned} \quad (5.23)$$

Let in the above equation $k = iM + n$ and let $s_n[i]$ change to s_k . Then, (5.23) can be written as

$$\begin{aligned} y_u &= \sum_{k=0}^{\infty} \sum_{l=0}^{L-1} s_k h_l \delta(u - k - l) \\ &= \sum_{k=0}^{\infty} s_k h_{u-k} \\ &= s_u * h_u \end{aligned} \quad (5.24)$$

Specifically, for the v th ($v > 1$) IDFT symbol

$$\mathbf{s}[v] = [s_0[v], s_1[v], \dots, s_{M-1}[v]]^T \quad (5.25)$$

the corresponding M number of samples is

$$\mathbf{y}[v] = [y_{vM}, y_{vM+1}, \dots, y_{vM+M-1}]^T \quad (5.26)$$

It can be shown that $\mathbf{y}[v]$ can be expressed as

$$\mathbf{y}[v] = \bar{\mathbf{H}}_{v-1} \mathbf{s}[v-1] + \mathbf{H}_v \mathbf{s}[v], \quad v = 1, 2, \dots \quad (5.27)$$

where \mathbf{H}_v is $(M \times M)$ and is given by

$$\mathbf{H}_v = \begin{bmatrix} h_0 & & & & & & \\ h_1 & h_0 & & & & & \\ \vdots & \vdots & \ddots & & & & \\ h_{L-1} & h_{L-2} & \cdots & h_0 & & & \\ 0 & h_{L-1} & \cdots & h_1 & h_0 & & \\ \vdots & \vdots & \cdots & \vdots & \vdots & \ddots & \\ 0 & 0 & \cdots & h_{L-1} & \cdots & h_1 & h_0 \end{bmatrix} \quad (5.28)$$

where the empty entries are zeros, while $\bar{\mathbf{H}}_{v-1}$ is an $(M \times M)$ upper triangle matrix given by

$$\bar{\mathbf{H}}_{v-1} = \begin{bmatrix} 0 & \cdots & 0 & h_{L-1} & h_{L-2} & \cdots & h_2 & h_1 \\ 0 & \cdots & 0 & 0 & h_{L-1} & \cdots & h_3 & h_2 \\ \vdots & \ddots & \vdots & \vdots & \vdots & \ddots & \vdots & \vdots \\ 0 & \cdots & 0 & 0 & 0 & \cdots & h_{L-1} & h_{L-2} \\ 0 & \cdots & 0 & 0 & 0 & \cdots & 0 & h_{L-1} \\ \mathbf{0} & \cdots & \mathbf{0} & \mathbf{0} & \mathbf{0} & \cdots & \mathbf{0} & \mathbf{0} \end{bmatrix} \quad (5.29)$$

From (5.10) we know that

$$\mathbf{s}[v] = \mathcal{F}^H \mathbf{x}[v] \quad (5.30)$$

When applying this to (5.27), we obtain

$$\mathbf{y}[v] = \bar{\mathbf{H}}_{v-1} \mathcal{F}^H \mathbf{x}[v-1] + \mathbf{H}_v \mathcal{F}^H \mathbf{x}[v], \quad v = 1, 2, \dots \quad (5.31)$$

Finally, carrying out the DFT on $\mathbf{y}[v]$, gives

$$\begin{aligned} z[v] &= \mathcal{F}\mathbf{y}[v] \\ &= \mathcal{F}\bar{\mathbf{H}}_{v-1}\mathcal{F}^H\mathbf{x}[v-1] + \mathcal{F}\mathbf{H}_v\mathcal{F}^H\mathbf{x}[v], \quad v = 1, 2, \dots \end{aligned} \quad (5.32)$$

Based on (5.32), the transmitted data $\mathbf{x}[v]$ can be estimated.

More specifically, the k th element of $z[v]$ can be expressed as

$$z_k[v] = \mathcal{F}_k^T \bar{\mathbf{H}}_{v-1} \mathcal{F}^H \mathbf{x}[v-1] + \mathcal{F}_k^T \mathbf{H}_v \mathcal{F}^H \mathbf{x}[v], \quad k = 0, 1, \dots, M-1 \quad (5.33)$$

where \mathcal{F}_k represents the k th column of \mathcal{F} . Equation (5.33) shows explicitly that $\mathbf{x}[v]$ experiences ISI, but only from a previous DFT symbol, provided that $L \leq M$. Let

$$\begin{aligned} \bar{H}_{km}(v) &= \mathcal{F}_k^T \mathbf{h}_{L-m}, \quad m = 1, 2, \dots, L-1 \\ H_{km}(v) &= \mathcal{F}_k^T \mathbf{h}_m^{(v)}, \quad m = 0, 1, \dots, M-1 \end{aligned} \quad (5.34)$$

where $\mathbf{h}_{L-m} = [h_{L-m}, h_{L-m+1}, \dots, h_{L-1}, 0, \dots, 0]^T$ and $\mathbf{h}_m^{(v)}$ represents the m th column of \mathbf{H}_v . Then, we can express (5.33) as

$$\begin{aligned} z_k[v] &= \frac{1}{\sqrt{M}} \sum_{i=0}^{M-1} \sum_{m=1}^{L-1} \bar{H}_{km}(v-1) \exp\left(j \frac{2\pi i(M-L+m)}{M}\right) x_i[v-1] \\ &\quad + \frac{1}{\sqrt{M}} \sum_{i=0}^{M-1} \sum_{m=0}^{M-1} H_{km}(v) \exp\left(j \frac{2\pi im}{M}\right) x_i[v] \\ &\quad k = 0, 1, \dots, M-1 \end{aligned} \quad (5.35)$$

The above equation can also be expressed as

$$\begin{aligned} z_k[v] &= \frac{1}{\sqrt{M}} \sum_{i=0}^{M-1} \sum_{m=1}^{L-1} \bar{H}_{km}(v-1) \exp\left(j \frac{2\pi i(M-L+m)}{M}\right) x_i[v-1] \\ &\quad - \frac{1}{\sqrt{M}} \sum_{i=0}^{M-1} \sum_{m=1}^{L-1} \bar{H}_{km}(v) \exp\left(j \frac{2\pi i(M-L+m)}{M}\right) x_i[v] \\ &\quad + \frac{1}{\sqrt{M}} \sum_{i=0}^{M-1} \sum_{m=0}^{M-1} H_{km}(v) \exp\left(j \frac{2\pi im}{M}\right) x_i[v] \\ &\quad + \frac{1}{\sqrt{M}} \sum_{i=0}^{M-1} \sum_{m=1}^{L-1} \bar{H}_{km}(v) \exp\left(j \frac{2\pi i(M-L+m)}{M}\right) x_i[v] \\ &\quad k = 0, 1, \dots, M-1 \end{aligned} \quad (5.36)$$

Let in the last sum and define $w = M - L + m$. Then, we can express (5.36) as

$$\begin{aligned} z_k[v] &= \frac{1}{\sqrt{M}} \sum_{i=0}^{M-1} \sum_{m=1}^{L-1} \bar{H}_{km}(v-1) \exp\left(j \frac{2\pi i(M-L+m)}{M}\right) x_i[v-1] \\ &\quad - \frac{1}{\sqrt{M}} \sum_{i=0}^{M-1} \sum_{m=1}^{L-1} \bar{H}_{km}(v) \exp\left(j \frac{2\pi i(M-L+m)}{M}\right) x_i[v] \end{aligned}$$

$$\begin{aligned}
& + \frac{1}{\sqrt{M}} \sum_{i=0}^{M-1} \sum_{m=0}^{M-1} H_{km}(v) \exp\left(j \frac{2\pi im}{M}\right) x_i[v] \\
& + \frac{1}{\sqrt{M}} \sum_{i=0}^{M-1} \sum_{w=M-L+1}^{M-1} \bar{H}_{k(L-M+w)}(v) \exp\left(j \frac{2\pi iw}{M}\right) x_i[v] \\
& k = 0, 1, \dots, M-1
\end{aligned} \tag{5.37}$$

Let us define

$$\check{H}_{km}(v) = \begin{cases} H_{km}(v) & \text{if } m \leq M-L \\ H_{km}(v) + \bar{H}_{k(L-M+m)}(v) & \text{if } m \geq M-L+1 \end{cases} \tag{5.38}$$

Then, we have

$$\begin{aligned}
z_k[v] = & \frac{1}{\sqrt{M}} \sum_{i=0}^{M-1} \sum_{m=1}^{L-1} \bar{H}_{km}(v-1) \exp\left(j \frac{2\pi i(M-L+m)}{M}\right) x_i[v-1] \\
& - \frac{1}{\sqrt{M}} \sum_{i=0}^{M-1} \sum_{m=1}^{L-1} \bar{H}_{km}(v) \exp\left(j \frac{2\pi i(M-L+m)}{M}\right) x_i[v] \\
& + \frac{1}{\sqrt{M}} \sum_{i=0}^{M-1} \sum_{m=0}^{M-1} \check{H}_{km}(v) \exp\left(j \frac{2\pi im}{M}\right) x_i[v] \\
& k = 0, 1, \dots, M-1
\end{aligned} \tag{5.39}$$

With the aid of (5.34) and (5.38), it can be shown that

$$\check{H}_{km}(v) = \frac{1}{\sqrt{M}} H_k(v) \exp\left(-j \frac{2\pi km}{M}\right) \tag{5.40}$$

where

$$H_k(v) = \sum_{l=0}^{L-1} h_l \exp\left(-j \frac{2\pi kl}{M}\right) \tag{5.41}$$

which represents the fading gain of the k th subcarrier. Applying (5.40) to (5.39), it can be shown that, except for the item corresponding to $i = k$, the last sum in (5.39) is zero. Hence, (5.39) can be simplified to

$$\begin{aligned}
z_k[v] = & H_k(v) x_k[v] \\
& - \frac{1}{\sqrt{M}} \sum_{i=0}^{M-1} \sum_{m=1}^{L-1} \bar{H}_{km}(v) \exp\left(j \frac{2\pi i(M-L+m)}{M}\right) x_i[v] \\
& + \frac{1}{\sqrt{M}} \sum_{i=0}^{M-1} \sum_{m=1}^{L-1} \bar{H}_{km}(v-1) \exp\left(j \frac{2\pi i(M-L+m)}{M}\right) x_i[v-1] \\
& k = 0, 1, \dots, M-1
\end{aligned} \tag{5.42}$$

where, at the right-hand side, the first term is the desired output, the second term represents the self-interference, while the last term is the ISI.

The decision variable of (5.42) shows that in frequency-selective fading channels, the multicarrier-based transmission is capable of significantly suppressing the ISI, provided that the multicarrier systems are designed satisfying $L \leq M$. Due to the delay spread of the frequency-selective fading channels, however, the IDFT–DFT operation introduces self-interference. In Section 5.3 we will show that the self-interference and ISI can cancel each other out, when the transmitted signals are carefully arranged. It can be shown that (5.42) will play an important role for us to gain insight into the design of the multicarrier schemes, so that the self-interference and ISI are fully removed.

5.3 Intersymbol Interference Suppression: Cyclic-Prefixing and Zero-Padding

ISI mitigation has been widely studied in the literature in the context of the OFDM or the frequency-domain spread MC-CDMA scheme [27, 29, 90, 132–142]. Main techniques include cyclic-prefixing (CP) and zero-padding (ZP) [30, 71, 90, 137]. In this section these two ISI mitigation techniques are investigated in the context of the generalized multicarrier scheme. It can be shown that the CP and ZP techniques might not be efficient for some multicarrier schemes.

As shown in (5.42) the self-interference and ISI are highly similar in structure. Hence, it is attractive to design the transmitted signals so that the self-interference and ISI can cancel out each other. To achieve this objective, let us assume that the channel is a frequency-selective slow fading channel whose gains maintain constants over at least two adjacent DFT symbols. In this case,

$$\bar{H}_{km}(v-1) = \bar{H}_{km}(v) \quad (5.43)$$

Thus, (5.42) can be expressed as

$$\begin{aligned} z_k[v] &= H_k(v)x_k[v] \\ &- \frac{1}{\sqrt{M}} \sum_{i=0}^{M-1} \sum_{m=1}^{L-1} \bar{H}_{km}(v) \exp\left(j \frac{2\pi i(M-L+m)}{M}\right) x_i[v] \\ &+ \frac{1}{\sqrt{M}} \sum_{i=0}^{M-1} \sum_{m=1}^{L-1} \bar{H}_{km}(v) \exp\left(j \frac{2\pi i(M-L+m)}{M}\right) x_i[v-1] \\ k &= 0, 1, \dots, M-1 \end{aligned} \quad (5.44)$$

According to (5.27)–(5.33), the above equation can be written as

$$\begin{aligned} z_k[v] &= H_k(v)x_k[v] - \mathcal{F}_k^T \bar{\mathbf{H}}_v s[v] + \mathcal{F}_k^T \bar{\mathbf{H}}_v s[v-1] \\ &= H_k(v)x_k[v] - \mathcal{F}_k^T \bar{\mathbf{H}}_v (s[v] - s[v-1]), \quad k = 0, 1, \dots, M-1 \end{aligned} \quad (5.45)$$

which shows that the self-interference and ISI can cancel out each other, if the multicarrier signal can be designed such that $\bar{\mathbf{H}}_v(s[v] - s[v-1]) = \mathbf{0}$. Observe that $\bar{\mathbf{H}}_v$ has only $(L-1)$ nonzero columns, which constitute the last $(L-1)$ columns of $\bar{\mathbf{H}}_v$, $\bar{\mathbf{H}}_v(s[v] - s[v-1])$ is a

zero vector, if the last $(L - 1)$ entries of $s[v]$ and $s[v - 1]$ are the same. Therefore, in order that the self-interference and ISI seen in (5.44) cancel out each other, the last $(L - 1)$ entries of $s[v]$ and $s[v - 1]$ should be the same, which can be achieved with the aid of the CP and ZP techniques to be analysed in detail below.

Let $z[v] = [z_0[v], z_1[v], \dots, z_{M-1}[v]]^T$. Then, after removing the self-interference and ISI, $z[v]$ can be expressed as

$$z[v] = \mathbf{H}[v]\mathbf{x}[v] \quad (5.46)$$

where

$$\mathbf{H}[v] = \text{diag}\{H_0(v), H_1(v), \dots, H_{M-1}(v)\} \quad (5.47)$$

Furthermore, according to our analysis in Section 5.2, it can be shown that $\mathbf{H}[v]$ can be expressed as

$$\mathbf{H}[v] = \mathcal{F}\check{\mathbf{H}}_v\mathcal{F}^H \quad (5.48)$$

where $\check{\mathbf{H}}_v$ is a $(M \times M)$ circulant matrix given by

$$\check{\mathbf{H}}_v = \begin{bmatrix} h_0 & 0 & \cdots & 0 & h_{L-1} & h_{L-2} & \cdots & h_2 & h_1 \\ h_1 & h_0 & \cdots & 0 & 0 & h_{L-1} & \cdots & h_3 & h_2 \\ \vdots & \vdots & \ddots & \vdots & \vdots & \vdots & \ddots & \vdots & \vdots \\ h_{L-3} & h_{L-4} & \cdots & h_0 & 0 & 0 & \cdots & h_{L-1} & h_{L-2} \\ h_{L-2} & h_{L-3} & \cdots & h_1 & h_0 & 0 & \cdots & 0 & h_{L-1} \\ h_{L-1} & h_{L-2} & \cdots & h_2 & h_1 & h_0 & \cdots & 0 & 0 \\ 0 & h_{L-1} & \cdots & h_3 & h_2 & h_1 & \cdots & 0 & 0 \\ \vdots & \vdots & \ddots & \vdots & \vdots & \vdots & \ddots & \vdots & \vdots \\ 0 & 0 & \cdots & h_{L-1} & h_{L-2} & h_{L-3} & \cdots & h_1 & h_0 \end{bmatrix} \quad (5.49)$$

It can be easily shown that

$$\check{\mathbf{H}}_v = \mathbf{H}_v + \bar{\mathbf{H}}_v \quad (5.50)$$

The CP technique can be understood by referring to Fig. 5.2. When the CP is employed, after the IDFT processing and P/S conversion at the transmitter, instead of transmitting M number of samples as shown in Fig. 5.1, $M + P_f$ number of samples are transmitted, where $P_f \geq L$ is the length of the added CP. As shown in Fig. 5.2, let

$$s[v] = [s_0[v], s_1[v], \dots, s_{M-1}[v]]^T, \quad v = 1, 2, \dots \quad (5.51)$$

the P_f -length prefix for the v th DFT symbol is given by

$$s_P[v] = [s_{M-P_f}[v], s_{M-P_f+1}[v], \dots, s_{M-1}[v]]^T, \quad v = 1, 2, \dots \quad (5.52)$$

At the receiver side, after the receiver obtains $M + P_f$ samples in the context of $s[v]$ and $s_P[v]$, the first P_f samples are discarded. In this case, by referring to (5.27), it can be shown that the M number of observation samples for recovering $\mathbf{x}[v] = [x_0[v], x_1[v], \dots, x_{M-1}[v]]^T$ are given by

$$\begin{aligned} \mathbf{y}[v] &= \bar{\mathbf{H}}_{v-1}s'[v-1] + \mathbf{H}_v s[v] \\ &= (\bar{\mathbf{H}}_{v-1} + \mathbf{H}_v)s[v] \\ &= \check{\mathbf{H}}[v]s[v], \quad v = 1, 2, \dots \end{aligned} \quad (5.53)$$

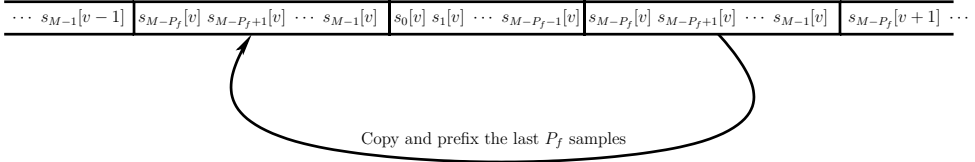


Figure 5.2: Illustration of cyclic prefixing (CP).

provided that $\tilde{\mathbf{H}}_{v-1} = \tilde{\mathbf{H}}_v$. Note that in (5.53) the second equality is because $s'[v-1]$ is in fact constituted by $s_P[v]$ prefixed with some zeros.

Based on (5.53) and according to our previous analysis ((5.46)–(5.50)), the ISI can be fully removed and the entries of $\mathbf{x}[v]$ are free of interference.

The principles of using ZP can be understood with the aid of Fig. 5.3. Here, following the transmission of the M number of desired samples, the transmitter stops transmission for a duration corresponding to P_f samples. In this case, the $M + P_f$ observation samples related to $s[v]$ can be expressed as

$$\mathbf{y}_P[v] = \begin{bmatrix} h_0 & & & & & \\ h_1 & h_0 & & & & \\ \vdots & \vdots & \ddots & & & \\ h_{L-1} & h_{L-2} & \cdots & h_0 & & \\ \vdots & \vdots & \dots & \vdots & \ddots & h_0 \\ & & & & & \vdots \\ & & & & & h_{L-1} \\ & & & & & h_{L-1} \end{bmatrix}_{(M+P_f) \times M} s[v], \quad v = 1, 2, \dots \quad (5.54)$$

If we divide $\mathbf{y}_P[v]$ into two vectors as

$$\mathbf{y}_P[v] = [\mathbf{y}_1^T[v], \mathbf{y}_2^T[v]]^T \quad (5.55)$$

where $\mathbf{y}_1[v]$ contains the first M entries of $\mathbf{y}_P[v]$, while $\mathbf{y}_2[v]$ contains the remaining P_f entries of $\mathbf{y}_P[v]$. Furthermore, let us extend $\mathbf{y}_2[v]$ to an M -length vector $\tilde{\mathbf{y}}_2[v]$ structured as

$$\tilde{\mathbf{y}}_2[v] = [\mathbf{y}_2^T[v], \mathbf{0}^T]^T \quad (5.56)$$

Then, it can be shown that

$$\begin{aligned} \mathbf{y}_1[v] &= \mathbf{H}_v s[v] \\ \tilde{\mathbf{y}}_2[v] &= \tilde{\mathbf{H}}_v s[v] \end{aligned} \quad (5.57)$$

Consequently, let us form $\mathbf{y}[v]$ as

$$\mathbf{y}[v] = \mathbf{y}_1[v] + \tilde{\mathbf{y}}_2[v] \quad (5.58)$$

$s_0[v]$	$s_1[v]$	\cdots	$s_{M-1}[v]$	$0 \ 0 \ \cdots \ 0$
P_f zeros				

Figure 5.3: Illustration of zero-padding (ZP).

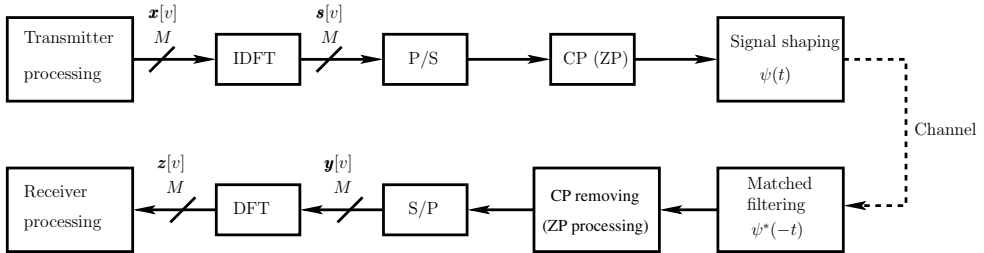


Figure 5.4: Schematic block diagram of the transmitter/receiver for multicarrier systems using IDFT/DFT assisted modulation/demodulation and cyclic-prefixing (CP) or zero-padding (ZP).

showing that

$$\begin{aligned} \mathbf{y}[v] &= (\bar{\mathbf{H}}_v + \mathbf{H}_v)\mathbf{s}[v] \\ &= \check{\mathbf{H}}[v]\mathbf{s}[v], \quad v = 1, 2, \dots \end{aligned} \quad (5.59)$$

Thus, after applying the DFT on $\mathbf{y}[v]$, both the self-interference and ISI can be fully removed.

Finally, the transmitter/receiver structure for multicarrier systems using IDFT/DFT assisted multicarrier modulation/demodulation and CP (or ZP) is shown in Fig. 5.4.

The CP or ZP technique demands more transmission bandwidth or transmission time. When the frequency selectivity of the fading channels is low, the extra bandwidth or time required by the CP or ZP is usually ignorable. This is often the case in OFDM and MC-CDMA systems. However, for MC DS-CDMA systems, especially when high chip-rate T-domain spreading is used, the employment of CP or ZP may waste much useful bandwidth or transmission time. This is because, in MC DS-CDMA systems, the IDFT/DFT has to be carried out within a chip duration, which is usually low. Fortunately, in MC DS-CDMA systems using high chip-rate T-domain spreading, a low number of subcarriers is usually available. When this is the case, other non-IDFT/DFT-based techniques may be used for implementing the multicarrier modulation/demodulation. In this case, powerful equalization at the receiver is usually required to mitigate the effect from possible interfering signals.

Note that, as our analysis in Section 5.2 shows, the κ value corresponding to the multitone DS-CDMA is $1/M$, which is significantly lower than one. Thus, no matter what we do, $L > M$ and the ISI cannot be suppressed by using CP or ZP. Hence, the IDFT/DFT-based techniques are not suitable for multicarrier modulation/demodulation in the multitone DS-CDMA. Note, furthermore, that, according to the analysis in Section 5.2 as well as that in this section, it can be implied that the ISI can be suppressed by using CP or ZP, provided that $L \leq M$.

5.4 Generation of Fading Statistics for Multicarrier Signals

This section introduces an approach for generating the fading statistics for multicarrier CDMA systems. This approach may be invoked when studying the performance of various multicarrier schemes by Monte Carlo simulation. Similar approaches can also be found in [143, 144].

The statistics generation is inspired by (5.41). Let

$$\mathbf{H}[v] = [H_0[v], H_1[v], \dots, H_{M-1}[v]]^T \quad (5.60)$$

contain the M number of channel gains of the M subcarriers. From (5.41) it can be readily shown that

$$\mathbf{H}[v] = \sqrt{M} \mathcal{F} \mathbf{h}[v], \quad v = 1, 2, \dots \quad (5.61)$$

where

$$\mathbf{h}[v] = [h_0[v], h_1[v], \dots, h_{L-1}[v], \underbrace{0, \dots, 0}_{M-L}]^T \quad (5.62)$$

represents the CIR with respect to the v th DFT symbol. Note that, in the CIR of $\mathbf{h}[v]$ it is usually assumed that

$$\sum_{l=0}^{L-1} E[|h_l|^2] = 1 \quad (5.63)$$

explaining that the transmitted power is distributed across the L number of resolvable multipath components.

If we assume that $\mathbf{h}[i]$ represents the CIR associated with the i th DFT symbol, and furthermore, we assume that $h_l[i]$ is a complex Gaussian process with the correlation function of [94]

$$E[h_l[i]h_v^*[j]] = \begin{cases} |h_l|^2 J_0(2\pi f_D(j-i)T), & \text{if } l = v \\ 0, & \text{otherwise} \end{cases} \quad (5.64)$$

where f_D denotes the maximum Doppler frequency shift. Then, the correlation between $H_k[i]$ and $H_k[i+n]$ can be expressed as

$$\begin{aligned} E[H_k[i]H_k^*[i+n]] &= \sum_{l=0}^{L-1} \sum_{v=0}^{L-1} E[h_l[i]h_v^*[i+n]] \exp\left(-j\frac{2\pi lk}{M}\right) \exp\left(j\frac{2\pi vk}{M}\right) \\ &= J_0(2\pi f_D n T) \sum_{l=0}^{L-1} |h_l|^2 \end{aligned} \quad (5.65)$$

This result implies that the fading experienced by the k th, $k = 0, 1, \dots, M-1$, subcarrier signal is flat fading.

Note that the above results have been derived when assuming that the number of resolvable paths is lower than the number of subcarriers of a multicarrier system, i.e. when $L \leq M$. Readers interested in the case of $L > M$ can also study the fading properties in the same way. In this case, we find that each subcarrier signal will experience frequency-selective fading.

We now investigate the BER performance of the OFDM communication scheme when communicating over frequency-selective Nakagami- m fading channels.

5.5 Performance of Orthogonal Frequency-Division Multiplexing

Let us consider the complex baseband equivalent OFDM signals. When communicating over frequency-selective Nakagami- m fading channels, then according to (5.53), the received observations can be expressed as

$$\mathbf{r} = \check{\mathbf{H}}\mathcal{F}^H\mathbf{x} + \mathbf{n} \quad (5.66)$$

after removing the CP or after the ZP processing. In (5.66) \mathbf{n} is an AWGN vector, the entries of which obey the Gaussian PDF with zero mean and a variance of $N_0/2E_\psi$ per dimension. Furthermore, in (5.66) $\check{\mathbf{H}}$ is given by (5.49).

Applying the DFT on \mathbf{r} , according to (5.46)–(5.48), we have

$$\begin{aligned} \mathbf{y} &= \mathcal{F}\mathbf{r} = \mathcal{F}\check{\mathbf{H}}\mathcal{F}^H\mathbf{x} + \mathcal{F}\mathbf{n} \\ &= \mathbf{H}\mathbf{x} + \mathcal{F}\mathbf{n} \end{aligned} \quad (5.67)$$

where $\mathbf{H} = \text{diag}\{H_0, H_1, \dots, H_{M-1}\}$. Finally, multiplying both sides of (5.67) by \mathbf{H}^H , we obtain the decision variable

$$\mathbf{z} = \mathbf{H}^2\mathbf{x} + \mathbf{n}' \quad (5.68)$$

where $\mathbf{n}' = \mathbf{H}^H\mathcal{F}^H\mathbf{n}$, which is an M -length Gaussian vector having zero mean and a covariance matrix given as $N_0/E_\psi \times \mathbf{H}^2$. Explicitly, the decision variable for x_m is

$$z_m = |H_m|^2 x_m + n'_m, \quad m = 0, 1, \dots, M-1 \quad (5.69)$$

where n'_m is Gaussian with zero mean and a variance of $|H_m|^2 N_0/2E_\psi$ per dimension.

Let us assume that $x_m = a_m + j b_m$, where $a_m, b_m \in \{+1, -1\}$ with equal probability. In this case, we have $E_\psi = E_b$. Then, the BER conditioned on H_m is given by

$$P_b(\gamma) = Q(\sqrt{2\gamma}) \quad (5.70)$$

where

$$\gamma = \frac{|H_m|^2}{\Omega} \gamma_c \quad (5.71)$$

and $\gamma_c = \Omega E_b / N_0$ and $\Omega = E[|H_m|^2]$.

When communicating over Nakagami- m fading channels, $|H_m|^2$ obeys the gamma distribution with the PDF given by (5.2). It can be shown that γ of (5.71) also obeys the gamma distribution, which has the PDF

$$f(\gamma) = \frac{1}{\Gamma(m)} \left(\frac{m}{\gamma_c} \right)^m \gamma^{m-1} \exp\left(-\frac{m\gamma}{\gamma_c}\right), \quad \gamma \geq 0 \quad (5.72)$$

The average bit-error rate (BER) can be obtained by integrating (5.70) with respect to γ from 0 to ∞ , yielding

$$P_b = \int_0^\infty Q(\sqrt{2\gamma}) f(\gamma) d\gamma \quad (5.73)$$

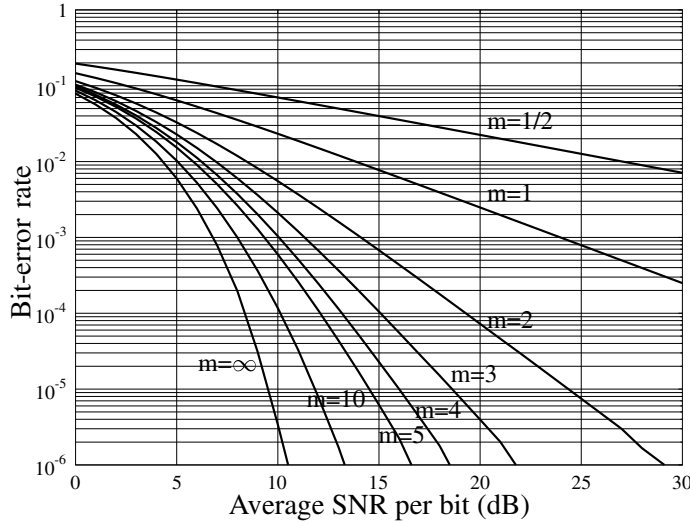


Figure 5.5: BER versus average SNR per bit performance for the OFDM scheme communicating over Nakagami- m fading channels associated with various m values.

After substituting (5.72) into (5.73), as shown in Appendix 5.A, we have

$$P_b = \frac{\Gamma(m + 1/2)}{2\sqrt{\pi}\Gamma(m + 1)} \sqrt{\frac{\gamma_c}{m + \gamma_c}} \left(\frac{m}{m + \gamma_c} \right)^m \times {}_2F_1\left(1, m + \frac{1}{2}; m + 1; \frac{m}{m + \gamma_c}\right) \quad (5.74)$$

where ${}_2F_1(a, b; c; z)$ is the hypergeometric function defined as [115] ${}_2F_1(a, b; c; z) = \sum_{k=0}^{\infty} \frac{(a)_k (b)_k z^k}{(c)_k k!}$ and $(a)_k = a(a+1)\cdots(a+k-1)$, $(a)_0 = 1$.

When communicating over Rayleigh fading channels associated with $m = 1$, as shown in Appendix 5.A, the average BER is then given by

$$P_b = \frac{1}{2} \left(1 - \sqrt{\frac{\gamma_c}{1 + \gamma_c}} \right) \quad (5.75)$$

Figure 5.5 shows the BER versus the average SNR per bit performance of the OFDM scheme, when communicating over Nakagami- m fading channels associated with various fading parameter values. Explicitly, when the m value increases, i.e. when the channel condition improves, the BER performance improves. When $m = 0.5$, which corresponds to the worst fading channel, the corresponding BER is the worst among the given results. By contrast, when $m \rightarrow \infty$, which corresponds with the AWGN channels, the OFDM system achieves its best BER performance.

5.6 Performance of Single-User Frequency-Domain Spread Multicarrier CDMA

From hereon, our analysis will ignore the IDFT/DFT operation and will be carried out directly for the sake of simplicity. Furthermore, the lower-case variables $\{h_i\}$ are used to represent the fading channel gains of the subcarriers. Note that, in the previous sections the fading channel gains of the subcarriers were represented by $\{H_i\}$. Therefore, $\{h_i\}$ in the following sections are actually the $\{H_i\}$ of the previous sections.

5.6.1 Representation of the Received Signals

When the MC-CDMA signal in the form of (3.32) is transmitted over frequency-selective Nakagami- m fading channels, the received complex baseband equivalent signal can be expressed as

$$R(t) = \sqrt{\frac{2P}{N_p}} \sum_{i=1}^q \sum_{j=1}^{N_p} h_{ij}^{(k)} b_i^{(k)}(t) c_k[j-1] \exp(j2\pi f_{ij} t + \varphi_{ij}^{(k)}) + n(t) \quad (5.76)$$

where $n(t)$ represents a complex Gaussian process, which has zero mean and a single-sided PSD of N_0 per dimension.

Similarly to (4.25), let

$$y_\lambda = (\sqrt{2P}T_s)^{-1} \int_0^{T_s} R(t) \exp(-j2\pi f_\lambda t + \varphi_\lambda^{(k)}) dt \quad (5.77)$$

be an observation sample. Then, when $\lambda = (i-1) + (j-1)q$, we have

$$y_{ij} = \frac{1}{\sqrt{N_p}} h_{ij} b_i^{(k)}[0] c_k[j-1] + n_{ij}, \quad i = 1, 2, \dots, q; \quad j = 1, 2, \dots, N_p \quad (5.78)$$

Let us define the vectors as in (4.28). Then, it can be shown that we have

$$\mathbf{y} = \mathbf{C}_k \mathbf{H}_k \mathbf{b}_k + \mathbf{n} \quad (5.79)$$

where \mathbf{C}_k is a $(qN_p \times qN_p)$ spreading matrix, which is now defined as

$$\mathbf{C}_k = \frac{1}{\sqrt{N_p}} \begin{bmatrix} \text{diag}\{\mathbf{c}_k\} & \mathbf{0} & \dots & \mathbf{0} \\ \mathbf{0} & \text{diag}\{\mathbf{c}_k\} & \dots & \mathbf{0} \\ \vdots & \vdots & \ddots & \vdots \\ \mathbf{0} & \mathbf{0} & \dots & \text{diag}\{\mathbf{c}_k\} \end{bmatrix} \quad (5.80)$$

where $\text{diag}\{\mathbf{c}_k\}$ is a diagonal matrix made up of the elements of \mathbf{c}_k , which is the spreading code assigned to the k th user. Furthermore, in (5.79), \mathbf{H}_k is the $(qN_p \times q)$ channel matrix given by

$$\mathbf{H}_k = \begin{bmatrix} \mathbf{h}_1 & \mathbf{0} & \dots & \mathbf{0} \\ \mathbf{0} & \mathbf{h}_2 & \dots & \mathbf{0} \\ \vdots & \vdots & \ddots & \vdots \\ \mathbf{0} & \mathbf{0} & \dots & \mathbf{h}_q \end{bmatrix} \quad (5.81)$$

where

$$\mathbf{h}_i = [h_{i1}, h_{i2}, \dots, h_{iN_p}]^T \quad (5.82)$$

5.6.2 MRC-Assisted Detection and Performance Analysis

When the maximal ratio combining (MRC) [2] scheme is considered, the decision variable for \mathbf{b}_k can be expressed as

$$\begin{aligned} z &= \Re\{(\mathbf{C}_k \mathbf{H}_k)^H \mathbf{y}\} \\ &= \Re\{\mathbf{H}_k^H \mathbf{C}_k^T \mathbf{C}_k \mathbf{H}_k \mathbf{b}_k + \mathbf{H}_k^H \mathbf{C}_k^T \mathbf{n}\} \\ &= \Re\left\{\frac{1}{N_p} \mathbf{H}_k^H \mathbf{H}_k \mathbf{b}_k + \mathbf{H}_k^H \mathbf{C}_k^T \mathbf{n}\right\} \end{aligned} \quad (5.83)$$

Substituting (5.81) into (5.83), explicitly, we have

$$z_i = \left(\frac{1}{N_p} \sum_{j=1}^{N_p} |h_{ij}|^2 \right) b_i^{(k)}[0] + \Re\{n_i\}, \quad i = 1, 2, \dots, q \quad (5.84)$$

where n_i is the i th element of $\mathbf{H}_k^H \mathbf{C}_k^T \mathbf{n}$, which has zero mean and a variance of $(N_0/2E_b) \sum_{j=1}^{N_p} |h_{ij}|^2 / N_p$ per dimension. Below, we derive the average BER expression.

Based on the above analysis, when conditioned on a set of channel fading amplitudes, the BER of the F-domain spread MC-CDMA can be expressed as

$$P_b(\gamma) = Q(\sqrt{2\gamma}) \quad (5.85)$$

where, since all the q bits have the same property, the index i is ignored. In (5.85)

$$\gamma = \sum_{j=1}^{N_p} \gamma_j \quad (5.86)$$

$$\gamma_j = \gamma_c \frac{|h_{ij}|^2}{\Omega} \quad (5.87)$$

$$\gamma_c = \frac{\Omega E_b}{N_p N_0} \quad (5.88)$$

When the Nakagami- m fading channel is considered, it can be shown that γ_j obeys the gamma distribution, which has the PDF of

$$f(\gamma_j) = \frac{1}{\Gamma(m)} \left(\frac{m}{\gamma_c} \right)^m \gamma_j^{m-1} \exp\left(-\frac{m\gamma_j}{\gamma_c}\right), \quad \gamma_j \geq 0 \quad (5.89)$$

When the instantaneous SNR is the sum of several component SNRs, such as the γ in (5.86), it is convenient to use the alternative form of the Q -function [109], which is defined as

$$Q(x) = \frac{1}{\pi} \int_0^{\pi/2} \exp\left(-\frac{x^2}{2 \sin^2 \theta}\right) d\theta, \quad x \geq 0 \quad (5.90)$$

This representation has the advantage of having finite integration limits that are independent of the argument x and hence allows us to obtain a convenient analytical expression for the average BER of the case, where the instantaneous SNR is the sum of several component SNRs, which may not be identically distributed [107, 109, 124].

When using (5.86) and (5.90) in (5.85), the conditional BER of (5.85) can be expressed as

$$P_b(\gamma) = \frac{1}{\pi} \int_0^{\pi/2} \exp\left(-\sum_{j=1}^{N_p} \frac{\gamma_j}{\sin^2 \theta}\right) d\theta \quad (5.91)$$

Since $\{\gamma_j\}$ are correlated random variables with respect to j , the average BER of the F-domain spread MC-CDMA should hence be evaluated in the context of the joint PDF of $\{\gamma_j\}$. Let $f(\gamma_1, \gamma_2, \dots, \gamma_{N_p})$ be the joint PDF. Then, the average BER of the F-domain spread MC-CDMA can be expressed as

$$\begin{aligned} P_b &= \underbrace{\int_0^\infty \cdots \int_0^\infty}_{N_p\text{-fold}} Q\left(\sqrt{2 \sum_{j=1}^{N_p} \gamma_j}\right) f(\gamma_1, \dots, \gamma_{N_p}) d\gamma_1, \dots, d\gamma_{N_p} \\ &= \underbrace{\int_0^\infty \cdots \int_0^\infty}_{N_p\text{-fold}} \frac{1}{\pi} \int_0^{\pi/2} \exp\left(-\sum_{j=1}^{N_p} \frac{\gamma_j}{\sin^2 \theta}\right) d\theta f(\gamma_1, \dots, \gamma_{N_p}) d\gamma_1, \dots, d\gamma_{N_p} \\ &= \frac{1}{\pi} \int_0^{\pi/2} \left[\underbrace{\int_0^\infty \cdots \int_0^\infty}_{N_p\text{-fold}} \exp\left(-\sum_{j=1}^{N_p} \frac{\gamma_j}{\sin^2 \theta}\right) f(\gamma_1, \dots, \gamma_{N_p}) d\gamma_1, \dots, d\gamma_{N_p} \right] d\theta \\ &= \frac{1}{\pi} \int_0^{\pi/2} E\left[\exp\left(-\sum_{j=1}^{N_p} \frac{\gamma_j}{\sin^2 \theta}\right)\right] d\theta \end{aligned} \quad (5.92)$$

where $E[\exp(-\sum_{j=1}^{N_p} (\gamma_j / \sin^2 \theta))]$ represents the expectation operation with respect to $\exp(-\sum_{j=1}^{N_p} (\gamma_j / \sin^2 \theta))$, which, according to Appendix 5.B, can be derived as

$$E\left[\exp\left(-\sum_{j=1}^{N_p} \frac{\gamma_j}{\sin^2 \theta}\right)\right] = \det\left(\mathbf{I} + \frac{\gamma_c}{m \sin^2 \theta} \mathbf{M}\right)^{-m} \quad (5.93)$$

where $\det(\mathbf{A})$ denotes the determinant of the square matrix \mathbf{A} , \mathbf{M} is the $(N_p \times N_p)$ covariance matrix of the ‘accompanying’ Gaussian distribution, which can be expressed as [145]

$$\mathbf{M} = \begin{bmatrix} 1 & \sqrt{\rho_{12}} & \cdots & \sqrt{\rho_{1N_p}} \\ \sqrt{\rho_{21}} & 1 & \cdots & \sqrt{\rho_{2N_p}} \\ \vdots & \vdots & \ddots & \vdots \\ \sqrt{\rho_{N_p 1}} & \sqrt{\rho_{N_p 2}} & \cdots & 1 \end{bmatrix} \quad (5.94)$$

where ρ_{ij} represents the correlation coefficient between $|h_i|^2$ and $|h_j|^2$. Hence, ρ_{ij} is given by (5.5) when the excess delay spread obeys the exponential distribution, while given by (5.8)

when the excess delay spread obeys the uniform distribution. Explicitly, we have $\rho_{ij} = \rho_{ji}$. Consequently, \mathbf{M} in (5.94) is a symmetric matrix.

Substituting (5.93) into (5.92), finally, the average BER of the single-user F-domain spread MC-CDMA can be expressed as

$$P_b = \frac{1}{\pi} \int_0^{\pi/2} \det\left(\mathbf{I} + \frac{\gamma_c}{m \sin^2 \theta} \mathbf{M}\right)^{-m} d\theta \quad (5.95)$$

Furthermore, let $\{\lambda_j\}$ be the eigenvalues of \mathbf{M} . Then, the average BER of (5.95) can be expressed alternatively as

$$\begin{aligned} P_b &= \frac{1}{\pi} \int_0^{\pi/2} \prod_{j=1}^{N_p} \left(1 + \frac{\lambda_j \gamma_c}{m \sin^2 \theta}\right)^{-m} d\theta \\ &= \frac{1}{\pi} \int_0^{\pi/2} \prod_{j=1}^{N_p} \left(\frac{m \sin^2 \theta}{\lambda_j \gamma_c + m \sin^2 \theta}\right)^m d\theta \end{aligned} \quad (5.96)$$

which shows that, once we have known the covariance matrix \mathbf{M} of (5.94), the average BER can be readily evaluated with the aid of (5.95).

Note that, since in (5.96) $(m \sin^2 \theta / (\lambda_j \gamma_c + m \sin^2 \theta)) \leq (m / (\lambda_j \gamma_c + m))$, it can be readily shown that the BER upper bound is given by

$$P_b \leq \frac{1}{2} \prod_{j=1}^{N_p} \frac{m}{\lambda_j \gamma_c + m} \quad (5.97)$$

Let us now consider some special cases. First, when the channel fading is sufficiently frequency selective, resulting in $\{\gamma_j\}$ being independent random variables obeying the common PDF of (5.89), then the covariance matrix \mathbf{M} is a unity matrix. Consequently, the average BER can be expressed as

$$P_b = \frac{1}{\pi} \int_0^{\pi/2} \left(\frac{m \sin^2 \theta}{\gamma_c + m \sin^2 \theta}\right)^{mN_p} d\theta \quad (5.98)$$

which, according to [53, 107, 115], can be expressed in a closed form as

$$\begin{aligned} P_b &= \sqrt{\frac{\gamma_c}{\gamma_c + m}} \frac{(1 + \gamma_c/m)^{-mN_p} \Gamma(mN_p + 1/2)}{2\sqrt{\pi} \Gamma(mN_p + 1)} \\ &\times {}_2F_1\left(1, mN_p + \frac{1}{2}; mN_p + 1; \frac{m}{m + \gamma_c}\right) \end{aligned} \quad (5.99)$$

Equations (5.98) and (5.99) show that when the subcarriers used for conveying one bit experience independent fading, the diversity order of N_p can be achieved.

Furthermore, if mN_p is a positive integer, (5.99) can be reduced following Alouini and Goldsmith [107] to

$$P_b = \left[\frac{1 - \mu}{2}\right]^{mN_p} \sum_{k=0}^{mN_p-1} \binom{mN_p - 1 + k}{k} \left[\frac{1 + \mu}{2}\right]^k \quad (5.100)$$

where $\mu = \sqrt{\gamma_c/(\gamma_c + m)}$.

Additionally, when each subcarrier signal experiences i.i.d Rayleigh fading associated with $m = 1$, (5.100) is further reduced to

$$P_b = \left[\frac{1 - \mu}{2} \right]^{N_p} \sum_{k=0}^{N_p-1} \binom{N_p - 1 + k}{k} \left[\frac{1 + \mu}{2} \right]^k \quad (5.101)$$

with $\mu = \sqrt{\gamma_c/(\gamma_c + 1)}$.

The second case is that when the channel fading is not frequency selective yielding $\gamma_1 = \gamma_2 = \dots = \gamma_{N_p}$, the covariance matrix \mathbf{M} is then singular and has only one eigenvalue, which is $\lambda = N_p$. Consequently, the average BER of the F-domain spread MC-CDMA can be expressed as

$$P_b = \frac{1}{\pi} \int_0^{\pi/2} \left(\frac{m \sin^2 \theta}{\gamma'_c + m \sin^2 \theta} \right)^m d\theta \quad (5.102)$$

where $\gamma'_c = N_p \gamma_c = \Omega E_b / N_0$. In this case, the F-domain spread MC-CDMA is unable to achieve frequency diversity.

Note that when the subcarrier signals conveying the same data bit experience correlated fading and correspondingly the BER is in the form of (5.96), the diversity order achieved is then within the range $(1, N_p)$, where N_p corresponds to the highest diversity order of the independent case of (5.99), while one corresponds to the fully correlated case of (5.102).

5.6.3 Performance Results

Figures 5.6 and 5.7 show the average BER versus the SNR per bit performance for the F-domain spread MC-CDMA, when communicating over either frequency-selective Rayleigh (Fig. 5.6) fading channels corresponding to $m = 1$, or frequency-selective Nakagami- m (Fig. 5.7) fading channels associated with $m = 1.5$. The excess delay spread was assumed to obey either the exponential distribution of (5.3) or the uniform distribution shown in (5.6). The results in these figures were evaluated using (5.96), when assuming that the normalized delay spread took various values. The normalized delay spread for the exponentially distributed excess delay spread is $\tau_{\text{Norm}} = \bar{\tau}/T_b$, while for the uniformly distributed excess delay spread is $\tau_{\text{Norm}} = T_m/T_b$. Furthermore, the BER curves are also shown in these figures, when the subcarriers conveying the same data bit experience the same frequency nonselective fading, or experience independent fading.

From the results of Figs 5.6 and 5.7, we can observe that, even though there exists slight frequency-selective fading, the BER performance achieved by the F-domain spread MC-CDMA system may be significantly improved. For example, compared with the case of non-selective fading as seen in Figs 5.6(a), the SNR gain corresponding to $\tau_{\text{Norm}} = 0.01$ is as high as 5 dB, which is achieved when the excess delay spread is only about 1 percent of the bit duration T_b . Furthermore, when the subcarrier signals conveying the same data bit experience independent fading, by comparing with Fig. 4.2, we can see that, at the BER of 10^{-6} , the BER performance for the Rayleigh fading case is about 3 dB difference from that achieved in AWGN channels, while the BER performance

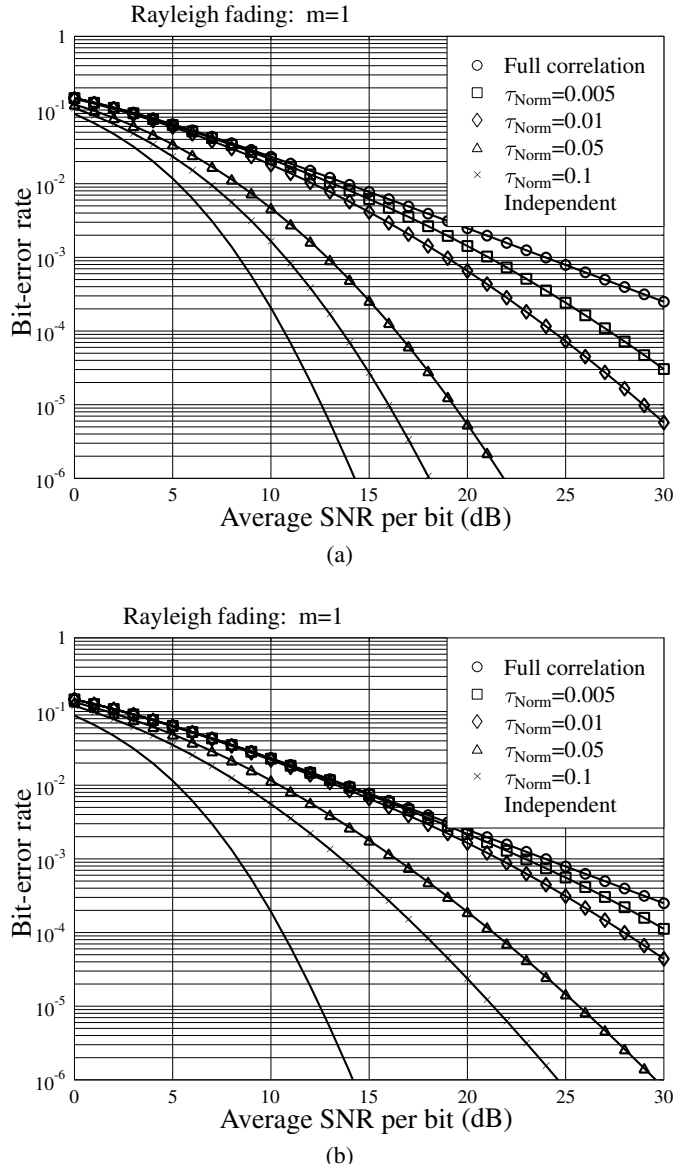


Figure 5.6: BER versus average SNR per bit performance for the F-domain spread MC-CDMA, when communicating over Rayleigh fading channels; (a) excess delay-spread obeys exponential distribution: $\tau_{\text{Norm}} = \bar{\tau} / T_b$; (b) excess delay-spread obeys uniform distribution: $\tau_{\text{Norm}} = T_m / T_b$.

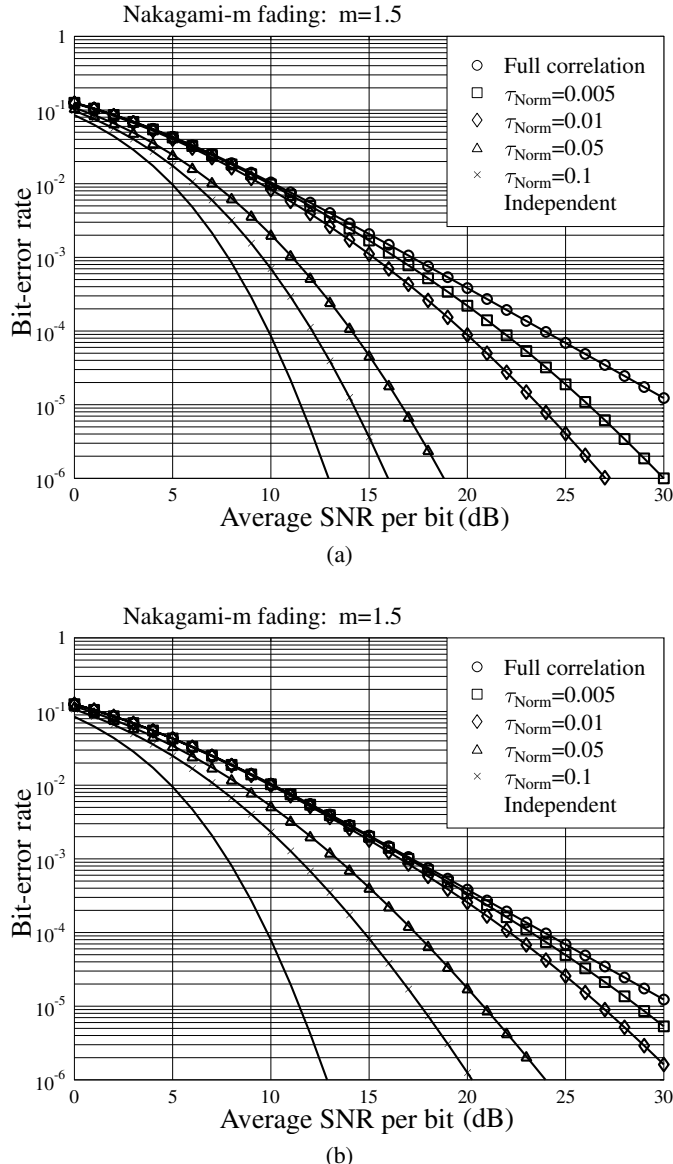


Figure 5.7: BER versus average SNR per bit performance for the F-domain spread MC-CDMA, when communicating over Nakagami- m fading channels associated with $m = 1.5$; (a) excess delay spread obeys exponential distribution: $\tau_{\text{Norm}} = \bar{\tau}/T_b$; (b) excess delay spread obeys uniform distribution: $\tau_{\text{Norm}} = T_m/T_b$.

for the Nakagami- m fading case is only about 2dB away from that achieved in AWGN channels. The reason for achieving the above BER performance is that when the subcarrier signals conveying the same data bit experience independent fading, as shown in (5.98), the diversity order equals the number of subcarriers conveying the same data bit, which is eight in these examples. Hence, it can be implied that when a higher number of subcarriers are used to transmit one data bit, a higher diversity order may be achieved if the channel is highly frequency selective. Consequently, the BER performance may be further improved and more closely approximates the BER bound achieved in AWGN channels.

Note that, as seen in Figs 5.6 and 5.7, the BER in Fig. 5.7 is lower than the corresponding BER in Fig. 5.6 for a given SNR value. This is because the channel condition considered in Fig. 5.7 is better than that considered in Fig. 5.6.

5.7 Performance of Single-Carrier Frequency-Division Multiple Access

In Section 3.4 of Chapter 3, the principles of both the IFDMA and LFDMA in the SC-FDMA schemes have been analysed in detail. In this section we consider the error performance of these two SC-FDMA schemes when considering frequency-selective Nakagami- m fading channels. The analysis is conducted using vector/matrix notations.

As in Section 3.4 of Chapter 3, we assume that the SC-FDMA uplink employs $U = MN$ subcarriers and supports $K \leq M$ users; each user transmits N data symbols within T_s seconds of the duration of a transmission block. Following Section 3.4 of Chapter 3, after the N -point DFT on \mathbf{x}_k containing the data symbols transmitted by user k , the output is

$$X_k = \mathcal{F}_N x_k, \quad k = 0, 1, \dots, K - 1 \quad (5.103)$$

As shown in Fig. 3.8 in Section 3.4 of Chapter 3, following the DFT, the N entries of X_k are mapped to N out of the U subcarriers. The mapping scheme for the IFDMA is given in (3.55), while that for the LFDMA is given in (3.56). When using vector/matrix notation, after the subcarrier mapping, the output for the k th user can be expressed as

$$\tilde{X}_k = P_k X_k, \quad k = 0, 1, \dots, K-1 \quad (5.104)$$

where \mathbf{P}_k is the k th user's subcarrier mapping matrix and it is a $(U \times N)$ -dimensional matrix. Specifically, for the IFDMA, \mathbf{P}_k is structured as: $\mathbf{P}_k(nM+k, n) = 1$ for $n = 0, 1, \dots, N-1$, the other entries of \mathbf{P}_k are zeros. For the LFDMA, $\mathbf{P}_k = [\mathbf{0}, \dots, \mathbf{0}, \mathbf{I}_N, \mathbf{0}, \dots, \mathbf{0}]^T$, where \mathbf{I}_N is located between row kN and $(k+1)N - 1$. As in the example considered in Section 3.4 of Chapter 3, the SC-FDMA has the parameters $U = 12$, $M = 3$, $N = 4$ and $k = 1$; accordingly, the subcarrier mapping matrix is

$$\mathbf{P}_k^T = \begin{bmatrix} 0 & 1 & 0 & 0 & 0 & 0 & 0 & 0 & 0 & 0 & 0 & 0 & 0 \\ 0 & 0 & 0 & 0 & 1 & 0 & 0 & 0 & 0 & 0 & 0 & 0 & 0 \\ 0 & 0 & 0 & 0 & 0 & 0 & 0 & 0 & 1 & 0 & 0 & 0 & 0 \\ 0 & 0 & 0 & 0 & 0 & 0 & 0 & 0 & 0 & 0 & 0 & 1 & 0 \end{bmatrix} \quad (5.105)$$

for the IFDMA and

$$\mathbf{P}_k^T = \begin{bmatrix} 0 & 0 & 0 & 0 & 1 & 0 & 0 & 0 & 0 & 0 & 0 \\ 0 & 0 & 0 & 0 & 0 & 1 & 0 & 0 & 0 & 0 & 0 \\ 0 & 0 & 0 & 0 & 0 & 0 & 1 & 0 & 0 & 0 & 0 \\ 0 & 0 & 0 & 0 & 0 & 0 & 0 & 1 & 0 & 0 & 0 \end{bmatrix} \quad (5.106)$$

for the LFDMA. It can be seen that for both the IFDMA and LFDMA, \mathbf{P}_k has the property

$$\mathbf{P}_k^T \mathbf{P}_l = \begin{cases} \mathbf{I}_N, & \text{for } k = l \\ \mathbf{0}, & \text{for } k \neq l \end{cases} \quad (5.107)$$

After the U -point IDFT on $\tilde{\mathbf{X}}_k$ as seen in Fig. 3.8 in Section 3.4 of Chapter 3, the output is denoted as

$$\tilde{\mathbf{x}}_k = \mathcal{F}_U^H \tilde{\mathbf{X}}_k, \quad k = 0, 1, \dots, K - 1 \quad (5.108)$$

Finally, $\tilde{\mathbf{x}}_k$ is transmitted by the k th user over the frequency-selective fading channel, which is assumed to have L number of resolvable paths, after adding the appropriate CP or appending a number of zeros, for the sake of removing the ISI at the receiver.

At the receiver side, following the principles discussed in Section 5.3, specifically according to (5.53), the received observations can be expressed as

$$\begin{aligned} \tilde{\mathbf{y}} &= \sum_{k=0}^{K-1} \check{\mathbf{H}}_k \tilde{\mathbf{x}}_k + \mathbf{n} \\ &= \sum_{k=0}^{K-1} \check{\mathbf{H}}_k \mathcal{F}_U^H \tilde{\mathbf{X}}_k + \mathbf{n} \end{aligned} \quad (5.109)$$

after removing the CP or after the ZP processing, where $\check{\mathbf{H}}_k$ is a $(U \times U)$ circulant matrix in the form of (5.49), while \mathbf{n} is a Gaussian noise vector distributed with zero mean and a covariance matrix $\sigma^2 \mathbf{I}_U$, where $\sigma^2 = 1/\text{SNR}$.

Applying the U -point DFT to $\tilde{\mathbf{y}}$ as shown in Fig. 3.11 in Section 3.4 of Chapter 3, we obtain

$$\begin{aligned} \mathbf{y} &= \sum_{k=0}^{K-1} \mathcal{F}_U \check{\mathbf{H}}_k \mathcal{F}_U^H \tilde{\mathbf{X}}_k + \tilde{\mathbf{n}} \\ &= \sum_{k=0}^{K-1} \mathbf{H}_k \mathbf{P}_k \mathbf{X}_k + \tilde{\mathbf{n}} \end{aligned} \quad (5.110)$$

where $\tilde{\mathbf{X}}_k = \mathbf{P}_k \mathbf{X}_k$ seen in (5.104) was applied with the second equality, $\tilde{\mathbf{n}} = \mathcal{F}_U \mathbf{n}$ is still Gaussian distributed with zero mean and a covariance matrix $\sigma^2 \mathbf{I}_U$ and, according to (5.48), we have

$$\begin{aligned} \mathbf{H}_k &= \text{diag}\{h_{k0}, h_{k1}, \dots, h_{k(U-1)}\} \\ &= \mathcal{F}_U \check{\mathbf{H}}_k \mathcal{F}_U^H \end{aligned} \quad (5.111)$$

Finally, the decision variables for the data symbols transmitted in \mathbf{x}_l of the l th user can be formed as

$$\begin{aligned} z_l &= \mathcal{F}_N^H \mathbf{P}_l^T \mathbf{W}_l^H \mathbf{y} \\ &= \mathcal{F}_N^H \mathbf{P}_l^T \mathbf{W}_l^H \mathbf{H}_l \mathbf{P}_l \mathbf{X}_l + \sum_{k \neq l} \mathcal{F}_N^H \mathbf{P}_l^T \mathbf{W}_l^H \mathbf{H}_k \mathbf{P}_k \mathbf{X}_k + \bar{\mathbf{n}}, \quad l = 0, 1, \dots, K-1 \end{aligned} \quad (5.112)$$

where the matrix \mathbf{W}_l is for the F-domain equalization of user l , the multiplication of \mathbf{P}_l^T implements subcarrier demapping, the multiplication of \mathcal{F}_N^H implements an N -point IDFT, $\bar{\mathbf{n}} = \mathcal{F}_N^H \mathbf{P}_l^T \mathbf{W}_l^H \tilde{\mathbf{n}}$. According to (5.111), \mathbf{H}_k is a diagonal matrix, implying that each of the U subcarriers experiences flat fading. Furthermore, according to Fig. 3.10 in Section 3.4 of Chapter 3 and (5.107) in this section, the K users are orthogonal in the F-domain. Hence, it can be shown that, provided that \mathbf{W}_l is a diagonal matrix, $\mathbf{P}_l^T \mathbf{W}_l^H \mathbf{H}_k \mathbf{P}_k = \mathbf{0}$, when $k \neq l$. In this case, remembering that $\mathbf{X}_l = \mathcal{F}_N \mathbf{x}_l$, (5.112) can be simplified to

$$z_l = \mathcal{F}_N^H \mathbf{P}_l^T \mathbf{W}_l^H \mathbf{H}_l \mathbf{P}_l \mathcal{F}_N \mathbf{x}_l + \bar{\mathbf{n}}, \quad l = 0, 1, \dots, K-1 \quad (5.113)$$

In (5.113) the matrix \mathbf{W}_l for the F-domain equalization can be chosen based on different criteria. Specifically, in the context of the matched-filtering (MF), zero-forcing (ZF) and minimum mean-square error (MMSE) principles, \mathbf{W}_l can be chosen respectively as [97, 103]

$$\text{MF : } \mathbf{W}_l = \mathbf{H}_l \quad (5.114)$$

$$\text{ZF : } \mathbf{W}_l = \left\{ \frac{1}{h_{l0}^*}, \frac{1}{h_{l1}^*}, \dots, \frac{1}{h_{l(U-1)}^*} \right\} \quad (5.115)$$

$$\text{MMSE : } \mathbf{W}_l = \left\{ \frac{h_{l0}}{|h_{l0}|^2 + \sigma^2}, \frac{h_{l1}}{|h_{l1}|^2 + \sigma^2}, \dots, \frac{h_{l(U-1)}}{|h_{l(U-1)}|^2 + \sigma^2} \right\} \quad (5.116)$$

It can be shown that, for both the MF and MMSE schemes, the data symbols within \mathbf{x}_l interfere with each other. By contrast, for the ZF scheme, applying (5.115) into (5.113), readily gives

$$z_l = \mathbf{x}_l + \bar{\mathbf{n}}, \quad l = 0, 1, \dots, K-1 \quad (5.117)$$

Explicitly, the interference among the symbols within \mathbf{x}_l is fully removed. However, we should realize that in the matrix \mathbf{W}_l for the ZF scheme, $1/h_{lu}$ might be a very high value, when the corresponding subcarrier experiences deep fading. In this case, multiplying \mathbf{W}_l with the noise sample will amplify the noise, yielding performance degradation. The characteristics of the MF-, ZF- and MMSE-based detection schemes will be studied in detail in Chapter 6 that explores multiuser detection. Below, we show some error performance results obtained by simulation.

Figures 5.8 and 5.9 depict the bit-error rate (BER) versus average SNR per bit performance of the IFDMA and LFDMA systems using the parameters $M = 8$ and $N = 8$, when communicating over frequency-selective Rayleigh ($m = 1$) or Nakagami- m ($m = 1.5$) fading channels. In both figures, three types of F-domain equalization scheme are considered that are based on the MF, ZF and MMSE principles, as shown in (5.114), (5.115) and (5.116), respectively. From the results shown in Figs 5.8 and 5.9, we observe the following. Note that when $L = 1$, the BER performance of the IFDMA or LFDMA system employing MF-, ZF- and MMSE-assisted F-domain equalization is the same, shown by curves marked with circles in Figs 5.8 and 5.9.

- From the analysis from (5.112) to (5.113), we know that both the IFDMA and LFDMA are free from MUI, provided that the matrix \mathbf{W}_l , $l = 0, 1, \dots, K - 1$, for the F-domain equalization is a diagonal matrix. However, for both the IFDMA and LFDMA, the symbols transmitted by a given user interfere with each other yielding intrauser interference, when the channel fading is frequency selective. As shown in Figs 5.8 and 5.9, when the MF-assisted F-domain equalization is used, the BER performance becomes worse, when the number of T-domain resolvable paths of the frequency-selective fading channels increases.
- Both the IFDMA and LFDMA systems may achieve certain diversity gain provided by the frequency-selective fading channels. However, the diversity gain is only achievable after the intra-user interference is efficiently mitigated. As shown in Figs 5.8 and 5.9, the diversity gain can only be noticed, when the MMSE-assisted F-domain equalization is used.
- Since in the IFDMA the subcarriers conveying the symbols of a user are separated in the F-domain by a maximum distance, while in the LFDMA a set of successive subcarriers are used for conveying the symbols of a user, the diversity gain of the IFDMA system is higher than that of the LFDMA (if there is some diversity gain observable).
- As our analysis in Section 5.5 shows, the OFDM scheme is incapable of achieving the frequency-diversity gain. Hence, in addition to being free of the PAPR problem, the SC-FDMA, especially the IFDMA, scheme also outperforms the OFDM scheme in terms of achievable BER performance, if some complexity can be invested for suppressing the intrauser interference.
- From the results shown in Figs 5.8 and 5.9, explicitly, there exists a trade-off between the diversity gain due to frequency-selective fading and the intrauser interference. Hence, better BER performance than that achieved by the MMSE equalization scheme may be obtained when the more advanced equalization scheme, such as that based on the maximum likelihood principles (see Chapter 6), is invoked.

5.8 Frequency-Domain Equalization in Single-Carrier DS-CDMA

In Section 4.7 we showed that, at the receiver, the observation signals in a (single-carrier) DS-CDMA system can be transformed to the F-domain. It can be shown that, after the transformation, a DS-CDMA scheme is in fact equivalent to a corresponding (F-domain spread) MC-CDMA scheme. Consequently, the advanced F-domain signal-processing techniques, which have conventionally been used in the MC-CDMA systems, may be implemented in the DS-CDMA systems in order to enhance their efficiency in terms of achievable error performance and/or implementational complexity. Note that when the fading channel scenarios are considered, we usually refer to the F-domain signal processing as F-domain equalization. In this section we consider in detail the principles and error performance of the DS-CDMA systems using F-domain equalization, when communicating

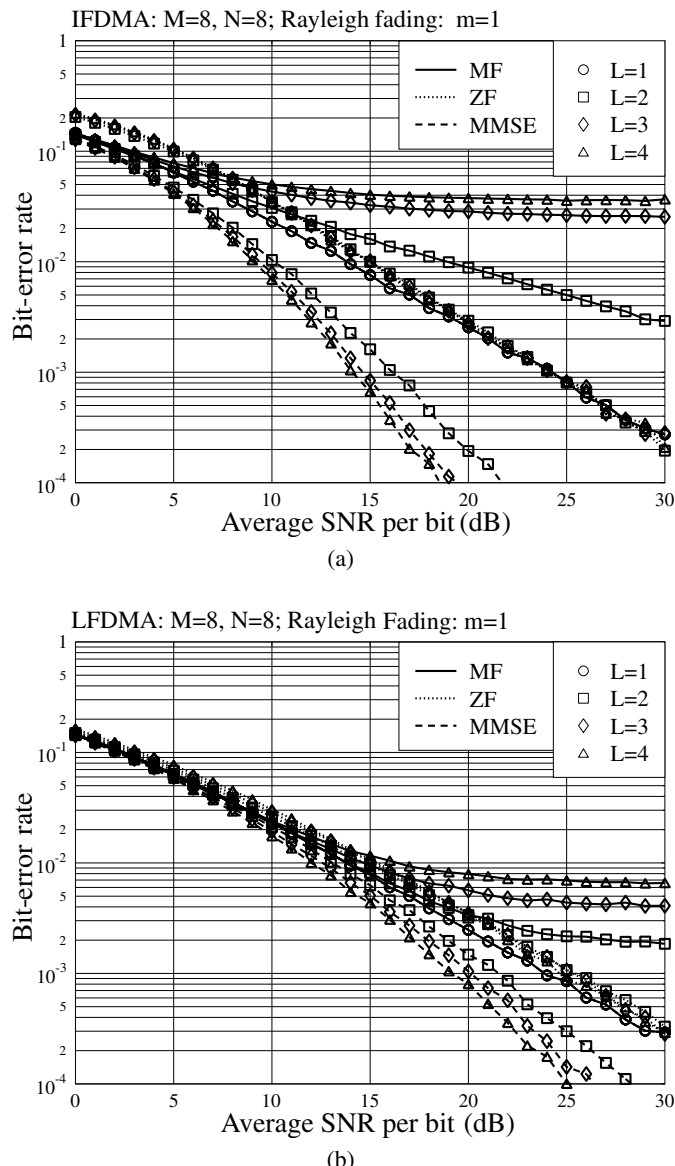


Figure 5.8: BER versus average SNR per bit performance for both the IFDMA and LFDMA systems communicating over Rayleigh fading channels; (a) IFDMA: $M = 8, N = 8$; (b) LFDMA: $M = 8, N = 8$.

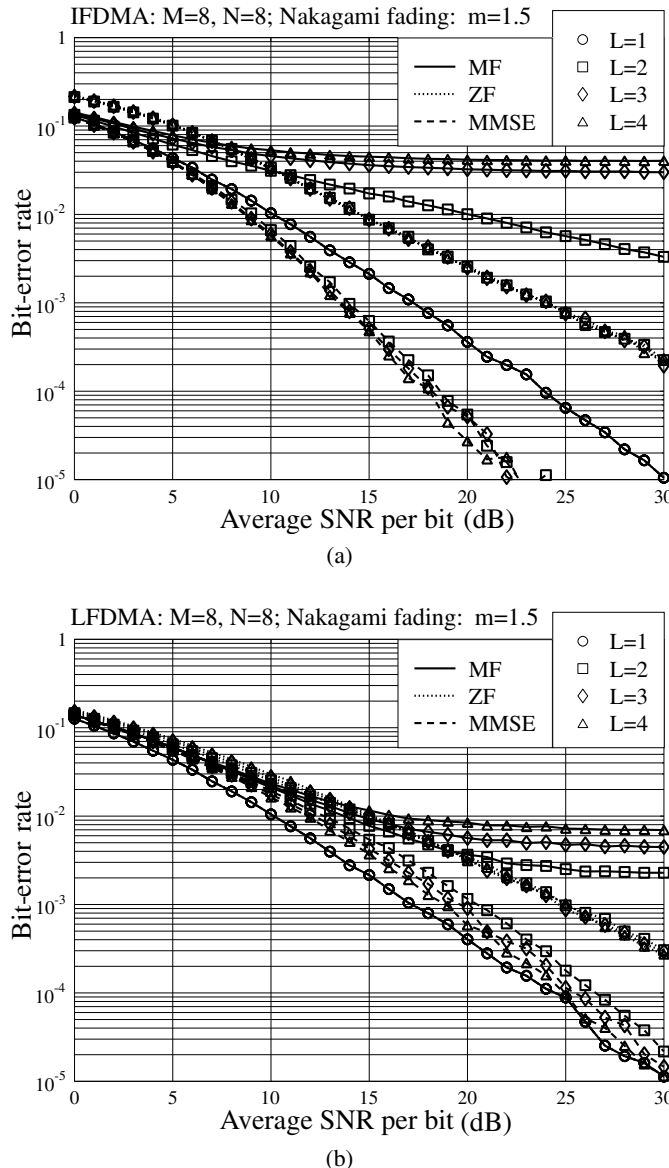


Figure 5.9: BER versus average SNR per bit performance for both the IFDMA and LFDMA systems communicating over Nakagami- m fading channels associated with $m = 1.5$; (a) IFDMA: $M = 8$, $N = 8$; (b) LFDMA: $M = 8$, $N = 8$.

over frequency-selective fading channels. F-domain equalization in DS-CDMA systems has been widely investigated in the literature as evidenced, e.g., by references [98–106].

Let us consider a DS-CDMA uplink system supporting K users. The K users transmit signals synchronously on a block-by-block basis, and each block consists of M data symbols. We assume the spreading factor of the DS-CDMA to be N . Furthermore, we assume that the user signals are transmitted associated with the CP or ZP, which is appropriately designed so that zero ISI can be achieved. Then, based on the above assumptions and the principles in Chapter 2, as well as implied by (4.213) and (4.218), the transmitted discrete spread-spectrum signal by the k th uplink user can be denoted in vector as

$$\mathbf{s}_k = \underbrace{\frac{1}{\sqrt{N}}(\mathbf{I}_M \otimes \mathbf{c}_k)}_{\mathbf{C}_k} \mathbf{b}_k, \quad k = 1, 2, \dots, K \quad (5.118)$$

where $\mathbf{s}_k = [s_{k0}, s_{k1}, \dots, s_{k(MN-1)}]^T$, $\mathbf{b}_k = [b_{k0}, b_{k1}, \dots, b_{k(M-1)}]^T$ contains the data symbols transmitted by the k th user, it is assumed that $E[|b_{km}|^2] = 1$, while $\mathbf{c}_k = [c_{k0}, c_{k1}, \dots, c_{k(N-1)}]^T$ is the spreading sequence assigned to the k th user and the element $c_{kn} \in \{+1, -1\}$. Furthermore, it can be shown that \mathbf{C}_k is a $(MN \times M)$ -dimensional matrix satisfying $\mathbf{C}_k^T \mathbf{C}_k = \mathbf{I}_M$.

Note that (5.118) only shows the part related to the useful data symbols, while the part related to the CP or ZP is ignored.

When the K signals in the form of (5.118) are transmitted independently over frequency-selective fading channels having L resolvable multipath components, the received discrete signal by the BS can then be expressed as

$$\mathbf{r} = \sum_{k=1}^K \check{\mathbf{H}}_k \mathbf{s}_k = \sum_{k=1}^K \check{\mathbf{H}}_k \mathbf{C}_k \mathbf{b}_k + \mathbf{n} \quad (5.119)$$

after removing the CP or after the ZP processing. Let $U = MN$. Then, in (5.119) $\check{\mathbf{H}}_k$ is a $(U \times U)$ circulant matrix expressed in the form of (5.49), whereas \mathbf{n} is a U -length Gaussian noise vector that obeys the multivariate Gaussian distribution with zero mean and a covariance matrix $\sigma^2 \mathbf{I}_U$, where $\sigma^2 = 1/\text{SNR}$.

Since $\check{\mathbf{H}}_k$ is a $(U \times U)$ circulant matrix, it can be decomposed into

$$\begin{aligned} \check{\mathbf{H}}_k &= \mathcal{F}_U^H \mathbf{H}_k \mathcal{F}_U \\ \mathbf{H}_k &= \text{diag}\{h_{k0}, h_{k1}, \dots, h_{k(U-1)}\} \end{aligned} \quad (5.120)$$

where \mathcal{F}_U is the U -point DFT matrix. Substituting $\check{\mathbf{H}}_k$ from (5.120) into (5.119) and then applying the DFT on \mathbf{r} , we obtain

$$\mathbf{y} = \mathcal{F}_U \mathbf{r} = \sum_{k=1}^K \mathbf{H}_k \mathcal{F}_U \mathbf{C}_k \mathbf{b}_k + \bar{\mathbf{n}} \quad (5.121)$$

where $\bar{\mathbf{n}} = \mathcal{F}_U \mathbf{n}$, which still obeys the multivariate Gaussian distribution with zero mean and a covariance matrix $\sigma^2 \mathbf{I}_U$.

It can be shown that the observation equation of (5.121) is equivalent to (5.79) for the F-domain spread MC-CDMA, when communicating over frequency-selective fading channels. In more detail, let us define

$$\begin{aligned}\mathcal{C}_k &= \mathcal{F}_U \mathbf{C}_k \\ &= [(\mathcal{C}_k^{(0)})^T, (\mathcal{C}_k^{(1)})^T, (\mathcal{C}_k^{(U-1)})^T]^T\end{aligned}\quad (5.122)$$

where $\mathcal{C}_k^{(u)}$ is the u th row of $\mathcal{F}_U \mathbf{C}_k$. Let us construct the matrices

$$\begin{aligned}\bar{\mathcal{C}}_k &= \text{diag}\{\mathcal{C}_k^{(0)}, \mathcal{C}_k^{(1)}, \dots, \mathcal{C}_k^{(U-1)}\} \\ \bar{\mathbf{H}}_k &= [h_{k0} \otimes \mathbf{I}_M, h_{k1} \otimes \mathbf{I}_M, \dots, h_{k(U-1)} \otimes \mathbf{I}_M]^T\end{aligned}\quad (5.123)$$

where $\bar{\mathcal{C}}_k$ is a $(U \times UM)$ -dimensional matrix, while $\bar{\mathbf{H}}_k$ is a $(UM \times M)$ -dimensional matrix. With the aid of the above definitions, it can be shown that (5.121) can be expressed as

$$\mathbf{y} = \sum_{k=1}^K \bar{\mathcal{C}}_k \bar{\mathbf{H}}_k \mathbf{b}_k + \bar{\mathbf{n}} \quad (5.124)$$

Explicitly, (5.124) is in the same form of (5.79) for the F-domain spread MC-CDMA. Hence, all the detection algorithms for the F-domain spread MC-CDMA can also be similarly applied to (5.124) for the single-carrier DS-CDMA.

Based on (5.121), various F-domain equalization schemes, such as those in [98–106], may be applied, in order to detect the transmitted information. Specifically, concerning the single-user detection, the decision variable vector for \mathbf{b}_k can be expressed as

$$\mathbf{z}_k = \mathbf{C}_k^T \mathcal{F}_U^H \mathbf{W}_k^H \mathbf{y}, \quad k = 1, 2, \dots, K \quad (5.125)$$

where the multiplication of \mathbf{W}_k^H , \mathcal{F}_U^H and \mathbf{C}_k^T implement, respectively, the F-domain equalization, IDFT and despreading operations. Specifically, for the MF-assisted detection schemes, \mathbf{W}_k is given by [97, 103]

$$\mathbf{W}_k = \mathbf{H}_k \quad (5.126)$$

Figure 5.10 illustrates the BER versus average SNR per bit performance of the single-carrier DS-CDMA system supporting one user, when the BPSK baseband modulation and the F-domain MF-based detection are used. Both the frequency-selective Rayleigh fading channels and the frequency-selective Nakagami- m fading channels associated with $m = 1.5$ were considered. In our simulations the random spreading sequence was assumed. Explicitly, the F-domain MF-based detection is capable of achieving the diversity provided by the frequency-selective fading channels.

When the single-carrier DS-CDMA system supports multiple users, it will then experience severe MUI, when the F-domain MF-based detection as shown in (5.125) associated with (5.126) is used. As shown in Fig. 5.11, the BER performance degrades significantly when the number of users supported increases. When the DS-CDMA system supports multiusers, advanced multiuser detection shown in Chapter 6 may be employed in order to enhance the achievable BER performance.

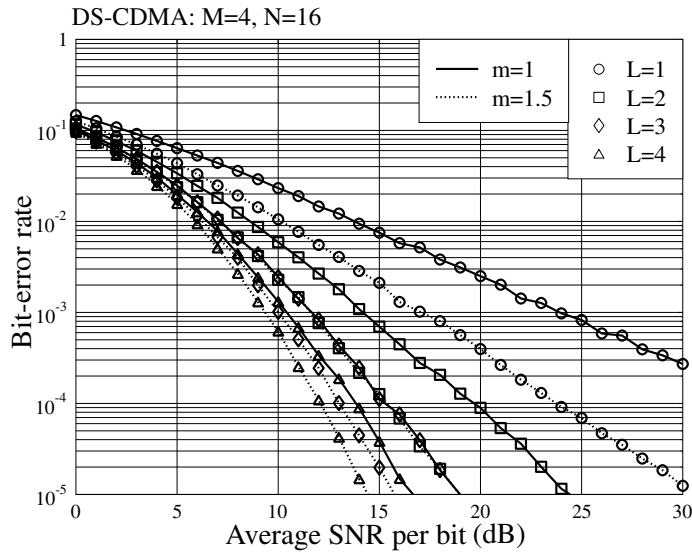


Figure 5.10: BER versus average SNR per bit performance for the single-carrier DS-CDMA systems using the F-domain MF-based detection, when communicating over Rayleigh ($m = 1$) and Nakagami- m ($m = 1.5$) fading channels.

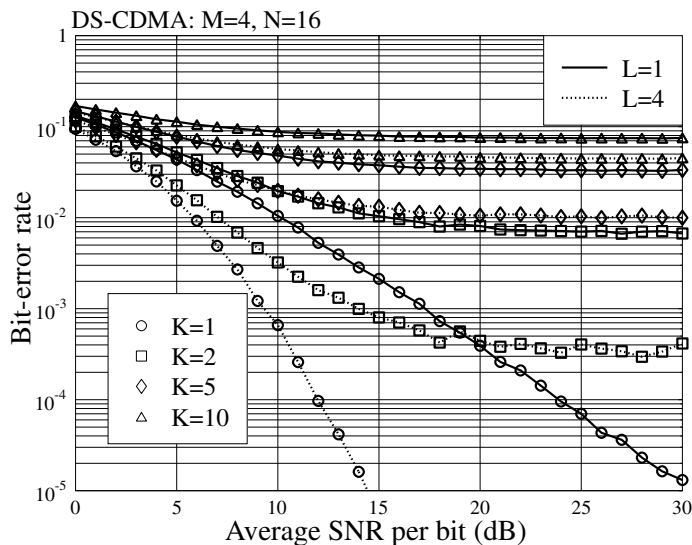


Figure 5.11: BER versus average SNR per bit performance for the single-carrier DS-CDMA systems using the F-domain MF-based detection, when communicating over Rayleigh ($m = 1$) and Nakagami- m ($m = 1.5$) fading channels.

The advantages of transforming the single-carrier DS-CDMA signals from the T-domain to the F-domain are at least twofold. First, it is beneficial to channel estimation/prediction [146]. This is because, after the single-carrier DS-CDMA signals experiencing frequency-selective fading are transformed to the multicarrier signals, each of the subcarrier signals experiences flat fading. Consequently, the subcarrier channels may be estimated/predicted more reliably with the aid of low-complexity F-domain channel estimation/prediction algorithms [147], in comparison with the single-carrier frequency-selective fading channels using T-domain channel estimation/prediction techniques. Second, after being transformed to the F-domain, a single-carrier DS-CDMA system may take advantage of the efficient F-domain signal processing at its receiver, whereas the transmitted single-carrier DS-CDMA signals suffer from no peak-to-average ratio (PAPR) problem.

5.9 Performance of Single-User Multicarrier DS-CDMA

In this section we derive the BER expression for the single-user MC DS-CDMA systems, when communicating over frequency-selective fading channels. The corresponding MC DS-CDMA system considered in the context of the AWGN channels can be found in Section 4.4 of Chapter 4.

When the k th user signal in a MC DS-CDMA system is transmitted over frequency-selective fading channels, according to Fig. 3.12 and (3.129), the received signal for the single-user case can be expressed as

$$R(t) = \sum_{i=1}^q \sum_{l=1}^p \sqrt{\frac{2P}{p}} h_{il}^{(k)} b_i^{(k)}(t) c_k(t) \exp(j2\pi f_{il} t) + n(t) \quad (5.127)$$

where $h_{il}^{(k)}$ represents the channel gain with respect to the il th subcarrier of the k th user. The details for the other terms in (5.127) can be found in association with (3.129) and (4.34). Note that, without loss of any generality, in (5.127) the initial phases of the subcarriers are absorbed into the channel gains. Furthermore, in obtaining (5.127) we used the assumption that each of the subcarrier signals experiences flat fading; even the overall MC DS-CDMA signal experiences frequency-selective fading. This assumption implies that the total bandwidth spanned by the MC DS-CDMA signal is higher than the coherence bandwidth of the corresponding wireless channel, while the bandwidth of a subcarrier signal alone is lower than the coherence bandwidth of the corresponding wireless channel. Let us first represent the received MC DS-CDMA signals in discrete forms.

5.9.1 Representation of the Received Signals

The detector considered in this section is the same as in Fig. 4.3. Hence, the n th observation with respect to the first transmitted symbol and the uv th subcarrier can be expressed as

$$y_{uv,n} = (\sqrt{2PN_e}T_c)^{-1} \int_{nT_c}^{(n+1)T_c} R(t) \exp(-j2\pi f_{uv}t) \psi^*(t) dt \\ u = 1, 2, \dots, q; v = 1, 2, \dots, p; n = 0, 1, \dots, N_e - 1 \quad (5.128)$$

where N_e represents the number of chips per symbol. Substituting (5.127) into (5.128), $y_{uv,n}$ can be expressed as

$$y_{uv,n} = \frac{c_n^{(k)}}{\sqrt{N_e p}} \sum_{i=1}^q b_i^{(k)}[0] \sum_{l=1}^p h_{il}^{(k)} \mu_{il,uv,n} + N_{uv,n} \quad (5.129)$$

where $N_{uv,n}$ represents the Gaussian noise given by

$$N_{uv,n} = (\sqrt{2PN_e T_c})^{-1} \int_{nT_c}^{(n+1)T_c} n(t) \exp(-j2\pi f_{uv}t) \psi^*(t) dt \quad (5.130)$$

which has zero mean and a variance of $N_0/2E_b$ per dimension. In (5.129)

$$\mu_{il,uv,n} = \frac{1}{T_c} \int_{nT_c}^{(n+1)T_c} \psi^2(t) \exp(j2\pi \Delta f_{il,uv} t) dt \quad (5.131)$$

where $\Delta f_{il,uv} = f_{il} - f_{uv}$. When the chip waveform $\psi(t)$ is periodic, i.e. when $\psi(nT_c + t) = \psi(t)$, we then have

$$\mu_{il,uv,n} = \hat{\mu}_{il,uv} \exp(j2\pi n \Delta f_{il,uv} T_c) \quad (5.132)$$

associated with

$$\hat{\mu}_{il,uv} = \frac{1}{T_c} \int_0^{T_c} \psi^2(t) \exp(j2\pi \Delta f_{il,uv} t) dt \quad (5.133)$$

Furthermore, it can be shown that, when $\exp(j2\pi \Delta f_{il,uv} T_c) \neq 1$, $\mu_{il,uv,n}$ in (5.132) has the property of

$$\sum_{n=0}^{N_e-1} \mu_{il,uv,n} = \hat{\mu}_{il,uv} \times \frac{1 - \exp(j2\pi \Delta f_{il,uv} T_s)}{1 - \exp(j2\pi \Delta f_{il,uv} T_c)} \quad (5.134)$$

Then, when the chip waveform $\psi(t)$ is periodic, $\sum_{n=0}^{N_e-1} \mu_{il,uv,n} = 0$, provided that $\Delta f_{il,uv} = i/T_s$, where $i \neq jN_e$ is an integer. However, when $\exp(j2\pi \Delta f_{il,uv} T_c) = 1$ implying that $f_{il,uv} = i/T_c$, we have $\mu_{il,uv,n} = \hat{\mu}_{il,uv}$.

It can be shown that $N_{uv,n}$ in (5.130) may not be independent with respect to the indices u and v . The correlation between $N_{uv,n}$ and $N_{il,m}$ can be obtained as

$$\begin{aligned} E[N_{uv,n} N_{il,m}^*] &= \frac{1}{2PN_e T_c^2} \int_{nT_c}^{(n+1)T_c} \int_{mT_c}^{(m+1)T_c} E[n(t) n^*(s)] \\ &\quad \times \exp(-j2\pi f_{uv}t) \exp(j2\pi f_{il}s) \psi^*(t) \psi(s) dt ds \end{aligned} \quad (5.135)$$

Explicitly, when $m \neq n$, we have

$$E[N_{uv,n} N_{il,m}^*] = 0 \quad (5.136)$$

By contrast, when $m = n$, we have

$$\begin{aligned}
 E[N_{uv,n}N_{il,n}^*] &= \frac{1}{2PN_e T_c^2} \int_{nT_c}^{(n+1)T_c} \int_{nT_c}^{(n+1)T_c} E[n(t)n^*(s)] \\
 &\quad \times \exp(-j2\pi f_{uv}t) \exp(j2\pi f_{il}s) \psi^*(t)\psi(s) dt ds \\
 &= \frac{1}{2PN_e T_c^2} \int_{nT_c}^{(n+1)T_c} E[n^2(t)]\psi^2(t) \exp(j2\pi \Delta f_{il,uv}t) dt \\
 &= \frac{N_0}{E_b} \times \frac{1}{T_c} \int_{nT_c}^{(n+1)T_c} \psi^2(t) \exp(j2\pi \Delta f_{il,uv}t) dt \\
 &= \frac{N_0}{E_b} \times \mu_{il,uv,n}
 \end{aligned} \tag{5.137}$$

Explicitly, $E[N_{uv,n}N_{il,n}^*] \neq 0$ if $\mu_{il,uv,n} \neq 0$, and in this case $N_{uv,n}$ is correlated with $N_{il,n}$.

Let

$$\begin{aligned}
 \mathbf{b}_k &= [b_1^{(k)}[0], b_2^{(k)}[0], \dots, b_q^{(k)}[0]]^T \\
 \boldsymbol{\mu}_{uv,n} &= [\mu_{11,uv,n}, \dots, \mu_{1p,uv,n}, \dots, \mu_{q1,uv,n}, \dots, \mu_{qp,uv,n}]^T \\
 \mathbf{h}_i^{(k)} &= [h_{i1}^{(k)}, h_{i2}^{(k)}, \dots, h_{ip}^{(k)}]^T \\
 \mathbf{H}_k &= \begin{bmatrix} \mathbf{h}_1^{(k)} & \mathbf{0} & \cdots & \mathbf{0} \\ \mathbf{0} & \mathbf{h}_2^{(k)} & \cdots & \mathbf{0} \\ \vdots & \vdots & \ddots & \vdots \\ \mathbf{0} & \mathbf{0} & \cdots & \mathbf{h}_q^{(k)} \end{bmatrix}
 \end{aligned} \tag{5.138}$$

Then, (5.129) can be expressed as

$$\begin{aligned}
 y_{uv,n} &= \frac{c_n^{(k)}}{\sqrt{N_e p}} \boldsymbol{\mu}_{uv,n}^T \mathbf{H}_k \mathbf{b}_k + N_{uv,n}, \\
 u &= 1, 2, \dots, q; \quad v = 1, 2, \dots, p; \quad n = 0, 1, \dots, N_e - 1
 \end{aligned} \tag{5.139}$$

Similarly, let

$$\begin{aligned}
 \mathbf{y}_{uv} &= [y_{uv,0}, y_{uv,1}, \dots, y_{uv,N_e-1}]^T \\
 \boldsymbol{\mu}_{uv} &= [\boldsymbol{\mu}_{uv,0}, \boldsymbol{\mu}_{uv,1}, \dots, \boldsymbol{\mu}_{uv,N_e-1}]^T \\
 \mathbf{C}_k &= \frac{1}{\sqrt{N_e}} \text{diag}\{c_0^{(k)}, c_1^{(k)}, \dots, c_{N_e-1}^{(k)}\} \\
 \mathbf{n}_{uv} &= [N_{uv,0}, N_{uv,1}, \dots, N_{uv,N_e-1}]^T
 \end{aligned} \tag{5.140}$$

where $\boldsymbol{\mu}_{uv}$ is a $(N_e \times pq)$ matrix. Then, we have

$$\begin{aligned}
 \mathbf{y}_{uv} &= \frac{1}{\sqrt{p}} \mathbf{C}_k \boldsymbol{\mu}_{uv} \mathbf{H}_k \mathbf{b}_k + \mathbf{n}_{uv}, \\
 u &= 1, 2, \dots, q; \quad v = 1, 2, \dots, p
 \end{aligned} \tag{5.141}$$

Finally, let

$$\begin{aligned}\mathbf{y} &= [\mathbf{y}_{11}^T, \dots, \mathbf{y}_{1p}^T, \dots, \mathbf{y}_{q1}^T, \dots, \mathbf{y}_{qp}^T]^T \\ \mathcal{C}_k &= \frac{1}{\sqrt{p}}(\mathbf{I}_{qp} \otimes \mathbf{C}_k) \\ \boldsymbol{\mu} &= [\boldsymbol{\mu}_{11}^T, \dots, \boldsymbol{\mu}_{1p}^T, \dots, \boldsymbol{\mu}_{q1}^T, \dots, \boldsymbol{\mu}_{qp}^T]^T \\ \mathbf{n} &= [\mathbf{n}_{11}^T, \dots, \mathbf{n}_{1p}^T, \dots, \mathbf{n}_{q1}^T, \dots, \mathbf{n}_{qp}^T]^T\end{aligned}\quad (5.142)$$

Then, the observation samples conveying the information of the first transmitted symbol can be expressed in matrix form as

$$\mathbf{y} = \mathcal{C}_k \boldsymbol{\mu} \mathbf{H}_k \mathbf{b}_k + \mathbf{n} \quad (5.143)$$

where, according to the previous analysis, it can be shown that $\boldsymbol{\mu}$ is independent of the user index k . In (5.143) \mathbf{n} is a qpN_e -length Gaussian noise vector, which has zero mean and a covariance matrix given by

$$E[\mathbf{n}\mathbf{n}^H] = \begin{bmatrix} E[\mathbf{n}_{11}\mathbf{n}_{11}^H] & \cdots & E[\mathbf{n}_{11}\mathbf{n}_{1p}^H] & \cdots & E[\mathbf{n}_{11}\mathbf{n}_{qp}^H] \\ \vdots & \ddots & \vdots & \ddots & \vdots \\ E[\mathbf{n}_{1p}\mathbf{n}_{11}^H] & \cdots & E[\mathbf{n}_{1p}\mathbf{n}_{1p}^H] & \cdots & E[\mathbf{n}_{1p}\mathbf{n}_{qp}^H] \\ \vdots & \ddots & \vdots & \ddots & \vdots \\ E[\mathbf{n}_{qp}\mathbf{n}_{11}^H] & \cdots & E[\mathbf{n}_{qp}\mathbf{n}_{1p}^H] & \cdots & E[\mathbf{n}_{qp}\mathbf{n}_{qp}^H] \end{bmatrix} \quad (5.144)$$

where, according to (5.135)–(5.137), we have

$$\begin{aligned}E[\mathbf{n}_{uv}\mathbf{n}_{uv}^H] &= \frac{N_0}{E_b} \mathbf{I}_{N_e} \\ E[\mathbf{n}_{uv}\mathbf{n}_{il}^H] &= \frac{N_0}{E_b} \text{diag}\{\mu_{il,uv,0}, \mu_{il,uv,1}, \dots, \mu_{il,uv,N_e-1}\}\end{aligned}\quad (5.145)$$

Hence, when the noise samples are correlated in the F-domain, as shown in (5.137), the noise covariance matrix of (5.144) is not diagonal.

However, when the subcarrier signals are designed such that $\hat{\mu}_{il,il} = 1$ and $\hat{\mu}_{il,uv} = 0$ whenever $u = i$ and $v = l$ do not hold simultaneously, then (5.143) can be simplified to

$$\mathbf{y} = \mathcal{C}_k \mathbf{H}_k \mathbf{b}_k + \mathbf{n} \quad (5.146)$$

where \mathcal{C}_k is still given by the equation in (5.142), but \mathcal{C}_k should now be defined as

$$\mathcal{C}_k = \frac{1}{\sqrt{N_e}} [c_0^{(k)}, c_1^{(k)}, \dots, c_{N_e-1}^{(k)}]^T \quad (5.147)$$

In this case the noise vector \mathbf{n} in (5.146) is a qpN_e -length Gaussian vector, which has zero mean and a diagonal covariance matrix given by

$$E[\mathbf{n}\mathbf{n}^H] = \frac{N_0}{E_b} \mathbf{I}_{qpN_e} \quad (5.148)$$

implying that the noise samples are independent in both the T-domain and the F-domain.

5.9.2 MRC-Assisted Detection and Performance Analysis

Let us now consider the correlation detection or the MF-assisted detection, where signals conveyed by the different subcarriers are combined based on the MRC principles. Then, according to (5.143), the decision vector for \mathbf{b}_k can be expressed as

$$\begin{aligned} \mathbf{z} &= (\mathcal{C}_k \boldsymbol{\mu} \mathbf{H}_k)^H \mathbf{y} \\ &= (\mathcal{C}_k \boldsymbol{\mu} \mathbf{H}_k)^H \mathcal{C}_k \boldsymbol{\mu} \mathbf{H}_k \mathbf{b}_k + \mathbf{n}' \end{aligned} \quad (5.149)$$

where $\mathbf{n}' = (\mathcal{C}_k \boldsymbol{\mu} \mathbf{H}_k)^H \mathbf{n}$, which is a Gaussian random vector having zero mean and a covariance matrix of $E[\mathbf{n}'(\mathbf{n}')^H] = (\mathcal{C}_k \boldsymbol{\mu} \mathbf{H}_k)^H E[\mathbf{n}\mathbf{n}^H] \mathcal{C}_k \boldsymbol{\mu} \mathbf{H}_k$. Using the fact that $\mathcal{C}_k^T \mathcal{C}_k = (1/N_e p) \mathbf{I}_{qpN_e}$, (5.149) can be expressed as

$$\mathbf{z} = \frac{1}{N_e p} \mathbf{H}_k^H \boldsymbol{\mu}^H \boldsymbol{\mu} \mathbf{H}_k \mathbf{b}_k + \mathbf{n}' \quad (5.150)$$

In more detail, it can be shown that we have

$$\boldsymbol{\mu}^H \boldsymbol{\mu} = \sum_{i=1}^q \sum_{j=1}^p \sum_{n=0}^{N_e-1} \boldsymbol{\mu}_{ij,n}^* \boldsymbol{\mu}_{ij,n}^T \quad (5.151)$$

Hence, substituting (5.151) into (5.150), we obtain

$$\mathbf{z} = \frac{1}{N_e p} \sum_{i=1}^q \sum_{j=1}^p \sum_{n=0}^{N_e-1} \mathbf{H}_k^H \boldsymbol{\mu}_{ij,n}^* \boldsymbol{\mu}_{ij,n}^T \mathbf{H}_k \mathbf{b}_k + \mathbf{n}' \quad (5.152)$$

Let us consider only the u th decision variable for $b_u^{(k)}[0]$. After simplifying (5.152), we have

$$\begin{aligned} z_u &= \frac{1}{N_e p} \sum_{i=1}^q \sum_{j=1}^p \sum_{n=0}^{N_e-1} \sum_{m=1}^q \sum_{l_1=1}^p \sum_{l_2=1}^p (h_{ul_1}^{(k)})^* h_{ml_2}^{(k)} \boldsymbol{\mu}_{ul_1,ij,n}^* \boldsymbol{\mu}_{ml_2,ij,n} b_m^{(k)}[0] + n'_u \\ u &= 1, 2, \dots, q \end{aligned} \quad (5.153)$$

where n'_u represents the u th element of \mathbf{n}' , which is Gaussian distributed with zero mean and one-dimensional variance of

$$\sigma^2 = \frac{1}{2} ((\mathcal{C}_k \boldsymbol{\mu} \mathbf{H}_k)^H E[\mathbf{n}\mathbf{n}^H] \mathcal{C}_k \boldsymbol{\mu} \mathbf{H}_k)_{u,u} \quad (5.154)$$

When decomposing (5.153) into the desired component, interference and noise, and when assuming periodic chip waveform, we then have

$$z_u = D_u + \text{ICBI}_u + n'_u \quad (5.155)$$

where D_u is the desired output, which is given by

$$\begin{aligned} D_u &= \left(\frac{1}{p} \sum_{i=1}^q \sum_{j=1}^p \sum_{l=1}^p |h_{ul}^{(k)}|^2 |\hat{\boldsymbol{\mu}}_{ul,ij}|^2 \right) b_u^{(k)}[0] \\ &= \left(\frac{1}{p} \sum_{l=1}^p \alpha_{ul} |h_{ul}^{(k)}|^2 \right) b_u^{(k)}[0] \end{aligned} \quad (5.156)$$

where $\alpha_{ul} = \sum_{i=1}^q \sum_{j=1}^p |\hat{\mu}_{ul,ij}|^2$. In (5.155) ICBI_u is the intercarrier plus interbit interference given by

$$\begin{aligned} \text{ICBI}_u &= \frac{1}{N_e p} \sum_{i=1}^q \sum_{j=1}^p \sum_{n=0}^{N_e-1} \sum_{m=1}^q \underbrace{\sum_{l_1=1}^p \sum_{l_2=1}^p}_{\substack{l_1 \neq l_2 \text{ if } m=u}} (h_{ul_1}^{(k)})^* h_{ml_2}^{(k)} \\ &\quad \times \hat{\mu}_{ul_1,ij}^* \hat{\mu}_{ml_2,ij} \exp(j2\pi n \Delta f_{ml_2,ul_1} T_c) b_m^{(k)}[0] \\ &= \frac{1}{N_e p} \sum_{i=1}^q \sum_{j=1}^p \sum_{m=1}^q \underbrace{\sum_{l_1=1}^p \sum_{l_2=1}^p}_{\substack{l_1 \neq l_2 \text{ if } m=u}} (h_{ul_1}^{(k)})^* h_{ml_2}^{(k)} \\ &\quad \times \frac{1 - \exp(j2\pi \Delta f_{ml_2,ul_1} T_s)}{1 - \exp(j2\pi \Delta f_{ml_2,ul_1} T_c)} \hat{\mu}_{ul_1,ij}^* \hat{\mu}_{ml_2,ij} b_m^{(k)}[0] \end{aligned} \quad (5.157)$$

Equation (5.157) shows that the MC DS-CDMA scheme can be readily designed so that $\text{ICBI}_u = 0$, i.e. so that there exists no interbit and intercarrier interference. According to (5.157), the zero interbit plus intercarrier interference may be achieved by configuring a normalized subcarrier spacing value, which yields $\exp(j2\pi \Delta f_{ml_2,ul_1} T_c) \neq 1$ and $\exp(j2\pi \Delta f_{ml_2,ul_1} T_s) = 1$. Additionally, the periodic chip waveform $\psi(t)$ and the subcarrier spacing can be jointly designed such that $\hat{\mu}_{ul,ij} = 0$, whenever $u \neq i$ or $l \neq j$. Hence, the forthcoming BER analysis is carried out by assuming that $\text{ICBI}_u = 0$. However, at the end of this section a MC DS-CDMA example using two subcarriers is provided so that we can gain insight into the interbit and intercarrier interference in the MC DS-CDMA systems.

When the subcarrier signals and/or the chip waveforms are designed such that $\text{ICBI}_u = 0$, it can be implied that the correlation matrix $(\mathcal{C}_k \boldsymbol{\mu} \mathbf{H}_k)^H \mathcal{C}_k \boldsymbol{\mu} \mathbf{H}_k$ in (5.149) is a diagonal matrix. Correspondingly, D_u in (5.156) is given by

$$D_u = \left(\frac{1}{p} \sum_{l=1}^p |h_{ul}^{(k)}|^2 \right) |b_u^{(k)}[0]| \quad (5.158)$$

In (5.155) n'_u is an independent Gaussian variable, which has zero mean and the single-dimensional variance of

$$\sigma^2 = \frac{N_0}{2E_b} \times \frac{1}{p} \sum_{l=1}^p |h_{ul}^{(k)}|^2 \quad (5.159)$$

Based on the above analysis, it can be shown that, given the fading amplitudes $h_{ul}^{(k)}$, the conditional BER of the MC DS-CDMA can be expressed as

$$P_b(\gamma) = Q(\sqrt{2\gamma}) \quad (5.160)$$

where the instantaneous SNR γ is given by

$$\gamma = \frac{D_u^2}{2\sigma^2} = \frac{1}{p} \sum_{l=1}^p |h_{ul}^{(k)}|^2 \times \frac{E_b}{N_0} \quad (5.161)$$

which can be expressed as

$$\begin{aligned}\gamma &= \sum_{l=1}^p \gamma_l \\ \gamma_l &= \frac{|h_{ul}^{(k)}|^2}{\Omega} \bar{\gamma}_c\end{aligned}\quad (5.162)$$

where $\Omega = E[|h_{ul}^{(k)}|^2]$ and $\bar{\gamma}_c = \Omega E_b / p N_0$.

Since in the considered MC DS-CDMA the p number of subcarriers used to convey the same data bit are not the adjacent subcarriers, and the two nearest subcarriers of these p subcarriers are separated by $q - 1$ subcarriers, therefore, it is reasonable for us to assume that the subcarriers conveying the same data bit experience independent fading. Consequently, when invoking the alternative definition for the Gaussian- Q function, as seen in (5.90), the average BER of the MC DS-CDMA supporting single-user can be expressed as

$$\begin{aligned}P_b &= \int_0^\infty P_b(\gamma) f(\gamma) d\gamma \\ &= \frac{1}{\pi} \int_0^{\pi/2} \int_0^\infty \exp\left(-\frac{\gamma}{\sin^2 \theta}\right) f(\gamma) d\gamma d\theta \\ &= \frac{1}{\pi} \int_0^{\pi/2} \prod_{l=1}^p I_l(\bar{\gamma}_c, \theta) d\theta\end{aligned}\quad (5.163)$$

where

$$\begin{aligned}I_l(\bar{\gamma}_c, \theta) &= E\left[\exp\left(-\frac{\gamma_l}{\sin^2 \theta}\right)\right] \\ &= \int_0^\infty \exp\left(-\frac{\gamma_l}{\sin^2 \theta}\right) f(\gamma_l) d\gamma_l\end{aligned}\quad (5.164)$$

When assuming the Nakagami- m fading channels, it can be shown that γ_l of (5.162) obeys the PDF of

$$f(\gamma_l) = \frac{1}{\Gamma(m)} \left(\frac{m}{\bar{\gamma}_c}\right)^m \gamma_l^{m-1} \exp\left(-\frac{m\gamma_l}{\bar{\gamma}_c}\right), \quad \gamma_l \geq 0 \quad (5.165)$$

Substituting the above PDF into (5.164), we can obtain $I_l(\bar{\gamma}_c, \theta)$, which is given by

$$I_l(\bar{\gamma}_c, \theta) = \left(\frac{m \sin^2 \theta}{\bar{\gamma}_c + m \sin^2 \theta}\right)^m \quad (5.166)$$

Finally, substituting (5.166) into (5.163), we obtain the average BER of the MC DS-CDMA supporting single-user, which is given by

$$\begin{aligned}P_b &= \frac{1}{\pi} \int_0^{\pi/2} \prod_{l=1}^p \left(\frac{m \sin^2 \theta}{\bar{\gamma}_c + m \sin^2 \theta}\right)^m d\theta \\ &= \frac{1}{\pi} \int_0^{\pi/2} \left(\frac{m \sin^2 \theta}{\bar{\gamma}_c + m \sin^2 \theta}\right)^{pm} d\theta\end{aligned}\quad (5.167)$$

From (5.167) we can find that the diversity order achieved by the MC DS-CDMA system is p , which is achieved when the p subcarriers conveying the same data bit experience independent fading.

Figures 5.12(a) and 5.12(b) show the BER versus SNR per bit performance of the MC DS-CDMA systems, when communicating over the Rayleigh fading channels (Fig. 5.12(a)) or the Nakagami- m fading channels (Fig. 5.12(b)) associated with $m = 1.5$. The results were evaluated using (5.167). In our evaluation various combinations of p and q values were used, when the product pq was a constant of 64. Note that when the value of q increases, the value of p decreases for a constant pq value. In this case the transmission information rate also increases. As the results in Figs 5.12(a) and 5.12(b) show, the BER performance improves when the p value increases, implying a high diversity gain. However, as above-mentioned, for a given value of pq , increasing the p value results in the transmission rate decreasing. Therefore, in MC DS-CDMA there exists a trade-off between the transmission rate and the achievable BER performance. In practice, this trade-off can readily be achieved through reconfiguration, such as on line, of the number of bits invoked in the S/P conversion and of the number of subcarriers for conveying the same data bit. When comparing the results in Fig. 5.12(a) with those in Fig. 5.12(b), we can observe that, for given p, q values, the BER performance improves when the channel fading becomes less severe, i.e. when the m value increases.

5.9.3 Interbit and Intercarrier Interference in MC DS-CDMA: An Example

In this section an example is provided in order to show the possible interbit and intercarrier interference in MC DS-CDMA systems. Then, the signalling design of the MC DS-CDMA is considered, in order that the interbit and intercarrier interference can be efficiently mitigated or fully removed.

In the example under discussion, we assume that the MC DS-CDMA uses only two subcarriers associated with two frequencies, f_1 and f_2 . Furthermore, we assume that each subcarrier transmits one separate bit, implying that there is no F-domain diversity achievable. In this case, the transmitted baseband equivalent MC DS-CDMA signal can be expressed in the form

$$s(t) = \sqrt{2P}b_1c_1(t)\exp(j2\pi f_1t + \phi_1) + \sqrt{2P}b_2c_1(t)\exp(j2\pi f_2t + \phi_2) \quad (5.168)$$

where b_1 and b_2 represent the two bits transmitted on the first and second subcarriers, respectively.

When $s(t)$ is transmitted over a fading channel, the received baseband equivalent MC DS-CDMA signal can be expressed as

$$R(t) = \sqrt{2Ph_1}b_1c_1(t)\exp(j2\pi f_1t) + \sqrt{2Ph_2}b_2c_1(t)\exp(j2\pi f_2t) + n(t) \quad (5.169)$$

where $n(t)$ represents the AWGN noise, while h_1 and h_2 represent the channel gains of the first and second subcarrier channels. Furthermore, in (5.169) the phases due to both the subcarrier modulation at the transmitter and the fading channel are absorbed in h_1 and h_2 .

The received MC DS-CDMA signal of (5.169) is sent to two chip waveform matched filters at frequencies f_1 and f_2 . Assume that the spreading gain is $N_e = T_s/T_c$, then, for

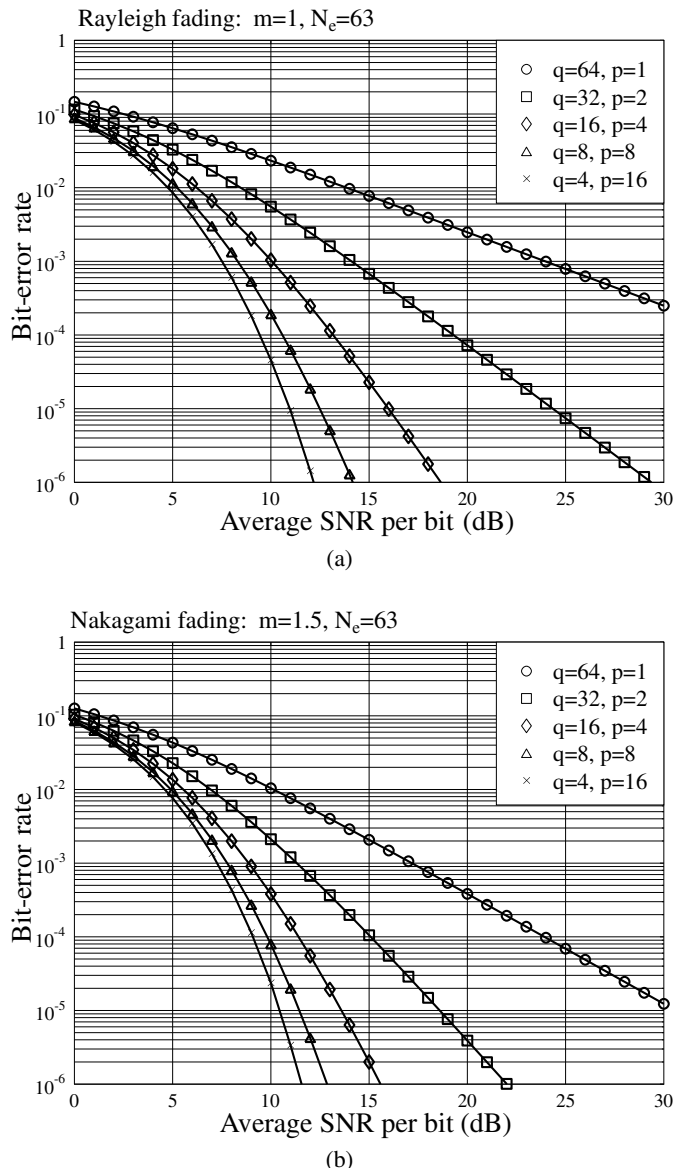


Figure 5.12: BER versus average SNR per bit performance for the MC DS-CDMA scheme supporting single-user; (a) Rayleigh fading channels; (b) Nakagami- m fading channels with $m = 1.5$.

each of the two subcarriers, the receiver can collect N_e observation samples, which can be expressed as

$$y_{u\lambda} = \frac{1}{\sqrt{2PN_e T_c}} \int_{\lambda T_c}^{(\lambda+1)T_c} R(t)\psi^*(t) \exp(-j2\pi f_u t) dt, \quad u = 1, 2 \quad (5.170)$$

Assuming periodic chip waveform, then on substituting (5.169) into (5.170), we obtain

$$\begin{aligned} y_{1\lambda} &= \frac{c_\lambda}{\sqrt{N_e}} [h_1 b_1 + h_2 \hat{\mu}_{21} \exp(j2\pi\lambda\Delta f_{21} T_c) b_2] + n_{1\lambda} \\ y_{2\lambda} &= \frac{c_\lambda}{\sqrt{N_e}} [h_1 \hat{\mu}_{12} \exp(j2\pi\lambda\Delta f_{12} T_c) b_1 + h_2 b_2] + n_{2\lambda} \end{aligned} \quad (5.171)$$

where $n_{u\lambda}$, $u = 1, 2$, is a Gaussian noise sample, which can be expressed as

$$n_{u\lambda} = \frac{1}{\sqrt{2PN_e T_c}} \int_{\lambda T_c}^{(\lambda+1)T_c} n(t)\psi^*(t) \exp(-j2\pi f_u t) dt, \quad u = 1, 2 \quad (5.172)$$

which has zero mean and a variance of $N_0/2E_b$ per dimension. In (5.171) $\Delta f_{ij} = (f_i - f_j)$ and

$$\hat{\mu}_{ij} = \frac{1}{T_c} \int_0^{T_c} \psi^2(t) \exp(j2\pi\Delta f_{ij} t) dt \quad (5.173)$$

It can be shown that $n_{1\lambda_1}$ and $n_{2\lambda_2}$ are uncorrelated, when $\lambda_1 \neq \lambda_2$. However, $n_{1\lambda}$ and $n_{2\lambda}$ might be correlated, since

$$\begin{aligned} E[n_{1\lambda} n_{2\lambda}^*] &= \frac{1}{2PN_e T_c^2} \int_{\lambda T_c}^{(\lambda+1)T_c} E[n(t)n^*(t)] \psi^2(t) \exp(-j2\pi\Delta f_{12} t) dt \\ &= \frac{N_0}{E_b} \hat{\mu}_{21} \exp(j2\pi\lambda\Delta f_{21} T_c) \end{aligned} \quad (5.174)$$

Similarly, we have

$$\begin{aligned} E[n_{2\lambda} n_{1\lambda}^*] &= \frac{N_0}{E_b} \hat{\mu}_{12} \exp(j2\pi\lambda\Delta f_{12} T_c) \\ &= \frac{N_0}{E_b} \hat{\mu}_{21}^* \exp(-j2\pi\lambda\Delta f_{21} T_c) \end{aligned} \quad (5.175)$$

Let

$$\mathbf{y} = [y_{10}, \dots, y_{1(N_e-1)}, y_{20}, \dots, y_{2(N_e-1)}]^T \quad (5.176)$$

Then, \mathbf{y} can be expressed as

$$\mathbf{y} = \mathcal{C}\boldsymbol{\mu}\mathbf{H}\mathbf{b} + \mathbf{n} \quad (5.177)$$

where, by definition, we have

$$\begin{aligned}
 \mathcal{C} &= \mathbf{I}_2 \otimes \mathbf{C} \\
 \mathbf{C} &= \frac{1}{\sqrt{N_e}} \text{diag}\{c_0, c_1, \dots, c_{N_e-1}\} \\
 \boldsymbol{\mu} &= \begin{bmatrix} 1 & \hat{\mu}_{21} \\ \vdots & \vdots \\ 1 & \hat{\mu}_{21} \exp(j2\pi(N_e-1)\Delta f_{21}T_c) \\ \hat{\mu}_{12} & 1 \\ \vdots & \vdots \\ \hat{\mu}_{12} \exp(j2\pi(N_e-1)\Delta f_{12}T_c) & 1 \end{bmatrix} \\
 \mathbf{H} &= \text{diag}\{h_1, h_2\} \\
 \mathbf{b} &= [b_1, b_2]^T \\
 \mathbf{n} &= [n_{10}, \dots, n_{1(N_e-1)}, n_{20}, \dots, n_{2(N_e-1)}]^T
 \end{aligned} \tag{5.178}$$

According to (5.177) and (5.178), explicitly, when the receiver has the knowledge about the spreading code \mathbf{C} , the chip waveform $\psi(t)$, the subcarrier frequencies f_1 and f_2 , as well as the channel, the receiver can then implement the MF-assisted demodulation by forming the decision variable as

$$z = (\mathcal{C}\boldsymbol{\mu}\mathbf{H})^H \mathbf{y} \tag{5.179}$$

which, by applying (5.177) and (5.178), can be expressed as

$$z = \mathbf{H}^H \begin{bmatrix} 1 + |\hat{\mu}_{12}|^2 & \rho_{12} \\ \rho_{21} & 1 + |\hat{\mu}_{21}|^2 \end{bmatrix} \mathbf{H} \mathbf{b} + \mathbf{n}' \tag{5.180}$$

$$= \begin{bmatrix} (1 + |\hat{\mu}_{12}|^2)|h_1|^2 + (h_1^* h_2) \rho_{12} \\ (h_2^* h_1) \rho_{21} + (1 + |\hat{\mu}_{21}|^2)|h_2|^2 \end{bmatrix} \mathbf{b} + \mathbf{n}' \tag{5.181}$$

where we have $|\hat{\mu}_{12}|^2 = |\hat{\mu}_{21}|^2, \rho_{ij}, i, j = 1, 2$ is given by

$$\rho_{ij} = \hat{\mu}_{ij}^* \sum_{n=0}^{N_e-1} \exp(-j2\pi n \Delta f_{ij} T_c) + \hat{\mu}_{ji} \sum_{n=0}^{N_e-1} \exp(j2\pi n \Delta f_{ji} T_c) \tag{5.182}$$

which is equal to zero, if we choose $\Delta f_{ij} = \lambda/T_s$, where $1 \leq \lambda \leq N_e - 1$ is an integer. Furthermore, we have $\rho_{ij} = \rho_{ji}^*$. In (5.181) $\mathbf{n}' = (\mathcal{C}\boldsymbol{\mu}\mathbf{H})^H \mathbf{n}$, which has zero mean and a covariance matrix given by

$$E[\mathbf{n}'(\mathbf{n}')^H] = (\mathcal{C}\boldsymbol{\mu}\mathbf{H})^H E[\mathbf{n}\mathbf{n}^H] \mathcal{C}\boldsymbol{\mu}\mathbf{H} \tag{5.183}$$

where

$$E[\mathbf{n}\mathbf{n}^H] = \frac{N_0}{E_b} \begin{bmatrix} \mathbf{I}_{N_e} & \boldsymbol{\mu}_{N_e} \\ \boldsymbol{\mu}_{N_e}^* & \mathbf{I}_{N_e} \end{bmatrix} \tag{5.184}$$

with $\boldsymbol{\mu}_{N_e} = \hat{\mu}_{21} \text{diag}\{1, \exp(j2\pi\Delta f_{21}T_c), \dots, \exp(j2\pi(N_e-1)\Delta f_{21}T_c)\}$.

According to (5.181), explicitly, there exists interbit or intercarrier interference, i.e. b_1 and b_2 interfere with each other, when the two subcarrier signals are correlated yielding

$\rho_{12} \neq 0$ and, certainly, also $\rho_{21} \neq 0$. However, the interbit and intercarrier interference can be mitigated with the aid of some efficient signal processing schemes such as the multiuser detection schemes that will be studied in Chapter 6. For example, if we form the decision variable vector using the operation

$$\mathbf{z} = \mathbf{H}^H [(\mathcal{C}\boldsymbol{\mu})^H \mathcal{C}\boldsymbol{\mu}]^{-1} (\mathcal{C}\boldsymbol{\mu})^H \mathbf{y} \quad (5.185)$$

then, we obtain

$$\mathbf{z} = \mathbf{H}^H \mathbf{H} \mathbf{b} + \mathbf{n}' = \begin{bmatrix} |h_1|^2 & 0 \\ 0 & |h_2|^2 \end{bmatrix} \mathbf{b} + \mathbf{n}' \quad (5.186)$$

where $\mathbf{n}' = \mathbf{H}^H [(\mathcal{C}\boldsymbol{\mu})^H \mathcal{C}\boldsymbol{\mu}]^{-1} (\mathcal{C}\boldsymbol{\mu})^H \mathbf{n}$. Explicitly, the interbit and intercarrier interference are fully removed. However, the noise samples in \mathbf{n}' are correlated after the operation, which may degrade the achievable BER performance.

5.10 Performance of Single-User Time-Hopping Multicarrier CDMA

In this section the error performance of the single-user TH/MC-CDMA is analysed. Readers interested in the performance analysis for noncoherent M -ary communication schemes may refer to references [2, 25, 110, 148–151].

5.10.1 Decision Variables and Their Statistics

When the TH/MC-CDMA signals in the form of (4.91) are transmitted over frequency-selective fading channels and assuming that the TH/MC-CDMA supports the single-user, the received complex low-pass equivalent signal can be expressed as

$$R(t) = \sqrt{\frac{2PM}{L}} \sum_{l=0}^{L-1} h_l^{(k)} \psi_{T_h}(t - y_k(l)T_h) \exp(j2\pi f_l t) + N(t) \quad (5.187)$$

where the initial phase $\varphi_l^{(k)}$ seen in (4.91) associated with the subcarrier modulation has been absorbed in $h_l^{(k)}$ for convenience, where $h_l^{(k)}$ represents the channel fading gain with respect to the k th user and the l th subcarrier, $N(t)$ represents the complex valued low-pass equivalent AWGN with zero mean and single-sided power spectral density (PSD) of N_0 per dimension.

As shown in Section 4.5.2, when the noncoherent detector shown in Fig. 3.21 in Section 3.8.3 is considered, the decision variable corresponding to the l th subcarrier and the m th time slot can be expressed as

$$R_{lm} = \left| \left(\sqrt{\frac{2PM}{L}} T_h \right)^{-1} \int_{mT_h}^{(m+1)T_h} R(t) \psi_{T_h}(t - mT_h) \exp(-j2\pi f_l t) dt \right|^2 \quad m = 0, 1, \dots, M-1; l = 0, 1, \dots, L-1 \quad (5.188)$$

Explicitly, we can obtain a total of ML number of observations. We assume that the time-domain pulse $\psi_{T_h}(t)$ and the subcarriers are designed so as to satisfy the condition of (4.114).

Then, substituting (5.187) into (5.188), it can be shown that we have

$$R_{lm} = |h_l^{(k)} \delta[y_k(l), m] + n_{lm}|^2, \quad m = 0, 1, \dots, M-1; l = 0, 1, \dots, L-1 \quad (5.189)$$

where n_{lm} is a complex Gaussian noise in the context of the l th subcarrier and the m th time slot, which is given by

$$n_{lm} = \left(\sqrt{\frac{2PM}{L}} T_h \right)^{-1} \int_{mT_h}^{(m+1)T_h} N(t) \psi_{T_h}(t - mT_h) \exp(-j2\pi f_l t) dt \quad (5.190)$$

which has zero mean and a variance of $LN_0/E_s = L/\gamma_s$, where $E_s = PT_s = PMT_h$ represents the transmitted energy per M -ary symbol, $\gamma_s = E_s/N_0 = bE_b/N_0$ represents the SNR per symbol.

Let us assume that the transmitted symbol is $x_k = 0$. Then, after the time de-hopping using the k th user's TH address and the subcarrier signal combining based on the equal-gain combining (EGC) principle [2], the decision variables can be expressed as

$$Z_0 = \sum_{l=0}^{L-1} |h_l^{(k)} + n_{l0}|^2; \quad Z_m = \sum_{l=0}^{L-1} |n_{lm}|^2, \quad m = 1, \dots, M-1 \quad (5.191)$$

Following Section 4.5.2, it can be shown that, conditioned on $h_l^{(k)}$, Z_0 obeys the noncentral χ^2 -distribution with $2L$ degrees of freedom and the PDF is given by [2]

$$f_{Z_0}(y|s^2) = \frac{\gamma_s}{L} \left(\frac{y}{s^2} \right)^{(L-1)/2} \exp\left(-\frac{\gamma_s(s^2 + y)}{L} \right) I_{L-1}\left(\frac{2\gamma_s\sqrt{ys^2}}{L} \right), \quad y \geq 0 \quad (5.192)$$

where s^2 is the non-centrality parameter of the χ^2 -distribution and is given by

$$s^2 = \sum_{l=0}^{L-1} |h_l^{(k)}|^2 \quad (5.193)$$

The decision variable Z_m , $m = 1, \dots, M-1$ obeys the central χ^2 -distribution with $2L$ degrees of freedom and the PDF is given by [2]

$$f_{Z_m}(y) = \frac{1}{(L-1)!} \left(\frac{\gamma_s}{L} \right)^L y^{L-1} \exp\left(-\frac{\gamma_s y}{L} \right), \quad y \geq 0, \quad m = 1, 2, \dots, M-1 \quad (5.194)$$

Invoking the variable transform of $z = \gamma_s y / L$ in (5.192) and (5.194), we obtain the more convenient forms of

$$f_{Z_0}(z|\gamma) = \left(\frac{z}{\gamma} \right)^{(L-1)/2} \exp(-\gamma - z) I_{L-1}(2\sqrt{\gamma z}), \quad z \geq 0 \quad (5.195)$$

$$f_{Z_m}(z) = \frac{1}{(L-1)!} z^{L-1} \exp(-z), \quad z \geq 0, \quad m = 1, 2, \dots, M-1 \quad (5.196)$$

In (5.195), by definition,

$$\gamma = \frac{\gamma_s}{L} \sum_{l=0}^{L-1} |h_l^{(k)}|^2 = \bar{\gamma}_s \sum_{l=0}^{L-1} \frac{|h_l^{(k)}|^2}{\Omega} \quad (5.197)$$

where $\bar{\gamma}_s = \Omega\gamma_s/L$ and $\Omega = E[|h_l^{(k)}|^2]$.

The condition in (5.195) can be averaged out by using

$$f_{Z_0}(z) = \int_0^\infty f_{Z_0}(z|\gamma) f(\gamma) d\gamma \quad (5.198)$$

where $f(\gamma)$ denotes the PDF of γ given by (5.197), which, according to [108, 115], can be expressed as

$$f(\gamma) = \frac{1}{\Gamma(mL)} \left(\frac{m}{\bar{\gamma}_s} \right)^{mL} \gamma^{mL-1} \exp\left(-\frac{m\gamma}{\bar{\gamma}_s}\right), \quad \gamma \geq 0 \quad (5.199)$$

Substituting (5.195) and (5.199) into (5.198) and after some simplification, we obtain

$$\begin{aligned} f_{Z_0}(z) &= \frac{1}{\Gamma(mL)} \left(\frac{m}{\bar{\gamma}_s} \right)^{mL} z^{(L-1)/2} \exp(-z) \\ &\times \int_0^\infty \gamma^{mL-L/2-1/2} \exp\left[-\left(\frac{\bar{\gamma}_s+m}{\bar{\gamma}_s}\right)\gamma\right] I_{L-1}(2\sqrt{\gamma z}) d\gamma \end{aligned} \quad (5.200)$$

which, by completing the integral with the aid of reference [152], can finally be expressed as

$$f_{Z_0}(z) = \frac{z^{L-1} \exp(-z)}{(L-1)!(1+\bar{\gamma}_s/m)^{mL}} {}_1F_1\left(mL; L; \frac{\bar{\gamma}_s z}{m+\bar{\gamma}_s}\right), \quad z \geq 0 \quad (5.201)$$

where ${}_1F_1(\cdot)$ is the confluent hypergeometric function, which is defined as [152]

$${}_1F_1(a; b; x) = \sum_{k=0}^{\infty} \frac{(a)_k x^k}{(b)_k k!} \quad (5.202)$$

where $b \neq 0, -1, -2, \dots$, and $(a)_k = a(a+1)(a+2)\cdots(a+k-1)$, $(a)_0 = 1$. However, ${}_1F_1(a; b; x)$ for $x \gg 0$ and $a > b > 0$ has a very high value, which may result in an overflow in the corresponding numerical computations. Hence, it is usually difficult to achieve sufficient accuracy for the estimation of (5.201). This predicament can be resolved by applying the relationship of ${}_1F_1(a; b; x) = e^x {}_1F_1(b-a; b; -x)$ [152] into (5.201), yielding

$$\begin{aligned} f_{Z_0}(z) &= \frac{z^{L-1}}{(L-1)!} \left(\frac{m}{m+\bar{\gamma}_s} \right)^{mL} \exp\left(-\frac{mz}{m+\bar{\gamma}_s}\right) \\ &\times {}_1F_1\left((1-m)L; L; -\frac{\bar{\gamma}_s z}{m+\bar{\gamma}_s}\right), \quad z \geq 0 \end{aligned} \quad (5.203)$$

Note that, since $(-n)_{n+1} = 0$ if n is a positive integer, then ${}_1F_1(-n, b, x)$ is the sum of only a limited number of terms, which can be expressed as ${}_1F_1(-n, b, x) = \sum_{k=0}^n ((-n)_k x^k)/((b)_k k!)$. Therefore, if m is a positive integer, (5.203) consists of the sum of limited terms. Furthermore, if a multipath Rayleigh fading channel model associated with $m = 1$ is considered, then, ${}_1F_1(0; b; x) = 1$ and, explicitly, (5.203) is reduced to

$$f_{Z_0}(z) = \frac{1}{(L-1)!} \left(\frac{1}{1+\bar{\gamma}_s} \right)^L z^{L-1} \exp\left(-\frac{z}{1+\bar{\gamma}_s}\right), \quad z \geq 0 \quad (5.204)$$

Having obtained the PDFs for the decision variables $\{Z_0, Z_1, \dots, Z_{M-1}\}$, as shown in (5.203) and (5.196), let us now derive the expression of the error probability.

5.10.2 Error Probability Analysis

Following our discussion in Section 4.5.2 of Chapter 4, the symbol error probability can be computed as

$$P_e = 1 - P_c \quad (5.205)$$

where P_c denotes the symbol correct probability. Since $\{Z_0, Z_1, \dots, Z_{M-1}\}$ are independent random variables, P_c can be expressed as

$$\begin{aligned} P_c &= P(Z_1 < Z_0, Z_2 < Z_0, \dots, Z_{M-1} < Z_0 | x_k = 0) \\ &= \int_0^\infty [P(Z_1 < y | Z_0 = y)]^{M-1} f_{Z_0}(y) dy \end{aligned} \quad (5.206)$$

where $P(Z_1 < y | Z_0 = y)$ is given by

$$P(Z_1 < y | Z_0 = y) = \int_0^y f_{Z_1}(x) dx \quad (5.207)$$

When substituting (5.196) into the above equation, we obtain

$$P(Z_1 < y | Z_0 = y) = 1 - \exp(-y) \sum_{n=0}^{L-1} \frac{y^n}{n!} \quad (5.208)$$

Substituting it into (5.206) yields

$$\begin{aligned} P_c &= \int_0^\infty \left[1 - \exp(-y) \sum_{n=0}^{L-1} \frac{y^n}{n!} \right]^{M-1} f_{Z_0}(y) dy \\ &= \frac{1}{(L-1)!} \left(\frac{m}{m + \bar{\gamma}_s} \right)^{mL} \int_0^\infty \left[1 - \exp(-y) \sum_{n=0}^{L-1} \frac{y^n}{n!} \right]^{M-1} \\ &\quad \times y^{L-1} \exp\left(-\frac{my}{m + \bar{\gamma}_s}\right) {}_1F_1\left((1-m)L; L; -\frac{\bar{\gamma}_s y}{m + \bar{\gamma}_s}\right) dy \end{aligned} \quad (5.209)$$

Invoking the binomial expansion,

$$\begin{aligned} \left[1 - \exp(-y) \sum_{n=0}^{L-1} \frac{y^n}{n!} \right]^{M-1} &= \sum_{k=0}^{M-1} (-1)^k \binom{M-1}{k} \left(\exp(-y) \sum_{n=0}^{L-1} \frac{y^n}{n!} \right)^k \\ &= \sum_{k=0}^{M-1} (-1)^k \binom{M-1}{k} \exp(-ky) \left(\sum_{n=0}^{L-1} \frac{y^n}{n!} \right)^k \end{aligned} \quad (5.210)$$

Furthermore, according to [2, 152, 153], in (5.210) we have

$$\left(\sum_{n=0}^{L-1} \frac{y^n}{n!} \right)^k = \sum_{n=0}^{k(L-1)} \beta_{nk} y^n \quad (5.211)$$

where β_{nk} is the set of coefficients in the above expansion, which can be computed recursively as

$$\beta_{nk} = \sum_{i=n-L+1}^n \beta_{i(k-1)} \frac{1}{(n-i)!} I_{[0, (k-1)(L-1)]}(i) \quad (5.212)$$

associated with

$$\begin{aligned}\beta_{00} &= \beta_{0k} = 1 \\ \beta_{n1} &= 1/n!, \quad \beta_{1k} = k \\ I_{[a,b]}(i) &= \begin{cases} 1, & \text{if } a \leq i \leq b \\ 0, & \text{otherwise} \end{cases}\end{aligned}$$

Applying (5.211) and (5.210) to (5.209), the symbol correct probability can be expressed as

$$\begin{aligned}P_c &= \int_0^\infty \left[1 - \exp(-y) \sum_{n=0}^{L-1} \frac{y^n}{n!} \right]^{M-1} f_{Z_0}(y) dy \\ &= \frac{1}{(L-1)!} \left(\frac{m}{m + \bar{\gamma}_s} \right)^{mL} \sum_{k=0}^{M-1} (-1)^k \binom{M-1}{k} \sum_{n=0}^{k(L-1)} \beta_{nk} \int_0^\infty y^{L+n-1} \\ &\quad \times \exp\left(-\frac{(k\bar{\gamma}_s + km + m)y}{m + \bar{\gamma}_s}\right) {}_1F_1\left((1-m)L; L; -\frac{\bar{\gamma}_s y}{m + \bar{\gamma}_s}\right) dy \quad (5.213)\end{aligned}$$

The integral in the above equation can be simplified by invoking the relationship of [7.621.4] in reference [152]¹, yielding the symbol correct probability

$$\begin{aligned}P_c &= \frac{1}{(L-1)!} \left(\frac{m}{m + \bar{\gamma}_s} \right)^{mL} \sum_{k=0}^{M-1} (-1)^k \binom{M-1}{k} \sum_{n=0}^{k(L-1)} \beta_{nk} (L+n-1)! \\ &\quad \times \left(\frac{m + \bar{\gamma}_s}{k\bar{\gamma}_s + km + m} \right)^{L+n} {}_2F_1\left((1-m)L, L+n; L; -\frac{\bar{\gamma}_s}{k\bar{\gamma}_s + km + m}\right) \quad (5.215)\end{aligned}$$

Correspondingly, the symbol error probability is given by

$$\begin{aligned}P_e &= \frac{1}{(L-1)!} \left(\frac{m}{m + \bar{\gamma}_s} \right)^{mL} \sum_{k=1}^{M-1} (-1)^{k+1} \binom{M-1}{k} \sum_{n=0}^{k(L-1)} \beta_{nk} (L+n-1)! \\ &\quad \times \left(\frac{m + \bar{\gamma}_s}{k\bar{\gamma}_s + km + m} \right)^{L+n} {}_2F_1\left((1-m)L, L+n; L; -\frac{\bar{\gamma}_s}{k\bar{\gamma}_s + km + m}\right) \quad (5.216)\end{aligned}$$

Finally, as shown in (4.128), when the random binary source is assumed, the BER can be computed as

$$P_b = \frac{2^{b-1}}{M-1} P_e \quad (5.217)$$

where $b = \log_2 M$.

¹

$$\int_0^\infty e^{-st} t^{b-1} {}_1F_1(a; c; kt) dt = \begin{cases} \Gamma(b) s^{-b} {}_2F_1(a, b; c; ks^{-1}), & \text{if } |s| > |k| \\ \Gamma(b) (s-k)^{-b} {}_2F_1(c-a, b; c; \frac{k}{k-s}), & \text{if } |s-k| > |k| \end{cases} \quad (5.214)$$

The symbol error probability of (5.216) has a range of special cases, which are summarized as follows. First, when m is an integer, (5.216) can be simplified to

$$\begin{aligned} P_e = & \frac{1}{(L-1)!} \left(\frac{m}{m + \bar{\gamma}_s} \right)^{mL} \sum_{k=1}^{M-1} (-1)^{k+1} \binom{M-1}{k} \\ & \times \sum_{n=0}^{k(L-1)} \beta_{nk} (L+n-1)! \left(\frac{m + \bar{\gamma}_s}{k\bar{\gamma}_s + km + m} \right)^{L+n} \\ & \times \sum_{u=0}^{L(m-1)} \frac{((1-m)L)_u (L+n)_u}{(L)_u u!} \left(-\frac{\bar{\gamma}_s}{k\bar{\gamma}_s + km + m} \right)^u \end{aligned} \quad (5.218)$$

which is the sum invoking only limited items. Second, let $L = 1$, then, with the aid of the relation of reference [152][9.131.1]

$$_2F_1(a, b; c; x) = (1-x)^{-a} {}_2F_1\left(a, c-b; c; \frac{x}{x-1}\right) \quad (5.219)$$

(5.216) can be reduced to

$$P_e = \sum_{k=1}^{M-1} \frac{(-1)^{k+1}}{k+1} \binom{M-1}{k} \left(\frac{(k+1)m}{k\bar{\gamma}_s + km + m} \right)^m \quad (5.220)$$

Third, when the Rayleigh fading channel corresponding to $m = 1$ is assumed, (5.216) is reduced to [2]

$$\begin{aligned} P_e = & \frac{1}{(L-1)!} \sum_{k=1}^{M-1} \frac{(-1)^{k+1}}{(k\bar{\gamma}_s + k+1)^L} \binom{M-1}{k} \\ & \times \sum_{n=0}^{k(L-1)} \beta_{nk} (L+n-1)! \left(\frac{1+\bar{\gamma}_s}{k\bar{\gamma}_s + k+1} \right)^n \end{aligned} \quad (5.221)$$

Furthermore, when $m = 1$ and $L = 1$, from (5.220) or (5.221) we can obtain the symbol error probability

$$P_e = \sum_{k=1}^{M-1} \frac{(-1)^{k+1}}{k\bar{\gamma}_s + k+1} \binom{M-1}{k} \quad (5.222)$$

5.10.3 Performance Results

In this section we show some numerical results computed using the equations derived in the last section, so as to characterize the BER performance of the single-user TH/MC-CDMA system.

Figure 5.13 shows the BER versus the average SNR per bit performance for the single-user TH/MC-CDMA associated with a different diversity order, when communicating over Rayleigh fading channels ($m = 1$). Specifically, in Fig. 5.13 both 16 PPM and 64 PPM were considered. Explicitly, the results in Fig. 5.13 show that, for a given M value, the BER performance improves when the diversity order increases. By comparing the BER of 16 PPM

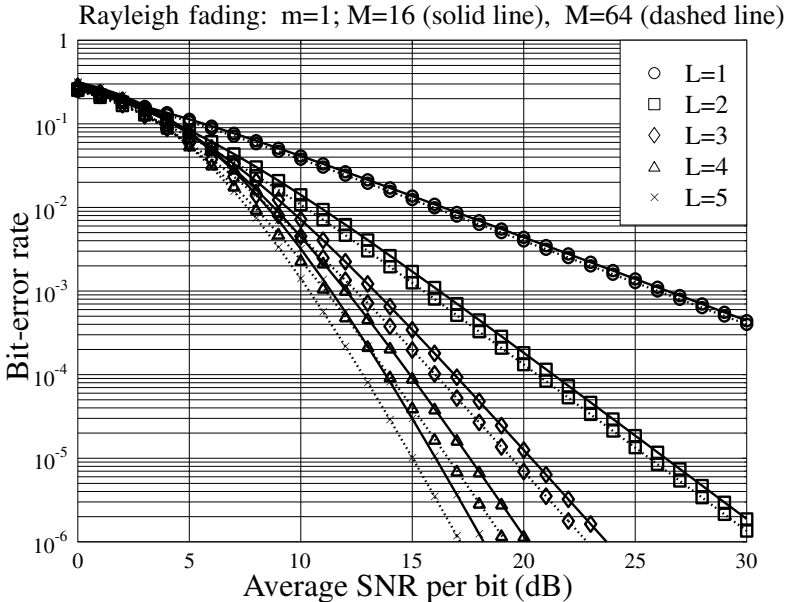


Figure 5.13: BER versus average SNR per bit performance for the TH/MC-CDMA communicating over Rayleigh fading channels associated with $m = 1$.

with that of 64 PPM, we can observe that, for a given diversity order, the BER of the 64 PPM is slightly lower than that of the 16 PPM. Note that, as the analysis in Section 3.8 shows, for a given transmitted data rate and a given M value, increasing the value of L results in more system bandwidth required. Furthermore, in M -ary noncoherent communications, such as in M -ary orthogonal signalling modulation [2], increasing the M value also implies that an increased system bandwidth is required.

Figure 5.14 shows the BER versus the average SNR per bit performance for the single-user TH/MC-CDMA associated with a different diversity order, when communicating over Nakagami- m fading channels with the fading parameter $m = 2$. Similarly to Fig. 5.13, the results in Fig. 5.14 show that, for a given M value, the BER performance improves when the diversity order increases. Furthermore, comparing the results in Fig. 5.14 with those in Fig. 5.13, the BER in Fig. 5.14 is lower than the corresponding BER observed in Fig. 5.13 for given values of L and M , since the channel considered in Fig. 5.14 was less faded than that considered in Fig. 5.13. This observation becomes more clear from the results shown in Fig. 5.15, where various fading parameter, i.e. m values were evaluated in the context of the TH/MC-CDMA systems.

5.11 Performance of Time-Frequency-Domain Spread Multicarrier DS-CDMA Supporting Multiusers

The communication principles of the TF-domain spread MC DS-CDMA were presented in Section 4.6 of Chapter 4, where the performance of the TF-domain spread MC DS-CDMA

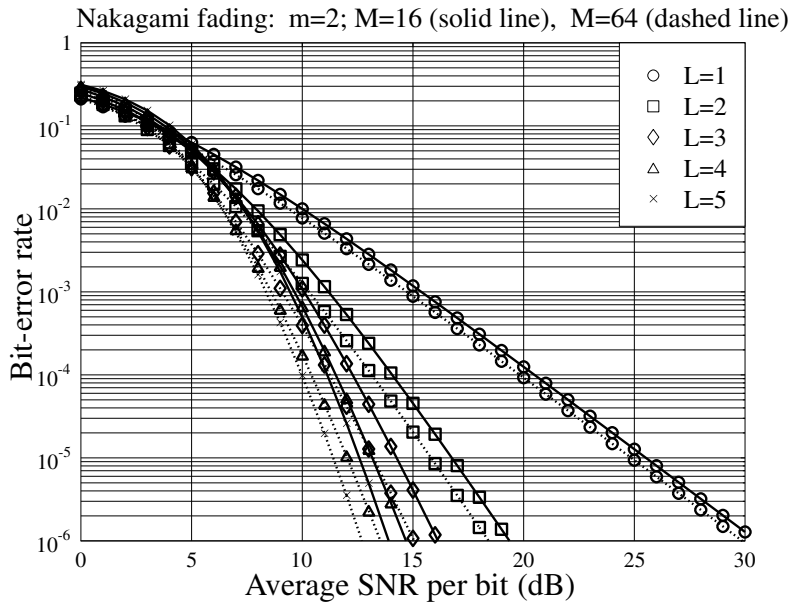


Figure 5.14: BER versus average SNR per bit performance for the TH/MC-CDMA communicating over Nakagami- m fading channels associated with $m = 1.5$.

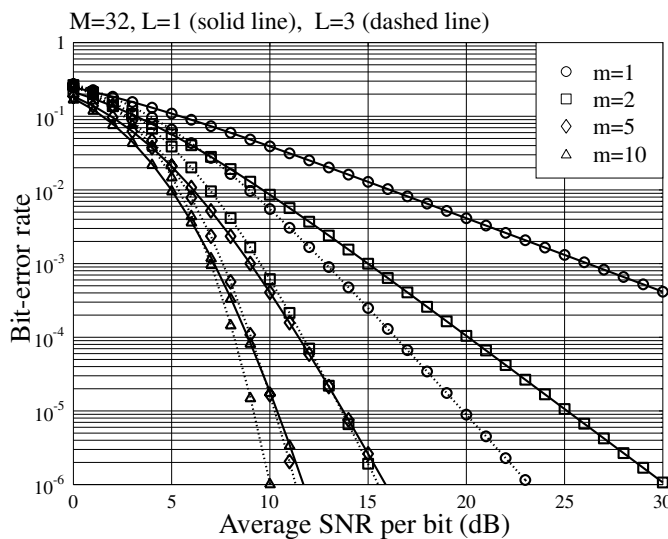


Figure 5.15: BER versus average SNR per bit performance for the TH/MC-CDMA communicating over Nakagami- m fading channels associated with various m values.

was also investigated, when communicating over the AWGN environment. In this section the BER performance of the TF-domain spread MC DS-CDMA, which supports multiple users, is investigated, when communicating over frequency-selective Nakagami fading channels. Note that the analytical approaches carried out in this section can be readily modified for the other types of multicarrier CDMA scheme, such as for the MC-CDMA in Section 5.6 and the MC DS-CDMA in Section 5.9, when these systems support multiple users.

The transmitter schematic block diagram of the TF-domain spread MC DS-CDMA is shown in Fig. 4.8. Correspondingly, the transmitted signal by the k th user is given by (4.134), which is copied here for convenience as

$$s_k(t) = \sqrt{\frac{2P}{N_p}} \sum_{u=0}^{U-1} \sum_{n_p=0}^{N_p-1} b_u^{(k)} c_{fu,n_p}^{(k)} c_k(t) \Re\{\exp(j[2\pi f_{n_p} t + \phi_{n_p}^{(k)}])\} \quad (5.223)$$

where we expressed $b_m^{(k)}[u]$ by $b_u^{(k)}$ for brevity, since we consider only the synchronous TF-domain spread MC DS-CDMA. Note, furthermore, that the details about the variables and parameters in the above equation can be found in the explanation with (4.134).

As in Section 4.6, we assume that the TF-domain spread MC DS-CDMA supports K number of users, and that all the users transmit at the same data rate. Furthermore, it is assumed that the average received power from each of the K users is the same, i.e. ideal power control is assumed. Consequently, when the K number of TF-domain spread MC DS-CDMA signals in the form of (5.223) are transmitted synchronously over the Nakagami- m fading channels, the received complex low-pass equivalent signal can be expressed as

$$R(t) = \sum_{k=1}^K \sqrt{\frac{2P}{N_p}} \sum_{u=0}^{U-1} \sum_{n_p=0}^{N_p-1} h_{n_p}^{(k)} b_u^{(k)} c_{fu,n_p}^{(k)} c_k(t) \exp(j[2\pi f_{n_p} t + \varphi_{n_p}^{(k)}]) + N(t) \quad (5.224)$$

where $h_{n_p}^{(k)}$ represents the fading channel gain corresponding to the n_p th subcarrier of the k th user. It is assumed that the channel fading associated with each of the subcarriers is time-invariant over at least one symbol duration of $T_s = UT_b$ seconds. Since frequency-selective Nakagami- m fading channels are considered, $h_i^{(k)}$ and $h_j^{(k)}$ for $i \neq j$ may or may not correlate. However, we assume that each of the subcarrier channels experiences flat Nakagami- m fading, and the amplitude of $h_{n_p}^{(k)}$ obeys the PDF as shown in (5.1).

5.11.1 Representation of the Received Signal

The receiver schematic block diagram considered in this section is the same as that shown in Fig. 4.10 in Section 4.6.3 of Chapter 4, i.e. each of the subcarrier signals is first input to a filter matched to the transmitted chip waveform $\psi(t)$, so that discrete observation samples are provided to the following detector. Specifically, according to Fig. 4.10, the n th sample of the v th subcarrier can be expressed as

$$y_{vn} = (\sqrt{2PN_t} T_c)^{-1} \int_{nT_c}^{(n+1)T_c} R(t) \exp(-j2\pi f_v t) \psi^*(t) dt \\ v = 0, 1, \dots, N_p - 1; n = 0, 1, \dots, N_t - 1 \quad (5.225)$$

Substituting (5.224) into the above equation, it can be shown that

$$y_{vn} = \sum_{k=1}^K \sum_{u=0}^{U-1} \sum_{n_p=0}^{N_p-1} \frac{1}{\sqrt{N_p N_t}} c_{fu,n_p}^{(k)} c_{kn} h_{n_p}^{(k)} \mu_{n_p v, n} b_u^{(k)} + N_{vn}$$

$$v = 0, 1, \dots, N_p - 1; n = 0, 1, \dots, N_t - 1 \quad (5.226)$$

where N_{vn} represents a Gaussian noise sample, which is Gaussian distributed with zero mean and a variance of $N_0/2E_b$ per dimension, and $E_b = PT_s = PN_t T_c$ represents the energy per bit. We assume that the periodic chip waveform of $\psi(t)$ is used; hence in (5.226) $\mu_{n_p v, n}$ is defined as

$$\mu_{n_p v, n} = \hat{\mu}_{n_p v} \exp(j2\pi n \Delta f_{n_p v} T_c), \quad n = 0, 1, \dots, N_t - 1 \quad (5.227)$$

$$\hat{\mu}_{n_p v} = \frac{1}{T_c} \int_0^{T_c} \psi^2(t) \exp(j2\pi \Delta f_{n_p v} t) dt \quad (5.228)$$

where it can be shown that we have $\Delta f_{n_p v} = f_{n_p} - f_v = i\lambda/T_s$, when the spacing between two adjacent subcarriers is λ/T_s .

Let us define

$$\mathbf{b}_k = [b_0^{(k)}, b_1^{(k)}, \dots, b_{U-1}^{(k)}]^T \quad (5.229)$$

$$\boldsymbol{\mu}_{v,n} = [\mu_{0v,n}, \mu_{1v,n}, \dots, \mu_{(N_p-1)v,n}]^T \quad (5.230)$$

$$\mathbf{H}_k = \text{diag}\{h_0^{(k)}, h_1^{(k)}, \dots, h_{N_p-1}^{(k)}\} \quad (5.231)$$

$$\begin{aligned} \mathbf{C}_f^{(k)} &= [\mathbf{c}_{f0}^{(k)}, \mathbf{c}_{f1}^{(k)}, \dots, \mathbf{c}_{f(U-1)}^{(k)}] \\ &= \frac{1}{\sqrt{N_p}} \begin{bmatrix} c_{f0,0}^{(k)} & c_{f1,0}^{(k)} & \cdots & c_{f(U-1),0}^{(k)} \\ c_{f0,1}^{(k)} & c_{f1,1}^{(k)} & \cdots & c_{f(U-1),1}^{(k)} \\ \vdots & \vdots & \ddots & \vdots \\ c_{f0,N_p-1}^{(k)} & c_{f1,N_p-1}^{(k)} & \cdots & c_{f(U-1),N_p-1}^{(k)} \end{bmatrix} \end{aligned} \quad (5.232)$$

Then, it can be shown that (5.226) can be expressed as

$$y_{vn} = \sum_{k=1}^K \frac{c_{kn}}{\sqrt{N_t}} (\boldsymbol{\mu}_{v,n})^T \mathbf{H}_k \mathbf{C}_f^{(k)} \mathbf{b}_k + N_{vn}$$

$$v = 0, 1, \dots, N_p - 1; n = 0, 1, \dots, N_t - 1 \quad (5.233)$$

Let us define

$$\begin{aligned} \mathbf{y}_v &= [y_{v0}, y_{v1}, \dots, y_{v(N_t-1)}]^T \\ \mathbf{n}_v &= [N_{v0}, N_{v1}, \dots, N_{v(N_t-1)}]^T \\ \mathbf{C}_k &= \text{diag}\{c_{k0}, c_{k1}, \dots, c_{k(N_t-1)}\}/\sqrt{N_t} \\ \boldsymbol{\mu}_v^T &= [\boldsymbol{\mu}_{v0}, \boldsymbol{\mu}_{v1}, \dots, \boldsymbol{\mu}_{v(N_t-1)}] \end{aligned} \quad (5.234)$$

Then, it can be shown that \mathbf{y}_v can be expressed as

$$\mathbf{y}_v = \sum_{k=1}^K \mathbf{C}_k \boldsymbol{\mu}_v \mathbf{H}_k \mathbf{C}_f^{(k)} \mathbf{b}_k + \mathbf{n}_v, \quad v = 0, 1, \dots, N_p - 1 \quad (5.235)$$

where, in summary, \mathbf{C}_k is $(N_t \times N_t)$, $\boldsymbol{\mu}_v$ is $(N_t \times N_p)$, \mathbf{H}_k is $(N_p \times N_p)$, $\mathbf{C}_f^{(k)}$ is $(N_p \times U)$ and \mathbf{n}_v is $(N_t \times 1)$.

Furthermore, defining

$$\begin{aligned} \mathbf{y} &= [\mathbf{y}_0^T, \mathbf{y}_1^T, \dots, \mathbf{y}_{N_p-1}^T]^T \\ \mathbf{n} &= [\mathbf{n}_0^T, \mathbf{n}_1^T, \dots, \mathbf{n}_{N_p-1}^T]^T \end{aligned} \quad (5.236)$$

then, \mathbf{y} can be expressed as

$$\mathbf{y} = \sum_{k=1}^K \mathbf{C}_k \boldsymbol{\mu} \mathbf{H}_k \mathbf{C}_f^{(k)} \mathbf{b}_k + \mathbf{n} \quad (5.237)$$

associated with \mathcal{C}_k and $\boldsymbol{\mu}$ being defined as

$$\begin{aligned} \mathcal{C}_k &= \text{diag}\{\mathbf{C}_k, \mathbf{C}_k, \dots, \mathbf{C}_k\} = \mathbf{I}_{N_p} \otimes \mathbf{C}_k \\ \boldsymbol{\mu} &= [\boldsymbol{\mu}_0^T, \boldsymbol{\mu}_1^T, \dots, \boldsymbol{\mu}_{N_p-1}^T]^T \end{aligned} \quad (5.238)$$

Notice that when the subcarrier signals are designed to be orthogonal with each other, yielding $\mu_{vv,n} = 1$ and $\mu_{n_p v, n} = 0$ for any $n_p \neq v$, then (5.226) is reduced to

$$\begin{aligned} y_{vn} &= \sum_{k=1}^K \sum_{u=0}^{U-1} \frac{1}{\sqrt{N_p N_t}} c_{fu,v}^{(k)} c_{kn} h_v^{(k)} b_u^{(k)} + N_{vn} \\ v &= 0, 1, \dots, N_p - 1; \quad n = 0, 1, \dots, N_t - 1 \end{aligned} \quad (5.239)$$

In this case, the observation equation of (5.237) can be simplified to

$$\mathbf{y} = \sum_{k=1}^K \mathbf{C}_k \mathbf{H}_k \mathbf{C}_f^{(k)} \mathbf{b}_k + \mathbf{n} \quad (5.240)$$

where \mathcal{C}_k is now defined as

$$\mathcal{C}_k = \mathbf{I}_{N_p} \otimes \mathbf{c}_k \quad (5.241)$$

where $\mathbf{c}_k = [c_{k0}, c_{k1}, \dots, c_{k(N_t-1)}]^T / \sqrt{N_t}$.

5.11.2 Single-User Detection and Analysis

Without loss of any generality, let us assume that the first user indexed by $k = 1$ is the reference user and our objective is to analyse the BER performance of the reference user, when the single-user detector, such as the correlation or MF-assisted detector, is considered. Furthermore, for the sake of simplicity, we only consider the case where the subcarrier signals

are orthogonal, corresponding to the observation equation of (5.240). In this case, the decision variable vector $\mathbf{Z}_1 = [Z_{10}, Z_{11}, \dots, Z_{1(U-1)}]^T$ for \mathbf{b}_1 can be expressed as

$$\mathbf{Z}_1 = (\mathcal{C}_1 \mathbf{H}_1 \mathbf{C}_f^{(1)})^H \mathbf{y} = (\mathbf{C}_f^{(1)})^T \mathbf{H}_1^H \mathcal{C}_1^T \mathbf{y} \quad (5.242)$$

Substituting (5.240) into the above equation, we can express \mathbf{Z}_1 as

$$\mathbf{Z}_1 = \mathbf{Z}_D + \sum_{k=2}^K \mathbf{Z}_{kI} + \mathbf{N}_1 \quad (5.243)$$

where

$$\begin{aligned} \mathbf{Z}_D &= (\mathbf{C}_f^{(1)})^T \mathbf{H}_1^H \mathcal{C}_1^T \mathcal{C}_1 \mathbf{H}_1 \mathbf{C}_f^{(1)} \mathbf{b}_1 \\ \mathbf{Z}_{kI} &= (\mathbf{C}_f^{(1)})^T \mathbf{H}_1^H \mathcal{C}_1^T \mathcal{C}_k \mathbf{H}_k \mathbf{C}_f^{(k)} \mathbf{b}_k \\ \mathbf{N}_1 &= (\mathbf{C}_f^{(1)})^T \mathbf{H}_1^H \mathcal{C}_1^T \mathbf{n} \end{aligned} \quad (5.244)$$

In (5.244) \mathbf{Z}_D contains the desired output and the self-interference among the bits of user 1, \mathbf{Z}_{kI} represents the interference imposed by the k th user on the reference user, while \mathbf{N}_1 is due to the Gaussian noise. Let us now analyse these terms in more detail.

First, using the definition of (5.241) for \mathcal{C}_k , we have $\mathcal{C}_1^T \mathcal{C}_1 = \mathbf{I}_{N_p}$. Hence, \mathbf{Z}_D can be expressed as

$$\mathbf{Z}_D = \underbrace{(\mathbf{C}_f^{(1)})^T \mathbf{H}_1^H \mathbf{H}_1 \mathbf{C}_f^{(1)}}_{\mathbf{R}_1} \mathbf{b}_1 \quad (5.245)$$

where $\mathbf{R}_1 = (\mathbf{C}_f^{(1)})^T \mathbf{H}_1^H \mathbf{H}_1 \mathbf{C}_f^{(1)}$ represents the autocorrelation within the reference user. Utilizing the definitions for \mathbf{H}_k and $\mathbf{C}_f^{(k)}$ as shown in (5.231) and (5.232), respectively, it can be shown that the (i, j) th entry of \mathbf{R}_1 can be expressed as

$$\mathbf{R}_1(i, j) = \frac{1}{N_p} \sum_{v=0}^{N_p-1} |h_v|^2 c_{fi,v} c_{fj,v}, \quad i, j = 0, 1, \dots, U-1 \quad (5.246)$$

where the superscripts concerning the reference user have been removed for simplicity.

Note that, as shown in (5.246), there exists interbit interference among the bits transmitted by the reference user; even the F-domain spreading sequences are orthogonal. This is because the frequency-selective fading associated with the N_p subcarriers destroys the orthogonality of the F-domain spreading sequences. Below, a range of approaches for mitigating the interbit interference are considered.

First, instead of carrying out the demodulation as shown in (5.242), the demodulation can be formed as

$$\begin{aligned} \mathbf{Z}_1 &= (\mathcal{C}_1 \mathbf{H}_1 (\mathbf{H}_1^H \mathbf{H}_1)^{-1} \mathbf{C}_f^{(1)})^H \mathbf{y} \\ &= (\mathbf{C}_f^{(1)})^T (\mathbf{H}_1^H \mathbf{H}_1)^{-1} \mathbf{H}_1^H \mathcal{C}_1^T \mathbf{y} \end{aligned} \quad (5.247)$$

In this case, it can be shown that

$$\mathbf{R}_1(i, j) = \begin{cases} 1, & \text{if } i = j \\ 0, & \text{otherwise} \end{cases} \quad (5.248)$$

provided that the F-domain spreading sequences are orthogonal. Correspondingly, \mathbf{Z}_D in (5.245) can be simplified to

$$\mathbf{Z}_D = \mathbf{b}_1 \quad (5.249)$$

Explicitly, the interbit interference is fully removed.

However, in the above scheme, if there exist small-value eigenvalues in $\mathbf{H}_1^H \mathbf{H}_1$, the multiplication operation on MUI and background noise will amplify the MUI as well as the noise, yielding performance degradation.

When the frequency selectivity of the fading channel is not high, and therefore the adjacent subcarriers experience similar fading, one alternative to mitigate the interbit interference of a given user is to assign the user U number of F-domain spreading sequences with the orthogonal variable spreading factor (OVSF) codes, such as the Walsh Hadamard codes [71]. More specifically, the OVSF sequences can be constructed by concatenation of one orthogonal code with another. For example, let \mathbf{C}_M be an orthogonal code of length M , the length- $2M$ orthogonal code can be constructed as

$$\mathbf{C}_{2M} = \begin{bmatrix} 1 & 1 \\ 1 & -1 \end{bmatrix} \otimes \mathbf{C}_M \quad (5.250)$$

This way, longer orthogonal codes can be constructed.

From the above constructions we can see that in an OVSF code, such as \mathbf{C}_{2M} , the sub-code \mathbf{C}_M is also an orthogonal code. Hence, in the TF-domain spread MC DS-CDMA, U number of orthogonal sequences having different subcodewords from \mathbf{C}_M may be assigned to the same user for signaturing the U bits. In this case, we can imply that, if $M \geq U$ and if the fading is frequency nonselective across M adjacent subcarriers, the orthogonality of the subcode will be retained and there will be no interbit interference within a given user.

Let us now turn to analyse the MUI as shown in (5.244). Since $\mathbf{C}_1^T \mathbf{C}_k = \mathbf{c}_1^T \mathbf{c}_k \mathbf{I}_{N_p}$, (5.244) can be simplified to

$$\begin{aligned} \mathbf{Z}_{kl} &= (\mathbf{C}_f^{(1)})^T \mathbf{H}_1^H \mathbf{C}_1^T \mathbf{c}_k \mathbf{H}_k \mathbf{C}_f^{(k)} \mathbf{b}_k \\ &= \mathbf{c}_1^T \mathbf{c}_k \underbrace{(\mathbf{C}_f^{(1)})^T \mathbf{H}_1^H \mathbf{H}_k \mathbf{C}_f^{(k)}}_{\mathbf{R}_{k1}} \mathbf{b}_k \end{aligned} \quad (5.251)$$

where \mathbf{R}_{k1} represents the cross-correlation between the k th interfering user and the reference user. It can be shown that the (i, j) th entry of \mathbf{R}_{k1} can be expressed as

$$\mathbf{R}_{k1}(i, j) = \frac{1}{N_p} \sum_{v=0}^{N_p-1} h_v^* h_v^{(k)} c_{fi,v} c_{ff,v}^{(k)}, \quad i, j = 0, 1, \dots, U-1 \quad (5.252)$$

Finally, in (5.244) \mathbf{N}_1 is a Gaussian random vector, which has zero mean and a covariance matrix given by $\mathbf{R}_1 \times (N_0/E_b)$, where \mathbf{R}_1 has been defined in (5.245).

5.11.3 Statistics Analysis

In this section we derive the statistics of the decision variables that are necessary for the BER analysis in the forthcoming discourse. Specifically, we consider the detection of the first bit

transmitted by the reference user. According to the results obtained in Section 5.11.2, it can be shown that the decision variable Z_{10} for the first bit of the reference user can be written as

$$Z_{10} = Z_{D0} + \sum_{u=1}^{U-1} Z_{Du} + \sum_{k=2}^K \sum_{u=0}^{U-1} Z_{kI,u} + N_{10} \quad (5.253)$$

where Z_{D0} is the desired output, which can be expressed as

$$Z_{D0} = \mathbf{R}_1(0, 0)b_0 = \left(\frac{1}{N_p} \sum_{v=0}^{N_p-1} |h_v|^2 \right) b_0 \quad (5.254)$$

In (5.253) Z_{Du} represents the interference imposed by the u th bit of the reference user on the desired bit, which is given by

$$Z_{Du} = \mathbf{R}_1(0, u)b_u = \left(\frac{1}{N_p} \sum_{v=0}^{N_p-1} |h_v|^2 c_{f0,v} c_{fu,v}^{(k)} \right) b_u \quad (5.255)$$

In (5.253) $Z_{kI,u}$ represents the interference imposed by the u th bit of the k th user on the desired bit, which, according to (5.251), can be represented as

$$Z_{kI,u} = \mathbf{R}_{k1}(0, u)(\mathbf{c}_1^T \mathbf{c}_k)b_u^{(k)} = \left(\frac{1}{N_p} \sum_{v=0}^{N_p-1} h_v^* h_v^{(k)} c_{f0,v} c_{fu,v}^{(k)} \right) (\mathbf{c}_1^T \mathbf{c}_k) b_u^{(k)} \quad (5.256)$$

where $\mathbf{c}_1^T \mathbf{c}_k$ is due to the cross-correlation between the T-domain spreading sequences \mathbf{c}_1 and \mathbf{c}_k , while $\sum_{v=0}^{N_p-1} h_v^* h_v^{(k)} c_{f0,v} c_{fu,v}^{(k)} / N_p$ is the result of the cross-correlation between the F-domain spreading sequences $\mathbf{c}_{f0}^{(1)}$ and $\mathbf{c}_{fu}^{(k)}$. Finally, in (5.253) N_{10} is a complex Gaussian random variable, which has zero mean and a variance of

$$\sigma_{10}^2 = \left(\frac{1}{N_p} \sum_{v=0}^{N_p-1} |h_v|^2 \right) \frac{N_0}{2E_b} \quad (5.257)$$

per dimension.

Let us assume that both the F-domain spreading sequences and T-domain spreading sequences are constituted by random sequences. Then Z_{Du} of (5.255) and $Z_{kI,u}$ of (5.256) can be expressed equivalently as

$$\begin{aligned} Z_{Du} &= \left(\frac{1}{N_p} \sum_{v=0}^{N_p-1} |h_v|^2 c_{fu,v} \right) b_u \\ Z_{kI,u} &= \left(\frac{1}{N_p} \sum_{v=0}^{N_p-1} h_v^* h_v^{(k)} c_{fu,v}^{(k)} \right) (\mathbf{c}_1^T \mathbf{c}_k) b_u^{(k)} \end{aligned} \quad (5.258)$$

Let the interbit interference plus the MUI be expressed as

$$I_{10} = \sum_{u=1}^{U-1} Z_{Du} + \sum_{k=2}^K \sum_{u=0}^{U-1} Z_{kI,u} \quad (5.259)$$

and let

$$\Psi = \text{Var}[I_{10} | \mathbf{H}_1, \mathcal{C}_f, \mathcal{C}_t] \quad (5.260)$$

where \mathcal{C}_f and \mathcal{C}_t contain all the possible F-domain and T-domain spreading sequences, while \mathbf{H}_1 contains the possible channel gains of the interfering users. Assuming that the source bits are i.i.d. random variables, then it can be shown that Ψ can be expressed as

$$\Psi = \sum_{u=1}^{U-1} |Z_{Du}|^2 + \sum_{k=2}^K \sum_{u=0}^{U-1} |Z_{kl,u}|^2 \quad (5.261)$$

Below, we derive the mean and variance of Ψ , which are expressed respectively as

$$\begin{aligned} \mu_\Psi &= E[\Psi] \\ \sigma_\Psi^2 &= E[(\Psi - \mu_\Psi)^2] \end{aligned} \quad (5.262)$$

Note that these terms are required to compute the BER, when the standard Gaussian approximation (SGA) [82, 94] or the simplified improved Gaussian approximation (SIGA) [94, 95] is invoked.

Let us first derive μ_Ψ . Due to the random characteristics of both the data bits and the T-domain as well as F-domain spreading sequences, with the aid of (5.258) and (5.259), it can be easily shown that μ_Ψ can be expressed as

$$\begin{aligned} \mu_\Psi &= \sum_{u=1}^{U-1} E[|Z_{Du}|^2] + \sum_{k=2}^K \sum_{u=0}^{U-1} E[|Z_{kl,u}|^2] \\ &= \frac{(U-1)}{N_p^2} \sum_{v=0}^{N_p-1} |h_v|^4 + \frac{U}{N_t N_p^2} \sum_{k=2}^K \sum_{v=0}^{N_p-1} |h_v|^2 E[|h_v^{(k)}|^2] \end{aligned} \quad (5.263)$$

Using the properties of the Nakagami- m distribution that $E[|h_v^{(k)}|^2] = \Omega$, as shown in (5.1), we arrive at

$$\mu_\Psi = \frac{(U-1)}{N_p^2} \sum_{v=0}^{N_p-1} |h_v|^4 + \frac{(K-1)U\Omega}{N_t N_p^2} \sum_{v=0}^{N_p-1} |h_v|^2 \quad (5.264)$$

$$= (U-1)\mu_1 + (K-1)U\mu_k \quad (5.265)$$

where, by definition,

$$\begin{aligned} \mu_1 &= \frac{1}{N_p^2} \sum_{v=0}^{N_p-1} |h_v|^4 \\ \mu_k &= \frac{\Omega}{N_t N_p^2} \sum_{v=0}^{N_p-1} |h_v|^2 \end{aligned} \quad (5.266)$$

The variance σ_Ψ^2 seen in (5.262) is derived in Appendix 5.C, which is

$$\sigma_\Psi^2 = \frac{2(U-1)}{N_p^4} \sum_{v=0}^{N_p-1} \sum_{m=0}^{N_p-1} |h_v|^4 |h_m|^4 + \frac{2(K-1)U\Omega^2}{N_t^2 N_p^4} \sum_{v=0}^{N_p-1} \sum_{m=0}^{N_p-1} |h_v|^2 |h_m|^2 \quad (5.267)$$

Having obtained the mean and variance of the interference power of Ψ , as shown in (5.264) and (5.267), below, we derive the BER expressions for the TF-domain spread MC DS-CDMA, when the SGA or SIGA is used.

5.11.4 Bit-Error Rate (BER) Analysis

In this section we derive the BER expression of the TF-domain spread MC DS-CDMA, when either the SGA or SIGA is invoked. We first derive the BER expression when the SGA is invoked for approximation of the interbit interference and MUI.

5.11.4.1 Standard Gaussian Approximation

When the SGA is invoked, the decision variable Z_{10} is approximated as a Gaussian random variable, whose mean and variance of the real part are given respectively by

$$E[\Re\{Z_{10}\}] = Z_{D0} = \left(\frac{1}{N_p} \sum_{v=0}^{N_p-1} |h_v|^2 \right) b_0 \quad (5.268)$$

$$\begin{aligned} \text{Var}[\Re\{Z_{10}\}] &= \sigma_{10}^2 + \frac{1}{2}\mu_\Psi \\ &= \left(\frac{1}{N_p} \sum_{v=0}^{N_p-1} |h_v|^2 \right) \frac{N_0}{2E_b} + \frac{(U-1)}{2N_p^2} \sum_{v=0}^{N_p-1} |h_v|^4 + \frac{(K-1)U\Omega}{2N_t N_p^2} \sum_{v=0}^{N_p-1} |h_v|^2 \end{aligned} \quad (5.269)$$

where the factor of $1/2$ before μ_Ψ is due to the fact that only the real part of Z_{10} is required in order to estimate b_0 of the reference user.

So that the problem is manageable, in (5.269) the term related to the interbit interference is approximated as

$$\frac{(U-1)}{2N_p^2} \sum_{v=0}^{N_p-1} |h_v|^4 = \frac{(U-1)\Omega}{2N_p^2} \sum_{v=0}^{N_p-1} |h_v|^2 \quad (5.270)$$

i.e. one of the $|h_v|^2$ is replaced by its average Ω . In this case, the variance of $\text{Var}[\Re\{Z_{10}\}]$ can be expressed as

$$\text{Var}[\Re\{Z_{10}\}] = \frac{1}{2} \left(\frac{1}{N_p} \sum_{v=0}^{N_p-1} |h_v|^2 \right) \Omega \left[\left(\frac{\Omega E_b}{N_0} \right)^{-1} + \frac{(U-1)}{N_p} + \frac{(K-1)U}{N_t N_p} \right] \quad (5.271)$$

Based on (5.268) and (5.271), the BER of the TF-domain spread MC DS-CDMA conditioned on $\{|h_v|^2\}_{v=0}^{N_p-1}$ can be represented as

$$\begin{aligned} P_b(|h_0|^2, |h_1|^2, \dots, |h_{N_p-1}|^2) &= Q\left(\sqrt{\frac{E^2[\Re\{Z_{10}\}]}{\text{Var}[\Re\{Z_{10}\}]}}\right) \\ &= Q(\sqrt{2\gamma}) \end{aligned} \quad (5.272)$$

where γ is the instantaneous SNR, which is given by

$$\begin{aligned}\gamma &= \frac{1}{2} \frac{E^2[\Re\{Z_{10}\}]}{\text{Var}[\Re\{Z_{10}\}]} = \sum_{v=0}^{N_p-1} \gamma_v \\ \gamma_v &= \frac{|h_v|^2}{\Omega} \gamma_c \\ \gamma_c &= \frac{1}{N_p} \left[\left(\frac{\Omega E_b}{N_0} \right)^{-1} + \frac{(U-1)}{N_p} + \frac{(K-1)U}{N_t N_p} \right]^{-1}\end{aligned}\quad (5.273)$$

where γ_c represents the average SNR observed on a subcarrier channel.

Invoking the representation of (5.90) for the Q -function and following the analysis in Section 5.6.2, it can be shown that the average BER of the TF-domain spread MC DS-CDMA when communicating over Nakagami- m fading channels can be expressed as

$$P_b = \frac{1}{\pi} \int_0^{\pi/2} \det \left(\mathbf{I} + \frac{\gamma_c}{m \sin^2 \theta} \mathbf{M} \right)^{-m} d\theta \quad (5.274)$$

where \mathbf{M} is a $(N_p \times N_p)$ symmetric covariance matrix of the ‘accompanying’ Gaussian distribution, which can be expressed as [145]

$$\mathbf{M} = \begin{bmatrix} 1 & \sqrt{\rho_{01}} & \cdots & \sqrt{\rho_{0(N_p-1)}} \\ \sqrt{\rho_{10}} & 1 & \cdots & \sqrt{\rho_{1(N_p-1)}} \\ \vdots & \vdots & \ddots & \vdots \\ \sqrt{\rho_{(N_p-1)0}} & \sqrt{\rho_{(N_p-1)1}} & \cdots & 1 \end{bmatrix} \quad (5.275)$$

where ρ_{ij} represents the correlation coefficient between $|h_i|^2$ and $|h_j|^2$ corresponding to the i th and j th subcarrier channels, respectively. The correlation coefficient ρ_{ij} is given by (5.5) when the excess delay spread obeys the exponential distribution, but given by (5.7) when the excess delay spread obeys the uniform distribution.

Let $\{\lambda_j\}_0^{N_p-1}$ be the eigenvalues of \mathbf{M} . Then, the average BER of (5.274) can alternatively be expressed as

$$\begin{aligned}P_b &= \frac{1}{\pi} \int_0^{\pi/2} \prod_{j=0}^{N_p-1} \left(1 + \frac{\lambda_j \gamma_c}{m \sin^2 \theta} \right)^{-m} d\theta \\ &= \frac{1}{\pi} \int_0^{\pi/2} \prod_{j=0}^{N_p-1} \left(\frac{m \sin^2 \theta}{\lambda_j \gamma_c + m \sin^2 \theta} \right)^m d\theta\end{aligned}\quad (5.276)$$

Hence, once the covariance matrix \mathbf{M} of (5.275) is known, the average BER can be readily evaluated using (5.276).

Note that in (5.276) $(m \sin^2 \theta / (\lambda_j \gamma_c + m \sin^2 \theta)) \leq (m / (\lambda_j \gamma_c + m))$. Hence the BER of the TF-domain spread MC DS-CDMA is upper-bounded as

$$P_b \leq \frac{1}{2} \prod_{j=0}^{N_p-1} \frac{m}{\lambda_j \gamma_c + m} \quad (5.277)$$

Note, furthermore, that the BER expressions for the special cases where the subcarriers experience independent fading and frequency nonselective fading can be obtained by following approaches similar to those shown in Section 5.6.2. Let us now derive the BER expression, when the SIGA is invoked.

5.11.4.2 Simplified Improved Gaussian Approximation

To derive the BER expression under the SIGA, the BER of the TF-domain spread MC DS-CDMA is expressed in terms of the variable Ψ as $P_b(\Psi)$, where the variable Ψ is given by (5.261). Then, following reference [95], $P_b(\Psi)$ can be expanded in differential form as

$$\begin{aligned} P_b(\Psi) &= P_b(\mu_\Psi) + (\Psi - \mu_\Psi) \frac{P_b(\mu_\Psi + h) - P_b(\mu_\Psi - h)}{2h} \\ &\quad + \frac{1}{2}(\Psi - \mu_\Psi)^2 \frac{P_b(\mu_\Psi + h) - 2P_b(\mu_\Psi) + P_b(\mu_\Psi - h)}{h^2} + \dots \end{aligned} \quad (5.278)$$

where μ_Ψ is given in (5.262). Taking the expectations with respect to Ψ and using the first three terms for the approximation, we can obtain the approximation to the BER, which is

$$P_b = E[P_b(\Psi)] \approx P_b(\mu_\Psi) + \frac{1}{2} \frac{P_b(\mu_\Psi + h) - 2P_b(\mu_\Psi) + P_b(\mu_\Psi - h)}{h^2} \sigma_\Psi^2 \quad (5.279)$$

where σ_Ψ^2 is given in (5.262).

The value of h in (5.279) may be chosen so that the BER computed according to (5.279) approximates the true BER value as closely as possible. According to reference [95], it is suggested that $h = \sqrt{3}\sigma_\Psi$ is appropriate, yielding

$$P_b \approx \frac{2}{3}P_b(\mu_\Psi) + \frac{1}{6}P_b(\mu_\Psi + \sqrt{3}\sigma_\Psi) + \frac{1}{6}P_b(\mu_\Psi - \sqrt{3}\sigma_\Psi) \quad (5.280)$$

In the context of the TF-domain spread MC DS-CDMA communicating over frequency-selective fading channels, the BER of (5.280) is still conditional on the channel gains of the N_p subcarriers, which can be represented explicitly as

$$P_b(|h_0|^2, |h_1|^2, \dots, |h_{N_p-1}|^2) \approx \frac{2}{3}P_b(\mu_\Psi) + \frac{1}{6}P_b(\mu_\Psi + \sqrt{3}\sigma_\Psi) + \frac{1}{6}P_b(\mu_\Psi - \sqrt{3}\sigma_\Psi) \quad (5.281)$$

where, according to our analysis previously in the context of SGA, $P_b(x)$ is defined as

$$P_b(x) = Q\left(\sqrt{\frac{E^2[\Re\{Z_{10}\}]}{0.5x + \sigma_{10}^2}}\right) \quad (5.282)$$

where x represents μ_Ψ , $\mu_\Psi + \sqrt{3}\sigma_\Psi$ or $\mu_\Psi - \sqrt{3}\sigma_\Psi$. Furthermore, from (5.282) we imply that $\sigma_{10}^2 + (\mu_\Psi - \sqrt{3}\sigma_\Psi)/2 \geq 0$ should be satisfied.

In more detail, in (5.281) $P_b(\mu_\Psi)$ can be denoted as

$$P_b(\mu_\Psi) = Q(\sqrt{2\gamma}) \quad (5.283)$$

where γ has been defined in (5.273). $P_b(\mu_\Psi + \sqrt{3}\sigma_\Psi)$ in (5.281) can be expressed as

$$P_b(\mu_\Psi + \sqrt{3}\sigma_\Psi) = Q(\sqrt{2\gamma_a}) \quad (5.284)$$

Let us approximate σ_Ψ^2 in (5.267) by

$$\begin{aligned}\sigma_\Psi^2 &\approx \frac{2(U-1)\Omega^2}{N_p^4} \sum_{v=0}^{N_p-1} \sum_{m=0}^{N_p-1} |h_v|^2 |h_m|^2 + \frac{2(K-1)U\Omega^2}{N_t^2 N_p^4} \sum_{v=0}^{N_p-1} \sum_{m=0}^{N_p-1} |h_v|^2 |h_m|^2 \\ &= \left(\frac{\Omega}{N_p} \sum_{v=0}^{N_p-1} |h_v|^2 \right)^2 \left[\frac{2(U-1)}{N_p^2} + \frac{2(K-1)U}{N_t^2 N_p^2} \right]\end{aligned}\quad (5.285)$$

Then, γ_a in (5.284) can be expressed as

$$\begin{aligned}\gamma_a &= \frac{1}{2} \frac{E^2[\Re\{Z_{10}\}]}{\text{Var}[\Re\{Z_{10}\}] + \sqrt{3}\sigma_\Psi/2} = \sum_{v=0}^{N_p-1} \gamma_{av} \\ \gamma_{av} &= \frac{|h_v|^2}{\Omega} \gamma_{ac} \\ \gamma_{ac} &= \frac{1}{N_p} \left[\left(\frac{\Omega E_b}{N_0} \right)^{-1} + \frac{(U-1)}{N_p} + \frac{(K-1)U}{N_t N_p} + \sqrt{6} \left[\frac{(U-1)}{N_p^2} + \frac{(K-1)U}{N_t^2 N_p^2} \right]^{1/2} \right]^{-1}\end{aligned}\quad (5.286)$$

Similarly, in (5.281) $P_b(\mu_\Psi - \sqrt{3}\sigma_\Psi)$ can be expressed as

$$P_b(\mu_\Psi - \sqrt{3}\sigma_\Psi) = Q(\sqrt{2\gamma_b}) \quad (5.287)$$

associated with

$$\begin{aligned}\gamma_b &= \frac{1}{2} \frac{E^2[\Re\{Z_{10}\}]}{\text{Var}[\Re\{Z_{10}\}] - \sqrt{3}\sigma_\Psi/2} = \sum_{v=0}^{N_p-1} \gamma_{bv} \\ \gamma_{bv} &= \frac{|h_v|^2}{\Omega} \gamma_{bc} \\ \gamma_{bc} &= \frac{1}{N_p} \left[\left(\frac{\Omega E_b}{N_0} \right)^{-1} + \frac{(U-1)}{N_p} + \frac{(K-1)U}{N_t N_p} - \sqrt{6} \left[\frac{(U-1)}{N_p^2} + \frac{(K-1)U}{N_t^2 N_p^2} \right]^{1/2} \right]^{-1}\end{aligned}\quad (5.288)$$

From (5.283), (5.284) and (5.287), we can see that the three parts in (5.281) for computing the BER of the TF-domain spread MC DS-CDMA are similar, which can be expressed in a general form as

$$P_b(|h_0|^2, |h_1|^2, \dots, |h_{N_p-1}|^2; \gamma_g) = Q(\sqrt{2\gamma_g}) \quad (5.289)$$

associated with

$$\begin{aligned}\gamma_g &= \sum_{v=0}^{N_p-1} \gamma_{gv} \\ \gamma_{gv} &= \frac{|h_v|^2}{\Omega} \gamma_{gc}\end{aligned}\quad (5.290)$$

According to the analysis under the SGA, after averaging $P_b(|h_0|^2, |h_1|^2, \dots, |h_{N_p-1}|^2; \gamma_g)$ with respect to $|h_0|^2, |h_1|^2, \dots, |h_{N_p-1}|^2$, we have

$$P_b(\gamma_{gc}) = \frac{1}{\pi} \int_0^{\pi/2} \prod_{j=0}^{N_p-1} \left(\frac{m \sin^2 \theta}{\lambda_j \gamma_{gc} + m \sin^2 \theta} \right)^m d\theta \quad (5.291)$$

where $\{\lambda_j\}_0^{N_p-1}$ are the eigenvalues of the matrix \mathbf{M} seen in (5.275).

Consequently, when the SIGA is invoked, the average BER of the TF-domain spread MC DS-CDMA can be expressed as

$$\begin{aligned} P_b \approx & \frac{2}{3\pi} \int_0^{\pi/2} \prod_{j=0}^{N_p-1} \left(\frac{m \sin^2 \theta}{\lambda_j \gamma_c + m \sin^2 \theta} \right)^m d\theta + \frac{1}{6\pi} \int_0^{\pi/2} \prod_{j=0}^{N_p-1} \left(\frac{m \sin^2 \theta}{\lambda_j \gamma_{ac} + m \sin^2 \theta} \right)^m d\theta \\ & + \frac{1}{6\pi} \int_0^{\pi/2} \prod_{j=0}^{N_p-1} \left(\frac{m \sin^2 \theta}{\lambda_j \gamma_{bc} + m \sin^2 \theta} \right)^m d\theta \end{aligned} \quad (5.292)$$

Note that in order to use (5.292), the condition of $\sigma_{10}^2 + (\mu_\Psi - \sqrt{3}\sigma_\Psi)/2 \geq 0$ should be satisfied, which requires in (5.288) that

$$\left(\frac{\Omega E_b}{N_0} \right)^{-1} + \frac{(U-1)}{N_p} + \frac{(K-1)U}{N_t N_p} - \sqrt{6} \left[\frac{(U-1)}{N_p^2} + \frac{(K-1)U}{N_t^2 N_p^2} \right]^{1/2} \geq 0 \quad (5.293)$$

Let us now demonstrate some performance results.

5.11.5 Performance Results

Figure 5.16 illustrates the BER performance results of the TF-domain spread MC DS-CDMA systems that were evaluated using SGA of (5.276) or SIGA of (5.292). Figure 5.16(a) considers the frequency-selective Rayleigh fading channels, while Fig. 5.16(b) the frequency-selective Nakagami- m fading channels associated with $m = 1.5$. In Fig. 5.16 the delay spread of the wireless channels denotes the normalized delay spread, which was obtained as $\tau_{\text{Norm}} = T_m/UT_b$, where T_m is the maximum delay spread of the wireless channels. In our evaluations in this section we assumed that the delay spread obeys the uniform distribution, which yields that the F-domain correlation coefficient between two subcarriers is given by (5.8). Note that, although no simulation results are shown in Fig. 5.16, however, as illustrated in [95], the BER evaluation based on the SIGA is usually very close to that obtained by simulation.

From the results in Fig. 5.16, we can observe that the SGA approach generally underestimates the BER that is achievable in practice or, in other words, the evaluated BER using the SGA is too optimistic in comparison with the actually achievable BER. However, the evaluated BER using the SGA is very close to that obtained based on the SIGA, when the average SNR per bit value is relatively low. This might be because, in this case, the background noise dominates the achievable BER performance. As shown in Fig. 5.16, the evaluated BER using the SGA approach is also very close to that obtained by the SIGA approach, when the number of supported users is relatively high. The reason for this observation is that the MUI is near-Gaussian distributed, when the number of supported users is high. Furthermore, the results of Fig. 5.16 show that the BER performance degrades significantly due to the increased MUI, when the number of supported users increases.

Figure 5.17 shows the effect of the frequency selectivity of communication channels on the achievable BER performance of the TF-domain spread MC DS-CDMA systems.

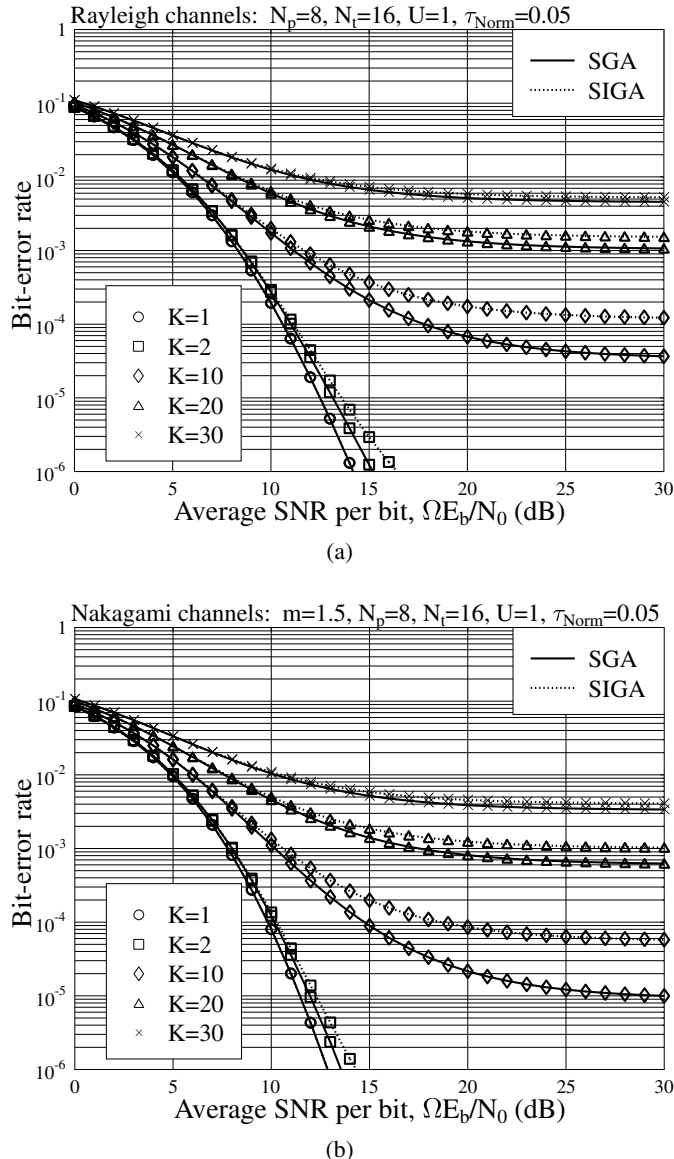


Figure 5.16: BER versus average SNR per bit performance of the TF-domain spread MC-DS CDMA systems over frequency-selective fading channels with the delay spread obeying the uniform distribution; (a) Rayleigh fading channels, $m = 1$; (b) Nakagami fading channels, $m = 1.5$.

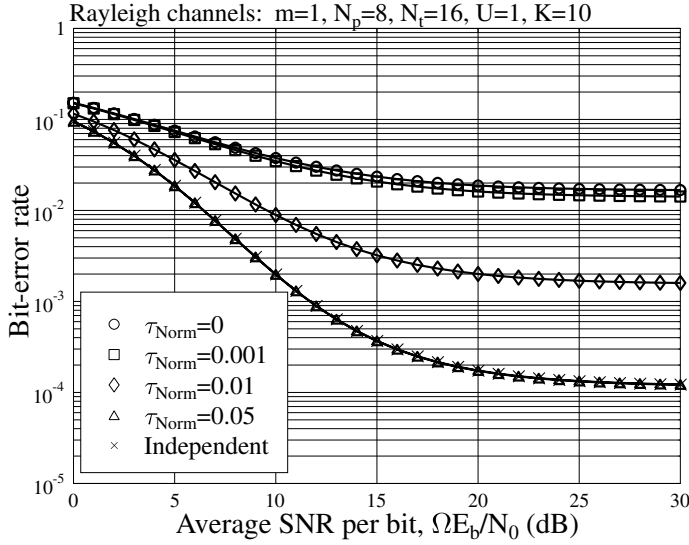


Figure 5.17: BER versus average SNR per bit performance of the TF-domain spread MC-DS CDMA systems, when communicating over frequency-selective Nakagami- m fading channels with various amounts of delay spread, assumed to obey the uniform distribution.

Since the frequency-diversity gain becomes higher, when the delay spread of the communication channels increases, as shown in Fig. 5.17, the BER performance improves as the delay spread of the communication channels increases. From Fig. 5.17, we can see that the subcarrier signals experience nearly independent fading, when the normalized delay spread of the communication channels is about $\tau_{Norm} = 0.05$. Accordingly, as shown in Fig. 5.17, the BER performance corresponding to $\tau_{Norm} = 0.05$ cannot be distinguished from that achieved by the TF-domain spread MC DS-CDMA, when communicating over the wireless channels, hence the subcarrier signals experience independent fading.

Finally, Fig. 5.18 shows the effect of the fading severity on the achievable BER performance of the TF-domain spread MC DS-CDMA systems. As shown in Fig. 5.18, the BER performance improves when the value of m increases, resulting in the subcarrier channels experiencing less severe fading.

5.12 Summary and Discussion

In this chapter the multicarrier communications in wireless frequency-selective fading channels have been considered. We first illustrate the impact of frequency-selective fading on the various multicarrier communications schemes. It is shown that, with the multicarrier transmission, except for the multitone DS-CDMA, the frequency-selective fading channels can be transformed to a range of parallel subcarrier channels conflicting flat fading. Consequently, the ISI may be readily mitigated with the aid of one-step low-complexity

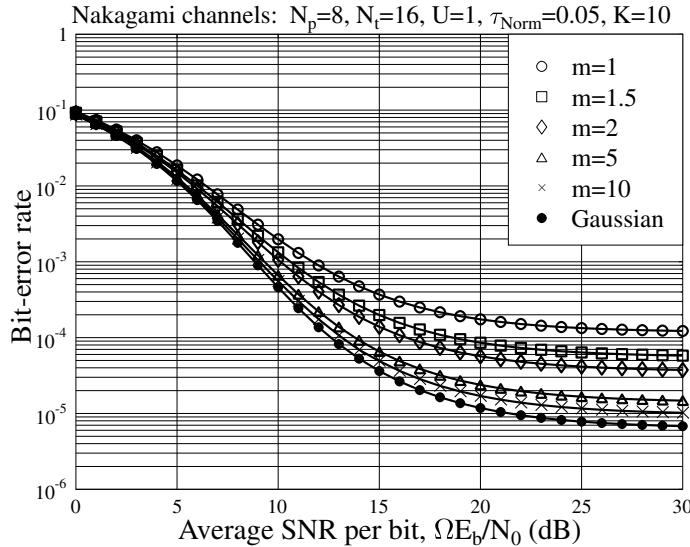


Figure 5.18: BER versus average SNR per bit performance of the TF-domain spread MC-DS CDMA systems, when communicating over frequency-selective Nakagami- m fading channels with various degrees of fading severity.

equalization. Then, the ISI-mitigation principles of using CP and ZP were established. The condition for using CP or ZP to control the ISI is analysed, and it is shown that the ISI in a conventional multitone DS-CDMA system cannot be removed by using CP or ZP techniques.

The BER performance of various multicarrier communication schemes is investigated over the frequency-selective Nakagami fading channels. Furthermore, the BER performance of the SC-FDMA and the single-carrier DS-CDMA using F-domain equalization is investigated. In Section 5.11 the BER performance of the generalized TF-domain spread MC DS-CDMA systems is analysed, when the SGA or SIGA is invoked in order to cope with the MUI. From this analysis and the performance results provided, the main characteristics of the various communication schemes considered in this chapter may be briefly summarized as follows.

The OFDM scheme considered in Section 5.5 can take the advantages of FFT/IFFT for implementation of multicarrier modulation/demodulation. It achieves the same BER performance as a corresponding conventional narrow-band communication scheme. However, it cannot make use of the frequency-selective fading to achieve frequency diversity, when without introducing redundancy by, such as, using error-control coding. If error-control coding is invoked for transmission, a certain frequency diversity may be achieved by sending the coded symbols of a codeword on different subcarriers. The OFDM scheme is not suitable for supporting multiple-access communications. Furthermore, the OFDM signals may experience severe PAPR problems.

The F-domain spread MC-CDMA scheme in Section 5.6 can be viewed as the extension of the OFDM scheme in Section 5.5 by introducing F-domain spreading. For this reason, F-domain spreading MC-CDMA is also referred to as the spreading OFDM. The F-domain

spread MC-CDMA scheme has all the advantages of the OFDM scheme. Additionally, the F-domain spread MC-CDMA scheme is suitable for supporting multiple-access communications and it is capable of achieving frequency diversity. The F-domain spread MC-CDMA signals may experience severe PAPR problems. Furthermore, due to the frequency-selective fading, the F-domain spread MC-CDMA systems may conflict severe MUI. Advanced detection schemes may be required in order to mitigate the MUI efficiently.

The MC DS-CDMA scheme in Section 5.9 can mitigate the PAPR problem, since the number of subcarriers is usually low after the employment of DS spreading associated with each subcarrier. It is capable of achieving frequency diversity by transmitting the same data symbol over several subcarrier channels. Since the number of subcarriers after using DS spreading is usually low, FFT-based multicarrier modulation/demodulation might not result in any benefits for complexity reduction. Furthermore, for a given system bandwidth, the spreading factor of each subcarrier decreases when a data symbol is repeated on more subcarriers for achieving higher frequency-diversity. This implies that there exists a trade-off between the number of users supportable and the frequency diversity achievable.

Therefore, F-domain spreading is invoked in the MC DS-CDMA scheme, yielding the TF-domain spread MC DS-CDMA scheme, as studied in Section 5.11. The TF-domain spread MC DS-CDMA scheme has all the advantages of the MC DS-CDMA scheme as detailed in Section 5.9. It is also free from the trade-off between the number of users supportable and the frequency diversity achievable. However, powerful detection schemes may be required in the TF-domain spread MC DS-CDMA systems, in order to suppress MUI. Note that the TF-domain MC DS-CDMA scheme represents the extension of the OFDM in Section 5.5, the F-domain spread MC-CDMA in Section 5.6 as well as the MC DS-CDMA in Section 5.9.

The SC-FDMA scheme in Section 5.7 can efficiently solve the PAPR problem conflicted by the OFDM systems. It is suitable for supporting uplink multiple-access communications. The SC-FDMA, especially the IFDMA scheme, is capable of achieving certain frequency diversity. Both the IFDMA and LFDMA are free from MUI. However, both of them conflict severe intrauser intersymbol interference, which is essential to mitigate in order to benefit from the frequency selectivity of the wireless channels.

Section 5.8 illustrates that in the single-carrier DS-CDMA system the receiver may take the advantage of the F-domain signal-processing techniques by transforming the single-carrier DS-CDMA signals from the T-domain to the F-domain, yielding the multicarrier-like signals. Since the single-carrier DS-CDMA scheme conflicts no PAPR problem, it is suitable for uplink transmission. Furthermore, the F-domain-based detection allows the single-carrier DS-CDMA scheme to achieve full diversity created by the frequency-selective fading.

All the above-mentioned communication schemes considered in this chapter are for coherent communications. In Section 5.10 the TH/MC-CDMA scheme is for noncoherent communications. The TH/MC-CDMA scheme can benefit from the multicarrier modulation of allowing to achieve frequency diversity. It does not conflict the PAPR problem. It is suitable for multiple-access communications. Furthermore, it may constitute a promising communications scheme for supporting UWB communications, due to the employment of MPPM modulation and time-hopping.

Of the above communication schemes, some may be extended or combined in order for them to be applied to practical systems to enhance their performance or mitigate some implementation problems. For example, the SC-FDMA scheme may be combined with the single-carrier DS-CDMA scheme in order to enhance the multiple-access capability

of the SC-FDMA system. The F-domain equalization principle may be extended to the various MC DS-CDMA schemes, such as to the MC DS-CDMA scheme considered in Section 5.9 or to the TF-domain spread MC DS-CDMA scheme considered in Section 5.11. The advantages of applying the F-domain equalization techniques to the MC DS-CDMA schemes are at least twofold. First, the F-domain equalization techniques may be applied to the existing MC DS-CDMA systems, such as that defined in the 3GPP cdma2000 standards, in order for them to take advantage of the F-domain signal processing. Second, the F-domain equalization techniques may be applied to the MC DS-CDMA systems to simplify their implementation, when broadband or UWB communications are considered. In OFDM-based or single-carrier DS-CDMA-based broadband or UWB communications, owing to the huge system bandwidth, the number of subcarriers in the OFDM systems will be very high, while the chip rate in the single-carrier DS-CDMA systems will also be very high. Both situations demand high-rate signal processing, remembering that, in an OFDM system, the chip rate of the T-domain transmitted signals is equivalent to that of the single-carrier DS-CDMA signals, which occupy the same bandwidth as the OFDM system. In order to reduce the signal processing rate, the MC DS-CDMA scheme without using the FFT-based multicarrier modulation/demodulation may be used to support the broadband or UWB communications. Since in the MC DS-CDMA broadband or UWB systems each subcarrier occupies only a fraction of the whole system bandwidth, the systems can use relative low-rate signal processing. At the receiver, after transformation of the subcarrier DS-CDMA signals from the T-domain to the F-domain, the MC DS-CDMA broadband or UWB systems can still benefit from the advantages provided by the F-domain equalization techniques.

Appendix 5.A $\int_0^\infty Q(\sqrt{2\gamma}) f(\gamma) d\gamma$

In this appendix we derive in detail the closed form for the average BER of

$$P_b = \int_0^\infty Q(\sqrt{2\gamma}) f(\gamma) d\gamma \quad (5.A.1)$$

After substituting $Q(x)$ and $f(\gamma)$ of (5.72) into the above equation, we have

$$P_b = \frac{1}{\sqrt{2\pi}\Gamma(m)} \left(\frac{m}{\gamma_c} \right)^m \int_0^\infty d\gamma \int_{\sqrt{2\gamma}}^\infty \exp\left(-\frac{t^2}{2}\right) \gamma^{m-1} \exp\left(-\frac{m\gamma}{\gamma_c}\right) dt \quad (5.A.2)$$

Exchanging the integration order gives

$$P_b = \frac{1}{\sqrt{2\pi}\Gamma(m)} \left(\frac{m}{\gamma_c} \right)^m \int_0^\infty \exp\left(-\frac{t^2}{2}\right) dt \int_0^{t^2/2} \gamma^{m-1} \exp\left(-\frac{m\gamma}{\gamma_c}\right) d\gamma \quad (5.A.3)$$

With the aid of (3.381.1) in [152], the second integral can be expressed as

$$\int_0^{t^2/2} \gamma^{m-1} \exp\left(-\frac{m\gamma}{\gamma_c}\right) d\gamma = \left(\frac{\gamma_c}{m} \right)^m \gamma\left(m, \frac{mt^2}{2\gamma_c}\right) \quad (5.A.4)$$

where $\gamma(\alpha, x)$ is the incomplete gamma function, which is defined as [152]

$$\gamma(\alpha, x) = \int_0^x e^{-t} t^{\alpha-1} dt, [\Re\{\alpha\} > 0] \quad (5.A.5)$$

Substitute (5.A.4) into (5.A.3),

$$P_b = \frac{1}{\sqrt{2\pi}\Gamma(m)} \int_0^\infty \exp\left(-\frac{t^2}{2}\right) \gamma\left(m, \frac{mt^2}{2\gamma_c}\right) dt \quad (5.A.6)$$

Using the variable transform of $y = t^2/2$, the above equation can be converted to

$$P_b = \frac{1}{2\sqrt{\pi}\Gamma(m)} \int_0^\infty y^{-1/2} e^{-y} \gamma\left(m, \frac{my}{\gamma_c}\right) dy \quad (5.A.7)$$

Now, we can use (6.455.2) of [152] to obtain

$$P_b = \frac{\Gamma(m + 1/2)}{2\sqrt{\pi}\Gamma(m + 1)} \sqrt{\frac{\gamma_c}{m + \gamma_c}} \left(\frac{m}{m + \gamma_c}\right)^m {}_2F_1\left(1, m + \frac{1}{2}; m + 1; \frac{m}{m + \gamma_c}\right) \quad (5.A.8)$$

where ${}_2F_1(a, b; c; z)$ is the hypergeometric function defined as [115] ${}_2F_1(a, b; c; z) = \sum_{k=0}^{\infty} \frac{(a)_k(b)_k z^k}{(c)_k k!}$ and $(a)_k = a(a+1)\cdots(a+k-1)$, $(a)_0 = 1$.

Note that if it is a Rayleigh fading channel associated with $m = 1$, from (5.A.3) we obtain

$$P_b = \frac{1}{\sqrt{2\pi}\gamma_c} \int_0^\infty \exp\left(-\frac{t^2}{2}\right) dt \int_0^{t^2/2} \exp\left(-\frac{\gamma}{\gamma_c}\right) d\gamma \quad (5.A.9)$$

It can be easily shown that in this case the average BER is given by

$$P_b = \frac{1}{2} \left(1 - \sqrt{\frac{\gamma_c}{1 + \gamma_c}} \right) \quad (5.A.10)$$

Furthermore, comparing (5.A.8) associated with $m = 1$ with (5.A.10), we obtain

$${}_2F_1\left(1, \frac{3}{2}; 2; x\right) = \frac{1}{x} \left(\sqrt{\frac{1}{1-x}} - 1 \right) \quad (5.A.11)$$

Appendix 5.B $E[\exp(-\sum_{j=1}^N (\gamma_j / \sin^2 \theta))]$ in Correlated Nakagami- m Fading

First, Nakagami in reference [108] showed that the Nakagami- m distribution, referred to as m -distribution in reference [108], could be obtained by generalization from the Rayleigh distribution. In more detail, let

$$r^2 = \alpha_1^2 + \alpha_2^2 + \cdots + \alpha_m^2 \quad (5.B.12)$$

where m at moment is assumed to be a positive number, and α_i is assume to obey the i.i.d. Rayleigh PDF given by

$$f_{\alpha_i}(r_i) = \frac{2r_i}{\Omega/m} \exp\left(-\frac{r_i^2}{\Omega/m}\right) \quad (5.B.13)$$

Then, according to [2], γ in (5.B.12) obeys the central χ^2 -distribution with $2m$ degrees of freedom and the PDF is

$$f(r) = \frac{2}{\Gamma(m)} \left(\frac{m}{\Omega} \right)^m r^{2m-1} \exp\left(-\frac{m}{\Omega}r^2\right), \quad R \geq 0 \quad (5.B.14)$$

which is the same as (5.1).

Although the Nakagami- m PDF of (5.B.14) is derived by assuming that m is a positive number, however, according the necessary and sufficient conditions of a probability distribution, the PDF of (5.B.14) is in fact valid for any positive m value, provided that $m \geq 1/2$. The reason for $m \geq 1/2$ becomes clear when we express (5.B.12) as

$$r^2 = \underbrace{X_{1I}^2 + X_{1Q}^2}_{\alpha_1^2} + \underbrace{X_{2I}^2 + X_{2Q}^2}_{\alpha_2^2} + \cdots + \underbrace{X_{mI}^2 + X_{mQ}^2}_{\alpha_m^2} \quad (5.B.15)$$

where X_{iI} 's and X_{iQ} 's obey the independent Gaussian distribution with zero mean and a common variance of $\Omega/2m$. Since r^2 is the sum of $2m$ Gaussian variables, the PDF of (5.B.14) is valid provided that $2m$ is not less than unity, i.e. provided that $m \geq 1/2$.

In order to derive $E[\exp(-\sum_{j=1}^N (\gamma_j / \sin^2 \theta))]$, where any γ_j obeys the Nakagami- m distribution with common parameters, let us express $\boldsymbol{\gamma} = [\gamma_1, \dots, \gamma_N]^T$ as

$$\boldsymbol{\gamma} = \underbrace{\begin{bmatrix} X_{1,1I}^2 \\ X_{2,1I}^2 \\ \vdots \\ X_{N,1I}^2 \end{bmatrix}}_{X_{1I}} + \underbrace{\begin{bmatrix} X_{1,1Q}^2 \\ X_{2,1Q}^2 \\ \vdots \\ X_{N,1Q}^2 \end{bmatrix}}_{X_{1Q}} + \cdots + \underbrace{\begin{bmatrix} X_{1,mI}^2 \\ X_{2,mI}^2 \\ \vdots \\ X_{N,mI}^2 \end{bmatrix}}_{X_{mI}} + \underbrace{\begin{bmatrix} X_{1,mQ}^2 \\ X_{2,mQ}^2 \\ \vdots \\ X_{N,mQ}^2 \end{bmatrix}}_{X_{mQ}} \quad (5.B.16)$$

where X_{iI} is independent of X_{jQ} and is also independent of X_{jI} if $j \neq i$, while X_{iI} or X_{iQ} is an N -length correlated vector. According to [145, 154], it can be shown that the characteristic function of X_{iI} or X_{iQ} can be expressed as

$$\phi_{X_{i.}}(t_1, t_2, \dots, t_N) = \det\left(\mathbf{I} - j \frac{\Omega}{m} \mathbf{D}_t \mathbf{M}\right)^{-1/2} \quad (5.B.17)$$

where $X_{i.}$ is either X_{iI} or X_{iQ} , \mathbf{D}_t is a diagonal matrix whose elements are t_1, t_2, \dots, t_N , while \mathbf{M} is the covariance matrix of $[X_{1,i.}, X_{2,i.}, \dots, X_{N,i.}]^T$. Applying the independence property among X_{iI} , X_{jQ} and X_{jI} , the characteristic function of $\boldsymbol{\gamma}$ of (5.B.16) is hence given by

$$\phi_{\boldsymbol{\gamma}}(t_1, t_2, \dots, t_N) = \det\left(\mathbf{I} - j \frac{\Omega}{m} \mathbf{D}_t \mathbf{M}\right)^{-m} \quad (5.B.18)$$

Let in (5.B.18) $t_1 = t_2 = \cdots = t_N = t$, we obtain the characteristic function of r^2 of (5.B.15), which is given by

$$\phi_{r^2}(t) = \det\left(\mathbf{I} - jt \frac{\Omega}{m} \mathbf{M}\right)^{-m} \quad (5.B.19)$$

Furthermore, from the characteristic function of r^2 the mathematical expectation of e^{-r^2} can be obtained, which is given by

$$E[e^{-r^2}] = \det\left(\mathbf{I} + \frac{\Omega}{m}\mathbf{M}\right)^{-m} \quad (5.B.20)$$

Finally, the expectation of $E[\exp(-\sum_{j=1}^N (\gamma_j / \sin^2 \theta))]$ can be obtained by replacing Ω in (5.B.20) by $\gamma_c / \sin^2 \theta$, yielding

$$E\left[\exp\left(-\sum_{j=1}^N \frac{\gamma_j}{\sin^2 \theta}\right)\right] = \det\left(\mathbf{I} + \frac{\gamma_c}{m \sin^2 \theta} \mathbf{M}\right)^{-m} \quad (5.B.21)$$

Appendix 5.C Derivation of the Variance of Ψ

With the aid of (5.261), (5.264), (5.265) and (5.266), the variance of σ_Ψ^2 defined in (5.262) can be expressed as

$$\begin{aligned} \sigma_\Psi^2 &= E[(\Psi - \mu_\Psi)^2] \\ &= E\left[\left(\sum_{u=1}^{U-1} (|Z_{Du}|^2 - \mu_1) + \sum_{k=2}^K \sum_{u=0}^{U-1} (|Z_{kl,u}|^2 - \mu_k)\right)^2\right] \\ &= \sum_{u=1}^{U-1} \sum_{j=1}^{U-1} E[(|Z_{Du}|^2 - \mu_1)(|Z_{Dj}|^2 - \mu_1)] \\ &\quad + 2 \times \sum_{u=1}^{U-1} \sum_{k=2}^K \sum_{j=0}^{U-1} E[(|Z_{Du}|^2 - \mu_1)(|Z_{kl,j}|^2 - \mu_k)] \\ &\quad + \sum_{k=2}^K \sum_{l=2}^K \sum_{u=0}^{U-1} \sum_{j=0}^{U-1} E[(|Z_{kl,u}|^2 - \mu_k)(|Z_{ll,j}|^2 - \mu_k)] \end{aligned} \quad (5.C.22)$$

In the above equation we have respectively

$$\begin{aligned} E[(|Z_{Du}|^2 - \mu_1)(|Z_{Dj}|^2 - \mu_1)] &= E[|Z_{Du}|^2 |Z_{Dj}|^2] - \mu_1^2 \\ &= \begin{cases} \frac{2}{N_p^4} \sum_{v=0}^{N_p-1} \sum_{m=0}^{N_p-1} |h_v|^4 |h_m|^4, & \text{when } u = j \\ 0, & \text{otherwise} \end{cases} \end{aligned} \quad (5.C.23)$$

$$E[(|Z_{Du}|^2 - \mu_1)(|Z_{kl,j}|^2 - \mu_k)] = 0 \quad (5.C.24)$$

$$\begin{aligned} E[(|Z_{kl,u}|^2 - \mu_k)(|Z_{ll,j}|^2 - \mu_k)] &= E[|Z_{kl,u}|^2 |Z_{ll,j}|^2] - \mu_k^2 \\ &= \begin{cases} 0, & \text{when } k \neq l \\ 0, & \text{when } k = l \text{ and } u \neq j \\ \frac{2\Omega^2}{N_t^2 N_p^4} \sum_{v=0}^{N_p-1} \sum_{m=0}^{N_p-1} |h_v|^2 |h_m|^2, & \text{when } k = l \text{ and } u = j \end{cases} \end{aligned} \quad (5.C.25)$$

Finally, applying the results in (5.C.23), (5.C.24) and (5.C.25) into (5.C.22), we arrive at

$$\sigma_{\Psi}^2 = \frac{2(U-1)}{N_p^4} \sum_{v=0}^{N_p-1} \sum_{m=0}^{N_p-1} |h_v|^4 |h_m|^4 + \frac{2(K-1)U\Omega^2}{N_t^2 N_p^4} \sum_{v=0}^{N_p-1} \sum_{m=0}^{N_p-1} |h_v|^2 |h_m|^2 \quad (5.C.26)$$

Coherent Multiuser Detection

6.1 Introduction

In wireless communications, when multiple users communicate over the same frequency band at the same time, the multiple users will interfere with each other. This type of interference is called multiuser interference (MUI) or multiple-access interference (MAI). When not taken care of, the MUI may significantly degrade the achievable error performance of the multiple-access system.

Code-division multiple access (CDMA) is a typical multiple-access scheme conflicting MUI, which may generate the near-far problem and degrade the achievable error performance. In CDMA systems the MUI can be efficiently mitigated with the aid of a technique known as multiuser detection (MUD) [88], which was originally invented by Verdu in 1983 (see reference [155]). Since its invention, the theory and application of MUD have been widely and intensively researched throughout the community of communications engineering and thousands of research papers have been published. Below, we first use a simple example to explain the principles behind MUD.

Let the considered CDMA system support two users, user 1 and user 2, and the signatures associated with these two users be \mathbf{h}_1 for user 1 and \mathbf{h}_2 for user 2. Furthermore, let the correlation coefficient between \mathbf{h}_1 and \mathbf{h}_2 be $0 \leq \rho < 1$, i.e. $\rho = \mathbf{h}_1^H \mathbf{h}_2 = \mathbf{h}_2^H \mathbf{h}_1$, when we assume that $\|\mathbf{h}_1\|^2 = \|\mathbf{h}_2\|^2 = 1$. Then, when communicating over an AWGN channel, the received CDMA signal can be expressed in the form

$$\mathbf{y} = A_1 \mathbf{h}_1 x_1 + A_2 \mathbf{h}_2 x_2 + \mathbf{n} \quad (6.1)$$

where \mathbf{y} , \mathbf{h}_1 , \mathbf{h}_2 and \mathbf{n} are all, say, N -length column vectors; \mathbf{y} is the vector observed by the receiver, \mathbf{n} is a noise vector included in the observation, x_1 and x_2 represent the symbols transmitted by users 1 and 2, and, finally, A_1 and A_2 are related to the transmission power of users 1 and 2.

From the discussion in the previous chapters, we know that when single-user detection is considered, which demodulates a given user using only the signature of the considered user,

the decision variables for users 1 and 2 can then be formed as

$$\begin{aligned} z_1 &= \mathbf{h}_1^H \mathbf{y} = A_1 x_1 + A_2 \rho x_2 + n_1 \\ z_2 &= \mathbf{h}_2^H \mathbf{y} = A_1 \rho x_1 + A_2 x_2 + n_2 \end{aligned} \quad (6.2)$$

where $n_i = \mathbf{h}_i^H \mathbf{n}$, $i = 1, 2$. The decision variables can also be expressed in matrix form as

$$\underbrace{\begin{bmatrix} z_1 \\ z_2 \end{bmatrix}}_z = \underbrace{\begin{bmatrix} 1 & \rho \\ \rho & 1 \end{bmatrix}}_R \underbrace{\begin{bmatrix} A_1 & 0 \\ 0 & A_2 \end{bmatrix}}_A \underbrace{\begin{bmatrix} x_1 \\ x_2 \end{bmatrix}}_x + \underbrace{\begin{bmatrix} n_1 \\ n_2 \end{bmatrix}}_n \quad (6.3)$$

Equation (6.2) or (6.3) shows that the detection of user 1 (or 2) conflicts interference from user 2 (or 1) through the correlation coefficient ρ . This type of interference is the so-called MUI. Typically, the MUI may result in the following negative effects on signal detection.

First, as seen in (6.2), when $\rho > 0$, then no matter how large the signal-to-noise ratio (SNR), there exist cases where user 1 and user 2 cannot be correctly detected simultaneously. In this case, the bit-error-rate (BER) curves of the CDMA system appear with error floor, which does not decrease when the SNR value increases.

Second, let us consider z_1 of user 1 and assume that $A_2 \rho \geq A_1$. In this case, user 1 cannot carry out the communication normally, since its signal $A_1 x_1$ is overwhelmed by the MUI of $A_2 \rho x_2$ and the detection for x_1 in this case is impossible. In wireless communications this phenomenon is known as the near-far problem that makes the detection of the weaker signals difficult due to the interference imposed by the relatively stronger signals.

The above-mentioned two problems can be efficiently solved by applying MUD, which jointly detects two users simultaneously or, in other words, detects one user by making use of information about the other user. For example, let us assume $A_2 > A_1$. As a result of this assumption, user 2 can be detected with a higher reliability than user 1 according to (6.2). Hence, the receiver can first detect user 2. Let the detected symbol for user 2 be \hat{x}_2 . Then, the receiver forms a new decision variable for user 1 according to

$$\begin{aligned} \hat{z}_1 &= z_1 - A_2 \rho \hat{x}_2 \\ &= A_1 x_1 + A_2 \rho (x_2 - \hat{x}_2) + n_1 \end{aligned} \quad (6.4)$$

From (6.4) we know that the decision for user 1 is MUI free, if the second user was detected correctly, i.e. if $\hat{x}_2 = x_2$. However, if $\hat{x}_2 \neq x_2$, the interference imposed by user 2 on user 1 is then enhanced. Nevertheless, due to the assumption of $A_2 > A_1$, yielding a high confidence on the second user's detection, the overall system error performance will be enhanced. This MUD is referred to as interference cancellation (IC) in the literature [88] and will be studied in the context of the multicarrier CDMA in Section 6.2.7.

Another example for MUD can be based on (6.3). Let us modify the decision variables for users 1 and 2 by multiplying both sides of (6.3) with the inverse of \mathbf{R} , giving

$$\begin{aligned} \hat{z} &= \mathbf{R}^{-1} z \\ &= \begin{bmatrix} A_1 & 0 \\ 0 & A_2 \end{bmatrix} \begin{bmatrix} x_1 \\ x_2 \end{bmatrix} + \mathbf{R}^{-1} \begin{bmatrix} n_1 \\ n_2 \end{bmatrix} \end{aligned} \quad (6.5)$$

Explicitly, the interference imposed by user 1 (2) on user 2 (1) is fully removed, and the detection hence becomes more reliable. This type of MUD is usually referred to as

decorrelating or zero-forcing (ZF) MUD [88], which will be studied in Sections 6.2.1, 6.3.1, 6.4.1 and 6.4.3 in the context of various multicarrier CDMA.

In addition to the above-mentioned two MUD schemes, there are many other types of MUD that can be derived based on certain optimization principles. The optimization criteria considered in this chapter for derivation of the MUDs are listed as follows:

- decorrelating or zero-forcing (ZF);
- minimum variance distortionless response (MVDR);
- minimum mean-square error (MMSE);
- maximum signal-to-interference-plus-noise ratio (MSINR);
- minimum power distortionless response (MPDR);
- decision feedback interference cancellation;
- maximum *a posteriori* probability (MAP);
- maximum likelihood decision (MLD);
- minimum symbol-error-rate (MSER).

Note that, although this chapter concentrates mainly on the principles, applications and performance of the MUDs in the context of the multicarrier CDMA, the MUD algorithms are, however, general, which represent the extension or modification of the existing MUD or, more generally, signal processing algorithms [88–90, 146]. Similarly, the MUD algorithms provided in this chapter may be extended to or applied for different multiple-input multiple-output (MIMO) scenarios, where signal detection may conflict interference.

Additionally, for the convenience of getting through the derivations, in Appendices 6.A and 6.B of this chapter, some matrix-related tools are provided. Furthermore in Appendix 6.C, we list ten search/non-search algorithms for the MLD-based MUD.

6.2 Multiuser Detection in Frequency-Domain Spread Multicarrier CDMA

In this section a range of MUD algorithms are derived in the context of the frequency (F)-domain spread MC-CDMA, which is referred to as MC-CDMA for the sake of brevity. We consider a synchronous MC-CDMA system like that considered in Section 5.6 of Chapter 5. The MC-CDMA system uses $U = qN_p$ number of subcarriers, where q represents the number of symbols (not necessarily binary) transmitted by an uplink user within one MC-CDMA symbol period, while N_p is the F-domain spreading factor. The MC-CDMA system supports K uplink users and the MC-CDMA signals are assumed to be transmitted over frequency-selective fading channels having a common number of resolvable paths, L .

Following the analysis in Section 5.6 of Chapter 5, after removing the cyclic prefixes (CPs), the observation vector obtained at the BS can be expressed as

$$\mathbf{y} = \sum_{k=1}^K \mathbf{C}_k \mathbf{H}_k \mathbf{x}_k + \mathbf{n} \quad (6.6)$$

where \mathbf{C}_k is a $(U \times U)$ spreading matrix, defined as

$$\mathbf{C}_k = \frac{1}{\sqrt{N_p}} \begin{bmatrix} \text{diag}\{\mathbf{c}_k\} & \mathbf{0} & \dots & \mathbf{0} \\ \mathbf{0} & \text{diag}\{\mathbf{c}_k\} & \dots & \mathbf{0} \\ \vdots & \vdots & \ddots & \vdots \\ \mathbf{0} & \mathbf{0} & \dots & \text{diag}\{\mathbf{c}_k\} \end{bmatrix} \quad (6.7)$$

where $\text{diag}\{\mathbf{c}_k\}$ is a $(N_p \times N_p)$ diagonal matrix constituted by the elements of \mathbf{c}_k , which is the N_p -length binary spreading code assigned to the k th user. Furthermore, in (6.6), \mathbf{H}_k is the $(U \times q)$ channel matrix, given by

$$\mathbf{H}_k = \begin{bmatrix} \tilde{\mathbf{h}}_{k1} & \mathbf{0} & \dots & \mathbf{0} \\ \mathbf{0} & \tilde{\mathbf{h}}_{k2} & \dots & \mathbf{0} \\ \vdots & \vdots & \ddots & \vdots \\ \mathbf{0} & \mathbf{0} & \dots & \tilde{\mathbf{h}}_{kq} \end{bmatrix} \quad (6.8)$$

where

$$\tilde{\mathbf{h}}_{ki} = [\tilde{h}_{i1}^{(k)}, \tilde{h}_{i2}^{(k)}, \dots, \tilde{h}_{iN_p}^{(k)}]^T, \quad i = 1, 2, \dots, q \quad (6.9)$$

where $\tilde{h}_{in}^{(k)}$ represents the k th user's F-domain fading gain associated with the subcarrier

$$u = (n - 1)q + i - 1, \quad n = 1, 2, \dots, N_p; \quad i = 1, 2, \dots, q \quad (6.10)$$

The above subcarrier arrangement makes it possible to achieve maximal diversity gain.

Furthermore, in (6.6) \mathbf{x}_k is in the form of

$$\mathbf{x}_k = [x_{k1}, x_{k2}, \dots, x_{kq}]^T \quad (6.11)$$

which contains the data transmitted by the k th user, while \mathbf{n} in (6.6) is the Gaussian noise vector given by

$$\mathbf{n} = [n_1, n_2, \dots, n_{qN_p}]^T \quad (6.12)$$

where $\{n_i\}$ are Gaussian random variables distributed with zero mean and a variance of $\sigma^2/2 = 1/2\text{SNR}$ per dimension.

In this section the frequency-selective fading channel applied for obtaining the simulation and numerical results has the channel impulse response (CIR)

$$h_k(\tau) = \sum_{l=0}^{L-1} h_l^{(k)} \delta(\tau - lT_\psi) \quad (6.13)$$

where $h_l^{(k)}$ is the complex channel gain of the l th resolvable path of user k . In our simulation and numerical examples, in this section the uniform multipath delay profile (MDP) is assumed. Hence, we have $E[|h_0^{(k)}|^2] = E[|h_1^{(k)}|^2] = \dots = E[|h_{L-1}^{(k)}|^2] = \Omega_0$. The number of multipaths is assumed to be either $L = 10$ or $L = 20$.

According to Section 5.2 of Chapter 5, the F-domain fading gain of the u th subcarrier can be expressed as

$$\tilde{h}_u^{(k)} = \sum_{l=0}^{L-1} h_l^{(k)} \exp\left(-j \frac{2\pi(u-1)l}{U}\right), \quad u = 1, \dots, U \quad (6.14)$$

Let us define

$$\mathbf{h}_k = \left[h_0^{(k)}, h_1^{(k)}, \dots, h_{L-1}^{(k)}, \underbrace{0, 0, \dots, 0}_{(U-L)0's} \right]^T \quad (6.15)$$

Then, it can be shown that $\tilde{\mathbf{h}}_{ki}$ in (6.9) can be expressed as

$$\tilde{\mathbf{h}}_{ki} = \mathbf{F}_i \mathbf{h}_k \quad (6.16)$$

where \mathbf{F}_i is a reduced discrete Fourier transform (DFT) matrix of size $(N_p \times qN_p)$, which can be expressed as

$$\mathbf{F}_i = \begin{bmatrix} 1 & \exp\left(-j\frac{2\pi(i-1)}{U}\right) & \dots & \exp\left(-j\frac{2\pi(i-1)(U-1)}{U}\right) \\ 1 & \exp\left(-j\frac{2\pi(q+i-1)}{U}\right) & \dots & \exp\left(-j\frac{2\pi(q+i-1)(U-1)}{U}\right) \\ \vdots & \vdots & \ddots & \vdots \\ 1 & \exp\left(-j\frac{2\pi((N_p-1)q+i-1)}{U}\right) & \dots & \exp\left(-j\frac{2\pi((N_p-1)q+i-1)(U-1)}{U}\right) \end{bmatrix} \quad i = 1, 2, \dots, q \quad (6.17)$$

It can be shown that (6.8) can be expressed as

$$\mathbf{H}_k = \mathbf{F}(\mathbf{I}_q \otimes \mathbf{h}_k) \quad (6.18)$$

where

$$\mathbf{F} = \text{diag}\{\mathbf{F}_1, \mathbf{F}_2, \dots, \mathbf{F}_q\} \quad (6.19)$$

Letting in (6.6), we define

$$\begin{aligned} \mathbf{x} &= [\mathbf{x}_1^T, \mathbf{x}_2^T, \dots, \mathbf{x}_K^T]^T \\ \mathbf{C} &= [\mathbf{C}_1, \mathbf{C}_2, \dots, \mathbf{C}_K] \\ \mathbf{H} &= \text{diag}\{\mathbf{H}_1, \mathbf{H}_2, \dots, \mathbf{H}_K\} \end{aligned} \quad (6.20)$$

where \mathbf{x} is a qK -length vector, \mathbf{C} is a $(U \times UK)$ matrix and \mathbf{H} is a $(UK \times qK)$ matrix. Then, (6.6) can be written as

$$\mathbf{y} = \mathbf{CHx} + \mathbf{n} \quad (6.21)$$

Note that when there is no intercarrier interference, (6.6) can also be divided into q independent detections, each of the detections includes K symbols with one symbol from each of the uplink users. Specifically, the observation vector for the i th symbol can be expressed as

$$\mathbf{y}_i = \frac{1}{\sqrt{N_p}} \sum_{k=1}^K \text{diag}\{\mathbf{c}_k\} \tilde{\mathbf{h}}_{ki} \mathbf{x}_{ki} + \mathbf{n}_i, \quad i = 1, 2, \dots, q \quad (6.22)$$

When applying (6.16) into (6.22), it can also be expressed as

$$\mathbf{y}_i = \frac{1}{\sqrt{N_p}} \sum_{k=1}^K \text{diag}\{\mathbf{c}_k\} \mathbf{F}_i \mathbf{h}_k \mathbf{x}_{ki} + \mathbf{n}_i, \quad i = 1, 2, \dots, q \quad (6.23)$$

Explicitly, when the channel is estimated in the F-domain, detection based on (6.6) is preferred. Otherwise, when the channel estimation is in the T-domain, then the detection can be built on (6.21). Furthermore, when there is no intercarrier interference, the detection based on (6.22) or (6.23) is preferred. This is because the matrices related to (6.22) or to (6.23) have lower ranks than those related to (6.6) or (6.21).

Apart from the above-mentioned differences, the detection algorithms based on (6.6) or (6.21), or on (6.22) or (6.23) are very similar. Therefore, in our forthcoming discussion, the detection algorithms are derived mainly according to (6.6) or (6.21), unless otherwise pointed out.

6.2.1 Decorrelating

Decorrelating MUD is also called zero-forcing (ZF) MUD. The decorrelating MUD belongs to the class of linear MUDs. It is capable of fully removing MUI.

Generally, for linear MUDs, the decision statistics for a given transmitted symbol or symbol vector is obtained by linearly processing the received observation vector, say \mathbf{y} . When the K number of users are jointly detected, the decision statistics can be expressed as

$$\mathbf{z} = \mathbf{W}^H \mathbf{y} \quad (6.24)$$

By contrast, when the K number of users are detected individually, the decision statistics can be expressed as

$$z_k = \mathbf{W}_k^H \mathbf{y}, \quad k = 1, 2, \dots, K \quad (6.25)$$

In (6.24) and (6.25), \mathbf{y} has been given by (6.21). Let us first consider the scenario of joint K -user detection.

Substituting (6.21) into (6.24), we have

$$\mathbf{z} = \mathbf{W}^H \mathbf{C} \mathbf{H} \mathbf{x} + \mathbf{W}^H \mathbf{n} \quad (6.26)$$

The decorrelating MUD is capable of fully suppressing the MUI, which can be achieved provided that \mathbf{W} is chosen to satisfy

$$\mathbf{W}^H \mathbf{C} \mathbf{H} = \mathbf{I}_{Kq} \quad (6.27)$$

Assuming that $K \leq N_p$, then it can be readily shown that a solution to \mathbf{W} is given by [88, 156]

$$\mathbf{W}_{\text{ZF}} = \mathbf{C} \mathbf{H} (\mathbf{H}^H \mathbf{C}^T \mathbf{C} \mathbf{H})^{-1} \quad (6.28)$$

Submitting (6.28) into (6.26) gives

$$\begin{aligned} \mathbf{z} &= (\mathbf{H}^H \mathbf{C}^T \mathbf{C} \mathbf{H})^{-1} \mathbf{H}^H \mathbf{C}^T \mathbf{C} \mathbf{H} \mathbf{x} + (\mathbf{H}^H \mathbf{C}^T \mathbf{C} \mathbf{H})^{-1} \mathbf{H}^H \mathbf{C}^T \mathbf{n} \\ &= \mathbf{x} + \underbrace{(\mathbf{H}^H \mathbf{C}^T \mathbf{C} \mathbf{H})^{-1} \mathbf{H}^H \mathbf{C}^T \mathbf{n}}_{\mathbf{n}'} \end{aligned} \quad (6.29)$$

Hence, the decorrelating MUD first carries out the correlation operation using $\mathbf{H}^H \mathbf{C}^T$, and then carries out the decorrelating operation by multiplying the inverse of the matrix $\mathbf{R} =$

$\mathbf{H}^H \mathbf{C}^T \mathbf{CH}$. As shown in (6.29), the MUI is fully removed. However, the Gaussian noise samples become correlated after the decorrelating detection. The covariance matrix of \mathbf{n}' can be expressed as

$$E[\mathbf{n}'(\mathbf{n}')^H] = \frac{1}{\text{SNR}} (\mathbf{H}^H \mathbf{C}^T \mathbf{CH})^{-1} = \frac{1}{\text{SNR}} \mathbf{R}^{-1} \quad (6.30)$$

In the context of the individual detection, when substituting (6.6) or (6.21) into (6.25), the decision statistics for the k th user can be expressed as

$$z_k = \mathbf{W}_k^H \mathbf{CHx} + \mathbf{W}_k^H \mathbf{n} \quad (6.31)$$

$$\begin{aligned} &= \mathbf{W}_k^H \sum_{l=1}^K \mathbf{C}_l \mathbf{H}_l \mathbf{x}_l + \mathbf{W}_k^H \mathbf{n} \\ &= \mathbf{W}_k^H \mathbf{C}_k \mathbf{H}_k \mathbf{x}_k + \sum_{l \neq k}^K \mathbf{W}_k^H \mathbf{C}_l \mathbf{H}_l \mathbf{x}_l + \mathbf{W}_k^H \mathbf{n}, \quad k = 1, 2, \dots, K \end{aligned} \quad (6.32)$$

where \mathbf{W}_k is a $(U \times q)$ weight matrix for detecting user k . The ZF-based detection requires that \mathbf{W}_k satisfies the following conditions simultaneously

$$\begin{aligned} \mathbf{W}_k^H \mathbf{C}_k \mathbf{H}_k &= \mathbf{I}_q \\ \mathbf{W}_k^H \mathbf{C}_l \mathbf{H}_l &= \mathbf{0}, \quad l = 1, 2, \dots, K; \quad l \neq k \end{aligned} \quad (6.33)$$

Below, we show the derivation of \mathbf{W}_k in three different ways.

The first derivation represents the extension of that in reference [90][pp. 30–31]. Let \mathbf{E}_k be a $(qK \times q)$ matrix in the form

$$\mathbf{E}_k^T = \left[\underbrace{\mathbf{0}, \dots, \mathbf{0}}_{(k-1)}, \mathbf{I}_q, \mathbf{0}, \dots, \mathbf{0} \right]^T \quad (6.34)$$

Then, it can be shown that a solution to \mathbf{W}_k can be expressed as

$$\mathbf{W}_{\text{ZF},k} = \mathbf{CH} (\mathbf{H}^H \mathbf{C}^T \mathbf{CH})^{-1} \mathbf{E}_k \quad (6.35)$$

This becomes explicit when we substitute (6.35) into (6.33), which yields

$$\begin{aligned} \mathbf{W}_{\text{ZF},k}^H \mathbf{C}_l \mathbf{H}_l &= \mathbf{E}_k^H (\mathbf{H}^H \mathbf{C}^T \mathbf{CH})^{-1} \mathbf{H}^H \mathbf{C}^T \mathbf{C}_l \mathbf{H}_l \\ &= \mathbf{E}_k^H (\mathbf{H}^H \mathbf{C}^T \mathbf{CH})^{-1} \mathbf{H}^H \mathbf{C}^T \mathbf{C} \mathbf{H} \mathbf{E}_l \\ &= \mathbf{E}_k^H \mathbf{E}_l = \begin{cases} \mathbf{I}_q, & \text{if } k = l \\ \mathbf{0}, & \text{otherwise} \end{cases} \end{aligned} \quad (6.36)$$

The second approach for deriving \mathbf{W}_k that achieves the ZF MUD first finds the null space to the interference subspace. The interference subspace can be expressed as

$$\mathbf{Q}_{\bar{k}} = [\mathbf{C}_1 \mathbf{H}_1, \dots, \mathbf{C}_{k-1} \mathbf{H}_{k-1}, \mathbf{C}_{k+1} \mathbf{H}_{k+1}, \dots, \mathbf{C}_K \mathbf{H}_K] \quad (6.37)$$

which is a $(U \times q(K - 1))$ matrix. Then, a subspace that is orthogonal to $\mathbf{Q}_{\bar{k}}$ can be constructed as reference [89]

$$\mathbf{Q}_{\bar{k}}^{\perp} = \mathbf{I}_U - \mathbf{Q}_{\bar{k}}(\mathbf{Q}_{\bar{k}}^H \mathbf{Q}_{\bar{k}})^{-1} \mathbf{Q}_{\bar{k}}^H \quad (6.38)$$

It can be easily proved that

$$\mathbf{Q}_{\bar{k}}^H \mathbf{Q}_{\bar{k}}^{\perp} = \mathbf{0}, \quad \mathbf{Q}_{\bar{k}}^{\perp} \mathbf{Q}_{\bar{k}} = \mathbf{0} \quad (6.39)$$

Furthermore, since $\mathbf{C}_l \mathbf{H}_l$ for $l \neq k$ is in the interference subspace, $\mathbf{C}_l \mathbf{H}_l$ for $l \neq k$ is hence orthogonal to $\mathbf{Q}_{\bar{k}}^{\perp}$.

Let us now define

$$\begin{aligned} \mathbf{W}_{\text{ZF},k} &= \mathbf{Q}_{\bar{k}}^{\perp} \mathbf{C}_k \mathbf{H}_k (\mathbf{H}_k^H \mathbf{C}_k^T \mathbf{Q}_{\bar{k}}^{\perp} \mathbf{C}_k \mathbf{H}_k)^{-1} \\ &= [\mathbf{I}_U - \mathbf{Q}_{\bar{k}}(\mathbf{Q}_{\bar{k}}^H \mathbf{Q}_{\bar{k}})^{-1} \mathbf{Q}_{\bar{k}}^H] \mathbf{C}_k \mathbf{H}_k \\ &\quad \times (\mathbf{H}_k^H \mathbf{C}_k^T [\mathbf{I}_U - \mathbf{Q}_{\bar{k}}(\mathbf{Q}_{\bar{k}}^H \mathbf{Q}_{\bar{k}})^{-1} \mathbf{Q}_{\bar{k}}^H] \mathbf{C}_k \mathbf{H}_k)^{-1}, \quad k = 1, 2, \dots, K \end{aligned} \quad (6.40)$$

Then, it can be shown that (6.40) satisfies the equations in (6.33). Therefore, (6.40) is a ZF solution.

The third approach for deriving the ZF solution of \mathbf{W}_k ($k = 1, 2, \dots, K$) first carries out the singular-value-decomposition (SVD) on $\mathbf{Q}_{\bar{k}}$ of (6.37) in order to obtain a subspace $\mathbf{Q}_{\bar{k}}^{\perp}$ that is orthogonal to the interference subspace. Let the SVD on $\mathbf{Q}_{\bar{k}}$ of (6.37) be expressed as

$$\mathbf{Q}_{\bar{k}} = \underbrace{[\mathbf{U}_{\bar{k},s} \mid \mathbf{U}_{\bar{k},n}]}_{\mathbf{U}_{\bar{k}}} \begin{bmatrix} \Sigma_{\bar{k},s}^{1/2} \\ \mathbf{0} \end{bmatrix} \mathbf{V}_{\bar{k}} \quad (6.41)$$

where $\mathbf{U}_{\bar{k}}$ and $\mathbf{V}_{\bar{k}}$ are $(U \times U)$ and $((K - 1)q \times (K - 1)q)$ unitary matrices, respectively, while $\Sigma_{\bar{k},s}$ is a $((K - 1)q \times (K - 1)q)$ diagonal matrix given by

$$\Sigma_{\bar{k},s} = \text{diag}\{\lambda_1, \lambda_2, \dots, \lambda_{(K-1)q}\} \quad (6.42)$$

which contains the eigenvalues of $\mathbf{Q}_{\bar{k}}^H \mathbf{Q}_{\bar{k}}$ or the nonzero eigenvalues of $\mathbf{Q}_{\bar{k}} \mathbf{Q}_{\bar{k}}^H$. Furthermore, in (6.42) $\mathbf{U}_{\bar{k},s}$ is a $(U \times (K - 1)q)$ matrix containing the eigenvectors corresponding to the nonzero eigenvalues of $\mathbf{Q}_{\bar{k}} \mathbf{Q}_{\bar{k}}^H$, while $\mathbf{U}_{\bar{k},n}$ is a $(U \times [U - (K - 1)q])$ matrix containing the eigenvectors corresponding to the zero eigenvalues of $\mathbf{Q}_{\bar{k}} \mathbf{Q}_{\bar{k}}^H$.

According to SVD theory [157], $\mathbf{U}_{\bar{k},n}$ is orthogonal to $\mathbf{U}_{\bar{k},s}$ and is the null subspace of that determined by the interfering signals, i.e. we can choose $\mathbf{Q}_{\bar{k}}^{\perp} = \mathbf{U}_{\bar{k},n}$. Therefore, the weight matrix \mathbf{W}_k can be constructed as

$$\mathbf{W}_{\text{ZF},k} = (\mathbf{U}_{\bar{k},n} \mathbf{U}_{\bar{k},n}^H) \mathbf{C}_k \mathbf{H}_k (\mathbf{H}_k^H \mathbf{C}_k^T (\mathbf{U}_{\bar{k},n} \mathbf{U}_{\bar{k},n}^H) \mathbf{C}_k \mathbf{H}_k)^{-1}, \quad k = 1, 2, \dots, K \quad (6.43)$$

It can be shown that (6.43) satisfies the equations in (6.33). Therefore, it is a ZF solution.

When \mathbf{W}_k achieves the ZF solution defined by the equations in (6.33), the decision statistics can be expressed as

$$z_k = \mathbf{x}_k + \mathbf{W}_k^H \mathbf{n}, \quad k = 1, 2, \dots, K \quad (6.44)$$

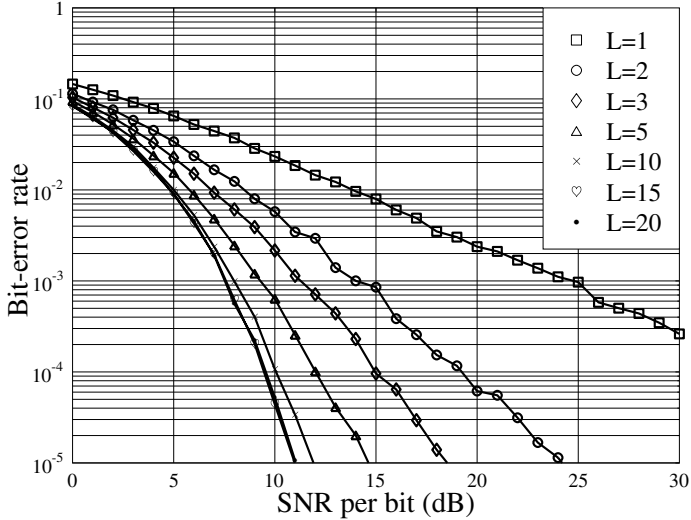


Figure 6.1: BER versus average SNR per bit performance for the MC-CDMA using $U = 64$ subcarriers, $q = 4$ bits per symbol per user and supporting $K = 1$ user, when communicating over frequency-selective Rayleigh fading channels obeying the uniform MDP. The simulations were based on (6.29).

which is free from MUI, but the Gaussian noise samples might become correlated after ZF-assisted linear processing, since $\mathbf{W}_k^H \mathbf{W}_k$ is usually not a diagonal matrix.

Figure 6.1 shows the BER versus average SNR per bit performance for the MC-CDMA using $U = 64$ subcarriers and supporting $K = 1$ uplink user, when communicating over the frequency-selective Rayleigh fading channels obeying the uniform MDP. The frequency-selective fading channels have different numbers of resolvable paths in the T-domain. It can be seen in Fig. 6.1 that the BER performance improves when the number of T-domain resolvable paths increases. This is because the F-domain diversity order increases when the number of T-domain resolvable paths increases. Since in the considered MC-CDMA one bit is conveyed by the $N_p = 16$ subcarriers having the largest F-domain spacing, the subcarrier signals conveying the same data bits hence become independent, when the number of T-domain resolvable paths is around $L = 16$. As seen in Fig. 6.1 the BER performance corresponding to $L = 15$ and $L = 20$ is typically indistinguishable.

Figure 6.2 shows the BER versus average SNR per bit performance for the MC-CDMA using random binary spreading sequences, when communicating over frequency-selective Rayleigh fading channels obeying the uniform MDP and having $L = 10$ or 20 T-domain resolvable paths. The MC-CDMA uses $U = 64$ subcarriers, and $q = 4$ bits is transmitted per symbol per user. The number of users supported is $K = 1, 4, 8, 16$. As shown in Fig. 6.2, the decorrelating MUD is capable of suppressing the MUI, and the BER versus SNR curves have no error floors, which were observed in the case of single user detection. However, the BER performance degrades when the number of users supported increases. This phenomenon can be explained as follows. First, the single-user BER bound performance is determined by the spreading factor N_p as well as the achievable diversity order. Second, it is well known [88]

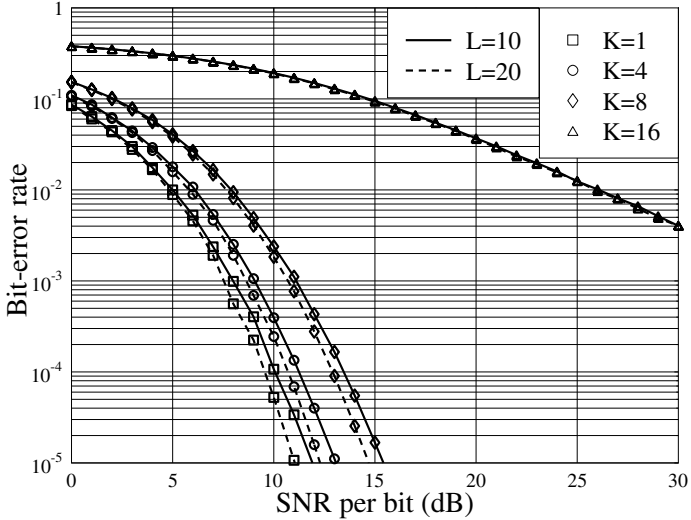


Figure 6.2: Decorrelating: BER versus average SNR per bit performance for the MC-CDMA using $U = 64$ subcarriers, $q = 4$ bits per symbol per user, when communicating over frequency-selective Rayleigh fading channels obeying the uniform MDP and having $L = 10$ or 20 resolvable paths in the T-domain. Random binary F-domain spreading sequences were assumed and the simulations were based on (6.29).

that the decorrelating MUD suppresses the MUI at the cost of amplifying the background noise, as will be explained in detail later in this section. In the considered MC-CDMA the degrees-of-freedom (DoFs) for achieving diversity as well as providing MUI suppression capability are determined by the spreading factor N_p forming a trade-off. When there are more multiuser signals required to suppress, the resulting diversity order becomes lower and hence the BER performance degrades. Otherwise, when the system supports a lower number of users requiring lower DoFs for MUI suppression, the diversity order achievable is then higher and correspondingly a better BER performance can be achieved.

As mentioned previously, the decorrelating MUD suppresses the MUI while amplifying background noise. This can be seen from (6.30), which implies that the variance for the i th element of n'_i is given by

$$\sigma_i^2 = \frac{1}{\text{SNR}} (\mathbf{R}^{-1})_{ii} \quad (6.45)$$

where $(\mathbf{R}^{-1})_{ii}$ represents the (i, i) th entry of \mathbf{R}^{-1} . Following reference [88][p. 196], it can be proved that

$$(\mathbf{R}^{-1})_{ii} = \left(\frac{1}{N_p} \sum_{n=1}^{N_p} |\tilde{h}_{in}^{(k)}|^2 - \mathbf{r}_i^H \mathbf{R}_i^{-1} \mathbf{r}_i \right)^{-1} \quad (6.46)$$

where \mathbf{R}_i is the $(Kq - 1) \times (Kq - 1)$ Hermitian matrix that obtained from \mathbf{R} by removing the i th column and i th row from \mathbf{R} ; \mathbf{R}_i is positive definite. By contrast, \mathbf{r}_i is a $(Kq - 1)$ -length vector formed from the i th column of \mathbf{R} after removing the (i, i) th entry of \mathbf{R} , which

is $N_p^{-1} \sum_{n=1}^{N_p} |\tilde{h}_{in}^{(k)}|^2$. When applying (6.46) into (6.45), it gives

$$\begin{aligned}\sigma_i^2 &= \frac{1}{\text{SNR}} \times \left(\frac{1}{N_p} \sum_{n=1}^{N_p} |\tilde{h}_{in}^{(k)}|^2 - \mathbf{r}_i^H \mathbf{R}_i^{-1} \mathbf{r}_i \right)^{-1} \\ &\geq \frac{1}{\text{SNR}} \times \left(\frac{1}{N_p} \sum_{n=1}^{N_p} |\tilde{h}_{in}^{(k)}|^2 \right)^{-1}\end{aligned}\quad (6.47)$$

where the last equation is the variance of the background noise, when the MC-CDMA system supports $K = 1$ user. Therefore, (6.47) shows that the variance of the background noise is amplified after the decorrelating MUD.

6.2.2 Minimum Variance Distortionless Response (MVDR)

The MVDR technique is capable of minimizing the variance of interference-plus-noise, while achieving the distortionless response of the desired signals. Let us first consider the scenario where the K number of uplink users are detected jointly. In this case, when substituting (6.21) into (6.24), the decision variable vector can be expressed as

$$\mathbf{z} = \mathbf{W}^H \mathbf{C} \mathbf{H} \mathbf{x} + \mathbf{W}^H \mathbf{n} \quad (6.48)$$

which shows that the variance of the noise can be expressed as

$$\text{Var}(\mathbf{z}) = \text{Trace}(E[\mathbf{W}^H \mathbf{n} \mathbf{n}^H \mathbf{W}]) = \sigma^2 \text{Trace}(\mathbf{W}^H \mathbf{W}) \quad (6.49)$$

where $\sigma^2 = 1/\text{SNR}$. The distortionless condition can be expressed as

$$\mathbf{W}^H \mathbf{C} \mathbf{H} = \mathbf{I}_{Kq} \quad (6.50)$$

Therefore, with the aid of the Lagrange multiplier, the minimization problem for the joint K -user MVDR-MUD can be expressed as

$$\mathbf{J} = \sigma^2 \times \mathbf{W}^H \mathbf{W} - (\mathbf{W}^H \mathbf{C} \mathbf{H} - \mathbf{I}_{Kq}) \boldsymbol{\lambda} - \boldsymbol{\lambda}^H (\mathbf{H}^H \mathbf{C}^T \mathbf{W} - \mathbf{I}_{Kq}) \quad (6.51)$$

Taking the complex gradient of $\text{Trace}(\mathbf{J})$ with respect to \mathbf{W}^* and equating the result to zero, the resulting equation can be solved to give

$$\mathbf{W} = \frac{1}{\sigma^2} \mathbf{C} \mathbf{H} \boldsymbol{\lambda} \quad (6.52)$$

where the multiplier $\boldsymbol{\lambda}$ can be obtained with the aid of the distortionless condition of (6.50),

$$\boldsymbol{\lambda} = \sigma^2 (\mathbf{H}^H \mathbf{C}^T \mathbf{C} \mathbf{H})^{-1} \quad (6.53)$$

Substituting it into (6.52) gives

$$\mathbf{W}_{\text{MVDR}} = \mathbf{C} \mathbf{H} (\mathbf{H}^H \mathbf{C}^T \mathbf{C} \mathbf{H})^{-1} \quad (6.54)$$

which is the same solution as (6.28) for the ZF-MUD.

In the context of the individual MVDR-MUD, when substituting (6.6) into (6.25), the decision statistics for the k th user is given by

$$\mathbf{z}_k = \mathbf{W}_k^H \mathbf{C}_k \mathbf{H}_k \mathbf{x}_k + \sum_{l \neq k}^K \mathbf{W}_k^H \mathbf{C}_l \mathbf{H}_l \mathbf{x}_l + \mathbf{W}_k^H \mathbf{n}, \quad k = 1, 2, \dots, K \quad (6.55)$$

where \mathbf{W}_k is a $(U \times q)$ weight matrix for detecting user k . In this case the variance of the interference-plus-noise is given by

$$\text{Var}(\mathbf{z}_k) = \text{Trace} \left(\mathbf{W}_k^H \underbrace{\left(\sum_{l \neq k}^K \mathbf{C}_l \mathbf{H}_l \mathbf{H}_l^H \mathbf{C}_l^T + \sigma^2 \mathbf{I}_U \right) \mathbf{W}_k}_{\mathbf{R}_I} \right) \quad (6.56)$$

where we assume that the data symbols are i.i.d. random variables, in order to obtain the results at the right-hand side.

For the individual MVDR-MUD, the distortionless criterion can be expressed as

$$\mathbf{W}_k^H \mathbf{C}_k \mathbf{H}_k = \mathbf{I}_q, \quad k = 1, 2, \dots, K \quad (6.57)$$

Therefore, the corresponding minimization problem can be formed as

$$\mathbf{J}_k = \mathbf{W}_k^H \mathbf{R}_I \mathbf{W}_k - (\mathbf{W}_k^H \mathbf{C}_k \mathbf{H}_k - \mathbf{I}_q) \boldsymbol{\lambda}_k - \boldsymbol{\lambda}_k^H (\mathbf{H}_k^H \mathbf{C}_k^T \mathbf{W}_k - \mathbf{I}_q) \quad (6.58)$$

Taking the complex gradient of trace(\mathbf{J}_k) with respect to \mathbf{W}_k^* , it can be shown that

$$\mathbf{W}_k = \mathbf{R}_I^{-1} \mathbf{C}_k \mathbf{H}_k \boldsymbol{\lambda}_k \quad (6.59)$$

where the multiplier $\boldsymbol{\lambda}_k$ can be obtained by substituting (6.59) into the distortionless condition of (6.57), which gives

$$\boldsymbol{\lambda}_k = (\mathbf{H}_k^H \mathbf{C}_k^T \mathbf{R}_I^{-1} \mathbf{C}_k \mathbf{H}_k)^{-1} \quad (6.60)$$

Finally, when substituting (6.60) into (6.59), we obtain the weight matrix for detecting the k th user, which is expressed as

$$\mathbf{W}_{\text{MVDR},k} = \mathbf{R}_I^{-1} \mathbf{C}_k \mathbf{H}_k (\mathbf{H}_k^H \mathbf{C}_k^T \mathbf{R}_I^{-1} \mathbf{C}_k \mathbf{H}_k)^{-1}, \quad k = 1, 2, \dots, K \quad (6.61)$$

Equation (6.61) implies that the individual MVDR-MUD is capable of suppressing the MUI and background noise. However, within a given user the detection is based on the ZF-MUD principles. This can be seen by setting $K = 1$ in (6.61), yielding $\mathbf{R}_I = \sigma^2 \mathbf{I}_U$. Applying this result into (6.61) gives $\mathbf{W}_k = \mathbf{C}_k \mathbf{H}_k (\mathbf{H}_k^H \mathbf{C}_k^T \mathbf{C}_k \mathbf{H}_k)^{-1}$, which is the ZF solution shown in the form of (6.28).

In order to suppress the MUI, background noise and intrauser interference in the MVDR sense, we may build the detection on a symbol-by-symbol basis. Let \mathbf{w}_{ki} ($i = 1, 2, \dots, q$) represent the i th column of \mathbf{W}_k and \mathbf{h}_{ki} ($i = 1, 2, \dots, q$) the i th column of $\mathbf{C}_k \mathbf{H}_k$. Then, following the equations from (6.55) to (6.61), it can be derived that

$$\begin{aligned} \mathbf{w}_{\text{MVDR},ki} &= \tilde{\mathbf{R}}_I^{-1} \mathbf{h}_{ki} (\mathbf{h}_{ki}^H \tilde{\mathbf{R}}_I^{-1} \mathbf{h}_{ki})^{-1} \\ &= \frac{\tilde{\mathbf{R}}_I^{-1} \mathbf{h}_{ki}}{\mathbf{h}_{ki}^H \tilde{\mathbf{R}}_I^{-1} \mathbf{h}_{ki}}, \quad i = 1, 2, \dots, q; k = 1, 2, \dots, K \end{aligned} \quad (6.62)$$

where

$$\tilde{\mathbf{R}}_I = \mathbf{R}_y - \mathbf{h}_{ki} \mathbf{h}_{ki}^H \quad (6.63)$$

and \mathbf{R}_y represents the autocorrelation matrix of the observation vector \mathbf{y} , which is given by

$$\mathbf{R}_y = \sum_{l=1}^K \mathbf{C}_l \mathbf{H}_l \mathbf{H}_l^H \mathbf{C}_l^T + \sigma^2 \mathbf{I}_U \quad (6.64)$$

When the MVDR-MUD uses the optimum weight vector of (6.62), the decision variable can be written as

$$z_{ki} = x_{ki} + \frac{\tilde{\mathbf{R}}_I^{-1} \mathbf{h}_{ki}}{\mathbf{h}_{ki}^H \tilde{\mathbf{R}}_I^{-1} \mathbf{h}_{ki}} (\mathbf{C} \mathbf{H} \mathbf{x} - \mathbf{h}_{ki} x_{ki} + \mathbf{n}) \quad (6.65)$$

In this case, when the interfering signals are approximated as i.i.d. Gaussian random variables with zero mean, then it can be shown that the variance of z_{ki} can be expressed as

$$\text{Var}[z_{ki}] = \frac{1}{\mathbf{h}_{ki}^H \tilde{\mathbf{R}}_I^{-1} \mathbf{h}_{ki}} \quad (6.66)$$

Correspondingly, the signal-to-interference-plus-noise ratio (SINR) for the MVDR-MUD based on (6.62) can be expressed as

$$\gamma_{ki} = \mathbf{h}_{ki}^H \tilde{\mathbf{R}}_I^{-1} \mathbf{h}_{ki} \quad (6.67)$$

Figure 6.3 shows the BER of the MC-CDMA using random binary spreading sequences, when communicating over frequency-selective Rayleigh fading channels obeying the uniform MDP. The simulations were based on (6.62). The MC-CDMA was assumed to use $U = 64$ subcarriers and each uplink user transmitted $q = 4$ bits per symbol. Furthermore, it was assumed that the frequency-selective fading channels had $L = 10$ or 20 T-domain resolvable paths. It can be seen from Fig. 6.3 that the BER performance degrades when the MC-CDMA supports an increased number of users, because of the trade-off existing between the number of users supported and the diversity gain achieved. Comparing the results in Fig. 6.3 with those in Fig. 6.2, we can observe that MVDR-MUD outperforms the decorrelating MUD in terms of the BER performance, since the MVDR-MUD based on (6.62) is capable of taking into account the background noise, while suppressing the MUI. By contrast, the decorrelating MUD amplifies the background noise when it concentrates solely on MUI suppression.

6.2.3 Minimum Mean-Square Error (MMSE)

When the MMSE-MUD is considered, the weight matrix \mathbf{W} (or \mathbf{W}_k) is chosen such that the mean-square error (MSE) between the transmitted signal vector \mathbf{x} (or \mathbf{x}_k) and its estimate \mathbf{z} (or \mathbf{z}_k) is minimized. Specifically, the minimization problem for the joint MMSE-MUD can be formed as

$$\begin{aligned} \mathbf{W}_{\text{MMSE}} &= \arg \min_{\mathbf{W}} E[\|\mathbf{x} - \mathbf{z}\|^2] \\ &= \arg \min_{\mathbf{W}} E[\|\mathbf{x} - \mathbf{W}^H \mathbf{y}\|^2] \\ &= \arg \min_{\mathbf{W}} E[\|\mathbf{x} - \mathbf{W}^H \mathbf{C} \mathbf{H} \mathbf{x} - \mathbf{W}^H \mathbf{n}\|^2] \end{aligned} \quad (6.68)$$

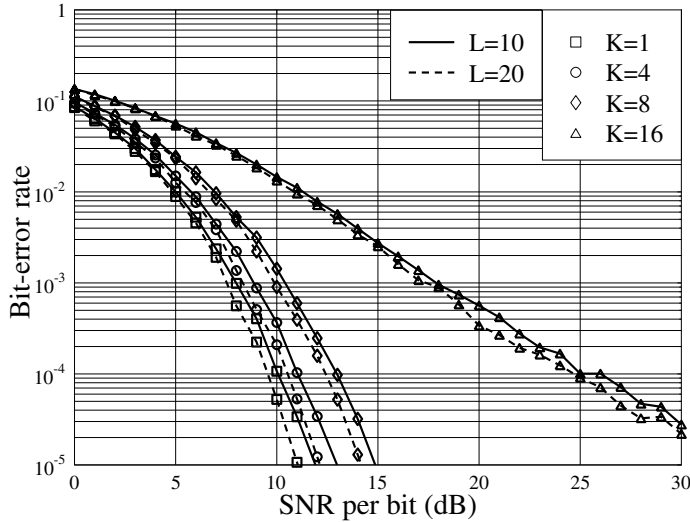


Figure 6.3: MVDR: BER versus average SNR per bit performance for the MC-CDMA using random binary spreading sequences, when communicating over frequency-selective Rayleigh fading channels obeying the uniform MDP and having $L = 10$ or 20 T-domain resolvable paths. The MC-CDMA system employs $U = 64$ subcarriers and $q = 4$ bits are transmitted per symbol per user. The simulations were based on the weight vector of (6.62).

where (6.26) was substituted. In (6.68) the expectation is taken with respect to the transmitted data symbols, which are assumed to be i.i.d. random variables, as well as to the AWGN, depending on whether the receiver uses their corresponding knowledge. Let the estimation error vector be expressed as

$$\Delta = \mathbf{x} - z = \mathbf{x} - \mathbf{W}^H \mathbf{y} \quad (6.69)$$

Then, the estimation error vector's covariance matrix can be expressed as

$$\begin{aligned} \mathbf{R}_\Delta &= E[(\mathbf{x} - \mathbf{W}^H \mathbf{y})(\mathbf{x} - \mathbf{W}^H \mathbf{y})^H] \\ &= \mathbf{I}_{Kq} - \mathbf{R}_{yx}^H \mathbf{W} - \mathbf{W}^H \mathbf{R}_{yx} + \mathbf{W}^H \mathbf{R}_y \mathbf{W} \end{aligned} \quad (6.70)$$

where \mathbf{R}_y is the autocorrelation matrix of the received signal vector \mathbf{y} of (6.6) or (6.21), which can be expressed as

$$\begin{aligned} \mathbf{R}_y &= E[\mathbf{y}\mathbf{y}^H] \\ &= \sum_{l=1}^K \mathbf{C}_l \mathbf{H}_l \mathbf{H}_l^H \mathbf{C}_l^T + \sigma^2 \mathbf{I}_U \\ &= \mathbf{C} \mathbf{H}^H \mathbf{C}^T + \sigma^2 \mathbf{I}_U \end{aligned} \quad (6.71)$$

In (6.70) \mathbf{R}_{yx} represents the cross-correlation matrix between the received signal vector \mathbf{y} and the desired symbol vector \mathbf{x} , which is given by

$$\begin{aligned}\mathbf{R}_{yx} &= E[\mathbf{y}\mathbf{x}^H] \\ &= \mathbf{C}\mathbf{H}\end{aligned}\quad (6.72)$$

The minimization of (6.68) is achieved when the complex gradient of the *trace* of the covariance matrix \mathbf{R}_Δ with respect to \mathbf{W}^* is a zero matrix, which yields

$$\mathbf{W}_{\text{MMSE}} = \mathbf{R}_y^{-1} \mathbf{R}_{yx} \quad (6.73)$$

In more detail, when substituting (6.71) and (6.72) into (6.73), the weight matrix achieving the MMSE-MUD can be expressed as

$$\mathbf{W}_{\text{MMSE}} = (\mathbf{C}\mathbf{H}\mathbf{H}^H\mathbf{C}^T + \sigma^2 \mathbf{I}_U)^{-1} \mathbf{C}\mathbf{H} \quad (6.74)$$

Furthermore, on invoking the *matrix inverse lemma* as shown in (6.B.5), in (6.74), we can obtain another solution for the MMSE MUD, which is

$$\mathbf{W}_{\text{MMSE}} = \mathbf{C}\mathbf{H}(\mathbf{H}^H\mathbf{C}^T\mathbf{C}\mathbf{H} + \sigma^2 \mathbf{I}_{Kq})^{-1} \quad (6.75)$$

In (6.75) the MMSE-MUD inverts a matrix of size $(Kq \times Kq)$, instead of inverting a $(U \times U)$ matrix in (6.74). When the number of users supported is relatively low, it can be shown that the complexity of the MMSE-MUD based on (6.75) may be significantly lower than that of the MMSE-MUD based on (6.74).

When applying the obtained results to (6.70), it can be shown that the MMSE normalized by the factor Kq , the number of symbols received, can be computed as

$$\begin{aligned}\text{MMSE} &= \frac{1}{Kq} \text{Trace}(\mathbf{I}_{Kq} - \mathbf{R}_{yx}^H \mathbf{W}) \\ &= \frac{1}{Kq} \text{Trace}(\mathbf{I}_{Kq} - \mathbf{H}^H \mathbf{C}^T \mathbf{C} \mathbf{H} [\mathbf{H}^H \mathbf{C}^T \mathbf{C} \mathbf{H} + \sigma^2 \mathbf{I}_{Kq}]^{-1}) \\ &= \frac{\sigma^2}{Kq} \text{Trace}([\mathbf{H}^H \mathbf{C}^T \mathbf{C} \mathbf{H} + \sigma^2 \mathbf{I}_{Kq}]^{-1})\end{aligned}\quad (6.76)$$

For the individual MMSE-MUD, let us consider the detection of the k th uplink user. In this case the weight matrix \mathbf{W}_k ($k = 1, 2, \dots, K$) for detecting the k th uplink user is determined such that the MSE between the transmitted vector \mathbf{x}_k and its estimate \mathbf{z}_k of (6.32) can be minimized. Specifically, the minimization problem can be formulated as

$$\begin{aligned}\mathbf{W}_{\text{MMSE},k} &= \arg \min_{\mathbf{W}_k} \{E[\|\mathbf{x}_k - \mathbf{z}_k\|^2]\} \\ &= \arg \min_{\mathbf{W}_k} \{E[\|\mathbf{x}_k - \mathbf{W}_k \mathbf{y}\|^2]\} \\ &= \arg \min_{\mathbf{W}_k} \left\{ E \left[\left\| \mathbf{x}_k - \sum_{l=1}^K \mathbf{W}_k^H \mathbf{C}_l \mathbf{H}_l \mathbf{x}_l - \mathbf{W}_k^H \mathbf{n} \right\|^2 \right] \right\}\end{aligned}\quad (6.77)$$

Following approaches for deriving \mathbf{W}_{MMSE} similar to those seen in (6.73), it can be shown that the solution to (6.77) is given by

$$\mathbf{W}_{\text{MMSE},k} = \mathbf{R}_y^{-1} \mathbf{R}_{yx_k} \quad (6.78)$$

where \mathbf{R}_y is given by (6.71), while \mathbf{R}_{yx_k} represents the cross-correlation matrix between the received signal vector \mathbf{y} and the desired symbol vector \mathbf{x}_k , which is given by

$$\begin{aligned} \mathbf{R}_{yx_k} &= E[\mathbf{y}\mathbf{x}_k^H] \\ &= \mathbf{C}_k \mathbf{H}_k \end{aligned} \quad (6.79)$$

Therefore, the weight matrix $\mathbf{W}_{\text{MMSE},k}$ can be expressed in detail as

$$\begin{aligned} \mathbf{W}_{\text{MMSE},k} &= (\mathbf{C} \mathbf{H} \mathbf{H}^H \mathbf{C}^T + \sigma^2 \mathbf{I}_U)^{-1} \mathbf{C}_k \mathbf{H}_k \\ &= \left(\sum_{l=1}^K \mathbf{C}_l \mathbf{H}_l \mathbf{H}_l^H \mathbf{C}_l^T + \sigma^2 \mathbf{I}_U \right)^{-1} \mathbf{C}_k \mathbf{H}_k, \quad k = 1, 2, \dots, K \end{aligned} \quad (6.80)$$

Let us represent the above equation as

$$\mathbf{W}_{\text{MMSE},k} = (\mathbf{C}_k \mathbf{H}_k \mathbf{H}_k^H \mathbf{C}_k^T + \mathbf{R}_I)^{-1} \mathbf{C}_k \mathbf{H}_k \quad (6.81)$$

where \mathbf{R}_I is given by (6.56). Then, by using the *matrix inverse lemma* of (6.B.3) in Appendix 6.B, the weight matrix for the individual MMSE-MUD can also be expressed as

$$\mathbf{W}_{\text{MMSE},k} = \mathbf{R}_I^{-1} \mathbf{C}_k \mathbf{H}_k (\mathbf{H}_k^H \mathbf{C}_k^T \mathbf{R}_I^{-1} \mathbf{C}_k \mathbf{H}_k + \mathbf{I}_q)^{-1}, \quad k = 1, 2, \dots, K \quad (6.82)$$

The normalized MMSE for the individual MMSE-MUD can be computed as

$$\begin{aligned} \text{MMSE}_k &= \frac{1}{q} \text{Trace}(\mathbf{I}_q - \mathbf{R}_{yx_k}^H \mathbf{W}_k) \\ &= \frac{1}{q} \text{Trace}(\mathbf{I}_q - \mathbf{H}_k^H \mathbf{C}_k^T \mathbf{R}_I^{-1} \mathbf{C}_k \mathbf{H}_k [\mathbf{H}_k^H \mathbf{C}_k^T \mathbf{R}_I^{-1} \mathbf{C}_k \mathbf{H}_k + \mathbf{I}_q]^{-1}) \\ &= \frac{1}{q} \text{Trace}([\mathbf{H}_k^H \mathbf{C}_k^T \mathbf{R}_I^{-1} \mathbf{C}_k \mathbf{H}_k + \mathbf{I}_q]^{-1}) \end{aligned} \quad (6.83)$$

It can be easily proved that the joint K -user MMSE-MUD and individual MMSE-MUD are equivalent. Using the definitions in (6.20), the weight matrix \mathbf{W}_{MMSE} of (6.74) for the joint K -user MMSE-MUD can be written as

$$\begin{aligned} \mathbf{W}_{\text{MMSE}} &= \mathbf{R}_y^{-1} [\mathbf{C}_1 \mathbf{H}_1, \mathbf{C}_2 \mathbf{H}_2, \dots, \mathbf{C}_K \mathbf{H}_K] \\ &= [\mathbf{R}_y^{-1} \mathbf{C}_1 \mathbf{H}_1, \mathbf{R}_y^{-1} \mathbf{C}_2 \mathbf{H}_2, \dots, \mathbf{R}_y^{-1} \mathbf{C}_K \mathbf{H}_K] \\ &= [\mathbf{W}_{\text{MMSE},1}, \mathbf{W}_{\text{MMSE},2}, \dots, \mathbf{W}_{\text{MMSE},K}] \end{aligned} \quad (6.84)$$

Therefore, both the joint and the individual optimizations result in the same (set of) linear processing matrices for detection of the K uplink users in the MMSE sense. Hence, we can imply that the minimum MSE can be computed either according to (6.76) or according to (6.83).

Furthermore, when we express $\mathbf{C}_k \mathbf{H}_k$ as

$$\mathbf{C}_k \mathbf{H}_k = [\mathbf{h}_{k1}, \mathbf{h}_{k2}, \dots, \mathbf{h}_{kq}] \quad (6.85)$$

the weight matrix (6.81) can be written as

$$\begin{aligned} \mathbf{W}_{\text{MMSE},k} &= \mathbf{R}_y^{-1} [\mathbf{h}_{k1}, \mathbf{h}_{k2}, \dots, \mathbf{h}_{kq}] \\ &= [\mathbf{R}_y^{-1} \mathbf{h}_{k1}, \mathbf{R}_y^{-1} \mathbf{h}_{k2}, \dots, \mathbf{R}_y^{-1} \mathbf{h}_{kq}] \\ &= [\mathbf{w}_{\text{MMSE},k1}, \mathbf{w}_{\text{MMSE},k2}, \dots, \mathbf{w}_{\text{MMSE},kq}] \end{aligned} \quad (6.86)$$

Consequently, the weight vector for detecting the symbol of x_{ki} is given by

$$\mathbf{w}_{\text{MMSE},ki} = \mathbf{R}_y^{-1} \mathbf{h}_{ki}, \quad i = 1, 2, \dots, q; k = 1, 2, \dots, K \quad (6.87)$$

Let $\mathbf{R}_y = \mathbf{h}_{ki} \mathbf{h}_{ki}^H + \tilde{\mathbf{R}}_I$, where $\tilde{\mathbf{R}}_I$ is given by (6.63). Then, with the aid of the *matrix inverse lemma* of (6.B.2), it can be shown that (6.87) can be expressed in detail as

$$\mathbf{w}_{\text{MMSE},ki} = \frac{\tilde{\mathbf{R}}_I^{-1} \mathbf{h}_{ki}}{1 + \mathbf{h}_{ki}^H \tilde{\mathbf{R}}_I^{-1} \mathbf{h}_{ki}}, \quad i = 1, 2, \dots, q; k = 1, 2, \dots, K \quad (6.88)$$

In this case the minimum MSE can now be expressed as

$$\begin{aligned} \text{MMSE} &= 1 - \mathbf{h}_{ki}^H \mathbf{R}_y^{-1} \mathbf{h}_{ki} \\ &= 1 - \frac{\mathbf{h}_{ki}^H \tilde{\mathbf{R}}_I^{-1} \mathbf{h}_{ki}}{1 + \mathbf{h}_{ki}^H \tilde{\mathbf{R}}_I^{-1} \mathbf{h}_{ki}} \\ &= \frac{1}{1 + \mathbf{h}_{ki}^H \tilde{\mathbf{R}}_I^{-1} \mathbf{h}_{ki}} \end{aligned} \quad (6.89)$$

When the MMSE-MUD is achieved, the decision variable based on the weight vector of (6.88) can be written as

$$z_{ki} = \mathbf{w}_{\text{MMSE},ki}^H \mathbf{h}_{ki} x_{ki} + \mathbf{w}_{\text{MMSE},ki}^H (\mathbf{C} \mathbf{H} \mathbf{x} - \mathbf{h}_{ki} x_{ki} + \mathbf{n}) \quad (6.90)$$

When the interfering signals are approximated as i.i.d. Gaussian random variables with zero mean, then the mean and variance of z_{ki} can be expressed as

$$\begin{aligned} E[z_{ki}] &= \mathbf{w}_{\text{MMSE},ki}^H \mathbf{h}_{ki} x_{ki} \\ \text{Var}[z_{ki}] &= \mathbf{w}_{\text{MMSE},ki}^H \tilde{\mathbf{R}}_I \mathbf{w}_{\text{MMSE},ki} \end{aligned} \quad (6.91)$$

Applying (6.88) into the above equations, they can be expressed in detail as

$$\begin{aligned} E[z_{ki}] &= \frac{\mathbf{h}_{ki}^H \tilde{\mathbf{R}}_I^{-1} \mathbf{h}_{ki}}{1 + \mathbf{h}_{ki}^H \tilde{\mathbf{R}}_I^{-1} \mathbf{h}_{ki}} \cdot x_{ki} \\ \text{Var}[z_{ki}] &= \frac{\mathbf{h}_{ki}^H \tilde{\mathbf{R}}_I^{-1} \mathbf{h}_{ki}}{(1 + \mathbf{h}_{ki}^H \tilde{\mathbf{R}}_I^{-1} \mathbf{h}_{ki})^2} \end{aligned} \quad (6.92)$$

Therefore, the SINR can be expressed as¹

$$\begin{aligned}\gamma_{ki} &= \frac{E^2[z_{ki}]}{\text{Var}[z_{ki}]} \\ &= \mathbf{h}_{ki}^H \tilde{\mathbf{R}}_I^{-1} \mathbf{h}_{ki}\end{aligned}\quad (6.93)$$

which is the same as (6.67) of the MVDR-MUD using the weight vector of (6.62). Comparing (6.93) with (6.89), we can see that

$$\gamma_{ki} = \text{MMSE}^{-1} - 1 \quad (6.94)$$

which is a general result [158] for the MMSE-MUD.

Figure 6.4 shows the BER of the MC-CDMA using random binary spreading sequences, when communicating over frequency-selective Rayleigh fading channels obeying the uniform MDP. The MC-CDMA was assumed to use $U = 64$ subcarriers and each uplink user transmitted $q = 4$ bits per symbol. Furthermore, it was assumed that the frequency-selective fading channels had $L = 10$ or 20 T-domain resolvable paths. As expected, the BER performance of the MMSE-MUD is the same as that of the symbol-by-symbol MVDR-MUD, as shown in Fig. 6.3, since both the MUD schemes result in the same output SNR value, as shown in (6.67) and (6.93).

6.2.4 Maximum Signal-to-Interference-plus-Noise Ratio (MSINR)

For the MSINR-MUD it is convenient to consider the detection on a symbol-by-symbol basis. Let \mathbf{w}_{ki} be the weight vector for detection of the i th symbol of the k th uplink user. Then, with the aid of (6.85) and (6.90), the decision statistics can be expressed as

$$\begin{aligned}z_{ki} &= \mathbf{w}_{ki}^H \mathbf{h}_{ki} x_{ki} + \mathbf{w}_{ki}^H (\mathbf{C} \mathbf{H} \mathbf{x} - \mathbf{h}_{ki} x_{ki} + \mathbf{n}) \\ i &= 1, 2, \dots, q; k = 1, 2, \dots, K\end{aligned}\quad (6.95)$$

Assume that the interfering signals after linear processing can be approximated as i.i.d. Gaussian random variables, the mean and variance of z_{ki} can be expressed as

$$\begin{aligned}E[z_{ki}] &= \mathbf{w}_{ki}^H \mathbf{h}_{ki} x_{ki} \\ \text{Var}[z_{ki}] &= \mathbf{w}_{ki}^H \tilde{\mathbf{R}}_I \mathbf{w}_{ki}\end{aligned}\quad (6.96)$$

Therefore, the SINR can be expressed as

$$\begin{aligned}\gamma_{ki} &= \frac{E^2[z_{ki}]}{\text{Var}[z_{ki}]} \\ &= \frac{\|\mathbf{w}_{ki}^H \mathbf{h}_{ki}\|^2}{\mathbf{w}_{ki}^H \tilde{\mathbf{R}}_I \mathbf{w}_{ki}}\end{aligned}\quad (6.97)$$

¹Note that, since z_{ki} is complex and the variance of z_{ki} is twice the variance of its real or imaginary part, the SINR is hence defined as $\gamma_{ki} = E^2[z_{ki}]/\text{Var}[z_{ki}]$, in accordance with the definition of $\gamma_{ki} = E^2[z_{ki}]/2\text{Var}[\Re[z_{ki}]]$ in the previous chapters.

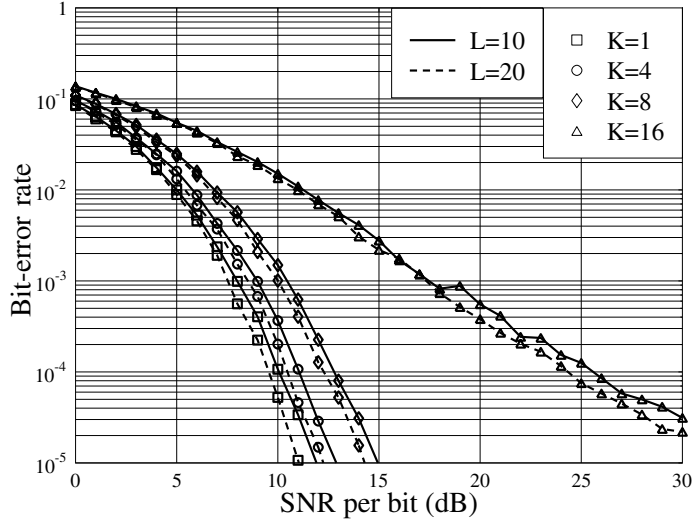


Figure 6.4: MMSE: BER versus average SNR per bit performance for the MC-CDMA using random binary spreading sequences, when communicating over frequency-selective Rayleigh fading channels obeying the uniform MDP and having $L = 10$ or 20 T-domain resolvable paths. The MC-CDMA system uses $U = 64$ subcarriers and $q = 4$ bits are transmitted per symbol per user. The simulations were based on the weight vector of (6.87).

The above equation can be written as

$$\gamma_{ki} = \frac{\|(\tilde{\mathbf{R}}_I^{1/2} \mathbf{w}_{ki})^H (\tilde{\mathbf{R}}_I^{-1/2} \mathbf{h}_{ki})\|^2}{\mathbf{w}_{ki}^H \tilde{\mathbf{R}}_I \mathbf{w}_{ki}} \quad (6.98)$$

Applying the Cauchy–Schwarz inequality [89, 156], (6.98) satisfies

$$\gamma_{ki} \leq \frac{\|(\tilde{\mathbf{R}}_I^{1/2} \mathbf{w}_{ki})^H\|^2 \|(\tilde{\mathbf{R}}_I^{-1/2} \mathbf{h}_{ki})\|^2}{\mathbf{w}_{ki}^H \tilde{\mathbf{R}}_I \mathbf{w}_{ki}} \quad (6.99)$$

with equality if and only if

$$\tilde{\mathbf{R}}_I^{1/2} \mathbf{w}_{ki} = c_{ki} \tilde{\mathbf{R}}_I^{-1/2} \mathbf{h}_{ki} \quad (6.100)$$

where c_{ki} is a nonzero constant. Therefore, the optimum weight vector in the MSINR sense can be expressed as

$$\mathbf{w}_{ki} = c_{ki} \tilde{\mathbf{R}}_I^{-1} \mathbf{h}_{ki}, \quad i = 1, 2, \dots, q; k = 1, 2, \dots, K \quad (6.101)$$

Correspondingly, the resultant maximum SINR can be obtained by applying (6.101) into (6.99), yielding

$$\gamma_{ki} = \mathbf{h}_{ki}^H \tilde{\mathbf{R}}_I^{-1} \mathbf{h}_{ki}, \quad i = 1, 2, \dots, q; k = 1, 2, \dots, K \quad (6.102)$$

It can be seen that the symbol-by-symbol MVDR-MUD in Section 6.2.2, MMSE-MUD in Section 6.2.3 and the symbol-by-symbol MSINR-MUD derived in this section all achieve the

same SINR value. Hence, the symbol-by-symbol MVDR-MUD is capable of achieving the maximum SINR while minimizing the variance of the interference plus noise. By contrast, the MMSE-MUD is capable of achieving the maximum SINR while minimizing the MSE between the desired signals and their estimates. The above arguments become clear if we substitute (6.101) into (6.95), which is

$$z_{ki} = c_{ki} \mathbf{h}_{ki}^H \tilde{\mathbf{R}}_I^{-1} \mathbf{h}_{ki} x_{ki} + c_{ki} \mathbf{h}_{ki}^H \tilde{\mathbf{R}}_I^{-1} (\mathbf{C} \mathbf{H} \mathbf{x} - \mathbf{h}_{ki} x_{ki} + \mathbf{n}) \quad (6.103)$$

Since c_{ki} is a nonzero arbitrary constant, it can be seen that, in order to achieve the distortionless criterion, c_{ki} should be chosen as

$$c_{ki} = \frac{1}{\mathbf{h}_{ki}^H \tilde{\mathbf{R}}_I^{-1} \mathbf{h}_{ki}} \quad (6.104)$$

In this case (6.101) is reduced to the solution of the MVDR-MUD, as shown in (6.62). By contrast, when we choose c_{ki} according to

$$c_{ki} \triangleq \arg \min_{c_{ki}} \{E[|z_{ki} - x_{ki}|^2]\} \quad (6.105)$$

it can be shown that

$$c_{ki} = \frac{1}{1 + \mathbf{h}_{ki}^H \tilde{\mathbf{R}}_I^{-1} \mathbf{h}_{ki}} \quad (6.106)$$

In this case (6.101) is reduced to the solution of the MMSE-MUD, as shown in (6.88).

Since the MSINR-MUD results in the same output SNR value as the symbol-by-symbol MVDR shown in (6.67), and as the MMSE-MUD as shown in (6.93), hence the MSINR-MUD has the same BER performance as shown in Figs. 6.3 and 6.4.

6.2.5 Minimum Power Distortionless Response (MPDR)

As shown in (6.61) and (6.62) the MVDR-MUDs require the knowledge of the autocorrelation matrix \mathbf{R}_I and $\tilde{\mathbf{R}}_I$ of the interfering signals and noise. In practice, this type of knowledge is sometimes difficult to acquire. For this reason, in array processing [89], when the receiver is unable to acquire the above-mentioned knowledge to carry out the MVDR-related processing, the MPDR assisted scheme [89] may be employed to derive the weight matrix or vector. As will be explained, in addition to the desired users' signatures, the MPDR-MUDs require only knowledge of the autocorrelation matrix \mathbf{R}_y of the received signals. This autocorrelation matrix can usually be estimated directly from the received signals. We start by considering the joint K -user MPDR-MUD.

Given the decision statistics for the K users as

$$\mathbf{z} = \mathbf{W}^H \mathbf{y} = \mathbf{W}^H \mathbf{C} \mathbf{H} \mathbf{x} + \mathbf{W}^H \mathbf{n} \quad (6.107)$$

the power of \mathbf{z} is given by

$$P_{ower} = E[\|\mathbf{z}\|^2] = \text{Trace}(\mathbf{W}^H \mathbf{R}_y \mathbf{W}) \quad (6.108)$$

where \mathbf{R}_y is the autocorrelation matrix of the observation vector \mathbf{y} , which is given by

$$\mathbf{R}_y = E[\mathbf{y} \mathbf{y}^H] = \mathbf{C} \mathbf{H} \mathbf{H}^H \mathbf{C}^T + \sigma^2 \mathbf{I}_U \quad (6.109)$$

The criterion of distortionless can be expressed as

$$\mathbf{W}^H \mathbf{C} \mathbf{H} = \mathbf{I}_{Kq} \quad (6.110)$$

Therefore, with the aid of the Lagrange multiplier, the minimization problem for the joint K -user MPDR-MUD can be expressed as

$$\mathbf{J} = \mathbf{W}^H \mathbf{R}_y \mathbf{W} - (\mathbf{W}^H \mathbf{C} \mathbf{H} - \mathbf{I}_{Kq}) \boldsymbol{\lambda} - \boldsymbol{\lambda}^H (\mathbf{H}^H \mathbf{C}^T \mathbf{W} - \mathbf{I}_{Kq}) \quad (6.111)$$

Taking the complex gradient of $\text{Trace}(\mathbf{J})$ with respect to \mathbf{W}^* and equating the result to zero, the resulting equation can be solved, which yields

$$\mathbf{W} = \mathbf{R}_y^{-1} \mathbf{C} \mathbf{H} \boldsymbol{\lambda} \quad (6.112)$$

where $\boldsymbol{\lambda}$ can be obtained by substituting (6.112) into (6.110), yielding $\boldsymbol{\lambda} = (\mathbf{H}^H \mathbf{C}^T \mathbf{R}_y^{-1} \mathbf{C} \mathbf{H})^{-1}$. Finally, when applying this $\boldsymbol{\lambda}$ into (6.112), the optimum weight matrix for the joint MPDR-MUD can be expressed as

$$\mathbf{W}_{\text{MPDR}} = \mathbf{R}_y^{-1} \mathbf{C} \mathbf{H} (\mathbf{H}^H \mathbf{C}^T \mathbf{R}_y^{-1} \mathbf{C} \mathbf{H})^{-1} \quad (6.113)$$

It can be proved that (6.113) is equivalent to the ZF solution of (6.28). With the aid of the *matrix inverse lemma* of (6.B.3), we obtain

$$\begin{aligned} \mathbf{R}_y^{-1} \mathbf{C} \mathbf{H} &= (\mathbf{C} \mathbf{H} \mathbf{H}^H \mathbf{C}^T + \sigma^2 \mathbf{I}_U)^{-1} \mathbf{C} \mathbf{H} \\ &= \mathbf{C} \mathbf{H} (\mathbf{H}^H \mathbf{C}^T \mathbf{C} \mathbf{H} + \sigma^2 \mathbf{I}_{Kq})^{-1} \end{aligned} \quad (6.114)$$

Applying it to (6.113) gives

$$\begin{aligned} \mathbf{W}_{\text{MPDR}} &= \mathbf{C} \mathbf{H} (\mathbf{H}^H \mathbf{C}^T \mathbf{C} \mathbf{H} + \sigma^2 \mathbf{I}_{Kq})^{-1} (\mathbf{H}^H \mathbf{C}^T \mathbf{C} \mathbf{H} (\mathbf{H}^H \mathbf{C}^T \mathbf{C} \mathbf{H} + \sigma^2 \mathbf{I}_{Kq})^{-1})^{-1} \\ &= \mathbf{C} \mathbf{H} (\mathbf{H}^H \mathbf{C}^T \mathbf{C} \mathbf{H} + \sigma^2 \mathbf{I}_{Kq})^{-1} (\mathbf{H}^H \mathbf{C}^T \mathbf{C} \mathbf{H} + \sigma^2 \mathbf{I}_{Kq}) (\mathbf{H}^H \mathbf{C}^T \mathbf{C} \mathbf{H})^{-1} \\ &= \mathbf{C} \mathbf{H} (\mathbf{H}^H \mathbf{C}^T \mathbf{C} \mathbf{H})^{-1} \end{aligned} \quad (6.115)$$

which is the same as (6.28), the weight matrix for the decorrelating MUD.

Explicitly, the detector based on (6.28) has a lower complexity than that based on (6.113).

In the context of the individual MPDR-MUD, the decision statistics for the k th user can be expressed as

$$\begin{aligned} z_k &= \mathbf{W}_k^H \mathbf{y} = \mathbf{W}_k^H \mathbf{C} \mathbf{H} \mathbf{x} + \mathbf{W}_k^H \mathbf{n} \\ &= \mathbf{W}_k^H \sum_{l=1}^K \mathbf{C}_l \mathbf{H}_l \mathbf{x}_l + \mathbf{W}_k^H \mathbf{n}, \quad k = 1, 2, \dots, K \end{aligned} \quad (6.116)$$

The power of z_k can be computed as

$$P_{\text{ower},k} = E[\|z_k\|^2] = \text{Trace}(\mathbf{W}_k^H \mathbf{R}_y \mathbf{W}_k) \quad (6.117)$$

The distortionless condition forces

$$\mathbf{W}_k^H \mathbf{C}_k \mathbf{H}_k = \mathbf{I}_q \quad (6.118)$$

Therefore, with the aid of the Lagrange multiplier, the minimization problem for the individual MPDR-MUD can be expressed as

$$\mathbf{J} = \mathbf{W}_k^H \mathbf{R}_y \mathbf{W}_k - (\mathbf{W}_k^H \mathbf{C}_k \mathbf{H}_k - \mathbf{I}_q) \boldsymbol{\lambda}_k - \boldsymbol{\lambda}_k^H (\mathbf{H}_k^H \mathbf{C}_k^T \mathbf{W}_k - \mathbf{I}_q) \quad (6.119)$$

Following the approaches for deriving the joint K -user MPDR-MUD, the weight matrix for the individual MPDR-MUD can be expressed as

$$\mathbf{W}_{\text{MPDR},k} = \mathbf{R}_y^{-1} \mathbf{C}_k \mathbf{H}_k (\mathbf{H}_k^H \mathbf{C}_k^T \mathbf{R}_y^{-1} \mathbf{C}_k \mathbf{H}_k)^{-1}, \quad k = 1, 2, \dots, K \quad (6.120)$$

As shown in (6.120), the individual MPDR-MUD requires only the knowledge about \mathbf{C}_k and \mathbf{H}_k . The autocorrelation matrix \mathbf{R}_y can be directly estimated from the observation vector \mathbf{y} .

With the aid of the *matrix inverse lemma* of (6.B.3), in (6.120) we can write $\mathbf{R}_y^{-1} \mathbf{C}_k \mathbf{H}_k$ as

$$\begin{aligned} \mathbf{R}_y^{-1} \mathbf{C}_k \mathbf{H}_k &= (\mathbf{C}_k \mathbf{H}_k \mathbf{H}_k^H \mathbf{C}_k^T + \mathbf{R}_I)^{-1} \mathbf{C}_k \mathbf{H}_k \\ &= \mathbf{R}_I^{-1} \mathbf{C}_k \mathbf{H}_k (\mathbf{H}_k^H \mathbf{C}_k^T \mathbf{R}_I^{-1} \mathbf{C}_k \mathbf{H}_k + \mathbf{I}_q)^{-1} \end{aligned} \quad (6.121)$$

where \mathbf{R}_I has been defined in (6.56). After substituting (6.121) into (6.120) and simplifying it, we can finally obtain

$$\mathbf{W}_{\text{MPDR},k} = \mathbf{R}_I^{-1} \mathbf{C}_k \mathbf{H}_k (\mathbf{H}_k^H \mathbf{C}_k^T \mathbf{R}_I^{-1} \mathbf{C}_k \mathbf{H}_k)^{-1}, \quad k = 1, 2, \dots, K \quad (6.122)$$

which is the same as (6.61) of the solution to the individual MVDR-MUD.

Furthermore, it can be readily shown that the optimum weight vector for the symbol-by-symbol MPDR-MUD can be expressed as

$$\mathbf{w}_{\text{MPDR},ki} = \frac{\mathbf{R}_y^{-1} \mathbf{h}_{ki}}{\mathbf{h}_{ki}^H \mathbf{R}_y^{-1} \mathbf{h}_{ki}}, \quad i = 1, 2, \dots, q; k = 1, 2, \dots, K \quad (6.123)$$

With the aid of the *matrix inverse lemma*, it can also be converted to

$$\mathbf{w}_{\text{MPDR},ki} = \frac{\tilde{\mathbf{R}}_I^{-1} \mathbf{h}_{ki}}{\mathbf{h}_{ki}^H \tilde{\mathbf{R}}_I^{-1} \mathbf{h}_{ki}}, \quad i = 1, 2, \dots, q; k = 1, 2, \dots, K \quad (6.124)$$

which is the same as (6.62) of the symbol-by-symbol MVDR-MUD. Hence, both the MPDR-MUD based on (6.123) and the MVDR-MUD of (6.62) should achieve the same BER performance.

6.2.6 Multiuser Detection in Subspaces

In the previous sections a range of MUDs have been derived under different optimization criteria. From these MUDs we can see that, when the receiver does not exploit the knowledge about the interfering users (except some fundamental assumptions about their corresponding channels and source data symbols), the receiver has to operate in a $U = qN_p$ dimensional space, where U represents the total number of subcarriers, q represents the number of bits transmitted within one MC-CDMA symbol by a user and N_p represents the F-domain spreading factor. In this case the detector must invert a matrix of size $(U \times U)$, such as

the autocorrelation matrix \mathbf{R}_y of the observation vector or the covariance matrix \mathbf{R}_I ($\tilde{\mathbf{R}}_I$) of the interference plus noise signals. Correspondingly, in these types of MUD the detection complexity is determined by inverting the matrix of rank ($U \times U$). In practice the rank of U (or N_p , more accurately) might be very high, when a MC-CDMA system employs a high number of subcarriers, in order to support a high number of users. Consequently, the complexity of the MUDs might be extreme. When these situations occur, multiuser detection can be designed in a reduced-rank subspace, so that the detection complexity can be less demanding. Therefore, in this section a range of rank-reduction approaches are suggested. Some approaches may be used to derive further MUDs in the following sections. Let us first consider the general theory.

Note that in this Section an ‘over-bar’ is used to indicate the operation within the reduced-rank subspace.

The observations in the subspace-based MUDs are obtained by projecting the received observation vector onto a lower dimensional subspace [89, 90, 146], which is referred to for brevity as *detection subspace*. Specifically, let \mathbf{P}_V be a ($U \times V$) matrix with its column vectors forming a basis for a V -dimensional subspace, where $V \leq U$. Then, for a given received U -dimensional vector \mathbf{y} , the V -dimensional vector in the subspace can be expressed as

$$\bar{\mathbf{y}} = \mathbf{P}_V^H \mathbf{y} \quad (6.125)$$

Note that, in this section, we refer to \mathbf{P}_V as the processing matrix, and the subspace determined by \mathbf{P}_V as the detection subspace. The processing matrix and detection subspace may be used without distinction. Furthermore, when normalization is necessary, $(\mathbf{P}_V^H \mathbf{P}_V)^{-1} \mathbf{P}_V^H$ can be used to replace \mathbf{P}_V^H in (6.125).

After the projection operation, the MUD can be operated based on $\bar{\mathbf{y}}$. As an example, let us consider the symbol-by-symbol MMSE-MUD. Applying (6.6) to (6.125), the observation vector in the subspace can be expressed as

$$\begin{aligned} \bar{\mathbf{y}} &= \mathbf{P}_V^H \mathbf{y} = \mathbf{P}_V^H \left(\sum_{k=1}^K C_k \mathbf{H}_k \mathbf{x}_k + \mathbf{n} \right) \\ &= \mathbf{P}_V^H (\mathbf{C} \mathbf{H} \mathbf{x} + \mathbf{n}) \end{aligned} \quad (6.126)$$

Let $\bar{\mathbf{w}}_{ki}$ be the weight vector for the detection of x_{ki} . Then, following the approaches discussed previously in Section 6.2.3, it can be shown that the decision statistics for x_{ki} can be expressed as

$$\bar{z}_{ki} = \bar{\mathbf{w}}_{\text{MMSE},ki}^H \times \bar{\mathbf{y}}, \quad i = 1, 2, \dots, q; k = 1, 2, \dots, K \quad (6.127)$$

where

$$\bar{\mathbf{w}}_{\text{MMSE},ki} = \mathbf{R}_{\bar{\mathbf{y}}}^{-1} \mathbf{r}_{\bar{\mathbf{y}}x_{ki}} = (\mathbf{P}_V^H \mathbf{R}_y \mathbf{P}_V)^{-1} \mathbf{P}_V^H \mathbf{h}_{ki} \quad (6.128)$$

$$\text{with } \mathbf{R}_{\bar{\mathbf{y}}} = E[\bar{\mathbf{y}} \bar{\mathbf{y}}^H] = \mathbf{P}_V^H \mathbf{R}_y \mathbf{P}_V,$$

$$\text{and } \mathbf{r}_{\bar{\mathbf{y}}x_{ki}} = \mathbf{P}_V^H \mathbf{R}_{yx_{ki}} = \mathbf{P}_V^H \mathbf{h}_{ki}$$

where \mathbf{h}_{ki} is the i th column of $\mathbf{C}_k \mathbf{H}_k$, as defined in the context of (6.62).

The minimum MSE of the subspace-based MMSE-MUD can be computed as

$$\begin{aligned}\text{MMSE} &= 1 - \mathbf{r}_{\bar{y}x_{ki}}^H \bar{\mathbf{w}}_{\text{MMSE},ki} \\ &= 1 - \mathbf{r}_{\bar{y}x_{ki}}^H \mathbf{R}_{\bar{y}}^{-1} \mathbf{r}_{\bar{y}x_{ki}} \\ &= 1 - \mathbf{h}_{ki}^H \mathbf{P}_V (\mathbf{P}_V^H \mathbf{R}_y \mathbf{P}_V)^{-1} \mathbf{P}_V^H \mathbf{h}_{ki}\end{aligned}\quad (6.129)$$

As can be seen in (6.127) and (6.128), the complexity of the reduced-rank MMSE-MUD is proportional to the rank V of the subspace, which is determined by \mathbf{P}_V . Hence, when $V \ll U$ is the case, the complexity of the subspace-based MUDs may be significantly lower than that of the MUDs based on the full observation space, which has a rank of U .

The problem left to consider is how we choose a $(U \times V)$ -dimensional processing matrix \mathbf{P}_V , so that the desired performance of a MUD in this detection subspace determined by \mathbf{P}_V can be the same or at least close to that of a corresponding MUD designed based on the full-rank space. From the information theory point of view, a detection subspace should be chosen so that the mutual information (or channel capacity) achieved in this reduced-rank detection subspace can be equal to (or close to) that achieved in the original full-rank space with a rank of the detection subspace as low as possible. In other words, a detection subspace \mathbf{P}_V should be chosen according to

$$\mathbf{P}_V \triangleq \arg \min_{\mathbf{P}'_V} \{ \mathcal{I}(\mathbf{x}, \mathbf{y}) - \mathcal{I}(\mathbf{x}, \bar{\mathbf{y}} \mid \mathbf{P}'_V) \} \quad (6.130)$$

when K users are jointly detected, or

$$\mathbf{P}_V \triangleq \arg \min_{\mathbf{P}'_V} \{ \mathcal{I}(\mathbf{x}_k, \mathbf{y}) - \mathcal{I}(\mathbf{x}_k, \bar{\mathbf{y}} \mid \mathbf{P}'_V) \}, \quad k = 1, 2, \dots, K \quad (6.131)$$

when K users are detected separately. In (6.130) and (6.131) $\mathcal{I}(\mathbf{x}, \mathbf{y})$ represents the mutual information between \mathbf{x} and \mathbf{y} , while $\mathcal{I}(\mathbf{x}, \bar{\mathbf{y}} \mid \mathbf{P}'_V)$ represents the mutual information between \mathbf{x} and $\bar{\mathbf{y}}$ conditional on the detection subspace \mathbf{P}'_V . Furthermore, it is worth noting that \mathbf{P}_V obtained in (6.131) might be different for different users.

In practice the detection subspace may be derived in the context of the specific scenarios considered. Below, a range of rank-reduction schemes are provided, where the processing matrices are derived based on the knowledge that is available to the detector and/or on the specific detection algorithm used by the detector.

6.2.6.1 Signal Subspace

The first subspace approach assumes that the receiver has knowledge about the signal subspace, such as the number of users as well as their signatures. First, when the receiver has the knowledge of \mathbf{CH} containing the signatures of the K users, the processing matrix can be chosen as

$$\mathbf{P}_V = \mathbf{CH} \quad (6.132)$$

which is a $(U \times V (= Kq))$ matrix determining a Kq -rank signal subspace. Applying the transform of (6.132) to (6.126), the Kq -length observation vector in the signal subspace determined by \mathbf{P}_V can be expressed as

$$\begin{aligned}\bar{\mathbf{y}} &= \mathbf{H}^H \mathbf{C}^T (\mathbf{CHx} + \mathbf{n}) \\ &= \mathbf{Rx} + \bar{\mathbf{n}}\end{aligned}\quad (6.133)$$

where $\mathbf{R} = \mathbf{H}^H \mathbf{C}^T \mathbf{C} \mathbf{H}$ is a correlation matrix of the signatures \mathbf{CH} , $\bar{\mathbf{n}} = \mathbf{H}^H \mathbf{C}^T \mathbf{n}$ is a Gaussian vector having zero mean and a covariance matrix of $\sigma^2 \mathbf{R}$.

In fact, the operation \mathbf{P}_V on \mathbf{y} shown in (6.133) is the correlation operation widely used for detection in CDMA systems [88]. It has been proved in reference [88] that $\bar{\mathbf{y}}$ is the sufficient statistic for detection of \mathbf{x} or \mathbf{x}_k in \mathbf{x} . It can be shown that the mutual information achieved in the signal subspace determined by \mathbf{P}_V is the same as that achieved in the full-rank observation space.

There are many other ways to derive the signal subspace that can be used to form a reduced-rank subspace for detection. For example, given the knowledge of \mathbf{CH} , the signal subspace can be obtained with the aid of the *singular-value-decomposition* (SVD) [157]. In detail, let us assume that \mathbf{CH} is column full-rank, i.e. the rank of \mathbf{CH} is Kq . Then, \mathbf{CH} can be expressed with the aid of SVD as

$$\begin{aligned}\mathbf{CH} &= \underbrace{[\mathbf{U}_s \mid \mathbf{U}_n]}_U \begin{bmatrix} \Lambda^{1/2} \\ \mathbf{0} \end{bmatrix} \mathbf{V} \\ &= \mathbf{U}_s \Lambda^{1/2} \mathbf{V}\end{aligned}\quad (6.134)$$

where \mathbf{U} and \mathbf{V} are both unitary matrices constituted by the eigenvectors of $\mathbf{CHH}^H \mathbf{C}^T$ and $\mathbf{H}^H \mathbf{C}^T \mathbf{CH}$, respectively, while $\Lambda = \text{diag}\{\lambda_1, \lambda_2, \dots, \lambda_{Kq}\}$ is a $(Kq \times Kq)$ diagonal matrix containing the eigenvalues of $\mathbf{H}^H \mathbf{C}^T \mathbf{CH}$ or the nonzero eigenvalues of $\mathbf{CHH}^H \mathbf{C}^T$. Furthermore, in (6.134) \mathbf{U}_s contains the Kq eigenvectors corresponding to the Kq nonzero eigenvalues of $\mathbf{CHH}^H \mathbf{C}^T$, \mathbf{U}_s determining the signal subspace. By contrast, \mathbf{U}_n contains the $(U - Kq)$ eigenvectors corresponding to the $(U - Kq)$ zero eigenvalues of $\mathbf{CHH}^H \mathbf{C}^T$, \mathbf{U}_n corresponding to the noise subspace.

Given the signal subspace \mathbf{U}_s of the observation space containing \mathbf{y} , the $V (= Kq)$ -rank processing matrix \mathbf{P}_V can be set as

$$\mathbf{P}_V = \mathbf{U}_s \quad (6.135)$$

Correspondingly, the observations in the signal subspace of \mathbf{U}_s can be represented by

$$\begin{aligned}\bar{\mathbf{y}} &= \mathbf{U}_s^H (\mathbf{CHx} + \mathbf{n}) \\ &= \mathbf{U}_s^H (\mathbf{U}_s \Lambda^{1/2} \mathbf{Vx} + \mathbf{n}) \\ &= \Lambda^{1/2} \mathbf{Vx} + \bar{\mathbf{n}}\end{aligned}\quad (6.136)$$

where $\bar{\mathbf{n}} = \mathbf{U}_s^H \mathbf{n}$.

Instead of carrying out the SVD decomposition on the signature matrix \mathbf{CH} , the signal subspace \mathbf{P}_V can also be obtained with the aid of the so-called QR-decomposition [157]. It has been proved that the QR-decomposition assisted approach is a highly useful approach for deriving the decision feedback MUDs. As shown in the forthcoming discourses, the QR-decomposition approach can also be employed for reducing the complexity of some MUDs, such as the maximum likelihood decision (MLD) MUD in Section 6.2.9.

With the QR-decomposition, the signature matrix \mathbf{CH} can be decomposed as

$$\mathbf{CH} = \mathbf{QM}^H \quad (6.137)$$

where \mathbf{Q} is a matrix satisfying $\mathbf{Q}^H \mathbf{Q} = \mathbf{I}_{Kq}$, while \mathbf{M} is a lower triangular matrix in the form of

$$\mathbf{M} = \begin{bmatrix} m_{11} & & & \\ m_{21} & m_{22} & & \\ \vdots & \vdots & \ddots & \\ m_{\mathcal{K}1} & m_{\mathcal{K}2} & \cdots & m_{\mathcal{KK}} \end{bmatrix} \quad (6.138)$$

where the empty entries are zeros and, for convenience, we let $\mathcal{K} = Kq$. In this case the $(U \times \mathcal{K})$ processing matrix \mathbf{P}_V can be set as

$$\mathbf{P}_V = \mathbf{Q} \quad (6.139)$$

Correspondingly, the observations in the subspace can be represented as

$$\begin{aligned} \bar{\mathbf{y}} &= \mathbf{Q}^H (\mathbf{C}\mathbf{H}\mathbf{x} + \mathbf{n}) \\ &= \mathbf{Q}^H (\mathbf{Q}\mathbf{M}^H \mathbf{x} + \mathbf{n}) \\ &= \mathbf{M}^H \mathbf{x} + \bar{\mathbf{n}} \end{aligned} \quad (6.140)$$

where $\bar{\mathbf{n}} = \mathbf{Q}^H \mathbf{n}$.

The above three approaches have been considered for deriving the processing matrix \mathbf{P}_V in the signal subspace. These approaches will be used in the following sections for derivation of some MUDs. Other approaches based on decomposition of \mathbf{CH} might also be found to be useful for some MUDs. As the above three approaches show, after the projection of the received signal vector \mathbf{y} onto the signal subspace results in $\bar{\mathbf{y}}$, the rank to be processed is reduced from $N_p q$ to Kq . Hence, we can imply that when $N_p \gg K$, the complexity of the MUDs built in the signal subspace may be significantly lower than that built in the original observation space.

6.2.6.2 Principal Components (PCs)

The principal components (PCs)-based subspace approach, based on the eigen-decomposition of the autocorrelation matrix, has had wide research and application [89, 146]. Specifically, the Hermitian autocorrelation matrix $\mathbf{R}_y = E[\mathbf{y}\mathbf{y}^H]$ (see, e.g., in (6.64)), which in practice may be replaced by its estimated version of $\hat{\mathbf{R}}_y$, can be expressed with the aid of its eigen-decomposition as

$$\mathbf{R}_y = \Phi \Lambda \Phi^H \quad (6.141)$$

where Φ is the orthonormal matrix whose columns are constituted by the eigenvectors of \mathbf{R}_y , i.e. Φ is in the form of

$$\Phi = [\phi_1, \phi_2, \dots, \phi_U] \quad (6.142)$$

where ϕ_i is the eigenvector corresponding to the eigenvalue of λ_i . In (6.141) Λ is the diagonal matrix, which is given by

$$\Lambda = \text{diag}\{\lambda_1, \lambda_2, \dots, \lambda_U\} \quad (6.143)$$

Let us assume that the eigenvalues are ordered as $\lambda_1 > \lambda_2 > \dots > \lambda_U$. Then, for a given dimension V of the detection subspace, the processing matrix \mathbf{P}_V in (6.125) in the context of PC is constituted by the first V columns of Φ , i.e.

$$\mathbf{P}_V = [\phi_1, \phi_2, \dots, \phi_V] \quad (6.144)$$

The PC-based technique can allow a significant reduction in rank for processing, provided that the dimension of the signal subspace is significantly lower than the original observation space spanned by the received signal \mathbf{y} , which is $U = Npq$ for the considered MC-CDMA system. When this is not the case, for example when the MC-CDMA system supports a high number of users, yielding $Kq > V$, then projecting the received signal vectors onto the subspace of V dimensions is likely to reduce the desired signal components. Consequently, the corresponding MUDs might conflict near-far problems [88]. In practical noise channels, when the MC-CDMA system supports a high number of users, the subspace \mathbf{P}_V with its dimension lower than Kq might also be utilized for achieving a low-complexity detection, while maintaining a satisfactory detection performance. In this case, the rank of the subspace \mathbf{P}_V can be determined based on the restriction [146, p. 826] of

$$\sum_{i=V+1}^U \lambda_{0i} < (U - V)\sigma^2 \quad (6.145)$$

where $\{\lambda_{0i}\}$ are the eigenvalues of the autocorrelation matrix of the received noiseless MC-CDMA signal vector, while σ^2 is the variance of the background noise.

It can be shown that the PC-based rank-reduction approach is capable of reaching the full-rank capacity, provided that the rank V of the subspace \mathbf{P}_V is not lower than the signal subspace's rank of Kq .

6.2.6.3 Cross-Spectral Metric (CSM)

The cross-spectral metric (CSM)-based technique for reduced-rank signal processing has been investigated, e.g., in references [89, 146, 159–161]. The principles behind the CSM-based reduced-rank filtering can be easily understood by referring to the MUDs derived based on the criteria of MVDR, MMSE, MSINR and MPDR. As shown previously in this chapter, the output SINR after the MUD-based processing can be expressed as

$$\gamma_{ki} = \mathbf{h}_{ki}^H \tilde{\mathbf{R}}_I^{-1} \mathbf{h}_{ki}, \quad i = 1, 2, \dots, q; \quad k = 1, 2, \dots, K \quad (6.146)$$

where \mathbf{h}_{ki} represents the signature of the transmitted symbol x_{ki} , while $\tilde{\mathbf{R}}_I$ represents the covariance matrix of interference plus noise. $\tilde{\mathbf{R}}_I$ is given in (6.63), which is repeated here for convenience:

$$\tilde{\mathbf{R}}_I = \mathbf{R}_y - \mathbf{h}_{ki} \mathbf{h}_{ki}^H \quad (6.147)$$

where \mathbf{R}_y represents the autocorrelation matrix of the observation vector \mathbf{y} .

Representing $\tilde{\mathbf{R}}_I$ using the eigen-analysis, it can be expressed as

$$\tilde{\mathbf{R}}_I = \tilde{\Phi} \tilde{\Lambda} \tilde{\Phi}^H = \sum_{i=1}^U \tilde{\lambda}_i \tilde{\phi}_i \tilde{\phi}_i^H \quad (6.148)$$

where $\tilde{\Lambda} = \text{diag}\{\tilde{\lambda}_1, \tilde{\lambda}_2, \dots, \tilde{\lambda}_U\}$, which are ordered such that $\tilde{\lambda}_1 \geq \tilde{\lambda}_2 \geq \dots \geq \tilde{\lambda}_U$, while $\tilde{\phi}_i$'s are the corresponding eigenvectors. From (6.148) we can know that

$$\tilde{\mathbf{R}}_I^{-1} = \sum_{j=1}^U \frac{\tilde{\phi}_j \tilde{\phi}_j^H}{\tilde{\lambda}_j} \quad (6.149)$$

Applying this result to (6.146), the output SINR can be expressed as

$$\gamma_{ki} = \sum_{j=1}^U \frac{\mathbf{h}_{ki}^H \tilde{\boldsymbol{\phi}}_j \tilde{\boldsymbol{\phi}}_j^H \mathbf{h}_{ki}}{\tilde{\lambda}_j} = \sum_{j=1}^U \frac{\|\mathbf{h}_{ki}^H \tilde{\boldsymbol{\phi}}_j\|^2}{\tilde{\lambda}_j}, \quad i = 1, 2, \dots, q; k = 1, 2, \dots, K \quad (6.150)$$

As can be seen in (6.150), for a given value of V , the V number of terms having the highest CSMs in the form of

$$\frac{\|\mathbf{h}_{ki}^H \tilde{\boldsymbol{\phi}}_j\|^2}{\tilde{\lambda}_j}, \quad j = 1, 2, \dots, U = N_p q \quad (6.151)$$

must be maintained, in order to achieve the highest available output SINR. Hence, the processing matrix \mathbf{P}_V must correspondingly be constituted by the V eigenvectors achieving these V highest CSMs.

The MMSE-MUD results in the minimum MSE of

$$\text{MMSE} = 1 - \mathbf{h}_{ki}^H \mathbf{R}_y^{-1} \mathbf{h}_{ki} \quad (6.152)$$

as shown in (6.89). With the aid of the eigen-analysis of (6.141), the MMSE can be expressed as

$$\text{MMSE} = 1 - \sum_{j=1}^U \frac{\|\mathbf{h}_{ki}^H \boldsymbol{\phi}_j\|^2}{\lambda_j} \quad (6.153)$$

Therefore, in order to minimize the MMSE after the rank-reduction, for a given value of V , the V number of terms having the highest CSMs in the form of

$$\frac{\|\mathbf{h}_{ki}^H \boldsymbol{\phi}_j\|^2}{\lambda_j}, \quad j = 1, 2, \dots, U = N_p q \quad (6.154)$$

must be maintained, and the processing matrix \mathbf{P}_V is hence made up of the V eigenvectors achieving these V highest CSMs.

The CSM-based subspace technique is more efficient than the PC-based approach, since the CSM takes into account the energy in the subspace contributed by the desired user. The subspace obtained based on the CSM is the optimum selection of $\binom{U}{V}$ eigenvectors for maximizing the output SINR or for minimizing the MSE. With the CSM technique, the rank of the subspace \mathbf{P}_V may be chosen to be below the dimension of the signal subspace without incurring a large penalty in the achievable performance, provided that the rank V of the subspace \mathbf{P}_V is sufficiently high.

Note that the PC technique does not need any information in the context of the user signals. By contrast, the CSM technique needs to invoke the knowledge of \mathbf{h}_{ki} of the desired symbol of the desired user, in order to select the subspace \mathbf{P}_V , as shown in (6.151) and (6.154).

It can be shown that the CSM-based rank-reduction approach is also capable of reaching the full-rank capacity, provided that the rank V of the subspace \mathbf{P}_V is not lower than the signal subspace of Kq .

6.2.6.4 Taylor Polynomial Approximation (TPA)

The rank-reduction processing matrix \mathbf{P}_V based on the Taylor polynomial approximation (TPA) is derived first by Taylor expanding the matrix $\mathbf{R}_y = E[\mathbf{y}\mathbf{y}^H]$ (see, e.g., in (6.64)), which, according to reference [157], can be described as follows. Let λ_{\max} be the maximum eigenvalue of \mathbf{R}_y . Let ρ be a constant satisfying $0 < \rho < 1/\lambda_{\max}$. Then, the matrix \mathbf{R}_y^{-1} can be Taylor expanded as

$$\begin{aligned}\mathbf{R}_y^{-1} &= \rho(\rho\mathbf{R}_y)^{-1} = \rho[\mathbf{I} - (\mathbf{I} - \rho\mathbf{R}_y)]^{-1} \\ &= \rho \sum_{n=0}^{\infty} (\mathbf{I} - \rho\mathbf{R}_y)^n\end{aligned}\quad (6.155)$$

Let the first V terms in (6.155) be used to approximate \mathbf{R}_y^{-1} . Then we have

$$\mathbf{R}_y^{-1} \approx \rho \sum_{n=0}^{V-1} (\mathbf{I} - \rho\mathbf{R}_y)^n \quad (6.156)$$

$$= a_0\mathbf{I} + a_1\mathbf{R}_y + \cdots + a_{V-1}\mathbf{R}_y^{V-1} \quad (6.157)$$

where the coefficients $\{a_n\}$ are determined by ρ associated with the expansion of (6.156). Considering the MMSE-MUD, when substituting (6.157) into (6.87), we obtain the weight vector

$$\mathbf{w}_{ki} \approx (a_0\mathbf{I} + a_1\mathbf{R}_y + \cdots + a_{V-1}\mathbf{R}_y^{V-1})\mathbf{h}_{ki} \quad (6.158)$$

and the decision statistics for x_{ki}

$$\begin{aligned}z_{ki} &\approx \mathbf{w}_{ki}^H \mathbf{y} \\ &= (a_0\mathbf{h}_{ki} + a_1\mathbf{R}_y\mathbf{h}_{ki} + \cdots + a_{V-1}\mathbf{R}_y^{V-1}\mathbf{h}_{ki})^H \mathbf{y}\end{aligned}\quad (6.159)$$

As shown in (6.159) there are V number of coefficients to be determined, which are dependent on the expansion of (6.156) as well as on the constant ρ selected. Furthermore, choosing the constant ρ depends on the eigen-decomposition of \mathbf{R}_y . Hence, determining the coefficients $\{a_n\}$ in (6.159) may result in a high complexity. Additionally, as noted in reference [162], the finite order approximations that result from tail-cutting of infinite order approximations generally do not lead to the best fit among all approximations of the same order. Hence, there should exist some weights such that the resulting linear detector is better than that based on solving $\{a_n\}$ in (6.159). Specifically, for the purpose of reduced-rank detection, we can design the subspace \mathbf{P}_V as

$$\mathbf{P}_V = [\mathbf{h}_{ki}, \mathbf{R}_y\mathbf{h}_{ki}, \dots, \mathbf{R}_y^{V-1}\mathbf{h}_{ki}] \quad (6.160)$$

which is a $(U \times V)$ -dimensional matrix. Then, the received observation vector \mathbf{y} is projected onto the subspace determined by the columns of \mathbf{P}_V , yielding the V -dimensional vector $\bar{\mathbf{y}} = (\mathbf{P}_V^H \mathbf{P}_V)^{-1} \mathbf{P}_V^H \mathbf{y}$. Finally, the vector $\bar{\mathbf{y}}$ in the subspace is processed in order to generate an estimate to x_{ki} .

The TPA technique was originally applied to derive the reduced-rank linear detectors for CDMA systems [88, 163]. The study in references [161, 164] has shown that the TPA-based reduced-rank MMSE detector is equivalent to the reduced-rank MMSE detector based

on the multistage Wiener filter (MSWF) [160]. In comparison with the other rank-reduction approaches based on PC and CSM, the TPA-assisted subspace approach does not depend on the eigen-decomposition of the autocorrelation matrix \mathbf{R}_y . According to [160, 161], the performance of the TPA-based MMSE detector is capable of converging to the full-rank performance with a rank of V significantly lower than that of the PC- and CSM-based reduced-rank MMSE detectors. Furthermore, the study in reference [161] shows that the rank V needed to achieve the full-rank performance does not scale with the system size, for example, determined by the number of users K and the rank U of the original observation space. Hence, the rank V can usually be significantly lower than the rank of the signal subspace, when the rank of the signal subspace is high.

Figures 6.5, 6.6 and 6.7 depict the BER versus average SNR per bit performance of the MC-CDMA systems employing the PC-, CSM- and TPA-assisted reduced-rank MMSE detection. The considered MC-CDMA systems employ $U = 64$ subcarriers, support $K = 10$ users, and $q = 4$ bits are transmitted per symbol per user. From the results of Figs. 6.5, 6.6 and 6.7, we make the following observations.

- The BER performance improves when increasing the rank, V of the detection subspace, provided that the rank V is lower than the rank of the signal subspace, which is K . When the rank V of the detection subspace reaches the rank $K = 10$ of the signal subspace, all the reduced-rank MMSE detectors are capable of achieving the BER performance of a corresponding full-rank MMSE detector.
- As shown in Figs. 6.5, 6.6, for the reduced-rank MMSE detectors designed based on PC (Fig. 6.5) and CSM (Fig. 6.6), when the rank V of the detection subspace is lower than the rank K of the signal subspace, i.e. when $V < K$, BER error floors may be observed. Typically, a lower rank of the detection subspace results in a higher BER floor. Hence, it is implied that the PC- and CSM-based reduced-rank MMSE detectors need to acquire knowledge about the rank of the signal subspace. Otherwise, they may experience the near-far problem.
- It can be observed that, for any given rank V of the detection subspace, the CSM-based reduced-rank MMSE detector outperforms the PC-based reduced-rank detector. Furthermore, as shown in Fig. 6.6, no BER floor is observed for the case of $V = 8$ within the SNR range considered; even in this case the rank $V = 8$ of the detection subspace is lower than the rank $K = 10$ of the signal subspace.
- Finally, it can be shown that the TPA-based reduced-rank MMSE detector outperforms all the other reduced-rank detectors and achieves the best BER performance for any given rank $V (< K)$ of the detection subspace. From the results of Fig. 6.7 we can see that the near full-rank BER performance can be achieved, when the rank of the detection subspace is about $V = 6$, which is significantly lower than $K = 10$ of the rank of the signal subspace.

Note again that the TPA-assisted reduced-rank MMSE detection does not depend on the complex eigen-decomposition of the autocorrelation matrix \mathbf{R}_y , in order to form the processing matrix \mathbf{P}_V , as shown in (6.160).

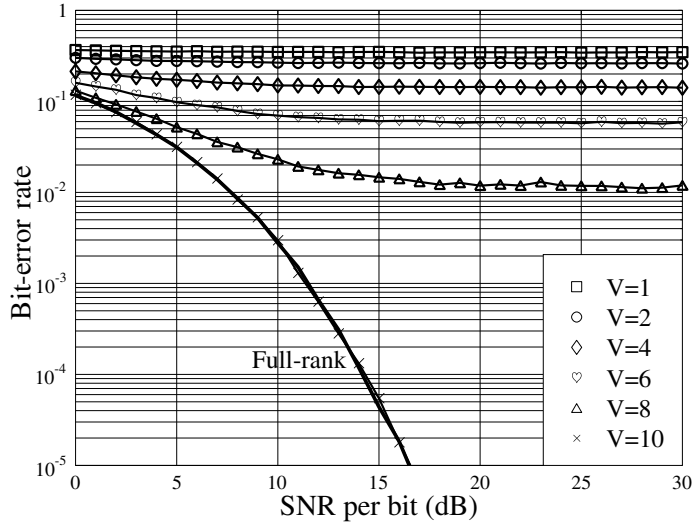


Figure 6.5: Reduced-rank MMSE (PC): BER versus average SNR per bit performance for the MC-CDMA using random binary spreading sequences, when communicating over frequency-selective Rayleigh fading channels obeying the uniform MDP and having $L = 10$ T-domain resolvable paths. The MC-CDMA system employs $U = 64$ subcarriers and $q = 4$ bits are transmitted per symbol per user.

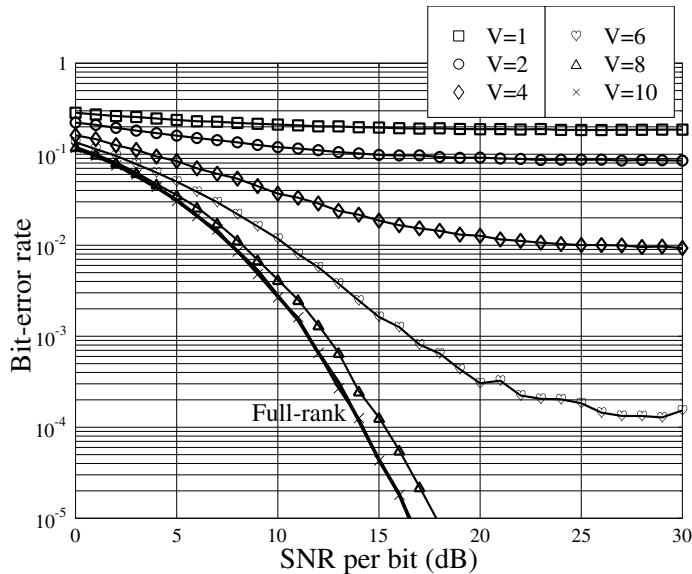


Figure 6.6: Reduced-rank MMSE (CSM): BER versus average SNR per bit performance for the MC-CDMA using random binary spreading sequences, when communicating over frequency-selective Rayleigh fading channels obeying the uniform MDP and having $L = 10$ T-domain resolvable paths. The MC-CDMA system employs $U = 64$ subcarriers and $q = 4$ bits are transmitted per symbol per user.

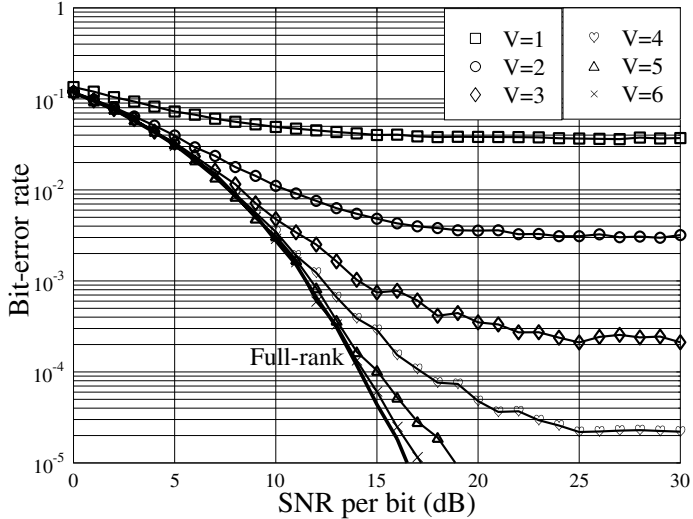


Figure 6.7: Reduced-rank MMSE (TPA): BER versus average SNR per bit performance for the MC-CDMA using random binary spreading sequences, when communicating over frequency-selective Rayleigh fading channels obeying the uniform MDP and having $L = 10$ T-domain resolvable paths. The MC-CDMA system employs $U = 64$ subcarriers and $q = 4$ bits are transmitted per symbol per user.

6.2.7 Decision Feedback Multiuser Detection

The decision feedback MUDs have been widely researched in the context of multiuser systems including the various CDMA systems. The basic principles behind the decision feedback MUDs is that, once a user is correctly detected, its impact on the other users can be removed with the aid of the knowledge related to the user detected. Decision feedback MUDs, which are also referred to as IC, can be carried out serially or in parallel. In this section the principles of a range of decision feedback MUDs are provided. As an example, let us first show the IC scheme based on the QR-decomposition of the signature matrix \mathbf{CH} , i.e. \mathbf{CH} can be expressed as (6.137) with the lower triangular matrix of (6.138). As shown in (6.140), after the processing by $\mathbf{P}_V = \mathbf{Q}$, the observation vector in the subspace can be expressed as

$$\bar{\mathbf{y}} = \mathbf{M}^H \mathbf{x} + \bar{\mathbf{n}} \quad (6.161)$$

In detail, the observations in (6.161) can be expressed as

$$\begin{aligned}\bar{y}_1 &= m_{11}x_1 + \sum_{i=2}^K m_{1i}x_i + \bar{n}_1 \\ \bar{y}_2 &= m_{22}x_2 + \sum_{i=3}^K m_{2i}x_i + \bar{n}_2 \\ &\dots\end{aligned}$$

$$\begin{aligned}\bar{y}_{\mathcal{K}-1} &= m_{(\mathcal{K}-1)(\mathcal{K}-1)}x_{\mathcal{K}-1} + m_{(\mathcal{K}-1)\mathcal{K}}x_{\mathcal{K}} + \bar{n}_{\mathcal{K}-1} \\ \bar{y}_{\mathcal{K}} &= m_{\mathcal{K}\mathcal{K}}x_{\mathcal{K}} + \bar{n}_{\mathcal{K}}\end{aligned}\quad (6.162)$$

where $m_{ij} = m_{ji}^*$ ($j > i$) was used. As can be seen from the above equation, $x_{\mathcal{K}}$ experiences no MUI. Hence, $x_{\mathcal{K}}$ can be first detected. Let its detected version be expressed as $\hat{x}_{\mathcal{K}}$. Now, since the receiver knows $\hat{x}_{\mathcal{K}}$ and since, as seen in (6.162), $x_{\mathcal{K}-1}$ conflicts MUI only from $x_{\mathcal{K}}$, the receiver can form a decision variable for $x_{\mathcal{K}-1}$ by trying to subtract the interference from $x_{\mathcal{K}}$ according to

$$\tilde{y}_{\mathcal{K}-1} = \bar{y}_{\mathcal{K}-1} - m_{(\mathcal{K}-1)\mathcal{K}}\hat{x}_{\mathcal{K}} \quad (6.163)$$

Explicitly, if $x_{\mathcal{K}}$ is correctly detected, i.e. if $\hat{x}_{\mathcal{K}} = x_{\mathcal{K}}$, the interference imposed by $x_{\mathcal{K}}$ on $x_{\mathcal{K}-1}$ is fully removed. Otherwise, if $x_{\mathcal{K}}$ is incorrectly detected, i.e. if $\hat{x}_{\mathcal{K}} \neq x_{\mathcal{K}}$, the interference from $x_{\mathcal{K}}$ will be doubled. Based on $\tilde{y}_{\mathcal{K}-1}$, let the detection for $x_{\mathcal{K}-1}$ be $\hat{x}_{\mathcal{K}-1}$. Then, the interference of $x_{\mathcal{K}-1}$ imposing on the other user symbols can similarly be cancelled as for $x_{\mathcal{K}-1}$. Finally, let the receiver employ the estimations of $x_2, x_3, \dots, x_{\mathcal{K}}$. Their interference on x_1 can be cancelled according to

$$\tilde{y}_1 = \bar{y}_1 - \sum_{i=2}^{\mathcal{K}} m_{1i}\hat{x}_i \quad (6.164)$$

In summary, we have

$$\begin{aligned}\tilde{y}_1 &= \bar{y}_1 - \sum_{i=2}^{\mathcal{K}} m_{1i}\hat{x}_i \\ \tilde{y}_2 &= \bar{y}_2 - \sum_{i=3}^{\mathcal{K}} m_{2i}\hat{x}_i \\ &\dots \\ \tilde{y}_{\mathcal{K}-1} &= \bar{y}_{\mathcal{K}-1} - m_{(\mathcal{K}-1)\mathcal{K}}\hat{x}_{\mathcal{K}} \\ \tilde{y}_{\mathcal{K}} &= \bar{y}_{\mathcal{K}}\end{aligned}\quad (6.165)$$

When the above operations are expressed in matrix form, we obtain

$$\begin{aligned}\tilde{\mathbf{y}} &= \bar{\mathbf{y}} - \bar{\mathbf{M}}^H \hat{\mathbf{x}} \\ &= \mathbf{Q}^H \mathbf{y} - \bar{\mathbf{M}}^H \hat{\mathbf{x}} \\ &= \mathbf{M}^H \mathbf{x} - \bar{\mathbf{M}}^H \hat{\mathbf{x}} + \bar{\mathbf{n}}\end{aligned}\quad (6.166)$$

where $\bar{\mathbf{M}}$ is obtained from \mathbf{M} by setting its diagonal entries to zero.

Let the diagonal matrix constituted by the diagonal elements of \mathbf{M} be expressed as $\text{diag}\{\mathbf{M}\}$. Then, the decision variable vector for the $\mathcal{K} = Kq$ data symbols can be expressed as

$$\begin{aligned}\mathbf{z} &= \text{diag}\{\mathbf{M}\} \tilde{\mathbf{y}} \\ &= \text{diag}\{\mathbf{M}\} \mathbf{Q}^H \mathbf{y} - \text{diag}\{\mathbf{M}\} \bar{\mathbf{M}}^H \hat{\mathbf{x}} \\ &= \text{diag}\{\mathbf{M}\} \mathbf{M}^H \mathbf{x} - \text{diag}\{\mathbf{M}\} \bar{\mathbf{M}}^H \hat{\mathbf{x}} + \text{diag}\{\mathbf{M}\} \bar{\mathbf{n}}\end{aligned}\quad (6.167)$$

The BER versus SNR per bit performance for a MC-CDMA system using the QR-decomposition assisted IC is shown in Fig. 6.8. The MC-CDMA supports $K = 4$ users, which

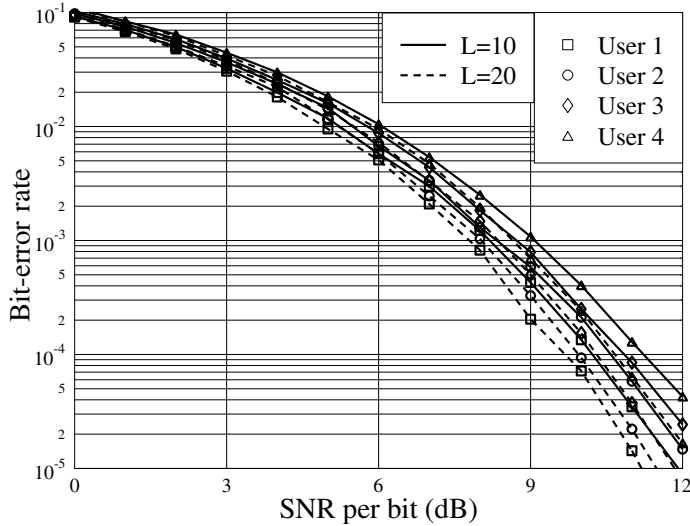


Figure 6.8: QR-decomposition assisted interference cancellation: BER versus average SNR per bit performance for the MC-CDMA using random binary spreading sequences, when communicating over frequency-selective Rayleigh fading channels obeying the uniform MDP and having $L = 10$ or 20 resolvable paths in the T-domain. The MC-CDMA system employs $U = 64$ subcarriers and $q = 4$ bits are transmitted per symbol per user. The simulations were based on (6.167).

are detected successively from user 4 to user 1 using (6.167). As shown in Fig. 6.8, the BER floors are removed due to the QR-decomposition and interference cancellation. However, four users are detected with four different BER values for a given SNR value, where the first detected user (the 4th user) has the highest BER, while the last detected user (the 1st user) achieves the lowest BER. The details for the explanation can be found in Sections 6.2.7.1 to 6.2.7.3.

In IC-assisted MUDs for CDMA systems, interference cancellation usually follows the first-stage correlation detection. Additionally, the interference cancellation can be carried out several times, yielding the so-called multistage interference cancellation (MSIC), in order to improve the error performance. In general, at each stage of the IC, the decision statistics can be expressed as

$$z(i) = \mathbf{G}(i)\mathbf{y}(i) - \mathbf{B}(i)\hat{\mathbf{x}}(i), \quad i = 1, 2, \dots \quad (6.168)$$

where i is for indexing the i th stage of IC. Let us now consider a range of decision feedback schemes.

6.2.7.1 Matched-Filtering Decision-Feedback

Interference cancellation can be carried out either successively or in parallel. Let us first consider the successive interference cancellation (SIC).

Given the observation vector

$$\mathbf{y} = \mathbf{C}\mathbf{H}\mathbf{x} + \mathbf{n} \quad (6.169)$$

after the correlation operation, the $\mathcal{K} = Kq$ -length decision vector can be expressed as

$$\bar{\mathbf{y}} = \underbrace{\mathbf{H}^H \mathbf{C}^T \mathbf{C} \mathbf{H} \mathbf{x}}_R + \mathbf{H}^H \mathbf{C}^T \mathbf{n} \quad (6.170)$$

where the autocorrelation matrix \mathbf{R} is expressed in detail as

$$\mathbf{R} = \begin{bmatrix} r_{11} & r_{12} & \cdots & r_{1\mathcal{K}} \\ r_{21} & r_{22} & \cdots & r_{2\mathcal{K}} \\ \vdots & \vdots & \ddots & \vdots \\ r_{\mathcal{K}1} & r_{\mathcal{K}2} & \cdots & r_{\mathcal{K}\mathcal{K}} \end{bmatrix} \quad (6.171)$$

Let the receiver start by detecting the \mathcal{K} th symbol, its estimation is given by

$$\begin{aligned} \hat{x}_{\mathcal{K}}(1) &= f_{\text{decision}}(\tilde{y}_{\mathcal{K}}(1)) \\ &= f_{\text{decision}}(\bar{y}_{\mathcal{K}}) \end{aligned} \quad (6.172)$$

where $f_{\text{decision}}(x)$ represents the decision making based on x .

After the receiver has the decision of $\hat{x}_{\mathcal{K}}(1)$, it tries to remove the impact of $x_{\mathcal{K}}$ on $x_{\mathcal{K}-1}$ using the operation

$$\tilde{y}_{\mathcal{K}-1}(1) = \bar{y}_{\mathcal{K}-1} - r_{(\mathcal{K}-1)\mathcal{K}} \hat{x}_{\mathcal{K}}(1) \quad (6.173)$$

Based on $\tilde{y}_{\mathcal{K}-1}(1)$ an estimation to $\hat{x}_{\mathcal{K}-1}(1)$ is formed as

$$\hat{x}_{\mathcal{K}-1}(1) = f_{\text{decision}}(\tilde{y}_{\mathcal{K}-1}(1)) \quad (6.174)$$

Following the above approaches, when the receiver has the estimations $\hat{x}_{i+1}(1), \hat{x}_{i+2}(1), \dots, \hat{x}_{\mathcal{K}}(1)$, the receiver forms the decision variable for x_i as

$$\tilde{y}_i(1) = \bar{y}_i - \sum_{j=i+1}^{\mathcal{K}} r_{ij} \hat{x}_j(1), \quad i = 1, 2, \dots, \mathcal{K}-1 \quad (6.175)$$

and makes the decision according to

$$\hat{x}_i(1) = f_{\text{decision}}(\tilde{y}_i(1)), \quad i = 1, 2, \dots, \mathcal{K}-1 \quad (6.176)$$

In summary, the procedure of SIC can be described in matrix form as

$$\begin{aligned} \tilde{\mathbf{y}}(1) &= \bar{\mathbf{y}} - \mathbf{B} \hat{\mathbf{x}}(1) \\ \hat{\mathbf{x}}(1) &= f_{\text{decision}}(\tilde{\mathbf{y}}(1)) \end{aligned} \quad (6.177)$$

where $\hat{\mathbf{x}}(1) = [\hat{x}_1, \hat{x}_2, \dots, \hat{x}_{\mathcal{K}}]^T$ and \mathbf{B} is given by

$$\mathbf{B} = \begin{bmatrix} 0 & r_{12} & r_{13} & \cdots & r_{1\mathcal{K}} \\ 0 & 0 & r_{23} & \cdots & r_{2\mathcal{K}} \\ \vdots & \vdots & \vdots & \ddots & \vdots \\ 0 & 0 & 0 & \cdots & r_{(\mathcal{K}-1)\mathcal{K}} \\ 0 & 0 & 0 & \cdots & 0 \end{bmatrix} \quad (6.178)$$

From the above analysis we can be implied that in SIC the MUI from the previous to the later users may be fully suppressed if the previous detections are correct. However, if a previous user is detected in error, the error will propagate to all the following detections. In order to minimize the events of error propagation, one strategy is to order the user signals from weak to strong. Another way is to use multistage interference cancellation.

Following the first-stage IC, it can be implied that, when the SNR is sufficiently high, x_1 is detected with the highest reliability, since all the other signals before its detection have been detected and their interference to x_1 might be subtracted. We can also be implied that $x_{\mathcal{K}}$ is detected with the lowest reliability, since the receiver makes no attempt to suppress the interference before detection of $x_{\mathcal{K}}$.

Since after the first-stage IC the reliability is in the order of $\hat{x}_1(1), \hat{x}_2(1), \dots, \hat{x}_{\mathcal{K}}(1)$, at the second-stage IC, the receiver can first detect x_2 by attempting to subtract the interference from x_1 , then, detect x_3 by attempting to subtract the interference from both x_1 and x_2 , and so on. To be more specific, we have

$$\begin{aligned}\tilde{y}_1(2) &= \tilde{y}_1(1) \\ \hat{x}_1(2) &= f_{\text{decision}}(\tilde{y}_1(2)) \\ \tilde{y}_i(2) &= \tilde{y}_i(1) - \sum_{j=1}^{i-1} r_{ij} \hat{x}_j(2), \quad i = 2, 3, \dots, \mathcal{K} \\ \hat{x}_i(2) &= f_{\text{decision}}(\tilde{y}_i(2)), \quad i = 2, 3, \dots, \mathcal{K}\end{aligned}\tag{6.179}$$

When expressed in matrix form, we have

$$\begin{aligned}\tilde{\mathbf{y}}(2) &= \tilde{\mathbf{y}}(1) - \mathbf{B}^H \hat{\mathbf{x}}(2) \\ \hat{\mathbf{x}}(2) &= f_{\text{decision}}(\tilde{\mathbf{y}}(2))\end{aligned}\tag{6.180}$$

where \mathbf{B}^H is used because \mathbf{R} is Hermitian.

Following the second-stage IC, the further stage of IC can be similarly carried out. The operation can be summarized as

$$\begin{cases} \tilde{\mathbf{y}}(2i-1) = \tilde{\mathbf{y}} - \mathbf{B} \hat{\mathbf{x}}(2i-1) \\ \hat{\mathbf{x}}(2i-1) = f_{\text{decision}}(\tilde{\mathbf{y}}(2i-1)) \end{cases} \quad ((2i-1)\text{-stage}) \tag{6.181}$$

$$\begin{cases} \tilde{\mathbf{y}}(2i) = \tilde{\mathbf{y}}(2i-1) - \mathbf{B}^H \hat{\mathbf{x}}(2i) \\ \hat{\mathbf{x}}(2i) = f_{\text{decision}}(\tilde{\mathbf{y}}(2i)) \end{cases} \quad (2i\text{-stage}) \tag{6.182}$$

for $i = 1, 2, \dots$

In Figs. 6.9 and 6.10 the BER performance of the considered MC-CDMA is depicted after the first- and second-stage SICs. From Fig. 6.9 we can see that user 4 has the worst BER performance, as there was no attempt at interference cancellation in its detection. By contrast, user 1 has the best BER performance among the four users because the receiver attempted to subtract interference from all the other users.

After the second-stage IC, as seen in Fig. 6.10, all four users achieve nearly the same BER performance. However, due to the detection of the fourth user at the first-stage and the error propagation property of SIC, the BER error-floors cannot be removed by the SICs

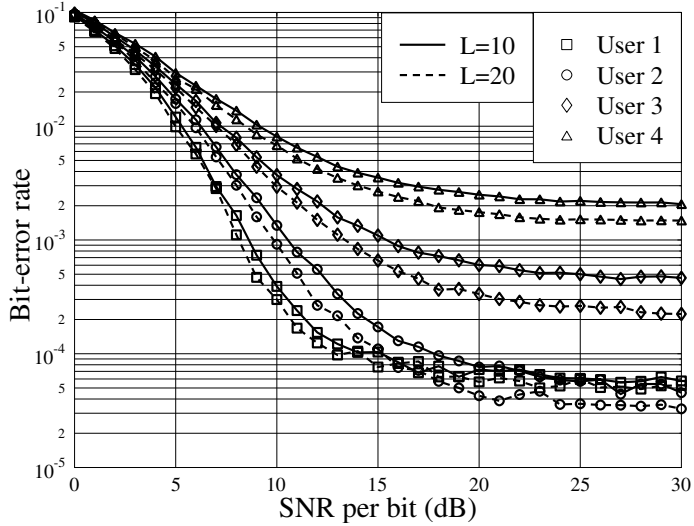


Figure 6.9: First-stage MF-SIC: BER versus average SNR per bit performance for the MC-CDMA using random binary spreading sequences, when communicating over frequency-selective Rayleigh fading channels obeying the uniform MDP and having $L = 10$ or 20 resolvable paths in the T-domain. The MC-CDMA system employs $U = 64$ subcarriers and $q = 4$ bits are transmitted per symbol per user. The simulations were based on (6.181) and (6.182).

following the matched-filtering operation. Later, we will show that the BER error floors can be efficiently removed when the SIC is carried out either by ZF (decorrelating) or MMSE principles.

In practice when the receiver has *a priori* knowledge of the reliabilities of the transmitted symbols by the K users, then the ordered detection can be applied and the symbols can be detected in order from higher to lower reliability. In CDMA systems the SIC technique is very suitable in situations where signals are received with different power levels. In this case signals are ordered according to their power levels and the detection is carried out in order from highest to lowest power level. In the considered MC-CDMA systems we assume that all the uplink signals are received with the same average power level, which can usually be achieved with the aid of power control [8]. Therefore, when long-term average is applied, all the uplink signals reach the BS with the same strength. In MC-CDMA systems the MC-CDMA signals usually experience frequency-selective fading, resulting in some signals being stronger than others in the relatively short term. When this is the case, the signals may be detected in order from the strongest to the weakest. However, when the fading selectivity of the channel is high and when each symbol is conveyed by a high number of subcarriers, the diversity order is then high. Consequently, it is hard to identify which signals are the more reliable ones. Furthermore, in MC-CDMA systems it can be that the reliability of detecting a symbol is not highly dependent on the signal's strength, but more on the signal's correlation with the other symbols. Hence, one strategy for extracting the reliability information might be based on assessing the correlation values with the other signals. Additionally, the SINR

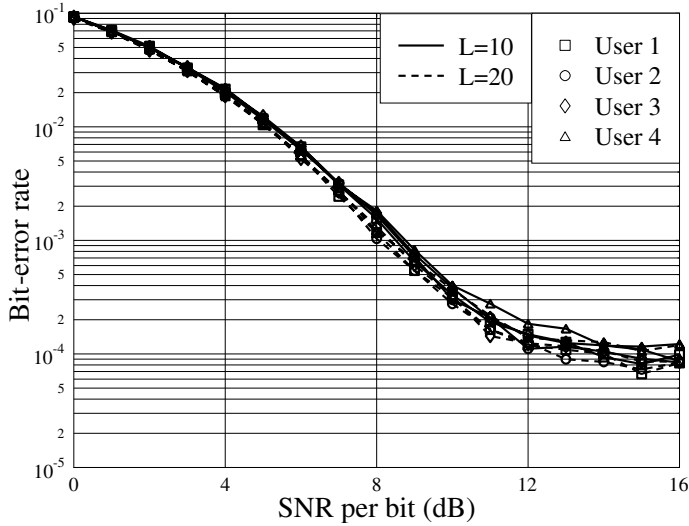


Figure 6.10: Second-stage MF-SIC: BER versus average SNR per bit performance for the MC-CDMA using random binary spreading sequences, when communicating over frequency-selective Rayleigh fading channels obeying the uniform MDP and having $L = 10$ or 20 resolvable paths in the T-domain. The MC-CDMA system employs $U = 64$ subcarriers and $q = 4$ bits are transmitted per symbol per user. The simulations were based on (6.181) and (6.182).

values can also serve as the measurements of the reliability, in order to improve the BER performance beyond that shown in Figs. 6.9 and 6.10.

Additionally, when all the detections have achieved a similar error floor, as seen in Fig. 6.10 after the second-stage IC, further IC stages usually do not improve BER performance. Let us now analyse the parallel interference cancellation (PIC).

The PIC can be described well using Fig. 6.11. Let the input to the i th stage of IC be expressed as $\tilde{\mathbf{y}}(i)$, where $\tilde{\mathbf{y}}(1) = \bar{\mathbf{y}}$. Then, based on $\tilde{\mathbf{y}}(i)$ the estimation to $\hat{\mathbf{x}}(i)$ can be expressed as

$$\hat{\mathbf{x}}(i) = f_{\text{decision}}(\tilde{\mathbf{y}}(i)) \quad (6.183)$$

As shown in Fig. 6.11, after the decision, interference cancellation is carried out, which generates output for the next stage. The interference cancellation procedure can be represented as [165]

$$\begin{aligned} \tilde{\mathbf{y}}(i+1) &= \bar{\mathbf{y}} - (\mathbf{R} - \text{diag}\{\mathbf{R}\})\hat{\mathbf{x}}(i) \\ &= \bar{\mathbf{y}} - (\mathbf{R} - \text{diag}\{\mathbf{R}\})f_{\text{decision}}(\tilde{\mathbf{y}}(i)) \\ i &= 1, 2, \dots \end{aligned} \quad (6.184)$$

It is explicit that in the multistage PIC the receiver attempts to suppress the MUI from all the interfering users. However, as with the SIC, if a signal at the current stage is detected in error, it will enhance its interference to the other signals in the following IC stage. For this reason, the so-called partial PIC has been proposed in reference [166]. Instead of making

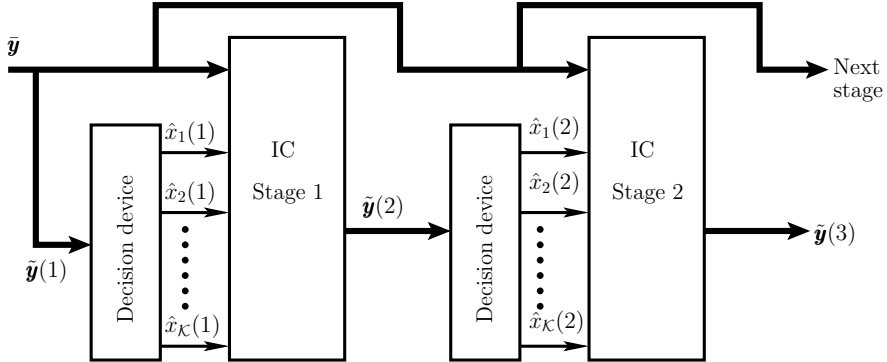


Figure 6.11: Schematic block diagram of multi-stage parallel interference cancellation.

full use of the estimated data as in (6.184), the partial PIC attempts only to subtract a fraction of the MUI at each stage. The partial PIC can be represented as

$$\begin{aligned}
 \tilde{\mathbf{y}}(i+1) &= \bar{\mathbf{y}} - \lambda(i)(\mathbf{R} - \text{diag}\{\mathbf{R}\})\hat{\mathbf{x}}(i) \\
 &= \bar{\mathbf{y}} - \lambda(i)(\mathbf{R} - \text{diag}\{\mathbf{R}\})f_{\text{decision}}(\tilde{\mathbf{y}}(i))
 \end{aligned} \quad i = 1, 2, \dots \quad (6.185)$$

where $0 < \lambda(i) \leq 1$ is a weight for the i th stage of IC.

Furthermore, if the *a priori* reliability information in the context of each symbol is available, different weights can be applied for different symbols. In this case the partial PIC can be represented as

$$\begin{aligned}
 \tilde{\mathbf{y}}(i+1) &= \bar{\mathbf{y}} - (\mathbf{R} - \text{diag}\{\mathbf{R}\})\lambda(i)\hat{\mathbf{x}}(i) \\
 &= \bar{\mathbf{y}} - (\mathbf{R} - \text{diag}\{\mathbf{R}\})\lambda(i)f_{\text{decision}}(\tilde{\mathbf{y}}(i))
 \end{aligned} \quad i = 1, 2, \dots \quad (6.186)$$

where $\lambda(i) = \text{diag}\{\lambda_1(i), \lambda_2(i), \dots, \lambda_K(i)\}$, $(0 < \lambda_k(i) \leq 1)$ contains the weights for the i th stage of IC.

Figure 6.12 shows the BER versus average SNR per bit performance for the considered MC-CDMA using the multistage PIC based on (6.184), when communicating over frequency-selective Rayleigh fading channels having, respectively, $L = 10$ or 20 T-domain resolvable paths. As can be seen from Fig. 6.12, the BER performance is significantly improved when the PIC-assisted MUD is employed, in contrast to the MC-CDMA using only the MF-assisted detection without using interference cancellation. As seen in Fig. 6.12, the first stage of PIC results in the most significant BER performance improvement. The second stage of PIC still provides some SNR gains over the first stage of PIC, especially in the relatively high SNR region. However, it seems that employing the PIC beyond stage 2 does not result in observable SNR gains in the considered SNR region.

Figure 6.13 shows the BER performance of the MC-CDMA system when the multistage partial MF-PIC is employed. The results of Fig. 6.13 show that the achieved BER is different for different values of $\lambda(i)$ in (6.185). In a relatively low SNR region, such as SNR < 10dB,

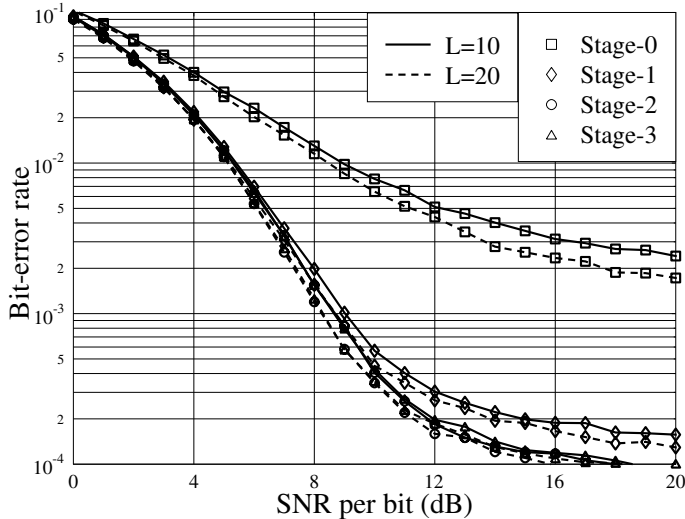


Figure 6.12: Multistage MF-PIC: BER versus average SNR per bit performance for the MC-CDMA using random binary spreading sequences, when communicating over frequency-selective Rayleigh fading channels obeying the uniform MDP and having $L = 10$ or 20 resolvable paths in the T-domain. The MC-CDMA system employs $U = 64$ subcarriers and $q = 4$ bits are transmitted per symbol per user. The simulations were based on (6.184).

a relatively higher $\lambda(i)$ value returns a better BER performance. Furthermore, it seems that, for a given SNR value, there exists an optimum $\lambda(i)$ value, which results in the lowest BER.

6.2.7.2 Zero-Forcing Decision-Feedback

ZF decision-feedback (ZF-DF) MUD, which is also referred to as decorrelating DF MUD, is designed so that the interference imposed by the latter detected signals on the early detected signals is suppressed based on the principles of the ZF-MUD (or decorrelating MUD) [167]. Since the ZF-DF MUD involves both the ZF and maximum likelihood principles, as shown in Section 6.2.9, the ZF-DF MUD usually outperforms the conventional ZF (decorrelating) MUD in terms of the achievable BER performance.

In the considered MC-CDMA system the output after the correlation operation is given by

$$\bar{\mathbf{y}} = \mathbf{R}\mathbf{x} + \bar{\mathbf{n}} \quad (6.187)$$

where $\bar{\mathbf{n}} = \mathbf{H}^H \mathbf{C}^T \mathbf{n}$, which is Gaussian distributed with zero mean and a covariance matrix given by $\sigma^2 \mathbf{R}$.

For the ZF-SIC, the correlation matrix \mathbf{R} is first factorized based on the Choleski decomposition [156], yielding $\mathbf{R} = \mathbf{M}\mathbf{M}^H$ and hence (6.187) can be expressed as

$$\bar{\mathbf{y}} = \mathbf{M}\mathbf{M}^H \mathbf{x} + \bar{\mathbf{n}} \quad (6.188)$$

where \mathbf{M} is a unique lower triangular matrix with real positive principal diagonal entries. Multiplying both sides of (6.188) by \mathbf{M}^{-1} , yields

$$\mathbf{z} = \mathbf{M}^H \mathbf{x} + \tilde{\mathbf{n}} \quad (6.189)$$

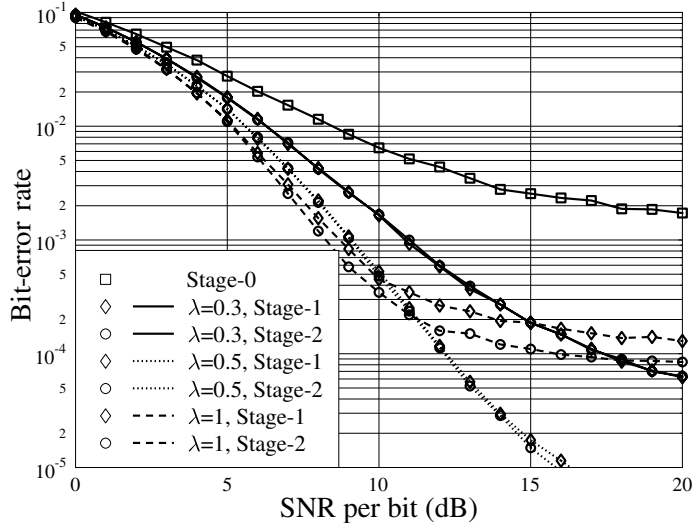


Figure 6.13: Multistage MF-PIC: BER versus average SNR per bit performance for the MC-CDMA using random binary spreading sequences, when communicating over frequency-selective Rayleigh fading channels obeying the uniform MDP and having $L = 20$ resolvable paths in the T-domain. The MC-CDMA system employs $U = 64$ subcarriers and $q = 4$ bits are transmitted per symbol per user. The simulations were based on (6.185).

where $\tilde{\mathbf{n}} = \mathbf{M}^{-1}\bar{\mathbf{n}} = \mathbf{M}^{-1}\mathbf{H}^H\mathbf{C}^T\mathbf{n}$. It can be shown that $\tilde{\mathbf{n}}$ is white Gaussian with a covariance matrix of $\sigma^2\mathbf{I}_{\mathcal{K}}$.

Let in (6.189) the upper triangular matrix be expressed as

$$\mathbf{M}^H = \begin{bmatrix} m_{11} & m_{12} & \cdots & m_{1\mathcal{K}} \\ 0 & m_{22} & \cdots & m_{2\mathcal{K}} \\ \vdots & \vdots & \ddots & \vdots \\ 0 & 0 & \cdots & m_{\mathcal{K}\mathcal{K}} \end{bmatrix} \quad (6.190)$$

Then, the interference cancellation can be represented as

$$\begin{aligned} \tilde{y}_{\mathcal{K}} &= z_{\mathcal{K}} \\ \hat{x}_{\mathcal{K}} &= f_{\text{decision}}(\tilde{y}_{\mathcal{K}}) \end{aligned} \quad (6.191)$$

$$\tilde{y}_k = z_k - \sum_{i=k+1}^{\mathcal{K}} m_{ki} \hat{x}_i, \quad k = \mathcal{K} - 1, \dots, 1$$

$$x_k = f_{\text{decision}}(\tilde{y}_k) \quad (6.192)$$

As can be seen from (6.191) and (6.192), $x_{\mathcal{K}}$ conflicts no MUI, x_i conflicts interference only from $x_{i+1}, \dots, x_{\mathcal{K}}$ and there is no interference from x_1, \dots, x_{i-1} . Therefore, the demodulation of x_i in the context of the ZF-SIC decorrelates against x_1, \dots, x_{i-1} .

The overall process for implementing the ZF-SIC can be represented in matrix form as

$$\begin{cases} \tilde{\mathbf{y}} = \mathbf{M}^{-1}\bar{\mathbf{y}} - (\mathbf{M}^H - \text{diag}\{\mathbf{M}^H\})\hat{\mathbf{x}} \\ \hat{\mathbf{x}} = f_{\text{decision}}(\tilde{\mathbf{y}}) \end{cases} \quad (6.193)$$

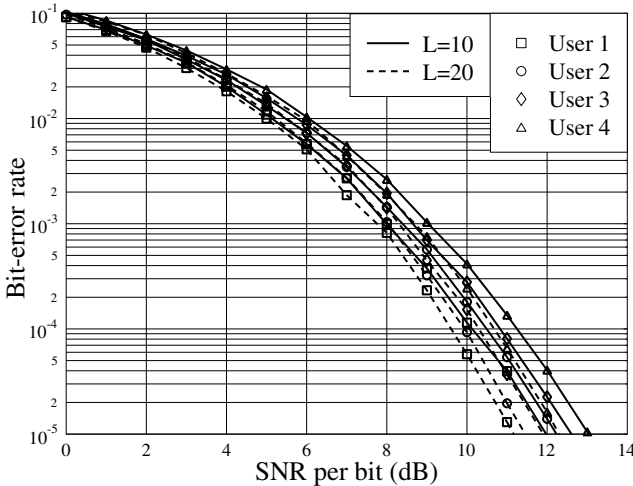


Figure 6.14: ZF-SIC: BER versus average SNR per bit performance for the MC-CDMA using random binary spreading sequences, when communicating over frequency-selective Rayleigh fading channels obeying the uniform MDP and having $L = 10$ or 20 resolvable paths in the T-domain. The MC-CDMA system employs $U = 64$ subcarriers and $q = 4$ bits are transmitted per symbol per user. The simulations were based on (6.193).

Figure 6.14 shows the BER performance of the MC-CDMA when using the ZF-SIC assisted MUD. It is clear that the BER performances of the four users are different, performing worse with the earlier detected user than with the latter. This is because the earlier detected user is demodulated, based more on the ZF principle than on the maximum likelihood principle. Conversely, the latter detected user is demodulated, based less on the ZF principle than on the maximum likelihood principles. It is well known that the maximum likelihood MUD results in a better BER performance than the ZF (decorrelating) MUD [88].

In order to make the BER performance for different users similar, one strategy is to arrange the user signals from weakest to strongest. In this way the relatively strong signals are detected, based more on the ZF principle, while the relatively weak signals are detected, based more on the maximum likelihood principle.

Alternatively, a further stage of IC can be carried out in order to make the BER performance for different users similar. At this IC stage the orders of the user signals are inverted. Then, the IC is carried out by invoking the data symbols estimated at the first IC stage.

In the context of the ZF-PIC, the first IC stage is based on the outputs of the conventional ZF-MUD. In this case, we have

$$\mathbf{z} = \mathbf{R}^{-1} \bar{\mathbf{y}} = \mathbf{x} + \tilde{\mathbf{n}} \quad (6.194)$$

and the decision is

$$\hat{\mathbf{x}} = f_{\text{decision}}(\mathbf{z}) = f_{\text{decision}}(\mathbf{R}^{-1} \bar{\mathbf{y}}) \quad (6.195)$$

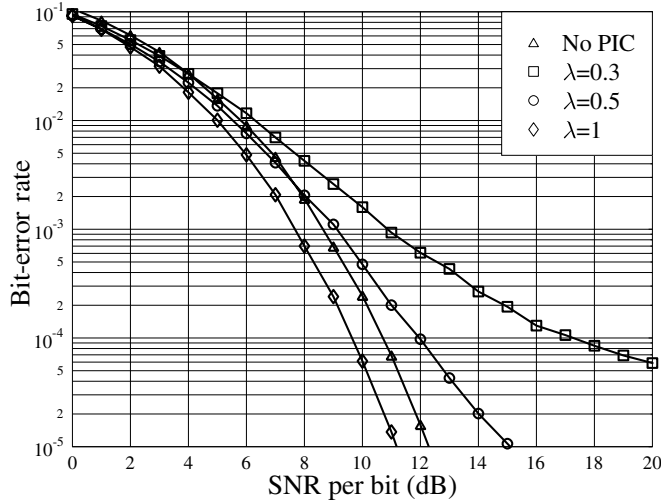


Figure 6.15: ZF-PIC: BER versus average SNR per bit performance for the MC-CDMA using random binary spreading sequences, when communicating over frequency-selective Rayleigh fading channels obeying the uniform MDP and having $L = 20$ resolvable paths in the T-domain. The MC-CDMA system employs $U = 64$ subcarriers and $q = 4$ bits are transmitted per symbol per user. The simulations were based on (6.196).

The ZF-PIC can be carried out in multistage fashion. The overall process of the ZF-PIC can be represented in matrix form as

$$\begin{cases} \tilde{\mathbf{y}}(i) = \bar{\mathbf{y}} - (\mathbf{R} - \text{diag}\{\mathbf{R}\})\lambda(i)\hat{\mathbf{x}}(i-1), & i = 1, 2, \dots \\ \hat{\mathbf{x}}(i) = f_{\text{decision}}(\tilde{\mathbf{y}}(i)) \end{cases} \quad (6.196)$$

where $\tilde{\mathbf{y}}(0) = \mathbf{R}^{-1}\bar{\mathbf{y}}$, $\lambda(i) = \text{diag}\{\lambda_1(i), \lambda_2(i), \dots, \lambda_K(i)\}$ contains the coefficients for weighting the estimated symbols.

Figure 6.15 illustrates the BER performance of the MC-CDMA system using the one-stage ZF-PIC, when different weight values are used associated with the ZF-PIC. In Fig. 6.15 the BER performance of the MC-CDMA using the conventional ZF (decorrelating) detector derived in Section 6.2.1 is also illustrated. As shown in Fig. 6.15, the ZF-PIC is capable of outperforming the conventional ZF-MUD, provided that an appropriate weight is applied.

6.2.7.3 Minimum Mean-Square Error Decision-Feedback

MMSE-DF can also be implemented successively or in parallel, yielding the MMSE-SIC and MMSE-PIC [88]. There are also other implementation structures for the MMSE-DF [168]. Let us first consider the MMSE-SIC.

Instead of factorizing the correlation matrix \mathbf{R} as in the ZF-SIC, as shown in (6.188), in the context of the MMSE-PIC we use the factorization [88] of

$$\mathbf{R} + \sigma^2 \mathbf{I}_K = \mathbf{M} \mathbf{M}^H \quad (6.197)$$

Multiplying both sides of (6.187) by \mathbf{M}^{-1} , the decision variable vector can be expressed as

$$\begin{aligned} \mathbf{z} &= \mathbf{M}^{-1}\bar{\mathbf{y}} \\ &= \mathbf{M}^{-1}\mathbf{R}\mathbf{x} + \tilde{\mathbf{n}} \\ &= \mathbf{M}^H\mathbf{x} - \sigma^2\mathbf{M}^{-1}\mathbf{x} + \tilde{\mathbf{n}} \end{aligned} \quad (6.198)$$

where $\tilde{\mathbf{n}} = \mathbf{M}^{-1}\bar{\mathbf{n}}$, while $\sigma^2\mathbf{M}^{-1}\mathbf{x}$ represents the ‘leaked’ MUI from the MMSE detection. Consequently, when without the knowledge of σ^2 , the MMSE-SIC can be represented as

$$\begin{cases} \tilde{\mathbf{y}}(1) = \mathbf{M}^{-1}\bar{\mathbf{y}} - (\mathbf{M}^H - \text{diag}\{\mathbf{M}^H\})\hat{\mathbf{x}}(1) \\ \hat{\mathbf{x}}(1) = f_{\text{decision}}(\tilde{\mathbf{y}}(1)) \end{cases} \quad (6.199)$$

where the detection order is from x_K to x_1 .

When the detector employs the knowledge of σ^2 , based on (6.199), the SIC can be carried out from x_1 to x_K according to

$$\begin{cases} \tilde{\mathbf{y}}(2) = \mathbf{M}^{-1}\tilde{\mathbf{y}}(1) + \sigma^2(\mathbf{M}^{-1} - \text{diag}\{\mathbf{M}^{-1}\})\hat{\mathbf{x}}(1) \\ \hat{\mathbf{x}}(2) = f_{\text{decision}}(\tilde{\mathbf{y}}(2)) \end{cases} \quad (6.200)$$

The MMSE-SIC also has the characteristic of different users having different resulted BER performances, as shown in Figs. 6.16 and 6.17. As the ZF-SIC, improved version of MMSE-SIC or multistage MMSE-SIC may be implemented, so that all the users achieve a similar BER performance.

As shown in Fig. 6.17, another IC stage for suppressing the ‘leaked’ MUI does not result in significant SNR gain. This in turn implies that the ‘leaked’ MUI after the MMSE detection is insignificant.

In the context of the MMSE-PIC, the first PIC stage uses the estimated data based on the conventional MMSE-MUD, derived in Section 6.2.3. In summary, the multistage MMSE-PIC can be represented as

$$\begin{cases} \tilde{\mathbf{y}}(i) = \bar{\mathbf{y}} - (\mathbf{R} - \text{diag}\{\mathbf{R}\})\lambda(i)\hat{\mathbf{x}}(i-1), & i = 1, 2, \dots \\ \hat{\mathbf{x}}(i) = f_{\text{decision}}(\tilde{\mathbf{y}}(i)) \end{cases} \quad (6.201)$$

where $\tilde{\mathbf{y}}(0) = (\mathbf{R} + \sigma^2\mathbf{I}_K)^{-1}\bar{\mathbf{y}}$, $\lambda(i) = \text{diag}\{\lambda_1(i), \lambda_2(i), \dots, \lambda_K(i)\}$ contains the coefficients for weighting the cancellation of the estimated symbols.

Figure 6.18 shows the BER performance of the MC-CDMA using the one-stage MMSE-PIC, when different weight values are employed associated with the MMSE-PIC. It is clear that when an appropriate weight value is applied, the MMSE-PIC outperforms the conventional MMSE-MUD studied in Section 6.2.3. Note that the BER performance may be further improved when more than one stage of PIC is invoked.

6.2.8 Maximum A Posteriori Probability Multiuser Detection

MAP-assisted MUD is capable of minimizing the probability of error. Hence, MAP-MUD is also referred to as the minimum error probability (MEP) MUD [88]. MAP-MUD makes use of the *a priori* information about the data symbols to be detected and outputs the soft

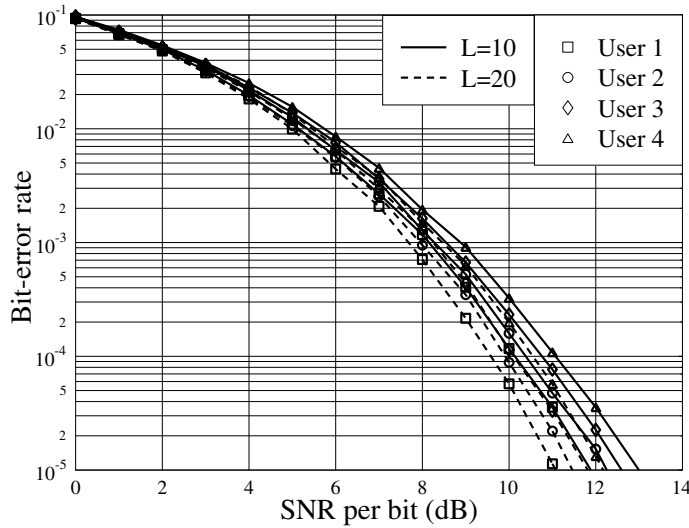


Figure 6.16: MMSE-SIC: BER versus average SNR per bit performance for the MC-CDMA using random binary spreading sequences, when communicating over frequency-selective Rayleigh fading channels obeying the uniform MDP and having $L = 10$ and 20 T-domain resolvable paths. The MC-CDMA system employs $U = 64$ subcarriers and $q = 4$ bits are transmitted per symbol per user. The simulations were based on (6.199).

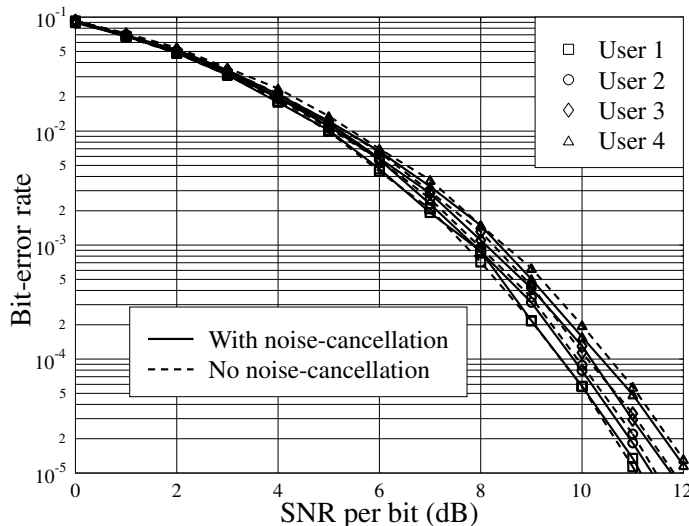


Figure 6.17: MMSE-SIC: BER versus average SNR per bit performance for the MC-CDMA using random binary spreading sequences, when communicating over frequency-selective Rayleigh fading channels obeying the uniform MDP and having $L = 20$ T-domain resolvable paths. The MC-CDMA system employs $U = 64$ subcarriers and $q = 4$ bits are transmitted per symbol per user. The simulations were based on (6.200).

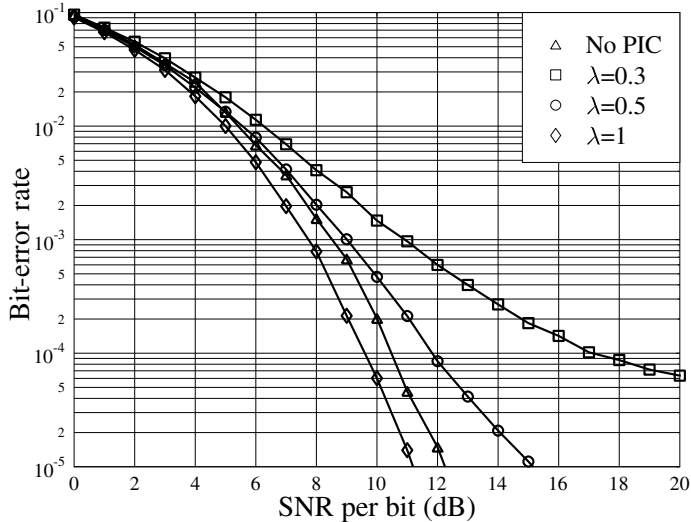


Figure 6.18: MMSE-PIC: BER versus average SNR per bit performance for the MC-CDMA using random binary spreading sequences, when communicating over frequency-selective Rayleigh fading channels obeying the uniform MDP and having $L = 20$ T-domain resolvable paths. The MC-CDMA system employs $U = 64$ subcarriers and $q = 4$ bits are transmitted per symbol per user. The simulations were based on (6.201).

estimations for these symbols. Hence, the MAP-MUD is beneficial to iterative (turbo) MUD and has been widely studied in conjunction with iterative (turbo) detection [90, 169]. In this section we consider the MAP-MUD at different levels as detailed below.

For the sake of generality, the MAP-MUDs are built on a block of $(U \times M)$ observations

$$\mathbf{Y} = [\mathbf{y}^{(1)}, \mathbf{y}^{(2)}, \dots, \mathbf{y}^{(M)}] \quad (6.202)$$

which correspond to $(\mathcal{K} \times M)$, where $\mathcal{K} = Kq$ data symbols transmitted by the K uplink users within the M MC-CDMA symbol periods, where M , for example, may represent the length of a codeword, if forward-error-correction (FEC) coding is invoked. The $(\mathcal{K} \times M)$ data symbols are expressed as

$$\mathbf{X} = [\mathbf{x}^{(1)}, \mathbf{x}^{(2)}, \dots, \mathbf{x}^{(M)}] \quad (6.203)$$

where $\mathbf{x}^{(m)}$ contains the symbols of the K users, which are transmitted within the m th MC-CDMA symbol period,

$$\begin{aligned} \mathbf{x}^{(m)} &= [(\mathbf{x}_1^{(m)})^T, \dots, (\mathbf{x}_K^{(m)})^T]^T, \quad m = 1, 2, \dots, M \\ \mathbf{x}_k^{(m)} &= [x_{k1}^{(m)}, \dots, x_{kq}^{(m)}]^T, \quad k = 1, 2, \dots, K \end{aligned} \quad (6.204)$$

Hence, $\mathbf{x}^{(m)}$ is a $(\mathcal{K} = Kq)$ -length vector.

According to (6.21) the observation vector $\mathbf{y}^{(m)}$ can be written as

$$\mathbf{y}^{(m)} = \mathbf{C}\mathbf{H}^{(m)}\mathbf{x}^{(m)} + \mathbf{n}^{(m)}, \quad m = 1, 2, \dots, M \quad (6.205)$$

We assume that the BS receiver employs the knowledge of $\mathbf{C}\mathbf{H}^{(m)}$. Hence, the MAP-MUDs can also be derived based on

$$\tilde{\mathbf{Y}} = [\tilde{\mathbf{y}}^{(1)}, \tilde{\mathbf{y}}^{(2)}, \dots, \tilde{\mathbf{y}}^{(M)}] \quad (6.206)$$

where $\tilde{\mathbf{y}}^{(m)}$ is given by

$$\begin{aligned} \tilde{\mathbf{y}}^{(m)} &= (\mathbf{C}\mathbf{H}^{(m)})^H \mathbf{y}^{(m)} \\ &= \mathbf{R}^{(m)} \mathbf{x}^{(m)} + \bar{\mathbf{n}}^{(m)}, \quad m = 1, 2, \dots, M \end{aligned} \quad (6.207)$$

where $\mathbf{R}^{(m)} = (\mathbf{C}\mathbf{H}^{(m)})^H \mathbf{C}\mathbf{H}^{(m)}$ and $\bar{\mathbf{n}}^{(m)} = (\mathbf{C}\mathbf{H}^{(m)})^H \mathbf{n}^{(i)}$, which is Gaussian distributed with zero-mean and a covariance matrix of $\sigma^2 \mathbf{R}^{(m)}$. Given $\mathbf{R}^{(m)}$ or $\mathbf{H}^{(m)}$, the probability density function (PDF) of $\tilde{\mathbf{y}}^{(m)}$ for a given $\mathbf{x}^{(m)}$ is given by

$$\begin{aligned} f(\tilde{\mathbf{y}}^{(m)} | \mathbf{x}^{(m)}) &= \frac{1}{(\pi\sigma^2)^K \det(\mathbf{R}^{(m)})} \\ &\times \exp[-(\tilde{\mathbf{y}}^{(m)} - \mathbf{R}^{(m)} \mathbf{x}^{(m)})^H (\mathbf{R}^{(m)})^{-1} (\tilde{\mathbf{y}}^{(m)} - \mathbf{R}^{(m)} \mathbf{x}^{(m)}) / \sigma^2] \end{aligned} \quad (6.208)$$

In order to distinguish between the different types of MAP-MUD, the following names are adopted:

- *K*-user block-based MAP-MUD (BMAP-MUD): the *K*-user BMAP-MUD detects $\mathbf{x}^{(m)}$ ($m = 1, 2, \dots, M$) based on the observation \mathbf{Y} or $\tilde{\mathbf{Y}}$;
- Single-user BMAP-MUD: the single-user BMAP-MUD detects $x_{kj}^{(m)}$ ($j = 1, \dots, q$; $k = 1, \dots, K$; $m = 1, \dots, M$) based on the observation \mathbf{Y} or $\tilde{\mathbf{Y}}$;
- *K*-user symbol-based MAP-MUD (SMAP-MUD): the *K*-user SMAP-MUD detects $\mathbf{x}^{(m)}$ ($m = 1, \dots, M$) based on the observation $\mathbf{y}^{(m)}$ or $\tilde{\mathbf{y}}^{(m)}$;
- Single-user symbol-based MAP-MUD (SMAP-MUD): the single-user SMAP-MUD detects $x_{kj}^{(m)}$ ($j = 1, \dots, q$; $k = 1, \dots, K$; $m = 1, \dots, M$) based on the observation $\mathbf{y}^{(m)}$ or $\tilde{\mathbf{y}}^{(m)}$;
- Bit-by-bit MAP-MUD (BitMAP-MUD): the BitMAP-MUD detects a bit in $x_{kj}^{(m)}$ ($j = 1, \dots, q$; $k = 1, \dots, K$; $m = 1, \dots, M$) based on the observation $\mathbf{y}^{(m)}$ or $\tilde{\mathbf{y}}^{(m)}$, where $x_{kj}^{(m)}$ is represented in binary as $x_{kj}^{(m)} \leftrightarrow [b_{kj}^{(m)}(b) \dots b_{kj}^{(m)}(1)]$ and b is the binary-length of a transmitted symbol.

The *assumptions* applied for the derivations of the MAP-MUDs are as follows. First, it is assumed that the channels in the context of the *K* number of uplink users are ideally estimated at the BS. Second, the transmitted data symbols of different users are assumed to be independent of each other and the data symbols as well as the information bits of a given user are ideally interleaved whenever necessary. Third, the signal set (constellation) is assumed to be $\mathcal{X} = \{X_0, X_1, \dots, X_{Q-1}\}$, where $X_i \in \mathcal{X}$ is complex and represents a legitimate point of the signal constellation, $Q = 2^b$ is the size of the constellation. Furthermore, it is assumed

that all the uplink transmissions use the same constellation and the *a priori* probability of $x_{kj}^{(m)} = X_s$ is given by

$$\begin{aligned} P_{kj}^{(m)}(s) &= P[x_{kj}^{(m)} = X_s], \quad s = 0, 1, \dots, Q-1; \quad m = 1, 2, \dots, M \\ j &= 1, 2, \dots, q; \quad k = 1, 2, \dots, K \end{aligned} \quad (6.209)$$

Explicitly, $P_{kj}^{(m)}(s)$ satisfies

$$\sum_{s=0}^{Q-1} P_{kj}^{(m)}(s) = 1 \quad (6.210)$$

Note that the K -user BMAP-MUD and single-user BMAP-MUD are optimum in the sense of maximizing the *a posteriori* probability by making use of the available information related to the whole data block, including the characteristics of the transmitted information as well as the channels conveying the information. By contrast, the other MAP-MUDs in the list are suboptimum, since the detection is based only on the observations that are directly related to the transmitted data. They are optimum only when the transmitted data as well as the communications channels are independent associated with the observations $\bar{\mathbf{y}}^{(1)}, \bar{\mathbf{y}}^{(2)}, \dots, \bar{\mathbf{y}}^{(M)}$. However, this is usually not the case, since in practice, correlation in sources usually cannot be fully removed and FEC coding is often employed, which also introduces correlation among the transmitted data.

Let us now derive in detail the MAP-MUDs in the list of this section.

For the K -user BMAP-MUD, the estimate to $\mathbf{x}^{(m)}$ maximizes its *a posteriori* probability when given the observation $\bar{\mathbf{Y}}$, which can be expressed as

$$\hat{\mathbf{x}}^{(m)} = \arg \max_{\mathbf{x}^{(t)} \in \mathcal{X}^{\mathcal{K}}} \{P(\mathbf{x}^{(t)} | \bar{\mathbf{Y}})\} \quad (6.211)$$

where $\mathbf{x}^{(t)}$ is a test symbol vector in the same form of $\mathbf{x}^{(m)}$ as seen in (6.204), $P(\mathbf{x}^{(t)} | \bar{\mathbf{Y}})$ is the *a posteriori* probability of $\mathbf{x}^{(t)}$ given the observation $\bar{\mathbf{Y}}$, which by the Bayes rule can be expressed as

$$\begin{aligned} P(\mathbf{x}^{(t)} | \bar{\mathbf{Y}}) &= \frac{P(\bar{\mathbf{Y}} | \mathbf{x}^{(t)}) P(\mathbf{x}^{(t)})}{P(\bar{\mathbf{Y}})} \\ &\propto \frac{f(\bar{\mathbf{Y}} | \mathbf{x}^{(t)}) P(\mathbf{x}^{(t)})}{f(\bar{\mathbf{Y}})} \end{aligned} \quad (6.212)$$

where the symbol ‘ \propto ’ is applied to the case that the probability law may not be satisfied. In (6.212) $f(\bar{\mathbf{Y}} | \mathbf{x}^{(t)})$ is the PDF of $\bar{\mathbf{Y}}$ given that $\mathbf{x}^{(t)}$ was transmitted, $P(\mathbf{x}^{(t)})$ is the *a priori* probability of $\mathbf{x}^{(t)} \in \mathcal{X}^{\mathcal{K}}$ and the denominator $f(\bar{\mathbf{Y}})$ does not depend on the transmitted data. In fact, $f(\bar{\mathbf{Y}})$ is just a normalization factor that can be expressed as

$$f(\bar{\mathbf{Y}}) = \sum_{\mathbf{x}^{(1)} \in \mathcal{X}^{\mathcal{K}}} \cdots \sum_{\mathbf{x}^{(M)} \in \mathcal{X}^{\mathcal{K}}} f(\bar{\mathbf{Y}} | \mathbf{x}^{(1)}, \dots, \mathbf{x}^{(M)}) P(\mathbf{x}^{(1)}, \dots, \mathbf{x}^{(M)}) \quad (6.213)$$

In (6.212) $f(\bar{Y} \mid \mathbf{x}^{(t)})$ is the PDF of observing \bar{Y} conditioned on the transmitted data $\mathbf{x}^{(m)} = \mathbf{x}^{(t)}$. It can be shown that $f(\bar{Y} \mid \mathbf{x}^{(t)})$ can be computed as

$$\begin{aligned} f(\bar{Y} \mid \mathbf{x}^{(t)}) &= f(\bar{y}^{(1)}, \dots, \bar{y}^{(m)}, \dots, \bar{y}^{(M)} \mid \mathbf{x}^{(t)}) \\ &= \underbrace{\sum_{\mathbf{x}^{(1)} \in \mathcal{X}^K} \dots \sum_{\mathbf{x}^{(M)} \in \mathcal{X}^K}}_{(M-1) \text{ terms}} f(\bar{Y} \mid \mathbf{x}^{(1)}, \dots, \mathbf{x}^{(t)}, \dots, \mathbf{x}^{(M)}) \\ &\quad \times P(\mathbf{x}^{(1)}, \dots, \mathbf{x}^{(m-1)}, \mathbf{x}^{(m+1)}, \dots, \mathbf{x}^{(M)} \mid \mathbf{x}^{(m)} = \mathbf{x}^{(t)}) \end{aligned} \quad (6.214)$$

Since the output $\mathbf{y}^{(l)}$ is only related to the input $\mathbf{x}^{(l)}$, the above equation can also be expressed as

$$\begin{aligned} f(\bar{Y} \mid \mathbf{x}^{(t)}) &= f(\bar{y}^{(m)} \mid \mathbf{x}^{(t)}) \underbrace{\sum_{\mathbf{x}^{(1)} \in \mathcal{X}^K} \dots \sum_{\mathbf{x}^{(M)} \in \mathcal{X}^K}}_{(M-1) \text{ terms}} \prod_{l \neq m}^M f(\bar{y}^{(l)} \mid \mathbf{x}^{(l)}) \\ &\quad \times P(\mathbf{x}^{(1)}, \dots, \mathbf{x}^{(m-1)}, \mathbf{x}^{(m+1)}, \dots, \mathbf{x}^{(M)} \mid \mathbf{x}^{(m)} = \mathbf{x}^{(t)}) \end{aligned} \quad (6.215)$$

Furthermore, when the transmitted data symbol vectors with respect to the index l are independent, we can further express (6.215) as

$$\begin{aligned} f(\bar{Y} \mid \mathbf{x}^{(t)}) &= f(\bar{y}^{(m)} \mid \mathbf{x}^{(t)}) \underbrace{\sum_{\mathbf{x}^{(1)} \in \mathcal{X}^K} \dots \sum_{\mathbf{x}^{(M)} \in \mathcal{X}^K}}_{(M-1) \text{ terms}} \prod_{l \neq m}^M f(\bar{y}^{(l)} \mid \mathbf{x}^{(l)}) P(\mathbf{x}^{(l)}) \\ &= f(\bar{y}^{(m)} \mid \mathbf{x}^{(t)}) \prod_{l \neq m}^M f(\bar{y}^{(l)}) \end{aligned} \quad (6.216)$$

where

$$f(\bar{y}^{(l)}) = \sum_{\mathbf{x}^{(l)} \in \mathcal{X}^K} f(\bar{y}^{(l)} \mid \mathbf{x}^{(l)}) P(\mathbf{x}^{(l)})$$

In (6.212) the probability of $P(\mathbf{x}^{(t)})$ can be expressed as

$$\begin{aligned} P(\mathbf{x}^{(t)}) &= P(\mathbf{x}^{(m)} = \mathbf{x}^{(t)}) \\ &= \prod_{k=1}^K P(x_k^{(m)} = x_k^{(t)}) \end{aligned} \quad (6.217)$$

since the symbols transmitted by different users are independent. Furthermore, when the symbols transmitted by the same user are independent, $P(\mathbf{x}^{(t)})$ can then be simplified to

$$P(\mathbf{x}^{(t)}) = \prod_{k=1}^K \prod_{l=1}^q P(x_{kl}^{(m)} = x_{kl}^{(t)}) \quad (6.218)$$

where $x_{kl}^{(t)}$ is a test symbol taken from \mathcal{X} .

According to the above analysis, we know that the estimate of $\mathbf{x}^{(m)}$ for the **K-user BMAP-MUD** maximizes the metric of

$$\hat{\mathbf{x}}^{(m)} = \arg \max_{\mathbf{x}^{(t)} \in \mathcal{X}^K} \{f(\bar{\mathbf{Y}} \mid \mathbf{x}^{(t)}) P(\mathbf{x}^{(t)})\} \quad (6.219)$$

When the transmitted data vectors corresponding to $\bar{\mathbf{y}}^{(1)}, \bar{\mathbf{y}}^{(2)}, \dots, \bar{\mathbf{y}}^{(M)}$ are independent, then, substituting (6.216) into (6.219), the K -user BMAP-MUD is reduced to the K -user SMAP-MUD, which can be expressed as

$$\hat{\mathbf{x}}^{(m)} = \arg \max_{\mathbf{x}^{(t)} \in \mathcal{X}^K} \{f(\bar{\mathbf{y}}^{(m)} \mid \mathbf{x}^{(t)}) P(\mathbf{x}^{(t)})\} \quad (6.220)$$

The K -user SMAP-MUD will be discussed later in this section.

Sometimes, it is more convenient to represent the quantities in the log domain. Defining a log-likelihood function of \mathbf{y} in the context of $\boldsymbol{\theta}$ as

$$\begin{aligned} L_y(\boldsymbol{\theta}) &= \ln[f(\mathbf{y} \mid \boldsymbol{\theta}) P(\boldsymbol{\theta})] \\ &= \ln f(\mathbf{y} \mid \boldsymbol{\theta}) + \ln P(\boldsymbol{\theta}) \end{aligned} \quad (6.221)$$

then the maximization problem of (6.219) can be modified to another maximization problem expressed as

$$\hat{\mathbf{x}}^{(m)} = \arg \max_{\mathbf{x}^{(t)} \in \mathcal{X}^K} \{\ln f(\bar{\mathbf{Y}} \mid \mathbf{x}^{(t)}) + \ln P(\mathbf{x}^{(t)})\} \quad (6.222)$$

where, by using (6.217), we have

$$\ln P(\mathbf{x}^{(t)}) = \sum_{k=1}^K \ln P(\mathbf{x}_k^{(m)} = \mathbf{x}_k^{(t)}) \quad (6.223)$$

while according to (6.215) we obtain

$$\begin{aligned} \ln f(\bar{\mathbf{Y}} \mid \mathbf{x}^{(t)}) &= \ln f(\bar{\mathbf{y}}^{(m)} \mid \mathbf{x}^{(t)}) + \ln \left[\underbrace{\sum_{\mathbf{x}^{(1)} \in \mathcal{X}^K} \dots \sum_{\mathbf{x}^{(M)} \in \mathcal{X}^K} \prod_{l \neq m}^M f(\bar{\mathbf{y}}^{(l)} \mid \mathbf{x}^{(l)})}_{(M-1) \text{ terms}} \right. \\ &\quad \times P(\mathbf{x}^{(1)}, \dots, \mathbf{x}^{(m-1)}, \mathbf{x}^{(m+1)}, \dots, \mathbf{x}^{(M)} \mid \mathbf{x}^{(m)} = \mathbf{x}^{(t)}) \Big] \\ &= L_c(\mathbf{x}^{(t)}) + L_e(\mathbf{x}^{(t)}) \end{aligned} \quad (6.224)$$

where

$$L_c(\mathbf{x}^{(t)}) = \ln f(\bar{\mathbf{y}}^{(m)} \mid \mathbf{x}^{(t)}) \quad (6.225)$$

denotes the reliability (information) provided by the communications channels, while

$$\begin{aligned} L_e(\mathbf{x}^{(t)}) &= \ln \left[\underbrace{\sum_{\mathbf{x}^{(1)} \in \mathcal{X}^K} \dots \sum_{\mathbf{x}^{(M)} \in \mathcal{X}^K} \prod_{l \neq m}^M f(\bar{\mathbf{y}}^{(l)} \mid \mathbf{x}^{(l)})}_{(M-1) \text{ terms}} \right. \\ &\quad \times P(\mathbf{x}^{(1)}, \dots, \mathbf{x}^{(m-1)}, \mathbf{x}^{(m+1)}, \dots, \mathbf{x}^{(M)} \mid \mathbf{x}^{(m)} = \mathbf{x}^{(t)}) \Big] \end{aligned} \quad (6.226)$$

denotes the reliability provided by the correlation existing among the transmitted data.

From (6.222) to (6.224), we can see that when $\mathbf{x}^{(1)}, \mathbf{x}^{(2)}, \dots, \mathbf{x}^{(M)}$ are correlated, which is usually the case when FEC coding is applied, the K -user BMAP-MUD depends on the whole block of observations, even though only one of the symbols in $\{\mathbf{x}^{(1)}, \mathbf{x}^{(2)}, \dots, \mathbf{x}^{(M)}\}$ is estimated. Hence, the complexity of the K -user BMAP-MUD is extremely high.

Note that when $\mathbf{x}^{(1)}, \mathbf{x}^{(2)}, \dots, \mathbf{x}^{(M)}$ are independent, then, using the relationship of (6.216), equation (6.224) can be simplified to

$$\ln f(\bar{\mathbf{Y}} | \mathbf{x}^{(t)}) = \ln f(\bar{\mathbf{y}}^{(m)} | \mathbf{x}^{(t)}) + \sum_{l \neq m}^M [\ln f(\bar{\mathbf{y}}^{(l)}) + \ln P(\mathbf{x}^{(l)})] \quad (6.227)$$

where, explicitly, the second term on the right-hand-side (r.h.s.) is a common term. It is not related to the optimization and hence can be ignored.

Additionally, with the aid of (6.208), the first term at the r.h.s. of (6.227) can be expressed as

$$\begin{aligned} \ln f(\bar{\mathbf{y}}^{(m)} | \mathbf{x}^{(t)}) &= -K \ln(\pi \sigma^2) - \ln[\det(\mathbf{R}^{(m)})] \\ &\quad - \sigma^{-2} (\bar{\mathbf{y}}^{(m)} - \mathbf{R}^{(m)} \mathbf{x}^{(t)})^H (\mathbf{R}^{(m)})^{-1} (\bar{\mathbf{y}}^{(m)} - \mathbf{R}^{(m)} \mathbf{x}^{(t)}) \\ &= -K \ln(\pi \sigma^2) - \ln[\det(\mathbf{R}^{(m)})] - \sigma^{-2} (\bar{\mathbf{y}}^{(m)})^H \mathbf{R}^{(m)} \bar{\mathbf{y}}^{(m)} \\ &\quad - \sigma^{-2} [(\mathbf{x}^{(t)})^H \mathbf{R}^{(m)} \mathbf{x}^{(t)} - 2\Re\{(\bar{\mathbf{y}}^{(m)})^H \mathbf{x}^{(t)}\}] \end{aligned} \quad (6.228)$$

where only the terms in the last bracket of $[\cdot]$ are related to the optimization, while the remaining terms are common and independent of $\mathbf{x}^{(t)}$. Consequently, when $\mathbf{x}^{(1)}, \mathbf{x}^{(2)}, \dots, \mathbf{x}^{(M)}$ are independent, after ignoring the common terms, the optimization problem of (6.222) can be converted to

$$\begin{aligned} \hat{\mathbf{x}}^{(m)} &= \arg \max_{\mathbf{x}^{(t)} \in \mathcal{X}^{\mathcal{K}}} \left\{ \ln f(\bar{\mathbf{y}}^{(m)} | \mathbf{x}^{(t)}) + \sum_{k=1}^K \ln P(\mathbf{x}_k^{(m)} = \mathbf{x}_k^{(t)}) \right\} \\ &\triangleq \arg \min_{\mathbf{x}^{(t)} \in \mathcal{X}^{\mathcal{K}}} \left\{ - \sum_{k=1}^K \ln P(\mathbf{x}_k^{(m)} = \mathbf{x}_k^{(t)}) + \sigma^{-2} [(\mathbf{x}^{(t)})^H \mathbf{R}^{(m)} \mathbf{x}^{(t)} \right. \\ &\quad \left. - 2\Re\{(\bar{\mathbf{y}}^{(m)})^H \mathbf{x}^{(t)}\}] \right\}, \quad m = 1, 2, \dots, M \end{aligned} \quad (6.229)$$

which is only dependent on the observation of $\bar{\mathbf{y}}^{(m)}$ and is independent of the other observations. The complexity of (6.229) is proportional to $O(Q^{\mathcal{K}})$.

The single-user BMAP-MUD can be readily obtained from the K -user BMAP-MUD. Following the approaches for the K -user BMAP-MUD, it can be shown that the single-user BMAP-MUD chooses the estimate to $x_{kj}^{(m)}$ according to

$$\begin{aligned} \hat{x}_{kj}^{(m)} &= \arg \max_{x_{kj}^{(t)} \in \mathcal{X}} \{ \ln f(\bar{\mathbf{Y}} | x_{kj}^{(t)}) + \ln P(x_{kj}^{(t)}) \}, \quad j = 1, 2, \dots, q \\ k &= 1, 2, \dots, K; \quad m = 1, 2, \dots, M \end{aligned} \quad (6.230)$$

where $P(x_{kj}^{(t)})$ is the *a priori* probability of the event $x_{kj}^{(m)} = x_{kj}^{(t)}$, while $f(\bar{\mathbf{Y}} \mid x_{kj}^{(t)})$ is the PDF of $\bar{\mathbf{Y}}$ given that $x_{kj}^{(m)} = x_{kj}^{(t)}$ was transmitted. The PDF of $f(\bar{\mathbf{Y}} \mid x_{kj}^{(t)})$ can be computed as

$$\begin{aligned} f(\bar{\mathbf{Y}} \mid x_{kj}^{(t)}) &= \sum_{\mathbf{x}_k^{(m)} \in \mathcal{X}^q: x_{kj}^{(m)} = x_{kj}^{(t)}} f(\bar{\mathbf{Y}} \mid \mathbf{x}_k^{(m)}) P(\mathbf{x}_k^{(m)} \mid x_{kj}^{(m)} = x_{kj}^{(t)}) \\ &= \sum_{\mathbf{x}^{(m)} \in \mathcal{X}^K: x_{kj}^{(m)} = x_{kj}^{(t)}} f(\bar{\mathbf{Y}} \mid \mathbf{x}^{(m)}) P(\mathbf{x}^{(m)} \mid \mathbf{x}_k^{(m)}) P(\mathbf{x}_k^{(m)} \mid x_{kj}^{(m)} = x_{kj}^{(t)}) \end{aligned} \quad (6.231)$$

Since $P(\mathbf{x}^{(m)} \mid \mathbf{x}_k^{(m)}) P(\mathbf{x}_k^{(m)} \mid x_{kj}^{(m)} = x_{kj}^{(t)}) = P(\mathbf{x}^{(m)} \mid x_{kj}^{(m)} = x_{kj}^{(t)})$, we have

$$f(\bar{\mathbf{Y}} \mid x_{kj}^{(t)}) = \sum_{\mathbf{x}^{(m)} \in \mathcal{X}^K: x_{kj}^{(m)} = x_{kj}^{(t)}} f(\bar{\mathbf{Y}} \mid \mathbf{x}^{(m)}) P(\mathbf{x}^{(m)} \mid x_{kj}^{(m)} = x_{kj}^{(t)}) \quad (6.232)$$

Similarly, the above equation can be further extended to

$$\begin{aligned} f(\bar{\mathbf{Y}} \mid x_{kj}^{(t)}) &= \sum_{\mathbf{x}^{(1)} \in \mathcal{X}^K} \cdots \sum_{\mathbf{x}^{(m)} \in \mathcal{X}^K: x_{kj}^{(m)} = x_{kj}^{(t)}} \cdots \sum_{\mathbf{x}^{(M)} \in \mathcal{X}^K} \prod_{l=1}^M f(\bar{\mathbf{y}}^{(l)} \mid \mathbf{x}^{(l)}) \\ &\times P(\mathbf{x}^{(1)}, \mathbf{x}^{(2)}, \dots, \mathbf{x}^{(M)} \mid x_{kj}^{(m)} = x_{kj}^{(t)}) \end{aligned} \quad (6.233)$$

Equation (6.233) is suitable in general where the transmitted data symbols are correlated. When the transmitted symbols are independent, from (6.232) or (6.233), it can be easily shown that

$$f(\bar{\mathbf{Y}} \mid x_{kj}^{(t)}) = \prod_{l \neq m}^M f(\bar{\mathbf{y}}^{(l)}) \sum_{\mathbf{x}^{(m)} \in \mathcal{X}^K: x_{kj}^{(m)} = x_{kj}^{(t)}} f(\bar{\mathbf{y}}^{(m)} \mid \mathbf{x}^{(m)}) P(\mathbf{x}^{(m)} \mid x_{kj}^{(m)} = x_{kj}^{(t)}) \quad (6.234)$$

Furthermore, since in the above equation the term $\prod_{l \neq m}^M f(\bar{\mathbf{y}}^{(l)})$ is common for any test symbol $x_{kj}^{(t)}$, it can be removed. Hence,

$$f(\bar{\mathbf{Y}} \mid x_{kj}^{(t)}) \propto \sum_{\mathbf{x}^{(m)} \in \mathcal{X}^K: x_{kj}^{(m)} = x_{kj}^{(t)}} f(\bar{\mathbf{y}}^{(m)} \mid \mathbf{x}^{(m)}) P(\mathbf{x}^{(m)} \mid x_{kj}^{(m)} = x_{kj}^{(t)}) \quad (6.235)$$

From the above analysis, we can be implied that the single-user BMAP-MUD is of similar detection complexity as the K -user BMAP-MUD. Although both of them are optimum in the sense of resulting in the minimum probability of error, their implementation complexity, however, is extremely high, which makes them impractical to implement. Below, the other types of MAP-MUD are explored. These MAP-MUDs are less complex. They are suboptimum, since they generally do not make use of all the information provided by the whole observation block for detection.

The K -user SMAP-MUD estimates $\mathbf{x}^{(m)}$ based on the observation $\bar{\mathbf{y}}^{(m)}$ obtained in the context of the m th MC-CDMA symbol. Specifically, the estimate to $\mathbf{x}^{(m)}$ can be represented as the optimization problem

$$\hat{\mathbf{x}}^{(m)} = \arg \max_{\mathbf{x}^{(t)} \in \mathcal{X}^K} \{ \ln f(\bar{\mathbf{y}}^{(m)} \mid \mathbf{x}^{(t)}) + \ln P(\mathbf{x}^{(t)}) \}, \quad m = 1, 2, \dots, M \quad (6.236)$$

where $P(\mathbf{x}^{(t)})$ represents the *a priori* probability of transmitting $\mathbf{x}^{(m)} = \mathbf{x}^{(t)}$. It can be computed as

$$P(\mathbf{x}^{(t)}) = \prod_{k=1}^K P(x_k^{(m)} = x_k^{(t)}) \quad (6.237)$$

when assuming that the data transmitted by different users is independent.

Applying (6.208) and the above result into (6.236), it can be shown that the optimization problem for detecting $\mathbf{x}^{(m)}$ can be simplified to

$$\begin{aligned} \hat{\mathbf{x}}^{(m)} = \arg \min_{\mathbf{x}^{(t)} \in \mathcal{X}^{\mathcal{K}}} & \left\{ (\mathbf{x}^{(t)})^H \mathbf{R}^{(m)} \mathbf{x}^{(t)} - 2\Re\{(\bar{\mathbf{y}}^{(m)})^H \mathbf{x}^{(t)}\} \right. \\ & \left. - \sigma^2 \sum_{k=1}^K \ln P(x_k^{(m)} = x_k^{(t)}) \right\}, \quad m = 1, 2, \dots, M \end{aligned} \quad (6.238)$$

where the common terms independent of the transmitted symbols are ignored. It can be seen that (6.238) is the same as (6.229).

For the single-user SMAP-MUD, the detection can be described as

$$\begin{aligned} \hat{x}_{kj}^{(m)} = \arg \max_{x_{kj}^{(t)} \in \mathcal{X}} & \{ \ln f(\bar{\mathbf{y}}^{(m)} | x_{kj}^{(t)}) + \ln P(x_{kj}^{(t)}) \} \\ j = 1, 2, \dots, q; \quad k = 1, 2, \dots, K; \quad m = 1, 2, \dots, M \end{aligned} \quad (6.239)$$

which detects $x_{kj}^{(m)}$ based on the observation vector $\bar{\mathbf{y}}^{(m)}$ corresponding to the m th MC-CDMA symbol. In (6.239) $f(\bar{\mathbf{y}}^{(m)} | x_{kj}^{(t)})$ can be computed as follows:

$$\begin{aligned} f(\bar{\mathbf{y}}^{(m)} | x_{kj}^{(t)}) &= \sum_{\mathbf{x}^{(m)} \in \mathcal{X}^{\mathcal{K}}: x_{kj}^{(m)} = x_{kj}^{(t)}} f(\bar{\mathbf{y}}^{(m)} | \mathbf{x}^{(m)}) P(\mathbf{x}^{(m)} | x_{kj}^{(m)} = x_{kj}^{(t)}) \\ &= \sum_{\mathbf{x}^{(m)} \in \mathcal{X}^{\mathcal{K}}: x_{kj}^{(m)} = x_{kj}^{(t)}} f(\bar{\mathbf{y}}^{(m)} | \mathbf{x}^{(m)}) \prod_{l \neq k}^K P(x_l^{(m)}) P(x_k^{(m)} | x_{kj}^{(m)} = x_{kj}^{(t)}) \end{aligned} \quad (6.240)$$

There are some special forms for (6.240). First, if $x_{kj}^{(m)}$'s are binary, then (6.240) can be expressed as

$$\begin{aligned} f(\bar{\mathbf{y}}^{(m)} | x_{kj}^{(t)} = \pm 1) &= \sum_{\mathbf{x}^{(m)} \in \{+1, -1\}^{\mathcal{K}}: x_{kj}^{(m)} = \pm 1} f(\bar{\mathbf{y}}^{(m)} | \mathbf{x}^{(m)}) \prod_{l \neq k}^K P(x_l^{(m)}) \\ &\quad \times P(x_k^{(m)} | x_{kj}^{(m)} = \pm 1) \end{aligned} \quad (6.241)$$

where $x_{kj}^{(t)} = \pm 1$ means $x_{kj}^{(t)} = +1$ or $x_{kj}^{(t)} = -1$. Second, when $x_{kj}^{(m)}$'s are i.i.d. binary random variables, (6.241) can be further simplified to

$$f(\bar{\mathbf{y}}^{(m)} | x_{kj}^{(t)} = \pm 1) = \frac{1}{2^{\mathcal{K}-1}} \sum_{\mathbf{x}^{(m)} \in \{+1, -1\}^{\mathcal{K}}: x_{kj}^{(m)} = \pm 1} f(\bar{\mathbf{y}}^{(m)} | \mathbf{x}^{(m)}) \quad (6.242)$$

Substituting (6.240) into (6.239), the estimate to $x_{kj}^{(m)}$ is in general represented by the optimization problem

$$\begin{aligned}\hat{x}_{kj}^{(m)} = \arg \max_{x_{kj}^{(t)} \in \mathcal{X}} & \left\{ \ln P(x_{kj}^{(t)}) + \ln \left[\sum_{x^{(m)} \in \mathcal{X}^{\mathcal{K}}: x_{kj}^{(m)} = x_{kj}^{(t)}} f(\bar{\mathbf{y}}^{(m)} | \mathbf{x}^{(m)}) \right. \right. \\ & \times \prod_{l \neq k}^K P(\mathbf{x}_l^{(m)}) P(\mathbf{x}_k^{(m)} | x_{kj}^{(m)} = x_{kj}^{(t)}) \left. \right] \left. \right\} \\ j = 1, 2, \dots, q; k = 1, 2, \dots, K; m = 1, 2, \dots, M\end{aligned}\quad (6.243)$$

The K -user or single-user SMAP-MUD detects $\mathbf{x}^{(m)}$ or $x_{kj}^{(m)}$ based on $\bar{\mathbf{y}}^{(m)}$, which is the observation corresponding only to the m th MC-CDMA symbol. Hence, both the K -user and single-user SMAP-MUDs are suboptimum, when the transmitted data symbols are correlated. In this case, iterative MUDs [90] may be employed for making further use of the information due to the correlation embedded in the data block. Readers interested in iterative MUDs or so-called turbo MUDs can refer to reference [90] for further details.

Finally, for the bit-by-bit MAP-MUD, i.e. for the BitMAP-MUD, assume that $x_{kj}^{(m)}$ is represented in binary as $x_{kj}^{(m)} \leftrightarrow [b_{kj}^{(m)}(b) \cdots b_{kj}^{(m)}(1)]$ according to a predefined mapping scheme, where b is the number of bits per transmitted symbol per user. The BitMAP-MUD estimates bit $b_{kj}^{(m)}(n)$ ($n = 1, \dots, b$) of $x_{kj}^{(m)}$ based on the observation $\bar{\mathbf{y}}^{(m)}$, which can be expressed as

$$\begin{aligned}\hat{b}_{kj}^{(m)}(n) = \arg \max_{b^{(t)}=\pm 1} & \{ \ln f(\bar{\mathbf{y}}^{(m)} | b^{(t)}) + \ln P(b^{(t)}) \} \\ n = 1, 2, \dots, b; j = 1, 2, \dots, q; k = 1, 2, \dots, K; m = 1, 2, \dots, M\end{aligned}\quad (6.244)$$

where $P(b^{(t)})$ represents the *a priori* probability of $b_{kj}^{(m)}(n) = b^{(t)}$. In (6.244) $f(\bar{\mathbf{y}}^{(m)} | b^{(t)})$ can be expressed as

$$f(\bar{\mathbf{y}}^{(m)} | b^{(t)}) = \sum_{x_{kj}^{(t)} \in \mathcal{X}: b_{kj}^{(t)}(n) = b^{(t)}} f(\bar{\mathbf{y}}^{(m)} | x_{kj}^{(t)}) P(x_{kj}^{(t)} | b_{kj}^{(t)}(n) = b^{(t)}) \quad (6.245)$$

Furthermore, according to (6.240), the above equation can be expressed as

$$\begin{aligned}f(\bar{\mathbf{y}}^{(m)} | b^{(t)}) = & \sum_{x_{kj}^{(t)} \in \mathcal{X}: b_{kj}^{(t)}(n) = b^{(t)}} \sum_{\mathbf{x}^{(m)} \in \mathcal{X}^{\mathcal{K}}: x_{kj}^{(m)} = x_{kj}^{(t)}} f(\bar{\mathbf{y}}^{(m)} | \mathbf{x}^{(m)}) \\ & \times \prod_{l \neq k}^K P(\mathbf{x}_l^{(m)}) P(\mathbf{x}_k^{(m)} | x_{kj}^{(m)} = x_{kj}^{(t)}) P(x_{kj}^{(t)} | b_{kj}^{(t)}(n) = b^{(t)})\end{aligned}\quad (6.246)$$

Figure 6.19 shows the BER versus average SNR per bit performance of a MC-CDMA system using BPSK modulation and K -user SMAP-MUD as shown in (6.238), when communicating over frequency-selective fading channels having $L = 20$ T-domain resolvable paths. The MC-CDMA system employs $U = 64$ subcarriers, $q = 16$ bits per symbol are transmitted, and it supports $K = 4$ uplink users. Furthermore, in our simulations we assumed

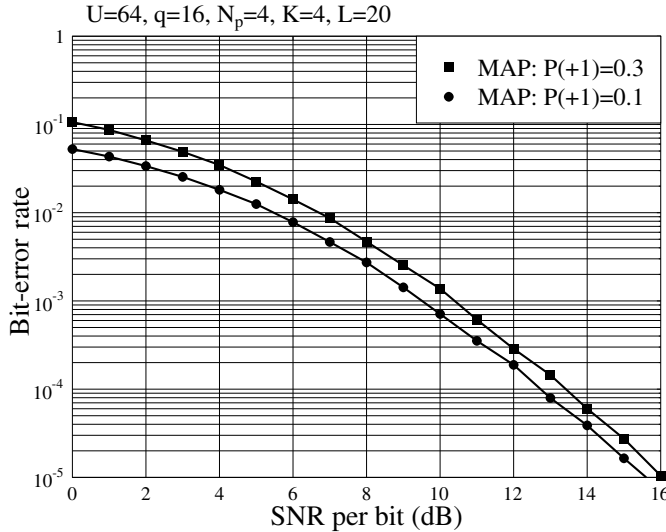


Figure 6.19: MAP-MUD: BER versus average SNR per bit performance for the MC-CDMA using random binary spreading sequences, when communicating over frequency-selective Rayleigh fading channels obeying the uniform MDP and having $L = 20$ T-domain resolvable paths. The MC-CDMA system employs $U = 64$ subcarriers and $q = 16$ bits are transmitted per symbol per user. The simulations were based on (6.238).

that the source symbols $+1$ and -1 were not uniformly distributed. Two cases of distribution were considered, where the first case assumed $P(+1) = 0.3$, $P(-1) = 0.7$ and the second case assumed $P(+1) = 0.1$, $P(-1) = 0.9$. From the results of Fig. 6.19 it can be observed that the MAP-MUD achieves different BER performances, when the source symbol obeys different distributions. When the source symbol is distributed more asymmetrically, a better BER performance is achieved.

6.2.9 Maximum Likelihood Decision Multiuser Detection

The MUD based on maximum likelihood decision (MLD), i.e. the MLD-MUD, detects the information transmitted by the uplink users in the maximum likelihood (ML) sense [88]. In MLD-MUD it is usually assumed that the source symbols (or vectors) are independent identically distributed (i.i.d.). If this is the case, the MLD-MUD is equivalent to the corresponding MAP-MUD and the MLD-MUD is hence optimum in a sense of achieving the MEP. However, when the sources cannot be modelled as the i.i.d. discrete random variables, the MLD-MUD is then not optimum in the MEP sense. Then the MAP-MUD outperforms the MLD-MUD with regard to the error rate performance achieved by these two MUDs.

Since MLD-MUD is equivalent to the MAP-MUD by assuming that in the MAP-MUD the source symbols are i.i.d. discrete random variables, the algorithms in the MLD-MUD can hence be readily obtained from the algorithms in the MAP-MUD by applying the assumption that the source symbols are i.i.d. discrete random variables. Below, a range of MLD-MUDs are provided in accordance with the MAP-MUDs as derived in Section 6.2.8.

First, for the **K -user BMLD-MUD**, the estimate to $\mathbf{x}^{(m)}$ is given by the optimization problem

$$\hat{\mathbf{x}}^{(m)} = \arg \max_{\mathbf{x}^{(t)} \in \mathcal{X}^K} \{\ln f(\bar{\mathbf{Y}} \mid \mathbf{x}^{(t)})\}, \quad m = 1, 2, \dots, M \quad (6.247)$$

where $\ln f(\bar{\mathbf{Y}} \mid \mathbf{x}^{(t)})$ is given by (6.224).

For the single-user BMLD-MUD, the estimate to $x_{kj}^{(m)}$ can be expressed as

$$\begin{aligned} \hat{x}_{kj}^{(m)} &= \arg \max_{x_{kj}^{(t)} \in \mathcal{X}} \{\ln f(\bar{\mathbf{Y}} \mid x_{kj}^{(t)})\}, \quad j = 1, 2, \dots, q \\ k &= 1, 2, \dots, K; \quad m = 1, 2, \dots, M \end{aligned} \quad (6.248)$$

where $f(\bar{\mathbf{Y}} \mid x_{kj}^{(t)})$ is given by (6.233).

For the K -user SMLD-MUD, the estimate to $\mathbf{x}^{(m)}$ is the solution to the optimization problem

$$\hat{\mathbf{x}}^{(m)} = \arg \max_{\mathbf{x}^{(t)} \in \mathcal{X}^K} \{\ln f(\bar{\mathbf{y}}^{(m)} \mid \mathbf{x}^{(t)})\}, \quad m = 1, 2, \dots, M \quad (6.249)$$

which, according to (6.238), can be represented as

$$\begin{aligned} \hat{\mathbf{x}}^{(m)} &= \arg \min_{\mathbf{x}^{(t)} \in \mathcal{X}^K} \{(\mathbf{x}^{(t)})^H \mathbf{R}^{(m)} \mathbf{x}^{(t)} - 2\Re\{(\bar{\mathbf{y}}^{(m)})^H \mathbf{x}^{(t)}\}\} \\ m &= 1, 2, \dots, M \end{aligned} \quad (6.250)$$

Similarly, in the context of the **single-user SMLD-MUD**, the estimate to $x_{kj}^{(m)}$ is the solution to the optimization problem

$$\begin{aligned} \hat{x}_{kj}^{(m)} &= \arg \max_{x_{kj}^{(t)} \in \mathcal{X}} \{\ln f(\bar{\mathbf{y}}^{(m)} \mid x_{kj}^{(t)})\}, \quad j = 1, 2, \dots, q \\ k &= 1, 2, \dots, K; \quad m = 1, 2, \dots, M \end{aligned} \quad (6.251)$$

where $f(\bar{\mathbf{y}}^{(m)} \mid x_{kj}^{(t)})$ is given in (6.240).

Finally, the **BitMLD-MUD** estimates bit $b_{kj}^{(m)}(n)$ ($n = 1, \dots, b$) of $x_{kj}^{(m)}$ based on the observation $\bar{\mathbf{y}}^{(m)}$ according to

$$\begin{aligned} \hat{b}_{kj}^{(m)}(n) &= \arg \max_{b^{(t)}=\pm 1} \{\ln f(\bar{\mathbf{y}}^{(m)} \mid b^{(t)})\}, \quad n = 1, 2, \dots, b \\ j &= 1, 2, \dots, q; \quad k = 1, 2, \dots, K; \quad m = 1, 2, \dots, M \end{aligned} \quad (6.252)$$

Figure 6.20 shows the BER performance of the MC-CDMA system using BPSK modulation, when communicating over frequency-selective fading channels, which have $L = 20$ T-domain resolvable paths. The MC-CDMA system employs $U = 64$ subcarriers, $q = 16$ bits per symbol are transmitted by each user, and the MC-CDMA supports $K = 4$ uplink users. For the sake of comparison, the BER of various pre-considered MUDs is also shown in Fig. 6.20. From the results of Fig. 6.20 it can be observed that the MLD-MUD is capable of achieving the best BER performance of the four detectors considered. The MF-assisted single-user detector has the worst BER performance, when the average SNR per

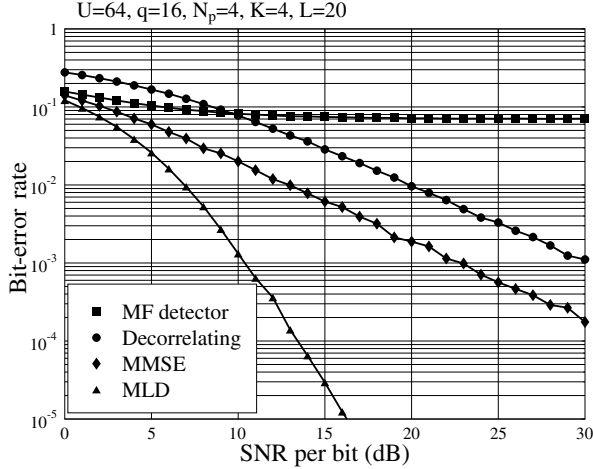


Figure 6.20: MLD-MUD: BER versus average SNR per bit performance for the MC-CDMA using random binary spreading sequences, when communicating over frequency-selective Rayleigh fading channels obeying the uniform MDP and having $L = 20$ T-domain resolvable paths. The MC-CDMA system employs $U = 64$ subcarriers and $q = 16$ bits are transmitted per symbol per user. The simulations for the MLD-MUD were based on (6.250).

bit is higher than 10 dB. However, when the average SNR per bit is lower than 10 dB, the decorrelating MUD is outperformed by the MF-assisted single-user detector. This observation is, as the analysis in Section 6.2.1 showed, the result of the decorrelating MUD enhancing the background noise while suppressing the MUI. By contrast, as shown in Fig. 6.20, the MMSE-MUD always outperforms the MF-assisted single-user detector.

Furthermore, when comparing the results in Fig. 6.20 with those in Fig. 6.19, it can be observed that the MAP-MUD outperforms the MLD-MUD when the source symbols are not i.i.d. variables.

In principle, the optimum solutions in the various classes of MAP-MUD or MLD-MUD can be found by carrying out exhaustive searches. However, in practice an exhaustive search is prohibitive for a large or even a moderate number of users because of its exponential increase of computational complexity. Hence, in multiuser detection there has been much research interest in finding the suboptimal but computationally efficient algorithms for the classes of MAP-MUD or MLD-MUD. In Appendix 6.C a range of suboptimal search-efficient algorithms of this kind are provided, in particular, for the MLD-MUDs where binary symbols are transmitted. These search-efficient algorithms have the computational complexity that is only polynomially difficult. However, they are often capable of achieving a BER performance that is similar to that obtained by the corresponding optimal MLD-MUDs.

6.2.10 Minimum Error-Probability Linear Multiuser Detection

In Section 6.2.8 various types of MAP-MUD were considered. They can minimize the block error probability, symbol error probability, or BER, depending on the specific MAP-MUDs

invoked. Although the MAP-MUDs considered in Section 6.2.8 are optimum in the sense of minimizing the corresponding error probability, the complexity of these MAP-MUDs is extreme and impractical when the number of users supported is relatively high. In this section, we consider the multiuser detection, which is capable of achieving the MSER or minimum BER (MBER) with an implementational complexity that linearly depends on the number of users supported. Hence, we refer to this type of MUD as the MSER-LMUD (or MBER-LMUD). As will be seen, in the MSER-LMUD (or MBER-LMUD) the multiuser detection is a linear operation associated with a weight vector (matrix). Instead, the complexity for computing the weight vector (matrix) is exponentially dependent on the number of users supported [170]. However, when the time-varying of wireless channels is not too fast, the rate of updating the weight vector (matrix) may be significantly lower than the data rate. Furthermore, the time-varying weight vector (or matrix) can be computed online using adaptive approaches [171].

In this section the principles of the linear multiuser detection under the criterion of MSER is first considered. After briefly introducing the principles, we then provide details of the derivation for the MBER-LMUD. Finally, the principles of MBER-LMUD are extended to the general MSER-LMUD.

For the sake of simplicity, let us modify the observation vector of (6.21) to

$$\begin{aligned} \mathbf{y} &= \bar{\mathbf{H}}\mathbf{x} + \mathbf{n} \\ &= \sum_{k=1}^{\mathcal{K}} \bar{\mathbf{h}}_k x_k + \mathbf{n} \end{aligned} \quad (6.253)$$

where $\bar{\mathbf{H}} = \mathbf{C}\mathbf{H}$ is a $(U \times \mathcal{K})$ matrix, $\mathcal{K} = qK$, and $\bar{\mathbf{H}} = [\bar{\mathbf{h}}_1, \bar{\mathbf{h}}_2, \dots, \bar{\mathbf{h}}_{\mathcal{K}}]$, \mathbf{x} is a \mathcal{K} -length vector, and \mathbf{n} is an U -length Gaussian noise vector that obeys the multivariate Gaussian distribution associated with zero mean and a covariance matrix given by $\sigma^2 \mathbf{I}_U$, where $\sigma^2 = 1/\text{SNR}$.

Let $\mathbf{W} = [\mathbf{w}_1, \dots, \mathbf{w}_{\mathcal{K}}]$ be a $(U \times \mathcal{K})$ weight matrix for detecting \mathbf{x} . Then, when the \mathcal{K} symbols in \mathbf{x} are detected simultaneously, the decision variable vector can be expressed as

$$\mathbf{z} = \mathbf{W}^H \mathbf{y} = \mathbf{W}^H \bar{\mathbf{H}}\mathbf{x} + \bar{\mathbf{n}} \quad (6.254)$$

where $\bar{\mathbf{n}} = \mathbf{W}^H \mathbf{n}$, which is still Gaussian with zero mean but with a covariance matrix of $\sigma^2 \mathbf{W}^H \mathbf{W}$. Let the signal set (constellation) be assumed to be $\mathcal{X} = \{X_0, X_1, \dots, X_{Q-1}\}$, where $X_i \in \mathcal{X}$ is complex and represents a legitimate point of the signal constellation, $Q = 2^b$ is the size of the constellation and b is the number of bits per symbol. Consequently, the PDF of \mathbf{z} conditioned on a given transmitted symbol $\mathbf{x} \in \mathcal{X}^{\mathcal{K}}$ can be expressed as

$$f(\mathbf{z} | \mathbf{x}) = \frac{1}{(\pi \sigma^2)^{\mathcal{K}} \det(\mathbf{W}^H \mathbf{W})} \exp[-(\mathbf{z} - \mathbf{W}^H \bar{\mathbf{H}}\mathbf{x})^H (\mathbf{W}^H \mathbf{W})^{-1} (\mathbf{z} - \mathbf{W}^H \bar{\mathbf{H}}\mathbf{x}) / \sigma^2] \quad (6.255)$$

Let $x_i = X_t \in \mathcal{X}$ be the i th symbol transmitted and $A(\mathbf{x} | x_i = X_t)$ be the range which yields the correct decision of $x_i = X_t$. Then, when assuming i.i.d. source symbols, the

average SER of detection can be expressed as

$$\begin{aligned} P_s(\mathbf{W}) &= \frac{1}{\mathcal{K}} \sum_{k=1}^{\mathcal{K}} \frac{1}{Q} \sum_{x_i=X_t \in \mathcal{X}} \frac{1}{Q^{\mathcal{K}-1}} \sum_{\mathbf{x} \in \mathcal{X}^{\mathcal{K}}; x_i=X_t} \left[1 - \int_{A(\mathbf{x}|x_i=X_t)} f(\mathbf{z} | \mathbf{x}) d\mathbf{z} \right] \\ &= \frac{1}{\mathcal{K}Q^{\mathcal{K}}} \sum_{k=1}^{\mathcal{K}} \sum_{x_i=X_t \in \mathcal{X}} \sum_{\mathbf{x} \in \mathcal{X}^{\mathcal{K}}; x_i=X_t} \left[1 - \int_{A(\mathbf{x}|x_i=X_t)} f(\mathbf{z} | \mathbf{x}) d\mathbf{z} \right] \end{aligned} \quad (6.256)$$

Consequently, the optimum weight matrix \mathbf{W}_o in the MSER sense can be obtained by solving the optimization problem

$$\mathbf{W}_o = \arg \min_{\mathbf{W}} \{P_s(\mathbf{W})\} \quad (6.257)$$

Explicitly, the computation of \mathbf{W}_o in (6.257) is exponentially hard.

When each of the \mathcal{K} symbols is detected separately, the decision variable for x_i can be expressed as

$$\begin{aligned} z_i &= \mathbf{w}_i^H \mathbf{y} = \mathbf{w}_i^H \bar{\mathbf{H}} \mathbf{x} + \mathbf{w}_i^H \mathbf{n} \\ &= \mathbf{w}_i^H \bar{\mathbf{h}}_i x_i + \sum_{k \neq i} \mathbf{w}_i^H \bar{\mathbf{h}}_k x_k + \mathbf{w}_i^H \mathbf{n}, \quad i = 1, 2, \dots, \mathcal{K} \end{aligned} \quad (6.258)$$

which is a Gaussian random variable with its mean given by

$$E[z_i] = \mathbf{w}_i^H \bar{\mathbf{h}}_i x_i + \sum_{k \neq i} \mathbf{w}_i^H \bar{\mathbf{h}}_k x_k \quad (6.259)$$

and its variance given by $\text{Var}[z_i] = \sigma^2 \mathbf{w}_i^H \mathbf{w}_i$. Hence, given $\mathbf{x} \in \mathcal{X}^{\mathcal{K}}$, the PDF of z_i can be expressed as

$$f(z_i | \mathbf{x}) = \frac{1}{\pi \sigma^2 \mathbf{w}_i^H \mathbf{w}_i} \exp \left(-\frac{[z_i - \sum_{k=1}^{\mathcal{K}} \mathbf{w}_i^H \bar{\mathbf{h}}_k x_k]^2}{\sigma^2 \mathbf{w}_i^H \mathbf{w}_i} \right) \quad (6.260)$$

Again, let $x_i = X_t \in \mathcal{X}$ be transmitted and $A(\mathbf{x} | x_i = X_t)$ be the range which yields the correct decision of $x_i = X_t$. Then, when assuming i.i.d. source symbols, the average SER for the detection of x_i can be expressed as

$$P_s(\mathbf{w}_i) = \frac{1}{Q^{\mathcal{K}}} \sum_{x_i=X_t \in \mathcal{X}} \sum_{\mathbf{x} \in \mathcal{X}^{\mathcal{K}}; x_i=X_t} \left[1 - \int_{A(\mathbf{x}|x_i=X_t)} f(z_i | \mathbf{x}) dz_i \right] \quad (6.261)$$

and the optimum weight vector \mathbf{w}_{io} in the MSER sense can be derived based on the optimization problem

$$\mathbf{w}_{io} = \arg \min_{\mathbf{w}_i} \{P_s(\mathbf{w}_i)\}, \quad i = 1, 2, \dots, \mathcal{K} \quad (6.262)$$

The computation for \mathbf{w}_{io} in (6.262) is also exponentially hard.

We now turn our attention to the MBER-LMUD, where we assume that $x_i \in \mathcal{X}$ is in binary. Furthermore, we consider the case where K users are detected separately. In this case the decision variable for $x_i = b_i$ can be expressed as

$$\begin{aligned} z_i &= \mathbf{w}_i^H \mathbf{y} = \mathbf{w}_i^H \bar{\mathbf{H}} \mathbf{b} + \mathbf{w}_i^H \mathbf{n} \\ &= \mathbf{w}_i^H \bar{\mathbf{h}}_i b_i + \sum_{k \neq i} \mathbf{w}_i^H \bar{\mathbf{h}}_k b_k + \mathbf{w}_i^H \mathbf{n}, \quad i = 1, 2, \dots, \mathcal{K} \end{aligned} \quad (6.263)$$

and the decision is based on

$$\hat{b}_i = \text{sgn}(\Re\{z_i\}), \quad i = 1, 2, \dots, \mathcal{K} \quad (6.264)$$

Let \mathbf{b}_i^- represent the binary vector, where the i th entry is $b_i = -1$. We also assume that the probability of $b_i = +1$ and that of $b_i = -1$ are equal to 0.5. Then, conditional on \mathbf{b}_i^- , the PDF of $\Re\{z_i\}$ can be expressed as

$$f_{\Re\{z_i\}}(z | \mathbf{b}_i^-) = \frac{1}{\sqrt{\pi\sigma^2 \mathbf{w}_i^H \mathbf{w}_i}} \exp\left(-\frac{[z - \Re\{\mathbf{w}_i^H \bar{\mathbf{H}} \mathbf{b}_i^-\}]^2}{\sigma^2 \mathbf{w}_i^H \mathbf{w}_i}\right) \quad (6.265)$$

The BER conditional on \mathbf{b}_i^- can be derived as

$$\begin{aligned} P_b(\mathbf{w}_i | \mathbf{b}_i^-) &= P(\Re\{z_i\} > 0 | \mathbf{b}_i^-) \\ &= P(\Re\{\mathbf{w}_i^H \bar{\mathbf{H}} \mathbf{b}_i^- + \mathbf{w}_i^H \mathbf{n}\} > 0) \\ &= \int_0^\infty f_{\Re\{z_i\}}(z | \mathbf{b}_i^-) dz \end{aligned} \quad (6.266)$$

When applying (6.265) into (6.266) and using the appropriate variable transform, it can be shown that

$$\begin{aligned} P_b(\mathbf{w}_i | \mathbf{b}_i^-) &= Q\left(-\frac{\sqrt{2}\Re\{\mathbf{w}_i^H \bar{\mathbf{H}} \mathbf{b}_i^-\}}{\sigma \sqrt{\mathbf{w}_i^H \mathbf{w}_i}}\right) \\ &= Q\left(\frac{\sqrt{2}\Re\{\mathbf{w}_i^H \bar{\mathbf{H}} \mathbf{b}_i^+\}}{\sigma \sqrt{\mathbf{w}_i^H \mathbf{w}_i}}\right) = P_b(\mathbf{w}_i | \mathbf{b}_i^+) \end{aligned} \quad (6.267)$$

where \mathbf{b}_i^+ represents the binary vector with its i th entry $b_i = +1$. Furthermore, the reason for the second equality in (6.267) is that the entries in \mathbf{b}_i^+ except $b_i = +1$ are binary uniform random variables.

Let $\bar{\mathbf{w}}_i = \mathbf{w}_i / \sqrt{\mathbf{w}_i^H \mathbf{w}_i}$, which represents the normalized weight vector, i.e. we have $\|\bar{\mathbf{w}}_i\|^2 = 1$. Then, (6.267) can also be written as

$$P_b(\bar{\mathbf{w}}_i | \mathbf{b}_i^+) = Q\left(\frac{\sqrt{2}\Re\{\bar{\mathbf{w}}_i^H \bar{\mathbf{H}} \mathbf{b}_i^+\}}{\sigma}\right) \quad (6.268)$$

When we consider that \mathbf{b}_i^+ is a \mathcal{K} -length random vector with its i th entry $b_i = +1$, the average BER of b_i can be expressed as

$$P_b(\bar{\mathbf{w}}_i) = \frac{1}{2^{\mathcal{K}-1}} \sum_{\mathbf{b}_i^+ \in \{+1, -1\}^{\mathcal{K}-1}} Q\left(\frac{\sqrt{2}\Re\{\bar{\mathbf{w}}_i^H \bar{\mathbf{H}} \mathbf{b}_i^+\}}{\sigma}\right) \quad (6.269)$$

Therefore, in the context of the MBER-LMUD, the optimum weight vector $\bar{\mathbf{w}}_{io}$ can be chosen according to the optimization problem

$$\bar{\mathbf{w}}_{io} = \arg \min_{\bar{\mathbf{w}}_i} P_b(\bar{\mathbf{w}}_i), \quad \text{subject to } \|\bar{\mathbf{w}}_i\|^2 = 1, \quad i = 1, 2, \dots, \mathcal{K} \quad (6.270)$$

In reference [170] it has been proved that the solution to the optimization problem of (6.270) is globally optimum. Furthermore, the optimum solution satisfies

$$\Re\{\bar{\mathbf{w}}_i^H \bar{\mathbf{H}} \mathbf{b}_i^+\} > 0 \quad (6.271)$$

for any $\mathbf{b}_i^+ \in \{+1, -1\}^{K-1}$ and $b_i = +1$. Therefore, the optimization problem in (6.270) can be restated as

$$\begin{aligned} \bar{\mathbf{w}}_{io} &= \arg \min_{\bar{\mathbf{w}}_i} P_b(\bar{\mathbf{w}}_i), \\ \text{subject to } \|\bar{\mathbf{w}}_i\|^2 &= 1, \quad \text{and} \quad \Re\{\bar{\mathbf{w}}_i^H \bar{\mathbf{H}} \mathbf{b}_i^+\} > 0 \end{aligned} \quad (6.272)$$

for $i = 1, 2, \dots, K$.

However, the problem in (6.272) is not a convex programming problem because $\|\bar{\mathbf{w}}_{io}\|^2 = 1$ is not convex. For this sake, as shown in reference [170], the above optimization problem can be modified to a convex programming problem

$$\begin{aligned} \bar{\mathbf{w}}_{io} &= \arg \min_{\bar{\mathbf{w}}_i} P_b(\bar{\mathbf{w}}_i), \\ \text{subject to } \|\bar{\mathbf{w}}_i\|^2 &\leq 1, \quad \text{and} \quad \Re\{\bar{\mathbf{w}}_i^H \bar{\mathbf{H}} \mathbf{b}_i^+\} > 0 \end{aligned} \quad (6.273)$$

The optimization problem of (6.273) can be used to represent (6.272), because once an $\bar{\mathbf{w}}_{io}$ satisfying $\|\bar{\mathbf{w}}_{io}\|^2 \leq 1$ is obtained, its normalized version will result in a smaller BER, i.e. $P_b(\bar{\mathbf{w}}_{io}) \geq P_b(\bar{\mathbf{w}}_{io}/\|\bar{\mathbf{w}}_{io}\|)$, as shown in reference [170].

Note that (6.273) is a convex programming problem that may be solved using some efficient algorithms.

As shown in reference [170, 171], the optimum weight vector can be obtained through the adaptive approaches. For example, the i th weight vector $\bar{\mathbf{w}}_i$ can be updated according to the steepest-descent gradient approach [171]

$$\bar{\mathbf{w}}_i(n+1) = \bar{\mathbf{w}}_i(n) - \mu \nabla P_b(\bar{\mathbf{w}}_i(n)) \quad (6.274)$$

associated with $\|\bar{\mathbf{w}}_i(n+1)\|^2 = 1$, where $\mu > 0$ represents the adaptation step size, while, according to reference [146],

$$\nabla P_b(\bar{\mathbf{w}}_i) = 2 \frac{\partial P_b(\bar{\mathbf{w}}_i)}{\partial \bar{\mathbf{w}}_i^*} \quad (6.275)$$

When expressing

$$\Re\{\bar{\mathbf{w}}_i^H \bar{\mathbf{H}} \mathbf{b}_i^+\} = \frac{1}{2} (\bar{\mathbf{w}}_i^H \bar{\mathbf{H}} \mathbf{b}_i^+ + (\mathbf{b}_i^+)^T \bar{\mathbf{H}}^H \bar{\mathbf{w}}) \quad (6.276)$$

it can be readily shown that

$$\nabla P_b(\bar{\mathbf{w}}_i) = -\frac{1}{2^{K-1} \sqrt{\pi} \sigma} \sum_{\mathbf{b}_i^+ \in \{+1, -1\}^{K-1}} \exp\left(-\frac{\Re^2\{\bar{\mathbf{w}}_i^H \bar{\mathbf{H}} \mathbf{b}_i^+\}}{\sigma^2}\right) \bar{\mathbf{H}} \mathbf{b}_i^+ \quad (6.277)$$

As (6.274) and (6.277) show, the computational burden for the weight vectors is still exponentially hard. Therefore, a sample-by-sample adaptive scheme assisted by a number of training symbols may be invoked in order to reduce the computational complexity [171].

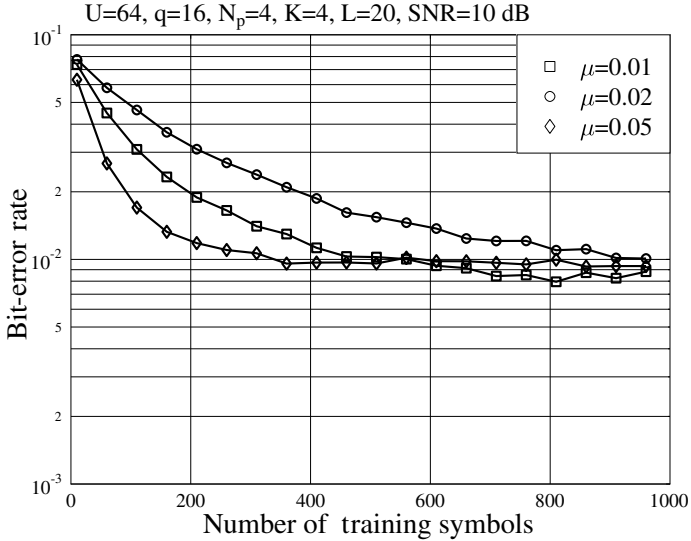


Figure 6.21: Illustration of the convergence behaviour of the adaptive MBER-MUD.

In this case, let the n th training vector be expressed as $\mathbf{b}(n)$. We then have $\mathbf{b}_i^+(n) = \text{sgn}(b_i)\mathbf{b}(n)$. Let (6.277) $\bar{\mathbf{H}}\mathbf{b}_i^+$ be approximated by the received observation vector as

$$\bar{\mathbf{H}}\mathbf{b}_i^+ \approx \text{sgn}(b_i)\mathbf{y} \quad (6.278)$$

Then, the one sample-based estimation to $\nabla P_b(\bar{\mathbf{w}}_i)$ can be expressed as

$$\nabla P_b(\bar{\mathbf{w}}_i) = -\frac{\text{sgn}(b_i)}{\sqrt{\pi}\sigma} \exp\left(-\frac{\Re^2\{\bar{\mathbf{w}}_i^H \mathbf{y}(n)\}}{\sigma^2}\right) \mathbf{y}(n) \quad (6.279)$$

Applying (6.279) to (6.274), we can finally obtain the adaptive equation

$$\begin{aligned} \bar{\mathbf{w}}_i(n+1) &= \bar{\mathbf{w}}_i(n) + \mu' \times \text{sgn}(b_i) \exp\left(-\frac{\Re^2\{\bar{\mathbf{w}}_i^H \mathbf{y}(n)\}}{\sigma^2}\right) \mathbf{y}(n) \\ \|\bar{\mathbf{w}}_i(n+1)\|^2 &= 1 \end{aligned} \quad (6.280)$$

where $\mu' = \mu/\sqrt{\pi}\sigma$.

Figure 6.21 shows the convergence behaviour of the adaptive MBER-MUD shown in (6.280), which shows that the step-size μ' has an explicit impact on the convergence speed of the adaptive MBER-MUD assisted by the steepest-descent gradient algorithm.

Figure 6.22 shows the comparison between the MMSE-MUD and MBER-MUD, when communicating over AWGN channels. In our simulations complex spreading sequences as shown in Fig. 6.22 were assumed. The data detection was begun after the training, using 10 000 symbols. As shown in Fig. 6.22, the MBER-MUD significantly outperforms the MMSE-MUD in terms of achievable BER performance.

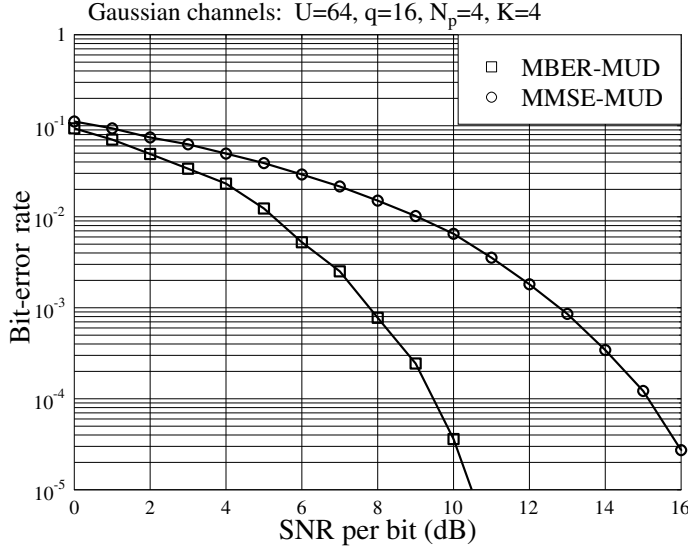


Figure 6.22: BER versus SNR per bit performance of the F-domain spread MC-CDMA communicating over AWGN channels. The simulations were based on (6.280) and assumed the complex spreading sequences: $c_1 = [-0.382748 + 0.312141i \quad -0.139761 + 0.585021i \quad 0.0773003 - 0.178344i \quad 0.537365 - 0.00576409i]^T$, $c_2 = [0.279948 + 0.135536i \quad -0.352868 - 0.49533i \quad -0.574009 + 0.179317i \quad -0.12719 + 0.365154i]^T$, $c_3 = [0.605558 + 0.168345i \quad -0.402689 + 0.0691333i \quad 0.485495 + 0.564371i \quad -0.162544 - 0.497239i]^T$, $c_4 = [-0.510056 + 0.0642861i \quad -0.159107 - 0.275855i \quad 0.210551 - 0.0450141i \quad 0.0208991 + 0.536272i]^T$. For the MBER-MUD, adaptive detection was employed, which assumed a step size $\mu' = 0.01$ and 10 000 training symbols.

We now try to extend the above derivation in the context of the MBER-LMUD to the general MSER-LMUD. The generalization is based on the finding [172] that the SER of many coherent digital communication schemes is a function of the formula

$$T[a, b, g; \gamma] = a \int_0^{b\pi} \exp\left(-\frac{g\gamma}{\sin^2 \theta}\right) d\theta, \quad a, b, g > 0 \quad (6.281)$$

where γ represents the (instantaneous) SNR. In (6.281) the parameters a , b and g are determined by the specific modulation scheme employed. Specifically, for the binary phase-shift keying (BPSK), binary frequency-shift keying (BFSK), multiple phase-shift keying (MPSK) and M -ary quadrature amplitude modulation (MQAM), etc. coherent modulation schemes, it can be shown that we have the following parameter configurations [91, 107, 172]:

BPSK:

$$P_s(\gamma) = T[a, b, g; \gamma] \quad \text{with } a = \frac{1}{\pi}, \quad b = \frac{1}{2}, \quad g = 1 \quad (6.282)$$

BFSK:

$$P_s(\gamma) = T[a, b, g; \gamma] \quad \text{with } a = \frac{1}{\pi}, \quad b = \frac{1}{2}, \quad \text{and} \\ g = \begin{cases} \frac{1}{2}, & \text{orthogonal BFSK} \\ 0.715, & \text{minimum correlation} \end{cases} \quad (6.283)$$

MPSK:

$$P_s(\gamma) = T[a, b, g; \gamma] \quad \text{with } a = \frac{1}{\pi}, \quad b = \frac{M-1}{M}, \quad g = \sin^2\left(\frac{\pi}{M}\right) \quad (6.284)$$

MQAM:

$$P_s(\gamma) = T[a_1, b_1, g_1; \gamma] - T[a_2, b_2, g_2; \gamma] \quad \text{with} \\ a_1 = \frac{4}{\pi} \left(1 - \frac{1}{\sqrt{M}}\right), \quad b_1 = \frac{1}{2}, \quad g_1 = \frac{3}{2(M-1)} \\ a_2 = \frac{4}{\pi} \left(1 - \frac{1}{\sqrt{M}}\right)^2, \quad b_2 = \frac{1}{4}, \quad g_2 = \frac{3}{2(M-1)} \quad (6.285)$$

There are also some other modulation schemes, such as the M -ary amplitude modulation (M-AM), whose SER can also be expressed as functions of (6.281).

Note that, since in (6.281) $\sin^2 \theta \leq 1$, we can readily obtain an SER upper-bound that can be expressed as

$$T[a, b, g; \gamma] \leq ab\pi \exp(-g\gamma) \quad (6.286)$$

Note, furthermore, that, since the integration range in (6.281) is fixed, the optimization can be based either on the accurate expression of (6.281) or on its upper-bound of (6.286).

As shown in (6.281) and (6.286), the SER is determined by γ of the instantaneous SNR. Let us consider the symbol-based linear MUD. Then, the decision variable for the i th symbol x_i can be written as

$$z_i = \left(\frac{\mathbf{w}_i^H \bar{\mathbf{H}} \mathbf{x} x_i^*}{\|x_i\|^2} \right) x_i + \mathbf{w}_i^H \mathbf{n}, \quad i = 1, 2, \dots, \mathcal{K} \quad (6.287)$$

where $\|x_i\|^2 = 1$ for the digital modulation schemes, such as BPSK, BFSK, MPSK, etc. having a constant transmission power. However, for the modulation schemes, such as MQAM, using non-uniform transmission power, $\|x_i\|^2 \neq 1$.

Using (6.287), it can be shown that for a given transmitted vector \mathbf{x} , the SNR γ for (6.281) or (6.286) conditional on the weight vector \mathbf{w}_i is given by

$$\gamma(\mathbf{w}_i) = \frac{\|\mathbf{w}_i^H \bar{\mathbf{H}} \mathbf{x} \|x_i\|^2\|^2}{\sigma^2 \|\mathbf{w}_i\|^2 \|x_i\|^4} = \frac{\|\mathbf{w}_i^H \bar{\mathbf{H}} \mathbf{x}\|^2}{\sigma^2 \|\mathbf{w}_i\|^2} \quad (6.288)$$

Again, let $\bar{\mathbf{w}}_i = \mathbf{w}_i / \|\mathbf{w}_i\|$ be the normalized weight vector satisfying $\|\bar{\mathbf{w}}_i\|^2 = 1$. The SNR γ for a given weight vector $\bar{\mathbf{w}}_i$ is then given by

$$\gamma(\bar{\mathbf{w}}_i) = \frac{\|\bar{\mathbf{w}}_i^H \bar{\mathbf{H}} \mathbf{x}\|^2}{\sigma^2}, \quad i = 1, 2, \dots, \mathcal{K} \quad (6.289)$$

Consequently, the SER conditioned on $\bar{\mathbf{w}}_i$ and \mathbf{x} can be expressed as

$$\begin{aligned} P_s(\bar{\mathbf{w}}_i \mid \mathbf{x}) &= T[a, b, g; \gamma(\bar{\mathbf{w}}_i)] \\ &= T\left[a, b, g; \gamma(\bar{\mathbf{w}}_i) = \frac{\|\bar{\mathbf{w}}_i^H \bar{\mathbf{H}} \mathbf{x}\|^2}{\sigma^2}\right] \end{aligned} \quad (6.290)$$

Let $\mathbf{x} \in \mathcal{X}^K$ and the size of \mathcal{X} is $Q = 2^b$, where b represents the number of bits per symbol. Furthermore, we assume that \mathbf{x} is an i.i.d. random vector in \mathcal{X}^K . Then, after taking the average in the context of \mathbf{x} , the SER conditional on $\bar{\mathbf{w}}_i$ can be expressed as

$$P_s(\bar{\mathbf{w}}_i) = \frac{1}{Q^K} \sum_{\mathbf{x} \in \mathcal{X}^K} T\left[a, b, g; \gamma(\bar{\mathbf{w}}_i) = \frac{\|\bar{\mathbf{w}}_i^H \bar{\mathbf{H}} \mathbf{x}\|^2}{\sigma^2}\right] \quad (6.291)$$

Correspondingly, when the SER upper-bound of (6.286) is used, we then have

$$\begin{aligned} P_s^{(U)}(\bar{\mathbf{w}}_i) &= \frac{ab\pi}{Q^K} \sum_{\mathbf{x} \in \mathcal{X}^K} \exp(-g\gamma(\bar{\mathbf{w}}_i)) \\ &= \frac{ab\pi}{Q^K} \sum_{\mathbf{x} \in \mathcal{X}^K} \exp\left(-\frac{g\|\bar{\mathbf{w}}_i^H \bar{\mathbf{H}} \mathbf{x}\|^2}{\sigma^2}\right) \end{aligned} \quad (6.292)$$

According to the principles of coherent communications and by referring to (6.287), we know that a valid optimum solution, say $\bar{\mathbf{w}}_{io}$, to $\bar{\mathbf{w}}_i$ should satisfy

$$\Re\{\bar{\mathbf{w}}_i^H \bar{\mathbf{H}} \mathbf{x}_i^*\} \geq 0, \quad \Im\{\bar{\mathbf{w}}_i^H \bar{\mathbf{H}} \mathbf{x}_i^*\} = 0 \quad (6.293)$$

Therefore, the optimum solution to $\bar{\mathbf{w}}_i$ can be derived with the aid of the optimization problem:

$$\begin{aligned} \bar{\mathbf{w}}_{io} &= \arg \min_{\bar{\mathbf{w}}_i} \{P_s(\bar{\mathbf{w}}_i)\} \\ &= \arg \min_{\bar{\mathbf{w}}_i} \left\{ \frac{1}{Q^K} \sum_{\mathbf{x} \in \mathcal{X}^K} T\left[a, b, g; \gamma(\bar{\mathbf{w}}_i) = \frac{\|\bar{\mathbf{w}}_i^H \bar{\mathbf{H}} \mathbf{x}\|^2}{\sigma^2}\right] \right\}, \\ \text{subject to } &\Re\{\bar{\mathbf{w}}_i^H \bar{\mathbf{H}} \mathbf{x}_i^*\} \geq 0, \quad \Im\{\bar{\mathbf{w}}_i^H \bar{\mathbf{H}} \mathbf{x}_i^*\} = 0 \text{ for } \mathbf{x} \in \mathcal{X}^K \\ \text{and } &\|\bar{\mathbf{w}}_i\|^2 = 1, \quad i = 1, 2, \dots, K \end{aligned} \quad (6.294)$$

Alternatively, when the SER upper-bound of (6.286) is considered, the above optimization problem can be modified to

$$\begin{aligned} \bar{\mathbf{w}}_{io} &= \arg \min_{\bar{\mathbf{w}}_i} \{P_s^{(U)}(\bar{\mathbf{w}}_i)\} \\ &= \arg \min_{\bar{\mathbf{w}}_i} \left\{ \frac{ab\pi}{Q^K} \sum_{\mathbf{x} \in \mathcal{X}^K} \exp\left(-\frac{g\|\bar{\mathbf{w}}_i^H \bar{\mathbf{H}} \mathbf{x}\|^2}{\sigma^2}\right) \right\} \\ \text{subject to } &\Re\{\bar{\mathbf{w}}_i^H \bar{\mathbf{H}} \mathbf{x}_i^*\} \geq 0, \quad \Im\{\bar{\mathbf{w}}_i^H \bar{\mathbf{H}} \mathbf{x}_i^*\} = 0 \text{ for } \mathbf{x} \in \mathcal{X}^K \\ \text{and } &\|\bar{\mathbf{w}}_i\|^2 = 1, \quad i = 1, 2, \dots, K \end{aligned} \quad (6.295)$$

Note that, as shown in (6.285) for the MQAM, the SER is related to two terms. The first term is the same as the above-discussed. The second term can be considered similarly. Specifically, the optimization problem for the MQAM case can be stated as

$$\begin{aligned}
 \bar{\mathbf{w}}_{io} &= \arg \min_{\bar{\mathbf{w}}_i} \{P_s(\bar{\mathbf{w}}_i)\} \\
 &= \arg \min_{\bar{\mathbf{w}}_i} \left\{ \frac{1}{Q^K} \sum_{\mathbf{x} \in \mathcal{X}^K} T \left(\left[a_1, b_1, g_1; \gamma(\bar{\mathbf{w}}_i) = \frac{\|\bar{\mathbf{w}}_i^H \bar{\mathbf{H}} \mathbf{x}\|^2}{\sigma^2} \right] \right. \right. \\
 &\quad \left. \left. - T \left[a_2, b_2, g_2; \gamma(\bar{\mathbf{w}}_i) = \frac{\|\bar{\mathbf{w}}_i^H \bar{\mathbf{H}} \mathbf{x}\|^2}{\sigma^2} \right] \right) \right\}, \\
 \text{subject to } &\Re\{\bar{\mathbf{w}}_i^H \bar{\mathbf{H}} \mathbf{x} \mathbf{x}_i^*\} \geq 0, \quad \Im\{\bar{\mathbf{w}}_i^H \bar{\mathbf{H}} \mathbf{x} \mathbf{x}_i^*\} = 0 \text{ for } \mathbf{x} \in \mathcal{X}^K \\
 \text{and } &\|\bar{\mathbf{w}}_i\|^2 = 1, \quad i = 1, 2, \dots, K
 \end{aligned} \tag{6.296}$$

Alternatively, using the fact that the second term in (6.285) is insignificant in comparison with the first term, the SER can be simply approximated by (6.294).

Below, we use a few examples to illustrate the behaviour of the general MSER-LMUD. Specifically, the BER performance of a BPSK-assisted CDMA scheme supporting two users is observed when different weight values are invoked. In Figs. 6.23 and 6.24 the BER versus weights surfaces are depicted for the CDMA systems using different sets of spreading code, as shown in Figs. 6.23 and 6.24, when communicating over AWGN channels. By contrast, in Figs. 6.25 and 6.26 the union-bound error probability versus weights surfaces are depicted, also when communicating over AWGN channels. From the error-rate surfaces in these figures, we can explicitly observe that there exist optimum solutions to the two weights. When the constraint of $\|\bar{\mathbf{w}}_i\|^2 = 1$ is applied, the optimum solution to $\bar{\mathbf{w}}_i$ is unique and globally optimum. Furthermore, when comparing Fig. 6.23 (or Fig. 6.24), which shows the exact BER, with Fig. 6.25 (or Fig. 6.26), which is the corresponding union-bound BER, we can observe that the shape of the BER surface of Fig. 6.23 (or Fig. 6.25) is very similar as the shape of the BER union-bound surface of Fig. 6.25 (or Fig. 6.26). It is noteworthy that this observation is not a surprise. As shown in Fig. 6.27, the exact SER of (6.281) and its corresponding SER union-bound of (6.286) are near-linearly dependent on each other. When the exact SER and its upper-bound are linearly dependent, it can be implied that the optimum solution obtained from (6.294) based on the exact SER should also be the optimum solution to the optimization problem (6.294), which is based on the SER upper-bound.

Therefore, in MSER-MUD the optimization problem may be designed based either on the exact SER or on its upper-bound (which is not necessarily the union-bound), depending on which form is more convenient for solving the problem. If the exact SER and its upper-bound are linearly dependent on each other, then the optimum solution obtained from the optimization problem based on the exact SER is also optimum to the optimization problem based on the SER upper-bound; conversely, the optimum solution obtained from the optimization problem based on the SER upper-bound is also optimum to the optimization problem based on the exact SER.

In this section various optimization algorithms have been considered for deriving the MUD algorithms for the F-domain spread MC-CDMA. The analysis and performance results show that all the MUD schemes are capable of efficiently mitigating the MUI. Furthermore, we have shown that there are some (different) optimization strategies that result in the same

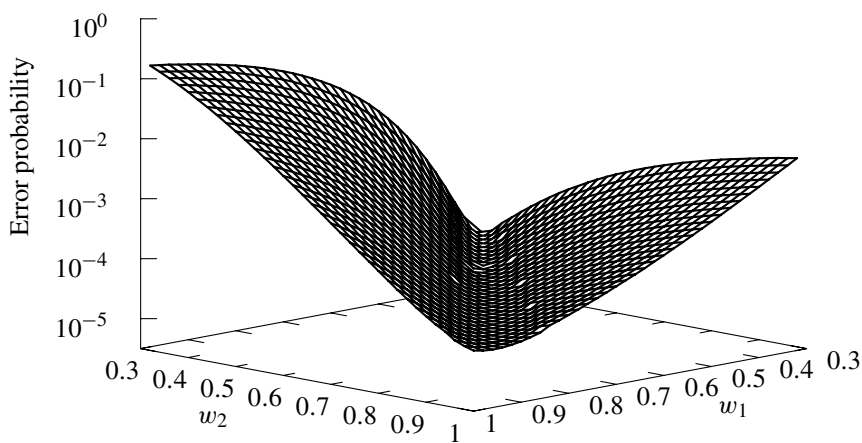


Figure 6.23: Exact error probability versus weights surface for a wireless communications system supporting two users associated with the user codes $c_1 = [1, 3]^T / \sqrt{10}$ and $c_2 = [-1, 1]^T / \sqrt{2}$, when communicating over Gaussian channels.

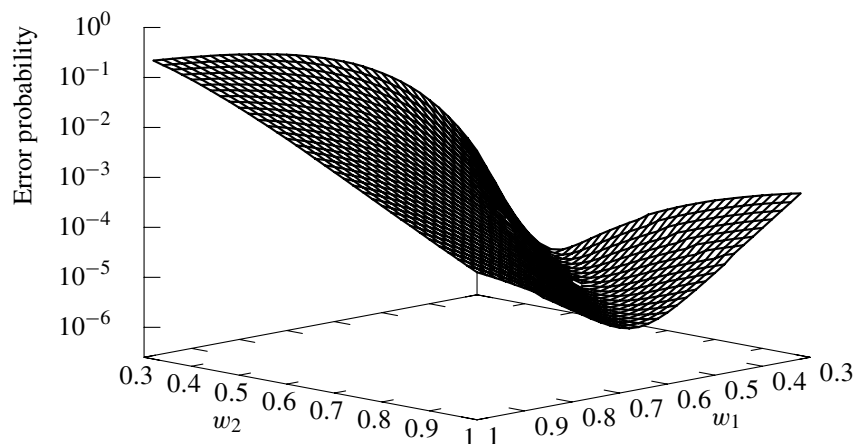


Figure 6.24: Exact error probability versus weights surface for a wireless communications system supporting two users associated with the user codes $c_1 = [1, 2]^T / \sqrt{5}$ and $c_2 = [-1.5, 1]^T / \sqrt{3.25}$, when communicating over Gaussian channels.

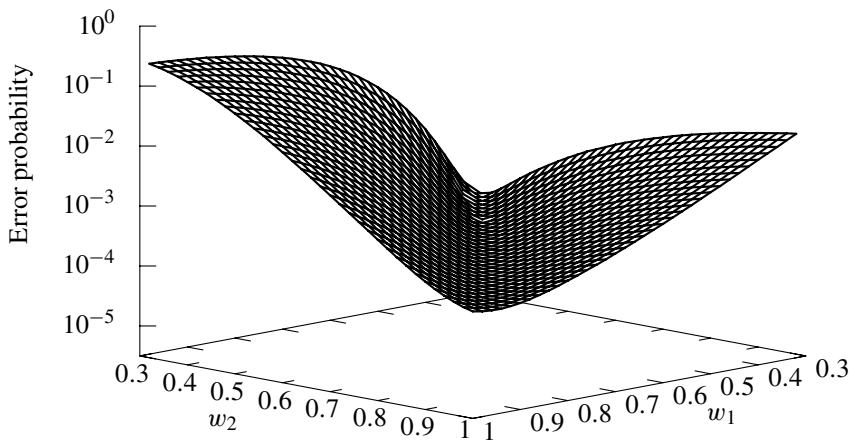


Figure 6.25: Error probability union-bound versus weights surface for a wireless communications system supporting two users associated with the user codes $c_1 = [1, 3]^T / \sqrt{10}$ and $c_2 = [-1, 1]^T / \sqrt{2}$, when communicating over Gaussian channels.

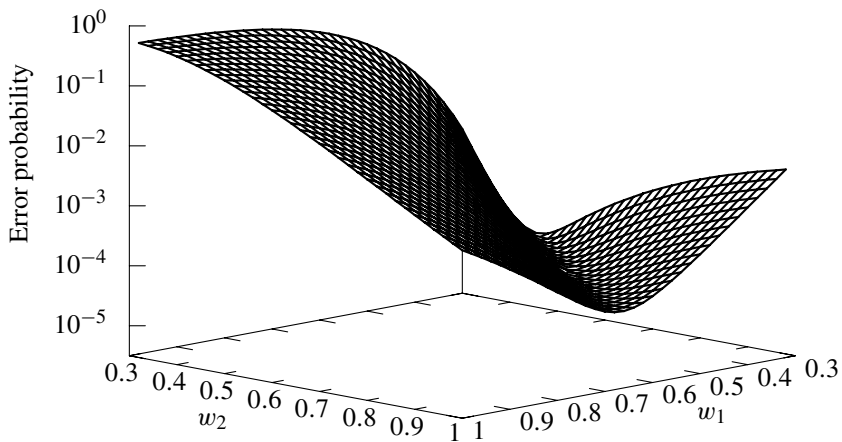


Figure 6.26: Error probability union-bound versus weights surface for a wireless communications system supporting two users associated with the user codes $c_1 = [1, 2]^T / \sqrt{5}$ and $c_2 = [-1.5, 1]^T / \sqrt{3.25}$, when communicating over Gaussian channels.

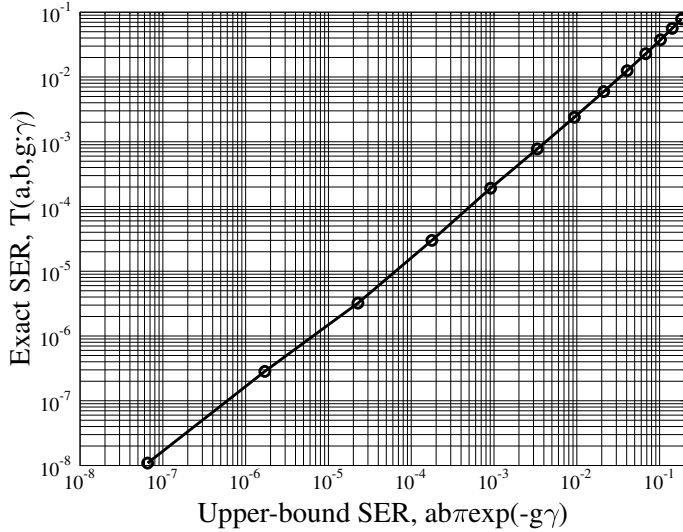


Figure 6.27: Illustration of the relationship between the exact SER in the form of (6.281) and its corresponding SER union-bound of (6.286).

MUD solutions. For example, the joint MVDR-MUD and joint MPDR-MUD are equivalent to the ZF-MUD, while the symbol-based individual MVDR-MUD and the symbol-based individual MPDR-MUD are equivalent to the MMSE-MUD. The MMSE-MUD can be equivalent to the MSINR-MUD. Furthermore, the MSINR-MUD also employs the similar solution as the symbol-based individual MVDR-MUD and the symbol-based individual MPDR-MUD. We now turn to consider the multiuser detection in the multicarrier DS-CDMA systems.

6.3 Multiuser Detection in Multicarrier DS-CDMA

In Section 6.2 various multiuser detection schemes were studied in the context of the F-domain spread MC-CDMA. In this section the multiuser detection in MC DS-CDMA systems is considered. Our emphasis is on the implementational issues of multiuser detection in MC DS-CDMA systems.

In Section 5.9 the observation equation in the context of the MC DS-CDMA supporting one user has been obtained. Straightforwardly, when the MC DS-CDMA supports K number of users and when a general baseband digital modulation scheme is employed, the observation equation can be written as

$$\mathbf{y} = \sum_{k=1}^K \mathcal{C}_k \boldsymbol{\mu} \mathbf{H}_k \mathbf{x}_k + \mathbf{n} \quad (6.297)$$

where \mathbf{x}_k contains the q number of data symbols transmitted by the k th user, \mathbf{y} is the qpN_e -length observation vector. Furthermore, according to Section 5.9, the vectors and matrices in (6.297) can be summarized as follows. The matrix \mathcal{C}_k is a $(qpN_e \times qpN_e)$ matrix composed

of the spreading sequence of the k th user. \mathcal{C}_k can be expressed as

$$\mathcal{C}_k = \frac{1}{\sqrt{p}}(\mathbf{I}_{qp} \otimes \mathbf{C}_k) \quad (6.298)$$

associated with \mathbf{C}_k given by

$$\mathbf{C}_k = \frac{1}{\sqrt{N_e}} \text{diag}\{c_0^{(k)}, c_1^{(k)}, \dots, c_{N_e-1}^{(k)}\} \quad (6.299)$$

The matrix $\boldsymbol{\mu}$ is a $(qpN_e \times qp)$ matrix that takes into account the intercarrier interference $\boldsymbol{\mu}$, given by

$$\begin{aligned} \boldsymbol{\mu} &= [\boldsymbol{\mu}_{11}^T, \dots, \boldsymbol{\mu}_{1p}^T, \dots, \boldsymbol{\mu}_{q1}^T, \dots, \boldsymbol{\mu}_{qp}^T]^T \\ \boldsymbol{\mu}_{uv} &= [\boldsymbol{\mu}_{uv,0}, \boldsymbol{\mu}_{uv,1}, \dots, \boldsymbol{\mu}_{uv,N_e-1}]^T \\ \boldsymbol{\mu}_{uv,n} &= [\mu_{11,uv,n}, \dots, \mu_{1p,uv,n}, \dots, \mu_{q1,uv,n}, \dots, \mu_{qp,uv,n}]^T \end{aligned} \quad (6.300)$$

and

$$\hat{\mu}_{il,uv,n} = \hat{\mu}_{il,uv} \exp(j2\pi n \Delta f_{il,uv} T_c) \quad (6.301)$$

associated with

$$\hat{\mu}_{il,uv} = \frac{1}{T_c} \int_0^{T_c} \psi^2(t) \exp(j2\pi \Delta f_{il,uv} t) dt \quad (6.302)$$

Note that $\boldsymbol{\mu}$ is determined by the subcarriers' locations but is independent of the specific users.

Furthermore, in (6.297) the matrix \mathbf{H}_k is related to the fading experienced by the qp subcarrier signals; it is a $(qp \times q)$ matrix and is given by

$$\mathbf{H}_k = \begin{bmatrix} \mathbf{h}_1^{(k)} & \mathbf{0} & \cdots & \mathbf{0} \\ \mathbf{0} & \mathbf{h}_2^{(k)} & \cdots & \mathbf{0} \\ \vdots & \vdots & \ddots & \vdots \\ \mathbf{0} & \mathbf{0} & \cdots & \mathbf{h}_q^{(k)} \end{bmatrix} \quad (6.303)$$

with $\mathbf{h}_i^{(k)}$ given by

$$\mathbf{h}_i^{(k)} = [h_{i1}^{(k)}, h_{i2}^{(k)}, \dots, h_{ip}^{(k)}]^T \quad (6.304)$$

Finally, in (6.297) \mathbf{n} is a complex Gaussian noise vector distributed with zero mean. Note that in \mathbf{n} , two samples obtained from two subcarriers might be correlated when these two subcarriers are close and non-orthogonal. However, for simplicity, in this section we assume (or approximate) that \mathbf{n} is an independent Gaussian noise vector and, correspondingly, has a covariance matrix of $\sigma^2 \mathbf{I}_{qpN_e} = (1/\text{SNR}) \mathbf{I}_{qpN_e}$.

When comparing equation (6.297) for the MC DS-CDMA with equation (6.6) for the F-domain spread MC-CDMA, we can observe that they have the same structure. It can be shown that all the MUD schemes considered in Section 6.2 for the F-domain spread MC-CDMA are applicable to the considered MC DS-CDMA, after some slight modifications. Therefore, details of multiuser detection based on (6.297) are not considered further here.

In the MC DS-CDMA systems the observation vector \mathbf{y} of (6.297) is a qpN_e -length vector. The value of qpN_e might be huge when the number of users supported is high and/or when each user transmits a high number of parallel symbols, or when the chip-level MUDs are considered. In these cases the complexity of the MUDs designed on the basis of (6.297) might be extreme.

According to our assumptions in Section 5.9 of Chapter 5, in the MC DS-CDMA all the subcarriers use the same spreading sequence of length N_e and each subcarrier signal of a given user experiences flat fading. When considering this characteristic of the MC DS-CDMA, the MUD in the MC DS-CDMA systems may be significantly simplified by appropriately distributing the signal processing burden in both the T-domain and F-domain. In this section we will make use of the above-mentioned characteristics for simplifying the MUDs in the MC DS-CDMA.

Following the derivation in Section 5.9 of Chapter 5, when the MC DS-CDMA supports K number of users, the observation vector obtained from the uv th subcarrier can be expressed as

$$\mathbf{y}_{uv} = \sum_{k=1}^K \frac{1}{\sqrt{p}} \mathbf{C}_k \boldsymbol{\mu}_{uv} \mathbf{H}_k \mathbf{x}_k + \mathbf{n}_{uv}, \quad u = 1, 2, \dots, q; v = 1, 2, \dots, p \quad (6.305)$$

With the aid of (5.140), we can divide (6.305) into the desired signal plus intercarrier interference (ICI) and noise as

$$\begin{aligned} \mathbf{y}_{uv} &= \sum_{k=1}^K \frac{h_{uv}^{(k)}}{\sqrt{p}} \mathbf{c}_k x_u^{(k)} + \sum_{k=1}^K \frac{1}{\sqrt{p}} (\mathbf{C}_k \boldsymbol{\mu}_{uv} \mathbf{H}_k \mathbf{x}_k - h_{uv} \mathbf{c}_k x_u^{(k)}) + \mathbf{n}_{uv} \\ &= \sum_{k=1}^K \frac{h_{uv}^{(k)}}{\sqrt{p}} \mathbf{c}_k x_u^{(k)} + \mathbf{I}_{uv} + \mathbf{n}_{uv}, \quad u = 1, 2, \dots, q; v = 1, 2, \dots, p \end{aligned} \quad (6.306)$$

where

$$\mathbf{I}_{uv} = \sum_{k=1}^K \frac{1}{\sqrt{p}} (\mathbf{C}_k \boldsymbol{\mu}_{uv} \mathbf{H}_k \mathbf{x}_k - h_{uv} \mathbf{c}_k x_u^{(k)}) \quad (6.307)$$

is due to the ICI, which is zero when the subcarrier signals are designed to be orthogonal with each other.

Let us express the observations in (6.305) in some desired form, so that they can be conveniently applied below. First, we define

$$\begin{aligned} \mathbf{y}_u &= [\mathbf{y}_{u1}^T, \mathbf{y}_{u2}^T, \dots, \mathbf{y}_{up}^T]^T \\ \mathbf{I}_u &= [\mathbf{I}_{u1}^T, \mathbf{I}_{u2}^T, \dots, \mathbf{I}_{up}^T]^T \\ \mathbf{n}_u &= [\mathbf{n}_{u1}^T, \mathbf{n}_{u2}^T, \dots, \mathbf{n}_{up}^T]^T \end{aligned} \quad (6.308)$$

for $u = 1, 2, \dots, q$. Then, \mathbf{y}_u can be expressed as

$$\mathbf{y}_u = \sum_{k=1}^K (\mathbf{h}_{ku} \otimes \mathbf{c}_k) x_u^{(k)} + \mathbf{I}_u + \mathbf{n}_u, \quad u = 1, 2, \dots, q \quad (6.309)$$

where, by definition

$$\mathbf{h}_{ku} = \frac{1}{\sqrt{p}} [h_{u1}^{(k)}, h_{u2}^{(k)}, \dots, h_{up}^{(k)}]^T \quad (6.310)$$

For $u = 1, 2, \dots, q$, we define

$$\begin{aligned}\mathbf{x}_u &= [x_u^{(1)}, x_u^{(2)}, \dots, x_u^{(K)}]^T \\ \mathbf{C} &= [\mathbf{c}_1, \mathbf{c}_2, \dots, \mathbf{c}_K] \\ \mathbf{H}_u &= [\mathbf{h}_{1u}, \mathbf{h}_{2u}, \dots, \mathbf{h}_{Ku}]\end{aligned}\quad (6.311)$$

Then, (6.309) can be alternatively expressed as

$$\mathbf{y}_u = (\mathbf{H}_u \square \mathbf{C}) \mathbf{x}_u + \mathbf{I}_u + \mathbf{n}_u, \quad u = 1, 2, \dots, q \quad (6.312)$$

where $(\mathbf{H}_u \square \mathbf{C})$ represents the *Khatri–Rao product*² between \mathbf{H}_u and \mathbf{C} .

Additionally, (6.306) can also be written as

$$\mathbf{y}_{uv} = \mathbf{C} \mathbf{H}_{uv} \mathbf{x}_u + \underbrace{\mathbf{I}_{uv} + \mathbf{n}_{uv}}_{\mathbf{J}_{uv}}, \quad u = 1, 2, \dots, q; v = 1, 2, \dots, p \quad (6.314)$$

where

$$\mathbf{H}_{uv} = \frac{1}{\sqrt{p}} \text{diag}\{h_{uv}^{(1)}, h_{uv}^{(2)}, \dots, h_{uv}^{(K)}\} \quad (6.315)$$

As shown in (6.312), the length of the observation vector \mathbf{y}_u is pN_e , and the spreading code matrix \mathbf{C} is certain once the users are given. The matrix \mathbf{H}_u denoting the CIRs is known, once the channels are estimated. Below, as three examples, we consider three types of MUD for the considered MC DS-CDMA that are derived based on equations (6.306) or (6.314), (6.309) or (6.312). The three types of MUD include the ZF-MUD, MMSE-MUD and MLD-MUD. We first consider the ZF-MUD.

6.3.1 Zero-Forcing Multiuser Detection

In MC DS-CDMA systems each subcarrier signal is constituted of K DS-CDMA signals belonging to K users and a data symbol of a given user is conveyed by a number of p subcarriers. Therefore, in MC DS-CDMA the linear MUD may be implemented by first carrying out the MUD in the context of each of the subcarriers. After the MUD, the subcarrier signals conveying the same data symbol are coherently combined in order to form a decision variable. When the linear MUDs in the MC DS-CDMA systems are designed following this philosophy, we will show that the corresponding MUD receivers have the lowest implementational complexity. However, they are often not optimum in terms of the achievable error probability performance. In order to achieve the lowest error probability, a linear MUD should make use of all the observations from the p subcarriers conveying the same data symbol at one optimization stage.

Specifically, when the sub-optimum ZF-MUD, which for brevity is referred to as SZF-MUD, is considered, for the u th symbol vector \mathbf{x}_u transmitted by the K users, the decision variable vector in the context of the uv th subcarrier can be formed as

$$\mathbf{z}_{uv} = \mathbf{W}_{uv}^H \mathbf{y}_{uv}, \quad u = 1, 2, \dots, q; v = 1, 2, \dots, p \quad (6.316)$$

²Khatri–Rao product [89]: Let \mathbf{A} and \mathbf{B} be $(N \times M)$ and $(P \times M)$ matrices, respectively. The Khatri–Rao product of \mathbf{A} and \mathbf{B} is defined as

$$\mathbf{A} \square \mathbf{B} = [\mathbf{a}_1 \otimes \mathbf{b}_1 \mid \mathbf{a}_2 \otimes \mathbf{b}_2 \mid \cdots \mid \mathbf{a}_M \otimes \mathbf{b}_M] \quad (6.313)$$

which is a $(NP \times M)$ matrix, \mathbf{a}_i denoting the i th column of \mathbf{A} .

where \mathbf{W}_{uv} is a weight matrix for processing the observation vector \mathbf{y}_{uv} of (6.314) obtained from the uv th subcarrier. After the MUD operation of (6.316), the p subcarrier signals conveying \mathbf{x}_u are then coherently combined to form the final decision variable vector

$$\mathbf{z}_u = \sum_{v=1}^p \mathbf{T}_{uv}^H \mathbf{z}_{uv}, \quad u = 1, 2, \dots, q \quad (6.317)$$

where the matrix \mathbf{T}_{uv} is a post-processing matrix carrying out the coherent combining.

It can be shown that for the ZF-MUD, the weight matrix and the post-processing matrix can be chosen as

$$\begin{aligned} \mathbf{W}_{uv} &= \mathbf{C}(\mathbf{C}^T \mathbf{C})^{-1} = \mathbf{C} \mathbf{R}_c^{-1} \\ \mathbf{T}_{uv} &= \mathbf{H}_{uv} \end{aligned} \quad (6.318)$$

where $\mathbf{R}_c = \mathbf{C}^T \mathbf{C}$ was defined.

Let $\mathbf{J}_{uv} = \mathbf{I}_{uv} + \mathbf{n}_{uv}$. Then, substituting (6.314), (6.316) and (6.318) into (6.317) the decision variable vector for \mathbf{x}_u can be expressed as

$$\begin{aligned} \mathbf{z}_u &= \sum_{v=1}^p \mathbf{T}_{uv}^H \mathbf{R}_c^{-1} \mathbf{C}^T \mathbf{y}_{uv} \\ &= \sum_{v=1}^p \mathbf{H}_{uv}^H \mathbf{H}_{uv} \mathbf{x}_u + \sum_{v=1}^p \mathbf{H}_{uv}^H \mathbf{R}_c^{-1} \mathbf{C}^T \mathbf{J}_{uv} \\ &= \begin{bmatrix} \sum_{v=1}^p |h_{uv}^{(1)}|^2 x_u^{(1)} \\ \sum_{v=1}^p |h_{uv}^{(2)}|^2 x_u^{(2)} \\ \vdots \\ \sum_{v=1}^p |h_{uv}^{(K)}|^2 x_u^{(K)} \end{bmatrix} + \sum_{v=1}^p \mathbf{H}_{uv}^H \mathbf{R}_c^{-1} \mathbf{C}^T \mathbf{J}_{uv}, \quad u = 1, 2, \dots, q \end{aligned} \quad (6.319)$$

Explicitly, the ZF-MUD fully removes the MUI; it is capable of implementing the maximal ratio combining (MRC) and achieving a diversity order of p .

In summary, the SZF-MUD having the processing weight matrices shown in (6.318) can be implemented as shown by the schematic block diagram of Fig. 6.28.

From (6.318) and Fig. 6.28 we know that the weight matrix \mathbf{W}_{uv} is time-invariant and common to any of the qp subcarriers. Hence, it can be computed ‘once for all’, provided that the active users remain unchanged. From this point of view, the ZF-MUD having the processing matrices in (6.318) in fact has an implementational complexity that is similar to the single-user matched-filter (MF) receiver. However, as mentioned previously and also as shown in Fig. 6.30, the above-derived ZF-MUD is only suboptimum in terms of achievable error probability performance in the ZF sense. An optimum ZF-MUD that is capable of achieving the lowest error probability in the ZF sense can be designed by considering all the observations across the p subcarriers conveying \mathbf{x}_u , i.e. by considering \mathbf{y}_u of both (6.309)

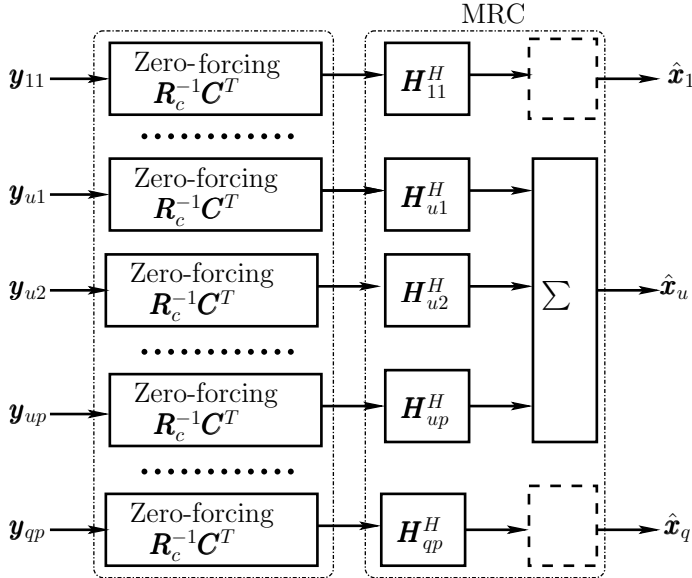


Figure 6.28: Schematic block diagram for implementation of the suboptimum ZF-MUD in MC DS-CDMA systems.

or (6.312). We now consider the optimum ZF-MUD, which, for the sake of brevity, is referred to as the OZF-MUD.

We derive the OZF-MUD based on (6.312). It can be shown that for the OZF-MUD the decision variable vector for \mathbf{x}_u can be described as

$$\mathbf{z}_u = \mathbf{W}_u^H \mathbf{y}_u, \quad u = 1, 2, \dots, q \quad (6.320)$$

where, according to (6.312), it can easily be shown that the weight matrix \mathbf{W}_u can be denoted

$$\mathbf{W}_u = (\mathbf{H}_u \square \mathbf{C}) [(\mathbf{H}_u \square \mathbf{C})^H (\mathbf{H}_u \square \mathbf{C})]^{-1} \quad (6.321)$$

Using the property of $(\mathbf{H}_u \square \mathbf{C})^H (\mathbf{H}_u \square \mathbf{C}) = (\mathbf{H}_u^H \mathbf{H}_u \odot \mathbf{C}^T \mathbf{C})$ [89], where \odot represents the Hadamard product operation³ [156], the above equation can be denoted as

$$\begin{aligned} \mathbf{W}_u &= (\mathbf{H}_u \square \mathbf{C}) [(\mathbf{H}_u^H \mathbf{H}_u \odot \mathbf{C}^T \mathbf{C})]^{-1} \\ &= (\mathbf{H}_u \square \mathbf{C}) [(\mathbf{H}_u^H \mathbf{H}_u \odot \mathbf{R}_c)]^{-1} \end{aligned} \quad (6.323)$$

In (6.323) the inverse term is a $(K \times K)$ matrix, which may be efficiently computed. This is because within the inverse matrix $\mathbf{R}_c = \mathbf{C}^T \mathbf{C}$ is a $(K \times K)$ time-invariant matrix, while

³Hadamard product: Let $\mathbf{A} = [a_{ij}]$ and $\mathbf{B} = [b_{ij}]$ be two $(M \times N)$ matrices, their Hadamard product is defined as

$$\mathbf{A} \odot \mathbf{B} = \begin{bmatrix} a_{11}b_{11} & a_{12}b_{12} & \cdots & a_{1N}b_{1N} \\ a_{21}b_{21} & a_{22}b_{22} & \cdots & a_{2N}b_{2N} \\ \vdots & \vdots & \ddots & \vdots \\ a_{M1}b_{M1} & a_{M2}b_{M2} & \cdots & a_{MN}b_{MN} \end{bmatrix} \quad (6.322)$$

$\mathbf{H}_u^H \mathbf{H}_u$ is a $(K \times K)$ matrix that may be updated at the fading rate of the wireless channels experienced by the subcarrier signals and, finally, the Hadamard product between $\mathbf{H}_u^H \mathbf{H}_u$ and $\mathbf{C}^T \mathbf{C}$ simply constitutes K^2 multiplications.

Upon applying (6.323) into (6.320), the decision variable vector is

$$\mathbf{z}_u = [(\mathbf{H}_u^H \mathbf{H}_u \odot \mathbf{R}_c)]^{-1} (\mathbf{H}_u \square \mathbf{C})^H \mathbf{y}_u \quad (6.324)$$

In (6.324), $(\mathbf{H}_u \square \mathbf{C})^H \mathbf{y}_u$ can be expressed as

$$\begin{aligned} (\mathbf{H}_u \square \mathbf{C})^H \mathbf{y}_u &= [\mathbf{h}_{1u} \otimes \mathbf{c}_1 \mid \mathbf{h}_{2u} \otimes \mathbf{c}_2 \mid \cdots \mathbf{h}_{Ku} \otimes \mathbf{c}_K]^H \begin{bmatrix} \mathbf{y}_{u1} \\ \mathbf{y}_{u2} \\ \vdots \\ \mathbf{y}_{up} \end{bmatrix} \\ &= \sum_{v=1}^p \mathbf{H}_{uv}^H \mathbf{C}^T \mathbf{y}_{uv} \end{aligned} \quad (6.325)$$

where \mathbf{H}_{uv} has been defined in (6.315) and \mathbf{y}_{uv} is given by (6.314).

Applying (6.325) to (6.324), we have

$$\mathbf{z}_u = [(\mathbf{H}_u^H \mathbf{H}_u \odot \mathbf{R}_c)]^{-1} \left(\sum_{v=1}^p \mathbf{H}_{uv}^H \mathbf{C}^T \mathbf{y}_{uv} \right), \quad u = 1, 2, \dots, q \quad (6.326)$$

Equation (6.326) shows that the OZF-MUD for \mathbf{x}_u can be divided into p MF operations in the context of the p number of subcarriers conveying \mathbf{x}_u and one decorrelating operation of multiplying a $(K \times K)$ matrix of $[(\mathbf{H}_u^H \mathbf{H}_u \odot \mathbf{R}_c)]^{-1}$ with the MFs' outputs. In summary, the OZF-MUD can be described by the schematic block diagram of Fig. 6.29

Figures 6.28 and 6.29 show that both the OZF-MUD and SZF-MUD have the modular structures. In Fig. 6.29 the operations in the MF modular components are subcarrier-by-subcarrier independent. The ZF operations for the q bits of a user are bit-by-bit independent but subcarrier-by-subcarrier dependent for a given bit. Conversely, in Fig. 6.28 the ZF operations are subcarrier-by-subcarrier independent. Except for the sum operation, the MRC operations are also subcarrier-by-subcarrier independent. Explicitly, the modular structures of the OZF-MUD and SZF-MUD as shown in Fig. 6.29 and Fig. 6.28 are beneficial to implementation and reconfiguration in practice. For example, in a dynamic communications environment, when certain frequency bands are occupied and some of the subcarriers in the MC DS-CDMA are sensed as having high interference temperature, the OZF-MUD in Fig. 6.29 and the SZF-MUD in Fig. 6.28 can be correspondingly reconfigured in order to adapt to the changed environment. Specifically, for the OZF-MUD as shown in Fig. 6.29, the subcarrier branches having the high interference temperature can be directly deleted from the receiver. However, the matrices implementing the ZF operations must be updated by removing the CIRs corresponding to the subcarriers having the high interference temperature. By contrast, the SZF-MUD as shown in Fig. 6.28 can be updated simply by deleting the subcarrier branches having the high interference temperature, i.e. by setting the corresponding observation vectors in the form of \mathbf{y}_{uv} to the zero vectors.

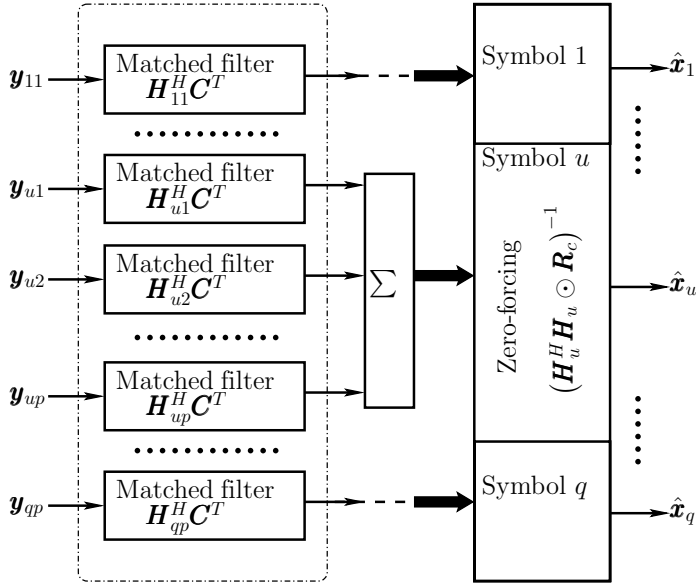


Figure 6.29: Schematic block diagram for implementation of the OZF-MUD in MC DS-CDMA systems.

Finally, when substituting (6.314) into (6.326), the decision variable vector for \mathbf{x}_u can be expressed as

$$\mathbf{z}_u = \mathbf{x}_u + [(\mathbf{H}_u^H \mathbf{H}_u \odot \mathbf{R}_c)]^{-1} \left(\sum_{v=1}^p \mathbf{H}_{uv}^H \mathbf{C}^T \mathbf{J}_{uv} \right), \quad u = 1, 2, \dots, q \quad (6.327)$$

where the MUI has been fully suppressed.

When comparing the SZF-MUD with the OZF-MUD, the OZF-MUD is capable of achieving a better error performance than the SZF-MUD, but at a cost of higher implementational complexity. As shown in (6.318) and (6.323), the matrix required to be inverted in (6.318) for the SZF-MUD is time-invariant, while that in (6.323) for the OZF-MUD is time-variant. However, when the number of users supported is not too high, the complexity of the OZF-MUD is still reasonable.

As an example, Fig. 6.30 shows the BER performance of the MC DS-CDMA system using both the OZF-MUD and SZF-MUD and supporting $K = 31$ users, when communicating over frequency-selective Rayleigh fading channels. From the results of Fig. 6.30 we can observe that when the Gold-sequences are employed for spreading, the OZF-MUD is capable of achieving the near single-user BER performance, when the number of subcarriers conveying a data bit is $p = 2, 4$ or 8 , or when the F-domain diversity order is $p = 2, 4$ and 8 . However, when not using the F-domain diversity corresponding to $p = 1$, the OZF-MUD cannot achieve the near single-user BER performance. Instead, as shown in Fig. 6.30, at the BER of 10^{-3} the BER performance of the OZF-MUD is more than 5 dB worse than the single-user BER performance. As shown in Fig. 6.30, although the SZF-MUD does have the

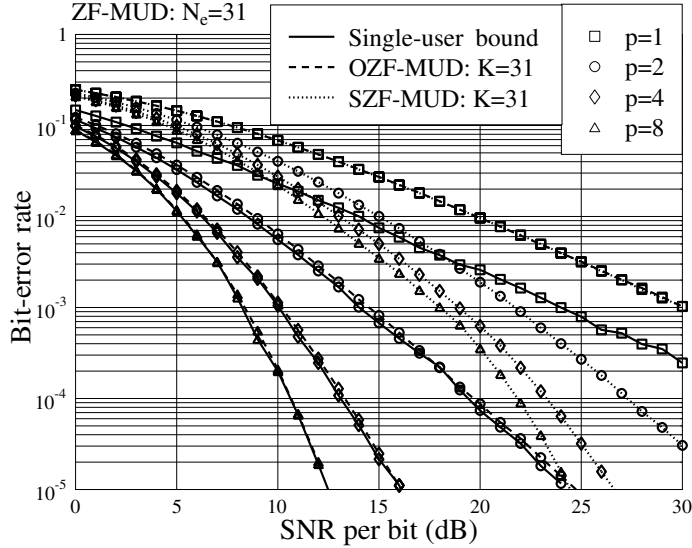


Figure 6.30: BER versus average SNR per bit performance for the MC DS-CDMA using orthogonal subcarriers having a T-domain spreading FACTOR of $N_e = 31$, when communicating over frequency-selective Rayleigh fading channels.

capability to suppress the MUI, its achievable BER performance is significantly worse than that achieved by the OZF-MUD, when the F-domain diversity order is higher than one. When $p = 1$ both the OZF-MUD and SZF-MUD achieve the same BER performance, since in this case the OZF-MUD is equivalent to the SZF-MUD.

However, as analysed previously, the SZF-MUD has the advantage of low complexity, similar to the single-user MF detector, and the advantage of robustness to the channel estimation errors. When we have a close look at (6.318) for the SZF-MUD and at (6.323) for the OZF-MUD, it is not hard to realize that the BER performance degradation of the SZF-MUD is because the ZF operation in the SZF-MUD cannot take channels into account.

The BER performance of the SZF-MUD can be significantly enhanced by employing an IC stage after the SZF-MUD. Since the IC stage does not invoke the channel-related matrix inverse operation, we can imply that the IC-assisted SZF-MUD, which is referred to as SZF-IC, should still be robust to the channel estimation errors. In detail, the SZF-IC can be operated by the following steps.

Step 1: SZF-MUD operation generating the decision variable vector \mathbf{z}_u ($u = 1, 2, \dots, q$) as shown in (6.319);

Step 2: Based on \mathbf{z}_u ($u = 1, 2, \dots, q$), make decisions as

$$\hat{\mathbf{x}}_u = f_{\text{decision}}(\mathbf{z}_u), \quad u = 1, 2, \dots, q \quad (6.328)$$

Step 3: For $k = 1, 2, \dots, K$, the IC is carried out, yielding

$$\mathbf{y}_{uv}^{(k)} = \mathbf{y}_{uv} - \mathbf{C} \mathbf{H}_{uv} \hat{\mathbf{x}}_u (\hat{x}_u^{(k)} = 0) \quad (6.329)$$

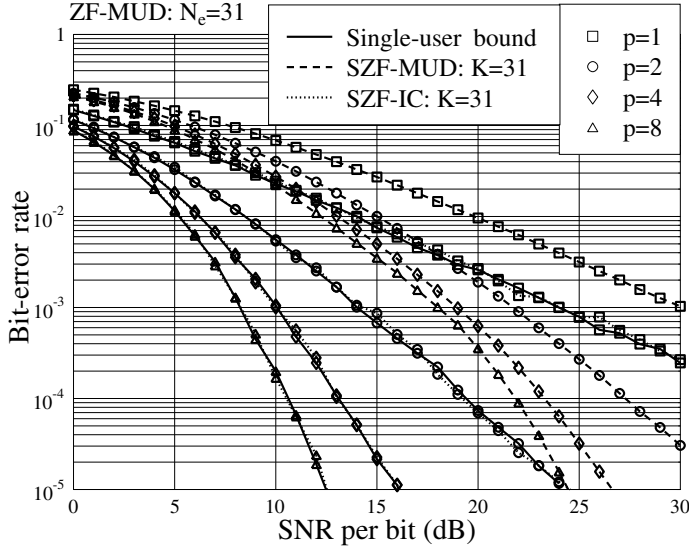


Figure 6.31: BER versus average SNR per bit performance for the MC DS-CDMA using orthogonal subcarriers having a T-domain spreading factor of $N_e = 31$, when communicating over frequency-selective Rayleigh fading channels.

where $\hat{\mathbf{x}}_u(\hat{x}_u^{(k)} = 0)$ is the result after setting $\hat{x}_u^{(k)} = 0$ in $\hat{\mathbf{x}}_u$;

Step 4: Forming the decision variable for $x_u^{(k)}$ as

$$\hat{z}_u^{(k)} = \frac{1}{\sqrt{p}} \sum_{v=1}^p (h_{uv}^{(k)})^* \mathbf{c}_k^T \mathbf{y}_{uv}^{(k)}, \quad u = 1, 2, \dots, q; k = 1, 2, \dots, K \quad (6.330)$$

The BER versus SNR per bit performance of the MC DS-CDMA using the SZF-IC is shown in Fig. 6.31 in conjunction with the BER performance of using the SZF-MUD and the single-user BER bound. As shown in Fig. 6.31, when an IC-stage is applied following the SZF-MUD, the near single-user BER performance can always be achievable regardless of the F-domain diversity order, even when the MC DS-CDMA supports $K = N_e = 31$ users, i.e. when the MC DS-CDMA is fully loaded.

Finally, the comparison among the ZF-related MUDs is summarized in Table 6.1. In this table the complexity denotes the complexity of detection per symbol per user. For example, for the OZF-MUD as shown in (6.326), it needs to compute the inverse of a time-variant ($K \times K$) matrix that has a complexity of $O(K^3)$, where $O(\cdot)$ means ‘proportional to’. Therefore, the complexity of detecting a symbol of a user is $O(K^3/K) = O(K^2)$. By contrast, for the SZF-MUD of (6.319) and the SZF-IC, since the inverse matrices are time-invariant, the highest complexity of detection in fact comes from the multiplication of a $(K \times N_e)$ matrix with an N_e -length vector, i.e. from $\mathbf{C}^T \mathbf{y}_{uv}$. Hence, when the number of multiplications is counted, the complexity per symbol per user is $O(KN_e/K) = O(N_e)$.

Table 6.1: Comparison of the OZF-MUD (6.326), SZF-MUD (6.319) and the SZF-IC.

	OZF-MUD	SZF-MUD	SZF-IC
Complexity	$O(K^2)$	$O(N_e)$	$O(N_e)$
Error performance	near-best	worst	best
Sensitivity to channel estimation error	high	low	low
Flexibility for adaptation	low	high	high

6.3.2 Minimum Mean-Square Error Multiuser Detection

Like the ZF-MUD studied in the above section, the MMSE-MUD can also be implemented first in the context of each of the qp subcarriers, and then by carrying out the combining across the subcarriers conveying the same data symbol. Alternatively, the MMSE-MUD can be derived by jointly considering all the observations related to the same data symbol. We first consider the former case.

When the MMSE detection principle is invoked for each subcarrier's detection, the decision variable vector for \mathbf{x}_u can be expressed as

$$\mathbf{z}_u = \sum_{v=1}^p (\mathbf{W}_{uv}^{(o)})^H \mathbf{y}_{uv}, \quad u = 1, 2, \dots, q \quad (6.331)$$

where the optimum weight matrix $\mathbf{W}_{uv}^{(o)}$ for the uv th subcarrier can be found by solving the optimization problem

$$\mathbf{W}_{uv}^{(o)} = \arg \min_{\mathbf{W}} \{ E[\|\mathbf{W}^H \mathbf{y}_{uv} - \mathbf{x}_u\|^2] \} \quad (6.332)$$

It can be shown that the optimum weight matrix $\mathbf{W}_{uv}^{(o)}$ can be expressed as

$$\mathbf{W}_{uv}^{(o)} = \mathbf{R}_{\mathbf{y}_{uv}}^{-1} \mathbf{R}_{\mathbf{y}_{uv} \mathbf{x}_u} \quad (6.333)$$

where $\mathbf{R}_{\mathbf{y}_{uv}}$ represents the autocorrelation matrix of \mathbf{y}_{uv} , while $\mathbf{R}_{\mathbf{y}_{uv} \mathbf{x}_u}$ represents the cross-correlation matrix between \mathbf{y}_{uv} and \mathbf{x}_u . The autocorrelation matrix $\mathbf{R}_{\mathbf{y}_{uv}}$ can be expressed as

$$\mathbf{R}_{\mathbf{y}_{uv}} = E[\mathbf{y}_{uv} \mathbf{y}_{uv}^H] = \mathbf{C} \mathbf{H}_{uv} \mathbf{H}_{uv}^H \mathbf{C}^T + \mathbf{R}_{\mathbf{J}_{uv}} \quad (6.334)$$

where $\mathbf{R}_{\mathbf{J}_{uv}} = E[\mathbf{J}_{uv} \mathbf{J}_{uv}^H]$ represents the autocorrelation matrix of \mathbf{J}_{uv} as seen in (6.314). The cross-correlation matrix $\mathbf{R}_{\mathbf{y}_{uv} \mathbf{x}_u}$ is given by

$$\mathbf{R}_{\mathbf{y}_{uv} \mathbf{x}_u} = E[\mathbf{y}_{uv} \mathbf{x}_u^H] = \mathbf{C} \mathbf{H}_{uv} \quad (6.335)$$

Consequently, substituting (6.334) and (6.335) into (6.333), the optimum weight matrix for the uv th subcarrier can be expressed as

$$\mathbf{W}_{uv}^{(o)} = (\mathbf{C} \mathbf{H}_{uv} \mathbf{H}_{uv}^H \mathbf{C}^T + \mathbf{R}_{\mathbf{J}_{uv}})^{-1} \mathbf{C} \mathbf{H}_{uv}, \quad v = 1, 2, \dots, p; u = 1, 2, \dots, q \quad (6.336)$$

Furthermore, when the *matrix inverse lemma* is invoked, we have

$$\begin{aligned} \mathbf{W}_{uv}^{(o)} &= \mathbf{R}_{J_{uv}}^{-1} \mathbf{C} \mathbf{H}_{uv} (\mathbf{H}_{uv}^H \mathbf{C}^T \mathbf{R}_{J_{uv}}^{-1} \mathbf{C} \mathbf{H}_{uv} + \mathbf{I}_K)^{-1} \\ v &= 1, 2, \dots, p; u = 1, 2, \dots, q \end{aligned} \quad (6.337)$$

The optimum weight matrix $\mathbf{W}_{uv}^{(o)}$ in (6.331) may be estimated directly from the observation vectors, it can also be found with the aid of adaptive approaches. Additionally, when there is no ICI, we have $\mathbf{R}_{J_{uv}} = \sigma^2 \mathbf{I}_{pN_e}$. Correspondingly, we have

$$\mathbf{W}_{uv}^{(o)} = (\mathbf{C} \mathbf{H}_{uv} \mathbf{H}_{uv}^H \mathbf{C}^T + \sigma^2 \mathbf{I}_N)^{-1} \mathbf{C} \mathbf{H}_{uv} \quad (6.338)$$

$$= \mathbf{C} \mathbf{H}_{uv} (\mathbf{H}_{uv}^H \mathbf{C}^T \mathbf{C} \mathbf{H}_{uv} + \sigma^2 \mathbf{I}_K)^{-1}, \quad v = 1, 2, \dots, p; u = 1, 2, \dots, q \quad (6.339)$$

Finally, if there is no ICI, then after substituting (6.314) and (6.339) into (6.331), the decision variable vector for \mathbf{x}_u when using the MMSE-MUD can be expressed as

$$\begin{aligned} z_u &= \sum_{v=1}^p [\mathbf{I}_K - (\mathbf{I}_K + \mathbf{H}_{uv}^H \mathbf{C}^T \mathbf{C} \mathbf{H}_{uv} / \sigma^2)^{-1}] \mathbf{x}_u \\ &\quad + \sum_{v=1}^p (\mathbf{H}_{uv}^H \mathbf{C}^T \mathbf{C} \mathbf{H}_{uv} + \sigma^2 \mathbf{I}_K)^{-1} \mathbf{H}_{uv}^H \mathbf{C}^T \mathbf{n}_{uv}, \quad u = 1, 2, \dots, q \end{aligned} \quad (6.340)$$

From the above analysis we can see that the autocorrelation matrix $\mathbf{R}_{y_{uv}}$ is a $(N_e \times N_e)$ matrix. When the receiver has no knowledge about the interfering users except for the desired user, implying that $\mathbf{R}_{y_{uv}}$ must be estimated from \mathbf{y}_{uv} , the receiver has to compute p number of inverse matrices of size $(N_e \times N_e)$ (as shown, e.g., in (6.338)) corresponding to the p subcarriers in order to detect one symbol vector of \mathbf{x}_u . By contrast, when the receiver employs the knowledge about all the active users, the receiver needs to compute p number of inverse matrices of size $(K \times K)$ (as shown, e.g., in (6.339)) in order to detect \mathbf{x}_u .

The autocorrelation matrix $\mathbf{R}_{y_{uv}}$ in the above derived MMSE-MUD is time-variant. In other words, $\mathbf{R}_{y_{uv}}$ can only be applied when the channels conveying \mathbf{x}_u , which include K users and p subcarriers for each user, stay unchanged. Otherwise, when an outdated version of $\mathbf{R}_{y_{uv}}$ is applied, the detection performance will degrade significantly, owing to the fact that the MMSE-MUD is sensitive to the channel estimation errors.

In the above derived MMSE-MUD, $\mathbf{R}_{y_{uv}}$ should be estimated within the time when the corresponding channels maintain unchanged. The average taken for estimating $\mathbf{R}_{y_{uv}}$ as shown in (6.334) is a short-term average. Furthermore, as shown in the forthcoming discourse, the above derived MMSE-MUD is suboptimum in terms of the best achievable error performance by the MMSE-MUD. Therefore, for convenience, we refer to this short-term average suboptimum MMSE-MUD as SMMSE-MUD-I.

It is well known that the single-user MF-assisted detector is often much more robust to the channel estimation error, in comparison with various multiuser detectors. For this reason, the detector for the MC DS-CDMA may be implemented by first carrying out the MMSE-MUD associated with each of the subcarriers, and then carrying out the coherent combining across the subcarriers conveying the same data symbol as the SZF-MUD. This type of MMSE-MUD can be obtained by taking the long average in estimation of $\mathbf{R}_{y_{uv}}$, yielding

$$\mathbf{R}_{y_{uv}} = E[\mathbf{y}_{uv} \mathbf{y}_{uv}^H] = \frac{\Omega}{p} \mathbf{C} \mathbf{C}^T + \mathbf{R}_{J_{uv}} \quad (6.341)$$

where $\Omega = E[\|h_{uv}^{(k)}\|^2]$ and $\mathbf{R}_{J_{uv}}$ is the long-term average version. In this case, we have

$$\mathbf{W}_{uv}^{(o)} = p(\Omega \mathbf{C} \mathbf{C}^T + p \mathbf{R}_{J_{uv}})^{-1} \mathbf{C} \mathbf{H}_{uv} \quad (6.342)$$

$$= p \mathbf{R}_{J_{uv}}^{-1} \mathbf{C} (\Omega \mathbf{C}^T \mathbf{R}_{J_{uv}}^{-1} \mathbf{C} + p \mathbf{I}_K)^{-1} \mathbf{H}_{uv}, \quad u = 1, 2, \dots, q \quad (6.343)$$

Furthermore, in this case, when there is no ICI, (6.338) and (6.339) can be simplified to

$$\mathbf{W}_{uv}^{(o)} = p(\Omega \mathbf{C} \mathbf{C}^T + p \sigma^2 \mathbf{I}_N)^{-1} \mathbf{C} \mathbf{H}_{uv} \quad (6.344)$$

$$= p \mathbf{C} (\Omega \mathbf{C}^T \mathbf{C} + p \sigma^2 \mathbf{I}_K)^{-1} \mathbf{H}_{uv}, \quad u = 1, 2, \dots, q \quad (6.345)$$

For convenience, we refer to the above long-term average suboptimum MMSE-MUD as the SMMSE-MUD-II. From the above analysis we know that the inverse matrices in the SMMSE-MUD-II are time-invariant, and the MRC-assisted coherent combining is achieved by the processing using matrix \mathbf{H}_{uv} . Since the time-varying dependent processing occurs only with the MRC, we can imply that the SMMSE-MUD-II should have the same robustness to the channel estimation error as the single-user MF detector. Furthermore, since the inverse matrix is only required to compute once when the active users maintain unchanged, the SMMSE-MUD-II also has an implementational complexity that is similar to that of the single-user MF detector. Let us now derive the MMSE-MUD achieving the best error performance, i.e. the optimum MMSE-MUD, which is referred to as the OMMSE-MUD in abbreviation.

The OMMSE-MUD is derived based on (6.312). In this case the decision variable vector can be expressed as

$$\mathbf{z}_u = (\mathbf{W}_u^{(o)})^H \mathbf{y}_u, \quad u = 1, 2, \dots, q \quad (6.346)$$

where the optimum weight matrix in the MMSE sense can be expressed as

$$\mathbf{W}_u^{(o)} = \mathbf{R}_{y_u}^{-1} \mathbf{R}_{y_u x_u} \quad (6.347)$$

where \mathbf{R}_{y_u} is the autocorrelation matrix of \mathbf{y}_u given by

$$\mathbf{R}_{y_u} = (\mathbf{H}_u \square \mathbf{C}) (\mathbf{H}_u \square \mathbf{C})^H + \mathbf{R}_{J_u} \quad (6.348)$$

where $\mathbf{R}_{J_u} = E[\mathbf{J}_u \mathbf{J}_u^H]$. \mathbf{R}_{y_u} is a $(pN_e \times pN_e)$ -dimensional matrix. In (6.347) $\mathbf{R}_{y_u x_u}$ is the crosscorrelation matrix given by

$$\mathbf{R}_{y_u x_u} = (\mathbf{H}_u \square \mathbf{C}) \quad (6.349)$$

which is a $(pN_e \times K)$ matrix. After substituting (6.348) and (6.349) into (6.347), the weight matrix for the OMMSE-MUD can be expressed as

$$\mathbf{W}_u^{(o)} = [(\mathbf{H}_u \square \mathbf{C}) (\mathbf{H}_u \square \mathbf{C})^H + \mathbf{R}_{J_u}]^{-1} (\mathbf{H}_u \square \mathbf{C}), \quad u = 1, 2, \dots, q \quad (6.350)$$

Therefore, when the receiver employs no channel knowledge about the interfering users (including their signature sequences and CIRs) except for the desired user, the receiver has to invert a matrix of size $(pN_e \times pN_e)$ -dimensional. In this case, the OMMSE-MUD has the highest implementational complexity. However, when the receiver has the knowledge about all the active users, all the K users can be estimated simultaneously. In this case, the *matrix inverse lemma* can be invoked, yielding

$$\mathbf{W}_u^{(o)} = \mathbf{R}_{J_u}^{-1} (\mathbf{H}_u \square \mathbf{C}) [(\mathbf{H}_u \square \mathbf{C})^H \mathbf{R}_{J_u}^{-1} (\mathbf{H}_u \square \mathbf{C}) + \mathbf{I}_K]^{-1}, \quad u = 1, 2, \dots, q \quad (6.351)$$

Furthermore, when there is no ICI, or when the ICI is ignored in the derivation of $\mathbf{W}_u^{(o)}$, equation (6.351) can be simplified to

$$\begin{aligned}\mathbf{W}_u^{(o)} &= (\mathbf{H}_u \square \mathbf{C})[(\mathbf{H}_u \square \mathbf{C})^H (\mathbf{H}_u \square \mathbf{C})^H + \sigma^2 \mathbf{I}_K]^{-1} \\ &= (\mathbf{H}_u \square \mathbf{C})[(\mathbf{H}_u^H \mathbf{H}_u \odot \mathbf{C}^T \mathbf{C}) + \sigma^2 \mathbf{I}_K]^{-1}\end{aligned}\quad (6.352)$$

where the matrix required to be inverted is a $(K \times K)$ matrix.

Substituting (6.352) into (6.346) and following (6.324) to (6.326), we have

$$z_u = [(\mathbf{H}_u^H \mathbf{H}_u \odot \mathbf{C}^T \mathbf{C}) + \sigma^2 \mathbf{I}_K]^{-1} \left(\sum_{v=1}^p \mathbf{H}_{uv}^H \mathbf{C}^T \mathbf{y}_{uv} \right), \quad u = 1, 2, \dots, q \quad (6.353)$$

Equation (6.353) shows that when the receiver employs knowledge about all the users, the OMMSE-MUD can be implemented in two stages: first, a correlation operation in the context of each of the subcarriers; second, a MMSE-based interference suppression across the subcarriers conveying the same data symbol vector of, say, \mathbf{x}_u .

The BER versus SNR per bit performance of the MC DS-CDMA employing various MMSE-MUDs is plotted in Figs. 6.32 and 6.33, when communicating over frequency-selective Rayleigh fading channels when the subcarrier channels conveying a data bit experience independent Rayleigh fading. Specifically, in Fig. 6.32 the BER of the MC DS-CDMA employing the OMMSE-MUD, SMMSE-MUD-I as well as the single-user BER bound are plotted, when the F-domain diversity order is $p = 1, 2, 4, 8$, respectively. By contrast, in Fig. 6.33 the BER performance of the MC DS-CDMA employing the SMMSE-MUD-I, SMMSE-MUD-II as well as the single-user BER bound are considered, also when the F-domain diversity order is $p = 1, 2, 4, 8$, respectively. From the results of Figs. 6.32, 6.33, explicitly, the SMMSE-MUD-I outperforms the SMMSE-MUD-II, and the OMMSE-MUD outperforms both the SMMSE-MUD-I and SMMSE-MUD-II, when considering the achievable BER performance. As shown in Fig. 6.32, the BER performance achieved by the OMMSE-MUD is very close to the single-user BER bound, when $p = 2, 3, 4$. By contrast, both the OMMSE-MUD and SMMSE-MUD-I achieve the same BER performance when $p = 1$. Furthermore, when $p = 1$, as shown in Fig. 6.33, the BER performance of the SMMSE-MUD-II is slightly worse than that achieved by the SMMSE-MUD-I or by the OMMSE-MUD.

As the ZF-IC, an IC-stage can be implemented after the SMMSE-MUD-II assisted multiuser detection, in order to achieve low complexity and robust detection, while also achieving the near single-user BER performance. The BER performance of the SMMSE-IC is depicted in Fig. 6.34 in conjunction with the BER of the corresponding SMMSE-MUD-II and the corresponding single-user BER bound. As can be seen in Fig. 6.34, when an IC stage is applied following the SMMSE-MUD-II detection, the MC DS-CDMA system is capable of achieving the near single-user BER performance.

In other words, the results of Fig. 6.31 and Fig. 6.34 show that, when an IC stage is employed after either the SZF-MUD or the SMMSE-MUD-II, the MC DS-CDMA system is capable of achieving a BER performance that is only achievable by the optimum MUD based on ML principles. However, as our analysis shows, both the SZF-IC and SMMSE-IC have an implementational complexity that is significantly lower than THAT of the ML-aided MUD, whose complexity is exponentially proportional to the number of users.

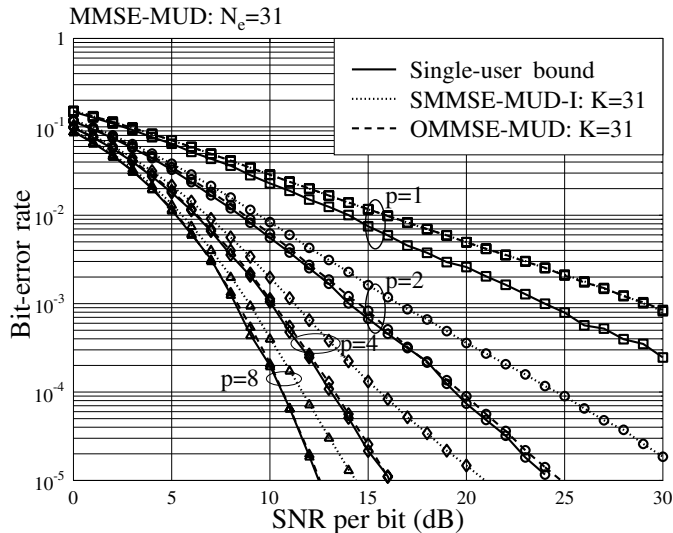


Figure 6.32: BER versus average SNR per bit performance for the MC DS-CDMA using orthogonal subcarriers having a T-domain spreading factor of $N_e = 31$, when communicating over frequency-selective Rayleigh fading channels.

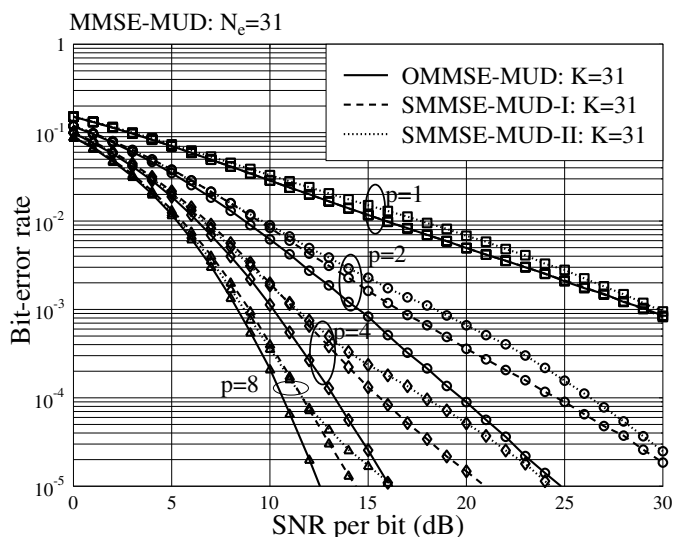


Figure 6.33: BER versus average SNR per bit performance for the MC DS-CDMA using orthogonal subcarriers having a T-domain spreading factor of $N_e = 31$, when communicating over frequency-selective Rayleigh fading channels.

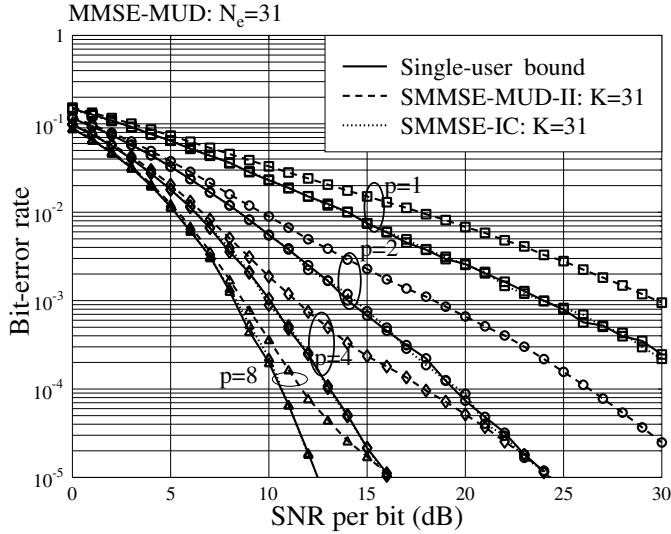


Figure 6.34: BER versus average SNR per bit performance for the MC DS-CDMA using orthogonal subcarriers having a T-domain spreading factor of $N_e = 31$, when communicating over frequency-selective Rayleigh fading channels.

Finally, a comparison of the above four types of MMSE-related MUD is summarized in Table 6.2, in terms of implementation complexity, error performance, robustness as well as flexibility. Again, the SMMSE-IC has the advantage of low complexity, high flexibility, robustness and also of achieving a low error probability.

In summary, in the last two subsections a range of low-complexity, high-flexibility and robust MUD schemes have been established for the MC DS-CDMA, constituting a multiple-access scheme suitable for operation in dynamic communications environments. The MUD schemes were derived based on the principles of ZF, MMSE and IC. The BER performance of the MC DS-CDMA in conjunction with the proposed MUD schemes was investigated by simulation. It can be shown that all the MUD schemes are capable of efficiently mitigating MUI. The study shows that the ZF-MUDs and MMSE-MUDs in MC DS-CDMA can usually be implemented using modular structures, where most modules are independent of each other. Moreover, it can be shown that the SZF-MUD, SZF-IC, SMMSE-MUD-II or SMMSE-IC has a fully subcarrier-by-subcarrier independent modular structure, where each of the modules may be reconfigured without effecting the others. Due to its high flexibility of both transmission and detection, the MC DS-CDMA aided by a proposed high-flexibility MUD constitutes one of the promising candidates for application in dynamic communications environments.

6.3.3 Maximum Likelihood Decision Multiuser Detection

We express (6.314) as

$$\mathbf{y}_{uv} = \mathbf{C}\mathbf{H}_{uv}\mathbf{x}_u + \mathbf{J}_{uv}, \quad u = 1, 2, \dots, q; v = 1, 2, \dots, p \quad (6.354)$$

Table 6.2: Comparison among the SMMSE-MUD-I (6.339), SMMSE-MUD-II (6.345), OMMSE-MUD (6.351) as well as the SMMSE-IC.

	OMMSE-MUD	SMMSE-MUD-I
Complexity	$O(p^3N_e^3)/K$ (no CIRs), $O(K^2)$ (CIRs)	$O(pN_e^3)/K$ (no CIRs) $O(pK^2)$ (CIRs)
Error performance	near-best	medium
Sensitivity to channel estimation error	high	high
Flexibility for adaptation	low	low
	SMMSE-MUD-II	SMMSE-IC
Complexity	$O(N_e)$	$O(N_e)$
Error performance	worst	best
Sensitivity to channel estimation error	low	low
Flexibility for adaptation	high	high

where $\mathbf{J}_{uv} = \mathbf{I}_{uv} + \mathbf{n}_{uv}$. Let \mathbf{J}_{uv} be approximated as a zero-mean Gaussian vector with a covariance matrix $\mathbf{R}_{\mathbf{J}_{uv}}$. Then, given \mathbf{H}_{uv} and \mathbf{x}_u , \mathbf{y}_{uv} is multivariate Gaussian distributed with a PDF

$$f(\mathbf{y}_{uv}) = \frac{1}{\pi^{N_e} \det(\mathbf{R}_{\mathbf{J}_{uv}})} \exp[-(\mathbf{y}_{uv} - \mathbf{C}\mathbf{H}_{uv}\mathbf{x}_u)^H \mathbf{R}_{\mathbf{J}_{uv}}^{-1} (\mathbf{y}_{uv} - \mathbf{C}\mathbf{H}_{uv}\mathbf{x}_u)] \\ u = 1, 2, \dots, q; v = 1, 2, \dots, p \quad (6.355)$$

Let

$$\mathbf{y}_u = [\mathbf{y}_{u1}^T, \mathbf{y}_{u2}^T, \dots, \mathbf{y}_{up}^T]^T, \quad u = 1, 2, \dots, q \quad (6.356)$$

Since the observations $\{\mathbf{y}_{uv}\}$ are independent random vectors, the PDF of \mathbf{y}_u can hence be expressed as

$$f(\mathbf{y}_u) = \prod_{v=1}^p \frac{1}{\pi^{N_e} \det(\mathbf{R}_{\mathbf{J}_{uv}})} \exp[-(\mathbf{y}_{uv} - \mathbf{C}\mathbf{H}_{uv}\mathbf{x}_u)^H \mathbf{R}_{\mathbf{J}_{uv}}^{-1} (\mathbf{y}_{uv} - \mathbf{C}\mathbf{H}_{uv}\mathbf{x}_u)] \\ = \frac{1}{\pi^{N_e p} \prod_{v=1}^p \det(\mathbf{R}_{\mathbf{J}_{uv}})} \exp\left[-\sum_{v=1}^p (\mathbf{y}_{uv} - \mathbf{C}\mathbf{H}_{uv}\mathbf{x}_u)^H \mathbf{R}_{\mathbf{J}_{uv}}^{-1} (\mathbf{y}_{uv} - \mathbf{C}\mathbf{H}_{uv}\mathbf{x}_u)\right] \\ u = 1, 2, \dots, q \quad (6.357)$$

With the MLD-MUD, the estimate to \mathbf{x}_u can be described by the optimization problem

$$\begin{aligned}\hat{\mathbf{x}}_u &= \arg \min_{\mathbf{x}_u} \left\{ \sum_{v=1}^p (\mathbf{y}_{uv} - \mathbf{C} \mathbf{H}_{uv} \mathbf{x}_u)^H \mathbf{R}_{J_{uv}}^{-1} (\mathbf{y}_{uv} - \mathbf{C} \mathbf{H}_{uv} \mathbf{x}_u) \right\} \\ u &= 1, 2, \dots, q\end{aligned}\quad (6.358)$$

After some simplification, the above optimization problem can be modified to

$$\begin{aligned}\hat{\mathbf{x}}_u &= \arg \min_{\mathbf{x}_u} \left\{ \sum_{v=1}^p [\mathbf{x}_u^H \mathbf{H}_{uv}^H \mathbf{C}^T \mathbf{R}_{J_{uv}}^{-1} \mathbf{C} \mathbf{H}_{uv} \mathbf{x}_u - 2\Re\{\mathbf{y}_{uv}^H \mathbf{R}_{J_{uv}}^{-1} \mathbf{C} \mathbf{H}_{uv} \mathbf{x}_u\}] \right\} \\ u &= 1, 2, \dots, q\end{aligned}\quad (6.359)$$

From (6.359) we can see that the MLD-MUD for the MC DS-CDMA can be treated as a joint optimization problem, which provides a feasible solution $\hat{\mathbf{x}}_u$ maximizing the overall likelihood function. Alternatively, for each given u , (6.359) can be divided into p parallel optimization subproblems, which can be stated as

$$\begin{aligned}\hat{\mathbf{x}}_u &= \arg \min_{\mathbf{x}_u} \{[\mathbf{x}_u^H \mathbf{H}_{uv}^H \mathbf{C}^H \mathbf{R}_{J_{uv}}^{-1} \mathbf{C} \mathbf{H}_{uv} \mathbf{x}_u - 2\Re\{\mathbf{y}_{uv}^H \mathbf{R}_{J_{uv}}^{-1} \mathbf{C} \mathbf{H}_{uv} \mathbf{x}_u\}]\} \\ v &= 1, 2, \dots, p\end{aligned}\quad (6.360)$$

For each given v , the optimization of (6.360) generates a feasible solution to \mathbf{x}_u . Hence, the detector can obtain a total of p number of feasible solutions for estimating \mathbf{x}_u , and the final solution to \mathbf{x}_u may be obtained by combining the p solutions based on some efficient schemes.

The fact that the MLD-MUD in the MC DS-CDMA can be treated as p parallel optimization subproblems may be applied in the design of novel search algorithms with high efficiency. For example, some of the search algorithms in Appendix 6.C may be modified so that they are suitable for p parallel searches. These parallel searches may cooperate with each other and learn from each other, in order to improve the efficiency and ultimately to enhance the error performance of the MC DS-CDMA system.

Above, the MLD-MUD has been built directly on the observations in the form of (6.354). Alternatively, the MLD-MUD can be carried out after the coherent combining of the observations seen in (6.354). Specifically, after the coherent combining of \mathbf{y}_{uv} for $v = 1, \dots, p$, the output can be expressed as

$$\mathbf{z}_u = \left(\sum_{v=1}^p \mathbf{H}_{uv}^H \mathbf{C}^T \mathbf{C} \mathbf{H}_{uv} \right) \mathbf{x}_u + \underbrace{\sum_{v=1}^p \mathbf{H}_{uv}^H \mathbf{C}^T \mathbf{J}_{uv}}_{\mathbf{J}_u}, \quad u = 1, 2, \dots, q \quad (6.361)$$

which is assumed to be Gaussian distributed with mean and covariance matrix given by

$$\begin{aligned}E[\mathbf{z}_u] &= \left(\sum_{v=1}^p \mathbf{H}_{uv}^H \mathbf{C}^T \mathbf{C} \mathbf{H}_{uv} \right) \mathbf{x}_u \\ \mathbf{R}_{J_u} &= \sum_{v=1}^p \sum_{w=1}^p \mathbf{H}_{uv}^H \mathbf{C}^T \mathbf{R}_{J_{uv}} \mathbf{C} \mathbf{H}_{uw}\end{aligned}\quad (6.362)$$

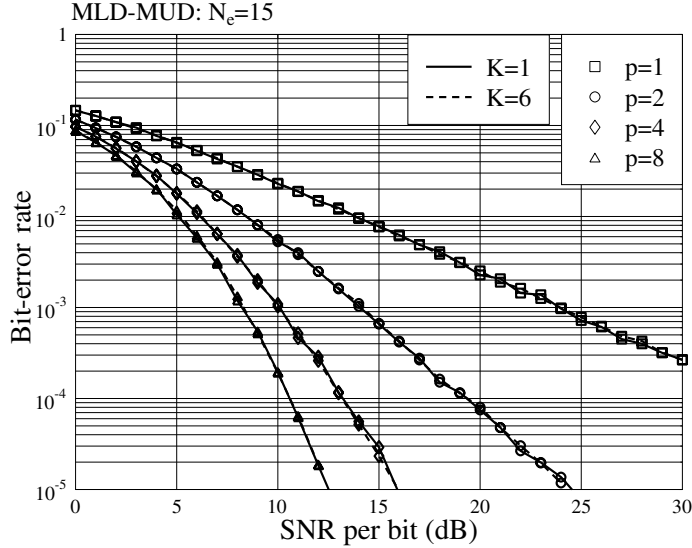


Figure 6.35: BER performance of the MLD-MUD for the MC DS-CDMA using orthogonal subcarriers having a T-domain spreading factor of $N_e = 15$, when communicating over frequency-selective Rayleigh fading channels. The simulations were based on (6.358).

Notice that, when \mathbf{J}_{uv} is independent with respect to v , we then have

$$\mathbf{R}_{J_u} = \sum_{v=1}^p \mathbf{H}_{uv}^H \mathbf{C}^T \mathbf{R}_{J_{uv}} \mathbf{C} \mathbf{H}_{uv} \quad (6.363)$$

Consequently, following the derivations in this section for (6.359) and (6.360), it can be shown that the estimate to \mathbf{x}_u in the MLD sense can be described as

$$\begin{aligned} \hat{\mathbf{x}}_u &= \arg \min_{\mathbf{x}_u} \left\{ \left[\mathbf{z}_u - \left(\sum_{v=1}^p \mathbf{H}_{uv}^H \mathbf{C}^T \mathbf{C} \mathbf{H}_{uv} \right) \mathbf{x}_u \right]^H \mathbf{R}_{J_u}^{-1} \right. \\ &\quad \times \left. \left[\mathbf{z}_u - \left(\sum_{v=1}^p \mathbf{H}_{uv}^H \mathbf{C}^T \mathbf{C} \mathbf{H}_{uv} \right) \mathbf{x}_u \right] \right\}, \quad u = 1, 2, \dots, q \end{aligned} \quad (6.364)$$

or

$$\hat{\mathbf{x}}_u = \arg \min_{\mathbf{x}_u} \{ [\mathbf{x}_u^H \mathbf{A}_u^H \mathbf{R}_{J_u}^{-1} \mathbf{A}_u \mathbf{x}_u - 2\Re\{\mathbf{z}_u^H \mathbf{R}_{J_u}^{-1} \mathbf{A}_u \mathbf{x}_u\}] \}, \quad u = 1, 2, \dots, q \quad (6.365)$$

where, by definition

$$\mathbf{A}_u = \sum_{v=1}^p \mathbf{H}_{uv}^H \mathbf{C}^T \mathbf{C} \mathbf{H}_{uv} \quad (6.366)$$

Figure 6.35 shows the BER performance of the MC DS-CDMA using MLD-MUD, when communicating over the frequency-selective Rayleigh fading channels, resulting in each subcarrier experiencing independent fading. The number of subcarriers conveying a data bit

was assumed to be $p = 1, 2, 4$ or 8 , yielding a corresponding diversity order of $1, 2, 4$ or 8 . As the curves in Fig. 6.35 shown, the MC DS-CDMA system supporting $K = 6$ users is capable of achieving the single-user performance, i.e. the BER performance of the MC DS-CDMA system supporting only one user.

6.4 Multiuser Detection in Time-Frequency-Domain Spread Multicarrier DS-CDMA

In Section 5.11 of Chapter 5 the performance of the TF-domain spread MC DS-CDMA has been investigated over frequency-selective fading channels. It has been shown that the TF-domain spread MC DS-CDMA is a highly generalized CDMA model that can easily be specified to another multicarrier CDMA scheme, such as to the F-domain spread MC-CDMA, the conventional DS-CDMA using only T-domain spreading, etc. The TF-domain spread MC DS-CDMA can make efficient use of the available resources provided by the wireless system.

In the TF-domain spread MC DS-CDMA, the general observation equation considering ICI was derived in Section 5.11.1 of Chapter 5, shown in (5.237). Here, we assume for brevity that the subcarrier signals are orthogonal and, in this case, the observation equation is given by (5.240), which is⁴

$$\mathbf{y} = \sum_{k=1}^K \mathbf{C}_k \mathbf{H}_k \mathbf{C}_f^{(k)} \mathbf{x}_k + \mathbf{n} \quad (6.367)$$

The vectors and matrices in (6.367) are defined as follows. The observation vector \mathbf{y} is a $N_p N_t$ -length vector, where $N_p N_t$ is the overall spreading factor of the TF-domain spread MC DS-CDMA system, and N_p and N_t represent the F-domain and T-domain spreading factors, respectively. The observation vector \mathbf{y} can be divided into the components

$$\begin{aligned} \mathbf{y} &= [\mathbf{y}_0^T, \mathbf{y}_1^T, \dots, \mathbf{y}_{N_p-1}^T]^T \\ \mathbf{y}_v &= [y_{v0}, y_{v1}, \dots, y_{v(N_t-1)}]^T, \quad v = 0, 1, \dots, N_p - 1 \end{aligned} \quad (6.368)$$

where \mathbf{y}_v contains the observations obtained in the context of the v th subcarrier, while y_{vn} is the observation corresponding to the n th chip on the v th subcarrier. The matrix \mathbf{C}_k in (6.367) is related to the T-domain spreading, which is a $(N_p N_t \times N_p)$ matrix given by

$$\begin{aligned} \mathbf{C}_k &= \mathbf{I}_{N_p} \otimes \mathbf{c}_k \\ \mathbf{c}_k &= \frac{1}{\sqrt{N_t}} [c_{k0}, c_{k1}, \dots, c_{k(N_t-1)}]^T \end{aligned} \quad (6.369)$$

where \mathbf{c}_k contains the T-domain spreading sequence assigned to the k th user. In (6.367) \mathbf{H}_k is a $(N_p \times N_p)$ diagonal matrix containing the channel gains of the N_p subcarriers, which can be expressed as

$$\mathbf{H}_k = \text{diag}\{h_0^{(k)}, h_1^{(k)}, \dots, h_{N_p-1}^{(k)}\} \quad (6.370)$$

⁴ \mathbf{c}_k in (5.240) is now represented by \mathbf{C}_k for convenience.

$\mathbf{C}_f^{(k)}$ is a $(N_p \times U)$ matrix related to the F-domain spreading of the k th user, $\mathbf{C}_f^{(k)}$ is given by

$$\begin{aligned} \mathbf{C}_f^{(k)} &= [\mathbf{c}_{f1}^{(k)}, \mathbf{c}_{f2}^{(k)}, \dots, \mathbf{c}_{f(U-1)}^{(k)}] \\ &= \frac{1}{\sqrt{N_p}} \begin{bmatrix} c_{f0,0}^{(k)} & c_{f1,0}^{(k)} & \cdots & c_{f(U-1),0}^{(k)} \\ c_{f0,1}^{(k)} & c_{f1,1}^{(k)} & \cdots & c_{f(U-1),1}^{(k)} \\ \vdots & \vdots & \ddots & \vdots \\ c_{f0,N_p-1}^{(k)} & c_{f1,N_p-1}^{(k)} & \cdots & c_{f(U-1),N_p-1}^{(k)} \end{bmatrix} \end{aligned} \quad (6.371)$$

where $\mathbf{c}_{fu}^{(k)}$ for $u = 1, \dots, U$ are the F-domain spreading sequences assigned to the k th user in order that the k th user transmit U data symbols simultaneously. In (6.367) \mathbf{x}_k contains the U data symbols transmitted by the k th user, which can be expressed as

$$\mathbf{x}_k = [x_{k1}, x_{k2}, \dots, x_{kU}]^T, \quad k = 1, 2, \dots, K \quad (6.372)$$

where it is assumed that $E[\|\mathbf{x}_{ki}\|^2] = 1$. Finally, in (6.367) the $N_p N_t$ -length noise vector \mathbf{n} is given by

$$\begin{aligned} \mathbf{n} &= [\mathbf{n}_0^T, \mathbf{n}_1^T, \dots, \mathbf{n}_{N_p-1}^T]^T \\ \mathbf{n}_v &= [n_{v0}, n_{v1}, \dots, n_{v(N_t-1)}]^T, \quad v = 0, 1, \dots, N_p - 1 \end{aligned} \quad (6.373)$$

which is Gaussian distributed with zero mean and a covariance matrix of⁵ $\sigma^2 \mathbf{I}$. Note that, when BPSK baseband modulation is employed, we have $\sigma^2 = N_0/E_b$.

Equation (6.367) can be expressed in a compact form as

$$\mathbf{y} = \mathbf{CHC}_f \mathbf{x} + \mathbf{n} \quad (6.374)$$

where

$$\begin{aligned} \mathbf{C} &= [\mathbf{C}_1, \mathbf{C}_2, \dots, \mathbf{C}_K] \\ \mathbf{H} &= \text{diag}\{\mathbf{H}_1, \mathbf{H}_2, \dots, \mathbf{H}_K\} \\ \mathbf{C}_f &= \text{diag}\{\mathbf{C}_f^{(1)}, \mathbf{C}_f^{(2)}, \dots, \mathbf{C}_f^{(K)}\} \\ \mathbf{x} &= [\mathbf{x}_1^T, \mathbf{x}_2^T, \dots, \mathbf{x}_K^T]^T \end{aligned} \quad (6.375)$$

where the dimensions of \mathbf{C} , \mathbf{H} , \mathbf{C}_f and \mathbf{x} are $(N_p N_t \times N_p K)$, $(N_p K \times N_p K)$, $(N_p K \times UK)$ and $(UK \times 1)$, respectively.

When the observation equation (6.367) for the TF-domain spread MC DS-CDMA is compared with (6.6) for the F-domain spread MC-CDMA, we can see that both of them have similar structures and also similar characteristics. Hence, all the MUD algorithms discussed in Section 6.2 for the F-domain spread MC-CDMA can be directly applied to the TF-domain spread MC DS-CDMA by correspondingly replacing $\mathbf{C}_k \mathbf{H}_k$ in (6.6) with the term $\mathbf{C}_k \mathbf{H}_k \mathbf{C}_f^{(k)}$ in (6.367). In this section we consider some modified MUD algorithms designed specifically for the TF-domain spread MC DS-CDMA. These MUD algorithms are designed

⁵Here the identity matrix \mathbf{I} should be $\mathbf{I}_{N_p N_t}$. However, it is expressed as \mathbf{I} for brevity.

with consideration of the unique characteristics of the TF-domain spread MC DS-CDMA. We first outline these observations in ways that are convenient to TF-domain detection.

The observation equation can be expressed in terms of the subcarriers, which, we will find later, is a more convenient way to derive the TF-domain MUD schemes. Let us define

$$\mathbf{c}_{f,n_p}^{(k)} = \frac{1}{\sqrt{N_p}} [c_{f0,n_p}^{(k)}, c_{f1,n_p}^{(k)}, \dots, c_{f(U-1),n_p}^{(k)}]^T \quad (6.376)$$

Then, for the n_p th subcarrier, where $n_p = 0, 1, \dots, N_p - 1$, the observation vector can be expressed as

$$\mathbf{y}_{n_p} = \sum_{k=1}^K h_{n_p}^{(k)} \mathbf{c}_k (\mathbf{c}_{f,n_p}^{(k)})^T \mathbf{x}_k + \mathbf{n}_{n_p}, \quad n_p = 0, 1, \dots, N_p - 1 \quad (6.377)$$

It can be shown that (6.377) can also be written as

$$\mathbf{y}_{n_p} = \mathcal{C} \mathcal{H}_{n_p} \mathbf{C}_{f,n_p} \mathbf{x} + \mathbf{n}_{n_p}, \quad n_p = 0, 1, \dots, N_p - 1 \quad (6.378)$$

where \mathbf{x} is given by (6.375), while \mathcal{C} , \mathcal{H}_{n_p} and \mathbf{C}_{f,n_p} are defined as

$$\begin{aligned} \mathcal{C} &= [\mathbf{c}_1, \mathbf{c}_2, \dots, \mathbf{c}_K] \\ \mathcal{H}_{n_p} &= \text{diag}\{h_{n_p}^{(1)}, h_{n_p}^{(2)}, \dots, h_{n_p}^{(K)}\} \\ \mathbf{C}_{f,n_p} &= \text{diag}\{(\mathbf{c}_{f,n_p}^{(1)})^T, (\mathbf{c}_{f,n_p}^{(2)})^T, \dots, (\mathbf{c}_{f,n_p}^{(K)})^T\} \end{aligned} \quad (6.379)$$

where \mathcal{C} is a $(N_t \times K)$ matrix, \mathcal{H}_{n_p} is a $(K \times K)$ diagonal matrix, while \mathbf{C}_{f,n_p} is a $(K \times UK)$ matrix.

Furthermore, it can be shown that the observation vector \mathbf{y} defined in (6.368) can be expressed as

$$\mathbf{y} = (\mathbf{I}_{N_p} \otimes \mathcal{C}) \mathcal{H} \mathbf{C}_f \mathbf{x} + \mathbf{n} \quad (6.380)$$

associated with

$$\begin{aligned} \mathcal{H} &= \text{diag}\{\mathcal{H}_0, \mathcal{H}_1, \dots, \mathcal{H}_{N_p-1}\} \\ \mathbf{C}_f &= [\mathbf{C}_{f,0}^T, \mathbf{C}_{f,1}^T, \dots, \mathbf{C}_{f,N_p-1}^T]^T \end{aligned} \quad (6.381)$$

where \mathcal{H} and \mathbf{C}_f are $(N_p K \times N_p K)$ and $(N_p K \times KU)$ dimensional matrices.

Additionally, it can be shown that (6.377) can be written as

$$\begin{aligned} \mathbf{y}_{n_p} &= \sum_{k=1}^K (h_{n_p}^{(k)} (\mathbf{c}_{f,n_p}^{(k)})^T \otimes \mathbf{c}_k) \mathbf{x}_k + \mathbf{n}_{n_p} \\ &= [(\mathbf{h}_{n_p}^T \mathbf{C}_{f,n_p}) \square \mathbf{S}] \mathbf{x} + \mathbf{n}_{n_p}, \quad n_p = 0, 1, \dots, N_p - 1 \end{aligned} \quad (6.382)$$

where, by definition, \mathbf{h}_{n_p} and \mathbf{S} are given by

$$\mathbf{h}_{n_p} = [h_{n_p}^{(1)}, h_{n_p}^{(2)}, \dots, h_{n_p}^{(K)}]^T \quad (6.383)$$

$$\begin{aligned} \mathbf{S} &= [\underbrace{\mathbf{c}_1, \dots, \mathbf{c}_1}_U, \underbrace{\mathbf{c}_2, \dots, \mathbf{c}_2}_U, \dots, \underbrace{\mathbf{c}_K, \dots, \mathbf{c}_K}_U] \\ &= [(\mathbf{1}_U^T \otimes \mathbf{c}_1), (\mathbf{1}_U^T \otimes \mathbf{c}_2), \dots, (\mathbf{1}_U^T \otimes \mathbf{c}_K)] \end{aligned} \quad (6.384)$$

where $\mathbf{1}_U = [1, 1, \dots, 1]^T$ is a U -length all ‘1’ vector. Hence, we know that \mathbf{S} is a $(N_t \times KU)$ matrix. Furthermore, in (6.382) \mathbf{C}_{f,n_p} is given in (6.379). With the aid of (6.382), it can be shown that the observation vector \mathbf{y} corresponding to all the qp subcarriers can be expressed as

$$\mathbf{y} = [(\mathbf{H}_f \mathbf{C}_f) \square \mathbf{S}] \mathbf{x} + \mathbf{n} \quad (6.385)$$

where \mathbf{C}_f is given in (6.381), which is a $(N_p K \times KU)$ matrix, \mathbf{n} is given by (6.373) and \mathbf{H}_f is defined as

$$\mathbf{H}_f = \text{diag}\{\mathbf{h}_0^T, \mathbf{h}_1^T, \dots, \mathbf{h}_{N_p-1}^T\} \quad (6.386)$$

which is a $(N_p \times N_p K)$ matrix. Note that, in (6.385) $[(\mathbf{H}_f \mathbf{C}_f) \square \mathbf{S}]$ is a $(N_p N_t \times KU)$ matrix.

Using the representations in the forms of (6.377) to (6.381) or of (6.382) to (6.386), we now consider the MUD in the TF-domain spread MC DS-CDMA by first deriving the ZF-MUD.

6.4.1 Time-Frequency-Domain Zero-Forcing Multiuser Detection

The TF-domain spread MC DS-CDMA has $N_p N_t$ degrees-of-freedom, hence, when linear multiuser detection is employed, the TF-domain spread MC DS-CDMA is capable of supporting up to $N_p N_t / U$ users, when we assume that each user transmits U parallel data symbols. However, for the T-domain spreading sequences of length- N_t , there are only N_t linearly independent sequences, and there usually only exist N_t sequences with good auto- and cross-correlation properties [6]. Hence, in TF-domain spread MC DS-CDMA systems we may only assign these N_t T-domain spreading sequences to the users requiring communications. This signature code assignment scheme implies that the same T-domain signature code may be assigned to multiple users, and these users sharing the same T-domain signature code can only be distinguished in the F-domain with the aid of their unique F-domain spreading codes.

Let us assume that the number of users $K (K \leq N_p N_t / U)$ supported by the TF-domain spread MC DS-CDMA can be expressed as $K = MK_1$, where $K_1 \leq N_t$ and M represents the number of users sharing the same T-domain spreading sequence. It can be shown that M should be chosen to satisfy $MU < N_p$, so that there are sufficient F-domain spreading sequences to distinguish the M users sharing the same T-domain spreading sequence. Furthermore, we assume that the T-domain spreading sequences are assigned to the users according to

$$\begin{array}{ccccccccccccc} \text{User :} & 1 & \dots & K_1 & K_1 + 1 & \dots & 2K_1 & \dots & (M - 1)K_1 + 1 & \dots & MK_1 \\ \text{Code :} & \mathbf{c}_1 & \dots & \mathbf{c}_{K_1} & \mathbf{c}_1 & \dots & \mathbf{c}_{K_1} & \dots & \mathbf{c}_1 & \dots & \mathbf{c}_{K_1} \end{array} \quad (6.387)$$

Let us construct a matrix using the K_1 different T-domain spreading codes as

$$\mathbf{C} = [\mathbf{c}_1, \mathbf{c}_2, \dots, \mathbf{c}_{K_1}] \quad (6.388)$$

Then, it can be shown that, after correlating \mathbf{y} of (6.380) using $(\mathbf{I}_{N_p} \otimes \mathbf{C}^T)$, the output can be expressed as

$$\bar{\mathbf{y}} = (\mathbf{I}_{N_p} \otimes \mathbf{R}_T) \mathcal{H} \mathbf{C}_f \mathbf{x} + \bar{\mathbf{n}} \quad (6.389)$$

where $\bar{\mathbf{n}} = (\mathbf{I}_{N_p} \otimes \mathbf{C}^T) \mathbf{n}$ and the matrix \mathbf{R}_T is the autocorrelation matrix of the T -domain spreading sequences, where the subscript T indicates the relation to the T -domain spreading sequences, \mathbf{R}_T is given by

$$\mathbf{R}_T = \mathbf{C}^T \mathbf{C} \quad (6.390)$$

which is a $(K_1 \times MK_1)$ matrix. With the code assignments as shown in (6.387), it can be shown that \mathbf{R}_T has the structure of

$$\mathbf{R}_T = [\mathbf{R}_t \quad \mathbf{R}_t \quad \cdots \quad \mathbf{R}_t] \quad (6.391)$$

which is composed of M number of subautocorrelation matrix \mathbf{R}_t given by

$$\mathbf{R}_t = \mathbf{C}^T \mathbf{C} \quad (6.392)$$

where \mathbf{R}_t is a $(K_1 \times K_1)$ autocorrelation matrix of \mathbf{C} given by (6.388).

Let $\bar{\mathbf{y}}$ be expressed as

$$\bar{\mathbf{y}} = [\bar{\mathbf{y}}_0^T, \bar{\mathbf{y}}_1^T, \dots, \bar{\mathbf{y}}_{N_p-1}^T]^T \quad (6.393)$$

$$\bar{\mathbf{y}}_v = [\bar{y}_{v1}, \bar{y}_{v2}, \dots, \bar{y}_{vK_1}]^T, \quad v = 0, 1, \dots, N_p - 1$$

$$\bar{\mathbf{n}} = [\bar{\mathbf{n}}_0^T, \bar{\mathbf{n}}_1^T, \dots, \bar{\mathbf{n}}_{N_p-1}^T]^T \quad (6.394)$$

$$\bar{\mathbf{n}}_v = [\bar{n}_{v1}, \bar{n}_{v2}, \dots, \bar{n}_{vK_1}]^T, \quad v = 0, 1, \dots, N_p - 1$$

where $\bar{\mathbf{y}}_v$ and $\bar{\mathbf{n}}_v$ contain, respectively, the components of $\bar{\mathbf{y}}$ and $\bar{\mathbf{n}}$ corresponding to the v th subcarrier. Then, expanding (6.389), $\bar{\mathbf{y}}_v$ can be denoted as

$$\bar{\mathbf{y}}_v = \mathbf{R}_T \mathcal{H}_v \mathbf{C}_{f,v} \mathbf{x} + \bar{\mathbf{n}}_v, \quad v = 0, 1, \dots, N_p - 1 \quad (6.395)$$

Let \mathcal{H}_v and $\mathbf{C}_{f,v}$ in (6.379) be partitioned as

$$\begin{aligned} \mathcal{H}_v &= \text{diag}\{\mathcal{H}_v[1], \mathcal{H}_v[2], \dots, \mathcal{H}_v[M]\} \\ \mathbf{C}_{f,v} &= \text{diag}\{\mathbf{C}_{f,v}[1], \mathbf{C}_{f,v}[2], \dots, \mathbf{C}_{f,v}[M]\} \end{aligned} \quad (6.396)$$

where both $\mathcal{H}_v[m]$ and $\mathbf{C}_{f,v}[m]$ contain the K_1 components related to K_1 users. Furthermore, let \mathbf{x} be correspondingly partitioned as

$$\mathbf{x} = [\mathbf{x}^T[1], \mathbf{x}^T[2], \dots, \mathbf{x}^T[M]]^T \quad (6.397)$$

Then, we can express (6.395) as

$$\bar{\mathbf{y}}_v = \sum_{m=1}^M \mathbf{R}_t \mathcal{H}_v[m] \mathbf{C}_{f,v}[m] \mathbf{x}[m] + \bar{\mathbf{n}}_v, \quad v = 0, 1, \dots, N_p - 1 \quad (6.398)$$

In the context of the v th subcarrier, where $v = 0, 1, \dots, N_p - 1$, executing the ZF operation by multiplying (6.398) with the matrix \mathbf{R}_t^{-1} , we obtain

$$\mathbf{z}_v = \sum_{m=1}^M \mathcal{H}_v[m] \mathbf{C}_{f,v}[m] \mathbf{x}[m] + \tilde{\mathbf{n}}_v \quad (6.399)$$

where $\tilde{\mathbf{n}}_v = \mathbf{R}_t^{-1} \bar{\mathbf{n}}_v$.

From (6.379) we know that $\mathcal{H}_v[m]$ and $\mathbf{C}_{f,v}[m]$ can be expressed as

$$\begin{aligned}\mathcal{H}_v[m] &= \text{diag}\{h_v^{((m-1)K_1+1)}, h_v^{((m-1)K_1+2)}, \dots, h_v^{(mK_1)}\} \\ \mathbf{C}_{f,v}[m] &= \text{diag}\{(\mathbf{c}_{f,v}^{((m-1)K_1+1)})^T, (\mathbf{c}_{f,v}^{((m-1)K_1+2)})^T, \dots, (\mathbf{c}_{f,v}^{(mK_1)})^T\}\end{aligned}\quad (6.400)$$

where $\mathcal{H}_v[m]$ is a $(K_1 \times K_1)$ matrix, while $\mathbf{C}_{f,v}[m]$ is a $(K_1 \times UK_1)$ matrix. When applying $\mathcal{H}_v[m]$ and $\mathbf{C}_{f,v}[m]$ into (6.399), it can be shown that interference exists only among the users sharing the same T-domain spreading sequence. When two users do not share the same T-domain spreading sequence, they are fully decorrelated by the T-domain ZF operation. Hence, the detection in the F-domain can be separated into K_1 groups with each group containing the M users sharing the same T-domain spreading code. More specifically, for the v th subcarrier, the k_1 th ($k_1 = 1, 2, \dots, K_1$) component can be expressed as

$$\begin{aligned}z_{v,k_1} &= \sum_{m=1}^M h_v^{((m-1)K_1+k_1)} (\mathbf{c}_{f,v}^{((m-1)K_1+k_1)})^T \mathbf{x}_{(m-1)K_1+k_1} + \tilde{n}_{v,k_1} \\ k_1 &= 1, 2, \dots, K_1; v = 0, 1, \dots, N_p - 1\end{aligned}\quad (6.401)$$

We define

$$\begin{aligned}\mathbf{z}_{f,k_1} &= [z_{0,k_1}, z_{1,k_1}, \dots, z_{(N_p-1),k_1}]^T, \quad k_1 = 1, 2, \dots, K_1 \\ \mathbf{n}_{f,k_1} &= [\tilde{n}_{0,k_1}, \tilde{n}_{1,k_1}, \dots, \tilde{n}_{(N_p-1),k_1}]^T, \quad k_1 = 1, 2, \dots, K_1\end{aligned}\quad (6.402)$$

where the subscript ‘ f ’ indicates specifically the relation to the F-domain. Then, we can express \mathbf{z}_{f,k_1} as

$$\mathbf{z}_{f,k_1} = \sum_{m=1}^M \mathbf{H}_{f,k_1}^{(m)} \mathbf{C}_{f,k_1}^{(m)} \mathbf{x}_{(m-1)K_1+k_1} + \mathbf{n}_{f,k_1}, \quad k_1 = 1, 2, \dots, K_1 \quad (6.403)$$

where

$$\begin{aligned}\mathbf{H}_{f,k_1}^{(m)} &= \text{diag}\{h_0^{((m-1)K_1+k_1)}, h_1^{((m-1)K_1+k_1)}, \dots, h_{N_p-1}^{((m-1)K_1+k_1)}\} \\ \mathbf{C}_{f,k_1}^{(m)} &= [\mathbf{c}_{f,0}^{((m-1)K_1+k_1)}, \mathbf{c}_{f,1}^{((m-1)K_1+k_1)}, \dots, \mathbf{c}_{f,N_p-1}^{((m-1)K_1+k_1)}]^T\end{aligned}\quad (6.404)$$

It can be shown that

$$\mathbf{C}_{f,k_1}^{(m)} = \mathbf{C}_f^{((m-1)K_1+k_1)} \quad (6.405)$$

where $\mathbf{C}_f^{((m-1)K_1+k_1)}$ is given by (6.376) and is the F-domain spreading matrix formed by the F-domain spreading codes assigned to the $((m-1)K_1+k_1)$ th user.

Furthermore, (6.403) can be expressed in a compact form as

$$\mathbf{z}_{f,k_1} = \mathbf{H}_{f,k_1} \mathbf{C}_{f,k_1} \mathbf{x}_{k_1} + \mathbf{n}_{f,k_1}, \quad k_1 = 1, 2, \dots, K_1 \quad (6.406)$$

where

$$\begin{aligned}\mathbf{H}_{f,k_1} &= [\mathbf{H}_{f,k_1}^{(1)}, \mathbf{H}_{f,k_1}^{(2)}, \dots, \mathbf{H}_{f,k_1}^{(M)}] \\ \mathbf{C}_{f,k_1} &= \text{diag}\{\mathbf{C}_{f,k_1}^{(1)}, \mathbf{C}_{f,k_1}^{(2)}, \dots, \mathbf{C}_{f,k_1}^{(M)}\} \\ \mathbf{x}_{k_1} &= [\mathbf{x}_{k_1}^T, \mathbf{x}_{K_1+k_1}^T, \dots, \mathbf{x}_{(M-1)K_1+k_1}^T]^T\end{aligned}\quad (6.407)$$

where \mathbf{H}_{f,k_1} is a $(N_p \times MN_p)$ matrix, \mathbf{C}_{f,k_1} is a $(MN_p \times MU)$ matrix, while \mathbf{x}_{k_1} is a MU -length vector containing the data symbols transmitted by the M users sharing the same T-domain sequence.

Finally, when we assume that $MU \leq N_p$, then, based on (6.406), the decision variable vector for \mathbf{x}_{k_1} after the ZF detection can be expressed as

$$\begin{aligned}\hat{\mathbf{x}}_{k_1} &= \mathbf{R}_{f,k_1}^{-1} \mathbf{C}_{f,k_1}^T \mathbf{H}_{f,k_1}^H \mathbf{z}_{f,k_1} \\ &= \mathbf{x}_{k_1} + \mathbf{R}_{f,k_1}^{-1} \mathbf{C}_{f,k_1}^T \mathbf{H}_{f,k_1}^H \mathbf{n}_{f,k_1}, \quad k_1 = 1, 2, \dots, K_1\end{aligned}\quad (6.408)$$

where

$$\mathbf{R}_{f,k_1} = \mathbf{C}_{f,k_1}^T \mathbf{H}_{f,k_1}^H \mathbf{H}_{f,k_1} \mathbf{C}_{f,k_1} \quad (6.409)$$

According to the above analysis, we know that the overall ZF operation includes N_p T-domain ZF operations in the context of each of the N_p subcarriers and K_1 F-domain ZF operations in the context of each of the K_1 user groups, where the users of the same group share the same T-domain spreading code. The ZF-related matrix in the T-domain is \mathbf{R}_t^{-1} , which is of size $(K_1 \times K_1)$ and is the same for all the N_p subcarriers. Furthermore, \mathbf{R}_t^{-1} is time-invariant. By contrast, the ZF-related matrix in the F-domain is \mathbf{R}_{f,k_1}^{-1} ($k_1 = 1, \dots, K_1$), the size of which is $(UM \times UM)$. However, the F-domain related ZF matrices in the form of \mathbf{R}_{f,k_1} are time-varying. Hence, the complexity of the above-derived TF-domain ZF-MUD is dominated mainly by the F-domain detection.

Above, the ZF operations have been carried out separately; first, in the T-domain, and then, in the F-domain. According to the analysis and simulation results in Section 6.3 in the context of the multicarrier DS-CDMA systems, the performance achieved by this type of ZF-MUD is suboptimum in terms of the best BER performance achievable by the optimum ZF-MUD. Hence, the above derived ZF-MUD is referred to as the SZF-MUD. The optimum ZF-MUD, referred to as the OZF-MUD, can be derived by considering the ZF operation in both the T-domain and F-domain jointly.

The OZF-MUD can be derived conveniently from equations (6.382) to (6.386). Based on (6.385) it can be easily shown that the weight matrix for the OZF-MUD is given by

$$\mathbf{W} = [(\mathbf{H}_f \mathbf{C}_f) \square \mathbf{S}] [(\mathbf{H}_f \mathbf{C}_f) \square \mathbf{S}]^H [(\mathbf{H}_f \mathbf{C}_f) \square \mathbf{S}]^{-1} \quad (6.410)$$

After invoking the relationship of $(\mathbf{A} \square \mathbf{B})^H (\mathbf{C} \square \mathbf{D}) = \mathbf{A}^H \mathbf{C} \odot \mathbf{B}^H \mathbf{D}$ [89], the above equation can be simplified to

$$\mathbf{W} = [(\mathbf{H}_f \mathbf{C}_f) \square \mathbf{S}] [(\mathbf{C}_f^T \mathbf{H}_f^H \mathbf{H}_f \mathbf{C}_f) \odot (\mathbf{S}^T \mathbf{S})]^{-1} \quad (6.411)$$

where both $(\mathbf{C}_f^T \mathbf{H}_f^H \mathbf{H}_f \mathbf{C}_f)$ and $(\mathbf{S}^T \mathbf{S})$ are the $(KU \times KU)$ matrices. Furthermore, it can be shown that we have

$$\mathbf{S}^T \mathbf{S} = (\mathbf{R}_C \otimes \mathbf{1}_{(U \times U)})$$

$$\mathbf{C}_f^T \mathbf{H}_f^H \mathbf{H}_f \mathbf{C}_f = \sum_{v=0}^{N_p-1} \mathbf{C}_{f,v}^T \mathbf{h}_v^* \mathbf{h}_v^T \mathbf{C}_{f,v} \quad (6.412)$$

where $\mathbf{1}_{(U \times U)}$ is a $(U \times U)$ matrix with all entries being one. Due to the above properties, in (6.411) the matrix required to be inverse is relatively easy to compute.

Finally, the decision variable vector for the KU data symbols can be formed as

$$\begin{aligned} z &= \mathbf{W}^H \mathbf{y} \\ &= [(\mathbf{C}_f^T \mathbf{H}_f^H \mathbf{H}_f \mathbf{C}_f) \odot (\mathbf{S}^T \mathbf{S})]^{-1} [(\mathbf{H}_f \mathbf{C}_f) \square \mathbf{S}]^H \mathbf{y} \end{aligned} \quad (6.413)$$

With the aid of the definitions in (6.386) for \mathbf{H}_f , (6.381) for \mathbf{C}_f and (6.384) for \mathbf{S} , it can be shown that we can express

$$[(\mathbf{H}_f \mathbf{C}_f) \square \mathbf{S}]^H \mathbf{y} = \sum_{v=0}^{N_p-1} \mathbf{C}_{f,v}^T \mathcal{H}_v^H \mathbf{C}^T \mathbf{y}_v \quad (6.414)$$

where $\mathbf{C}_{f,v}$, \mathcal{H}_v and \mathbf{C} are all defined in (6.379). After substituting (6.414) into (6.413), the OZF-MUD for the TF-domain spread MC DS-CDMA can be written as

$$z = [(\mathbf{C}_f^T \mathbf{H}_f^H \mathbf{H}_f \mathbf{C}_f) \odot (\mathbf{S}^T \mathbf{S})]^{-1} \left(\sum_{v=0}^{N_p-1} \mathbf{C}_{f,v}^T \mathcal{H}_v^H \mathbf{C}^T \mathbf{y}_v \right) \quad (6.415)$$

According to (6.415), the OZF-MUD in the TF-domain spread MC DS-CDMA can be implemented in the following steps. First, the correlation or matched-filtering operations are implemented with respect to each of the N_p subcarriers by multiplying the observations of a subcarrier with its corresponding matrix in the form

$$\mathbf{C}_{f,v}^T \mathcal{H}_v^H \mathbf{C}^T$$

The correlation outputs with respect to the N_p subcarriers are then summed to form

$$\sum_{v=0}^{N_p-1} \mathbf{C}_{f,v}^T \mathcal{H}_v^H \mathbf{C}^T \mathbf{y}_v$$

Finally, as shown in (6.415) one ZF-processing is invoked for removing the MUI.

$$\begin{bmatrix} 1 & -1 & -1 & -1 & -1 & 1 & 1 & -1 & -1 & 1 & -1 & 1 & -1 & 1 & 1 & -1 \\ -1 & -1 & -1 & -1 & 1 & 1 & 1 & 1 & -1 & 1 & -1 & 1 & -1 & 1 & -1 & -1 \\ -1 & -1 & -1 & 1 & 1 & 1 & -1 & 1 & 1 & -1 & 1 & -1 & 1 & -1 & -1 & -1 \\ 1 & -1 & -1 & -1 & -1 & -1 & -1 & 1 & 1 & -1 & 1 & 1 & 1 & 1 & 1 & 1 \\ 1 & 1 & -1 & 1 & -1 & 1 & -1 & -1 & 1 & -1 & -1 & -1 & 1 & -1 & 1 & -1 \\ -1 & -1 & 1 & 1 & 1 & 1 & 1 & -1 & 1 & 1 & 1 & -1 & -1 & -1 & 1 & 1 \\ 1 & -1 & 1 & -1 & 1 & 1 & -1 & 1 & 1 & -1 & 1 & 1 & 1 & 1 & -1 & 1 \\ -1 & 1 & -1 & -1 & 1 & -1 & 1 & -1 & -1 & 1 & 1 & -1 & 1 & 1 & 1 & 1 \\ -1 & 1 & -1 & -1 & 1 & 1 & -1 & 1 & -1 & -1 & 1 & 1 & -1 & 1 & 1 & 1 \\ -1 & 1 & -1 & -1 & 1 & 1 & 1 & 1 & 1 & 1 & 1 & 1 & 1 & 1 & -1 & -1 \\ -1 & 1 & 1 & 1 & -1 & 1 & -1 & 1 & -1 & -1 & 1 & -1 & 1 & -1 & 1 & -1 \\ 1 & -1 & 1 & -1 & -1 & 1 & 1 & -1 & -1 & 1 & 1 & 1 & -1 & -1 & -1 & -1 \\ -1 & -1 & -1 & -1 & -1 & 1 & -1 & -1 & 1 & -1 & -1 & 1 & 1 & -1 & 1 & 1 \\ -1 & -1 & 1 & -1 & -1 & 1 & 1 & -1 & -1 & -1 & 1 & 1 & 1 & -1 & -1 & -1 \\ -1 & -1 & 1 & 1 & 1 & -1 & 1 & -1 & -1 & 1 & 1 & 1 & 1 & -1 & -1 & 1 \\ -1 & -1 & -1 & 1 & 1 & -1 & -1 & 1 & 1 & -1 & 1 & 1 & 1 & 1 & 1 & 1 \end{bmatrix} \quad (6.416)$$

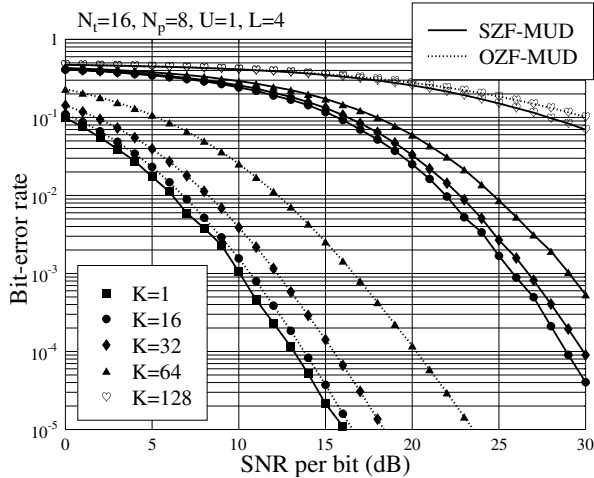


Figure 6.36: SZF-MUD and OZF-MUD: BER versus average SNR per bit performance for the TF-domain spread MC DS-CDMA using random F-domain spreading sequences with a spreading factor of $N_p = 8$, T-domain spreading factor of $N_t = 16$ and $U = 1$ bit per user, when communicating over frequency-selective Rayleigh fading channels having $L = 4$ T-domain resolvable paths. The T-domain spreading sequences for the simulations are given by (6.416).

Figures 6.36 and 6.37 show the BER versus average SNR per bit performance of the TF-domain spread MC DS-CDMA, which uses the parameters $N_p = 8$, $N_t = 16$, $U = 1$, when communicating over frequency-selective fading channels having $L = 4$ T-domain resolvable multipath components. Since $N_p N_t = 128$ and $U = 1$, the maximum number of users supportable is $K = 128$, when considering a linear MUD scheme. Note that when the SZF-MUD is considered, using random T-domain spreading sequences may result in a high probability that two user sequences are linearly correlated. For this reason, in our simulations for Fig. 6.36, the T-domain spreading sequences were fixed and given by (6.416). The F-domain spreading sequences for Fig. 6.36 were random sequences. However, in the context of Fig. 6.37 both the T-domain and F-domain spreading sequences were made up of random sequences.

The results in Fig. 6.36 show that the OZF-MUD significantly outperforms the SZF-MUD in terms of BER performance, when the number of users supported is $K = 16, 32$ or 64 . However, when $K = 128$, the OZF-MUD is outperformed by the SZF-MUD, which might be the result of the specific set of T-domain spreading sequences as shown in (6.416) used in the simulations. Fig. 6.37 illustrates the BER performance of the TF-domain spread MC DS-CDMA using OZF-MUD associated with random T-domain and F-domain spreading sequences. We observe that the BER performance in Fig. 6.37 is better than the corresponding BER performance of the OZF-MUD scheme shown in Fig. 6.36.

Note that for the implementational complexity, the OZF-MUD is $O(U^2 K^2)$ per symbol per user, where $O(\cdot)$ means proportional to. By contrast, the complexity of the SZF-MUD is $O(K_1 U^2 M^2) + O(U^2 K^2 / K_1)$ per symbol per user. Hence, the SZF-MUD may have a significantly lower complexity than the OZF-MUD when the value of K_1 is high. Note,

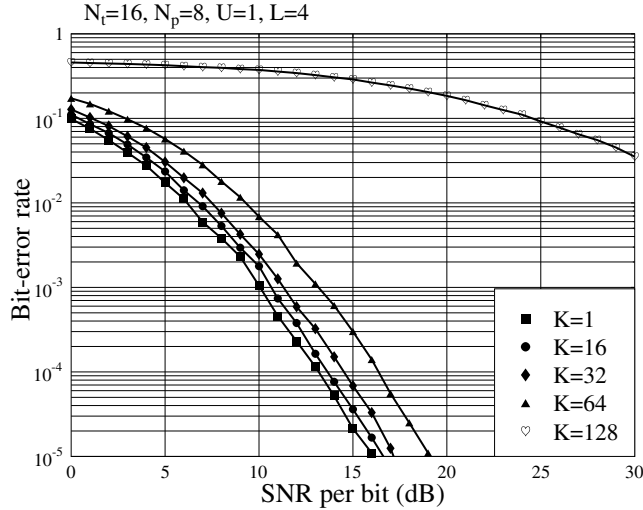


Figure 6.37: OZF-MUD: BER versus average SNR per bit performance for the TF-domain spread MC DS-CDMA using random spreading sequences, F-domain spreading factor of $N_p = 8$, T-domain spreading factor of $N_t = 16$ and $U = 1$ bit per user, when communicating over frequency-selective Rayleigh fading channels having $L = 4$ T-domain resolvable paths.

furthermore, that the T-domain ZF operation in SZF-MUD is low-complexity, since the matrix \mathbf{R}_t as seen in (6.392) is time-invariant and its inverse is only required to compute once during the detection.

6.4.2 Time-Frequency-Domain MMSE Multiuser Detection

For the MMSE-MUDs in the TF-domain spread MC DS-CDMA, we also consider the SMMSE-MUD and OMMSE-MUD. The SMMSE-MUD carries out two stages of detection, one in the T-domain and one in the F-domain. By contrast, the OMMSE-MUD carries out joint TF-domain detection, which treats all the available observations jointly without regarding to the specific subcarriers. Let us first consider the SMMSE-MUD.

The SMMSE-MUD is derived based on (6.382), which can also be expressed as

$$\mathbf{y}_v = \sum_{k=1}^K h_v^{(k)} \mathbf{c}_k (\mathbf{c}_{f,v}^{(k)})^T \mathbf{x}_k + \mathbf{n}_v, \quad v = 0, 1, \dots, N_p - 1 \quad (6.417)$$

where \mathbf{n}_v is a N_t -length Gaussian noise vector distributed with zero mean and a covariance matrix $\sigma^2 \mathbf{I}_{N_t}$. Considering the code assignment scheme in (6.387), (6.417) becomes

$$\begin{aligned} \mathbf{y}_v &= \sum_{k_1=1}^{K_1} \mathbf{c}_{k_1} \left[\sum_{m=0}^{M-1} h_v^{(k_1+mK_1)} (\mathbf{c}_{f,v}^{(k_1+mK_1)})^T \mathbf{x}_{(k_1+mK_1)} \right] + \mathbf{n}_v \\ &= \sum_{k_1=1}^{K_1} \mathbf{c}_{k_1} \tilde{x}_{k_1 v} + \mathbf{n}_v, \quad v = 0, 1, \dots, N_p - 1 \end{aligned} \quad (6.418)$$

where, for brevity, we define

$$\tilde{x}_{k_1 v} = \sum_{m=0}^{M-1} h_v^{(k_1+mK_1)} (\mathbf{c}_{f,v}^{(k_1+mK_1)})^T \mathbf{x}_{(k_1+mK_1)}, \quad k_1 = 1, 2, \dots, K_1 \quad (6.419)$$

The SMMSE-MUD first carries out the MUI suppression in the T-domain in the context of each of the N_p subcarriers and then carries out the MUI suppression in the F-domain concerning all the N_p subcarriers, both using MMSE principles.

In the context of the T-domain MMSE detection, $\tilde{x}_{k_1 v}$, ($k_1 = 1, 2, \dots, K_1$) in the form of (6.419) is detected under the MMSE principles. Let $\mathbf{w}_{k_1 v}^{(o)}$ be the optimum weight vector in the MMSE sense for processing the v th subcarrier, in order to detect $\tilde{x}_{k_1 v}$. Then, the output of the detector can be expressed as

$$z_{k_1 v} = (\mathbf{w}_{k_1 v}^{(o)})^H \mathbf{y}_v, \quad v = 0, 1, \dots, N_p - 1; \quad k_1 = 1, 2, \dots, K_1 \quad (6.420)$$

where the optimum weight matrix $\mathbf{w}_{k_1 v}^{(o)}$ in the MMSE sense can be expressed as

$$\mathbf{w}_{k_1 v}^{(o)} = \mathbf{R}_{\mathbf{y}_v}^{-1} \mathbf{R}_{\mathbf{y}_v \tilde{x}_{k_1 v}} \quad (6.421)$$

where $\mathbf{R}_{\mathbf{y}_v}$ denotes the autocorrelation matrix of \mathbf{y}_v , which can be expressed as

$$\mathbf{R}_{\mathbf{y}_v} = E \left[\left(\sum_{k_1=1}^{K_1} \mathbf{c}_{k_1} \tilde{x}_{k_1 v} \right) \left(\sum_{k_1=1}^{K_1} \mathbf{c}_{k_1} \tilde{x}_{k_1 v} \right)^H \right] + \sigma^2 \mathbf{I}_{N_t} \quad (6.422)$$

When assuming random source data symbols and the random F-domain spreading sequence, it can be shown that

$$\begin{aligned} \mathbf{R}_{\mathbf{y}_v} &= \frac{MU\Omega}{N_p} \sum_{k_1=1}^{K_1} \mathbf{c}_{k_1} \mathbf{c}_{k_1}^T + \sigma^2 \mathbf{I}_{N_t} \\ &= \frac{MU\Omega}{N_p} \mathbf{R}_t + \sigma^2 \mathbf{I}_{N_t} \end{aligned} \quad (6.423)$$

where \mathbf{R}_t is given by (6.392) and $\Omega = E[|h_v^{(k_1+mK_1)}|^2]$. $\mathbf{R}_{\mathbf{y}_v}$ is a $(N_t \times N_t)$ matrix. In (6.421) $\mathbf{R}_{\mathbf{y}_v \tilde{x}_{k_1}}$ denotes the cross-correlation matrix between \mathbf{y}_v and \tilde{x}_{k_1} , which can be expressed as

$$\begin{aligned} \mathbf{R}_{\mathbf{y}_v \tilde{x}_{k_1}} &= E[\mathbf{y}_v \tilde{x}_{k_1}^H] \\ &= \frac{MU\Omega}{N_p} \mathbf{c}_{k_1} \end{aligned} \quad (6.424)$$

which is an N_t -length vector. When substituting (6.423) and (6.424) into (6.421), we obtain

$$\begin{aligned} \mathbf{w}_{k_1 v}^{(o)} &= \frac{MU\Omega}{N_p} \left(\frac{MU\Omega}{N_p} \mathbf{R}_t + \sigma^2 \mathbf{I}_{N_t} \right)^{-1} \mathbf{c}_{k_1} \\ &= \left(\mathbf{R}_t + \frac{N_p \sigma^2}{MU\Omega} \mathbf{I}_{N_t} \right)^{-1} \mathbf{c}_{k_1}, \quad k_1 = 1, 2, \dots, K_1 \end{aligned} \quad (6.425)$$

Equation (6.425) shows that $\mathbf{w}_{k_1v}^{(o)}$ is time-invariant once the active users are certain.

From (6.425) we can observe that when the TF-domain spread MC DS-CDMA system employs a higher number of subcarriers, i.e. the value of N_p is higher, the T-domain MMSE detector then puts a greater emphasis on background noise suppression than on MUI suppression. By contrast, when the number of users M sharing the same T-domain spreading code increases or/and when the number of data symbols U per user transmitted increases, the T-domain MMSE detector then emphasizes MUI suppression more than background noise suppression.

Given the optimum weight matrix in (6.425), it can be shown that, in the context of the v th subcarrier, the output of the MMSE detector corresponding to x_{k_1v} can be expressed as

$$\begin{aligned} z_{k_1v} &= (\mathbf{w}_{k_1v}^{(o)})^H \mathbf{y}_v = \tilde{x}_{k_1v} + J_{k_1v} \\ &= \sum_{m=0}^{M-1} h_v^{(k_1+mK_1)} (\mathbf{c}_{f,v}^{(k_1+mK_1)})^T \mathbf{x}_{(k_1+mK_1)} + J_{k_1v} \\ v &= 0, 1, \dots, N_p - 1 \end{aligned} \quad (6.426)$$

and, correspondingly, the minimum MSE is given by

$$\begin{aligned} \sigma_J^2 &= E[\|(\mathbf{w}_{k_1v}^{(o)})^H \mathbf{y}_v - \tilde{x}_{k_1v}\|^2] \\ &= E[\|\tilde{x}_{k_1v}\|^2] - (\mathbf{R}_{\mathbf{y}_v \tilde{x}_{k_1}})^H \mathbf{w}_{k_1v}^{(o)} \\ &= \frac{MU\Omega}{N_p} \left[1 - \mathbf{c}_{k_1}^T \left(\mathbf{R}_t + \frac{N_p\sigma^2}{MU\Omega} \mathbf{I}_{N_t} \right)^{-1} \mathbf{c}_{k_1} \right] \end{aligned} \quad (6.427)$$

which is a constant once the T-domain spreading codes and the noise variance σ^2 are given. In (6.426) J_{k_1v} contains the unsuppressed MUI and Gaussian noise; J_{k_1v} can usually be approximated as a Gaussian noise with zero mean and a variance given by σ_J^2 of (6.427).

We now consider the F-domain MMSE detection. Specifically, the detection of the users sharing the T-domain spreading code with user k_1 is considered. The F-domain MMSE detection begins with defining

$$\begin{aligned} \mathbf{z}_{f,k_1} &= [z_{k_10}, z_{k_11}, \dots, z_{k_1(N_p-1)}]^T \\ \mathbf{C}_f^{(k_1+mK_1)} &= \text{diag}\{(\mathbf{c}_{f,0}^{(k_1+mK_1)})^T, (\mathbf{c}_{f,1}^{(k_1+mK_1)})^T, \dots, (\mathbf{c}_{f,N_p-1}^{(k_1+mK_1)})^T\} \\ \mathbf{H}_f^{(k_1+mK_1)} &= [\mathbf{I}_U \otimes h_0^{(k_1+mK_1)}, \mathbf{I}_U \otimes h_1^{(k_1+mK_1)}, \dots, \mathbf{I}_U \otimes h_{N_p-1}^{(k_1+mK_1)}]^T \\ \mathbf{J}_{f,k_1} &= [J_{k_10}, J_{k_11}, \dots, J_{k_1(N_p-1)}]^T \end{aligned} \quad (6.428)$$

where $\mathbf{C}_f^{(k_1+mK_1)}$ and $\mathbf{H}_f^{(k_1+mK_1)}$ are $(N_p \times UN_p)$ and $(UN_p \times U)$ matrices, respectively. Based on the above definitions, \mathbf{z}_{f,k_1} can be represented as

$$\mathbf{z}_{f,k_1} = \sum_{m=0}^{M-1} \mathbf{C}_f^{(k_1+mK_1)} \mathbf{H}_f^{(k_1+mK_1)} \mathbf{x}_{(k_1+mK_1)} + \mathbf{J}_{f,k_1}, \quad k_1 = 1, 2, \dots, K_1 \quad (6.429)$$

Based on the representation in (6.429), we now derive the F-domain MMSE detector for the TF-domain MC DS-CDMA system. Specifically, let the $(N_p \times U)$ matrix $\mathbf{W}_{f,mk_1}^{(o)}$

($m = 0, \dots, M - 1$, $k_1 = 1, \dots, K_1$) be the optimum weight matrix for detecting $\mathbf{x}_{(mK_1+k_1)}$ in the MMSE sense. Then, the corresponding decision variable vector can be expressed as

$$\hat{\mathbf{x}}_{(k_1+mK_1)} = (\mathbf{W}_{f,mk_1}^{(o)})^H \mathbf{z}_{f,k_1}, \quad m = 0, 1, \dots, M - 1; \quad k_1 = 1, 2, \dots, K_1 \quad (6.430)$$

The optimum weight matrix $\mathbf{W}_{f,mk_1}^{(o)}$ can be expressed as

$$\mathbf{W}_{f,mk_1}^{(o)} = \mathbf{R}_{\mathbf{z}_{f,k_1}}^{-1} \mathbf{R}_{\mathbf{z}_{f,k_1} \mathbf{x}_{(k_1+mK_1)}} \quad (6.431)$$

where $\mathbf{R}_{\mathbf{z}_{f,k_1}}$ is the autocorrelation matrix of \mathbf{z}_{f,k_1} , i.e.

$$\mathbf{R}_{\mathbf{z}_{f,k_1}} = [\mathbf{z}_{f,k_1} \mathbf{z}_{f,k_1}^H] \quad (6.432)$$

The autocorrelation matrix $\mathbf{R}_{\mathbf{z}_{f,k_1}}$ in practice may be estimated when a sufficient number of observation samples for \mathbf{z}_{f,k_1} are available. However, when the receiver employs knowledge of the F-domain and T-domain spreading codes of all the users, and when the receiver also has knowledge of the fading channels of all the N_p subcarriers regarding all the users, an expression for the autocorrelation matrix $\mathbf{R}_{\mathbf{z}_{f,k_1}}$ can also be obtained by analysis. Specifically, when in (6.429) the elements in \mathbf{J}_{f,k_1} are approximated as independent Gaussian random variables having a common variance σ_J^2 , it can be easily shown that

$$\mathbf{R}_{\mathbf{z}_{f,k_1}} = \sum_{m=0}^{M-1} \mathbf{C}_f^{(k_1+mK_1)} \mathbf{H}_f^{(k_1+mK_1)} (\mathbf{H}_f^{(k_1+mK_1)})^H (\mathbf{C}_f^{(k_1+mK_1)})^T + \sigma_J^2 \mathbf{I}_{N_p} \quad (6.433)$$

when random F-domain spreading codes and random source data symbols are assumed.

Note that the approximation of the elements in \mathbf{J}_{f,k_1} as independent Gaussian random variables is reasonable, since, first, $J_{k_1 i}$ can be closely Gaussian approximated after the MMSE detection, and, second, for $i \neq j$

$$E[J_{k_1 i} J_{k_1 j}^*] = E[((\mathbf{w}_{k_1 i}^{(o)})^H \mathbf{y}_i - \tilde{x}_{k_1 i}) ((\mathbf{w}_{k_1 j}^{(o)})^H \mathbf{y}_j - \tilde{x}_{k_1 j})^*] = 0 \quad (6.434)$$

due to the random channels and random F-domain spreading codes.

In (6.431) $\mathbf{R}_{\mathbf{z}_{f,k_1} \mathbf{x}_{(k_1+mK_1)}}$ represents the cross-correlation matrix between \mathbf{z}_{f,k_1} and $\mathbf{x}_{(k_1+mK_1)}$, which, with the aid of (6.429), can be expressed as

$$\mathbf{R}_{\mathbf{z}_{f,k_1} \mathbf{x}_{(mK_1+k_1)}} = \mathbf{C}_f^{(k_1+mK_1)} \mathbf{H}_f^{(k_1+mK_1)} \quad (6.435)$$

Finally, when substituting (6.433) and (6.435) into (6.431), the optimum weight matrix for estimating $\mathbf{x}_{(mK_1+k_1)}$ can be expressed as

$$\begin{aligned} \mathbf{W}_{f,mk_1}^{(o)} &= \left(\sum_{l=0}^{M-1} \mathbf{C}_f^{(k_1+lK_1)} \mathbf{H}_f^{(k_1+lK_1)} (\mathbf{H}_f^{(k_1+lK_1)})^H (\mathbf{C}_f^{(k_1+lK_1)})^T + \sigma_J^2 \mathbf{I}_{N_p} \right)^{-1} \\ &\times \mathbf{C}_f^{(k_1+mK_1)} \mathbf{H}_f^{(k_1+mK_1)}, \quad m = 0, 1, \dots, M - 1; \quad k_1 = 1, 2, \dots, K_1 \end{aligned} \quad (6.436)$$

Let express

$$\mathbf{R}_{\mathbf{z}_{f,k_1}} = \mathbf{C}_f^{(k_1+mK_1)} \mathbf{H}_f^{(k_1+mK_1)} (\mathbf{H}_f^{(k_1+mK_1)})^H (\mathbf{C}_f^{(k_1+mK_1)})^T + \mathbf{R}_{\mathbf{z}_{f,k_1}}^{(I)} \quad (6.437)$$

where $\mathbf{R}_{z_{f,k_1}}^{(I)}$ denotes the autocorrelation matrix of interference plus noise, which can be expressed as

$$\mathbf{R}_{z_{f,k_1}}^{(I)} = \sum_{l \neq m}^{M-1} \mathbf{C}_f^{(k_1+lK_1)} \mathbf{H}_f^{(k_1+lK_1)} (\mathbf{H}_f^{(k_1+lK_1)})^H (\mathbf{C}_f^{(k_1+lK_1)})^T + \sigma_J^2 \mathbf{I}_{N_p} \quad (6.438)$$

Then, applying (6.437) to (6.436) and invoking the *matrix inverse lemma* as shown in (6.B.6) in Appendix 6.B, we obtain

$$\begin{aligned} \mathbf{W}_{f,mk_1}^{(o)} &= (\mathbf{R}_{z_{f,k_1}}^{(I)})^{-1} \mathbf{C}_f^{(k_1+mK_1)} \mathbf{H}_f^{(k_1+mK_1)} \\ &\times [(\mathbf{H}_f^{(k_1+lK_1)})^H (\mathbf{C}_f^{(k_1+lK_1)})^T (\mathbf{R}_{z_{f,k_1}}^{(I)})^{-1} \mathbf{C}_f^{(k_1+mK_1)} \mathbf{H}_f^{(k_1+mK_1)} + \mathbf{I}_U]^{-1} \\ m &= 0, 1, \dots, M-1; k_1 = 1, 2, \dots, K_1 \end{aligned} \quad (6.439)$$

After the F-domain MMSE detection, the minimum MSE can be expressed as

$$\begin{aligned} \sigma_{mk_1}^2 &= \left[1 - \frac{1}{U} \mathbf{R}_{z_{f,k_1}}^H \mathbf{x}_{(mK_1+k_1)} \mathbf{W}_{f,mk_1}^{(o)} \right] \\ &= \left[1 - \frac{1}{U} (\mathbf{H}_f^{(k_1+lK_1)})^H (\mathbf{C}_f^{(k_1+lK_1)})^T (\mathbf{R}_{z_{f,k_1}}^{(I)})^{-1} \mathbf{C}_f^{(k_1+mK_1)} \mathbf{H}_f^{(k_1+mK_1)} \right] \\ m &= 0, 1, \dots, M-1; k_1 = 1, 2, \dots, K_1 \end{aligned} \quad (6.440)$$

which clearly depends on the channel state.

We now turn to consider the OMMSE-MUD. The OMMSE-MUD is derived below based on (6.382) to (6.386). Let $\mathbf{W}^{(o)}$ be the optimum weight matrix in the MMSE sense for detecting \mathbf{x} . The decision vector corresponding to \mathbf{x} can then be expressed as

$$\mathbf{z} = (\mathbf{W}^{(o)})^H \mathbf{y} \quad (6.441)$$

In the MMSE sense, the optimum weight matrix $\mathbf{W}^{(o)}$ is given by

$$\mathbf{W}^{(o)} = \mathbf{R}_y^{-1} \mathbf{R}_{yx} \quad (6.442)$$

where \mathbf{R}_y is the autocorrelation matrix of \mathbf{y} , which, with the aid of (6.385), can be obtained as

$$\mathbf{R}_y = E[\mathbf{y}\mathbf{y}^H] = [(\mathbf{H}_f \mathbf{C}_f) \square \mathbf{S}] [(\mathbf{H}_f \mathbf{C}_f) \square \mathbf{S}]^H + \sigma^2 \mathbf{I}_{N_p N_t} \quad (6.443)$$

In (6.442) \mathbf{R}_{yx} is the cross-correlation matrix between \mathbf{y} and \mathbf{x} , which can be expressed as

$$\mathbf{R}_{yx} = E[\mathbf{y}\mathbf{x}^H] = [(\mathbf{H}_f \mathbf{C}_f) \square \mathbf{S}] \quad (6.444)$$

Consequently, when substituting (6.443) and (6.444) into (6.442), the optimum weight matrix $\mathbf{W}^{(o)}$ can be expressed as

$$\mathbf{W}^{(o)} = [(\mathbf{H}_f \mathbf{C}_f) \square \mathbf{S}] [(\mathbf{H}_f \mathbf{C}_f) \square \mathbf{S}]^H + \sigma^2 \mathbf{I}_{N_p N_t} \quad (6.445)$$

When invoking the *Matrix inverse lemma*, we obtain

$$\begin{aligned} \mathbf{W}^{(o)} &= [(\mathbf{H}_f \mathbf{C}_f) \square \mathbf{S}] [(\mathbf{H}_f \mathbf{C}_f) \square \mathbf{S}]^H [(\mathbf{H}_f \mathbf{C}_f) \square \mathbf{S}] + \sigma^2 \mathbf{I}_K)^{-1} \\ &= [(\mathbf{H}_f \mathbf{C}_f) \square \mathbf{S}] [(\mathbf{C}_f^T \mathbf{H}_f^H \mathbf{H}_f \mathbf{C}_f) \odot (\mathbf{S}^T \mathbf{S}) + \sigma^2 \mathbf{I}_K]^{-1} \end{aligned} \quad (6.446)$$

which shows that when the receiver employs the knowledge about all the K users including their CIRs and spreading sequences, the OMMSE-MUD has to invert a $(UK \times UK)$ matrix. Furthermore, after some simplifications with the aid of equations (6.382) to (6.386), it can be shown that in (6.446) $\mathbf{C}_f^T \mathbf{H}_f^H \mathbf{H}_f \mathbf{C}_f$ and $\mathbf{S}^T \mathbf{S}$ can be expressed in the same way as in (6.412).

After substituting (6.446) into (6.441), the OMMSE-MUD can be expressed as

$$\mathbf{z} = [(\mathbf{C}_f^T \mathbf{H}_f^H \mathbf{H}_f \mathbf{C}_f) \odot (\mathbf{S}^T \mathbf{S}) + \sigma^2 \mathbf{I}_K]^{-1} [(\mathbf{H}_f \mathbf{C}_f) \square \mathbf{S}]^H \mathbf{y} \quad (6.447)$$

It can be shown that

$$[(\mathbf{H}_f \mathbf{C}_f) \square \mathbf{S}]^H \mathbf{y} = \sum_{v=0}^{N_p-1} \mathbf{C}_{f,v}^T \mathbf{H}_v^H \mathbf{C}^T \mathbf{y}_v \quad (6.448)$$

where $\mathbf{C}_{f,v}$, \mathbf{H}_v and \mathbf{C} have been defined associated with (6.379). Consequently, the decision variable vector for the OMMSE-MUD can also be represented as

$$\mathbf{z} = [(\mathbf{C}_f^T \mathbf{H}_f^H \mathbf{H}_f \mathbf{C}_f) \odot (\mathbf{S}^T \mathbf{S}) + \sigma^2 \mathbf{I}_K]^{-1} \times \sum_{v=0}^{N_p-1} \mathbf{C}_{f,v}^T \mathbf{H}_v^H \mathbf{C}^T \mathbf{y}_v \quad (6.449)$$

According to (6.449), when the receiver employs the knowledge about the active users concerning their CIRs and T-domain as well as F-domain spreading codes, the detector can be decomposed into two parts. The first part carries out the correlation operations with regard to each of the N_p subcarriers with the aid of the K users' T-, F-domain spreading codes and their CIRs, and the correlation outputs of all the N_p subcarriers are summed together. By contrast, the second part carries out the MMSE operation, which multiplies the result of the above-mentioned sum with the inverse matrix as shown in (6.449).

Note that in the above derivation for the OMMSE-MUD, the K number of users are detected jointly. In the OMMSE-MUD each user can also be detected separately. Specifically, let the m th user be detected. Then, from (6.445) the corresponding optimum weight matrix can be expressed as

$$\begin{aligned} \mathbf{W}_m^{(o)} &= [(\mathbf{H}_f \mathbf{C}_f) \square \mathbf{S}] [(\mathbf{H}_f \mathbf{C}_f) \square \mathbf{S}]^H + \sigma^2 \mathbf{I}_{N_p N_t}^{-1} \underbrace{[(\mathbf{H}_f \mathbf{C}_f) \square \mathbf{S}]}_{\text{the terms related to the } m\text{th user}} \\ &= [(\mathbf{H}_f \mathbf{C}_f) \square \mathbf{S}] [(\mathbf{H}_f \mathbf{C}_f) \square \mathbf{S}]^H + \sigma^2 \mathbf{I}_{N_p N_t}^{-1} [(\mathbf{H}_m (\mathbf{C}_f^{(m)})^T) \square (\mathbf{I}_U^T \otimes \mathbf{c}_m)] \end{aligned} \quad (6.450)$$

where \mathbf{H}_m is given by (6.370), while $\mathbf{C}_f^{(m)}$ is given in (6.371). One of the advantages of employing the separate OMMSE-MUD is that the OMMSE-MUD can be easily implemented using adaptive techniques. However, as seen in (6.450) the receiver must invert a matrix of size $(N_p N_t \times N_p N_t)$, which might be extreme when $N_p N_t$ is big. In order to circumvent this dilemma, the reduced-rank assisted MUDs – considered in Section 6.2.6 – may be used.

Figure 6.38 shows the BER performance of the TF-domain spread MC DS-CDMA using the proposed SMMSE- and OMMSE-MUDs, when communicating over frequency-selective Rayleigh fading channels having $L = 4$ T-domain resolvable paths. The considered TF-domain spread MC DS-CDMA employed a total $N_p = 8$ number of subcarriers and its T-domain spreading factor was $N_t = 16$. Furthermore, it was assumed that $U = 1$. From the

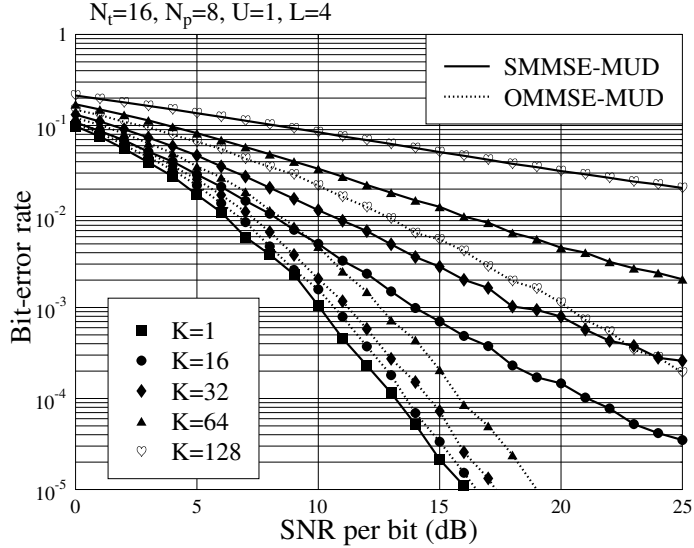


Figure 6.38: SMMSE-MUD, OMMSE-MUD: BER versus average SNR per bit performance for the TF-domain spread MC DS-CDMA using random spreading sequences, F-domain spreading factor of $N_p = 8$, T-domain spreading factor of $N_t = 16$ and $U = 1$ bit per user, when communicating over frequency-selective Rayleigh fading channels having $L = 4$ T-domain resolvable paths.

results in Fig. 6.38, we observe that although the BER performance achieved by the SMMSE-MUD is worse than that by the OMMSE-MUD, the SMMSE-MUD is capable of efficiently suppressing MUI. Note that although the SMMSE-MUD can only achieve the suboptimum BER performance in the MMSE sense, when considering practical applications, however, we should take into account the advantages of the SMMSE-MUD. First, the SMMSE-MUD may provide a low-complexity implementation, since the T-domain MMSE operation is based on a time-invariant matrix as shown (6.425), and the size of the inverse matrix in the F-domain MMSE is usually relatively small in comparison with that of the inverse matrix in the OMMSE-MUD. Additionally, the SMMSE-MUD may be more robust to channel estimation error than the OMMSE-MUD, which can have similar arguments as those for the SMMSE-MUD in Section 6.3.2.

6.4.3 Hybrid Time-Frequency-Domain ZF-MMSE Multiuser Detection

The MUDs in the TF-domain spread MC DS-CDMA may also be implemented in hybrid ways, where the MUDs in the T-domain and F-domain are operated under different criteria. As two examples, in this section we consider the hybrid TF-domain ZF/MMSE and MMSE/ZF MUDs. For the hybrid TF-domain ZF/MMSE-MUDs, the ZF-MUD is applied in the T-domain, while the MMSE-MUD is applied in the F-domain. Conversely, in the hybrid TF-domain MMSE/ZF-MUDs the MMSE-MUD is applied in the T-domain, while the ZF-MUD is applied in the F-domain. Furthermore, these hybrid TF-domain MUDs are derived

by assuming that the T-domain MUDs have the lowest complexity, corresponding to the SZF-MUD and SMMSE-MUD, studied in Section 6.4.1 and Section 6.4.2, respectively.

For the hybrid TF-domain ZF/MMSE-MUD, upon following the SZF-MUD in Section 6.4.1, after the T-domain ZF operation, as shown in (6.403), the outputs in the context of the N_p subcarriers can be expressed as

$$\mathbf{z}_{f,k_1} = \sum_{m=1}^M \mathbf{H}_{f,k_1}^{(m)} \mathbf{C}_{f,k_1}^{(m)} \mathbf{x}_{(m-1)K_1+k_1} + \mathbf{n}_{f,k_1}, \quad k_1 = 1, 2, \dots, K_1 \quad (6.451)$$

where

$$\begin{aligned} \mathbf{H}_{f,k_1}^{(m)} &= \text{diag}\{h_0^{((m-1)K_1+k_1)}, h_1^{((m-1)K_1+k_1)}, \dots, h_{N_p-1}^{((m-1)K_1+k_1)}\} \\ \mathbf{C}_{f,k_1}^{(m)} &= [\mathbf{c}_{f,0}^{((m-1)K_1+k_1)}, \mathbf{c}_{f,1}^{((m-1)K_1+k_1)}, \dots, \mathbf{c}_{f,N_p-1}^{((m-1)K_1+k_1)}]^T \\ \mathbf{n}_{f,k_1} &= [\tilde{n}_{0,k_1}, \tilde{n}_{1,k_1}, \dots, \tilde{n}_{(N_p-1),k_1}]^T \end{aligned} \quad (6.452)$$

and \tilde{n}_{v,k_1} is given by (6.402). It can be shown that \tilde{n}_{v,k_1} is Gaussian distributed with zero mean and a variance of $\sigma^2 \mathbf{R}_t^{-1}(k_1, k_1)$, where $\mathbf{R}_t^{-1}(k_1, k_1)$ is the (k_1, k_1) -th element of \mathbf{R}_t^{-1} . The variance is common to all the subcarriers.

As shown in (6.406), equation (6.451) can also be expressed as

$$\mathbf{z}_{f,k_1} = \mathbf{H}_{f,k_1} \mathbf{C}_{f,k_1} \mathbf{x}_{k_1} + \mathbf{n}_{f,k_1}, \quad k_1 = 1, 2, \dots, K_1 \quad (6.453)$$

with the matrices defined in (6.407).

With the aid of (6.451) or (6.453) we can now derive the MMSE detection in the F-domain. Let $\mathbf{W}_{f,k_1}^{(o)}$ be the optimum weight matrix for detection of the M users sharing the same T-domain spreading code as user k_1 . Then, the decision variable vector can be expressed as

$$\bar{\mathbf{z}}_{f,k_1} = (\mathbf{W}_{f,k_1}^{(o)})^H \mathbf{z}_{f,k_1} \quad (6.454)$$

where $\mathbf{W}_{f,k_1}^{(o)}$ is given by

$$\begin{aligned} \mathbf{W}_{f,k_1}^{(o)} &= \mathbf{R}_{\mathbf{z}_{f,k_1}}^{-1} \mathbf{R}_{\mathbf{z}_{f,k_1} \mathbf{x}_{k_1}} \\ &= [\mathbf{H}_{f,k_1} \mathbf{C}_{f,k_1} \mathbf{C}_{f,k_1}^T \mathbf{H}_{f,k_1}^H + \sigma^2 \mathbf{R}_t^{-1}(k_1, k_1) \mathbf{I}_{N_p}]^{-1} \mathbf{H}_{f,k_1} \mathbf{C}_{f,k_1} \end{aligned} \quad (6.455)$$

which needs to invert a $(N_p \times N_p)$ -dimensional matrix.

Again, when the receiver employs the knowledge about the CIRs and the T-domain as well as F-domain spreading sequences of all the users, the optimum weight matrix $\mathbf{W}_{f,k_1}^{(o)}$ can then be expressed as

$$\begin{aligned} \mathbf{W}_{f,k_1}^{(o)} &= \mathbf{H}_{f,k_1} \mathbf{C}_{f,k_1} [\mathbf{C}_{f,k_1}^T \mathbf{H}_{f,k_1}^H \mathbf{H}_{f,k_1} \mathbf{C}_{f,k_1} + \sigma^2 \mathbf{R}_t^{-1}(k_1, k_1) \mathbf{I}_{UM}]^{-1} \\ k_1 &= 1, 2, \dots, K_1 \end{aligned} \quad (6.456)$$

In the context of the hybrid TF-domain MMSE/ZF-MUD, following the SMMSE-MUD in Section 6.4.2, after the T-domain MMSE operation, the outputs of the N_p subcarriers have been given in (6.429) as

$$\mathbf{z}_{f,k_1} = \sum_{m=0}^{M-1} \mathbf{C}_f^{(k_1+mK_1)} \mathbf{H}_f^{(k_1+mK_1)} \mathbf{x}_{(k_1+mK_1)} + \mathbf{J}_{f,k_1}, \quad k_1 = 1, 2, \dots, K_1 \quad (6.457)$$

where the corresponding matrices have been defined associated with (6.429).

Explicitly, (6.457) can be expressed in a compact form as

$$\mathbf{z}_{f,k_1} = \mathbf{C}_f^{(k_1)} \mathbf{H}_f^{(k_1)} \mathbf{x}^{(k_1)} + \mathbf{J}_{f,k_1}, \quad k_1 = 1, 2, \dots, K_1 \quad (6.458)$$

where, by definition

$$\begin{aligned} \mathbf{C}_f^{(k_1)} &= [(\mathbf{C}_f^{(k_1)})^T, (\mathbf{C}_f^{(k_1+K_1)})^T, \dots, (\mathbf{C}_f^{(k_1+(M-1)K_1)})^T]^T \\ \mathbf{H}_{f,k_1} &= \text{diag}\{\mathbf{H}_f^{(k_1)}, \mathbf{H}_f^{(k_1+K_1)}, \dots, \mathbf{H}_f^{(k_1+(M-1)K_1)}\} \\ \mathbf{x}^{(k_1)} &= [\mathbf{x}_{(k_1)}^T, \mathbf{x}_{(k_1+K_1)}^T, \dots, \mathbf{x}_{(k_1+(M-1)K_1)}^T]^T \end{aligned} \quad (6.459)$$

Based on (6.458), consequently, the decision variable vector after the F-domain ZF detection can be expressed as

$$\begin{aligned} \bar{\mathbf{z}}_{f,k_1} &= [(\mathbf{C}_f^{(k_1)} \mathbf{H}_f^{(k_1)})^H \mathbf{C}_f^{(k_1)} \mathbf{H}_f^{(k_1)}]^{-1} (\mathbf{C}_f^{(k_1)} \mathbf{H}_f^{(k_1)})^H \mathbf{z}_{f,k_1} \\ &= \mathbf{x}^{(k_1)} + [(\mathbf{C}_f^{(k_1)} \mathbf{H}_f^{(k_1)})^H \mathbf{C}_f^{(k_1)} \mathbf{H}_f^{(k_1)}]^{-1} (\mathbf{C}_f^{(k_1)} \mathbf{H}_f^{(k_1)})^H \mathbf{J}_{f,k_1} \\ k_1 &= 1, 2, \dots, K_1 \end{aligned} \quad (6.460)$$

Figures 6.39 and 6.40 show the BER performance of the TF-domain spread MC DS-CDMA systems using hybrid ZF/MMSE-MUD or MMSE/ZF-MUD. Again, in order to avoid the event that the random generated T-domain spreading sequences are linearly dependent, yielding ill-conditioned ZF operation, the T-domain spreading sequences for the simulations of ZF/MMSE-MUD (Fig. 6.39) were fixed and given by (6.416). Furthermore, for the sake of comparison, the BER performance of the corresponding hybrid MMSE/ZF-MUD is also shown in Fig. 6.39, although in the hybrid MMSE/ZF-MUD both the T-domain and F-domain spreading sequences can be random sequences. By contrast, in the simulations for Fig. 6.40 random T-domain and F-domain spreading sequences were used.

The results in Figs 6.39 and 6.40 show that both the ZF/MMSE-MUD and MMSE/ZF-MUD are efficient for MUI suppression, and there are no error-floors observed, even when the TF-domain spread MC DS-CDMA system is fully loaded supporting $K = 128$ users. The results in Fig. 6.39 show that when multiple users are supported, the MMSE/ZF-MUD may significantly outperform the ZF/MMSE-MUD, when the SNR value is relatively low. This observation is mainly because in the MMSE/ZF-MUD the first-stage T-domain MMSE operation can efficiently mitigate both the MUI, which is generated by the T-domain spreading sequences, and background noise, while the second-stage F-domain ZF operation can efficiently mitigate the MUI in the F-domain. By contrast, in the ZF/MMSE-MUD, although the first-stage ZF operation is capable of fully removing the MUI in the T-domain, it also greatly amplifies the background noise. Consequently, the second stage of the F-domain MMSE has to operate in a very low SNR region, yielding the degraded BER performance as observed in Fig. 6.39. Note that, since each data symbol is transmitted on N_p subcarriers, the signal received associated with a subcarrier hence has a relatively low SNR value, in comparison with the scenario where one data symbol is transmitted on one subcarrier. Therefore, in the hybrid TF-domain MUDs it is desirable that the earlier stage MUD(s) are efficient to mitigate of background noise.

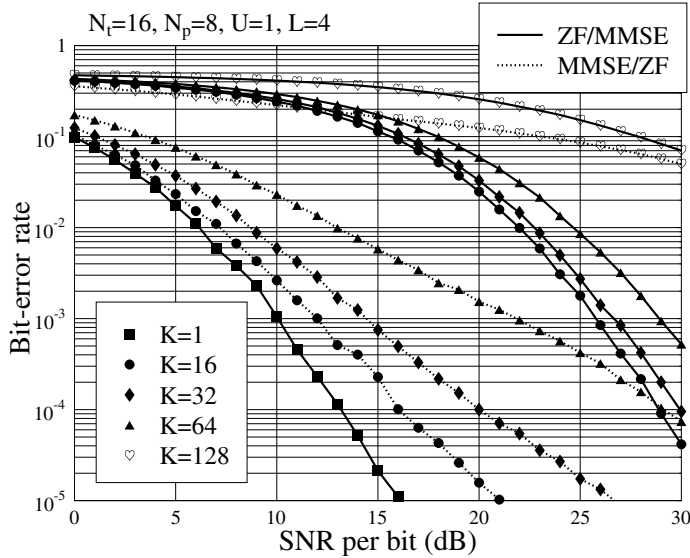


Figure 6.39: ZF/MMSE-MUD, MMSE/ZF-MUD: BER versus average SNR per bit performance for the TF-domain spread MC DS-CDMA using random F-domain spreading sequences with spreading factor of $N_p = 8$, T-domain spreading factor of $N_t = 16$ and $U = 1$ bit per user, when communicating over frequency-selective Rayleigh fading channels having $L = 4$ T-domain resolvable paths. The T-domain spreading sequences for the simulations are given by (6.416).

Note that the hybrid TF-domain MUD may be implemented in various ways apart from the two considered in this section. The criteria associated with the T-domain and F-domain detections may be chosen according to the specific requirements as well as the constraints in practice. Let us now consider the MLD-MUD for the TF-domain spread MC DS-CDMA.

6.4.4 Maximum-Likelihood Decision Multiuser Detection

Referring to (6.385), the MLD-MUD chooses the estimate to \mathbf{x} according to the optimization problem of

$$\begin{aligned}\hat{\mathbf{x}} &= \arg \min_{\mathbf{x}} \{ \| \mathbf{y} - [(\mathbf{H}_f \mathcal{C}_f) \square \mathbf{S}] \mathbf{x} \|^2 \} \\ &\triangleq \arg \min_{\mathbf{x}} \{ \mathbf{x}^H [(\mathcal{C}_f^T \mathbf{H}_f^H \mathbf{H}_f \mathcal{C}_f) \odot (\mathbf{S}^T \mathbf{S})] \mathbf{x} - 2\Re \{ \mathbf{x}^H [(\mathbf{H}_f \mathcal{C}_f) \square \mathbf{S}] \mathbf{y} \} \}\end{aligned}\quad (6.461)$$

Invoking the relationship in (6.414), the above optimization problem can also be represented as

$$\hat{\mathbf{x}} = \arg \min_{\mathbf{x}} \left\{ \mathbf{x}^H [(\mathcal{C}_f^T \mathbf{H}_f^H \mathbf{H}_f \mathcal{C}_f) \odot (\mathbf{S}^T \mathbf{S})] \mathbf{x} - 2\Re \left\{ \mathbf{x}^H \times \left(\sum_{v=0}^{N_p-1} \mathcal{C}_{f,v}^T \mathcal{H}_v^H \mathcal{C}_f^T \mathbf{y}_v \right) \right\} \right\} \quad (6.462)$$

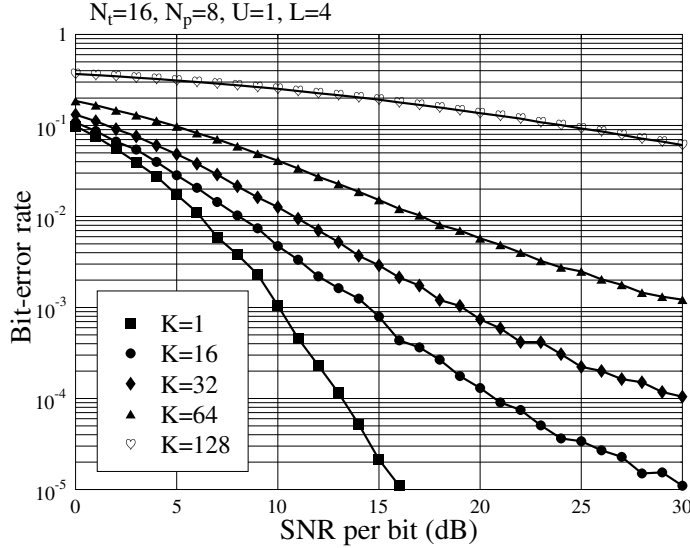


Figure 6.40: MMSE/ZF-MUD: BER versus average SNR per bit performance for the TF-domain spread MC DS-CDMA using random spreading sequences, F-domain spreading factor of $N_p = 8$, T-domain spreading factor of $N_t = 16$ and $U = 1$ bit per user, when communicating over frequency-selective Rayleigh fading channels having $L = 4$ T-domain resolvable paths.

Note that in (6.462) the terms of $\mathbf{C}_f^T \mathbf{H}_f^H \mathbf{H}_f \mathbf{C}_f$ and $\mathbf{S}^T \mathbf{S}$ may be simply represented by that shown in (6.412). Furthermore, in (6.462) the term in $\sum_{v=0}^{N_p-1} \mathbf{C}_{f,v}^T \mathcal{H}_v^H \mathbf{C}_f^T \mathbf{y}_v$ can be computed in parallel with respect to the N_p number of subcarriers.

The complexity for solving the optimization problem of (6.462) is exponentially proportional to the value of UK . The complexity may be decreased by introducing some efficient search algorithms as shown in Appendix 6.C. Alternatively, the MLD scheme may be implemented associated with another linear MUD scheme, such as the ZF-MUD or MMSE-MUD, to form the hybrid TF-domain MUDs. Specifically, in the T-domain the linear ZF-MUD or MMSE-MUD may be operated in order to remove the majority of MUI. After the MUI suppression in the T-domain, the MLD-MUD operated in the F-domain only needs to consider the M users sharing the same T-domain spreading sequence. Consequently, the complexity of the overall MUD is only exponentially proportional to the value of M , which is usually significantly lower than the value of UK .

6.5 Summary and Discussion

In this chapter various MUD schemes have been investigated in the context of three classes of multicarrier CDMA scheme, namely the F-domain spread MC-CDMA, MC DS-CDMA and the TF-domain spread MC DS-CDMA. The main MUD schemes considered in this chapter are summarized in Table 6.3, and can be generally classified as linear and nonlinear MUDs. As shown in Table 6.3, the linear MUDs can be obtained through the optimization criteria of

decorrelating (ZF), MVDR, MMSE, MSINR, MPDR, MSER, etc. The nonlinear MUDs are obtained according to the principles of IC depending on decision-feedback, MLD and MAP, etc. Linear MUDs generate their estimates through linear processing of the observations by a weight matrix or vector. Hence, they have typical implementation complexity that is linearly dependent on the number of users. In the linear MUD family, excepting the MSER-MUD, the weight matrices (vectors) can be formed by the correlation matrix of the user signatures, autocorrelation matrix of the observations, or the autocorrelation matrix of the interference plus background noise, associated with the cross-correlation matrix between the observations and the desired data. The MSER-LMUD also linearly processes the observations with a weight matrix (vector). However, the computation for its weight matrix or vector may be demanding, which may be obtained through exhaustive search, nonlinear programming optimization, adaptive optimization, etc. approaches. In linear MUDs, the received observations may first be projected onto a carefully designed subspace, and then signal detection is carried out in this subspace, forming the so-called reduced-rank detection. The reduced-rank detection may be optimized under any linear or nonlinear criterion. The reduced-rank detection often results in lower implementation complexity, in comparison with the corresponding detection in the original full-rank space.

In the nonlinear MUD family, the IC schemes aided by decision feedback (DF) information constitute a class of low-complexity high-efficiency MUD schemes. In the IC-based MUDs, the first detection stage is usually a conventional MF detector, or a low-complexity linear MUD, such as the decorrelating, MMSE, etc. detector. During the second detection stage, the data obtained during the first stage of detection are used by the detector to form a signal trying to resemble the interference, with the aid of the information about the interfering signals including their spreading sequences and CSI, etc. Then, this interference-resemblance signal is subtracted from the original received signal. In the IC-based MUDs, if the first stage of detection is sufficiently reliable, most MUIs can be removed in the following IC stage(s). For those incorrectly detected symbols, they will enhance their interference on the others and they may also generate error propagation. IC can be carried out in successive, in parallel, or in hybrid successive/parallel mode including several stages. Instead of building the IC based on all the detected data, IC may also be executed in the context of only the data reliably detected, if side-information about reliability is available. By doing partial IC, the error-propagation problem in IC-based MUDs may be efficiently mitigated.

The MLD-MUD based on the maximum-likelihood sequence estimation (MLSE) [2] principles is an overall optimum MUD, when the transmitted data is i.i.d. and when the required knowledge for MLD-MUD is ideal. When the transmitted data is not i.i.d. data, then the MAP-MUD is overall optimum, when the required knowledge for MAP-MUD is ideal. Although the nonlinear MLD-MUD and MAP-MUD are capable of significantly outperforming the linear MUDs and the nonlinear IC as seen in Table 6.3, they often demand much stricter knowledge about the user signatures and CSI than the linear MUDs and nonlinear IC. Their performance would be degraded significantly if the required knowledge is nonideal. Furthermore, the complexity of MLD-MUD and MAP-MUD may be extreme, being exponentially dependent on the number of users. The complexity of the MLD-MUD and MAP-MUD may be significantly mitigated when an efficient search algorithm as given in Section 6.C is invoked.

The MAP-MUDs may be implemented on the basis of block-by-block, symbol-by-symbol or bit-by-bit. Since the MAP-MUDs are soft-input soft-output (SISO) detectors,

Table 6.3: A summary of multiuser detection schemes.

MUD class	MUD scheme	Description
Linear	Decorrelating (ZF)	Zero MUI, noise amplification
	MVDR	Minimum variance of interference plus noise given distortionless constraint
	MMSE	Minimum mean-square error between a signal and its estimate, noise suppression
	MSINR	Maximum SNR, noise suppression
	MPDR	Minimum power of detector output given distortionless constraint
	MSER	Minimum probability of error, weights may be obtained through exhaustive search, nonlinear programming, adaptive, etc. optimization approach
Reduced-rank	Signal space	Project received signals onto a reduced-rank subspace, then detection is carried out in MMSE, MSINR, MPDR, etc. principles
	PC	
	CSM	
	TPA	
Nonlinear	Decision feedback (IC)	MF Decorrelating (MMSE) Operated in successive, parallel, or in hybrid model, outperforms the corresponding linear detector
	MLD	Optimized in maximum likelihood sense, equivalent to MAP when assuming i.i.d. sources
	MAP	Minimum probability of error, soft information outputs, easy to integrate with iterative decoding/detection

which make use of the *a priori* knowledge about the data being detected and generate the soft estimates for them, the MAP-MUDs may be readily integrated with various iterative algorithms implementing iterative (turbo) detection.

Appendix 6.A Derivatives with Respect to Complex Vector/Matrix

In advanced wireless signal processing, there are many optimization problems that require the derivatives of a real-valued function, such as the cost-functions, with respect to a complex

vector/matrix to be computed. In this Appendix we summarize the results of this kind of derivative, which may be used in Chapter 8 also.

Let $f(\theta, \theta^*)$ be a function of $\theta = \alpha + j\beta$. Then, according to [173], the partial derivative of $f(\theta)$ with respect to θ is given by

$$\frac{\partial f(\theta, \theta^*)}{\partial \theta} = \frac{1}{2} \left[\frac{\partial f(\alpha, \beta)}{\partial \alpha} - j \frac{\partial f(\alpha, \beta)}{\partial \beta} \right] \quad (6.A.1)$$

while with respect to θ^* is given by

$$\frac{\partial f(\theta, \theta^*)}{\partial \theta^*} = \frac{1}{2} \left[\frac{\partial f(\alpha, \beta)}{\partial \alpha} + j \frac{\partial f(\alpha, \beta)}{\partial \beta} \right] \quad (6.A.2)$$

Based on the above definition, when $f(\theta, \theta^*)$ is a function of vector $\theta = [\theta_1, \theta_2, \dots, \theta_N]^T$, the partial derivative of $f(\theta, \theta^*)$ with respect to θ is defined by

$$\frac{\partial f(\theta, \theta^*)}{\partial \theta} = \left[\frac{\partial f(\theta, \theta^*)}{\partial \theta_1}, \frac{\partial f(\theta, \theta^*)}{\partial \theta_2}, \dots, \frac{\partial f(\theta, \theta^*)}{\partial \theta_N} \right]^T \quad (6.A.3)$$

where

$$\frac{\partial f(\theta, \theta^*)}{\partial \theta_n} = \frac{1}{2} \left[\frac{\partial f(\alpha_1, \beta_1, \dots, \alpha_N, \beta_N)}{\partial \alpha_n} - j \frac{\partial f(\alpha_1, \beta_1, \dots, \alpha_N, \beta_N)}{\partial \beta_n} \right]$$

$$n = 1, 2, \dots, N \quad (6.A.4)$$

In a similar way, we have

$$\frac{\partial f(\theta, \theta^*)}{\partial \theta^*} = \left[\frac{\partial f(\theta, \theta^*)}{\partial \theta_1^*}, \frac{\partial f(\theta, \theta^*)}{\partial \theta_2^*}, \dots, \frac{\partial f(\theta, \theta^*)}{\partial \theta_N^*} \right]^T \quad (6.A.5)$$

where

$$\frac{\partial f(\theta, \theta^*)}{\partial \theta_n^*} = \frac{1}{2} \left[\frac{\partial f(\alpha_1, \beta_1, \dots, \alpha_N, \beta_N)}{\partial \alpha_n} + j \frac{\partial f(\alpha_1, \beta_1, \dots, \alpha_N, \beta_N)}{\partial \beta_n} \right]$$

$$n = 1, 2, \dots, N \quad (6.A.6)$$

Furthermore, when $f(\theta, \theta^*)$ is a function of the matrix θ given by

$$\theta = \begin{bmatrix} \theta_{11} & \theta_{12} & \dots & \theta_{1N} \\ \theta_{21} & \theta_{22} & \dots & \theta_{2N} \\ \vdots & \vdots & \ddots & \vdots \\ \theta_{M1} & \theta_{M2} & \dots & \theta_{MN} \end{bmatrix} = [\theta_{mn}]_{M \times N} \quad (6.A.7)$$

then the partial derivative of $f(\theta, \theta^*)$ with respect to θ is defined by

$$\frac{\partial f(\theta, \theta^*)}{\partial \theta} = \begin{bmatrix} \frac{\partial f(\theta, \theta^*)}{\partial \theta_{11}} & \frac{\partial f(\theta, \theta^*)}{\partial \theta_{12}} & \dots & \frac{\partial f(\theta, \theta^*)}{\partial \theta_{1N}} \\ \frac{\partial f(\theta, \theta^*)}{\partial \theta_{21}} & \frac{\partial f(\theta, \theta^*)}{\partial \theta_{22}} & \dots & \frac{\partial f(\theta, \theta^*)}{\partial \theta_{2N}} \\ \vdots & \vdots & \ddots & \vdots \\ \frac{\partial f(\theta, \theta^*)}{\partial \theta_{M1}} & \frac{\partial f(\theta, \theta^*)}{\partial \theta_{M2}} & \dots & \frac{\partial f(\theta, \theta^*)}{\partial \theta_{MN}} \end{bmatrix} \quad (6.A.8)$$

where

$$\frac{\partial f(\boldsymbol{\theta}, \boldsymbol{\theta}^*)}{\partial \theta_{mn}} = \frac{1}{2} \left[\frac{\partial f([\alpha_{ij}]_{M \times N}, [\beta_{ij}]_{M \times N})}{\partial \alpha_{mn}} - j \frac{\partial f([\alpha_{ij}]_{M \times N}, [\beta_{ij}]_{M \times N})}{\partial \beta_{mn}} \right] \\ m = 1, 2, \dots, M; n = 1, 2, \dots, N \quad (6.A.9)$$

Similarly, the partial derivative of $f(\boldsymbol{\theta}, \boldsymbol{\theta}^*)$ with respect to $\boldsymbol{\theta}^*$ is defined by

$$\frac{\partial f(\boldsymbol{\theta}, \boldsymbol{\theta}^*)}{\partial \boldsymbol{\theta}^*} = \begin{bmatrix} \frac{\partial f(\boldsymbol{\theta}, \boldsymbol{\theta}^*)}{\partial \theta_{11}^*} & \frac{\partial f(\boldsymbol{\theta}, \boldsymbol{\theta}^*)}{\partial \theta_{12}^*} & \dots & \frac{\partial f(\boldsymbol{\theta}, \boldsymbol{\theta}^*)}{\partial \theta_{1N}^*} \\ \frac{\partial f(\boldsymbol{\theta}, \boldsymbol{\theta}^*)}{\partial \theta_{21}^*} & \frac{\partial f(\boldsymbol{\theta}, \boldsymbol{\theta}^*)}{\partial \theta_{22}^*} & \dots & \frac{\partial f(\boldsymbol{\theta}, \boldsymbol{\theta}^*)}{\partial \theta_{2N}^*} \\ \vdots & \vdots & \ddots & \vdots \\ \frac{\partial f(\boldsymbol{\theta}, \boldsymbol{\theta}^*)}{\partial \theta_{M1}^*} & \frac{\partial f(\boldsymbol{\theta}, \boldsymbol{\theta}^*)}{\partial \theta_{M2}^*} & \dots & \frac{\partial f(\boldsymbol{\theta}, \boldsymbol{\theta}^*)}{\partial \theta_{MN}^*} \end{bmatrix} \quad (6.A.10)$$

where

$$\frac{\partial f(\boldsymbol{\theta}, \boldsymbol{\theta}^*)}{\partial \theta_{mn}^*} = \frac{1}{2} \left[\frac{\partial f([\alpha_{ij}]_{M \times N}, [\beta_{ij}]_{M \times N})}{\partial \alpha_{mn}} + j \frac{\partial f([\alpha_{ij}]_{M \times N}, [\beta_{ij}]_{M \times N})}{\partial \beta_{mn}} \right] \\ m = 1, 2, \dots, M; n = 1, 2, \dots, N \quad (6.A.11)$$

For a function of complex vectors/matrices, its partial derivatives have the following properties [89, 173–175]:

1.

$$\frac{\partial f(\boldsymbol{\theta})}{\partial \boldsymbol{\theta}^*} = \mathbf{0}, \quad \frac{\partial f(\boldsymbol{\theta}^*)}{\partial \boldsymbol{\theta}} = \mathbf{0} \quad (6.A.12)$$

where $f(\boldsymbol{\theta})$ is a function of $\boldsymbol{\theta}$ alone, while $f(\boldsymbol{\theta}^*)$ is a function of $\boldsymbol{\theta}^*$ alone.

2.

$$\frac{\partial (\mathbf{a}^H \boldsymbol{\theta})}{\partial \boldsymbol{\theta}} = \mathbf{a}^*, \quad \frac{\partial (\boldsymbol{\theta}^H \mathbf{a})}{\partial \boldsymbol{\theta}} = \mathbf{0} \\ \frac{\partial (\mathbf{a}^H \boldsymbol{\theta})}{\partial \boldsymbol{\theta}^*} = \mathbf{0}, \quad \frac{\partial (\boldsymbol{\theta}^H \mathbf{a})}{\partial \boldsymbol{\theta}^*} = \mathbf{a} \quad (6.A.13)$$

3.

$$\frac{\partial (\boldsymbol{\theta}^H \mathbf{A} \boldsymbol{\theta})}{\partial \boldsymbol{\theta}} = (\mathbf{A} \boldsymbol{\theta})^*, \quad \text{if } \mathbf{A}^H = \mathbf{A} \\ \frac{\partial (\boldsymbol{\theta}^H \mathbf{A} \boldsymbol{\theta})}{\partial \boldsymbol{\theta}^*} = \mathbf{A} \boldsymbol{\theta}, \quad \text{if } \mathbf{A}^H = \mathbf{A} \quad (6.A.14)$$

4.

$$\frac{\partial (\boldsymbol{\theta}^T \mathbf{A} \boldsymbol{\theta})}{\partial \boldsymbol{\theta}} = (\mathbf{A} + \mathbf{A}^T) \boldsymbol{\theta}, \quad \frac{\partial (\boldsymbol{\theta}^T \mathbf{A} \boldsymbol{\theta})}{\partial \boldsymbol{\theta}^*} = \mathbf{0} \quad (6.A.15)$$

5.

$$\frac{\partial(\boldsymbol{\theta}^H \mathbf{A} \boldsymbol{\theta}^*)}{\partial \boldsymbol{\theta}} = \mathbf{0}, \quad \frac{\partial(\boldsymbol{\theta}^H \mathbf{A} \boldsymbol{\theta}^*)}{\partial \boldsymbol{\theta}^*} = (\mathbf{A} + \mathbf{A}^T) \boldsymbol{\theta}^* \quad (6.A.16)$$

6.

$$\begin{aligned} \frac{\partial \text{Trace}(\boldsymbol{\theta})}{\partial \boldsymbol{\theta}} &= \mathbf{I}, & \frac{\partial \text{Trace}(\boldsymbol{\theta})}{\partial \boldsymbol{\theta}^*} &= \mathbf{0} \\ \frac{\partial \text{Trace}(\boldsymbol{\theta}^*)}{\partial \boldsymbol{\theta}} &= \mathbf{0}, & \frac{\partial \text{Trace}(\boldsymbol{\theta}^*)}{\partial \boldsymbol{\theta}^*} &= \mathbf{I} \end{aligned} \quad (6.A.17)$$

7.

$$\begin{aligned} \frac{\partial \text{Trace}(\mathbf{A} \boldsymbol{\theta})}{\partial \boldsymbol{\theta}} &= \mathbf{A}^T, & \frac{\partial \text{Trace}(\mathbf{A} \boldsymbol{\theta})}{\partial \boldsymbol{\theta}^*} &= \mathbf{0} \\ \frac{\partial \text{Trace}(\mathbf{A} \boldsymbol{\theta}^H)}{\partial \boldsymbol{\theta}} &= \mathbf{0}, & \frac{\partial \text{Trace}(\mathbf{A} \boldsymbol{\theta}^H)}{\partial \boldsymbol{\theta}^*} &= \mathbf{A} \end{aligned} \quad (6.A.18)$$

8.

$$\frac{\partial \text{Trace}(\boldsymbol{\theta}^H \boldsymbol{\theta})}{\partial \boldsymbol{\theta}} = \boldsymbol{\theta}^*, \quad \frac{\partial \text{Trace}(\boldsymbol{\theta}^H \boldsymbol{\theta})}{\partial \boldsymbol{\theta}^*} = \boldsymbol{\theta} \quad (6.A.19)$$

9.

$$\frac{\partial \text{Trace}(\boldsymbol{\theta}^H \mathbf{A} \boldsymbol{\theta})}{\partial \boldsymbol{\theta}} = \mathbf{A}^T \boldsymbol{\theta}^*, \quad \frac{\partial \text{Trace}(\boldsymbol{\theta}^H \mathbf{A} \boldsymbol{\theta})}{\partial \boldsymbol{\theta}^*} = \mathbf{A} \boldsymbol{\theta} \quad (6.A.20)$$

10.

$$\frac{\partial \text{Trace}(\boldsymbol{\theta}^H \mathbf{A} \boldsymbol{\theta} \mathbf{B})}{\partial \boldsymbol{\theta}} = \mathbf{A}^T \boldsymbol{\theta}^* \mathbf{B}^T, \quad \frac{\partial \text{Trace}(\boldsymbol{\theta}^H \mathbf{A} \boldsymbol{\theta} \mathbf{B})}{\partial \boldsymbol{\theta}^*} = \mathbf{A} \boldsymbol{\theta} \mathbf{B} \quad (6.A.21)$$

Appendix 6.B Matrix Inversion

The equations listed in this appendix are mainly from references [89, 156, 175]. Some of their extensions are also listed for convenience.

1. *Matrix Inverse Lemma:* Assume that \mathbf{A} is $(N \times N)$, \mathbf{B} is $(N \times M)$, \mathbf{C} is $(M \times M)$ and \mathbf{D} is $(M \times N)$, then we have

$$(\mathbf{A} + \mathbf{B} \mathbf{C} \mathbf{D})^{-1} = \mathbf{A}^{-1} - \mathbf{A}^{-1} \mathbf{B} (\mathbf{D} \mathbf{A}^{-1} \mathbf{B} + \mathbf{C}^{-1})^{-1} \mathbf{D} \mathbf{A}^{-1} \quad (6.B.1)$$

2. Assume that \mathbf{A} is $(N \times N)$, \mathbf{h} is an N -dimensional column vector, then,

$$(\mathbf{A} + \mathbf{h} \mathbf{h}^H)^{-1} = \mathbf{A}^{-1} - \frac{\mathbf{A}^{-1} \mathbf{h} \mathbf{h}^H \mathbf{A}^{-1}}{1 + \mathbf{h}^H \mathbf{A}^{-1} \mathbf{h}} \quad (6.B.2)$$

3. Assume that \mathbf{A} is $(N \times N)$, \mathbf{B} is $(N \times M)$, \mathbf{C} is $(M \times M)$ and \mathbf{D} is $(M \times N)$, then we have

$$(\mathbf{A} + \mathbf{B} \mathbf{C} \mathbf{D})^{-1} \mathbf{B} = \mathbf{A}^{-1} \mathbf{B} (\mathbf{D} \mathbf{A}^{-1} \mathbf{B} + \mathbf{C}^{-1})^{-1} \mathbf{C}^{-1} \quad (6.B.3)$$

4. Assume that \mathbf{B} is $(N \times M)$ and \mathbf{C} is $(M \times M)$, then we have

$$(\sigma^2 \mathbf{I}_N + \mathbf{B} \mathbf{C} \mathbf{B}^H)^{-1} = \frac{1}{\sigma^2} [\mathbf{I}_N - \mathbf{B} (\mathbf{B}^H \mathbf{B} + \sigma^2 \mathbf{C}^{-1})^{-1} \mathbf{B}^H] \quad (6.B.4)$$

5. Assume that \mathbf{B} is $(N \times M)$ and \mathbf{D} is $(M \times N)$, then we have

$$(\mathbf{B} \mathbf{D} + \sigma^2 \mathbf{I}_N)^{-1} \mathbf{B} = \mathbf{B} (\mathbf{D} \mathbf{B} + \sigma^2 \mathbf{I}_M)^{-1} \quad (6.B.5)$$

6. Assume that \mathbf{A} is $(N \times N)$ and \mathbf{B} is $(N \times M)$, then we have

$$(\mathbf{A} + \mathbf{B} \mathbf{B}^H)^{-1} \mathbf{B} = \mathbf{A}^{-1} \mathbf{B} (\mathbf{B}^H \mathbf{A}^{-1} \mathbf{B} + \mathbf{I}_M)^{-1} \quad (6.B.6)$$

7. When \mathbf{A} is a $(N \times N)$ positive definite matrix, then, according to the *Choleski decomposition*, we can express \mathbf{A} as

$$\mathbf{A} = \mathbf{F} \mathbf{F}^H \quad (6.B.7)$$

where \mathbf{F} is a unique lower or upper triangular matrix with real positive diagonal entries. Hence, the inverse of \mathbf{A} can be expressed as

$$\mathbf{A}^{-1} = (\mathbf{F}^{-1})^H \mathbf{F}^{-1} \quad (6.B.8)$$

8. When \mathbf{A} is a $(N \times N)$ Hermitian matrix, then \mathbf{A} can be decomposed as

$$\mathbf{A} = \mathbf{\Phi} \mathbf{\Lambda} \mathbf{\Phi}^H = \sum_{n=1}^N \lambda_n \boldsymbol{\phi}_n \boldsymbol{\phi}_n^H \quad (6.B.9)$$

where $\mathbf{\Lambda} = \text{diag}\{\lambda_1, \lambda_2, \dots, \lambda_N\}$ containing the eigenvalues of \mathbf{A} , $\mathbf{\Phi} = [\boldsymbol{\phi}_1, \boldsymbol{\phi}_2, \dots, \boldsymbol{\phi}_N]$ is the unitary matrix and $\boldsymbol{\phi}_n$ is an eigenvector corresponding to λ_n . The inverse of \mathbf{A} can be expressed as

$$\mathbf{A}^{-1} = \mathbf{\Phi} \mathbf{\Lambda}^{-1} \mathbf{\Phi}^H = \sum_{n=1}^N \frac{\boldsymbol{\phi}_n \boldsymbol{\phi}_n^H}{\lambda_n} \quad (6.B.10)$$

10 *The Moore–Penrose Inverse*: If \mathbf{A} is a $(N \times M)$ matrix with rank M , then

$$\mathbf{A}^\dagger = (\mathbf{A}^H \mathbf{A})^{-1} \mathbf{A}^H \quad (6.B.11)$$

If \mathbf{A} is a $(N \times M)$ matrix with rank N , then

$$\mathbf{A}^\dagger = \mathbf{A}^H (\mathbf{A} \mathbf{A}^H)^{-1} \quad (6.B.12)$$

Appendix 6.C Suboptimal Algorithms for Maximum Likelihood Decision Multiuser Detection

In this appendix a range of suboptimal algorithms for solving the optimization problem in MLD-MUD are summarized. Specifically, the optimization problem to be attacked is

$$\hat{\mathbf{b}} = \arg \min_{\mathbf{b} \in \{+1, -1\}^{\mathcal{K}}} \{ \mathbf{b}^T \mathbf{R} \mathbf{b} - 2\Re\{\mathbf{y}^H \mathbf{b}\} \} \quad (6.C.1)$$

where \mathbf{R} is a $(\mathcal{K} \times \mathcal{K})$ full rank Hermitian matrix, \mathbf{y} is the \mathcal{K} -length observation vector given by

$$\mathbf{y} = \mathbf{R} \mathbf{b} + \mathbf{n} \quad (6.C.2)$$

where \mathbf{n} is Gaussian with zero mean and a covariance matrix $\sigma^2 \mathbf{R}$, while \mathbf{b} in (6.C.1) and (6.C.2) is in the form

$$\mathbf{b} = [b_1, b_2, \dots, b_{\mathcal{K}}]^T \quad (6.C.3)$$

where b_k ($k = 1, 2, \dots, \mathcal{K}$) takes value in $\mathcal{B} = \{+1, -1\}$, i.e. only binary data symbols are considered in this Appendix, although extensions to the general non-binary cases are straightforward.

The optimum solution to (6.C.1) requires an exhaustive search over all the $2^{\mathcal{K}}$ possible combinations of the components of the binary data vector $\mathbf{b} \in \mathcal{B}^{\mathcal{K}}$. Explicitly, the computational complexity increases exponentially with the number of users or the value of \mathcal{K} .

The algorithms considered in the following subsections aim to find the solutions to $\mathbf{b} \in \mathcal{B}^{\mathcal{K}}$, such that the resulted value of the argument at the r.h.s of (6.C.1) is as low as possible, but with a computational complexity that is not NP-hard.

In this Appendix both the suboptimal search algorithms and non-search algorithms are considered, in order to find the solution to the MLD-MUD problem. Let us first consider the search-assisted algorithms.

6.C.1 Search Algorithms

In order to describe the various search algorithms for the MLD-MUD, as shown in (6.C.1), we invoke the following definitions.

A search space \mathbf{B} is defined as

$$\mathbf{B} = \{\mathbf{b}_1, \mathbf{b}_2, \dots, \mathbf{b}_{2^{\mathcal{K}}}\} \quad (6.C.4)$$

which contains the $2^{\mathcal{K}}$ candidates representing the possible data vectors that might be transmitted. In (6.C.4) $\mathbf{b}_i \in \mathcal{B}^{\mathcal{K}}$ for $i = 1, 2, \dots, 2^{\mathcal{K}}$.

A test vector \mathbf{b} is chosen from \mathbf{B} , where \mathbf{b} is in the form of (6.C.3).

A cost function is defined as

$$L(\mathbf{b}) = \mathbf{b}^T \mathbf{R} \mathbf{b} - 2\Re\{\mathbf{y}^H \mathbf{b}\} \quad (6.C.5)$$

when the test vector \mathbf{b} is applied.

An *a priori* information related vector is defined as

$$\boldsymbol{\lambda}(n) = \begin{bmatrix} \lambda_{1+}(n) & \lambda_{2+}(n) & \cdots & \lambda_{\mathcal{K}+}(n) \\ \lambda_{1-}(n) & \lambda_{2-}(n) & \cdots & \lambda_{\mathcal{K}-}(n) \end{bmatrix}, \quad n = 1, \dots \quad (6.C.6)$$

where $\lambda_{i+}(n)$ and $\lambda_{i-}(n)$ are related to the reliabilities that $b_i \in \mathbf{b}$ is decided as +1 or -1, respectively, before the n th round of search.

Explicitly, with the aid of $\lambda(n)$ defined in (6.C.6), the search process may exploit the *a priori* information for enhancing the search and ultimately saving the search time. Specifically, for the MLD-MUD, the search process may be started following a low-complexity linear single-user or multiuser detection procedure. In this case, after the single-user or multiuser detection, the receiver has obtained a certain amount of information about the transmitted bits that may be exploited to improve the search procedure.

Finally, we define a decision-risk (DR) function as

$$\mathbf{D}(n) = \begin{bmatrix} D_{1+}(n) & D_{2+}(n) & \cdots & D_{\mathcal{K}+}(n) \\ D_{1-}(n) & D_{2-}(n) & \cdots & D_{\mathcal{K}-}(n) \end{bmatrix}, \quad n = 0, 1, \dots \quad (6.C.7)$$

where $D_{i+}(n) \geq 0$ and $D_{i-}(n) \geq 0$ represent the risks in the context of making the decision that $b_i = +1$ and $b_i = -1$, respectively, based on $D_{i+}(n)$ and $D_{i-}(n)$, or $\lambda_{i+}(n)$ and $\lambda_{i-}(n)$. The decision is in favour of a DR that is as low as possible.

6.C.1.1 QRD-M Tree-Search Algorithm

In reference [176] a tree search algorithm for the MLD in MIMO systems has been derived, when the QR-decomposition is applied to the MIMO CIR matrix. When considering the observation equation (6.C.2), we can equivalently execute the decomposition on \mathbf{R} as

$$\mathbf{R} = \mathbf{F}\mathbf{F}^H \quad (6.C.8)$$

where \mathbf{F} is a unique lower or upper triangular matrix with real positive diagonal entries. Specifically, let us assume that \mathbf{F} is an upper triangular matrix. In this case, \mathbf{F}^H can be expressed as

$$\mathbf{F}^H = \begin{bmatrix} f_{11} & & & \\ f_{12}^* & f_{22} & & \\ \vdots & \ddots & & \\ f_{1\mathcal{K}}^* & f_{2\mathcal{K}}^* & \cdots & f_{\mathcal{K}\mathcal{K}} \end{bmatrix} \quad (6.C.9)$$

When multiplying (6.C.2) by \mathbf{F}^{-1} , we obtain

$$\begin{aligned} \tilde{\mathbf{y}} &= \mathbf{F}^{-1}\mathbf{y} \\ &= \mathbf{F}^H\mathbf{b} + \tilde{\mathbf{n}} \end{aligned} \quad (6.C.10)$$

where $\tilde{\mathbf{n}} = \mathbf{F}^{-1}\mathbf{n}$, which is now a zero-mean Gaussian vector with a covariance matrix of $\sigma^2 \mathbf{I}_{\mathcal{K}}$. Hence, the noise is now white Gaussian.

The QRD-M tree search algorithm can be designed based on (6.C.10), which, instead of maintaining all the possible branches when using exhaustive search, only (at most) M number of branches are maintained at each step. The QRD-M tree search algorithm can be described in detail as follows.

Since b_1 experiences no MUI, the search starts from $k = 1$ by computing the cost value

$$L(\hat{b}_1) = \|\tilde{\mathbf{y}}_1 - f_{11}\hat{b}_1\|^2, \quad \hat{b}_1 = \pm 1 \quad (6.C.11)$$

These $2^1 = 2$ values will be set as the initial values.

We define

$$\begin{aligned}\tilde{\mathbf{y}}_k &= [\tilde{y}_1, \tilde{y}_2, \dots, \tilde{y}_k]^T \\ \hat{\mathbf{b}}_k &= [\hat{b}_1, \hat{b}_2, \dots, \hat{b}_k]^T = [\hat{\mathbf{b}}_{k-1}^T, \hat{b}_k]^T \\ L(\hat{\mathbf{b}}_k) &= \|\tilde{\mathbf{y}}_k - \mathbf{F}_k^H \hat{\mathbf{b}}_k\|^2 + L(\hat{\mathbf{b}}_{k-1})\end{aligned}\quad (6.C.12)$$

where \mathbf{F}_k^H is formed by the k th row of \mathbf{F}^H by removing the elements of zeros. Then, for $k = 2, 3, \dots, \mathcal{K}$, the search process can be described by the following steps:

Step 1: Set $\hat{b}_k = +1, -1$ and compute

$$L(\hat{\mathbf{b}}_k) = \|\tilde{\mathbf{y}}_k - \mathbf{F}_k^H \hat{\mathbf{b}}_k\|^2 + L(\hat{\mathbf{b}}_{k-1}) \quad (6.C.13)$$

associated with all the 2^{k-1} combinations of $\hat{\mathbf{b}}_{k-1}$, yielding 2^k number of branches with certain cost values.

Step 2: If $2^k \leq M$, set $k \leftarrow (k+1)$ and return to Step 1. Otherwise, go to Step 3 if $2^k > M$.

Step 3: Find the M number of branches which have the lowest cost values computed in (6.C.13) and store their corresponding cost values. Delete all the other branches and their cost values. Then, set $k \leftarrow (k+1)$ and go to Step 4.

Step 4: Set $\hat{b}_k = +1, -1$ and compute

$$L(\hat{\mathbf{b}}_k) = \|\tilde{\mathbf{y}}_k - \mathbf{F}_k^H \hat{\mathbf{b}}_k\|^2 + L(\hat{\mathbf{b}}_{k-1}) \quad (6.C.14)$$

associated with all the left M number of branches, yielding $2M$ number of branches with certain cost values.

Step 5: If $k < \mathcal{K}$, find the M number of branches which have the lowest cost values computed in (6.C.14) and store their corresponding cost values. Delete all the other branches and their cost values. Then, set $k \leftarrow (k+1)$ and return to Step 4. Otherwise, if $k = \mathcal{K}$, go to Step 6.

Step 6: Find the branch having the lowest cost value. Its corresponding binary sequence $\hat{\mathbf{b}}_{\mathcal{K}}$ is taken as the estimate to the transmitted binary sequence \mathbf{b} .

Based on the above description, it can be implied that the complexity of the QRD-M tree search algorithm is in the order of $O(2M)$ for the detection of one bit.

6.C.1.2 Greedy Search Algorithm

In MUD the greedy search can usually be referred to as the ordered greedy search. It starts with ordering the bits to be detected according to their reliabilities obtained intrinsically from the available knowledge, such as the relative power levels, relative log-likelihood ratios

(LLRs), etc. For our current search problem, let us assume that the reliabilities associated with the bits to be detected are arranged in descent as

$$\delta_1 \geq \delta_2 \geq \cdots \geq \delta_K \quad (6.C.15)$$

and after the ordering the bits to be detected are expressed as

$$\tilde{\mathbf{b}} = [\tilde{b}_1, \tilde{b}_2, \dots, \tilde{b}_K]^T \quad (6.C.16)$$

Furthermore, let us assume that the corresponding DR function is given by (6.C.7).

For greedy search, each search cycle detects one bit, say \tilde{b}_k ($k = 1, 2, \dots, K$), by choosing $\tilde{b}_k = +1$ or -1 , which yields the lower risk or lower accumulative risk, until all the K bits are detected.

Greedy search can be built on the reliabilities, as shown in (6.C.15), ordered at the beginning of the search. Alternatively, the order may be updated every time after one bit is detected. Usually, the latter greedy search scheme using real-time updated reliabilities outperforms the former greedy search scheme without using reliability updating, at a cost of higher implementational complexity. Additionally, the DR-function of the remaining bits may also be updated whenever a bit is detected, so that the error performance can be enhanced.

It has been shown [177] that, when the available *a priori* knowledge in favour of the detection is efficiently exploited, the greedy search-based MUD is capable of achieving an error performance that is very close to that achieved by the optimum MLD-MUD. This near-optimum error performance is achieved with the detection complexity significantly lower than that of the optimum MLD-MUD.

6.C.1.3 Sphere-Decoding-Based Search

When the sphere-decoding (SD)-based search is invoked, the search is limited to the binary vectors that lie inside a hypersphere, instead of testing all the binary vectors in \mathbf{B} [178]. Therefore, the optimization problem concerned can be represented as

$$\hat{\mathbf{b}} = \arg \min_{\mathbf{b} \in \mathbf{B}} \{ \| \mathbf{y} - \mathbf{R}\mathbf{b} \|^2 \} \leq r^2 \quad (6.C.17)$$

where r denotes the radius of the sphere where the search is operated.

When the QR-decomposition is invoked as shown in Section 6.C.1.1, the above-stated problem can be expressed as

$$\hat{\mathbf{b}} = \arg \min_{\mathbf{b} \in \mathbf{B}} \left\{ \sum_{k=1}^K \| \tilde{\mathbf{y}}_k - \mathbf{F}_k^H \mathbf{b} \|^2 \right\} \leq r^2 \quad (6.C.18)$$

where \mathbf{F}_k^H now denotes the k th row of \mathbf{F}^H , since \mathbf{b} is a K -length binary vector. Let $\tilde{\mathbf{y}} = \mathbf{F}^H \tilde{\mathbf{y}}$, where $\tilde{\mathbf{y}} = \mathbf{F}^{-H} \tilde{\mathbf{y}}$ is hence the ZF solution. Then, (6.C.18) can be written as

$$\begin{aligned} \hat{\mathbf{b}} &= \arg \min_{\mathbf{b} \in \mathbf{B}} \left\{ \sum_{k=1}^K \| \mathbf{F}_k^H \tilde{\mathbf{y}} - \mathbf{F}_k^H \mathbf{b} \|^2 \right\} \leq r^2 \\ &= \arg \min_{\mathbf{b} \in \mathbf{B}} \left\{ \sum_{k=1}^K \left\| f_{kk}(\tilde{y}_k - b_k) + \sum_{l=1}^{k-1} f_{lk}^*(\tilde{y}_l - b_l) \right\|^2 \right\} \leq r^2 \\ &= \arg \min_{\mathbf{b} \in \mathbf{B}} \left\{ \sum_{k=1}^K f_{kk}^2 (\tilde{y}_k - b_k)^2 + \sum_{l=1}^{k-1} \frac{f_{lk}^*}{f_{kk}} (\tilde{y}_l - b_l)^2 \right\} \leq r^2 \end{aligned} \quad (6.C.19)$$

Based on (6.C.19) the SD-based search starts with $k = 1$ and finds the valid b_1 's that satisfy $f_{kk}^2 \|\bar{y}_k - b_k\| \leq r^2$, which are recorded by the search process. Once having obtained the valid b_1 's, the SD-based search then finds the valid b_2 's that satisfy $\sum_{k=1}^2 f_{kk}^2 \|\bar{y}_k - b_k\| + \sum_{l=1}^{k-1} \frac{f_{lk}^*}{f_{kk}} (\bar{y}_l - b_l)^2 \leq r^2$ associated with all the recorded b_1 's. The combinations of $(b_1 b_2)$'s that fulfill the above-mentioned condition are recorded. The above search process continues in the same way until it generates the valid combinations of $(b_1 b_2, \dots, b_K)$, or until there are no valid solutions in the considered hypersphere. If there are no valid binary vectors can be found in the considered hypersphere, the search restarts with an enlarged radius. If there are valid binary vectors in the currently considered hypersphere, the search restarts but with a smaller radius. This search process continues until there is only one valid binary vector in the hypersphere.

In the above-described search process, \bar{y} is the ZF solution. Hence, this search process can be referred to as the ZF-assisted SD. Alternatively, the solutions obtained from the other types of MUD may be invoked in the search process as above stated. Specifically, when the MMSE-MUD is considered, we can carry out the decomposition as

$$\mathbf{R} + \sigma^2 \mathbf{I}_k = \mathbf{F} \mathbf{F}^H \quad (6.C.20)$$

In this case, it can be shown that $\bar{y} = \mathbf{F}^{-H} \tilde{\mathbf{y}}$ is the MMSE solution. With the aid of the decomposition of (6.C.20), the MMSE-assisted SD can now be carried out in the same way as the ZF-assisted SD.

6.C.1.4 Coordinate Descent Search Algorithm

Given the observation vector of (6.C.2), since the detector has the knowledge about the autocorrelation matrix \mathbf{R} , the observation vector can be modified to

$$\tilde{\mathbf{y}} = \frac{1}{2}(\mathbf{y} + \mathbf{R}\mathbf{e}) \quad (6.C.21)$$

where $\mathbf{e} = [1, 1, \dots, 1]^T$. Let $\tilde{\mathbf{b}} = (\mathbf{b} + \mathbf{e})/2$. Then, applying (6.C.2), (6.C.21) can be expressed as

$$\tilde{\mathbf{y}} = \mathbf{R}\tilde{\mathbf{b}} + \frac{1}{2}\mathbf{n} \quad (6.C.22)$$

When the MLD-MUD is operated in the context of (6.C.22), we obtain an equivalent quadratic 0-1 programming problem, which can be expressed as

$$\hat{\tilde{\mathbf{b}}} = \arg \min_{\tilde{\mathbf{b}} \in \{0, 1\}^K} \{\tilde{\mathbf{b}}^T \mathbf{R} \tilde{\mathbf{b}} - 2\Re\{\tilde{\mathbf{y}}^H \tilde{\mathbf{b}}\}\} \quad (6.C.23)$$

$$= \arg \min_{\tilde{\mathbf{b}} \in \{0, 1\}^K} \left\{ \sum_{i=1}^K \sum_{j \neq i}^K R_{ij} \tilde{b}_i \tilde{b}_j + \sum_{i=1}^K (R_{ii} \tilde{b}_i - 2\Re\{\tilde{y}_i^*\}) \tilde{b}_i \right\} \quad (6.C.24)$$

where R_{ij} denotes the (i, j) th element of \mathbf{R} . Furthermore, since either $\tilde{b}_i = 0$ or $\tilde{b}_i = 1$, (6.C.24) can be written as

$$\begin{aligned}\hat{\tilde{\mathbf{b}}} &= \arg \min_{\tilde{\mathbf{b}} \in \{0, 1\}^K} \left\{ \sum_{i=1}^K \sum_{j \neq i}^K R_{ij} \tilde{b}_i \tilde{b}_j + \sum_{i=1}^K (R_{ii} - 2\Re\{\tilde{y}_i^*\}) \tilde{b}_i \right\} \\ &= \arg \min_{\tilde{\mathbf{b}} \in \{0, 1\}^K} \left\{ \sum_{i=1}^K \left(\sum_{j \neq i}^K R_{ij} \tilde{b}_j + R_{ii} - 2\Re\{\tilde{y}_i^*\} \right) \tilde{b}_i \right\}\end{aligned}\quad (6.C.25)$$

The coordinate descent search (CDS) algorithm is based on the following observation. According to (6.C.25), let us assume that a temporary solution to $\tilde{\mathbf{b}}$ is given by $\tilde{\mathbf{b}} = [\tilde{b}_1, \tilde{b}_2, \dots, \tilde{b}_K]^T$. Then, when \tilde{b}_k is flipped from 0(1) to 1(0), the cost value variation is given by $(\sum_{j \neq k}^K R_{kj} \tilde{b}_j + R_{kk} - 2\Re\{\tilde{y}_k^*\})$. In this case, if \tilde{b}_k in $\tilde{\mathbf{b}}$ is in error, the resultant cost value after the flipping will decrease. Therefore, let us express

$$\begin{aligned}J(n) &= \sum_{i=1}^K \left(\sum_{j \neq i}^K R_{ij} \tilde{b}_j(n) + R_{ii} - 2\Re\{\tilde{y}_i^*\} \right) \tilde{b}_i(n) \\ J_k(n) &= \left(\sum_{j \neq k}^K R_{kj} \tilde{b}_j(n) + R_{kk} - 2\Re\{\tilde{y}_k^*\} \right) (2\tilde{b}_k(n) - 1), \quad k = 1, 2, \dots, K\end{aligned}\quad (6.C.26)$$

Then, in the context of the CDS algorithm, the bit, say $\tilde{b}_l(n)$, corresponding to the highest value in $\{J_k(n) > 0\}$ is flipped. After the flipping, the terms in (6.C.26) can be updated to $(n+1)$ and the search process can be proceeded, until for all k we have $J_k(n) \leq 0$.

The above search process may be simplified with the aid of the properties of the related matrices. Please refer to reference [179] for the details. The above-described CDS algorithm flips one bit each time; this algorithm is hence referred to as the *Descent I* algorithm. Explicitly, the CDS algorithm may flip two, three, etc. bits each time, yielding the *Descent II*, *III*, etc. algorithm.

Note that the CDS algorithm can be viewed as searching for a discrete local minimum in the neighbourhood of the point $\tilde{\mathbf{b}} = [\tilde{b}_1, \tilde{b}_2, \dots, \tilde{b}_K]^T$. As indicated in reference [179], the *Descent I* algorithm in the worst case may require an exponential number of iterations. However, the complexity of the *Descent I* algorithm in practice is polynomial.

6.C.1.5 Evolutionary Programming Algorithm

In reference [180] the evolutionary programming (EP) algorithm has been introduced to attack the problem of MLD-MUD. The EP algorithm can be described as follows.

Let

$$\mathcal{T}_M = \{\tilde{\mathbf{b}}_1, \tilde{\mathbf{b}}_2, \dots, \tilde{\mathbf{b}}_M\} \quad (6.C.27)$$

be a set containing M number of binary vectors for the initial test. The M binary vectors may be randomly selected from \mathbf{B} seen in (6.C.4). However, in order to improve the convergence speed, \mathcal{T}_M may include the vector, say, $\hat{\mathbf{b}}$, which is estimated based on a conventional single-user or a low-complexity linear multiuser detector, such as that studied in Sections 6.2.1 to 6.2.6.

The cost values for the binary trial vectors in (6.C.27) can be computed using (6.C.5) as

$$L(\tilde{\mathbf{b}}_i) = \tilde{\mathbf{b}}_i^T \mathbf{R} \tilde{\mathbf{b}}_i - 2\Re\{\mathbf{y}^H \tilde{\mathbf{b}}_i\}, \quad i = 1, 2, \dots, M \quad (6.C.28)$$

Based on (6.C.27) and (6.C.28), the EP algorithm can now be implemented by the following steps:

Step 1: Based on \mathcal{T}_M , a set of \mathcal{T}_{2M} containing $2M$ binary vectors is formed as

$$\mathcal{T}_{2M} = \{\tilde{\mathbf{b}}_1, \tilde{\mathbf{b}}_2, \dots, \tilde{\mathbf{b}}_M; \tilde{\mathbf{b}}_{M+1}, \tilde{\mathbf{b}}_{M+2}, \dots, \tilde{\mathbf{b}}_{2M}\} \quad (6.C.29)$$

where for each given i , $\tilde{\mathbf{b}}_{M+i}$ is formed as

$$\tilde{\mathbf{b}}_{M+i} = \text{sign}(\tilde{\mathbf{b}}_i + \mathbf{n}_i) \quad (6.C.30)$$

where \mathbf{n}_i is a Gaussian random vector with zero mean and a covariance matrix $\sigma^2 \mathbf{I}_K$, $\text{sign}(x)$ is a sign function satisfying $\text{sign}(x) = +1$ if $x > 0$ and $\text{sign}(x) = -1$, otherwise.

Step 2: Compute the cost values of the added binary vectors $\tilde{\mathbf{b}}_{M+1}, \tilde{\mathbf{b}}_{M+2}, \dots, \tilde{\mathbf{b}}_{2M}$ as

$$L(\tilde{\mathbf{b}}_{M+i}) = \tilde{\mathbf{b}}_{M+i}^T \mathbf{R} \tilde{\mathbf{b}}_{M+i} - 2\Re\{\mathbf{y}^H \tilde{\mathbf{b}}_{M+i}\}, \quad i = 1, 2, \dots, M \quad (6.C.31)$$

and form a cost value set as

$$\mathcal{L} = \{L(\tilde{\mathbf{b}}_1), L(\tilde{\mathbf{b}}_2), \dots, L(\tilde{\mathbf{b}}_{2M})\} \quad (6.C.32)$$

Step 3: Arrange the parents and offspring, $\tilde{\mathbf{b}}_i, i = 1, 2, \dots, 2M$, in ascending order of their cost values, and form an updated binary test vector set by the first M vectors as

$$\mathcal{T}_M = \{\tilde{\mathbf{b}}_1, \tilde{\mathbf{b}}_2, \dots, \tilde{\mathbf{b}}_M\} \quad (6.C.33)$$

which contains the M number of vectors in (6.C.29) corresponding to the M lowest cost values in (6.C.32).

Step 4: Return to Step 1, unless the preset conditions have been achieved or the available execution time is reached.

Note that one of the preset conditions might be a preset cost value. Note, furthermore, that the variance σ^2 for generating \mathbf{n}_i in (6.C.30) determines the range of locality of the offspring around its parents.

6.C.1.6 Genetic Algorithm

The genetic algorithm (GA) is in fact another evolutionary search algorithm. It belongs to the family of stochastic search algorithms. In reference [181] the GA has been employed to find the solution of the MLD-MUD in CDMA systems. In summary, the GA for multiuser detection in CDMA systems includes the following operations.

Step 1 (Initialization): The GA selects the initial population randomly from the solution space \mathcal{B} as shown in (6.C.4), which can be expressed as

$$\mathcal{T}_M = \{\tilde{\mathbf{b}}_1, \tilde{\mathbf{b}}_2, \dots, \tilde{\mathbf{b}}_M\} \quad (6.C.34)$$

for a population size M . Note that in order to enhance the search speed, a solution to a conventional single-user detector or a low-complexity linear multiuser detector may be included in the initial population of (6.C.34).

Step 2 (Fitness evaluation): Computing the fitness values of the population in \mathcal{T}_M according to

$$L(\tilde{\mathbf{b}}_i) = C + 2\Re\{\mathbf{y}^H \tilde{\mathbf{b}}_i\} - \tilde{\mathbf{b}}_i^T \mathbf{R} \tilde{\mathbf{b}}_i, \quad i = 1, 2, \dots, M \quad (6.C.35)$$

where a constant C is applied such that the fitness value is positive. The fitness values are then mapped into probabilities, say $\{P_1, P_2, \dots, P_M\}$, according to a given (user defined) mapping algorithm. A higher fitness value is associated with a higher probability. For example, one fitness-to-probability mapping approach can be as follows:

$$P_i = \frac{L(\tilde{\mathbf{b}}_i)}{\sum_{l=1}^M L(\tilde{\mathbf{b}}_l)}, \quad i = 1, 2, \dots, M \quad (6.C.36)$$

Step 3 (Genetic operation): This step can further be divided into the following substeps:

- Parent selection: According to the probability values of $\{P_1, P_2, \dots, P_M\}$, parents in the form of $\tilde{\mathbf{b}}_i$ are selected from \mathcal{T}_M : $\tilde{\mathbf{b}}_i$ is selected as a parent with a probability of P_i . Since some probability values are higher than the others, it is possible that [71, 181] a $\tilde{\mathbf{b}}_i$ with relatively high probability (high fitness value) may be selected more than one time, while a $\tilde{\mathbf{b}}_i$ with relatively low probability (low fitness value) may not be selected at all;
- Crossover: The crossover operation creates two offsprings by combining the subparts of the bit strings of the two selected parents in the form of $(\tilde{\mathbf{b}}_i, \tilde{\mathbf{b}}_j)$. For example, as shown in reference [181], some bits in $\tilde{\mathbf{b}}_i$ are exchanged with the corresponding bits in $\tilde{\mathbf{b}}_j$. Explicitly, there are various ways to implement the crossover. The simplest way is the one-point crossover, where only one subpart of the bit strings of the two selected parents are exchanged. The crossover position can usually be selected randomly.

The crossover probability, say P_c , is user defined, which is usually set to a high value (> 0.9). If the crossover is not allowed between two parents, the parents are then forwarded directly to the next generation without any change.

- Mutation: The mutation operation inverts each data bit of a parent controlled by a so-called mutation probability, say P_m . The probability of mutation is usually set to a low value, such as 0.01.

Step 4 (New generation forming): The fitness values of all the offspring candidate binary sequences are computed. Then, \mathcal{T}_M is updated by replacing all or part of its binary sequences by their offspring candidate sequences with the highest fitness values, in order to form a new generation.

Step 5: The search process continues by returning to Step 3, or terminates, when the convergence condition is satisfied or the maximum search time is reached.

Note that the performance and search speed of the GA can be improved if *a priori* information, such as that in the form of (6.C.6) or (6.C.7), is available. The performance and search speed of the GA can also be improved when it is implemented with the decision-feedback multiuser detection [181]. It has been shown [181] that the complexity of the GA is of the order of $O(K^2)$ for a large K value. Furthermore, the GA can be invoked for joint multiuser detection and channel estimation [71].

6.C.1.7 Ant-Colony-Inspired Search

The search approach inspired by the behaviour of an ant-colony, ACS for short, is a high-efficiency optimization approach for solving the exponentially hard discrete problems such as the MLD-MUD problem [182]. It belongs to the family of statistical searches. The ACS has been considered for MLD-MUD, e.g., in reference [183]. In order to describe the ACS algorithm, let us first define some arguments.

A cost function is defined by (6.C.5). The reliability-related *a priori* matrix $\lambda(n)$ for the n th round search is defined in (6.C.6), where $\lambda(1)$ represents the *a priori* information obtained from other ways, such as from a low-complexity linear detector. The reliability $\lambda(n)$ is analogous to the pheromone laid on the trails by the ants before the $(n+1)$ th round explores. Additionally, we define

$$\begin{aligned}\mathbf{b}_0^{(m)} &= [\emptyset]^T, \\ \mathbf{b}_k^{(m)} &= [\mathbf{b}_{k-1}^{(m)}, b_k^{(m)}]^T, \quad k = 1, 2, \dots, \mathcal{K}; m = 1, 2, \dots, M\end{aligned}\quad (6.C.37)$$

where \emptyset means empty, M represents the number of parallel searches (ants) carried out simultaneously.

Before starting a new search round, the reliabilities (pheromones) are mapped to the form of probabilities according to a user-defined function. This mapping function should be defined by considering both the convergence speed and the availability of finding the global optimal solution. After the mapping, let the probabilities be

$$\mathbf{P}(n) = \begin{bmatrix} P_{1+}(n) & P_{2+}(n) & \cdots & P_{\mathcal{K}+}(n) \\ P_{1-}(n) & P_{2-}(n) & \cdots & P_{\mathcal{K}-}(n) \end{bmatrix}, \quad n = 1, \dots \quad (6.C.38)$$

With the ACS algorithm, each of the M ants tries to build a solution $\mathbf{b}_{\mathcal{K}}^{(m)}$ ($m = 1, 2, \dots, M$) from $\mathbf{b}_0^{(m)}$ with the aid of the *a priori* information of (6.C.38). The procedure can be described as follows:

Step 1: Initialization: $\mathbf{b}_0^{(m)}$, $\mathbf{P}(n)$, $k = 1, m = 1, 2, \dots, M$;

Step 2: For all $m = 1, 2, \dots, M$, the ants construct $\mathbf{b}_k^{(m)} = [\mathbf{b}_{k-1}^{(m)}, b_k^{(m)}]^T$, where $b_k^{(m)}$ is chosen to be +1 with a probability of $P_{k+}(n)$, while chosen to be -1 with a probability of $P_{k-}(n)$;

Step 3: If $k < \mathcal{K}$, set $k = k + 1$ and return to Step 2; otherwise, if $k = \mathcal{K}$, stop.

Explicitly, the above process generates M number of candidate solutions $\{\mathbf{b}_{\mathcal{K}}^{(1)}, \mathbf{b}_{\mathcal{K}}^{(2)}, \dots, \mathbf{b}_{\mathcal{K}}^{(M)}\}$. Let the costs in the context of these candidate solutions obtained at the n th round

search be computed as

$$L(\mathbf{b}_{\mathcal{K}}^{(m)}) = (\mathbf{b}_{\mathcal{K}}^{(m)})^T \mathbf{R} \mathbf{b}_{\mathcal{K}}^{(m)} - 2\Re\{\mathbf{y}^H \mathbf{b}_{\mathcal{K}}^{(m)}\}, \quad m = 1, 2, \dots, M \quad (6.C.39)$$

With the cost values computed in (6.C.39), the reliabilities (pheromones) in $\lambda(n)$ are updated to $\lambda(n+1)$ to be more reliable. The updating algorithm is user-defined and should take into account both the convergence speed and global optimal. For example, $\lambda_{k+}(n+1)$ and $\lambda_{k-}(n+1)$ can be updated according to

$$\begin{aligned} \lambda_{k+}(n+1) &= (1-\rho)\lambda_{k+}(n) + \sum_{\text{for all } m: b_k^{(m)}=+1} \Delta\lambda_{k+}^{(m)} + \Delta\tilde{\lambda}_{k+} \\ \lambda_{k-}(n+1) &= (1-\rho)\lambda_{k-}(n) + \sum_{\text{for all } m: b_k^{(m)}=-1} \Delta\lambda_{k-}^{(m)} + \Delta\tilde{\lambda}_{k-} \\ k &= 1, 2, \dots, \mathcal{K} \end{aligned} \quad (6.C.40)$$

where ρ is a forgetting factor (*evaporation rate*). The forgetting factor ρ is used to avoid unlimited accumulation of the reliability and also to avoid convergence to a local optimum solution. In (6.C.40) $\Delta\lambda_{k+}^{(m)}$ is the quantity of reliability (pheromone) added to $b_k = +1$, when $b_k^{(m)} = +1$, while $\Delta\lambda_{k-}^{(m)}$ is the quantity of reliability (pheromone) added to $b_k = -1$, if $b_k^{(m)} = -1$. $\Delta\lambda_{k+}^{(m)}$ and $\Delta\lambda_{k-}^{(m)}$ may be chosen as

$$\Delta\lambda_{k+}^{(m)} = \Delta\lambda_{k-}^{(m)} = C/L(\mathbf{b}_{\mathcal{K}}^{(m)}) \quad (6.C.41)$$

where C is a constant. Equation (6.C.41) implies that higher reliability is added if the cost is lower. Furthermore, if $b_k = +1$ or $b_k = -1$ is the solution of the best of the M solutions, a quantity of extra reliability of $\Delta\tilde{\lambda}_{k+}$ or $\Delta\tilde{\lambda}_{k-}$ is then added, where $\Delta\tilde{\lambda}_{k+}$ and $\Delta\tilde{\lambda}_{k-}$ can be set as

$$\Delta\tilde{\lambda}_{k+} = \Delta\tilde{\lambda}_{k-} = C'/L_{\text{Lowest}} \quad (6.C.42)$$

with L_{Lowest} being the lowest cost in $\{L(\mathbf{b}_{\mathcal{K}}^{(m)})\}$.

Having obtained the updated reliabilities of $\lambda(n+1)$, the detector can start a new round of search based on $\lambda(n+1)$, if the preset constraints are not satisfied. When the preset constraints are satisfied, decisions of the \mathcal{K} bits can be made based on $\lambda(n+1)$ by finding the path corresponding to the higher reliability. Specifically, the decision can be made according to

$$b_k = \begin{cases} +1, & \text{if } \lambda_{k+}(n+1) > \lambda_{k-}(n+1) \\ -1, & \text{if } \lambda_{k+}(n+1) \leq \lambda_{k-}(n+1) \end{cases} \quad (6.C.43)$$

Note that one scheme for mapping the reliabilities to probabilities is [182]

$$\begin{aligned} P_{k+}(n) &= \frac{\lambda_{k+}^\alpha(n)\eta_{k+}^\beta}{\lambda_{k+}^\alpha(n)\eta_{k+}^\beta + \lambda_{k-}^\alpha(n)\eta_{k-}^\beta} \\ P_{k-}(n) &= \frac{\lambda_{k-}^\alpha(n)\eta_{k-}^\beta}{\lambda_{k+}^\alpha(n)\eta_{k+}^\beta + \lambda_{k-}^\alpha(n)\eta_{k-}^\beta} \end{aligned} \quad (6.C.44)$$

where the parameters α and β control the relative importance of the observed reliability $\lambda_{k+}(n)$ ($\lambda_{k-}(n)$) versus the heuristic information η_{k+} (η_{k-}). The heuristic information η_{k+} (η_{k-}) can be any available *a priori* concerning $b_k = +1$ ($b_k = -1$). For the MLD-MUD, the heuristic information η_{k+} (η_{k-}) can be set as the *a priori* information about $b_k = +1$ ($b_k = -1$) after a low-complexity linear detector.

6.C.2 Non-Search Algorithms

So far, a range of search algorithms have been considered for tackling the MLD-MUD problem. In this section a few approaches not using search for the MLD-MUD are considered. Specifically, the EP algorithm, probabilistic data associated algorithm (PDA) and the semidefinite programming relaxation (SDPR) algorithm are derived. Let us first consider the EP algorithm.

6.C.2.1 Expectation Maximization

The principles of the expectation maximization (EM) algorithm can be found, e.g., in [175], which, when connecting it with the MLD-MUD, can be described as follows.

Let us consider the \mathcal{K} -length observation vector

$$\mathbf{y} = \mathbf{R}\mathbf{b} + \mathbf{n} \quad (6.C.45)$$

where \mathbf{R} is the correlation matrix of the user signatures, \mathbf{n} is zero-mean Gaussian with a covariance matrix $\sigma^2 \mathbf{R}$, while \mathbf{b} is in the form

$$\mathbf{b} = [b_1, b_2, \dots, b_{\mathcal{K}}]^T \quad (6.C.46)$$

We define

$$\begin{aligned} \mathbf{y}^{(k)} &= [y_1^{(k)}, y_2^{(k)}, \dots, y_{\mathcal{K}}^{(k)}]^T \\ \mathbf{n}^{(k)} &= [n_1^{(k)}, n_2^{(k)}, \dots, n_{\mathcal{K}}^{(k)}]^T, \quad k = 1, 2, \dots, \mathcal{K} \end{aligned} \quad (6.C.47)$$

where $\mathbf{n}^{(k)}$ is a zero-mean Gaussian vector with a covariance matrix $\sigma_k^2 \mathbf{R}$ and satisfies

$$\sum_{k=1}^{\mathcal{K}} \sigma_k^2 = \sigma^2 \quad (6.C.48)$$

Furthermore, it can be shown that $\mathbf{n}^{(k)}$ is independent of $\mathbf{n}^{(l)}$ when $l \neq k$. This is because $\mathbf{n}^{(k)}$ is in the form of $\mathbf{n}^{(k)} = \mathbf{H}^H \tilde{\mathbf{n}}^{(k)}$, where $\tilde{\mathbf{n}}^{(k)}$ represents the component noise vector before the correlation operation. Hence, when $l \neq k$, $\tilde{\mathbf{n}}^{(k)}$ is independent of $\tilde{\mathbf{n}}^{(l)}$, yielding $\mathbf{n}^{(k)}$ is independent of $\mathbf{n}^{(l)}$ when $l \neq k$. Let \mathbf{R}_k represents the k th column of \mathbf{R} . Furthermore, let

$$\mathbf{y}^{(k)} = \mathbf{R}_k b_k + \mathbf{n}^{(k)}, \quad k = 1, 2, \dots, \mathcal{K} \quad (6.C.49)$$

Then, it can be shown that (6.C.45) can be written as

$$\mathbf{y} = \sum_{k=1}^{\mathcal{K}} \mathbf{y}^{(k)} = \sum_{k=1}^{\mathcal{K}} \mathbf{R}_k b_k + \sum_{k=1}^{\mathcal{K}} \mathbf{n}^{(k)} \quad (6.C.50)$$

where $\mathbf{n} = \sum_{k=1}^{\mathcal{K}} \mathbf{n}^{(k)}$ has zero mean and a covariance matrix of $\sigma^2 \mathbf{R}$.

It can be readily shown that $\mathbf{y}^{(k)}$ is an independent Gaussian random vector obeying the PDF of

$$f(\mathbf{y}^{(k)}; b_k) = \frac{1}{(\pi \sigma_k^2)^{\mathcal{K}} \det(\mathbf{R})} \exp[-(\mathbf{y}^{(k)} - \mathbf{R}_k b_k)^H \mathbf{R}^{-1} (\mathbf{y}^{(k)} - \mathbf{R}_k b_k)/\sigma_k^2] \\ k = 1, 2, \dots, \mathcal{K} \quad (6.C.51)$$

Consequently, the joint PDF of $\mathbf{y}^{(1)}, \mathbf{y}^{(2)}, \dots, \mathbf{y}^{(\mathcal{K})}$ can be expressed as

$$f(\mathbf{y}^{(1)}, \mathbf{y}^{(2)}, \dots, \mathbf{y}^{(\mathcal{K})}; \mathbf{b}) = \frac{1}{\det(\mathbf{R}) \prod_{k=1}^{\mathcal{K}} (\pi \sigma_k^2)^{\mathcal{K}}} \\ \times \exp \left[- \sum_{k=1}^{\mathcal{K}} \frac{1}{\sigma_k^2} (\mathbf{y}^{(k)} - \mathbf{R}_k b_k)^H \mathbf{R}^{-1} (\mathbf{y}^{(k)} - \mathbf{R}_k b_k) \right] \quad (6.C.52)$$

According to the principles of EP, for the MLD-MUD problem, the problem described in (6.C.1) is equivalent to the problem of

$$\hat{\mathbf{b}} = \arg \max_{\mathbf{b} \in \mathbf{B}} \{E[\ln f(\mathbf{y}^{(1)}, \mathbf{y}^{(2)}, \dots, \mathbf{y}^{(\mathcal{K})}; \mathbf{b} | \mathbf{y})]\} \quad (6.C.53)$$

Applying (6.C.52) and ignoring the items that are not related to \mathbf{b} , we obtain

$$\ln f(\mathbf{y}^{(1)}, \mathbf{y}^{(2)}, \dots, \mathbf{y}^{(\mathcal{K})}; \mathbf{b} | \mathbf{y}) = \sum_{k=1}^{\mathcal{K}} \frac{1}{\sigma_k^2} (2 \Re \{(\mathbf{y}^{(k)})^H \mathbf{R}^{-1} \mathbf{R}_k b_k\}) \\ = \sum_{k=1}^{\mathcal{K}} \frac{2b_k}{\sigma_k^2} (\Re \{\mathbf{R}_k^H \mathbf{R}^{-1} \mathbf{y}^{(k)}\}) \quad (6.C.54)$$

Hence, (6.C.53) can be described as

$$\hat{\mathbf{b}} = \arg \max_{\mathbf{b} \in \mathbf{B}} \left\{ E \left[\sum_{k=1}^{\mathcal{K}} \frac{2b_k}{\sigma_k^2} (\Re \{\mathbf{R}_k^H \mathbf{R}^{-1} \mathbf{y}^{(k)}\}) \right] \right\} \\ = \arg \max_{\mathbf{b} \in \mathbf{B}} \left\{ \sum_{k=1}^{\mathcal{K}} \frac{2b_k}{\sigma_k^2} (\Re \{\mathbf{R}_k^H \mathbf{R}^{-1} E[\mathbf{y}^{(k)}]\}) \right\} \quad (6.C.55)$$

Since in the above problem each term in the sum contains only one of the \mathcal{K} bits, therefore it is sufficient to maximize each term separately in order to maximize the whole sum. Consequently, (6.C.55) shows that the optimization problem in (6.C.1) is divided into \mathcal{K} parallel optimization problems

$$\hat{b}_k = \arg \max_{b_k \in \{+1, -1\}} \left\{ \frac{2b_k}{\sigma_k^2} (\Re \{\mathbf{R}_k^H \mathbf{R}^{-1} E[\mathbf{y}^{(k)}]\}) \right\}, \quad k = 1, 2, \dots, \mathcal{K} \quad (6.C.56)$$

However, in (6.C.56) $\mathbf{y}^{(k)}$ is unobservable and hence the term $E[\mathbf{y}^{(k)}]$ cannot be computed. For this sake, the problems in (6.C.56) are suggested [184, 185] to be optimized

in an iterative way. Specifically, let at the n th iteration the estimations to \mathbf{b} be represented by $\hat{\mathbf{b}}(n) = [\hat{b}_1(n), \hat{b}_2(n), \dots, \hat{b}_{\mathcal{K}}(n)]^T$. Then, $E[\mathbf{y}^{(k)}]$ can be approximated as

$$E[\mathbf{y}^{(k)}] = \mathbf{R}_k \hat{b}_k(n) + \frac{\sigma_k^2}{\sigma^2} [\mathbf{y} - \mathbf{R}\hat{\mathbf{b}}(n)], \quad k = 1, 2, \dots, \mathcal{K} \quad (6.C.57)$$

With the aid of (6.C.57), the estimation to \mathbf{b} at the $(n+1)$ th iteration can be formed as

$$\begin{aligned} \hat{b}_k(n+1) &= \arg \max_{b_k \in \{+1, -1\}} \left\{ \frac{2b_k}{\sigma_k^2} \left(\Re \left\{ \mathbf{R}_k^H \mathbf{R}^{-1} \left(\mathbf{R}_k \hat{b}_k(n) + \frac{\sigma_k^2}{\sigma^2} [\mathbf{y} - \mathbf{R}\hat{\mathbf{b}}(n)] \right) \right\} \right) \right\} \\ k &= 1, 2, \dots, \mathcal{K} \end{aligned} \quad (6.C.58)$$

Furthermore, since b_k is binary, the estimation to $\hat{b}_k(n+1)$ at the $(n+1)$ th iteration can be decided as

$$\begin{aligned} \hat{b}_k(n+1) &= \text{sign} \left(\Re \left\{ \mathbf{R}_k^H \mathbf{R}^{-1} \left(\mathbf{R}_k \hat{b}_k(n) + \frac{\sigma_k^2}{\sigma^2} [\mathbf{y} - \mathbf{R}\hat{\mathbf{b}}(n)] \right) \right\} \right) \\ k &= 1, 2, \dots, \mathcal{K} \end{aligned} \quad (6.C.59)$$

Note that the EP algorithm has a complexity that is only linear in \mathcal{K} . However, it may converge to a local optimum solution. In [185] there are some other modified algorithms that may be used to improve the convergence speed or yield a global optimum solution.

Note, furthermore, that the above derivation is based on the conventional correlation detector's output as seen in (6.C.45). The derivation can also be based directly on the zero-forcing solution. In this case, we have

$$\mathbf{y} = \mathbf{b} + \mathbf{n} \quad (6.C.60)$$

where \mathbf{n} is zero-mean Gaussian but with a covariance matrix $\sigma^2 \mathbf{R}^{-1}$. Let $\mathbf{1}_k$ represent a vector with zero entries except the k th position, which is 1. Then, following the above steps, it can be shown that (6.C.59) can be modified to

$$\hat{b}_k(n+1) = \text{sign} \left(\Re \left\{ \mathbf{1}_k^H \mathbf{R} \left(\mathbf{1}_k \hat{b}_k(n) + \frac{\sigma_k^2}{\sigma^2} [\mathbf{y} - \hat{\mathbf{b}}(n)] \right) \right\} \right), \quad k = 1, 2, \dots, \mathcal{K} \quad (6.C.61)$$

6.C.2.2 Probabilistic Data Associated Algorithm

The PDA algorithm [186] is an iterative algorithm. The PDA algorithm usually starts the iteration following a conventional linear decorrelating (zero-forcing) MUD, although extension to using other linear MUDs is explicit. Let the observation vector be given by (6.C.2). Then, after the decorrelating operation, the observation vector can be expressed as

$$\tilde{\mathbf{y}} = \mathbf{b} + \tilde{\mathbf{n}} = b_k \mathbf{e}_k + \sum_{l \neq k} b_l \mathbf{e}_l + \tilde{\mathbf{n}} \quad (6.C.62)$$

where $\tilde{\mathbf{n}} = \mathbf{R}^{-1} \mathbf{n}$ is coloured Gaussian with zero mean and a covariance matrix of $\sigma^2 \mathbf{R}^{-1}$. Furthermore, in (6.C.62) \mathbf{e}_l ($l = 1, 2, \dots, \mathcal{K}$) is a \mathcal{K} -length column vector with zero entries except the l th entry of one.

The PDA algorithm associates each of the bits in \mathbf{b} with a probability, which is expressed as

$$\mathbf{P}_+(n) = \{P_{1+}(n), P_{2+}(n), \dots, P_{\mathcal{K}+}(n)\}, \quad n \geq 0 \quad (6.C.63)$$

where $P_{k+}(n)$ is the probability that $b_k = +1$ after the n th iteration. Correspondingly, the $P_{k-}(n)$ is the probability that $b_k = -1$, $P_{k-}(n) = 1 - P_{k+}(n)$.

The PDA algorithm requires the *a posteriori* probability to be computed

$$P_{k+}(n) = P(b_k = +1 | \tilde{\mathbf{y}}, \{P_{l+}(n)\}_{l \neq k}), \quad k = 1, 2, \dots, \mathcal{K} \quad (6.C.64)$$

which depends on the $2^{\mathcal{K}-1}$ combinations of $\{b_l\}_{l \neq k}$ and hence the computation is exponentially hard with the value of \mathcal{K} .

In order to simplify the computation, a Gaussian approximation may be invoked to compute $P_{k+}(n)$ in (6.C.64). Specifically, from (6.C.62) we have

$$b_k \mathbf{e}_k = \tilde{\mathbf{y}} - \sum_{l \neq k} b_l \mathbf{e}_l + \tilde{\mathbf{n}} \quad (6.C.65)$$

When the Gaussian approximation is invoked, $b_k \mathbf{e}_k$ can be approximated as a Gaussian vector with a PDF expressed as $\mathcal{N}(\boldsymbol{\mu}_k, \boldsymbol{\Omega}_k)$, where

$$\begin{aligned} \boldsymbol{\mu}_k &= E[b_k \mathbf{e}_k] \\ &= \tilde{\mathbf{y}} - \sum_{l \neq k} (2P_{l+}(n) - 1) \mathbf{e}_l \end{aligned} \quad (6.C.66)$$

$$\begin{aligned} \boldsymbol{\Omega}_k &= E[(b_k \mathbf{e}_k - \boldsymbol{\mu}_k)(b_k \mathbf{e}_k - \boldsymbol{\mu}_k)^T] \\ &= E\left[\left(-\sum_{l \neq k} b_l \mathbf{e}_l - \sum_{l \neq k} (2P_{l+}(n) - 1) \mathbf{e}_l + \tilde{\mathbf{n}}\right)\right. \\ &\quad \times \left.\left(-\sum_{l \neq k} b_l \mathbf{e}_l - \sum_{l \neq k} (2P_{l+}(n) - 1) \mathbf{e}_l + \tilde{\mathbf{n}}\right)^T\right] \\ &= \sum_{l \neq k} 4P_{l+}(n)(1 - P_{l+}(n)) \mathbf{e}_l \mathbf{e}_l^T + \sigma^2 \mathbf{R}^{-1} \end{aligned} \quad (6.C.67)$$

Consequently, the PDF of $\mathcal{N}(\boldsymbol{\mu}_k, \boldsymbol{\Omega}_k)$ can be expressed as

$$\mathcal{N}(\boldsymbol{\mu}_k, \boldsymbol{\Omega}_k) \sim \exp\left[-\frac{1}{2}(b_k \mathbf{e}_k - \boldsymbol{\mu}_k)^T \boldsymbol{\Omega}_k^{-1} (b_k \mathbf{e}_k - \boldsymbol{\mu}_k)\right] \quad (6.C.68)$$

Furthermore, it can be shown that we have

$$\frac{P_{k+}(n)}{1 - P_{k+}(n)} = \exp(-2\boldsymbol{\mu}_k^T \boldsymbol{\Omega}_k^{-1} \mathbf{e}_k), \quad k = 1, 2, \dots, \mathcal{K} \quad (6.C.69)$$

As shown in reference [186], $\boldsymbol{\mu}_k$ and $\boldsymbol{\Omega}_k$ can be computed in an iterative way. Let

$$\begin{aligned} \boldsymbol{\mu} &= \tilde{\mathbf{y}} - \sum_l (2P_{l+}(n) - 1) \mathbf{e}_l \\ &= \boldsymbol{\mu}_k - (2P_{k+}(n) - 1) \mathbf{e}_k \end{aligned} \quad (6.C.70)$$

$$\begin{aligned}\boldsymbol{\Omega} &= \sum_{l \neq k} 4P_{l+}(n)(1 - P_{l+}(n))\mathbf{e}_l\mathbf{e}_l^T + \sigma^2\mathbf{R}^{-1} \\ &= \boldsymbol{\Omega}_k + 4P_{k+}(n)(1 - P_{k+}(n))\mathbf{e}_k\mathbf{e}_k^T\end{aligned}\quad (6.C.71)$$

Then, with the aid of the *matrix inverse lemma* seen in (6.B.2), we obtain

$$\boldsymbol{\Omega}^{-1} = \boldsymbol{\Omega}_k^{-1} - \frac{4P_{k+}(n)(1 - P_{k+}(n))\boldsymbol{\Omega}_k^{-1}\mathbf{e}_k\mathbf{e}_k^T\boldsymbol{\Omega}_k^{-1}}{1 + 4P_{k+}(n)(1 - P_{k+}(n))\mathbf{e}_k^T\boldsymbol{\Omega}_k^{-1}\mathbf{e}_k} \quad (6.C.72)$$

Therefore, the iteration equations can be described as follows: given $\boldsymbol{\mu}(n)$, $\boldsymbol{\Omega}(n)$ and $P_{k+}(n)$, $\boldsymbol{\mu}_k(n)$ and $\boldsymbol{\Omega}_k(n)$ are updated to $\boldsymbol{\mu}_k(n+1)$ and $\boldsymbol{\Omega}_k(n+1)$ as

$$\begin{aligned}\boldsymbol{\mu}_k(n+1) &= \boldsymbol{\mu}(n) + (2P_{k+}(n) - 1)\mathbf{e}_k \\ \boldsymbol{\Omega}_k^{-1}(n+1) &= \boldsymbol{\Omega}_k^{-1}(n) + \frac{4P_{k+}(n)(1 - P_{k+}(n))\boldsymbol{\Omega}_k^{-1}(n)\mathbf{e}_k\mathbf{e}_k^T\boldsymbol{\Omega}_k^{-1}(n)}{1 + 4P_{k+}(n)(1 - P_{k+}(n))\mathbf{e}_k^T\boldsymbol{\Omega}_k^{-1}(n)\mathbf{e}_k}\end{aligned}\quad (6.C.73)$$

With the updated $\boldsymbol{\mu}_k(n+1)$ and $\boldsymbol{\Omega}_k(n+1)$, the probability $P_{k+}(n)$ can now be recomputed using (6.C.69) yielding its updated version of $P_{k+}(n+1)$. With the updated versions of $\boldsymbol{\mu}_k(n+1)$, $\boldsymbol{\Omega}_k(n+1)$ and $P_{k+}(n+1)$, $\boldsymbol{\mu}(n)$ and $\boldsymbol{\Omega}(n)$ can be updated to $\boldsymbol{\mu}(n+1)$ and $\boldsymbol{\Omega}(n+1)$ as

$$\begin{aligned}\boldsymbol{\mu}(n+1) &= \boldsymbol{\mu}_k(n+1) - (2P_{k+}(n+1) - 1)\mathbf{e}_k \\ \boldsymbol{\Omega}^{-1}(n+1) &= \boldsymbol{\Omega}_k^{-1}(n+1) - \frac{4P_{k+}(n+1)(1 - P_{k+}(n+1))\boldsymbol{\Omega}_k^{-1}(n+1)\mathbf{e}_k\mathbf{e}_k^T\boldsymbol{\Omega}_k^{-1}(n+1)}{1 + 4P_{k+}(n+1)(1 - P_{k+}(n+1))\mathbf{e}_k^T\boldsymbol{\Omega}_k^{-1}(n+1)\mathbf{e}_k}\end{aligned}\quad (6.C.74)$$

With the aid of the above-obtained quantities, the PDA algorithm can now be executed in the following steps.

Step 1: Set $n = 0$, initialize

$$\mathbf{P}_+(0) = \{P_{1+}(0) = 0.5, P_{2+}(0) = 0.5, \dots, P_{\mathcal{K}+}(0) = 0.5\} \quad (6.C.75)$$

and compute $\boldsymbol{\mu}(0)$ and $\boldsymbol{\Omega}^{-1}(0)$;

Step 2: Compute $P_{k+}(n)$ using the iteration equations in (6.C.73) and (6.C.74) for $k = 1, 2, \dots, \mathcal{K}$;

Step 3: If $\{P_{k+}(n)\}$ have converged, go to Step 4, otherwise, set $n \leftarrow n + 1$ and return to Step 2;

Step 4: Make decisions:

$$b_k = \begin{cases} +1, & \text{if } P_{k+}(n) > 0.5 \\ -1, & \text{otherwise} \end{cases} \quad (6.C.76)$$

for $k = 1, 2, \dots, \mathcal{K}$.

Note that the stop (convergence) condition can be set as

$$P_{k+}(n) \in [0, \epsilon] \cup [1 - \epsilon, 1] \quad (6.C.77)$$

where ϵ is a sufficiently small positive value, so that $P_{k+}(n)$ is either close to zero or to one.

The PDA algorithm is one of the simplest and highly effective algorithms for attacking the MLD-MUD problem. It can be shown that the error performance of the CDMA systems using the PDA-assisted detection is very close to that achieved by the optimal MLD-MUD [186].

6.C.2.3 Semidefinite Programming Relaxation

The semidefinite programming (SDP) is an efficient approximation approach for solving many non-polynomial (NP)-hard combinatorial problems, by converting them into convex problems that have the complexity of polynomial-hard [187]. The SDPR for maximum likelihood multiuser detection has been studied, e.g., in references [188–190].

In order to facilitate the SDP for solving the MLD-MUD problem, let us modify the MLD-MUD problem as shown in (6.C.1) into

$$\hat{\mathbf{b}} = \arg \min_{\mathbf{b}} \{\mathbf{b}^T \tilde{\mathbf{R}} \mathbf{b} - 2\tilde{\mathbf{y}}^T \mathbf{b}\}, \quad \text{s.t. } \mathbf{b} \in \{+1, -1\}^{\mathcal{K}} \quad (6.C.78)$$

where s.t. is for *subject to*, $\tilde{\mathbf{R}} = \Re\{\mathbf{R}\}$ and $\tilde{\mathbf{y}} = \Re\{\mathbf{y}\}$. Note that, if \mathbf{b} is complex, the optimization problem in (6.C.1) can also be converted to the form of (6.C.78), by correspondingly extending the \mathcal{K} -length complex vectors \mathbf{b} and \mathbf{y} into the $2\mathcal{K}$ -length real vectors $\tilde{\mathbf{b}}$ and $\tilde{\mathbf{y}}$, and the $(\mathcal{K} \times \mathcal{K})$ -dimensional complex matrix \mathbf{R} into the $(2\mathcal{K} \times 2\mathcal{K})$ -dimensional real matrix $\tilde{\mathbf{R}}$ [190].

Let define

$$\begin{aligned} \mathbf{x} &= [\mathbf{b}^T, b_0 = 1]^T \\ \mathbf{Q} &= \begin{bmatrix} \tilde{\mathbf{R}} & -\tilde{\mathbf{y}} \\ -\tilde{\mathbf{y}}^T & 0 \end{bmatrix} \end{aligned} \quad (6.C.79)$$

where $b_0 = 1$ is a redundant dummy variable and \mathbf{x} is a $(\mathcal{K} + 1)$ -length vector. Then, the optimization problem in (6.C.78) can be described as

$$\hat{\mathbf{x}} = \arg \min_{\mathbf{x}} \{\mathbf{x}^T \mathbf{Q} \mathbf{x}\}, \quad \text{s.t. } \mathbf{b} \in \{+1, -1\}^{\mathcal{K}}, \quad b_0 = 1 \quad (6.C.80)$$

In (6.C.80) the argument to be minimized has the property of $\mathbf{x}^T \mathbf{Q} \mathbf{x} = \text{Trace}(\mathbf{Q} \mathbf{X})$, where $\mathbf{X} = \mathbf{x} \mathbf{x}^T$. It can be shown that \mathbf{X} is a positive semidefinite matrix with diagonal entries of ones and, furthermore, with a rank of one [187]. Consequently, the optimization problem of (6.C.80) can be restated as

$$\hat{\mathbf{X}} = \arg \min_{\mathbf{X}} \{\text{Trace}(\mathbf{Q} \mathbf{X})\}, \quad \text{s.t. } \text{diag}\{\mathbf{X}\} = \mathbf{1}, \quad \text{rank}(\mathbf{X}) = 1, \quad \mathbf{X} \geq 0 \quad (6.C.81)$$

where $\mathbf{1}$ is an all-one vector of length $(\mathcal{K} + 1)$, while $\mathbf{X} \geq 0$ implies positive semidefinite.

With the SDPR, the rank one constraint is relaxed in order to yield a basic convex optimization problem of

$$\hat{\mathbf{X}} = \arg \min_{\mathbf{X}} \{\text{Trace}(\mathbf{Q}\mathbf{X})\}, \text{ s.t. } \text{diag}\{\mathbf{X}\} = \mathbf{1}, \quad \mathbf{X} \geq 0 \quad (6.C.82)$$

which is now a linear optimization problem with linear constraints. This optimization problem can be solved in polynomial complexity using, for example, the interior-point method or cutting plane method [187]. In reference [187] a range of methods for solving the optimization problem of (6.C.82) have been studied. Some of these approaches have been successfully applied to solving the MLD-MUD problem, as shown, e.g., in references [188–190].

Chapter 7

Noncoherent Multiuser Detection

In TH/MC-CDMA systems the carrier phases of the received signal are difficult to estimate due to the time-hopping characteristics of the M -ary pulse-position modulation (MPPM). Hence, the TH/MC-CDMA system studied in the previous chapters uses noncoherent demodulation. The TH/MC-CDMA system allows multiple users to share a single frequency band through assigning each user a unique TH pattern. However, when different users transmit signals within the same time slot on the same subcarrier, they generate so-called ‘hits’ or, more generally, multiuser interference (MUI), which may significantly degrade the achievable BER performance of the TH/MC-CDMA system when not taken care of. One of the approaches for mitigating the MUI is to design the TH patterns so that the average number of hits is as low as possible. One such class of TH patterns, which is optimum in the sense of minimizing the number of hits, has been designed and studied in reference [191]. Another way of mitigating the MUI is to use multiuser detection (MUD) [88] to demodulate all user signals simultaneously. As shown in Chapter 6, with MUD, a user is demodulated by making use of (at least part of) the knowledge about the other users. Therefore, the MUD often demands much higher detection complexity than the single-user detector (SUD), which demodulates a user without invoking the knowledge about the other users.

The noncoherent MUDs may be broadly classified into two classes, namely the prior noncoherent MUDs and the posterior noncoherent MUDs. In the prior noncoherent MUDs the MUD-related operations are carried out before the (square-law) noncoherent processing. The noncoherent MUDs proposed and studied, e.g., in references [192–199] belong to this class. By contrast, for the posterior noncoherent MUDs, the MUD-related operations are executed after the (square-law) noncoherent processing. The posterior noncoherent MUDs have been investigated, e.g., in references [86, 87, 200–204].

In this chapter the prior noncoherent MUDs are first discussed in Sections 7.3, 7.4 and 7.5. Then, the posterior noncoherent MUDs are investigated in Sections 7.6, 7.7 and 7.8.

Note that in this chapter the noncoherent MUDs are established only in the context of the TH/MC-CDMA systems. However, the noncoherent MUD algorithms established in this chapter can be readily extended to the other types of noncoherent multiuser system, including the fast frequency-hopping (FFH) systems using M -ary frequency shift-keying

(MFSK) baseband modulation, the time-hopping-assisted ultra-wide bandwidth (TH-UWB) systems using MPPM, etc.

7.1 Representation of Discrete Time-Hopping Multicarrier CDMA Signals

In this section we provide a feasible signal model for the representation of the TH/MC-CDMA signals, so that multiuser detection can conveniently be derived, when based on it. The TH/MC-CDMA scheme was considered in detail in Section 3.8. In Section 4.5 the power-spectral density (PSD) of the TH/MC-CDMA signals and the error performance of the TH/MC-CDMA communicating over additive white Gaussian noise (AWGN) channels were investigated. By contrast, in Section 5.10 the single-user error performance of the TH/MC-CDMA was investigated when communicating over Nakagami- m fading channels.

In the TH/MC-CDMA system considered in this chapter, we assume that one data symbol is conveyed by L subcarriers and one symbol duration is divided into Q number of time slots. Furthermore, we assume that MPPM is used for data modulation, where $M \leq Q$. Then, when the TH/MC-CDMA supports K number of multiple-access users having the transmitted signals in the form of (4.91), the received complex low-pass equivalent signal in frequency-selective fading channels can be expressed as

$$R(t) = \sum_{k=1}^K \sqrt{\frac{2PQ}{L}} \sum_{l=0}^{L-1} h_l^{(k)} \psi_{T_h}(t - y_k(l)T_h) \exp(j2\pi f_l t) + N(t) \quad (7.1)$$

where P represents the transmission power per dimension, L represents the number of subcarriers conveying the same data symbol and T_h is the duration of a time slot or chip duration. In (7.1) f_l , $l = 0, \dots, L-1$, is the l th subcarrier frequency, $\psi_{T_h}(t)$ is the time domain pulse-waveform defined within $[0, T_h]$, which is normalized to satisfy $\int_0^{T_h} \psi_{T_h}^2(t) dt = T_h$, $h_l^{(k)}$ represents the channel's fading gain with respect to the l th subcarrier and the k th user, and $N(t)$ represents the complex valued low-pass equivalent AWGN with zero mean and single-sided power spectral density of N_0 per dimension. Furthermore, as shown in Section 3.8 of Chapter 3, let $x_k \in [0, M]$ be an M -ary symbol transmitted by the k th user and $\mathbf{a}_k = [a_0^{(k)}, a_1^{(k)}, \dots, a_{L-1}^{(k)}]$, where $a_l^{(k)} \in GF(Q)$ ($l = 0, \dots, L-1$), be the k th user's TH address. Then, $\{y_k(l)\}$ in (7.1) are obtained according to the operation

$$\mathbf{Y}_k = [y_k(0), y_k(1), \dots, y_k(L-1)] = x_k \cdot \mathbf{1} \oplus \mathbf{a}_k \quad (7.2)$$

where $\mathbf{1}$ represents an all-one vector of length L , $y_k(l)$ ($l = 0, \dots, L-1$) is also an element in $GF(Q)$, and \oplus denotes the addition operation in $GF(Q)$.

The schematic block diagram of the prior noncoherent multiuser receiver for the TH/MC-CDMA is shown in Fig. 7.1. As shown, the prior noncoherent multiuser receiver can be divided into three sub-blocks implementing front-end processing, multiuser processing (MUP) and post-processing, respectively. The front-end processing sub-block carries out the multicarrier demodulation and generates observation samples for the MUP. The MUP sub-block functions to mitigate the MUI with the aid of certain signal processing algorithms, as will be detailed later. Finally, the post-processing sub-block executes the conventional

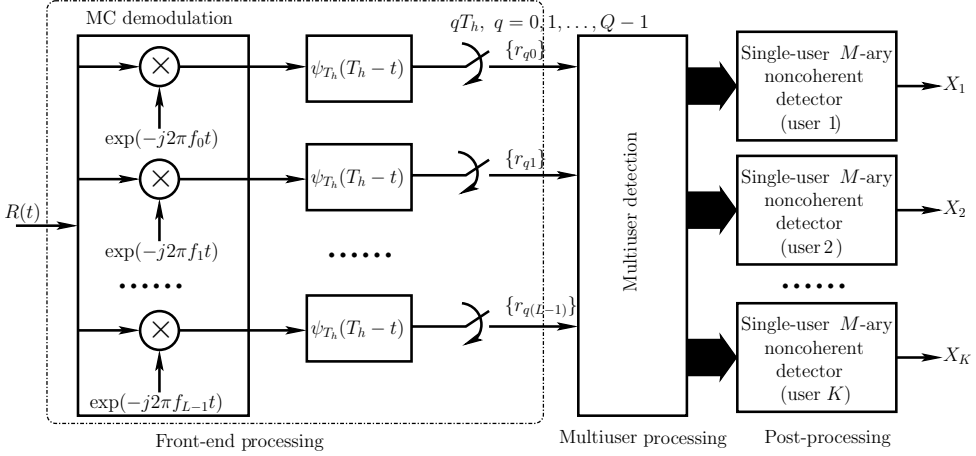


Figure 7.1: Receiver block diagram of the TH/MC-CDMA system using prior noncoherent multiuser detection and single-user noncoherent M -ary detection.

(single-user) noncoherent M -ary detection in order to recover the transmitted M -ary data symbol, which will also be detailed subsequently in the forthcoming discourse.

As shown in Fig. 7.1 the observation samples input to the MUP sub-block can be expressed as

$$r_{lm} = \left(\sqrt{\frac{2PQ}{L}} T_h \right)^{-1} \int_{mT_h}^{(m+1)T_h} R(t) \psi_{T_h}^*(t - mT_h) \exp(-j2\pi f_l t) dt \\ m = 0, 1, \dots, Q-1; l = 0, 1, \dots, L-1 \quad (7.3)$$

Assuming that the time-domain pulse $\psi_{T_h}(t)$ and the subcarriers are designed to satisfy the condition of (4.114), then, substituting (7.1) into (7.3), it can be shown that the observation samples can be expressed as

$$r_{lm} = \sum_{k=1}^K h_l^{(k)} \delta[y_k(l), m] + n_{lm}, \quad m = 0, 1, \dots, Q-1; l = 0, 1, \dots, L-1 \quad (7.4)$$

where n_{lm} is a complex Gaussian noise observed in the context of the l th subcarrier and the m th time slot, n_{lm} is given by

$$n_{lm} = \left(\sqrt{\frac{2PQ}{L}} T_h \right)^{-1} \int_{mT_h}^{(m+1)T_h} N(t) \psi_{T_h}^*(t - mT_h) \exp(-j2\pi f_l t) dt \quad (7.5)$$

which is Gaussian distributed with zero mean and a variance of $\sigma^2/2 = LN_0/2E_s = L/2\gamma_s$ per dimension, where $E_s = PT_s = PQT_h$ represents the transmitted energy per M -ary symbol, $\gamma_s = E_s/N_0 = bE_b/N_0$ represents the SNR per symbol.

Let us define

$$\mathbf{r} = [r_0^T, r_1^T, \dots, r_{L-1}^T]^T \\ \mathbf{r}_l = [r_{l0}, r_{l1}, \dots, r_{l(Q-1)}]^T \quad (7.6)$$

In order to take advantage of the MUD principles in coherent multiuser systems [88], the observation vector \mathbf{r} should be represented in a form that is linearly dependent on the transmitted information symbols [199]. Below, we provide a representation of the observation vector \mathbf{r} with the aid of the Hadamard transform [205]. In our derivation an accompanying example is utilized in order to explain the principles behind it. In this example, we assume that $Q = 8$, $M = 4$ and $L = 4$, the TH address for user k is $\mathbf{a}_k = [4, 3, 6, 7]$. Let $X_k = 2$ be the 4-ary symbol transmitted and let the system support only a single user. Then, we have

$$\begin{aligned} \mathbf{Y}_k &= [y_k(0), y_k(1), y_k(2), y_k(3)] = X_k \cdot \mathbf{1} \oplus \mathbf{a}_k \\ &= [6, 5, 0, 1] \end{aligned} \quad (7.7)$$

Correspondingly, the received observations in the form of (7.4) can be expressed as

$$r_{lm} = h_l^{(k)} \delta[y_k(l), m] + n_{lm}, \quad m = 0, 1, \dots, 7; l = 0, 1, 2, 3 \quad (7.8)$$

Furthermore, it can be shown that \mathbf{r}_0 , \mathbf{r}_1 , \mathbf{r}_2 , and \mathbf{r}_3 can be denoted as

$$\mathbf{r}_0 = \begin{bmatrix} n_{00} \\ n_{01} \\ n_{02} \\ n_{03} \\ n_{04} \\ n_{05} \\ h_0^{(k)} + n_{06} \\ n_{07} \end{bmatrix}, \mathbf{r}_1 = \begin{bmatrix} n_{10} \\ n_{11} \\ n_{12} \\ n_{13} \\ n_{14} \\ h_1^{(k)} + n_{15} \\ n_{16} \\ n_{17} \end{bmatrix}, \mathbf{r}_2 = \begin{bmatrix} h_2^{(k)} + n_{20} \\ n_{21} \\ n_{22} \\ n_{23} \\ n_{24} \\ n_{25} \\ n_{26} \\ n_{27} \end{bmatrix}, \mathbf{r}_3 = \begin{bmatrix} n_{30} \\ h_3^{(k)} + n_{31} \\ n_{32} \\ n_{33} \\ n_{34} \\ n_{35} \\ n_{36} \\ n_{37} \end{bmatrix} \quad (7.9)$$

Let

$$\mathbb{H}_2 = \frac{1}{\sqrt{2}} \begin{bmatrix} +1 & +1 \\ +1 & -1 \end{bmatrix} \quad (7.10)$$

be a second-order normalized Sylvester-type Hadamard matrix. Then, the Sylvester-type Hadamard matrix of order $M = 2^b$, where b denotes the number of bits per symbol, can be obtained through the concatenation operation of

$$\mathbb{H}_M = \mathbb{H}_2 \otimes \mathbb{H}_{M/2}, \quad M \geq 4 \quad (7.11)$$

where \otimes denotes the Kronecker product operation [89, 156].

For example, in the context of the considered example corresponding to $M = 4$, the normalized Hadamard matrix is

$$\mathbb{H}_4 = \frac{1}{\sqrt{4}} \begin{bmatrix} +1 & +1 & +1 & +1 \\ +1 & -1 & +1 & -1 \\ +1 & +1 & -1 & -1 \\ +1 & -1 & -1 & +1 \end{bmatrix} \quad (7.12)$$

Again, let

$$\mathbf{a}_k = [a_0^{(k)}, a_1^{(k)}, \dots, a_{L-1}^{(k)}] \quad (7.13)$$

be the TH address assigned to the k th user, where $a_l^{(k)} \in GF(Q)$. Let $\mathbf{F}_0^{(k)}, \mathbf{F}_1^{(k)}, \dots, \mathbf{F}_{L-1}^{(k)}$ be the k th user's L number of TH-matrices of dimension $(Q \times M)$, which have the following structures:

- each column has one and only one nonzero element of ‘1’; all the other $(Q - 1)$ elements are zero elements;
- for the m th column, where $m = 0, 1, \dots, M - 1$, the position of the nonzero element is at $(m \oplus a_l^{(k)}, m)$, where $l = 0, 1, \dots, L - 1$.

Specifically, for the example considered above, we have $\mathbf{F}_0^{(k)}$, $\mathbf{F}_1^{(k)}$, $\mathbf{F}_2^{(k)}$ and $\mathbf{F}_3^{(k)}$ as follows.

$$\mathbf{F}_0^{(k)} = \begin{bmatrix} 0 & 0 & 0 & 0 \\ 0 & 0 & 0 & 0 \\ 0 & 0 & 0 & 0 \\ 0 & 0 & 0 & 0 \\ 1 & 0 & 0 & 0 \\ 0 & 1 & 0 & 0 \\ 0 & 0 & 1 & 0 \\ 0 & 0 & 0 & 1 \end{bmatrix}, \quad \mathbf{F}_1^{(k)} = \begin{bmatrix} 0 & 0 & 0 & 0 \\ 0 & 0 & 0 & 0 \\ 0 & 0 & 0 & 0 \\ 1 & 0 & 0 & 0 \\ 0 & 1 & 0 & 0 \\ 0 & 0 & 1 & 0 \\ 0 & 0 & 0 & 1 \\ 0 & 0 & 0 & 0 \end{bmatrix} \quad (7.14)$$

$$\mathbf{F}_2^{(k)} = \begin{bmatrix} 0 & 0 & 1 & 0 \\ 0 & 0 & 0 & 1 \\ 0 & 0 & 0 & 0 \\ 0 & 0 & 0 & 0 \\ 0 & 0 & 0 & 0 \\ 1 & 0 & 0 & 0 \\ 0 & 1 & 0 & 0 \end{bmatrix}, \quad \mathbf{F}_3^{(k)} = \begin{bmatrix} 0 & 1 & 0 & 0 \\ 0 & 0 & 1 & 0 \\ 0 & 0 & 0 & 1 \\ 0 & 0 & 0 & 0 \\ 0 & 0 & 0 & 0 \\ 0 & 0 & 0 & 0 \\ 1 & 0 & 0 & 0 \end{bmatrix} \quad (7.15)$$

Now let the nature binary representation of the k th user’s transmitted symbol be denoted as

$$X_k = \tilde{b}_{b-1}^{(k)} \tilde{b}_{b-2}^{(k)} \cdots \tilde{b}_0^{(k)} \quad (7.16)$$

where logical ‘zero’ is represented by $+1$ and logical ‘one’ is by -1 . Then, as shown in [205], based on the representation of (7.16), the X_k -th column in \mathbb{H}_M of (7.11) can be formed by

$$\mathbf{x}_k = \frac{1}{\sqrt{M}} \begin{bmatrix} 1 \\ \tilde{b}_{b-1}^{(k)} \\ \vdots \\ \tilde{b}_0^{(k)} \end{bmatrix} \otimes \begin{bmatrix} 1 \\ \tilde{b}_{b-2}^{(k)} \\ \vdots \\ \tilde{b}_0^{(k)} \end{bmatrix} \otimes \cdots \otimes \begin{bmatrix} 1 \\ \tilde{b}_0^{(k)} \end{bmatrix} \quad (7.17)$$

With the aid of the above definitions, it can now be shown that the observation vector \mathbf{r}_l can be represented as

$$\mathbf{r}_l = \sum_{k=1}^K h_l^{(k)} \mathbf{F}_l^{(k)} \mathbb{H}_M \mathbf{x}_k + \mathbf{n}_l, \quad l = 0, 1, \dots, L - 1 \quad (7.18)$$

where we have defined

$$\mathbf{n}_l = [n_{l0}, n_{l1}, \dots, n_{l(Q-1)}]^T \quad (7.19)$$

which is a Gaussian vector with zero mean and a covariance matrix $\sigma^2 \mathbf{I}_Q$.

The representation of (7.18) can be justified by the fact that in (7.18) $\mathbb{H}_M \mathbf{x}_k$ returns an M -length column vector having a single nonzero element ‘1’ at the location X_k . Hence,

right-multiplying $\mathbb{H}_M \mathbf{x}_k$ on $\mathbf{F}_l^{(k)}$ selects the X_k th column of $\mathbf{F}_l^{(k)}$, which yields Q number of outputs corresponding to a column having single nonzero element 1 at the location $X_k \otimes a_l^{(k)}$.

Specifically, for the example considered, since the transmitted symbol is $X_k = 2 = -1 + 1$, we have \mathbf{x}_k given by

$$\mathbf{x}_k = \frac{1}{\sqrt{4}} \begin{bmatrix} 1 \\ -1 \end{bmatrix} \otimes \begin{bmatrix} 1 \\ 1 \end{bmatrix} = \frac{1}{\sqrt{4}} [1, 1, -1, -1]^T \quad (7.20)$$

Applying the TH matrices seen in (7.14) and (7.15), it can be easily shown that $\mathbf{r}_0 - \mathbf{r}_3$ in (7.9) can be expressed as

$$\begin{aligned} \mathbf{r}_0 &= h_0^{(k)} \mathbf{F}_0^{(k)} \mathbb{H}_4 \mathbf{x}_k + \mathbf{n}_0, \quad \mathbf{r}_1 = h_1^{(k)} \mathbf{F}_1^{(k)} \mathbb{H}_4 \mathbf{x}_k + \mathbf{n}_1 \\ \mathbf{r}_2 &= h_2^{(k)} \mathbf{F}_2^{(k)} \mathbb{H}_4 \mathbf{x}_k + \mathbf{n}_2, \quad \mathbf{r}_3 = h_3^{(k)} \mathbf{F}_3^{(k)} \mathbb{H}_4 \mathbf{x}_k + \mathbf{n}_3 \end{aligned} \quad (7.21)$$

Below, we represent the observations shown in (7.18) in different forms, in order that they can be conveniently used for our derivation of various detection schemes. First, let $\mathbf{H}_l^{(k)} = h_l^{(k)} \mathbf{I}_M$ and $\tilde{\mathbf{x}}_k = \mathbb{H}_M \mathbf{x}_k$. Then, the Q observations obtained from the l th subcarrier can be represented as

$$\mathbf{r}_l = \sum_{k=1}^K \mathbf{F}_l^{(k)} \mathbf{H}_l^{(k)} \tilde{\mathbf{x}}_k + \mathbf{n}_l, \quad l = 0, 1, \dots, L-1 \quad (7.22)$$

Let us define

$$\begin{aligned} \mathbf{F}_l &= [\mathbf{F}_l^{(1)}, \mathbf{F}_l^{(2)}, \dots, \mathbf{F}_l^{(K)}] \\ \mathbf{H}_l &= \text{diag}\{\mathbf{H}_l^{(1)}, \mathbf{H}_l^{(2)}, \dots, \mathbf{H}_l^{(K)}\} \\ \tilde{\mathbf{x}} &= [\tilde{\mathbf{x}}_1^T, \tilde{\mathbf{x}}_2^T, \dots, \tilde{\mathbf{x}}_K^T]^T \end{aligned} \quad (7.23)$$

where \mathbf{F}_l , \mathbf{H}_l and $\tilde{\mathbf{x}}$ are $(Q \times MK)$, $(MK \times MK)$ and $(MK \times 1)$ matrices, respectively. Then, \mathbf{r}_l of (7.22) can be represented in a compact form as

$$\mathbf{r}_l = \mathbf{F}_l \mathbf{H}_l \tilde{\mathbf{x}} + \mathbf{n}_l, \quad l = 0, 1, \dots, L-1 \quad (7.24)$$

Second, let us define

$$\begin{aligned} \mathbf{F}^{(k)} &= \text{diag}\{\mathbf{F}_0^{(k)}, \mathbf{F}_1^{(k)}, \dots, \mathbf{F}_{L-1}^{(k)}\} \\ \mathbf{H}^{(k)} &= [(\mathbf{H}_0^{(k)})^T, (\mathbf{H}_1^{(k)})^T, \dots, (\mathbf{H}_{L-1}^{(k)})^T]^T \end{aligned} \quad (7.25)$$

which are respectively $(QL \times ML)$ and $(ML \times M)$ matrices. Then, the observation vector \mathbf{r} seen in (7.6), which contains QL observation samples from the L subcarriers, can be expressed as

$$\mathbf{r} = \sum_{k=1}^K \mathbf{F}^{(k)} \mathbf{H}^{(k)} \tilde{\mathbf{x}}_k + \mathbf{n} \quad (7.26)$$

associated with

$$\mathbf{n} = [\mathbf{n}_0^T, \mathbf{n}_1^T, \dots, \mathbf{n}_{L-1}^T]^T \quad (7.27)$$

which is a Gaussian vector with zero mean and a covariance matrix $\sigma^2 \mathbf{I}_{QL}$.

Furthermore, the channel impulse response (CIR) matrix $\mathbf{H}^{(k)}$ can be expressed as the product of an amplitude matrix and a phase matrix, i.e.

$$\mathbf{H}^{(k)} = \mathbf{A}^{(k)} \Psi^{(k)}, \quad k = 1, 2, \dots, K \quad (7.28)$$

where $\mathbf{A}^{(k)}$ and $\Psi^{(k)}$ contain the amplitudes and phases of $\mathbf{H}^{(k)}$, which are respectively expressed as

$$\begin{aligned} \mathbf{A}^{(k)} &= \text{diag}\{\mathbf{A}_0^{(k)}, \mathbf{A}_1^{(k)}, \dots, \mathbf{A}_{L-1}^{(k)}\} \\ \Psi^{(k)} &= [(\Psi_0^{(k)})^T, (\Psi_1^{(k)})^T, \dots, (\Psi_{L-1}^{(k)})^T]^T \end{aligned} \quad (7.29)$$

Assume that $h_l^{(k)} = |h_l^{(k)}| \exp(j\theta_l^{(k)})$, then, in (7.29) we have $\mathbf{A}_l^{(k)} = |h_l^{(k)}| \mathbf{I}_M$ and $\Psi_l^{(k)} = \exp(j\theta_l^{(k)}) \mathbf{I}_M$. Then, (7.26) can be written as

$$\mathbf{r} = \sum_{k=1}^K \mathbf{F}^{(k)} \mathbf{A}^{(k)} \Psi^{(k)} \tilde{\mathbf{x}}_k + \mathbf{n} \quad (7.30)$$

Additionally, (7.30) can be represented in a compact form as

$$\mathbf{r} = \mathbf{F} \mathbf{A} \Psi \tilde{\mathbf{x}} + \mathbf{n} \quad (7.31)$$

where $\tilde{\mathbf{x}}$ has been defined in (7.23) and the other related matrices are defined as

$$\begin{aligned} \mathbf{F} &= [\mathbf{F}^{(1)}, \mathbf{F}^{(2)}, \dots, \mathbf{F}^{(K)}] \\ \mathbf{A} &= \text{diag}\{\mathbf{A}^{(1)}, \mathbf{A}^{(2)}, \dots, \mathbf{A}^{(K)}\} \\ \Psi &= \text{diag}\{\Psi^{(1)}, \Psi^{(2)}, \dots, \Psi^{(K)}\} \end{aligned} \quad (7.32)$$

where \mathbf{F} is a $(QL \times MLK)$ -dimensional matrix, \mathbf{A} is a $(MLK \times MLK)$ -dimensional matrix, while Ψ is a $(MLK \times MK)$ -dimensional matrix.

Having obtained the representations for the observations in the TH/MC-CDMA system, as shown in (7.22), (7.24), (7.26) or (7.28), let us now discuss the detection in the TH/MC-CDMA systems by first considering the single-user detection.

7.2 Noncoherent Single-User Detection

In this section, noncoherent SUD is considered to illustrate the detection procedure in the TH/MC-CDMA system using MPPM. As shown in reference [199], in multiuser systems using M -ary modulation the noncoherent detection can usually be divided into two detection stages: the first detection stage aims at MUI mitigation, while the second detection stage carries out the conventional M -ary noncoherent detection for recovering transmitted symbols.

Let us assume that the first user of $k = 1$ is to be detected. Based on the observations as shown in (7.18), the time dehopping (TDH) can be achieved by multiplying $\mathbf{F}_l^{(1)}$ on \mathbf{r}_l , where

$l = 0, 1, \dots, L - 1$, yielding

$$\begin{aligned} z_l &= (\mathbf{F}_l^{(1)})^T \mathbf{r}_l \\ &= h_l^{(1)} (\mathbf{F}_l^{(1)})^T \mathbf{F}_l^{(1)} \mathbb{H}_M \mathbf{x}_1 + \sum_{k=2}^K h_l^{(k)} (\mathbf{F}_l^{(1)})^T \mathbf{F}_l^{(k)} \mathbb{H}_M \mathbf{x}_k + (\mathbf{F}_l^{(1)})^T \mathbf{n}_l \\ l &= 0, 1, \dots, L - 1 \end{aligned} \quad (7.33)$$

It can be easily shown that the TH-matrices have the properties

$$\begin{aligned} (\mathbf{F}_l^{(k)})^T \mathbf{F}_l^{(k)} &= \mathbf{I}_M \\ (\mathbf{F}_l^{(k)})^T \mathbf{F}_l^{(j)} &= \mathbf{R}_{kj}^{(l)}, \quad k \neq j \end{aligned} \quad (7.34)$$

where $\mathbf{R}_{kj}^{(l)}$ is the cross-correlation matrix of $\mathbf{F}_l^{(k)}$ and $\mathbf{F}_l^{(j)}$, the nonzero elements in $\mathbf{R}_{kj}^{(l)}$ may generate MUI. After applying (7.34) to (7.33), we obtain

$$z_l = h_l^{(1)} \mathbb{H}_M \mathbf{x}_1 + \sum_{k=2}^K h_l^{(k)} \mathbf{R}_{1k}^{(l)} \mathbb{H}_M \mathbf{x}_k + \tilde{\mathbf{n}}_l, \quad l = 0, 1, \dots, L - 1 \quad (7.35)$$

where $\tilde{\mathbf{n}}_l = (\mathbf{F}_l^{(1)})^T \mathbf{n}_l$, which is Gaussian distributed with zero mean and a covariance matrix of $\sigma^2 \mathbf{I}_M$, since $(\mathbf{F}_l^{(1)})^T \mathbf{F}_l^{(1)} = \mathbf{I}_M$.

Note that, due to the TH characteristics of the TH/MC-CDMA, a nonzero element in $\mathbf{R}_{1k}^{(l)}$ does not mean that there is always MUI from the k th user. This is because, as analysed previously, the processing of $\mathbb{H}_M \mathbf{x}_k$ has ‘selection’ capability. More specifically, the processing of $\mathbb{H}_M \mathbf{x}_k$ on $\mathbf{R}_{1k}^{(l)}$ selects only one column from $\mathbf{R}_{1k}^{(l)}$ and which column is selected depends on the M -ary transmitted data symbol. Hence, if in $\mathbf{R}_{1k}^{(l)}$ a column with a nonzero element is selected, then the reference user conflicts interference from the l th subcarrier of the k th user. Otherwise, if an all-zero column in $\mathbf{R}_{1k}^{(l)}$ is selected, there will be no interference imposing on the reference user by the l th subcarrier of the k th user.

After the TDH, let us construct L decision vectors in the form

$$\begin{aligned} \mathbf{q}_l &= [q_{l0}, q_{l1}, \dots, q_{l(M-1)}]^T \\ q_{li} &= |z_{li}|^2, \quad i = 0, 1, \dots, M - 1; \quad l = 0, 1, \dots, L - 1 \end{aligned} \quad (7.36)$$

where z_{li} is the i th element of \mathbf{z}_l . Based on $\mathbf{q}_0, \mathbf{q}_1, \dots, \mathbf{q}_{L-1}$, various diversity combining schemes for the M -ary orthogonal signalling may be invoked to form M decision variables, in order to receive the transmitted information. In Appendix 7.9 a range of noncoherent diversity combining schemes for the M -ary orthogonal signalling are summarized. Specifically, as shown in Appendix 7.9, when the equal-gain combining (EGC) is applied, we form M number of decision variables as [2]

$$Q_m = \sum_{l=0}^{L-1} q_{lm}, \quad m = 0, 1, \dots, M - 1 \quad (7.37)$$

After obtaining M number of decision variables as shown in (7.37), the largest of them is chosen as that corresponding to the transmitted symbol, which can be mapped to $b = \log_2 M$ binary bits representing the transmitted information.

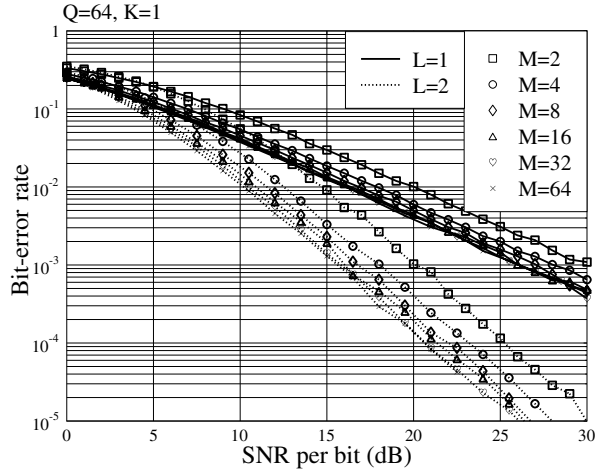


Figure 7.2: BER versus average SNR per bit performance of the TH/MC-CDMA system supporting $K = 1$ user and using $Q = 64$ time slots per symbol duration, when communicating over Rayleigh fading channels.

Instead of using EGC-aided diversity combining, the majority logic decision approach as discussed in Chapter 2 may also be invoked to extract transmitted information. With the majority logic decision we can form a $(M \times L)$ frequency-time (FT) matrix \mathbf{D}_1 for the desired user as follows. Let $\lambda > 0$ be a preset threshold, which may be optimized for a given SNR value according to a specific communications environment. Then, whenever q_{lm} ($m = 0, \dots, M - 1$; $l = 0, \dots, L - 1$) exceeds the threshold λ , the corresponding FT element of the FT matrix is flagged by a marker (or logical 1), or otherwise by a space (or logical 0). Based on \mathbf{D}_1 , the majority logic decision-based detector makes a decision in favour of the particular M -ary symbol \hat{X}_1 corresponding to the specific row, which has the highest number of nonzero entries, in order to provide an estimate for the transmitted symbol X_1 of the reference user.

Figures 7.2 and 7.3 show the BER versus average SNR per bit performance of the TH/MC-CDMA systems supporting $K = 1$ user, when communicating over Rayleigh fading channels. In the considered TH/MC-CDMA system, a symbol duration was assumed to be divided into $Q = 64$ time slots. Different modulation levels of M and different diversity orders of L were considered. The results in Figs 7.2 and 7.3 show that using diversity can significantly enhance the BER performance of the TH/MC-CDMA systems.

By contrast, in Fig. 7.4 the BER versus average SNR per bit performance of the TH/MC-CDMA systems supporting multiple users is depicted, when communicating over Rayleigh fading channels. Again, in the corresponding evaluations $Q = 64$ time slots per symbol duration and $M = 8$ -ary modulation were assumed, and one 8-ary symbol was transmitted on $L = 3$ subcarriers. Furthermore, it was assumed that random TH patterns were employed by the TH/MC-CDMA system to support multiple users. Explicitly, as seen in Fig. 7.4, the TH/MC-CDMA system conflicts severe MUI, which results in the BER performance becoming worse, when the number of users supported increases.

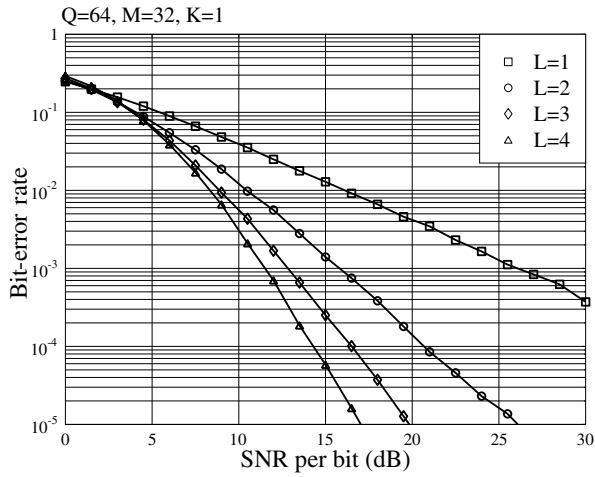


Figure 7.3: BER versus average SNR per bit performance of the TH/MC-CDMA system supporting $K = 1$ user, using $Q = 64$ time slots per symbol duration and $M = 8$ -ary modulation, when communicating over Rayleigh fading channels.

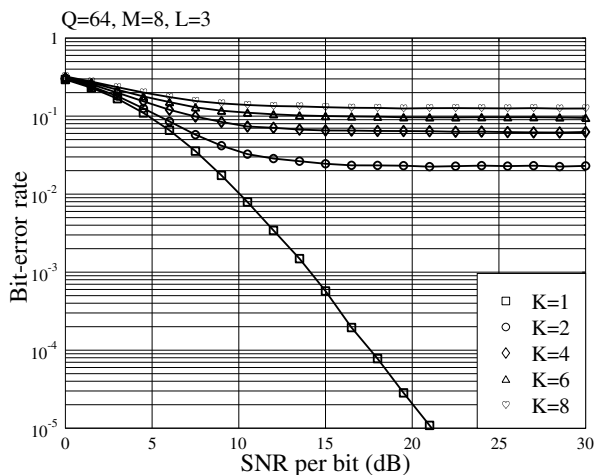


Figure 7.4: BER versus average SNR per bit performance of the TH/MC-CDMA system using $Q = 64$ time slots per symbol duration, $M = 8$ -ary modulation, and transmitting one symbol on $L = 3$ subcarriers, when communicating over Rayleigh fading channels.

The severe MUI conflicted by the TH/MC-CDMA may be mitigated with the aid of various MUD schemes, as analysed in the following sections. Let us first consider the optimum noncoherent MUD for the TH/MC-CDMA.

7.3 Optimum Prior Noncoherent Multiuser Detection

The optimum MUD, especially the optimum prior noncoherent MUD, in multiuser systems using M -ary modulations has been investigated, e.g., in references [196, 197, 199]. In this section we consider the optimum prior noncoherent MUD for the TH/MC-CDMA system by extending the optimum noncoherent MUD schemes considered in references [196, 197, 199].

In the TH/MC-CDMA system having the observation vector expressed by (7.31), given the transmitted information vector $\tilde{\mathbf{x}}$, the amplitude \mathbf{A} and the phase Ψ , the observation vector \mathbf{r} of (7.31) obeys the multivariate Gaussian distribution with zero mean and a covariance matrix of $\sigma^2 \mathbf{I}_{QL}$, which can be expressed as

$$\begin{aligned} f(\mathbf{r} | \tilde{\mathbf{x}}, \mathbf{A}, \Psi) &= \frac{1}{(\pi\sigma^2)^{QL}} \exp\left[-\frac{(\mathbf{r} - \mathbf{F}\mathbf{A}\Psi\tilde{\mathbf{x}})^H(\mathbf{r} - \mathbf{F}\mathbf{A}\Psi\tilde{\mathbf{x}})}{\sigma^2}\right] \\ &= C \exp\left[-\frac{\|\mathbf{r} - \mathbf{F}\mathbf{A}\Psi\tilde{\mathbf{x}}\|^2}{\sigma^2}\right] \end{aligned} \quad (7.38)$$

where $C = 1/(\pi\sigma^2)^{QL}$ is a constant.

First, when *coherent* detection is applied, which implies that the knowledge about \mathbf{A} and Ψ is available, the optimum MUD for $\tilde{\mathbf{x}}$ is the MAP-MUD, which can be described as

$$\begin{aligned} \hat{\tilde{\mathbf{x}}} &= \arg \max_{\tilde{\mathbf{x}}} \{f(\tilde{\mathbf{x}} | \mathbf{r}, \mathbf{A}, \Psi)\} \\ &\triangleq \arg \max_{\tilde{\mathbf{x}}} \{P(\tilde{\mathbf{x}})f(\mathbf{r} | \tilde{\mathbf{x}}, \mathbf{A}, \Psi)\} \end{aligned} \quad (7.39)$$

where $P(\tilde{\mathbf{x}})$ denotes the *a priori* probability of transmitting the M -ary symbol $\tilde{\mathbf{x}}$.

When the transmitted symbols are equal-probable yielding $P(\tilde{\mathbf{x}}) = 1/M$, the MAP-MUD represented by (7.39) is then reduced to the maximum likelihood decision (MLD)-based MUD (MLD-MUD), which finds the optimum solution according to

$$\hat{\tilde{\mathbf{x}}} = \arg \max_{\tilde{\mathbf{x}}} \{f(\mathbf{r} | \tilde{\mathbf{x}}, \mathbf{A}, \Psi)\} \quad (7.40)$$

When applying (7.38) to (7.40), the optimization problem for the MLD-MUD can then be written as

$$\begin{aligned} \hat{\tilde{\mathbf{x}}} &= \arg \min_{\tilde{\mathbf{x}}} \{\|\mathbf{r} - \mathbf{F}\mathbf{A}\Psi\tilde{\mathbf{x}}\|^2\} \\ &= \arg \max_{\tilde{\mathbf{x}}} \{2\Re\{\mathbf{r}^H \mathbf{F}\mathbf{A}\Psi\tilde{\mathbf{x}}\} - \tilde{\mathbf{x}}^H \Psi^* \mathbf{A} \mathbf{F}^T \mathbf{F}\mathbf{A}\Psi\tilde{\mathbf{x}}\} \end{aligned} \quad (7.41)$$

Second, when communicating over the communications environments where the knowledge about Ψ is not available but that about \mathbf{A} is available, the MLD-MUD can be formed as

$$\hat{\tilde{\mathbf{x}}} = \arg \max_{\tilde{\mathbf{x}}, \Psi} \{2\Re\{\mathbf{r}^H \mathbf{F}\mathbf{A}\Psi\tilde{\mathbf{x}}\} - \tilde{\mathbf{x}}^H \Psi^* \mathbf{A} \mathbf{F}^T \mathbf{F}\mathbf{A}\Psi\tilde{\mathbf{x}}\} \quad (7.42)$$

which is in fact a joint maximum-likelihood (ML) estimator of $\tilde{\mathbf{x}}$ and Ψ .

Furthermore, when the knowledge about both Ψ and \mathbf{A} is not available, the MLD-MUD is then a joint estimator of $\tilde{\mathbf{x}}$, Ψ and \mathbf{A} .

In M -ary communications such as in our TH/MC-CDMA systems, the above optimum MUDs only provide an estimate of $\hat{\tilde{\mathbf{x}}}$ for $\tilde{\mathbf{x}}$, but not directly for the transmitted information. Hence, after obtaining the estimate $\hat{\tilde{\mathbf{x}}}$, a second detection stage is required in order to provide an estimate for the transmitted M -ary symbol, say X_k , $k = 1, \dots, K$. Specifically, from our previous analysis, $\hat{\tilde{\mathbf{x}}}_k$ can be expressed as

$$\hat{\tilde{\mathbf{x}}}_k = \mathbb{H}_M \hat{\tilde{\mathbf{x}}}_k, \quad k = 1, 2, \dots, K \quad (7.43)$$

which is an M -length vector having single nonzero element ‘1’ at the location X_k of a column. Therefore, the estimate of \hat{X}_k for X_k can be obtained from the location of the nonzero element in $\hat{\tilde{\mathbf{x}}}_k$.

Explicitly, all the above-mentioned optimum MUDs have an extremely high complexity, which typically increases exponentially with the number of users K as well as with the symbol size M . Furthermore, when the signal amplitudes in \mathbf{A} and phases in Ψ are unknowns, the joint optimum MUDs become even more complex. Therefore, in practice, suboptimum MUDs with reasonable complexity are usually desirable. Hence, from Section 7.4 to Section 7.6 in this chapter, the suboptimum MUDs with linear complexity are derived in the context of the TH/MC-CDMA.

The above optimum MUDs are symbol-level optimum detectors, which might not be optimum at the bit level. Sometimes, the bit-level optimum detectors are desirable. First, the bit-level optimum detectors may outperform the symbol-level optimum detectors in terms of achievable bit-error probability. Second, in some cases, e.g., in binary coded M -ary communications, the bit-level soft-input soft-output (SISO) detection is convenient for implementing the iterative detection and decoding algorithms. Therefore, we now derive the optimum bit-level MUD based on MAP principles, which uses soft *a priori* information and provides soft *a posteriori* information, i.e. it is a SISO detector. Hence, the expressions obtained can be directly invoked in the joint or iterative detection and decoding schemes in coded M -ary communications systems.

Let us assume that the receiver employs the knowledge about both \mathbf{A} and Ψ . Let the signal set be expressed as $\mathcal{X} = \{X_0, X_1, \dots, X_{M-1}\}$. Furthermore, let \mathcal{X}_k^{i+} ($i = 0, 1, \dots, b - 1$) be a symbol set of user k , the members of which correspond to those X_k 's whose i th bit in its binary representation $\tilde{b}_{b-1}^{(k)} \tilde{b}_{b-2}^{(k)} \cdots \tilde{b}_0^{(k)}$ is $\tilde{b}_i^{(k)} = +1$. Similarly, let \mathcal{X}_k^{i-} ($i = 0, 1, \dots, b - 1$) be a symbol set of user k , the members of which correspond to those X_k 's whose i th bit in its binary representation $\tilde{b}_{b-1}^{(k)} \tilde{b}_{b-2}^{(k)} \cdots \tilde{b}_0^{(k)}$ is $\tilde{b}_i^{(k)} = -1$. Explicitly, the size of both \mathcal{X}_k^{i+} and \mathcal{X}_k^{i-} is $M/2$. Based on the above assumptions, the bit-level MAP-MUD computes the log-likelihood ratio (LLR) or information $\Lambda(\tilde{b}_i^{(k)})$ for bit $\tilde{b}_i^{(k)}$ as [90]

$$\Lambda(\tilde{b}_i^{(k)}) \triangleq \ln \frac{P(\tilde{b}_i^{(k)} = +1 | \mathbf{r})}{P(\tilde{b}_i^{(k)} = -1 | \mathbf{r})}, \quad i = 0, 1, \dots, b - 1; \quad k = 1, 2, \dots, K \quad (7.44)$$

Invoking the Bayes rules [206], the above LLR can be written as

$$\begin{aligned}\Lambda(\tilde{b}_i^{(k)}) &= \ln \frac{P(\mathbf{r} \mid \tilde{b}_i^{(k)} = +1)}{P(\mathbf{r} \mid \tilde{b}_i^{(k)} = -1)} + \ln \frac{P(\tilde{b}_i^{(k)} = +1)}{P(\tilde{b}_i^{(k)} = -1)} \\ &\triangleq \ln \frac{f(\mathbf{r} \mid \tilde{b}_i^{(k)} = +1)}{f(\mathbf{r} \mid \tilde{b}_i^{(k)} = -1)} + \ln \frac{P(\tilde{b}_i^{(k)} = +1)}{P(\tilde{b}_i^{(k)} = -1)} \\ &= \Lambda_e(\mathbf{r} \mid \tilde{b}_i^{(k)}) + \Lambda_a(\tilde{b}_i^{(k)})\end{aligned}\quad (7.45)$$

where $\Lambda_a(\tilde{b}_i^{(k)}) = P(\tilde{b}_i^{(k)} = +1)/P(\tilde{b}_i^{(k)} = -1)$ is the *a priori* information concerning $\tilde{b}_i^{(k)} = +1$ and $\tilde{b}_i^{(k)} = -1$, while $\Lambda_e(\mathbf{r} \mid \tilde{b}_i^{(k)}) = P(\mathbf{r} \mid \tilde{b}_i^{(k)} = +1)/P(\mathbf{r} \mid \tilde{b}_i^{(k)} = -1)$ is the *extrinsic* information [90] of $\tilde{b}_i^{(k)} = \pm 1$, which is provided by the communications channel.

Generally, in (7.45) $\Lambda_a(\tilde{b}_i^{(k)})$ represents the soft-input and $\Lambda(\tilde{b}_i^{(k)})$ represents the soft-output. Hence, the MAP-MUD represented by (7.45) is a SISO detector, where the increased information due to the detection process is $\Lambda_e(\mathbf{r} \mid \tilde{b}_i^{(k)})$, which reflects the reliability of the communications channel. Equation (7.45) can be conveniently implemented as a component of an iterative detector in M -ary communications, where iterations are operated between the detection and channel decoding.

As shown in (7.45), in order to compute the extrinsic information $\Lambda_e(\mathbf{r} \mid \tilde{b}_i^{(k)})$, the probability density functions (PDFs) of $f(\mathbf{r} \mid \tilde{b}_i^{(k)} = +1)$ and $f(\mathbf{r} \mid \tilde{b}_i^{(k)} = -1)$ must first be computed. The PDF $f(\mathbf{r} \mid \tilde{b}_i^{(k)} = +1)$ can be expressed as

$$\begin{aligned}f(\mathbf{r} \mid \tilde{b}_i^{(k)} = +1) &= \sum_{\mathbf{x}_k \in \mathcal{X}_k^{i+}} P(\mathbf{x}_k) f(\mathbf{r} \mid \mathbf{x}_k) \\ &= \sum_{\mathbf{x}_1 \in \mathcal{X}} \cdots \sum_{\mathbf{x}_k \in \mathcal{X}_k^{i+}} \cdots \sum_{\mathbf{x}_K \in \mathcal{X}} \prod_{i=1}^K P(\mathbf{x}_i) f(\mathbf{r} \mid \mathbf{x}_1, \mathbf{x}_2, \dots, \mathbf{x}_K) \\ &\triangleq \sum_{\mathbf{x}_1 \in \mathcal{X}} \cdots \sum_{\mathbf{x}_k \in \mathcal{X}_k^{i+}} \cdots \sum_{\mathbf{x}_K \in \mathcal{X}} \prod_{i=1}^K P(\mathbf{x}_i) f(\mathbf{r} \mid \tilde{\mathbf{x}}, \mathbf{A}, \Psi)\end{aligned}\quad (7.46)$$

where $f(\mathbf{r} \mid \tilde{\mathbf{x}}, \mathbf{A}, \Psi)$ has been given by (7.38). In a similar way, the PDF of $f(\mathbf{r} \mid \tilde{b}_i^{(k)} = -1)$ can be expressed as

$$f(\mathbf{r} \mid \tilde{b}_i^{(k)} = -1) \triangleq \sum_{\mathbf{x}_1 \in \mathcal{X}} \cdots \sum_{\mathbf{x}_k \in \mathcal{X}_k^{i-}} \cdots \sum_{\mathbf{x}_K \in \mathcal{X}} \prod_{i=1}^K P(\mathbf{x}_i) f(\mathbf{r} \mid \tilde{\mathbf{x}}, \mathbf{A}, \Psi)\quad (7.47)$$

Consequently, with the aid of (7.46) and (7.47), when the *a priori* information $\Lambda_a(\tilde{b}_i^{(k)})$ is given, the *a posteriori* LLR $\Lambda(\tilde{b}_i^{(k)})$ can be computed. Finally, the estimate to $\tilde{b}_i^{(k)}$ can be decided as the sign of $\Lambda(\tilde{b}_i^{(k)})$, i.e.

$$\hat{b}_i^{(k)} = \text{sign}\{\Lambda(\tilde{b}_i^{(k)})\}, \quad i = 0, 1, \dots, b-1; k = 1, 2, \dots, K\quad (7.48)$$

From the above derivation we know that the complexity of the detection based on (7.45) with the aid of (7.46) and (7.47) is extremely high (proportional to $O(M^K)$), which renders the above-derived bit-level MAP-MUD or SISO-based MUD impractical. In the forthcoming sections the linear MUDs with reasonable complexity are considered. The above-derived bit-level SISO algorithm will be revisited, in order to obtain the SISO detectors that are practically meaningful.

7.4 Prior Noncoherent Decorrelating Multiuser Detection

The prior noncoherent decorrelating MUD for the multiuser systems using the general M -ary orthogonal/nonorthogonal modulations has been studied, e.g., in reference [199]. By contrast, in references [193, 194] the decorrelating MUD has been investigated in the context of the DS-CDMA using M -ary orthogonal modulation. This section extends the decorrelating MUD considered in reference [199] to the TH/MC-CDMA, in order to demodulate the TH/MC-CDMA signals with, relatively, a lower complexity, in comparison with the optimum MUDs considered in Section 7.3.

As in reference [199] the prior noncoherent decorrelating MUD for the TH/MC-CDMA can be divided into two detection stages: a decorrelating MUD stage and a single-user noncoherent detection stage. The decorrelating MUD stage carries out the decorrelating operation aimed at removing the MUI, while the single-user noncoherent detection carries out the conventional M -ary noncoherent detection, which may include diversity combining, decision variable forming as well as decision making.

Let us consider the observation vector of (7.24), which, for convenience, is copied here as

$$\mathbf{r}_l = \mathbf{F}_l \mathbf{H}_l \tilde{\mathbf{x}} + \mathbf{n}_l, \quad l = 0, 1, \dots, L - 1 \quad (7.49)$$

where \mathbf{F}_l , \mathbf{H}_l and $\tilde{\mathbf{x}}$ are $(Q \times MK)$, $(MK \times MK)$ and $(MK \times 1)$ matrices, respectively. We assume that $Q \geq MK$. On carrying out the correlation operation by multiplying both sides of (7.49) with \mathbf{F}_l^T , we obtain an MK -length vector

$$\mathbf{y}_l = \mathbf{R}_l \mathbf{H}_l \tilde{\mathbf{x}} + \bar{\mathbf{n}}_l, \quad l = 0, 1, \dots, L - 1 \quad (7.50)$$

where $\mathbf{R}_l = \mathbf{F}_l^T \mathbf{F}_l$ is an autocorrelation matrix of \mathbf{F}_l and $\bar{\mathbf{n}}_l = \mathbf{F}_l^T \mathbf{n}_l$.

The autocorrelation matrix \mathbf{R}_l is generally a matrix of high dimensions, $(MK \times MK)$. However, as seen, e.g., in (7.15), the TH matrices \mathbf{F}_l 's are typically sparse, where each of the \mathbf{F}_l 's has only MK number of nonzero elements. Hence, although the dimensions of \mathbf{R}_l 's are high, the complexity of the decorrelating MUD in TH/MC-CDMA might be still reasonable. This is because the sparsity property of the TH matrices can be beneficial to fast computation of the autocorrelation matrices \mathbf{R}_l 's as well as the other matrices with \mathbf{F}_l 's as components [207].

The decorrelating MUD is achieved by multiplying both sides of (7.50) with the inverse of \mathbf{R}_l , i.e. with \mathbf{R}_l^{-1} , which yields

$$\begin{aligned} \mathbf{z}_l &= \mathbf{R}_l^{-1} \mathbf{y}_l \\ &= \mathbf{H}_l \tilde{\mathbf{x}} + \tilde{\mathbf{n}}_l, \quad l = 0, 1, \dots, L - 1 \end{aligned} \quad (7.51)$$

where $\tilde{\mathbf{n}}_l = \mathbf{R}_l^{-1} \bar{\mathbf{n}}_l$, which is Gaussian with zero mean and a covariance matrix of

$$\begin{aligned} E[\tilde{\mathbf{n}}_l \tilde{\mathbf{n}}_l^H] &= \mathbf{R}_l^{-1} E[\bar{\mathbf{n}}_l \bar{\mathbf{n}}_l^H] \mathbf{R}_l^{-1} \\ &= \sigma^2 \mathbf{R}_l^{-1} \end{aligned} \quad (7.52)$$

Note that when some of the columns in \mathbf{R}_l are linearly dependent, \mathbf{R}_l^{-1} does not exist. In this case, we can replace \mathbf{R}_l^{-1} by the Moore–Penrose generalized inverse [156]. However, for simplicity, our forthcoming discussion is based on the assumption that the columns in \mathbf{R}_l are linearly independent, implying that \mathbf{R}_l^{-1} exists.

After the first stage of decorrelating MUD, let us now consider the second stage of single-user detection. Both the optimum and suboptimum detections are considered. Without loss of any generality, let us consider the detection of the first user (reference user). Furthermore, when without generating confusion, the superscripts or subscripts related to the reference user are deleted for convenience.

For the first user, the corresponding sufficient statistics are constituted by the first M terms of \mathbf{z}_l , which can be expressed as

$$\begin{aligned} \mathbf{z}_l^{(1)} &= \mathbf{H}_l^{(1)} \tilde{\mathbf{x}}_1 + \tilde{\mathbf{n}}_l^{(1)} \\ &= |h_l| e^{j\theta_l} \mathbb{H}_M \mathbf{x}_1 + \tilde{\mathbf{n}}_l^{(1)}, \quad l = 0, 1, \dots, L - 1 \end{aligned} \quad (7.53)$$

where $\tilde{\mathbf{n}}_l^{(1)}$ is Gaussian with zero mean and a covariance matrix expressed as $\sigma^2 \mathbf{Q}_l$. The covariance matrix \mathbf{Q}_l ($l = 0, \dots, L - 1$) is a $(M \times M)$ matrix, which is constructed by the $(M \times M)$ submatrix at the top-left corner of \mathbf{R}_l^{-1} .

According to the properties of $\mathbb{H}_M \mathbf{x}_k$, it can be shown that when the i th symbol is transmitted by the reference user, $\mathbf{z}_l^{(1)}$, $l = 0, 1, \dots, L - 1$ is then complex Gaussian distributed with mean given by

$$\boldsymbol{\mu}_l = [0, \dots, 0, \underbrace{|h_l| e^{j\theta_l}}_{\text{Position } i}, 0, \dots, 0]^T, \quad l = 0, 1, \dots, L - 1 \quad (7.54)$$

and a covariance matrix of $\sigma^2 \mathbf{Q}_l$, $l = 0, 1, \dots, L - 1$. Hence, the PDF of $\mathbf{z}_l^{(1)}$ given \mathbf{x}_i and h_l can be expressed as

$$\begin{aligned} f(\mathbf{z}_l^{(1)} | \mathbf{x}_i, h_l) &= \frac{1}{(\pi \sigma^2)^M \det(\mathbf{Q}_l)} \exp\left(-\frac{(\mathbf{z}_l^{(1)} - \boldsymbol{\mu}_l)^H \mathbf{Q}_l^{-1} (\mathbf{z}_l^{(1)} - \boldsymbol{\mu}_l)}{\sigma^2}\right) \\ &= C_l \exp\left(-\frac{1}{\sigma^2} \left[(\mathbf{z}_l^{(1)})^H \mathbf{Q}_l^{-1} \mathbf{z}_l^{(1)} + |h_l|^2 q_{l,ii} - 2|h_l| \Re \left\{ e^{j\theta_l} \sum_{n=0}^{M-1} (\mathbf{z}_{ln}^{(1)})^* q_{l,ni} \right\} \right]\right) \\ &\quad l = 0, 1, \dots, L - 1 \end{aligned} \quad (7.55)$$

where C_l is a normalization factor, $\mathbf{z}_{ln}^{(1)}$ is the n th element of $\mathbf{z}_l^{(1)}$, while $q_{l,ni}$ is the (n, i) th element of \mathbf{Q}_l^{-1} .

Let

$$\mathbf{z}^{(1)} = [(\mathbf{z}_0^{(1)})^T, (\mathbf{z}_1^{(1)})^T, \dots, (\mathbf{z}_{L-1}^{(1)})^T]^T \quad (7.56)$$

where $\{z_l^{(1)}\}$ are independent random vectors in terms of the index l , since it has been assumed that each subcarrier in the TH/MC-CDMA experiences independent fading. Hence, the PDF of $z^{(1)}$ can be expressed as

$$\begin{aligned} f(z^{(1)} | \mathbf{x}_i, \{h_l\}) &= \prod_{l=0}^{L-1} f(z_l^{(1)} | \mathbf{x}_i, h_l) \\ &= C \prod_{l=0}^{L-1} \exp\left(-\frac{1}{\sigma^2} \left[(z_l^{(1)})^H \mathbf{Q}_l^{-1} z_l^{(1)} + |h_l|^2 q_{l,ii} - 2|h_l| \Re \left\{ e^{j\theta_l} \sum_{n=0}^{M-1} (z_{ln}^{(1)})^* q_{l,ni} \right\} \right] \right) \end{aligned} \quad (7.57)$$

where $C = \prod_{l=0}^{L-1} C_l$.

As the receiver does not use the knowledge about the phases $\{\theta_l\}$, in this case, the marginal PDF independent of $\{\theta_l\}$ can be used to achieve the detection. Let us assume that $\{\theta_l\}$ are independent random variables uniformly distributed in $[0, 2\pi)$. Then, the marginal PDF of $z^{(1)}$ conditioned on the channel amplitudes $\{|h_l|\}$ can be obtained by averaging out the conditions of $\{\theta_l\}$, which can be expressed as

$$f(z^{(1)} | \mathbf{x}_i, \{|h_l|\}) = \frac{1}{(2\pi)^L} \underbrace{\int_0^{2\pi} \cdots \int_0^{2\pi}}_{L \text{ terms}} f(z^{(1)} | \mathbf{x}_i, \{h_l\}) d\theta_0, \dots, d\theta_{L-1} \quad (7.58)$$

Applying (7.57) to (7.58), we can express it as

$$\begin{aligned} f(z^{(1)} | \mathbf{x}_i, \{|h_l|\}) &= C \prod_{l=0}^{L-1} \exp\left(-\frac{1}{\sigma^2} [(z_l^{(1)})^H \mathbf{Q}_l^{-1} z_l^{(1)} + |h_l|^2 q_{l,ii}] \right) \\ &\times \frac{1}{2\pi} \int_0^{2\pi} \exp\left(\frac{2|h_l|}{\sigma^2} \Re \left\{ e^{j\theta_l} \sum_{n=0}^{M-1} (z_{ln}^{(1)})^* q_{l,ni} \right\}\right) d\theta_l \end{aligned} \quad (7.59)$$

Let us express in the above equation

$$\sum_{n=0}^{M-1} (z_{ln}^{(1)})^* q_{l,ni} = \left| \sum_{n=0}^{M-1} (z_{ln}^{(1)})^* q_{l,ni} \right| \exp(j\phi_i)$$

where $\phi_i = \tan^{-1}(\sum_{n=0}^{M-1} (z_{ln}^{(1)})^* q_{l,ni})$. Then, (7.59) can be rewritten as

$$\begin{aligned} f(z^{(1)} | \mathbf{x}_i, \{|h_l|\}) &= C \prod_{l=0}^{L-1} \exp\left(-\frac{1}{\sigma^2} \left[(z_l^{(1)})^H \mathbf{Q}_l^{-1} z_l^{(1)} + |h_l|^2 q_{l,ii} \right] \right) \\ &\times \frac{1}{2\pi} \int_0^{2\pi} \exp\left(\frac{2|h_l|}{\sigma^2} \left| \sum_{n=0}^{M-1} (z_{ln}^{(1)})^* q_{l,ni} \right| \cos(\theta_l + \phi_i)\right) d\theta_l \\ &= C \prod_{l=0}^{L-1} \exp\left(-\frac{1}{\sigma^2} \left[(z_l^{(1)})^H \mathbf{Q}_l^{-1} z_l^{(1)} + |h_l|^2 q_{l,ii} \right] \right) \\ &\times I_0\left(\frac{2|h_l|}{\sigma^2} \left| \sum_{n=0}^{M-1} (z_{ln}^{(1)})^* q_{l,ni} \right| \right) \end{aligned} \quad (7.60)$$

where $I_0(x)$ is the modified zeroth-order Bessel function of the first kind defined as $I_0(x) = (2\pi)^{-1} \int_0^{2\pi} \exp(x \cos \alpha) d\alpha$ [152].

Having obtained the marginal PDF of $\mathbf{z}^{(1)}$ conditioned on a transmitted symbol and the channel amplitudes, as shown in (7.60), the noncoherent MAP-based single-user detector yielding the minimum symbol error probability can now be described as

$$\begin{aligned}\hat{X}_1 &= \arg \max_{X_1=i \leftrightarrow \mathbf{x}_i} \{f(\mathbf{x}_i | \mathbf{z}^{(1)}, \{|h_l|\})\} \\ &\triangleq \arg \max_{X_1=i \leftrightarrow \mathbf{x}_i} \{P(\mathbf{x}_i) f(\mathbf{z}^{(1)} | \mathbf{x}_i, \{|h_l|\})\} \\ &\triangleq \arg \max_{X_1=i \leftrightarrow \mathbf{x}_i} \{P(X_1 = i) f(\mathbf{z}^{(1)} | \mathbf{x}_i, \{|h_l|\})\}\end{aligned}\quad (7.61)$$

Substituting (7.60) into (7.61) and after ignoring the common terms, the MAP-assisted optimization problem can now be expressed as

$$\hat{X}_1 = \arg \max_{X_1=i \leftrightarrow \mathbf{x}_i} \left\{ P(X_1 = i) \prod_{l=0}^{L-1} \exp\left(-\frac{|h_l|^2 q_{l,ii}}{\sigma^2}\right) I_0\left(\frac{2|h_l|}{\sigma^2} \left| \sum_{n=0}^{M-1} (z_{ln}^{(1)})^* q_{l,ni} \right| \right) \right\} \quad (7.62)$$

The above optimization problem can also be described in the logarithm domain as

$$\begin{aligned}\hat{X}_1 &= \arg \max_{X_1=i \leftrightarrow \mathbf{x}_i} \left\{ \ln P(X_1 = i) \right. \\ &\quad \left. + \sum_{l=0}^{L-1} \left(-\frac{|h_l|^2 q_{l,ii}}{\sigma^2} + \ln \left[I_0\left(\frac{2|h_l|}{\sigma^2} \left| \sum_{n=0}^{M-1} (z_{ln}^{(1)})^* q_{l,ni} \right| \right) \right] \right) \right\}\end{aligned}\quad (7.63)$$

Furthermore, when assuming that the transmitted symbol obeys the i.i.d. distribution, the MAP-based single-user noncoherent detector is reduced to the MLD-based single-user noncoherent detector formed as

$$\hat{X}_1 = \arg \max_{X_1=i \leftrightarrow \mathbf{x}_i} \left\{ \sum_{l=0}^{L-1} \left(-\frac{|h_l|^2 q_{l,ii}}{\sigma^2} + \ln \left[I_0\left(\frac{2|h_l|}{\sigma^2} \left| \sum_{n=0}^{M-1} (z_{ln}^{(1)})^* q_{l,ni} \right| \right) \right] \right) \right\} \quad (7.64)$$

Above, the MAP- or MLD-assisted noncoherent detector is optimum in terms of the achievable minimum symbol error probability, when the noise samples in $\mathbf{z}_l^{(1)}$ as seen in (7.53) are correlated. If we ignore the correlation among the noise samples, the conventional M -ary detector may be used to recover the transmitted data. More specifically, when the EGC-based combining scheme is invoked, we can form M number of decision variables as

$$Z_m = \sum_{l=0}^{L-1} |z_{lm}^{(1)}|^2, \quad m = 0, 1, \dots, M-1 \quad (7.65)$$

where $z_{lm}^{(1)}$ is the m th element of $\mathbf{z}_l^{(1)}$. According to the noncoherent demodulation principles of the conventional M -ary orthogonal modulation [2], the largest of $\{Z_m\}$ is selected and mapped to an M -ary symbol, which denotes the estimate of the transmitted M -ary symbol.

This summarizes the second-stage symbol-level single-user detection. Let us now derive a second-stage bit-level detector, which is essentially a SISO detector, that may be implemented

as a component of an iterative detection scheme. Let the transmitted symbol by the reference user be expressed as

$$X_1 \longleftrightarrow \tilde{b}_{b-1} \tilde{b}_{b-2} \cdots \tilde{b}_0 \quad (7.66)$$

Then, for the λ th bit, the single-user SISO detector computes

$$\begin{aligned} \Lambda(\tilde{b}_\lambda) &= \ln \left[\frac{f(z^{(1)} | \tilde{b}_\lambda = +1, \{|h_l|\})}{f(z^{(1)} | \tilde{b}_\lambda = -1, \{|h_l|\})} \right] + \ln \left[\frac{P(\tilde{b}_\lambda = +1)}{P(\tilde{b}_\lambda = -1)} \right] \\ &= \Lambda_e(\tilde{b}_\lambda) + \Lambda_a(\tilde{b}_\lambda), \quad \lambda = 0, 1, \dots, b-1 \end{aligned} \quad (7.67)$$

where $\Lambda_a(\tilde{b}_\lambda) = \ln[P(\tilde{b}_\lambda = +1)/P(\tilde{b}_\lambda = -1)]$ represents the *a priori* information about \tilde{b}_λ , while

$$\Lambda_e(\tilde{b}_\lambda) = \ln \left[\frac{f(z^{(1)} | \tilde{b}_\lambda = +1, \{|h_l|\})}{f(z^{(1)} | \tilde{b}_\lambda = -1, \{|h_l|\})} \right] \quad (7.68)$$

is the extrinsic information measuring the reliability of the channel without using the information about the phase. In (7.67) the conditional PDFs $f(z^{(1)} | \tilde{b}_\lambda = \pm 1, \{|h_l|\})$ can be obtained as follows.

Let \mathcal{X}_λ^+ be a symbol set that contains the $M/2$ number of M -ary symbols with $\tilde{b}_\lambda = +1$ in their binary representations. Let \mathcal{X}_λ^- be a symbol set that contains the $M/2$ number of M -ary symbols with $\tilde{b}_\lambda = -1$ in their binary representations. Then, the (marginal) PDFs of $f(z^{(1)} | \tilde{b}_\lambda = \pm 1, \{|h_l|\})$ can be computed as

$$\begin{aligned} &f(z^{(1)} | \tilde{b}_\lambda = +1, \{|h_l|\}) \\ &= \sum_{X_1=i \in \mathcal{X}_\lambda^+ \leftrightarrow \mathbf{x}_i} P(X_1 = i) f(z^{(1)} | \mathbf{x}_i, \{|h_l|\}) \\ &= C \sum_{X_1=i \in \mathcal{X}_\lambda^+ \leftrightarrow \mathbf{x}_i} P(X_1 = i) \prod_{l=0}^{L-1} \exp \left(-\frac{1}{\sigma^2} [(\mathbf{z}_l^{(1)})^H \boldsymbol{\Omega}_l^{-1} \mathbf{z}_l^{(1)} + |h_l|^2 q_{l,ii}] \right) \\ &\quad \times I_0 \left(\frac{2|h_l|}{\sigma^2} \left| \sum_{n=0}^{M-1} (\mathbf{z}_{ln}^{(1)})^* q_{l,ni} \right| \right) \end{aligned} \quad (7.69)$$

$$\begin{aligned} &f(z^{(1)} | \tilde{b}_\lambda = -1, \{|h_l|\}) \\ &= \sum_{X_1=j \in \mathcal{X}_\lambda^- \leftrightarrow \mathbf{x}_j} P(X_1 = j) f(z^{(1)} | \mathbf{x}_j, \{|h_l|\}) \\ &= C \sum_{X_1=j \in \mathcal{X}_\lambda^- \leftrightarrow \mathbf{x}_j} P(X_1 = j) \prod_{l=0}^{L-1} \exp \left(-\frac{1}{\sigma^2} [(\mathbf{z}_l^{(1)})^H \boldsymbol{\Omega}_l^{-1} \mathbf{z}_l^{(1)} + |h_l|^2 q_{l,jj}] \right) \\ &\quad \times I_0 \left(\frac{2|h_l|}{\sigma^2} \left| \sum_{n=0}^{M-1} (\mathbf{z}_{ln}^{(1)})^* q_{l,nj} \right| \right) \end{aligned} \quad (7.70)$$

When substituting (7.69) and (7.70) into (7.68), it can be shown that the extrinsic information can be simplified to

$$\begin{aligned} \Lambda_e(\tilde{b}_\lambda) = & \ln \left[\sum_{i \in \mathcal{X}_\lambda^+ \leftrightarrow \mathbf{x}_i} P(X_1 = i) \prod_{l=0}^{L-1} \exp \left(-\frac{|h_l|^2 q_{l,ii}}{\sigma^2} \right) \right. \\ & \times I_0 \left(\frac{2|h_l|}{\sigma^2} \left| \sum_{n=0}^{M-1} (z_{ln}^{(1)})^* q_{l,ni} \right| \right) \Big] \\ & - \ln \left[\sum_{j \in \mathcal{X}_\lambda^- \leftrightarrow \mathbf{x}_j} P(X_1 = j) \prod_{l=0}^{L-1} \exp \left(-\frac{|h_l|^2 q_{l,jj}}{\sigma^2} \right) \right. \\ & \times I_0 \left(\frac{2|h_l|}{\sigma^2} \left| \sum_{n=0}^{M-1} (z_{ln}^{(1)})^* q_{l,nj} \right| \right) \Big] \end{aligned} \quad (7.71)$$

Finally, when the *a posteriori* information as shown in (7.67) is obtained, the λ th bit of X_1 can be decided according to

$$\hat{b}_\lambda = \text{sgn}(\Lambda(\tilde{b}_\lambda)), \quad \lambda = 0, 1, \dots, b-1 \quad (7.72)$$

This concludes the derivation of the second-stage bit-level SISO detector. As shown in (7.71), the complexity of the single-user SISO detector is determined mainly by the symbol size M as well as by the diversity order L .

Figure 7.5 illustrates the BER versus average SNR per bit performance of the TH/MC-CDMA system employing the noncoherent decorrelating detection, when communicating over Rayleigh fading channels. In the simulations, it was assumed that the $M = 8$ -ary data symbols were transmitted, one symbol duration was divided into $Q = 64$ time slots, and each data symbol was conveyed by $L = 3$ subcarriers. Furthermore, random TH addresses were assumed. However, in the simulations the TH addresses generating a singular cross-correlation matrix of \mathbf{R}_l as seen in (7.50) were excluded from the simulations, since these sets of TH addresses constitute the ‘bad’ TH addresses in terms of achievable BER performance. Note that for the simulation conditions considered in Fig. 7.5, there is about 30 per cent of ‘bad’ TH addresses. From the results of Fig. 7.5, it can be seen that, after removing the ‘bad’ TH addresses from the simulations, the TH/MC-CDMA is capable of achieving the single-user BER performance bound, regardless of the number of users supported, which is $K = 1, 2, 4, 6, 8$. It has been well recognized that the decorrelating MUD operation generally amplifies the background noise, hence the BER performance degrades when increasing the number of users supported, as shown in Chapter 6. For the TH/MC-CDMA employing the prior noncoherent decorrelating MUD, this noise-amplification phenomenon is not observed in Fig. 7.5. Instead, the TH/MC-CDMA supporting a different number of users achieves a similar BER performance. The reason behind this observation is that \mathbf{R}_l ’s for the considered cases are sparse matrices, resulting in the diagonal entries of \mathbf{R}_l^{-1} being approximately one.

7.5 Prior Noncoherent MMSE Multiuser Detection

The prior noncoherent MMSE-MUD for multiuser systems using general nonorthogonal multipulse modulation (NMM) has been investigated in reference [195]. Furthermore, in

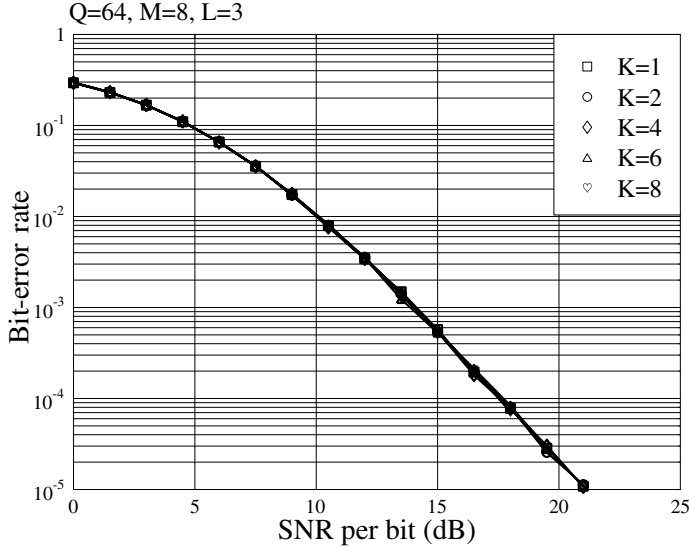


Figure 7.5: BER versus average SNR per bit performance of the TH/MC-CDMA system using prior noncoherent decorrelating detection, when communicating over Rayleigh fading channels. The parameters used in simulations were $Q = 64$, $M = 8$ -ary and $L = 3$.

reference [195] the blind adaptive implementation of the prior noncoherent MMSE-MUD has been investigated. In this section we extend the principles of the prior noncoherent MMSE-MUD in reference [195] for the detection of TH/MC-CDMA signals, where orthogonal MPPM and frequency (F)-domain diversity are employed.

Our prior noncoherent MMSE-MUDs are derived based on the observations:

$$\mathbf{r}_l = \mathbf{F}_l \mathbf{H}_l \tilde{\mathbf{x}} + \mathbf{n}_l \quad (7.73)$$

$$= \sum_{k=1}^K \mathbf{F}_l^{(k)} \mathbf{H}_l^{(k)} \tilde{\mathbf{x}}_k + \mathbf{n}_l, \quad l = 0, 1, \dots, L-1 \quad (7.74)$$

where, again, \mathbf{F}_l , \mathbf{H}_l and $\tilde{\mathbf{x}}$ are respectively $(Q \times MK)$, $(MK \times MK)$ and $(MK \times 1)$ matrices, while $\mathbf{F}_l^{(k)}$, $\mathbf{H}_l^{(k)}$ and $\tilde{\mathbf{x}}_k$ are respectively $(Q \times M)$, $(M \times M)$ and $(M \times 1)$ matrices. The overall detection procedure is also divided into two detection stages: the MMSE-MUD stage and the single-user detection stage. In the context of the MMSE-MUD, both joint MMSE-MUDs and individual MMSE-MUDs are considered, where by joint MMSE-MUDs we mean that all the K users are detected together based on MMSE-MUD principles. By contrast, the individual MMSE-MUD aims to detect only the desired user while suppressing the MUI from the other $(K-1)$ users. We first consider the joint MMSE-MUD, which is derived based on the observation equation (7.73).

One of the typical characteristics of the prior noncoherent MMSE-MUD is that, instead of estimating directly $\tilde{\mathbf{x}}$ in (7.73), the term $\mathbf{H}_l \tilde{\mathbf{x}}$ seen in (7.73) is estimated based on the observations obtained from the l th subcarrier. Specifically, let $\mathbf{W}_{o,l}$ be an optimum $(Q \times MK)$ linear matrix for processing \mathbf{r}_l for $l = 0, 1, \dots, L-1$. Then, the output \mathbf{y}_l denoting the

estimate of $\mathbf{H}_l \tilde{\mathbf{x}}$ can be expressed as

$$\mathbf{y}_l = \mathbf{W}_{o,l}^H \mathbf{r}_l \quad (7.75)$$

where the optimum linear processing matrix $\mathbf{W}_{o,l}$ in MMSE principle is obtained from the optimization problem

$$\mathbf{W}_{o,l} = \arg \min_{\mathbf{W}_l} \{ E[\|\mathbf{W}_l^H \mathbf{r}_l - \mathbf{H}_l \tilde{\mathbf{x}}\|^2] \} \quad (7.76)$$

Following the MMSE principles as shown in Chapter 6, the optimum linear processing matrix can be expressed as

$$\mathbf{W}_{o,l} = \mathcal{R}_l^{-1} \mathcal{R}_{rx,l}, \quad l = 0, 1, \dots, L-1 \quad (7.77)$$

where \mathcal{R}_l is the autocorrelation matrix of \mathbf{r}_l , which can be expressed as

$$\begin{aligned} \mathcal{R}_l &= E[\mathbf{r}_l \mathbf{r}_l^H] \\ &= \mathbf{F}_l \underbrace{E[\mathbf{H}_l \tilde{\mathbf{x}} \tilde{\mathbf{x}}^T \mathbf{H}_l^H]}_{\mathbf{E}_l} \mathbf{F}_l^T + \sigma^2 \mathbf{I}_Q \end{aligned} \quad (7.78)$$

When using the definitions in (7.23), it can be shown that the mathematics expectation in (7.78) can be expressed as

$$\mathbf{E}_l = E[\mathbf{H}_l \tilde{\mathbf{x}} \tilde{\mathbf{x}}^T \mathbf{H}_l^H] = \frac{1}{M} \text{diag}\{|h_l^{(1)}|^2 \mathbf{I}_M, |h_l^{(2)}|^2 \mathbf{I}_M, \dots, |h_l^{(K)}|^2 \mathbf{I}_M\} \quad (7.79)$$

Note that when the receiver does not use the knowledge about $\{h_l^{(k)}\}$, \mathbf{E}_l of (7.79) can be replaced by its average, which can be expressed as

$$E[\mathbf{E}_l] = \frac{\Omega}{M} \mathbf{I}_{KM} \quad (7.80)$$

where $\Omega = E[|h_l^{(k)}|^2]$.

In (7.77) $\mathcal{R}_{rx,l}$ denotes the cross-correlation matrix between \mathbf{r} and $\mathbf{H}_l \tilde{\mathbf{x}}$, i.e.

$$\mathcal{R}_{rx,l} = E[\mathbf{r}_l \tilde{\mathbf{x}}^T \mathbf{H}_l^H] = \mathbf{F}_l \mathbf{E}_l \quad (7.81)$$

Finally, substituting (7.78) and (7.81) into (7.77), the optimum linear processing matrix in the MMSE sense can be expressed as

$$\mathbf{W}_{o,l} = (\mathbf{F}_l \mathbf{E}_l \mathbf{F}_l^T + \sigma^2 \mathbf{I}_Q)^{-1} \mathbf{F}_l \mathbf{E}_l, \quad l = 0, 1, \dots, L-1 \quad (7.82)$$

Furthermore, when invoking the *matrix inverse lemma* [156], (7.82) can also be expressed as

$$\mathbf{W}_{o,l} = \mathbf{F}_l (\mathbf{F}_l^T \mathbf{F}_l + \sigma^2 \mathbf{E}_l^{-1})^{-1}, \quad l = 0, 1, \dots, L-1 \quad (7.83)$$

In comparison with the prior noncoherent decorrelating MUD investigated in Section 7.4, where the inverse matrix \mathbf{R}_l^{-1} might not exist, in the prior noncoherent MMSE-MUD the inverse matrix in (7.82) or (7.83) always exists. Let us now turn to consider the individual MMSE-MUD, which is derived based on (7.74).

Let $\mathbf{W}_{ol}^{(i)}$ be a $(Q \times M)$ -dimensional linear processing matrix that is optimum in the MMSE sense for detection of the i th user. Then, the estimate to $\mathbf{H}_l^{(k)}\tilde{\mathbf{x}}_k$ can be expressed as

$$\mathbf{y}_l^{(i)} = (\mathbf{W}_{ol}^{(i)})^H \mathbf{r}_l, \quad l = 0, 1, \dots, L-1; i = 1, 2, \dots, K \quad (7.84)$$

where, when following similar derivations for the joint MMSE-MUD, the optimum linear processing matrix can be expressed as

$$\mathbf{W}_{o,l}^{(i)} = \mathcal{R}_l^{-1} \mathcal{R}_{rx_i,l}, \quad l = 0, 1, \dots, L-1; i = 1, 2, \dots, K \quad (7.85)$$

where \mathcal{R}_l is given by (7.78). However, from (7.74), \mathcal{R}_l can also be expressed as

$$\begin{aligned} \mathcal{R}_l &= E[\mathbf{r}_l \mathbf{r}_l^H] \\ &= \sum_{k=1}^K \mathbf{F}_l^{(k)} E[\mathbf{H}_l^{(k)} \tilde{\mathbf{x}}_k \tilde{\mathbf{x}}_k^H (\mathbf{H}_l^{(k)})^H] (\mathbf{F}_l^{(k)})^T + \sigma^2 \mathbf{I}_Q \\ &= \sum_{k=1}^K \frac{|h_l^{(k)}|^2}{M} \mathbf{F}_l^{(k)} (\mathbf{F}_l^{(k)})^T + \sigma^2 \mathbf{I}_Q \end{aligned} \quad (7.86)$$

In (7.85) $\mathcal{R}_{rx_i,l}$ denotes the cross-correlation matrix between \mathbf{r} and $\mathbf{H}_l^{(i)}\tilde{\mathbf{x}}_i$, which can be expressed as

$$\mathcal{R}_{rx_i,l} = E[\mathbf{r}_l \tilde{\mathbf{x}}_i^H (\mathbf{H}_l^{(i)})^H] = \frac{|h_l^{(i)}|^2}{M} \times \mathbf{F}_l^{(i)} \quad (7.87)$$

Finally, when substituting (7.86) and (7.87) into (7.85), the optimum linear processing matrix for the l th subcarrier and the i th user can be expressed as

$$\begin{aligned} \mathbf{W}_{o,l}^{(i)} &= \left(\sum_{k=1}^K \frac{|h_l^{(k)}|^2}{M} \mathbf{F}_l^{(k)} (\mathbf{F}_l^{(k)})^T + \sigma^2 \mathbf{I}_Q \right)^{-1} \frac{|h_l^{(i)}|^2}{M} \times \mathbf{F}_l^{(i)} \\ l &= 0, 1, \dots, L-1; i = 1, 2, \dots, K \end{aligned} \quad (7.88)$$

In (7.88) let us express the autocorrelation matrix \mathcal{R}_l as

$$\mathcal{R}_l = \frac{|h_l^{(i)}|^2}{M} \left[\mathbf{F}_l^{(i)} (\mathbf{F}_l^{(i)})^T + \underbrace{\sum_{k \neq i}^K \frac{|h_l^{(k)}|^2}{|h_l^{(i)}|^2} \mathbf{F}_l^{(k)} (\mathbf{F}_l^{(k)})^T + \frac{M}{|h_l^{(i)}|^2} \sigma^2 \mathbf{I}_Q}_{\Sigma_l} \right] \quad (7.89)$$

where Σ_l denotes the autocorrelation matrix of the MUI plus Gaussian noise. In this case, the optimum linear processing matrix of (7.88) can also be expressed as

$$\mathbf{W}_{o,l}^{(i)} = [\mathbf{F}_l^{(i)} (\mathbf{F}_l^{(i)})^T + \Sigma_l]^{-1} \mathbf{F}_l^{(i)}, \quad l = 0, 1, \dots, L-1; i = 1, 2, \dots, K \quad (7.90)$$

Having completed the first stage MMSE-MUD, the second stage of single-user detection can be carried out as follows. Let us consider specifically the i th user. After the MMSE-MUD,

the outputs in the context of the L number of subcarriers can be expressed as

$$\begin{aligned}
 \mathbf{y}_l^{(i)} &= (\mathbf{F}_l^{(i)})^T [\mathbf{F}_l^{(i)}(\mathbf{F}_l^{(i)})^T + \boldsymbol{\Sigma}_l]^{-1} \mathbf{r}_l \\
 &= \underbrace{(\mathbf{F}_l^{(i)})^T [\mathbf{F}_l^{(i)}(\mathbf{F}_l^{(i)})^T + \boldsymbol{\Sigma}_l]^{-1} \mathbf{F}_l^{(i)} \mathbf{H}_l^{(i)} \tilde{\mathbf{x}}_i}_{\text{Desired output}} \\
 &\quad + \underbrace{(\mathbf{F}_l^{(i)})^T [\mathbf{F}_l^{(i)}(\mathbf{F}_l^{(i)})^T + \boldsymbol{\Sigma}_l]^{-1} \left(\sum_{k \neq i}^K \mathbf{F}_l^{(k)} \mathbf{H}_l^{(k)} \tilde{\mathbf{x}}_k + \mathbf{n}_l \right)}_{\text{MUI+noise}}, \\
 l &= 0, 1, \dots, L-1; i = 1, 2, \dots, K
 \end{aligned} \tag{7.91}$$

As shown in (7.91), explicitly, the prior noncoherent MMSE-MUD does not fully remove the MUI. In this case, deriving the accurate PDF of the MMSE-MUD's output is highly involving, even though it might not be impossible. Consequently, the optimum second-stage single-user detection in TH/MC-CDMA using the prior MMSE-MUD cannot be implemented similarly to the TH/MC-CDMA using the decorrelating MUD, as analysed in Section 7.4. Therefore, we analyse the second stage of single-user detection with the aid of Gaussian approximation, which approximates the leaked MUI as additive Gaussian noise that is independent of the background Gaussian noise.

First, when the Gaussian approximation on the leaked MUI is assumed and when we ignore the noise correlations, the conventional SUD for M -ary orthogonal modulation – which is suboptimum – can be invoked for the second-stage detection. Let us assume for simplicity that the EGC-assisted diversity combining scheme is used. Then, based on (7.91), the M number of decision variables can be formed as

$$Z_m^{(i)} = \sum_{l=0}^{L-1} |y_{lm}^{(i)}|^2, \quad m = 0, 1, \dots, M-1; i = 1, 2, \dots, K \tag{7.92}$$

where $y_{lm}^{(i)}$ is the m th element of $\mathbf{y}_l^{(i)}$. Finally, the maximum of $\{Z_m^{(i)}\}_{m=0}^{M-1}$ is chosen and mapped to an M -ary symbol, which denotes the estimate of the transmitted symbol by the i th user.

Second, in order to implement the second stage of single-user detection in an ‘optimum’ way as for the decorrelating MUD discussed in Section 7.4, the PDF of the MMSE-MUD’s output should first be derived. It can be shown that, when the Gaussian approximation on the leaked MUI is assumed, $\mathbf{y}_l^{(i)}$ of (7.91) can be approximated as a Gaussian vector with mean given by

$$\boldsymbol{\mu}_l^{(i)} = E[\mathbf{y}_l^{(i)}] = \mathbf{H}_l^{(i)} \tilde{\mathbf{x}}_i \tag{7.93}$$

and the covariance matrix given by

$$\begin{aligned}
 \mathbf{C}_l &= E[(\mathbf{y}_l^{(i)} - \boldsymbol{\mu}_l^{(i)})(\mathbf{y}_l^{(i)} - \boldsymbol{\mu}_l^{(i)})^H] \\
 &= E[((\mathbf{W}_{ol}^{(i)})^H \mathbf{r}_l - \mathbf{H}_l^{(i)} \tilde{\mathbf{x}}_i)((\mathbf{W}_{ol}^{(i)})^H \mathbf{r}_l - \mathbf{H}_l^{(i)} \tilde{\mathbf{x}}_i)^H]
 \end{aligned}$$

$$\begin{aligned}
&= \underbrace{(\mathbf{W}_{ol}^{(i)})^H \mathcal{R}_l \mathbf{W}_{ol}^{(i)} - (\mathbf{W}_{ol}^{(i)})^H \mathcal{R}_{rx_i,l}}_0 - \mathcal{R}_{rx_i,l}^H \mathbf{W}_{ol}^{(i)} + \frac{|h_l^{(i)}|^2}{M} \mathbf{I}_M \\
&= \frac{|h_l^{(i)}|^2}{M} \mathbf{I}_M - \mathcal{R}_{rx_i,l}^H \mathcal{R}_l^{-1} \mathcal{R}_{rx_i,l}
\end{aligned} \tag{7.94}$$

Substituting (7.86) and (7.87) into the above equation, it can be shown that

$$\mathbf{C}_l = \frac{|h_l^{(i)}|^2}{M} [\mathbf{I}_M - (\mathbf{F}_l^{(i)})^T [\mathbf{F}_l^{(i)} (\mathbf{F}_l^{(i)})^T + \boldsymbol{\Sigma}_l]^{-1} \mathbf{F}_l^{(i)}] \tag{7.95}$$

where $\boldsymbol{\Sigma}_l$ was defined in (7.89). Furthermore, when invoking the *matrix inverse lemma*, the covariance matrix can be simplified to

$$\mathbf{C}_l = \frac{|h_l^{(i)}|^2}{M} [(\mathbf{F}_l^{(i)})^T \boldsymbol{\Sigma}_l^{-1} \mathbf{F}_l^{(i)} + \mathbf{I}_M]^{-1} \tag{7.96}$$

Having obtained the mean as shown in (7.93) as well as the covariance matrix as shown in (7.96) of the MMSE-MUD's output $\mathbf{y}_l^{(i)}$, then, for a given transmitted symbol \mathbf{x}_m by the i th user and a channel gain h_l , the PDF of using Gaussian approximation can now be expressed as

$$\begin{aligned}
f(\mathbf{y}_l^{(i)} | \mathbf{x}_m, h_l) &= \frac{1}{\pi^M \det(\mathbf{C}_l)} \exp[-(\mathbf{y}_l^{(i)} - \boldsymbol{\mu}_l)^H \mathbf{C}_l^{-1} (\mathbf{y}_l^{(i)} - \boldsymbol{\mu}_l)] \\
l &= 0, 1, \dots, L-1; \quad i = 1, 2, \dots, K
\end{aligned} \tag{7.97}$$

With the aid of (7.97), the ‘optimum’ second stage of single-user detection in the context of the MMSE-MUD can be analysed by following steps similar to those for the decorrelating MUD studied in Section 7.4. Hence, the details are left to the reader.

Figure 7.6 illustrates the BER versus average SNR per bit performance of the TH/MC-CDMA system employing the prior noncoherent MMSE detection, when communicating over Rayleigh fading channels. In the simulations it was assumed that the $M = 8$ -ary data symbols were transmitted, one symbol duration was divided into $Q = 64$ time slots, and each data symbol was conveyed by $L = 3$ subcarriers. Furthermore, the random TH addresses were assumed. Again, in the simulations the TH addresses generating a singular cross-correlation matrix of \mathbf{R}_l as seen in (7.50) were excluded from the simulations, since these sets of TH addresses constitute the ‘bad’ TH addresses in terms of achievable BER performance. The results of Fig. 7.6 show that the TH/MC-CDMA is capable of achieving the single-user BER performance bound, regardless of the number of users supported, which is $K = 1, 2, 4, 6, 8$.

So far, a range of optimum and suboptimum prior noncoherent MUDs have been developed as shown in Sections 7.3, 7.4 and 7.5. All these prior noncoherent MUDs are derived based on the extended linear representations as shown in (7.22), (7.24), (7.26), (7.30) or (7.31), in order to take advantage of the MUD principles in coherent systems. In these prior noncoherent MUDs, such as in the prior noncoherent decorrelating MUD and the prior noncoherent MMSE-MUD, one of the common characteristics is that the MUD is operated prior to the noncoherent M -ary detection. Hence, this class of noncoherent MUDs is referred to as the prior noncoherent MUD.

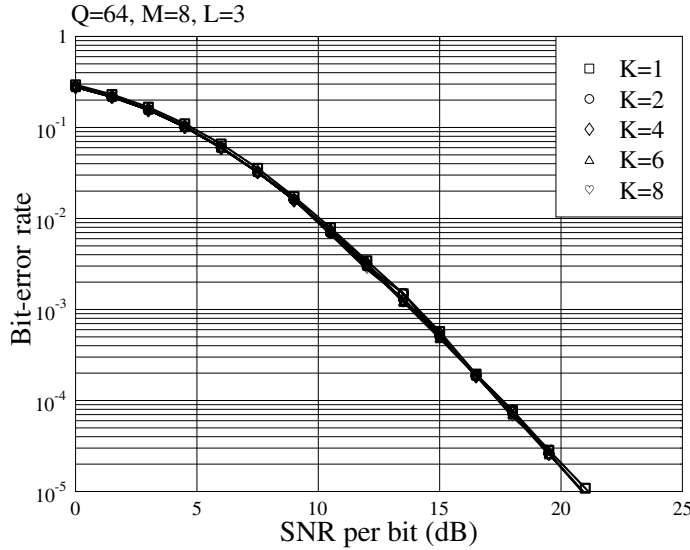


Figure 7.6: BER versus average SNR per bit performance of the TH/MC-CDMA system using prior noncoherent MMSE detection, when communicating over Rayleigh fading channels. The parameters used in simulations were $Q = 64$, $M = 8$ -ary and $L = 3$.

In the prior noncoherent MUDs the number of users supportable, or the MUI suppression capability, is mainly determined by the degrees-of-freedom of Q , which is the number of time slots per symbol-duration. The diversity order achieved is L of the number of subcarriers conveying the same data symbol. In other words, in the prior noncoherent MUDs the diversity order cannot be used to trade-off the MUI suppression capability.

In the following sections a class of noncoherent MUD is developed in the context of the TH/MC-CDMA systems. In this class of noncoherent MUDs the square-law-based noncoherent processing is first executed, which generates a set of observations for the following MUD operations. Since, in this class of noncoherent MUDs, the MUD-related operations are carried out after the square-law-based noncoherent processing, this class of noncoherent MUDs is hence referred to as the posterior noncoherent MUDs, in order to distinguish them from the prior noncoherent MUDs considered in Sections 7.3, 7.4 and 7.5.

According to the analysis in our forthcoming discourse, it can be shown that in the posterior noncoherent MUDs there exists a trade-off between the number of time slots Q per symbol duration and the MUI suppression capability as well as a trade-off between the diversity order L and the MUI suppression capability. In other words there exists a trade-off between the MUI suppression capability and the total QL number of degrees-of-freedom, which are provided by the TH/MC-CDMA system.

7.6 Optimum Posterior Noncoherent Multiuser Detection

In this and the following two sections the posterior noncoherent MUDs are established, where the MUD is operated after the square-law noncoherent processing. Specifically, in

this section, the optimum posterior noncoherent MUDs are investigated. These optimum posterior noncoherent MUDs are derived based on the MAP principles associated with considering various assumptions about the TH/MC-CDMA systems. Section 7.7 considers the suboptimum posterior noncoherent MUD, which has a relatively lower complexity than the optimum posterior noncoherent MUDs. Finally, in Section 7.8 various posterior noncoherent interference cancellation (IC) schemes are studied in the context of the TH/MC-CDMA systems.

The posterior noncoherent MUDs have been widely investigated in the literature, e.g. in references [86, 87, 201–204, 208, 209], in the context of the FFH systems with MFSK baseband modulations (MFSK-FFH). Specifically, in reference [208] Timor has presented a two-stage demodulation scheme for the MFSK-FFH system that is capable of efficiently removing most of the multiuser interference, when the effect from the background noise can be ignored. In reference [201] the MLD-MUD has been developed and investigated for the MFSK-FFH system supporting multiple users, when communicating over Rayleigh fading channels in addition to Gaussian noise. In reference [209] the optimum combining in the MFSK-FFH has been studied, when the non-Gaussian approximation of the MUI is invoked. It is shown [209] that the optimum combiner is a soft-limiting combiner, which significantly outperforms the hard-limiting combiner and also the linear combiner. In reference [203] a MUD scheme based on cancelling co-channel interference has been proposed by Mabuchi *et al.* In this proposed MUD scheme the candidates of all the users' data symbols are exploited to form the estimates to the received time-frequency (TF) matrix, and the set of data symbols yielding a TF matrix having the most number of coincident entries with the received TF matrix is selected as the estimates to the transmitted symbols. Explicitly, the computational effort of this MUD scheme is extremely high for a large number of users. In reference [86] Fiebig proposed an IC scheme for the MFSK-FFH system. In this IC scheme the candidate matrices are reduced in a recursive way. Fiebig's IC scheme is capable of achieving near optimum performance with low complexity, when communicating over interference-only channels. By contrast, in the IC scheme proposed by Halford and Brandt-Pearce [87] the knowledge about the received signal amplitudes is required for carrying out the IC. In contrast to the bulk of research, which assumes synchronous MFSK-FFH systems, in reference [204] the optimum MUD as well as multistage IC have been investigated for the asynchronous MFSK-FFH systems. In reference [202] several noncoherent MUD schemes have also been proposed and investigated in the context of the MFSK-FFH systems.

The receiver schematic block diagram in the TH/MC-CDMA system using posterior noncoherent MUD is shown in Fig. 7.7. In contrast to the receiver block diagram of Fig. 7.1 corresponding to the TH/MC-CDMA using prior noncoherent MUD, where the receiver is divided into three sub-blocks, Fig. 7.7 constitutes two sub-blocks: front-end processing and MUP. The front-end processing is a noncoherent processing stage that derives observations that are independent of the random phases introduced by carrier modulation and fading. As shown in Fig. 7.7 the random phases are removed by the square-law operations in the context of each of the L subcarriers. In Fig. 7.7, the MUP is a noncoherent MUD stage, which carries out the MUD in order to suppress the MUI. As shown in Fig. 7.7 the estimates to the transmitted symbols by the K users are directly extracted by the MUP. By contrast, in Fig. 7.1 a post-processing stage following the MUP is required in order to extract the transmitted information.

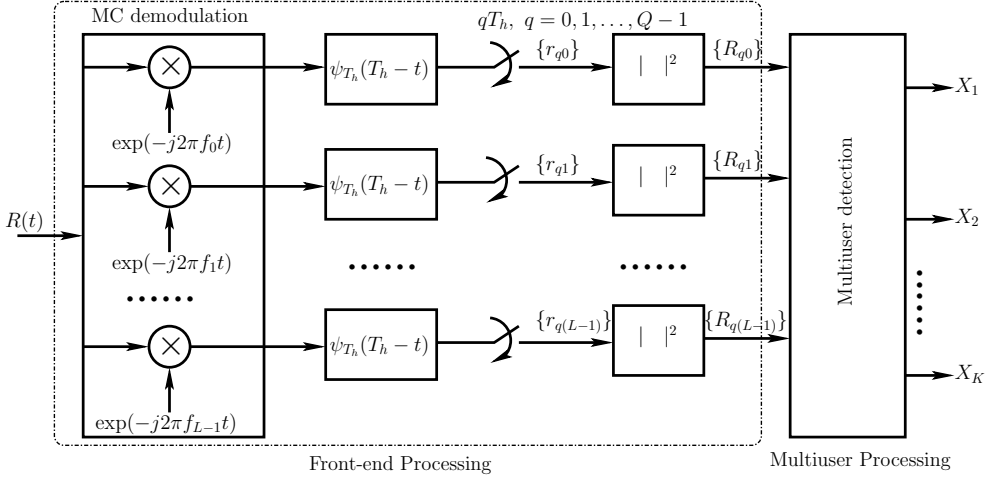


Figure 7.7: Receiver schematic block diagram of the TH/MC-CDMA system using the posterior noncoherent MUD.

According to our analysis in Section 7.1, the observations before the square-law operation can be expressed as

$$\mathbf{r}_l = \sum_{k=1}^K h_l^{(k)} \mathbf{F}_l^{(k)} \mathbb{H}_M \mathbf{x}_k + \mathbf{n}_l, \quad l = 0, 1, \dots, L-1 \quad (7.98)$$

where the q th element of \mathbf{r}_l can be denoted in detail as¹

$$r_{ql} = \sum_{k=1}^K h_l^{(k)} \delta[y_k(l), q] + n_{ql}, \quad q = 0, 1, \dots, Q-1; \quad l = 0, 1, \dots, L-1 \quad (7.99)$$

which shows that interference occurs only when two or more users activate the same time slot on a given subcarrier.

After the square-law operation, as shown in Fig. 7.7, the observations can be expressed as

$$\begin{aligned} R_{ql} &= |r_{ql}|^2 \\ &= \left| \sum_{k=1}^K h_l^{(k)} \delta[y_k(l), q] + n_{ql} \right|^2, \quad q = 0, 1, \dots, Q-1; \quad l = 0, 1, \dots, L-1 \end{aligned} \quad (7.100)$$

In posterior noncoherent MUDs, the MUDs are often operated based on a so-called FT matrix, as shown, for example, in Figs 7.8 or 7.9, where in the TH/MC-CDMA one symbol duration is divided into $Q = M = 8$ time slots and one symbol is conveyed by $L = 4$ subcarriers. The posterior noncoherent MUDs can be based either on soft-decision or hard-decision observations. Correspondingly, the FT matrices can be formed as follows.

¹Note that in the previous sections of Sections 7.1 to 7.5, r_{lq} was used as the prior noncoherent MUDs often operated on a column-by-column basis. For the posterior noncoherent MUDs, the MUD operations are generally based on FT matrices. Hence, we use the variable r_{ql} in order to relate it to the (q, l) th entry of the FT matrices.

	<i>R</i>			
7	R_{70}	R_{71}	R_{72}	R_{73}
6	R_{60}	R_{61}	R_{62}	R_{63}
5	R_{50}	R_{51}	R_{52}	R_{53}
4	R_{40}	R_{41}	R_{42}	R_{43}
3	R_{30}	R_{31}	R_{32}	R_{33}
2	R_{20}	R_{21}	R_{22}	R_{23}
1	R_{10}	R_{11}	R_{12}	R_{13}
0	R_{00}	R_{01}	R_{02}	R_{03}
	0	1	2	3

Figure 7.8: FT matrix for posterior noncoherent multiuser detection based on soft-decision observations.

	<i>R</i>			
7		■	■	
6				
5	■			■
4		■	■	
3				■
2	■			
1				■
0	■		■	
	0	1	2	3

Figure 7.9: FT matrix for posterior noncoherent multiuser detection based on hard-decision observations.

In the context of the posterior noncoherent MUDs using soft-decision observations, the FT matrix as shown in Fig. 7.8 is a $(Q \times L)$ matrix, where the rows are in the time (T)-domain with Q denoting the number of time slots per symbol duration per subcarrier, while the columns are in the frequency (F)-domain with L representing the number of subcarriers conveying the same data symbol. In the context of the posterior noncoherent MUDs using the soft-decision observations, the input to the (q, l) th element of the FT matrix is simply R_{ql} , which is an analog value. Note that we may also refer to the FT elements as cells, FT cells, etc. for clarity.

In the context of the posterior noncoherent MUDs using hard-decision observations, the FT matrix shown in Fig. 7.9 is also a $(Q \times L)$ matrix. However, the inputs to the elements

in the FT matrix are binary representing two states: ‘1’ (or ‘marked’) and ‘0’ (or ‘empty’). In more detail, the FT matrix in this case can be formed as follows. Let λ be a preset threshold. Then, whenever $R_{ql} \geq \lambda$, where $q = 0, 1, \dots, Q - 1; l = 0, 1, \dots, L - 1$, the (q, l) th entry of the FT matrix is input ‘1’ (or ‘marked’). Otherwise, if $R_{ql} < \lambda$, the input to the (q, l) th element of the FT matrix is then ‘0’ (or ‘empty’). In this way the FT matrix obtained at the receiver is in the form of Fig. 7.9.

Based on the FT matrices in the forms as shown in Figs 7.8 and 7.9, let us now investigate a range of posterior noncoherent MUDs.

7.6.1 Optimum Posterior Noncoherent Multiuser Detection in Noiseless Rayleigh Fading Channels

Let the transmitted M -ary symbols by the K number of users be collected into a vector expressed as

$$\mathbf{s} = [X_1, X_2, \dots, X_K]^T \quad (7.101)$$

Then, for a given transmitted symbol vector \mathbf{s} and a set of TH addresses of $\{\mathbf{a}_k\}$, the PDF of the received FT matrix \mathbf{R} can be expressed as $f(\mathbf{R} | \mathbf{s}, \{\mathbf{a}_k\})$. Hence, for the K -user symbol-by-symbol MAP-MUD, the transmitted symbol vector can be estimated according to the optimization problem

$$\begin{aligned} \hat{\mathbf{s}} &= \max_{\mathbf{s} \in \mathcal{X}^K} f(\mathbf{s} | \mathbf{R}, \{\mathbf{a}_k\}) \\ &\triangleq \max_{\mathbf{s} \in \mathcal{X}^K} \{P(\mathbf{s}) f(\mathbf{R} | \mathbf{s}, \{\mathbf{a}_k\})\} \end{aligned} \quad (7.102)$$

where $\mathcal{X} = \{0, 1, \dots, M - 1\}$ is a set containing the M possible transmitted symbols.

When the K users’ transmitted symbols are independent random variables, we then have

$$P(\mathbf{s}) = \prod_{k=1}^K P(X_k) \quad (7.103)$$

Furthermore, using the fact that the QL entries in the FT matrix \mathbf{R} are independent, $f(\mathbf{R} | \mathbf{s}, \{\mathbf{a}_k\})$ can be written as

$$f(\mathbf{R} | \mathbf{s}, \{\mathbf{a}_k\}) = \prod_{q=0}^{Q-1} \prod_{l=0}^{L-1} f(R_{ql} | \mathbf{s}, \{\mathbf{a}_k\}) \quad (7.104)$$

Substituting (7.103) and (7.104) into (7.102), the MAP-assisted optimization can be modified to

$$\hat{\mathbf{s}} = \max_{\{\mathbf{X}_k \in \mathcal{X}\}_{k=1}^K} \left\{ \prod_{k=1}^K \prod_{q=0}^{Q-1} \prod_{l=0}^{L-1} P(X_k) f(R_{ql} | \mathbf{s}, \{\mathbf{a}_k\}) \right\} \quad (7.105)$$

Furthermore, when the transmitted symbols are uniformly distributed, the K -user symbol-by-symbol MAP-MUD is reduced to the K -user symbol-by-symbol MLD-MUD and the corresponding optimization problem can be expressed as

$$\hat{\mathbf{s}} = \max_{\{\mathbf{X}_k \in \mathcal{X}\}_{k=1}^K} \left\{ \prod_{q=0}^{Q-1} \prod_{l=0}^{L-1} f(R_{ql} | \mathbf{s}, \{\mathbf{a}_k\}) \right\} \quad (7.106)$$

When the TH/MC-CDMA is operated in a noiseless communications environment, from (7.100) the square-law output R_{ql} is given by

$$R_{ql} = \left| \sum_{k=1}^K h_l^{(k)} \delta[y_k(l), q] \right|^2, \quad q = 0, 1, \dots, Q-1; l = 0, 1, \dots, L-1 \quad (7.107)$$

In this case, the PDF of R_{ql} can be derived as follows. First, when the (q, l) th cell in \mathbf{R} is not activated by any user, we have in (7.107) $\delta[y_k(l), q] = 0$ for any k . Hence, the corresponding PDF is given by

$$f(R_{ql} = 0 | s, \{\mathbf{a}_k\}) = 1 \quad \text{and} \quad f(R_{ql} \neq 0 | s, \{\mathbf{a}_k\}) = 0 \quad (7.108)$$

Therefore, when communicating over noiseless channels, the search space's size in the MAP-MUD or MLD-MUD, which is M^K as shown in (7.105) or (7.106), can be significantly reduced. Only those transmitted symbols yielding nonzero entries in the FT matrix \mathbf{R} are required to be tested in (7.105) or (7.106). Specifically, for the example having the FT matrix \mathbf{R} as shown in Fig. 7.8, there are at most KL nonzero elements in the FT matrix, when the K user signals are transmitted over noiseless channels. Hence, the MAP-MUD or MLD-MUD only needs to test those symbols which activate the FT elements corresponding to the nonzero elements.

Second, when the (q, l) th FT element is activated by K_{ql} users, according to (7.107), the decision variable is then given by

$$\begin{aligned} R_{ql} &= \left| \sum_{k=1}^{K_{ql}} h_l^{(k)} \right|^2 \\ &= \left(\Re \left\{ \sum_{k=1}^{K_{ql}} h_l^{(k)} \right\} \right)^2 + \left(\Im \left\{ \sum_{k=1}^{K_{ql}} h_l^{(k)} \right\} \right)^2 \end{aligned} \quad (7.109)$$

where both $h_R = \Re \left\{ \sum_{k=1}^{K_{ql}} h_l^{(k)} \right\}$ and $h_I = \Im \left\{ \sum_{k=1}^{K_{ql}} h_l^{(k)} \right\}$ are the sum of K_{ql} independent Gaussian random variables. Since, when communicating over flat Rayleigh fading channels, both the real and imaginary parts of $h_l^{(k)}$ obey the Gaussian distributions with zero mean and a common variance of $1/2$, h_R and h_I are Gaussian random variables having zero mean and a common variance of $K_{ql}/2$. Hence, R_{ql} obeys the χ^2 -distribution with two degrees-of-freedom, i.e. the exponential distribution, which can be expressed as

$$f(R_{ql} | s, \{\mathbf{a}_k\}) = \frac{1}{K_{ql}} \exp \left(-\frac{R_{ql}}{K_{ql}} \right), \quad R_{ql} \geq 0 \quad (7.110)$$

Consequently, on applying the above results to (7.105) or (7.106), the K -user symbol-by-symbol MAP-MUD can be described as

$$\hat{s} = \max_{\{X_k \in \mathcal{X}\}_{k=1}^K : \{K_{ql} \geq 1\}} \left\{ \prod_{k=1}^K P(X_k) \underbrace{\prod_{q=0}^{Q-1} \prod_{l=0}^{L-1} \frac{1}{K_{ql}} \exp \left(-\frac{R_{ql}}{K_{ql}} \right)}_{K_{ql} \geq 1} \right\} \quad (7.111)$$

and the K -user symbol-by-symbol MLD-MUD can be stated as

$$\hat{s} = \max_{\{X_k \in \mathcal{X}\}_{k=1}^K; \{K_{ql} \geq 1\}} \left\{ \underbrace{\prod_{q=0}^{Q-1} \prod_{l=0}^{L-1} \frac{1}{K_{ql}} \exp\left(-\frac{R_{ql}}{K_{ql}}\right)}_{K_{ql} \geq 1} \right\} \quad (7.112)$$

When using the log-likelihood, (7.112) can also be expressed as

$$\hat{s} = \min_{\{X_k \in \mathcal{X}\}_{k=1}^K; \{K_{ql} \geq 1\}} \left\{ \underbrace{\sum_{q=0}^{Q-1} \sum_{l=0}^{L-1} \left[\ln K_{ql} + \frac{R_{ql}}{K_{ql}} \right]}_{K_{ql} \geq 1} \right\} \quad (7.113)$$

For the single-user symbol-by-symbol MAP-MUD, let us assume that the first user is the desired user to be detected. Based on (7.111), the MAP-assisted optimization problem can be stated as

$$\hat{X}_1 = \max_{X_1 \in \mathcal{X}; \{K_{ql} \geq 1\}} \left\{ \underbrace{\sum_{X_2 \in \mathcal{X}} \cdots \sum_{X_K \in \mathcal{X}} \left(\prod_{k=1}^K P(X_k) \right)}_{\{K_{ql} \geq 1\}} \underbrace{\prod_{q=0}^{Q-1} \prod_{l=0}^{L-1} \frac{1}{K_{ql}} \exp\left(-\frac{R_{ql}}{K_{ql}}\right)}_{K_{ql} \geq 1} \right\} \quad (7.114)$$

Similarly, based on (7.112), the single-user symbol-by-symbol MLD-MUD can be stated as the optimization problem of

$$\hat{X}_1 = \max_{X_1 \in \mathcal{X}; \{K_{ql} \geq 1\}} \left\{ \underbrace{\sum_{X_2 \in \mathcal{X}} \cdots \sum_{X_K \in \mathcal{X}} \prod_{q=0}^{Q-1} \prod_{l=0}^{L-1} \frac{1}{K_{ql}} \exp\left(-\frac{R_{ql}}{K_{ql}}\right)}_{\{K_{ql} \geq 1\}} \right\} \quad (7.115)$$

or expressed in log-likelihood as

$$\hat{X}_1 = \min_{X_1 \in \mathcal{X}; \{K_{ql} \geq 1\}} \left\{ \underbrace{\sum_{X_2 \in \mathcal{X}} \cdots \sum_{X_K \in \mathcal{X}} \sum_{q=0}^{Q-1} \sum_{l=0}^{L-1} \left[\ln K_{ql} + \frac{R_{ql}}{K_{ql}} \right]}_{\{K_{ql} \geq 1\}} \right\} \quad (7.116)$$

Finally, for the single-user bit-level MAP-MUD and MLD-MUD, the symbol transmitted by the k th user can be expressed in binary as (7.16). Let us consider the λ th bit in the binary representation as shown in (7.16). Let \mathcal{X}^+ contain the M -ary symbols, the λ th bit in their binary representations is +1. Similarly, let \mathcal{X}^- contain the M -ary symbols, the λ th bit in their binary representations is -1. Explicitly, the size of both \mathcal{X}^+ and \mathcal{X}^- is $M/2$. Consequently, for the λ th bit transmitted by the reference user, the detector computes

$$\begin{aligned} \Lambda(\tilde{b}_\lambda) &= \ln \left[\frac{f(\mathbf{R} | \tilde{b}_\lambda = +1; s, \{\mathbf{a}_k\})}{f(\mathbf{R} | \tilde{b}_\lambda = -1; s, \{\mathbf{a}_k\})} \right] + \ln \left[\frac{P(\tilde{b}_\lambda = +1)}{P(\tilde{b}_\lambda = -1)} \right] \\ &= \Lambda_e(\tilde{b}_\lambda) + \Lambda_a(\tilde{b}_\lambda), \quad \lambda = 0, 1, \dots, b-1 \end{aligned} \quad (7.117)$$

where $\Lambda_a(\tilde{b}_\lambda) = \ln[P(\tilde{b}_\lambda = +1)/P(\tilde{b}_\lambda = -1)]$ represents the *a priori* information about \tilde{b}_λ , while

$$\Lambda_e(\tilde{b}_\lambda) = \ln \left[\frac{f(\mathbf{R} | \tilde{b}_\lambda = +1; s, \{\mathbf{a}_k\})}{f(\mathbf{R} | \tilde{b}_\lambda = -1; s, \{\mathbf{a}_k\})} \right] \quad (7.118)$$

is the extrinsic information obtained from the detection. In (7.118) the conditional PDFs $f(\mathbf{R} | \tilde{b}_\lambda = \pm 1; s, \{\mathbf{a}_k\})$ can be computed as

$$\begin{aligned} f(\mathbf{R} | \tilde{b}_\lambda = \pm 1; s, \{\mathbf{a}_k\}) &= \underbrace{\sum_{X_1 \in \mathcal{X}^\pm} \sum_{X_2 \in \mathcal{X}} \cdots \sum_{X_K \in \mathcal{X}}}_{\{K_{ql} \geq 1\}} \prod_{k=1}^K P(X_k) \\ &\times \underbrace{\prod_{q=0}^{Q-1} \prod_{l=0}^{L-1} \frac{1}{K_{ql}}}_{K_{ql} \geq 1} \exp \left(-\frac{R_{ql}}{K_{ql}} \right) \end{aligned} \quad (7.119)$$

where the set \mathcal{X}^+ or \mathcal{X}^- is applied in corresponding to $\tilde{b}_\lambda = +1$ or $\tilde{b}_\lambda = -1$, respectively.

Note that (7.117) can efficiently be computed by the log-MAP algorithm, e.g., as stated in reference [90].

7.6.2 Optimum Posterior Noncoherent Multiuser Detection in Noisy Rayleigh Fading Channels

In the last section the optimum posterior MUDs have been derived, when assuming that the TH/MC-CDMA signals are transmitted over noiseless Rayleigh fading channels. When the TH/MC-CDMA signals are transmitted over Rayleigh fading channels with AWGN, the K -user symbol-by-symbol MAP-MUD and MLD-MUD can also be expressed as (7.105) and (7.106). However, in this case the output R_{ql} of the square-law detector is given by

$$R_{ql} = \left| \sum_{k=1}^K h_l^{(k)} \delta[y_k(l), q] + n_{ql} \right|^2, \quad q = 0, 1, \dots, Q-1; l = 0, 1, \dots, L-1 \quad (7.120)$$

where n_{ql} is Gaussian distributed with zero mean and a variance of $\sigma^2/2 = LN_0/2E_s = L/2\gamma_s$ per dimension, where $E_s = PT_s = PQT_h$ represents the received energy per M -ary symbol, $\gamma_s = E_s/N_0 = bE_b/N_0$ represents the SNR per symbol.

Let us assume that, for a given set of transmitted symbols by the K users, the number of users activating the (q, l) th FT element is K_{ql} ($0 \leq K_{ql} \leq K$). Then, (7.120) can be expressed as

$$R_{ql} = \left| \sum_{k=1}^{K_{ql}} h_l^{(k)} + n_{ql} \right|^2, \quad q = 0, 1, \dots, Q-1; l = 0, 1, \dots, L-1 \quad (7.121)$$

Since $h_l^{(k)}$ as well as n_{ql} are independent Gaussian random variables, it can be easily shown that the PDF of R_{ql} can be expressed as

$$f(R_{ql} | s, \{a_k\}) = \frac{1}{K_{ql} + \sigma^2} \exp\left(-\frac{R_{ql}}{K_{ql} + \sigma^2}\right), \quad q = 0, 1, \dots, Q-1 \\ l = 0, 1, \dots, L-1 \quad (7.122)$$

Applying the PDFs as shown in (7.122) to (7.105) and (7.106), the optimization problem for the K -user symbol-by-symbol MAP-MUD can now be stated as

$$\hat{s} = \max_{\{X_k \in \mathcal{X}\}_{k=1}^K} \left\{ \prod_{k=1}^K P(X_k) \prod_{q=0}^{Q-1} \prod_{l=0}^{L-1} \frac{1}{K_{ql} + \sigma^2} \exp\left(-\frac{R_{ql}}{K_{ql} + \sigma^2}\right) \right\} \\ \triangleq \min_{\{X_k \in \mathcal{X}\}_{k=1}^K} \left\{ \left(-\sum_{k=1}^K \ln P(X_k) \right) + \sum_{q=0}^{Q-1} \sum_{l=0}^{L-1} \left[\ln(K_{ql} + \sigma^2) + \frac{R_{ql}}{K_{ql} + \sigma^2} \right] \right\} \quad (7.123)$$

and that for the symbol-by-symbol MLD-MUD as

$$\hat{s} = \max_{\{X_k \in \mathcal{X}\}_{k=1}^K} \left\{ \prod_{q=0}^{Q-1} \prod_{l=0}^{L-1} \frac{1}{K_{ql} + \sigma^2} \exp\left(-\frac{R_{ql}}{K_{ql} + \sigma^2}\right) \right\} \\ \triangleq \min_{\{X_k \in \mathcal{X}\}_{k=1}^K} \left\{ \sum_{q=0}^{Q-1} \sum_{l=0}^{L-1} \left[\ln(K_{ql} + \sigma^2) + \frac{R_{ql}}{K_{ql} + \sigma^2} \right] \right\} \quad (7.124)$$

Notice that, in the FT matrix there might be many FT elements that are not activated by any users, when their transmitted symbols are given. Let the number of FT elements having not been activated be $\mathcal{N}(x)$ conditional on $x = [X_1, X_2, \dots, X_K]^T$. Then, the optimization problems stated in (7.123) and (7.124) can also be written as

$$\hat{s} = \max_{\{X_k \in \mathcal{X}\}_{k=1}^K} \left\{ \prod_{k=1}^K P(X_k) \underbrace{\prod_{q=0}^{Q-1} \prod_{l=0}^{L-1} \frac{1}{K_{ql} + \sigma^2} \exp\left(-\frac{R_{ql}}{K_{ql} + \sigma^2}\right)}_{K_{ql} \geq 1} \right. \\ \times \left. \frac{1}{\sigma^{2\mathcal{N}(x)}} \exp\left(-\frac{\mathcal{N}(x)R_{ql}}{\sigma^2}\right) \right\} \\ \triangleq \min_{\{X_k \in \mathcal{X}\}_{k=1}^K} \left\{ -\sum_{k=1}^K \ln P(X_k) + \underbrace{\sum_{q=0}^{Q-1} \sum_{l=0}^{L-1} \left[\ln(K_{ql} + \sigma^2) + \frac{R_{ql}}{K_{ql} + \sigma^2} \right]}_{K_{ql} \geq 1} \right. \\ \left. + \mathcal{N}(x) \ln \sigma^2 + \frac{\mathcal{N}(x)R_{ql}}{\sigma^2} \right\} \quad (7.125)$$

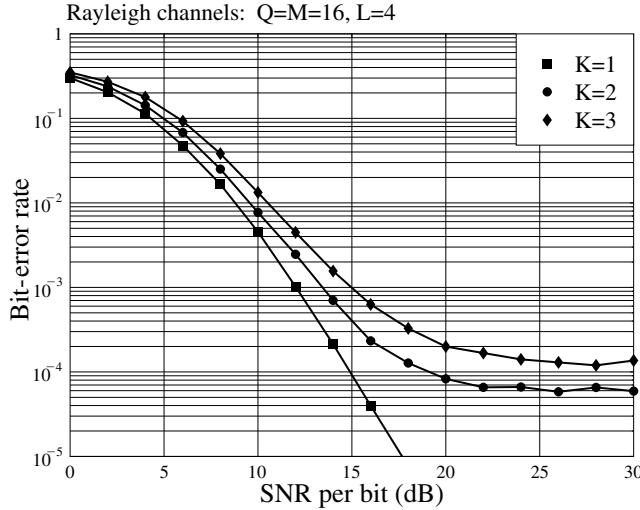


Figure 7.10: BER versus average SNR per bit performance for the TH/MC-CDMA system employing the optimum posterior noncoherent MLD-MUD, when communicating Rayleigh fading channels.

and

$$\begin{aligned} \hat{s} &= \max_{\{\mathbf{x}_k \in \mathcal{X}\}_{k=1}^K} \left\{ \frac{1}{\sigma^{2\mathcal{N}(\mathbf{x})}} \exp\left(-\frac{\mathcal{N}(\mathbf{x})R_{ql}}{\sigma^2}\right) \underbrace{\prod_{q=0}^{Q-1} \prod_{l=0}^{L-1} \frac{1}{K_{ql} + \sigma^2} \exp\left(-\frac{R_{ql}}{K_{ql} + \sigma^2}\right)}_{K_{ql} \geq 1} \right\} \\ &\triangleq \min_{\{\mathbf{x}_k \in \mathcal{X}\}_{k=1}^K} \left\{ \mathcal{N}(\mathbf{x}) \ln \sigma^2 + \frac{\mathcal{N}(\mathbf{x})R_{ql}}{\sigma^2} + \underbrace{\sum_{q=0}^{Q-1} \sum_{l=0}^{L-1} \left[\ln(K_{ql} + \sigma^2) + \frac{R_{ql}}{K_{ql} + \sigma^2} \right]}_{K_{ql} \geq 1} \right\} \quad (7.126) \end{aligned}$$

Based on (7.123) and (7.124) or (7.125) and (7.126), the single-user symbol-by-symbol MAP-MUD and MLD-MUD as well as the bit-level MAP-MUD and MLD-MUD can be easily derived by following the same principles as shown in Section 7.6.1. Hence, the details are ignored.

Figure 7.10 shows the BER performance of the TH/MC-CDMA system using the optimum posterior noncoherent MLD-MUD. The parameters with the considered TH/MC-CDMA were $Q = M = 16$ and $L = 4$, $K = 1, 2, 3$ users were supported and random TH patterns were assumed. The simulations were based on (7.124). As shown in Fig. 7.10, the optimum posterior noncoherent detector is capable of efficiently mitigating the MUI and yielding the best achievable BER performance in comparison with other types of noncoherent MUD as discussed, for example, in Section 7.8.

When the number of users supported is $K = 2$ or 3 , as shown in Fig. 7.10, there is a BER floor observed. The BER floor is not due to the optimum posterior noncoherent detector, but the result of the random TH patterns. In more detail, when the random TH patterns are used, there are chances that the TH patterns of two or more users are linearly dependent. In this

case the optimum posterior noncoherent detector is incapable of distinguishing between the symbols transmitted by the linearly dependent users. Note that when linearly independent TH patterns are used, the BER floors seen in Fig. 7.10 will disappear and the BER performance for $K = 2$ or 3 should be similar to that for $K = 1$.

It can be derived that, for the TH/MC-CDMA supporting $K = 2$ users, the BER floor occurs at around

$$P_b(\text{floor}) = \frac{1}{2} \cdot \frac{1}{2} \cdot \frac{M-1}{M} \cdot \frac{1}{M^{L-1}} \quad (7.127)$$

where the first $1/2$ reflects the relationship between the bit error probability and symbol error probability in M -ary signalling, the second $1/2$ is due to the fact that when the two TH patterns are linearly dependent, the detector randomly selects one symbol from two and hence the error probability is $1/2$, $(M-1)/M$ takes into account the symbols transmitted by two users being different and, finally, $1/M^{L-1}$ is the probability of the event that the two TH patterns are linearly dependent. Applying $M = 16$ and $L = 4$ to (7.127), we obtain $P_b(\text{floor}) = 5.7 \times 10^{-5}$, which is the BER floor corresponding to $K = 2$, as shown in Fig. 7.10.

The BER floors for the other sets of parameters may be deduced similarly. Equation (7.127) implies that the BER floors can be decreased by increasing the value of M and/or of L . Additionally, as mentioned previously, the BER floors can be fully removed by employing the linearly independent TH patterns.

7.7 Suboptimum Posterior Noncoherent Multiuser Detection in Rayleigh Fading Channels

As shown in (7.123) and (7.124), or (7.125) and (7.126), it can be seen that, when communicating over Rayleigh fading channels with noise, the number of candidates for both the optimum MAP-MUD and MLD-MUD to test is M^K , implying that the complexity of these optimum MUDs increases exponentially with the number of users. Hence, these optimum MUDs are impractical when the number of users supported is high. In this section the suboptimum posterior noncoherent MAP-MUDs and MLD-MUDs are considered. These suboptimum MUDs can significantly reduce the search space's size in comparison with the corresponding optimum MAP-MUDs or MLD-MUDs.

The detection in suboptimum MAP-MUDs or MLDs starts with finding an appropriate search space through hard-decision as follows.

1. Based on the received FT matrix of \mathbf{R} , as shown in Fig. 7.8, a FT matrix is formed by comparing each of the soft entries in Fig. 7.8 with a preset threshold.² If an entry in \mathbf{R} is higher than the threshold, the corresponding entry in the hard-decision-based FT matrix is then set as ‘1’ (marked). Otherwise, if a soft entry in \mathbf{R} is not higher than the threshold, the corresponding entry in the hard-decision-based FT matrix is then set as ‘0’ (empty). Let the resultant hard-decision-based accompanying FT matrix be expressed as \mathbf{R}_a , which is in the form of \mathbf{R}_a as shown in Fig. 7.11.

²Note that the threshold can be determined by considering the signal-to-noise ratio (SNR) as well as the affordable detection complexity. Generally, the threshold should be set to minimize the miss probability for a given false-alarm probability. A bigger false-alarm probability will result in a larger search space of candidates.

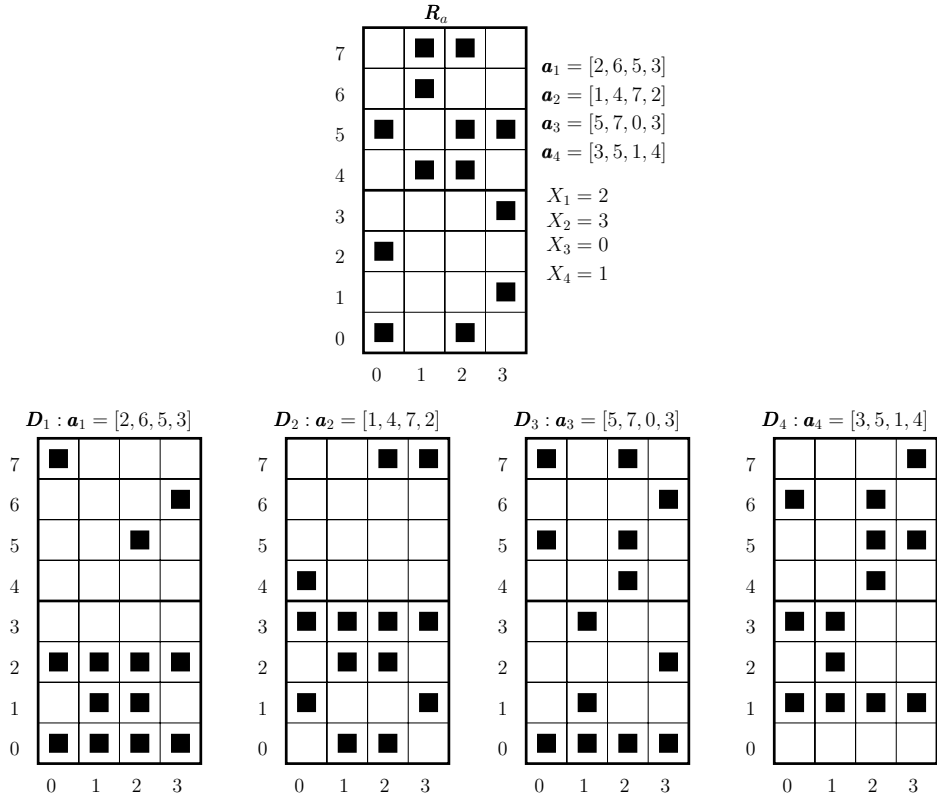


Figure 7.11: Received hard-decision based FT matrix R_a as well as the FT matrices formed after the time-dehopping operations using the TH addresses of users 1, 2, 3 and 4.

2. The accompanying FT matrix R_a is de-hopped by the TH addresses of the K users, yielding K de-hopped matrices expressed as D_1 , D_2 , ..., D_K , respectively. In the example of Fig. 7.11, these matrices are shown as D_1 , D_2 , D_3 , D_4 .
3. Based on the de-hopped matrices D_1 , D_2 , ..., D_K , the possible symbols transmitted by the K users are identified. Specifically, depending on the affordable detection complexity, the symbols generating the complete rows with L entries per row and the symbols generating the rows with $(L-1)$, $(L-2)$, etc., entries per row are identified as the possible symbols transmitted. For the example considered in Fig. 7.11, the possible transmitted symbols can be identified as $\{X_1 \in \{0, 2\}; X_2 \in \{3\}; X_3 \in \{0\}; X_4 \in \{1\}\}$, when both the complete rows and the rows with three entries (there are no rows with three entries) are considered. Let the set of the possible symbols transmitted be expressed as $\{X_i \in \mathcal{X}_i\}_{i=1}^K$.

Having obtained a set $\{X_i \in \mathcal{X}_i\}_{i=1}^K$ for the possible symbols transmitted, we re-encode these possible symbols by invoking the TH addresses of the K users, in order to form a FT matrix R_t , which shows the FT entries that are possibly activated by the K users. R_t is in the form of R_a as shown in Fig. 7.11 for the example considered. Furthermore, it can be shown

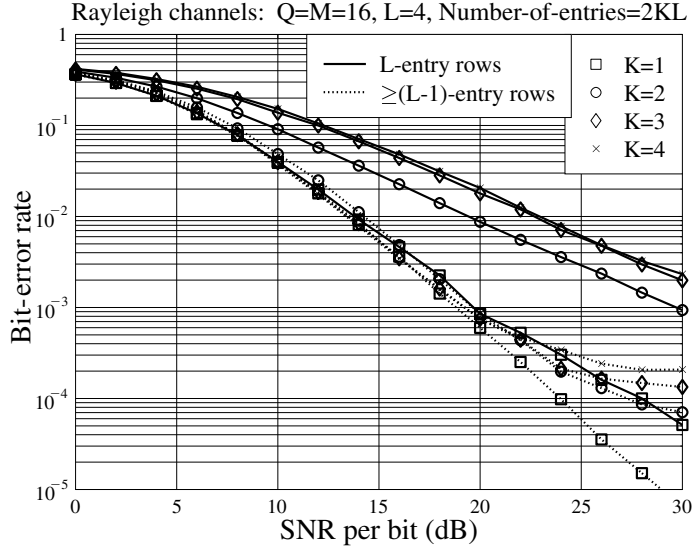


Figure 7.12: BER versus average SNR per bit performance for the TH/MC-CDMA system employing the suboptimum MLD-MUD, when communicating over Rayleigh fading channels. The number-of-entries shown in the figure represents the number of entries in the hard-decision-based FT matrix \mathbf{R}_a , as seen, e.g., in Fig. 7.11.

that \mathbf{R}_t might be different from the accompanying matrix \mathbf{R}_a , since the possible symbols transmitted may also include those which generate the rows with $(L - 1)$ or fewer entries. Let the marked elements in \mathbf{R}_t be collected in a set defined as \mathcal{M} .

Based on the set $\{X_i \in \mathcal{X}_i\}_{i=1}^K$ of the possible symbols transmitted and the set \mathcal{M} containing the elements possibly activated, the (suboptimum) MAP-MUD can now be stated as

$$\hat{s} = \min_{\{X_k \in \mathcal{X}_k\}_{k=1}^K} \left\{ -\sum_{k=1}^K \ln P(X_k) + \underbrace{\sum_{q=0}^{Q-1} \sum_{l=0}^{L-1} \left[\ln(K_{ql} + \sigma^2) + \frac{R_{ql}}{K_{ql} + \sigma^2} \right]}_{(q,l) \in \mathcal{M}} \right\} \quad (7.128)$$

and the (suboptimum) MLD-MUD as

$$\hat{s} = \min_{\{X_k \in \mathcal{X}_k\}_{k=1}^K} \left\{ \underbrace{\sum_{q=0}^{Q-1} \sum_{l=0}^{L-1} \left[\ln(K_{ql} + \sigma^2) + \frac{R_{ql}}{K_{ql} + \sigma^2} \right]}_{(q,l) \in \mathcal{M}} \right\} \quad (7.129)$$

Note that, as for the example considered in Fig. 7.11, there are only two symbol vectors needing to be detected associated with the marked elements in \mathbf{R}_t as shown in Fig. 7.11. The first symbol vector is $\{X_1, X_2, X_3, X_4\} = \{0, 3, 0, 1\}$ and the second is $\{X_1, X_2, X_3, X_4\} = \{2, 3, 0, 1\}$.

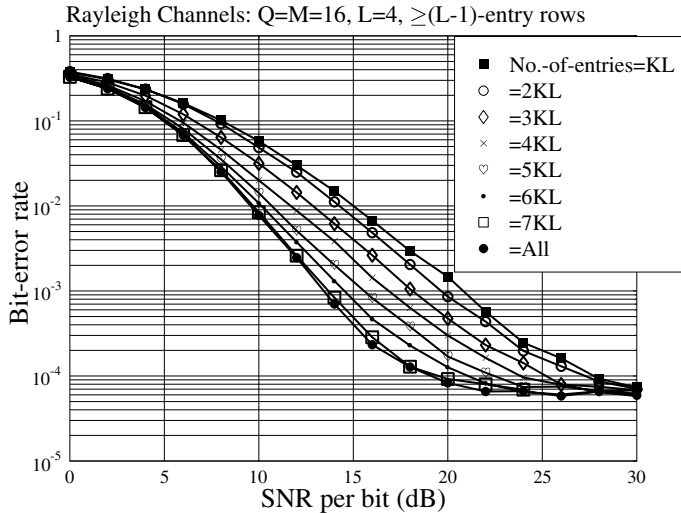


Figure 7.13: BER versus average SNR per bit performance for the TH/MC-CDMA system employing the suboptimum MLD-MUD, when communicating over Rayleigh fading channels. The number of users supported is $K = 2$. The number-of-entries shown in the figure represents the number of entries in hard-decision-based FT matrix \mathbf{R}_a , as seen, e.g., in Fig. 7.11.

Figure 7.12 shows the BER versus average SNR per bit performance of the TH/MC-CDMA using the suboptimum MLD-MUD considered in this subsection, when communicating over Rayleigh fading channels. In the TH/MC-CDMA system considered, we assumed $Q = M = 16$, one 16-ary symbol was transmitted by $L = 4$ subcarriers, and the random TH patterns were assumed. The number of users supported was $K = 1, 2, 3, 4$. Additionally, as noted in Fig. 7.12, the number of entries used for finding the possible candidate symbols was $2KL$, which were chosen from the received FT matrix of \mathbf{R} as shown in Fig. 7.8. Instead of using the threshold-assisted selection, from \mathbf{R} the $2KL$ entries having the largest values were selected to form \mathbf{R}_a , which is in the form as shown in Fig. 7.11. Furthermore, as shown in Fig. 7.12, the candidate symbols were determined by the rows having L entries, or by the rows having $(L - 1)$ or L entries.

The results of Fig. 7.12 show that the BER performance degrades explicitly when the candidate symbols are selected only according to the complete rows having L entries. By contrast, when the candidate symbols are selected according to the rows having L as well as $(L - 1)$ entries, the BER performance corresponding to different K is similar, when the SNR per bit value is lower than 20 dB. When the SNR per bit value is higher than 20 dB, the BER performance degrades when increasing the number of users, and, when $K > 1$, the BER floors are observed due to the reasons as discussed in the context of Fig. 7.10. Additionally, Fig. 7.12 shows that when $K > 1$, the BER performance of the detector searching the candidates based on the rows having L and $(L - 1)$ entries is much better than that of the detector searching the candidates based only on the complete rows.

Figure 7.13 illustrates the trade-off between the achievable BER performance and the number of entries – which is proportional to the implementational complexity – in \mathbf{R}_a used for finding the candidate symbols. The candidate symbols were formed based on the rows

having either L entries or $(L - 1)$ entries. As shown in Fig. 7.13, when more entries are used yielding more candidate symbols for search by the suboptimum MLD-MUD, better BER performance is achievable.

7.8 Posterior Noncoherent Interference Cancellation

Having considered the optimum and suboptimum posterior noncoherent MUDs in Sections 7.6 and 7.7, in this section we consider a range of noncoherent IC schemes for detection of the TH/MC-CDMA signals. The IC schemes considered here have either been studied, e.g., in references [86, 87, 202, 203], in the context of the MFSK-FFH systems, or represent the extensions of the IC schemes proposed in these references. Generally, the IC schemes are operated on the basis of the hard-decision-based TF- or FT-matrices. A noncoherent IC scheme is usually constituted of two stages. The first stage carries out the conventional noncoherent detection, hence we refer to it as the conventional detection stage (CD-stage). The second stage implements the MUI cancellation and hence it is referred to as the IC-stage. Let us first illustrate the principles of the conventional single-user posterior noncoherent detection based on the FT-matrix principles.

7.8.1 Conventional Single-User Posterior Noncoherent Detection

The conventional single-user posterior detection, which is referred to as SUD for simplicity, for the multiuser FFH systems using MFSK modulation has been investigated, e.g., by Goodman *et al.* in reference [13]. For our TH/MC-CDMA system using MPPM modulation, the conventional SUD can be carried out in a similar procedure as that stated in reference [13]. As described previously in this chapter, the conventional SUD operations in the TH/MC-CDMA system can be illustrated by means of FT matrices having Q rows and L columns, where the Q rows correspond to the Q distinct time slots, while the L columns represent the L number of subcarriers conveying the same M -ary symbol. Specifically, the conventional SUD for the TH/MC-CDMA system using MPPM can be well understood by referring to Fig. 7.14, where the TH/MC-CDMA system supporting four users was assumed, one symbol duration was divided into $Q = M = 8$ time slots and the number of subcarriers conveying the same data symbol was $L = 4$. As shown in Fig. 7.14, when the received FT matrix \mathbf{R} is obtained, four FT matrices denoted by \mathbf{D}_1 , \mathbf{D}_2 , \mathbf{D}_3 and \mathbf{D}_4 can be obtained by the subtraction operation in $GF(8)$ with the aid of the unique TH addresses \mathbf{a}_1 , \mathbf{a}_2 , \mathbf{a}_3 and \mathbf{a}_4 from the marked elements of \mathbf{R} according to $q \ominus a_{kl}$ on the column-by-column basis, i.e. the element at (q, l) is moved to the location of $(q \ominus a_{kl}, l)$. Based on \mathbf{D}_1 , \mathbf{D}_2 , \mathbf{D}_3 and \mathbf{D}_4 the majority vote-based decoder can be used for detection, opting to decide in favour of the particular 8-ary symbols corresponding to the specific row with the highest number of non-zero entries in \mathbf{D}_1 , \mathbf{D}_2 , \mathbf{D}_3 and \mathbf{D}_4 , to provide estimates of the transmitted symbols by users $k = 1, 2, 3$ and 4 . For example, for users $k = 1, 2, 3$ and 4 , based on the FT matrices of \mathbf{D}_1 , \mathbf{D}_2 , \mathbf{D}_3 as well as \mathbf{D}_4 in Fig. 7.14, we find that the transmitted symbols by users 1, 2, 3 and 4 were 2, 3, 0, 1, which can be correctly decoded with the aid of the unambiguous majority vote.

However, when there are two or more rows in a FT matrix for detection that have the same number of maximum entries, for example, as shown in \mathbf{D}_1 in Figs 7.18 and 7.20 in the following subsections, the detector has to select randomly one of the rows with the

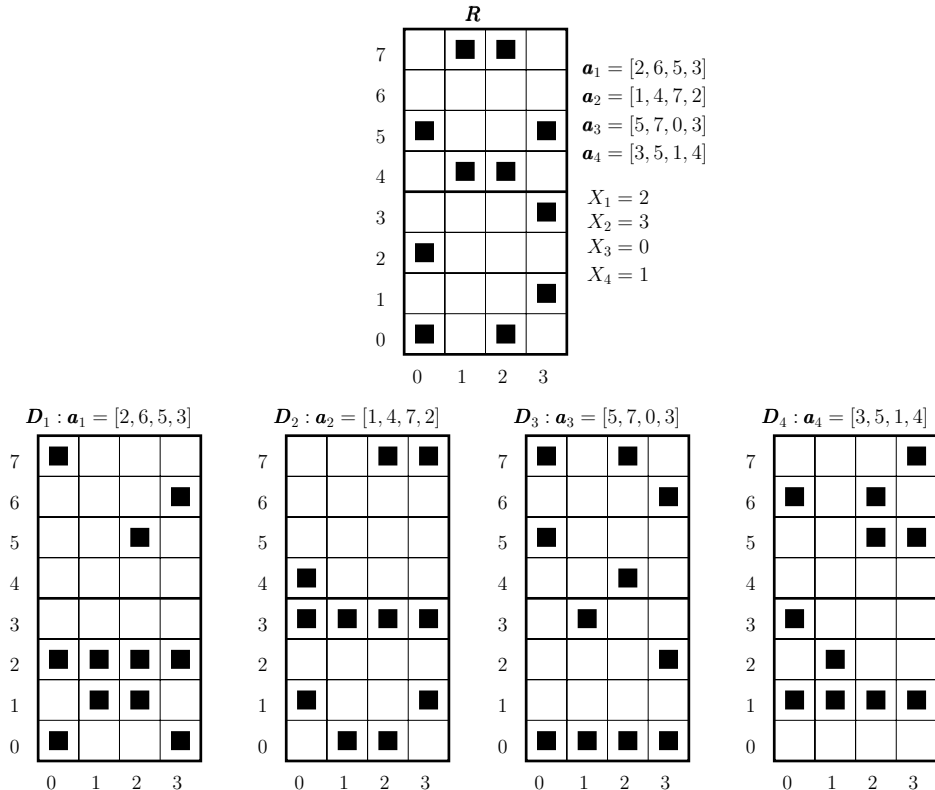


Figure 7.14: Illustration of the conventional SUD operations in the TH/MC-CDMA system, which employs $Q = M = 8$ time-slots per symbol and transmits one symbol on $L = 4$ subcarriers. $K = 4$ users are supported using the TH addresses $\mathbf{a}_1, \mathbf{a}_2, \mathbf{a}_3$ and \mathbf{a}_4 . It can be shown that, after the time de-hopping of the received matrix \mathbf{R} using the TH addresses $\mathbf{a}_1, \mathbf{a}_2, \mathbf{a}_3$ and \mathbf{a}_4 , respectively, the four symbols transmitted can be correctly recovered with the aid of the majority vote-assisted detection.

maximum entries. Since the detector does not have explicit knowledge as to which users activated the individual time slots, this detection scheme may result in detection errors. Hence, when the conventional SUD is used, it can be implied that even in the absence of noise, the detection may still make erroneous decisions concerning the transmitted symbols, owing to the presence of multiuser interference. Therefore, more potent multiuser detection, such as those considered in Sections 7.3 to 7.7, is required, in order to improve the detection performance of the TH/MC-CDMA system. The optimum or suboptimum MUDs considered in Sections 7.3 to 7.7 have been built based on the soft-valued observations that are obtained before or after the noncoherent (square-law) operations. By contrast, in Sections 7.8.2 to 7.8.4, a range of posterior IC schemes are investigated in the context of the TH/MC-CDMA, which, except for the IC scheme considered in Section 7.8.4, are developed based on the hard-decision observations.

Note that when the ‘marked’ entries of the received matrix \mathbf{R} , such as the \mathbf{R} in Fig. 7.14, are soft values, such as the square-law outputs, then, in addition to the majority vote decoding, various other noncoherent diversity combining schemes as described in Appendix 7.9 may be invoked to assist detection of the TH/MC-CDMA signals.

Let us now analyse the error probability of the TH/MC-CDMA system using conventional SUD when communicating over noiseless or noisy Rayleigh fading channels. In our analysis we assume that unique random TH addresses are employed by the active users.

When communicating over noiseless channels, the only source of generating errors is when the conventional SUD has to choose among multiple (more than one) complete rows. Let us consider the detection of the first user with the detection matrix after the de-hopping expressed as \mathbf{D}_1 as shown in Fig. 7.14. Then, when the TH/MC-CDMA system supports K users with the aid of random TH addresses, the probability that a FT element in the interference rows of \mathbf{D}_1 is marked is

$$P_M = 1 - \left(1 - \frac{1}{Q}\right)^{K-1} \quad (7.130)$$

The probability that an interfering row is a complete row is given by

$$P_M^L = \left[1 - \left(1 - \frac{1}{Q}\right)^{K-1}\right]^L \quad (7.131)$$

Furthermore, the probability that there are exactly j number of complete interfering rows in the first M rows³ of \mathbf{D}_1 is given by

$$\begin{aligned} P_J(j) &= \binom{M-1}{j} (P_M^L)^j (1 - P_M^L)^{M-1-j} \\ &= \binom{M-1}{j} P_M^{Lj} (1 - P_M^L)^{M-1-j}, \quad j = 0, 1, \dots, M-1 \end{aligned} \quad (7.132)$$

When assuming that the conventional SUD randomly selects one of the complete rows, when there is more than one complete row in the detection matrix of \mathbf{D}_1 , the symbol error rate (SER) of the TH/MC-CDMA system in noiseless channels can hence be expressed as

$$P_s = 1 - \sum_{j=0}^{M-1} \frac{1}{j+1} P_J(j) \quad (7.133)$$

Correspondingly, the BER of the TH/MC-CDMA system in noiseless channels can hence be computed as

$$P_b = \frac{M/2}{M-1} P_s \quad (7.134)$$

When communicating over the Rayleigh fading channels in addition to the AWGN, the detection probability P_D , miss probability P_m , and the false-alarm probability P_F are required in order to derive the SER expression. Specifically, the detection probability P_D

³If a complete row occurs within row M to row $(Q-1)$, this complete row does not introduce erroneous detection, since $M < Q$.

is defined as the probability that a FT element is detected (marked), conditional on the FT element being activated by one or several users. The miss probability P_m is defined as the probability that a FT element is not detected (marked), conditional on the FT element being activated by one or several users. Finally, the false-alarm probability P_F is defined as the probability that a FT element is detected (marked), when the FT element was actually not activated by any of the users.

As shown in Section 7.6.2, when the (q, l) th FT element in \mathbf{R} is activated by K_{ql} users, the PDF of R_{ql} is given by (7.122). Let λ be the preset threshold. Then, the detection probability conditional on K_{ql} can be expressed as

$$P_D(K_{ql}) = \int_{\lambda}^{\infty} f(R_{ql} | \mathbf{s}, \{\mathbf{a}_k\}) dR_{ql} \quad (7.135)$$

Substituting (7.122) into the above equation, we obtain

$$P_D(K_{ql}) = \exp\left(-\frac{\lambda}{K_{ql} + \sigma^2}\right) \quad (7.136)$$

Explicitly, the detection probability P_D is a function of the number of users K_{ql} activating the (q, l) th element, which may take a value of $1, 2, \dots, K$. It can be shown that the analysis of SER becomes highly complicated, when all the combinations of $\{P_D(K_{ql})\}_{k=1}^K$ are invoked in the analysis. Therefore, in the following analysis, we only consider the average detection probability, which can be computed as

$$\begin{aligned} P_D &= \left[\sum_{K_{ql}=1}^K P(K_{ql}) P_D(K_{ql}) \right] \left[\sum_{K_{ql}=1}^K P(K_{ql}) \right]^{-1} \\ &= \left[\sum_{K_{ql}=1}^K \binom{K}{K_{ql}} \left(\frac{1}{Q}\right)^{K_{ql}} \left(1 - \frac{1}{Q}\right)^{K-K_{ql}} \exp\left(-\frac{\lambda}{K_{ql} + \sigma^2}\right) \right] \\ &\times \left[\sum_{K_{ql}=1}^K \binom{K}{K_{ql}} \left(\frac{1}{Q}\right)^{K_{ql}} \left(1 - \frac{1}{Q}\right)^{K-K_{ql}} \right]^{-1} \end{aligned} \quad (7.137)$$

The average miss probability can be expressed as

$$P_m = 1 - P_D \quad (7.138)$$

Finally, the false-alarm probability P_F can be straightforwardly obtained from (7.136) by setting $K_{ql} = 0$, which gives

$$P_F = P_D(0) = \exp\left(-\frac{\lambda}{\sigma^2}\right) \quad (7.139)$$

Following the analysis in reference [13], the probability that a FT element in the interfering rows of \mathbf{D}_1 is marked can be expressed as

$$\bar{P}_M = P_A + P_F - P_A P_F \quad (7.140)$$

where P_A is the probability that a FT element is marked on condition that the element was activated by at least one user. P_A can be expressed as

$$P_A = \left[1 - \left(1 - \frac{1}{Q} \right)^{K-1} \right] P_D \quad (7.141)$$

The probability that there are u entries in an interfering row is given by

$$P_I(u) = \binom{L}{u} \bar{P}_M^u (1 - \bar{P}_M)^{L-u} \quad (7.142)$$

Among the $M - 1$ interfering rows, the probability that u is the maximum number of entries of a row and that there are exactly v interfering rows containing u entries can be expressed as

$$P_I(u, v) = \binom{M-1}{v} [P_I(u)]^v \left(\sum_{m=0}^{u-1} P_I(m) \right)^{M-1-v}, \quad u > 0 \quad (7.143)$$

It can be shown that

$$\begin{aligned} P_I(0, M-1) &= [P_I(0)]^{M-1} \\ P_I(0, m) &= 0, \quad \text{for } m \neq M-1 \end{aligned} \quad (7.144)$$

For the correct row of \mathbf{D}_1 , the probability that there are w entries can be expressed as

$$P_1(w) = \binom{L}{w} P_D^w (1 - P_D)^{L-w} \quad (7.145)$$

Consequently, given w the number of entries in the correct row, the probability of correct detection can be expressed as

$$P_c(w) = \sum_{v=0}^{M-1} \frac{1}{v+1} P_I(w, v) \quad (7.146)$$

Therefore, the average SER is

$$\begin{aligned} P_s &= 1 - P_c = 1 - \sum_{w=0}^L P_1(w) P_c(w) \\ &= 1 - \sum_{w=0}^L P_1(w) \sum_{v=0}^{M-1} \frac{1}{v+1} P_I(w, v) \end{aligned} \quad (7.147)$$

and the BER can be obtained from (7.134).

Below, we illustrate a range of BER performance results for the TH/MC-CDMA using the conventional single-user posterior noncoherent detector, when communicating over Rayleigh fading channels. In the TH/MC-CDMA system under consideration, the number of time slots per symbol duration was assumed to be $Q = 64$, which is the same as the baseband

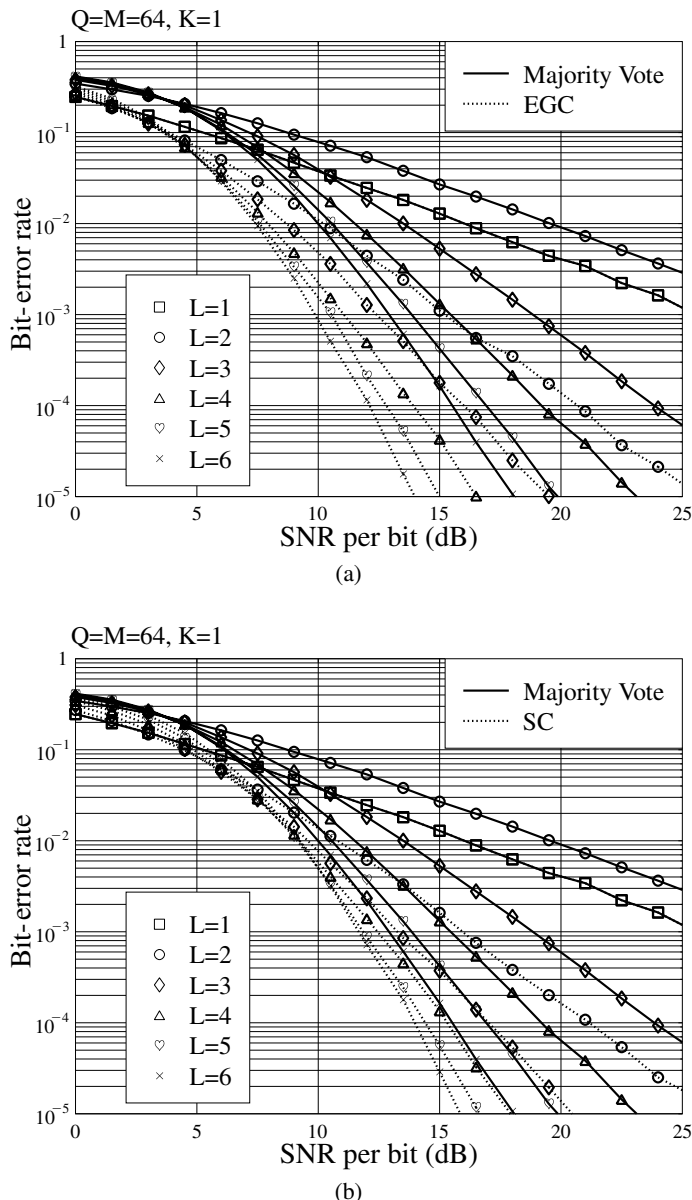


Figure 7.15: BER versus average SNR per bit performance for the single-user TH/MC-CDMA system using the conventional SUD associated with majority vote decoding, EGC or SC, when communicating over Rayleigh fading channels in addition to AWGN; (a) majority vote decoding and equal gain combining; (b) majority vote decoding and selection combining.

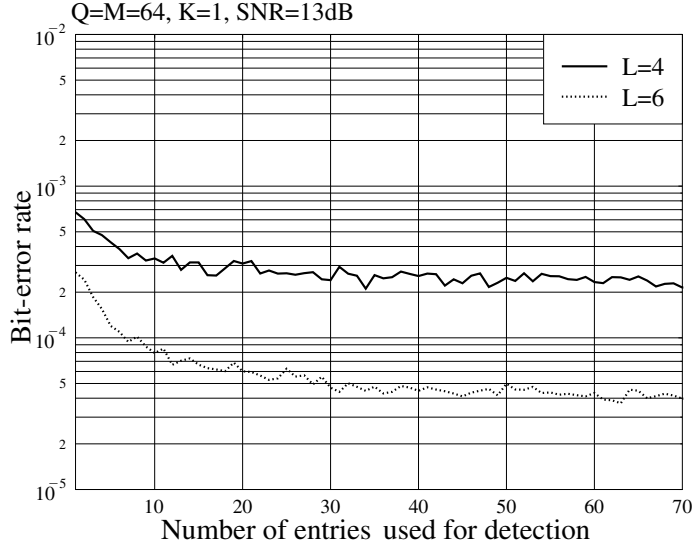


Figure 7.16: BER performance of the single-user TH/MC-CDMA system using the conventional SUD associated with hybrid selection/equal gain combining (SC/EGC), when communicating over Rayleigh fading channels in addition to AWGN.

modulation level, i.e. $M = Q = 64$. First, in Fig. 7.15 the BER performance of the single-user TH/MC-CDMA systems with different diversity combining schemes is evaluated. The diversity combining schemes include majority vote decoding, EGC and selection combining (SC). Additionally, for the SC scheme, the maximum of the QL entries of \mathbf{R} is selected for detection. By contrast, for the majority vote decoding, the L number of largest entries in \mathbf{R} are first selected, and then decoded based on the majority vote principles. The results in Fig. 7.15 show that the majority vote decoding is outperformed by both the EGC and SC, and the EGC achieves the best BER performance among the three diversity combining schemes. Furthermore, it can be observed that both the SC and the majority vote decoding, especially the latter, are not efficient at a relatively low SNR region. As shown in Fig. 7.15, for the majority vote decoding, the BER performance corresponding to $L = 2$ is always worse than that corresponding to $L = 1$; the BER performance corresponding to $L = 3$ becomes better than that corresponding to $L = 1$ only if the SNR per bit value is higher than approximately 1.05 dB. However, the BER performance of the majority vote decoding with $L = 3$ is still significantly worse than the BER performance of the EGC (or SC) with $L = 2$. Considering that the majority vote decoding, which needs to find L maximums, has a relatively higher complexity than the SC, which only needs to find one maximum, therefore, the majority vote decoding is not an efficient diversity combining scheme for the single-user TH/MC-CDMA systems.

Figure 7.16 shows the BER performance of the TH/MC-CDMA against the number of entries used for detection, when the hybrid SC/EGC assisted diversity combining is invoked for detection in Rayleigh fading channels. The number of entries for detection are made up the set of entries having the highest values. It is noteworthy that when only the one

largest entry of \mathbf{R} is considered, the SC/EGC is then reduced to the SC. Hence, in Fig. 7.16 the points corresponding to one entry for detection represent the BER of the TH/MC-CDMA using SC. By contrast, when all the ML entries of \mathbf{R} are invoked for detection, the SC/EGC is then reduced to the EGC. The results of Fig. 7.16 show that the BER performance improves, when increasing the number of largest entries invoked for detection. This observation implies that the (pure) SC scheme using only one entry for detection achieves the worst BER performance, while the (pure) EGC using all the ML entries for detection achieves the best BER performance. The BER performance achieved by the hybrid SC/EGC lies between that achieved by the pure SC and EGC. However, as shown in Fig. 7.16, the BER performance of the TH/MC-CDMA using the SC/EGC tends to become stable when an efficient number, which is, however, significantly lower than ML , of entries are chosen for detection. Specifically, as seen in Fig. 7.16, for $L = 4, 20\text{--}30$ entries are sufficient to achieve the BER performance of the TH/MC-CDMA using the pure EGC, while for $L = 6$, it is sufficient to choose 30–50 entries for carrying out the SC/EGC detection.

In Fig. 7.17 the BER performance of the multiuser TH/MC-CDMA systems using the conventional SUD is depicted, when communicating over Rayleigh fading channels. Explicitly, when the TH/MC-CDMA supports multiple users and employs the conventional SUD for detection, the BER performance degrades significantly as the number of users increases, which yields the increased MUI.

The MUI may be mitigated with the aid of various posterior noncoherent MUD schemes, which are now studied in the following subsections.

7.8.2 Minimum-Distance Decoding Based Interference Cancellation

In reference [203] Mabuchi *et al.* proposed a posterior noncoherent MUD scheme for the MFSK-FFH systems based on cancelling the co-channel interference. The processing in this noncoherent MUD scheme is in fact equivalent to examining the Hamming distance between the received TF matrix \mathbf{R} , as, for example, shown in Fig. 7.18, and a range of test TF matrices. A test matrix is formed by K user symbols in conjunction with the K users' FH patterns. The K specific user symbols generating a TF matrix which has the minimum Hamming distance from the received TF matrix \mathbf{R} are chosen as the estimates of the transmitted K user symbols. Therefore, we refer to this noncoherent MUD scheme as the minimum-distance decoding-based interference cancellation (MDD-IC). Below, we first consider the principles of the Mabuchi's MDD-IC in the context of the TH/MC-CDMA system. Then, the principles are extended to the general MDD-IC.

With the aid of Fig. 7.18, the Mabuchi's MDD-IC can be explained as follows.

1. Based on the received hard-decision observation matrix \mathbf{R} , the receiver decodes the K users using their TH patterns, generating the detection matrices $\mathbf{D}_1, \mathbf{D}_2, \dots, \mathbf{D}_K$.
2. Decide the candidates for the transmitted symbols. As shown in Fig. 7.18, the data symbols corresponding to the majority rows are identified as the candidates of the transmitted symbols. For the example, in Fig. 7.18, where interference-only channels are assumed, the data symbols corresponding to the complete rows are decided as the candidates of the transmitted symbols, which are $\hat{X}_1 = \{1, 2\}, \hat{X}_2 = 3, \hat{X}_3 = 0, \hat{X}_4 = 0$. Explicitly, $\hat{X}_2 = 3, \hat{X}_3 = 0$ and $\hat{X}_4 = 0$ can be correctly decoded using the conventional SUD. However, the decision for user 1 at this stage is ambiguous.

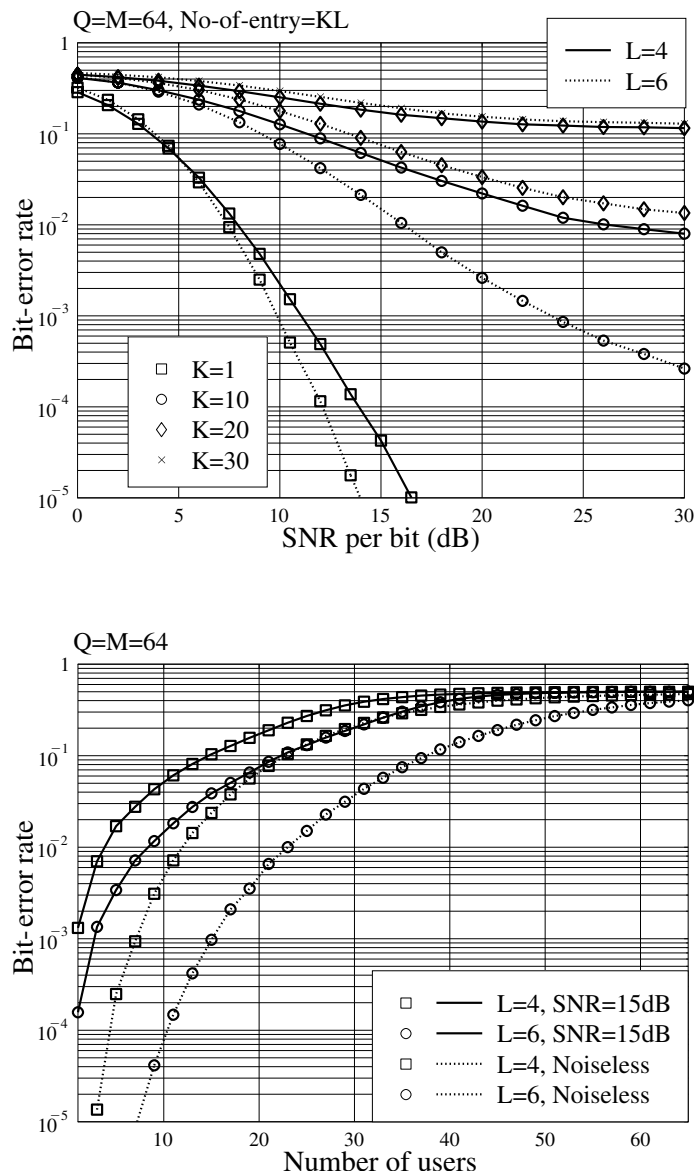


Figure 7.17: BER performance of the multiuser TH/MC-CDMA system using the conventional SUD associated with majority vote decoding, when communicating over Rayleigh fading channels in addition to AWGN.

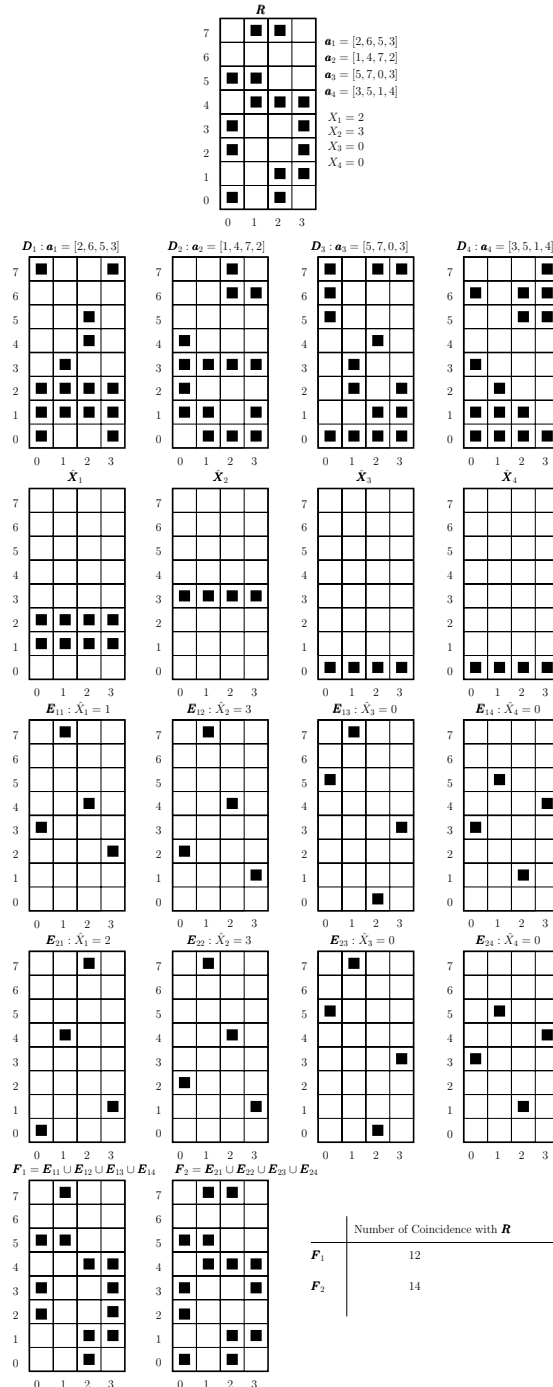


Figure 7.18: Illustration of the noncoherent MUD based on the minimum-distance decoding assisted interference cancellation (MDD-IC).

3. Each of the candidates of the user data symbols is re-encoded by its corresponding TH patterns and then added using logical OR operation with the other re-encoded candidates of the other $(K - 1)$ users, in order to form a range of candidate matrices for the observation matrix \mathbf{R} . For example as shown in Fig. 7.18, after re-encoding the candidates, we obtain the matrices $\{\mathbf{E}_{11}, \mathbf{E}_{12}, \mathbf{E}_{13}, \mathbf{E}_{14}\}$ for the candidates $\hat{X}_1 = 1$, $\hat{X}_2 = 3$, $\hat{X}_3 = 0$ and $\hat{X}_4 = 0$, as well as $\{\mathbf{E}_{21}, \mathbf{E}_{22}, \mathbf{E}_{23}, \mathbf{E}_{24}\}$ for the candidates $\hat{X}_1 = 2$, $\hat{X}_2 = 3$, $\hat{X}_3 = 0$ and $\hat{X}_4 = 0$. After adding $\{\mathbf{E}_{11}, \mathbf{E}_{12}, \mathbf{E}_{13}, \mathbf{E}_{14}\}$ on the element-by-element basis using the logical OR operation, we obtain \mathbf{F}_1 . In the same way, by adding $\{\mathbf{E}_{21}, \mathbf{E}_{22}, \mathbf{E}_{23}, \mathbf{E}_{24}\}$ on the element-by-element basis using the logical OR operation, we obtain \mathbf{F}_2 . \mathbf{F}_1 and \mathbf{F}_2 are the candidate matrices of the observation matrix \mathbf{R} .
4. Compare the observation matrix \mathbf{R} with its candidate matrices, and the one having the most coincidences with the observation matrix \mathbf{R} is selected. Finally, the data symbols generating the selected candidate matrix form the estimates of the K transmitted symbols. As shown in Fig. 7.18, \mathbf{F}_2 has more coincidences than \mathbf{F}_1 with the observation matrix \mathbf{R} . Hence, the corresponding symbols $\hat{X}_1 = 2$, $\hat{X}_2 = 3$, $\hat{X}_3 = 0$ and $\hat{X}_4 = 0$ are finally decided as the estimates of the transmitted symbols. Explicitly, they are all correctly detected.

The MDD-IC is capable of achieving the optimum error performance, when communicating over interference-only channels. However, the detection may become computationally intensive, when a large number of users are supported. Additionally, when in the presence of fading and noise, the correct rows may not be the majority rows due to the miss of detection. In this case, the detection considering only the majority rows may significantly degrade the error performance. The detection performance can be improved by considering the majority rows as well as the rows having fewer entries. However, increasing the number of rows considered, which implies that the number of candidates to be examined is increased, will further result in an increase of computational complexity.

For the general MDD-IC, as mentioned previously, it is equivalent to finding the K symbols that form a candidate matrix having the minimum distance from the observation matrix \mathbf{R} . Let us now explain the principle.

In the observation matrix \mathbf{R} , let the marked entries be replaced by 1's, while the empty entries by 0's, i.e. modify the matrix \mathbf{R} in the form seen in Fig. 7.18 to an observation matrix with entries of 1's and 0's. Then, for the general case, the MDD-IC can be described as

$$\{\hat{X}_1, \hat{X}_2, \dots, \hat{X}_K\} = \arg \min_{\tilde{\mathbf{R}}: X_1, X_2, \dots, X_K; \mathbf{a}_1, \mathbf{a}_2, \dots, \mathbf{a}_K} \left\{ \sum_{i=0}^{Q-1} \sum_{j=0}^{L-1} \mathbf{R}_{ij} \oplus \tilde{\mathbf{R}}_{ij} \right\} \quad (7.148)$$

where the candidate matrix $\tilde{\mathbf{R}}$ is formed by the test symbols X_1, X_2, \dots, X_K associated with the K users' TH addresses $\mathbf{a}_1, \mathbf{a}_2, \dots, \mathbf{a}_K$, and \oplus denotes the operation of binary addition.

Note that the algorithm of (7.148) has a computational complexity proportional to $O(M^K)$. In order to mitigate the computational burden, the algorithm may only consider the candidates that generate the majority rows, as well as the candidates that generate the rows having one or two fewer entries than the majority rows.

Figure 7.19 shows the BER versus the number of users performance of the TH/MC-CDMA employing the MDD-IC and conventional majority vote-based SUD, when commu-

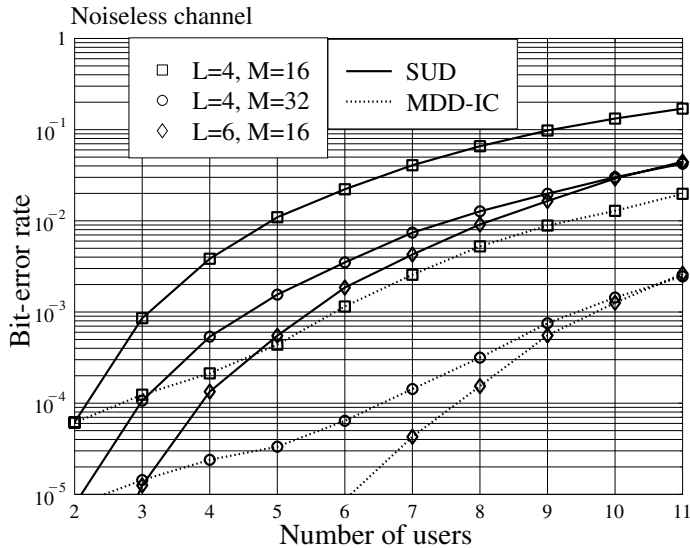


Figure 7.19: BER versus the number of users performance of the TH/MC-CDMA system employing the MDD-IC or conventional majority vote assisted detection, when communicating over noiseless channels.

nicipating over noiseless channels. In this case the candidate matrix formed by the correct candidate symbols is the same as the observation matrix \mathbf{R} and hence the distance between the correct candidate matrix and the observation matrix \mathbf{R} is zero. This fact implies that errors occur only when there are other candidate symbols that form the candidate matrices with a distance zero from the observation matrix. Hence, in our simulations, the ‘stop’ conditions are set as follows:

- when the detection matrix \mathbf{D}_1 of the desired user has only one complete row (explicitly, the detection is correct), or
- when there is a set of candidate symbols found, which form a candidate matrix having a distance zero from the observation matrix \mathbf{R} , or
- when the maximum number of iterations is reached.

Additionally, random TH codes were assumed in the simulations. The other parameters used for simulations are shown on the top of the figure.

The results of Fig. 7.19 illustrate that the BER performance of the TH/MC-CDMA systems can be significantly improved, when the MDD-IC is used instead of the conventional majority vote-based SUD. As Fig. 7.19 shown, for both $L = 4$, $M = 16$ and $L = 4$, $M = 32$, the BER performance for the MDD-IC and the conventional majority vote-assisted SUD is the same, when the TH/MC-CDMA system supports $K = 2$ users. The reason for this observation is that when the system supports two users, an erroneous decision is made only when the two TH addresses are linearly dependent. In this case, both the MDD-IC and the conventional majority vote-assisted SUD are incapable of distinguishing the symbols

transmitted by the two users. Hence, it can be concluded that, when random TH patterns are assumed, both the MDD-IC and conventional majority vote-assisted SUD achieve the same BER, when the TH/MC-CDMA system supports two users. Otherwise, if the number of users supported is high, as shown in Fig. 7.19, the MDD-IC significantly outperforms the conventional majority vote-assisted SUD.

7.8.3 Iterative Posterior Interference Cancellation

The conventional noncoherent SUD considered in Section 7.8.1 makes erroneous decisions when there are multiple rows in the detection matrices that contain the same or more number of entries than the correct row. As shown in Fig. 7.20, in the detection matrix \mathbf{D}_1 , both the first and second rows have the maximum $L = 4$ entries. In this case, the conventional noncoherent SUD has to choose randomly from these two complete rows, yielding an error probability of $1/2$. In order to improve the detection performance of the TH/MC-CDMA, the iterative interference cancellation (IIC) algorithm proposed by Fiebig [86] may be employed. The IIC algorithm can be stated as follows.

1. Conventional noncoherent SUD: a conventional noncoherent SUD stage to generate all the detection matrices $\mathbf{D}_1, \mathbf{D}_2, \dots, \mathbf{D}_K$, as shown in Fig. 7.20.
2. Based on the detection matrices $\mathbf{D}_1, \mathbf{D}_2, \dots, \mathbf{D}_K$, a decision is made for any of the users, whose corresponding detection matrix contains only one majority row. Here the majority row is defined as the row with the maximum number of entries. The symbol is decided as the index of the majority row.
3. At the i th iteration of IIC, where $i = 1, 2, \dots, i_{\max}$, the following two steps are executed:
 - (a) Form a reference matrix $\tilde{\mathbf{R}}$ by re-encoding the detected symbols at the $(i - 1)$ th stage using their corresponding TH addresses. Modify the received matrix $\mathbf{R}^{(i-1)}$ to $\mathbf{R}^{(i)}$, where $\mathbf{R}^{(0)} = \mathbf{R}$, with referring to the reference matrix $\tilde{\mathbf{R}}$. Specifically, $\mathbf{R}^{(i)}$ is obtained from $\mathbf{R}^{(i-1)}$ by deleting those entries whose corresponding elements in $\tilde{\mathbf{R}}$ are marked.
 - (b) For each of the users whose symbols have not yet been detected, generate a detection matrix in the form of $\mathbf{D}_{k'}^{(i)}$ by despread $\mathbf{R}^{(i)}$ using its TH address. If there exists only one majority row in $\mathbf{D}_{k'}^{(i)}$, the decision on the corresponding symbol is made. Otherwise, the detection is left until the next stage.
4. The iteration of IIC stops, when all the users are detected during the iterations or the iteration does not yield any further symbol decisions, or when the maximum number of iterations allowed is reached.

The operation of the IIC in the TH/MC-CDMA systems may be understood by referring to Fig. 7.20. As shown in Fig. 7.20, after the zeroth stage of conventional noncoherent SUD, the first user's symbol of 2 might be erroneously detected as symbol 1, since both row 1 and row 2 in \mathbf{D}_1 are complete rows. By contrast, all the other three users can be correctly detected, since in each of their detection matrices there is only one complete row. Based on $\mathbf{D}_2, \mathbf{D}_3$ and \mathbf{D}_4 , the transmitted symbols can be decided as $\hat{X}_2 = 3, \hat{X}_3 = 0$ and $\hat{X}_4 = 0$.

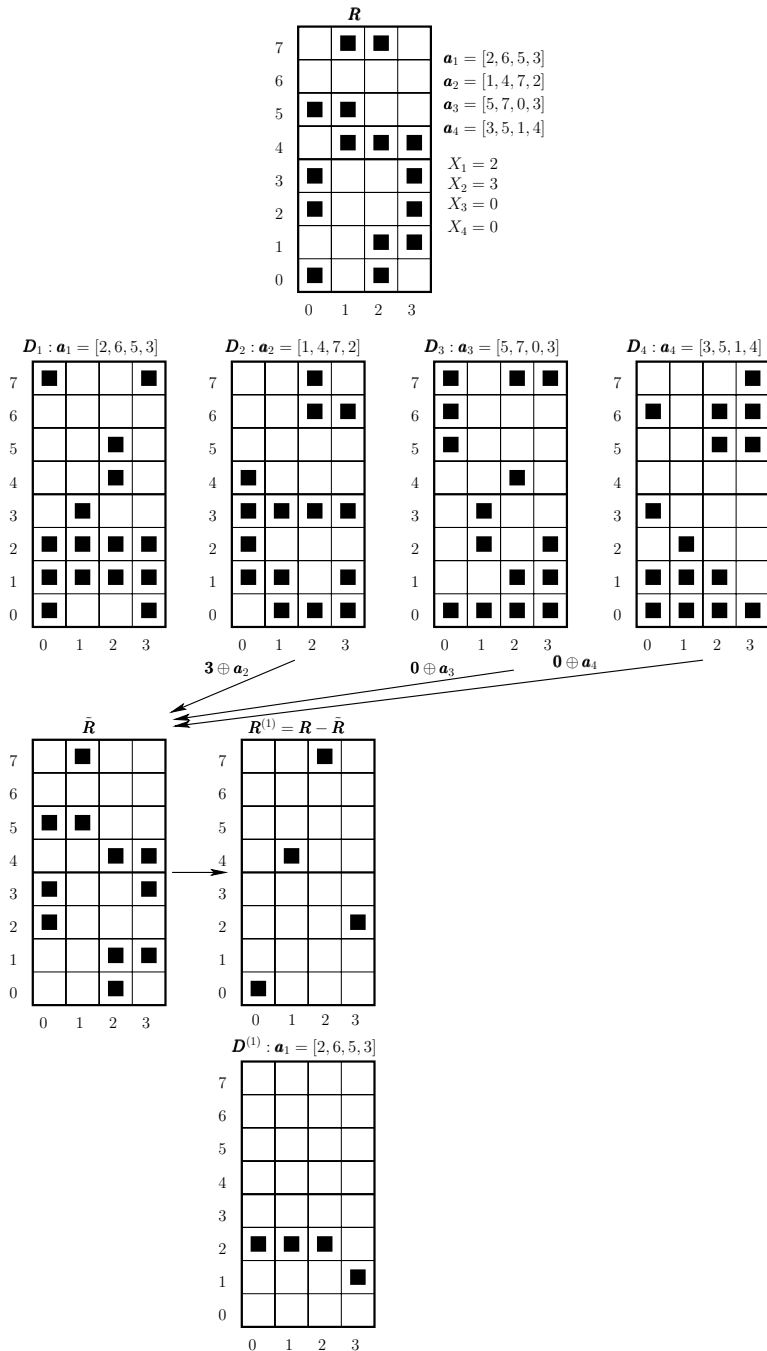


Figure 7.20: Illustration of iterative interference cancellation for the TH/MC-CDMA systems.

As shown in Fig. 7.20, based on the IIC algorithm as above-described, the multiuser interference inflicted upon the first user's signal by user 2, 3 and 4 can be cancelled by jointly exploiting the information of all four users. Specifically, following a tentative zeroth stage detection concerning all reliably detected users, a reference matrix $\tilde{\mathbf{R}}$ is constructed by re-encoding the reliably detected symbols 3, 0 and 0 using the TH addresses of users 2, 3 and 4, which are shown in the matrix $\tilde{\mathbf{R}}$ of Fig. 7.20. Once the reference matrix $\tilde{\mathbf{R}}$ is generated, the detector compares it with the received matrix \mathbf{R} , and cancels this reference matrix from the received matrix, yielding the matrix $\mathbf{R}^{(1)}$ seen in Fig. 7.20. Finally, by decoding $\mathbf{R}^{(1)}$ using the TH address $\mathbf{a}_1 = \{2, 6, 5, 3\}$ of the first user, the FT matrix of $\mathbf{D}_1^{(1)}$ is obtained. Accordingly, symbol 2 transmitted by the first user can now be reliably detected based on the majority vote principles.

The above-stated IIC algorithm has a complexity that only increases linearly with the number of users, and it is capable of achieving the near optimum performance, when communicating over interference-only channels [86]. However, when communicating over fading channels with noise, the above-stated IIC algorithm might not be efficient. First, a decoding error occurs if the desired data symbol corresponds to a row with fewer entries than the majority rows. Second, an erroneous detection in the previous iterations may severely affect the detections of the following iterations.

Instead of cancelling at the same time all the users having majority rows at the last iteration, the IIC algorithm may be operated by cancelling one user, assumed to be the most reliable user detected, at each iteration. The reliability of detection may be measured in different ways, such as by the number of entries in the majority rows, etc.

Below, we analyse the error performance of the TH/MC-CDMA systems with IIC by following the approaches by reference [86], when the TH/MC-CDMA signals are transmitted over noiseless channels or interference-only channels. We analyse the error probability after the first iteration, as well as the lower-bound of the error probability.

Let us focus on the first user of $k = 1$, which has the detection matrix \mathbf{D}_1 . The detection matrices of the $(K - 1)$ interfering users are $\mathbf{D}_2, \mathbf{D}_3, \dots, \mathbf{D}_K$. Before the IIC, the possible outcomes in a detection matrix (either the desired user or an interfering user) can be classified as

- E_1 : there is one complete row corresponding to the correct row;
- $E_2(j)$, $j = 1, \dots, M - 1$: there are j complete rows due to the MUI;
- $E_2 = \{\cup E_2(j)\}$: there is at least one complete row generated by the MUI.

Let the probabilities of the events E_1 , $E_2(j)$ and E_2 be expressed as P_{E_1} , $P_{E_2}(j)$ and P_{E_2} , respectively. Then, these probabilities can be expressed as

$$\begin{aligned} P_{E_1} &= (1 - P_M^L)^{M-1} \\ P_{E_2}(j) &= \binom{M-1}{j} P_M^{Lj} (1 - P_M^L)^{M-1-j} \\ P_{E_2} &= \sum_{j=1}^{M-1} P_{E_2}(j) = 1 - P_{E_1} \end{aligned} \tag{7.149}$$

where P_M is given by (7.130) in Section 7.8.1. It can be shown that the SER when the conventional noncoherent SUD (see Section 7.8.1) is used can alternatively be expressed as

$$P_s = 1 - P_{E_1} - \sum_{j=1}^{M-1} \frac{1}{j+1} P_{E_2}(j) \quad (7.150)$$

The detection process for user 1 continues to the first iteration, when the event E_2 associated with user 1 occurs and also when there is at least one interfering user correctly detected. This probability is given by

$$P(S_0 \rightarrow S_1) = [1 - (1 - P_{E_1})^{K-1}] P_{E_2} \quad (7.151)$$

where $S_0 \rightarrow S_1$ means from iteration zero to iteration one. Correspondingly, the probability that the detection process cannot be continued to iteration one even when the event E_2 occurs with user 1 is given by

$$P(S_0 \rightarrow S_0) = (1 - P_{E_1})^{K-1} P_{E_2} \quad (7.152)$$

After the first iteration, let the possible outcomes of the detection matrix $\mathbf{D}_1^{(1)}$ be expressed as

- F_1 : there is one majority row corresponding to the correct row;
- F_2 : the correct row is not a majority row;
- $F_3(j)$, $j = 1, \dots, M - 1$: there are $(j + 1)$ majority rows, one is the correct row and the other j are the interfering rows;
- $F_3 = \{\cup F_3(j)\}$: in addition to the correct row (which is a majority row), there is at least one majority row generated by the MUI.

Let the probabilities of the events F_1 , F_2 , $F_3(j)$ and F_3 be denoted as P_{F_1} , P_{F_2} , $P_{F_3}(j)$ and P_{F_3} , respectively. Then, it can be shown that the above-mentioned events produce the following results:

- Event F_1 results in an unambiguous correct detection after the first iteration. Its contribution to the symbol correct probability is $P(S_0 \rightarrow S_1)P_{F_1}$;
- Event F_2 yields an unambiguous erroneous detection after the first iteration. Its contribution to the symbol error probability is $P(S_0 \rightarrow S_1)P_{F_2}$;
- Event F_3 yields ambiguity. The probability $P(S_0 \rightarrow S_1)P_{F_3}$ is the probability that the detection of user 1 continues to the second iteration, conditional on there being further interfering users detected during the first iteration. If the detection carries out after the first iteration, the contributions of event F_3 to the symbol error and correct probabilities are

$$\begin{aligned} P_{E,1} &= P(S_0 \rightarrow S_1) \times \sum_{j=1}^{M-1} \frac{j}{j+1} P_{F_3}(j) \\ P_{C,1} &= P(S_0 \rightarrow S_1) \times \sum_{j=1}^{M-1} \frac{1}{j+1} P_{F_3}(j) \end{aligned} \quad (7.153)$$

respectively.

Based on the above analysis, after the first iteration, the overall symbol correct probability can be expressed as

$$\begin{aligned} P_c^{(1)} &= P_{E_1} + (1 - P_{E_1})^{K-1} \sum_{j=1}^{M-1} \frac{1}{j+1} P_{E_2}(j) \\ &\quad + P(S_0 \rightarrow S_1) \left(P_{F_1} + \sum_{j=1}^{M-1} \frac{1}{j+1} P_{F_3}(j) \right) \end{aligned} \quad (7.154)$$

where the second term at the r.h.s. is the probability that the symbol is correctly detected, when there are ambiguous rows in \mathbf{D}_1 and the detection process cannot be continued to the first iteration. By contrast, the third term at the r.h.s. of (7.154) is the correct probability contributed by the first iteration, when the detection stops after the first iteration. The overall SER after the first iteration is given by

$$\begin{aligned} P_s^{(1)} &= (1 - P_{E_1})^{K-1} \sum_{j=1}^{M-1} \frac{j}{j+1} P_{E_2}(j) \\ &\quad + P(S_0 \rightarrow S_1) \left(P_{F_2} + \sum_{j=1}^{M-1} \frac{j}{j+1} P_{F_3}(j) \right) \end{aligned} \quad (7.155)$$

where the first term at the r.h.s. is the result that the detection process of user 1 cannot be continued to the first iteration when the event E_2 occurs, and the third term at the right-hand side is the symbol error probability added by the first iteration, when the detection of user 1 stops after the first iteration. Straightforwardly, $P_c^{(1)}$ and $P_s^{(1)}$ satisfies

$$P_c^{(1)} = 1 - P_s^{(1)} \quad (7.156)$$

Furthermore, it can be shown that a SER lower-bound can be expressed as

$$P_{s,\text{L-bound}}^{(1)} = (1 - P_{E_1})^{K-1} \sum_{j=1}^{M-1} \frac{j}{j+1} P_{E_2}(j) + P(S_0 \rightarrow S_1) P_{F_2} \quad (7.157)$$

which is obtained from (7.155) assuming that the detection is always correct, if the detection process continues to the second iteration.

From (7.154) to (7.157), it is implied that, in order to compute the SER (7.155) after the first iteration or the SER lower-bound of (7.157), we must first obtain either P_{F_1} and $\{P_{F_3}(j)\}$ or P_{F_2} and $\{P_{F_3}(j)\}$. Below, let us derive P_{F_2} and $P_{F_3}(j)$ for $j \geq 1$.

Let us assume that there are K_c interfering users that are correctly detected before the first iteration. The probability of this event is

$$P(K_c) = \binom{K-1}{K_c} P_{E_1}^{K_c} (1 - P_{E_1})^{K-1-K_c}, \quad K_c = 0, 1, 2, \dots, K-1 \quad (7.158)$$

Let the number of complete rows in \mathbf{D}_1 be $(j+1)$, $j \geq 1$. Then, it can be implied that the event F_2 in the context of user 1 is equivalent to the joint of the following subevents:

- G_1 : one or more entries in the correct row are deleted, due to the coincidence (hit) with the K_c correctly detected users;
- G_2 : there is at least one row in the j interfering rows that has more entries than the correct row.

Given K_c the correctly detected users, the probability that a specific FT element is hit by the correctly detected users can be expressed as

$$P_{\text{hit}}(K_c) = 1 - \left(1 - \frac{1}{Q}\right)^{K_c} \quad (7.159)$$

The probability that there are i number of FT elements in the correct row that are hit by the K_c correctly detected users, can be expressed as

$$P_{\text{hit}}^{(c)}(L, i, P_{\text{hit}}(K_c)) = \binom{L}{i} P_{\text{hit}}^i(K_c) [1 - P_{\text{hit}}(K_c)]^{L-i} \quad (7.160)$$

Let us assume that g_l users hit the l th element of the correct row, where $0 \leq g_l \leq K_c$, $l = 0, 1, \dots, L-1$ and $g_0 + g_1 + \dots + g_{L-1} = i$. Then, after the first iteration, the probability that an interfering element of the l th column is removed by the $(K_c - g_l)$ correctly detected users can be expressed as

$$P_Q(g_l) = 1 - \left(1 - \frac{1}{Q-1}\right)^{K_c - g_l}, \quad l = 0, 1, \dots, L-1 \quad (7.161)$$

The probability that there are m elements in a complete interfering row are removed after the first iteration can be expressed as

$$P_G(m; g_0, g_1, \dots, g_{L-1}) = \sum_{\mathcal{C}(L)_m} \prod_{j=0}^{m-1} P_Q(g_{i_j}) \prod_{j=m}^{L-1} [1 - P_Q(g_{i_j})] \quad (7.162)$$

where $\sum_{\mathcal{C}(L)_m}$ denotes the sum over the $\binom{L}{m}$ number of combinations, where m out of L elements in the complete interfering row are removed after the first iteration. Based on (7.162), the probability that there are i or fewer elements in a complete interfering row that are removed can be expressed as

$$P_i(g_0, g_1, \dots, g_{L-1}) = \sum_{m=0}^i P_G(m; g_0, g_1, \dots, g_{L-1}) \quad (7.163)$$

Consequently, the probability of event G_2 on condition that there are j complete interfering rows and that, in the correct row, there are i elements being deleted can be approximately⁴ denoted as

$$P_{G_2}(i; g_0, g_1, \dots, g_{L-1}) = 1 - [1 - P_i(g_0, g_1, \dots, g_{L-1})]^j \quad (7.164)$$

⁴Explicitly, the events concerning the j interfering rows are also not independent. However, it is too complicated to consider all possible events.

Finally, the probability of event F_2 in (7.155) can be expressed as

$$P_{F_2} = \sum_{j=1}^{M-1} \sum_{i=1}^L \sum_{g_0=0}^i \sum_{g_1=0}^{i-g_0} \cdots \sum_{g_{L-1}=0}^{i-\sum_{k=0}^{L-2} g_k} \binom{M-1}{j} P_{\text{hit}}^{(c)}(L, i, P_{\text{hit}}(K_c)) \\ \times \frac{i!}{g_0! \cdots g_{L-1}!(i - \sum_{k=0}^{L-1} g_k)!} P_{G_2}(i; g_0, g_1, \dots, g_{L-1}) \quad (7.165)$$

In order to derive the probability of event F_3 , we can first derive the probability that after the first iteration, there are t ($1 \leq t \leq j$) interfering rows having the same number of entries, which is i , as the correct row, while any of the other $(j-t)$ interfering rows has, at most, $(i-1)$ entries. This probability can be expressed as

$$P_{G_3}(i, j, t; g_0, g_1, \dots, g_{L-1}) = \binom{j}{t} [P_G(i; g_0, g_1, \dots, g_{L-1})]^t \\ \times [1 - P_i(g_0, g_1, \dots, g_{L-1})]^{j-t} \quad (7.166)$$

Therefore, $P_{F_3}(j)$ in (7.155) can be expressed as

$$P_{F_3}(j) = \sum_{j=1}^{M-1} \sum_{i=1}^L \sum_{t=1}^j \sum_{g_0=0}^i \sum_{g_1=0}^{i-g_0} \cdots \sum_{g_{L-1}=0}^{i-\sum_{k=0}^{L-2} g_k} \binom{M-1}{j} P_{\text{hit}}^{(c)}(L, i, P_{\text{hit}}(K_c)) \\ \times \frac{i!}{g_0! \cdots g_{L-1}!(i - \sum_{k=0}^{L-1} g_k)!} P_{G_3}(i, j, t; g_0, g_1, \dots, g_{L-1}) \quad (7.167)$$

As an example, the BER performance of the TH/MC-CDMA using the IIC-assisted detection is shown in Fig. 7.21 associated with $L = 4$ and $L = 6$, when communicating over noiseless channels. In both figures the BER curves corresponding to Iteration 0 represent the BER performance of the TH/MC-CDMA using the conventional majority vote-assisted SUD. Explicitly, the BER performance improves when the IIC-assisted detection is invoked. However, Fig. 7.21 shows that the BER performance improvement is marginal, when more than one iteration of IIC is utilized.

7.8.4 Posterior Multistage Interference Cancellation

In reference [87] a multistage interference cancellation (MIC) scheme has been proposed for the MFSK-FFH systems. In this subsection we extend the principles of MIC to the TH/MC-CDMA, in order to mitigate the MUI.

In the MIC scheme proposed in reference [87], it is assumed that the receiver uses the knowledge about the energy level of each of the FT elements, and this knowledge is exploited to form the receiver matrix \mathbf{R} . Specifically, given the energy level of the received signal, an entry in \mathbf{R} is classified into one of the three types, which are:

- there is no user signal presents at a FT element, and the corresponding FT element is marked as ‘0’ or empty;
- there is only one user signal presents at a FT element. Correspondingly, the FT element is marked as ‘1’;

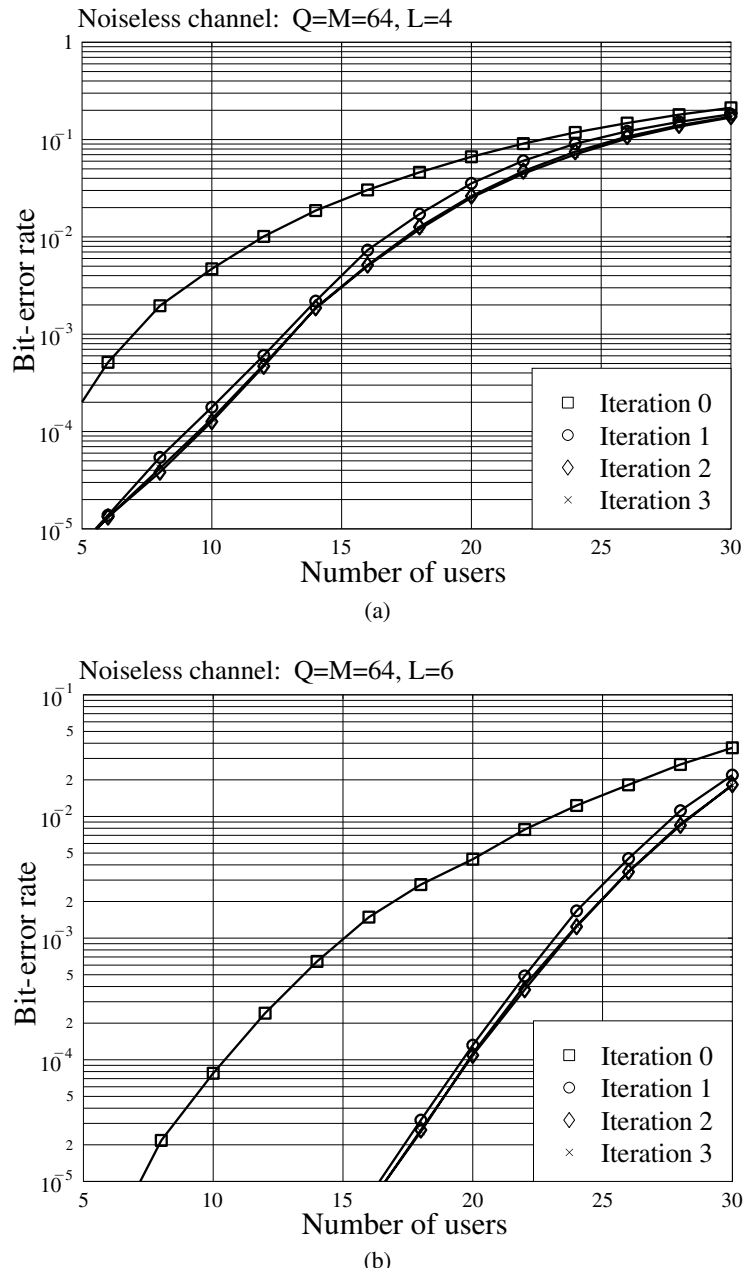


Figure 7.21: BER versus the number of users performance of the TH/MC-CDMA system employing the IIC assisted detection, when communicating over interference-only channels. (a) $L = 4$; (b) $L = 6$.

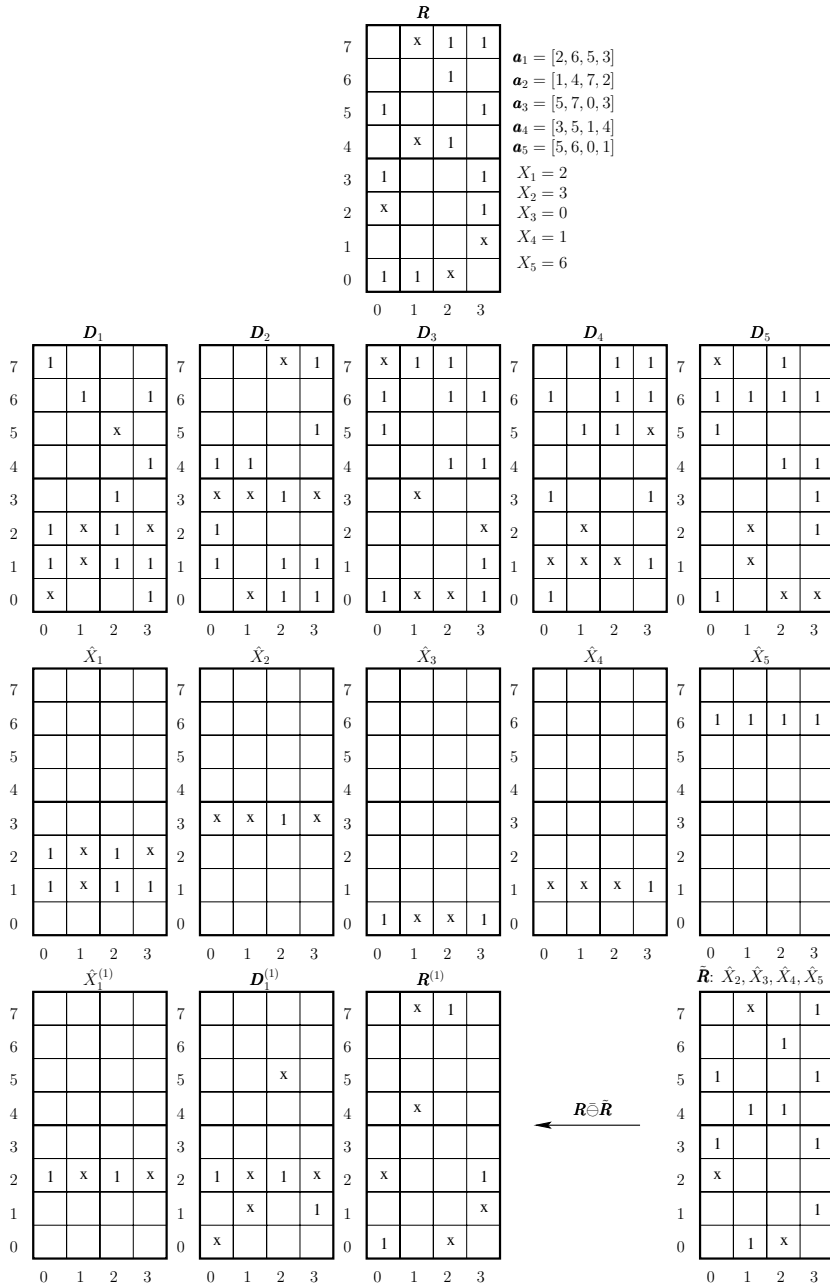


Figure 7.22: Illustration of the principles of MUD based on posterior multistage interference cancellation.

- for any of the other cases, such as there are several user signals presenting at a FT element, the FT element is marked as ‘x’.

The received observation matrix is in the form of \mathbf{R} as shown in Fig. 7.22, where the TH/MC-CDMA supports $K = 5$ users associated with the TH addresses $\mathbf{a}_1 = [2, 6, 5, 3]$, $\mathbf{a}_2 = [1, 4, 7, 2]$, $\mathbf{a}_3 = [5, 7, 0, 3]$, $\mathbf{a}_4 = [3, 5, 1, 4]$ and $\mathbf{a}_5 = [5, 6, 0, 1]$. In this example the user symbols transmitted are $X_1 = 2$, $X_2 = 3$, $X_3 = 0$, $X_4 = 1$ and $X_5 = 6$.

Assisted by the example shown in Fig. 7.22, the MIC algorithm can be stated as follows. Let $\mathbf{R}^{(0)} = \mathbf{R}$, $\mathbf{D}_k^{(0)} = \mathbf{D}_k$, $k = 1, 2, \dots, K$. Then, at the i th stage of the MIC algorithm, where $i = 0, 1, 2, \dots, i_{max}$, the following operation steps are executed:

1. Decode the observation matrix $\mathbf{R}^{(i)}$ using the TH addresses of the K users to generate the detection matrices $\mathbf{D}_1^{(i)}, \mathbf{D}_2^{(i)}, \dots, \mathbf{D}_K^{(i)}$. In the example considered, as shown in Fig. 7.22, the detection matrices for users 1–5 are $\mathbf{D}_1, \mathbf{D}_2, \dots, \mathbf{D}_5$ at the zeroth stage.
2. For a user with its detection matrix having one majority row, an estimate to the transmitted symbol is decided as the symbol corresponding to the majority row. As shown in the example of Fig. 7.22, at the zeroth stage the estimates to the symbols transmitted by users 2, 3, 4, 5 are $\hat{X}_2 = 3$, $\hat{X}_3 = 0$, $\hat{X}_4 = 1$ and $\hat{X}_5 = 6$, respectively. By contrast, for the users corresponding to the detection matrices each of which has multiple majority rows, their detections are left until the following detection stages.
3. Form a reference matrix $\tilde{\mathbf{R}}$ by re-encoding the detected symbols at the i th stage with the aid of their corresponding TH addresses. Then, update the observation matrix $\mathbf{R}^{(i)}$ at the i th stage to $\mathbf{R}^{(i+1)}$ of the $(i + 1)$ th stage with the aid of the reference matrix $\tilde{\mathbf{R}}$. Specifically, if an element, say $\tilde{\mathbf{R}}(m, n)$, in $\tilde{\mathbf{R}}$ is marked as ‘1’ and if this element is activated by only one user, i.e. it is an element ‘1’ in \mathbf{R} , then the corresponding element $\mathbf{R}^{(i)}(m, n)$ in $\mathbf{R}^{(i)}$ is deleted to form $\mathbf{R}^{(i+1)}(m, n)$. In the example shown in Fig. 7.22, the reference matrix $\tilde{\mathbf{R}}$ was formed by re-encoding $\hat{X}_2 = 3$, $\hat{X}_3 = 0$, $\hat{X}_4 = 1$ and $\hat{X}_5 = 6$ associated with the TH patterns $\mathbf{a}_2, \mathbf{a}_3, \mathbf{a}_4$ and \mathbf{a}_5 . Note that in Fig. 7.22 \ominus represents the operations as the above-stated.
4. Return to Step (1), unless all the users are detected, or the current stage does not yield any further symbol decisions, or the maximum number of stages allowed is reached.

Let us now derive the expression for the SER of the TH/MC-CDMA systems, when communicating over interference-only channels. Specifically, we derive the SER after the first stage of MIC as well as the lower- and upper-bound of the SER.

Let us assume that $M \leq Q$, the FT matrix is $(Q \times L)$ dimensional, and random TH patterns are employed. As in Section 7.8.3 let us classify the possible outcomes of $\mathbf{D}_k^{(0)}$, $k = 1, 2, \dots, K$ into the following events:

- E_1 : there is one complete row corresponding to the correct row, the probability of this event is P_{E_1} ;
- $E_2(j)$, $j = 1, \dots, M - 1$: there are j complete rows due to the MUI, and the corresponding probability is $P_{E_2}(j)$;
- $E_2 = \{\cup E_2(j)\}$: there is at least one complete row generated by the MUI, and the probability of this event is P_{E_2} .

Let us assume that user 1 is the desired user. Then, in a similar way as in Section 7.8.3, let us classify the possible outcomes of $\mathbf{D}_k^{(1)}$, $k = 1, 2, \dots, K$ into the following events:

- F_1 : there is one majority row corresponding to the correct row, the probability of the event is P_{F_1} .
- F_2 : the correct row is not a majority row. For the considered MIC, it can be shown that the probability of this event is $P_{F_2} = 0$, when communicating over interference-only channels.
- $F_3(j)$, $j = 1, \dots, M - 1$: there are $(j + 1)$ majority rows, one is the correct row and the other j are the interfering rows. The probability of this event is $P_{F_3}(j)$.
- $F_3 = \{\cup F_3(j)\}$: in addition to the correct row (which is a majority row), there is at least one majority row generated by the MUI. Correspondingly, the probability of this event is P_{F_3} .

Note that P_{F_3} is the probability of the desired user continuing to the second MIC stage, provided that there are other users detected correctly at the first MIC stage. Furthermore, we have $P_{F_3} = 1 - P_{F_1}$.

Moreover, following the derivation in Section 7.8.3, it can be shown that the SER after the first MIC stage (if the detection process stops) can be expressed as

$$P_s^{(1)} = (1 - P_{E_1})^{K-1} \sum_{j=1}^{M-1} \frac{j}{j+1} P_{E_2}(j) + P(S_0 \rightarrow S_1) \times \sum_{j=1}^{M-1} \frac{j}{j+1} P_{F_3}(j) \quad (7.168)$$

where $P(S_0 \rightarrow S_1)$ represents the probability of the event that the detection of the desired user continues to the first MIC stage, $P(S_0 \rightarrow S_1)$ is given in (7.151). $P_s^{(1)}$ of (7.168) can be viewed as one upper-bound SER of the TH/MC-CDMA using MIC, when communicating over interference-only channels.

The probability that there are K_c interfering users correctly detected at the zeroth MIC stage can be denoted as

$$P_I(K_c) = \binom{K-1}{K_c} P_{E_1}^{K_c} (1 - P_{E_1})^{K-1-K_c}, \quad K_c = 0, 1, \dots, K-1 \quad (7.169)$$

Consequently, the lower-bound SER and another SER upper-bound can be expressed as

$$\begin{aligned} P_{L,s}^{(1)} &= (1 - P_{E_1})^{K-1} \sum_{j=1}^{M-1} \frac{j}{j+1} P_{E_2}(j) \\ &\quad + P(S_0 \rightarrow S_1) \times \sum_{K_c=1}^{K-2} P_I(K_c) P_{F_3}^{K-1-K_c} \sum_{j=1}^{M-1} \frac{j}{j+1} P_{F_3}(j) \end{aligned} \quad (7.170)$$

$$P_{U,s}^{(1)} = (1 - P_{E_1})^{K-1} \sum_{j=1}^{M-1} \frac{j}{j+1} P_{E_2}(j)$$

$$\begin{aligned}
& + P(S_0 \rightarrow S_1) \times \sum_{K_c=1}^{K-2} P_I(K_c) P_{F_3}^{K-1-K_c} \sum_{j=1}^{M-1} \frac{j}{j+1} P_{F_3}(j) \\
& + P(S_0 \rightarrow S_1) \times \sum_{K_c=1}^{K-2} P_I(K_c) (1 - P_{F_3})^{K-1-K_c} P_{F_3}
\end{aligned} \tag{7.171}$$

where $P_{F_3}^{K-1-K_c}$ in (7.170) and (7.171) is the probability that the detection of the desired user cannot be continued to the second MIC stage, since all the $(K - 1 - K_c)$ users that were not correctly detected at the zeroth stage, also cannot be correctly detected at the first stage. By contrast, $(1 - P_{F_3})^{K-1-K_c} P_{F_3}$ in (7.171) is the probability that the detection of the desired user will be continued to the second MIC stage, due to at least one out of the $(K - 1 - K_c)$ users being correctly detected at the first MIC stage.

Below, we derive the probability $P_{F_3}(j)$, which is required for evaluating (7.168), (7.170) and (7.171), by following the approaches developed in reference [87].

The probability that in $D_k^{(0)}$ there are i users which do not collide with the other users on a given subcarrier has been given in reference [87] and is also derived in detail in Appendix 7.9, which can be expressed as

$$P_{NC}(i) = \sum_{[g_2, g_3, \dots, g_n] \in \mathcal{G}_i} \left[\frac{K!}{Q^K (2!)^{g_2} (3!)^{g_3} \cdots (n!)^{g_n}} \right] \cdot \left[\frac{Q!}{f(g_2, g_3, \dots, g_n)} \right] \tag{7.172}$$

where the set \mathcal{G}_i contains all possible combinations satisfying the constraint that there are i users which do not collide with the other users, i.e.

$$\mathcal{G}_i = \{[g_2, g_3, \dots, g_n] : 2g_2 + \cdots + ng_n = K - i\} \tag{7.173}$$

Furthermore, in (7.172) $f(g_2, g_3, \dots, g_n)$ is defined as

$$f(g_2, g_3, \dots, g_n) = i! g_2! \cdots g_n! (Q - K + g_2 + 2g_3 + \cdots + (n-1)g_n)! \tag{7.174}$$

When there are K_c reliably detected users and there are i users which do not collide with the other users on a given subcarrier, the probability that a user is a reliably detected user and does not collide with the other users on a given subcarrier is given by

$$P_{NH}(K_c, i) = \frac{i}{K} \cdot \frac{K_c}{K-1} \tag{7.175}$$

Therefore, the probability that l users on a given subcarrier are removed – implying that these l users are both reliably detected and do not collide with the other users – can be expressed as

$$\begin{aligned}
P_R(l) &= \sum_{i=l}^K \sum_{K_c=l}^{K-1} [P_{NH}(K_c, i)]^l [1 - P_{NH}(K_c, i)]^{K-1-l} P_{NC}(i) P_I(K_c) \\
&\quad l = 1, 2, \dots, L-2
\end{aligned} \tag{7.176}$$

It can be shown that, for $l = 0$, we have

$$\begin{aligned}
P_R(0) &= P_{NC}(0) P_I(0) + P_{NC}(1) P_I(0) + P_{NC}(0) P_I(1) \\
&\quad + \sum_{i=1}^K \sum_{K_c=1}^{K-1} [1 - P_{NH}(K_c, i)]^{K-1} P_{NC}(i) P_I(K_c)
\end{aligned} \tag{7.177}$$

and for $l = K - 1$, we have

$$P_R(K - 1) = P_{NC}(K)P_I(K - 1) + P_{NH}(K - 1, K - 1)P_{NC}(K - 1)P_I(K - 1) \quad (7.178)$$

After considering the users removed during the zeroth MIC stage, the probability that an entry in $\mathbf{D}_k^{(1)}$ is a marked entry due to the interference can be expressed as

$$P_M^{(1)} = \sum_{l=0}^{K-1} \left[1 - \left(1 - \frac{1}{Q} \right)^{K-1-l} \right] P_R(l) \quad (7.179)$$

Consequently, the probability that there is a complete interfering row is $(P_M^{(1)})^L$. Hence, the probability that there are j complete interfering rows (the event of F_3) can be expressed as

$$P_{F_3}(j) = \binom{M-1}{j} [(P_M^{(1)})^L]^j [1 - (P_M^{(1)})^L]^{M-1-j}, \quad j = 0, 1, \dots, M-1 \quad (7.180)$$

With the aid of (7.180), the SER after the first MIC stage, the SER lower-bound and the SER upper-bound can be evaluated using equations (7.168), (7.170) and (7.171), respectively.

The BER performance of the TH/MC-CDMA using the MIC-assisted detection is shown in Fig. 7.23 associated with $L = 4$ and $L = 6$, when communicating over interference-only channels. Note that the BER performance corresponding to Iteration 0 represents the BER performance of the TH/MC-CDMA using the conventional majority vote-assisted SUD. The results of Fig. 7.23 show that the BER performance improves significantly when the MIC-assisted detection is invoked. Furthermore, the BER performance improves when more iterations of MIC are applied, but the improvement becomes less and less significant.

When we compare Fig. 7.21 for IIC with Fig. 7.23 for MIC, we observe that the MIC outperforms the IIC. However, as previously mentioned, the MIC needs the knowledge about the energy level of each of the FT elements, which is usually hard to obtain in practice.

7.9 Summary and Discussion

In this chapter we have developed a range of noncoherent MUD schemes. Although the study as well as the performance results are in the context of the TH/MC-CDMA, the detection algorithms are, however, general and suitable for many noncoherent communications schemes, such as for the FFH using MFSK, using hopping pattern assisted user signatures and orthogonal baseband modulation. In this chapter, both the prior and posterior noncoherent MUDs have been considered:

- for the class of prior noncoherent MUDs, the MUI suppression is carried out before the (square-law) noncoherent operations;
- for the class of posterior noncoherent MUDs, the MUI suppression is carried out after the (square-law) noncoherent operations.

The prior noncoherent MUDs can usually achieve the full diversity gain. However, the number of users supportable is usually low. The diversity gain cannot be used as a trade-off for supporting more users. By contrast, the posterior noncoherent MUDs are capable

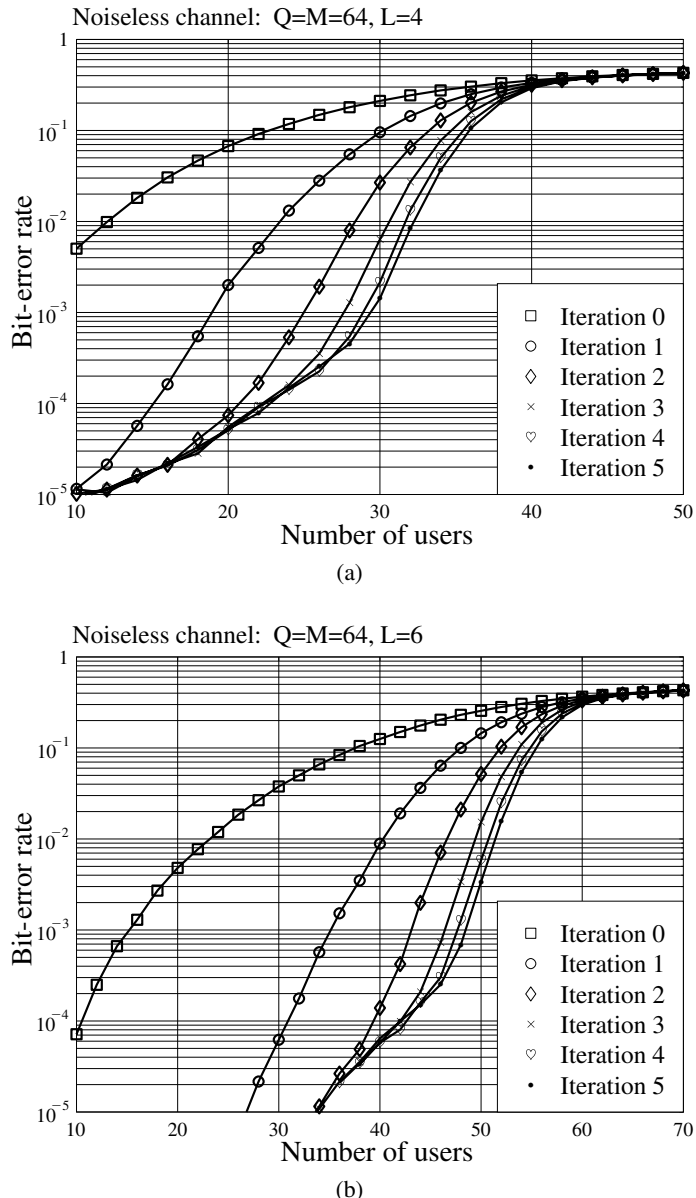


Figure 7.23: BER versus the number of users performance of the TH/MC-CDMA system employing the posterior MIC-assisted detection, when communicating over interference-only channels; (a) $L = 4$; (b) $L = 6$.

of supporting a high number of users by making a trade-off between the number of users supportable and the diversity gain achievable.

In this chapter both the optimum and suboptimum noncoherent MUDs have been derived. The optimum noncoherent MUDs can retain an optimum BER performance, but usually with an extremely high complexity, rendering them impractical for implementation. The suboptimum noncoherent MUDs are outperformed by the optimum noncoherent MUD in terms of achievable BER performance. However, the suboptimum noncoherent MUDs often have relatively low complexity, and hence they are relatively easy to implement in practice.

Appendix 7.A Noncoherent Diversity Combining Schemes for M -ary Orthogonal Signalling

Given the observations shown in (7.36), which are

$$\begin{aligned} \mathbf{q}_l &= [q_{l0}, q_{l1}, \dots, q_{l(M-1)}]^T, \quad l = 0, 1, \dots, L-1 \\ q_{lm} &= |z_{lm}|^2, \quad m = 0, 1, \dots, M-1; \quad l = 0, 1, \dots, L-1 \end{aligned} \quad (7.A.1)$$

any of the following diversity combining schemes may be applied to form the M decision variables for detection of the M -ary transmitted symbol.

1. **Equal Gain Combining (EGC).** For the EGC-aided diversity combining, the M decision variables are formed as [210]

$$Q_m = \sum_{l=0}^{L-1} q_{lm}, \quad m = 0, 1, \dots, M-1 \quad (7.A.2)$$

2. **Majority Logic Decision or Majority Vote** [13]. With the majority logic decision assisted diversity combining, we first form a $(M \times L)$ FT matrix \mathbf{D} . Let $\lambda > 0$ be a preset threshold. Then, whenever q_{lm} ($m = 0, \dots, M-1$; $l = 0, \dots, L-1$) in (7.A.1) exceeds the threshold λ , the corresponding FT entry of the FT matrix is flagged by a marker (or a logical one), otherwise by a space, empty or a logical zero. Based on \mathbf{D} , the detector makes a decision in favour of the particular M -ary symbol \hat{X} corresponding to the specific row, which has the highest number of nonzero entries, in order to provide an estimate to the transmitted symbol X .

3. **Selection Combining (SC).** For the SC-aided diversity combining, the M number of decision variables are formed as

$$Q_m = \max\{q_{0m}, q_{1m}, \dots, q_{(L-1)m}\}, \quad m = 0, 1, \dots, M-1 \quad (7.A.3)$$

where Q_m is the maximum of $\{q_{0m}, q_{1m}, \dots, q_{(L-1)m}\}$. Finally, the estimate to the transmitted symbol is decided as

$$\hat{X} \leftrightarrow \max\{Q_0, Q_1, \dots, Q_{M-1}\} \quad (7.A.4)$$

The above-described SC scheme is equivalent to

$$\hat{X} \leftrightarrow \max \left\{ \begin{array}{cccc} q_{00}, & q_{10}, & \cdots, & q_{(L-1)0} \\ q_{01}, & q_{11}, & \cdots, & q_{(L-1)1} \\ \vdots & \vdots & \ddots & \vdots \\ q_{0(M-1)}, & q_{1(M-1)}, & \cdots, & q_{(L-1)(M-1)} \end{array} \right\} \quad (7.A.5)$$

4. **Product Combining (PC).** For the PC-aided diversity combining, the M decision variables are formed as [211]

$$Q_m = \prod_{l=0}^{L-1} q_{lm}, \quad m = 0, 1, \dots, M-1 \quad (7.A.6)$$

5. **Noise-Normalization Combining (NNC).** Let σ_{lm}^2 be the interference-plus-noise power of z_{lm} . Then, for the NNC-aided diversity combining, the M decision variables are formed as [212, 213]

$$Q_m = \sum_{l=0}^{L-1} \frac{q_{lm}}{\sigma_{lm}^2}, \quad m = 0, 1, \dots, M-1 \quad (7.A.7)$$

6. **Self-Normalization Combining (SNC).** For the SNC-aided diversity combining, the M decision variables are formed as [214]

$$Q_m = \sum_{l=0}^{L-1} \frac{q_{lm}}{q_{l0} + q_{l1} + \cdots + q_{l(M-1)}}, \quad m = 0, 1, \dots, M-1 \quad (7.A.8)$$

7. **Soft-Limiting Combining (SLC).** SLC is also referred to as clipping combining [212]. For the SNC-aided diversity combining the square-law outputs are clipped by a soft-limiter before their combining. Specifically, let h be a threshold, which is set as the value minimizing the probability of error for given conditions, such as a given SNR value. Then, the square-law outputs $\{q_{lm}\}$ are clipped to yield

$$q'_{lm} = \begin{cases} q_{lm}, & \text{when } q_{lm} \leq h \\ h, & \text{when } q_{lm} > h \end{cases} \quad (7.A.9)$$

After the clipping, the M number of decision variables are formed according to [212, 215]

$$Q_m = \sum_{l=0}^{L-1} q'_{lm}, \quad m = 0, 1, \dots, M-1 \quad (7.A.10)$$

8. **Optimum Diversity Combining (ODC).** The ODC has been studied, e.g., in references [209, 216, 217], which has been derived based on the maximum likelihood

principles. Let us assume that $\{q_{li}\}$ are independent random variables.⁵ Then, the conditional joint PDF of $\{q_{li}\}$ can be expressed as

$$f[\{q_{li}\} | j] = \prod_{l=0}^{L-1} \prod_{i=0}^{Q-1} f[q_{li} | j] \quad (7.A.11)$$

given symbol j was transmitted, where $j = 0, 1, \dots, M - 1$.

According to the maximum likelihood principles, the hypothesis H_m of the m th symbol is transmitted is accepted, if

$$f[\{q_{li}\} | m] \geq f[\{q_{li}\} | j], \quad \text{for all } j \neq m \quad (7.A.12)$$

Substituting (7.A.11) into (7.A.12), the maximum likelihood estimator accepts H_m if

$$\prod_{l=0}^{L-1} \prod_{i=0}^{Q-1} f[q_{li} | m] \geq \prod_{l=0}^{L-1} \prod_{i=0}^{Q-1} f[q_{li} | j], \quad \text{for all } j \neq m \quad (7.A.13)$$

which is also equivalent to accepting the hypothesis H_m if

$$\sum_{l=0}^{L-1} \sum_{i=0}^{Q-1} \ln f[q_{li} | m] \geq \sum_{l=0}^{L-1} \sum_{i=0}^{Q-1} \ln f[q_{li} | j], \quad \text{for all } j \neq m \quad (7.A.14)$$

Statistically, we can assume that $f[q_{li} | m] = f[q_{li} | j]$ for $i \neq m \neq j$. Using this fact, (7.A.14) can be simplified to

$$\begin{aligned} & \sum_{l=0}^{L-1} (\ln f[q_{lm} | m] + \ln f[q_{lj} | m]) \\ & \geq \sum_{l=0}^{L-1} (\ln f[q_{lj} | j] + \ln f[q_{lm} | j]), \quad \text{for all } j \neq m \end{aligned} \quad (7.A.15)$$

When rearranging it, we obtain

$$\sum_{l=0}^{L-1} \ln \left(\frac{f[q_{lm} | m]}{f[q_{lm} | j]} \right) \geq \sum_{l=0}^{L-1} \ln \left(\frac{f[q_{lj} | j]}{f[q_{lj} | m]} \right), \quad \text{for all } j \neq m \quad (7.A.16)$$

Based on (7.A.16), the M decision variables for the ODC can be formed as

$$Q_m = \sum_{l=0}^{L-1} h(q_{lm}), \quad m = 0, 1, \dots, M - 1 \quad (7.A.17)$$

where the nonlinear function $h(q_{lm})$ is defined as

$$h(q_{lm}) = \ln \left(\frac{f[q_{lm} | m]}{f[q_{lm} | j]} \right) \quad (7.A.18)$$

Note that, as shown in references [209, 216], when there is no MUI, the above-derived ODC is reduced to the EGC. Additionally, it has been shown in references [209, 216] that the clipped combining represents an approximation of the ODC.

⁵Note that, strictly speaking, $\{q_{li}\}$ are not independent, since the number of users supported by the TH/MC-CDMA is finite. However, when both $Q \gg 1$ and $K \gg 1$, the assumption that $\{q_{li}\}$ are independent is reasonable.

Appendix 7.B Derivation of $P_{NC}(i)$

In this appendix, we derive Equation (7.172) in Section 7.8.4.

In the TH/MC-CDMA system using MPPM and assuming that one data symbol is conveyed by L subcarriers, the probability that i users do not collide with any other ($K - i$) users on a given subcarrier is equivalent to the probability of the event that K pigeons live in Q pigeon holes, there are i pigeon holes each of which accommodates only one pigeon. The probability can be derived as follows.

First, when without any constraint, there are Q^K different ways for K pigeons to live in Q pigeon holes.

Let us assume

$$\left. \begin{array}{l} i \text{ holes: each pigeon hole has one pigeon;} \\ g_2 \text{ holes: each pigeon hole has two pigeons;} \\ g_3 \text{ holes: each pigeon hole has three pigeons;} \\ \vdots \\ g_n \text{ holes: each pigeon hole has } n \text{ pigeons;} \end{array} \right\} i + 2g_2 + \cdots + ng_n = K \quad (7.B.1)$$

It can be implied that the number of pigeon holes without pigeons is $(Q - i - g_2 - \cdots - g_n)$.

Let the set \mathcal{G}_i contain all the possible combinations that there are i pigeon holes each of which accommodates one pigeon, i.e.

$$\mathcal{G}_i = \{[g_2, g_3, \dots, g_n] : 2g_2 + \cdots + ng_n = K - i\} \quad (7.B.2)$$

Therefore, when selecting $i + g_2 + \cdots + g_n$ from Q pigeon holes, the number of combinations is

$$\begin{aligned} A &= \binom{Q}{i} \binom{Q-i}{g_2} \binom{Q-i-g_2}{g_3} \cdots \binom{Q-i-g_2-\cdots-g_{n-1}}{g_n} \\ &= \frac{Q!}{i!g_2!\cdots g_n!(Q-i-g_2-\cdots-g_n)!} \\ &= \frac{Q!}{i!g_2!\cdots g_n!(Q-K+g_2+2g_3+\cdots+(n-1)g_n)!} \end{aligned} \quad (7.B.3)$$

The number of combinations of assigning the K pigeons to the $i + g_2 + \cdots + g_n$ pigeon holes under the constraint of (7.B.1) is

$$\begin{aligned} B &= \binom{K}{1} \cdots \binom{K-i+1}{1} \binom{K-i}{2} \cdots \binom{K-i-2g_2+2}{2} \\ &\quad \times \binom{K-i-2g_2-\cdots-(n-1)g_{n-1}}{n} \\ &\quad \times \cdots \binom{K-i-2g_2-\cdots-(n-1)g_{n-1}-ng_n+n}{n} \\ &= \frac{K!}{(2!)^{g_2}(3!)^{g_3}\cdots(n!)^{g_n}} \end{aligned} \quad (7.B.4)$$

Consequently, the probability of the joint event that K pigeons live in Q pigeon holes and that there are i pigeon holes, each of which accommodates one pigeon, is given by

$$\begin{aligned} P_{NC}(i) &= \frac{1}{Q^K} \sum_{[g_2, g_3, \dots, g_n] \in \mathcal{G}_i} AB \\ &= \sum_{[g_2, g_3, \dots, g_n] \in \mathcal{G}_i} \left[\frac{K!}{Q^K (2!)^{g_2} (3!)^{g_3} \cdots (n!)^{g_n}} \right] \cdot \left[\frac{Q!}{f(g_2, g_3, \dots, g_n)} \right] \end{aligned} \quad (7.B.5)$$

where

$$f(g_2, g_3, \dots, g_n) = i! g_2! \cdots g_n! (Q - K + g_2 + 2g_3 + \cdots + (n-1)g_n)! \quad (7.B.6)$$

Chapter 8

Multiuser Transmitter Preprocessing

In the last two chapters we have developed a range of multiuser detection (MUD) schemes in the context of various classes of multicarrier CDMA schemes. It has been shown that, when a multicarrier CDMA system supports multiple users interfering with each other, the MUD is capable of significantly enhancing the achievable error performance and allowing the multicarrier CDMA systems to support more users, than do the corresponding multicarrier CDMA systems not using MUD. As can be seen in the last two chapters, all the MUDs so far considered aim to separate the multiuser signals or suppress the multiuser interference (MUI) with high efficiency at the receiver end. Explicitly, this type of MUD is feasible for uplink transmission, since in this case the base-station (BS) is usually capable of acquiring the knowledge for carrying out the MUDs and is also capable of managing the increased computation burden generated by the MUD algorithms. However, for downlink transmissions, low-complexity mobile terminals (MTs) with high power-efficiency are usually preferable. Furthermore, in practice it is usually much harder for the MTs to acquire the corresponding knowledge for implementing high-efficiency MUDs than for the BS's. When taking into account the affordable complexity, the size and the battery life of the MTs, and the practical availability of acquiring knowledge, implementing MUDs at the MTs is practically less feasible and unattractive than implementing them at the BS's.

Due to the above-mentioned reasons, the concepts of transmitter preprocessing, such as prefiltering, transmitter MUD (TMUD), multiuser transmission (MUT), etc. have been developed [218–225] and various transmitter preprocessing algorithms as well as their corresponding performance have attracted wide research. In this chapter the transmitter preprocessing is investigated in association with two types of representative multicarrier CDMA scheme, namely the frequency (F)-domain spread MC-CDMA and the time-frequency (TF)-domain spread MC DS-CDMA. Since in wireless communications, the transmitter usually does not carry out ‘detection’, instead of using terminology such as transmitter detection (detector) (TD) or transmitter multiuser detection (detector) (TMUD), we will use the terminologies: *transmitter preprocessing (preprocessor)* (TP), *single-user transmitter preprocessing (preprocessor)* (SUTP) or *multiuser transmitter preprocessing (preprocessor)* (MUTP), etc. Furthermore, in the case of MUTP, we may sometimes instead use the terminology of *transmitter multiuser interference (TMUI) suppression* without

explicit notification. Specifically, in this chapter the transmitter preprocessing techniques considered include:

- transmitter matched-filter (TMF) or pre-RAKE, which is a type of SUTP scheme;
- zero-forcing multiuser transmitter preprocessing (ZF-MUTP);
- minimum mean-square error multiuser transmitter preprocessing (MMSE-MUTP);
- maximum signal-to-interference-plus-noise ratio multiuser transmitter preprocessing (MSINR-MUTP);
- minimum variance distortionless response multiuser transmitter preprocessing (MVDR-MUTP);
- minimum power distortionless response multiuser transmitter preprocessing (MPDR-MUTP);
- eigenspace-based multiuser transmitter preprocessing;
- minimum bit error rate multiuser transmitter preprocessing (MBER-MUTP);
- maximum mutual information multiuser transmitter preprocessing (MMI-MUTP);
- transmitter MUI cancellation.

In the context of the practical implementation, since carrying out transmitter preprocessing requires full or at least partial knowledge of the channels connecting the BS with the downlink MTs as well as knowledge about the MTs' signature waveforms, hence transmitter preprocessing techniques are more applicable in time-division duplex (TDD) systems than in frequency-division duplex (FDD) systems. In TDD systems both the uplink and downlink communicate within the same frequency band, the uplink and downlink channels are hence reciprocal. Therefore, the channel knowledge required for implementing the downlink transmitter preprocessing may be obtained through estimation of the uplink channels at the BS. In this chapter the transmitter preprocessing algorithms are derived by assuming that the BS transmitter employs the ideal knowledge whenever it is required.

Finally, in this chapter the acquisition of the channel knowledge for transmitter preprocessing is discussed in the context of the TDD- and FDD-assisted wireless systems. Furthermore, a novel multicarrier-division duplex (MDD) technique is developed for the multicarrier CDMA systems, in order to acquire the channel knowledge for their transmitter preprocessing. Let us use a simple example to show the basic principles of transmitter preprocessing.

8.1 Principles of Transmitter Preprocessing: An Example

As shown in Fig. 8.1, in this example under consideration, it is a system whose transmitter constitutes two transmission elements, such as two transmit antennas, a CDMA system with a spreading factor of two, etc. The system supports two remote MTs, each of which employs one receive antenna. Let $\mathbf{x} = [x_1, x_2]^T$ be the two symbols that will be transmitted to MT1

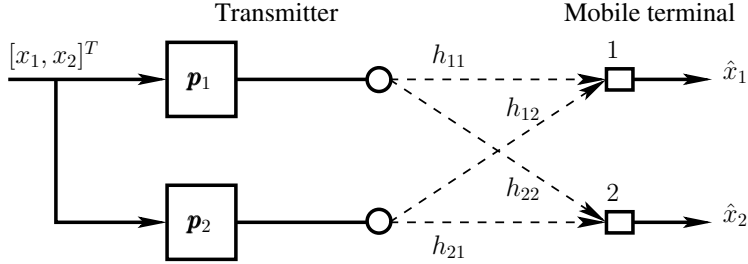


Figure 8.1: A transmitter preprocessing example, where the transmitter transmits information to the two remote mobile terminals through two transmission elements.

and MT2, respectively. As shown in Fig. 8.1, these two symbols are first input to each of the two transmission elements, where they are processed by the preprocessing vectors \mathbf{p}_1 and \mathbf{p}_2 , respectively. After the preprocessing, the signals are transmitted from the two transmission elements to the two remote MTs. Therefore, the signals transmitted by the first and second transmission channels can be written as

$$\begin{aligned} s_1 &= \mathbf{p}_1^T \mathbf{x} \\ s_2 &= \mathbf{p}_2^T \mathbf{x} \end{aligned} \quad (8.1)$$

where, for convenience, we may assume that $E[|x_i|^2] = 1$ for $i = 1, 2$.

Let $\mathbf{s} = [s_1 \ s_2]^T$. Then, (8.1) can be expressed as

$$\mathbf{s} = \mathbf{P}\mathbf{x} \quad (8.2)$$

where

$$\mathbf{P} = \begin{bmatrix} \mathbf{p}_1^T \\ \mathbf{p}_2^T \end{bmatrix} = [\mathbf{P}_1 \ \mathbf{P}_2] \quad (8.3)$$

which is a (2×2) matrix, while \mathbf{P}_1 and \mathbf{P}_2 represent the first and second columns of \mathbf{P} .

Note that, in order to maintain that the transmission power is unchanged after using preprocessing, the matrix \mathbf{P} should be normalized to satisfy

$$E[\|\mathbf{s}\|^2] = E[\|\mathbf{P}\mathbf{x}\|^2] = E[\|\mathbf{x}\|^2] \quad (8.4)$$

After substituting \mathbf{P} from (8.3) into (8.4) and assuming that x_1 and x_2 are independent, we can, in fact, equivalently have

$$E[\|\mathbf{P}_i x_i\|^2] = E[\|x_i\|^2] = 1 \quad (8.5)$$

for $i = 1, 2$.

Assume that the channel from the i th, $i = 1, 2$, transmission element to the k th, $k = 1, 2$, MT is expressed as h_{ki} . Then, the signal received by the first and second MTs can be expressed as

$$\begin{aligned} r_1 &= h_{11}s_1 + h_{12}s_2 + n_1 \\ r_2 &= h_{21}s_1 + h_{22}s_2 + n_2 \end{aligned} \quad (8.6)$$

which can be further expressed using matrix notation as

$$\begin{aligned} r_1 &= \mathbf{h}_1^T s + n_1 \\ r_2 &= \mathbf{h}_2^T s + n_2 \end{aligned} \quad (8.7)$$

where $\mathbf{h}_i = [h_{i1} \ h_{i2}]^T$, n_i is the AWGN with zero mean and a variance of $1/2\text{SNR}$ per dimension. Let $\mathbf{r} = [r_1 \ r_2]^T$, which is a length-2 vector. Then, when applying (8.2), we have

$$\begin{aligned} \mathbf{r} &= \begin{bmatrix} \mathbf{h}_1^T \\ \mathbf{h}_2^T \end{bmatrix} s + \begin{bmatrix} n_1 \\ n_2 \end{bmatrix} \\ &= \mathbf{H}s + \mathbf{n} \end{aligned} \quad (8.8)$$

$$= \mathbf{H}\mathbf{P}\mathbf{x} + \mathbf{n} \quad (8.9)$$

where $\mathbf{H} = [\mathbf{h}_1 \ \mathbf{h}_2]^T$ is a (2×2) matrix, while \mathbf{n} is an AWGN vector having zero mean and a covariance matrix of $(1/\text{SNR})\mathbf{I}_2$.

When substituting \mathbf{H} and \mathbf{P} , it can be shown that we have

$$\mathbf{H}\mathbf{P} = \begin{bmatrix} \mathbf{h}_1^T \mathbf{P}_1 & \mathbf{h}_1^T \mathbf{P}_2 \\ \mathbf{h}_2^T \mathbf{P}_1 & \mathbf{h}_2^T \mathbf{P}_2 \end{bmatrix} \quad (8.10)$$

Hence, \mathbf{r} in (8.9) can be expressed as

$$\mathbf{r} = \begin{bmatrix} \mathbf{h}_1^T \mathbf{P}_1 & \mathbf{h}_1^T \mathbf{P}_2 \\ \mathbf{h}_2^T \mathbf{P}_1 & \mathbf{h}_2^T \mathbf{P}_2 \end{bmatrix} \mathbf{x} + \mathbf{n} \quad (8.11)$$

In order to carry out the transmitter preprocessing, the transmitter must determine a preprocessing matrix \mathbf{P} . Let us choose

$$\begin{aligned} \mathbf{P}_1 &= \beta_1 \mathbf{h}_1^* \\ \mathbf{P}_2 &= \beta_2 \mathbf{h}_2^* \end{aligned} \quad (8.12)$$

where β_i for $i = 1, 2$ represent the normalization constants, which can be derived according to the constraint of (8.5), yielding

$$\beta_1 = \beta_2 = \frac{1}{\sqrt{|h_{11}|^2 + |h_{12}|^2}} \quad (8.13)$$

Consequently, when substituting (8.12) associated with (8.13) into (8.3), it can be shown that the preprocessing matrix is given by

$$\mathbf{P} = \begin{bmatrix} \frac{\mathbf{h}_1^*}{\sqrt{|h_{11}|^2 + |h_{12}|^2}} & \frac{\mathbf{h}_2^*}{\sqrt{|h_{21}|^2 + |h_{22}|^2}} \end{bmatrix} \quad (8.14)$$

Furthermore, when substituting (8.14) into (8.11), it can be shown that the decision variables r_1 and r_2 with respect to x_1 and x_2 can be expressed as

$$\begin{bmatrix} r_1 \\ r_2 \end{bmatrix} = \begin{bmatrix} \frac{|h_{11}|^2 + |h_{12}|^2}{\sqrt{|h_{11}|^2 + |h_{12}|^2}} & \frac{h_{11}h_{21}^* + h_{12}h_{22}^*}{\sqrt{|h_{21}|^2 + |h_{22}|^2}} \\ \frac{h_{21}h_{11}^* + h_{22}h_{12}^*}{\sqrt{|h_{11}|^2 + |h_{12}|^2}} & \frac{|h_{21}|^2 + |h_{22}|^2}{\sqrt{|h_{21}|^2 + |h_{22}|^2}} \end{bmatrix} \begin{bmatrix} x_1 \\ x_2 \end{bmatrix} + \begin{bmatrix} n_1 \\ n_2 \end{bmatrix} \quad (8.15)$$

It can be shown from (8.15) that the transmitter preprocessing carries out the maximal ratio combining (MRC) [2] of the signals transmitted by the two transmission elements. Furthermore, according to (8.15), for both x_1 and x_2 a diversity order of two has been achieved, which is shown by the elements at (1, 1) for x_1 and (2,2) for x_2 . However, the two symbols x_1 and x_2 interfere with each other, when \mathbf{h}_1 is not orthogonal to \mathbf{h}_2 . This is indicated in (8.15) by the elements (1,2) for x_1 and (2,1) for x_2 .

The transmitter preprocessing discussed above in fact belongs to the class of TMF-SUTP, which cannot suppress the multiuser interference. As shown in our forthcoming discourse, when the advanced MUTPs are employed, the multiuser interference may be efficiently mitigated at the MT receivers, and the resulting performance can be close to the single-user performance bound, even when the concerned system supports multiple downlink users.

8.2 Transmitter Preprocessing in Frequency-Domain Spread MC-CDMA

8.2.1 Transmitted Signal

The transmitter schematic block diagram for the F-domain spread MC-CDMA using transmitter preprocessing is shown in Fig. 8.2. We assume that the F-domain spread MC-CDMA supports K number of downlink users, and that the transmitter of the F-domain spread MC-CDMA invokes serial-to-parallel (S/P) conversion, as shown in Fig. 3.5. As shown in Fig. 8.2, let

$$\mathbf{x}_k = [x_1^{(k)}, x_2^{(k)}, \dots, x_q^{(k)}]^T, \quad k = 1, 2, \dots, K \quad (8.16)$$

contain the q number of symbols that will be transmitted to user k . Let

$$\mathbf{c}_k = \frac{1}{\sqrt{N_p}}[c_k[0], c_k[1], \dots, c_k[N_p - 1]]^T, \quad k = 1, 2, \dots, K \quad (8.17)$$

be the F-domain spreading code assigned to the k th downlink user. Furthermore, let us construct a F-domain spreading matrix for the k th user as

$$\begin{aligned} \mathbf{C}_k &= \text{diag}\{\mathbf{c}_k, \mathbf{c}_k, \dots, \mathbf{c}_k\} \\ &= \mathbf{I}_q \otimes \mathbf{c}_k, \quad k = 1, 2, \dots, K \end{aligned} \quad (8.18)$$

which is a $(N_p q \times q)$ matrix. Then, the F-domain spreading for the k th user can be expressed as

$$\mathbf{C}_k \mathbf{x}_k, \quad k = 1, 2, \dots, K \quad (8.19)$$

When combining in the context of the K downlink users, the F-domain spreading signal can be expressed as

$$\sum_{k=1}^K \mathbf{C}_k \mathbf{x}_k = \mathbf{C} \mathbf{x} \quad (8.20)$$

where

$$\begin{aligned} \mathbf{C} &= [\mathbf{C}_1, \mathbf{C}_2, \dots, \mathbf{C}_K] \\ \mathbf{x} &= [\mathbf{x}_1^T, \mathbf{x}_2^T, \dots, \mathbf{x}_K^T]^T \end{aligned} \quad (8.21)$$

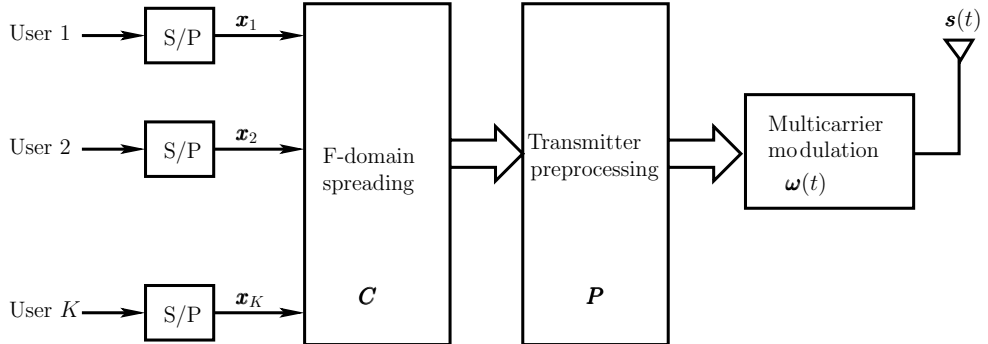


Figure 8.2: Transmitter block diagram of the frequency-domain spreading MC-CDMA using transmitter preprocessing or multiuser transmitter preprocessing.

Finally, as shown in Fig. 8.2, after the transmitter preprocessing and multicarrier modulation, the transmitted MC-CDMA signal in the context of the $N_p q$ subcarriers can be expressed as

$$\mathbf{s}(t) = \boldsymbol{\omega}(t) \mathbf{P} \mathbf{C} \mathbf{x} \quad (8.22)$$

where \mathbf{P} represents the preprocessing matrix to be determined, such as, using the techniques that will be developed in our forthcoming discourse in this section, $\mathbf{s}(t)$ represents the $N_p q$ -length transmitted vector, which is expressed as

$$\mathbf{s}(t) = [s_1(t), s_2(t), \dots, s_{N_p q}(t)]^T \quad (8.23)$$

Furthermore, in (8.22) $\boldsymbol{\omega}(t)$ represents the multicarrier modulation matrix, which is given by

$$\boldsymbol{\omega}(t) = \text{diag}\{\exp(j2\pi f_1 t), \exp(j2\pi f_2 t), \dots, \exp(j2\pi f_{N_p q} t)\} \quad (8.24)$$

Since $\boldsymbol{\omega}(t)$ is a $(N_p q \times N_p q)$ matrix and \mathbf{C} is a $(N_p q \times qK)$ matrix, we can know that the preprocessing matrix \mathbf{P} is a $(N_p q \times N_p q)$ matrix. Let us express (8.22) as

$$\mathbf{s}(t) = \boldsymbol{\omega}(t) \bar{\mathbf{P}} \mathbf{x} \quad (8.25)$$

where $\bar{\mathbf{P}}$ is a $(N_p q \times qK)$ matrix defined as

$$\bar{\mathbf{P}} = \mathbf{P} \mathbf{C} \quad (8.26)$$

Later, we will assume that $K \leq N_p$, i.e. the number of downlink users supported is lower than the length of the F-domain spreading codes. In this case, once $\bar{\mathbf{P}}$ is obtained, the preprocessing matrix \mathbf{P} can be determined by the following operation [89]:

$$\mathbf{P} = \bar{\mathbf{P}} (\mathbf{C}^T \mathbf{C})^{-1} \mathbf{C}^T \quad (8.27)$$

Therefore, in Sections 8.2.3 to 8.2.6, we focus our attention on deriving the matrix $\bar{\mathbf{P}}$, instead of the original preprocessing matrix \mathbf{P} .

Note, furthermore, that in CDMA systems the spreading and transmitter preprocessing can be implemented jointly. The transmitter processing can be understood as the spreading

operation based on a channel-related spreading matrix $\bar{\mathbf{P}}$. Alternatively, it may also be viewed as the preprocessing based on a spreading-related preprocessing matrix $\bar{\mathbf{P}}$.

Moreover, for the sake of performance comparison, the transmission power in the F-domain spread MC-CDMA should be retained as constant no matter whether the transmitter preprocessing is employed. The constant transmission power after using transmitter preprocessing can be achieved by normalizing the derived preprocessing matrix, \mathbf{P} , or its modified version $\bar{\mathbf{P}}$. Specifically, we assume that the transmitted symbol $x_i^{(k)}$ is normalized to satisfy $E[|x_i^{(k)}|^2] = 1$. Hence, when assuming that the transmitted symbols are i.i.d. variables, we have

$$E[\|\mathbf{x}\|^2] = Kq \quad (8.28)$$

Furthermore, according to our previous definitions for \mathbf{C}_k and \mathbf{C} , it can be shown that [89]

$$E[\|\mathbf{Cx}\|^2] = E[\|\mathbf{x}\|^2] = Kq \quad (8.29)$$

Therefore, in order to maintain a constant transmission power, the preprocessing matrix $\bar{\mathbf{P}}$ should be normalized to satisfy

$$E[\|\bar{\mathbf{P}}\mathbf{x}\|^2] = E[\|\mathbf{PCx}\|^2] = E[\|\mathbf{Cx}\|^2] = E[\|\mathbf{x}\|^2] = Kq \quad (8.30)$$

yielding

$$\text{Trace}(\|\bar{\mathbf{P}}\|^2) = E[\|\mathbf{x}\|^2] = Kq \quad (8.31)$$

Alternatively, \mathbf{P} should be normalized to satisfy

$$\text{Trace}(\|\mathbf{PC}\|^2) = E[\|\mathbf{x}\|^2] = Kq \quad (8.32)$$

Let us now derive the signal representation observed at the K number of mobile terminals.

8.2.2 Representation of the Received Signal

We assume that each of the subcarrier channels experiences flat fading. The channel vector connecting the BS transmitter and the k th MT in the context of the N_{pq} subcarrier channels is expressed as

$$\mathbf{h}_k = [h_1^{(k)}, h_2^{(k)}, \dots, h_{N_{pq}}^{(k)}]^T, \quad k = 1, 2, \dots, K \quad (8.33)$$

Then, when the transmitted signal vector is given by (8.25), the received signal at the k th MT can be expressed as

$$\begin{aligned} r_k(t) &= \mathbf{h}_k^T s(t) + n(t) \\ &= \mathbf{h}_k^T \boldsymbol{\omega}(t) \bar{\mathbf{P}} \mathbf{x} + n(t), \quad k = 1, 2, \dots, K \end{aligned} \quad (8.34)$$

where $n(t)$ represents the zero mean complex baseband equivalent Gaussian noise.

The receiver schematic block diagram for the k th MT, $k = 1, 2, \dots, K$, is given by Fig. 8.3. In order to make the MTs as simple as possible, we assume that the MTs employ the low-complexity SUD. Specifically, as shown in Fig. 8.3, the k th MT first carries out the multicarrier demodulation, and then the SUD.

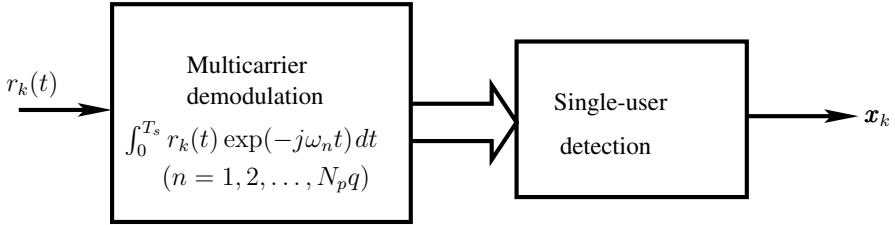


Figure 8.3: Receiver block diagram for the FR-domain spreading MC-CDMA using transmitter preprocessing, where low-complexity single-user detection is assumed.

At the k th MT receiver, let the $N_p q$ number of outputs after the multicarrier demodulation be collected in an observation vector expressed as

$$\mathbf{r}_k = [r_1^{(k)}, r_2^{(k)}, \dots, r_{N_p q}^{(k)}]^T \quad (8.35)$$

We assume that the subcarrier signals are designed to be orthogonal with each other, i.e.

$$\begin{aligned} \rho_{uv} &= \frac{1}{T_s} \int_0^{T_s} \exp(j\omega_u t) \exp(-j\omega_v t) dt \\ &= \begin{cases} 1, & \text{if } u = v \\ 0, & \text{otherwise} \end{cases} \end{aligned} \quad (8.36)$$

Then, we have

$$r_u^{(k)} = \frac{1}{T_s} \int_0^{T_s} r_k(t) \exp(-j\omega_u t) dt, \quad u = 1, 2, \dots, N_p q; k = 1, 2, \dots, K \quad (8.37)$$

Substituting (8.34) into the above equation, it can be shown that

$$r_u^{(k)} = (\bar{\mathbf{h}}_k^{(u)})^T \bar{\mathbf{P}} \mathbf{x} + N_u^{(k)}, \quad u = 1, 2, \dots, N_p q; k = 1, 2, \dots, K \quad (8.38)$$

where $\bar{\mathbf{h}}_k^{(u)}$ is formed from \mathbf{h}_k by setting all its elements except $h_u^{(k)}$ to zero, while $N_u^{(k)}$ is a Gaussian noise sample that has zero mean and a variance of $\sigma_s^2/2 = N_0/2E_s$ per dimension, and E_s denotes the transmitted energy per symbol.

Explicitly, based on (8.38), we know that the observation vector \mathbf{r}_k at MT k can be expressed as

$$\mathbf{r}_k = \mathbf{H}_k \bar{\mathbf{P}} \mathbf{x} + \mathbf{n}_k \quad (8.39)$$

where

$$\mathbf{H}_k = \text{diag}\{h_1^{(k)}, h_2^{(k)}, \dots, h_{N_p q}^{(k)}\} \quad (8.40)$$

and

$$\mathbf{n}_k = [N_1^{(k)}, N_2^{(k)}, \dots, N_{N_p q}^{(k)}]^T \quad (8.41)$$

which is a zero-mean complex vector, and its covariance matrix can be expressed as

$$\mathbf{R}_{n_k} = E[\mathbf{n}_k \mathbf{n}_k^H] = \frac{N_0}{E_s} \mathbf{I}_{N_p q} = \sigma_s^2 \mathbf{I}_{N_p q} \quad (8.42)$$

As shown in Fig. 8.3, after the multicarrier demodulation, the k th MT carries out single-user detection. Specifically, the decision variables for the q number of transmitted symbols in \mathbf{x}_k as seen in (8.16), are formed by carrying out the correlation operation, which can be expressed as

$$\begin{aligned}\mathbf{y}_k &= \mathbf{C}_k^T \mathbf{r}_k \\ &= \mathbf{C}_k^T \mathbf{H}_k \bar{\mathbf{P}} \mathbf{x} + \mathbf{n}'_k, \quad k = 1, 2, \dots, K\end{aligned}\quad (8.43)$$

where $\mathbf{n}'_k = \mathbf{C}_k^T \mathbf{n}_k$, which is zero-mean Gaussian and has a covariance matrix of

$$\mathbf{R}_{\mathbf{n}'_k} = E[(\mathbf{n}'_k)(\mathbf{n}'_k)^H] = \sigma_s^2 \mathbf{I}_q \quad (8.44)$$

since we have $\mathbf{C}_k^T \mathbf{C}_k = \mathbf{I}_q$.

Finally, in order to assist the choice of transmitter preprocessing matrix $\bar{\mathbf{P}}$ or \mathbf{P} , we collect the decision variables in the context of the K MTs into a Kq -length vector \mathbf{y} , defined as

$$\mathbf{y} = [\mathbf{y}_1^T, \mathbf{y}_2^T, \dots, \mathbf{y}_K^T]^T \quad (8.45)$$

Then, it can be readily shown that \mathbf{y} can be expressed as

$$\mathbf{y} = \mathcal{C}^T \mathbf{H} \bar{\mathbf{P}} \mathbf{x} + \mathbf{n} \quad (8.46)$$

where, by definition, \mathcal{C} , \mathbf{H} and \mathbf{n} are expressed as

$$\mathcal{C} = \text{diag}\{\mathbf{C}_1, \mathbf{C}_2, \dots, \mathbf{C}_K\} \quad (8.47)$$

$$\mathbf{H} = [\mathbf{H}_1^T, \mathbf{H}_2^T, \dots, \mathbf{H}_K^T]^T \quad (8.48)$$

$$\mathbf{n} = [(\mathbf{n}'_1)^T, (\mathbf{n}'_2)^T, \dots, (\mathbf{n}'_K)^T]^T \quad (8.49)$$

where \mathbf{n} is a zero-mean complex Gaussian vector, which has a covariance matrix of

$$\mathbf{R}_n = E[\mathbf{n}\mathbf{n}^H] = \sigma_s^2 \mathbf{I}_{Kq} \quad (8.50)$$

Note that, in (8.46) \mathcal{C} is a $(N_p K q \times K q)$ -dimensional matrix, \mathbf{H} is a $(N_p K q \times N_p q)$ -dimensional matrix and $\bar{\mathbf{P}}$ is a $(N_p q \times K q)$ -dimensional matrix.

Above, we have obtained the representation of the decision variables for the K MTs, as shown in (8.46). When employing transmitter preprocessing, the preprocessing matrix \mathbf{P} must be first derived according to certain criteria. We now consider the derivation of $\bar{\mathbf{P}} = \mathbf{P}\mathcal{C}$ for the downlink F-domain spread MC-CDMA in the following subsections.

8.2.3 Transmitter Matched-Filtering Single-User Preprocessor

For the SUTP, the preprocessing for a given user is derived based on the information related only to this user, including possibly its signature sequences and its corresponding channel impulse responses (CIRs). In this case, the preprocessing scheme for maximizing the achievable BER performance is to maximize the signal-to-noise ratio (SNR) by treating the interference from the other users as Gaussian noise, yielding the so-called TMF.

It can be shown that, when the TMF-assisted preprocessing is considered, according to (8.46), the preprocessing matrix $\bar{\mathbf{P}}$ can be chosen as

$$\bar{\mathbf{P}} = (\mathbf{C}^T \mathbf{H})^H \boldsymbol{\beta} = \mathbf{H}^H \mathbf{C} \boldsymbol{\beta} \quad (8.51)$$

where $\boldsymbol{\beta}$ is a $(Kq \times Kq)$ matrix for normalization, which will be discussed later in this section.

Substituting $\bar{\mathbf{P}}$ of (8.51) into (8.46), it can be shown that the decision variables for the reference user corresponding to $k = 1$ can be expressed as

$$\mathbf{y}_1 = \mathbf{C}_1^T \mathbf{H}_1 \mathbf{H}_1^H \mathbf{C}_1 \boldsymbol{\beta}_1 \mathbf{x}_1 + \sum_{k=2}^K \mathbf{C}_1^T \mathbf{H}_1 \mathbf{H}_k^H \mathbf{C}_k \boldsymbol{\beta}_k \mathbf{x}_k + \mathbf{n}'_1 \quad (8.52)$$

where $\boldsymbol{\beta}_k = \text{diag}\{\beta_1^{(k)}, \dots, \beta_q^{(k)}\}$. According to (8.40), we have

$$\begin{aligned} \mathbf{H}_k \mathbf{H}_k^H &= \text{diag}\{|h_1^{(k)}|^2, |h_2^{(k)}|^2, \dots, |h_{N_p q}^{(k)}|^2\} \\ \mathbf{H}_k \mathbf{H}_j^H &= \text{diag}\{h_1^{(k)}(h_1^{(j)})^*, h_2^{(k)}(h_2^{(j)})^*, \dots, h_{N_p q}^{(k)}(h_{N_p q}^{(j)})^*\} \end{aligned} \quad (8.53)$$

which yield in (8.52)

$$\begin{aligned} \mathbf{C}_1^T \mathbf{H}_1 \mathbf{H}_1^H \mathbf{C}_1 &= \frac{1}{N_p} \text{diag} \left\{ \sum_{j=1}^{N_p} |h_j^{(1)}|^2, \sum_{j=1}^{N_p} |h_{(N_p+j)}^{(1)}|^2, \dots, \sum_{j=1}^{N_p} |h_{(N_p(q-1)+j)}^{(1)}|^2 \right\} \\ \mathbf{C}_1^T \mathbf{H}_1 \mathbf{H}_k^H \mathbf{C}_k &= \frac{1}{N_p} \text{diag} \left\{ \sum_{j=1}^{N_p} h_j^{(1)}(h_j^{(k)})^* c_1[j-1] c_k[j-1] \right. \\ &\quad \sum_{j=1}^{N_p} h_{(N_p+j)}^{(1)}(h_{(N_p+j)}^{(k)})^* c_1[j-1] c_k[j-1], \dots \\ &\quad \left. \dots, \sum_{j=1}^{N_p} h_{(N_p(q-1)+j)}^{(1)}(h_{(N_p(q-1)+j)}^{(k)})^* c_1[j-1] c_k[j-1] \right\} \end{aligned} \quad (8.54)$$

The above results show that a given symbol, say $x_u^{(1)}$, of the desired user is interfered only by the corresponding symbol $x_u^{(k)}$ of an interfering user, which is transmitted by the same set of subcarriers conveying $x_u^{(1)}$. Therefore, the decision variable for $x_u^{(1)}$ can be expressed as

$$\begin{aligned} y_u^{(1)} &= \frac{\beta_u^{(1)}}{N_p} \sum_{j=1}^{N_p} |h_{(N_p(u-1)+j)}^{(1)}|^2 x_u^{(1)} \\ &\quad + \sum_{k=2}^K \frac{\beta_u^{(k)}}{N_p} \sum_{j=1}^{N_p} h_{(N_p(u-1)+j)}^{(1)}(h_{(N_p(u-1)+j)}^{(k)})^* c_1[j-1] c_k[j-1] x_u^{(k)} \\ &\quad + (n_u^{(1)})', \quad u = 1, 2, \dots, q \end{aligned} \quad (8.55)$$

We now derive the normalization coefficients in $\boldsymbol{\beta}$ as seen in (8.51). We can also alternatively derive the normalization matrix $\boldsymbol{\beta}_k$, which is seen in (8.52). Specifically, without

considering the multiuser case, according to (8.51) and (8.52), it can be easily shown that the preprocessing matrix for the k th user is given by

$$\bar{\mathbf{P}}_k = \mathbf{H}_k^H \mathbf{C}_k \boldsymbol{\beta}_k \quad (8.56)$$

Correspondingly, the normalization coefficient should satisfy

$$E[\|\bar{\mathbf{P}}_k \mathbf{x}_k\|^2] = E[\|\mathbf{H}_k^H \mathbf{C}_k \boldsymbol{\beta}_k \mathbf{x}_k\|^2] = E[\|\mathbf{x}_k\|^2] = q \quad (8.57)$$

or

$$\text{Trace}(\mathbf{H}_k^H \mathbf{C}_k \boldsymbol{\beta}_k^2 \mathbf{C}_k^T \mathbf{H}_k) = \text{Trace}(\boldsymbol{\beta}_k^2 \mathbf{C}_k^T \mathbf{H}_k \mathbf{H}_k^H \mathbf{C}_k) = q \quad (8.58)$$

which gives

$$\boldsymbol{\beta}_k = \text{diag}((\mathbf{C}_k^T \mathbf{H}_k \mathbf{H}_k^H \mathbf{C}_k)^{-1/2}) \quad (8.59)$$

where the operation $\text{diag}(\mathbf{A})$ returns a diagonal matrix having the diagonal entries constituted by the diagonal entries of \mathbf{A} . Finally, with the aid of (8.53) and (8.54), it can be shown that

$$\beta_u^{(k)} = \sqrt{\frac{N_p}{\sum_{j=1}^{N_p} |h_{(N_p(u-1)+j)}^{(k)}|^2}}, \quad k = 1, 2, \dots, K; \quad u = 1, 2, \dots, q \quad (8.60)$$

Substituting the above results into (8.55), the decision variable for $x_u^{(1)}$ can be expressed as

$$\begin{aligned} y_u^{(1)} &= \left(\sqrt{\frac{1}{N_p} \sum_{j=1}^{N_p} |h_{(N_p(u-1)+j)}^{(1)}|^2} \right) x_u^{(1)} \\ &\quad + \sum_{k=2}^K \left(\sqrt{N_p \sum_{j=1}^{N_p} |h_{(N_p(u-1)+j)}^{(k)}|^2} \right)^{-1} \sum_{j=1}^{N_p} h_{(N_p(u-1)+j)}^{(1)} (h_{(N_p(u-1)+j)}^{(k)})^* \\ &\quad \times c_1[j-1] c_k[j-1] x_u^{(k)} + (n_u^{(1)})', \quad u = 1, 2, \dots, q \end{aligned} \quad (8.61)$$

where the first term is the desired output, the second term is the MUI inflicted on the desired user by the other ($K - 1$) users and the final term is the Gaussian noise.

When the F-domain spread MC-CDMA system supports one user, (8.61) is then reduced to

$$y_u^{(1)} = \left(\sqrt{\frac{1}{N_p} \sum_{j=1}^{N_p} |h_{(N_p(u-1)+j)}^{(1)}|^2} \right) x_u^{(1)} + (n_u^{(1)})' \quad (8.62)$$

Explicitly, from the MT's view, the TMF-assisted transmitter preprocessing achieves the MRC of the N_p number of subcarrier signals conveying the same data bit. Hence, the transmitter preprocessing tends to concentrate more transmission power on the subcarriers that do not suffer from deep fading, but to transmit less power on the subcarriers that conflict deep fading.

When the BPSK baseband modulation scheme is assumed, according to (8.62), the instantaneous SNR can be expressed as

$$\begin{aligned}\gamma &= \sum_{j=1}^{N_p} \gamma_j \\ \gamma_j &= \frac{|h_{(N_p(u-1)+j)}^{(1)}|^2}{\Omega} \gamma_c\end{aligned}\quad (8.63)$$

where $\Omega = E[|h_{(N_p(u-1)+j)}^{(1)}|^2]$ and $\gamma_c = \Omega E_b / N_p N_0$. According to (8.63), explicitly, the TMF-assisted SUTP results in a diversity order of N_p being achieved at the MTs. Furthermore, when the transmission information rate is sufficiently high, and hence the subcarriers conveying the same data bit experience independent Nakagami- m fading, then, according to (5.99), the average BER can be expressed as

$$\begin{aligned}P_b &= \sqrt{\frac{\gamma_c}{\gamma_c + m}} \frac{(1 + \gamma_c/m)^{-mN_p} \Gamma(mN_p + 1/2)}{2\sqrt{\pi} \Gamma(mN_p + 1)} \\ &\quad \times {}_2F_1\left(1, mN_p + \frac{1}{2}; mN_p + 1; \frac{m}{m + \gamma_c}\right)\end{aligned}\quad (8.64)$$

The BER obtained from evaluating (8.64) represents the best (lowest) BER that the F-domain spread MC-CDMA system is capable of achieving. When the subcarriers conveying the same data bit experience correlated fading, the corresponding BER performance will be worse in comparison with that achieved by (8.64), even the system supports only one user. Figure 8.4 shows the single-user (bound) BER performance of the F-domain spread MC-CDMA using the TMF-assisted SUTP, when each subcarrier is assumed to experience independent Nakagami fading. The F-domain spread MC-CDMA system employs $N_p q = 64$ subcarriers and $q = 4$ bits are transmitted to the downlink user, and the results were evaluated based on (8.64). The results in Fig. 8.4 show that the TMF-SUTP is capable of achieving the transmit diversity, which is on the order of 16 (=64/4), yielding that the BER performance is close to that achieved by a BPSK scheme in AWGN channels, even when communicating over Rayleigh fading channels.

Figure 8.5 shows the BER versus average SNR per bit performance for the MC-CDMA using the TMF-SUTP and supporting multiple users, when communicating over frequency-selective Rayleigh fading channels having $L = 10$ or 20 T-domain resolvable paths. The MC-CDMA system employs $N_p q = 64$ subcarriers and $q = 4$ bits are transmitted to each of the downlink users. The results of Fig. 8.5 show that when the F-domain spread MC-CDMA supports multiple downlink MTs, the achievable BER performance degrades significantly due to the MUI. Therefore, from the results of Figs 8.4 and 8.5, we know that the F-domain spread MC-CDMA using the TMF-assisted preprocessing is capable of achieving the frequency diversity, but conflicts severe MUI. This is because the TMF-assisted preprocessing belongs to the SUTPs, which do not utilize the knowledge about the other MTs for preprocessing; only make use of that about the desired MT. Let us now derive the various MUTP schemes, which can efficiently mitigate the MUI.

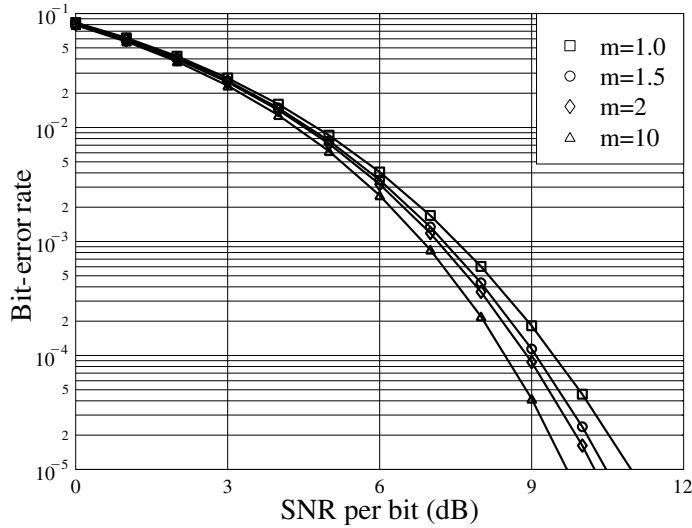


Figure 8.4: Single-user BER performance for the F-domain spread MC-CDMA using the TMF-assisted SUTP, when communicating over frequency-selective Nakagami- m fading channels where each subcarrier experiences independent fading. The MC-CDMA system employs $N_p q = 64$ subcarriers and $q = 4$ bits are transmitted to the downlink user. The results were computed according to (8.64).

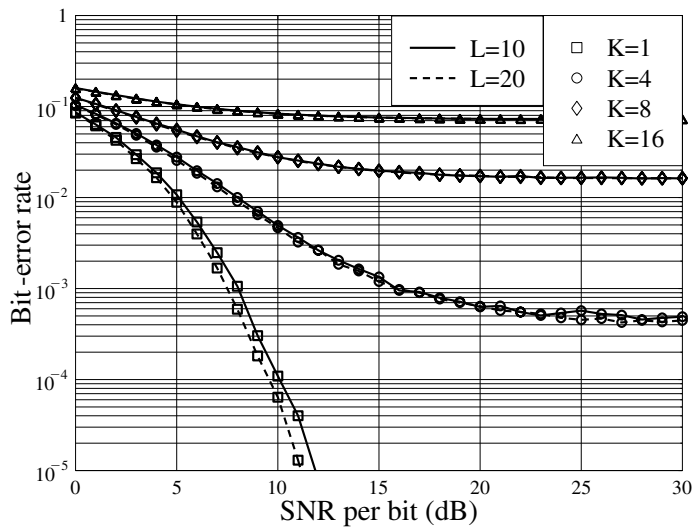


Figure 8.5: BER versus average SNR per bit performance for the MC-CDMA using the TMF-assisted SUTP, when communicating over frequency-selective Rayleigh fading channels having $L = 10$ or 20 T-domain resolvable paths. The MC-CDMA system employs $N_p q = 64$ subcarriers and $q = 4$ bits are transmitted to each of the downlink users. The simulations were based on the preprocessing matrix (8.51) associated with using the normalization of (8.59).

8.2.4 Zero-Forcing Multiuser Transmitter Preprocessor

In the last section it was shown that the TMF-assisted SUTP is capable of achieving the frequency diversity, when the channel experiences a frequency-selective fading, but suffers from severe MUI, as shown in (8.61). In this section the first MUTP scheme, namely the ZF-MUTP, is derived. We will show that the ZF-MUTP is capable of fully suppressing the MUI, yielding that the detection for each MT is free from MUI. Assuming that there are $K \leq N_p$ number of downlink MTs, the ZF preprocessing in the ZF-MUTP is in fact equivalent to decomposing the downlink channels into K number of parallel channels that are independent of each other, each of the parallel channels is for transmission of one downlink MT.

The objective of the ZF-MUTP is to choose the preprocessing matrix $\bar{\mathbf{P}}$, so that each of the MTs is MUI free. Below, the preprocessing matrix $\bar{\mathbf{P}}$ is derived using different approaches.

First, according to (8.46), if the preprocessing matrix $\bar{\mathbf{P}}$ is chosen to satisfy

$$\mathcal{C}^T \mathbf{H} \bar{\mathbf{P}} = \boldsymbol{\beta} \quad (8.65)$$

where $\boldsymbol{\beta}$ is $(Kq \times Kq)$ diagonal, then the decision variable vector \mathbf{y} in (8.46) is correspondingly given by

$$\mathbf{y} = \boldsymbol{\beta} \mathbf{x} + \mathbf{n} \quad (8.66)$$

which explicitly shows that the MUI imposed on each of the MTs is fully eliminated.

Solving the linear equation of (8.65), the preprocessing matrix $\bar{\mathbf{P}}$ is given by

$$\bar{\mathbf{P}} = (\mathcal{C}^T \mathbf{H})^\dagger \boldsymbol{\beta} \quad (8.67)$$

where \mathbf{A}^\dagger represents the Moore–Penrose generalized inverse of \mathbf{A} [156, 157].

When assuming that $K \leq N_p$, yielding $\mathcal{C}^T \mathbf{H}$ to be row-full, i.e. the rank of $\mathcal{C}^T \mathbf{H}$ is equal to the number of its rows. Then, we have [156]

$$\begin{aligned} \bar{\mathbf{P}} &= (\mathcal{C}^T \mathbf{H})^H (\mathcal{C}^T \mathbf{H} \mathbf{H}^H \mathcal{C})^{-1} \boldsymbol{\beta} \\ &= \mathbf{H}^H \mathcal{C} \mathbf{R}^{-1} \boldsymbol{\beta} \end{aligned} \quad (8.68)$$

where, by definition, $\mathbf{R} = \mathcal{C}^T \mathbf{H} \mathbf{H}^H \mathcal{C}$, expressed in more detail,

$$(\mathcal{C}^T \mathbf{H})^H = [\mathbf{H}_1^H \mathcal{C}_1, \mathbf{H}_2^H \mathcal{C}_2, \dots, \mathbf{H}_K^H \mathcal{C}_K] \quad (8.69)$$

$$\mathbf{R} = \begin{bmatrix} \mathcal{C}_1^T \mathbf{H}_1 \mathbf{H}_1^H \mathcal{C}_1 & \mathcal{C}_1^T \mathbf{H}_1 \mathbf{H}_2^H \mathcal{C}_2 & \dots & \mathcal{C}_1^T \mathbf{H}_1 \mathbf{H}_K^H \mathcal{C}_K \\ \mathcal{C}_2^T \mathbf{H}_2 \mathbf{H}_1^H \mathcal{C}_1 & \mathcal{C}_2^T \mathbf{H}_2 \mathbf{H}_2^H \mathcal{C}_2 & \dots & \mathcal{C}_2^T \mathbf{H}_2 \mathbf{H}_K^H \mathcal{C}_K \\ \vdots & \vdots & \ddots & \vdots \\ \mathcal{C}_K^T \mathbf{H}_K \mathbf{H}_1^H \mathcal{C}_1 & \mathcal{C}_K^T \mathbf{H}_K \mathbf{H}_2^H \mathcal{C}_2 & \dots & \mathcal{C}_K^T \mathbf{H}_K \mathbf{H}_K^H \mathcal{C}_K \end{bmatrix} \quad (8.70)$$

which is a $(Kq \times Kq)$ matrix. Therefore, the added complexity for the transmitter preprocessing is dominated by the inverse operation of \mathbf{R} , which might be extreme, when the K and q values are high.

For the considered F-domain spread MC-CDMA, it can be shown that the matrix \mathbf{R} employs a special structure that can simplify the inverse of \mathbf{R} . Specifically, the terms in \mathbf{R} are in the form

$$\begin{aligned} \mathbf{C}_i^T \mathbf{H}_i \mathbf{H}_k^H \mathbf{C}_k &= \frac{1}{N_p} \text{diag} \left\{ \sum_{j=1}^{N_p} h_j^{(i)} (h_j^{(k)})^* c_i[j-1] c_k[j-1] \right. \\ &\quad \sum_{j=1}^{N_p} h_{(N_p+j)}^{(i)} (h_{(N_p+j)}^{(k)})^* c_i[j-1] c_k[j-1], \dots \\ &\quad \left. \dots, \sum_{j=1}^{N_p} h_{(N_p(q-1)+j)}^{(i)} (h_{(N_p(q-1)+j)}^{(k)})^* c_i[j-1] c_k[j-1] \right\}, \\ i, k &= 1, 2, \dots, K \end{aligned} \quad (8.71)$$

In other words, \mathbf{R} is structured by K^2 number of diagonal matrices having the same size of $(q \times q)$. Therefore, according to the matrix theory [89, 157], there exists an orthogonal (permutation) matrix \mathbf{E} of size $(Kq \times Kq)$, which satisfies $\mathbf{E}\mathbf{E}^T = \mathbf{I}_{Kq}$, such that

$$\mathbf{R} = \mathbf{E} \tilde{\mathbf{R}} \mathbf{E}^T \quad (8.72)$$

and $\tilde{\mathbf{R}}$ takes the form

$$\tilde{\mathbf{R}} = \text{diag}\{\tilde{\mathbf{R}}_1, \tilde{\mathbf{R}}_2, \dots, \tilde{\mathbf{R}}_q\} \quad (8.73)$$

where $\tilde{\mathbf{R}}_i$, $i = 1, 2, \dots, q$ is a $(K \times K)$ matrix with its (m, n) th element given by

$$\tilde{\mathbf{R}}_i(m, n) = \frac{1}{N_p} \sum_{j=1}^{N_p} h_{(N_p(i-1)+j)}^{(m)} (h_{(N_p(i-1)+j)}^{(n)})^* c_m[j-1] c_n[j-1] \quad (8.74)$$

Consequently, upon substituting (8.72) into (8.68), the preprocessing matrix can now be computed as

$$\begin{aligned} \bar{\mathbf{P}} &= \mathbf{H}^H \mathcal{C} (\mathbf{E} \tilde{\mathbf{R}} \mathbf{E}^T)^{-1} \boldsymbol{\beta} \\ &= \mathbf{H}^H \mathcal{C} \mathbf{E} \tilde{\mathbf{R}}^{-1} \mathbf{E}^T \boldsymbol{\beta} \end{aligned} \quad (8.75)$$

where

$$\tilde{\mathbf{R}}^{-1} = \text{diag}\{\tilde{\mathbf{R}}_1^{-1}, \tilde{\mathbf{R}}_2^{-1}, \dots, \tilde{\mathbf{R}}_q^{-1}\} \quad (8.76)$$

which shows that the inverse of a $(Kq \times Kq)$ matrix is replaced by the inverse of q number of $(K \times K)$ matrices.

Note that the above simplification is because of the fact that, in the considered F-domain spread MC-CDMA, there exists no intersymbol interference within a user. In other words, a symbol of a reference user is only interfered by the symbols transmitted by the interfering users, which are transmitted on the same set of subcarriers as this considered symbol of the reference user, but not by any other symbols of the interfering users. Furthermore, when substituting $\bar{\mathbf{P}}$ of (8.68) into (8.46) and rearranging it by invoking the permutation matrix, we

obtain

$$\begin{aligned}
 \mathbf{y} &= (\mathcal{C}^T \mathbf{H})(\mathbf{H}^H \mathcal{C} \mathbf{R}^{-1})(\boldsymbol{\beta} \mathbf{x}) + \mathbf{n} \\
 &= \mathbf{E} \underbrace{(\mathbf{E}^T \mathcal{C}^T \mathbf{H})(\mathbf{H}^H \mathcal{C} \mathbf{E} \mathbf{E}^T \mathbf{R}^{-1} \mathbf{E})}_{\mathbf{I}_{Kq}} (\mathbf{E}^T \boldsymbol{\beta} \mathbf{x}) + \mathbf{n} \\
 &= (\mathcal{C}^T \mathbf{H})(\mathbf{H}^H \mathcal{C} \mathbf{E} \tilde{\mathbf{R}}^{-1}) \boldsymbol{\beta}' (\mathbf{E} \mathbf{x}) + \mathbf{n}
 \end{aligned} \tag{8.77}$$

where $\mathbf{E}^T \boldsymbol{\beta}$ is converted to $\boldsymbol{\beta}' \mathbf{E}$, and $\boldsymbol{\beta}'$ is also a diagonal matrix to be determined. The above equation implies that, instead of using the transmitter block diagram of Fig. 8.2, the transmitter can first map \mathbf{x} to $\mathbf{E} \mathbf{x}$. In this case, the preprocessing matrix $\tilde{\mathbf{P}}$ can be derived based on the simplified matrix inversion, as shown in (8.76). The corresponding receiver is still simple and no de-permutation is required.

We now consider the normalization issue to derive the normalization matrix $\boldsymbol{\beta}$. In the F-domain spread MC-CDMA, the transmission powers for the Kq number of symbols transmitted by the K users can be normalized jointly or individually. For joint normalization, all the user bits are normalized using the same factor and the normalization matrix can simply be expressed as

$$\boldsymbol{\beta} = \beta \mathbf{I}_{Kq} \tag{8.78}$$

Consequently, substituting (8.68) associated with (8.78) into (8.31), it can be easily shown that

$$\beta = \sqrt{\frac{Kq}{\text{Trace}(\mathbf{R}^{-1})}} \tag{8.79}$$

Furthermore, according to (8.72), the normalization factor can be expressed as

$$\begin{aligned}
 \beta &= \sqrt{\frac{Kq}{\text{Trace}(\tilde{\mathbf{R}}^{-1})}} \\
 &= \sqrt{\frac{Kq}{\sum_{i=1}^q \text{Trace}(\tilde{\mathbf{R}}_i^{-1})}}
 \end{aligned} \tag{8.80}$$

By contrast, the normalization matrix $\boldsymbol{\beta}$ achieving individual normalization can be derived as follows. Substituting (8.68) into (8.31), we obtain

$$\begin{aligned}
 \text{Trace}(\tilde{\mathbf{P}}^H \tilde{\mathbf{P}}) &= \text{Trace}(\boldsymbol{\beta} \mathbf{R}^{-1} \mathcal{C}^T \mathbf{H} \mathbf{H}^H \mathcal{C} \mathbf{R}^{-1} \boldsymbol{\beta}) \\
 &= \text{Trace}(\boldsymbol{\beta}^2 \mathbf{R}^{-1}) \\
 &= Kq
 \end{aligned} \tag{8.81}$$

Let $\mathbf{R}^{-1}(i, i)$ be the (i, i) th element of \mathbf{R}^{-1} . Explicitly, the above condition can be satisfied, provided that

$$\beta_i^2 \mathbf{R}^{-1}(i, i) = 1, \text{ resulting in } \beta_i = \sqrt{\frac{1}{\mathbf{R}^{-1}(i, i)}}, \quad i = 1, 2, \dots, Kq \tag{8.82}$$

Note that, for the joint normalization approach of (8.79) or (8.80), no matter whether the channels corresponding to the individual users are good or bad, all the users' transmitted

signals are equally weighted at the transmitter. This normalization approach in fact emphasizes the good channels and higher power is transmitted over these good channels, provided that the total transmission power is a constant. By contrast, for the individual normalization approach of (8.82), all the channels transmit using the same power. The performance results at the end of this section show that these two normalization approaches may result in different BER performance results, as shown in Figs 8.6 and 8.7.

Above, the transmitter preprocessing matrix $\bar{\mathbf{P}}$ achieving the ZF-MUTP was derived according to (8.46). As shown in (8.66), the MUI at any given MT is fully removed. Below, we derive the transmitter preprocessing matrix $\bar{\mathbf{P}}$ using an alternative approach, which also results in a preprocessing matrix $\bar{\mathbf{P}}$ that is capable of achieving the zero-forcing transmitter preprocessing.

Let us first express the preprocessing matrix $\bar{\mathbf{P}}$ as

$$\bar{\mathbf{P}} = [\bar{\mathbf{P}}_1, \bar{\mathbf{P}}_2, \dots, \bar{\mathbf{P}}_K] \quad (8.83)$$

where $\bar{\mathbf{P}}_i$, $i = 1, 2, \dots, K$ is $(N_p q \times q)$ dimensional. Then, according to (8.43), the decision variable vector for the k th user can be expressed as

$$\mathbf{y}_k = \mathbf{C}_k^T \mathbf{H}_k \bar{\mathbf{P}}_k \mathbf{x}_k + \sum_{i \neq k}^K \mathbf{C}_k^T \mathbf{H}_k \bar{\mathbf{P}}_i \mathbf{x}_i + \mathbf{n}'_k, \quad k = 1, 2, \dots, K \quad (8.84)$$

In this case, the ZF-MUTP can be achieved if the component matrices in $\bar{\mathbf{P}}$ of (8.83) are chosen to satisfy

$$\mathbf{C}_k^T \mathbf{H}_k \bar{\mathbf{P}}_k = \boldsymbol{\beta}_k, \quad \text{while } \mathbf{C}_i^T \mathbf{H}_i \bar{\mathbf{P}}_k = \mathbf{0} \text{ for } i \neq k \quad (8.85)$$

for $k = 1, 2, \dots, K$, where $\boldsymbol{\beta}_k$ is a $(q \times q)$ diagonal matrix for normalization. The requirements in (8.85) imply that \mathbf{P}_k , $k = 1, 2, \dots, K$ should be chosen in the q -rank subspace determined by $\mathbf{C}_k^T \mathbf{H}_k$ but this subspace is orthogonal to the $(K - 1)q$ -rank subspace determined by all $\mathbf{C}_i^T \mathbf{H}_i$ for $i = 1, 2, \dots, K$; $i \neq k$. Note that the preprocessing matrix $\bar{\mathbf{P}}_k$ for user k is not unique, provided that it satisfies the constraints of (8.85) and has a rank equating to q . One method for constructing $\bar{\mathbf{P}}_k$ is described as follows. First, we define a $(N_p q \times (K - 1)q)$ -dimensional matrix

$$\mathbf{W}_{\bar{k}} = [\mathbf{H}_1^H \mathbf{C}_1, \dots, \mathbf{H}_{k-1}^H \mathbf{C}_{k-1}, \mathbf{H}_{k+1}^H \mathbf{C}_{k+1}, \dots, \mathbf{H}_K^H \mathbf{C}_K] \quad (8.86)$$

invoking all the MTs except the desired k th MT. Then, we construct a $(N_p q \times q)$ matrix of $\mathbf{Q}_{\mathbf{W}_{\bar{k}}}^\perp$, which can be expressed as

$$\mathbf{Q}_{\mathbf{W}_{\bar{k}}}^\perp = [\mathbf{I}_{N_p q} - \mathbf{W}_{\bar{k}} (\mathbf{W}_{\bar{k}}^H \mathbf{W}_{\bar{k}})^{-1} \mathbf{W}_{\bar{k}}^H] \mathbf{H}_k^H \mathbf{C}_k \quad (8.87)$$

Explicitly, $\mathbf{Q}_{\mathbf{W}_{\bar{k}}}^\perp$ is orthogonal to $\mathbf{W}_{\bar{k}}$, since

$$(\mathbf{W}_{\bar{k}})^H \mathbf{Q}_{\mathbf{W}_{\bar{k}}}^\perp = \mathbf{0} \quad \text{and} \quad (\mathbf{Q}_{\mathbf{W}_{\bar{k}}}^\perp)^H \mathbf{W}_{\bar{k}} = \mathbf{0} \quad (8.88)$$

but

$$\mathbf{C}_k^T \mathbf{H}_k \mathbf{Q}_{\mathbf{W}_{\bar{k}}}^\perp = \mathbf{C}_k^T \mathbf{H}_k [\mathbf{I}_{N_p q} - \mathbf{W}_{\bar{k}} (\mathbf{W}_{\bar{k}}^H \mathbf{W}_{\bar{k}})^{-1} \mathbf{W}_{\bar{k}}^H] \mathbf{H}_k^H \mathbf{C}_k \neq \mathbf{0} \quad (8.89)$$

Hence, $\mathbf{H}_k^H \mathbf{C}_k$ has power being projected on the subspace determined by $\mathbf{Q}_{\bar{\mathbf{W}}_k}^\perp$. Therefore, the preprocessing matrix $\bar{\mathbf{P}}_k$ can be chosen as

$$\begin{aligned}\bar{\mathbf{P}}_k &= \mathbf{Q}_{\bar{\mathbf{W}}_k}^\perp \boldsymbol{\beta}_k \\ &= [\mathbf{I}_{N_p q} - \mathbf{W}_{\bar{k}} (\mathbf{W}_{\bar{k}}^H \mathbf{W}_{\bar{k}})^{-1} \mathbf{W}_{\bar{k}}^H] \mathbf{H}_k^H \mathbf{C}_k \boldsymbol{\beta}_k, \quad k = 1, 2, \dots, K\end{aligned}\quad (8.90)$$

where the normalization matrix can be obtained according to

$$\text{Trace}(\bar{\mathbf{P}}_k \bar{\mathbf{P}}_k^H) = q \quad (8.91)$$

which, when jointly normalized, is given by

$$\boldsymbol{\beta}_k = \sqrt{\frac{q}{\text{Trace}(\mathbf{H}_k^H \mathbf{C}_k \mathbf{C}_k^T \mathbf{H}_k [\mathbf{I}_{N_p q} - \mathbf{W}_{\bar{k}} (\mathbf{W}_{\bar{k}}^H \mathbf{W}_{\bar{k}})^{-1} \mathbf{W}_{\bar{k}}^H]^2)}}, \quad k = 1, 2, \dots, K \quad (8.92)$$

or, when individually normalized, is given by

$$\beta_i^{(k)} = \sqrt{\frac{1}{Q(i, i)}}, \quad i = 1, 2, \dots, q; k = 1, 2, \dots, K \quad (8.93)$$

where by definition

$$\mathbf{Q} = \mathbf{C}_k^T \mathbf{H}_k [\mathbf{I}_{N_p q} - \mathbf{W}_{\bar{k}} (\mathbf{W}_{\bar{k}}^H \mathbf{W}_{\bar{k}})^{-1} \mathbf{W}_{\bar{k}}^H]^2 \mathbf{H}_k^H \mathbf{C}_k \quad (8.94)$$

Above, two types of TP schemes have been derived, both of which are capable of fully removing the MUI at any of the MTs supported. Hence, both of them belong to the family of ZF-MUTP. When comparing the first ZF-MUTP, which computes the preprocessing matrix using (8.68), with the second ZF-MUTP, which derives the preprocessing matrix using (8.90) in the context of each of the K users, we find that, instead of inverting a matrix of size $(Kq \times Kq)$ in (8.68), the second ZF-MUTP inverts K number of matrices of size $[(K-1)q \times (K-1)q]$, each of which is for one downlink user. It is well recognized that the complexity of computing the inverse of a matrix of size $(N \times N)$ is typically proportional to $O(N^3)$. It can be shown that the complexity of the first ZF-MUTP corresponding to (8.68) is of the order of $O(K^3 q^3)$, while that of the second ZF-MUTP corresponding to (8.90) is of the order of $O(K(K-1)^3 q^3) = O(K^3 q^3 \times (K-1)^3 / K^2)$. Since $(K-1)^3 / K^2 > 1$ provided that $K > 3$, therefore, the second ZF-MUTP does not have the implementation advantage over the first ZF-MUTP, when $K > 3$.

The evaluation of the BER performance of the F-domain spread MC-CDMA using these two ZF-MUTPs may be obtained by using a so-called semi-numerical method, as analysed below.

Let us assume that the BPSK baseband modulation is employed. Then, for the first ZF-MUTP corresponding to (8.68), the decision variable for the i th bit of the k th MT can be expressed as

$$y_i^{(k)} = \beta_i^{(k)} b_i^{(k)} + n_i^{(k)}, \quad i = 1, 2, \dots, q; k = 1, 2, \dots, K \quad (8.95)$$

where $n_i^{(k)}$ is the Gaussian noise with zero mean and a variance of $N_0/2E_b$, and the normalization coefficient $\beta_i^{(k)}$ is given by (8.79) or (8.80), when the joint normalization is employed, while given by (8.82), when the individual normalization is utilized.

By contrast, for the second ZF-MUTP corresponding to (8.90), the decision variable vector for the k th user can be obtained by substituting (8.90) into (8.84), which yields

$$\mathbf{y}_k = \mathbf{C}_k^T \mathbf{H}_k [\mathbf{I}_{N_p q} - \mathbf{W}_{\bar{k}} (\mathbf{W}_{\bar{k}}^H \mathbf{W}_{\bar{k}})^{-1} \mathbf{W}_{\bar{k}}^H] \mathbf{H}_k^H \mathbf{C}_k \boldsymbol{\beta}_k \mathbf{b}_k + \mathbf{n}'_k, \quad k = 1, 2, \dots, K \quad (8.96)$$

Hence, the decision variable for the i th bit of the k th user can be expressed as

$$\begin{aligned} y_i^{(k)} &= [(\mathbf{H}_k^H \mathbf{C}_k)(i)]^H [\mathbf{I}_{N_p q} - \mathbf{W}_{\bar{k}} (\mathbf{W}_{\bar{k}}^H \mathbf{W}_{\bar{k}})^{-1} \mathbf{W}_{\bar{k}}^H] \mathbf{H}_k^H \mathbf{C}_k \boldsymbol{\beta}_k \mathbf{b}_k + n_i^{(k)} \\ i &= 1, 2, \dots, q; \quad k = 1, 2, \dots, K \end{aligned} \quad (8.97)$$

where $\mathbf{X}(i)$ represents the i th column of \mathbf{X} and the normalization coefficient $\beta_i^{(k)}$ is given by (8.92) or (8.93), when the joint or individual normalization is employed. Furthermore, since there exists no interference among the q bits of the same user, (8.97) can be also be reduced to

$$\begin{aligned} y_i^{(k)} &= [(\mathbf{H}_k^H \mathbf{C}_k)(i)]^H [\mathbf{I}_{N_p q} - \mathbf{W}_{\bar{k}} (\mathbf{W}_{\bar{k}}^H \mathbf{W}_{\bar{k}})^{-1} \mathbf{W}_{\bar{k}}^H] (\mathbf{H}_k^H \mathbf{C}_k)(i) \beta_i^{(k)} b_i^{(k)} + n_i^{(k)} \\ &= \tilde{\beta}_i^{(k)} b_i^{(k)} + n_i^{(k)}, \quad Di = 1, 2, \dots, q; \quad k = 1, 2, \dots, K \end{aligned} \quad (8.98)$$

where, by definition

$$\tilde{\beta}_i^{(k)} = [(\mathbf{H}_k^H \mathbf{C}_k)(i)]^H [\mathbf{I}_{N_p q} - \mathbf{W}_{\bar{k}} (\mathbf{W}_{\bar{k}}^H \mathbf{W}_{\bar{k}})^{-1} \mathbf{W}_{\bar{k}}^H] (\mathbf{H}_k^H \mathbf{C}_k)(i) \beta_i^{(k)} \quad (8.99)$$

Consequently, based on (8.95) and (8.99), the conditional BER can be expressed using the Gaussian Q -function as

$$P_b(\lambda) = Q\left(\sqrt{\frac{2\lambda^2 E_b}{N_0}}\right) \quad (8.100)$$

where $\lambda = \beta_i^{(k)}$ for the first ZF-MUTP and $\lambda = \tilde{\beta}_i^{(k)}$ for the second ZF-MUTP. Finally, the average BER of the F-domain spread MC-CDMA using ZF-MUTP can be evaluated as

$$P_b = \int_0^\infty Q\left(\sqrt{\frac{2y^2 E_b}{N_0}}\right) f_\lambda(y) dy \quad (8.101)$$

which requires the PDF of λ that is difficult to derive. In this case, the average BER may be obtained based on a sufficient number of realizations for λ , and then computed as

$$P_b \approx \frac{1}{N} \sum_{n=1}^N Q\left(\sqrt{\frac{2\lambda_n^2 E_b}{N_0}}\right) \quad (8.102)$$

where λ_n represents a realization of $\beta_i^{(k)}$ or $\tilde{\beta}_i^{(k)}$, correspondingly, for the first and second ZF-MUTPs.

Note that, the BER for both the cases can also be obtained using Monte-Carlo simulations based on (8.95) and (8.98), respectively.

Figures 8.6 and 8.7 show the BER versus SNR per bit performance of the BPSK-assisted MC-CDMA system using the ZF-MUTP, when communicating over frequency-selective Rayleigh fading channels having $L = 10$ or 20 T-domain resolvable paths. The MC-CDMA system was assumed to employ $N_p q = 64$ subcarriers and $q = 4$ bits were

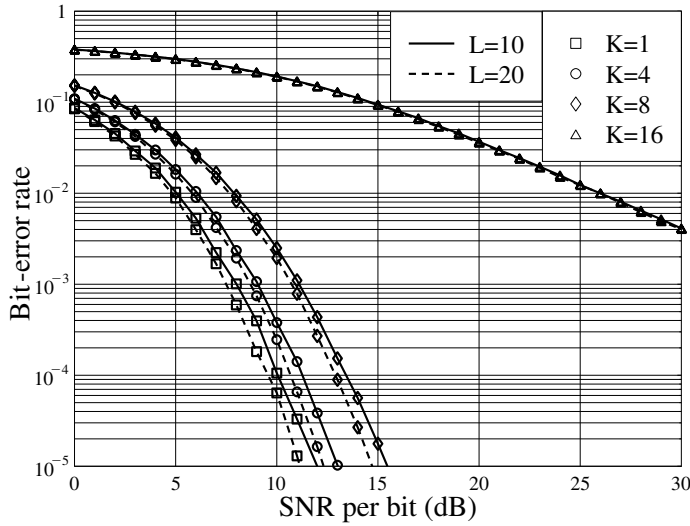


Figure 8.6: BER versus average SNR per bit performance for the MC-CDMA using the ZF-MUTP, when communicating over frequency-selective Rayleigh fading channels having $L = 10$ or 20 T-domain resolvable paths. The MC-CDMA system employs $N_{pq} = 64$ subcarriers and $q = 4$ bits are transmitted to each of the downlink users. The simulations were based on the preprocessing matrix (8.68) associated with using the individual normalization of (8.82).

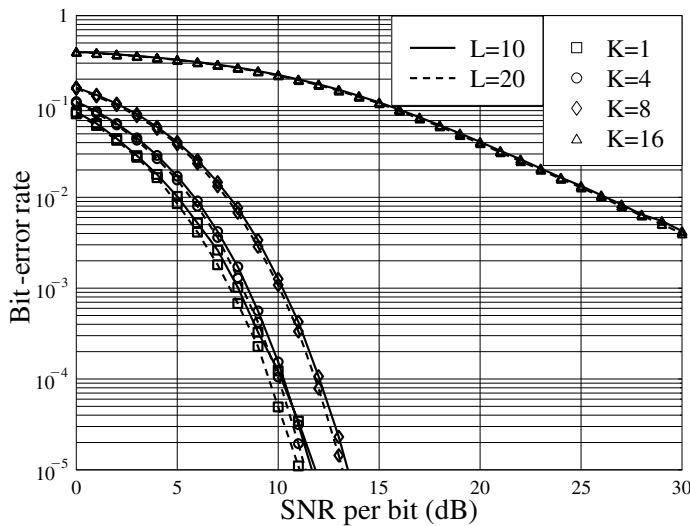


Figure 8.7: BER versus average SNR per bit performance for the MC-CDMA using the ZF-MUTP, when communicating over frequency-selective Rayleigh fading channels having $L = 10$ or 20 T-domain resolvable paths. The MC-CDMA system employs $N_{pq} = 64$ subcarriers and $q = 4$ bits are transmitted to each of the downlink users. The simulations were based on the preprocessing matrix (8.68) associated with using the joint normalization of (8.79).

transmitted to each of the downlink users. Therefore, each data bit was conveyed by $N_p = 16$ subcarriers, implying that the highest diversity order achievable is 16. Furthermore, in Fig. 8.6 the transmission power was normalized based on the individual normalization of (8.82), while in Fig. 8.7 it was normalized based on the joint normalization of (8.79). Comparing Figs 8.6 and 8.7 with Fig. 8.5 in Section 8.2.3, we observe that the ZF-MUTP is capable of removing the MUI. However, when the number of users supported becomes higher, the BER performance becomes poorer. This is because the ZF-MUTP amplifies background noise, while providing the MUI suppression. The results of Figs 8.6 and 8.7 show that the BER performance corresponding to $L = 20$ is slightly better than that of $l = 10$. Furthermore, when comparing Fig. 8.6 with Fig. 8.7, it can be observed that the joint transmission power normalization slightly outperforms the individual transmission power normalization.

8.2.5 Minimum Mean-Square Error (MMSE) Multiuser Transmitter Preprocessing

For convenience, let us copy here the decision variable vector of (8.46)

$$\mathbf{y} = \mathcal{C}^T \mathbf{H} \bar{\mathbf{P}} \mathbf{x} + \mathbf{n} \quad (8.103)$$

where \mathbf{n} is Gaussian and has a covariance matrix $\mathbf{R}_n = \sigma_s^2 \mathbf{I}_{Kq}$.

For the MUTP derived based on the minimum mean-square error (MMSE) criterion, i.e. for the MMSE-MUTP, the transmitter preprocessing matrix $\bar{\mathbf{P}}$ in (8.103) is chosen, so that the mean-square error (MSE) associated with the K number of remote MTs is minimized, under the constraint that the total transmission power is constant. Based on (8.103), the minimization problem can be stated as

$$\begin{aligned} \bar{\mathbf{P}} &= \arg \min_{E[\|\bar{\mathbf{P}}\mathbf{x}\|^2] = E[\|\mathbf{x}\|^2]} \{E[\|\mathbf{x} - \mathbf{y}\|^2]\} \\ &= \arg \min_{E[\|\bar{\mathbf{P}}\mathbf{x}\|^2] = E[\|\mathbf{x}\|^2]} \{E[\|\mathbf{x} - \mathcal{C}^T \mathbf{H} \bar{\mathbf{P}} \mathbf{x} - \mathbf{n}\|^2]\} \end{aligned} \quad (8.104)$$

Let the estimation error vector be expressed as

$$\Delta = \mathbf{x} - \mathcal{C}^T \mathbf{H} \bar{\mathbf{P}} \mathbf{x} - \mathbf{n} \quad (8.105)$$

Then, the variance of the estimation error associated with K MTs can be expressed as

$$\begin{aligned} J &= E[\|\Delta\|^2] = E[(\mathbf{x} - \mathcal{C}^T \mathbf{H} \bar{\mathbf{P}} \mathbf{x} - \mathbf{n})^H (\mathbf{x} - \mathcal{C}^T \mathbf{H} \bar{\mathbf{P}} \mathbf{x} - \mathbf{n})] \\ &= \text{Trace}(E[(\mathbf{x} - \mathcal{C}^T \mathbf{H} \bar{\mathbf{P}} \mathbf{x} - \mathbf{n})(\mathbf{x} - \mathcal{C}^T \mathbf{H} \bar{\mathbf{P}} \mathbf{x} - \mathbf{n})^H]) \\ &= \text{Trace}(\mathbf{R}_\Delta) \end{aligned} \quad (8.106)$$

where \mathbf{R}_Δ is the covariance matrix of the estimation error vector of (8.105) and, by definition,

$$\mathbf{R}_\Delta = E[(\mathbf{x} - \mathcal{C}^T \mathbf{H} \bar{\mathbf{P}} \mathbf{x} - \mathbf{n})(\mathbf{x} - \mathcal{C}^T \mathbf{H} \bar{\mathbf{P}} \mathbf{x} - \mathbf{n})^H] \quad (8.107)$$

Expanding it and completing the necessary expectations, we obtain

$$\mathbf{R}_\Delta = \mathbf{I}_{Kq} - \bar{\mathbf{P}}^H \mathbf{H}^H \mathcal{C} - \mathcal{C}^T \mathbf{H} \bar{\mathbf{P}} + \mathcal{C}^T \mathbf{H} \bar{\mathbf{P}} \bar{\mathbf{P}}^H \mathbf{H}^H \mathcal{C} + \sigma_s^2 \mathbf{I}_{Kq} \quad (8.108)$$

The transmitter preprocessing matrix $\bar{\mathbf{P}}$ can be derived, accordingly, based on whether the BS transmitter uses the knowledge about the variance σ_s^2 of the noise presenting at the remote MTs. Let us first consider the case where we assume that the BS transmitter does not employ the knowledge of the noise variance σ_s^2 . In this case, taking the derivative of $\text{Trace}(\mathbf{R}_\Delta)$ with respect to $\bar{\mathbf{P}}^*$ using the relations in Appendix 6.A, and setting the derivative result to equal a zero matrix, we obtain

$$\mathbf{H}^H \mathcal{C} \mathcal{C}^T \mathbf{H} \bar{\mathbf{P}} = \mathbf{H}^H \mathcal{C} \boldsymbol{\beta} \quad (8.109)$$

where $\boldsymbol{\beta}$ is a diagonal matrix for power normalization. It can be observed that in (8.109) $\mathbf{H}^H \mathcal{C} \mathcal{C}^T \mathbf{H}$ is singular and is not invertible. However, the above equation is solvable, since the columns of the matrix $\mathbf{H}^H \mathcal{C}$ lie in the span of the matrix $\mathbf{H}^H \mathcal{C} \mathcal{C}^T \mathbf{H}$. According to the matrix theory [157], one possible solution achieving the minimum norm is given by

$$\bar{\mathbf{P}} = \mathbf{H}^H \mathcal{C} (\mathcal{C}^T \mathbf{H} \mathbf{H}^H \mathcal{C})^{-1} \boldsymbol{\beta} \quad (8.110)$$

which is in fact the zero-forcing solution given by (8.68).

In the context of the communications environments where the BS transmitter is capable of acquiring the knowledge of the noise variance σ_s^2 , using the power constraint of $E[\|\bar{\mathbf{P}}\mathbf{x}\|^2] = E[\|\mathbf{x}\|^2]$ or $\text{Trace}(\bar{\mathbf{P}}^H \bar{\mathbf{P}}) = Kq$, \mathbf{R}_Δ can be modified to

$$\mathbf{R}_\Delta = \mathbf{I}_{Kq} - \bar{\mathbf{P}}^H \mathbf{H}^H \mathcal{C} - \mathcal{C}^T \mathbf{H} \bar{\mathbf{P}} + \mathcal{C}^T \mathbf{H} \bar{\mathbf{P}} \bar{\mathbf{P}}^H \mathbf{H}^H \mathcal{C} + \rho \sigma_s^2 \bar{\mathbf{P}}^H \bar{\mathbf{P}} \quad (8.111)$$

where $\rho = 1/Kq$ for the above case. However, ρ can in general be defined as the *noise-suppression factor*, the value of which determines how much the noise suppression is emphasized.

Taking the derivative of $\text{Trace}(\mathbf{R}_\Delta)$ with respect to $\bar{\mathbf{P}}^*$ and setting the result to equal zero gives

$$\frac{\partial \text{Trace}(\mathbf{R}_\Delta)}{\partial \bar{\mathbf{P}}^*} = -\mathbf{H}^H \mathcal{C} + \mathbf{H}^H \mathcal{C} \mathcal{C}^T \mathbf{H} \bar{\mathbf{P}} + \rho \sigma_s^2 \bar{\mathbf{P}} = \mathbf{0} \quad (8.112)$$

which yields the preprocessing matrix

$$\bar{\mathbf{P}} = (\mathbf{H}^H \mathcal{C} \mathcal{C}^T \mathbf{H} + \rho \sigma_s^2 \mathbf{I}_{N_p q})^{-1} \mathbf{H}^H \mathcal{C} \boldsymbol{\beta} \quad (8.113)$$

where the diagonal matrix $\boldsymbol{\beta}$ is for power normalization. Furthermore, invoking the *matrix inverse lemma* seen in (6.B.1) of Appendix 6.B, the preprocessing matrix can be expressed as

$$\bar{\mathbf{P}} = \mathbf{H}^H \mathcal{C} (\mathcal{C}^T \mathbf{H} \mathbf{H}^H \mathcal{C} + \rho \sigma_s^2 \mathbf{I}_{Kq})^{-1} \boldsymbol{\beta} \quad (8.114)$$

which is a preprocessing matrix required to invert a matrix of size $(Kq \times Kq)$.

Note that (8.114) may not always result in the MMSE solution. However, the factor ρ can be optimized, so that the best error performance can be achieved. Furthermore, the result of (8.114) can be written in a more general form as

$$\bar{\mathbf{P}} = \mathbf{H}^H \mathcal{C} (\rho_1 \mathcal{C}^T \mathbf{H} \mathbf{H}^H \mathcal{C} + \rho_2 \sigma_s^2 \mathbf{I}_{Kq})^{-1} \boldsymbol{\beta} \quad (8.115)$$

where $0 \leq \rho_1, \rho_2 \leq 1$ are the parameters that may be optimized according to the specific cases in practice, so that the best error performance can be achieved.

It can be shown that (8.114) is reduced to the zero-forcing solution seen in (8.110) when $\rho = 0$. When $\rho = 1$ and $\sigma_s^2 = (1/\text{SNR})$, (8.114) becomes

$$\bar{\mathbf{P}} = \mathbf{H}^H \mathcal{C} \left(\mathcal{C}^T \mathbf{H} \mathbf{H}^H \mathcal{C} + \frac{1}{\text{SNR}} \mathbf{I}_{Kq} \right)^{-1} \boldsymbol{\beta} \quad (8.116)$$

which is the MMSE solution derived in references [226, 227]. Furthermore, when in (8.114) $\rho \rightarrow \infty$ or in (8.115) $\rho_1 = 0$ and $\rho_2 = 1$, the preprocessing matrix is reduced to

$$\bar{\mathbf{P}} = \mathbf{H}^H \mathcal{C} \boldsymbol{\beta} \quad (8.117)$$

which is the solution for the TMF, as shown in (8.51).

Finally, in (8.114) $\boldsymbol{\beta}$ can be expressed as

$$\boldsymbol{\beta} = \sqrt{\frac{Kq}{\text{Trace}(\mathbf{H}^H \mathcal{C} [\mathcal{C}^T \mathbf{H} \mathbf{H}^H \mathcal{C} + \rho \sigma_s^2 \mathbf{I}_{Kq}]^{-2} \mathcal{C}^T \mathbf{H})}} \times \mathbf{I}_{Kq} \quad (8.118)$$

for using the joint power normalization, and expressed as

$$\boldsymbol{\beta}(i, i) = \sqrt{\|(\mathbf{H}^H \mathcal{C} (\mathcal{C}^T \mathbf{H} \mathbf{H}^H \mathcal{C} + \rho \sigma_s^2 \mathbf{I}_{Kq})^{-1})(i)\|^{-2}}, \quad i = 1, 2, \dots, Kq \quad (8.119)$$

for using the individual power normalization.

Figures 8.8 and 8.9 show the BER against SNR per bit performance for the MC-CDMA using MMSE-MUTP, when communicating over frequency-selective Rayleigh fading channels having $L = 10$ or 20 T-domain resolvable paths. The MC-CDMA system under consideration uses $N_p q = 64$ subcarriers. The number of bits per symbol is $q = 4$ and the F-domain spreading factor is $N_p = 16$. In Fig. 8.8 the simulations were based on the preprocessing matrix (8.114) associated with $\rho = 1$ and the individual power normalization of (8.119). By contrast, in Fig. 8.9 the simulations were based on the preprocessing matrix (8.114) associated with $\rho = 1$ and the joint power normalization of (8.118). From the results of Figs. 8.8 and 8.9, we may make the following observations. First, the MMSE-MUTP using either the individual power normalization of (8.119) or the joint power normalization of (8.118) is capable of mitigating the downlink MUI efficiently. Second, when the downlink channels become more frequency selective, better BER performance can be achieved. This observation implies that the MMSE-MUTP is capable of achieving the frequency diversity gain, in addition to suppressing the MUI. Third, when comparing Figs 8.8 and 8.9, the BER performance of the MMSE-MUTP using the joint power normalization of (8.118) is better than that of a corresponding MMSE-MUTP using the individual power normalization of (8.119). Finally, the MMSE-MUTP using either the individual or joint power normalization trades the diversity gain for MUI suppression, resulting in the BER performance degrading when the number of users supported increases.

When comparing the BER performance of the MMSE-MUTP seen in Figs 8.8 and 8.9 with that of the ZF-MUTP as seen in Figs 8.6 and 8.7 in Section 8.2.4, we find that the MMSE-MUTP outperforms the ZF-MUTP in terms of achievable BER performance. The ZF-MUTP discussed in Section 8.2.4 amplifies the background noise, when fully removing the downlink MUI. Conversely, the MMSE-MUTP does not fully remove the downlink MUI, but it is capable of suppressing the background noise. However, the MMSE-MUTP needs the knowledge of noise variance in order to carry out the preprocessing.

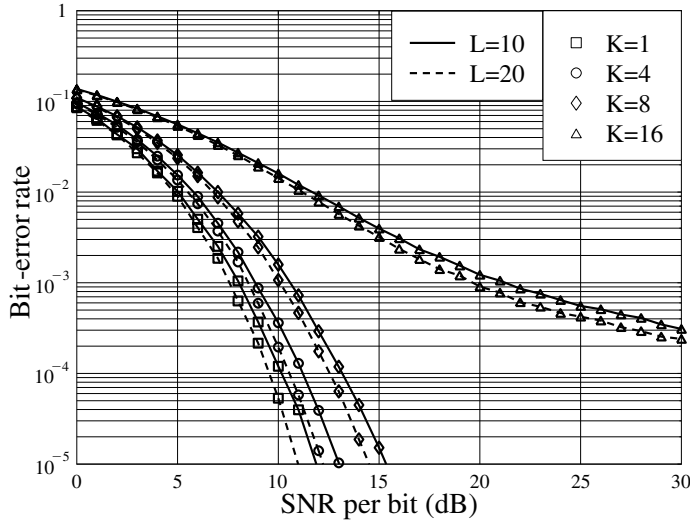


Figure 8.8: BER versus average SNR per bit performance for the MC-CDMA using the MMSE-MUTP, when communicating over frequency-selective Rayleigh fading channels having $L = 10$ or 20 T-domain resolvable paths. The MC-CDMA system employs $N_p q = 64$ subcarriers and $q = 4$ bits are transmitted to each of the downlink users. The simulations were based on the preprocessing matrix (8.114) associated with $\rho = 1$ and the individual power normalization of (8.119).

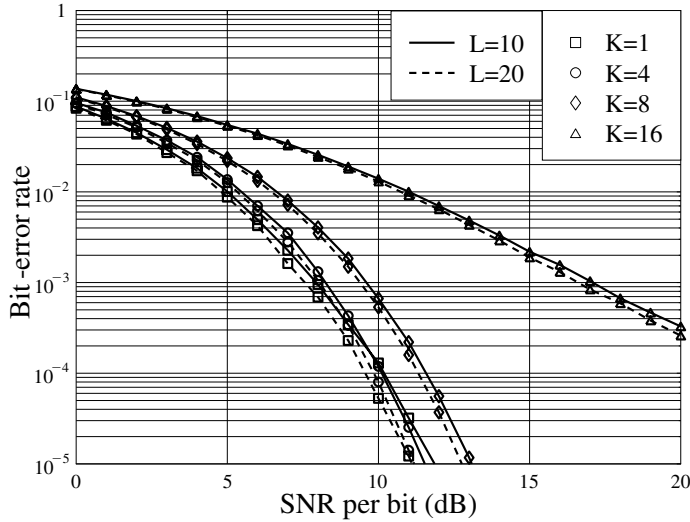


Figure 8.9: BER versus average SNR per bit performance for the MC-CDMA using the MMSE-MUTP, when communicating over frequency-selective Rayleigh fading channels having $L = 10$ or 20 T-domain resolvable paths. The MC-CDMA system employs $N_p q = 64$ subcarriers and $q = 4$ bits are transmitted to each of the downlink users. The simulations were based on the preprocessing matrix (8.114) associated with $\rho = 1$ and the joint power normalization of (8.118).

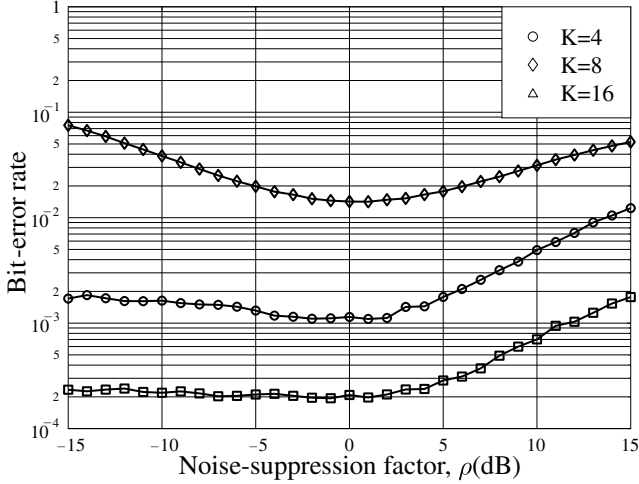


Figure 8.10: BER versus noise-suppression factor performance for the MC-CDMA using the MMSE-MUTP, when communicating over frequency-selective Rayleigh fading channels having $L = 20$ T-domain resolvable paths. The MC-CDMA system employs $N_p q = 64$ subcarriers and $q = 4$ bits are transmitted to each of the downlink users. The simulations were based on the preprocessing matrix (8.114) associated with the individual power normalization of (8.119).

In Fig. 8.10 we illustrate the effect of the noise-suppression factor, ρ , on the achievable BER performance of the MC-CDMA, when it supports the number of users of $K = 4, 8$ and 16 . Note that the MMSE-MUTP is reduced to the ZF-MUTP, when $\rho = 0$. When the ρ value of the noise suppression factor increases, the preprocessing aims its power more at background noise suppression. When $\rho \rightarrow \infty$, the MMSE-MUTP is reduced to the TMF-SUTP. For example, as shown in Fig. 8.10, when $\rho = 15$ dB, the BS preprocessing deliberately emphasizes the noise suppression by a factor of 15 dB, implying that the noise variance invoked in the MMSE-assisted preprocessing is approximately 15 dB higher than the actual noise variance of the downlink channels.

From the results of Fig. 8.10, we may make the following observations. First, for any given K value, generally, there is an optimum ρ value that results in the lowest BER. Second, the BER performance only loosely depends on the ρ value of the noise-suppression factor. It can be seen that there is a range within which the achievable BER performance is better than that of the corresponding ZF-MUTP. This implies that the achievable BER performance of the MMSE-MUTP is generally insensitive to the noise variance set in the preprocessing matrix, as seen, for example, in (8.114).

8.2.6 Maximum Signal-to-Interference-Plus-Noise Ratio (MSINR) Multiuser Transmitter Preprocessing

Again, we copy here the decision variable vector of (8.46)

$$\mathbf{y} = \mathcal{C}^T \mathbf{H} \bar{\mathbf{P}} \mathbf{x} + \mathbf{n} \quad (8.120)$$

where the decision variable vector for \mathbf{x}_k can be expressed as

$$\mathbf{y}_k = \mathbf{C}_k^T \mathbf{H}_k \bar{\mathbf{P}}_k \mathbf{x}_k + \sum_{i \neq k}^K \mathbf{C}_k^T \mathbf{H}_k \bar{\mathbf{P}}_i \mathbf{x}_i + \mathbf{n}'_k, \quad k = 1, 2, \dots, K \quad (8.121)$$

and $\bar{\mathbf{P}}_i$, $i = 1, 2, \dots, K$ is for the preprocessing of \mathbf{x}_i . Let $y_i^{(k)}$ be the i th entry of \mathbf{y}_k , and $E[y_i^{(k)}]$ and $\text{Var}[y_i^{(k)}]$ be the mean and variance of $y_i^{(k)}$, where $i = 1, 2, \dots, q$. Then, the SINR for detection of the data symbol $x_i^{(k)}$ can be expressed as

$$\text{SINR}_i^{(k)} = \frac{1}{2} \frac{E^2[y_i^{(k)}]}{\text{Var}[y_i^{(k)}]} \quad (8.122)$$

However, for downlink preprocessing, the maximization of (8.122) is extremely difficult. For this sake, we may alternatively minimize the cost function [228] of

$$J = \sum_{k=1}^K \sum_{i=1}^q (\text{SINR}_i^{(k)})^{-1} \quad (8.123)$$

under the power constraint and given that the ZF condition has been achieved, i.e. given that

$$\mathbf{C}_k^T \mathbf{H}_k \bar{\mathbf{P}}_i = \mathbf{0}, \quad \text{for any } k \neq i \quad (8.124)$$

In this case, one of the solutions to the problem is given by (8.68), which, for simplicity, can be rewritten as

$$\bar{\mathbf{P}} = \tilde{\mathbf{P}} \boldsymbol{\beta} \quad (8.125)$$

where $\tilde{\mathbf{P}} = (\mathbf{C}^T \mathbf{H})^H (\mathbf{C}^T \mathbf{H} \mathbf{H}^H \mathbf{C})^{-1}$. When substituting (8.125) into (8.120), the decision variable vector can now be expressed as

$$\mathbf{y} = \boldsymbol{\beta} \mathbf{x} + \mathbf{n}' \quad (8.126)$$

Consequently, the problem is now reduced to choosing the power normalization matrix $\boldsymbol{\beta}$ under the power constraint, so that the overall SINR is maximized, or alternatively, the cost function of (8.123) is minimized.

First, let us assume that \mathbf{n}' is Gaussian and that the common variance of its elements is σ^2 . Then, it can be shown that the cost function of (8.123) is given by

$$J = \sigma^2 \sum_{k=1}^K \sum_{i=1}^q \frac{1}{(\beta_i^{(k)})^2} \quad (8.127)$$

When taking into account the power constraint, the solution to the problem can be derived by finding the minimum of the augmented cost function

$$\mathcal{J} = \sigma^2 \sum_{k=1}^K \sum_{i=1}^q \frac{1}{(\beta_i^{(k)})^2} + \mu \left[\sum_{k=1}^K \sum_{i=1}^q (\beta_i^{(k)})^2 \|\tilde{\mathbf{p}}_i^{(k)}\|^2 - Kq \right] \quad (8.128)$$

where $\tilde{\mathbf{p}}_i^{(k)}$ is a column of $\tilde{\mathbf{P}}$, which preprocesses the data symbol $x_i^{(k)}$, μ is the Lagrange multiplier. Taking the derivative of \mathcal{J} with respect to $\beta_i^{(k)}$ and setting it to zero gives [228]

$$\beta_i^{(k)} = \frac{\bar{\mu}}{\sqrt{\|\tilde{\mathbf{p}}_i^{(k)}\|}} \quad (8.129)$$

where $\bar{\mu}$ is independent of i and k , which can be obtained by the power constraint of $E[\text{Trace}(\tilde{\mathbf{P}}\tilde{\mathbf{P}}^H)] = Kq$, yields

$$\bar{\mu} = \sqrt{\frac{Kq}{\sum_{k'=1}^K \sum_{i'=1}^q \|\tilde{\mathbf{p}}_{i'}^{(k')}\|}} \quad (8.130)$$

Finally, when substituting (8.130) into (8.129) and then applying the result to (8.125), we obtain the preprocessing vector $\tilde{\mathbf{p}}_i^{(k)}$ for $x_i^{(k)}$, which can be expressed as

$$\tilde{\mathbf{p}}_i^{(k)} = \sqrt{\frac{Kq}{\sum_{k'=1}^K \sum_{i'=1}^q \|\tilde{\mathbf{p}}_{i'}^{(k')}\| \|\tilde{\mathbf{p}}_i^{(k)}\|}} \times \tilde{\mathbf{p}}_i^{(k)} \quad (8.131)$$

Based on (8.131), the overall preprocessing matrix for the MSINR-MUTP can be formed as

$$\tilde{\mathbf{P}} = [\tilde{\mathbf{p}}_0^{(1)} \ \cdots \ \tilde{\mathbf{p}}_{q-1}^{(1)} \ \cdots \cdots \ \tilde{\mathbf{p}}_0^{(K)} \ \cdots \ \tilde{\mathbf{p}}_{q-1}^{(K)}] \quad (8.132)$$

Figure 8.11 compares the BER performance of the MC-CDMA using the MSINR-MUTP with that of the MC-CDMA using the ZF-MUTP. It can be seen that the MSINR-MUTP slightly outperforms the ZF-MUTP.

8.2.7 Minimum Variance Distortionless Response (MVDR) Multiuser Transmitter Preprocessing

In this section we derive the optimum preprocessing matrix $\tilde{\mathbf{P}}$ based on the minimum variance distortionless response (MVDR) principles, which have received wide research in signal detection for CDMA, multiple antenna, antenna array, etc. systems. The MVDR-assisted transmitter preprocessing for DS-CDMA systems has been studied in reference [218] without making the effort to mitigate background noise.

As shown in (8.121) the decision variable vector for \mathbf{x}_k of the k th user's transmitted symbols can be expressed as

$$\mathbf{y}_k = \mathbf{C}_k^T \mathbf{H}_k \tilde{\mathbf{P}}_k \mathbf{x}_k + \sum_{i \neq k}^K \mathbf{C}_k^T \mathbf{H}_k \tilde{\mathbf{P}}_i \mathbf{x}_i + \mathbf{n}'_k, \quad k = 1, 2, \dots, K \quad (8.133)$$

where $\tilde{\mathbf{P}}_i$, $i = 1, 2, \dots, K$ is for the preprocessing of \mathbf{x}_i . From (8.133) we imply that the total interference imposed by user k on the other $(K - 1)$ users plus the background noise

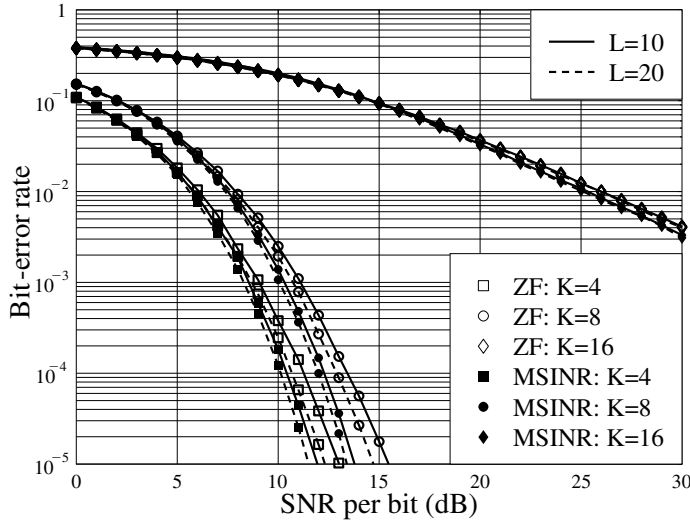


Figure 8.11: BER versus average SNR per bit performance for the MC-CDMA using the MSINR-assisted MUTP, when communicating over frequency-selective Rayleigh fading channels having $L = 10$ or 20 T-domain resolvable paths. The MC-CDMA system employs $N_p q = 64$ subcarriers and $q = 4$ bits are transmitted to each of the downlink users. The simulations were based on the preprocessing matrix (8.125). In this figure the results of the ZF-MUTP shown in Fig. 8.6 are also included.

can be expressed as

$$\mathbf{I}_k = \sum_{i \neq k}^K \mathbf{C}_i^T \mathbf{H}_i \bar{\mathbf{P}}_k \mathbf{x}_k + \mathbf{n}'_k, \quad k = 1, 2, \dots, K \quad (8.134)$$

Assuming that \mathbf{x}_k is constituted by i.i.d symbols satisfying $E[|x_i^{(k)}|^2] = 1$, then the variance of \mathbf{I}_k is given by

$$E[\|\mathbf{I}_k\|^2] = \text{Trace}\left(\bar{\mathbf{P}}_k^H \underbrace{\left[\sum_{i \neq k}^K \mathbf{H}_i^H \mathbf{C}_i \mathbf{C}_i^T \mathbf{H}_i \right]}_{\mathbf{R}_{\bar{k}}} \bar{\mathbf{P}}_k\right) + \sigma_s^2 q, \quad k = 1, 2, \dots, K \quad (8.135)$$

where

$$\mathbf{R}_{\bar{k}} = \sum_{i \neq k}^K \mathbf{H}_i^H \mathbf{C}_i \mathbf{C}_i^T \mathbf{H}_i \quad (8.136)$$

When invoking the power constraint $\text{Trace}(\bar{\mathbf{P}}_k \bar{\mathbf{P}}_k^H) = q$ on the transmitted signals, (8.135) can be written as

$$E[\|\mathbf{I}_k\|^2] = \text{Trace}(\bar{\mathbf{P}}_k^H [\mathbf{R}_{\bar{k}} + \sigma_s^2 \mathbf{I}_{N_p q}] \bar{\mathbf{P}}_k), \quad k = 1, 2, \dots, K \quad (8.137)$$

According to (8.133), the distortionless condition can be expressed as¹

$$\mathbf{C}_k^T \mathbf{H}_k \bar{\mathbf{P}}_k = \boldsymbol{\beta}_k, \quad k = 1, 2, \dots, K \quad (8.138)$$

The preprocessing matrix for the MVDR-MUTP can be found by minimizing $E[\|\mathbf{I}_k\|^2]$ while providing distortionless response to the k th MT. Hence, the preprocessing matrix $\bar{\mathbf{P}}_k$ corresponding to \mathbf{x}_k can be found by minimizing the cost function

$$\mathbf{J}_k = \bar{\mathbf{P}}_k^H [\mathbf{R}_{\bar{k}} + \rho \sigma_s^2 \mathbf{I}_{N_p q}] \bar{\mathbf{P}}_k + \boldsymbol{\lambda}_k^H (\boldsymbol{\beta}_k - \mathbf{C}_k^T \mathbf{H}_k \bar{\mathbf{P}}_k) + (\boldsymbol{\beta}_k - \bar{\mathbf{P}}_k^H \mathbf{H}_k^H \mathbf{C}_k) \boldsymbol{\lambda}_k \quad (8.139)$$

where the noise-suppression factor ρ is introduced. Taking the derivative of \mathbf{J}_k with respect to $\bar{\mathbf{P}}_k^*$, it can be shown that the matrix for preprocessing \mathbf{x}_k can be expressed as

$$\bar{\mathbf{P}}_k = (\mathbf{R}_{\bar{k}} + \rho \sigma_s^2 \mathbf{I}_{N_p q})^{-1} \mathbf{H}_k^H \mathbf{C}_k \boldsymbol{\lambda}_k, \quad k = 1, 2, \dots, K \quad (8.140)$$

where $\boldsymbol{\lambda}_k$ can be found by substituting (8.140) into (8.138), yielding

$$\boldsymbol{\lambda}_k = (\mathbf{C}_k^T \mathbf{H}_k (\mathbf{R}_{\bar{k}} + \rho \sigma_s^2 \mathbf{I}_{N_p q})^{-1} \mathbf{H}_k^H \mathbf{C}_k)^{-1} \boldsymbol{\beta}_k \quad (8.141)$$

Substituting (8.141) into (8.140), we finally obtain the preprocessing matrix in the MVDR sense as

$$\begin{aligned} \bar{\mathbf{P}}_k &= (\mathbf{R}_{\bar{k}} + \rho \sigma_s^2 \mathbf{I}_{N_p q})^{-1} \mathbf{H}_k^H \mathbf{C}_k (\mathbf{C}_k^T \mathbf{H}_k (\mathbf{R}_{\bar{k}} + \rho \sigma_s^2 \mathbf{I}_{N_p q})^{-1} \mathbf{H}_k^H \mathbf{C}_k)^{-1} \boldsymbol{\beta}_k \\ k &= 1, 2, \dots, K \end{aligned} \quad (8.142)$$

where $\boldsymbol{\beta}_k$ can be found by invoking the power constraint, which gives

$$\begin{aligned} \boldsymbol{\beta}_k &= \boldsymbol{\beta}_k \mathbf{I}_q \\ \boldsymbol{\beta}_k &= \sqrt{\frac{q}{\text{Trace}(\bar{\mathbf{P}}_k^H \bar{\mathbf{P}}_k)}} \end{aligned} \quad (8.143)$$

for using the joint power normalization, while, for the individual power normalization, $\boldsymbol{\beta}(i, i)$ can be obtained from

$$(\bar{\mathbf{P}}_k(i))^H (\bar{\mathbf{P}}_k(i)) = 1 \quad (8.144)$$

where $\bar{\mathbf{P}}_k(i)$ is the i th column of $\bar{\mathbf{P}}_k$.

Finally, the overall preprocessing matrix for the MVDR-MUTP can be formed as

$$\bar{\mathbf{P}} = [\bar{\mathbf{P}}_1, \bar{\mathbf{P}}_2, \dots, \bar{\mathbf{P}}_K] \quad (8.145)$$

where $\bar{\mathbf{P}}_k$ is given by (8.142).

Equation (8.142) shows that the MVDR-MUTP is capable of fully removing the MUI, while taking into account the noise suppression. Hence, the MVDR-MUTP shown in (8.142) can be interpreted as a joint MMSE-MUTP and ZF-MUTP.

Figure 8.12 shows the BER performance of the MC-CDMA using the MVDR-MUTP, when communicating over frequency-selective Rayleigh fading channels. It can be seen that the MVDR-MUTP can efficiently mitigate the downlink MUI.

¹Note that instead of using the conventional distortionless condition [89] of $\mathbf{C}_k^T \mathbf{H}_k \bar{\mathbf{P}}_k = \mathbf{I}_q$, we use the constraint of $\mathbf{C}_k^T \mathbf{H}_k \bar{\mathbf{P}}_k = \boldsymbol{\beta}_k$ as the distortionless condition, in order to match the constraint on the transmission power. Explicitly, the former is a special case of the latter.

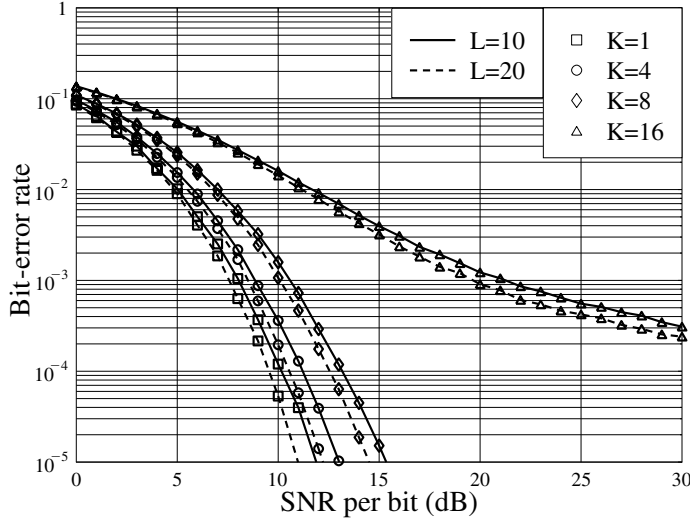


Figure 8.12: BER versus average SNR per bit performance for the MC-CDMA using the MVDR-assisted MUTP, when communicating over frequency-selective Rayleigh fading channels having $L = 10$ or 20 T-domain resolvable paths. The MC-CDMA system employs $N_p q = 64$ subcarriers and $q = 4$ bits are transmitted to each of the downlink users. The simulations were based on the preprocessing matrix (8.142) associated with $\rho = 1$ and using the individual power normalization of (8.144).

8.2.8 Minimum Power Distortionless Response (MPDR) Multiuser Transmitter Preprocessing

In this section the optimum preprocessing matrix $\bar{\mathbf{P}}$ is found by minimizing the total power received by the K number of MTs, under the condition that the MTs' received signals are distortionless.

Given the decision variable vector of (8.46), i.e.

$$\mathbf{y} = \mathcal{C}^T \mathbf{H} \bar{\mathbf{P}} \mathbf{x} + \mathbf{n} \quad (8.146)$$

the average output power is given by

$$\begin{aligned} P_o &= E[\|\mathbf{y}\|^2] = E[\|\mathcal{C}^T \mathbf{H} \bar{\mathbf{P}} \mathbf{x} + \mathbf{n}\|^2] \\ &= \text{Trace}(\mathcal{C}^T \mathbf{H} \bar{\mathbf{P}} \bar{\mathbf{P}}^H \mathbf{H}^H \mathcal{C} + \sigma_s^2 \mathbf{I}_{Kq}) \end{aligned} \quad (8.147)$$

The condition of distortionless can be expressed as

$$\mathcal{C}^T \mathbf{H} \bar{\mathbf{P}} = \boldsymbol{\beta} \quad (8.148)$$

where $\boldsymbol{\beta}$ is a diagonal matrix for achieving the power constraints. Based on (8.147) and (8.148), we can constitute the cost function as

$$\mathbf{J} = \mathcal{C}^T \mathbf{H} \bar{\mathbf{P}} \bar{\mathbf{P}}^H \mathbf{H}^H \mathcal{C} + \sigma_s^2 \mathbf{I}_{Kq} + \boldsymbol{\lambda}^H (\boldsymbol{\beta} - \mathcal{C}^T \mathbf{H} \bar{\mathbf{P}}) + (\boldsymbol{\beta} - \bar{\mathbf{P}}^H \mathbf{H}^H \mathcal{C}) \boldsymbol{\lambda} \quad (8.149)$$

Since it is the trace of \mathbf{J} that is minimized, using the fact of $\text{Trace}(\bar{\mathbf{P}}\bar{\mathbf{P}}^H) = \text{Trace}(\mathbf{I}_{Kq}) = Kq$, equation (8.149) can also be written as

$$\mathbf{J} = \mathbf{C}^T \mathbf{H} \bar{\mathbf{P}} \bar{\mathbf{P}}^H \mathbf{H}^H \mathbf{C} + \sigma_s^2 \bar{\mathbf{P}}^H \bar{\mathbf{P}} + \lambda^H (\boldsymbol{\beta} - \mathbf{C}^T \mathbf{H} \bar{\mathbf{P}}) + (\boldsymbol{\beta} - \bar{\mathbf{P}}^H \mathbf{H}^H \mathbf{C}) \lambda \quad (8.150)$$

Taking the derivative of $\text{Trace}(\mathbf{J})$ with respect to $\bar{\mathbf{P}}^*$ and setting the result to equal to zero, we obtain

$$\frac{\partial \text{Trace}(\mathbf{J})}{\partial \bar{\mathbf{P}}^*} = \mathbf{H}^H \mathbf{C} \mathbf{C}^T \mathbf{H} \bar{\mathbf{P}} + \rho \sigma_s^2 \bar{\mathbf{P}} - \mathbf{H}^H \mathbf{C} \lambda = \mathbf{0} \quad (8.151)$$

which yields the preprocessing matrix

$$\bar{\mathbf{P}} = (\mathbf{H}^H \mathbf{C} \mathbf{C}^T \mathbf{H} + \rho \sigma_s^2 \mathbf{I}_{N_p q})^{-1} \mathbf{H}^H \mathbf{C} \lambda \quad (8.152)$$

Substituting (8.152) into (8.148), we obtain

$$\lambda = (\mathbf{C}^T \mathbf{H} (\mathbf{H}^H \mathbf{C} \mathbf{C}^T \mathbf{H} + \rho \sigma_s^2 \mathbf{I}_{N_p q})^{-1} \mathbf{H}^H \mathbf{C})^{-1} \boldsymbol{\beta} \quad (8.153)$$

Finally, when applying (8.153) into (8.152), the preprocessing matrix for the MUTP-MPDR is given by

$$\begin{aligned} \bar{\mathbf{P}} &= (\mathbf{H}^H \mathbf{C} \mathbf{C}^T \mathbf{H} + \rho \sigma_s^2 \mathbf{I}_{N_p q})^{-1} \mathbf{H}^H \mathbf{C} \\ &\quad \times (\mathbf{C}^T \mathbf{H} (\mathbf{H}^H \mathbf{C} \mathbf{C}^T \mathbf{H} + \rho \sigma_s^2 \mathbf{I}_{N_p q})^{-1} \mathbf{H}^H \mathbf{C})^{-1} \boldsymbol{\beta} \end{aligned} \quad (8.154)$$

where $\boldsymbol{\beta}$ can be obtained by applying the power constraint, and ρ is the noise-suppression factor, as discussed in the previous sections.

When the *matrix inverse lemma* is invoked, the preprocessing matrix of (8.154) can also be expressed as

$$\begin{aligned} \bar{\mathbf{P}} &= \mathbf{H}^H \mathbf{C} (\mathbf{C}^T \mathbf{H} \mathbf{H}^H \mathbf{C} + \rho \sigma_s^2 \mathbf{I}_{Kq})^{-1} \\ &\quad \times (\mathbf{C}^T \mathbf{H} \mathbf{H}^H \mathbf{C} (\mathbf{C}^T \mathbf{H} \mathbf{H}^H \mathbf{C} + \rho \sigma_s^2 \mathbf{I}_{Kq})^{-1})^{-1} \boldsymbol{\beta} \end{aligned} \quad (8.155)$$

Furthermore, since both $\mathbf{C}^T \mathbf{H} \mathbf{H}^H \mathbf{C}$ and $(\mathbf{C}^T \mathbf{H} \mathbf{H}^H \mathbf{C} + \rho \sigma_s^2 \mathbf{I}_{Kq})^{-1}$ in the above equation are invertible, we have

$$\begin{aligned} \bar{\mathbf{P}} &= \mathbf{H}^H \mathbf{C} (\mathbf{C}^T \mathbf{H} \mathbf{H}^H \mathbf{C} + \rho \sigma_s^2 \mathbf{I}_{Kq})^{-1} \\ &\quad \times (\mathbf{C}^T \mathbf{H} \mathbf{H}^H \mathbf{C} + \rho \sigma_s^2 \mathbf{I}_{Kq}) (\mathbf{C}^T \mathbf{H} \mathbf{H}^H \mathbf{C})^{-1} \boldsymbol{\beta} \\ &= \mathbf{H}^H \mathbf{C} (\mathbf{C}^T \mathbf{H} \mathbf{H}^H \mathbf{C})^{-1} \boldsymbol{\beta} \end{aligned} \quad (8.156)$$

Hence, the MPDR-MUTP results in the same solution as (8.2.4) obtained in Section 8.2.4 in the context of the ZF-MUTP. The fact that the MPDR-MUTP of (8.156) is equivalent to the ZF-MUTP of (8.2.4) implies that the MPDR-MUTP derived is unable to suppress the background noise, even though the noise variance has been invoked in the derivation at the start.

Note that the result of (8.156) has been derived when K downlink users are jointly considered. When the transmitter preprocessing is optimized on a user-by-user basis in the MPDR sense, as shown in reference [229], the resulting MPDR-MUTP solution is then equivalent to that of the MMSE-MUTP, which was studied in Section 8.2.5. In this case, the MPDR-MUTP has the potential of mitigating background noise.

8.2.9 Eigenspace-Based Multiuser Transmitter Preprocessing

In this section we show that the preprocessing matrix $\bar{\mathbf{P}}$ derived in the previous sections may be either derived or expressed in the context of the eigenspace of certain matrices invoked. First, we derive the preprocessing matrix $\bar{\mathbf{P}}$ for the ZF-MUTP that has been discussed in Section 8.2.4, based on the eigen-decomposition [230]. As shown in (8.85) the conditions for achieving the ZF-MUTP can be described as

$$\mathbf{C}_k^T \mathbf{H}_k \bar{\mathbf{P}}_k = \boldsymbol{\beta}_k, \quad \text{while } \mathbf{C}_i^T \mathbf{H}_i \bar{\mathbf{P}}_k = \mathbf{0} \text{ for any } i \neq k \quad (8.157)$$

where $k = 1, 2, \dots, K$, where $\boldsymbol{\beta}_k$ is a $(q \times q)$ diagonal matrix for achieving the power constraints. In other words, the preprocessing matrix $\bar{\mathbf{P}}_k$ corresponding to the k th MT is a $(N_p q \times q)$ matrix, which lies in the subspace determined by $\mathbf{C}_k^T \mathbf{H}_k$ and is orthogonal to the $(K - 1)q$ -rank subspace determined by all $\mathbf{C}_i^T \mathbf{H}_i$ for $i = 1, 2, \dots, K$; $i \neq k$. Here, we can define a $(N_p q \times (K - 1)q)$ -dimensional matrix as (8.86), which is

$$\mathbf{W}_{\bar{k}} = [\mathbf{H}_1^H \mathbf{C}_1, \dots, \mathbf{H}_{k-1}^H \mathbf{C}_{k-1}, \mathbf{H}_{k+1}^H \mathbf{C}_{k+1}, \dots, \mathbf{H}_K^H \mathbf{C}_K], \quad k = 1, 2, \dots, K \quad (8.158)$$

Let the singular-value-decomposition (SVD) [157] on $\mathbf{W}_{\bar{k}}$ be expressed as

$$\mathbf{W}_{\bar{k}} = \underbrace{[\mathbf{U}_{\bar{k},s} \mid \mathbf{U}_{\bar{k},n}]}_{\mathbf{U}_{\bar{k}}} \begin{bmatrix} \Sigma_{\bar{k},s}^{1/2} \\ \mathbf{0} \end{bmatrix} \mathbf{V}_{\bar{k}}^H, \quad k = 1, 2, \dots, K \quad (8.159)$$

where $\mathbf{U}_{\bar{k}}$ and $\mathbf{V}_{\bar{k}}$ are $(N_p q \times N_p q)$ and $((K - 1)q \times (K - 1)q)$ unitary matrices, respectively, while $\Sigma_{\bar{k},s}$ is a $((K - 1)q \times (K - 1)q)$ diagonal matrix given by

$$\Sigma_{\bar{k},s} = \text{diag}\{\lambda_1, \lambda_2, \dots, \lambda_{(K-1)q}\} \quad (8.160)$$

which contains the eigenvalues of $\mathbf{W}_{\bar{k}}^H \mathbf{W}_{\bar{k}}$. Furthermore, in (8.159) $\mathbf{U}_{\bar{k},s}$ is a $(N_p q \times (K - 1)q)$ matrix containing the eigenvectors corresponding to the nonzero eigenvalues of $\mathbf{W}_{\bar{k}} \mathbf{W}_{\bar{k}}^H$, while $\mathbf{U}_{\bar{k},n}$ is a $(N_p q \times (N_p - K + 1)q)$ matrix containing the eigenvectors corresponding to the zero eigenvalues of $\mathbf{W}_{\bar{k}} \mathbf{W}_{\bar{k}}^H$.

According to the theory of the SVD [157], the columns of $\mathbf{U}_{\bar{k}}$ are made up of the eigenvectors of $\mathbf{W}_{\bar{k}} \mathbf{W}_{\bar{k}}^H$, while the columns of $\mathbf{V}_{\bar{k}}$ consist of the eigenvectors of $\mathbf{W}_{\bar{k}}^H \mathbf{W}_{\bar{k}}$. Hence, it can be shown that $\mathbf{U}_{\bar{k},n}$ is orthogonal to $\mathbf{U}_{\bar{k},s}$ and is the null subspace of that determined by $\mathbf{W}_{\bar{k}}$. Therefore, let

$$\bar{\mathbf{P}}_k = \mathbf{U}_{\bar{k},n} \xi_k, \quad k = 1, 2, \dots, K \quad (8.161)$$

where ξ_k is a $((N_p - K + 1)q \times q)$ matrix to be discussed in detail later. Then, it can be shown that $\bar{\mathbf{P}}_k$ satisfies the conditions of $\mathbf{C}_i^T \mathbf{H}_i \bar{\mathbf{P}}_k = \mathbf{0}$ for $i \neq k$, as required in (8.157).

In (8.161) the operation of ξ_k on $\mathbf{U}_{\bar{k},n}$ maps the $(N_p - K + 1)q$ -dimensional subspace determined by $\mathbf{U}_{\bar{k},n}$ to the desired q -dimensional subspace of $\bar{\mathbf{P}}_k$. Hence, ξ_k should be chosen to satisfy:

- $\mathbf{C}_k^T \mathbf{H}_k \bar{\mathbf{P}}_k = \boldsymbol{\beta}_k \neq \mathbf{0}$, the first condition in (8.157), and
- the transmission power constraint, i.e. $\text{Trace}(\bar{\mathbf{P}}_k \bar{\mathbf{P}}_k^H) = q$.

Considering (8.161) in the context of the first condition as above-mentioned, we have

$$\mathbf{C}_k^T \mathbf{H}_k \mathbf{U}_{\bar{k},n} \boldsymbol{\xi}_k \neq \mathbf{0}, \quad k = 1, 2, \dots, K \quad (8.162)$$

Explicitly, $\boldsymbol{\xi}_k$ is not unique, provided that it satisfies (8.162) as well as the second condition of $\text{Trace}(\bar{\mathbf{P}}_k \bar{\mathbf{P}}_k^H) = q$. Specifically, one of the solutions is

$$\boldsymbol{\xi}_k = \mathbf{U}_{\bar{k},n}^H \mathbf{H}_k^H \mathbf{C}_k \boldsymbol{\beta}_k \quad (8.163)$$

where the $(q \times q)$ diagonal matrix $\boldsymbol{\beta}_k$ is for the normalization of the transmission power associated with the k th MT, which can be obtained as follows.

Since $\mathbf{U}_{\bar{k},n}$ is orthonormal, it can be shown that we have

$$\begin{aligned} q &= \text{Trace}(\bar{\mathbf{P}}_k \bar{\mathbf{P}}_k^H) = \text{Trace}(\bar{\mathbf{P}}_k^H \bar{\mathbf{P}}_k) \\ &= \text{Trace}(\boldsymbol{\xi}_k^H \boldsymbol{\xi}_k) \end{aligned} \quad (8.164)$$

Let $\boldsymbol{\beta}_k = \beta_k \mathbf{I}_q$, i.e. when the joint power normalization is applied. Then, substituting (8.163) into (8.164), we can obtain

$$\beta_k = \sqrt{\frac{q}{\text{Trace}(\mathbf{C}_k^T \mathbf{H}_k \mathbf{U}_{\bar{k},n} \mathbf{U}_{\bar{k},n}^H \mathbf{H}_k^H \mathbf{C}_k)}}, \quad k = 1, 2, \dots, K \quad (8.165)$$

Finally, in summary, when substituting (8.163) into (8.161) and also applying (8.165), the preprocessing matrix derived based on the SVD for achieving the ZF-MUTP can be expressed as

$$\bar{\mathbf{P}} = [\bar{\mathbf{P}}_1, \bar{\mathbf{P}}_2, \dots, \bar{\mathbf{P}}_K] \quad (8.166)$$

$$\bar{\mathbf{P}}_k = \sqrt{\frac{q}{\text{Trace}(\mathbf{C}_k^T \mathbf{H}_k \mathbf{U}_{\bar{k},n} \mathbf{U}_{\bar{k},n}^H \mathbf{H}_k^H \mathbf{C}_k)}} \times (\mathbf{U}_{\bar{k},n} \mathbf{U}_{\bar{k},n}^H) \mathbf{H}_k^H \mathbf{C}_k \quad (8.167)$$

Note that in our considered MC-CDMA downlink transmission, there exists no inter-carrier interference and also no intersymbol interference within the same user. Hence, the columns of $\mathbf{H}_k^H \mathbf{C}_k$ in (8.167) are orthogonal and, therefore, no further processing is required. In case the columns of $\mathbf{H}_k^H \mathbf{C}_k$ in (8.167) are not orthogonal, which yields intersymbol interference among the symbols transmitted by the same user, we can decompose the term $\mathbf{H}_k^H \mathbf{C}_k$ using the SVD as

$$\mathbf{H}_k^H \mathbf{C}_k = [\mathbf{U}_s^{(k)} \mid \mathbf{U}_n^{(k)}] \begin{bmatrix} \Sigma_k^{1/2} & \mathbf{0} \\ \mathbf{0} & \mathbf{0} \end{bmatrix} \begin{bmatrix} (\mathbf{V}_s^{(k)})^H \\ (\mathbf{V}_n^{(k)})^H \end{bmatrix} \quad (8.168)$$

and express the preprocessing matrix as

$$\bar{\mathbf{P}}_k = \sqrt{\frac{q}{\text{Trace}([\mathbf{U}_s^{(k)}]^H \mathbf{U}_{\bar{k},n} \mathbf{U}_{\bar{k},n}^H \mathbf{U}_s^{(k)})}} \times (\mathbf{U}_{\bar{k},n} \mathbf{U}_{\bar{k},n}^H) \mathbf{U}_s^{(k)} \quad (8.169)$$

Above, we derived the preprocessing matrix $\bar{\mathbf{P}}$ for the ZF-MUTP, as shown in (8.166), with the aid of the eigen-analysis principles. As we mentioned at the beginning of this section,

the eigen-analysis principles may also be invoked to represent the preprocessing matrix of the other types of MUTP scheme. As an example, below, we show the eigen-representation of the preprocessing matrix in the MMSE-MUTP.

The preprocessing matrix of the MMSE-MUTP is given by (8.114), which is

$$\bar{\mathbf{P}} = \mathbf{H}^H \mathcal{C} (\mathcal{C}^T \mathbf{H} \mathbf{H}^H \mathcal{C} + \rho \sigma_s^2 \mathbf{I}_{Kq})^{-1} \boldsymbol{\beta} \quad (8.170)$$

Let us express $\mathbf{H}^H \mathcal{C}$ using the SVD as

$$\mathbf{H}^H \mathcal{C} = \underbrace{[\mathbf{U}_s \mid \mathbf{U}_n]}_{\mathbf{U}} \begin{bmatrix} \Sigma^{1/2} \\ \mathbf{0} \end{bmatrix} \mathbf{V}^H = \mathbf{U}_s \Sigma^{1/2} \mathbf{V}^H \quad (8.171)$$

where \mathbf{U} and \mathbf{V} are unitary matrices of size $(N_p q \times N_p q)$ and $(Kq \times Kq)$, respectively, while Σ is a diagonal matrix given by

$$\Sigma = \text{diag}\{\lambda_1, \lambda_2, \dots, \lambda_{Kq}\} \quad (8.172)$$

where $\lambda_1, \lambda_2, \dots, \lambda_{Kq}$ are the eigenvalues of $\mathbf{H}^H \mathcal{C} \mathcal{C}^T \mathbf{H}$. Furthermore, in (8.171) the columns of \mathbf{U}_s are made up of the eigenvectors corresponding to the nonzero eigenvalues of $\mathbf{H}^H \mathcal{C} \mathcal{C}^T \mathbf{H}$. \mathbf{U}_s is $(N_p q \times Kq)$ -dimensional. By contrast, the columns of \mathbf{U}_n are made up of the eigenvectors corresponding to the zero eigenvalues of $\mathbf{H}^H \mathcal{C} \mathcal{C}^T \mathbf{H}$, and \mathbf{U}_n is $(N_p q \times (N_p - K)q)$ -dimensional.

When substituting (8.171) into (8.170), we have the preprocessing matrix

$$\begin{aligned} \bar{\mathbf{P}} &= \mathbf{U} \begin{bmatrix} \Sigma^{1/2} \\ \mathbf{0} \end{bmatrix} \mathbf{V}^H \left(\mathbf{V} \begin{bmatrix} \Sigma^{1/2} & \mathbf{0}^T \end{bmatrix} \underbrace{\mathbf{U}^H \mathbf{U}}_{I_{N_p q}} \begin{bmatrix} \Sigma^{1/2} \\ \mathbf{0} \end{bmatrix} \mathbf{V}^H + \rho \sigma_s^2 \mathbf{I}_{Kq} \right)^{-1} \boldsymbol{\beta} \\ &= \mathbf{U} \begin{bmatrix} \Sigma^{1/2} \\ \mathbf{0} \end{bmatrix} \mathbf{V}^H (\mathbf{V} \Sigma \mathbf{V}^H + \rho \sigma_s^2 \mathbf{I}_{Kq})^{-1} \boldsymbol{\beta} \\ &= \mathbf{U} \begin{bmatrix} \Sigma^{1/2} \\ \mathbf{0} \end{bmatrix} \underbrace{\mathbf{V}^H \mathbf{V}}_{I_{Kq}} \Sigma_{s+n}^{-1} \mathbf{V}^H \boldsymbol{\beta} \\ &= \mathbf{U} \begin{bmatrix} \Sigma^{1/2} \\ \mathbf{0} \end{bmatrix} \Sigma_{s+n}^{-1} \mathbf{V}^H \boldsymbol{\beta} = \mathbf{U} \begin{bmatrix} \Sigma^{1/2} \Sigma_{s+n}^{-1} \\ \mathbf{0} \end{bmatrix} \mathbf{V}^H \boldsymbol{\beta} \end{aligned} \quad (8.173)$$

where

$$\Sigma_{s+n} = \Sigma + \rho \sigma_s^2 \mathbf{I}_{Kq} \quad (8.174)$$

Finally, when applying $\mathbf{U} = [\mathbf{U}_s \mid \mathbf{U}_n]$ to (8.173), an alternative representation of the preprocessing matrix seen in (8.170) for the MMSE-MUTP is given by

$$\begin{aligned} \bar{\mathbf{P}} &= \mathbf{U}_s \Sigma^{1/2} \Sigma_{s+n}^{-1} \mathbf{V}^H \boldsymbol{\beta} \\ &= \mathbf{U}_s \boldsymbol{\Lambda} \mathbf{V}^H \boldsymbol{\beta} \end{aligned} \quad (8.175)$$

where

$$\begin{aligned} \boldsymbol{\Lambda} &= \Sigma^{1/2} \Sigma_{s+n}^{-1} \\ &= \text{diag} \left\{ \frac{\sqrt{\lambda_1}}{\lambda_1 + \rho \sigma_s^2}, \frac{\sqrt{\lambda_2}}{\lambda_2 + \rho \sigma_s^2}, \dots, \frac{\sqrt{\lambda_{Kq}}}{\lambda_{Kq} + \rho \sigma_s^2} \right\} \end{aligned} \quad (8.176)$$

Furthermore, β in (8.175) can be obtained from the transmission power constraint

$$\text{Trace}(\bar{\mathbf{P}}\bar{\mathbf{P}}^H) = \text{Trace}(\bar{\mathbf{P}}^H\bar{\mathbf{P}}) = Kq \quad (8.177)$$

Specifically, for using the joint power constraint assisted normalization, we have

$$\begin{aligned} \beta &= \beta \mathbf{I}_{Kq} \\ \beta &= \sqrt{\frac{Kq}{\text{Trace}(\Lambda^2)}} = \sqrt{Kq \left(\sum_{i=1}^{Kq} \frac{\lambda_i}{[\lambda_i + \rho\sigma_s^2]^2} \right)^{-1}} \end{aligned} \quad (8.178)$$

By contrast, when the individual power constraint assisted normalization is applied, $\beta(i, i)$ is determined by the (i, i) th element of

$$\mathbf{V}\Lambda^2\mathbf{V}^H \quad (8.179)$$

and is given by

$$\beta(i, i) = \frac{\lambda_i + \rho\sigma_s^2}{\sqrt{\lambda_i}} \quad (8.180)$$

Consequently, when applying (8.178) and (8.180), respectively, into (8.175), the corresponding preprocessing matrix for using the joint power constraint assisted normalization is given by

$$\bar{\mathbf{P}} = \sqrt{Kq \left(\sum_{i=1}^{Kq} \frac{\lambda_i}{(\lambda_i + \rho\sigma_s^2)^2} \right)^{-1}} \times \mathbf{U}_s \Lambda \mathbf{V}^H \quad (8.181)$$

while the preprocessing matrix for using the individual power constraint assisted normalization is given by

$$\bar{\mathbf{P}} = \mathbf{U}_s \Lambda \mathbf{V}^H \beta \quad (8.182)$$

where β is given by

$$\beta = \text{diag} \left\{ \frac{\lambda_1 + \rho\sigma_s^2}{\sqrt{\lambda_1}}, \frac{\lambda_2 + \rho\sigma_s^2}{\sqrt{\lambda_2}}, \dots, \frac{\lambda_{Kq} + \rho\sigma_s^2}{\sqrt{\lambda_{Kq}}} \right\} \quad (8.183)$$

Note that, from (8.181) and (8.182) the eigen-representations of the preprocessing matrices in the ZF-MUTP can be readily obtained by setting $\rho = 0$ in these and their related equations. In summary, the eigen-representation of the preprocessing matrix in the ZF-MUTP using the joint power constraint assisted normalization can be expressed as

$$\bar{\mathbf{P}} = \sqrt{Kq \left(\sum_{i=1}^{Kq} \frac{1}{\lambda_i} \right)^{-1}} \times \mathbf{U}_s \tilde{\Lambda} \mathbf{V}^H \quad (8.184)$$

By contrast, when the individual power constraint assisted normalization is employed, the eigen-representations of the preprocessing matrix in the ZF-MUTP can be written as

$$\bar{\mathbf{P}} = \mathbf{U}_s \tilde{\Lambda} \mathbf{V}^H \beta \quad (8.185)$$

associated with β given by

$$\beta = \text{diag}\{\sqrt{\lambda_1}, \sqrt{\lambda_2}, \dots, \sqrt{\lambda_{Kq}}\} \quad (8.186)$$

In (8.184) and (8.185) $\tilde{\Lambda}$ is obtained from (8.176) by setting $\rho = 0$, yielding

$$\tilde{\Lambda} = \text{diag}\left\{\frac{1}{\sqrt{\lambda_1}}, \frac{1}{\sqrt{\lambda_2}}, \dots, \frac{1}{\sqrt{\lambda_{Kq}}}\right\} \quad (8.187)$$

Let us now consider the transmitter preprocessing schemes aimed at achieving the minimum BER.

8.2.10 Minimum Bit-Error Rate (MBER) Multiuser Transmitter Preprocessing

In this section the transmitter preprocessing matrix is designed so that the remote MTs are capable of achieving the minimum bit-error rate (MBER), given the constraint on the total transmission power. The transmitter preprocessing under the MBER criterion has been investigated, e.g., in references [231, 232]. The contents in this section represent the extension of the work in references [231, 232] to the transmitter preprocessing in the considered MC-CDMA.

For the sake of simplifying our discussion, given the MIMO equation of (8.46), i.e.

$$\mathbf{y} = \mathcal{C}^T \mathbf{H} \bar{\mathbf{P}} \mathbf{x} + \mathbf{n} \quad (8.188)$$

for the MC-CDMA using F-domain spreading, let us define

$$\tilde{\mathbf{H}} = \mathbf{H}^T \mathcal{C} = [\tilde{\mathbf{h}}_1, \tilde{\mathbf{h}}_2, \dots, \tilde{\mathbf{h}}_{Kq}] \quad (8.189)$$

which is a $(N_p q \times Kq)$ matrix. Then, (8.188) can be expressed as

$$\mathbf{y} = \tilde{\mathbf{H}}^T \bar{\mathbf{P}} \mathbf{x} + \mathbf{n} \quad (8.190)$$

Furthermore, let $\mathcal{K} = Kq$, $\mathcal{N} = N_p q$ in the above equation. Then, the dimensions of the arguments in (8.190) are \mathbf{y} , \mathbf{x} , \mathbf{n} : $(\mathcal{K} \times 1)$; $\tilde{\mathbf{H}}$ and $\bar{\mathbf{P}}$: $(\mathcal{N} \times \mathcal{K})$.

For simplicity, we assume that the entries of \mathbf{x} are taken from a BPSK constellation, where x_k , $k = 1, \dots, \mathcal{K}$ are independent of each other and take a value of $+1$ or -1 with equal probability. Furthermore, it is assumed that $\mathcal{N} \geq \mathcal{K}$.

From (8.190), we know that the decision variable for the i th bit is given by

$$\begin{aligned} y_i &= \tilde{\mathbf{h}}_i^T \bar{\mathbf{P}} \mathbf{x} + n_i \\ &= \sum_{k=1}^{\mathcal{K}} \tilde{\mathbf{h}}_i^T \bar{\mathbf{p}}_k x_k + n_i, \quad i = 1, 2, \dots, \mathcal{K} \end{aligned} \quad (8.191)$$

where n_i is complex Gaussian distributed with zero mean and a variance of σ_s^2 , and $\bar{\mathbf{p}}_k$ is for preprocessing of x_k . It can be seen that the decision variable y_i is complex Gaussian with its mean given by $\tilde{\mathbf{h}}_i^T \bar{\mathbf{P}} \mathbf{x}$ and a variance of σ_s^2 . Hence, when BPSK baseband modulation is

considered, for a given realization \mathbf{x}_i of \mathbf{x} with its i th entry $x_i = +1$, which is expressed as \mathbf{x}_i^+ , it can be shown that the BER can be expressed as [2]

$$\begin{aligned} \text{BER}_i &= P(\Re\{y_i\} < 0) \\ &= P(\Re\{\bar{\mathbf{h}}_i^T \bar{\mathbf{P}} \mathbf{x}_i^+ + n_i\} < 0) \\ &= P(\Re\{-n_i\} > \Re\{\bar{\mathbf{h}}_i^T \bar{\mathbf{P}} \mathbf{x}_i^+\}) \\ &= Q\left(\frac{\sqrt{2}\Re\{\bar{\mathbf{h}}_i^T \bar{\mathbf{P}} \mathbf{x}_i^+\}}{\sigma_s}\right) \end{aligned} \quad (8.192)$$

where $\Re\{\cdot\}$ represents the real part of the argument, while $Q(x)$ is the Gaussian Q -function.

Since, except for $x_i = +1$, the other components in \mathbf{x}_i^+ are binary random variables, the average BER of x_i can be expressed as

$$\overline{\text{BER}}_i = \frac{1}{2^{K-1}} \sum_{k=1}^{2^{K-1}} Q\left(\frac{\sqrt{2}\Re\{\bar{\mathbf{h}}_i^T \bar{\mathbf{P}} \mathbf{x}_i^+\}}{\sigma_s}\right) \quad (8.193)$$

The overall average BER can be expressed as

$$\overline{\text{BER}} = \frac{1}{K} \sum_{i=1}^K \frac{1}{2^{K-1}} \sum_{k=1}^{2^{K-1}} Q\left(\frac{\sqrt{2}\Re\{\bar{\mathbf{h}}_i^T \bar{\mathbf{P}} \mathbf{x}_i^+\}}{\sigma_s}\right) \quad (8.194)$$

Therefore, the optimization problem for the MBER-MUTP can be formed as

$$\tilde{\mathbf{P}}_{\text{MBER}} = \arg \min_{\tilde{\mathbf{P}}} \overline{\text{BER}} \quad \text{subject to} \quad \text{Trace}(\tilde{\mathbf{P}} \tilde{\mathbf{P}}^H) = K \quad (8.195)$$

Note that, since $\partial^2 Q(x)/\partial^2 x > 0$ only when $x > 0$, then $x > 0$ should be satisfied, so that the function $Q(x)$ is a convex function. Therefore, the optimum preprocessing matrix $\tilde{\mathbf{P}}_{\text{MBER}}$ lies in the area, resulting in $\Re\{\bar{\mathbf{h}}_i^T \bar{\mathbf{P}} \mathbf{x}_i^+\} \geq 0$ for any given i and k .

Using (8.191), the term $\bar{\mathbf{h}}_i^T \bar{\mathbf{P}} \mathbf{x}_i^+$ in (8.194) can be written as

$$\begin{aligned} \bar{\mathbf{h}}_i^T \bar{\mathbf{P}} \mathbf{x}_i^+ &= \bar{\mathbf{h}}_i^T \bar{\mathbf{p}}_i (x_i = +1) + \sum_{k \neq i}^K \bar{\mathbf{h}}_i^T \bar{\mathbf{p}}_k x_k \\ &= (\mathbf{x}_i^+)^T (\mathbf{I}_K \otimes \bar{\mathbf{h}}_i^T) \text{vec}(\bar{\mathbf{P}}) \end{aligned} \quad (8.196)$$

where the operator $\text{vec}(\cdot)$ stacks the columns of the argument matrix to form a long column vector. Specifically, $\text{vec}(\bar{\mathbf{P}})$ is a NK -length column vector. In (8.196) let us define

$$\mathbf{V}_i = \mathbf{I}_K \otimes \bar{\mathbf{h}}_i \quad (8.197)$$

which is a $(NK \times K)$ matrix. Alternatively, (8.194) can be modified to

$$\overline{\text{BER}} = \frac{1}{K} \sum_{i=1}^K \frac{1}{2^{K-1}} \sum_{k=1}^{2^{K-1}} Q\left(\frac{\sqrt{2}\Re\{(\mathbf{x}_i^+)^T \mathbf{V}_i^T \text{vec}(\bar{\mathbf{P}})\}}{\sigma_s}\right) \quad (8.198)$$

The above expression is similar as the corresponding equations derived in references [170, 171, 232].

According to the above analysis, the unconstraint objective function to be minimized can be expressed as

$$J = \overline{\text{BER}} + \lambda(\|\text{vec}(\bar{\mathbf{P}})\|^2 - \mathcal{K}) \quad (8.199)$$

Taking the derivative of J with respect to $\text{vec}(\bar{\mathbf{P}}^*)$ and setting the result to equal a $(\mathcal{N}\mathcal{K} \times 1)$ zero matrix, we obtain

$$\begin{aligned} \frac{\partial J}{\partial \text{vec}(\bar{\mathbf{P}}^*)} &= \frac{-1}{\sqrt{\pi}\mathcal{K}2^{\mathcal{K}-1}} \sum_{i=1}^{\mathcal{K}} \sum_{k=1}^{2^{\mathcal{K}-1}} \exp(-\Re^2\{(\mathbf{x}_i^+)^T \mathbf{V}_i^T \text{vec}(\bar{\mathbf{P}})\}) \\ &\quad \times \frac{\partial}{\partial \text{vec}(\bar{\mathbf{P}}^*)} \Re\{(\mathbf{x}_i^+)^T \mathbf{V}_i^T \text{vec}(\bar{\mathbf{P}})\} + \lambda \text{vec}(\bar{\mathbf{P}}) = \mathbf{0} \end{aligned} \quad (8.200)$$

Using the expression

$$\Re\{(\mathbf{x}_i^+)^T \mathbf{V}_i^T \text{vec}(\bar{\mathbf{P}})\} = \frac{1}{2}[(\mathbf{x}_i^+)^T \mathbf{V}_i^T \text{vec}(\bar{\mathbf{P}}) + \text{vec}(\bar{\mathbf{P}})^H \mathbf{V}_i^* (\mathbf{x}_i^+)] \quad (8.201)$$

we have in (8.200)

$$\frac{\partial}{\partial \text{vec}(\bar{\mathbf{P}}^*)} \Re\{(\mathbf{x}_i^+)^T \mathbf{V}_i^T \text{vec}(\bar{\mathbf{P}})\} = \frac{1}{2} \mathbf{V}_i^* (\mathbf{x}_i^+) \quad (8.202)$$

Hence, (8.200) can be expressed as

$$\begin{aligned} \frac{\partial J}{\partial \text{vec}(\bar{\mathbf{P}}^*)} &= \frac{-1}{2\sqrt{\pi}\mathcal{K}2^{\mathcal{K}-1}} \sum_{i=1}^{\mathcal{K}} \sum_{k=1}^{2^{\mathcal{K}-1}} \exp(-\Re^2\{(\mathbf{x}_i^+)^T \mathbf{V}_i^T \text{vec}(\bar{\mathbf{P}})\}) \mathbf{V}_i^* (\mathbf{x}_i^+) \\ &\quad + \lambda \text{vec}(\bar{\mathbf{P}}) = \mathbf{0} \end{aligned} \quad (8.203)$$

which gives

$$\text{vec}(\bar{\mathbf{P}}) = \frac{1}{2\lambda\sqrt{\pi}\mathcal{K}2^{\mathcal{K}-1}} \sum_{i=1}^{\mathcal{K}} \sum_{k=1}^{2^{\mathcal{K}-1}} \exp(-\Re^2\{(\mathbf{x}_i^+)^T \mathbf{V}_i^T \text{vec}(\bar{\mathbf{P}})\}) \mathbf{V}_i^* (\mathbf{x}_i^+) \quad (8.204)$$

Furthermore, using the power constraint in (8.195), we can obtain the Lagrange multiplier λ , which can be expressed as

$$\lambda = \frac{1}{2\sqrt{\pi}\mathcal{K}2^{\mathcal{K}-1}} \left\| \sum_{i=1}^{\mathcal{K}} \sum_{k=1}^{2^{\mathcal{K}-1}} \exp(-\Re^2\{(\mathbf{x}_i^+)^T \mathbf{V}_i^T \text{vec}(\bar{\mathbf{P}})\}) \mathbf{V}_i^* (\mathbf{x}_i^+) \right\| \quad (8.205)$$

Explicitly, it is extremely difficult to derive a closed form for the preprocessing matrix $\bar{\mathbf{P}}$. As indicated in reference [232], the optimum solution to the preprocessing matrix lies in the set ξ , which can be expressed as

$$\xi = \left\{ \sum_{i=1}^{\mathcal{K}} \sum_{k=1}^{2^{\mathcal{K}-1}} a_{k,i} \mathbf{V}_i^* (\mathbf{x}_i^+) \mid a_{k,i} > 0 \right\} \quad (8.206)$$

Alternatively, a numerical optimization solution may be obtained through the steepest-descent gradient approach [171, 232]. According to the steepest descent method, the preprocessing vectors are updated as

$$\text{vec}(\bar{\mathbf{P}})(n+1) = \text{vec}(\bar{\mathbf{P}})(n) + \mu \frac{\partial J}{\partial \text{vec}(\bar{\mathbf{P}}^*)}, \quad n = 1, 2, \dots \quad (8.207)$$

where

$$\begin{aligned} \frac{\partial J}{\partial \text{vec}(\bar{\mathbf{P}}^*)} &= \frac{-1}{2\sqrt{\pi}\mathcal{K}2^{\mathcal{K}-1}} \sum_{i=1}^{\mathcal{K}} \sum_{k=1}^{2^{\mathcal{K}-1}} \exp(-\Re^2\{(\mathbf{x}_i^+)^T \mathbf{V}_i^T \text{vec}(\bar{\mathbf{P}})\}) \mathbf{V}_i^*(\mathbf{x}_i^+) \\ &\quad + \lambda \times \text{vec}(\bar{\mathbf{P}}) \end{aligned} \quad (8.208)$$

and λ is obtained using (8.205). Note that at the start of the iteration, other optimum preprocessing matrices for $\bar{\mathbf{P}}$, such as the ZF solution, obtained in the previous sections may be used as the initial preprocessing matrix to search for the MBER solution.

Above, we considered the MBER-MUTP in the general context without stressing constraint on the preprocessing matrix $\bar{\mathbf{P}}$. It has been shown that in this case there is no closed-form solution to the MBER-MUTP. Below, we consider the MBER-MUTP given that the preprocessing matrix $\bar{\mathbf{P}}$ is also a ZF solution. It can be shown that under this constraint a closed-form solution to $\bar{\mathbf{P}}$ can be obtained, when the SNR value is sufficiently high.

According to Section 8.2.4, when the preprocessing matrix $\bar{\mathbf{P}}$ is a ZF solution, then, for the signal form of (8.190), $\bar{\mathbf{P}}$ can be expressed as

$$\begin{aligned} \bar{\mathbf{P}} &= (\bar{\mathbf{H}}^T)^\dagger \boldsymbol{\beta} \\ &= \bar{\mathbf{H}}^* (\bar{\mathbf{H}}^T \bar{\mathbf{H}}^*)^{-1} \boldsymbol{\beta} \end{aligned} \quad (8.209)$$

Substituting the above equation into (8.190), the decision variable vector for the MTs can be expressed as

$$\mathbf{y} = \boldsymbol{\beta} \mathbf{x} + \mathbf{n} \quad (8.210)$$

where the diagonal matrix $\boldsymbol{\beta}$ is to achieve constraint on the transmission power. According to the transmission power constraint of

$$\text{Trace}(\bar{\mathbf{P}} \bar{\mathbf{P}}^H) = \mathcal{K} \quad (8.211)$$

it can be easily shown that

$$\text{Trace}(\boldsymbol{\beta}^2 (\bar{\mathbf{H}}^T \bar{\mathbf{H}}^*)^{-1}) = \mathcal{K} \quad (8.212)$$

Carrying out the LDL-decomposition on $\bar{\mathbf{H}}^T \bar{\mathbf{H}}^*$, i.e. letting $\bar{\mathbf{H}}^T \bar{\mathbf{H}}^* = \mathbf{L} \mathbf{D} \mathbf{L}^H$, where \mathbf{L} is a lower triangular matrix with unity diagonal entries, while $\mathbf{D} = \text{diag}\{d_1, d_2, \dots, d_{\mathcal{K}}\}$ is a diagonal matrix, then, (8.212) can be written as

$$\text{Trace}(\boldsymbol{\beta}^2 \mathbf{D}^{-1}) = \mathcal{K} \quad (8.213)$$

Let $\boldsymbol{\beta} = \text{diag}\{\beta_1, \beta_2, \dots, \beta_{\mathcal{K}}\}$. Then the above equation can be expressed as

$$\sum_{i=1}^{\mathcal{K}} \frac{\beta_i^2}{d_i} = \mathcal{K} \quad (8.214)$$

According to (8.210), it can be shown that the decision variable for x_i is

$$y_i = \beta_i x_i + n_i, \quad i = 1, 2, \dots, \mathcal{K} \quad (8.215)$$

Correspondingly, when BPSK baseband modulation is assumed, the BER of x_i can be expressed as

$$\text{BER}_i = Q\left(\sqrt{\frac{2\beta_i^2}{\sigma_s^2}}\right) \quad (8.216)$$

and the average BER over all the received \mathcal{K} bits can be expressed as

$$\overline{\text{BER}} = \frac{1}{\mathcal{K}} \sum_{i=1}^{\mathcal{K}} Q\left(\sqrt{\frac{2\beta_i^2}{\sigma_s^2}}\right) \quad (8.217)$$

Consequently, the constraint optimization problem to be solved can be stated as

$$\boldsymbol{\beta} = \arg \min_{\boldsymbol{\beta}} \overline{\text{BER}} \quad \text{subject to} \quad \sum_{i=1}^{\mathcal{K}} \frac{\beta_i^2}{d_i} = \mathcal{K} \quad (8.218)$$

Explicitly, the above optimization tries to assign an appropriate amount of power to transmit each of $\{x_i\}$, so that the minimum average BER is achieved.

Alternatively, the unconstraint objective function to be minimized can be expressed as

$$J = \overline{\text{BER}} + \lambda \left(\sum_{i=1}^{\mathcal{K}} \frac{\beta_i^2}{d_i} - \mathcal{K} \right) \quad (8.219)$$

Since $\beta_i > 0$, we know that $\overline{\text{BER}}$ in (8.217) is a convex function. Therefore, the minimum of J exists. Taking the derivative of J with respect to β_i for $i = 1, 2, \dots, \mathcal{K}$, setting the result equal to zero, and considering the power constraint of (8.214), we obtain a set of equations

$$\begin{aligned} -\frac{1}{\sqrt{\pi} \mathcal{K} \sigma_s} \exp\left(-\frac{\beta_1^2}{\sigma_s^2}\right) + \frac{2\lambda\beta_1}{d_1} &= 0 \\ -\frac{1}{\sqrt{\pi} \mathcal{K} \sigma_s} \exp\left(-\frac{\beta_2^2}{\sigma_s^2}\right) + \frac{2\lambda\beta_2}{d_2} &= 0 \\ &\dots \\ -\frac{1}{\sqrt{\pi} \mathcal{K} \sigma_s} \exp\left(-\frac{\beta_{\mathcal{K}}^2}{\sigma_s^2}\right) + \frac{2\lambda\beta_{\mathcal{K}}}{d_{\mathcal{K}}} &= 0 \\ \sum_{i=1}^{\mathcal{K}} \frac{\beta_i^2}{d_i} &= \mathcal{K} \end{aligned} \quad (8.220)$$

Therefore, the $(\mathcal{K} + 1)$ variables can be solved with the aid of the above $(\mathcal{K} + 1)$ equations. However, there are still no closed-form solutions to β_2 . Instead, these equations may be solved by numerical approaches.

When the SNR with respect to each of the transmitted bits, i.e. when β_i^2/σ_s^2 for $i = 1, 2, \dots, \mathcal{K}$, is sufficiently high, the approximation of $\exp(-\beta_i^2/\sigma_s^2) \approx 1 - \beta_i^2/\sigma_s^2$ may be invoked, which, after some arrangement, yields

$$\beta_i^2 + \frac{2\sqrt{\pi}\mathcal{K}\sigma_s^3\lambda\beta_i}{d_i} - \sigma_s^2 = 0, \quad i = 1, 2, \dots, \mathcal{K} \quad (8.221)$$

Solving this equation gives

$$\beta_i = -\frac{\sqrt{\pi}\mathcal{K}\sigma_s^3\lambda}{d_i} + \frac{\sigma_s}{d_i}\sqrt{\pi\mathcal{K}^2\sigma_s^4\lambda^2 + d_i^2}, \quad i = 1, 2, \dots, \mathcal{K} \quad (8.222)$$

where λ can be found numerically with the aid of (8.214).

Note that another strategy for optimally assigning power to the corresponding transmitted bits so as to achieve the minimum BER can be found by first applying Jensen's inequality [233] to the average BER of (8.217). Readers interested in the scheme can see reference [231] for details.

8.2.11 Maximum Mutual Information (MMI) Multiuser Transmitter Preprocessing

In this section the transmitter preprocessing matrix is designed to achieve the maximum information rate. Two scenarios are considered. For the first scenario, the overall information rate of the MC-CDMA system is maximized, regardless of the information rate transmitted to each of the individual MTs. For clarity, we refer to this scheme as the joint MMI-MUTP. By contrast, the second scenario maximizes the information rate of each individual MT when there is no MUI among the downlink users. Hence, this preprocessing scheme is referred to as the ZF/MMI-MUTP for convenience.

In the context of the joint MMI-MUTP, given the transmission MIMO equation

$$\mathbf{y} = \mathbf{C}^T \mathbf{H} \bar{\mathbf{P}} \mathbf{x} + \mathbf{n} \quad (8.223)$$

of the MC-CDMA system, the mutual information can be expressed as [234]

$$\mathcal{I}(\mathbf{y}, \mathbf{x}) = \log_2[\det(\mathbf{I}_{Kq} + \mathbf{C}^T \mathbf{H} \bar{\mathbf{Q}} \bar{\mathbf{P}}^H \mathbf{H}^H \mathbf{C})] \text{ bits/transmission} \quad (8.224)$$

where $\bar{\mathbf{Q}}_{\bar{\mathbf{P}}} = \bar{\mathbf{P}} \bar{\mathbf{P}}^H$. Note that the mutual information of (8.224) is achieved, when the elements of \mathbf{x} are i.i.d. Gaussian variables with unity variance.

Therefore, for the joint MMI-MUTP, the preprocessing matrix $\bar{\mathbf{P}}$ is chosen according to the optimization problem

$$\bar{\mathbf{P}}_{\text{JMMI}} = \arg \max_{\bar{\mathbf{P}}: \text{Trace}(\bar{\mathbf{P}} \bar{\mathbf{P}}^H) \leq Kq} \{\mathcal{I}(\mathbf{y}, \mathbf{x}) = \log_2[\det(\mathbf{I}_{Kq} + \mathbf{C}^T \mathbf{H} \bar{\mathbf{Q}} \bar{\mathbf{P}}^H \mathbf{H}^H \mathbf{C})]\} \quad (8.225)$$

When invoking the relationship of $\det(\mathbf{I} + \mathbf{AB}) = \det(\mathbf{I} + \mathbf{BA})$ [156], the above optimization problem can be expressed as

$$\bar{\mathbf{P}}_{\text{JMMI}} = \arg \max_{\bar{\mathbf{P}}: \text{Trace}(\bar{\mathbf{P}} \bar{\mathbf{P}}^H) \leq Kq} \{\mathcal{I}(\mathbf{y}, \mathbf{x}) = \log_2[\det(\mathbf{I}_{N_p q} + \bar{\mathbf{Q}} \bar{\mathbf{P}}^H \mathbf{C} \mathbf{C}^T \mathbf{H})]\} \quad (8.226)$$

Let the SVD on $\mathbf{H}^H \mathcal{C}$ be expressed as

$$\mathbf{H}^H \mathcal{C} = \underbrace{[\mathbf{U}_s \mid \mathbf{U}_n]}_U \begin{bmatrix} \boldsymbol{\Sigma}^{1/2} \\ \mathbf{0} \end{bmatrix} \mathbf{V}^H = \mathbf{U}_s \boldsymbol{\Sigma}^{1/2} \mathbf{V}^H \quad (8.227)$$

where \mathbf{U} and \mathbf{V} are unitary matrices of size $(N_p q \times N_p q)$ and $(Kq \times Kq)$, respectively, while $\boldsymbol{\Sigma}$ is a diagonal matrix given by

$$\boldsymbol{\Sigma} = \text{diag}\{\lambda_1, \lambda_2, \dots, \lambda_{Kq}\} \quad (8.228)$$

where $\lambda_1, \lambda_2, \dots, \lambda_{Kq}$ are the nonzero eigenvalues of $\mathbf{H}^H \mathcal{C} \mathcal{C}^T \mathbf{H}$. Furthermore, in (8.227) the columns of the $(N_p q \times Kq)$ matrix \mathbf{U}_s are made up of the eigenvectors corresponding to the nonzero eigenvalues of $\mathbf{H}^H \mathcal{C} \mathcal{C}^T \mathbf{H}$. By contrast, the columns of the $(N_p q \times (N_p - K)q)$ matrix \mathbf{U}_n are made up of the eigenvectors corresponding to the zero eigenvalues of $\mathbf{H}^H \mathcal{C} \mathcal{C}^T \mathbf{H}$. After substituting (8.227) into (8.226), we obtain

$$\mathcal{I}(\mathbf{y}, \mathbf{x}) = \log_2[\det(\mathbf{I}_{N_p q} + \mathbf{Q}_{\bar{P}} \mathbf{U}_s \boldsymbol{\Sigma} \mathbf{U}_s^H)] \quad (8.229)$$

Reapplying the relationship of $\det(\mathbf{I} + \mathbf{AB}) = \det(\mathbf{I} + \mathbf{BA})$, the above equation can be written as

$$\mathcal{I}(\mathbf{y}, \mathbf{x}) = \log_2[\det(\mathbf{I}_{Kq} + \boldsymbol{\Sigma}^{1/2} \mathbf{U}_s^H \mathbf{Q}_{\bar{P}} \mathbf{U}_s \boldsymbol{\Sigma}^{1/2})] \quad (8.230)$$

In (8.230), since $\mathbf{Q}_{\bar{P}} = \bar{P} \bar{P}^H$ is non-negative definite, hence $\tilde{\mathbf{Q}}_{\bar{P}} = \mathbf{U}_s^H \mathbf{Q}_{\bar{P}} \mathbf{U}_s$ is also non-negative definite. Furthermore, we have $\text{Trace}(\tilde{\mathbf{Q}}_{\bar{P}}) = \text{Trace}(\mathbf{Q}_{\bar{P}})$, since \mathbf{U}_s is a unitary matrix. Therefore, the maximization over $\mathbf{Q}_{\bar{P}}$ is equivalent to the maximization over $\tilde{\mathbf{Q}}_{\bar{P}}$. Consequently, with the aid of Hadamard's inequality [156], which states that when \mathbf{A} is a $(M \times M)$ non-negative definite square matrix, then

$$\det(\mathbf{A}) \leq \prod_{m=1}^M a_{mm}$$

with equality when \mathbf{A} is diagonal, we have

$$\begin{aligned} \mathcal{I}(\mathbf{y}, \mathbf{x}) &\leq \log_2 \left[\prod_{i=1}^{Kq} (1 + \lambda_i \tilde{\mathbf{Q}}_{\bar{P}}(i, i)) \right] \\ &= \sum_{i=1}^{Kq} \log_2(1 + \lambda_i \tilde{\mathbf{Q}}_{\bar{P}}(i, i)) \end{aligned} \quad (8.231)$$

where $\tilde{\mathbf{Q}}_{\bar{P}}(i, i)$ is the (i, i) th element of $\tilde{\mathbf{Q}}_{\bar{P}}$, and the equality is achieved when $\tilde{\mathbf{Q}}_{\bar{P}}$ is diagonal. Therefore, the maximum mutual information is given by

$$\mathcal{I}_{\max}(\mathbf{y}, \mathbf{x}) = \sum_{i=1}^{Kq} \log_2[1 + \lambda_i \tilde{\mathbf{Q}}_{\bar{P}}(i, i)] \quad (8.232)$$

which is achieved when $\tilde{\mathbf{Q}}_{\bar{P}} = \mathbf{U}_s^H \mathbf{Q}_{\bar{P}} \mathbf{U}_s$ is a diagonal matrix. Explicitly, the condition for $\tilde{\mathbf{Q}}_{\bar{P}}$ to be a diagonal matrix is satisfied, when we set the preprocessing matrix as

$$\bar{\mathbf{P}}_{\text{JMMI}} = \mathbf{U}_s \boldsymbol{\beta}^{1/2} \quad (8.233)$$

where $\boldsymbol{\beta} = \text{diag}\{\beta_1, \dots, \beta_{Kq}\}$. Substituting (8.233) into (8.232) finally gives

$$\mathcal{I}_{\max}(\mathbf{y}, \mathbf{x}) = \sum_{i=1}^{Kq} \log_2(1 + \lambda_i \beta_i) \quad (8.234)$$

In (8.234) β_i for $i = 1, 2, \dots, Kq$ can be found via the ‘water-filling’ principles [233, pp. 250–233], under the constraint

$$\text{Trace}(\bar{\mathbf{P}} \bar{\mathbf{P}}^H) = \text{Trace}(\mathbf{U}_s \boldsymbol{\beta}^{1/2} \boldsymbol{\beta}^{1/2} \mathbf{U}_s^H) = \sum_{i=1}^{Kq} \beta_i \leq Kq \quad (8.235)$$

Specifically, according to the ‘water-filling’ principles, β_i is given by

$$\beta_i = \left(v - \frac{1}{\lambda_i} \right)^+, \quad i = 1, 2, \dots, Kq \quad (8.236)$$

where $(x)^+$ is defined as

$$(x)^+ = \begin{cases} x & \text{if } x > 0 \\ 0 & \text{if } x \leq 0 \end{cases} \quad (8.237)$$

and v is chosen such that

$$\sum_{i=1}^{Kq} \beta_i = \sum_{i=1}^{Kq} \left(v - \frac{1}{\lambda_i} \right)^+ \leq Kq \quad (8.238)$$

Finally, when applying (8.236) to (8.234), we obtain the maximum mutual information, which is given by

$$\mathcal{I}_{\max}(\mathbf{y}, \mathbf{x}) = \sum_{i=1}^{Kq} \log_2(v\lambda_i)^+ \quad (8.239)$$

Note that when Gaussian noise is invoked, the channel capacity of the MC-CDMA downlink using the joint MMI-MUTP can be expressed as [233]

$$\mathcal{I}_{\max}(\mathbf{y}, \mathbf{x}) = \sum_{i=1}^{Kq} \log_2 \left[\frac{(v\lambda_i)^+}{\sigma_s^2} \right] \text{ (bits/transmission)} \quad (8.240)$$

Furthermore, since the multicarrier channels are time variant, the channel capacity of (8.240) is hence time variant and depends on instantaneous channel realizations. Therefore, we may evaluate the ergodic channel capacity of the MC-CDMA [234] by taking the average of (8.240), yielding

$$\tilde{\mathcal{I}}_{\max}(\mathbf{y}, \mathbf{x}) = E[\mathcal{I}_{\max}(\mathbf{y}, \mathbf{x})] \quad (8.241)$$

From the above analysis, we observe that the joint MMI-MUTP converts the transmission multicarrier channels into Kq parallel subchannels that are orthogonal with each other. According to (8.236), in the joint MMI-MUTP the transmitter allocates more power to the subchannels having relatively higher eigenvalues.

The capacity (8.241) represents the upper-bound information rate of the MC-CDMA system, which can only be achievable when the K downlink MTs employ ideal knowledge

about the downlink channels and when they also cooperate with each other, in addition to the channels' knowledge known to the BS transmitter for carrying out the MMI-MUTP. Below, we consider the ZF/MMI-MUTP, where the information rate in the context of each of the downlink MTs is maximized, when there is no MUI among the MTs. The capacity of the MC-CDMA using ZF/MMI-MUTP can be achievable without requiring cooperation from the downlink MTs. Furthermore, if $q = 1$, then the capacity can be achieved even if a MT does not know its channels. Otherwise, if $q > 1$, a MT must then have knowledge about its channels in order to achieve the capacity of the MC-CDMA using ZF/MMI-MUTP.

Since the ZF/MMI-MUTP maximizes the information rate of each of the downlink MTs, conditional on there being no multiuser interference among the MTs, our analysis can start with the ZF-MUTP. In this case, according to (8.169) in Section 8.2.9, the preprocessing matrix for the k th MT can be expressed as

$$\bar{\mathbf{P}}_k = (\mathbf{U}_{\bar{k},n} \mathbf{U}_{\bar{k},n}^H) \mathbf{U}_s^{(k)} \boldsymbol{\beta}_k^{1/2}, \quad k = 1, 2, \dots, K \quad (8.242)$$

where we used $\boldsymbol{\beta}_k = \text{diag}\{\beta_{k1}, \beta_{k2}, \dots, \beta_{kq}\}$. Correspondingly, the decision vector for the k th MT can be expressed as

$$\mathbf{y}_k = \mathbf{C}_k^T \mathbf{H}_k (\mathbf{U}_{\bar{k},n} \mathbf{U}_{\bar{k},n}^H) \mathbf{U}_s^{(k)} \boldsymbol{\beta}_k^{1/2} \mathbf{x}_k + \mathbf{n}_k, \quad k = 1, 2, \dots, K \quad (8.243)$$

Consequently, the optimization problem for achieving the maximum mutual information can be formulated as

$$\begin{aligned} \bar{\mathbf{P}}_{\text{ZMMI},k} = \arg \max_{\bar{\mathbf{P}}_k : \text{Trace}(\bar{\mathbf{P}}_k \bar{\mathbf{P}}_k^H) \leq q} \{ & \mathcal{I}(\mathbf{y}_k, \mathbf{x}_k) = \log_2 [\det(\mathbf{I}_q + (\mathbf{C}_k^T \mathbf{H}_k (\mathbf{U}_{\bar{k},n} \mathbf{U}_{\bar{k},n}^H) \mathbf{U}_s^{(k)}) \\ & \times \boldsymbol{\beta}_k (\mathbf{C}_k^T \mathbf{H}_k (\mathbf{U}_{\bar{k},n} \mathbf{U}_{\bar{k},n}^H) \mathbf{U}_s^{(k)})^H)] \} \end{aligned} \quad (8.244)$$

On invoking the SVD to express

$$(\mathbf{C}_k^T \mathbf{H}_k (\mathbf{U}_{\bar{k},n} \mathbf{U}_{\bar{k},n}^H) \mathbf{U}_s^{(k)})^H (\mathbf{C}_k^T \mathbf{H}_k (\mathbf{U}_{\bar{k},n} \mathbf{U}_{\bar{k},n}^H) \mathbf{U}_s^{(k)}) = \bar{\mathbf{U}}_s^{(k)} \boldsymbol{\Sigma}_k (\bar{\mathbf{U}}_s^{(k)})^H \quad (8.245)$$

where $\boldsymbol{\Sigma}_k = \text{diag}\{\lambda_{k1}, \lambda_{k2}, \dots, \lambda_{kq}\}$, we can modify the problem of (8.244) to

$$\begin{aligned} \mathcal{I}(\mathbf{y}_k, \mathbf{x}_k) &= \log_2 [\det(\mathbf{I}_q + \boldsymbol{\beta}_k \boldsymbol{\Sigma}_k)] \\ &= \log_2 \left[\prod_{i=1}^q (1 + \beta_{ki} \lambda_{ki}) \right] \\ &= \sum_{i=1}^q \log_2 [1 + \beta_{ki} \lambda_{ki}] \end{aligned} \quad (8.246)$$

With the aid of (8.242), the constraint in the above equation can be expressed as

$$\begin{aligned} \text{Trace}(\bar{\mathbf{P}}_k \bar{\mathbf{P}}_k^H) &= \text{Trace}(\mathbf{U}_{\bar{k},n}^H \mathbf{U}_s^{(k)} \boldsymbol{\beta}_k (\mathbf{U}_s^{(k)})^H \mathbf{U}_{\bar{k},n}) \leq q \\ \text{or } \text{Trace}((\mathbf{U}_s^{(k)})^H \mathbf{U}_{\bar{k},n} \mathbf{U}_{\bar{k},n}^H \mathbf{U}_s^{(k)} \boldsymbol{\beta}_k) &\leq q, \quad k = 1, 2, \dots, K \end{aligned} \quad (8.247)$$

Let us express

$$\boldsymbol{\alpha}^{(k)} = (\mathbf{U}_s^{(k)})^H \mathbf{U}_{\bar{k},n} \mathbf{U}_{\bar{k},n}^H \mathbf{U}_s^{(k)} \quad (8.248)$$

then the constraint on the transmission power can be formulated as

$$\sum_{i=1}^q \alpha_{ii}^{(k)} \beta_{ki} \leq q, \quad k = 1, 2, \dots, K \quad (8.249)$$

where $\alpha_{ii}^{(k)}$ is the (i, i) th element of $\boldsymbol{\alpha}^{(k)}$. Consequently, the cost function for obtaining the maximal mutual information can be formed as

$$J = \sum_{i=1}^q \log_2[1 + \beta_{ki} \lambda_{ki}] - \mu_k \left(\sum_{i=1}^q \alpha_{ii}^{(k)} \beta_{ki} - q \right) \quad (8.250)$$

Taking the derivative of J with respect to β_{ki} and setting the derivative result equal to zero, we obtain

$$\beta_{ki} = \frac{1}{\mu_k \alpha_{ii}^{(k)} \ln 2} - \frac{1}{\lambda_{ki}}, \quad i = 1, 2, \dots, q \quad (8.251)$$

where μ_k can be found by substituting (8.251) into (8.249), which yields

$$v_k = \frac{1}{\mu_k} = \frac{q + \sum_{i=1}^q 1/\lambda_{ki}}{\sum_{i=1}^q 1/(\alpha_{ii}^{(k)} \ln 2)} \quad (8.252)$$

However, the above optimization may result in negative values for some β_{ki} 's. In this case, β_{ki} for $i = 1, 2, \dots, q$ can be found via ‘water-filling’ and β_{ki} can be chosen according to

$$\beta_{ki} = \left(\frac{v_k}{\alpha_{ii}^{(k)} \ln 2} - \frac{1}{\lambda_{ki}} \right)^+ \quad (8.253)$$

After absorbing $\ln 2$ into v_k , (8.253) can be equivalently expressed as

$$\beta_{ki} = \left(\frac{v_k}{\alpha_{ii}^{(k)}} - \frac{1}{\lambda_{ki}} \right)^+, \quad i = 1, 2, \dots, q \quad (8.254)$$

where v_k is chosen so that

$$\begin{aligned} \sum_{i=1}^q \alpha_{ii}^{(k)} \left(\frac{v_k}{\alpha_{ii}^{(k)}} - \frac{1}{\lambda_{ki}} \right)^+ &\leq q \\ \text{or } \sum_{i=1}^q \left(v_k - \frac{\alpha_{ii}^{(k)}}{\lambda_{ki}} \right)^+ &\leq q \end{aligned} \quad (8.255)$$

Finally, when applying (8.254) into (8.246), it can be shown that the corresponding maximum mutual information is given by

$$\mathcal{I}_{\max}(\mathbf{y}_k, \mathbf{x}_k) = \sum_{i=1}^q \log_2 \left(\frac{v_k \lambda_{ki}}{\alpha_{ii}^{(k)}} \right)^+, \quad k = 1, 2, \dots, K \quad (8.256)$$

where $(\cdot)^+$ means that only those terms satisfying $\beta_{ki} > 0$ are invoked.

Furthermore, it can be shown that when the Gaussian channels are considered, the capacity of the MC-CDMA system using the ZF/MMI-MUTP can be expressed as [233]

$$\mathcal{I}_{\max}(\mathbf{y}_k, \mathbf{x}_k) = \sum_{i=1}^q \log_2 \left[\left(\frac{v_k \lambda_{ki}}{\alpha_{ii}^{(k)}} \right)^+ \Big/ \sigma_s^2 \right] \text{ (bits/transmission/user), } k = 1, 2, \dots, K \quad (8.257)$$

and, correspondingly, the ergodic channel capacity of the MC-CDMA system using the ZF/MMI-MUTP can be evaluated as

$$\bar{\mathcal{I}}_{\max}(\mathbf{y}_k, \mathbf{x}_k) = E[\mathcal{I}_{\max}(\mathbf{y}_k, \mathbf{x}_k)] \text{ (bits/transmission/user), } k = 1, 2, \dots, K \quad (8.258)$$

The above analysis shows that the ZF/MMI-MUTP also divides the overall transmission multicarrier channels into Kq parallel subchannels without interfering with each other; there are q sub-channels for each downlink user. For each downlink user, the transmission power is allocated to the q subchannels according to (8.254) under the constraint of (8.255). The power is allocated by taking into account jointly the q number of eigenvalues associated with the q subchannels as well as the q number of coefficients $\{\alpha_{ii}^{(k)}\}$ produced by the ZF preprocessing. As seen in (8.254), the power allocation aims to reach an optimum balance between the eigenvalues and the coefficients due to the ZF preprocessing, in order to maximize the capacity. The power allocation emphasizes the subchannels having high eigenvalues, while simultaneously de-emphasizes the subchannels having high coefficients of $\{\alpha_{ii}^{(k)}\}$.

Below, we provide a range of simulation results showing the capacity of the MC-CDMA systems using the preprocessing schemes derived in this section.

Figure 8.13 shows the capacity (normalized by $N_p q$) of the MC-CDMA system using the joint MMI-MUTP (Fig. 8.13(a)) or ZF/MMI-MUTP (Fig. 8.13(b)), when communicating over the frequency-selective fading channels with $L = 10$ T-domain resolvable paths. From the results of Fig. 8.13, we observe that, for the joint MMI-MUTP, the capacity increases, when increasing the number of the downlink MTs supported. However, this is not always the case for the ZF/MMI-MUTP. As shown in Fig. 8.13(b) the MC-CDMA supporting $K = 8$ MTs achieves the highest capacity within the considered SNR region. When $K = 16$ the capacity achieved is the lowest, when $\text{SNR} < 10$ dB. When further increasing the SNR, the capacity of the MC-CDMA system supporting $K = 16$ may become better than in the other scenarios. From the results of Fig. 8.13(b), it can be implied that, for a given SNR value, there may exist an optimum value of K , which results in the MC-CDMA achieving the highest possible capacity. Furthermore, the results of Figs 8.13(a) and 8.13(b) show that for any given K and SNR values, the capacity achieved by the joint MMI-MUTP is higher than that achieved by the ZF/MMI-MUTP; the difference becomes significant, either when the number of MTs supported increases or when the SNR increases.

Figure 8.14 shows the impact of the spreading factor N and the number of MTs K on the capacity of the MC-CDMA downlink. In our simulations we assumed that the MC-CDMA employed $N_p q = 64$ subcarriers, when the symbol rate associated with each downlink MT changed. However, the total symbol rate was retained as a constant, which was $N_p q = 64$ symbols/transmission, implying, as shown in Fig. 8.14, that $K = N_p$ and satisfies $Kq = 64$. The results of Fig. 8.14(a) show that the MC-CDMA using the joint MMI-MUTP is capable of achieving a similar capacity for all the scenarios considered, except in the case of

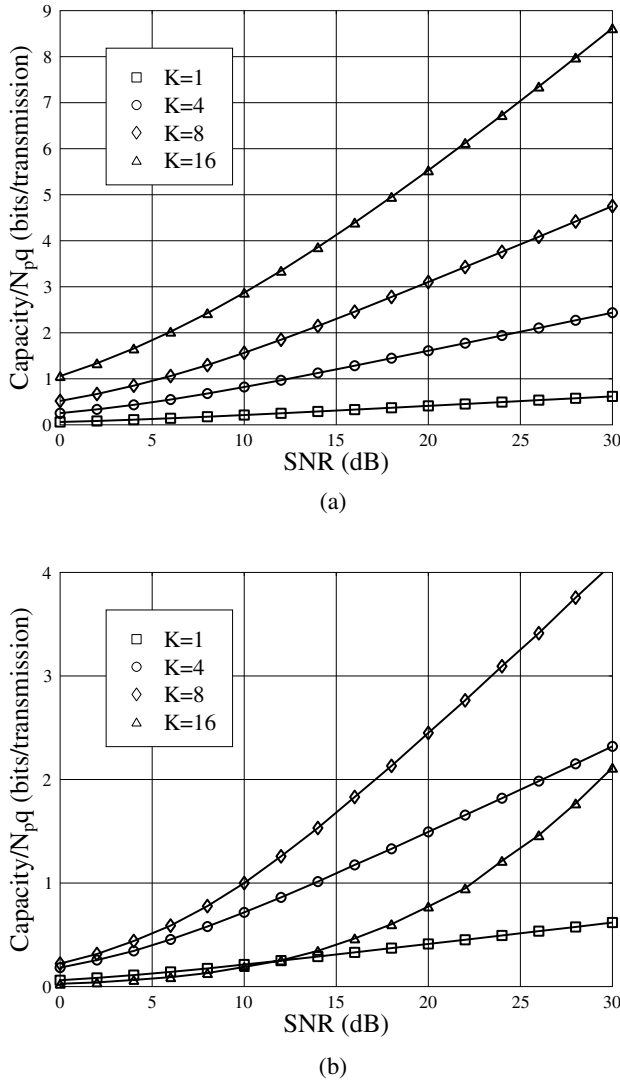


Figure 8.13: Capacity of the MC-CDMA using MMI-MUTP, when communicating over frequency-selective Rayleigh fading channels having $L = 10$ T-domain resolvable paths. The MC-CDMA system employs $N_p q = 64$ subcarriers and $q = 4$ symbols are transmitted to each of the downlink users. The simulations were based on (8.241) for the joint MMI-MUTP and (8.258) for the ZF/MMI-MUTP; (a) joint MMI-MUTP; (b) ZF/MMI-MUTP.

$q = 64$, $N_p = 1$, $K = 1$, which achieves a capacity that is slightly higher. From the results of Fig. 8.14(b) we see that the ZF-MUTP significantly degrades the capacity of the MC-CDMA. When the number of MTs K increases, implying more powerful ZF processing, the capacity of the MC-CDMA system decreases explicitly.

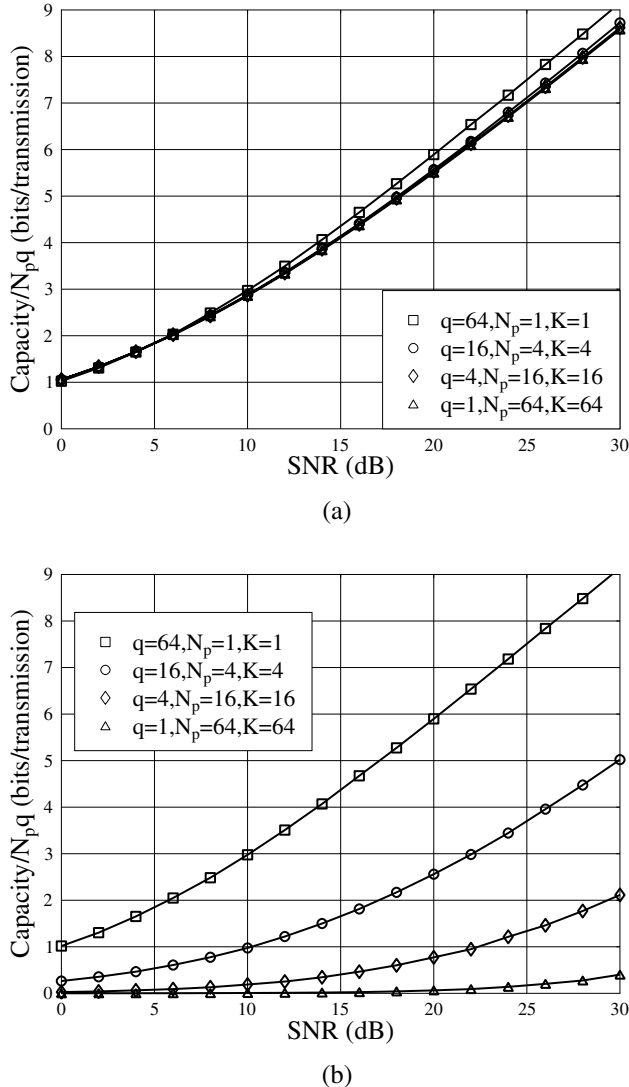


Figure 8.14: Capacity of the MC-CDMA using MMI-MUTP, when communicating over frequency-selective Rayleigh fading channels having $L = 10$ T-domain resolvable paths. The MC-CDMA system employs $N_{pq} = 64$ subcarriers. The simulations were based on (8.241) for the joint MMI-MUTP and (8.258) for the ZF/MMI-MUTP; (a) joint MMI-MUTP; (b) ZF/MMI-MUTP.

The results of Fig. 8.14 imply that in multiuser communications, it is desirable to let fewer users transmit at higher rate. As shown in Fig. 8.14, when $K = 1$, the ZF/MMI-MUTP scheme is equivalent to the joint MMI-MUTP scheme, and the highest capacity can be achieved. In this case, the MC-CDMA scheme is reduced to the OFDM scheme without spreading. From this point of view, the conventional OFDM scheme without spreading is

optimum. However, the conventional OFDM scheme is not suitable for supporting multiuser communications. When multiuser communications are considered, it seems that the desirable strategies might be the TDMA-based OFDM or FDMA-based OFDM, which can make the multiuser signals orthogonal either in the T-domain or in the F-domain.

In Fig. 8.15 we illustrate the impact of the number of T-domain resolvable paths (or the frequency-selectivity) of the frequency-selective fading channels on the capacity of the MC-CDMA using joint MMI-MUTP (Fig. 8.15(a)) or ZF/MMI-MUTP (Fig. 8.15(b)). It can be seen that the number of T-domain resolvable paths has only an insignificant effect on the capacity of the MC-CDMA using both joint MMI-MUTP and ZF/MMI-MUTP. Note that, due to the simulation problem, in Fig. 8.15(b) the capacity curve corresponding to $L = 1$ was not drawn. This is because, in this case, the random F-domain spreading codes generate a deficient channel matrix with a relatively high probability.

Finally, in Fig. 8.16 we illustrate the relationship between the capacity of the MC-CDMA system and the number of MTs it supports. As shown in Fig. 8.16(a), for the joint MMI-MUTP, the capacity increases nearly linearly with the number of MTs supported. By contrast, for the ZF/MMI-MUTP, the capacity of the MC-CDMA system first increases, when the number of MTs supported increases, as shown in Fig. 8.16(b). After a certain value of K , as shown in Fig. 8.16(b), the capacity then decreases, when further increasing the number of MTs supported. Hence, for a MC-CDMA system using ZF/MMI-MUTP, if given N_p , q and SNR, there usually exists an optimum value for the number of MTs supported, which results in the MC-CDMA being capable of achieving the highest capacity. Note that this observation has also been implied by the results shown in Fig. 8.13(b).

8.2.12 Transmitter Multiuser Interference Cancellation

The schematic block diagram for a general transmitter preprocessing scheme using transmitter multiuser interference cancellation (TMU-IC) is shown in Fig. 8.17, where \mathbf{S} carries out the feedforward transform and generates output for the multicarrier modulator. By contrast, \mathbf{F} is a feedback filter, through which $\tilde{\mathbf{x}}$ is fed back to the input, where the MUI is cancelled. Therefore, according to Fig. 8.17 we can express the preprocessed data as

$$\bar{\mathbf{P}}\mathbf{x} = \mathbf{S}(\tilde{\mathbf{x}} - \mathbf{F}\bar{\mathbf{x}}) \quad (8.259)$$

where $\tilde{\mathbf{x}} = \boldsymbol{\beta}\mathbf{x}$. After substituting the above equation into

$$\mathbf{y} = \mathbf{C}^T \mathbf{H} \bar{\mathbf{P}}\mathbf{x} + \mathbf{n} \quad (8.260)$$

the decision variables observed at the MTs can be expressed as

$$\mathbf{y} = \mathbf{C}^T \mathbf{H} \mathbf{S}(\tilde{\mathbf{x}} - \mathbf{F}\bar{\mathbf{x}}) + \mathbf{n} \quad (8.261)$$

$$= \mathbf{C}^T \mathbf{H} \mathbf{S} \tilde{\mathbf{x}} + \mathbf{n} \quad (8.262)$$

where (8.261) to (8.262) is due to $\bar{\mathbf{x}} = \tilde{\mathbf{x}} - \mathbf{F}\bar{\mathbf{x}}$, as seen in Fig. 8.17.

Let us first consider the TMU-IC based on the QR-decomposition, which has been considered in reference [235] in the context of the downlink MC-CDMA systems. Let the QR-decomposition on $\mathbf{H}^H \mathbf{C}$ be expressed as [156]

$$\mathbf{H}^H \mathbf{C} = \mathbf{Q} \mathbf{R} \quad (8.263)$$

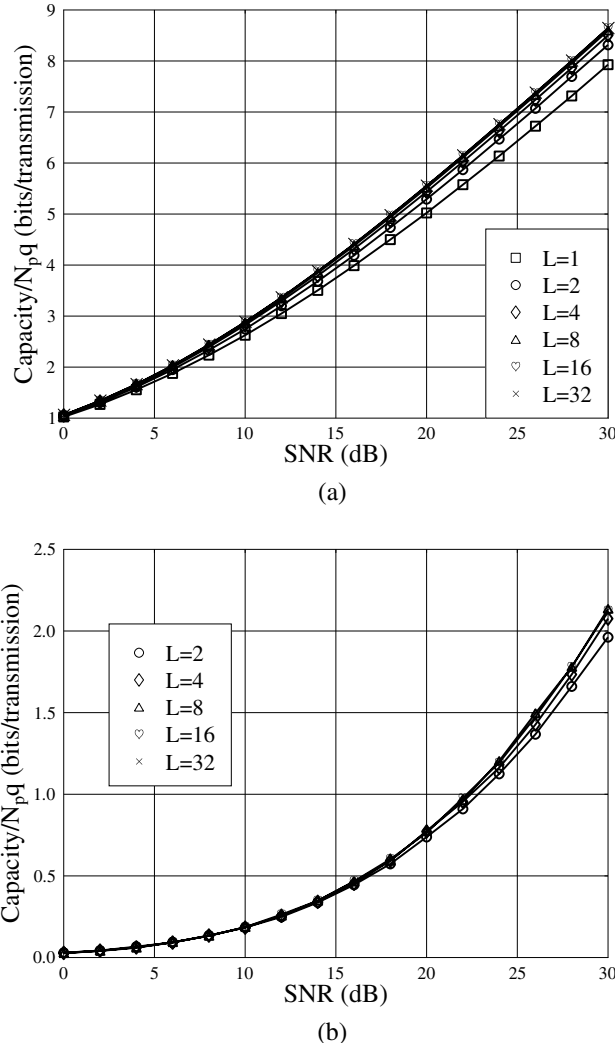


Figure 8.15: Capacity of the MC-CDMA using MMI-MUTP, when communicating over frequency-selective Rayleigh fading channels. The MC-CDMA system employs $N_p q = 64$ subcarriers, supports $K = 16$ users and transmits $q = 4$ symbols to each of the downlink users. The simulations were based on (8.241) for the joint MMI-MUTP and (8.258) for the ZF/MMI-MUTP; (a) joint MMI-MUTP; (b) ZF/MMI-MUTP.

where \mathcal{R} is a $(Kq \times Kq)$ upper triangular matrix, \mathbf{Q} is a $(N_p q \times Kq)$ orthonormal matrix. Then, letting in (8.261) and (8.262) $\mathbf{S} = \mathbf{Q}$, and when substituting (8.263) into (8.262), we obtain

$$\mathbf{y} = \mathcal{R}^H \bar{\mathbf{x}} + \mathbf{n} = \mathbf{M} \bar{\mathbf{x}} + \mathbf{n} \quad (8.264)$$

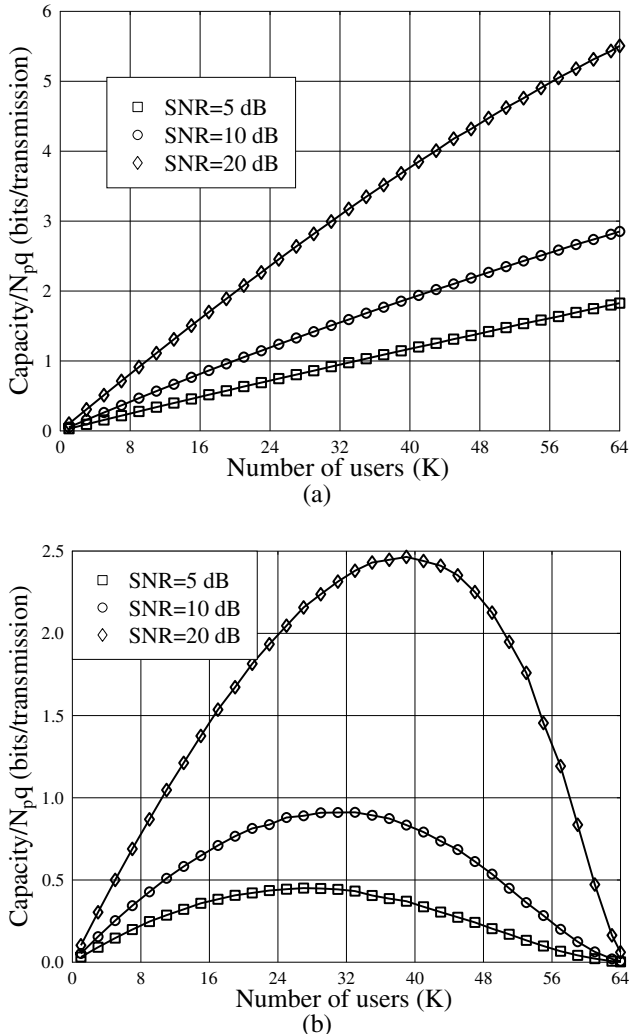


Figure 8.16: Capacity of the MC-CDMA using MMI-MUTP, when communicating over frequency-selective Rayleigh fading channels having $L = 10$ T-domain resolvable paths. The MC-CDMA system employs $N_{pq} = 64$ subcarriers and $q = 1$ symbol is transmitted to each of the downlink users. The simulations were based on (8.241) for the joint MMI-MUTP and (8.258) for the ZF/MMI-MUTP; (a) joint MMI-MUTP; (b) ZF/MMI-MUTP.

where $\mathbf{M} = \mathcal{R}^H$ is a lower triangular matrix. In more detail, let $N = Kq$, then \mathbf{M} can be expressed as

$$\mathbf{M} = \begin{bmatrix} m_{11} & & & \\ m_{21} & m_{22} & & \\ \vdots & \vdots & \ddots & \\ m_{N1} & m_{N2} & \cdots & m_{NN} \end{bmatrix} \quad (8.265)$$

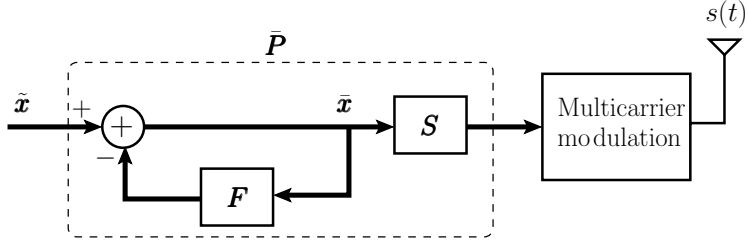


Figure 8.17: Schematic block diagram of the transmitter preprocessing using transmitter multiuser interference cancellation.

where the empty entries are zeros. When applying (8.265) to (8.264) and expanding it with respect to each of the transmitted bits, the decision variables can be expressed as

$$\begin{aligned}
 y_1 &= m_{11}\bar{x}_1 + n_1 \\
 y_2 &= m_{22}\bar{x}_2 + m_{21}\bar{x}_1 + n_2 \\
 &\dots &&\dots \\
 y_i &= m_{ii}\bar{x}_i + \sum_{j=1}^{i-1} m_{ij}\bar{x}_j + n_i \\
 &\dots &&\dots \\
 y_N &= m_{NN}\bar{x}_N + \sum_{j=1}^{N-1} m_{Nj}\bar{x}_j + n_N
 \end{aligned} \tag{8.266}$$

In the above equations, if we set

$$\begin{aligned}
 \bar{x}_1 &= \tilde{x}_1 \\
 \bar{x}_2 &= \tilde{x}_2 - \frac{1}{m_{22}}m_{21}\bar{x}_1 \\
 \bar{x}_3 &= \tilde{x}_3 - \frac{1}{m_{33}}(m_{32}\bar{x}_2 + m_{31}\bar{x}_1) \\
 &\dots &&\dots \\
 \bar{x}_i &= \tilde{x}_i - \frac{1}{m_{ii}}\left(\sum_{j=1}^{i-1} m_{ij}\bar{x}_j\right), \quad i = 2, \dots, N
 \end{aligned} \tag{8.267}$$

we obtain the decision variables given as

$$\begin{aligned}
 y_1 &= m_{11}\tilde{x}_1 + n_1 \\
 y_2 &= m_{22}\tilde{x}_2 + n_2 \\
 &\dots \\
 y_i &= m_{ii}\tilde{x}_i + n_i, \quad i = 1, 2, \dots, N
 \end{aligned} \tag{8.268}$$

Explicitly, the downlink MUI is fully removed in terms of each of the transmitted bits.

When expressing (8.267) in matrix form, we obtain

$$\mathbf{M}\tilde{\mathbf{x}} = \mathbf{M}_d\tilde{\mathbf{x}} \quad (8.269)$$

where $\mathbf{M}_d = \text{diag}\{m_{11}, m_{22}, \dots, m_{NN}\}$ associated with $N = Kq$. Hence, we have

$$\tilde{\mathbf{x}} = \mathbf{M}^{-1}\mathbf{M}_d\tilde{\mathbf{x}} \quad (8.270)$$

Substituting (8.270) into (8.262) and remembering that $\mathbf{S} = \mathbf{Q}$ and $\tilde{\mathbf{x}} = \boldsymbol{\beta}\mathbf{x}$, \mathbf{y} can be expressed as

$$\mathbf{y} = \mathbf{C}^T \mathbf{H} \mathbf{Q} \mathbf{M}^{-1} \mathbf{M}_d \boldsymbol{\beta} \mathbf{x} + \mathbf{n} \quad (8.271)$$

From (8.271) we can deduce that the transmitter preprocessing matrix $\bar{\mathbf{P}}$ can be expressed as

$$\bar{\mathbf{P}} = \mathbf{Q} \mathbf{M}^{-1} \mathbf{M}_d \boldsymbol{\beta} \quad (8.272)$$

where $\boldsymbol{\beta}$ can be determined by the constraint on the transmission power.

From (8.270) we can also obtain the following relation

$$\tilde{\mathbf{x}} = \tilde{\mathbf{x}} - \mathbf{M}_d^{-1}(\mathbf{M} - \mathbf{M}_d)\tilde{\mathbf{x}} \quad (8.273)$$

from which we can deduce that \mathbf{F} in (8.259) is given by

$$\mathbf{F} = \mathbf{M}_d^{-1}(\mathbf{M} - \mathbf{M}_d) \quad (8.274)$$

Additionally, substituting (8.270) into (8.264), it can be shown that the decision variable vector for \mathbf{x} is given by

$$\begin{aligned} \mathbf{y} &= \mathbf{M}_d\tilde{\mathbf{x}} + \mathbf{n} \\ &\triangleq \boldsymbol{\beta}\mathbf{x} + \mathbf{n} \end{aligned} \quad (8.275)$$

which shows that the downlink MUI is fully removed in terms of each transmitted symbol. Therefore, the TMU-IC can be viewed as another type of ZF-MUTP and the preprocessing with a feedback filter shown in Fig. 8.17 can be interpreted as an efficient implementation of the (Moore–Penrose) matrix inversion in the ZF-MUTP seen in (8.67).

Above, we have derived the TMU-IC scheme for the MC-CDMA system without considering its inherent characteristics. Therefore, the above-obtained results are suitable for the general MIMO systems using TMU-IC. However, the MC-CDMA system considered in this section employs some special features; for example, there is no intercarrier and interbit interference, which might be exploited for simplifying the computation of the transmitter preprocessing matrix $\bar{\mathbf{P}}$. To be more specific, it can be shown that $\mathbf{C}^T \mathbf{H}$ can be expressed as

$$\mathbf{C}^T \mathbf{H} = \begin{bmatrix} \mathbf{C}_1^T \mathbf{H}_1 \\ \mathbf{C}_2^T \mathbf{H}_2 \\ \vdots \\ \mathbf{C}_K^T \mathbf{H}_K \end{bmatrix} = \mathbf{C}_k^T \mathbf{H}_k = \begin{bmatrix} \mathbf{C}_1^T \mathbf{H}_1 & & & \\ \vdots & & & \\ \mathbf{c}_k^T \mathbf{H}_1^{(k)} & 0 & & \\ 0 & \mathbf{c}_k^T \mathbf{H}_2^{(k)} & 0 & \\ \vdots & \vdots & \ddots & \\ 0 & 0 & \cdots & \mathbf{c}_k^T \mathbf{H}_q^{(k)} \\ & & \vdots & \\ & & & \mathbf{C}_K^T \mathbf{H}_K \end{bmatrix} \quad (8.276)$$

where $\tilde{\mathbf{H}}_i^{(k)}$ is a $(N_p \times N_p)$ diagonal matrix with the diagonal entries being the N_p channel gains of the subcarriers conveying the i th, $i = 1, 2, \dots, q$, bit of MT k . Therefore, the MIMO equation seen in (8.260) can be decomposed into q independent MIMO equations

$$\tilde{\mathbf{y}}_i = \tilde{\mathbf{C}}^T \tilde{\mathbf{H}}_i \tilde{\mathbf{P}}_i \tilde{\mathbf{x}}_i + \tilde{\mathbf{n}}_i, \quad i = 1, 2, \dots, q \quad (8.277)$$

where

$$\begin{aligned} \tilde{\mathbf{C}} &= \text{diag}\{\mathbf{c}_1, \mathbf{c}_2, \dots, \mathbf{c}_K\} \\ \tilde{\mathbf{H}}_i &= [(\mathbf{H}_i^{(1)})^T, (\mathbf{H}_i^{(2)})^T, \dots, (\mathbf{H}_i^{(K)})^T]^T \\ \tilde{\mathbf{P}}_i &= [\mathbf{p}_i^{(1)}, \mathbf{p}_i^{(2)}, \dots, \mathbf{p}_i^{(K)}] \\ \tilde{\mathbf{x}}_i &= [x_{1i}, x_{2i}, \dots, x_{Ki}]^T \end{aligned} \quad (8.278)$$

where $\mathbf{p}_i^{(k)}$ is the N_p -length preprocessing vector for processing x_{ki} .

When comparing (8.277) with (8.260) and following the same approach in this section for deriving \mathbf{S} and \mathbf{F} in (8.259), it can be shown that, when the QR-decomposition of $\tilde{\mathbf{H}}_i^H \tilde{\mathbf{C}}$ is given by

$$\tilde{\mathbf{H}}_i^H \tilde{\mathbf{C}} = \mathbf{Q}_i (\mathbf{M}_i)^H \quad (8.279)$$

the corresponding matrices for the TMU-IC can be expressed as

$$\begin{aligned} \mathbf{S}_i &= \mathbf{Q}_i \\ \mathbf{F}_i &= \mathbf{M}_{id}^{-1} (\mathbf{M}_i - \mathbf{M}_{id}), \quad i = 1, 2, \dots, q \end{aligned} \quad (8.280)$$

where \mathbf{M}_{id} is a diagonal matrix having the same diagonal entries as \mathbf{M}_i . Furthermore, it can be shown that the preprocessing matrix can be expressed as

$$\tilde{\mathbf{P}}_i = \mathbf{Q}_i (\mathbf{M}_i)^{-1} \mathbf{M}_{id} \boldsymbol{\beta}_i, \quad i = 1, 2, \dots, q \quad (8.281)$$

where, again, $\tilde{\mathbf{P}}_i$ is $(N_p \times K)$ -dimensional.

Note that the TMU-IC has the advantage that there is no error propagation, since the IC operation is performed at the transmitter where signals and transmitted symbols are perfectly known. By contrast, as shown in Chapter 6, the MUD-IC conflicts error propagation, since in this case the IC operation has to be carried out based on the symbols detected from the noisy and/or faded observations, which might hence be wrong.

The above approach for deriving the ZF-type TMU-IC can be extended generally, where the transmitter preprocessing may be implemented under various optimization criteria. First, it can be shown that the matrix \mathbf{F} of (8.274) or \mathbf{F}_i in (8.280) can be expressed in a general form as

$$\mathbf{F} = \mathbf{B} - \mathbf{I} \quad (8.282)$$

where $\mathbf{B} = \mathbf{M}_d^{-1} \mathbf{M}$ or $\mathbf{B} = \mathbf{M}_{id}^{-1} \mathbf{M}_i$ is explicitly a lower triangular matrix with unity diagonal entries. Second, from $\tilde{\mathbf{P}}$ of (8.272) or $\tilde{\mathbf{P}}_i$ of (8.281), we know that the preprocessing matrix is in the form

$$\bar{\mathbf{P}} = \mathbf{S} \mathbf{B}^{-1} \boldsymbol{\beta} \quad (8.283)$$

where we only considered that $\bar{\mathbf{P}}$ and $\tilde{\mathbf{P}}_i$ can be derived in the same way as below.

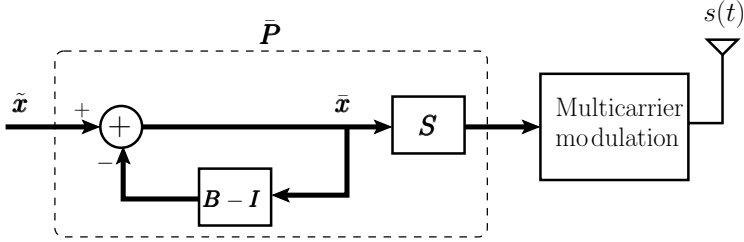


Figure 8.18: Schematic block diagram of the transmitter preprocessing using transmitter multiuser interference cancellation.

Based on (8.282) and (8.283), the TMU-IC can in general be implemented as Fig. 8.18, where the matrices S and B can be determined according to the preprocessing matrices derived in the previous sections. Specifically, for the ZF-MUTP and MMSE-MUTP, their corresponding S and B matrices can be derived as follows.

In the context of the ZF-MUTP, the preprocessing matrix is given by (8.68), which is

$$\bar{P} = \mathbf{H}^H \mathcal{C} (\mathcal{C}^T \mathbf{H} \mathbf{H}^H \mathcal{C})^{-1} \boldsymbol{\beta} \quad (8.284)$$

Invoking the QR-decomposition [157], the matrix $\mathbf{H}^H \mathcal{C}$ can be expressed as

$$\mathbf{H}^H \mathcal{C} = \mathbf{Q} \mathbf{R} = \mathbf{Q} \mathbf{D}^{1/2} \mathbf{L}^H \quad (8.285)$$

where \mathbf{L} is a lower triangular matrix with unity diagonal entries, \mathbf{D} is a diagonal matrix with positive diagonal entries. Applying the above result to (8.284), we obtain

$$\begin{aligned} \bar{P} &= \mathbf{Q} \mathbf{D}^{1/2} \mathbf{L}^H (\mathbf{L} \mathbf{D} \mathbf{L}^H)^{-1} \boldsymbol{\beta} \\ &= \mathbf{Q} \mathbf{D}^{-1/2} \mathbf{L}^{-1} \boldsymbol{\beta} \end{aligned} \quad (8.286)$$

where $\mathbf{D}^{-1/2}$ can be absorbed into $\boldsymbol{\beta}$. Hence, when comparing (8.283) with (8.286), it can be shown that for the ZF-assisted TMU-IC, we have

$$\begin{aligned} \mathbf{B} &= \mathbf{L} \\ \mathbf{S} &= \mathbf{Q} \end{aligned} \quad (8.287)$$

which are the same results obtained previously in this section for the ZF-assisted TMU-IC.

In the context of the MMSE-MUTP, the transmitter preprocessing matrix is given by

$$\bar{P} = \mathbf{H}^H \mathcal{C} (\mathcal{C}^T \mathbf{H} \mathbf{H}^H \mathcal{C} + \rho \sigma_s^2 \mathbf{I}_{Kq})^{-1} \boldsymbol{\beta} \quad (8.288)$$

Invoking the LDL-decomposition [157] on the autocorrelation matrix $\mathcal{C}^T \mathbf{H} \mathbf{H}^H \mathcal{C} + \rho \sigma_s^2 \mathbf{I}_{Kq}$, the preprocessing matrix of (8.288) can be expressed as

$$\begin{aligned} \bar{P} &= \mathbf{H}^H \mathcal{C} (\mathbf{L} \mathbf{D} \mathbf{L}^H)^{-1} \boldsymbol{\beta} \\ &= \mathbf{H}^H \mathcal{C} (\mathbf{L}^{-1})^H \mathbf{D}^{-1} \mathbf{L}^{-1} \boldsymbol{\beta} \end{aligned} \quad (8.289)$$

Correspondingly, after absorbing \mathbf{D}^{-1} into $\boldsymbol{\beta}$ and comparing (8.283) with (8.289), it can be shown that, for the MMSE-assisted TMU-IC, we have

$$\begin{aligned}\mathbf{B} &= \mathbf{L} \\ \mathbf{S} &= \mathbf{H}^H \mathcal{C} (\mathbf{L}^{-1})^H\end{aligned}\quad (8.290)$$

Similarly, the other transmitter preprocessing schemes considered in this chapter may also be implemented as shown in Fig. 8.18. Readers interested in their implementation may derive the corresponding matrices of \mathbf{B} and \mathbf{S} by following the same approaches as above.

Since the ZF-assisted TMU-IC and MMSE-assisted TMU-IC belong to the family of ZF-MUTP and the family of MMSE-MUTP, respectively, the ZF-assisted TMU-IC and MMSE-assisted TMU-IC achieve the BER performance of the ZF-MUTP studied in Section 8.2.4 and the MMSE-MUTP in Section 8.2.5, respectively. In comparison with the MUD considered in Chapter 6, both the ZF-IC in Section 6.2.7.2 and MMSE-IC in Section 6.2.7.3 are the approximates of the MLD-MUD. In Chapter 6 we showed that both the ZF-IC and MMSE-IC are capable of achieving BER performance that is very close to that achieved by the MLD-MUD.

Finally, note that, since, according to Fig. 8.18, $\bar{\mathbf{x}} = \tilde{\mathbf{x}} - (\mathbf{B} - \mathbf{I})\tilde{\mathbf{x}}$, hence the data vector $\bar{\mathbf{x}}$ after the MUI cancellation can be expressed as

$$\bar{\mathbf{x}} = \mathbf{B}^{-1} \tilde{\mathbf{x}} \quad (8.291)$$

As shown in the context of both the ZF- and MMSE-assisted TMU-ICs, \mathbf{B} is obtained from decomposing the channel-related autocorrelation matrix. Hence, it can be implied that some elements in $\bar{\mathbf{x}}$ might have very high amplitudes, when \mathbf{B} is ill-conditioned. To overcome this problem, the Tomlinson–Harashima precoding [236] approach can be used to map the amplitudes into a desired range. Specifically, using the M -ary quadrature amplitude modulation (MQAM) as an example, the Tomlinson–Harashima precoding computes

$$\mathbf{v} = -2\sqrt{M} \left\lfloor \frac{\bar{\mathbf{x}} - \sqrt{M}}{2\sqrt{M}} \right\rfloor \quad (8.292)$$

and then replaces $\bar{\mathbf{x}}$ by

$$\mathbf{d} = \bar{\mathbf{x}} + \mathbf{v} \quad (8.293)$$

After the Tomlinson–Harashima precoding-based mapping, the real and imaginary parts of the entries in

$$\begin{aligned}\bar{\mathbf{x}} &= \mathbf{d} - (\mathbf{B} - \mathbf{I})\bar{\mathbf{x}} \\ &= \bar{\mathbf{x}} + \mathbf{v} - (\mathbf{B} - \mathbf{I})\bar{\mathbf{x}}\end{aligned}\quad (8.294)$$

will be in the desired range $(-\sqrt{M}, \sqrt{M}]$.

8.3 Transmitter Preprocessing in Frequency-Domain Spread MC DS-CDMA Systems

In the previous section a range of transmitter preprocessing schemes were investigated in the context of the F-domain spread MC-CDMA. It can be shown that the transmitter

preprocessing may be designed to achieve various objectives, such as to mitigate the multiuser interference (MUI) presenting at the remote MTs, to maximize the information rate, etc. In this section we extend the study to the TF-domain spread MC DS-CDMA, which represents a highly general CDMA scheme. As shown previously, by setting the corresponding parameters appropriate values, the TF-domain spread MC DS-CDMA can be readily converted to another CDMA scheme, such as single-carrier DS-CDMA, F-domain spread MC-CDMA, MC DS-CDMA without F-domain spreading, etc. Let us first consider the system model of the TF-domain spread MC DS-CDMA using transmitter preprocessing.

8.3.1 Transmitted Signal

For simplicity, the TF-domain spread MC DS-CDMA considered in this section is constituted of an orthogonal MC DS-CDMA scheme that employs orthogonal subcarrier signals, as shown in Section 3.5 of Chapter 3. The transmitter schematic block diagram of the TF-domain spread MC DS-CDMA using transmitter preprocessing is shown in Fig. 8.19, which consists of S/P conversion, TF-domain spreading, preprocessing and MC modulation, etc. components. Below, the operation details of the components seen in Fig. 8.19 are provided. First, the main parameters used by the TF-domain spread MC DS-CDMA system are listed as follows:

- U : number of bits (symbols) invoked in the S/P conversion, or the number of bits per symbol transmitted to a remote MT;
- N_p : total number of subcarriers, and length of the F-domain spreading codes;
- T_c , T_b , T_s : chip duration, bit duration and symbol duration of the corresponding signals in the TF-domain spread MC DS-CDMA;
- $N_t = T_s/T_c$: number of chips per symbol-duration or length of the T-domain spreading codes;
- $\mathbf{C}_f^{(k)}$: F-domain spreading matrix, which is $(N_p \times U)$ dimensional. Each column of $\mathbf{C}_f^{(k)}$ constitutes a F-domain spreading code, which is expressed as $\mathbf{c}_{fu}^{(k)} = [c_{fu,1}^{(k)}, c_{fu,2}^{(k)}, \dots, c_{fu,N_p}^{(k)}]^T / \sqrt{N_p}$;
- $c_k(t)$: T-domain spreading code waveform of the k th downlink MT, which is formed based on the sequence $\mathbf{c}_k = [c_{k0}, c_{k1}, \dots, c_{k(N_t-1)}]^T / \sqrt{N_t}$ assigned to the k th downlink MT.

Second, in our forthcoming analysis the following assumptions are applied:

- orthogonal subcarrier signals: the spacing between two adjacent subcarriers is $1/T_c$;
- K number of downlink MTs are supported, $KU \leq N_p N_t$;
- the same T-domain spreading code may be assigned to several MTs, the same F-domain spreading code may also be assigned to several MTs. However, no two MTs are assigned the same T-domain spreading code and the same set of F-domain spreading codes, simultaneously;

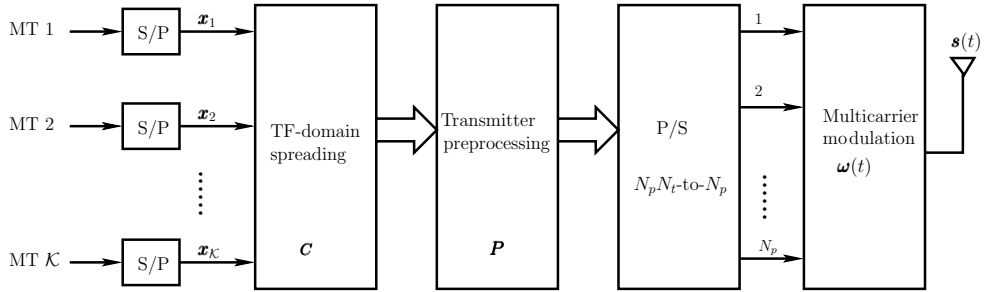


Figure 8.19: Transmitter schematic block diagram of the TF-domain spread MC DS-CDMA using transmitter preprocessing.

- the subcarrier signals are arranged so that each subcarrier signal experiences frequency non-selective (flat) fading;
- the BS transmitter uses the knowledge of the channels connecting the BS with all the MTs. The BS has knowledge of both the T-domain and F-domain spreading codes of all the MTs. By contrast, each MT knows only its own T-domain and F-domain spreading codes. Furthermore, the MTs do not exploit the fading-channel knowledge for detection.

Let the KU symbols transmitted to the K MTs be expressed as

$$\begin{aligned} \mathbf{x} &= [x_1^T, x_2^T, \dots, x_K^T]^T \\ \mathbf{x}_k &= [x_{k1}, x_{k2}, \dots, x_{kU}]^T \end{aligned} \quad (8.295)$$

As shown in Fig. 8.19, after the S/P conversion, the data symbol to be transmitted are first spread in the TF-domain. Let

$$\begin{aligned} \mathbf{C}_f^{(k)} &= [\mathbf{c}_{f1}^{(k)}, \mathbf{c}_{f2}^{(k)}, \dots, \mathbf{c}_{fU}^{(k)}] \\ &= \frac{1}{\sqrt{N_p}} \begin{bmatrix} c_{f1,1}^{(k)} & c_{f2,1}^{(k)} & \cdots & c_{fU,1}^{(k)} \\ c_{f1,2}^{(k)} & c_{f2,2}^{(k)} & \cdots & c_{fU,2}^{(k)} \\ \vdots & \vdots & \ddots & \vdots \\ c_{f1,N_p}^{(k)} & c_{f2,N_p}^{(k)} & \cdots & c_{fU,N_p}^{(k)} \end{bmatrix} \end{aligned} \quad (8.296)$$

be the set of F-domain spreading codes assigned to the k th MT. Then, the output after the F-domain spreading can be expressed as

$$\mathbf{s}_f^{(k)} = \mathbf{C}_f^{(k)} \mathbf{x}_k, \quad k = 1, 2, \dots, K \quad (8.297)$$

which is an N_p -length vector and each entry of $\mathbf{s}_f^{(k)}$ corresponds to a subcarrier. Let

$$\mathbf{c}_k = \frac{1}{\sqrt{N_t}} [c_{k0}, c_{k1}, \dots, c_{k(N_t-1)}]^T \quad (8.298)$$

be the T-domain spreading code assigned to the k th MT. Then, each of the entries in $\mathbf{s}_f^{(k)}$ of (8.297) is further spread using this T-domain spreading code, yielding

$$\begin{aligned}\mathbf{s}_t^{(k)} &= (\mathbf{I}_{N_p} \otimes \mathbf{c}_k) \mathbf{s}_f^{(k)} \\ &= (\mathbf{I}_{N_p} \otimes \mathbf{c}_k) \mathbf{C}_f^{(k)} \mathbf{x}_k, \quad k = 1, 2, \dots, K\end{aligned}\quad (8.299)$$

which is an $N_p N_t$ -length vector. Let

$$\mathbf{C}^{(k)} = (\mathbf{I}_{N_p} \otimes \mathbf{c}_k) \mathbf{C}_f^{(k)} \quad (8.300)$$

be the spreading matrix of MT k . It can be seen that $\mathbf{C}^{(k)}$ is a $(N_p N_t \times U)$ matrix. Then, we obtain

$$\mathbf{s}_t^{(k)} = \mathbf{C}^{(k)} \mathbf{x}_k, \quad k = 1, 2, \dots, K \quad (8.301)$$

After adding $\mathbf{s}_t^{(k)}$ with $k = 1, 2, \dots, K$, it yields

$$\begin{aligned}\mathbf{s}_t &= \sum_{k=1}^K \mathbf{C}^{(k)} \mathbf{x}_k \\ &= [\mathbf{C}^{(1)}, \mathbf{C}^{(2)}, \dots, \mathbf{C}^{(K)}] \mathbf{x} \\ &= \mathbf{C} \mathbf{x}\end{aligned}\quad (8.302)$$

where, by definition,

$$\mathbf{C} = [\mathbf{C}^{(1)}, \mathbf{C}^{(2)}, \dots, \mathbf{C}^{(K)}] \quad (8.303)$$

which is a $(N_p N_t \times KU)$ spreading matrix.

As shown in Fig. 8.19, following the TF-domain spreading, the transmitter preprocessing is carried out by multiplying the signal \mathbf{s}_t with a $(N_p N_t \times N_p N_t)$ dimensional preprocessing matrix \mathbf{P} , giving

$$\begin{aligned}\mathbf{d} &= \mathbf{P} \mathbf{s}_t = \mathbf{P} \mathbf{C} \mathbf{x} \\ &= \bar{\mathbf{P}} \mathbf{x}\end{aligned}\quad (8.304)$$

where we define

$$\bar{\mathbf{P}} = \mathbf{P} \mathbf{C} \quad (8.305)$$

which includes the F-domain spreading, T-domain spreading as well as the transmitter preprocessing.

Finally, as shown in Fig. 8.19, after the P/S conversion in the context of each subcarrier, the multicarrier modulation is operated, in order to form the time-frequency transmitted signal. Specifically, let \mathbf{d} be expressed as

$$\begin{aligned}\mathbf{d} &= [\mathbf{d}_1^T, \mathbf{d}_2^T, \dots, \mathbf{d}_{N_p}^T]^T \\ \mathbf{d}_n &= [d_{n1}, d_{n2}, \dots, d_{nN_t}]^T, \quad n = 1, 2, \dots, N_p\end{aligned}\quad (8.306)$$

where \mathbf{d}_n , ($n = 1, 2, \dots, N_p$) is transmitted by the n th subcarrier within N_t chip durations. Let the T-domain signal corresponding to \mathbf{d}_n be expressed as $d_n(t) = \sum_{j=0}^{N_t-1} d_{n(j+1)} \psi_{T_c}$

$(t - jT_c)$, where $\psi_{T_c}(t)$ is the chip waveform. Then, the normalized transmitted baseband equivalent MC DS-CDMA signal can be expressed as

$$s(t) = \sum_{n=1}^{N_p} d_n(t) \exp(j2\pi f_n t) \quad (8.307)$$

Above, we have derived the transmitted signal for the TF-domain spread MC DS-CDMA without putting any constraint on the spreading codes, except to satisfy the assumption that no two data symbols sharing the same T-domain and F-domain spreading codes, or that the spreading matrix \mathbf{C} seen in (8.303) is column-rank full. In other words, the above described scheme with the transmitted signal of (8.307) is suitable for where correlations exist among the T-domain spreading codes and also among the F-domain spreading codes. However, for the considered TF-domain spread MC DS-CDMA, the transmitter can be easily designed so that each subcarrier signal experiences flat fading. In this case, orthogonal T-domain spreading codes can be assigned to different MTs so that there exists no interference in the T-domain among these MTs. This is because, when the communications channels are flat fading, the transmitted orthogonality can be reserved by the received signals. Specifically, in the TF-domain spread MC DS-CDMA the T-domain orthogonal spreading codes, such as the Walsh–Hadamard codes, can be first assigned to different MTs. If the T-domain orthogonal spreading codes are not sufficient, then the same T-domain spreading code can be shared by several MTs, and these MTs sharing the same T-domain spreading code are distinguished by assigning them unique F-domain spreading codes. To be more specific, let us assume that the TF-domain spread MC DS-CDMA supports a total $\mathcal{K} = KN_t$ number of MTs and that there are N_t orthogonal T-domain spreading codes available. Then, each orthogonal T-domain spreading code is shared by K MTs. The K MTs sharing the same T-domain spreading code are then distinguished by assigning them unique F-domain spreading codes.

For the above-described scenario, it can be shown that there is no MUI in the T-domain. Hence, the preprocessing in the context of the T-domain spreading codes is redundant and only the F-domain preprocessing is required. In this case the transmitter schematic block diagram can be shown as Fig. 8.20, where the transmitter preprocessing is carried out following the F-domain spreading. Specifically, after the F-domain spreading and transmitter preprocessing, the output signals can be expressed as

$$\mathbf{s}_p^{(k)} = \mathbf{P}_k \mathbf{C}_f^{(k)} \mathbf{x}_k, \quad k = 1, 2, \dots, \mathcal{K} \quad (8.308)$$

where \mathbf{P}_k is a $(N_p \times N_p)$ matrix and $\mathbf{s}_p^{(k)}$ is an N_p -length vector. We define

$$\bar{\mathbf{P}}_k = \mathbf{P}_k \mathbf{C}_f^{(k)}, \quad k = 1, 2, \dots, \mathcal{K} \quad (8.309)$$

Then, (8.308) can be rewritten as

$$\mathbf{s}_p^{(k)} = \bar{\mathbf{P}}_k \mathbf{x}_k, \quad k = 1, 2, \dots, \mathcal{K} \quad (8.310)$$

As shown in Fig. 8.20, after the preprocessing, $\mathbf{s}_p^{(k)}$ is converted to N_p branches, each corresponding to one subcarrier and spread using T-domain spreading codes. Let $\mathbf{s}_p^{(k)}$ be expressed as

$$\mathbf{s}_p^{(k)} = [s_{p1}^{(k)}, s_{p2}^{(k)}, \dots, s_{pN_p}^{(k)}]^T \quad (8.311)$$

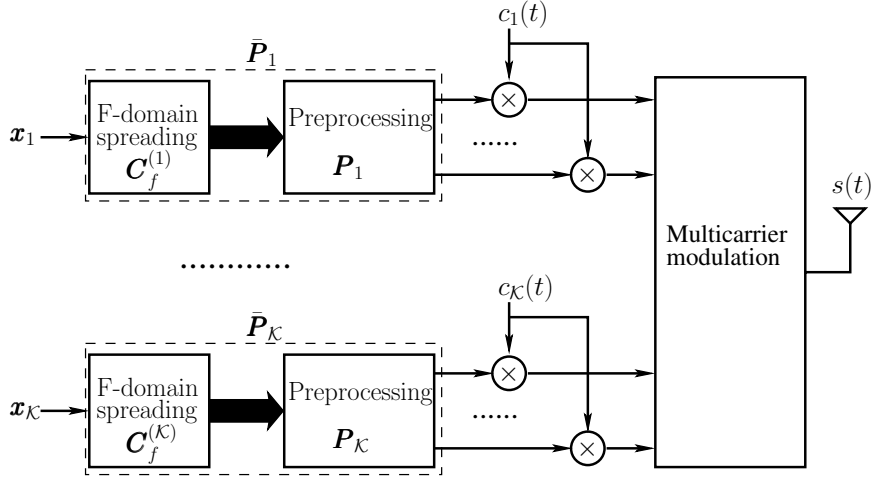


Figure 8.20: Transmitter schematic block diagram of the TF-domain spread MC DS-CDMA using transmitter preprocessing.

Then, for the k th MT, after the T-domain spreading, the signal on the n th branch can be expressed as

$$s_n^{(k)}(t) = s_{pn}^{(k)} c_k(t), \quad k = 1, 2, \dots, \mathcal{K}; n = 1, 2, \dots, N_p \quad (8.312)$$

where $c_k(t) = (\sqrt{N_t})^{-1} \sum_{j=0}^{N_t-1} c_{kj} \psi_{T_c}(t - jT_c)$. Then, the \mathcal{K} number of signals with the same n index are added together and multiplied by the n th subcarrier having a frequency f_n , in order to form the signal transmitted on the n th subcarrier. Finally, all the subcarrier signals are summed together to form the transmitted signal, which can be expressed as

$$\begin{aligned} s(t) &= \sum_{n=1}^{N_p} \sum_{k=1}^{\mathcal{K}} s_n^{(k)}(t) \exp(j2\pi f_n t) \\ &= \sum_{n=1}^{N_p} \sum_{k=1}^{\mathcal{K}} s_{pn}^{(k)} c_k(t) \exp(j2\pi f_n t) \end{aligned} \quad (8.313)$$

In order to distinguish the above two preprocessing schemes, we refer to the first one having the transmitted signal of (8.307) as the TF-preprocessing, while to the second one with the transmitted signal of (8.313) as the F-preprocessing. Let us now analyse their received signal forms.

8.3.2 Representation of the Received Signal

When assuming that each subcarrier signal experiences flat slow fading, the received signal at the k th MT can be expressed as

$$r_k(t) = \sum_{n=1}^{N_p} h_n^{(k)} d_n(t) \exp(j2\pi f_n t) + n_k(t), \quad k = 1, 2, \dots, \mathcal{K} \quad (8.314)$$

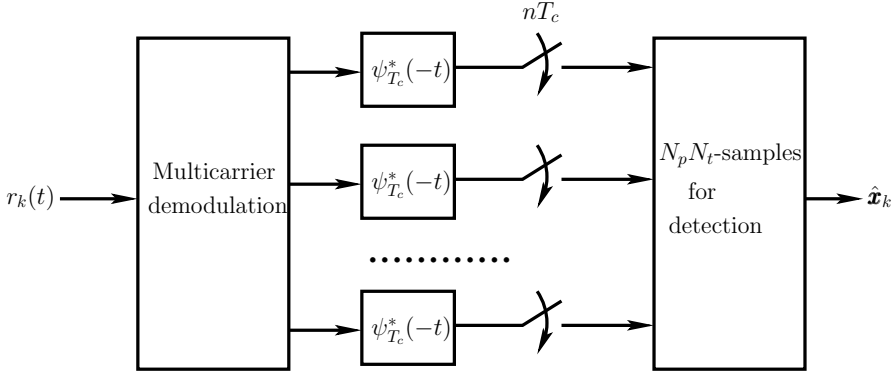


Figure 8.21: Receiver block diagram of the k th MT.

for the MC DS-CDMA using the TF-preprocessing, while

$$r_k(t) = \sum_{n=1}^{N_p} \sum_{l=1}^{\mathcal{K}} h_n^{(k)} s_{pn}^{(l)} c_l(t) \exp(j2\pi f_n t) + n_k(t), \quad k = 1, 2, \dots, \mathcal{K} \quad (8.315)$$

for the MC DS-CDMA using the F-preprocessing. In both (8.314) and (8.315) $h_n^{(k)}$ represents the fading gain of the n th subcarrier channel with respect to the k th MT. It is assumed that $E[h_n^{(k)}] = 0$ and $E[|h_n^{(k)}|^2] = 1$. In both (8.314) and (8.315) $n_k(t)$ represents the AWGN noise with zero mean and a single-sided PSD of $\sigma_s^2/2 = N_0/2E_s = 1/2\text{SNR}$ per dimension, where E_s represents the energy per symbol and SNR is the SNR per symbol.

The receiver structures for both the preprocessing schemes are the same, as shown in Fig. 8.21. In detail, first, multicarrier demodulation is carried out to recover the N_p branches corresponding to the N_p subcarriers. Then, corresponding to each of the N_p branches the carrierless signal is input to a filter matched to the transmitted chip waveform. The filter output is sampled at the chip rate, providing N_t observation samples per branch per symbol duration. Hence, the k th MT can obtain a total of $N_p N_t$ observation samples for detecting its data. We assume that the detection scheme at the MTs is low-complexity. Specifically, the data transmitted to the k th MT are recovered by despreading the $N_p N_t$ observations in both the T-domain and F-domain in order to form the decision variables for decision making.

In mathematical description, the output of the chip matched filters can be expressed as

$$\begin{aligned} r_{nm}^{(k)} &= \frac{1}{T_c} \int_{(m-1)T_c}^{mT_c} r_k(t) \psi_{T_c}^*(t - (m-1)T_c) \exp(-j2\pi f_n t) dt \\ m &= 1, 2, \dots, N_t; \quad n = 1, 2, \dots, N_p \end{aligned} \quad (8.316)$$

Substituting (8.314) into the above equation and bearing in mind that the subcarrier signals are orthogonal, it can be shown that for the TF-preprocessing scheme we have

$$r_{nm}^{(k)} = h_n^{(k)} d_{nm} + N_{nm}^{(k)}, \quad m = 1, 2, \dots, N_t; \quad n = 1, 2, \dots, N_p \quad (8.317)$$

where

$$N_{nm}^{(k)} = \frac{1}{T_c} \int_{(m-1)T_c}^{mT_c} n_k(t) \psi_{T_c}^*(t - (m-1)T_c) \exp(-j2\pi f_n t) dt \quad (8.318)$$

is the Gaussian noise sample, which has zero mean and a variance of $\sigma_s^2/2$ per dimension. Furthermore, it can be shown that $N_{nm}^{(k)}$ is independent in terms of the indices n, m and k .

Similarly, when substituting (8.315) into (8.316) and remembering that the subcarrier signals are orthogonal, it can be shown that for the F-preprocessing scheme, we have

$$\begin{aligned} r_{nm}^{(k)} &= \frac{1}{\sqrt{N_t}} \sum_{l=1}^{\mathcal{K}} h_n^{(k)} s_{pn}^{(l)} c_{lm} + N_{nm}^{(k)} \\ &= h_n^{(k)} s_{pn}^{(l)} \times \frac{1}{\sqrt{N_t}} \sum_{l=1}^{\mathcal{K}} c_{lm} + N_{nm}^{(k)} \\ m &= 1, 2, \dots, N_t; n = 1, 2, \dots, N_p \end{aligned} \quad (8.319)$$

In the context of the TF-domain spread MC DS-CDMA using the TF-preprocessing, let us define

$$\begin{aligned} \mathbf{r}^{(k)} &= [r_{11}^{(k)}, \dots, r_{1N_t}^{(k)}; \dots; r_{N_p 1}^{(k)}, \dots, r_{N_p N_t}^{(k)}]^T \\ \mathbf{n}^{(k)} &= [N_{11}^{(k)}, \dots, N_{1N_t}^{(k)}; \dots; N_{N_p 1}^{(k)}, \dots, N_{N_p N_t}^{(k)}]^T \\ \mathbf{H}^{(k)} &= \text{diag}\{\mathbf{I}_{N_t} \otimes h_1^{(k)}, \mathbf{I}_{N_t} \otimes h_2^{(k)}, \dots, \mathbf{I}_{N_t} \otimes h_{N_p}^{(k)}\} \end{aligned} \quad (8.320)$$

Then, we can express $\mathbf{r}^{(k)}$ as

$$\mathbf{r}^{(k)} = \mathbf{H}^{(k)} \mathbf{d} + \mathbf{n}^{(k)}, \quad k = 1, 2, \dots, \mathcal{K} \quad (8.321)$$

When substituting \mathbf{d} from (8.304) into the above equation, we obtain

$$\mathbf{r}^{(k)} = \mathbf{H}^{(k)} \bar{\mathbf{P}} \mathbf{x} + \mathbf{n}^{(k)}, \quad k = 1, 2, \dots, \mathcal{K} \quad (8.322)$$

In the context of the TF-domain spread MC DS-CDMA using the F-preprocessing, since the T-domain spreading codes assigned to different MTs are orthogonal, the MT receivers can first despread the received signal in the T-domain, in order to remove those multiuser signals having their T-domain spreading codes that are different from the k th MT's. Hence, after the despreading and applying (8.319), we obtain

$$\begin{aligned} r_n^{(k)} &= \frac{1}{\sqrt{N_t}} \sum_{m=1}^{N_t} c_{km} r_{nm}^{(k)} \\ &= \sum_{l=1}^{\mathcal{K}} h_n^{(k)} s_{pn}^{(l)} + N_n^{(k)}, \quad n = 1, 2, \dots, N_p; k = 1, 2, \dots, K \end{aligned} \quad (8.323)$$

where $K = \mathcal{K}/N_t$ is the number of MTs sharing the same T-domain spreading code. Since there is no interference from the other MTs, whose T-domain spreading codes are different

from that of MT k , explicitly, the transmitter preprocessing for MT k only needs to consider those MTs sharing the same T-domain spreading code of the k th MT. Therefore, only the K MTs sharing the same T-domain spreading code will be considered here. In (8.323), the noise term is given by

$$N_n^{(k)} = \frac{1}{\sqrt{N_t}} \sum_{m=1}^{N_t} c_{km} N_{nm}^{(k)}$$

which is still a Gaussian random variable and is independent in terms of the indices n and k .

Let us define

$$\begin{aligned}\underline{\mathbf{r}}^{(k)} &= [r_1^{(k)}, r_2^{(k)}, \dots, r_{N_p}^{(k)}]^T \\ \underline{\mathbf{H}}^{(k)} &= \text{diag}\{h_1^{(k)}, h_2^{(k)}, \dots, h_{N_p}^{(k)}\} \\ \underline{\mathbf{n}}^{(k)} &= [N_1^{(k)}, N_2^{(k)}, \dots, N_{N_p}^{(k)}]^T\end{aligned}\quad (8.324)$$

Then, with the aid of (8.310), it can be shown that for the F-preprocessing scheme we have

$$\begin{aligned}\underline{\mathbf{r}}^{(k)} &= \underline{\mathbf{H}}^{(k)} \sum_{l=1}^K s_p^{(l)} + \underline{\mathbf{n}}^{(k)} \\ &= \underline{\mathbf{H}}^{(k)} \sum_{l=1}^K \bar{\mathbf{P}}_k \mathbf{x}_k + \underline{\mathbf{n}}^{(k)} \\ &= \underline{\mathbf{H}}^{(k)} \underline{\mathbf{P}} \underline{\mathbf{x}} + \underline{\mathbf{n}}^{(k)}\end{aligned}\quad (8.325)$$

where, by definition, we have

$$\begin{aligned}\underline{\mathbf{P}} &= [\bar{\mathbf{P}}_1, \bar{\mathbf{P}}_2, \dots, \bar{\mathbf{P}}_K] \\ \underline{\mathbf{x}} &= [\mathbf{x}_1^T, \mathbf{x}_2^T, \dots, \mathbf{x}_K^T]^T\end{aligned}\quad (8.326)$$

where $\underline{\mathbf{P}}$ is a $(N_p \times KU)$ matrix, while $\underline{\mathbf{x}}$ is a KU -length column vector.

Finally, for the TF-preprocessing, based on the observation vector (8.322), the k th MT forms its decision variable vector by carrying out the despreading operations in both the T-domain and F-domain using its T-domain and F-domain spreading codes. When considering jointly the T-domain and F-domain despreading, the decision variable vector for the k th MT can be expressed as

$$\mathbf{y}_k = (\mathbf{C}^{(k)})^T \underline{\mathbf{H}}^{(k)} \bar{\mathbf{P}} \underline{\mathbf{x}} + \mathbf{n}_k, \quad k = 1, 2, \dots, \mathcal{K} \quad (8.327)$$

where \mathbf{y}_k is the U -length decision variable vector, $\mathbf{C}^{(k)}$ is given by (8.300) and

$$(\mathbf{C}^{(k)})^T = (\mathbf{C}_f^{(k)})^T (\mathbf{I}_{N_p} \otimes \mathbf{c}_k^T) \quad (8.328)$$

Hence, the MT receivers first carry out the T-domain despreading and then the F-domain despreading. Furthermore, in (8.327)

$$\mathbf{n}_k = (\mathbf{C}^{(k)})^T \underline{\mathbf{n}}^{(k)}, \quad k = 1, 2, \dots, \mathcal{K} \quad (8.329)$$

which is a Gaussian noise vector having zero mean and its covariance matrix can be expressed as

$$\begin{aligned}\mathbf{R}_n^{(k)} &= E[\mathbf{n}_k \mathbf{n}_k^H] = E[(\mathbf{C}^{(k)})^T \mathbf{n}^{(k)} (\mathbf{n}^{(k)})^H \mathbf{C}^{(k)}] \\ &= \sigma_s^2 \mathbf{R}_c^{(k)}, \quad k = 1, 2, \dots, K\end{aligned}\quad (8.330)$$

where $\mathbf{R}_c^{(k)}$ is given by

$$\begin{aligned}\mathbf{R}_c^{(k)} &= (\mathbf{C}^{(k)})^T \mathbf{C}^{(k)} \\ &= (\mathbf{C}_f^{(k)})^T (\mathbf{I}_{N_p} \otimes \mathbf{c}_k^T) (\mathbf{I}_{N_p} \otimes \mathbf{c}_k) \mathbf{C}_f^{(k)} \\ &= (\mathbf{C}_f^{(k)})^T (\mathbf{I}_{N_p} \otimes \mathbf{c}_k^T \mathbf{c}_k) \mathbf{C}_f^{(k)} \\ &= (\mathbf{C}_f^{(k)})^T \mathbf{C}_f^{(k)}, \quad k = 1, 2, \dots, K\end{aligned}\quad (8.331)$$

which is the $(U \times U)$ cross-correlation matrix of the F-domain spreading codes assigned to the k th MT. From (8.329) to (8.331), we know that the noise samples in \mathbf{n}_k are coloured and correlated if the F-domain spreading codes assigned to one MT are not orthogonal. In this case the noise covariance matrix is given by (8.330). If the F-domain spreading codes assigned to one MT are orthogonal, then the noise samples in \mathbf{n}_k are white and independent. In this case, $\mathbf{R}_c^{(k)} = \mathbf{I}_U$ and the corresponding noise covariance matrix can be expressed as

$$\mathbf{R}_n^{(k)} = \sigma_s^2 \mathbf{I}_U, \quad k = 1, 2, \dots, K \quad (8.332)$$

Let us define

$$\begin{aligned}\mathbf{y} &= [\mathbf{y}_1^T, \mathbf{y}_2^T, \dots, \mathbf{y}_K^T]^T \\ \mathbf{n} &= [\mathbf{n}_1^T, \mathbf{n}_2^T, \dots, \mathbf{n}_K^T]^T\end{aligned}\quad (8.333)$$

Then, when collecting all the MTs' decision variable vectors into \mathbf{y} , we obtain

$$\mathbf{y} = \mathbf{C}^T \mathbf{H} \bar{\mathbf{P}} \mathbf{x} + \mathbf{n} \quad (8.334)$$

where

$$\begin{aligned}\mathbf{C} &= \text{diag}\{\mathbf{C}^{(1)}, \mathbf{C}^{(2)}, \dots, \mathbf{C}^{(K)}\} \\ \mathbf{H} &= [(\mathbf{H}^{(1)})^T, (\mathbf{H}^{(2)})^T, \dots, (\mathbf{H}^{(K)})^T]^T\end{aligned}\quad (8.335)$$

In the context of the TF-domain spread MC DS-CDMA system using F-preprocessing, after the F-domain despreading, the k th MT's decision variable vector can be expressed as

$$\begin{aligned}\underline{\mathbf{y}}_k &= (\mathbf{C}_f^{(k)})^T \underline{\mathbf{r}}^{(k)} \\ &= (\mathbf{C}_f^{(k)})^T \underline{\mathbf{H}}^{(k)} \underline{\mathbf{P}} \mathbf{x} + \underline{\mathbf{n}}_k, \quad k = 1, 2, \dots, K\end{aligned}\quad (8.336)$$

where $\underline{\mathbf{y}}_k$ is a U -length vector and $\underline{\mathbf{n}}_k$ is given by

$$\underline{\mathbf{n}}_k = (\mathbf{C}_f^{(k)})^T \underline{\mathbf{n}}^{(k)} \quad (8.337)$$

which is also a zero-mean Gaussian vector having the covariance matrix given by (8.330). Hence, the elements of \underline{n}_k are independent only when the F-domain spreading codes assigned to one MT are orthogonal.

Again let us define

$$\begin{aligned}\underline{y} &= [\underline{y}_1^T, \underline{y}_2^T, \dots, \underline{y}_K^T]^T \\ \underline{n} &= [\underline{n}_1^T, \underline{n}_2^T, \dots, \underline{n}_K^T]^T\end{aligned}\quad (8.338)$$

Then, when collecting all the decision variables into \underline{y} , it can be expressed as

$$\underline{y} = \underline{C}^T \underline{H} \underline{P} \underline{x} + \underline{n} \quad (8.339)$$

where we have defined

$$\begin{aligned}\underline{C} &= \text{diag}\{\underline{C}_f^{(1)}, \underline{C}_f^{(2)}, \dots, \underline{C}_f^{(K)}\} \\ \underline{H} &= [(\underline{H}^{(1)})^T, (\underline{H}^{(2)})^T, \dots, (\underline{H}^{(K)})^T]^T\end{aligned}\quad (8.340)$$

Above, the representations for the TF-domain spread MC DS-CDMA systems using either the TF-preprocessing or the F-preprocessing have been derived, as shown in (8.334) and (8.339), respectively. Comparing (8.334) with (8.339), it can be found that both the preprocessing related MIMO equations have the same structure and properties, except the size difference. Hence, in the next section the preprocessing is considered only in the context of the TF-domain spread MC DS-CDMA systems using TF-preprocessing, which has the MIMO representation of (8.334). The obtained results can be directly converted to the TF-domain spread MC DS-CDMA systems using the F-preprocessing by replacing the corresponding matrices.

Furthermore, when comparing the MIMO equation of (8.46) for the F-domain spread MC-CDMA with the MIMO equation (8.334) of the TF-domain spread MC DS-CDMA, their structures are also the same. Hence, all the preprocessing matrices derived based on (8.46) in the previous sections can be directly applied for the transmitter preprocessing in the TF-domain spread MC DS-CDMA system, if the noise samples are white and independent Gaussian noise. However, if the F-domain spreading codes assigned to a MT are not orthogonal, then the noise samples from that MT are correlated. In this case the preprocessing matrices for the TF-domain spread MC DS-CDMA may be different from that derived in the previous sections. Hence, in the forthcoming discourse the transmitter preprocessing for the TF-domain spread MC DS-CDMA is studied in the context of several typical preprocessing schemes, when assuming that the F-domain spreading codes assigned to one MT are correlated.

8.3.3 Minimum Mean-Square Error Multiuser Transmitter Preprocessing

In Section 8.2.5 we showed that both the MF-SUTP and the ZF-MUTP constitute the special examples of the MMSE-MUTP. Hence, in this section we derive preprocessing matrix in the TF-domain spread MC DS-CDMA, when the MMSE-MUTP is considered. The preprocessing matrices for the MF-SUTP and ZF-MUTP are then directly given from modifying the preprocessing matrix for the MMSE-MUTP.

The derivation starts with (8.327), which is given by

$$\mathbf{y}_k = (\mathbf{C}^{(k)})^T \mathbf{H}^{(k)} \bar{\mathbf{P}} \mathbf{x} + \mathbf{n}_k, \quad k = 1, 2, \dots, \mathcal{K} \quad (8.341)$$

where \mathbf{n}_k is Gaussian but is correlated and has the covariance matrix given by (8.330). In order for the transmitter preprocessing to invoke the noise variance in the preprocessing matrix, so that it has the potential to suppress the noise signals presenting at the remote MTs, we carry out the *Cholesky factorization* [88, 156] on the cross-correlation matrix $\mathbf{R}_c^{(k)}$, which gives

$$\mathbf{R}_c^{(k)} = \mathbf{F}_k \mathbf{F}_k^H \quad (8.342)$$

where \mathbf{F}_k is a lower triangular matrix with positive diagonal elements. If we process \mathbf{y}_k by the matrix \mathbf{F}_k^{-1} , we obtain an equivalent equation for the decision variable vector, which can be expressed as

$$\begin{aligned} \bar{\mathbf{y}}_k &= \mathbf{F}_k^{-1} \mathbf{y}_k = \mathbf{F}_k^{-1} (\mathbf{C}^{(k)})^T \mathbf{H}^{(k)} \bar{\mathbf{P}} \mathbf{x} + \mathbf{F}_k^{-1} \mathbf{n}_k \\ &= \mathbf{F}_k^{-1} (\mathbf{C}^{(k)})^T \mathbf{H}^{(k)} \bar{\mathbf{P}} \mathbf{x} + \bar{\mathbf{n}}_k, \quad k = 1, 2, \dots, \mathcal{K} \end{aligned} \quad (8.343)$$

where

$$\bar{\mathbf{n}}_k = \mathbf{F}_k^{-1} \mathbf{n}_k, \quad k = 1, 2, \dots, \mathcal{K} \quad (8.344)$$

The covariance matrix of $\bar{\mathbf{n}}_k$ can be expressed as

$$\begin{aligned} E[\bar{\mathbf{n}}_k \bar{\mathbf{n}}_k^H] &= E[\mathbf{F}_k^{-1} \mathbf{n}_k \mathbf{n}_k^H \mathbf{F}_k^{-H}] \\ &= \mathbf{F}_k^{-1} [\mathbf{n}_k \mathbf{n}_k^H] \mathbf{F}_k^{-H} \\ &= \sigma_s^2 \mathbf{F}_k^{-1} \mathbf{R}_c^{(k)} \mathbf{F}_k^{-H} \\ &= \sigma_s^2 \mathbf{I}_U \end{aligned} \quad (8.345)$$

Therefore, $\bar{\mathbf{n}}_k$ is now white and its elements are independent. Hence, the operation in (8.343) is usually referred to as noise whitening.

Let us define

$$\begin{aligned} \bar{\mathbf{y}} &= [\bar{\mathbf{y}}_1^T, \bar{\mathbf{y}}_2^T, \dots, \bar{\mathbf{y}}_{\mathcal{K}}^T]^T \\ \bar{\mathbf{n}} &= [\bar{\mathbf{n}}_1^T, \bar{\mathbf{n}}_2^T, \dots, \bar{\mathbf{n}}_{\mathcal{K}}^T]^T \\ \mathbf{F} &= \text{diag}\{\mathbf{F}_1, \mathbf{F}_2, \dots, \mathbf{F}_{\mathcal{K}}\} \end{aligned} \quad (8.346)$$

Then, we obtain a whitened representation

$$\bar{\mathbf{y}} = \mathbf{F}^{-1} \mathbf{C}^T \mathbf{H} \bar{\mathbf{P}} \mathbf{x} + \bar{\mathbf{n}} \quad (8.347)$$

based on which we can now derive the preprocessing matrix under the MMSE criterion.

As in Section 8.2.5 the preprocessing matrix $\bar{\mathbf{P}}$ can be obtained by minimizing the MSE between $\bar{\mathbf{y}}$ and \mathbf{x} under the constraint on the transmission power, which can be formed as

$$\begin{aligned} \bar{\mathbf{P}} &= \arg \min_{E[\|\bar{\mathbf{P}} \mathbf{x}\|^2] = E[\|\mathbf{x}\|^2]} E[\|\mathbf{x} - \bar{\mathbf{y}}\|^2] \\ &= \arg \min_{E[\|\bar{\mathbf{P}} \mathbf{x}\|^2] = E[\|\mathbf{x}\|^2]} E[\|\mathbf{x} - \mathbf{F}^{-1} \mathbf{C}^T \mathbf{H} \bar{\mathbf{P}} \mathbf{x} - \bar{\mathbf{n}}\|^2] \end{aligned} \quad (8.348)$$

Following the approaches in Section 8.2.5, it can be shown that the preprocessing matrix $\bar{\mathbf{P}}$ for the MMSE-MUTP can be represented as

$$\bar{\mathbf{P}} = [\mathbf{H}^H \mathbf{C} \mathbf{F}^{-H} \mathbf{F}^{-1} \mathbf{C}^T \mathbf{H} + \rho \sigma_s^2 \mathbf{I}_{N_p N_t}]^{-1} \mathbf{H}^H \mathbf{C} \mathbf{F}^{-H} \boldsymbol{\beta} \quad (8.349)$$

where $\boldsymbol{\beta}$ is for achieving the constraint on the transmission power; this will be discussed in detail in Section 8.3.5.

When invoking the *matrix inverse lemma*, the preprocessing matrix in the MMSE-MUTP for the TF-domain spread MC DS-CDMA can also be expressed as

$$\bar{\mathbf{P}} = \mathbf{H}^H \mathbf{C} \mathbf{F}^{-H} [\mathbf{F}^{-1} \mathbf{C}^T \mathbf{H} \mathbf{H}^H \mathbf{C} \mathbf{F}^{-H} + \rho \sigma_s^2 \mathbf{I}_{K_U}]^{-1} \boldsymbol{\beta} \quad (8.350)$$

Having obtained the preprocessing matrix $\bar{\mathbf{P}}$ for the MMSE-MUTP, the corresponding preprocessing matrix for the MF-SUTP and ZF-MUTP can be easily obtained. Specifically, the preprocessing matrix for the MF-SUTP can be obtained from (8.350) by letting $\rho \rightarrow \infty$, which, after absorbing the constant terms into the power normalization matrix $\boldsymbol{\beta}$, yields

$$\bar{\mathbf{P}} = \mathbf{H}^H \mathbf{C} \mathbf{F}^{-H} \boldsymbol{\beta} \quad (8.351)$$

When the preprocessing does not care about the correlation between the noise samples at the MT's receivers, the preprocessing can be built based on (8.334) and the corresponding preprocessing matrix for the MF-SUTP can be further simplified to

$$\bar{\mathbf{P}} = \mathbf{H}^H \mathbf{C} \boldsymbol{\beta} \quad (8.352)$$

In the context of the ZF-MUTP, the preprocessing matrix can be obtained from (8.350) by letting $\rho = 0$, which gives

$$\bar{\mathbf{P}} = \mathbf{H}^H \mathbf{C} \mathbf{F}^{-H} (\mathbf{F}^{-1} \mathbf{C}^T \mathbf{H} \mathbf{H}^H \mathbf{C} \mathbf{F}^{-H})^{-1} \boldsymbol{\beta} \quad (8.353)$$

Since \mathbf{F} and $\mathbf{C}^T \mathbf{H} \mathbf{H}^H \mathbf{C}$ are invertible, we have

$$\begin{aligned} \bar{\mathbf{P}} &= \mathbf{H}^H \mathbf{C} \mathbf{F}^{-H} \mathbf{F}^H (\mathbf{C}^T \mathbf{H} \mathbf{H}^H \mathbf{C})^{-1} \mathbf{F} \boldsymbol{\beta} \\ &= \mathbf{H}^H \mathbf{C} (\mathbf{C}^T \mathbf{H} \mathbf{H}^H \mathbf{C})^{-1} \mathbf{F} \boldsymbol{\beta} \end{aligned} \quad (8.354)$$

Again, it can be easily shown that, when the preprocessing for the ZF-MUTP is built on (8.334), the corresponding preprocessing matrix can be expressed as

$$\bar{\mathbf{P}} = \mathbf{H}^H \mathbf{C} (\mathbf{C}^T \mathbf{H} \mathbf{H}^H \mathbf{C})^{-1} \boldsymbol{\beta} \quad (8.355)$$

However, in this case the noise samples of a given user may be correlated.

Below, we investigate in detail the characteristics of the TF-domain spread MC DS-CDMA, when it employs the above-derived MF-SUTP, ZF-MUTP or MMSE-MUTP, which has the preprocessing matrix of (8.351), (8.354) or (8.350), respectively.

8.3.3.1 Matched Filtering

When substituting (8.351) into (8.343), the decision variable vector for the k th MT can be expressed as

$$\bar{\mathbf{y}}_k = \mathbf{F}_k^{-1} (\mathbf{C}^{(k)})^T \mathbf{H}^{(k)} \mathbf{H}^H \mathbf{C} \mathbf{F}^{-H} \boldsymbol{\beta} \mathbf{x} + \bar{\mathbf{n}}_k \quad (8.356)$$

After applying \mathbf{C} and \mathbf{H} from (8.335) as well as \mathbf{F} from (8.346) into the above equation, we have

$$\begin{aligned}\bar{\mathbf{y}}_k &= \mathbf{F}_k^{-1}(\mathbf{C}^{(k)})^T \mathbf{H}^{(k)} \sum_{l=1}^{\mathcal{K}} (\mathbf{H}^{(l)})^H \mathbf{C}^{(l)} \mathbf{F}_l^{-H} \boldsymbol{\beta}_l \mathbf{x}_l + \bar{\mathbf{n}}_k \\ &= \mathbf{F}_k^{-1}(\mathbf{C}^{(k)})^T \mathbf{H}^{(k)} (\mathbf{H}^{(k)})^H \mathbf{C}^{(k)} \mathbf{F}_k^{-H} \boldsymbol{\beta}_k \mathbf{x}_k \\ &\quad + \underbrace{\mathbf{F}_k^{-1}(\mathbf{C}^{(k)})^T \mathbf{H}^{(k)} \sum_{l \neq k}^{\mathcal{K}} (\mathbf{H}^{(l)})^H \mathbf{C}^{(l)} \mathbf{F}_l^{-H} \boldsymbol{\beta}_l \mathbf{x}_l}_{\mathbf{I}_{MUI}} + \bar{\mathbf{n}}_k\end{aligned}\quad (8.357)$$

where we expressed $\boldsymbol{\beta} = \text{diag}\{\boldsymbol{\beta}_1, \boldsymbol{\beta}_2, \dots, \boldsymbol{\beta}_{\mathcal{K}}\}$. Since

$$\mathbf{H}^{(k)}(\mathbf{H}^{(k)})^H = \text{diag}\{\mathbf{I}_{N_t} \otimes |h_1^{(k)}|^2, \mathbf{I}_{N_t} \otimes |h_2^{(k)}|^2, \dots, \mathbf{I}_{N_t} \otimes |h_{N_p}^{(k)}|^2\} \quad (8.358)$$

we have

$$\begin{aligned}\mathcal{R}_k &= (\mathbf{C}^{(k)})^T \mathbf{H}^{(k)} (\mathbf{H}^{(k)})^H \mathbf{C}^{(k)} \\ &= (\mathbf{C}_f^{(k)})^T \mathbf{M} \mathbf{C}_f^{(k)}\end{aligned}\quad (8.359)$$

where, by definition, \mathbf{M} is a diagonal matrix given by

$$\mathbf{M} = \text{diag}\{|h_1^{(k)}|^2, |h_2^{(k)}|^2, \dots, |h_{N_p}^{(k)}|^2\} \quad (8.360)$$

Furthermore, according to (8.296), it can be shown that

$$\mathcal{R}_k(i, j) = \begin{cases} \frac{1}{N_p} \sum_{n=1}^{N_p} |h_n^{(k)}|^2 & \text{if } i = j \\ \frac{1}{N_p} \sum_{n=1}^{N_p} c_{fi,n}^{(k)} c_{fj,n}^{(k)} |h_n^{(k)}|^2 & \text{otherwise} \end{cases} \quad (8.361)$$

Hence, (8.357) can be expressed as

$$\bar{\mathbf{y}}_k = \mathbf{F}_k^{-1} \mathcal{R}_k \mathbf{F}_k^{-H} \boldsymbol{\beta}_k \mathbf{x}_k + \mathbf{I}_{MUI} + \bar{\mathbf{n}}_k \quad (8.362)$$

where \mathbf{I}_{MUI} represents the MUI.

Since the inverse of a lower triangular matrix is also a lower triangular matrix, we can express \mathbf{F}_k^{-1} as

$$\mathbf{F}_k^{-1} = \mathbf{L} = \begin{bmatrix} l_{11} & 0 & \cdots & 0 \\ l_{21} & l_{22} & \cdots & 0 \\ \vdots & \vdots & \ddots & \vdots \\ l_{U1} & l_{U2} & \cdots & l_{UU} \end{bmatrix} \quad (8.363)$$

Then, it can be shown that

$$\mathbf{F}_k^{-H} \boldsymbol{\beta}_k \mathbf{x}_k = \begin{bmatrix} \sum_{m=1}^U l_{m1}^* \beta_{km} x_{km} \\ \sum_{m=2}^U l_{m2}^* \beta_{km} x_{km} \\ \vdots \\ l_{(U-1)(U-1)}^* \beta_{k(U-1)} x_{k(U-1)} + l_{U(U-1)}^* \beta_{kU} x_{kU} \\ l_{UU}^* \beta_{kU} x_{kU} \end{bmatrix} \quad (8.364)$$

Therefore, the decision variables for the symbols in \mathbf{x}_k can be expressed in detail as

$$\bar{y}_{kj} = \sum_{u=1}^U \left(\sum_{n=1}^j l_{jn} \mathcal{R}_k(j, u) \right) \left(\sum_{m=u}^U l_{mu}^* \beta_{km} x_{km} \right) + \mathbf{I}_{MUI}(j) + \bar{\mathbf{n}}_k(j), \quad j = 1, 2, \dots, U \quad (8.365)$$

where $\mathbf{I}_{MUI}(j)$ denotes the j th entry of \mathbf{I}_{MUI} . When decomposing the above equation into the desired term and interference terms, we can express it as

$$\bar{y}_{kj} = |l_{jj}|^2 \mathcal{R}_k(j, j) \beta_{kj} x_{kj} + I_{SI}(j) + \mathbf{I}_{MUI}(j) + \bar{\mathbf{n}}_k(j), \quad j = 1, 2, \dots, U \quad (8.366)$$

where $I_{SI}(j)$ represents the interference from the k th MT itself, which can be expressed as

$$\begin{aligned} I_{SI}(j) &= \left(\sum_{n=1}^{j-1} l_{jn} \mathcal{R}_k(j, j) \right) \left(\sum_{m=j+1}^U l_{mu}^* \beta_{km} x_{km} \right) \\ &\quad + \sum_{u \neq j}^U \left(\sum_{n=1}^j l_{jn} \mathcal{R}_k(j, u) \right) \left(\sum_{m=u}^U l_{mu}^* \beta_{km} x_{km} \right) \end{aligned} \quad (8.367)$$

Finally, when applying (8.361) to (8.366), the decision variables for the symbols transmitted to the k th MT can be expressed as

$$\bar{y}_{kj} = \left(\frac{1}{N_p} \sum_{n=1}^{N_p} |h_n^{(k)}|^2 \right) \times |l_{jj}|^2 \beta_{kj} x_{kj} + I_{SI}(j) + \mathbf{I}_{MUI}(j) + \bar{\mathbf{n}}_k(j), \quad j = 1, 2, \dots, U \quad (8.368)$$

which shows that a diversity order of N_p can be achieved by the TF-domain spread MC DS-CDMA using the MF-SUTP.

Another way to express the decision variables of the k MT can be obtained by first expressing $\mathbf{C}_f^{(k)}$ using the QR-decomposition as

$$\mathbf{C}_f^{(k)} = \mathbf{Q}_k \mathbf{F}_k^H \quad (8.369)$$

where \mathbf{Q}_k is an $(N_p \times U)$ orthonormal matrix. In this case we have

$$\mathcal{R}_k = (\mathbf{C}_f^{(k)})^H \mathbf{M} \mathbf{C}_f^{(k)} = \mathbf{F}_k \mathbf{Q}_k^H \mathbf{M} \mathbf{Q}_k \mathbf{F}_k^H \quad (8.370)$$

Hence, the decision variables in (8.362) can be expressed as

$$\begin{aligned}\bar{\mathbf{y}}_k &= \mathbf{F}_k^{-1} \mathbf{F}_k \mathbf{Q}_k^H \mathbf{M} \mathbf{Q}_k \mathbf{F}_k^H \mathbf{F}_k^{-H} \boldsymbol{\beta}_k \mathbf{x}_k + \mathbf{I}_{MUI} + \bar{\mathbf{n}}_k \\ &= \mathbf{Q}_k^H \mathbf{M} \mathbf{Q}_k \boldsymbol{\beta}_k \mathbf{x}_k + \mathbf{I}_{MUI} + \bar{\mathbf{n}}_k\end{aligned}\quad (8.371)$$

Let $\mathbf{Q}_k = [q_{ij}]$. Then we have

$$\begin{aligned}\bar{y}_{kj} &= \left(\sum_{n=1}^{N_p} |q_{nj}|^2 |h_n^{(k)}|^2 \right) \beta_{kj} x_{kj} + \underbrace{\sum_{l \neq j}^U \left(\sum_{n=1}^{N_p} q_{nj}^* q_{nl} |h_n^{(k)}|^2 \right) \beta_{kl} x_{kl}}_{I_{SI}(j)} \\ &\quad + \mathbf{I}_{MUI}(j) + \bar{\mathbf{n}}_k(j), \quad j = 1, 2, \dots, U\end{aligned}\quad (8.372)$$

Again, it is shown that a diversity order of N_p can be achieved by the TF-domain spread MC DS-CDMA using the MF-SUTP.

Note that when communicating over AWGN channels having $h_n^{(k)} = 1$ for $n = 1, 2, \dots, N_p$, then \mathcal{R}_k in (8.359) is given by

$$\mathcal{R}_k = (\mathbf{C}_f^{(k)})^T \mathbf{C}_f^{(k)} = \mathcal{R}_c^{(k)} = \mathbf{F}_k \mathbf{F}_k^H \quad (8.373)$$

Applying it to (8.362), we obtain the decision variables for the TF-domain spread MC DS-CDMA communicating over AWGN channels, which is

$$\bar{\mathbf{y}}_k = \boldsymbol{\beta}_k \mathbf{x}_k + \mathbf{I}_{MUI} + \bar{\mathbf{n}}_k, \quad k = 1, 2, \dots, K \quad (8.374)$$

which is free from the self-interference from a MT itself. Hence, the whitening processing at a MT can assist the transmitter preprocessing to suppress the interference from the MT itself, when communicating over AWGN channels.

The BER performance of the TF-domain spread MC DS-CDMA using the MF-MUTP is shown in Fig. 8.22, when communicating over frequency-selective Rayleigh fading channels having $L = 8$ T-domain resolvable paths. The details of the parameters used in the simulations can be found in the figure. As shown in Fig. 8.22, the BER performance degrades significantly when the system supports more users. The BER floors observed in Fig. 8.22 reflect that the MF-MUTP is unable to mitigate the downlink MUI.

8.3.3.2 Zero-Forcing

The decision variables in the TF-domain spread MC DS-CDMA using the ZF-MUTP can be obtained by substituting (8.354) into (8.347), which yields

$$\bar{\mathbf{y}} = \boldsymbol{\beta} \mathbf{x} + \bar{\mathbf{n}} \quad (8.375)$$

Explicitly, the preprocessing of the ZF-MUTP fully removes the downlink MUI and makes the decision variables have the Gaussian distributions, which are conditioned on $\boldsymbol{\beta}$. Therefore, as shown in Section 8.3.5, the performance of the TF-domain spread MC DS-CDMA systems using the ZF-MUTP is dependent on the specific power normalization scheme applied.

Figures 8.23 and 8.24 show the BER performance of the TF-domain spread MC DS-CDMA using the ZF-MUTP, when communicating over frequency-selective Rayleigh fading

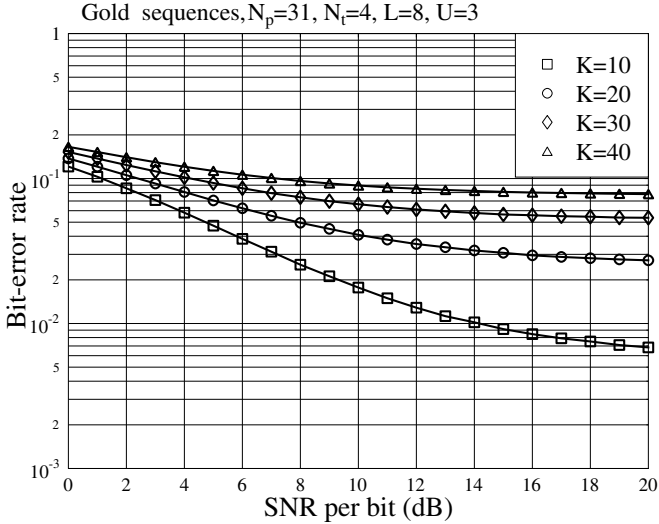


Figure 8.22: BER performance of the TF-domain spread MC DS-CDMA using the MF-MUTP, when communicating over frequency-selective Rayleigh fading channels having $L = 8$ T-domain resolvable paths. The simulations were based on the preprocessing matrix (8.351) associated with using the joint power normalization.

channels having $L = 8$ T-domain resolvable paths. In the simulations for Fig. 8.23, it was assumed that both the T-domain and F-domain spreading sequences were constituted of random sequences. However, due to the problem with the simulations, constraint was added to the generation of the F-domain random sequences. Specifically, only those randomly generated sequences yielding $\mathbf{R}_c^{(k)}$ for $k = 1, 2, \dots, K$ full-rank were simulated. By contrast, in the simulations for Fig. 8.24, it was assumed that the T-domain spreading sequences were orthogonal sequences, while the F-domain spreading sequences were Gold-sequences. In comparison with Fig. 8.22 for the MF-MUTP, we can see that the ZF-MUTP outperforms significantly the MF-MUTP. However, for any given number of users of $K > 1$, the TF-domain spread MC DS-CDMA using T-domain orthogonal sequences and F-domain Gold-sequences is much better than that using random sequences for both the T-domain and F-domain spreading.

8.3.3.3 Minimum Mean-Square Error

After substituting (8.350) into (8.347) the decision variable vector for the TF-domain spread MC DS-CDMA using the MMSE-MUTP can be expressed as

$$\bar{\mathbf{y}} = \mathbf{F}^{-1} \mathbf{C}^T \mathbf{H} \mathbf{H}^H \mathbf{C} \mathbf{F}^{-H} [\mathbf{F}^{-1} \mathbf{C}^T \mathbf{H} \mathbf{H}^H \mathbf{C} \mathbf{F}^{-H} + \rho \sigma_s^2 \mathbf{I}_{KU}]^{-1} \boldsymbol{\beta} \mathbf{x} + \bar{\mathbf{n}} \quad (8.376)$$

Using the eigen-analysis we express

$$\mathbf{F}^{-1} \mathbf{C}^T \mathbf{H} \mathbf{H}^H \mathbf{C} \mathbf{F}^{-H} = \mathbf{U} \boldsymbol{\Sigma}_s \mathbf{U}^H \quad (8.377)$$

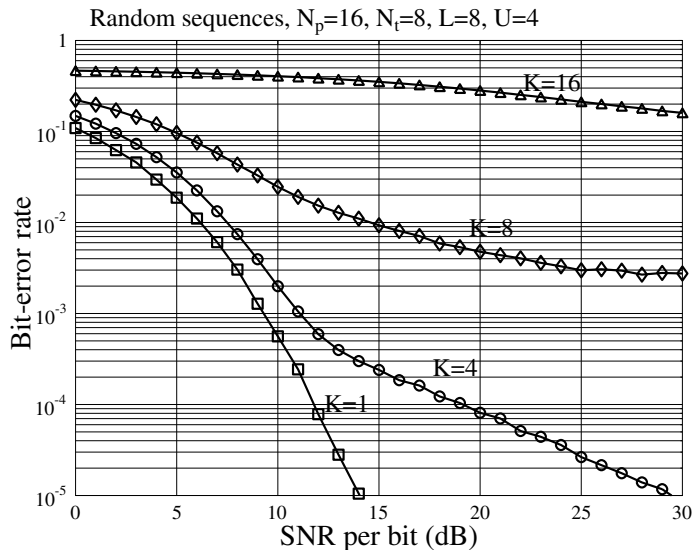


Figure 8.23: BER performance of the TF-domain spread MC DS-CDMA using the ZF-MUTP, when communicating over frequency-selective Rayleigh fading channels having $L = 8$ T-domain resolvable paths. The simulations were based on the preprocessing matrix (8.353) associated with using the joint power normalization.

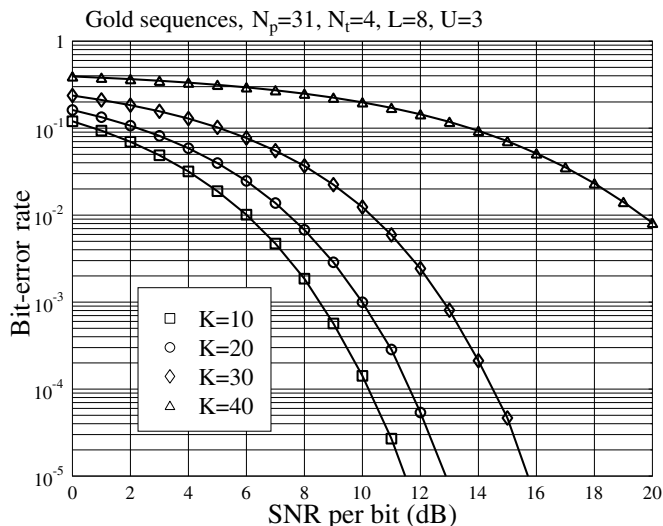


Figure 8.24: BER performance of the TF-domain spread MC DS-CDMA using the ZF-MUTP, when communicating over frequency-selective Rayleigh fading channels having $L = 8$ T-domain resolvable paths. The simulations were based on the preprocessing matrix (8.353) associated with using the joint power normalization.

where $\Sigma_s = \text{diag}\{\lambda_1, \lambda_2, \dots, \lambda_{\mathcal{K}U}\}$ contains the eigenvalues, while the columns of \mathbf{U} are the corresponding eigenvectors. Then, applying (8.377) to (8.376), it can be shown that

$$\begin{aligned}\bar{\mathbf{y}} &= \mathbf{U} \Sigma_s \mathbf{U}^H \mathbf{U} \Sigma_{s+n}^{-1} \mathbf{U}^H \boldsymbol{\beta} \mathbf{x} + \bar{\mathbf{n}} \\ &= \mathbf{U} \boldsymbol{\Lambda} \mathbf{U}^H \boldsymbol{\beta} \mathbf{x} + \bar{\mathbf{n}}\end{aligned}\quad (8.378)$$

where Σ_{s+n} and $\boldsymbol{\Lambda}$ are, respectively, defined as

$$\begin{aligned}\Sigma_{s+n} &= \text{diag}\{\lambda_1 + \rho\sigma_s^2, \lambda_2 + \rho\sigma_s^2, \dots, \lambda_{\mathcal{K}U} + \rho\sigma_s^2\} \\ \boldsymbol{\Lambda} &= \text{diag}\left\{\frac{\lambda_1}{\lambda_1 + \rho\sigma_s^2}, \frac{\lambda_2}{\lambda_2 + \rho\sigma_s^2}, \dots, \frac{\lambda_{\mathcal{K}U}}{\lambda_{\mathcal{K}U} + \rho\sigma_s^2}\right\}\end{aligned}\quad (8.379)$$

Let $\mathbf{U} = [u_{ij}]$. Then, the decision variable for the k th symbol can be expressed as

$$\bar{y}_k = \sum_{j=1}^{\mathcal{K}U} \frac{\lambda_j |u_{kj}|^2}{\lambda_j + \rho\sigma_s^2} \beta_k x_k + \sum_{l \neq k}^{\mathcal{K}U} \sum_{j=1}^{\mathcal{K}U} \frac{\lambda_j}{\lambda_j + \rho\sigma_s^2} u_{kj} u_{lj}^* \beta_l x_l + \bar{n}_k, \quad k = 1, 2, \dots, \mathcal{K}U\quad (8.380)$$

where the first term at the right-hand side (r.h.s.) represents the desired component, the second term at the r.h.s. represents the interference imposed by a MT itself as well as by the other MTs, while the last term is due to the background noise. By using the MMSE-MUTP, the second term at the r.h.s. of (8.380) should be insignificant.

Another way to represent the decision variables of the MMSE-MUTP scheme can be started by decomposing the preprocessing matrix of (8.349) into \mathcal{K} component preprocessing matrices, each of which corresponds to one MT. Specifically, the preprocessing matrix of (8.349) can be written as

$$\begin{aligned}\bar{\mathbf{P}} &= [\mathbf{H}^H \mathbf{C} \mathbf{F}^{-H} \mathbf{F}^{-1} \mathbf{C}^T \mathbf{H} + \rho\sigma_s^2 \mathbf{I}_{N_p N_t}]^{-1} \\ &\quad \times [(\mathbf{H}^{(1)})^H \mathbf{C}^{(1)} \mathbf{F}_1^{-H} \boldsymbol{\beta}_1, (\mathbf{H}^{(2)})^H \mathbf{C}^{(2)} \mathbf{F}_2^{-H} \boldsymbol{\beta}_2, \dots, (\mathbf{H}^{(\mathcal{K})})^H \mathbf{C}^{(\mathcal{K})} \mathbf{F}_{\mathcal{K}}^{-H} \boldsymbol{\beta}_{\mathcal{K}}]\end{aligned}\quad (8.381)$$

From the above equation, explicitly, we can express the preprocessing matrix for the k th MT as

$$\bar{\mathbf{P}}_k = [\mathbf{H}^H \mathbf{C} \mathbf{F}^{-H} \mathbf{F}^{-1} \mathbf{C}^T \mathbf{H} + \rho\sigma_s^2 \mathbf{I}_{N_p N_t}]^{-1} (\mathbf{H}^{(k)})^H \mathbf{C}^{(k)} \mathbf{F}_k^{-H} \boldsymbol{\beta}_k, \quad k = 1, 2, \dots, \mathcal{K}\quad (8.382)$$

Furthermore, it can be shown that

$$\mathbf{H}^H \mathbf{C} \mathbf{F}^{-H} \mathbf{F}^{-1} \mathbf{C}^T \mathbf{H} = \sum_{k=1}^{\mathcal{K}} (\mathbf{H}^{(k)})^H \mathbf{C}^{(k)} \mathbf{F}_k^{-H} \mathbf{F}_k^{-1} (\mathbf{C}^{(k)})^T \mathbf{H}^{(k)}\quad (8.383)$$

Hence, (8.382) can be written as

$$\bar{\mathbf{P}}_k = [(\mathbf{H}^{(k)})^H \mathbf{C}^{(k)} \mathbf{F}_k^{-H} \mathbf{F}_k^{-1} (\mathbf{C}^{(k)})^T \mathbf{H}^{(k)} + \mathbf{R}_I^{(k)}]^{-1} (\mathbf{H}^{(k)})^H \mathbf{C}^{(k)} \mathbf{F}_k^{-H} \boldsymbol{\beta}_k\quad (8.384)$$

where $\mathbf{R}_I^{(k)}$ represents the covariance matrix of the MUI plus background noise, which can be expressed as

$$\mathbf{R}_I^{(k)} = \sum_{l \neq k}^{\mathcal{K}} (\mathbf{H}^{(l)})^H \mathbf{C}^{(l)} \mathbf{F}_l^{-H} \mathbf{F}_l^{-1} (\mathbf{C}^{(l)})^T \mathbf{H}^{(l)} + \rho\sigma_s^2 \mathbf{I}_{N_p N_t}\quad (8.385)$$

After applying the *matrix inverse lemma* on (8.384) we finally obtain the desired preprocessing matrix for the k th MT, which can be expressed as

$$\begin{aligned}\bar{\mathbf{P}}_k &= (\mathbf{R}_I^{(k)})^{-1} (\mathbf{H}^{(k)})^H \mathbf{C}^{(k)} \mathbf{F}_k^{-H} \\ &\quad \times [\mathbf{F}_k^{-1} (\mathbf{C}^{(k)})^T \mathbf{H}^{(k)} (\mathbf{R}_I^{(k)})^{-1} (\mathbf{H}^{(k)})^H \mathbf{C}^{(k)} \mathbf{F}_k^{-H} + \mathbf{I}_U]^{-1} \boldsymbol{\beta}_k \\ k &= 1, 2, \dots, \mathcal{K}\end{aligned}\quad (8.386)$$

Note that if $U = 1$, then the second line in (8.386) can be absorbed into $\boldsymbol{\beta}_k$, and, correspondingly, we have

$$\bar{\mathbf{P}}_k = (\mathbf{R}_I^{(k)})^{-1} (\mathbf{H}^{(k)})^H \mathbf{C}^{(k)} \mathbf{F}_k^{-H} \boldsymbol{\beta}_k, \quad k = 1, 2, \dots, \mathcal{K} \quad (8.387)$$

The preprocessing matrix of (8.386) or (8.387) processes the data to be transmitted to the k th MT in such a way that the k th MT imposes the lowest interference in the MMSE sense on the other $(\mathcal{K} - 1)$ MTs. For a given MT, this type of preprocessing does not seek an optimum solution for maximizing the considered MT's performance, but seeks an optimum solution for minimizing its impact on the other MTs. Hence, we may refer to this type of optimization as the *altruistic (A)-optimization* and its corresponding solution is referred to as A-optimum [229]. Although this type of optimization is not optimum when considering any individual MT, however, the overall optimization is optimum or the system is *overall (O)-optimum*, when all the MTs involved in the system have achieved their corresponding A-optimum solutions.

Based on (8.386), the decision vector for the k th MT can be expressed with the assistance of (8.343) as

$$\begin{aligned}\bar{\mathbf{y}}_k &= \mathbf{F}_k^{-1} (\mathbf{C}^{(k)})^T \mathbf{H}^{(k)} (\mathbf{R}_I^{(k)})^{-1} (\mathbf{H}^{(k)})^H \mathbf{C}^{(k)} \mathbf{F}_k^{-H} \\ &\quad \times [\mathbf{F}_k^{-1} (\mathbf{C}^{(k)})^T \mathbf{H}^{(k)} (\mathbf{R}_I^{(k)})^{-1} (\mathbf{H}^{(k)})^H \mathbf{C}^{(k)} \mathbf{F}_k^{-H} + \mathbf{I}_U]^{-1} \boldsymbol{\beta}_k \mathbf{x}_k \\ &\quad + \mathbf{I}_{MUI} + \bar{\mathbf{n}}_k, \quad k = 1, 2, \dots, \mathcal{K}\end{aligned}\quad (8.388)$$

where \mathbf{I}_{MUI} represents the MUI term, which can be expressed as

$$\mathbf{I}_{MUI} = \mathbf{F}_k^{-1} (\mathbf{C}^{(k)})^T \mathbf{H}^{(k)} \sum_{l \neq k}^{\mathcal{K}} \bar{\mathbf{P}}_l \boldsymbol{\beta}_l \mathbf{x}_l \quad (8.389)$$

where $\bar{\mathbf{P}}_l$ is given by (8.386).

It can be implied that the first term at the r.h.s. of (8.388) generates the desired decision variable, while suppressing the interference from MT k itself. Let us use the eigen-representation of

$$\mathbf{F}_k^{-1} (\mathbf{C}^{(k)})^T \mathbf{H}^{(k)} (\mathbf{R}_I^{(k)})^{-1} (\mathbf{H}^{(k)})^H \mathbf{C}^{(k)} \mathbf{F}_k^{-H} = \boldsymbol{\Phi} \boldsymbol{\Sigma} \boldsymbol{\Phi}^H \quad (8.390)$$

where $\boldsymbol{\Phi} = [\boldsymbol{\phi}_1, \boldsymbol{\phi}_2, \dots, \boldsymbol{\phi}_U]$ is an $(U \times U)$ unitary matrix and $\boldsymbol{\Sigma} = \text{diag}\{\lambda_1, \lambda_2, \dots, \lambda_U\}$. Then, (8.388) can be expressed as

$$\bar{\mathbf{y}}_k = \boldsymbol{\Phi} \boldsymbol{\Lambda} \boldsymbol{\Phi}^H \boldsymbol{\beta}_k \mathbf{x}_k + \mathbf{I}_{MUI} + \bar{\mathbf{n}}_k, \quad k = 1, 2, \dots, \mathcal{K} \quad (8.391)$$

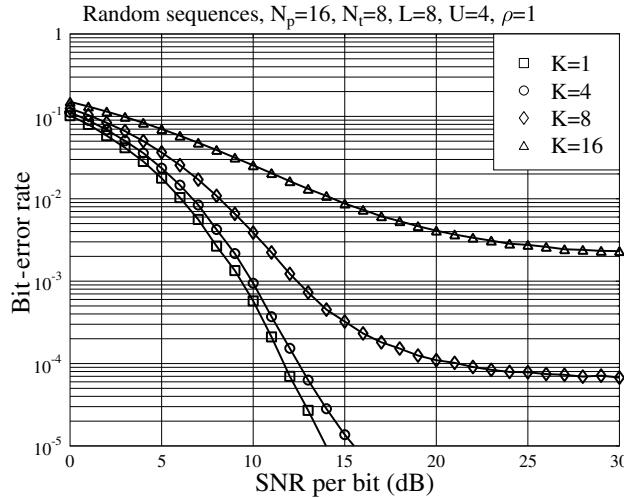


Figure 8.25: BER performance of the TF-domain spread MC DS-CDMA using the MMSE-MUTP, when communicating over frequency-selective Rayleigh fading channels having $L = 8$ T-domain resolvable paths. The simulations were based on the preprocessing matrix (8.350) associated with using the joint power normalization.

where

$$\boldsymbol{\Lambda} = \text{diag}\left\{\frac{\lambda_1}{\lambda_1 + 1}, \frac{\lambda_2}{\lambda_2 + 1}, \dots, \frac{\lambda_U}{\lambda_U + 1}\right\} \quad (8.392)$$

In more detail, when substituting (8.392) into (8.391), we obtain

$$\bar{\mathbf{y}}_k = \sum_{n=1}^U \left(\frac{\lambda_n}{\lambda_n + 1} \right) \boldsymbol{\phi}_n \boldsymbol{\phi}_n^H \boldsymbol{\beta}_k \mathbf{x}_k + \mathbf{I}_{MUI} + \bar{\mathbf{n}}_k, \quad k = 1, 2, \dots, K \quad (8.393)$$

Figures 8.25 and 8.26 depict the BER versus average SNR per bit performance for the TF-domain spread MC DS-CDMA using the MMSE-MUTP, when communicating over frequency-selective Rayleigh fading channels having $L = 8$ T-domain resolvable paths. In Fig. 8.25 random sequences were assumed, while in Fig. 8.26 T-domain orthogonal sequences and F-domain Gold-sequences were assumed. Furthermore, as for the ZF-MUTP, in our simulations for Fig. 8.25 only the randomly generated sequences, which satisfied that $\mathbf{R}_c^{(k)}$ for $k = 1, 2, \dots, K$ were full-rank, were simulated. From the results of Figs 8.25 and 8.26 we can see that the MMSE-MUTP is capable of efficiently mitigating the MUI. It outperforms both the MF-MUTP and the ZF-MUTP. Note that in Fig. 8.25, error-floors for both $K = 8$ and $K = 16$ are observed. This is because when random spreading sequences are employed, the probability that an interfering MT has one or more spreading sequences, which are the same as that of the desired MT, is sufficiently high. This probability results in the error floors being observable within the BER region considered.

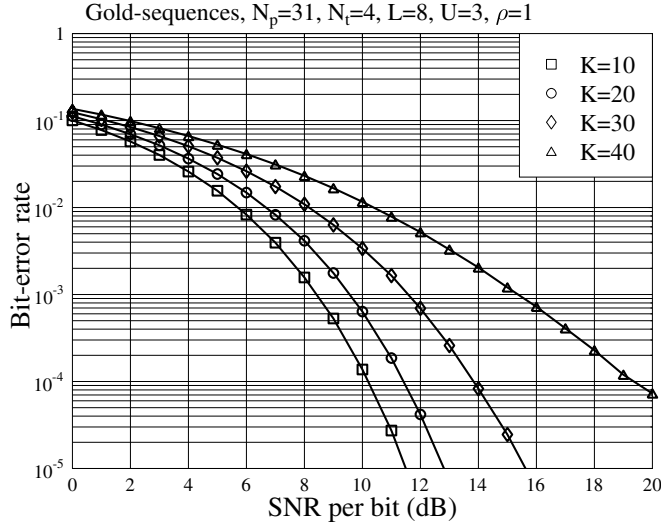


Figure 8.26: BER performance of the TF-domain spread MC DS-CDMA using the MMSE-MUTP, when communicating over frequency-selective Rayleigh fading channels having $L = 8$ T-domain resolvable paths. The simulations were based on the preprocessing matrix (8.350) associated with using the joint power normalization.

8.3.4 Maximum Mutual Information Multiuser Transmitter Preprocessing

The analysis in this section follows that in Section 8.2.11. Two MMI-MUTPs are considered: the joint MMI-MUTP and the ZF/MMI-MUTP. The joint MMI-MUTP maximizes the overall information rate of the TF-domain spread MC DS-CDMA system regardless of the information rate of each individual MT. By contrast, the ZF/MMI-MUTP maximizes the information rate of each individual MT after removing the downlink MUI.

In the context of the joint MMI-MUTP, the decision variable vector of the \mathcal{K} downlink symbols is given by

$$\bar{\mathbf{y}} = \mathbf{F}^{-1} \mathbf{C}^T \mathbf{H} \bar{\mathbf{P}} \mathbf{x} + \bar{\mathbf{n}} \quad (8.394)$$

Hence, following the steps in Section 8.2.11, it can be shown that the optimization problem can be expressed as

$$\begin{aligned} \bar{P}_{\text{JMMI}} &= \arg \max_{\bar{\mathbf{P}}: \text{Trace}(\bar{\mathbf{P}} \bar{\mathbf{P}}^H) \leq \mathcal{K}U} \{ \mathcal{I}(\bar{\mathbf{y}}, \mathbf{x}) = \log_2 [\det(\mathbf{I}_{N_p N_t} + \mathbf{Q}_{\bar{\mathbf{P}}} \mathbf{H}^H \mathbf{C} (\mathbf{F} \mathbf{F}^H)^{-1} \mathbf{C}^T \mathbf{H})] \\ &\quad = \log_2 [\det(\mathbf{I}_{N_p N_t} + \mathbf{Q}_{\bar{\mathbf{P}}} \mathbf{H}^H \mathbf{C} \mathbf{R}_c^{-1} \mathbf{C}^T \mathbf{H})] \} \end{aligned} \quad (8.395)$$

where $\mathbf{Q}_{\bar{\mathbf{P}}} = \bar{\mathbf{P}} \bar{\mathbf{P}}^H$, and

$$\mathbf{R}_c = \mathbf{F} \mathbf{F}^H = \text{diag}\{\mathbf{R}_c^{(1)}, \mathbf{R}_c^{(2)}, \dots, \mathbf{R}_c^{(\mathcal{K})}\} \quad (8.396)$$

and $\mathbf{R}_c^{(k)}$ is given by (8.342).

Lets use the eigen-representation to express $\mathbf{H}^H \mathbf{C} \mathbf{R}_c^{-1} \mathbf{C}^T \mathbf{H}$ as

$$\mathbf{H}^H \mathbf{C} \mathbf{R}_c^{-1} \mathbf{C}^T \mathbf{H} = \mathbf{U}_s \boldsymbol{\Sigma} \mathbf{U}_s^H \quad (8.397)$$

where \mathbf{U}_s is a unitary matrix of size $(N_p N_t \times \mathcal{K}U)$ and $\boldsymbol{\Sigma}$ is a diagonal matrix given by

$$\boldsymbol{\Sigma} = \text{diag}\{\lambda_1, \lambda_2, \dots, \lambda_{\mathcal{K}U}\} \quad (8.398)$$

where $\lambda_1, \lambda_2, \dots, \lambda_{\mathcal{K}U}$ are the eigenvalues of $\mathbf{H}^H \mathbf{C} \mathbf{R}_c^{-1} \mathbf{C}^T \mathbf{H}$. Substituting (8.397) into (8.395), we obtain

$$\mathcal{I}(\bar{\mathbf{y}}, \mathbf{x}) = \log_2[\det(\mathbf{I}_{N_p N_t} + \mathbf{Q}_{\bar{P}} \mathbf{U}_s \boldsymbol{\Sigma} \mathbf{U}_s^H)] \quad (8.399)$$

Applying the relationship of $\det(\mathbf{I} + \mathbf{AB}) = \det(\mathbf{I} + \mathbf{BA})$, the above equation can be written as

$$\mathcal{I}(\bar{\mathbf{y}}, \mathbf{x}) = \log_2[\det(\mathbf{I}_{\mathcal{K}U} + \boldsymbol{\Sigma}^{1/2} \mathbf{U}_s^H \mathbf{Q}_{\bar{P}} \mathbf{U}_s \boldsymbol{\Sigma}^{1/2})] \quad (8.400)$$

Hence, following the same principles in Section 8.2.11, the transmitter preprocessing matrix for the joint MMI-MUTP should be chosen as

$$\bar{\mathbf{P}}_{\text{JMMI}} = \mathbf{U}_s \boldsymbol{\beta}^{1/2} \quad (8.401)$$

where $\boldsymbol{\beta} = \text{diag}\{\beta_1, \dots, \beta_{\mathcal{K}U}\}$. According to the ‘water-filling’ principles [233, pp. 250–3], β_i is chosen to be

$$\beta_i = \left(v - \frac{1}{\lambda_i} \right)^+, \quad i = 1, 2, \dots, \mathcal{K}U \quad (8.402)$$

and v is chosen so that

$$\sum_{i=1}^{\mathcal{K}U} \beta_i = \sum_{i=1}^{\mathcal{K}U} \left(v - \frac{1}{\lambda_i} \right)^+ \leq \mathcal{K}U \quad (8.403)$$

Furthermore, according to Section 8.2.11, the maximum mutual information of the TF-domain spread MC DS-CDMA system can be expressed as

$$\mathcal{I}_{\max}(\bar{\mathbf{y}}, \mathbf{x}) = \sum_{i=1}^{\mathcal{K}U} \log_2(v\lambda_i)^+ \text{ (bits/transmission)} \quad (8.404)$$

and the maximum ergodic mutual information of the TF-domain spread MC DS-CDMA can be expressed as

$$\bar{\mathcal{I}}_{\max}(\bar{\mathbf{y}}, \mathbf{x}) = E[\mathcal{I}_{\max}(\bar{\mathbf{y}}, \mathbf{x})] \text{ (bits/transmission)} \quad (8.405)$$

For the ZF/MMI-MUTP, where the mutual information of each MT is maximized after the MUI suppression, we can start with (8.388) by representing $\mathbf{R}_I^{(k)}$ using the eigen-analysis as

$$\mathbf{R}_I^{(k)} = [\mathbf{U}_I \mid \mathbf{U}_n] \begin{bmatrix} \boldsymbol{\Lambda}_I & \mathbf{0} \\ \mathbf{0} & \sigma_s^2 \mathbf{I} \end{bmatrix} \begin{bmatrix} \mathbf{U}_I^H \\ \mathbf{U}_n^H \end{bmatrix} \quad (8.406)$$

where $\boldsymbol{\Lambda}_I$ is a diagonal matrix containing $(\mathcal{K}-1)U$ eigenvalues contributed by the interfering users, \mathbf{U}_I contains the eigenvectors corresponding to these eigenvalues. By contrast, \mathbf{U}_n

contains the $(N_p N_t - (\mathcal{K} - 1)U)$ eigenvectors of the noise subspace. Hence, when the preprocessing matrix for the k th MT is set in the form

$$\tilde{\mathbf{P}}_{\text{ZMMI},k} = (\mathbf{U}_n \mathbf{U}_n^H) \tilde{\mathbf{P}}_k \quad (8.407)$$

it can be implied that the interference imposed by the interfering MTs on the k th MT is fully removed, since the interference subspace is orthogonal to the noise subspace, while $\tilde{\mathbf{P}}_k$ lies in the noise subspace of \mathbf{U}_n . Therefore, the decision vector for the k th MT can be expressed as

$$\bar{\mathbf{y}}_k = \mathbf{F}_k^{-1}(\mathbf{C}^{(k)})^T \mathbf{H}^{(k)} (\mathbf{U}_n \mathbf{U}_n^H) \tilde{\mathbf{P}}_k \mathbf{x}_k + \bar{\mathbf{n}}_k, \quad k = 1, 2, \dots, \mathcal{K} \quad (8.408)$$

Now, the problem of maximizing the mutual information of the k th MT can be formulated as

$$\begin{aligned} \tilde{\mathbf{P}}_k = \arg \max_{\tilde{\mathbf{P}}_k : \text{Trace}(\tilde{\mathbf{P}}_k \tilde{\mathbf{P}}_k^H) \leq U} & \{ \mathcal{I}(\bar{\mathbf{y}}_k, \mathbf{x}_k) = \log_2 [\det(\mathbf{I}_U + \\ & + (\mathbf{F}_k^{-1}(\mathbf{C}^{(k)})^T \mathbf{H}^{(k)} (\mathbf{U}_n \mathbf{U}_n^H)) \tilde{\mathbf{P}}_k \tilde{\mathbf{P}}_k^H (\mathbf{F}_k^{-1}(\mathbf{C}^{(k)})^T \mathbf{H}^{(k)} (\mathbf{U}_n \mathbf{U}_n^H))^H)] \} \end{aligned} \quad (8.409)$$

Invoking the SVD to express

$$(\mathbf{F}_k^{-1}(\mathbf{C}^{(k)})^T \mathbf{H}^{(k)} (\mathbf{U}_n \mathbf{U}_n^H))^H (\mathbf{F}_k^{-1}(\mathbf{C}^{(k)})^T \mathbf{H}^{(k)} (\mathbf{U}_n \mathbf{U}_n^H)) = \mathbf{U}_s^{(k)} \boldsymbol{\Sigma}_k (\mathbf{U}_s^{(k)})^H \quad (8.410)$$

where $\boldsymbol{\Sigma}_k = \text{diag}\{\lambda_{k1}, \lambda_{k2}, \dots, \lambda_{kU}\}$, we can modify the problem of (8.409) to

$$\mathcal{I}(\bar{\mathbf{y}}_k, \mathbf{x}_k) = \log_2 [\det(\mathbf{I}_U + \boldsymbol{\Sigma}_k^{1/2} (\mathbf{U}_s^{(k)})^H \tilde{\mathbf{P}}_k \tilde{\mathbf{P}}_k^H \mathbf{U}_s^{(k)} \boldsymbol{\Sigma}_k^{1/2})] \quad (8.411)$$

Consequently, by following the approaches in Section 8.2.11, it can be shown that $\tilde{\mathbf{P}}_k$ should be chosen to be

$$\tilde{\mathbf{P}}_k = \mathbf{U}_s^{(k)} \boldsymbol{\beta}_k^{1/2} \quad (8.412)$$

in order to maximize the information rate. Furthermore, when substituting (8.412) into (8.407), the desired preprocessing matrix for the k th MT can be expressed as

$$\tilde{\mathbf{P}}_{\text{ZMMI},k} = (\mathbf{U}_n \mathbf{U}_n^H) \mathbf{U}_s^{(k)} \boldsymbol{\beta}_k^{1/2} \quad (8.413)$$

where, also in (8.412), $\boldsymbol{\beta}_k = \text{diag}\{\beta_{k1}, \beta_{k2}, \dots, \beta_{kU}\}$.

Let us now apply (8.412) to (8.411). Then, the mutual information of the k th MT can be expressed as

$$\mathcal{I}(\bar{\mathbf{y}}_k, \mathbf{x}_k) = \log_2 [\det(\mathbf{I}_U + \boldsymbol{\Sigma}_k \boldsymbol{\beta}_k)], \quad k = 1, 2, \dots, \mathcal{K} \quad (8.414)$$

Expressing

$$\boldsymbol{\alpha}^{(k)} = (\mathbf{U}_s^{(k)})^H (\mathbf{U}_n \mathbf{U}_n^H) \mathbf{U}_s^{(k)} \quad (8.415)$$

and following the ‘water-filling’ principles for the ZF/MMI-MUTP as studied in Section 8.2.11, β_{ki} for $i = 1, 2, \dots, U$; $k = 1, 2, \dots, \mathcal{K}$ can be chosen as

$$\beta_{ki} = \left(\frac{v_k}{\alpha_{ii}^{(k)}} - \frac{1}{\lambda_{ki}} \right)^+, \quad i = 1, 2, \dots, U; k = 1, 2, \dots, \mathcal{K} \quad (8.416)$$

where v_k is chosen so that

$$\sum_{i=1}^U \left(v_k - \frac{\alpha_{ii}^{(k)}}{\lambda_{ki}} \right) \leq U \quad (8.417)$$

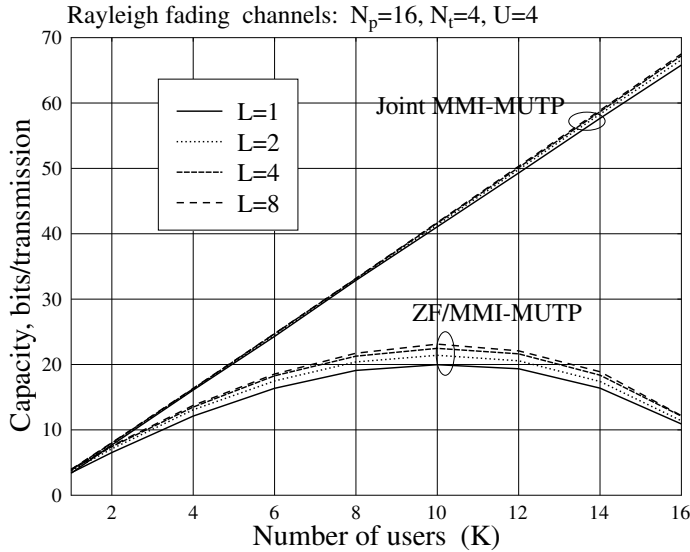


Figure 8.27: Capacity of the TF-domain spread MC DS-CDMA using MMI-MUTP, when communicating over frequency-selective Rayleigh fading channels having various number of T-domain resolvable paths. The simulations were based on (8.405) and (8.419).

Furthermore, it can be shown that the maximum mutual information of MT k is given by

$$\mathcal{I}_{\max}(\bar{\mathbf{y}}_k, \mathbf{x}_k) = \sum_{i=1}^U \log_2 \left(\frac{v_k \lambda_{ki}}{\alpha_{ii}^{(k)}} \right)^+ \quad (\text{bits/transmission/user}), \quad k = 1, 2, \dots, \mathcal{K} \quad (8.418)$$

Correspondingly, the maximum ergodic mutual information of MT k can be expressed as

$$\bar{\mathcal{I}}_{\max}(\bar{\mathbf{y}}_k, \mathbf{x}_k) = E[\mathcal{I}_{\max}(\bar{\mathbf{y}}_k, \mathbf{x}_k)] \quad (\text{bits/transmission/user}), \quad k = 1, 2, \dots, \mathcal{K} \quad (8.419)$$

In Figs 8.27 and 8.28 the capacity of the TF-domain spread MC-CDMA using either the joint MMI-MUTP or ZF/MMI-MUTP was drawn versus the number of MTs supported, when communicating over frequency-selective Rayleigh fading channels having various numbers of T-domain resolvable paths. Like the F-domain spread MC-CDMA using MMI-MUTP, as discussed in Section 8.2.11, the ZF operation significantly degrades the capacity of the TF-domain spread MC-CDMA systems. Furthermore, as the results in Figs 8.27 and 8.28 show, the number of T-domain resolvable paths has an insignificant impact on the capacity of the TF-domain spread MC-CDMA system, when either the joint MMI-MUTP or the ZF/MMI-MUTP is used.

Above, several typical optimization schemes have been invoked to derive the preprocessing matrix for the TF-domain spread MC DS-CDMA. Below, we use a separate section to discuss the transmission power allocation in the TF-domain spread MC DS-CDMA using transmitter preprocessing.

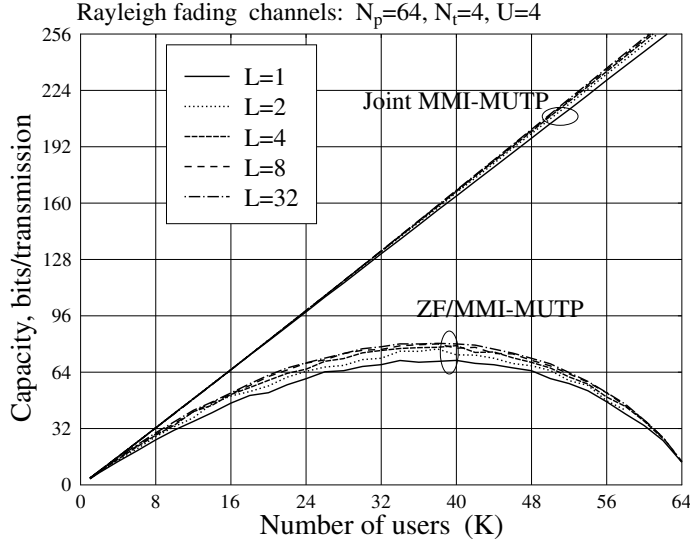


Figure 8.28: Capacity of the TF-domain spread MC DS-CDMA using MMI-MUTP, when communicating over frequency-selective Rayleigh fading channels having various numbers of T-domain resolvable paths. The simulations were based on (8.405) and (8.419).

8.3.5 Transmission Power Allocation

In this section we summarize a range of power-allocation schemes that may be employed by the transmitter preprocessing schemes, namely MF-SUTP, ZF-MUTP and MMSE-MUTP, derived in Section 8.3.3. Given a preprocessing scheme, the power allocation is equivalent to choosing the corresponding component values in β under the constraint of the total transmission power. Note that Section 8.3.4 considered the power allocation that achieves the maximum mutual information of the TF-domain spread MC DS-CDMA systems.

8.3.5.1 Joint Power Normalization

The joint power normalization is suitable for all of the above-mentioned preprocessing schemes. For the joint power normalization, let us express the preprocessing matrix as

$$\bar{\mathbf{P}} = \tilde{\mathbf{P}}\beta \quad (8.420)$$

where $\tilde{\mathbf{P}}$ represents the determinate part of the preprocessing matrix. For example, in the preprocessing matrix of (8.351) for the MF-SUTP, $\tilde{\mathbf{P}} = \mathbf{H}^H \mathbf{C} \mathbf{F}^{-H}$. Then, according to the constraint on the transmission power, which is given by

$$\text{Trace}(\bar{\mathbf{P}} \bar{\mathbf{P}}^H) = \mathcal{K}U \quad (8.421)$$

it can be easily shown that β in (8.420) can be chosen as

$$\beta = \sqrt{\frac{\mathcal{K}U}{\text{Trace}(\tilde{\mathbf{P}} \tilde{\mathbf{P}}^H)}} \quad (8.422)$$

8.3.5.2 Individual Power Normalization

The individual power normalization is also suitable for all of the above three types of preprocessing scheme. Let the preprocessing matrix $\bar{\mathbf{P}}$ be expressed as

$$\bar{\mathbf{P}} = [\bar{\mathbf{p}}_1, \bar{\mathbf{p}}_2, \dots, \bar{\mathbf{p}}_{\mathcal{K}U}] \quad (8.423)$$

Furthermore, let $\bar{\mathbf{p}}_i$ be expressed as

$$\bar{\mathbf{p}}_i = \tilde{\mathbf{p}}_i \beta_i, \quad i = 1, 2, \dots, \mathcal{K}U \quad (8.424)$$

where $\tilde{\mathbf{p}}_i$ is determinate. Then, for the individual power normalization, β_i is chosen to be

$$\beta_i = \sqrt{\frac{1}{\tilde{\mathbf{p}}_i^H \tilde{\mathbf{p}}_i}} \quad (8.425)$$

8.3.5.3 Maximal SNR Assisted Normalization for ZF-MUTP

The downlink MUI is fully removed when the ZF-MUTP is used. In this case the preprocessing matrix is given by (8.354) and the decision variable vector can be expressed as

$$\bar{\mathbf{y}} = \boldsymbol{\beta} \mathbf{x} + \bar{\mathbf{n}} \quad (8.426)$$

where $\boldsymbol{\beta} = \text{diag}\{\beta_1, \beta_2, \dots, \beta_{\mathcal{K}U}\}$ and $\bar{\mathbf{n}}$ is Gaussian with zero mean and a covariance matrix of $\sigma_s^2 \mathbf{I}_{\mathcal{K}U}$. Consequently, following Section 8.2.6, the optimization problem can be formed as

$$\boldsymbol{\beta} \triangleq \arg \min_{\{\beta_i\}} \left\{ \sigma_s^2 \sum_{i=1}^{\mathcal{K}U} \frac{1}{\beta_i^2} \right\} \quad (8.427)$$

under the power constraint

$$\text{Trace}(\bar{\mathbf{P}} \bar{\mathbf{P}}^H) = \mathcal{K}U \quad (8.428)$$

Applying (8.354) to (8.428), we obtain

$$\text{Trace}(\bar{\mathbf{P}} \bar{\mathbf{P}}^H) = \text{Trace}(\mathbf{F}^H (\mathbf{C}^T \mathbf{H} \mathbf{H}^H \mathbf{C})^{-1} \mathbf{F} \boldsymbol{\beta}^2) = \mathcal{K}U \quad (8.429)$$

Let us define

$$\mathbf{F}^H (\mathbf{C}^T \mathbf{H} \mathbf{H}^H \mathbf{C})^{-1} \mathbf{F} = \mathbf{A} = [a_{ij}] \quad (8.430)$$

Then, (8.429) can be rewritten as

$$\sum_{i=1}^{\mathcal{K}U} a_{ii} \beta_i^2 = \mathcal{K}U \quad (8.431)$$

Consequently, with the aid of (8.431), the conditional optimization problem of (8.427) can be formulated as an unconditional optimization problem with the cost function given by

$$J = \sigma_s^2 \sum_{i=1}^{\mathcal{K}U} \frac{1}{\beta_i^2} + \mu \left(\sum_{i=1}^{\mathcal{K}U} a_{ii} \beta_i^2 - \mathcal{K}U \right) \quad (8.432)$$

Taking the derivative of J with respect to β_i and setting the derivative result to equal zero, we obtain

$$\beta_i = \left(\frac{\sigma_s^2}{\mu a_{ii}} \right)^{1/4}, \quad i = 1, 2, \dots, \mathcal{K}U \quad (8.433)$$

Applying β_i from (8.433) to (8.431), we can compute μ , which is

$$\mu = \frac{\sigma_s^2}{\mathcal{K}^2 U^2} \left(\sum_{i=1}^{\mathcal{K}U} \sqrt{a_{ii}} \right)^2 \quad (8.434)$$

Substituting it into (8.433), we can finally obtain β_i

$$\beta_i = \sqrt{\mathcal{K}U} \left(\sum_{j=1}^{\mathcal{K}U} \sqrt{a_{ii} a_{jj}} \right)^{-1/2}, \quad i = 1, 2, \dots, \mathcal{K}U \quad (8.435)$$

Furthermore, it can be shown that the minimum of the cost function is

$$\begin{aligned} J_{\min} &= \sigma_s^2 \sum_{i=1}^{\mathcal{K}U} \frac{1}{\beta_i^2} \\ &= \frac{\sigma_s^2}{\mathcal{K}U} \sum_{i=1}^{\mathcal{K}U} \sum_{j=1}^{\mathcal{K}U} \sqrt{a_{ii} a_{jj}} \\ &= \frac{\sigma_s^2}{\mathcal{K}U} \left(\sum_{i=1}^{\mathcal{K}U} \sqrt{a_{ii}} \right)^2 \end{aligned} \quad (8.436)$$

Above, the transmission power of the TF-domain spread MC DS-CDMA using transmitter preprocessing has been normalized according to the principles of the MSINR, given that ZF-MUTP is used. When BPSK is used as the baseband modulation, as shown in Section 8.2.10, the transmission power can also be normalized so as to achieve the minimum BER (MBER) for the TF-domain spread MC DS-CDMA using the ZF-MUTP. Note that the derivation of the MBER-assisted power normalization is very similar to that considered in Section 8.2.10, which is hence not repeated here.

8.4 Relationship Between Linear Multiuser Transmission and Linear Multiuser Detection

In Chapter 6 a wide range of linear MUD algorithms were derived. Correspondingly, in Sections 8.2 and 8.3 of the current chapter, a range of linear MUTP algorithms have been derived. In this section we develop the relationship between the linear MUD and linear MUTP by following the findings in reference [229]. The main conclusions concerning the relationship between the linear MUD and linear MUTP are as follows [229]: for any given linear MUD scheme, there exists a counterpart linear MUTP scheme. The counterpart linear MUTP can be easily designed from the original linear MUD associated with considering the constraint on the transmission power as well as the availability of the knowledge about the noise presenting at the remote MTs.

Our analysis starts with considering both the uplink and downlink of a wireless system simultaneously and expressing both the uplink MIMO equation and downlink MIMO equation in their general forms. From Chapter 6, we know that, for any given multicarrier scheme considered, the MIMO equation governing the uplink can be expressed as

$$\mathbf{y}_U = \mathcal{H}\mathbf{x} + \mathbf{n}_U = \sum_{k=1}^{\mathcal{K}} \mathbf{h}_k x_k + \mathbf{n}_U \quad (8.437)$$

where the subscript ‘ U ’ is used explicitly to indicate the uplink. Let us assume that \mathbf{y}_U of the \mathcal{N} -length vector observed is properly normalized. Then, the other arguments in (8.437) can be described as follows. The data vector \mathbf{x} contains the \mathcal{K} symbols transmitted by the uplink MTs to the BS; it can be expressed as

$$\mathbf{x} = [x_1, x_2, \dots, x_{\mathcal{K}}]^T \quad (8.438)$$

and we assume that $E[|x_k|^2] = 1$ and x_k is an i.i.d. uniform random variable. In (8.437) \mathcal{H} is the $(\mathcal{N} \times \mathcal{K})$ MIMO transform matrix, which is in the form

$$\mathcal{H} = [\mathbf{h}_1, \mathbf{h}_2, \dots, \mathbf{h}_{\mathcal{K}}] \quad (8.439)$$

where \mathbf{h}_k is the signature for x_k , \mathbf{h}_k is given by

$$\mathbf{h}_k = [h_{k1}, h_{k2}, \dots, h_{k\mathcal{N}}]^T, \quad k = 1, 2, \dots, \mathcal{K} \quad (8.440)$$

and it is normalized to satisfy $E[\|\mathbf{h}_k\|^2] = 1$. Furthermore, in (8.437) \mathbf{n}_U is the \mathcal{N} -length noise vector, each element of which is a complex Gaussian random variable with zero mean and a variance of $\sigma_U^2/2 = 1/2\text{SNR}_U$ per dimension, where SNR_U represents the SNR of the uplink.

It can be shown that the observation equation (6.21) in Chapter 6 for the MUD in the F-domain spread MC-CDMA can be represented in the form of (8.437) after letting $\mathcal{H} = \mathbf{C}\mathbf{H}$.

When a linear detector is used to detect the uplink transmitted symbols, the decision variable vector for the \mathcal{K} transmitted symbols in \mathbf{x} can be formed as

$$\mathbf{z} = \mathbf{W}^H \mathbf{y}_U = \mathbf{W}^H \mathcal{H}\mathbf{x} + \mathbf{W}^H \mathbf{n}_U \quad (8.441)$$

where \mathbf{W} is a $(\mathcal{N} \times \mathcal{K})$ matrix, which, for convenience, is referred to as the receiver *post-processing matrix*. The post-processing matrix \mathbf{W} has the structure

$$\mathbf{W} = [\mathbf{w}_1, \mathbf{w}_2, \dots, \mathbf{w}_{\mathcal{K}}] \quad (8.442)$$

where \mathbf{w}_k , $k = 1, 2, \dots, \mathcal{K}$ is the *post-processing vector* for detection of x_k .

Let us now consider a corresponding multicarrier downlink scheme that is dual to the multicarrier uplink scheme. After some required processing, such as de-spreading, etc. at the MTs, it can be shown that the MIMO equation describing the observations for detection of the \mathcal{K} symbols transmitted by the BS to the MTs can be represented as

$$\mathbf{y}_D = \mathcal{H}^T \mathbf{P}\mathbf{x} + \mathbf{n}_D \quad (8.443)$$

where the subscript ‘ D ’ is used to specify the downlink. Again, let us assume that proper normalization has been invoked for \mathbf{y}_D . Then, in (8.443) \mathbf{x} having the same form of (8.438)

containing the \mathcal{K} symbols transmitted by the BS to the MTs, \mathbf{P} is the $(\mathcal{N} \times \mathcal{K})$ transmitter preprocessing matrix, which is given by

$$\mathbf{P} = [\mathbf{p}_1, \mathbf{p}_2, \dots, \mathbf{p}_{\mathcal{K}}] \quad (8.444)$$

where \mathbf{p}_k is for preprocessing x_k , $k = 1, \dots, \mathcal{K}$. Additionally, in (8.443) \mathbf{n}_D is the \mathcal{K} -length noise vector, each entry of which is assumed to be a complex Gaussian random variable with zero mean and a variance of $\sigma_D^2/2 = 1/2\text{SNR}_D$ per dimension, where SNR_D denotes the downlink SNR.

Note that both the matrices \mathbf{H} in (8.437) and (8.443) are the same, when the dual uplink and downlink systems are considered.

It can be shown that the observation equation (8.46) in Section 8.2.2 for the MUTP in the F-domain spread MC-CDMA can be represented in the form of (8.443) after letting $\mathbf{H} = (\mathbf{C}^T \mathbf{H})^T$. Furthermore, a reader who is interested in the details may check to confirm that the transpose of $\mathbf{C}^T \mathbf{H}$ in (8.46), i.e. $(\mathbf{C}^T \mathbf{H})^T$ is the same as the \mathbf{CH} in (6.21) of Chapter 6.

Let us now consider the relationship between the MUD and MUTP, or between the post-processing matrix \mathbf{W} and the preprocessing matrix \mathbf{P} . From the theory of linear MUD, we find that in nearly all the linear MUDs,² the post-processing matrix \mathbf{W} has the property of making $\mathbf{W}^H \mathbf{H}$ a Hermitian matrix. If this property is satisfied, then, after setting $\mathbf{P} = \mathbf{W}^*$, (8.443) can be expressed as

$$\begin{aligned} \mathbf{y}_D &= \mathbf{H}^T \mathbf{W}^* \mathbf{x} + \mathbf{n}_D \\ &= (\mathbf{W}^H \mathbf{H})^T \mathbf{x} + \mathbf{n}_D \end{aligned} \quad (8.445)$$

Comparing (8.441) with (8.445), it can be easily shown that, after ignoring the noise term, both \mathbf{z} of (8.441) and \mathbf{y}_D of (8.445) have the same statistical properties due to the randomness of \mathbf{x} . Hence, when $\mathbf{W}^H \mathbf{H}$ is Hermitian and \mathbf{W} is efficient for the uplink MUD, then, $\mathbf{P} = \mathbf{W}^*$ will make $\mathbf{H}^T \mathbf{P}$ Hermitian and will be similarly efficient as the uplink MUD, concerning the capability of MUI suppression.

The above observation suggests that the transmitter preprocessing matrix \mathbf{P} in (8.443) may be designed based on deriving the receiver post-processing matrix \mathbf{W} in (8.441), and similarly, the receiver post-processing matrix \mathbf{W} in (8.441) may also be designed based on finding the preprocessing matrix \mathbf{P} of (8.443), according to the simple relation of $\mathbf{P} = \mathbf{W}^*$ and $\mathbf{W} = \mathbf{P}^*$, respectively. However, we should notice that the downlink noise power σ_D^2 is not necessarily equal to the uplink noise power σ_U^2 . Furthermore, the preprocessing is carried out under the power constraint, so that the total transmission power before and after the preprocessing remains unchanged. When taking into account these two facts, we may design the preprocessing matrix \mathbf{P} or post-processing matrix \mathbf{W} from the post-processing matrix \mathbf{W} or the preprocessing matrix \mathbf{P} as follows:

$$\begin{aligned} \mathbf{P} &= \text{Modified}(\mathbf{W}^* | \sigma_D^2 \rightarrow \sigma_U^2) \boldsymbol{\beta} \\ \mathbf{W} &= \text{Modified}(\mathbf{P}^* | \sigma_U^2 \rightarrow \sigma_D^2) \boldsymbol{\beta}^{-1} \end{aligned} \quad (8.446)$$

where $\boldsymbol{\beta} = \text{diag}\{\beta_1, \beta_2, \dots, \beta_{\mathcal{K}}\}$ is for achieving the constraint on the transmission power, while $a \rightarrow b$ means using a to replace b .

²Note that we use the word ‘nearly’, since we cannot make sure that any linear MUDs satisfy the property as described here.

More specifically, when considering the design of the preprocessing matrix \mathbf{P} or the preprocessing vector $\{\mathbf{p}_k\}$ from the post-processing matrix \mathbf{W} or the post-processing vector $\{\mathbf{w}_k\}$, the approaches can be summarized as follows. Let the post-processing be expressed as

$$\begin{aligned} z &= \mathbf{W}^H \mathbf{y} = \mathbf{W}^H \mathcal{H} \mathbf{x} + \mathbf{W}^H \mathbf{n}_U, \\ z_k &= \mathbf{w}_k^H \mathbf{h}_k x_k + \underbrace{\mathbf{w}_k^H \left(\sum_{l \neq k} \mathbf{h}_l x_l + \mathbf{n}_U \right)}_{\mathbf{n}_l^{(k)}}, \quad k = 1, 2, \dots, \mathcal{K} \end{aligned} \quad (8.447)$$

Then, once the post-processing matrix \mathbf{W} or vectors $\{\mathbf{w}_k\}$ are obtained with the aid of an optimization scheme, the preprocessing matrix \mathbf{P} or vectors $\{\mathbf{p}_k\}$ can then be obtained according to

$$\begin{aligned} \mathbf{P} &= \text{Modified}(\mathbf{W}^* | \sigma_D^2 \rightarrow \sigma_U^2) \boldsymbol{\beta} \\ \mathbf{p}_k &= \beta_k \times \text{Modified}(\mathbf{w}_k^* | \sigma_D^2 \rightarrow \sigma_U^2), \quad k = 1, 2, \dots, \mathcal{K} \end{aligned} \quad (8.448)$$

Let us below use the above-provided approaches to design the preprocessing matrices (vectors) for several MUTP schemes. First, in the context of the MF-assisted single-user detector, the receiver post-processing matrix \mathbf{W} in (8.441) is given by

$$\mathbf{W}_{\text{MF}} = \mathcal{H} \quad (8.449)$$

Correspondingly, according to (8.448), for the MF-assisted single-user transmitter preprocessing, the preprocessing matrix \mathbf{P} in (8.443) can be expressed as

$$\mathbf{P}_{\text{MF}} = \mathcal{H}^* \boldsymbol{\beta} \quad (8.450)$$

Specifically, for the F-domain spread MC-CDMA having the downlink MIMO equation (8.46) as seen in Section 8.2.2, we have $\mathcal{H} = (\mathcal{C}^T \mathbf{H})^T$. Applying it to (8.450), we obtain

$$\mathbf{P}_{\text{MF}} = (\mathcal{C}^T \mathbf{H})^H \boldsymbol{\beta} = \mathbf{H}^H \mathcal{C} \boldsymbol{\beta} \quad (8.451)$$

which is the same as (8.51).

Second, based on (8.441), it can be easily shown that the receiver post-processing matrix \mathbf{W} in the ZF sense can be expressed as

$$\mathbf{W}_{\text{ZF}} = \mathcal{H} (\mathcal{H}^H \mathcal{H})^{-1} \quad (8.452)$$

Correspondingly, according to (8.448), the transmitter preprocessing matrix \mathbf{P} in the sense of achieving ZF can be expressed as

$$\mathbf{P}_{\text{ZF}} = \mathcal{H}^* (\mathcal{H}^T \mathcal{H}^*)^{-1} \boldsymbol{\beta} \quad (8.453)$$

For the F-domain spread MC-CDMA having the downlink MIMO equation of (8.46), after substituting $\mathcal{H} = (\mathcal{C}^T \mathbf{H})^T$ into (8.453), the preprocessing matrix is given by

$$\mathbf{P}_{\text{ZF}} = (\mathcal{C}^T \mathbf{H})^H (\mathcal{C}^T \mathbf{H} \mathbf{H}^H \mathcal{C})^{-1} \boldsymbol{\beta} \quad (8.454)$$

which is the same as (8.68).

Finally, let us consider the MUD and MUTP that are based on the MMSE principles. From (8.441) it can be shown that the optimum receiver post-processing matrix in the MMSE sense is given by

$$\begin{aligned} \mathbf{W}_{\text{MMSE}} &= (\mathcal{H}\mathcal{H}^H + \sigma_U^2 \mathbf{I}_{\mathcal{N}})^{-1} \mathcal{H} \\ &= \mathcal{H}(\mathcal{H}^H \mathcal{H} + \sigma_U^2 \mathbf{I}_{\mathcal{K}})^{-1} \end{aligned} \quad (8.455)$$

Correspondingly, according to (8.448), the preprocessing matrix can be expressed as

$$\begin{aligned} \mathbf{P}_{\text{MMSE}} &= (\mathcal{H}^* \mathcal{H}^T + \rho \sigma_D^2 \mathbf{I}_{\mathcal{N}})^{-1} \mathcal{H}^* \boldsymbol{\beta} \\ &= \mathcal{H}^* (\mathcal{H}^T \mathcal{H}^* + \rho \sigma_D^2 \mathbf{I}_{\mathcal{K}})^{-1} \boldsymbol{\beta} \end{aligned} \quad (8.456)$$

where ρ is the noise-suppression factor. It is set to zero, when the BS transmitter does not have the knowledge about the noise variance of the downlink. Alternatively, $\rho \sigma_D^2$ can be set to a small value, even the BS transmitter does not employ the knowledge about the background noise. As seen in Fig. 8.10, when $\rho > 0$ and it is not very big, the BER performance of the MC-CDMA is usually better than that when $\rho = 0$, which is the BER performance of the MC-CDMA using ZF-MUTP.

Furthermore, for the F-domain spread MC-CDMA having the downlink MIMO equation of (8.46), after substituting $\mathcal{H} = (\mathcal{C}^T \mathbf{H})^T$ and $\sigma_D^2 = \sigma_s^2$ into (8.456), we can find that the preprocessing matrix in the MMSE sense can be expressed as

$$\mathbf{P}_{\text{MMSE}} = (\mathbf{H}^H \mathcal{C} \mathcal{C}^T \mathbf{H} + \rho \sigma_s^2 \mathbf{I}_{N_{pq}})^{-1} \mathbf{H}^H \mathcal{C} \boldsymbol{\beta} \quad (8.457)$$

$$= \mathbf{H}^H \mathcal{C} (\mathcal{C}^T \mathbf{H} \mathbf{H}^H \mathcal{C} + \rho \sigma_s^2 \mathbf{I}_{Kq})^{-1} \boldsymbol{\beta} \quad (8.458)$$

which are the same as (8.113) and (8.114), respectively.

Similarly, we can derive the preprocessing matrices for the other types of MUTP scheme based on their corresponding MUD schemes, according to the relationship between the MUD and MUTP obtained in this section.

8.5 Extraction of Channel Knowledge for Transmitter Preprocessing in Multicarrier CDMA Systems

In Sections 8.2 and 8.3, various transmitter preprocessing schemes were established in conjunction with both the F-domain spread MC-CDMA and TF-domain spread MC DS-CDMA. It can be seen that a basic requirement for the BS to carry out the transmitter preprocessing is that the transmitter uses knowledge about both the spreading sequences (code signatures) and the CIRs, which can also be referred to as the *spatial signatures*, in the context of all the downlink MTs. While the BS always employs the code signatures of all the downlink MTs, to obtain the knowledge about the CIRs of the downlink channels is not straightforward. Hence, in this section the extraction of channel knowledge is addressed, when various communication scenarios are considered. Specifically, three types of communication duplexing scenarios will be considered in this section. The first two are the well-known TDD and FDD. The third one is the MDD, which is proposed specifically for the multicarrier communications systems, where the transmitters require the CIR information for carrying out transmitter preprocessing.

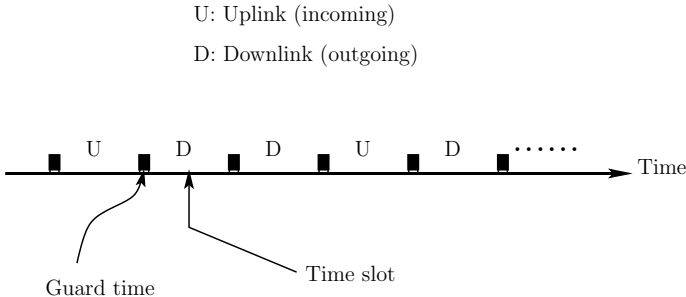


Figure 8.29: Illustrate of the TDD.

8.5.1 Time-Division Duplex (TDD)

In the context of the wireless communications systems based on TDD, the uplink and downlink are separated (orthogonal) in the time domain, while communicating within the same frequency band. Specifically, as shown in Fig. 8.29, in the TDD-based wireless systems the time axis is first divided into frames. Each frame is then further divided into a number of time slots. A time slot can be assigned either for the uplink (U) transmission or for the downlink (D) transmission. Due to the fact that wireless channels experience delay spread, which results in intersymbol interference (ISI), a certain amount of guard-time is usually inserted between two adjacent time slots.

TDD has a typical advantage in the communications scenario where the uplink and downlink data rates are asymmetric and variable. In this case, as shown in Fig. 8.29, as the amount of downlink data increases and that of the uplink data decreases, more time slots (bandwidth) can be dynamically allocated to the downlink, while fewer time slots (bandwidth) are correspondingly allocated to the uplink.

Another advantage of using TDD is that the uplink and downlink channels in TDD-based systems are reciprocal. In this case, the broadcast downlink channels from BS to MTs can be estimated or predicted using its reciprocity with the uplink channels from MTs to BS. As shown in Fig. 8.29, provided that the channel fading is sufficiently slow, the channel knowledge required for downlink preprocessing can be extracted from the uplink channels with the aid of efficient channel estimation or prediction approaches [146]. However, when the channel fading is fast, resulting in the estimation or prediction of the downlink channels insufficiently accurate, more frame time slots might be allocated for uplink transmission in order for the BS to have more observations for providing relatively more accurate channel estimation or prediction for the downlink channels.

While the TDD-based wireless communication systems employ the above-mentioned advantages, especially the advantage of facilitating the downlink channel estimation at BS, the TDD-based systems also have some disadvantages, especially with regard to cellular communications. First, the TDD mode is very demanding on system synchronization. Second, the TDD mode is not efficient when the uplink and downlink transmissions are symmetric. In this case, the TDD mode tends to waste bandwidth while switching frequently between transmitting and receiving. Furthermore, the fast switching between transmitting and receiving requires complex and power-hungry circuitry, and, since

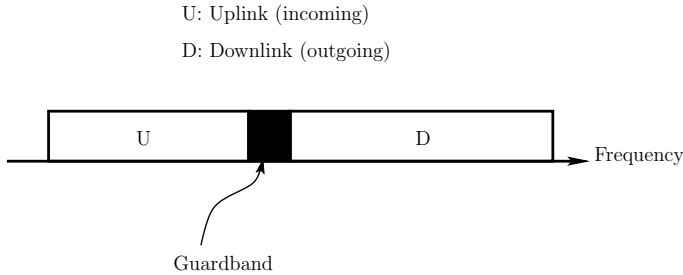


Figure 8.30: Illustrate of the frequency-division duplex (FDD).

in the TDD-based systems the uplink and downlink are operated within the same frequency band, the TDD mode tends to conflict severe intracell and intercell interference. In a multicell TDD-based wireless system, an uplink (downlink) signal experiences interference not only from the other uplink (downlink) signals of its own cell but also from both the uplink and downlink signals of the other cells.

8.5.2 Frequency-Division Duplex (FDD)

For the wireless communications systems based on FDD, the uplink and downlink are separated (orthogonal) in the frequency-domain. The principles of FDD can be well understood with the aid of Fig. 8.30. In FDD-assisted wireless communications, the available frequency band is divided into two sub-bands, one is for the uplink and the other is for the downlink, which are supported by the carrier frequencies f_U and f_D , respectively. The uplink and downlink sub-bands are separated by a so-called guardband.

The FDD mode is efficient for the transmission of symmetric traffics of the uplink and downlink. Another advantage of the FDD is that it makes radio planning easier and more efficient. In FDD-based wireless systems, in principle there is no interference between uplink and downlink signals. An uplink signal conflicts interference only from the uplink signals of the intracell and intercells, while a downlink signal conflicts interference only from the downlink signals of the intracell and intercells.

Since in FDD-based systems the uplink and downlink are operated on two separate frequency bands, the uplink and downlink channels are not reciprocal. Therefore, applying the CIR-dependent transmitter preprocessing techniques in FDD-based systems is much more difficult than applying them in TDD-based systems. In FDD-based systems the channel knowledge required to carry out the preprocessing might have to be fed back from the receiver(s) to the transmitter(s). However, feeding back the channel knowledge requires extra bandwidth, which substantially reduces the communications efficiency.

An alternative way for FDD-based systems to utilize transmitter preprocessing is that, instead of carrying out transmitter full-preprocessing, transmitter partial-preprocessing might be used. Here, we refer to the transmitter full-preprocessing as those types of preprocessing which invoke all the knowledge, including code signatures, CIRs, etc. for the preprocessing, so that the transmitters are capable of doing anything except match filter for the receiver(s). By contrast, the transmitter partial-preprocessing uses only the part of available knowledge, such as code signatures, for carrying out preprocessing. As an example, in FDD-based MC

DS-CDMA systems the channel knowledge is usually not available at the BS transmitter without using feedback, but the BS knows the T-domain spreading sequences of all the downlink MTs. In this case, the preprocessing can be carried out in the T-domain in the context of each of the subcarriers, in order to mitigate the multiuser interference generated by the T-domain spreading sequences. At the MTs, receiver processing can be carried out to further suppress the MUI and also to implement the coherent combining in order to achieve frequency-domain diversity.

8.5.3 Multicarrier-Division Duplex (MDD)

In the last two subsections two types of duplexing scheme, namely the TDD and FDD, were discussed. Clearly, both of them have some advantages and some disadvantages, depending on the specific communications environments concerned. Specifically, the TDD mode is beneficial to transmitter preprocessing use, since in the TDD-based systems the uplink and downlink channels are reciprocal and the channel knowledge for transmitter preprocessing can be relatively easy to obtain, being directly estimated from the received signals. Comparing with the TDD-mode, in FDD-based systems transmitter preprocessing techniques are not straightforward to apply. This is mainly because in FDD-based systems, in most cases, the channel knowledge required for carrying out transmitter preprocessing cannot be extracted at the transmitter side and has to be fed back from the receiver(s). However, in cellular wireless communications the FDD mode is usually capable of providing higher (total) throughput than the TDD mode, since a user signal communicating in FDD mode usually conflicts (or imposes) lower interference from (or on) the other user signals, in comparison with a user signal communicating in TDD mode.

When multicarrier communications are considered, MDD, as shown in Fig. 8.31 might be employed for the uplink and downlink transmissions. MDD essentially belongs to the family of FDD. Specifically, in multicarrier systems both the uplink and downlink can be operated within the same frequency band. A fraction of the sub-bands (subcarriers) can be allocated to support the uplink communications, the remainder are for the downlink communications. Explicitly, the MDD-mode has all the advantages of the TDD-mode. First, the MDD-mode is capable of supporting asymmetric and variable traffics for the uplink and downlink. This can be easily achieved by dynamically allocating the corresponding number of sub-bands. Second, in MDD-mode the channel knowledge required to carry out transmitter preprocessing can be easily obtained with the aid of the frequency-domain channel estimation or prediction, as will be shown in detail below. The MDD-mode also inherits some of the merits of the FDD-mode. For example, in FDD-mode there is no switchover between transmitting and receiving. In MDD-mode there is no or only a very low chance of switchover between transmitting and receiving. Furthermore, the MDD-mode may have some merits that the TDD and FDD modes are incapable of providing. The MDD-mode has the highest flexibility for design or online reconfiguration, since, in comparison with the TDD and FDD modes, the MDD-mode uses a higher number of parameters that can be adjusted according to requirement. Furthermore, it seems that the MDD-mode is suitable for many types of communication environment, including short-distance and long-distance communications, different types of cellular wireless communication, indoor and outdoor, etc.

One typical problem with MDD-mode is the added intercarrier interference, which may degrade the achievable performance significantly when the channel fading becomes time-

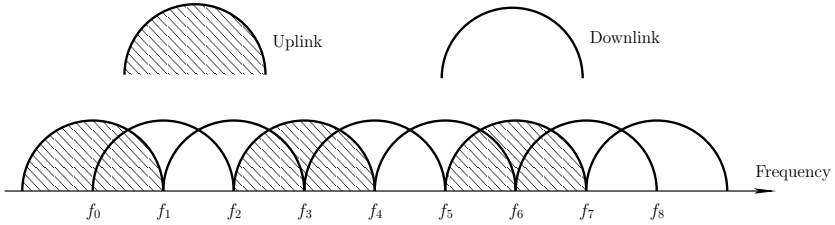


Figure 8.31: Illustrate of the multicarrier-division duplex (MDD).

selective or when there is frequency offset. Hence, in MDD-mode the intercarrier interference should be taken care of, which may be mitigated with the aid of some advanced signal processing techniques.

Below, the details of the MDD-mode in conjunction with transmitter preprocessing are provided, when considering various communications scenarios. Let us first consider the principles of MDD.

8.5.3.1 Principles of MDD: Gaussian Channels

In this section the principles of MDD are established, when assuming that the communication channels are Gaussian. Let us assume that in the considered MDD-based system the total bandwidth for both the uplink and downlink transmissions is divided into \mathcal{U} sub-bands associated with \mathcal{U} number of subcarriers with their frequencies indexed by $f_1, f_2, \dots, f_{\mathcal{U}}$. Let the \mathcal{U} number of subcarriers be divided into G sets, each set having M subcarriers, i.e. $\mathcal{U} = GM$, where ($G \geq 2$) is an integer. Let $V_U = \mu_U M$ ($1 \leq \mu_U < G$) represent the number of subcarriers for supporting the uplink transmission, while $V_D = \mu_D M$ ($\mu_D = G - \mu_U$) represents the number of subcarriers for supporting the downlink transmission. Assume an orthogonal multicarrier scheme and the subcarrier signals are arranged in a form as shown in Fig. 8.31, where $G = 3$ and one-third of the sub-bands are allocated to support the uplink, while the remaining two-thirds of the sub-bands are allocated to support the downlink. Furthermore, it is assumed that the spacing between two adjacent subcarriers is $1/T_c$, where T_c represents the chip duration of the spreading sequences and the value of T_c controls the sub-bands' bandwidth.

Explicitly, the MDD scheme based on the above-assumed settings employs the flexibility for supporting asymmetric and variable traffics. This can be achieved simply by allocating an appropriate number of subcarriers for the up- and downlinks.

After the transmitter processing (Fig. 5.4), let the signals transmitted by the k th MT on the uplink subcarriers be denoted as

$$\begin{aligned} \mathbf{d}_g^{(k)} &= [d_{g0}^{(k)}, d_{g1}^{(k)}, \dots, d_{g(M-1)}^{(k)}]^T \\ g &= 1, 2, \dots, \mu_U; k = 1, 2, \dots, K \end{aligned} \quad (8.459)$$

where K represents the number of MTs supported by the uplink. After the transmitter preprocessing, let the signals transmitted by the BS to the k 'th MT on the downlink

subcarriers be denoted as

$$\begin{aligned}\mathbf{d}_{g'}^{(k')} &= [d_{g'0}^{(k')}, d_{g'1}^{(k')}, \dots, d_{g'(M-1)}^{(k')}]^T \\ g' &= 1, 2, \dots, \mu_D; k' = 1, 2, \dots, K'\end{aligned}\quad (8.460)$$

where K' represents the number of MTs supported by the downlink.

For convenience, let us introduce the concepts of reduced-DFT (RDFT) and reduced-IDFT (RIDFT), the meaning of which will become explicit following our analysis. Carrying out the RIDFT processing in the context of the g th or g' th set of frequencies on $\mathbf{d}_g^{(k)}$ or $\mathbf{d}_{g'}^{(k')}$, the output signals can be expressed respectively as

$$\begin{aligned}s_g^{(k)} &= \mathbf{A}_g^* \mathbf{F}^* \mathbf{d}_g^{(k)}, \quad g = 1, 2, \dots, \mu_U; k = 1, 2, \dots, K \\ s_{g'}^{(k')} &= \mathbf{A}_{g'}^* \mathbf{F}^* \mathbf{d}_{g'}^{(k')}, \quad g' = 1, 2, \dots, \mu_D; k' = 1, 2, \dots, K'\end{aligned}\quad (8.461)$$

where by definition

$$\begin{aligned}s_a^{(b)} &= [s_a^{(b)}[0], s_a^{(b)}[1], \dots, s_a^{(b)}[\mathcal{U}-1]]^T \\ \mathbf{A}_a &= \text{diag} \left\{ 1, \exp \left(-j \frac{2\pi G(a)}{\mathcal{U}} \right), \dots, \exp \left(-j \frac{2\pi G(a)(\mathcal{U}-1)}{\mathcal{U}} \right) \right\}\end{aligned}\quad (8.462)$$

where $a \in \{g, g'\}$, $b \in \{k, k'\}$ and $G(a)$ represent the mapping of a to an index in $\{0, 1, \dots, G-1\}$ for frequency sets. For example, in a MDD system there are $G = 2N$ sets of frequencies. Let the odd sets of frequencies, i.e. sets $1, 3, \dots, 2N-1$, be assigned for the uplink transmissions, while the even sets of frequencies, i.e. sets $0, 2, \dots, 2N$, be assigned for the downlink transmissions. Then, we may have the mapping

$$G(g) = 2g - 1, \quad g = 1, 2, \dots, N; \quad G(g') = 2g', \quad g' = 0, 1, \dots, N-1 \quad (8.463)$$

In (8.461) \mathbf{F} is a $(\mathcal{U} \times M)$ RDFT matrix, which is given by

$$\mathbf{F} = \frac{1}{\sqrt{\mathcal{U}}} \begin{bmatrix} 1 & 1 & \cdots & 1 \\ 1 & \exp \left(-j \frac{2\pi G}{\mathcal{U}} \right) & \cdots & \exp \left(-j \frac{2\pi G \cdot (M-1)}{\mathcal{U}} \right) \\ 1 & \exp \left(-j \frac{2\pi G \cdot 2}{\mathcal{U}} \right) & \cdots & \exp \left(-j \frac{2\pi G \cdot (M-1)2}{\mathcal{U}} \right) \\ \vdots & \vdots & \ddots & \vdots \\ 1 & \exp \left(-j \frac{2\pi G \cdot (\mathcal{U}-1)}{\mathcal{U}} \right) & \cdots & \exp \left(-j \frac{2\pi G \cdot (M-1)(\mathcal{U}-1)}{\mathcal{U}} \right) \end{bmatrix} \quad (8.464)$$

which is in fact constituted by M (i.e. 0th, G th, ..., $G(M - 1)$ th columns) out of the \mathcal{U} columns of the DFT matrix \mathcal{F} given by

$$\mathcal{F} = \frac{1}{\sqrt{\mathcal{U}}} \begin{bmatrix} 1 & 1 & \cdots & 1 \\ 1 & \exp\left(-j\frac{2\pi}{\mathcal{U}}\right) & \cdots & \exp\left(-j\frac{2\pi(\mathcal{U}-1)}{\mathcal{U}}\right) \\ 1 & \exp\left(-j\frac{2\pi^2}{\mathcal{U}}\right) & \cdots & \exp\left(-j\frac{2\pi(\mathcal{U}-1)^2}{\mathcal{U}}\right) \\ \vdots & \vdots & \ddots & \vdots \\ 1 & \exp\left(-j\frac{2\pi(\mathcal{U}-1)}{\mathcal{U}}\right) & \cdots & \exp\left(-j\frac{2\pi(\mathcal{U}-1)(\mathcal{U}-1)}{\mathcal{U}}\right) \end{bmatrix} \quad (8.465)$$

Since the DFT matrix \mathcal{F} has the property of $\mathcal{F}\mathcal{F}^H = \mathcal{F}^H\mathcal{F} = I_{\mathcal{U}}$, explicitly, we have $\mathcal{F}^H\mathbf{F} = I_M$ and also $\mathbf{F}^T\mathbf{F}^* = I_M$.

Let us assume that both the uplink and downlink signals are ideally synchronized. Then, for a given receiver terminal indexed by κ , which is either the BS or one of the MTs, the received signal after the matched filtering and S/P conversion (Fig. 5.4) can be expressed as

$$\begin{aligned} \mathbf{r}_\kappa &= \sum_{k=1}^K h_k s_g^{(k)} + h_\kappa \sum_{k'=1}^{K'} s_{g'}^{(k')} + \mathbf{n}_\kappa \\ &= \sum_{k=1}^K h_k \mathbf{A}_g^* \mathcal{F}^* \mathbf{d}_g^{(k)} + h_\kappa \sum_{k'=1}^{K'} \mathbf{A}_{g'}^* \mathcal{F}^* \mathbf{d}_{g'}^{(k')} + \mathbf{n}_\kappa \end{aligned} \quad (8.466)$$

where \mathbf{r}_κ is a \mathcal{U} -length vector. Note that, to obtain (8.466) we assumed that the receiver terminal κ may also receive the signal transmitted by itself, if it is the BS or one of the MTs transmitting signals. However, in practice a terminal may be designed so that it does not receive its own transmitted signals. In (8.466) h_k represents the uplink channel gain, h_κ represents the channel gain connecting the BS to the receiver terminal κ , both h_k and h_κ are assumed to be given constants, since the AWGN channels are considered in this section. Furthermore, in (8.466) \mathbf{n}_κ is a \mathcal{U} -length AWGN vector, the entries of \mathbf{n}_κ are Gaussian distributed with zero mean and a variance of $\sigma^2/2$ per dimension.

Since the columns of the RDFT matrix $\mathbf{A}_a\mathbf{F}$ are chosen from the DFT matrix \mathcal{F} of (8.465), hence $\mathbf{A}_a\mathbf{F}$ has the properties that, if $i \in \{g\}$ and $j \in \{g'\}$, then

$$\mathbf{F}^T \mathbf{A}_i \mathbf{A}_j^* \mathbf{F}^* = \mathbf{0} \quad (8.467)$$

if $i, j \in \{g\}$ or $i, j \in \{g'\}$, then

$$\mathbf{F}^T \mathbf{A}_i \mathbf{A}_j^* \mathbf{F}^* = \begin{cases} I_M, & \text{if } i = j \\ \mathbf{0}, & \text{if } i \neq j \end{cases} \quad (8.468)$$

Applying the RDFT to \mathbf{r}_κ associated with the matrix $\mathbf{A}_i \mathbf{F}$, which characterizes the $G(i)$ th set of frequencies, we obtain

$$\begin{aligned} \mathbf{y}_\kappa &= \mathbf{F}^T \mathbf{A}_i \mathbf{r}_\kappa \\ &= \sum_{k_i=1}^{K_i} h_{k_i} \mathbf{F}^T \mathbf{A}_i \mathbf{A}_i^* \mathbf{F}^* \mathbf{d}_i^{(k_i)} + \sum_{k=1, G(g) \neq G(i)}^K h_k \mathbf{F}^T \mathbf{A}_i \mathbf{A}_g^* \mathbf{F}^* \mathbf{d}_g^{(k)} \\ &\quad + h_\kappa \sum_{k'=1}^{K'} \mathbf{F}^T \mathbf{A}_i \mathbf{A}_{g'}^* \mathbf{F}^* \mathbf{d}_{g'}^{(k')} + \mathbf{F}^T \mathbf{A}_i \mathbf{n}_\kappa \end{aligned} \quad (8.469)$$

when $i \in \{g\}$, i.e. when the receiver terminal is the BS, and

$$\begin{aligned} \mathbf{y}_\kappa &= \mathbf{F}^T \mathbf{A}_i \mathbf{r}_\kappa \\ &= h_\kappa \sum_{k_i=1}^{K_i} \mathbf{F}^T \mathbf{A}_i \mathbf{A}_i^* \mathbf{F}^* \mathbf{d}_i^{(k_i)} + \sum_{k=1}^K h_k \mathbf{F}^T \mathbf{A}_i \mathbf{A}_g^* \mathbf{F}^* \mathbf{d}_g^{(k)} \\ &\quad + h_\kappa \sum_{k'=1, G(g') \neq G(i)}^{K'} \mathbf{F}^T \mathbf{A}_i \mathbf{A}_{g'}^* \mathbf{F}^* \mathbf{d}_{g'}^{(k')} + \mathbf{F}^T \mathbf{A}_i \mathbf{n}_\kappa \end{aligned} \quad (8.470)$$

when $i \in \{g'\}$, i.e. when the receiver terminal is a MT. In (8.469) and (8.470) K_i represents the number of MTs supported by the $G(i)$ th set of frequencies. Note, furthermore, that \mathbf{y}_κ in (8.469) and (8.470) are M -length vectors. Applying the results in (8.467) and (8.468) into the above two equations, it can be easily shown that

$$\mathbf{y}_\kappa = \sum_{k_i=1}^{K_i} h_{k_i} \mathbf{d}_i^{(k_i)} + \mathbf{F}^T \mathbf{A}_i \mathbf{n}_\kappa \quad (8.471)$$

when the receiver terminal is the BS, and

$$\mathbf{y}_\kappa = h_\kappa \sum_{k_i=1}^{K_i} \mathbf{d}_i^{(k_i)} + \mathbf{F}^T \mathbf{A}_i \mathbf{n}_\kappa \quad (8.472)$$

when the receiver terminal is a MT.

The results of (8.471) and (8.472) show that the RDFT processing based on $\mathbf{A}_i \mathbf{F}$ successfully recovers the multiuser signals transmitted on the $G(i)$ th set of frequencies. By contrast, the multiuser signals transmitted on the other ($G - 1$) sets of frequencies are fully removed, regardless of that they are for the uplink or downlink. Therefore, when communicating over AWGN channels, the uplink (or incoming) and downlink (or outgoing) in wireless communications can be duplexed based on the MDD principles as above-described. We now turn to show that the MDD is also valid when communicating over frequency-selective fading channels.

8.5.3.2 MDD Systems in Frequency-Selective Fading Channels

Let the CIR of the frequency-selective fading channel be expressed as

$$h_k(\tau) = \sum_{l=0}^{L_k-1} h_l^{(k)} \delta(\tau - lT_\psi) \quad (8.473)$$

where L_k represents the number of resolvable paths in terms of the k th MT, $h_l^{(k)}$ is the complex channel gain of the l th resolvable path, and T_ψ is the duration of a transmitted sample and $T_\psi = 1/W_s$, where W_s is the overall frequency bandwidth supporting both the uplink and downlink.

Again, let us assume that both the uplink and downlink signals are ideally synchronized. Let the transmitted signals be in the form of (8.461). Then, for a given receiver terminal of κ , which is either the BS or one of the MTs, after the matched filtering, removing the cyclic prefixing (CP) samples (or zero padding (ZP) processing), and S/P conversion, as shown in Fig. 5.4, the received signal of terminal κ can be expressed as

$$\mathbf{r}_\kappa = \sum_{k=1}^K \check{\mathbf{H}}^{(k)} \mathbf{A}_g^* \mathcal{F}^* \mathbf{d}_g^{(k)} + \check{\mathbf{H}}^{(\kappa)} \sum_{k'=1}^{K'} \mathbf{A}_{g'}^* \mathcal{F}^* \mathbf{d}_{g'}^{(k')} + \mathbf{n}_\kappa \quad (8.474)$$

where $\check{\mathbf{H}}^{(k)}$ is a $(\mathcal{U} \times \mathcal{U})$ circulant matrix representing the channels connecting the k th transmitter to terminal κ , while $\check{\mathbf{H}}^{(\kappa)}$ is a $(\mathcal{U} \times \mathcal{U})$ circulant matrix representing the channels connecting the BS transmitter to terminal κ , both $\check{\mathbf{H}}^{(k)}$ and $\check{\mathbf{H}}^{(\kappa)}$ are in the form of (5.49) shown in Chapter 5.

Let us assume that the κ th receiver terminal aims to detect the information on the $G(i)$ th set of frequencies, which might support the uplink if terminal κ is the BS or support the downlink if terminal κ is one of the MTs. Then, as the AWGN channel case seen in (8.469) and (8.470), terminal κ uses $\mathbf{A}_i \mathbf{F}$ to recover the signals transmitted on the $G(i)$ th set of frequencies, while suppressing the signals transmitted on the other sets of frequencies. Following (8.469) and (8.470), this operation can be expressed as

$$\begin{aligned} \mathbf{y}_\kappa &= \mathbf{F}^T \mathbf{A}_i \mathbf{r}_\kappa \\ &= \sum_{k_i=1}^{K_i} \mathbf{F}^T \mathbf{A}_i \check{\mathbf{H}}^{(k_i)} \mathbf{A}_i^* \mathbf{F}^* \mathbf{d}_i^{(k_i)} + \sum_{k=1, G(g) \neq G(i)}^K \mathbf{F}^T \mathbf{A}_i \check{\mathbf{H}}^{(k)} \mathbf{A}_g^* \mathbf{F}^* \mathbf{d}_g^{(k)} \\ &\quad + \sum_{k'=1}^{K'} \mathbf{F}^T \mathbf{A}_i \check{\mathbf{H}}^{(\kappa)} \mathbf{A}_{g'}^* \mathbf{F}^* \mathbf{d}_{g'}^{(k')} + \mathbf{F}^T \mathbf{A}_i \mathbf{n}_\kappa \end{aligned} \quad (8.475)$$

when $i \in \{g\}$, i.e. when the receiver terminal is the BS, and

$$\begin{aligned} \mathbf{y}_\kappa &= \mathbf{F}^T \mathbf{A}_i \mathbf{r}_\kappa \\ &= \sum_{k_i=1}^{K_i} \mathbf{F}^T \mathbf{A}_i \check{\mathbf{H}}^{(k_i)} \mathbf{A}_i^* \mathbf{F}^* \mathbf{d}_i^{(k_i)} + \sum_{k=1}^K \mathbf{F}^T \mathbf{A}_i \check{\mathbf{H}}^{(k)} \mathbf{A}_g^* \mathbf{F}^* \mathbf{d}_g^{(k)} \\ &\quad + \sum_{k'=1, G(g') \neq G(i)}^{K'} \mathbf{F}^T \mathbf{A}_i \check{\mathbf{H}}^{(\kappa)} \mathbf{A}_{g'}^* \mathbf{F}^* \mathbf{d}_{g'}^{(k')} + \mathbf{F}^T \mathbf{A}_i \mathbf{n}_\kappa \end{aligned} \quad (8.476)$$

when $i \in \{g'\}$, i.e. when the receiver terminal is a MT.

According to (5.48) in Chapter 5, the circulant matrix $\check{\mathbf{H}}^{(k)}$ satisfies

$$\mathcal{F} \check{\mathbf{H}}^{(k)} \mathcal{F}^H = \mathbf{H}^{(k)} \quad (8.477)$$

where

$$\mathbf{H}^{(k)} = \text{diag}\{H_0^{(k)}, H_1^{(k)}, \dots, H_{\mathcal{U}-1}^{(k)}\} \quad (8.478)$$

associated with

$$H_u^{(k)} = \sum_{l=0}^{L_k-1} h_l^{(k)} \exp\left(-j \frac{2\pi ul}{\mathcal{U}}\right), \quad u = 0, 1, \dots, \mathcal{U}; k = 1, 2, \dots, K \quad (8.479)$$

which is the fading gain corresponding to the u th subcarrier of the k th MT.

The property of (8.477) implies that

$$\mathbf{F}^T \mathbf{A}_i \check{\mathbf{H}}^{(k)} \mathbf{A}_j^* \mathbf{F}^* = \begin{cases} \mathbf{H}_i^{(k)} & \text{if } i = j \\ \mathbf{0} & \text{otherwise} \end{cases} \quad (8.480)$$

where $\mathbf{H}_i^{(k)} = \text{diag}\{H_{i0}^{(k)}, H_{i1}^{(k)}, \dots, H_{i(M-1)}^{(k)}\}$ and

$$H_{ij}^{(k)} = \sum_{l=0}^{L_k-1} h_l^{(k)} \exp\left(-j \frac{2\pi[Gj + G(i)]l}{\mathcal{U}}\right) \quad (8.481)$$

where $i \in \{g, g'\}$. Explicitly, $\mathbf{H}_i^{(k)}$ contains the M number of fading gains of the subcarriers indexed by $\{G(i), G+G(i), \dots, G(M-1)+G(i)\}$.

After applying the results of (8.480) into (8.475) and (8.476), they can be simplified to

$$\mathbf{y}_\kappa = \sum_{k_i=1}^{K_i} \mathbf{H}_i^{(k_i)} \mathbf{d}_i^{(k_i)} + \underbrace{\mathbf{F}^T \mathbf{A}_i \mathbf{n}_\kappa}_{\mathbf{n}'_\kappa} \quad (8.482)$$

when the receiver terminal is the BS, and

$$\mathbf{y}_\kappa = \mathbf{H}_i^{(\kappa)} \sum_{k_i=1}^{K_i} \mathbf{d}_i^{(k_i)} + \underbrace{\mathbf{F}^T \mathbf{A}_i \mathbf{n}_\kappa}_{\mathbf{n}'_\kappa} \quad (8.483)$$

when the receiver terminal is a MT. It can be shown that $\mathbf{n}'_\kappa = \mathbf{F}^T \mathbf{A}_i \mathbf{n}_\kappa$ is an M -length complex Gaussian vector, which is distributed with zero mean and a covariance matrix of $\sigma^2 \mathbf{I}_M$.

Below, we analyse the correlation properties of the fading gains $\{H_u^{(k)}\}$ seen in (8.479). Therefore, we relate the fading gains to time as $\{h_l^{(k)}[i]\}$ and $\{H_u^{(k)}[i]\}$, where i is the time index. Furthermore, we assume that the maximum Doppler frequency shift is f_D and that the IDFT/DFT duration is T , which is in fact T_c when the orthogonal MC DS-CDMA is considered.

Based on the above assumptions, it can be shown that the autocorrelation in the time domain can be computed as [131]

$$\begin{aligned}
E[H_u^{(k)}[i](H_u^{(k)}[i+n])^*] &= \sum_{l=0}^{L_k-1} \sum_{v=0}^{L_k-1} E[h_l^{(k)}[i](h_v^{(k)}[i+n])^*] \\
&\quad \times \exp\left(-j \frac{2\pi ul}{\mathcal{U}}\right) \exp\left(j \frac{2\pi uv}{\mathcal{U}}\right) \\
&= \sum_{l=0}^{L_k-1} E[h_l^{(k)}[i](h_l^{(k)}[i+n])^*] \\
&= J_0(2\pi f_D n T) \sum_{l=0}^{L_k-1} |h_l^{(k)}[i]|^2
\end{aligned} \tag{8.484}$$

where $J_0(x)$ is the 0th order Bessel function of the first kind. Explicitly, the above autocorrelation function is independent of the index u . Hence, the time-domain correlation coefficient can be expressed as

$$\rho_t^{(k)}(n) = J_0(2\pi f_D n T) \tag{8.485}$$

The autocorrelation function in the frequency domain can be computed as

$$\begin{aligned}
E[H_u^{(k)}[i](H_v^{(k)}[i])^*] &= \sum_{l=0}^{L_k-1} \sum_{n=0}^{L_k-1} E[h_l^{(k)}[i](h_n^{(k)}[i])^*] \\
&\quad \times \exp\left(-j \frac{2\pi ul}{\mathcal{U}}\right) \exp\left(j \frac{2\pi vn}{\mathcal{U}}\right) \\
&= \sum_{l=0}^{L_k-1} |h_l^{(k)}[i]|^2 \exp\left(-j \frac{2\pi(u-v)l}{\mathcal{U}}\right)
\end{aligned} \tag{8.486}$$

which is related to the time index of i . Therefore, the frequency-domain correlation coefficient can be expressed as

$$\rho_f^{(k)}(i) = \left(\sum_{l=0}^{L_k-1} |h_l^{(k)}[i]|^2 \right)^{-1} \sum_{l=0}^{L_k-1} |h_l^{(k)}[i]|^2 \exp\left(-j \frac{2\pi(u-v)l}{\mathcal{U}}\right) \tag{8.487}$$

Note that the correlation coefficients considered in (8.485) and (8.487) take into account both the amplitude and phase correlations. By contrast, in the Introduction of Chapter 5, the correlation coefficient given in (5.4) or (5.7) is the envelope correlation coefficient of the wireless channels.

Figures 8.32 and 8.33 show the TF fading characteristics of a frequency-selective fading channel, when the available bandwidth is divided into $\mathcal{U} = 256$ sub-bands. In Fig. 8.32 it was assumed that the number of resolvable paths was $L = 10$ and the multipaths obeyed a uniform multipath delay profile (MDP), i.e. all the multipath components have the same average power. By contrast, in the context of Fig. 8.33, the number of resolvable paths was $L = 20$ and the multipaths obeyed an exponential MDP, where the first resolvable path has the highest

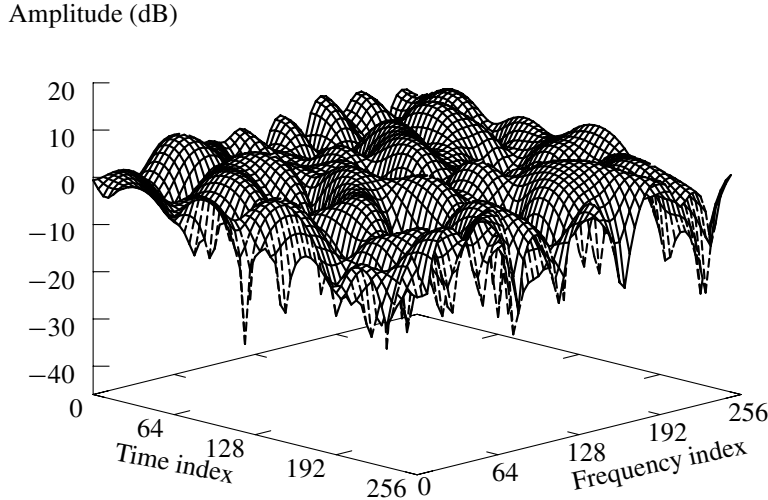


Figure 8.32: Uniform multipath delay profile: Time-frequency fading envelope of a MC signal using $\mathcal{U} = 256$ subcarriers, when communicating over a frequency-selective fading channel having $L = 10$ resolvable paths and assuming a normalized Doppler frequency-shift of $f_D T = 0.01$.

average power and the average power of the other resolvable paths decreases exponentially with the delay. Figures 8.32 and 8.33 show that the fading varies in both the T-domain and F-domain. In the T-domain the varying (fading) rate is determined by the maximum Doppler frequency-shift f_D , while in the F-domain the varying rate is determined by the number of resolvable paths as well as the distribution of the MDPs. Usually, the T-domain varying becomes faster when the maximum Doppler frequency shift increases; the F-domain varying becomes faster when the number of resolvable paths increases. When Fig. 8.32 is compared with Fig. 8.33, we can see that in the F-domain the channel corresponding to Fig. 8.32 varies faster than that corresponding to Fig. 8.33, even the number of resolvable paths for Fig. 8.32 is only half that for Fig. 8.33. This is because when exponential MDP is experienced, only the first several multipaths dominate the fading characteristics in the F-domain. In practice, frequency-selective fading channels usually follow the exponential MDP.

In Fig. 8.34 the F-domain envelope and phase of a frequency-selective fading channel with $L = 10$ resolvable paths are depicted, when a MC scheme having $\mathcal{U} = 256$ subcarriers is considered. It can be seen that the fading amplitude and phase are highly correlated in the F-domain.

8.5.3.3 Channel Estimation/Prediction in MDD Systems

Based on the analysis in Section 8.5.3.2 and also the results shown in Figs 8.32 to 8.34, it can be implied that, when the MDD is employed, the downlink (uplink) channels can be estimated through the uplink (downlink) channels. In this way the channel state information for carrying out transmitter preprocessing can be acquired. Below, we show the principles of channel estimation/prediction in MDD-based wireless communications systems. Two

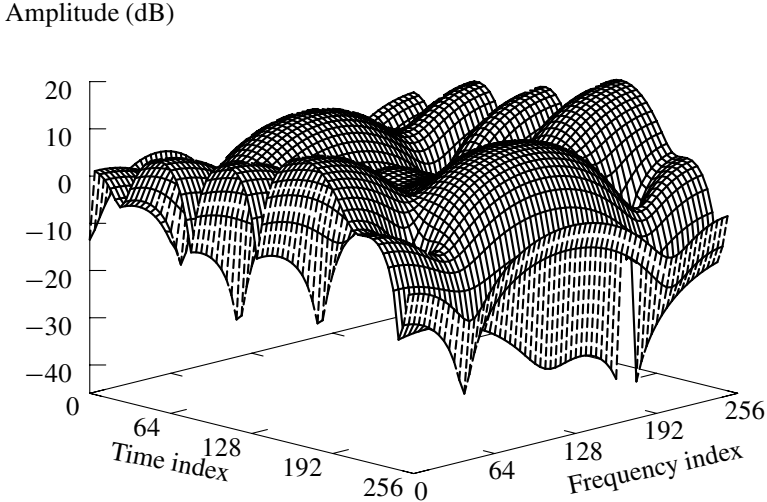


Figure 8.33: Exponential multipath delay profile: Time-frequency fading envelope of a multicarrier signal using $\mathcal{U} = 256$ subcarriers, when communicating over a frequency-selective fading channel having $L = 20$ resolvable paths and assuming a normalized Doppler frequency-shift of $f_D T = 0.01$.

cases are considered: the first case assumes ideal estimation of the uplink channels, while the second case assumes that the estimator can only access the observations of the uplink channels. In the context of the second case, the channel estimation/prediction is based on the Wiener filter theory [146]. The channel estimation is first carried out in the F-domain and then enhanced in the T-domain. Finally, future channel states for transmitter preprocessing are predicted.

The downlink channel estimation problem can be described in principle as shown in Fig. 8.35, where the filled boxes are the observations obtained from the uplink, and the empty boxes corresponding to the downlink are estimated with the aid of the information provided by the filled boxes. Finally, a prediction stage is applied in order to obtain the CIR information corresponding to the boxes filled with the cross-lines, as shown in Fig. 8.35. Having obtained the required CIR information, transmitter preprocessing for the boxes filled with cross-lines can then be operated.

Let us first consider the ideal case, which assumes that the uplink channels are ideally estimated. Let the uplink channels of a desired user at time i are collected to a vector of

$$\mathbf{H}_U[i] = [H_{U,0}[i], H_{U,1}[i], \dots, H_{U,(\mu_U M-1)}[i]]^T, \quad i = 0, 1, \dots, N-1 \quad (8.488)$$

where $\mu_U M$ is the number of subcarriers supporting the uplink. Furthermore, for simplicity, the user index k is ignored in (8.488) as well as in the forthcoming analysis. Since the uplink channels have been ideally estimated, then, according to (8.479), the elements in (8.488) can be expressed as

$$H_{U,u}[i] = \sum_{l=0}^{L-1} h_l[i] \exp\left(-j \frac{2\pi u l}{\mathcal{U}}\right), \quad u = 0, 1, \dots, \mu_U M - 1 \quad (8.489)$$

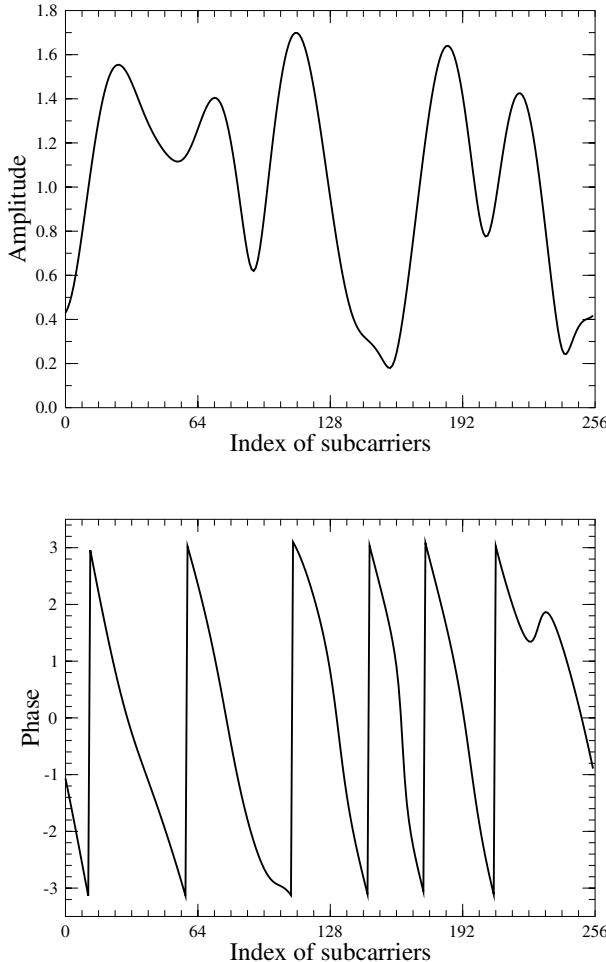


Figure 8.34: Uniform power delay profile: Envelope and phase of a multicarrier system using $\mathcal{U} = 256$ subcarriers, when communicating over a frequency-selective fading channel having $L = 10$ resolvable paths.

for $i = 0, 1, \dots, N - 1$. Hence, it can be easily shown that, for a given i , $\mathbf{H}_U[i]$ of (8.488) can be represented in a form as

$$\mathbf{H}_U[i] = \mathbf{Q}\mathbf{h}[i] \quad (8.490)$$

where \mathbf{Q} is a $(\mu_U M \times L)$ matrix, its elements are made up of the elements in the DFT matrix \mathcal{F} . Furthermore, it can be shown that \mathbf{Q} is independent of the time index i . In (8.490), $\mathbf{h}[i]$ is defined as

$$\mathbf{h}[i] = [h_0[i], h_1[i], \dots, h_{L-1}[i]]^T, \quad i = 0, 1, \dots, N - 1 \quad (8.491)$$

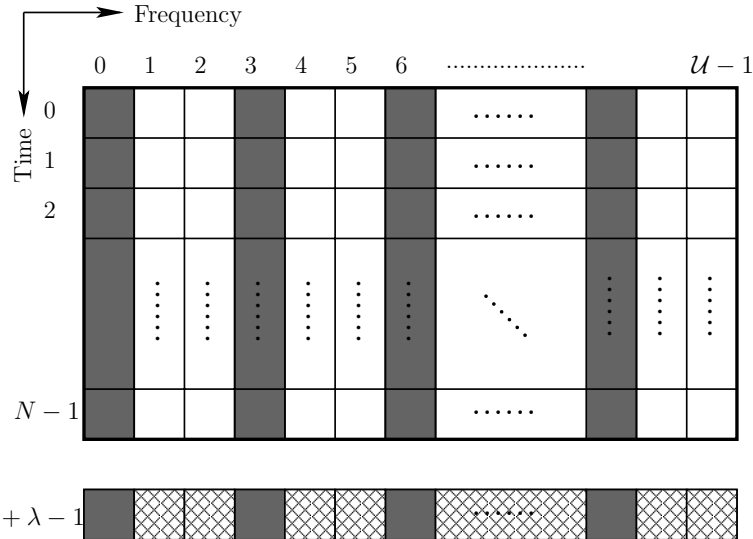


Figure 8.35: TF-domain illustration of the uplink and downlink channels in a MDD system using a total of \mathcal{U} subcarriers.

Based on (8.490), it can be shown that, provided that $\mu_U M \geq L$, we can solve the equation for $\mathbf{h}[i]$, which can be expressed as

$$\mathbf{h}[i] = (\mathbf{Q}^H \mathbf{Q})^{-1} \mathbf{Q}^H \mathbf{H}_U[i], \quad i = 0, 1, \dots, N - 1 \quad (8.492)$$

Once $\mathbf{h}[i]$ is obtained, the fading gain associated with a downlink subcarrier channel can be estimated as

$$H_{D,v}[i] = \sum_{l=0}^{L-1} h_l[i] \exp\left(-j \frac{2\pi v l}{\mathcal{U}}\right), \quad v = 0, 1, \dots, (G - \mu_U)M - 1 \quad (8.493)$$

for $i = 0, 1, \dots, N - 1$. Consequently, $\{H_{D,v}[i]\}$ can be used to predict the future channel states required for the transmitter preprocessing, as will be discussed later.

In the context of the second case where the estimator has only the observation of the uplink channels, the observation equation (8.490) can be modified to

$$\tilde{\mathbf{H}}_U[i] = \mathbf{Q}\mathbf{h}[i] + \mathbf{n}[i], \quad i = 0, 1, \dots, N - 1 \quad (8.494)$$

where $\mathbf{n}[i]$ denotes the channel noise. In order to obtain (8.494), we assumed that the data symbols transmitted on the uplink channels are detected correctly. Hence, equation (8.494) is independent of the data symbols conveyed by the uplink. Based on (8.494), $\mathbf{h}[i]$ may be estimated with the aid of many available optimization algorithms, such as those considered in Chapter 6. Below, as an example, the Wiener filter principles [146] are invoked for the channel estimation/prediction in the MDD-based systems.

Let $\mathbf{w}_u[i]$ be a weight vector for forming the estimation to the downlink channel gain $H_{D,u}[i]$ ($u = 0, 1, \dots, (G - \mu_U)M - 1$). Given (8.494), the estimation to $H_{D,u}[i]$ can be

formed as

$$\hat{H}_{D,u}[i] = \mathbf{w}_u^H[i] \bar{\mathbf{H}}_U[i], \quad u = 0, 1, \dots, (G - \mu_U)M - 1; \quad i = 0, 1, \dots, N - 1 \quad (8.495)$$

According to the MMSE principles, $\mathbf{w}_u[i]$ can be chosen as

$$\mathbf{w}_u[i] = \arg \min_{\mathbf{w}} \{E[\|H_{D,u}[i] - \mathbf{w}^H \bar{\mathbf{H}}_U[i]\|^2]\} \quad (8.496)$$

which can be readily solved and it can be shown that the solution can be expressed as

$$\mathbf{w}_u[i] = \mathbf{R}_U^{-1}[i] \mathbf{r}_{UD}^{(u)}[i] \quad (8.497)$$

where $\mathbf{R}_U[i]$ is the $(\mu_U M \times \mu_U M)$ autocorrelation matrix of $\bar{\mathbf{H}}_U[i]$, which is given by

$$\begin{aligned} \mathbf{R}_U[i] &= E[\bar{\mathbf{H}}_U[i] \bar{\mathbf{H}}_U^H[i]] \\ &= [E[\bar{H}_{U,m}[i] \bar{H}_{U,n}^*[i]]], \quad m, n = 0, 1, \dots, \mu_U M - 1 \end{aligned} \quad (8.498)$$

where $E[\bar{H}_{U,m}[i] \bar{H}_{U,n}^*[i]]$ is the (m, n) th entry of $\mathbf{R}_U[i]$. According to (8.494) and (8.489), it can be shown that we have

$$E[H_{U,m}[i] H_{U,n}^*[i]] = \begin{cases} \sum_{l=0}^{L-1} \Omega_l \exp\left(-j \frac{2\pi(f_U(m) - f_U(n))l}{\mathcal{U}}\right), & \text{if } m \neq n \\ \sum_{l=0}^{L-1} \Omega_l + \sigma^2, & \text{if } m = n \end{cases} \quad (8.499)$$

where $\Omega_l = E[|h_l[i]|^2]$, σ^2 is the variance of the complex noise, $f_U(m)$ maps the index of m to a subcarrier index used by the uplink. Similarly, $f_D(m)$ used below maps the index of m to a subcarrier index used by the downlink.

By contrast, in (8.497) $\mathbf{r}_{UD}^{(u)}[i]$ represents the $(\mu_U M \times 1)$ cross-correlation matrix between $\bar{\mathbf{H}}_U[i]$ and $H_{D,u}[i]$, which can be expressed as

$$\mathbf{r}_{UD}^{(u)}[i] = [r_{UD,0}^{(u)}[i], r_{UD,1}^{(u)}[i], \dots, r_{UD,\mu_U M-1}^{(u)}[i]]^T \quad (8.500)$$

where

$$\begin{aligned} r_{UD,m}^{(u)}[i] &= E[\bar{H}_{U,m}[i] H_{D,u}^*[i]] \\ &= \sum_{l=0}^{L-1} \Omega_l \exp\left(-j \frac{2\pi(f_U(m) - f_D(u))l}{\mathcal{U}}\right) \end{aligned} \quad (8.501)$$

It can be shown that the minimum MSE for the F-domain estimation as above described is given by

$$\begin{aligned} M_{MSE} &= E[H_{D,u}[i] H_{D,u}^*[i]] - (\mathbf{r}_{UD}^{(u)}[i])^H \mathbf{R}_U^{-1}[i] \mathbf{r}_{UD}^{(u)}[i] \\ &= \sum_{l=0}^{L-1} |h_l[i]|^2 - (\mathbf{r}_{UD}^{(u)}[i])^H \mathbf{R}_U^{-1}[i] \mathbf{r}_{UD}^{(u)}[i] \end{aligned} \quad (8.502)$$

After the F-domain channel estimation associated with all the time indices $i = 0, 1, \dots, N - 1$ of all the downlink channels, we then have the estimates

$$\begin{aligned}\hat{\mathbf{H}}_{D,u} &= [\hat{H}_{D,u}[0], \hat{H}_{D,u}[1], \dots, \hat{H}_{D,u}[N-1]]^T \\ u &= 0, 1, \dots, (G - \mu_U)M - 1\end{aligned}\quad (8.503)$$

Based on these, the estimation to the channel of a given time-index of a given downlink channel may be further enhanced in the T-domain. For example, in (8.503), $\hat{H}_{D,u}[0]$ may be enhanced using the information conveyed by $\hat{H}_{D,u}[1], \dots, \hat{H}_{D,u}[N-1]$, etc.

After the above-mentioned T-domain estimation, further rounds of estimation in the F-and/or T-domain may be carried out, in order to make the estimation as accurate as possible.

When the estimation to the downlink channels is sufficiently reliable, the future downlink channel states can now be predicted. Specifically, let us consider the u th downlink subcarrier channel and let the N number of most recently estimated channel states be expressed as (8.503) for simplicity. Then, as shown in Fig. 8.35, the λ -step ($\lambda \geq 1$) prediction to the channel state $H_{D,u}[N + \lambda - 1]$ at time $(N + \lambda - 1)$ can be expressed as

$$\tilde{H}_{D,u}[N + \lambda - 1] = \hat{\mathbf{w}}_u^H \hat{\mathbf{H}}_{D,u}, \quad u = 0, 1, \dots, (G - \mu_U)M - 1 \quad (8.504)$$

where, again, according to the MMSE principles, the weight vector $\hat{\mathbf{w}}_u$ can be chosen as

$$\hat{\mathbf{w}}_u = \arg \min_{\mathbf{w}} \{E[\|\mathbf{H}_{D,u}[N + \lambda - 1] - \mathbf{w}^H \hat{\mathbf{H}}_{D,u}\|^2]\} \quad (8.505)$$

It can be shown that the optimum solution can be expressed as

$$\hat{\mathbf{w}}_u = \mathbf{R}_D^{-1} \mathbf{r}_{D,\lambda}^{(u)} \quad (8.506)$$

where \mathbf{R}_D is the autocorrelation matrix of $\hat{\mathbf{H}}_{D,u}$ of (8.503), which can be computed as

$$\mathbf{R}_D = E[\hat{\mathbf{H}}_{D,u} \hat{\mathbf{H}}_{D,u}^H] \quad (8.507)$$

With the aid of (8.484), it can be shown that \mathbf{R}_D can be expressed as

$$\mathbf{R}_D = \sum_{l=0}^{L-1} \Omega_l^2 \times \begin{bmatrix} 1 & J_0(2\pi f_D T) & \cdots & J_0(2\pi f_D [N-1]T) \\ J_0(2\pi f_D T) & 1 & \cdots & J_0(2\pi f_D [N-2]T) \\ \vdots & \vdots & \ddots & \vdots \\ J_0(2\pi f_D [N-1]T) & J_0(2\pi f_D [N-2]T) & \cdots & 1 \end{bmatrix} \quad (8.508)$$

In (8.506) $\mathbf{r}_{D,\lambda}^{(u)}$ represents the cross-correlation function between $\hat{\mathbf{H}}_{D,u}$ and $H_{D,u}[N + \lambda - 1]$, which is given by

$$\begin{aligned}\mathbf{r}_{D,\lambda}^{(u)} &= E[\hat{\mathbf{H}}_{D,u} H_{D,u}^*[N + \lambda - 1]] \\ &= \sum_{l=0}^{L-1} \Omega_l^2 [J_0(2\pi f_D [N + \lambda - 1]T), J_0(2\pi f_D [N + \lambda - 2]T), \dots, J_0(2\pi f_D [\lambda]T)]^T\end{aligned}\quad (8.509)$$

The minimum MSE for the prediction is given by

$$MSE = E[\|H_{D,u}[N + \lambda - 1]\|^2] - (\mathbf{r}_{D,\lambda}^{(u)})^H \mathbf{R}_D^{-1} \mathbf{r}_{D,\lambda}^{(u)} \quad (8.510)$$

Based on the estimates $\{\tilde{H}_{D,u}[N + \lambda - 1]\}$, as shown in (8.504), the transmitter preprocessing for the symbols to be transmitted within the time indexed by λ can then be accomplished.

8.6 Summary and Discussion

In this chapter the principles of MUTP have been established and a range of MUTP schemes have been derived and analysed in the context of both the F-domain spread MC-CDMA and the TF-domain spread MC DS-CDMA. The error performance of the F-domain spread MC-CDMA systems and TF-domain spread MC DS-CDMA systems, which use various MUTP schemes, has been demonstrated, when communicating over frequency-selective fading channels. The equivalency between the MUD and MUTP has been developed. Furthermore, the acquisition of channel knowledge for carrying out MUTP has been discussed in the context of the TDD-, FDD- and MDD-based wireless communications systems, respectively.

From the MUD theory established in Chapter 6 and the MUTP theory provided in this chapter, it seems that there always exists a counterpart MUTP scheme for any given MUD scheme. In most cases, the MUD scheme and its counterpart MUTP scheme, which are derived under the same optimization criterion, have a similar impact on the achievable error performance. However, there are MUD schemes and their counterparts that have an explicitly different impact on the achievable error performance. For example, the interference cancellation assisted MUD scheme approximates the maximum likelihood MUD. It is capable of achieving an error performance that is very close to that achieved by the maximum likelihood MUD. By contrast, in MUTP the transmitter interference cancellation scheme actually represents an alternative implementation of the ZF-MUTP, and it achieves a similar error performance as the ZF-MUTP.

It has been shown that for any given linear MUD scheme, there exists a counterpart linear MUTP scheme. The counterpart linear MUTP scheme can be readily derived from the original linear MUD scheme associated with consideration of the constraint on the transmission power as well as the availability of the knowledge about the statistics of the background noise presenting at the remote receivers.

In various MUTP arrangements, power allocation can play a significant role in attaining the best performance. The transmission power can be allocated for achieving the lowest error rate. It can also be allocated in a way so that the system is capable of obtaining the highest throughput.

The key issue in MUTP is the acquisition of channel knowledge required for transmitter preprocessing. In TDD-based wireless systems, the channel knowledge required for carrying out the transmitter preprocessing may be readily extracted using the fact that in TDD-based wireless systems the uplink (incoming) and downlink (outgoing) channels are reciprocal. Applying the CIR-dependent transmitter preprocessing techniques in FDD-based systems is much more difficult than applying them in TDD-based systems. This is because in FDD-based systems the channel knowledge for carrying out transmitter preprocessing is hard to obtain, as the uplink and downlink channels are operated on two separate frequency bands.

In MC communications, it seems that the MDD-mode constitutes a promising duplex mode that may employ the advantages of both the TDD as well as the FDD-modes.

Chapter 9

Multiantenna Multicarrier Code-Division Multiple Access

In wireless communications multiple-input multiple-output (MIMO) systems equipped with multiple antennas at both the transmitter and receiver hold the promise of attaining substantial spectral-efficiency improvements relative to what can be achieved by the conventional single-input single-output (SISO) wireless systems, which employ single antenna at both the transmitter and receiver. Since the proposal of MIMO concept, MIMO systems have attracted intense interests in the context of both MIMO theory and applications, as indicated, for example, by the references [237–239] and also by the references therein. It has been widely recognized that MIMO systems can be used to achieve high capacity and high diversity order, to mitigate the effects of various types of interfering signal and to support space-division multiple-access (SDMA). The core principle behind the high spectral-efficiency achieved by the MIMO systems is that the multiple antennas used by the transmitter and/or receiver are capable of providing extra degrees-of-freedom in the spatial domain, in addition to the degrees-of-freedom available in the more conventionally exploited time domain and frequency domain. These increased degrees-of-freedom provide novel techniques for increasing the achievable capacity and diversity order of wireless communication systems, as well as for mitigating the effects of intentional or unintentional interfering signals.

In this chapter we begin by studying the capacity that is achievable by MIMO channels and analyse this in the context of two communications scenarios. For the first scenario, the MIMO systems are operated under the CSI/CSI mode, which assumes that both the transmitter and receiver employ the channel state information (CSI). By contrast, for the second scenario, we assume that the MIMO transmitter employs only the channel distribution information (CDI) and the CSI is only known to the receiver, yielding the so-called CDI/CSI mode. Following the capacity of MIMO channels, in Section 9.2 we provide a comprehensive overview of the spatial-diversity techniques that may be applied to the MIMO systems, which include transmit diversity, receive diversity and MIMO diversity. In the context of the transmit diversity techniques, we deal with the space–time coding (STC) and space–time spreading (STS) in a unified perspective, and illustrate that various STS schemes can be

readily designed based on the STC schemes. We illustrate that, for any given STC scheme, there exists a corresponding STS scheme, which has similar properties as the STC and is capable of achieving the same order of diversity as the STC. Furthermore, we show that STC can be viewed as a special class of STS, and STS as the generalization of STC. After the overview of spatial diversity, the principles of SDMA are considered briefly in Section 9.3.

The applications of MIMO principles in multicarrier CDMA systems are then investigated. Specifically, in Section 9.4 we consider the applications of STC in the orthogonal frequency-division multiplexing (OFDM) and the frequency (F)-domain spread MC-CDMA systems. In Section 9.5 the performance of the time-frequency (TF)-domain spread MC DS-CDMA systems using STS is investigated. Finally, in Section 9.6, as an example, we design and investigate a space-time transmission scheme for the multiantenna MC DS-CDMA downlink, when it is operated in the communications environments experiencing both frequency selective fading and time-selective fading. It can be shown that the proposed space-time transmission scheme is capable of simultaneously exploiting both the frequency selectivity and time selectivity of wireless channels, in addition to achieving the full spatial diversity.

9.1 Multiple-Input Multiple-Output Communications

In this section we develop the theory of MIMO communications with the emphasis on the capacity of MIMO channels. Let us first describe a general channel model for MIMO systems.

9.1.1 Multiple-Input Multiple-Output System Model

Let us consider a MIMO system employing M transmit antennas and N receive antennas as shown in Fig. 9.1. The output–input relationship of the MIMO system can be described by the equation

$$\mathbf{y} = \mathbf{H}\mathbf{x} + \mathbf{n} \quad (9.1)$$

$$= \sum_{m=1}^M \mathbf{h}_m x_m + \mathbf{n} \quad (9.2)$$

where, by assuming M inputs and N outputs, we may express the arguments in (9.1) as follows:

$$\mathbf{x} = [x_1, x_2, \dots, x_M]^T \quad (9.3)$$

$$\begin{aligned} \mathbf{H} &= [\mathbf{h}_1, \mathbf{h}_2, \dots, \mathbf{h}_M] \\ &= \begin{bmatrix} h_{11} & h_{12} & \dots & h_{1M} \\ h_{21} & h_{22} & \dots & h_{2M} \\ \vdots & \vdots & \ddots & \vdots \\ h_{N1} & h_{N2} & \dots & h_{NM} \end{bmatrix} \end{aligned} \quad (9.4)$$

$$\mathbf{n} = [n_1, n_2, \dots, n_N]^T \quad (9.5)$$

$$\mathbf{y} = [y_1, y_2, \dots, y_N]^T \quad (9.6)$$

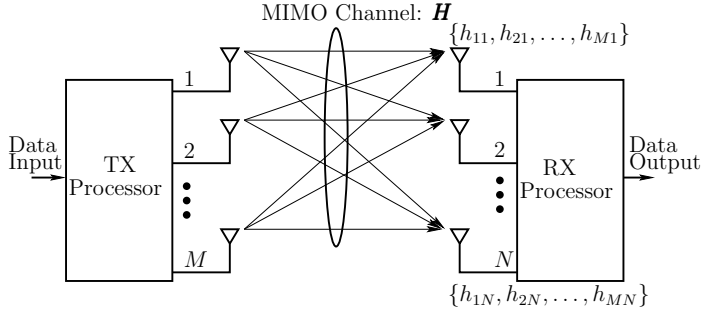


Figure 9.1: Schematic diagram for multiantenna MIMO wireless systems.

where \mathbf{x} is the M -length transmitted (input) signal vector, \mathbf{H} is the $(N \times M)$ channel matrix connecting the inputs with the outputs of the MIMO system, \mathbf{h}_m represents the signature of symbol x_m for $m = 1, 2, \dots, M$, \mathbf{n} is the N -length noise vector and, finally, \mathbf{y} is the N -length received (output) signal vector or the observation vector.

Throughout this section, the following assumptions are applied.

1. The M number of transmitted symbols constituting the transmitted signal vector \mathbf{x} are drawn from an independent identically distributed (i.i.d.) discrete source with zero mean and a common variance of $1/M$, i.e. $E[x_m] = 0$ and $E[x_m^2] = 1/M$. Note that, $E[x_m^2] = 1/M$ is used to constrain the total transmission power to a constant regardless of the number of transmit antennas.
2. The channels are memoryless, implying that an independent realization of \mathbf{H} is drawn for each use of the channels. Furthermore, it is assumed that each element of \mathbf{H} obeys the complex Gaussian distribution with zero mean and a variance 0.5 per dimension. In other words, the channel from any transmit antenna to any receive antenna is assumed to experience (flat) Rayleigh fading.
3. The noise vector \mathbf{n} is assumed to be the complex Gaussian noise vector, each element of \mathbf{n} is modelled as an i.i.d. complex Gaussian random variable with zero mean and a variance of $\sigma^2/2 = 1/2\text{SNR}$ per dimension, where SNR represents the average signal-to-noise ratio (SNR) per receive antenna.

Let us first consider the capacity of the MIMO systems.

9.1.2 Capacity of Multiple-Input Multiple-Output Channels

According to references [233, 234, 240], given the MIMO equation of (9.1) and the channel matrix \mathbf{H} , the capacity of the MIMO system can be obtained by solving the optimization problem:

$$C(\mathbf{H}) = \arg \max_{\mathbf{x}: \text{Trace}(\mathbf{Q}_x) \leq 1} \{\mathcal{I}(\mathbf{x}; \mathbf{y} | \mathbf{H})\} \quad (9.7)$$

where $\mathbf{Q}_x = E[\mathbf{x}\mathbf{x}^H]$ denotes the covariance matrix of the transmitted vector \mathbf{x} , while $\mathcal{I}(\mathbf{x}; \mathbf{y} | \mathbf{H})$ is the mutual information between \mathbf{x} and \mathbf{y} , when \mathbf{H} is given. According

to (9.7), finding the capacity $C(\mathbf{H})$ is equivalent to designing a suitable \mathbf{x} , which maximizes the mutual information $\mathcal{I}(\mathbf{x}; \mathbf{y} | \mathbf{H})$, while satisfying the power constraint of $\text{Trace}(\mathbf{Q}_x) \leq 1$.

In (9.7) the mutual information can be expressed as [233, 234, 240]

$$\begin{aligned}\mathcal{I}(\mathbf{x}; \mathbf{y} | \mathbf{H}) &= h(\mathbf{y} | \mathbf{H}) - h(\mathbf{y} | \mathbf{x}, \mathbf{H}) \\ &= h(\mathbf{y} | \mathbf{H}) - h(\mathbf{Hx} + \mathbf{n} | \mathbf{x}, \mathbf{H}) \\ &= h(\mathbf{y} | \mathbf{H}) - h(\mathbf{n} | \mathbf{x}, \mathbf{H}) \\ &= h(\mathbf{y} | \mathbf{H}) - h(\mathbf{n})\end{aligned}\quad (9.8)$$

where $h(\cdot)$ represents the differential entropy of the corresponding argument [233]. In (9.8), $h(\mathbf{n})$ is a constant given by [234, 240]

$$h(\mathbf{n}) = \log_2[(\pi e)^N \det(\sigma^2 \mathbf{I}_N)] = \log_2[(\pi e \sigma^2)^N] \quad (9.9)$$

where $\det(\mathbf{A})$ denotes the determinant of the square matrix \mathbf{A} . Hence, maximizing the mutual information $\mathcal{I}(\mathbf{x}; \mathbf{y} | \mathbf{H})$ is equivalent to maximizing $h(\mathbf{y} | \mathbf{H})$, which is achieved if and only if (iff) \mathbf{y} is a circularly symmetric complex Gaussian vector [233, 234]. In this case, the $h(\mathbf{y} | \mathbf{H})$ is given as

$$h(\mathbf{y} | \mathbf{H}) = \log_2[(\pi e)^N \det(\mathbf{R}_y)] \quad (9.10)$$

where the covariance matrix \mathbf{R}_y is

$$\begin{aligned}\mathbf{R}_y &= E[\mathbf{y}\mathbf{y}^H] \\ &= \sigma^2 \mathbf{I}_N + \mathbf{H} E[\mathbf{x}\mathbf{x}^H] \mathbf{H}^H \\ &= \sigma^2 \mathbf{I}_N + \mathbf{H} \mathbf{Q}_x \mathbf{H}^H\end{aligned}\quad (9.11)$$

Substituting (9.9) and (9.10) into (9.8), we obtain

$$\begin{aligned}\mathcal{I}(\mathbf{x}; \mathbf{y} | \mathbf{H}) &= \log_2[(\pi e)^N \det(\sigma^2 \mathbf{I}_N + \mathbf{H} \mathbf{Q}_x \mathbf{H}^H)] - \log_2[(\pi e)^N \det(\sigma^2 \mathbf{I}_N)] \\ &= \log_2 \left[\frac{\det(\sigma^2 \mathbf{I}_N + \mathbf{H} \mathbf{Q}_x \mathbf{H}^H)}{\det(\sigma^2 \mathbf{I}_N)} \right] \\ &= \log_2 \left[\det \left(\mathbf{I}_N + \frac{1}{\sigma^2} \mathbf{H} \mathbf{Q}_x \mathbf{H}^H \right) \right]\end{aligned}\quad (9.12)$$

Note that, in the above derivations some properties, see, e.g., reference [156], for the determinant operations have been applied.

Finally, when substituting (9.12) into (9.7), the capacity of the MIMO system can be obtained by solving the optimization problem of

$$C(\mathbf{H}) = \arg \max_{\mathbf{x}: \text{Trace}(\mathbf{Q}_x) \leq 1} \left\{ \mathcal{I}(\mathbf{x}; \mathbf{y} | \mathbf{H}) = \log_2 \left[\det \left(\mathbf{I}_N + \frac{1}{\sigma^2} \mathbf{H} \mathbf{Q}_x \mathbf{H}^H \right) \right] \right\} \quad (9.13)$$

Below, let us analyse the capacity of the MIMO systems, when we assume that either both the transmitter and receiver employ perfect CSI, or only the receiver employs perfect CSI, while the transmitter can only access the CDI. For convenience, the former is referred to as the CSI/CSI mode, the latter as the CDI/CSI mode.

In the context of the MIMO systems working under the CSI/CSI mode, both the transmitter and receiver can perfectly track the MIMO channel matrix \mathbf{H} . In this case, the transmitter can use the information about \mathbf{H} to carry out transmitter preprocessing, as shown in Chapter 8, in order to maximize the mutual information in (9.13), and ultimately to achieve the capacity of the MIMO system. Following Section 8.2.11 of Chapter 8, the mutual information in (9.13) can be written as

$$\mathcal{I}(\mathbf{x}; \mathbf{y} | \mathbf{H}) = \log_2 \left[\det \left(\mathbf{I}_M + \frac{1}{\sigma^2} \mathbf{H}^H \mathbf{H} \mathbf{Q}_x \right) \right] \quad (9.14)$$

where $\mathbf{H}^H \mathbf{H}$ is a Hermitian matrix of non-negative definite. Let the rank of \mathbf{H} be G , so is the rank of $\mathbf{H}^H \mathbf{H}$. Note that, for a MIMO system described by (9.1), we have $G \leq \min\{M, N\}$. However, $G = \min\{M, N\}$ with a probability of one, when each element in \mathbf{H} is assumed to be an i.i.d. complex Gaussian random variable. Using the eigen-decomposition, we can express $\mathbf{H}^H \mathbf{H}$ as

$$\begin{aligned} \mathbf{H}^H \mathbf{H} &= \mathbf{U} \boldsymbol{\Sigma} \mathbf{U}^H = [\mathbf{U}_s \mathbf{U}_n] \begin{bmatrix} \boldsymbol{\Sigma}_s & \mathbf{0} \\ \mathbf{0} & \mathbf{0} \end{bmatrix} \begin{bmatrix} \mathbf{U}_s^H \\ \mathbf{U}_n^H \end{bmatrix} \\ &= \mathbf{U}_s \boldsymbol{\Sigma}_s \mathbf{U}_s^H \end{aligned} \quad (9.15)$$

where \mathbf{U} is a $(M \times M)$ unitary matrix, \mathbf{U}_s is constituted by the G columns of \mathbf{U} corresponding to the G nonzero diagonal entries in $\boldsymbol{\Sigma}$, while \mathbf{U}_n is made up of $(M - G)$ columns of \mathbf{U} corresponding to the $(M - G)$ zero diagonal entries in $\boldsymbol{\Sigma}$. In (9.15), $\boldsymbol{\Sigma}_s = \text{diag}\{\lambda_1, \lambda_2, \dots, \lambda_G\}$ is a $(G \times G)$ diagonal matrix containing the G nonzero eigenvalues. Substituting (9.15) into (9.14) and after some rearrangements, we obtain

$$\mathcal{I}(\mathbf{x}; \mathbf{y} | \mathbf{H}) = \log_2 \left[\det \left(\mathbf{I}_G + \frac{1}{\sigma^2} \boldsymbol{\Sigma}_s \mathbf{U}_s^H \mathbf{Q}_x \mathbf{U}_s \right) \right] \quad (9.16)$$

According to references [233, 234] as well as our analysis in Section 8.2.11 of Chapter 8, the maximum of $\mathcal{I}(\mathbf{x}; \mathbf{y} | \mathbf{H})$ is achieved, only when $\mathbf{U}_s^H \mathbf{Q}_x \mathbf{U}_s$ is a diagonal matrix, i.e. when

$$\mathbf{U}_s^H \mathbf{Q}_x \mathbf{U}_s = \boldsymbol{\beta} \quad (9.17)$$

where $\boldsymbol{\beta} = \text{diag}\{\beta_1, \beta_2, \dots, \beta_G\}$ is for achieving the transmission power constraint. After applying (9.17) to (9.16), we arrive at

$$\begin{aligned} \mathcal{I}(\mathbf{x}; \mathbf{y} | \mathbf{H}) &= \log_2 \left[\det \left(\mathbf{I}_G + \frac{1}{\sigma^2} \boldsymbol{\Sigma}_s \boldsymbol{\beta} \right) \right] \\ &= \sum_{g=1}^G \log_2 \left(1 + \frac{\lambda_g \beta_g}{\sigma^2} \right) \end{aligned} \quad (9.18)$$

From this equation, we can spot that in a MIMO system employing M transmit and N receive antennas that are sufficiently separated, the MIMO channel can be decomposed into $G = \min\{M, N\}$ parallel independent SISO channels. The power conveyed by each of the SISO channels can be allocated in such a way that the maximum mutual information of the

MIMO system is targeted. Specifically, in (9.18) β_g for $g = 1, 2, \dots, G$ can be obtained according to the ‘water-filling’ principles under the constraint of

$$\sum_{g=1}^G \beta_g = \text{Trace}(\boldsymbol{\beta}) = \text{Trace}(\mathbf{U}_s^H \mathbf{Q}_x \mathbf{U}_s) = \text{Trace}(\mathbf{Q}_x) \leq 1 \quad (9.19)$$

which gives

$$\beta_g = \left(\mu - \frac{\sigma^2}{\lambda_g} \right)^+, \quad g = 1, 2, \dots, G \quad (9.20)$$

where μ is a constant chosen to satisfy (9.19).

Finally, the maximum mutual information or the capacity of the MIMO system can be obtained by substituting (9.20) into (9.18), which gives

$$C(\mathbf{H}) = \mathcal{I}_{\max}(\mathbf{x}; \mathbf{y} | \mathbf{H}) = \sum_{g=1}^G \log_2 \left[\frac{\mu \lambda_g}{\sigma^2} \right]^+ \quad (9.21)$$

The capacity of (9.21) represents the capacity of the MIMO system, when \mathbf{H} is deterministic, or when one realization of \mathbf{H} is given in fading channels. For the fading channels, the ergodic (unconditional) capacity C can be obtained by averaging the conditional capacity $C(\mathbf{H})$ over different realizations of \mathbf{H} , which can be expressed as

$$C = E_{\mathbf{H}}\{C(\mathbf{H})\} \text{ [bits/transmission]} \quad (9.22)$$

In the context of the MIMO systems operated under the CDI/CSI mode, the receiver employs ideal knowledge about \mathbf{H} , but the transmitter knows only the MIMO channel’s distribution information. In this case, the transmitter can only process the transmitted signals using the distribution information. In reference [234] it was proved that, in order to achieve the capacity of the MIMO channel under the CDI/CSI mode, the transmitted signal vector \mathbf{x} should be circularly symmetric complex Gaussian with zero mean and a covariance matrix

$$\mathbf{Q}_x = \frac{1}{M} \mathbf{I}_M \quad (9.23)$$

The detailed proof for the above results can be found in reference [234]. Below, we provide some discussion for the result of (9.23) from another angle. As a result, an upper-bound for the capacity of the MIMO channels in the CDI/CSI mode is obtained.

The discussion starts with maximizing (9.14) under the CDI/CSI mode. Since the transmitter employs only the distribution information of the MIMO channel \mathbf{H} , it can only seek a solution to maximize

$$\mathcal{I}(\mathbf{x}; \mathbf{y}) = E_{\mathbf{H}}\{\mathcal{I}(\mathbf{x}; \mathbf{y} | \mathbf{H})\} = E_{\mathbf{H}} \left\{ \log_2 \left[\det \left(\mathbf{I}_M + \frac{1}{\sigma^2} \mathbf{H}^H \mathbf{H} \mathbf{Q}_x \right) \right] \right\} \quad (9.24)$$

As under the CDI/CSI mode, the transmitter cannot make use of the information about \mathbf{H} , \mathbf{H} is independent of the transmitted signal \mathbf{x} . In this case, $\log_2[\det(\mathbf{I}_M + (1/\sigma^2)\mathbf{H}^H \mathbf{H} \mathbf{Q}_x)]$

in (9.24) is concave in terms of $\mathbf{H}^H \mathbf{H}$. Consequently, on invoking Jensen's inequality [233], we have

$$\begin{aligned}\mathcal{I}(\mathbf{x}; \mathbf{y}) &= E_{\mathbf{H}} \left\{ \log_2 \left[\det \left(\mathbf{I}_M + \frac{1}{\sigma^2} \mathbf{H}^H \mathbf{H} \mathbf{Q}_x \right) \right] \right\} \\ &\leq \log_2 \left[\det \left(\mathbf{I}_M + \frac{1}{\sigma^2} E_{\mathbf{H}} [\mathbf{H}^H \mathbf{H}] \mathbf{Q}_x \right) \right] \\ &= \log_2 \left[\det \left(\mathbf{I}_M + \frac{N}{\sigma^2} \mathbf{Q}_x \right) \right]\end{aligned}\quad (9.25)$$

Furthermore, according to the random matrix theory [241], given that $\text{Trace}(\mathbf{A}) = \alpha$, the determinant of the $(M \times M)$ positive definite matrix \mathbf{A} is maximized when $\mathbf{A} = (\alpha/M)\mathbf{I}_M$. Hence, given that $\text{Trace}(\mathbf{Q}_x) = 1$, (9.25) satisfies

$$\begin{aligned}\log_2 \left[\det \left(\mathbf{I}_M + \frac{N}{\sigma^2} \mathbf{Q}_x \right) \right] &\leq \log_2 \left[\det \left(\mathbf{I}_M + \frac{N}{M\sigma^2} \mathbf{I}_M \right) \right] \\ &= M \log_2 \left(1 + \frac{N}{M\sigma^2} \right)\end{aligned}\quad (9.26)$$

with equality if $\mathbf{Q}_x = (1/M)\mathbf{I}_M$, implying that the transmission power should be uniformly distributed over the M number of transmit antennas, in order to achieve the maximum of mutual information, i.e., the capacity of the MIMO channel.

Finally, after combining (9.25) and (9.26), it can be shown that

$$C = \arg \max_{\mathbf{x}: \text{Trace}(\mathbf{Q}_x)=1} \{\mathcal{I}(\mathbf{x}; \mathbf{y})\} \leq M \log_2 \left(1 + \frac{N}{M\sigma^2} \right) = C_{\max} \text{ [bits/transmission]} \quad (9.27)$$

where C_{\max} is one of the capacity upper-bounds of the MIMO system using M transmit antennas and N receive antennas, when it is operated under the CDI/CSI mode.

Furthermore, when applying (9.23) into (9.24), the ergodic capacity of the MIMO system under the CDI/CSI mode can be evaluated as

$$C = E_{\mathbf{H}} \left\{ \log_2 \left[\det \left(\mathbf{I}_M + \frac{1}{M\sigma^2} \mathbf{H}^H \mathbf{H} \right) \right] \right\} \text{ [bits/transmission]} \quad (9.28)$$

$$= E_{\mathbf{H}} \left\{ \log_2 \left[\det \left(\mathbf{I}_N + \frac{1}{M\sigma^2} \mathbf{H} \mathbf{H}^H \right) \right] \right\} \text{ [bits/transmission]} \quad (9.29)$$

Note that, for some distribution cases, closed-form analytical results for (9.28) or (9.29) are available. However, evaluation of these analytical results is often highly involving. Alternatively, Monte Carlo based simulations can be used for evaluating (9.28) or (9.29).

From (9.28) and (9.29), we can obtain the results for the following special cases. First, when a single-input multiple-output (SIMO) case is considered, the corresponding capacity can be obtained by setting $M = 1$ in (9.28), yielding

$$C = E_{\{h_n\}} \left[\log_2 \left(1 + \frac{1}{\sigma^2} \sum_{n=1}^N |h_n|^2 \right) \right] \text{ [bits/transmission]} \quad (9.30)$$

Second, when a multiple-input single-output (MISO) case is considered, the corresponding capacity can be obtained by setting $N = 1$ in (9.29), which results in

$$C = E_{\{h_m\}} \left[\log_2 \left(1 + \frac{1}{M\sigma^2} \sum_{m=1}^M |h_m|^2 \right) \right] \text{ [bits/transmission]} \quad (9.31)$$

Third, when in (9.29) N is fixed, by the law of large number, we have

$$\lim_{M \rightarrow \infty} \frac{1}{M} \mathbf{H} \mathbf{H}^H = \mathbf{I}_N \quad (9.32)$$

with a probability of one. In this case,

$$\begin{aligned} C &= \lim_{M \rightarrow \infty} E_{\mathbf{H}} \left\{ \log_2 \left[\det \left(\mathbf{I}_N + \frac{1}{M\sigma^2} \mathbf{H} \mathbf{H}^H \right) \right] \right\} \\ &= \log_2 \left[\det \left(\mathbf{I}_N + \frac{1}{\sigma^2} \mathbf{I}_N \right) \right] \\ &= N \times \log_2 \left(1 + \frac{1}{\sigma^2} \right) \text{ [bits/transmission]} \end{aligned} \quad (9.33)$$

which shows that the capacity of the MIMO system increases linearly with the number of receive antennas.

Fourth, when in (9.28) M is fixed by the law of large number, we have

$$\lim_{N \rightarrow \infty} \frac{1}{N} \mathbf{H}^H \mathbf{H} = \mathbf{I}_M \quad (9.34)$$

with a probability of one. In this case,

$$\begin{aligned} C &= \lim_{N \rightarrow \infty} E_{\mathbf{H}} \left\{ \log_2 \left[\det \left(\mathbf{I}_M + \frac{1}{M\sigma^2} \mathbf{H}^H \mathbf{H} \right) \right] \right\} \\ &= \lim_{N \rightarrow \infty} E_{\mathbf{H}} \left\{ \log_2 \left[\det \left(\mathbf{I}_M + \frac{N}{M\sigma^2} \frac{1}{N} \mathbf{H}^H \mathbf{H} \right) \right] \right\} \\ &= \log_2 \left[\det \left(\mathbf{I}_M + \frac{N}{M\sigma^2} \mathbf{I}_M \right) \right] \\ &\geq M \times \log_2 \left(1 + \frac{1}{\sigma^2} \right) \text{ [bits/transmission]} \end{aligned} \quad (9.35)$$

which shows that the capacity of the MIMO system increases at least linearly with the number of transmit antennas.

From the above results, it is implied that if both M and N simultaneously become large, the capacity of the MIMO system then grows at least linearly with $G = \min(M, N)$.

Finally, let $M = N$ in (9.28) or (9.29). Then, if the value of $M = N$ is sufficiently high, using the result of (9.34), we have

$$\det \left(\mathbf{I}_M + \frac{1}{M\sigma^2} \mathbf{H}^H \mathbf{H} \right) \geq \det \left(\mathbf{I}_M + \frac{1}{M\sigma^2} \mathbf{I}_M \right) \quad (9.36)$$

with a probability of one. Hence, when $M = N \rightarrow \infty$, the capacity of the MIMO system satisfies

$$\begin{aligned} C &= \lim_{M \rightarrow \infty} E_H \left\{ \log_2 \left[\det \left(\mathbf{I}_M + \frac{1}{M\sigma^2} \mathbf{H}^H \mathbf{H} \right) \right] \right\} \\ &\geq \lim_{M \rightarrow \infty} E_H \left\{ \log_2 \left[\det \left(\mathbf{I}_M + \frac{1}{M\sigma^2} \mathbf{I}_M \right) \right] \right\} \\ &= \lim_{M \rightarrow \infty} \log_2 \left[\left(1 + \frac{1}{M\sigma^2} \right)^M \right] \\ &= \frac{1}{\sigma^2} \log_2 e = \text{SNR} \times \log_2 e \text{ [bits/transmission]} \end{aligned} \quad (9.37)$$

Therefore, when the values of both M and N are sufficiently high, then the capacity of the MIMO system using M transmit antennas and N receive antennas increases at least linearly with the SNR value.

Below, we show the relationship between (9.12) and the covariance matrix of the estimation error in the MMSE detection, which has been studied in reference [242]. In reference [242] a more general case and intuitive discussion have been addressed. Let (9.12) be rewritten as

$$\begin{aligned} \mathcal{I}(\mathbf{x}; \mathbf{y} | \mathbf{H}) &= \log_2 \left[\det \left(\mathbf{Q}_x \left[\mathbf{Q}_x^{-1} + \frac{1}{\sigma^2} \mathbf{H}^H \mathbf{H} \right] \right) \right] \\ &= \log_2 \det(\mathbf{Q}_x) + \log_2 \left[\det \left(\mathbf{Q}_x^{-1} + \frac{1}{\sigma^2} \mathbf{H}^H \mathbf{H} \right) \right] \end{aligned} \quad (9.38)$$

With the MMSE detection, as shown in Section 6.2.3 in Chapter 6, the covariance matrix Δ of the estimation error vector is given by

$$\Delta = E[(\mathbf{x} - \mathbf{W}^H \mathbf{y})(\mathbf{x} - \mathbf{W}^H \mathbf{y})^H] \quad (9.39)$$

Applying the optimum solution of $\mathbf{W} = \mathbf{R}_y^{-1} \mathbf{R}_{yx}$ to the above equation, it can be shown that

$$\Delta = \mathbf{Q}_x - \mathbf{R}_{yx}^H \mathbf{R}_y^{-1} \mathbf{R}_{yx} \quad (9.40)$$

where \mathbf{R}_{yx} is the cross-correlation matrix between \mathbf{y} and \mathbf{x} , which is

$$\mathbf{R}_{yx} = E[\mathbf{y}\mathbf{x}^H] = \mathbf{H}\mathbf{Q}_x \quad (9.41)$$

Substituting the above equation and \mathbf{R}_y from (9.11) into (9.40) yields

$$\Delta = \mathbf{Q}_x - \mathbf{Q}_x \mathbf{H}^H (\sigma^2 \mathbf{I}_N + \mathbf{H} \mathbf{Q}_x \mathbf{H}^H)^{-1} \mathbf{H} \mathbf{Q}_x \quad (9.42)$$

Finally, when using the *matrix inverse lemma*, as seen in Appendix 6.B of Chapter 6, to express

$$\mathbf{H}^H (\sigma^2 \mathbf{I}_N + \mathbf{H} \mathbf{Q}_x \mathbf{H}^H)^{-1} \mathbf{H} = \mathbf{Q}_x^{-1} - \mathbf{Q}_x^{-1} \left(\mathbf{Q}_x^{-1} + \frac{1}{\sigma^2} \mathbf{H}^H \mathbf{H} \right)^{-1} \mathbf{Q}_x^{-1} \quad (9.43)$$

and then submitting it into (9.42), we can simplify it to

$$\Delta = \left(Q_x^{-1} + \frac{1}{\sigma^2} H^H H \right)^{-1} \quad (9.44)$$

From (9.38) and (9.44), we can readily find that the mutual information of (9.38) can be expressed as

$$\begin{aligned} \mathcal{I}(x; y | H) &= \log_2 \det(Q_x) + \log_2 \det(\Delta^{-1}) \\ &= \log_2 \left[\frac{\det(Q_x)}{\det(\Delta)} \right] \end{aligned} \quad (9.45)$$

which relates, in a simple manner, the mutual information to the covariance matrix of the estimation error in MMSE detection.

Following the discussion in reference [242], in order to maximize the mutual information $\mathcal{I}(x; y | H)$, the matrix Δ^{-1} in (9.45) should be a diagonal matrix, so is the covariance matrix Δ . However, as shown in (9.44), Δ is not usually diagonal when without transmitter preprocessing. In this case, to use the MMSE detection followed by separate decoding is not a capacity-achieving scheme – there is information loss [242]. When in a MIMO system the CSI is available to the transmitter, then, the transmitter can modify the transmitted signal vector, as in Chapter 8, such that the resultant covariance matrix Δ is diagonal. In this case, the MMSE detector is optimum and is capable of achieving lossless information processing. Below, we provide a range of simulation results in order to characterize the capacity of the MIMO systems when they are operated under either the CSI/CSI or CDI/CSI mode.

Figure 9.2 shows the capacity versus SNR for the MIMO systems using various number transmit/receive antennas, when they are operated under the CDI/CSI mode. In Fig. 9.2(a) we evaluated the capacity when the MIMO system employed, at most, four transmit/receive antennas. Note that the error rate performance of these MIMO schemes will be investigated in Section 9.4 in the context of the F-domain spread MC-CDMA or OFDM systems. In Fig. 9.2(b) the capacity of the MIMO system was evaluated when different combinations of transmit/receive antennas were assumed, while retaining $MN = 12$. From the results of Fig. 9.2, we can observe that the capacity of the MIMO system is different for different transmit/receive antenna configurations, even when the product MN retains a constant. As shown in Fig. 9.2, at low SNR region, the MIMO system is generally capable of providing higher capacity, when the receiver employs more antennas. For example, as shown in Fig. 9.2(a), the highest capacity is achieved by the configuration ($M = 1, N = 4$), when $\text{SNR} \leq 5 \text{ dB}$. By contrast, at high SNR region, the highest capacity is usually achieved by the MIMO system, where both the transmitter and receiver employ a similar number of antennas. As shown in Figs 9.2(a) and 9.2(b), given that $MN = 4$ and 12, respectively, the highest capacity is achieved when ($M = 2, N = 2$) for Fig. 9.2(a) and ($M = 3, N = 4$) for Fig. 9.2(b) at the high SNR region.

In Fig. 9.3 the capacity of the same MIMO systems as for Fig. 9.2 is evaluated, when assuming that the MIMO systems are operated in CSI/CSI mode. Comparing the results in Fig. 9.3 with those in Fig. 9.2, we find that, in Fig. 9.3, in CSI/CSI mode, the capacity of the MIMO system using M transmit antennas and N receive antennas is the same as that of the MIMO system using N transmit antennas and M receive antennas, regardless of the values of M and N . However, in Fig. 9.2 in CDI/CSI mode, if $M > N$, the capacity of the MIMO

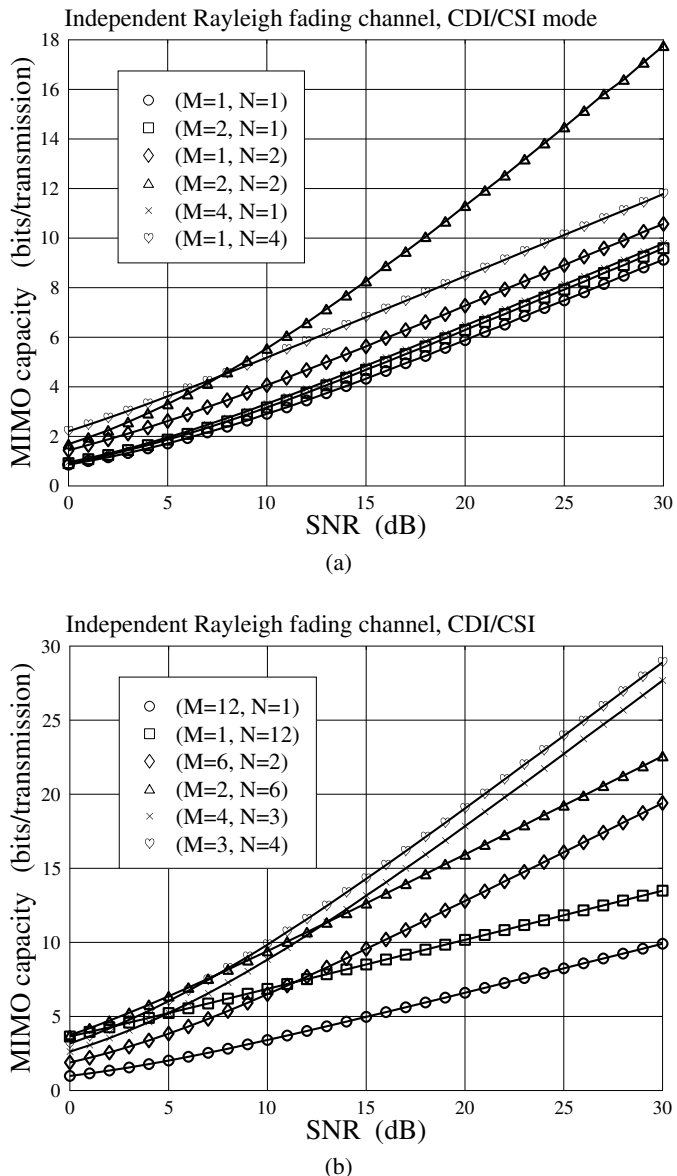


Figure 9.2: Capacity versus SNR for the MIMO systems operated in CDI/CSI mode, when communicating over Rayleigh fading channels; (a) $MN \leq 4$; (b) $MN = 12$.

system using M transmit antennas and N receive antennas is lower than that of the MIMO system using N transmit antennas and M receive antennas: when the difference between M and N is bigger, the difference of the capacity is also bigger. Furthermore, it can be implied from the results of Fig. 9.3 that, in CSI/CSI mode, it is always desirable to make the number of transmit antennas equal to the number of receive antennas.

In Fig. 9.4 the capacity of the MIMO system under the CDI/CSI mode is drawn against the number of transmit antennas in Fig. 9.4(a) with respect to a different number of receive antennas, or drawn against the number of receive antennas in Fig. 9.4(b) with respect to a different number of transmit antennas. In Fig. 9.5 the capacity of the MIMO system under the CDI/CSI mode is presented in three dimension (3D) against the number of transmit/receive antennas. In all these figures, we assumed that $\sigma^2 = \text{SNR} = 1$. From the results of Fig. 9.4(a) and Fig. 9.5 we can see that, once the number of transmit antennas reaches the number of receive antennas, further increasing the number of transmit antennas only results in a marginal increase of capacity, when the MIMO system is operated in CDI/CSI mode. The reason for this observation may be as follows. From (9.29), we know that, once $M \geq N$, the ergodic capacity of the MIMO system can be expressed as

$$\begin{aligned} C &= E_{\mathbf{H}} \left\{ \log_2 \left[\det \left(\mathbf{I}_N + \frac{1}{M\sigma^2} \mathbf{H} \mathbf{H}^H \right) \right] \right\} \\ &= E_{\mathbf{H}} \left\{ \log_2 \left[\det \left(\mathbf{I}_N + \frac{1}{\sigma^2} \frac{1}{M} \mathbf{H} \mathbf{H}^H \right) \right] \right\} \end{aligned} \quad (9.46)$$

Using the approximation of $\mathbf{H} \mathbf{H}^H / M \approx \mathbf{I}_N$, (9.46) can be approximated as

$$\begin{aligned} C &\approx E_{\mathbf{H}} \left\{ \log_2 \left[\det \left(\mathbf{I}_N + \frac{1}{\sigma^2} \mathbf{I}_N \right) \right] \right\} \\ &= \log_2 \left[\det \left(\mathbf{I}_N + \frac{1}{\sigma^2} \mathbf{I}_N \right) \right] \\ &= N \log_2 \left(1 + \frac{1}{\sigma^2} \right) \end{aligned} \quad (9.47)$$

which suggests that the capacity of the MIMO system stays nearly constant, once the number of transmit antennas is sufficiently high.

From the results of Fig. 9.4(b) and Fig. 9.5 we observe that the capacity of the MIMO system increases nearly linearly with the number of receive antennas, when the number of receive antennas does not exceed the number of transmit antennas. This phenomenon is well explained by (9.33) and by (9.47). However, when the number of receive antennas exceeds the number of transmit antennas, the capacity of the MIMO system increases more or less following the logarithm law. This observation can also be demonstrated by analysis. According to (9.28), if $N > M$, the ergodic capacity of the MIMO system under the CDI/CSI mode can be expressed as

$$\begin{aligned} C &= E_{\mathbf{H}} \left\{ \log_2 \left[\det \left(\mathbf{I}_M + \frac{1}{M\sigma^2} \mathbf{H}^H \mathbf{H} \right) \right] \right\} \\ &= E_{\mathbf{H}} \left\{ \log_2 \left[\det \left(\mathbf{I}_M + \frac{N}{M\sigma^2} \frac{1}{N} \mathbf{H}^H \mathbf{H} \right) \right] \right\} \end{aligned} \quad (9.48)$$

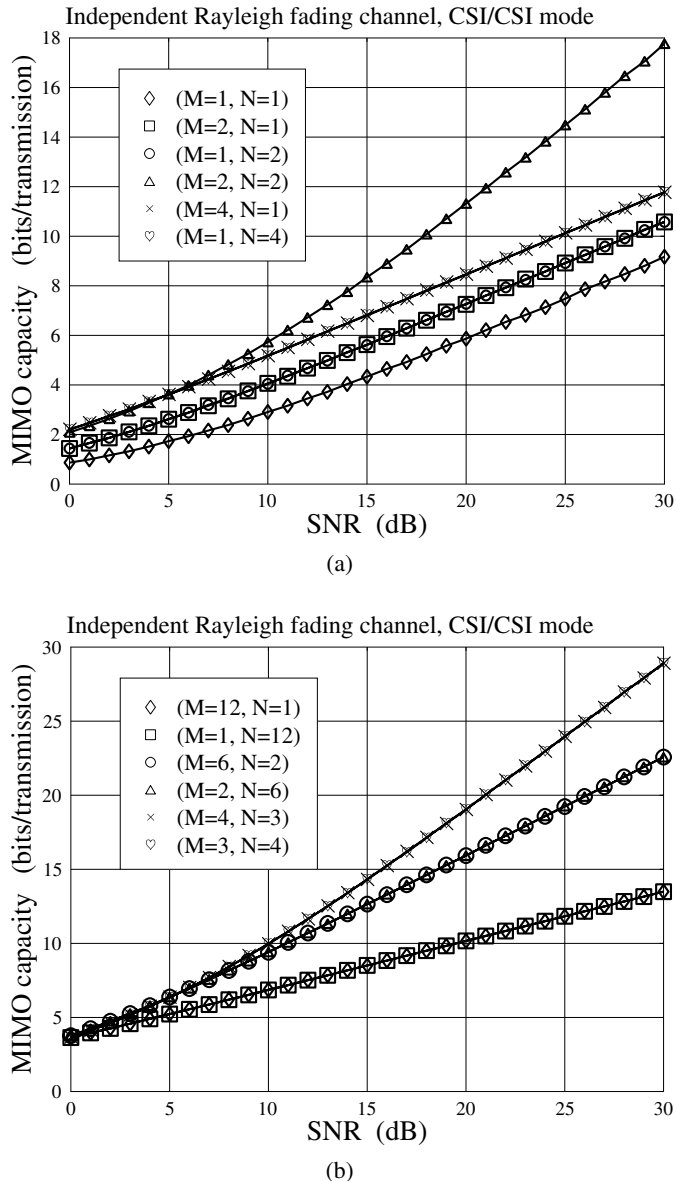


Figure 9.3: Capacity versus SNR for the MIMO systems operated in CSI/CSI mode, when communicating over Rayleigh fading channels; (a) $MN \leq 4$; (b) $MN = 12$.

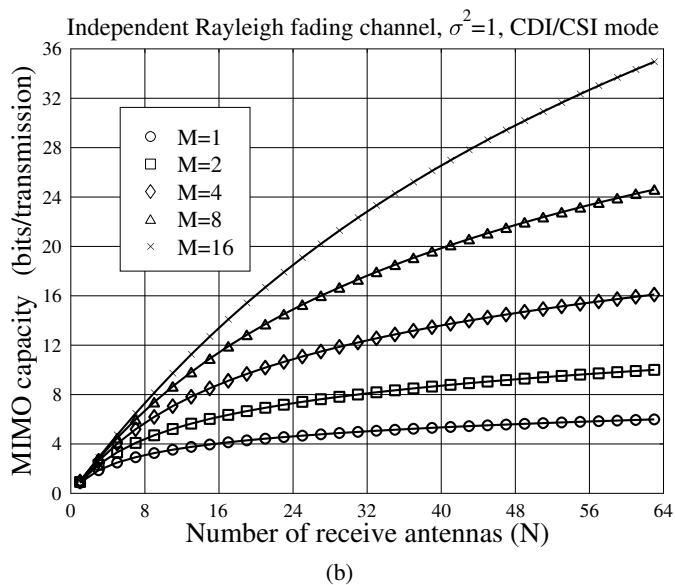
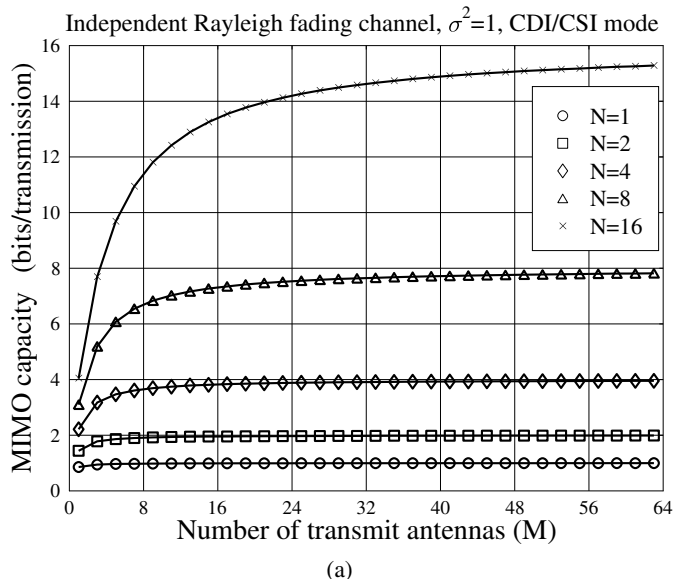


Figure 9.4: Capacity versus the number of transmit/receive antennas for the MIMO systems operated in CDI/CSI mode, when communicating over Rayleigh fading channels with $\sigma^2 = \text{SNR} = 1$; (a) capacity versus M ; (b) capacity versus N .

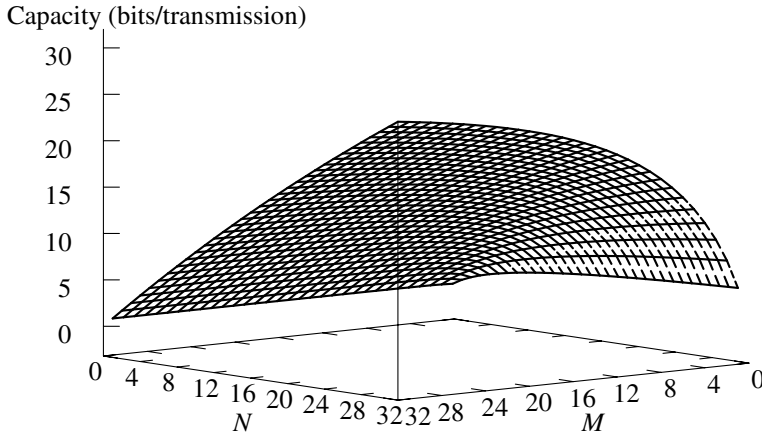


Figure 9.5: Capacity versus the number of transmit/receive antennas for the MIMO systems operated in CDI/CSI mode, when communicating over Rayleigh fading channels with $\sigma^2 = \text{SNR} = 1$.

Again, using $\mathbf{H}^H \mathbf{H}/N = \mathbf{I}_M$, we can approximate (9.48) as

$$\begin{aligned} C &\approx E_{\mathbf{H}} \left\{ \log_2 \left[\det \left(\mathbf{I}_M + \frac{N}{M\sigma^2} \mathbf{I}_M \right) \right] \right\} \\ &= \log_2 \left[\det \left(\mathbf{I}_M + \frac{N}{M\sigma^2} \mathbf{I}_M \right) \right] \\ &= M \log_2 \left(1 + \frac{N}{M\sigma^2} \right) \end{aligned} \quad (9.49)$$

Explicitly, for a fixed value of M , the capacity of the MIMO system increases with the logarithm function of N representing the number of receive antennas.

The impact of the number of transmit/receive antennas on the capacity of the MIMO systems operated in CSI/CSI mode is shown in Figs 9.6 and 9.7. Note again that, in CSI/CSI mode, the capacity of the MIMO system using M transmit antennas and N receive antennas is the same as that of the MIMO system using N transmit antennas and M receive antennas. In comparison with the results shown in Figs 9.4 and 9.5, we can observe that, when the MIMO system uses multiple transmit antennas and when the number of receive antennas is relatively low, such as when $N \leq M$, the capacity of the MIMO system operated in CSI/CSI mode can be significantly higher than the capacity of the MIMO system operated in CDI/CSI mode. However, when the number of receive antennas is significantly higher than the number of transmit antennas, i.e. when $N \gg M$, as shown in Fig. 9.4(b) and Fig. 9.6, e.g., for $N = 63$, the capacity of the MIMO systems under both the operation modes is similar. In this case, it can be implied that the capacity of the MIMO system is dominated by the number of receive antennas. In Fig. 9.7 we see that the capacity surface is symmetric in terms of M and N , which again reflects that the capacity of the MIMO system using M transmit antennas and N receive antennas is the same as that of the MIMO system using N transmit antennas and M receive antennas, when the MIMO system is operated under the CSI/CSI mode. By contrast,

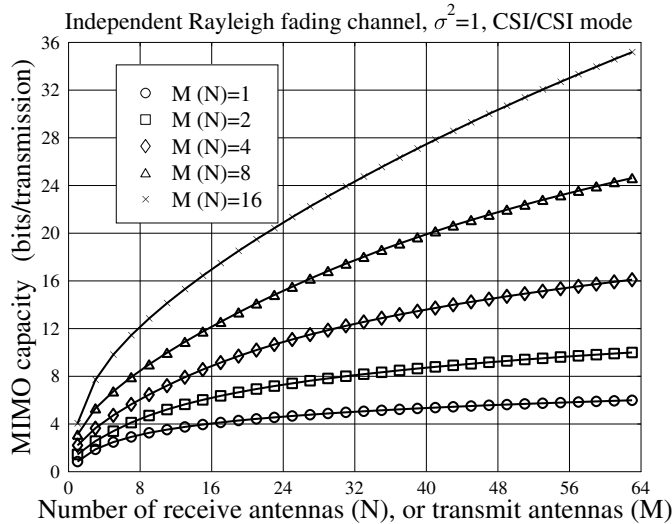


Figure 9.6: Capacity versus the number of transmit/receive antennas for the MIMO systems operated under the CSI/CSI mode, when transmitting over Rayleigh fading channels and assuming $\sigma^2 = \text{SNR} = 1$.

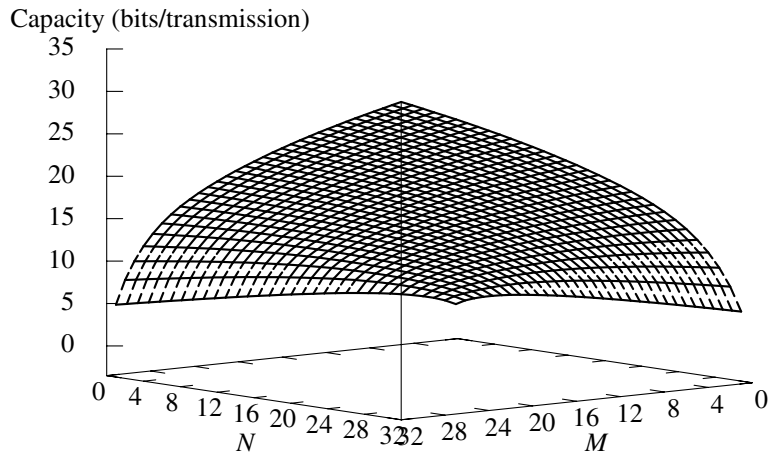


Figure 9.7: Capacity versus the number of transmit/receive antennas for the MIMO systems operated in CSI/CSI mode, when communicating over Rayleigh fading channels and assuming that $\sigma^2 = \text{SNR} = 1$.

as seen in Fig. 9.5, the capacity surface for the MIMO system operated in CDI/CSI mode is asymmetric, which explains that, in CDI/CSI mode, it is desirable to use more receive antennas when MN is a constant.

9.2 Spatial Diversity

It is well known that signals transmitted over wireless channels experience fading, which may be efficiently mitigated by exploiting various types of diversity. In recent years, spatial diversity has received a lot of attention as an effective diversity technique used for combatting fading in wireless communications [243–246]. In advanced high data rate wireless communications, spatial diversity is particularly attractive, since the diversity can be achieved without incurring an expenditure of transmission time and bandwidth. Spatial diversity can be achieved by transmitting the same signal from geographically sufficiently separated transmit antennas, in order to assist the receiver to generate several replicas experiencing independent fading. This type of spatial diversity, which depends mainly on the transmitter preprocessing, is usually referred to as *transmit diversity*. Spatial diversity can also be achieved by generating observations of the same transmitted signal from geographically sufficiently separated receive antennas, yielding *receive diversity*. Furthermore, in a same wireless system, both transmit and receive diversity can be achieved simultaneously by deployment of multiple transmit antennas and also multiple receive antennas. For simplicity, we refer below to this type of diversity as MIMO diversity.

In this section we review the principles of a range of spatial diversity schemes. For clarity, we say that a diversity scheme is capable of achieving a diversity order M , if the decision variable, say z , for the transmitted symbol, say x , is represented by the sum of squares of M random variables, which are preferred to be independent in order to obtain maximum diversity gain.

Note that starting from this section, we assume that the transmitted symbols, say $\{x_i\}$, are independent random variables satisfying $E[x_i] = 0$ and $E[\|x_i\|^2] = 1$. Notice that this assumption is different from the assumption for the $\{x_i\}$ in (9.3). This is because, when considering the channel capacity, $\{x_i\}$ in (9.3) in fact represent the transmitted signals, which we have known should be Gaussian distributed random variables in order to achieve the channel capacity. By contrast, in this and the following sections, $\{x_i\}$ denote phasors of constellations in certain modulation schemes. For example, in BPSK baseband modulation, we have $\{x_i = \pm 1\}$.

Let us first consider the receive diversity.

9.2.1 Receive Diversity

Receive diversity (RD) is achieved by a SIMO system; it is a straightforward way to obtain spatial diversity. RD is feasible to implement for the uplink, since it is usually easy to deploy multiple antennas at the BS. Let us assume that the SIMO system employs N receive antennas. Let the transmitted symbol be x . Then, according to (9.1), the SIMO equation can be expressed as

$$\mathbf{y} = \mathbf{h}x + \mathbf{n} \quad (9.50)$$

where $\mathbf{h} = [h_1, h_2, \dots, h_N]^T$ contains the channel gains of the SIMO channels.

Assuming that the receiver employs the CSI then the decision variable for x can be formed as

$$z = \mathbf{h}^H \mathbf{y} = \sum_{n=1}^N |h_n|^2 x + n \quad (9.51)$$

where $n = \mathbf{h}^H \mathbf{n}$, which is a Gaussian random variable distributed with zero mean and a variance of $\sigma^2 \sum_{n=1}^N |h_n|^2$.

According to (9.51), explicitly, the diversity order achieved is N .

The combining carried out in (9.51) follows the principles of maximal ratio combining (MRC), which is optimum and referred to as MRC-RD. In order to reduce the implementation complexity, suboptimum combining schemes may be invoked. Suboptimum combining may include section combining (SC) and generalized MRC/SC (MRC/SC) schemes. For the SC, the receiver selects only the best of N ; for example, with the highest SNR, to demodulate the transmitted signal. For the generalized MRC/SC, the receiver first selects L best observations out of N , and then combines the L best observations based on the MRC principles.

In practice, finding L best observations out of N coherently, e.g. based on their SNR values or $\{h_n\}$ directly, may not result in complexity reduction, since the receiver has to estimate all the channels in order to make the selection. As power is often easy to estimate, instead, the receiver can make the selection according to the output power of the N receive antennas at the cost of a little loss of performance.

9.2.2 Transmit Diversity

Transmit diversity is beneficial to downlink transmission, where the BS employs multiple, say M , transmit antennas and a mobile terminal (MT) employs one receive antenna, forming a MISO system. In order to achieve transmit diversity, the transmitter of a MISO system needs to carry out certain preprocessing, so that the receiver can form the decision variables, which are functions of the sum of squares of the channel gains involved. Therefore, transmit diversity can be classified into *closed-loop transmit diversity* and *open-loop transmit diversity*. In the context of the closed-loop transmit diversity, the corresponding transmitter preprocessing makes use of the CSI, which may be directly estimated at the transmitter side, or fed back from the receiver to the transmitter. For the open-loop transmit diversity, the transmitter does not use the CSI for preprocessing. Below, we analyse the principles of transmit diversity in the order as follows.

- Closed-loop transmit diversity:
 - ❑ SWitched Transmit Diversity (SWiTD);
 - ❑ Transmitter MRC assisted Transmit Diversity (TMRC-TD).
- Open-loop transmit diversity:
 - ❑ Orthogonal Transmit Diversity (OTD);
 - ❑ Transmit Diversity based on Space–Time Code (Coding) (STC-TD);
 - ❑ Transmit Diversity based on Space–Time Spreading (STS-TD).

Let us first consider the closed-loop transmit diversity.

9.2.2.1 Switched Transmit Diversity

For the switched transmit diversity (SWiTD), signals are only transmitted from one of the transmit antennas that is assumed to be the best or as told by the receiver. Switched

transmit diversity implements transmitter selection combining (TSC). More specifically, if the transmitter employs ideal CSI of the M channels, the transmitter can then choose the best of the M channels to transmit signals. In TDD mode, the transmitter may obtain the CSI of its outgoing channels through estimation/prediction of its incoming channels. Alternatively, channel estimation/prediction can be carried out at the receiver with the aid of pilot signals transmitted by the transmitter. After the receiver makes a decision as to which of the M channels is the best, the receiver informs the transmitter of its decision using a feedback channel, and the transmitter then transmits signals from the corresponding antenna.

In order to avoid switching too frequently, which possibly results in high complexity and bandwidth wasting, the switching may only occur until the quality of the current channel drops below a preset threshold.

9.2.2.2 TMRC-Assisted Transmit Diversity

The TMRC-assisted transmit diversity (TMRC-TD) scheme requires CSI at the transmitter for carrying out transmitter preprocessing, so that the MRC can be achieved at the receiver. Let us assume a MISO system with M transmit antennas and transmitter preprocessing. Then, according to Chapter 8, the decision variable at the receiver can be expressed as

$$z = \mathbf{h}^T \mathbf{p}x + n \quad (9.52)$$

where $\mathbf{h} = [h_1, h_2, \dots, h_M]^T$, \mathbf{p} is an M -length preprocessing vector and n is a noise variable. According to Chapter 8, in order to achieve the MRC combining, \mathbf{p} can be chosen as

$$\mathbf{p} = \frac{\mathbf{h}^*}{\sqrt{\|\mathbf{h}\|^2}} \quad (9.53)$$

where $1/\sqrt{\|\mathbf{h}\|^2}$ is for achieving the constraint on the transmission power. Substituting (9.53) into (9.52), the decision variable can be expressed as

$$\begin{aligned} z &= \frac{1}{\sqrt{\|\mathbf{h}\|^2}} \mathbf{h}^T \mathbf{h}^* x + n \\ &= \left(\frac{1}{\sqrt{\|\mathbf{h}\|^2}} \sum_{m=1}^M |h_m|^2 \right) x + n \\ &= \left(\sqrt{\sum_{m=1}^M |h_m|^2} \right) x + n \end{aligned} \quad (9.54)$$

Therefore, the TMRC-TD scheme is capable of achieving a diversity order of M .

We now turn to consider the open-loop transmit diversity.

9.2.2.3 Orthogonal Transmit Diversity

In orthogonal transmit diversity (OTD) signals transmitted by different transmit antennas are separated using orthogonal signals. The concept of OTD can be found in references [244, 248]. The principle behind the OTD can be understood with the aid of the following example considering a space–time system using $M = 2$ transmit antennas and $N = 1$ receive antenna.

Let \mathbf{c}_1 and \mathbf{c}_2 be two normalized orthogonal codewords, i.e. $\mathbf{c}_1^H \mathbf{c}_2 = 0$ and $\|\mathbf{c}_1\|^2 = \|\mathbf{c}_2\|^2 = 1$. Let $\{x_1\}$ and $\{x_2\}$ be two data streams, where $\{x_1\}$ is constituted by the even indexed symbols, while $\{x_2\}$ by the odd indexed symbols, of the original data. Then, $\{x_1\}$ and $\{x_2\}$ are transmitted respectively by the first and second transmit antennas as

$$\begin{aligned} \text{Antenna 1 : } s_1 &= \mathbf{c}_1 x_1 \\ \text{Antenna 2 : } s_2 &= \mathbf{c}_2 x_2 \end{aligned} \quad (9.55)$$

Assuming flat fading channels and that the channel gains corresponding to the first and second transmit antennas are h_1 and h_2 , then the observation vector extracted at the receive antenna is

$$\begin{aligned} \mathbf{r} &= h_1 s_1 + h_2 s_2 + \mathbf{n} \\ &= h_1 \mathbf{c}_1 x_1 + h_2 \mathbf{c}_2 x_2 + \mathbf{n} \end{aligned} \quad (9.56)$$

Based on (9.56), the receiver recovers x_1 by forming the decision variable

$$z_1 = h_1^* \mathbf{c}_1^H \mathbf{r} = |h_1|^2 x_1 + n_1 (= h_1^* \mathbf{c}_1^H \mathbf{n}) \quad (9.57)$$

and the receiver recovers x_2 by forming the decision variable

$$z_2 = h_2^* \mathbf{c}_2^H \mathbf{r} = |h_2|^2 x_2 + n_2 (= h_2^* \mathbf{c}_2^H \mathbf{n}) \quad (9.58)$$

From (9.57) and (9.58), we can see that the decision variables for x_1 and x_2 are the same as the conventional BPSK-assisted SISO scheme. When we consider only two symbols, there is no diversity gain at all, since the decision variable z_1 only depends on $|h_1|^2$, while z_2 only depends on $|h_2|^2$. Therefore, in OTD-based space-time systems, channel coding is usually used in order to achieve diversity, as detailed in reference [248].

9.2.2.4 Transmit Diversity Based on Space-Time Coding

STC assisted transmit diversity (STC-TD) is a type of open-loop transmit diversity scheme, which has received wide research and application [243–246, 249–252]. For the purpose of explaining the principles of the STC, let us consider a MISO system employing M transmit antennas and one receive antenna. Let

$$\mathbf{x} = [x_1, x_2, \dots, x_G]^T \quad (9.59)$$

be the information symbols to be transmitted. Then, a STC can generally be structured as [245, 246]

$$\mathcal{G} = \beta \times \begin{bmatrix} a_{11} & a_{12} & \cdots & a_{1M} \\ a_{21} & a_{22} & \cdots & a_{2M} \\ \vdots & \vdots & \ddots & \vdots \\ a_{L,1} & a_{L,2} & \cdots & a_{L,M} \end{bmatrix} \quad (9.60)$$

where a_{lm} , $l = 1, \dots, L_t$; $m = 1, \dots, M$ is a linear combination of the symbols x_1, x_2, \dots, x_G as well as their conjugate versions $x_1^*, x_2^*, \dots, x_G^*$. In (9.60) L_t denotes the number of time slots for transmitting a STC, each column is transmitted by one

transmit antenna using L_t time slots, and each row is simultaneously transmitted by M transmit antennas. Furthermore, in (9.60) the factor β is for achieving the constraint on the transmission power by considering both the number of transmit antennas and the STC's coding rate, β can be determined using the relationship

$$\text{Trace}(E[\mathcal{G}^H \mathcal{G}]) = G \quad (9.61)$$

Let us assume that h_m ($m = 1, 2, \dots, M$) is the fading gain of the channel from the m th transmit antenna to the receive antenna. Furthermore, we assume that the M channels from the M transmit antennas to the receive antenna maintain static over at least a STC block of L_t time slots. Then, the observations obtained by the receiver from the L_t time slots can be expressed as

$$\mathbf{y} = \mathcal{G}\mathbf{h} + \mathbf{n} \quad (9.62)$$

where

$$\mathbf{h} = [h_1, h_2, \dots, h_M]^T, \quad (9.63)$$

while \mathbf{n} is an L_t -length Gaussian noise vector, each component of which is complex Gaussian distributed with zero mean and a variance of $\sigma^2/2 = 1/2\text{SNR}$ per dimension.

Let us assume that the receiver employs ideal knowledge about the fading channels, i.e. about \mathbf{h} . Then, according to the maximum-likelihood principles, as shown in Chapter 6, the receiver estimates the transmitted G symbols according to

$$\hat{\mathbf{x}} = \arg \min_{\mathbf{x}} \{\|\mathbf{y} - \mathcal{G}(\mathbf{x})\mathbf{h}\|^2\} \quad (9.64)$$

where $\mathcal{G}(\mathbf{x})$ is a STC codeword in the form of (9.60), which is constructed from the testing symbol vector \mathbf{x} .

From (9.64) it can be implied that, in order to minimize the decoding error probability, the STC must be designed to maximize the minimum Euclidean distance [246], which can be described by the optimization problem

$$\mathcal{G} = \arg \max \{\min \{\|\mathcal{G}(\mathbf{x}_i)\mathbf{h} - \mathcal{G}(\mathbf{x}_j)\mathbf{h}\|^2\}\}, \quad \text{for any } \mathbf{x}_i \neq \mathbf{x}_j \quad (9.65)$$

where \mathbf{x}_i represents one of the possible symbol vectors transmitted.

Space-time codes can be classified into space-time trellis codes (STTCs) [246] and space-time block codes (STBCs) [243, 245, 251]. The STTC is capable of achieving both diversity gain and coding gain, while the STBC can usually achieve the diversity gain, but either no coding gain at all or very low coding gain. However, by virtue of its special structure, STBC can be decoded using low-complexity linear processing at the receiver. By contrast, STTC decoding is much more complex, requiring relatively high-complexity algorithms, such as the vector Viterbi algorithm, for decoding.

Note that, for STBC, the observation equation seen in (9.62) can usually be converted to the form

$$\mathbf{y} = \mathbf{H}\mathbf{x} + \mathbf{n} \quad (9.66)$$

where \mathbf{H} is a $(L_t \times G)$ channel matrix constructed by channel gains. Based on (9.66) the maximum-likelihood decoding can be described as

$$\hat{\mathbf{x}} = \arg \min_{\mathbf{x}} \{\|\mathbf{y} - \mathbf{H}\mathbf{x}\|^2\} \quad (9.67)$$

Below, our discussion focuses solely on the STBC. Let us first use the well-known Alamouti STC [243] to show the principles. Alamouti STC is for two transmit antennas, given by [243]

$$\mathcal{G}_2 = \frac{1}{\sqrt{2}} \begin{bmatrix} x_1 & x_2 \\ -x_2^* & x_1^* \end{bmatrix} \quad (9.68)$$

The Alamouti STC is transmitted in the following way: during the first time slot, the first antenna transmits x_1 and the second antenna transmits x_2 ; during the second time slot, the first antenna transmits $-x_2^*$ while the second antenna transmits x_1^* .

When the STC of (9.68) is transmitted over flat-fading channels with the channel gains h_1 , h_2 , respectively, from the first and second transmit antennas to the receiver, the two observations obtained by the receiver from the two time slots can then be expressed as

$$\begin{bmatrix} y_1 \\ y_2 \end{bmatrix} = \frac{1}{\sqrt{2}} \begin{bmatrix} x_1 & x_2 \\ -x_2^* & x_1^* \end{bmatrix} \begin{bmatrix} h_1 \\ h_2 \end{bmatrix} + \begin{bmatrix} n_1 \\ n_2 \end{bmatrix} \quad (9.69)$$

Straightforwardly, after taking the conjugate on y_2 , we have

$$\underbrace{\begin{bmatrix} y_1 \\ y_2^* \end{bmatrix}}_y = \underbrace{\frac{1}{\sqrt{2}} \begin{bmatrix} h_1 & h_2 \\ h_2^* & -h_1^* \end{bmatrix}}_H \underbrace{\begin{bmatrix} x_1 \\ x_2 \end{bmatrix}}_x + \underbrace{\begin{bmatrix} n_1 \\ n_2^* \end{bmatrix}}_n \quad (9.70)$$

The decoding of \mathcal{G}_2 is achieved simply by multiplying both sides of (9.70) by H^H , which gives

$$\begin{aligned} \begin{bmatrix} z_1 \\ z_2 \end{bmatrix} &= H^H y \\ &= \frac{1}{2} \begin{bmatrix} |h_1|^2 + |h_2|^2 & 0 \\ 0 & |h_1|^2 + |h_2|^2 \end{bmatrix} \begin{bmatrix} x_1 \\ x_2 \end{bmatrix} + H^H n \end{aligned} \quad (9.71)$$

Explicitly, \mathcal{G}_2 has the properties of

$$\mathcal{G}_2^H \mathcal{G}_2 = \frac{(|x_1|^2 + |x_2|^2)}{2} \mathbf{I}_2 \longleftrightarrow H^H H = \frac{(|h_1|^2 + |h_2|^2)}{2} \mathbf{I}_2 \quad (9.72)$$

and of the decoding of x_1 being independent of that of x_2 . Furthermore, the diversity order for detection of both x_1 and x_2 is two.

Below, we provide a summary of a range of STBCs that have been designed in the literature. We also summarize some of their properties. Let us first consider the real-domain STBCs.

STBCs for Real Signal Constellations The following STBCs are derived from orthogonal design by Tarokh *et al.* in reference [251].

$$\mathbf{G}_2 = \frac{1}{\sqrt{2}} \begin{bmatrix} x_1 & x_2 \\ -x_2 & x_1 \end{bmatrix}, \quad \mathbf{G}_4 = \frac{1}{\sqrt{4}} \begin{bmatrix} x_1 & x_2 & x_3 & x_4 \\ -x_2 & x_1 & -x_4 & x_3 \\ -x_3 & x_4 & x_1 & -x_2 \\ -x_4 & -x_3 & x_2 & x_1 \end{bmatrix} \quad (9.73)$$

$$\mathbf{G}_3 = \frac{1}{\sqrt{3}} \begin{bmatrix} x_1 & x_2 & x_3 \\ -x_2 & x_1 & -x_4 \\ -x_3 & x_4 & x_1 \\ -x_4 & -x_3 & x_2 \end{bmatrix}, \quad \mathbf{G}_5 = \frac{1}{\sqrt{5}} \begin{bmatrix} x_1 & x_2 & x_3 & x_4 & x_5 \\ -x_2 & x_1 & x_4 & -x_3 & x_6 \\ -x_3 & -x_4 & x_1 & x_2 & x_7 \\ -x_4 & x_3 & -x_2 & x_1 & x_8 \\ -x_5 & -x_6 & -x_7 & -x_8 & x_1 \\ -x_6 & x_5 & -x_8 & x_7 & -x_2 \\ -x_7 & x_8 & x_5 & -x_6 & -x_3 \\ -x_8 & -x_7 & x_6 & x_5 & -x_4 \end{bmatrix} \quad (9.74)$$

$$\mathbf{G}_7 = \frac{1}{\sqrt{7}} \begin{bmatrix} x_1 & x_2 & x_3 & x_4 & x_5 & x_6 & x_7 \\ -x_2 & x_1 & x_4 & -x_3 & x_6 & -x_5 & -x_8 \\ -x_3 & -x_4 & x_1 & x_2 & x_7 & x_8 & -x_5 \\ -x_4 & x_3 & -x_2 & x_1 & x_8 & -x_7 & x_6 \\ -x_5 & -x_6 & -x_7 & -x_8 & x_1 & x_2 & x_3 \\ -x_6 & x_5 & -x_8 & x_7 & -x_2 & x_1 & -x_4 \\ -x_7 & x_8 & x_5 & -x_6 & -x_3 & x_4 & x_1 \\ -x_8 & -x_7 & x_6 & x_5 & -x_4 & -x_3 & x_2 \end{bmatrix} \quad (9.75)$$

$$\mathbf{G}_8 = \frac{1}{\sqrt{8}} \begin{bmatrix} x_1 & x_2 & x_3 & x_4 & x_5 & x_6 & x_7 & x_8 \\ -x_2 & x_1 & x_4 & -x_3 & x_6 & -x_5 & -x_8 & x_7 \\ -x_3 & -x_4 & x_1 & x_2 & x_7 & x_8 & -x_5 & -x_6 \\ -x_4 & x_3 & -x_2 & x_1 & x_8 & -x_7 & x_6 & -x_5 \\ -x_5 & -x_6 & -x_7 & -x_8 & x_1 & x_2 & x_3 & x_4 \\ -x_6 & x_5 & -x_8 & x_7 & -x_2 & x_1 & -x_4 & x_3 \\ -x_7 & x_8 & x_5 & -x_6 & -x_3 & x_4 & x_1 & -x_2 \\ -x_8 & -x_7 & x_6 & x_5 & -x_4 & -x_3 & x_2 & x_1 \end{bmatrix} \quad (9.76)$$

The above STBCs from orthogonal design have the following properties:

1. $\mathbf{G}_M \mathbf{G}_M^T = \mathbf{G}_M^T \mathbf{G}_M = (\frac{1}{M} \sum_{m=1}^M x_m^2) \mathbf{I}_M$ for $M = 2, 4, 8, \dots, 2^b$, where b is an integer.
2. $\mathbf{G}_3^T \mathbf{G}_3 = (\frac{1}{3} \sum_{m=1}^4 x_m^2) \mathbf{I}_3$, $\mathbf{G}_5^T \mathbf{G}_5 = (\frac{1}{5} \sum_{m=1}^8 x_m^2) \mathbf{I}_5$ and $\mathbf{G}_7^T \mathbf{G}_7 = (\frac{1}{7} \sum_{m=1}^8 x_m^2) \mathbf{I}_7$.
3. After ignoring the normalization factor, \mathbf{G}_3 is obtained from \mathbf{G}_4 by deleting the last column, \mathbf{G}_5 is obtained from \mathbf{G}_8 by deleting the last three columns and \mathbf{G}_7 is obtained from \mathbf{G}_8 by deleting the last column. Similarly, we can obtain \mathbf{G}_6 from \mathbf{G}_8 by deleting any two columns in \mathbf{G}_8 .
4. The coding rate of all the above STBCs is one.
5. All the above STBCs achieve full diversity.

6. For all the above STBCs, the observations at the receiver can be represented by a MIMO equation in the form

$$\mathbf{y} = \mathbf{H}\mathbf{x} + \mathbf{n} \quad (9.77)$$

7. The transmitted symbols can be detected simply by first forming the decision variables as

$$\begin{aligned} z &= \Re\{\mathbf{H}^H \mathbf{y}\} \\ &= \Re\{\mathbf{H}^H \mathbf{H}\}\mathbf{x} + \Re\{\mathbf{H}^H \mathbf{n}\} \\ &= \left(\frac{1}{M} \sum_{m=1}^M |h_m|^2 \right) \mathbf{x} + \Re\{\mathbf{H}^H \mathbf{n}\} \end{aligned} \quad (9.78)$$

Explicitly, all the above STBCs achieve full diversity.

STBCs for Complex Signal Constellations The following STBCs are suitable for complex signal constellations.

1. Alamouti STBC for two transmit antennas [243], coding rate= 1:

$$\mathcal{G}_2 = \frac{1}{\sqrt{2}} \begin{bmatrix} x_1 & x_2 \\ -x_2^* & x_1^* \end{bmatrix} \quad (9.79)$$

2. STBCs for three and four transmit antennas [245, 251], coding rate= 1/2:

$$\mathcal{G}_3 = \frac{1}{\sqrt{6}} \begin{bmatrix} x_1 & x_2 & x_3 \\ -x_2 & x_1 & -x_4 \\ -x_3 & x_4 & x_1 \\ -x_4 & -x_3 & x_2 \\ x_1^* & x_2^* & x_3^* \\ -x_2^* & x_1^* & -x_4^* \\ -x_3^* & x_4^* & x_1^* \\ -x_4^* & -x_3^* & x_2^* \end{bmatrix} \quad (9.80)$$

$$\mathcal{G}_4 = \frac{1}{\sqrt{8}} \begin{bmatrix} x_1 & x_2 & x_3 & x_4 \\ -x_2 & x_1 & -x_4 & x_3 \\ -x_3 & x_4 & x_1 & -x_2 \\ -x_4 & -x_3 & x_2 & x_1 \\ x_1^* & x_2^* & x_3^* & x_4^* \\ -x_2^* & x_1^* & -x_4^* & x_3^* \\ -x_3^* & x_4^* & x_1^* & -x_2^* \\ -x_4^* & -x_3^* & x_2^* & x_1^* \end{bmatrix} \quad (9.81)$$

Explicitly, when ignoring the normalization factor, \mathcal{G}_3 can be constructed from \mathcal{G}_4 by deleting the last column in \mathcal{G}_4 .

3. STBCs for three and four transmit antennas [245, 251], coding rate = 3/4:

$$\mathcal{H}_3 = \frac{1}{\sqrt{3}} \begin{bmatrix} x_1 & x_2 & \frac{x_3}{\sqrt{2}} \\ -x_2^* & x_1^* & \frac{x_3}{\sqrt{2}} \\ \frac{x_3^*}{\sqrt{2}} & \frac{x_3^*}{\sqrt{2}} & \frac{-x_1 - x_1^* + x_2 - x_2^*}{2} \\ \frac{x_3^*}{\sqrt{2}} & -\frac{x_3^*}{\sqrt{2}} & \frac{x_2 + x_2^* + x_1 - x_1^*}{2} \end{bmatrix} \quad (9.82)$$

$$\mathcal{H}_4 = \frac{1}{\sqrt{4}} \begin{bmatrix} x_1 & x_2 & \frac{x_3}{\sqrt{2}} & \frac{x_3}{\sqrt{2}} \\ -x_2^* & x_1^* & \frac{x_3}{\sqrt{2}} & -\frac{x_3}{\sqrt{2}} \\ \frac{x_3^*}{\sqrt{2}} & \frac{x_3^*}{\sqrt{2}} & \frac{-x_1 - x_1^* + x_2 - x_2^*}{2} & \frac{-x_2 - x_2^* + x_1 - x_1^*}{2} \\ \frac{x_3^*}{\sqrt{2}} & -\frac{x_3^*}{\sqrt{2}} & \frac{x_2 + x_2^* + x_1 - x_1^*}{2} & -\frac{x_1 + x_1^* + x_2 - x_2^*}{2} \end{bmatrix} \quad (9.83)$$

Again, when ignoring the normalization factor, \mathcal{H}_3 can be obtained from \mathcal{H}_4 by deleting its last column.

4. The STBC $\tilde{\mathcal{H}}_4$ below is from reference [253], $\tilde{\mathcal{H}}_3$ is obtained from $\tilde{\mathcal{H}}_4$ by deleting its last column. Both codes have a coding rate of 3/4, and they have simpler structures and lower encoding complexity than their counterpart codes of \mathcal{H}_3 and \mathcal{H}_4 .

$$\tilde{\mathcal{H}}_3 = \frac{1}{\sqrt{3}} \begin{bmatrix} x_1 & 0 & x_2 \\ 0 & x_1 & x_3^* \\ -x_2^* & -x_3 & x_1^* \\ x_3^* & -x_2 & 0 \end{bmatrix} \quad (9.84)$$

$$\tilde{\mathcal{H}}_4 = \frac{1}{\sqrt{4}} \begin{bmatrix} x_1 & 0 & x_2 & -x_3 \\ 0 & x_1 & x_3^* & x_2^* \\ -x_2^* & -x_3 & x_1^* & 0 \\ x_3^* & -x_2 & 0 & x_1^* \end{bmatrix} \quad (9.85)$$

The above STBCs for complex signal constellations have the following properties:

1. All the above STBCs achieve full diversity.
2. Except the Alamouti STBC of \mathcal{G}_2 , the coding rate of all the other STBCs is lower than one. Furthermore, it has been proved in reference [251] that there exist no orthogonal STBCs having a unity coding rate for complex signal constellations with linear processing (complexity), when $M \geq 4$.
3. All the STBCs are orthogonal codes, $\mathcal{G}_M^T \mathcal{G}_M = c(\sum_{g=1}^G |x_g|^2) \mathbf{I}_M$ and $\mathcal{H}_M^T \mathcal{H}_M = c(\sum_{g=1}^G |x_g|^2) \mathbf{I}_M$ where c is a constant and G is the number of symbols included in the STBC considered.

4. For \mathcal{G}_2 , \mathcal{G}_3 and \mathcal{G}_4 , the corresponding observations at the receiver can be represented by a MIMO equation in the form

$$\mathbf{y} = \mathbf{H}\mathbf{x} + \mathbf{n} \quad (9.86)$$

where the vector $\mathbf{y} = [y_0, \dots, y_{L_t/2-1}, y_{L_t/2}^*, \dots, y_{L_t-1}^*]^T$, L_t denotes the number of time slots conveying the STBC and y_i^* represents the conjugate of the observation obtained from the i th time slot.

5. The transmitted symbols in the context of \mathcal{G}_2 , \mathcal{G}_3 and \mathcal{G}_4 can be simply detected by forming the decision variables as

$$\begin{aligned} z &= \mathbf{H}^H \mathbf{y} \\ &= \mathbf{H}^H \mathbf{H}\mathbf{x} + \mathbf{H}^H \mathbf{n} \\ &= \left(\mu \sum_{m=1}^M |h_m|^2 \right) \mathbf{x} + \mathbf{H}^H \mathbf{n} \end{aligned} \quad (9.87)$$

where M denotes the number of transmit antennas and μ is a constant determined by the specific STBC considered.

6. For the STBCs \mathcal{H}_3 , \mathcal{H}_4 and $\tilde{\mathcal{H}}_3$, $\tilde{\mathcal{H}}_4$, we can form the MIMO equation as

$$\tilde{\mathbf{y}} = \tilde{\mathbf{H}}\tilde{\mathbf{x}} + \tilde{\mathbf{n}} \quad (9.88)$$

where, by construction,

$$\begin{aligned} \tilde{\mathbf{y}} &= [\mathbf{y}^T, \mathbf{y}^H]^T, \quad (2L_t \times 1) \\ \tilde{\mathbf{x}} &= [\mathbf{x}^T, \mathbf{x}^H]^T, \quad (2G \times 1) \\ \tilde{\mathbf{n}} &= [\mathbf{n}^T, \mathbf{n}^H]^T, \quad (2L_t \times 1) \end{aligned} \quad (9.89)$$

where \mathbf{y} contains the L_t observations obtained directly by the receiver, \mathbf{y}^H is the Hermitian (transpose conjugate) of \mathbf{y} . Similarly, we can obtain $\tilde{\mathbf{n}}$ from \mathbf{n} . Furthermore, in (9.88) $\tilde{\mathbf{H}}$ is determined by the specific STBC considered.

7. With the representation of (9.88), it can be shown that $\tilde{\mathbf{H}}$ has the property

$$\tilde{\mathbf{H}}^H \tilde{\mathbf{H}} = \mu \left(\sum_{m=1}^M |h_m|^2 \right) \mathbf{I}_{2G} \quad (9.90)$$

Hence, we have

$$\tilde{\mathbf{z}} = \tilde{\mathbf{H}}^H \tilde{\mathbf{y}} = \mu \left(\sum_{m=1}^M |h_m|^2 \right) \tilde{\mathbf{x}} + \tilde{\mathbf{H}}^H \tilde{\mathbf{n}} \quad (9.91)$$

which shows that there is no interference among the transmitted symbols and their conjugate versions. Consequently, the decision variable vector \mathbf{z} for \mathbf{x} can be formed as

$$\begin{aligned} \mathbf{z} &= [z_0, z_1, \dots, z_{G-1}]^T \\ z_i &= \tilde{z}_i + \tilde{z}_{i+G}^*, \quad i = 0, 1, \dots, G-1 \end{aligned} \quad (9.92)$$

where \tilde{z}_i is the i th element of $\tilde{\mathbf{z}}$.

Since there are no full-rate full-diversity orthogonal STBCs for complex signal constellations with linear processing, research attention has been turned to design the full-rate full-diversity quasi-orthogonal STBCs, which may require a little more decoding complexity than the linear processing. For example, the following quasi-orthogonal STBC from reference [254] is for four transmit antennas and has full rate and achieves full diversity.

$$\mathcal{A}_4 = \frac{1}{\sqrt{4}} \begin{bmatrix} a_1 & a_2 & a_3 & a_4 \\ -a_2^* & a_1^* & -a_4^* & a_3^* \\ a_1 & a_2 & -a_3 & -a_4 \\ -a_2^* & a_1^* & a_4^* & -a_3^* \end{bmatrix} \quad (9.93)$$

where a_1, a_2, a_3 and a_4 are constructed by the transmitted symbols x_1, x_2, x_3 and x_4 as

$$\begin{aligned} a_1 &= \frac{x_1 + x_2}{\sqrt{2}}, & a_2 &= \frac{x_3 + x_4}{\sqrt{2}} \\ a_3 &= \frac{x_1 - x_2}{\sqrt{2}}, & a_4 &= \frac{x_3 - x_4}{\sqrt{2}} \end{aligned} \quad (9.94)$$

When the code \mathcal{A}_4 is transmitted over flat-fading channels using four transmit antennas, the observations at the receiver can be expressed as

$$\mathbf{y} = \frac{1}{2} \underbrace{\begin{bmatrix} h_1 & h_2 & h_3 & h_4 \\ h_2^* & -h_1^* & h_4^* & -h_3^* \\ h_1 & h_2 & -h_3 & -h_4 \\ h_2^* & -h_1^* & -h_4^* & h_3^* \end{bmatrix}}_{\mathbf{H}} \begin{bmatrix} a_1 \\ a_2 \\ a_3 \\ a_4 \end{bmatrix} + \mathbf{n} \quad (9.95)$$

Processing the above equation using \mathbf{H} , we obtain

$$\begin{aligned} \mathbf{r} &= \mathbf{H}^H \mathbf{y} \\ &= \frac{1}{2} \begin{bmatrix} |h_1|^2 + |h_2|^2 & 0 & 0 & 0 \\ 0 & |h_1|^2 + |h_2|^2 & 0 & 0 \\ 0 & 0 & |h_3|^2 + |h_4|^2 & 0 \\ 0 & 0 & 0 & |h_3|^2 + |h_4|^2 \end{bmatrix} \begin{bmatrix} a_1 \\ a_2 \\ a_3 \\ a_4 \end{bmatrix} + \bar{\mathbf{n}} \end{aligned} \quad (9.96)$$

Explicitly, there is no interference among a_1, a_2, a_3 and a_4 . Furthermore, as shown in (9.94), x_1 and x_2 are only involved in a_1 and a_3 , while x_3 and x_4 are only related to a_2 and a_4 . Hence, (9.96) can be decoupled into two independent equations as

$$\begin{aligned} \underbrace{\begin{bmatrix} r_1 \\ r_3 \end{bmatrix}}_{\mathbf{r}_a} &= \frac{1}{\sqrt{8}} \underbrace{\begin{bmatrix} |h_1|^2 + |h_2|^2 & |h_1|^2 + |h_2|^2 \\ |h_3|^2 + |h_4|^2 & -(|h_3|^2 + |h_4|^2) \end{bmatrix}}_{\mathbf{H}_c} \underbrace{\begin{bmatrix} x_1 \\ x_2 \end{bmatrix}}_{\mathbf{x}_a} + \underbrace{\begin{bmatrix} \bar{n}_1 \\ \bar{n}_2 \end{bmatrix}}_{\mathbf{n}_a} \\ \underbrace{\begin{bmatrix} r_2 \\ r_4 \end{bmatrix}}_{\mathbf{r}_b} &= \frac{1}{\sqrt{8}} \underbrace{\begin{bmatrix} |h_1|^2 + |h_2|^2 & |h_1|^2 + |h_2|^2 \\ |h_3|^2 + |h_4|^2 & -(|h_3|^2 + |h_4|^2) \end{bmatrix}}_{\mathbf{H}_c} \underbrace{\begin{bmatrix} x_3 \\ x_4 \end{bmatrix}}_{\mathbf{x}_b} + \underbrace{\begin{bmatrix} \bar{n}_1 \\ \bar{n}_2 \end{bmatrix}}_{\mathbf{n}_b} \end{aligned} \quad (9.97)$$

In (9.97) \mathbf{H}_c is not an orthogonal matrix, hence, x_1 and x_2 are correlated, so are x_3 and x_4 . In this case, the optimum decoding scheme is the maximum likelihood decoding (MLD), which solves the optimization problems for x_1 and x_2 , as well as x_3 and x_4 according to

$$\begin{aligned}\hat{\mathbf{x}}_a &= \arg \min_{\mathbf{x}_t} \{ \| \mathbf{r}_a - \mathbf{H}_c \mathbf{x}_t \|^2 \} \\ \hat{\mathbf{x}}_b &= \arg \min_{\mathbf{x}_t} \{ \| \mathbf{r}_b - \mathbf{H}_c \mathbf{x}_t \|^2 \}\end{aligned}\quad (9.98)$$

where \mathbf{x}_t is a length-2 complex testing vector.

The STBC \mathcal{A}_4 shown in (9.93) is capable of achieving full rate and full diversity. However, it is not an orthogonal STBC. One of the advantages of this STBC is that it does not require CSI for carrying out the encoding. However, its decoding complexity is slightly higher than that of a corresponding orthogonal STBC. If in practice partial CSI is available at the transmitter, as shown in reference [255], full-rate full-diversity STBCs are available for complex signal constellations with linear processing. Below are a few examples taken from reference [255] that are the STBCs for three or four transmit antennas.

Two full-rate full-diversity STBCs for three transmit antennas are given by reference [255]

$$\begin{aligned}\mathbf{T}_3^{(1)} &= \frac{1}{\sqrt{3}} \begin{bmatrix} x_1 & x_2 & ax_2 \\ -x_2^* & x_1^* & ax_1^* \end{bmatrix} \\ \mathbf{T}_3^{(2)} &= \frac{1}{\sqrt{3}} \begin{bmatrix} x_1 & x_2 & ax_1 \\ x_2^* & -x_1^* & ax_2^* \end{bmatrix}\end{aligned}\quad (9.99)$$

where $a = \pm 1$ is determined by the partial CSI fed back from the receiver that will become clear in our later analysis.

When the above two STBCs are transmitted over flat-fading channels, the received observations can be expressed using the MIMO equations respectively as

$$\begin{aligned}\mathbf{y}^{(1)} &= \underbrace{\frac{1}{\sqrt{3}} \begin{bmatrix} h_1 & h_2 + ah_3 \\ h_2^* + ah_3^* & -h_1^* \end{bmatrix}}_{\mathbf{H}^{(1)}} \begin{bmatrix} x_1 \\ x_2 \end{bmatrix} + \mathbf{n}^{(1)} \\ \mathbf{y}^{(2)} &= \underbrace{\frac{1}{\sqrt{3}} \begin{bmatrix} h_1 + ah_3 & h_2 \\ -h_2^* & h_1^* + ah_3^* \end{bmatrix}}_{\mathbf{H}^{(2)}} \begin{bmatrix} x_1 \\ x_2 \end{bmatrix} + \mathbf{n}^{(2)}\end{aligned}\quad (9.100)$$

Furthermore, when using $\mathbf{H}^{(1)}$ and $\mathbf{H}^{(2)}$ to process $\mathbf{y}^{(1)}$ and $\mathbf{y}^{(2)}$, respectively, we obtain

$$\begin{aligned}\mathbf{r}^{(1)} &= (\mathbf{H}^{(1)})^H \mathbf{y}^{(1)} \\ &= \frac{1}{3} \begin{bmatrix} |h_1|^2 + |h_2|^2 + |h_3|^2 + 2a\Re\{h_2h_3^*\} & 0 \\ 0 & |h_1|^2 + |h_2|^2 + |h_3|^2 + 2a\Re\{h_2h_3^*\} \end{bmatrix} \begin{bmatrix} x_1 \\ x_2 \end{bmatrix} \\ &\quad + \bar{\mathbf{n}}^{(1)}\end{aligned}\quad (9.101)$$

$$\begin{aligned}\mathbf{r}^{(2)} &= (\mathbf{H}^{(2)})^H \mathbf{y}^{(2)} \\ &= \frac{1}{3} \begin{bmatrix} |h_1|^2 + |h_2|^2 + |h_3|^2 + 2a\Re\{h_1h_3^*\} & 0 \\ 0 & |h_1|^2 + |h_2|^2 + |h_3|^2 + 2a\Re\{h_1h_3^*\} \end{bmatrix} \begin{bmatrix} x_1 \\ x_2 \end{bmatrix} \\ &\quad + \bar{\mathbf{n}}^{(2)}\end{aligned}\quad (9.102)$$

From (9.101) we see that the gain achieved by the STBC $\mathcal{T}_3^{(1)}$ will be higher than the gain achieved by the three order of diversity, provided that a is chosen to make $2a\Re\{h_2h_3^*\} > 0$. Similarly, from (9.102) we see that the gain achieved by the STBC $\mathcal{T}_3^{(2)}$ will be higher than the gain achieved by the three order of diversity, if a is chosen to satisfy $2a\Re\{h_1h_3^*\} > 0$. Hence, when the space–time system uses one-bit feedback, either $\mathcal{T}_3^{(1)}$ or $\mathcal{T}_3^{(2)}$ can be used. Correspondingly, the receiver uses one feedback bit to inform the transmitter whether $\Re\{h_2h_3^*\} > 0$ for $\mathcal{T}_3^{(1)}$ or whether $\Re\{h_1h_3^*\} > 0$ for $\mathcal{T}_3^{(2)}$. With the aid of this one-bit information fed back from the receiver, the transmitter can decide an appropriate value of a , so that $2a\Re\{h_2h_3^*\} > 0$ or $2a\Re\{h_1h_3^*\} > 0$ is always satisfied.

Furthermore, it can be implied from (9.101) and (9.102) that, when using only one-bit feedback, both $\mathcal{T}_3^{(1)}$ and $\mathcal{T}_3^{(2)}$ achieve the same BER performance. However, if two feedback bits are available, the transmitter can then choose between $\mathcal{T}_3^{(1)}$ and $\mathcal{T}_3^{(2)}$, in order to achieve better BER performance. This is an interesting transmission scheme proposed in reference [255]. Specifically, as shown in (9.101) and (9.102), if $|\Re\{h_1h_3^*\}| < |\Re\{h_2h_3^*\}|$, the STBC $\mathcal{T}_3^{(1)}$ is then preferred, since it can yield higher output SNR than the STBC $\mathcal{T}_3^{(2)}$. Otherwise, the STBC $\mathcal{T}_3^{(2)}$ is preferred to the STBC $\mathcal{T}_3^{(1)}$, if $|\Re\{h_1h_3^*\}| > |\Re\{h_2h_3^*\}|$. Therefore, when two feedback bits are available, one bit is then used to indicate whether $|\Re\{h_1h_3^*\}| > |\Re\{h_2h_3^*\}|$, so that the transmitter can choose between $\mathcal{T}_3^{(1)}$ and $\mathcal{T}_3^{(2)}$. The second bit is used to convey the information about whether $\Re\{h_1h_3^*\} > 0$ or $\Re\{h_2h_3^*\} > 0$ depending on the STBC chosen, so that the transmitter can decide an appropriate value for a .

The above principles may be extended to the case using more than two STBCs or to the space–time system using more than three transmit antennas. For example, in reference [255] there is another STBC for three transmit antennas, which is

$$\mathcal{T}_3^{(3)} = \frac{1}{\sqrt{3}} \begin{bmatrix} x_1 & ax_2 & x_2 \\ x_2^* & ax_2^* & -x_1^* \end{bmatrix} \quad (9.103)$$

Hence, if three feedback bits are available, the space–time system can choose one from the three STBCs $\mathcal{T}_3^{(1)}$, $\mathcal{T}_3^{(2)}$ and $\mathcal{T}_3^{(3)}$, in order to achieve a further enhanced BER performance.

In the context of the STBCs for four transmit antennas, reference [255] has designed the following full-rate full-diversity STBCs for complex signal constellations with linear processing.

$$\mathcal{T}_4^{(1)} = \frac{1}{\sqrt{4}} \begin{bmatrix} x_1 & x_2 & ax_1 & bx_2 \\ -x_2^* & x_1^* & -ax_2^* & bx_1^* \end{bmatrix} \quad (9.104)$$

$$\mathcal{T}_4^{(2)} = \frac{1}{\sqrt{4}} \begin{bmatrix} x_1 & x_2 & ax_2 & bx_1 \\ -x_2^* & x_1^* & ax_1^* & -bx_2^* \end{bmatrix} \quad (9.105)$$

$$\mathcal{T}_4^{(3)} = \frac{1}{\sqrt{4}} \begin{bmatrix} x_1 & ax_1 & x_2 & bx_2 \\ -x_2^* & -ax_2^* & x_1^* & bx_1^* \end{bmatrix} \quad (9.106)$$

In the above three equations $a = \pm 1$ and $b = \pm 1$, which are determined based on the information fed back from the receiver.

The operation principles of the \mathcal{T}_4 family are similar to those of the \mathcal{T}_3 family. However, for the \mathcal{T}_4 family, a minimum of two feedback bits are required. Specifically, if two feedback bits are available, the space–time system may use any one of the above three STBCs, any

of which will achieve a similar BER performance. The two feedback bits are used for the transmitter to decide the corresponding values for a and b .

As discussed in reference [255], when three or four feedback bits are available, then the space–time system can choose one best STBC from two (any two of the above three) or three STBCs, in order that the best BER performance can be achieved.

Below, we discuss another type of open-loop transmit diversity scheme that is suitable for the space–time systems using spread-spectrum techniques.

9.2.2.5 Transmit Diversity Based on Space–Time Spreading

STS-assisted transmit diversity (STS-TD) is a type of open-loop transmit diversity scheme designed specifically for spread-spectrum-based CDMA systems [256–258]. Let us first use an example to show the principles of STS. In this example we consider a spread-spectrum system employing $M = 2$ transmit antennas and $N = 1$ receive antenna, and the spreading code \mathbf{c} (which is not necessary orthogonal) of length S , where \mathbf{c} is normalized to satisfy $\|\mathbf{c}\|^2 = 1$. Based on \mathbf{c} we can construct two orthogonal codes of length $2S$:

$$\begin{aligned} \mathbf{c}_1 &= [\mathbf{c}^T \ \mathbf{c}^T]^T / \sqrt{2} \\ \mathbf{c}_2 &= [\mathbf{c}^T \ -\mathbf{c}^T]^T / \sqrt{2} \end{aligned} \quad (9.107)$$

Let x_1 and x_2 be two consecutive symbols to be transmitted. With the STS, the two signals transmitted by the two transmit antennas are formed as

$$\mathbf{S} = [s_1 \ s_2] = \underbrace{[\mathbf{c}_1 \ \mathbf{c}_2]}_{\mathbf{C}} \underbrace{\frac{1}{\sqrt{2}} \begin{bmatrix} x_1 & x_2 \\ -x_2^* & x_1^* \end{bmatrix}}_{\mathbf{g}_2} \quad (9.108)$$

When transmitting \mathbf{S} over flat-fading channels with the channel gains corresponding to the first and second transmit antennas being h_1 and h_2 , the $2S$ observations obtained at the receiver can be expressed as

$$\begin{aligned} \mathbf{r} &= [s_1 \ s_2] \begin{bmatrix} h_1 \\ h_2 \end{bmatrix} \\ &= [\mathbf{c}_1 \ \mathbf{c}_2] \frac{1}{\sqrt{2}} \begin{bmatrix} x_1 & x_2 \\ -x_2^* & x_1^* \end{bmatrix} \begin{bmatrix} h_1 \\ h_2 \end{bmatrix} + \mathbf{n} \end{aligned} \quad (9.109)$$

Carrying out the de-spread operation using \mathbf{C} and using the result of $\mathbf{C}^H \mathbf{C} = \mathbf{I}_2$, we obtain

$$\mathbf{y} = \mathbf{C}^H \mathbf{r} = \frac{1}{\sqrt{2}} \begin{bmatrix} x_1 & x_2 \\ -x_2^* & x_1^* \end{bmatrix} \begin{bmatrix} h_1 \\ h_2 \end{bmatrix} + \bar{\mathbf{n}} \quad (9.110)$$

where $\bar{\mathbf{n}} = \mathbf{C}^H \mathbf{n}$. Furthermore, (9.110) can be represented as

$$\tilde{\mathbf{y}} = \underbrace{\frac{1}{\sqrt{2}} \begin{bmatrix} h_1 & h_2 \\ h_2^* & -h_1^* \end{bmatrix}}_{\mathbf{H}} \underbrace{\begin{bmatrix} x_1 \\ x_2 \end{bmatrix}}_{\mathbf{x}} + \tilde{\mathbf{n}} \quad (9.111)$$

which is the same as (9.70) for the STBC \mathcal{G}_2 . Hence, the above STS scheme is capable of achieving a diversity order of two, like the STBC \mathcal{G}_2 .

Let us now generalize the STS for the space–time systems with M number of transmit antennas. From the generalization, we can conclude the following:

- For any given STC (either STBC or STTC), there exists a corresponding STS scheme. STS can be viewed as the generalization of STC. By contrast, STC can be viewed as a special case of the STS, which employs a spreading matrix \mathbf{I} .
- If the STC is full-rate, the corresponding STS is also full-rate.
- The STS scheme is capable of achieving the same order of diversity as the STC on which the STS design is based.

The generalization starts with (9.60), i.e.

$$\mathcal{G} = \beta \begin{bmatrix} a_{11} & a_{12} & \cdots & a_{1M} \\ a_{21} & a_{22} & \cdots & a_{2M} \\ \vdots & \vdots & \ddots & \vdots \\ a_{L_t 1} & a_{L_t 2} & \cdots & a_{L_t M} \end{bmatrix} \quad (9.112)$$

which is the STC for M transmit antennas that transmits G symbols using L_t time slots. Based on the value of L_t , we can form a $(\mathcal{L} \times L_t)$ -dimensional spreading matrix

$$\mathbf{C} = [c_1 \ c_2 \ \cdots \ c_{L_t}] \quad (9.113)$$

where $\|c_i\|^2 = 1$. For the spreading matrix \mathbf{C} , the number of columns L_t is determined by the number of time slots for transmission of the STC, while the number of rows \mathcal{L} depends on the design objective. Let us assume that the number of chips per symbol (before the STC) is S . If the design intends that the data-rate of the systems with and without the STS is the same, then we have $\mathcal{L} = GS$. Since for length \mathcal{L} there are only \mathcal{L} orthogonal codes and, furthermore, since each user requires L_t orthogonal codes for the STS, in this case the maximum number of users supportable by the space–time system is $K_{\max} = \mathcal{L}/L_t = GS/L_t$. It can be shown that, for the full-rate STCs, we have $K_{\max} = S$ due to $G = L_t$. Otherwise, if the rate of the STCs is lower than one, i.e. $G/L_t < 1$, then the maximum number of users supportable by the STS system is lower than S .

If the design intends that the maximum number of users supported by the systems with and without STS is the same, which is S , then we can let $\mathcal{L} = L_t S$. Since in this case there are $\mathcal{L} = L_t S$ orthogonal codes and each user requires L_t orthogonal codes for STS, the maximum number of users supportable by the STS system is hence $K_{\max} = \mathcal{L}/L_t = S$. However, since the STS system transmits G symbols using L_t time slots, the rate of the STS system is hence G/L_t . Furthermore, it can be shown that for the full-rate STC, the STS scheme is also full-rate. Otherwise, the rate of the STS scheme is lower than one.

From the above analysis, we can conclude that the STS schemes designed based on the full-rate STCs are also the full-rate STS schemes. The full-rate can be achieved without requiring trade-off of the maximum number of users supportable by the STS system, of the achievable diversity order, as shown below, etc. In practice, the STS schemes having

the above properties of full-rate, full-diversity and requiring no extra spreading codes are desirable.

Based on the spreading matrix \mathbf{C} of (9.113) and the STC of (9.112), the STS signals transmitted by the M number of transmit antennas are formed as

$$\mathbf{S} = [s_1 \ s_2, \dots, \ s_M] = \mathbf{CG} \quad (9.114)$$

where s_m ($m = 1, 2, \dots, M$) is transmitted by the m th transmit antenna. It can be shown that

$$\text{Trace}(\mathbf{S}^H \mathbf{S}) = \text{Trace}(\mathbf{G}^H \mathbf{G}) = G \quad (9.115)$$

implying that (9.114) is a normalized STS scheme.

Assuming flat-fading channels and the channel gains of

$$\mathbf{h} = [h_1 \ h_2, \dots, \ h_M]^T \quad (9.116)$$

corresponding to the M transmit antennas, the observations obtained by the receiver can then be expressed as

$$\begin{aligned} \mathbf{r} &= \mathbf{Sh} + \mathbf{n} \\ &= \mathbf{CGh} + \mathbf{n} \end{aligned} \quad (9.117)$$

De-spreading \mathbf{r} using the spreading matrix \mathbf{C} and assuming that $\mathbf{c}_i^H \mathbf{c}_j = 0$ for $i \neq j$, the receiver generates

$$\begin{aligned} \mathbf{y} &= \mathbf{C}^H \mathbf{r} \\ &= \mathbf{Gh} + \bar{\mathbf{n}} \end{aligned} \quad (9.118)$$

where $\bar{\mathbf{n}} = \mathbf{C}^H \mathbf{n}$, which is a complex Gaussian noise vector distributed with zero mean and a covariance matrix $\sigma^2 \mathbf{I}_{L_r}$.

It can be seen that (9.118) is the same as (9.62). Hence, the following operations are the same as the decoding operations of the STC for (9.62). Furthermore, it can be implied from (9.118) and (9.62) that the STS scheme designed based on a given STC is capable of achieving the same diversity gain as the STC.

Above, we have assumed that the spreading matrix \mathbf{C} is constructed by the orthogonal spreading codes, satisfying $\mathbf{C}^H \mathbf{C} = \mathbf{I}$. In the case where \mathbf{C} is not an orthogonal matrix, we obtain after the de-spreading operation

$$\mathbf{y} = \mathbf{R}_C \mathbf{Gh} + \bar{\mathbf{n}} \quad (9.119)$$

where $\mathbf{R}_C = \mathbf{C}^H \mathbf{C}$ is the autocorrelation matrix of \mathbf{C} . In order to return to the same form as the STC decoding, the receiver can carry out the decorrelating operation by multiplying (9.119) with \mathbf{R}_C^{-1} , yielding

$$\begin{aligned} \tilde{\mathbf{y}} &= \mathbf{R}_C^{-1} \mathbf{y} \\ &= \mathbf{Gh} + \tilde{\mathbf{n}} \end{aligned} \quad (9.120)$$

where $\tilde{\mathbf{n}} = \mathbf{R}_C^{-1} \bar{\mathbf{n}}$, which is still a complex Gaussian noise vector distributed with zero mean and a covariance matrix $\sigma^2 \mathbf{R}_C^{-1}$, implying that the noise samples in $\tilde{\mathbf{n}}$ may become correlated if $\mathbf{C}^H \mathbf{C} \neq \mathbf{I}$.

Nevertheless, (9.120) has the same structure as (9.62) of the original STC. Hence, the following decoding/detection operations are the same as the decoding of STC.

Additionally, based on (9.117), it seems that the STS and STC may be jointly designed, in order to achieve the best performance, such as to achieve coding gain in addition to diversity gain.

Finally, it is worth noting explicitly that the STC \mathcal{G} in (9.112) can be any STC, it can be a STTC in reference [246] or a STBC chosen, for example, from those listed in Section 9.2.2.4.

9.2.3 MIMO Diversity

Thus far, we have considered many schemes for achieving either transmit diversity or receive diversity. In MIMO systems multiple transmit and receiver antennas can be simultaneously employed for achieving a high order of diversity, which we refer to as MIMO diversity. It can be shown that, in a rich scattering environment resulting in independent fading from each transmit antenna to each receive antenna, a MIMO system having M transmit antennas and N receive antennas is capable of achieving a diversity order of MN . Below, we use a simple example to illustrate the principles.

Let us assume a MIMO system using $M = 2$ transmit antennas and N receive antennas. Let the two consecutive symbols x_1 and x_2 be transmitted based on the Alamouti STBC scheme. Furthermore, let us assume that the channel from either of the transmit antennas to any of the receive antennas experience flat fading. Then, according to Section 9.2.2.4, the observation vector at the n th receive antenna can be expressed as

$$\mathbf{r}_n = \begin{bmatrix} r_{1n} \\ r_{2n}^* \end{bmatrix} = \underbrace{\frac{1}{\sqrt{2}} \begin{bmatrix} h_{1n} & h_{2n} \\ h_{2n}^* & -h_{1n}^* \end{bmatrix}}_{\mathbf{H}_n} \underbrace{\begin{bmatrix} x_1 \\ x_2 \end{bmatrix}}_{\mathbf{x}} + \underbrace{\begin{bmatrix} n_{1n} \\ n_{2n}^* \end{bmatrix}}_{\mathbf{n}_n} \quad (9.121)$$

We define

$$\mathbf{r} = [\mathbf{r}_1^T, \mathbf{r}_2^T, \dots, \mathbf{r}_N^T]^T, \quad (2N \times 1) \quad (9.122)$$

$$\mathbf{H} = [\mathbf{H}_1^T, \mathbf{H}_2^T, \dots, \mathbf{H}_N^T]^T, \quad (2N \times 2) \quad (9.123)$$

$$\mathbf{n} = [\mathbf{n}_1^T, \mathbf{n}_2^T, \dots, \mathbf{n}_N^T]^T, \quad (2N \times 1) \quad (9.124)$$

Then, when considering the N number of receive antennas, the observations associated with two consecutive symbol intervals can be expressed in matrix form as

$$\mathbf{r} = \mathbf{H}\mathbf{x} + \mathbf{n} \quad (9.125)$$

Using the fact that the Alamouti STBC satisfies

$$\begin{aligned} \mathbf{H}_n^H \mathbf{H}_n &= \frac{1}{2} \begin{bmatrix} |h_{1n}|^2 + |h_{2n}|^2 & 0 \\ 0 & |h_{1n}|^2 + |h_{2n}|^2 \end{bmatrix} \\ &= \frac{(|h_{1n}|^2 + |h_{2n}|^2)}{2} \mathbf{I}_2 \end{aligned} \quad (9.126)$$

after the space–time combining completed by multiplying \mathbf{H}^H with \mathbf{r} , the decision variable for \mathbf{x} can be expressed as

$$\begin{aligned} z &= \mathbf{H}^H \mathbf{r} \\ &= \frac{1}{2} \sum_{n=1}^N (|h_{1n}|^2 + |h_{2n}|^2) \mathbf{x} + \mathbf{H}^H \mathbf{n} \end{aligned} \quad (9.127)$$

Explicitly, the diversity order achieved is $2N$.

Similarly, it can be shown that when a MIMO system uses M transmit antennas and N receive antennas, then the diversity order achieved by the MIMO system can be as high as MN , provided that a full-diversity space–time scheme (STC, STS, etc.) is used.

Let us now consider the principles of spatial-division multiple-access (SDMA).

9.3 Spatial-Division Multiple Access

In wireless communications multiuser signals arriving at a point (for example, a base-station (BS)) may be distinguished by the location-related information of the transmitters, resulting in the so-called SDMA. The SDMA techniques make multiuser communications possible in those wireless systems, such as the OFDM system, which themselves are not suitable for supporting multiple-access communications. Furthermore, the SDMA techniques are capable of adding degrees-of-freedom to the existing multiple-access systems, such as CDMA systems, in order to provide higher capacity or to support a higher number of users [259]. In SDMA systems different users may be distinguished by making use of the characteristics of the wireless channels experienced by these users. It is well known that the wireless channels of different users separated geographically by a sufficient distance will experience uncorrelated fading, yielding different channel impulse responses (CIRs) observed by a receiver. Once the receiver obtains the CIR information of the users, these CIRs can be viewed as the signature codes of the users as in the CDMA systems. Consequently, the receiver is capable of distinguishing between the users with the aid of their unique CIRs. Below, we use an example to show the principles of SDMA.

Let us assume a SDMA system where K users communicate with a common BS using narrow-band signals. Let us assume that the BS employs N number of receive antennas, while a MT employs M transmit antennas. Let \mathbf{x}_k be the data vector transmitted by the k th MT. Furthermore, the k th MT may transmit the space–time coded information in order to achieve transmit diversity. After considering all the above assumptions and following the principles of MIMO in Section 9.1 and that of spatial diversity in Section 9.2, the MIMO equation connecting the k th MT to the BS is then in the form of $\mathbf{H}_k \mathbf{x}_k$. The overall observations obtained by the N receive antennas over a certain number of time slots conveying the transmitted STCs can be expressed as

$$\mathbf{y} = \sum_{k=1}^K \mathbf{H}_k \mathbf{x}_k + \mathbf{n} \quad (9.128)$$

where \mathbf{n} is a complex Gaussian noise vector distributed with zero mean and a covariance matrix $\sigma^2 \mathbf{I} = (\text{SNR})^{-1} \mathbf{I}$, when the STCs and \mathbf{x}_k are represented by their normalized

versions, as shown in Sections 9.1 and 9.2. Furthermore, it can be shown that (9.128) can also be expressed in a compact form as

$$\mathbf{y} = \mathbf{H}\mathbf{x} + \mathbf{n} \quad (9.129)$$

associated with defining

$$\begin{aligned} \mathbf{H} &= [\mathbf{H}_1, \mathbf{H}_2, \dots, \mathbf{H}_K] \\ \mathbf{x} &= [\mathbf{x}_1^T, \mathbf{x}_2^T, \dots, \mathbf{x}_K^T]^T \end{aligned} \quad (9.130)$$

In (9.128) and (9.129) \mathbf{H}_k is the spatial signature of MT k and the K users are distinguished at the BS by their corresponding unique spatial signatures. Furthermore, it can be implied that the number of users supportable by the SDMA system is mainly determined by the rank of the channel state matrix \mathbf{H} .

When comparing the MIMO equations in (9.128) and (9.129) with the corresponding equations in Chapter 6 for various multicarrier CDMA schemes, we find that they are basically in the same form. Furthermore, we show that all the detection schemes considered in Chapter 6 for the multicarrier CDMA system can be readily extended for detection in the SDMA systems. For example, based on (9.129), in SDMA systems the correlation detection can be implemented as

$$\begin{aligned} z &= \mathbf{H}^H \mathbf{y} \\ &= \mathbf{H}^H \mathbf{H} \mathbf{x} + \mathbf{H}^H \mathbf{n} \end{aligned} \quad (9.131)$$

the zero-forcing (ZF) detection can be implemented as

$$\begin{aligned} z &= (\mathbf{H}^H \mathbf{H})^{-1} \mathbf{H}^H \mathbf{y} \\ &= (\mathbf{H}^H \mathbf{H})^{-1} \mathbf{H}^H \mathbf{H} \mathbf{x} + (\mathbf{H}^H \mathbf{H})^{-1} \mathbf{H}^H \mathbf{n} \\ &= \mathbf{x} + (\mathbf{H}^H \mathbf{H})^{-1} \mathbf{H}^H \mathbf{n} \end{aligned} \quad (9.132)$$

and the minimum mean-square error (MMSE) detection can be implemented as

$$\begin{aligned} z &= (\mathbf{H}^H \mathbf{H} + \sigma^2 \mathbf{I})^{-1} \mathbf{H}^H \mathbf{y} \\ &= (\mathbf{H}^H \mathbf{H} + \sigma^2 \mathbf{I})^{-1} \mathbf{H}^H \mathbf{H} \mathbf{x} + (\mathbf{H}^H \mathbf{H} + \sigma^2 \mathbf{I})^{-1} \mathbf{H}^H \mathbf{n} \end{aligned} \quad (9.133)$$

However, we should realize the differences existing between the SDMA and the CDMA based on spread-spectrum techniques. In CDMA systems user signatures are usually premeditated, time-invariant and can be optimized during system design and may be reconfigured during communications. By contrast, in SDMA systems the users' spatial signatures (CIRs) are determined by the wireless communication channels, which are random, time-varying and cannot be controlled. Hence, in SDMA systems powerful channel estimation (prediction) and detection are usually required, this may demand significantly higher complexity than the conventional CDMA systems.

Let us now consider the space-time processing in various MC-CDMA systems.

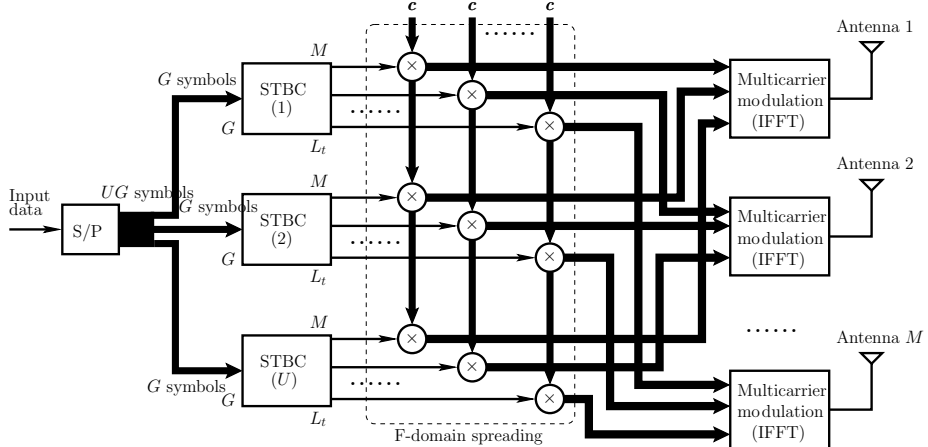


Figure 9.8: Schematic block diagram for the frequency-domain spread MC-CDMA employing multiple transmit/receive antennas, where thick and thin lines denote vector- and scalar-based connections, respectively.

9.4 Performance of Multicarrier CDMA Using Space–Time Coding

In this section we consider the principles and performance of the F-domain spread space–time MC-CDMA, which employs multiple transmit/receive antennas. We assume that the CSI is only known to the receiver and the transmitter uses STBCs for the receiver to achieve transmit diversity. In order to focus our attention mainly on the space–time issues, we assume that the F-domain spread MC-CDMA supports only the single user. In this section the performance of the OFDM system using multiple transmit/receive antennas is investigated as a special example of the F-domain spread MC-CDMA.

9.4.1 Transmission Scheme

The transmitter schematic block diagram for the F-domain spread MC-CDMA with multiple transmit antennas is shown in Fig. 9.8. The F-domain spread MC-CDMA employs a total of $\mathcal{U} = UN_p$ subcarriers. We assume that the transmitter employs M antennas for transmission and the receiver employs N antennas for receiving. We assume that the transmitter uses a 1-to- U serial-to-parallel (S/P) converter, that the STBC used at the transmitter invokes G symbols and that a STBC is transmitted using L_t time slots. Furthermore, we assume that the F-domain spreading code is $\mathbf{c} = [c_1, c_2, \dots, c_{N_p}]^T$, which is an N_p -length vector and is normalized to satisfy $\|\mathbf{c}\|^2 = 1$.

Let a block of UG data symbols to be transmitted be expressed as

$$\begin{aligned} \mathbf{x}_1 &= [x_{11}, x_{12}, \dots, x_{1G}]^T \\ \mathbf{x}_2 &= [x_{21}, x_{22}, \dots, x_{2G}]^T \\ &\vdots \\ \mathbf{x}_U &= [x_{U1}, x_{U2}, \dots, x_{UG}]^T \end{aligned} \tag{9.134}$$

As shown in Fig. 9.8, the UG data symbols are converted into U branches, each branch has G data symbols and \mathbf{x}_u in (9.134) contains the G data symbols of the u th branch.

As shown in Fig. 9.8, at each of the U branches the G data symbols are encoded according to the principles of the STBC shown in Section 9.2.2.4. Specifically, for the u th branch, the STBC generates $L_t M$ number of outputs expressed as

$$\mathbf{G}^{(u)} = \beta \begin{bmatrix} a_{11}^{(u)} & a_{12}^{(u)} & \cdots & a_{1M}^{(u)} \\ a_{21}^{(u)} & a_{22}^{(u)} & \cdots & a_{2M}^{(u)} \\ \vdots & \vdots & \ddots & \vdots \\ a_{L_t 1}^{(u)} & a_{L_t 2}^{(u)} & \cdots & a_{L_t M}^{(u)} \end{bmatrix} \quad (9.135)$$

where β is a power normalization coefficient, which can be found through (9.61) in Section 9.2.2.4. In (9.135) the l th row is transmitted within the l th time slot, while the m th column is transmitted by the m th transmit antenna using L_t time slots. Therefore, within the l th time slot a total of UM coded symbols are transmitted, which can be expressed as

$$\begin{array}{ccccccccc} \text{Antenna :} & & 1 & & 2 & & \cdots & & M \\ \\ \text{Branch 1 :} & \beta a_{l1}^{(1)} & \beta a_{l2}^{(1)} & \cdots & \beta a_{lM}^{(1)} & & & & \\ \text{Branch 2 :} & \beta a_{l1}^{(2)} & \beta a_{l2}^{(2)} & \cdots & \beta a_{lM}^{(2)} & & & & \\ \cdots & \cdots & \cdots & & \ddots & & \cdots & & \\ \text{Branch } U : & \beta a_{l1}^{(U)} & \beta a_{l2}^{(U)} & \cdots & \beta a_{lM}^{(U)} & & & & \end{array} \quad (9.136)$$

where the U coded symbols under antenna m ($m = 1, \dots, M$) are transmitted simultaneously by the m th transmit antenna.

As shown in Fig. 9.8, following the STBC, each of the coded symbols is spread using a common F-domain spreading code \mathbf{c} . Correspondingly, the outputs after F-domain spreading can be expressed as

$$\begin{array}{ccccccccc} \text{Antenna :} & & 1 & & 2 & & \cdots & & M \\ \\ \text{Branch 1 :} & \beta a_{l1}^{(1)} \mathbf{c} & \beta a_{l2}^{(1)} \mathbf{c} & \cdots & \beta a_{lM}^{(1)} \mathbf{c} & & & & \\ \text{Branch 2 :} & \beta a_{l1}^{(2)} \mathbf{c} & \beta a_{l2}^{(2)} \mathbf{c} & \cdots & \beta a_{lM}^{(2)} \mathbf{c} & & & & \\ \cdots & \cdots & \cdots & & \ddots & & \cdots & & \\ \text{Branch } U : & \beta a_{l1}^{(U)} \mathbf{c} & \beta a_{l2}^{(U)} \mathbf{c} & \cdots & \beta a_{lM}^{(U)} \mathbf{c} & & & & \end{array} \quad (9.137)$$

Explicitly, the m th column under Antenna m has a total of $\mathcal{U} = UN_p$ chips, which are transmitted on the \mathcal{U} subcarriers of the m th transmit antenna after the multicarrier modulation, as seen in Fig. 9.8, according to the principles discussed in Chapter 5.

Let the \mathcal{U} subcarriers, which we assume are orthogonal to each other, be expressed as

$$\{f\} = \{f_1, f_2, \dots, f_{\mathcal{U}}\} \quad (9.138)$$

from the lowest to the highest frequencies. Then, for the m th transmit antenna, the N_p chips at the u th branch of (9.137) are transmitted on the N_p subcarriers

$$\{f\}_u = \{f_u, f_{u+U}, \dots, f_{u+(N_p-1)U}\}, \quad u = 1, 2, \dots, U \quad (9.139)$$

In other words, the N_p chips of a given coded symbol are transmitted on the N_p frequencies that are separated with the maximum spacing, so that maximum frequency diversity can be achieved, when the MC-CDMA signals experience frequency-selective fading.

Note that the above-discussed scheme is reduced to the OFDM scheme, if we set the spreading factor $N_p = 1$. In this case, each space-time block transmits GU data symbols. Therefore, the performance of the space-time coded OFDM system can be studied as a special example of the space-time coded MC-CDMA system considered in this section. Furthermore, all the analytical results obtained in our forthcoming discourse in the context of the MC-CDMA system are also suitable for the OFDM system, after setting $N_p = 1$ and using \mathcal{U} to replace U .

9.4.2 Receiver Scheme

Let us assume that the channels from the transmitter to receiver maintain constancy during one space-time block, but are independent from one block to another. Let the gain of the channel in terms of the $(u + n_p U)$ th subcarrier, the m th transmit antenna and the n th receive antenna be expressed as $h_{u,n_p}^{(n,m)}$. Then, after the multicarrier demodulation, as shown in Fig. 9.9, and removal of the cyclic prefixes, etc. the signal received by the n th receive antenna from the $(u + n_p U)$ th subcarrier within the l th time slot can be expressed in discrete form as

$$\begin{aligned} r_{u,n_p,l}^{(n)} &= \beta \sum_{m=1}^M a_{lm}^{(u)} c_{n_p} h_{u,n_p}^{(n,m)} + n_{u,n_p,l}^{(n)}, \quad n = 1, 2, \dots, N \\ u &= 1, 2, \dots, U; n_p = 1, 2, \dots, N_p; l = 1, 2, \dots, L_t \end{aligned} \quad (9.140)$$

where $n_{u,n_p,l}^{(n)}$ is a complex Gaussian random variable distributed with zero mean and a variance $\sigma^2/2 = 1/2\text{SNR}$ per dimension. Carrying out the de-spread by multiplying $r_{u,n_p,l}^{(n)}$ with c_{n_p} and using the result $|c_{n_p}|^2 = 1/N_p$, we obtain

$$\begin{aligned} y_{u,n_p,l}^{(n)} &= \frac{\beta}{N_p} \sum_{m=1}^M a_{lm}^{(u)} h_{u,n_p}^{(n,m)} + \bar{n}_{u,n_p,l}^{(n)}, \quad n = 1, 2, \dots, N \\ u &= 1, 2, \dots, U; n_p = 1, 2, \dots, N_p; l = 1, 2, \dots, L_t \end{aligned} \quad (9.141)$$

where $\bar{n}_{u,n_p,l}^{(n)} = c_{n_p} n_{u,n_p,l}^{(n)}$, which is a complex Gaussian random variable distributed with zero mean and a variance $\sigma^2/2N_p$ per dimension. Note that since the fading experienced by one subcarrier might be different from that by another subcarrier, as shown in Fig. 9.9, within one time slot, the UN_p subcarriers of a given receiver antenna provide UN_p observations to the blocks, which implement STBC decoding, combining and detection. Let us define

$$\begin{aligned} \mathbf{a}_l^{(u)} &= \beta [a_{l1}^{(u)}, a_{l2}^{(u)}, \dots, a_{lM}^{(u)}]^T \\ \mathbf{h}_{u,n_p}^{(n)} &= [h_{u,n_p}^{(n,1)}, h_{u,n_p}^{(n,2)}, \dots, h_{u,n_p}^{(n,M)}]^T \end{aligned} \quad (9.142)$$

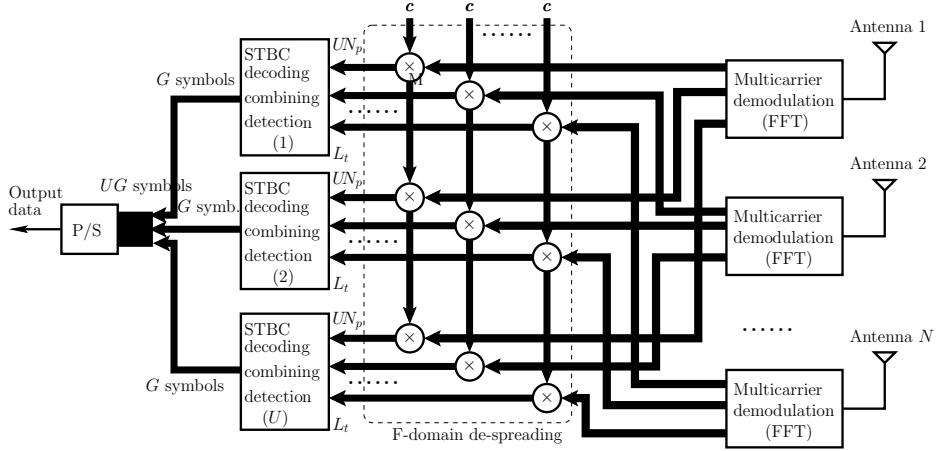


Figure 9.9: Receiver schematic block diagram for the frequency-domain spread MC-CDMA employing multiple transmit/receive antennas, where thick and thin lines denote vector- and scalar-based connections, respectively.

Then, (9.141) can be expressed as

$$\begin{aligned} y_{u,n_p,l}^{(n)} &= \frac{1}{N_p} (\mathbf{a}_l^{(u)})^T \mathbf{h}_{u,n_p}^{(n)} + \bar{n}_{u,n_p,l}^{(n)}, \quad n = 1, 2, \dots, N \\ u &= 1, 2, \dots, U; n_p = 1, 2, \dots, N_p; l = 1, 2, \dots, L_t \end{aligned} \quad (9.143)$$

Let us now consider a space–time block of L_t time slots and define

$$\begin{aligned} \mathbf{y}_{u,n_p}^{(n)} &= [y_{u,n_p,1}^{(n)}, y_{u,n_p,2}^{(n)}, \dots, y_{u,n_p,L_t}^{(n)}]^T \\ \mathbf{n}_{u,n_p}^{(n)} &= [\bar{n}_{u,n_p,1}^{(n)}, \bar{n}_{u,n_p,2}^{(n)}, \dots, \bar{n}_{u,n_p,L_t}^{(n)}]^T \end{aligned} \quad (9.144)$$

where $\mathbf{n}_{u,n_p}^{(n)}$ is an L_t -length Gaussian noise vector distributed with zero mean and a covariance matrix $\frac{\sigma^2}{N_p} \mathbf{I}_{L_t}$. Then, it can be shown that

$$\begin{aligned} \mathbf{y}_{u,n_p}^{(n)} &= \frac{1}{N_p} \mathcal{G}^{(u)} \mathbf{h}_{u,n_p}^{(n)} + \mathbf{n}_{u,n_p}^{(n)}, \quad n = 1, 2, \dots, N \\ u &= 1, 2, \dots, U; n_p = 1, 2, \dots, N_p \end{aligned} \quad (9.145)$$

where $\mathcal{G}^{(u)}$ is the STBC given by (9.135).

In this section we consider only the class of STBCs that satisfies

$$\mathcal{G}^{(u)} \mathbf{h}_{u,n_p}^{(n)} = \mathbf{H}_{u,n_p}^{(n)} \mathbf{x}_u \quad (9.146)$$

where \mathbf{x}_u has been defined in (9.134). In this case, (9.145) can be modified to

$$\begin{aligned} \mathbf{y}_{u,n_p}^{(n)} &= \frac{1}{N_p} \mathbf{H}_{u,n_p}^{(n)} \mathbf{x}_u + \mathbf{n}_{u,n_p}^{(n)}, \quad n = 1, 2, \dots, N \\ u &= 1, 2, \dots, U; n_p = 1, 2, \dots, N_p \end{aligned} \quad (9.147)$$

Let us consider those subcarrier branches conveying the same STBC and define

$$\begin{aligned}\mathbf{y}_u^{(n)} &= [(\mathbf{y}_{u,1}^{(n)})^T, (\mathbf{y}_{u,2}^{(n)})^T, \dots, (\mathbf{y}_{u,N_p}^{(n)})^T]^T \\ \mathbf{n}_u^{(n)} &= [(\mathbf{n}_{u,1}^{(n)})^T, (\mathbf{n}_{u,2}^{(n)})^T, \dots, (\mathbf{n}_{u,N_p}^{(n)})^T]^T \\ \mathbf{H}_u^{(n)} &= [(\mathbf{H}_{u,1}^{(n)})^T, (\mathbf{H}_{u,2}^{(n)})^T, \dots, (\mathbf{H}_{u,N_p}^{(n)})^T]^T\end{aligned}\quad (9.148)$$

Then, the observation vector $\mathbf{y}_u^{(n)}$ can be expressed as

$$\mathbf{y}_u^{(n)} = \frac{1}{N_p} \mathbf{H}_u^{(n)} \mathbf{x}_u + \mathbf{n}_u^{(n)}, \quad n = 1, 2, \dots, N; u = 1, 2, \dots, U \quad (9.149)$$

Finally, let us consider the N number of receive antennas and define

$$\begin{aligned}\mathbf{y}_u &= [(\mathbf{y}_u^{(1)})^T, (\mathbf{y}_u^{(2)})^T, \dots, (\mathbf{y}_u^{(N)})^T]^T \\ \mathbf{n}_u &= [(\mathbf{n}_u^{(1)})^T, (\mathbf{n}_u^{(2)})^T, \dots, (\mathbf{n}_u^{(N)})^T]^T \\ \mathbf{H}_u &= [(\mathbf{H}_u^{(1)})^T, (\mathbf{H}_u^{(2)})^T, \dots, (\mathbf{H}_u^{(N)})^T]^T\end{aligned}\quad (9.150)$$

the observations for detection of \mathbf{x}_u can now be expressed by

$$\mathbf{y}_u = \frac{1}{N_p} \mathbf{H}_u \mathbf{x}_u + \mathbf{n}_u, \quad u = 1, 2, \dots, U \quad (9.151)$$

In (9.151) the dimension of both \mathbf{y}_u and \mathbf{n}_u is $(L_t N_p N \times 1)$, while the dimension of \mathbf{H}_u is $(L_t N_p N \times G)$. Furthermore, it is worth mentioning that the U blocks of data symbols seen in (9.134) can be detected separately, since we assumed that the subcarriers were orthogonal, implying that there is no intercarrier interference.

Based on (9.151), the STBC decoding, diversity combining and detection, as seen in Fig. 9.9, can be implemented. Specifically, in this section we consider only the full-diversity orthogonal STBCs. For this class of STBCs, they have the property

$$(\mathbf{H}_{u,n_p}^{(n)})^H \mathbf{H}_{u,n_p}^{(n)} = \beta^2 \left(\sum_{m=1}^M |h_{u,n_p}^{(n,m)}|^2 \right) \mathbf{I}_M \quad (9.152)$$

Consequently, after the STBC decoding and diversity combining, the decision variable vector for \mathbf{x}_u can be formed as

$$\mathbf{z}_u = (\mathbf{H}_u)^H \mathbf{y}_u \quad (9.153)$$

Substituting (9.151) into (9.153) and using the result of (9.152), we can express \mathbf{z}_u as

$$\mathbf{z}_u = \frac{\beta^2}{N_p} \left(\sum_{n_p=1}^{N_p} \sum_{n=1}^N \sum_{m=1}^M |h_{u,n_p}^{(n,m)}|^2 \right) \mathbf{x}_u + \boldsymbol{\eta}_u, \quad u = 1, 2, \dots, U \quad (9.154)$$

where $\boldsymbol{\eta}_u = (\mathbf{H}_u)^H \mathbf{n}_u$, which is a complex Gaussian random variable vector distributed with zero mean and a covariance matrix

$$E[\boldsymbol{\eta}_u \boldsymbol{\eta}_u^H] = \sigma^2 \times \frac{\beta^2}{N_p} \left(\sum_{n_p=1}^{N_p} \sum_{n=1}^N \sum_{m=1}^M |h_{u,n_p}^{(n,m)}|^2 \right) \mathbf{I}_G \quad (9.155)$$

As seen in (9.154) the F-domain spread MC-CDMA may achieve a diversity order that is as high as $N_p MN$, if the subcarrier signals conveying a given STBC experience independent fading, yielding $h_{u,n_p}^{(n,m)}$ to be an independent random variable in terms of the indices n_p , n and m . However, if the subcarrier signals conveying a given STBC experience flat fading resulting in $h_{u,n_p}^{(n,m)} = h_u^{(n,m)}$, then (9.154) reduces to

$$\mathbf{z}_u = \beta^2 \left(\sum_{n=1}^N \sum_{m=1}^M |h_u^{(n,m)}|^2 \right) \mathbf{x}_u + \boldsymbol{\eta}_u, \quad u = 1, 2, \dots, U \quad (9.156)$$

In this case, the space–time F-domain spread MC-CDMA system is capable of achieving a diversity order of MN . In other words, the space–time F-domain spread MC-CDMA system is only capable of achieving the spatial diversity, but no frequency diversity.

Furthermore, when a space–time OFDM system is considered, as mentioned previously, we only need to set $N_p = 1$ and use \mathcal{U} to replace U in the results for the space–time F-domain spread MC-CDMA system. Specifically, for the space–time OFDM system, the decision variable vector for \mathbf{x}_u can be obtained from (9.156) by changing U to \mathcal{U} , i.e.

$$\mathbf{z}_u = \beta^2 \left(\sum_{n=1}^N \sum_{m=1}^M |h_u^{(n,m)}|^2 \right) \mathbf{x}_u + \boldsymbol{\eta}_u, \quad u = 1, 2, \dots, \mathcal{U} \quad (9.157)$$

Let us now analyse the error probability of the space–time F-domain spread MC-CDMA system as well as that of the space–time OFDM system in the next subsection.

9.4.3 Analysis of Probability of Error

From (9.154) and (9.155) we know that the instantaneous SNR of the decision variables is given by

$$\begin{aligned} \gamma &= \frac{1}{\sigma^2} \times \frac{\beta^2}{N_p} \left(\sum_{n_p=1}^{N_p} \sum_{n=1}^N \sum_{m=1}^M |h_{u,n_p}^{(n,m)}|^2 \right) \\ &= \sum_{n_p=1}^{N_p} \sum_{n=1}^N \sum_{m=1}^M \gamma_{n_p,mn} \end{aligned} \quad (9.158)$$

where, by definition,

$$\begin{aligned} \gamma_{n_p,mn} &= \frac{|h_{u,n_p}^{(n,m)}|^2}{\Omega} \times \gamma_c \\ \gamma_c &= \frac{\Omega}{\sigma^2} \times \frac{\beta^2}{N_p} \end{aligned} \quad (9.159)$$

where $\Omega = E[|h_{u,n_p}^{(n,m)}|^2]$ and γ_c represents the average SNR of a subcarrier channel from one transmit antenna to one receive antenna. Note that, starting from the equation of (9.158) the index of u has been ignored, since all the transmitted symbols have the same error probability in statistics.

In this section we aim at deriving a generalized closed-form expression for various baseband modulation schemes. Our generalization is based on the finding [172] that the symbol-error-rate (SER) of many coherent modulation schemes is a function of the formula

$$T[a, b, g; \gamma] = a \int_0^{b\pi} \exp\left(-\frac{g\gamma}{\sin^2 \theta}\right) d\theta, \quad a, b, g > 0 \quad (9.160)$$

where γ represents the instantaneous SNR of (9.158). In (9.160) the parameters a , b and g are determined by the specific modulation scheme considered. Specifically, for the BPSK, BFSK, multiple phase-shift keying (MPSK) and M -ary quadrature amplitude modulation (MQAM), etc. coherent modulation schemes, the parameters a , b and g have the following configurations [91, 107, 172]:

BPSK:

$$P_s(\gamma) = T[a, b, g; \gamma] \text{ with } a = \frac{1}{\pi}, \quad b = \frac{1}{2}, \quad g = 1 \quad (9.161)$$

BFSK:

$$\begin{aligned} P_s(\gamma) &= T[a, b, g; \gamma] \text{ with } a = \frac{1}{\pi}, \quad b = \frac{1}{2}, \quad \text{and} \\ g &= \begin{cases} \frac{1}{2}, & \text{orthogonal BFSK} \\ 0.715, & \text{minimum correlation} \end{cases} \end{aligned} \quad (9.162)$$

MPSK:

$$P_s(\gamma) = T[a, b, g; \gamma] \text{ with } a = \frac{1}{\pi}, \quad b = \frac{M-1}{M}, \quad g = \sin^2\left(\frac{\pi}{M}\right) \quad (9.163)$$

MQAM:

$$\begin{aligned} P_s(\gamma) &= T[a_1, b_1, g_1; \gamma] - T[a_2, b_2, g_2; \gamma] \text{ with} \\ a_1 &= \frac{4}{\pi} \left(1 - \frac{1}{\sqrt{M}}\right), \quad b_1 = \frac{1}{2}, \quad g_1 = \frac{3}{2(M-1)} \\ a_2 &= \frac{4}{\pi} \left(1 - \frac{1}{\sqrt{M}}\right)^2, \quad b_2 = \frac{1}{4}, \quad g_2 = \frac{3}{2(M-1)} \end{aligned} \quad (9.164)$$

We note, furthermore, that there are some other modulation schemes, such as the M -ary amplitude modulation (M-AM), whose SER can also be expressed as functions of (9.160).

Additionally, since in (9.160) $\sin^2 \theta \leq 1$, we can readily obtain the corresponding SER upper-bounds of various coherent modulation schemes through the expression

$$T[a, b, g; \gamma] \leq ab\pi \exp(-g\gamma) \quad (9.165)$$

In order to evaluate the average SER of the above-mentioned coherent modulation schemes, the instantaneous SNR seen in (9.160) must be averaged out. This can be done

by integrating (9.160) with respect to the distribution of the instantaneous SNR, which can be evaluated as

$$\begin{aligned}
 T[a, b, g] &= \int_0^\infty T[a, b, g; \gamma] f(\gamma) d\gamma \\
 &= \int_0^\infty \left[a \int_0^{b\pi} \exp\left(-\frac{g\gamma}{\sin^2 \theta}\right) d\theta \right] f(\gamma) d\gamma \\
 &= a \int_0^{b\pi} \left[\int_0^\infty \exp\left(-\frac{g\gamma}{\sin^2 \theta}\right) f(\gamma) d\gamma \right] d\theta \\
 &= a \int_0^{b\pi} E_\gamma \left[\exp\left(-\frac{g\gamma}{\sin^2 \theta}\right) \right] d\theta
 \end{aligned} \tag{9.166}$$

where $E_\gamma[\exp(-g\gamma/\sin^2 \theta)]$ denotes the expectation of $\exp(-g\gamma/\sin^2 \theta)$ with respect to the instantaneous SNR γ .

Assuming that the subcarrier channels in the considered space-time MC-CDMA system experience Nakagami- m fading, then $|h_{u,n_p}^{(n,m)}|^2$ obeys the gamma distribution [109] and has the PDF given by (5.2) in Chapter 5. Furthermore, it can be shown that the PDF of $\gamma_{n_p,mn}$ in (9.159) can be expressed as

$$f(\gamma_{n_p,mn}) = \frac{1}{\Gamma(m)} \left(\frac{m}{\gamma_c} \right)^m \gamma_{n_p,mn}^{m-1} \exp\left(-\frac{m\gamma_{n_p,mn}}{\gamma_c}\right), \quad \gamma_{n_p,mn} \geq 0 \tag{9.167}$$

where $\Gamma(\cdot)$ is the gamma function [2] and m is the Nakagami- m fading parameter.

Let us express

$$\begin{aligned}
 \gamma &= \sum_{n_p=1}^{N_p} \gamma_{n_p} \\
 \gamma_{n_p} &= \sum_{n=1}^N \sum_{m=1}^M \gamma_{n_p,mn}
 \end{aligned} \tag{9.168}$$

We assume that the channel from any of the transmit antennas to any of the receive antennas experiences independent fading. Then, γ_{n_p} in (9.168) represents the sum of MN independent random variables obeying the common gamma distribution having the PDF as shown in (9.167). According to reference [108], the sum of gamma-distributed random variables is also a gamma-distributed random variable, the PDF of γ_{n_p} in (9.168) can be expressed as

$$f(\gamma_{n_p}) = \frac{1}{\Gamma(MNm)} \left(\frac{m}{\gamma_c} \right)^{MNm} \gamma_{n_p}^{MNm-1} \exp\left(-\frac{m\gamma_{n_p}}{\gamma_c}\right), \quad \gamma_{n_p} \geq 0 \tag{9.169}$$

which is equivalent to a gamma distribution having the fading parameter MNm and the second-order moment of $MNm\gamma_c$.

With the aid of (9.168) and (9.169) and following our derivation in Section 5.6.2 of Chapter 5, it can be shown that we have

$$E_\gamma \left[\exp\left(-\frac{g\gamma}{\sin^2 \theta}\right) \right] = \det \left(\mathbf{I} + \frac{g\gamma_c}{m \sin^2 \theta} \mathbf{M} \right)^{-MNm} \tag{9.170}$$

where \mathbf{M} is the $(N_p \times N_p)$ symmetric covariance matrix of the ‘accompanying’ Gaussian distribution, which can be expressed as [145]

$$\mathbf{M} = \begin{bmatrix} 1 & \sqrt{\rho_{12}} & \cdots & \sqrt{\rho_{1N_p}} \\ \sqrt{\rho_{21}} & 1 & \cdots & \sqrt{\rho_{2N_p}} \\ \vdots & \vdots & \ddots & \vdots \\ \sqrt{\rho_{N_p1}} & \sqrt{\rho_{N_p2}} & \cdots & 1 \end{bmatrix} \quad (9.171)$$

In (9.171) ρ_{ij} represents the correlation coefficient between the squares of the two fading envelopes corresponding to the i th and j th subcarriers, as discussed in Chapter 5. Specifically, ρ_{ij} is given by (5.5) of Chapter 5 when the excess delay spread of the wireless channels obeys the exponential distribution, while given by (5.8) of Chapter 5 when the excess delay spread obeys the uniform distribution.

Substituting (9.170) into (9.166), we finally obtain

$$T[a, b, g] = a \int_0^{b\pi} \det\left(\mathbf{I} + \frac{g\gamma_c}{m \sin^2 \theta} \mathbf{M}\right)^{-MNd} d\theta \quad (9.172)$$

Furthermore, let $\lambda_1, \lambda_2, \dots, \lambda_D$ be the D number of nonzero eigenvalues of \mathbf{M} . Then, (9.170) can be written as

$$\begin{aligned} T[a, b, g] &= a \int_0^{b\pi} \prod_{j=1}^D \left(1 + \frac{\lambda_j g \gamma_c}{m \sin^2 \theta}\right)^{-MNd} d\theta \\ &= a \int_0^{b\pi} \prod_{j=1}^D \left(\frac{m \sin^2 \theta}{\lambda_j g \gamma_c + m \sin^2 \theta}\right)^{MNd} d\theta \end{aligned} \quad (9.173)$$

which is the desired expression for us to evaluate the error rate performance of the space–time MC-CDMA systems using, possibly, various coherent modulation schemes as discussed in the context of the equations from (9.160) to (9.164). As shown in (9.173), the diversity order achieved by a space–time MC-CDMA system is MND , where M and N are the results of using the M transmit antennas and N receive antennas, while D is the contribution of the frequency-selective fading channel.

Below, let us consider several special cases. First, when a space–time OFDM system is considered, we have $N_p = 1$. Hence, \mathbf{M} is reduced to a scalar and its single eigenvalue is $\lambda_1 = 1$. In this case, (9.173) is reduced to

$$T[a, b, g] = a \int_0^{b\pi} \left(\frac{m \sin^2 \theta}{g \gamma_c + m \sin^2 \theta}\right)^{MNd} d\theta \quad (9.174)$$

which shows that the space–time OFDM systems can achieve full spatial diversity, but no frequency diversity. Consequently, the error-rate performance of the space–time OFDM systems using various coherent modulation schemes can be evaluated using the equations from (9.160) to (9.164) associated with (9.174).

Second, when all the subcarriers conveying a STBC experience flat fading, then \mathbf{M} is a rank one matrix with one eigenvalue of $\lambda_1 = N_p$. In this case, (9.173) is reduced to

$$T[a, b, g] = a \int_0^{b\pi} \left(\frac{m \sin^2 \theta}{N_p g \gamma_c + m \sin^2 \theta}\right)^{MNd} d\theta \quad (9.175)$$

which shows that the space–time MC-CDMA systems can achieve only full spatial diversity, but there is no frequency diversity.

Finally, when all the subcarriers conveying a STBC experience independent fading, then $\mathbf{M} = \mathbf{I}_{N_p}$. Consequently, (9.173) can be expressed as

$$T[a, b, g] = a \int_0^{b\pi} \left(\frac{m \sin^2 \theta}{g\gamma_c + m \sin^2 \theta} \right)^{MNN_p m} d\theta \quad (9.176)$$

In this case the space–time MC-CDMA systems can achieve not only the full spatial diversity, but also the full frequency diversity.

Let us now provide a range of performance results for the space–time MC-CDMA and OFDM systems.

9.4.4 Performance Results

In this section we provide the error-rate performance only for a few representative examples. However, it is worth mentioning again that the error-rate performance of various space–time OFDM or MC-CDMA systems using possibly various coherent digital modulation schemes may be readily evaluated by the expressions derived in Section 9.4.3.

Figure 9.10 illustrates the error-rate performance of the space–time OFDM system using either BPSK or 16QAM baseband modulation, when communicating over Rayleigh fading channels corresponding to $m = 1$ or Nakagami- m fading channels associated with $m = 1.5$. The results in Fig. 9.10 were evaluated from (9.174) associated with (9.161) for the BPSK and (9.164) for the 16QAM schemes. Note that in Fig. 9.10 the legend (aT_x, bRx) means that the space–time system employs a transmit antennas and b receive antennas. From the results of Fig. 9.10, generally, we can observe that the error-rate performance improves when the total number of antennas increases. However, for a given total number of antennas, different configurations of the number of transmit/receive antennas may result in a different error-rate performance. Usually, a better error-rate performance can be achieved, when using more receive antennas. Note that the bit-error rate (BER) performance presented by the solid lines in Fig. 9.10(a) has been given in reference [243]. Additionally, as predicted, the results of Fig. 9.10 show that the error-rate performance improves when the channel becomes less faded, i.e. when the value of m increases.

Figure 9.11 shows the impact of frequency selectivity of the wireless channels on the achievable BER performance of the space–time MC-CDMA systems. In principle, the wireless channel becomes more frequency selective, when its delay spread increases. In Fig. 9.11 the excess delay spread obeys the uniform distribution as shown in (5.8). The normalized delay spread τ_{Norm} equals the delay spread of the corresponding wireless channel divided by the symbol duration after the S/P conversion. In more detail, $\tau_{\text{Norm}} = \tau/T_s = \tau/UT_b$, where T_s is the symbol duration after the S/P conversion, while T_b denotes the bit duration before the S/P conversion. As seen in Fig. 9.11, the BER performance improves when the delay spread of the wireless channels increases, resulting in higher frequency-diversity gain.

Finally, in Fig. 9.12 the BER versus average SNR per bit performance of the space–time MC-CDMA system was evaluated, when communicating over frequency-selective Rayleigh fading channels associated with a normalized delay spread $\tau_{\text{Norm}} = 0.1$. When comparing

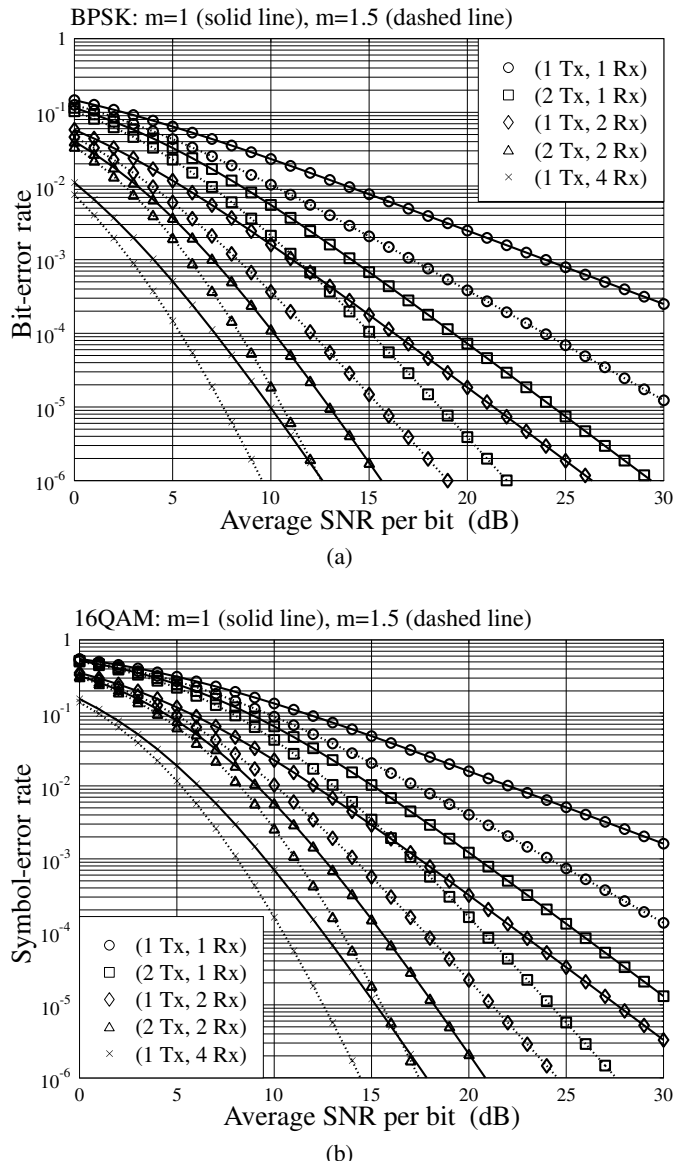


Figure 9.10: BER versus average SNR per bit performance for the space–time OFDM systems, when communicating over Rayleigh ($m = 1$) or Nakagami ($m = 1.5$) fading channels; (a) BPSK; (b) 16QAM.

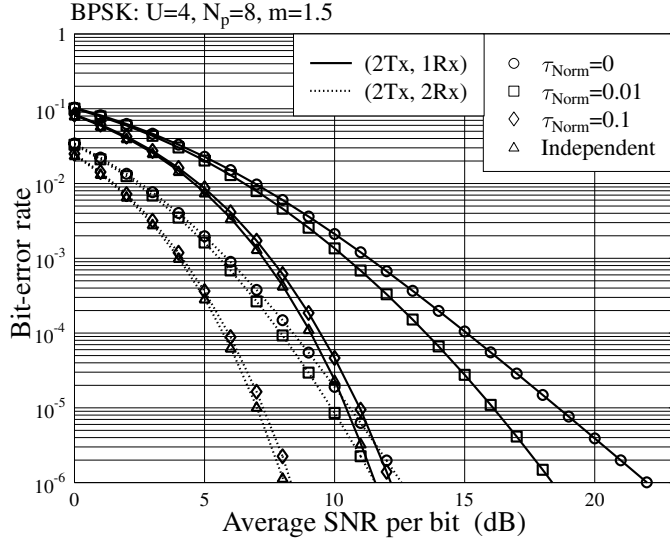


Figure 9.11: BER versus average SNR per bit performance for the space–time MC-CDMA systems using 32 subcarriers, when communicating over Nakagami ($m = 1.5$) fading channels associated with different delay spread. The excess delay spread obeys the uniform distribution.

the results of Fig. 9.12 with the corresponding results in Fig. 9.10(a), it can be shown that the space–time MC-CDMA system is capable of achieving a significant frequency-diversity gain, in addition to the spatial-diversity gain.

9.5 Time-Frequency-Domain Space–Time Spread Multicarrier DS-CDMA

In the previous section we investigated the applications of STBC in the F-domain spread MC-CDMA systems. In this section we consider the applications of STS in the TF-domain spread MC DS-CDMA system, and refer to it for convenience as the TF-domain STS/MC DS-CDMA. We first describe in detail the TF-domain STS/MC DS-CDMA systems, including both the transmitter and receiver principles. Then, the closed-form expressions for the error probability of the TF-domain STS/MC DS-CDMA systems are derived, when considering the generalized Nakagami- m fading channels. Finally, performance results are provided in order to illustrate the achievable error-rate performance of the TF-domain STS/MC DS-CDMA systems. Again, for simplicity of showing the principles and of carrying out the analysis, in this section we consider only the TF-domain STS/MC DS-CDMA supporting single-user. Hence, the performance obtained in this section represents the upper-bound performance, which may be achievable by using optimum multiuser detection (MUD) in the TF-domain STS/MC DS-CDMA systems. Additionally, in practice it is usually the case that transmit diversity is mainly to enhance the downlink transmission, where MUI can be removed by

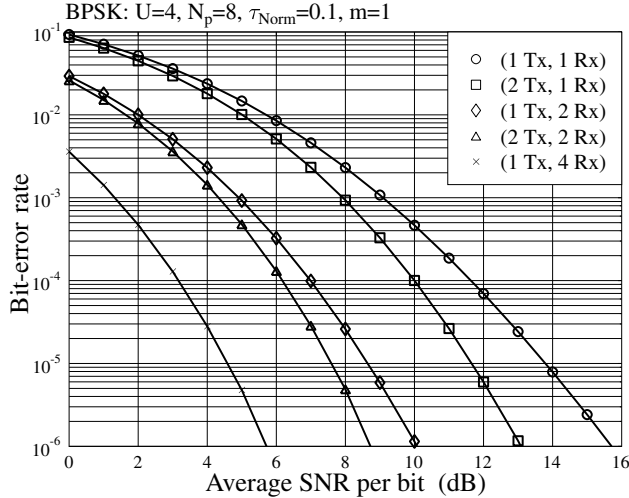


Figure 9.12: BER versus average SNR per bit performance for the space–time MC-CDMA systems using 32 subcarriers, when communicating over Rayleigh ($m = 1$) fading channels associated with a normalized delay spread $\tau_{\text{Norm}} = 0.1$, and the excess delay spread obeys the uniform distribution.

assigning orthogonal spreading sequences to different downlink users. If this is the case, then the closed-form expressions and performance results obtained in this section are also suitable for the TF-domain STS/MC DS-CDMA systems supporting multiple users.

Note that from the previous contents, we know that the TF-domain spread MC DS-CDMA represents a generalized CDMA scheme, which can be readily configured to some other special CDMA schemes. Furthermore, in Section 9.2.2.5 we showed that the STS represents a generalized transmit diversity scheme with the STBC-based transmit diversity scheme in Section 9.2.2.4 being a special class that corresponds to the STS using an identity matrix for spreading. Hence, the TF-domain STS/MC DS-CDMA system considered in this section as well as the closed-form expressions obtained in Section 9.5.3 can be easily modified for many other CDMA schemes using possibly different transmit diversity schemes based on either STS or STC. Let us first describe the transmission scheme of the TF-domain STS/MC DS-CDMA.

9.5.1 Transmission Scheme

The transmitter schematic block diagram for the TF-domain STS/MC DS-CDMA employing multiple transmit/receive antennas is shown in Fig. 9.13. We assume that the TF-domain STS/MC DS-CDMA uses orthogonal subcarriers and employs the following system parameters and settings:

M and N : number of transmit and receive antennas;

L_t : number of time slots for transmitting a STS block;

N_p : number of subcarriers for F-domain spreading;

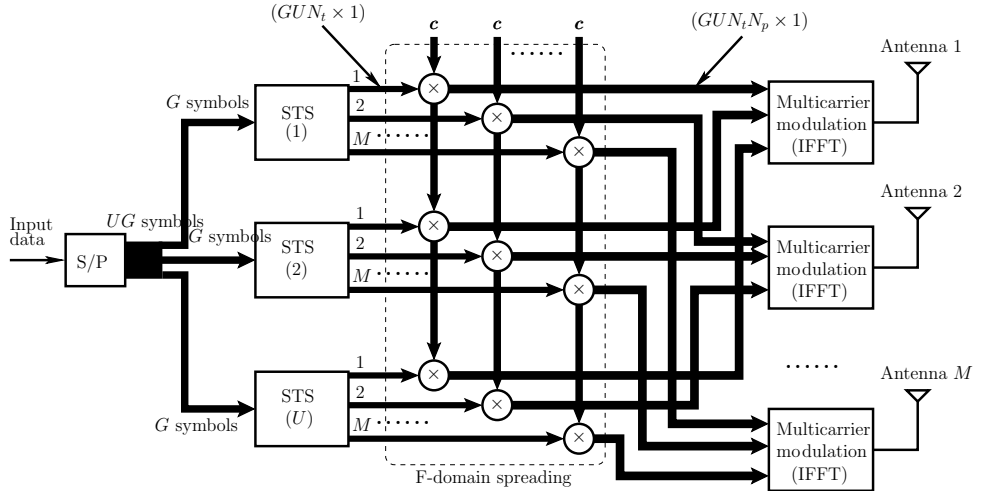


Figure 9.13: Schematic block diagram for the TF-domain STS/MC DS-CDMA using space–time spreading, where thick and thin lines denote vector- and scalar-based connections, respectively.

U : number of substreams after S/P conversion;

G : number of symbols invoked in a STS block;

T_c : chip duration of the spreading sequences;

T : symbol duration before S/P conversion;

T_s : symbol duration of a STS symbol (block). Since each transmission invokes UG symbols, we have $T_s = UGT$;

$N_t = T/T_c$: number of chips transmitted within a symbol duration before S/P conversion. Correspondingly, the number of chips transmitted within a symbol duration after the S/P is UN_t ;

C_u , $u = 1, 2, \dots, U$: $(GUN_t \times L_t)$ -dimensional STS matrix for the u th substream. It is assumed that $C_u^H C_u = I$ and $C_u^H C_v = 0$ for any $u \neq v$.

From the above settings, it can be implied that the TF-domain STS/MC DS-CDMA is always full-rate, no matter whether or not the STS is designed based on the full-rate STC. However, as our discussion in Section 9.2.2.5 showed, if the STS is designed based on a full-rate STC, which results in $L_t = G$, then the STS-based system and that not using STS can support the same maximum number of users. Otherwise, if the STS is designed based on a STC with its rate less than one, then the STS-based system has $L_t > G$. In this case, the maximum number of users supportable by the STS-based system will be lower than that supportable by the corresponding system without using STS, as a user in the STS-based system requires more spreading sequences than the corresponding system without STS.

As shown in Fig. 9.13 each STS block transmits UG data symbols. Let these UG data symbols be represented by

$$\begin{aligned}\mathbf{x}_1 &= [x_{11}, x_{12}, \dots, x_{1G}]^T \\ \mathbf{x}_2 &= [x_{21}, x_{22}, \dots, x_{2G}]^T \\ &\quad \dots \dots \\ \mathbf{x}_U &= [x_{U1}, x_{U2}, \dots, x_{UG}]^T\end{aligned}\tag{9.177}$$

where \mathbf{x}_u contains the G data symbols to be processed by the u th substream. After the STBC of \mathbf{x}_u let the output $(L_t \times M)$ -dimensional codeword be given by

$$\mathcal{G}^{(u)} = \beta \begin{bmatrix} a_{11}^{(u)} & a_{12}^{(u)} & \dots & a_{1M}^{(u)} \\ a_{21}^{(u)} & a_{22}^{(u)} & \dots & a_{2M}^{(u)} \\ \vdots & \vdots & \ddots & \vdots \\ a_{L_t 1}^{(u)} & a_{L_t 2}^{(u)} & \dots & a_{L_t M}^{(u)} \end{bmatrix}, \quad u = 1, 2, \dots, U\tag{9.178}$$

where β is a power normalization coefficient that can be found through (9.61) in Section 9.2.2.4. Then, on invoking the STS according to the principles seen in Section 9.2.2.5, we obtain a $(GUN_t \times M)$ space–time matrix

$$\mathbf{S}^{(u)} = [s_1^{(u)}, s_2^{(u)}, \dots, s_M^{(u)}] = \mathbf{C}_u \mathcal{G}^{(u)}, \quad u = 1, 2, \dots, U\tag{9.179}$$

where s_m will be transmitted from the m th transmit antenna using GUN_t chip durations.

As shown in Fig. 9.13, following the STS, the signals are spread in the F-domain. Since we have assumed that the signals of the same user are orthogonal in the T-domain, different substreams may use the same F-domain spreading codes. Let the N_p -length F-domain spreading code be

$$\mathbf{c} = [c_1, c_2, \dots, c_{N_p}]^T\tag{9.180}$$

which satisfies $\|\mathbf{c}\|^2 = 1$. Then, after the F-domain spreading, the signals from the u th substream, which will be transmitted on the n_p th subcarrier by the M transmit antennas, can be expressed as

$$S_{n_p}^{(u)} = c_{n_p} \mathbf{C}_u \mathcal{G}^{(u)}, \quad u = 1, 2, \dots, U; n_p = 1, 2, \dots, N_p\tag{9.181}$$

Finally, as shown in Fig. 9.13, the STS signals are transmitted from the M transmit antennas after the multicarrier modulation.

9.5.2 Receiver Scheme

The receiver schematic block diagram for the TF-domain STS/MC DS-CDMA using N receive antennas is shown in Fig. 9.14, where the received signals are first carried out the MC demodulation and then followed by a matched filter (MF) matching to the transmitted chip-waveform. Let us assume that each subcarrier signal experiences flat fading, and that the channel gain with respect to the m th transmit antenna, the n th receive antenna and n_p th subcarrier is expressed as $h_{n_p}^{(n,m)}$. Since it has been assumed that the subcarrier signals are

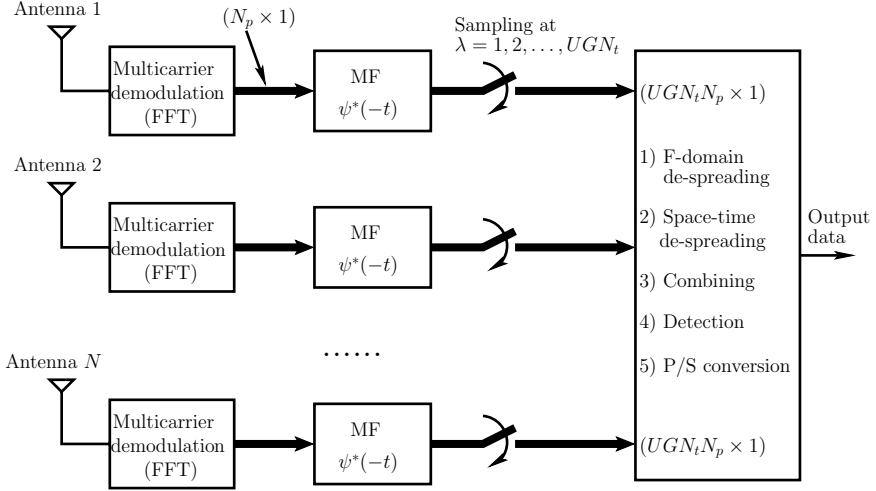


Figure 9.14: Receiver schematic block diagram for the TF-domain STS/MC DS-CDMA, where thick and thin lines denote vector- and scalar-based connections, respectively.

orthogonal to each other, there is no intercarrier interference and it is hence sufficient for us to consider only the n_p th subcarrier in detail. Let

$$\mathbf{h}_{n_p}^{(n)} = [h_{n_p}^{(n,1)}, h_{n_p}^{(n,2)}, \dots, h_{n_p}^{(n,M)}]^T \quad (9.182)$$

Consequently, after the multicarrier demodulation and chip-waveform matched filtering, the observations obtained from the GN_t chip durations of the n_p th subcarrier can be expressed as

$$\begin{aligned} \mathbf{r}_{n_p}^{(n)} &= \sum_{u=1}^U \mathbf{S}_{n_p}^{(u)} \mathbf{h}_{n_p}^{(n)} + \mathbf{n}_{n_p}^{(n)} \\ &= \sum_{u=1}^U c_{n_p} \mathbf{C}_u \mathcal{G}^{(u)} \mathbf{h}_{n_p}^{(n)} + \mathbf{n}_{n_p}^{(n)}, \quad n = 1, 2, \dots, N; n_p = 1, 2, \dots, N_p \end{aligned} \quad (9.183)$$

where $\mathbf{n}_{n_p}^{(n)}$ is a GN_t -length complex Gaussian random vector distributed with zero mean and a covariance matrix $\sigma^2 \mathbf{I}$, where $\sigma^2 = 1/\text{SNR}$ and SNR represents the SNR.

Let us consider the class of attractive STBCs, which satisfy

$$\mathcal{G}^{(u)} \mathbf{h}_{n_p}^{(n)} = \mathbf{H}_{n_p}^{(n)} \mathbf{x}_u, \quad u = 1, 2, \dots, U \quad (9.184)$$

Then, (9.183) can be written as

$$\mathbf{r}_{n_p}^{(n)} = \sum_{u=1}^U c_{n_p} \mathbf{C}_u \mathbf{H}_{n_p}^{(n)} \mathbf{x}_u + \mathbf{n}_{n_p}^{(n)}, \quad n = 1, 2, \dots, N; n_p = 1, 2, \dots, N_p \quad (9.185)$$

Based on (9.185), the detection procedure can be started by first carrying out the F-domain de-spreading, which generates the observations from the n_p th subcarrier as

$$\begin{aligned} \mathbf{y}_{n_p}^{(n)} &= c_{n_p} \mathbf{r}_{n_p}^{(n)} = \frac{1}{N_p} \sum_{u=1}^U \mathbf{C}_u \mathbf{H}_{n_p}^{(n)} \mathbf{x}_u + \bar{\mathbf{n}}_{n_p}^{(n)} \\ n &= 1, 2, \dots, N; \quad n_p = 1, 2, \dots, N_p \end{aligned} \quad (9.186)$$

where we have used the result of $\|c_{n_p}\|^2 = 1/N_p$. In the above equation $\bar{\mathbf{n}}_{n_p}^{(n)} = c_{n_p} \mathbf{n}_{n_p}^{(n)}$ is a complex Gaussian random vector, which is distributed with zero mean and a covariance matrix $N_p^{-1} \sigma^2 \mathbf{I}$.

Let us define

$$\begin{aligned} \mathbf{y}^{(n)} &= [(\mathbf{y}_1^{(n)})^T, (\mathbf{y}_2^{(n)})^T, \dots, (\mathbf{y}_{N_p}^{(n)})^T]^T \\ \mathbf{H}^{(n)} &= [(\mathbf{H}_1^{(n)})^T, (\mathbf{H}_2^{(n)})^T, \dots, (\mathbf{H}_{N_p}^{(n)})^T]^T \\ \mathbf{n}^{(n)} &= [(\bar{\mathbf{n}}_1^{(n)})^T, (\bar{\mathbf{n}}_2^{(n)})^T, \dots, (\bar{\mathbf{n}}_{N_p}^{(n)})^T]^T \end{aligned} \quad (9.187)$$

Then, the observations from the N_p subcarriers can be expressed as

$$\mathbf{y}^{(n)} = \frac{1}{N_p} \sum_{u=1}^U (\mathbf{C}_u \otimes \mathbf{I}_{N_p}) \mathbf{H}^{(n)} \mathbf{x}_u + \mathbf{n}^{(n)}, \quad n = 1, 2, \dots, N \quad (9.188)$$

Furthermore, let us define

$$\begin{aligned} \mathbf{y} &= [(\mathbf{y}^{(1)})^T, (\mathbf{y}^{(2)})^T, \dots, (\mathbf{y}^{(N)})^T]^T \\ \mathbf{H} &= [(\mathbf{H}^{(1)})^T, (\mathbf{H}^{(2)})^T, \dots, (\mathbf{H}^{(N)})^T]^T \\ \mathbf{n} &= [(\bar{\mathbf{n}}^{(1)})^T, (\bar{\mathbf{n}}^{(2)})^T, \dots, (\bar{\mathbf{n}}^{(N)})^T]^T \end{aligned} \quad (9.189)$$

Then, the overall observations from the N number of receive antennas can be expressed as

$$\mathbf{y} = \frac{1}{N_p} \sum_{u=1}^U (\mathbf{C}_u \otimes \mathbf{I}_{N_p N}) \mathbf{H} \mathbf{x}_u + \mathbf{n} \quad (9.190)$$

where \mathbf{y} is a $N_p N U G N_t$ -length observation vector, \mathbf{H} is a $(N_p N L_t \times G)$ -dimensional channel matrix, \mathbf{x}_u is a G -length data symbol vector, and, finally, \mathbf{n} is a $N_p N U G N_t$ -length noise vector.

Based on (9.190) the decision variable vector for \mathbf{x}_u can be formed in a way as

$$\mathbf{z}_u = [(\mathbf{C}_u \otimes \mathbf{I}_{N_p N}) \mathbf{H}]^H \mathbf{y}, \quad u = 1, 2, \dots, U \quad (9.191)$$

Substituting (9.190) into the above equation and using the facts of $\mathbf{C}_u^H \mathbf{C}_u = \mathbf{I}_{N_t}$ and $\mathbf{C}_u^H \mathbf{C}_v = \mathbf{0}$ for $u \neq v$, we can express \mathbf{z}_u as

$$\mathbf{z}_u = \frac{1}{N_p} \mathbf{H}^H \mathbf{H} \mathbf{x}_u + \bar{\mathbf{n}}, \quad u = 1, 2, \dots, U \quad (9.192)$$

where $\bar{\mathbf{n}} = [(C_u \otimes \mathbf{I}_{N_p N}) \mathbf{H}]^H \mathbf{n}$. It can be shown that there is no interference among the transmitted symbols $\{\mathbf{x}_u\}$.

Let us assume that the STBC of the STS designed based on belongs to the class of full-diversity orthogonal STBCs. In this case, \mathbf{z}_u can be further simplified to

$$\mathbf{z}_u = \frac{\beta^2}{N_p} \left(\sum_{n_p=1}^{N_p} \sum_{n=1}^N \sum_{m=1}^M |h_{n_p}^{(n,m)}|^2 \right) \mathbf{x}_u + \bar{\mathbf{n}}, \quad u = 1, 2, \dots, U \quad (9.193)$$

where $\bar{\mathbf{n}}$ is a complex Gaussian random vector, which is distributed with zero mean and a covariance matrix

$$E[\bar{\mathbf{n}} \bar{\mathbf{n}}^H] = \sigma^2 \times \frac{\beta^2}{N_p} \left(\sum_{n_p=1}^{N_p} \sum_{n=1}^N \sum_{m=1}^M |h_{n_p}^{(n,m)}|^2 \right) \mathbf{I}_G \quad (9.194)$$

With the obtained decision variable vector as shown in (9.193), let us now analyse the error probability of the TF-domain STS/MC DS-CDMA system, when communicating over Nakagami- m fading channels.

9.5.3 Analysis of Probability of Error

From the decision variable vector of (9.193) we can know that the instantaneous SNR for detection of \mathbf{x}_u is given by

$$\begin{aligned} \gamma &= \frac{1}{\sigma^2} \times \frac{\beta^2}{N_p} \left(\sum_{n_p=1}^{N_p} \sum_{n=1}^N \sum_{m=1}^M |h_{n_p}^{(n,m)}|^2 \right) \\ &= \sum_{n_p=1}^{N_p} \sum_{n=1}^N \sum_{m=1}^M \gamma_{n_p,mn} \end{aligned} \quad (9.195)$$

where

$$\begin{aligned} \gamma_{n_p,mn} &= \frac{|h_{n_p}^{(n,m)}|^2}{\Omega} \times \gamma_c \\ \gamma_c &= \frac{\Omega}{\sigma^2} \times \frac{\beta^2}{N_p} \end{aligned} \quad (9.196)$$

where $\Omega = E[|h_{n_p}^{(n,m)}|^2]$ and γ_c represents the average SNR of a subcarrier channel from one transmit antenna to one receive antenna.

When comparing (9.195) and (9.196) with (9.158) and (9.159), we can find that they are in the same forms and also have the same meaning. Hence, the error probability analysis for the TF-domain STS/MC DS-CDMA can be carried out by following the same steps as that for the space-time MC-CDMA in Section 9.4.3. It can be shown that, when a special baseband modulation scheme shown in (9.161) to (9.164) is considered, the average probability of error of the TF-domain STS/MC DS-CDMA can be evaluated by the equation in association with

$$T[a, b, g] = a \int_0^{b\pi} \det \left(\mathbf{I} + \frac{g\gamma_c}{m \sin^2 \theta} \mathbf{M} \right)^{-MNm} d\theta \quad (9.197)$$

where \mathbf{M} is in the same form as (9.171). Furthermore, let $\lambda_1, \lambda_2, \dots, \lambda_D$ be the D number of non-zero eigenvalues of \mathbf{M} . Then, $T[a, b, g]$ can be evaluated by the expression

$$\begin{aligned} T[a, b, g] &= a \int_0^{b\pi} \prod_{j=1}^D \left(1 + \frac{\lambda_j g \gamma_c}{m \sin^2 \theta}\right)^{-MNm} d\theta \\ &= a \int_0^{b\pi} \prod_{j=1}^D \left(\frac{m \sin^2 \theta}{\lambda_j g \gamma_c + m \sin^2 \theta}\right)^{MNm} d\theta \end{aligned} \quad (9.198)$$

With the aid of (9.196) to (9.198), the error probability of the TF-domain STS/MC DS-CDMA using various baseband modulation schemes and various STS schemes can be readily evaluated. Specifically, in (9.196) β is determined by the STS scheme, which is the only parameter required from the STS for evaluation of the error probability. By contrast, in (9.197) and (9.198) the parameters a, b and g are determined by the specific modulation scheme considered as shown in (9.161) to (9.164).

Below we specialize (9.198) to some special cases. First, for a single-carrier DS-CDMA system experiencing flat fading, we have $D = 1$ and $\lambda_j = 1$. Correspondingly, we have

$$T[a, b, g] = a \int_0^{b\pi} \left(\frac{m \sin^2 \theta}{g \gamma_c + m \sin^2 \theta}\right)^{MNm} d\theta \quad (9.199)$$

which achieves a diversity order of MN from the space-domain.

Second, when each of the N_p subcarriers experiences independent fading, then $\mathbf{M} = \mathbf{I}$. In this case, (9.198) is reduced to

$$T[a, b, g] = a \int_0^{b\pi} \left(\frac{m \sin^2 \theta}{g \gamma_c + m \sin^2 \theta}\right)^{N_p MNm} d\theta \quad (9.200)$$

which is capable of achieving a diversity order of $N_p MN$ contributed from both space-domain and frequency-domain.

Finally, when the N_p subcarriers experience flat fading, then the rank of \mathbf{M} is one and the only non-zero eigenvalue is $\lambda_1 = N_p$. In this case, (9.198) is reduced to

$$T[a, b, g] = a \int_0^{b\pi} \left(\frac{m \sin^2 \theta}{g N_p \gamma_c + m \sin^2 \theta}\right)^{MNm} d\theta \quad (9.201)$$

which can only achieve the diversity order of MN provided by the space-domain.

When comparing the expression (9.198) for the error rate of the STS/MC DS-CDMA with (9.173) for the error rate of the F-domain spread MC-CDMA using STC, we can see that they are the same. Hence, the error rate performance of the STS/MC DS-CDMA system considered in this section appears with the same behaviour as that seen in Figs. 9.11 and 9.12, when the same system parameters are utilized. However, we should realize that in the STS/MC DS-CDMA systems the frequency spacing between two adjacent subcarriers is $1/T_c$, which is usually much higher than the spacing of two adjacent subcarriers in the F-domain spread MC-CDMA systems. Hence, in the STS/MC DS-CDMA systems, the fading associated with different subcarriers may readily become uncorrelated, even the delay-spread of the wireless channels is small. As an example to show this concern, in Fig. 9.15 the

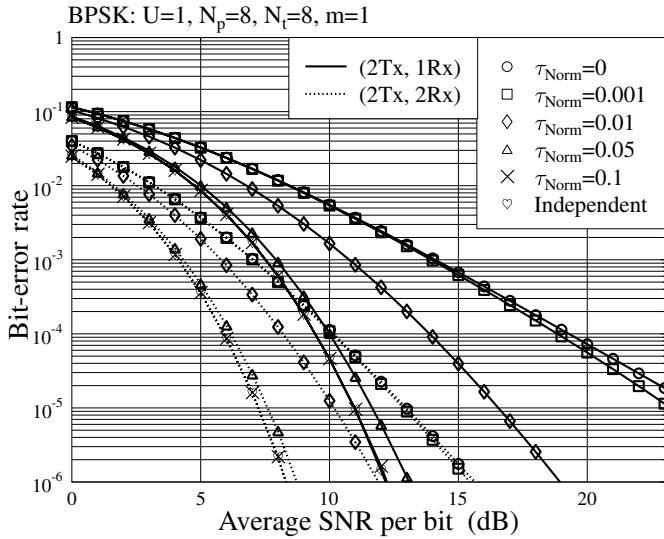


Figure 9.15: BER versus average SNR per bit performance for the STS/MC DS-CDMA systems using 8 subcarriers, when communicating over Rayleigh ($m = 1$) fading channels associated with different delay-spread. The delay-spread was assumed to obey the uniform distribution.

impact of the delay-spread of the wireless channels on the achievable BER performance of the STS/MC DS-CDMA systems is depicted, where the excess delay-spread obeys the uniform distribution shown in (5.8) and the normalized delay-spread is defined as $\tau_{\text{Norm}} = \tau/UT$. As seen in Fig. 9.15, the BER performance improves, when the delay-spread of the wireless channels increases, resulting in higher frequency-diversity gain. It can be seen that, even the normalized delay-spread is as low as $\tau_{\text{Norm}} = 0.1$, the fading of subcarrier channels becomes nearly independent, and the BER performance is the same as that of the STS/MC DS-CDMA systems, where the subcarrier signals experience independent fading.

9.6 Space–Time Multicarrier DS-CDMA over Fast Time-Varying Fading Channels¹

In wireless communications multicarrier CDMA schemes employ a range of advantages, which include low intersymbol interference (ISI) due to invoking S/P conversion at the transmitter, low implementation complexity of carrier modulation/demodulation for the sake of using FFT techniques, etc. In multicarrier CDMA systems frequency diversity can usually be achieved by repeating (spreading) the same transmitted signal in the frequency (F)-domain on several subcarriers, as shown in references [15, 37, 41, 54, 260] or in Chapter 5

¹This section is based on and reproduced with permission from Lie-Liang Yang: ‘Performance of Multiantenna Multicarrier Direct-Sequence Code-Division Multiple-Access Using Orthogonal Variable Spreading Factor Codes Assisted Space–Time Spreading in Time-Selective Fading Channels’ from *IET Proceedings Communications*, Vol. 2, No. 5, pp. 708–719, May 2008. © Institution of Engineering & Technology.

and Sections 9.4 and 9.5 of this chapter. Spatial diversity can be achieved by deployment of multiple transmit antennas or/and multiple receive antennas with the aid of, for example, space–time coding [245], space–time spreading [256], etc. transmitter processing schemes, as shown in the previous sections of this chapter.

It is well recognized that broadband wireless mobile channels are typically time-varying and the received signals may experience both frequency-selective fading and time selective fading. The multicarrier CDMA schemes considered so far, which include the F-domain spread MC-CDMA [15, 71] and MC DS-CDMA [41, 53, 71], have been designed without consideration of the time-selectivity of the wireless channels. When a multicarrier CDMA system employs both S/P conversion and transmitter processing for achieving transmit diversity [256, 258], as shown in Sections 9.4 and 9.5, the symbol duration, T_s , of the transmitted signals is usually many times the bit duration, T_b , of the signals observed before the S/P conversion, even when the BPSK baseband modulation is assumed. More specifically, let the S/P converter carry out the 1-to- U conversion and the transmitter employ M transmit antennas. Then, the symbol duration after the S/P conversion is $T_s = UT_b$ [71]. When the STS-assisted transmit diversity scheme, which invokes G symbols, is used, as shown in Section 9.5, the symbol duration is then further extended, yielding $T_s = UGT_b$. Therefore, when using both S/P conversion and (open-loop) transmit diversity scheme, the multicarrier CDMA signals may be very sensitive to time-selective fading.

Therefore, in this section one of our objectives is to design and investigate a space–time transmission scheme for the multiantenna MC DS-CDMA downlink, so that it is capable of simultaneously exploiting both the frequency selectivity and the time selectivity of the wireless channels, in addition to achieving the full transmit diversity. Specifically, in the considered multiantenna MC DS-CDMA system the BS transmitter uses a STS-assisted transmit diversity scheme. This is because, as shown in Section 9.2.2.5, the STS-assisted transmit diversity scheme is capable of providing maximal transmit diversity without requiring extra STS spreading codes, when the number of transmit antennas obeys $M = G = 2, 4, 8$, etc. and when real-valued data symbols are transmitted. In this section we assume that the orthogonal STS codes are made up of a class of orthogonal variable spreading factor (OVSF) codes [261]. It can be shown that the employment of the OVSF codes is capable of providing the facilities for exploiting the time-selectivity of wireless channels, as will become apparent.

In this section we consider specifically the multiuser multiantenna MC DS-CDMA using BPSK baseband modulation. The benchmark single-user BER bound of the multiantenna MC DS-CDMA using BPSK modulation is first investigated, so as to gain insight into the achievable BER performance, when the space–time MC DS-CDMA signals experience various levels of time-selective fading. It can be shown that, even when slight time-selective fading exists, it may be exploited to significantly improve the achievable BER performance of the multiantenna MC DS-CDMA. Then, the BER performance of the multiantenna MC DS-CDMA system supporting multiple users is investigated, when a single-user correlation detector [88] is used. Due to time-selective fading, our analysis and results show that even when orthogonal STS codes are employed, multiuser interference (MUI) may be conflicted and may significantly degrade the achievable BER performance. In this case, a low-complexity multiuser detector discussed in Chapter 6 may be used to suppress the MUI. In this section a MMSE MUD is investigated, which shows that the MUI can be efficiently suppressed, while simultaneously achieving the diversity provided by multiple transmit/receive antennas and that by time-selective fading.

Note that, in this section, in order to focus our attention mainly on the spatial- and time-diversity, we do not try to make use of the frequency diversity.

9.6.1 System Model

9.6.1.1 Transmitter Model

The downlink of a digital mobile radio communications system is considered, where the BS consists of M number of transmit antennas. The BS transmitter uses BPSK modulation and STS, and the space–time signal is transmitted to the MTs with the aid of multicarrier modulation. The diagram for the BS transmitter is shown in Fig. 9.16, which uses U subcarriers and M transmit antennas, where we assume that $M = G = 2, 4, 8, \dots$, since in these cases the corresponding STS schemes are capable of providing maximal transmit diversity without requiring extra STS spreading sequences, as shown in Section 9.2.2.5. Furthermore, it is assumed that the downlink of the multiantenna MC DS-CDMA system supports K number of users. As shown in Fig. 9.16, for the k th user, a block of UM data bits having a bit duration of T_b is S/P converted to U parallel substreams. Each substream has M data bits, which are space–time spread using the schemes shown in Section 9.2.2.5 [256–258] with the aid of M orthogonal spreading codes of $\{c_{k1}(t), c_{k2}(t), \dots, c_{kM}(t)\}$, $k = 1, 2, \dots, K$ and mapped to the M transmit antennas. In order to exploit the time-selective fading for achieving the time diversity, in this section the orthogonal STS codes are assumed to belong to the family of Walsh–Hadamard codes [71] or to the other families of orthogonal codes, which have the properties of OVSF codes [71, 261]. The reason for using the STS codes with the properties of OVSF codes will become clear.

According to the above analysis, we can know that the symbol duration of the STS signals is UMT_b and the discrete period of the orthogonal codes is $UMT_b/T_c = UMN_t$, where $N_t = T_b/T_c$ and T_c represents the chip duration of the orthogonal spreading codes. The orthogonal STS codes take the form of $c_{ki}(t) = \sum_{j=0}^{UMN_t-1} c_{ki}[j]\psi_{T_c}(t - jT_c)$, where $c_{ki}[j] \in \{+1, -1\}$ and they obey the relationship of $\sum_{l=0}^{UMN_t-1} c_{im}[l]c_{jn}[l] = 0$, whenever $i \neq j$ or $m \neq n$. Furthermore, $\psi_{T_c}(t)$ represents the chip impulse waveform defined over the interval of $[0, T_c]$. As seen in Fig. 9.16, following STS, each STS block generates M parallel signals to be mapped to the M transmit antennas. Finally, as seen in Fig. 9.16, for each of the M transmit antennas, the K number of user signals are multiplexed and multicarrier modulated with the aid of the U number of subcarriers, in order to form the downlink transmitted signal.

Note that in the multiantenna MC DS-CDMA systems considered in this paper the same space–time signal may be transmitted on several subcarriers to further achieve the frequency diversity, when communicating over frequency-selective fading channels. However, for the sake of having our concentration mainly on the time-selective fading, we assume that each of the subcarrier signals experiences flat fading and each space–time signal is only transmitted on one subcarrier, i.e. no frequency-diversity is considered. Furthermore, in order that the description is simple to follow, let us first consider the MC DS-CDMA system using two transmit antennas and derive in detail the transmitted signal as well as the received signal models. This special case will then be extended to the general multiantenna MC DS-CDMA system, which employs M transmit antennas.

For the multiantenna MC DS-CDMA system using $M = 2$ transmit antennas at the BS and supporting K users, the STS operation and carrier modulation in the context of

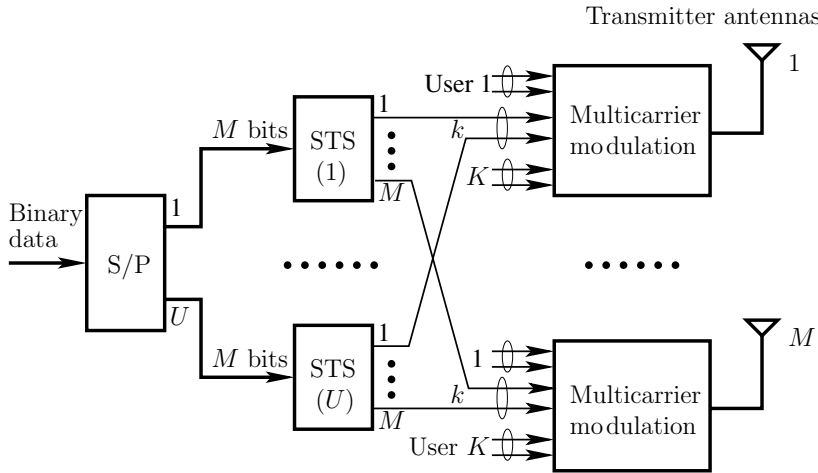


Figure 9.16: BS transmitter block diagram of the multiantenna MC DS-CDMA system using the OVSF codes assisted space-time spreading. (Reproduced with permission from Lie-Liang Yang: ‘Performance of Multiantenna Multicarrier Direct-Sequence Code-Division Multiple-Access Using Orthogonal Variable Spreading Factor Codes Assisted Space-Time Spreading in Time-Selective Fading Channels’ from *IET Proceedings Communications*, Vol. 2, No. 5, pp. 708–719, May 2008. © Institution of Engineering & Technology.)

the u th subcarrier of the MC DS-CDMA can be shown as Fig. 9.17, where P represents the transmission power per transmit antenna. According to Fig. 9.17, the downlink MC DS-CDMA signals transmitted by antenna 1 and 2 of the BS can be expressed as [256, 258]

$$\begin{bmatrix} s_1(t) \\ s_2(t) \end{bmatrix} = \Re \left\{ \sum_{k=1}^K \sum_{u=1}^U \sqrt{\frac{2E_b}{M^2 U T_b}} \begin{bmatrix} [c_{k1}(t)b_{k,u1} + c_{k2}(t)b_{k,u2}] \exp[j(2\pi f_u t + \phi_{u1})] \\ [c_{k1}(t)b_{k,u2} - c_{k2}(t)b_{k,u1}] \exp[j(2\pi f_u t + \phi_{u2})] \end{bmatrix} \right\} \quad (9.202)$$

where $\Re\{x\}$ represents the real part of x , $E_b = PT_b$ represents the transmitted energy per bit, $M^2 U = 2 \times 2 \times U$ is a power normalization factor, due to using M number of transmit antennas and also the symbol duration of $T_s = UMT_b$. It can be shown that, after the normalization, each subcarrier of a transmit antenna emits KE_b Joule within a symbol duration of T_s and the total energy emitted within T_s is given by $K \times UME_b$. Additionally, in (9.202) $b_{k,u1}$ and $b_{k,u2}$ represent the two bits of the k th user, which are invoked in the STS with respect to the u th subcarrier, f_u is the frequency of the u th subcarrier, while $\{\phi_{ul}, m = 1, 2\}$ represent the phases introduced by multicarrier modulations.

Let us assume that each subcarrier signal experiences correlated Nakagami- m fading. Then, the received baseband equivalent signal by the n th receive antenna of the desired MT can be expressed as

$$\begin{aligned} r_n(t) = & \sum_{k=1}^K \sum_{u=1}^U \sqrt{\frac{2E_b}{M^2 U T_b}} \{ h_{1nu}(t)[c_{k1}(t)b_{k,u1} + c_{k2}(t)b_{k,u2}] \exp[j(2\pi f_u t + \phi_{u1})] \\ & + h_{2nu}(t)[c_{k1}(t)b_{k,u2} - c_{k2}(t)b_{k,u1}] \exp[j(2\pi f_u t + \phi_{u2})] \} + n_n(t) \end{aligned} \quad (9.203)$$

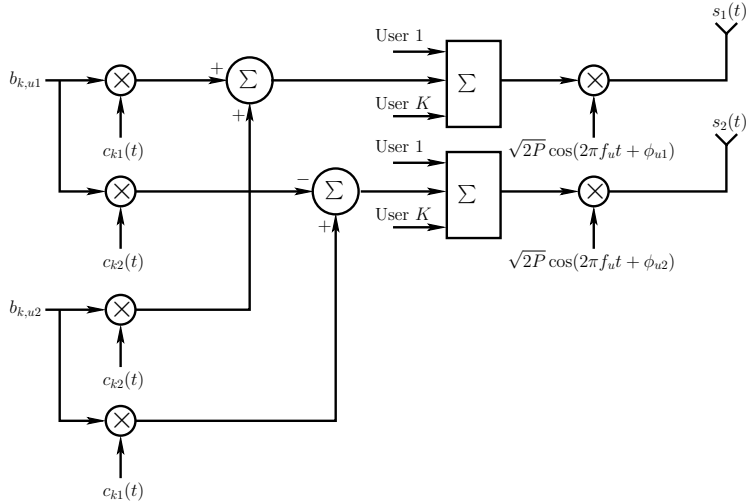


Figure 9.17: Illustration of space–time spreading for the u th subcarrier of the MC DS-CDMA using two transmit antennas. (Reproduced with permission from Lie-Liang Yang: ‘Performance of Multiantenna Multicarrier Direct-Sequence Code-Division Multiple-Access Using Orthogonal Variable Spreading Factor Codes Assisted Space–Time Spreading in Time-Selective Fading Channels’ from *IET Proceedings Communications*, Vol. 2, No. 5, pp. 708–719, May 2008. © Institution of Engineering & Technology.)

where $n = 1, 2, \dots, N$ and N represents the number of receive antennas of the k th MT, $n_n(t)$ is the complex-valued additive white Gaussian noise (AWGN) received by the n th receive antenna, which has zero mean and a single-sided PSD of N_0 per dimension. In (9.203) $h_{mn}(t)$ represents the time-variant channel gain with respect to the m th transmit antenna, the n th receive antenna and the u th subcarrier. The time-variant channel gain $h_{mn}(t)$ is assumed to be a correlated complex random process, which can be expressed as $h_{mn}(t) = |h_{mn}(t)|\exp[j\varphi_{mn}(t)]$, where $|h_{mn}(t)|$ and $\varphi_{mn}(t)$ represent respectively the time-variant envelope and phase of the corresponding fast-fading channel.

Furthermore, according to reference [131], the correlation factors $\rho_h(\tau)$ of the channel gain, $\rho_{|h|}(\tau)$ of the channel envelope and $\rho_{|h|^2}(\tau)$ of the squared channel envelope are given by

$$\rho_h(\tau) \approx J_0(2\pi f_D \tau) \quad (9.204)$$

$$\rho_{|h|}(\tau) = \rho_{|h|^2}(\tau) = J_0^2(2\pi f_D \tau) \quad (9.205)$$

respectively, where $J_0(x)$ is the zero-order Bessel function of the first kind, f_D is the Doppler frequency shift, while τ is the relative delay.

9.6.1.2 Receiver Model

The receiver structure for detection of the multiantenna MC DS-CDMA signal is shown in Fig. 9.18. As shown in Fig. 9.18 the receiver comprises of N receive antennas. Let us consider the n th receive antenna in detail. As mentioned previously in Section 9.6.1.1, the STS codes

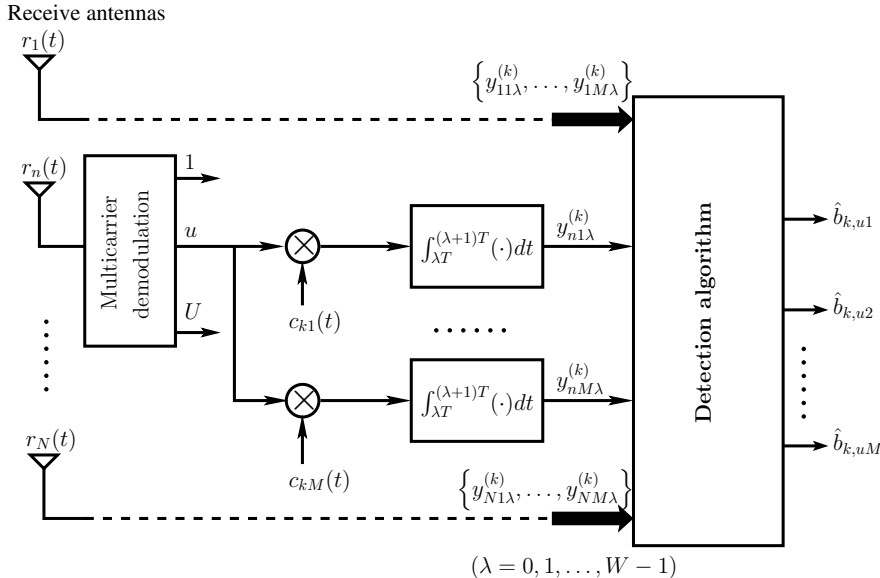


Figure 9.18: Receiver block diagram for the k th MT supported by the multiantenna MC DS-CDMA system. (Reproduced with permission from Lie-Liang Yang: ‘Performance of Multiantenna Multicarrier Direct-Sequence Code-Division Multiple-Access Using Orthogonal Variable Spreading Factor Codes Assisted Space–Time Spreading in Time-Selective Fading Channels’ from *IET Proceedings Communications*, Vol. 2, No. 5, pp. 708–719, May 2008. © Institution of Engineering & Technology.)

belong to the family of OVSF codes, hence any of the STS codewords, for example 1 – 1 1 – 1 – 1 1 – 1, can be expressed as the concatenation of a mother codeword, such as 1 – 1 1 – 1, based on another codeword, which we refer to as a generating codeword and it is 1 – 1 for this specific example. More specifically, for our multiantenna MC DS-CDMA, we assume that the spreading factor UMN_t can be factorized as $UMN_t = W (= 2^{k_1}) \times V (= 2^{k_2})$, where k_1 and k_2 are integers. Additionally, we assume that $V \geq M$, since each user requires M STS codewords. Let \mathbf{C}_V be the matrix that contains the mother orthogonal code of length V , \mathbf{C}_W be the matrix containing the generating orthogonal code of length W . Then, the $UMN_t = WV$ number of OVSF codewords of length UMN_t can be expressed as

$$\mathbf{C}_{WV} = \mathbf{C}_W \otimes \mathbf{C}_V \quad (9.206)$$

where \otimes represents the *Kronecker product* operation [89].

Let us assume that the channels stay constant over at least the time duration of $T = VT_c$ seconds, which is referred to as a *fraction*. Then, the orthogonality among the subcarriers can be retained and there exists no intercarrier interference (ICI) within the observation of one fraction [53]. Hence, for brevity, we consider only one subcarrier, such as the u th subcarrier. As shown in Fig. 9.18, the variables $y_{n1\lambda}^{(k)}$ and $y_{n2\lambda}^{(k)}$ in the context of the λ th fraction can be

expressed as

$$y_{n1\lambda}^{(k)} = \left(\sqrt{\frac{2E_b}{M^2 U T_b}} \right)^{-1} \frac{1}{T} \int_{\lambda T}^{(\lambda+1)T} r_n(t) c_{k1}(t) \exp(-j2\pi f_u t) dt \quad (9.207)$$

$$y_{n2\lambda}^{(k)} = \left(\sqrt{\frac{2E_b}{M^2 U T_b}} \right)^{-1} \frac{1}{T} \int_{\lambda T}^{(\lambda+1)T} r_n(t) c_{k2}(t) \exp(-j2\pi f_u t) dt \quad (9.208)$$

where $k = 1, 2, \dots, K$, $n = 1, 2, \dots, N$ and $\lambda = 0, 1, \dots, W - 1$.

Let us assume that the first user corresponding to $k = 1$ is the desired user. We also assume that the orthogonal STS codes are assigned to users under the following constraints:

1. The STS codes assigned to the same user are made up of different mother codes, implying that $V \geq M$. Hence, the STS codes assigned to a given user are orthogonal on the fraction level.
2. The same set of mother codes are assigned to K_1 users to generate their STS codes with the aid of their unique generating codes, respectively.

Based on the above constraints and remembering that the channels stay constant over at least a fraction, it can be shown that the desired user may conflict interference from, at most, the $(K_1 - 1)$ users who share the same set of mother codes as the desired user. The remaining $K_2 (= K - K_1)$ users impose no interference on the desired user, since their mother codes are orthogonal to those of the desired user on the fraction level. Furthermore, the interference from the $(K_1 - 1)$ users depends on the fading rate of the channel. Specifically, if the channels remain time-invariant over a symbol duration of $UMN_t T_c$ seconds, there will exist no MUI at all in the multiantenna MC DS-CDMA system, since in this case all the UMN_t -length STS codes are orthogonal. Therefore, the multiantenna MC DS-CDMA considered in this section employs a self-adjustment capability. As will become evident, when the fading of the wireless channels becomes more time-selective, the multiantenna MC DS-CDMA conflicts higher MUI, but, simultaneously, it is capable of achieving a higher diversity gain due to the severe time-selective fading. By contrast, when the fading becomes less time-selective, the achievable time-diversity gain will also be lower, but in this case the MUI also becomes lower since the STS codes become more orthogonal.

Let us consider the K_1 number of users sharing the common set of mother codes of the desired user and assume that $k = 1$ in (9.207) and (9.208). Then, substituting $r_n(t)$ of (9.203) into (9.207) and (9.208) and using a vector notation to denote the transmitted and received signals, the observations from the n th receive antenna can be expressed as

$$\mathbf{y}_{n\lambda} = \sum_{j=1}^{K_1} \mathbf{C}_j^{(\lambda)} \mathbf{H}_{nu}^{(\lambda)} \mathbf{b}_{j,u} + \mathbf{n}_{nu}^{(\lambda)} \quad (9.209)$$

where

$$\mathbf{y}_{n\lambda} = \begin{bmatrix} y_{n1\lambda}^{(1)} \\ y_{n2\lambda}^{(1)} \end{bmatrix}, \quad \mathbf{C}_j^{(\lambda)} = \begin{bmatrix} C_j^{(\lambda)} C_1^{(\lambda)} & 0 \\ 0 & C_j^{(\lambda)} C_1^{(\lambda)} \end{bmatrix} = C_j^{(\lambda)} C_1^{(\lambda)} \mathbf{I}_2, \quad \mathbf{b}_{j,u} = \begin{bmatrix} b_{j,u1} \\ b_{j,u2} \end{bmatrix} \quad (9.210)$$

$$\mathbf{H}_{nu}^{(\lambda)} = \begin{bmatrix} h_{1nu}^{(\lambda)} & h_{2nu}^{(\lambda)} \\ -h_{2nu}^{(\lambda)} & h_{1nu}^{(\lambda)} \end{bmatrix}, \quad \mathbf{n}_{nu}^{(\lambda)} = \begin{bmatrix} n_{1nu}^{(\lambda)} \\ n_{2nu}^{(\lambda)} \end{bmatrix} \quad (9.211)$$

In (9.210) and (9.211) $C_j = [C_j^{(1)}, \dots, C_j^{(\lambda)}, \dots, C_j^{(W-1)}]$, $j = 1, \dots, K_1$ is the j th MT's generating code and $C_j^{(\lambda)}$ is the λ th chip of the generating code C_j , $\mathbf{H}_{nu}^{(\lambda)}$ is the CIR matrix corresponding to the λ th fraction, while $\mathbf{n}_{nu}^{(\lambda)}$ represents the AWGN vector, where

$$n_{mn\mu}^{(\lambda)} = \left(\sqrt{\frac{2E_b}{M^2 U T_b}} \right)^{-1} \frac{1}{T} \int_{\lambda T}^{(\lambda+1)T} n_n(t) c_{km}(t) \exp(-2\pi f_u t) dt, \quad m = 1, 2 \quad (9.212)$$

which is a zero-mean complex Gaussian random variable with a variance of $WMN_0/2E_b$ per dimension. Furthermore, by observing (9.210) and (9.211), it can be shown that (9.209) can be easily extended for the general multiantenna MC DS-CDMA employing M transmit antennas. Specifically, for the general multiantenna MC DS-CDMA using $M = 2, 4, 8, \dots$ transmit antennas, $\mathbf{y}_{n\lambda}$, $\mathbf{b}_{j,u}$, $\mathbf{n}_{nu}^{(\lambda)}$ are M -dimensional vectors, $\mathbf{C}_j^{(\lambda)}$ is a $(M \times M)$ diagonal matrix, while $\mathbf{H}_{nu}^{(\lambda)}$ is a $(M \times M)$ channel matrix determined by the STS scheme employed by the transmitter. Below, we turn to consider the general multiantenna MC DS-CDMA using M transmit antennas and N receive antennas.

Let us define

$$\mathbf{y}_n = [\mathbf{y}_{n0}^T, \mathbf{y}_{n1}^T, \dots, \mathbf{y}_{n(W-1)}^T]^T \quad (9.213)$$

$$\mathbf{C}_j = \text{diag}\{\mathbf{C}_j^{(0)}, \mathbf{C}_j^{(1)}, \dots, \mathbf{C}_j^{(W-1)}\} \quad (9.214)$$

$$\mathbf{H}_{nu} = [(\mathbf{H}_{nu}^{(0)})^T, (\mathbf{H}_{nu}^{(1)})^T, \dots, (\mathbf{H}_{nu}^{(W-1)})^T]^T \quad (9.215)$$

$$\mathbf{n}_{nu} = [(\mathbf{n}_{nu}^{(0)})^T, (\mathbf{n}_{nu}^{(1)})^T, \dots, (\mathbf{n}_{nu}^{(W-1)})^T]^T \quad (9.216)$$

where \mathbf{y}_n and \mathbf{n}_{nu} are the MW -length vectors, \mathbf{C}_j is a $(MW \times MW)$ diagonal matrix related to the generating codes of users j and 1, and, finally, \mathbf{H}_{nu} is a $(MW \times M)$ channel matrix. Based on the above definition, we have

$$\mathbf{y}_n = \sum_{j=1}^{K_1} \mathbf{C}_j \mathbf{H}_{nu} \mathbf{b}_{j,u} + \mathbf{n}_{nu}, \quad n = 1, 2, \dots, N \quad (9.217)$$

Furthermore, let us consider the N number of receive antennas and define

$$\mathbf{y} = [\mathbf{y}_1^T, \mathbf{y}_2^T, \dots, \mathbf{y}_N^T]^T \quad (9.218)$$

$$\mathbf{H}_u = [\mathbf{H}_{1u}^T, \mathbf{H}_{2u}^T, \dots, \mathbf{H}_{Nu}^T]^T \quad (9.219)$$

$$\mathbf{n}_u = [\mathbf{n}_{1u}^T, \mathbf{n}_{2u}^T, \dots, \mathbf{n}_{Nu}^T]^T \quad (9.220)$$

Then, the received samples from the N number of receive antennas, which are sufficient for detecting $\{\mathbf{b}_{j,u}\}_{j=1}^{K_1}$, can be expressed as

$$\mathbf{y} = \sum_{j=1}^{K_1} (\mathbf{I}_N \otimes \mathbf{C}_j) \mathbf{H}_u \mathbf{b}_{j,u} + \mathbf{n}_u \quad (9.221)$$

Let us now consider the detection of the multiantenna MC DS-CDMA signals.

9.6.2 Detection Schemes

Two types of detection scheme are considered: the single-user correlation detector and the MMSE MUD. In the context of the single-user correlation detector, let

$$\mathbf{z} = [z_1^T, z_2^T, \dots, z_{K_1}^T]^T \quad (9.222)$$

be the $K_1 M$ -length vector containing the decision variables for the K_1 number of users sharing the same set of mother codes, where

$$\begin{aligned} \mathbf{z}_k &= [z_{k1}, z_{k2}, \dots, z_{kM}]^T \\ &= \Re \left\{ \frac{1}{W} ((\mathbf{I}_N \otimes \mathbf{C}_k) \mathbf{H}_u)^H \mathbf{y} \right\}, \quad k = 1, 2, \dots, K_1 \end{aligned} \quad (9.223)$$

is a M -length vector containing the decision variables for the M data bits transmitted by the k th user.

Substituting (9.221) into (9.223) and after some simplification, we obtain

$$\begin{aligned} \mathbf{z}_k &= \Re \left\{ \sum_{j=1}^{K_1} \sum_{n=1}^N \frac{1}{W} \sum_{w=0}^{W-1} C_k^{(w)} C_j^{(w)} (\mathbf{H}_{nu}^{(w)})^H \mathbf{H}_{nu}^{(w)} \mathbf{b}_{j,u} \right. \\ &\quad \left. + \sum_{n=1}^N \frac{1}{W} \sum_{w=0}^{W-1} C_k^{(w)} (\mathbf{H}_{nu}^{(w)})^H \mathbf{n}_{nu}^{(w)} \right\} \end{aligned} \quad (9.224)$$

According to (9.211) and the principles of STS shown in Section 9.2.2.5, it can be shown that we have

$$\Re \{(\mathbf{H}_{nu}^{(w)})^H \mathbf{H}_{nu}^{(w)}\} = \left(\sum_{m=1}^M |h_{mn}^{(w)}|^2 \right) \mathbf{I}_M \quad (9.225)$$

Hence, (9.224) can be expressed as

$$\mathbf{z}_k = \sum_{j=1}^{K_1} \frac{1}{W} \sum_{w=0}^{W-1} C_k^{(w)} C_j^{(w)} \left(\sum_{n=1}^N \sum_{m=1}^M |h_{mn}^{(w)}|^2 \right) \mathbf{b}_{j,u} + \sum_{n=1}^N \frac{1}{W} \sum_{w=0}^{W-1} C_k^{(w)} \mathbf{n}_{R,nu}^{(w)} \quad (9.226)$$

for $k = 1, \dots, K_1$, where $\mathbf{n}_{R,nu}^{(w)} = \Re \{(\mathbf{H}_{nu}^{(w)})^H \mathbf{n}_{nu}^{(w)}\}$, which is a M -length Gaussian vector having zero mean and a covariance matrix of $(WMN_0 \sum_{m=1}^M |h_{mn}^{(w)}|^2 / 2E_b) \mathbf{I}_M$. Finally, let us normalize \mathbf{z}_k in (9.226) using $W^{-1} \sum_{w=0}^{W-1} \sum_{n=1}^N \sum_{m=1}^M |h_{mn}^{(w)}|^2$ and expressing

$$\eta_{jk} = \frac{\sum_{w=0}^{W-1} C_k^{(w)} C_j^{(w)} (\sum_{n=1}^N \sum_{m=1}^M |h_{mn}^{(w)}|^2)}{\sum_{w=0}^{W-1} \sum_{n=1}^N \sum_{m=1}^M |h_{mn}^{(w)}|^2} \quad (9.227)$$

where we have $\eta_{kk} = 1$. Then, (9.226) can equivalently be expressed as

$$\mathbf{z}_k = \sum_{j=1}^{K_1} \eta_{jk} \mathbf{b}_{j,u} + \mathbf{n}_k, \quad k = 1, 2, \dots, K_1 \quad (9.228)$$

where \mathbf{n}_k is a M -length real Gaussian vector with zero mean and a covariance matrix given by

$$E[\mathbf{n}_k \mathbf{n}_k^T] = \underbrace{\left(2\gamma_c \sum_{w=0}^{W-1} \sum_{n=1}^N \sum_{m=1}^M \frac{|h_{lmn}^{(w)}|^2}{\Omega} \right)^{-1}}_{\sigma^2} \mathbf{I}_M \quad (9.229)$$

with definition of $\gamma_c = \Omega E_b / MWN_0$ and $\Omega = E[|h_{mn}^{(w)}|^2]$.

In (9.228), η_{jk} represents the cross-correlation coefficient between user j and user k . Since both C_k and C_j belong to the orthogonal code \mathbf{C}_W , $[C_k^{(0)} C_j^{(0)}, \dots, C_k^{(W-1)} C_j^{(W-1)}]$ is hence an orthogonal code belonging to \mathbf{C}_W . Consequently, when the channels are time-invariant implying that $|h_{mn}^{(w)}|^2$ in (9.227) is independent of the index of w , η_{jk} for any values of $j \neq k$ is zero, and hence there exists no MUI. However, when the downlink channels are time-variant resulting in $\sum_{n=1}^N \sum_{m=1}^M |h_{mn}^{(w)}|^2$ being different for different values of w , then η_{jk} for $j \neq k$ is nonzero and consequently MUI exists. Furthermore, according to (9.227) and the properties of orthogonal codes, it can be implied that only the time-varying parts in $\{\sum_{n=1}^N \sum_{m=1}^M |h_{mn}^{(w)}|^2\}_{w=0}^{W-1}$ contribute MUI, while the common part of them generates no MUI. To be more specific, let us express $\sum_{n=1}^N \sum_{m=1}^M |h_{mn}^{(w)}|^2 = A + B^{(w)}$, where A represents the common part, which is independent of the index w , while $B^{(w)}$ represents the time-variant part dependent on w . Then, after substituting $A + B^{(w)}$ into (9.227), it can be easily seen that A makes no contribution to η_{jk} , and the MUI is only generated by $B^{(w)}$.

In case MUI exists due to fast time-varying fading, a low-complexity MUD may be used to mitigate the MUI. In this section the MMSE-based MUD is used, since it has the advantages of low-complexity and of being able to be implemented using adaptive techniques [146]. Let the d th, where $d = 1, \dots, M$, bit of the reference user be detected. When the MMSE-MUD is used, the decision variable for $b_{1,ud}$ can be expressed as

$$z_d = \Re(\mathbf{W}_0^H \mathbf{y}) \quad (9.230)$$

where \mathbf{y} is given by (9.221), \mathbf{W}_0 represents the optimum weight matrix in the MMSE sense, which as shown in Chapter 6 can be expressed as

$$\mathbf{W}_0 = \mathbf{R}_y^{-1} \mathbf{r}_{yb_d} \quad (9.231)$$

where \mathbf{R}_y is the autocorrelation matrix of \mathbf{y} of (9.221), which, when assuming independent transmitted binary data, can be expressed as

$$\begin{aligned} \mathbf{R}_y &= E[\mathbf{y} \mathbf{y}^H] \\ &= \mathbf{h}_{ud} \mathbf{h}_{ud}^H + \mathbf{H}_{ud} \mathbf{H}_{ud}^H + \underbrace{\sum_{j=2}^{K_1} (\mathbf{I}_N \otimes \mathbf{C}_j) \mathbf{H}_u \mathbf{H}_u^H (\mathbf{I}_N \otimes \mathbf{C}_j)^T}_{\Sigma} + \frac{WMN_0}{E_b} \mathbf{I}_{MNW} \end{aligned} \quad (9.232)$$

where \mathbf{h}_{ud} represents the d th column of \mathbf{H}_u , while $\mathbf{H}_{u\bar{d}}$ represents the matrix formed from \mathbf{H}_u after removing the d th column. In (9.231) \mathbf{r}_{yb_d} represents the cross-correlation vector between \mathbf{y} and the desired bit $b_{1,ud}$, which is given by

$$\begin{aligned}\mathbf{r}_{yb_d} &= E[\mathbf{y}b_{1,ud}^H] \\ &= (\mathbf{I}_N \otimes \mathbf{C}_{11})\mathbf{h}_{ud} = \mathbf{h}_{ud}\end{aligned}\quad (9.233)$$

where the last equation is due to $\mathbf{C}_{11} = \mathbf{I}_{MW}$. Therefore, after substituting (9.232) and (9.233) into (9.231), the optimum weight matrix is given by

$$\mathbf{W}_0 = (\mathbf{h}_{ud}\mathbf{h}_{ud}^H + \Sigma)^{-1}\mathbf{h}_{ud}\quad (9.234)$$

Above, the MMSE detector is directly derived based on the observations \mathbf{y} of (9.221). This MMSE detector is practically implementable, since both \mathbf{R}_y and \mathbf{r}_{yb_d} can be estimated from the observations \mathbf{y} with the aid of only the desired user's information but without using the other users' information. However, for performance evaluation, the MMSE detection form of (9.230) is not very convenient, since, as shown in (9.206), it invokes the inversion of matrices having the dimensions of $NMW \times NMW$. For the sake of performance evaluation, the MMSE detector can in fact be derived based on (9.228). We note that the MMSE detector derived based on (9.228) may not be realizable on the downlink, since it requires the information of the orthogonal STS codes of all the K_1 users. However, in comparison with the MMSE detector of (9.230), the BER performance of the MMSE detector derived based on (9.228) may be more easily evaluated. Furthermore, as indicated in reference [88], both the MMSE detectors discussed above achieve the same BER performance.

An important advantage of using (9.228) for BER performance evaluation is that, according to (9.228), the d th data bit of the k th user conflicts interference only from the d th bit of an interfering user, since the mother codes of the same user are orthogonal. Hence, we can only consider the d th data bits of the K_1 users. Specifically, let $\mathbf{z}_d = [z_{1d}, z_{2d}, \dots, z_{K_1d}]^T$ and \mathbf{n}_d be the decision variable vector and the noise vector corresponding to the d th data bits of all the K_1 users. Then, \mathbf{z}_d can be expressed as

$$\mathbf{z}_d = \mathbf{R}\mathbf{b}_d + \mathbf{n}_d, \quad d = 1, 2, \dots, M \quad (9.235)$$

where $\mathbf{b}_d = [b_{1,ud}, b_{2,ud}, \dots, b_{K_1,ud}]^T$, while the correlation matrix \mathbf{R} is given by

$$\mathbf{R} = \begin{bmatrix} 1 & \eta_{21} & \cdots & \eta_{K_11} \\ \eta_{12} & 1 & \cdots & \eta_{K_12} \\ \vdots & \vdots & \ddots & \vdots \\ \eta_{1K_1} & \eta_{2K_1} & \cdots & 1 \end{bmatrix} \quad (9.236)$$

With the aid of (9.235), now we can easily show that the optimum weight vector for achieving the MMSE solution can be expressed as

$$\bar{\mathbf{W}}_0 = (\mathbf{R}^2 + \sigma^2 \mathbf{I}_{K_1})^{-1} \mathbf{R} \quad (9.237)$$

which is the same for any value of $d = 1, 2, \dots, M$. Finally, the decision variable for $\mathbf{b}_d = [b_{1,ud}, b_{2,ud}, \dots, b_{K_1,ud}]^T$ can be expressed as

$$\bar{\mathbf{z}}_d = \bar{\mathbf{W}}_0^T \mathbf{z}_d = \mathbf{R}(\mathbf{R}^2 + \sigma^2 \mathbf{I}_{K_1})^{-1} \mathbf{z}_d, \quad d = 1, 2, \dots, M \quad (9.238)$$

Let us now analyse the benchmark single-user BER performance bound of the multi-antenna MC DS-CDMA system.

9.6.3 Analysis of Single-User Bit-Error-Rate

The single-user BER bound may be achieved either when the multiantenna MC DS-CDMA system supports only one user, i.e. when $K = 1$, or when there are no two users sharing the same set of orthogonal mother codes, indicating $K_1 = 1$ and hence no MUI. As seen from the results in Section 9.6.4, from the benchmark BER performance, we can gain insight into the achievable BER performance of the multiantenna MC DS-CDMA system, when communicating over time-variant channels. According to (9.228), the conditional BER of the multiantenna MC DS-CDMA system supporting $K = 1$ user or corresponding to $K_1 = 1$ can be written as

$$P_b(\gamma) = Q(\sqrt{2\gamma}) \quad (9.239)$$

where $Q(x)$ is the Gaussian Q -function, while the instantaneous SNR γ is given by

$$\gamma = \left(\sum_{n=1}^N \sum_{m=1}^M \sum_{w=0}^{W-1} \frac{|h_{mnw}^{(w)}|^2}{\Omega} \right) \gamma_c \quad (9.240)$$

with $\gamma_c = \Omega E_b / MN N_0$.

Note that when the fading of the channel is sufficiently slow so that $|h_{mnw}^{(w)}|^2$ is independent of the index w , then the instantaneous SNR γ can be expressed as $\gamma = (\sum_{n=1}^N \sum_{m=1}^M |h_{mnw}|^2 / \Omega) \gamma'_c$ associated with $\gamma'_c = \Omega E_b / MN N_0$. In this case the multiantenna MC DS-CDMA system is capable of achieving a diversity order of MN . By contrast, when the fading of the channel is sufficiently fast resulting in $\{|h_{mnw}^{(w)}|^2\}$ in (9.240) being independent random variables with respect to the index w , then the multiantenna MC DS-CDMA system is capable of achieving a maximum diversity order of MNW . According to the above analysis, it can be expected that, when $\{|h_{mnw}^{(w)}|^2\}$ with respect to w maintain correlated but the channels become more time-selective, the BER performance of the single-user multiantenna MC DS-CDMA system will improve.

Due to the fact that $\{h_{mnw}^{(w)}\}$ are i.i.d. random variables with respect to the indices of m and n , (9.240) can be expressed as the sum of W number of correlated random variables, which can be expressed as

$$\gamma = \sum_{w=0}^{W-1} \gamma_w \quad (9.241)$$

where $\gamma_w = (\sum_{n=1}^N \sum_{m=1}^M |h_{mnw}^{(w)}|^2 / \Omega) \gamma_c$. Let us assume that $|h_{mnw}^{(w)}|$ obeys the Nakagami- m distribution and that $|h_{mnw}^{(w)}|^2$ has the PDF given by (5.2) in Chapter 5. Then, as shown in Section 9.4, γ_w obeys the *gamma distribution* with $2MNm$ degrees-of-freedom, which can be expressed with the PDF given by

$$f(\gamma_w) = \frac{1}{\Gamma(MN m)} \left(\frac{m}{\gamma_c} \right)^{MN m} \gamma_w^{MN m - 1} \exp\left(-\frac{m \gamma_w}{\gamma_c}\right), \quad \gamma_w \geq 0 \quad (9.242)$$

where m is the fading parameter of the Nakagami- m fading. It can be seen that $f(\gamma_w)$ is also a gamma distribution having the fading parameter $MN m$ and the second-order moment of $MN \gamma_c$.

Using the definition of $Q(x) = \pi^{-1} \int_0^{\pi/2} \exp(-x^2/2 \sin^2 \theta) d\theta$ [107], the average BER can be expressed as

$$\begin{aligned}
 P_b &= \underbrace{\int_0^\infty \cdots \int_0^\infty}_{W-\text{fold}} Q\left(\sqrt{2 \sum_{w=0}^{W-1} \gamma_w}\right) f(\gamma_0, \dots, \gamma_{W-1}) d\gamma_0 \dots d\gamma_{W-1} \\
 &= \underbrace{\int_0^\infty \cdots \int_0^\infty}_{W-\text{fold}} \frac{1}{\pi} \int_0^{\pi/2} \exp\left(-\sum_{w=0}^{W-1} \frac{\gamma_w}{\sin^2 \theta}\right) d\theta f(\gamma_0, \dots, \gamma_{W-1}) d\gamma_0 \dots d\gamma_{W-1} \\
 &= \frac{1}{\pi} \int_0^{\pi/2} \left[\underbrace{\int_0^\infty \cdots \int_0^\infty}_{W-\text{fold}} \exp\left(-\sum_{w=0}^{W-1} \frac{\gamma_w}{\sin^2 \theta}\right) f(\gamma_0, \dots, \gamma_{W-1}) d\gamma_0 \dots d\gamma_{W-1} \right] d\theta \\
 &= \frac{1}{\pi} \int_0^{\pi/2} E\left\{\exp\left(-\sum_{w=0}^{W-1} \frac{\gamma_w}{\sin^2 \theta}\right)\right\} d\theta
 \end{aligned} \tag{9.243}$$

In the above equation $f(\gamma_0, \dots, \gamma_{W-1})$ represents the joint PDF of the variables $\gamma_0, \dots, \gamma_{W-1}$, while $E\{\exp(-\sum_{w=0}^{W-1} \gamma_w/\sin^2 \theta)\}$ represents the expectation associated with $\exp(-\sum_{w=0}^{W-1} \gamma_w/\sin^2 \theta)$, which, according to [145], can be evaluated as

$$E\left\{\exp\left(-\sum_{w=0}^{W-1} \frac{\gamma_w}{\sin^2 \theta}\right)\right\} = \det\left(\mathbf{I}_W + \frac{\gamma_c}{m \sin^2 \theta} \mathbf{M}\right)^{-MNm} \tag{9.244}$$

where \mathbf{M} is the $(W \times W)$ covariance matrix of the ‘accompanying’ Gaussian distribution, which can be expressed as [145]

$$\mathbf{M} = \begin{bmatrix} 1 & \sqrt{\rho_{01}} & \cdots & \sqrt{\rho_{0(W-1)}} \\ \sqrt{\rho_{10}} & 1 & \cdots & \sqrt{\rho_{1(W-1)}} \\ \vdots & \vdots & \ddots & \vdots \\ \sqrt{\rho_{(W-1)0}} & \sqrt{\rho_{(W-1)1}} & \cdots & 1 \end{bmatrix} \tag{9.245}$$

where ρ_{ij} represents the correlation coefficient between $|h_{mn}^{(i)}|^2$ and $|h_{mn}^{(j)}|^2$, which can be expressed as $\rho_{ij} = J_0^2(2\pi f_D \Delta t_{ij})$ [131], where Δt_{ij} represents the time-spacing between $h_{mn}^{(i)}$ and $h_{mn}^{(j)}$, f_D is the Doppler-frequency shift, while $J_0(x)$ is the zero-order Bessel function of the first kind. Explicitly, we have $\rho_{ij} = \rho_{ji}$. Consequently, \mathbf{M} in (9.245) is a symmetric matrix.

Upon substituting (9.244) into (9.243), finally, the average single-user BER bound for the multiantenna MC DS-CDMA can be expressed as

$$P_b = \frac{1}{\pi} \int_0^{\pi/2} \det\left(\mathbf{I}_W + \frac{\gamma_c}{m \sin^2 \theta} \mathbf{M}\right)^{-MNm} d\theta \tag{9.246}$$

Furthermore, let $\{\lambda_w\}$ be the eigenvalues of \mathbf{M} . Then, the average BER of (9.246) can be alternatively expressed as

$$\begin{aligned} P_b &= \frac{1}{\pi} \int_0^{\pi/2} \prod_{w=0}^{W-1} \left(1 + \frac{\lambda_w \gamma_c}{m \sin^2 \theta} \right)^{-MNm} d\theta \\ &= \frac{1}{\pi} \int_0^{\pi/2} \prod_{w=0}^{W-1} \left(\frac{m \sin^2 \theta}{\lambda_w \gamma_c + m \sin^2 \theta} \right)^{MNm} d\theta \end{aligned} \quad (9.247)$$

which shows that, once we have known the covariance matrix \mathbf{M} of (9.245), the average single-user BER bound can be readily evaluated with the aid of (9.247).

Let us now consider two extreme cases. First, when the channel fading is sufficiently fast, resulting in that $\{\gamma_w\}$ in (9.243) are independent random variables obeying the common PDF of (9.242), then the average single-user BER bound can be expressed as

$$P_b = \frac{1}{\pi} \int_0^{\pi/2} \left(\int_0^\infty \exp\left(-\frac{\gamma_w}{m \sin^2 \theta}\right) f(\gamma_w) d\gamma_w \right)^W d\theta \quad (9.248)$$

When applying the PDF of (9.242) into the above equation, it can be shown that in this case the average single-user BER bound can be expressed as

$$P_b = \frac{1}{\pi} \int_0^{\pi/2} \left(\frac{m \sin^2 \theta}{\gamma_c + m \sin^2 \theta} \right)^{MNWm} d\theta \quad (9.249)$$

which, if $MNWm$ is an integer, according to [53, 107, 115], can be further simplified to

$$P_b = \left[\frac{1-\mu}{2} \right]^{MNWm} \sum_{k=0}^{MNWm-1} \binom{MNWm-1+k}{k} \left[\frac{1+\mu}{2} \right]^k \quad (9.250)$$

where $\mu = \sqrt{\gamma_c/(1+\gamma_c)}$. (9.250) shows that a diversity order of MNW can be achievable.

The second case is that, when the channel fading is sufficiently slow such that $\gamma_1 = \gamma_2 = \dots = \gamma_W$, then, the average single-user BER bound can be expressed as

$$P_b = \frac{1}{\pi} \int_0^{\pi/2} \left(\int_0^\infty \exp\left(-\frac{\gamma}{m \sin^2 \theta}\right) f(\gamma) d\gamma \right) d\theta \quad (9.251)$$

where γ also has the PDF of (9.242), but γ_c in (9.242) should now be replaced by $\gamma'_c = \Omega E_b / MN_0$. Following the same approach for deriving (9.250), it can be shown that in this case the average single-user BER bound can be expressed as

$$P_b = \frac{1}{\pi} \int_0^{\pi/2} \left(\frac{m \sin^2 \theta}{\gamma'_c + m \sin^2 \theta} \right)^{MNm} d\theta \quad (9.252)$$

Again, when MNm is an integer, (9.252) can be simplified to

$$P_b = \left[\frac{1-\mu'}{2} \right]^{MNm} \sum_{k=0}^{MNm-1} \binom{MNm-1+k}{k} \left[\frac{1+\mu'}{2} \right]^k \quad (9.253)$$

where $\mu' = \sqrt{\gamma'_c/(1 + \gamma'_c)}$. In this case, as shown in (9.252) and (9.253), the diversity order achievable is MN . Let us now show a range of performance results for characterizing the multiantenna MC DS-CDMA system.

Note that, when the Gaussian approximation [82] is invoked for approximating the MUI components in (9.226) as zero-mean additive Gaussian variables, the above-derived single-user BER bound expressions are then suitable for the BER evaluation of the general multiantenna MC DS-CDMA supporting multiple users. In this case, the average BER is also given by (9.247) or (9.250), but with γ_c given by $\gamma_c = [\sigma_{MUI}^2 + (\Omega E_b/MWN_0)^{-1}]^{-1}$, where σ_{MUI}^2 represents the variance of the MUI. However, due to the inaccuracy of the Gaussian approximation [88], in Section 9.6.4 our BER results for the multiuser multiantenna MC DS-CDMA were obtained by simulation. It is also worth mentioning that (9.253) is an accurate expression even when the multiantenna MC DS-CDMA supports multiple users. This is because, when the fading is sufficiently slow resulting in the fading over one symbol duration of T_s being constant, all the STS codes are orthogonal at the symbol level and hence there is no MUI.

As shown in Section 9.6.4, when there is MUI, the BER performance of the correlation detection-assisted multiantenna MC DS-CDMA degrades when the number of users sharing the same set of mother codes increases. In this case a MUD scheme may be used to suppress the MUI. As an example, in Section 9.6.4 the BER performance of the multiantenna MC DS-CDMA is investigated, when the MMSE-MUD is considered.

9.6.4 Performance Results

In this section we show some BER performance results of the multiantenna MC DS-CDMA, so as to demonstrate the effect of time-varying fading channels on the achievable BER. In this section only correlated Rayleigh fading channels are considered. A reader who is interested in the performance over the more general correlated Nakagami- m fading channels can obtain the BER performance results using the equations obtained in the previous sections or following the simulation method carried out in this section.

For convenience, the parameters used in the context of the multiantenna MC DS-CDMA, which are also shown in the following figures, are summarized as follows:

- $f_D T_s$: normalized Doppler frequency shift;
- U : number of branches after the S/P conversion;
- M : number of transmit antennas;
- N : number of receive antennas;
- N_t : number of bits per bit duration;
- V : length of the orthogonal mother codes;
- W : length of the orthogonal generating codes;
- K_1 : number of users sharing the same set of orthogonal mother codes.

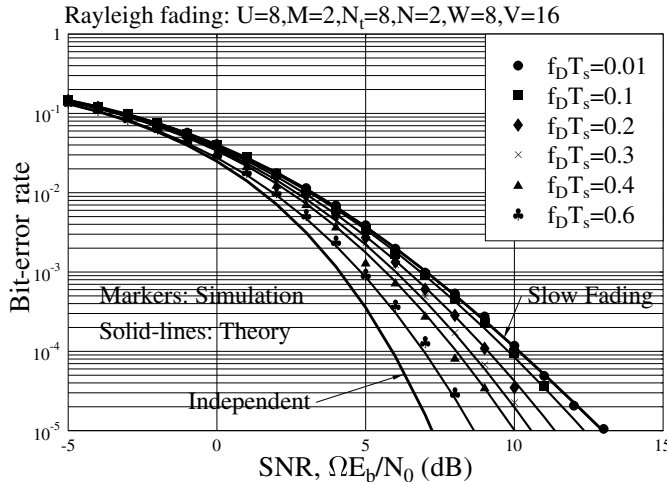


Figure 9.19: Single-user BER performance of the STS-assisted multiantenna MC DS-CDMA system using $M = 2$ transmit antennas and $N = 2$ receive antennas, when communicating over various fast fading channels. (Reproduced with permission from Lie-Liang Yang: ‘Performance of Multiantenna Multicarrier Direct-Sequence Code-Division Multiple-Access Using Orthogonal Variable Spreading Factor Codes Assisted Space–Time Spreading in Time-Selective Fading Channels’ from *IET Proceedings Communications*, Vol. 2, No. 5, pp. 708–719, May 2008. © Institution of Engineering & Technology.)

In Figs 9.19 and 9.20 we show the single-user BER bound of the multiantenna MC DS-CDMA system associated with various values of the normalized Doppler frequency shift f_{DT_s} , as shown in the figures. Specifically, in Fig. 9.19 we assume that the length of the orthogonal mother codes was $V = 16$ and that the length of the orthogonal generating codes was $W = 8$. By contrast, in Fig. 9.20 these parameters were assumed to be $V = 32$, $W = 16$. In both figures the solid lines were evaluated by (9.247) associated with their corresponding f_{DT_s} values, while the markers in Fig. 9.19 were obtained by simulation. From the results of Figs 9.19 and 9.20, we observe that even the slight time-selective fading may be exploited by the multiantenna MC DS-CDMA system, resulting in a significantly improved BER performance. For example, as seen in Figs 9.19 and 9.20, when the value of f_{DT_s} changes from 0.01, which corresponds to a nearly time non-selective fading channel, to 0.6 of slight time-selective fading channel, the SNR gain is 4.5 dB at the BER of 10^{-5} in Fig. 9.19 and is 6 dB at the BER of 10^{-5} in Fig. 9.20. Note that we imply here that $f_{DT_s} = 0.6$ is the slight time-selective fading, since in this case the number of resolvable paths due to the time-selectivity is only $[2f_{DT_s}] + 1 = 2$ [262]. When the channels are highly time-selective resulting in $\{\gamma_w\}$ seen in (9.241) being independent random variables, as shown in Figs 9.19 and 9.20, the SNR gains at the BER of 10^{-5} in Fig. 9.19 and of 10^{-5} in Fig. 9.20 are about 6 dB and 9 dB, respectively. Correspondingly, the number of resolvable paths due to the time-selective fading should be about 8 for Fig. 9.19 and 16 for Fig. 9.20.

In Fig. 9.21 the single-user BER versus normalized Doppler-frequency shift, f_{DT_s} , performance was evaluated, when $W = 8$, 16 or 32, and $V = 64$, 32 or 16. As shown in Fig. 9.21, the total spreading factor $UMN_t = WV$ was assumed to be a constant, which was

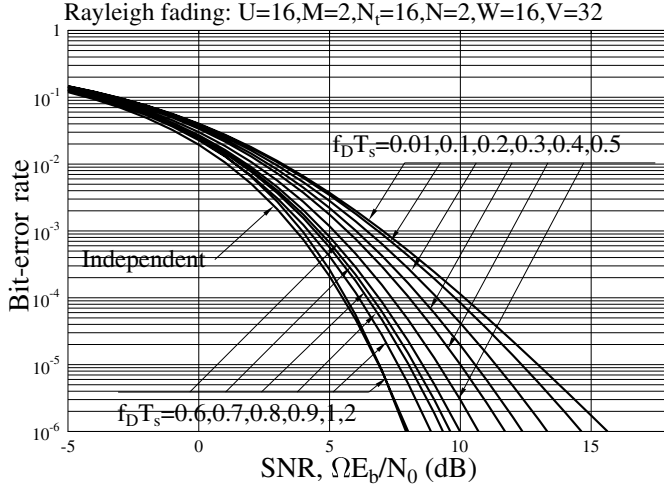


Figure 9.20: Single-user BER performance for the STS-assisted multiantenna MC DS-CDMA system using $M = 2$ transmit antennas and $N = 2$ receive antennas, when communicating over various fast fading channels. (Reproduced with permission from Lie-Liang Yang: 'Performance of Multiantenna Multicarrier Direct-Sequence Code-Division Multiple-Access Using Orthogonal Variable Spreading Factor Codes Assisted Space-Time Spreading in Time-Selective Fading Channels' from *IET Proceedings Communications*, Vol. 2, No. 5, pp. 708–719, May 2008. © Institution of Engineering & Technology.)

$UMN_t = WV = 512$. From the results in Fig. 9.21, we observe that when the normalized Doppler-frequency shift is lower than 0.5, the above-mentioned three types of scheme achieve a similar BER performance. However, as seen in Fig. 9.21, when the normalized Doppler-frequency shift is relatively high, such as $f_D T_s > 1$, usually a higher W value results in a lower BER. Note that the fluctuation of the BER curves seen in Fig. 9.21 is mainly because the Bessel function $J_0(x)$ of (9.245) does not monotonously decrease by increasing the value of x [131].

Figure 9.22 shows the single-user BER performance with respect to different settings of the values of V and W , when communicating over the time-selective fading channels having a normalized Doppler frequency shift of $f_D T_s = 0.5$ or $f_D T_s = 2$. As shown in Fig. 9.22, the length of the generating codes was assumed to be $W = 4, 8, 16$ or 32 , and correspondingly, the length of the mother codes was $V = 128, 64, 32$ and 16 . From the results of Fig. 9.22 we observe that, except $W = 4, V = 128$, all the other cases considered achieve a similar BER performance, when the normalized Doppler frequency shift is $f_D T_s = 0.5$, implying a relatively slow fading channel. By contrast, when $f_D T_s = 2$, which corresponds to a relative fast fading channel, the BER performance improves when the value of W increases from $W = 4$ to $W = 8$ and further to 16 . However, there is no further improvement when increasing the value of W from $W = 16$ to $W = 32$. The above observations imply that when $f_D T_s = 0.5$, the length of the generating codes should at least be set to $W = 8$, in order to achieve the full diversity gain resulting from the time-selective fading. However, when $f_D T_s = 2$, the length of the generating codes should then be set to $W = 16$ at the lowest, in order to achieve the full time-selective diversity gain.

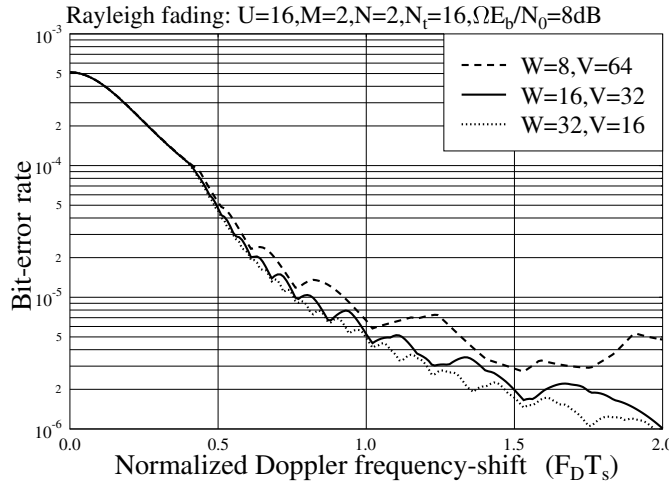


Figure 9.21: Single-user BER bound versus normalized Doppler frequency shift $f_D T_s$ for the STS-assisted multiantenna MC DS-CDMA system using $M = 2$ transmit antennas and $N = 2$ receive antennas, when assuming various lengths of orthogonal mother and generating codes, while maintaining $WV = 512$. (Reproduced with permission from Lie-Liang Yang: ‘Performance of Multiantenna Multicarrier Direct-Sequence Code-Division Multiple-Access Using Orthogonal Variable Spreading Factor Codes Assisted Space–Time Spreading in Time-Selective Fading Channels’ from *IET Proceedings Communications*, Vol. 2, No. 5, pp. 708–719, May 2008. © Institution of Engineering & Technology.)

Note that when a system supporting multiple users is considered, the single-user BER performance shown in Figs 9.21 and 9.22 may be achieved, when advanced MUD is invoked for detection. However, according to the MUD principles discussed in Chapter 6 and our previous analysis, the complexity of the MUD for the multiantenna MC DS-CDMA is determined by the length, W of the orthogonal generating codes. The complexity becomes higher when the value of W is higher. Hence, from the results of Figs 9.21 and 9.22, we know that the length of W and V should be adjusted to correspond to the Doppler frequency shift or the fading rate, in order to achieve the highest achievable diversity gain but at the lowest cost for detection. Given WV a constant, a relatively low W value may be utilized to reduce the implementation complexity, when the normalized Doppler-frequency shift is low. By contrast, when the normalized Doppler-frequency shift becomes higher, a relatively higher W value is then required in order to achieve the resulting higher diversity gain.

In Fig. 9.23 we investigated the BER performance of the correlation based SUD, when in the multiantenna MC DS-CDMA system there are $K_1 = 8$ users sharing the same set of orthogonal mother codes. Specifically, in our simulations the normalized Doppler-frequency shift was assumed to be $f_D T_s = 0.01, 0.1, 0.2, 0.3, 0.4, 0.6$. Furthermore, Fig. 9.23 also shows the BER curve, when each of the W fractions experienced independent fading. As expected, the results of Fig. 9.23 show that the BER performance degrades when the normalized Doppler-frequency shift increases, i.e. when the channel fading becomes more time-selective. This is because, as the channel fading becomes more time-selective, the

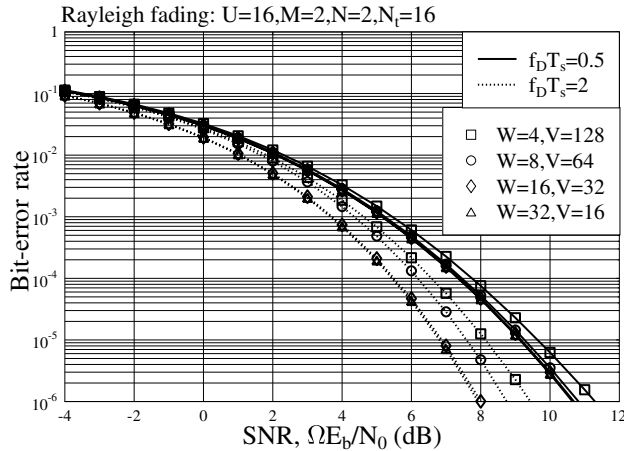


Figure 9.22: Single-user BER performance of the STS-assisted multiantenna MC DS-CDMA system using $M = 2$ transmit antennas and $N = 2$ receive antennas, when communicating over the time-selective fading channels having a normalized Doppler frequency of $f_D T_s = 0.5$ or $f_D T_s = 2$. (Reproduced with permission from Lie-Liang Yang: ‘Performance of Multiantenna Multicarrier Direct-Sequence Code-Division Multiple-Access Using Orthogonal Variable Spreading Factor Codes Assisted Space–Time Spreading in Time-Selective Fading Channels’ from *IET Proceedings Communications*, Vol. 2, No. 5, pp. 708–719, May 2008. © Institution of Engineering & Technology.)

orthogonality of the generating codes is destroyed to a greater degree, resulting in higher MUI. Consequently, when the multiantenna MC DS-CDMA system supports multiple users, the BER performance improvement from the time-selective diversity is overwhelmed by the BER performance degradation due to the time-selectivity resulting MUI. Hence, when the channel fading becomes highly time-selective, MUI suppression is necessary in order to enhance the achievable BER performance.

Therefore, in Fig. 9.24 we investigated the BER performance of the MMSE based MUD, when $K_1 = 8$ users shared the same set of orthogonal mother codes. Note that all the simulations parameters of Fig. 9.24 were the same as those for Fig. 9.23. Explicitly, when the MMSE-based MUD is used, the MUI can be mitigated efficiently. As shown by the results of Fig. 9.24, the BER performance tendency is similar to that in Fig. 9.19, which improves when the normalized Doppler-frequency increases.

Without doubt, when the more advanced maximum likelihood MUD is used, the near single-user BER performance as shown in Figs 9.19 and 9.21 can then be achieved.

9.6.5 Conclusions

In this section a downlink multiantenna MC DS-CDMA system using OVSF-codes-assisted-STS has been designed and investigated, when communicating over fast time-selective fading channels. The performance results show that the multiantenna MC DS-CDMA using OVSF-codes-assisted-STS is a high-efficiency downlink space–time transmission

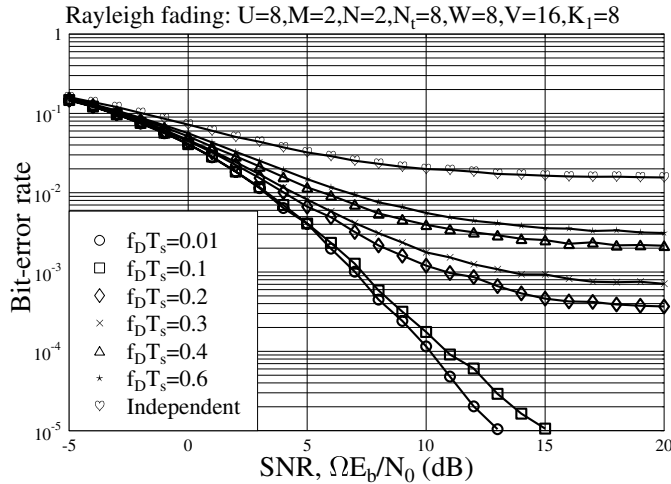


Figure 9.23: BER versus average SNR per bit performance for the STS-assisted multiantenna MC DS-CDMA system using correlation-based SUD, when communicating over time-selective Rayleigh fading channels having different values of normalized Doppler frequency. (Reproduced with permission from Lie-Liang Yang: ‘Performance of Multiantenna Multicarrier Direct-Sequence Code-Division Multiple-Access Using Orthogonal Variable Spreading Factor Codes Assisted Space-Time Spreading in Time-Selective Fading Channels’ from *IET Proceedings Communications*, Vol. 2, No. 5, pp. 708–719, May 2008. © Institution of Engineering & Technology.)

scheme. This space–time transmission scheme is capable of achieving time diversity owing to time-selective fading, in addition to achieving full transmit/receive diversity. It has been shown that even the slight time-selectivity of wireless channels may be exploited in order to significantly enhance the achievable BER performance of the multiantenna MC DS-CDMA system. Furthermore, the study shows that the length of the orthogonal generating codes and mother codes should be adjusted to correspond with the Doppler frequency shift or the fading rate of the wireless channels, in order to achieve the highest achievable diversity gain but at the lowest cost for detection. Specifically, given that the spreading factor of the system is a constant, relatively short generating codes may be utilized to reduce the implementation complexity, when the normalized Doppler-frequency shift is low. When the normalized Doppler-frequency shift becomes higher, then relatively longer generating codes are required in order to achieve a higher diversity gain.

Note that although for simplicity the frequency-diversity has not been considered in the context of the multiantenna MC DS-CDMA, however, as mentioned in Section 9.6.1.1, in the considered multiantenna MC DS-CDMA system the frequency diversity can be achieved by transmitting the same space–time signal on several subcarriers. Hence, the proposed space–time transmission scheme is capable of simultaneously exploiting both the frequency-selectivity and time-selectivity of the wireless channels, while achieving full spatial-diversity.

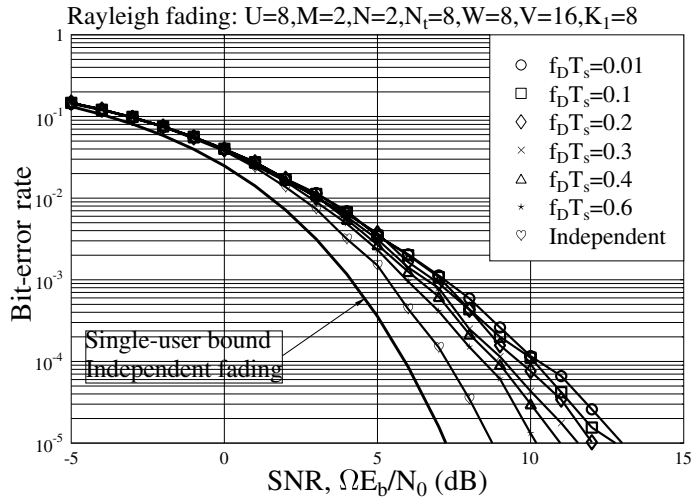


Figure 9.24: BER versus average SNR per bit performance for the STS-assisted multiantenna MC DS-CDMA system using MMSE MUD, when communicating over time-selective Rayleigh fading channels having different values of normalized Doppler frequency. (Reproduced with permission from Lie-Liang Yang: ‘Performance of Multiantenna Multicarrier Direct-Sequence Code-Division Multiple-Access Using Orthogonal Variable Spreading Factor Codes Assisted Space–Time Spreading in Time-Selective Fading Channels’ from *IET Proceedings Communications*, Vol. 2, No. 5, pp. 708–719, May 2008. © Institution of Engineering & Technology.)

9.7 Summary and Discussion

In this chapter we have explored the theory of MIMO communications and the space–time processing techniques. Furthermore, three typical multiantenna multicarrier CDMA schemes have been investigated associated with various space–time processing schemes, in order to illustrate the impact of space–time processing on the performance enhancement of these multicarrier CDMA systems. From the study and performance results provided in this chapter, we may need to be aware of the following issues in MIMO wireless communications.

First, in theory the performance of MIMO systems is maximized, when the MIMO channels experience independent fading. In practice, however, highly independent fading channels usually demand highly complex techniques for channel estimation and/or prediction.

Second, a MIMO system with CSI known to the transmitter usually significantly outperforms a corresponding MIMO system without using CSI at the transmitter. For example, the capacity of the MIMO system with the CSI known to both the transmitter and receiver can be significantly higher than that of the corresponding MIMO system, where the CSI is only known to the receiver. Also, for a given number of transmit antennas, the closed-loop transmit diversity scheme can often achieve a higher diversity gain than the corresponding open-loop transmit diversity scheme. Hence, in wireless communications high-efficiency techniques for the transmitters to acquire CSI are very important. In Section 8.5 of Chapter 8, different techniques for the extraction of transmitter CSI were explored. One point of which we may need to be aware is that extraction of

transmitter CSI often results in trade-off of bandwidth, power and complexity. In practice, low-complexity, high-efficiency transmitter preprocessing schemes depending only on partial transmitter CSI may be highly attractive.

Third, this chapter has shown that STC and STS can be unified to one generalized space-time coding (GSTC) scheme. Hence, one straightforward question is that in space-time spread-spectrum communications, such as in space-time MC-CDMA systems, does there exist some (open-loop) space-time processing schemes that are more efficient than the existing STS scheme, so that they are capable of achieving certain coding gains, in addition to the full-diversity gains?

Finally, it is worth mentioning that when considering the parallel transmission scenarios, such as in OFDM, further research might be required in order to develop the communications schemes that can make efficient use of both the frequency-selectivity and time-selectivity of wireless channels.

Bibliography

- [1] Lee, W. C. Y. (2002) The most spectrum-efficient duplexing system: CDD. *IEEE Communications Magazine*, **3**(3), 163–6, March.
- [2] Proakis, J. G. (1995) *Digital Communications*, 3rd edn. McGraw-Hill: New York, USA.
- [3] Simon, M. K., Omura, J. K., Scholtz, R. A. and Levitt, B. K. (1985) *Spread Spectrum Communications: Volume I*, Computer Science Press: Maryland, USA.
- [4] Simon, M. K., Omura, J. K., Scholtz, R. A. and Levitt, B. K. (1985) *Spread Spectrum Communications: Volume II*, Computer Science Press: Maryland, USA.
- [5] Simon, M. K., Omura, J. K., Scholtz, R. A. and Levitt, B. K. (1985) *Spread Spectrum Communications: Volume III*, Computer Science Press: Maryland, USA.
- [6] Ziener, R. E. and Peterson, R. L. (1985) *Digital Communications and Spread Spectrum Systems*, Macmillan Publishing Company: New York, USA, Collier Macmillan: London, U.K. Publishers.
- [7] Lee, J. S. and Miller, L. E. (1998) *CDMA Systems Engineering Handbook*, Artech House: Boston-London.
- [8] Viterbi, A. J. (1995) *Principle of Spread Spectrum Multiple Access Communications*, Addison-Wesley: New York, USA.
- [9] Geraniotis, E. A. (1985) Coherent hybrid DS-SFH spread-spectrum multiple-access communications. *IEEE Journal on Selected Areas in Communications*, **3**(5), 695–705, September.
- [10] Geraniotis, E. A. (1986) NonCoherent hybrid DS-SFH spread-spectrum multiple-access communications. *IEEE Transactions on Communications*, **34**(9), 862–72, September.
- [11] Liu, T., Li, E. and Xiang, H. (1998) *A Hybrid TH/DS Spread Spectrum System Supporting Multirate Services*. Proceedings of IEEE International Symposium on Spread Spectrum Techniques and Applications, **1**, 309–13, 2–4 September.
- [12] Polydoros, A. and Weber, C. (1985) Detection Performance Considerations for Direct-Sequence and Time-Hopping LPI Waveforms. *IEEE Journal on Selected Areas in Communications*, **3**(5), 727–44, September.
- [13] Goodman, D. J., Henry, P. S. and Prabhu, V. K. (1980) Frequency-hopped multilevel FSK for mobile radio. *The Bell System Technical Journal*, **59**(7), 1257–75, September.
- [14] Blogh, J. and Hanzo, L *Third-Generation Systems and Intelligent Wireless Networking: Smart Antennas and Adaptive Modulation*, John Wiley & Sons – IEEE Press, 2002.
- [15] Gui, X. and Ng, T. S. (1999) Performance of asynchronous orthogonal multicarrier CDMA system in frequency selective fading channel. *IEEE Transactions on Communications*, **47**(7), 1084–91, July.
- [16] Tomba, L. and Krzymien, W. A. (1996) Downlink detection schemes for MC-CDMA systems in indoor environments. *IEICE Transactions on Communications*, **E79-B**(9), 1351–60, September.
- [17] Leam, A. W. and Sarwate, D. P. Time-hopping and frequency-hopping multiple-access packet communications. *IEEE Transactions on Communications*, **38**(6), 875–88, June.

- [18] Wittman, J. H. (1968) Analysis of a hybrid frequency-time hopping random-access satellite communication system. *IEEE Transactions on Communications Technology*, **COM-16**(2), 303–10, April.
- [19] Abeta, S., Atarashi, H. et al. (2000) *Coherent Multicarrier/DS-CDMA and MC-CDMA for Broadband Packet Wireless Access*. Proceedings of IEEE VTC'2000-Spring, Vol. 3, pp. 1918–22.
- [20] Ramirez-Mireles, F. (2001) Performance of ultrawideband SSMA using time hopping and M -ary PPM. *IEEE Journal on Selected Areas in Communications*, **19**(6), 1186–96, June.
- [21] Win, M. Z. and Scholtz, R. A. (2000) Ultra-wide bandwidth time-hopping spread-spectrum impulse radio for wireless multiple-access communications. *IEEE Transactions on Communications*, **48**(4), 679–91,
- [22] Yang, L. L. and Hanzo, L. (2002) Residue number system assisted fast frequency-hopped synchronous ultra-wideband spread-spectrum multiple-access: a design alternative to impulse radio. *IEEE Journal on Selected Areas in Communications*, **20**(9), 1652–63, December.
- [23] Hara, S. and Prasad, R. (1997) Overview of multicarrier CDMA. *IEEE Communications Magazine*, **35**(12), 126–33, December.
- [24] Enge, P. K. and Sarwate, D. P. (1987) Spread-spectrum multiple-access performance of orthogonal codes: Linear receivers. *IEEE Transactions on Communications*, **35**(12), 1309–19, December.
- [25] Jalloul, L. M. A. and Holtzman, J. M. (1994) Performance analysis of DS/CDMA with noncoherent M -ary orthogonal modulation in multipath fading channels. *IEEE Journal on Selected Areas in Communications*, **12**(5), 862–70, June.
- [26] Bird, J. S. and Felstead, E. B. (1986) Antijam performance of fast frequency-hopped M -ary NCFSK – An overview. *IEEE Journal on Selected Areas in Communications*, **4**(2), 216–33, March.
- [27] Bingham, J. A. C. (1990) Multicarrier modulation for data transmission: An idea whose time has come. *IEEE Communications Magazine*, 5–14, May.
- [28] Kalet, I. (1989) The multitone channel. *IEEE Transactions on Communications*, **37**(2), 119–24, February.
- [29] Weinstein, S. B. and Ebert, P. M. (1971) Data transmission by frequency-division multiplexing using the discrete Fourier transform. *IEEE Transactions on Communication Technology*, **COM-19**(5), 628–34, October.
- [30] Hanzo, L., Webb, W. and Keller, T. (1999) *Single- and Multi-carrier Quadrature Amplitude Modulation: Principles and Applications for Personal Communications, WLANs and Broadcasting*, 2nd edn. IEEE Press and John Wiley & Sons: London, UK.
- [31] Chouly, A., Brajal, A. and Jourdan, S. (1993) *Orthogonal Multicarrier Techniques Applied to Direct Sequence Spread Spectrum CDMA Systems*. Proceedings of IEEE GLOBECOM'1993, Vol. 3, pp. 1723–8.
- [32] Popovic, B. M. (1998) *Spreading Waveforms for Multi-carrier CDMA Systems*. IEEE International Symposium on Spread Spectrum Techniques and Applications, **1**, 205–9.
- [33] Yee, N. and Linnartz, J.-P. (1993) *BER of Multi-carrier CDMA in an Indoor Rician Fading Channel*. Proceedings of The Asilomar Conference on Signals, Systems and Computers, **1**, 426–30.
- [34] Yee, N., Linnartz, J.-P. and Fettweis, G. (1994) Multi-carrier CDMA in indoor wireless radio network. *IEICE Transactions on Communications*, **E77-B**(7), 900–4.
- [35] Kim, Y. H., Song, I. et al. (2000) Design and performance analysis of a convolutionally coded overlapping multicarrier DS/CDMA system. *IEEE Transactions on Vehicular Technology*, **49**(5), 1950–67, September.
- [36] Kondo, S. and Milstein, L. B. (1993) *On the Use of Multicarrier Direct Sequence Spread Spectrum Systems*. Proceedings of IEEE MILCOM'93, Boston, MA, USA, pp. 52–6, October.
- [37] Kondo, S. and Milstein, L. B. (1996) Performance of multicarrier DS CDMA systems. *IEEE Transactions on Communications*, **44**(2), 238–46, February.
- [38] Dasilva, V. M. and Sousa, E. S. (1993) *Performance of Orthogonal CDMA Codes for Quasi-synchronous Communication Systems*. Proceedings of IEEE ICUPC'93, Ottawa, Canada, pp. 995–9.
- [39] Dasilva, V. M. and Sousa, E. S. (1994) Multicarrier orthogonal CDMA signals for quasi-synchronous communication systems. *IEEE Journal on Selected Areas in Communications*, **12**(5), 842–52, June.
- [40] Matsutani, H., Sanada, Y. and Nakagawa, M. (1997) Orthogonalization using multicarrier pre-decorrelation in a multipath fading channel. *IEICE Transactions on Fundamentals*, **E80-A**(12), 2470–6, December.

- [41] Sourour, E. A. and Nakagawa, M. (1996) Performance of orthogonal multicarrier CDMA in a multipath fading channel. *IEEE Transactions on Communications*, **44**(3), 356–67, March.
- [42] Sousa, E. S. (1993) Performance of a direct sequence spread spectrum multiple access system utilizing unequal carrier frequencies. *IEICE Transactions on Communications*, **E76-B**(8), 906–12, August.
- [43] Vandendorpe, L. (1995) Multitone spread spectrum multiple access communications system in a multipath Rician fading channel. *IEEE Transactions on Vehicular Technology*, **44**(2), 327–37, May.
- [44] Vandendorpe, L. and Van de Wiel, O. (1996) MIMO DFE equalization for multitone DS/SS systems over multipath channels. *IEEE Journal on Selected Areas in Communications*, **14**(3), 502–11, April.
- [45] Vandendorpe, L. and Van de Wiel, O. (1997) Fractionally spaced decision feedback joint detection for multitone CDMA systems. *IEEE Transactions on Communications*, **45**(8), 906–9, August.
- [46] Chen, Q., Sousa, E. S. and Pasupathy, S. (1996) Multicarrier CDMA with adaptive frequency hopping for mobile radio systems. *IEEE Journal on Selected Areas in Communications*, **14**(9), 1852–8, December.
- [47] Kim, Y. H., Song, I. et al. (1999) *An Adaptive Multicarrier DS/CDMA System for Forward Links*. Proceedings of IEEE MILCOM'1999, Vol. 2, pp. 1095–9.
- [48] Kim, Y. H., Song, I., Yoon, S. and Park, S. R. (1999) A multicarrier CDMA system with adaptive subchannel allocation for forward links. *IEEE Transactions on Vehicular Technology*, **48**(5), 1428–36, September.
- [49] Yang, L. L. and Hanzo, L. (1999) *Blind Joint Soft-detection Assisted Slow Frequency-hopping Multicarrier DS-CDMA*. Proceedings of IEEE GLOBECOM, Rio de Janeiro, Brazil, pp. 842–6, December.
- [50] Yang, L. L. and Hanzo, L. (2000) Blind joint soft-detection assisted slow frequency-hopping multicarrier DS-CDMA. *IEEE Transactions on Communications*, **48**(9), 1520–9, September.
- [51] Yang, L. L. and Hanzo, L. (2001) Slow frequency-hopping multicarrier DS-CDMA for transmission over Nakagami multipath fading channels. *IEEE Journal on Selected Areas in Communications*, **19**(7), 1211–21, July.
- [52] Yang, L. L. and Hanzo, L. (2001) *Multirate Transmission in Frequency-hopping Multicarrier Direct Sequence Code Division Multiple Access Systems*. Proceedings of IEEE VTC'2001-Fall, Vol. 1, pp. 52–6.
- [53] Yang, L. L. and Hanzo, L. (2002) Performance of generalized multicarrier DS-CDMA over Nakagami-m fading channels. *IEEE Transactions on Communications*, **50**(6), 956–66, June.
- [54] Yang, L. L. and Hanzo, L. (2003) Multicarrier DS-CDMA: A multiple-access scheme for ubiquitous broadband wireless communications. *IEEE Communications Magazine*, **41**(10), 116–24.
- [55] Yang, L. L., Hua, W. and Hanzo, L. (2003) *Multiuser Detection in Multicarrier CDMA Systems Employing both Time-Domain and Frequency-Domain Spreading*. Proceedings of IEEE PIMRC'2003, Beijing, China, 7–10 September.
- [56] Yang, L. L., Hua, W. and Hanzo, L. (2003) *A Multicarrier DS-CDMA System using both Time-domain and Frequency-domain Spreading*. Proceeding of IEEE VTC'2003 Fall, Orlando, USA, 6–9 October.
- [57] Paterson, K. G. and Tarokh, V. (2000) On the existence and construction of good codes with low peak-to-average power ratios. *IEEE Transactions on Information Theory*, **46**(6), 1974–87, September.
- [58] Tarokh, V. and Jafarkhani, H. (2000) On the computation and eduction of the peak-to-average power ratio in multicarrier communications. *IEEE Transactions on Communications*, **48**(1), 37–44, January.
- [59] Benvenuto, N. and Tomasin, S. (2002) On the comparison between OFDM and single-carrier modulation with a DFE using a frequency-domain feedforward filter. *IEEE Transactions on Communications*, **50**(6), 947–55, June.
- [60] Frank, T., Klein, A. and Costa, E. (2007) IFDMA: A scheme combining the advantages of OFDMA and CDMA. *IEEE Wireless Communications*, 9–17, June.
- [61] Horlin, F. et al. (2008) Single-carrier FDMA or cyclic-prefix CDMA with optimized spreading sequences? *IEEE Transactions on Vehicular Technology*, accepted for publication.
- [62] Myung, H. G., Lim, J. and Goodman, D. J. (2006) Single-carrier FDMA for uplink wireless transmission. *IEEE Vehicular Technology Magazine*, 30–8, September.
- [63] Myung, H. G., Lim, J. and Goodman, D. J. (2006) *Peak-to-average Power Ratio of Single-carrier FDMA Signals with Pulse Shaping*. IEEE PIMRC'06, Helsinki, Finland, September.

- [64] Sorger, U., Broeck, I. De and Schnell, M. (1998) *Interleaved FDMA: A New Spread Spectrum Multiple-access Scheme*. Proceedings of IEEE ICC'98, **2**, 1013–7.
- [65] Proakis, J. G. and Manolakis, D. G. (1996) *Digital Signal Processing: Principles, Algorithms, and Applications*, 3rd edn. Prentice-Hall: New Jersey, USA.
- [66] Ruiz, A., Cioffic, J. M. and Kasturia, A. (1992) Discrete multiple tone modulation with Coset coding for the spectral shaped channel. *IEEE Transactions on Communications*, **40**(6), 1012–9, June.
- [67] Popovic, B. M. (1999) Spreading sequences for multicarrier CDMA systems. *IEEE Transactions on Communications*, **47**(6), 918–26, June.
- [68] Sanada, Y. and Nakagawa, M. (1996) A multiuser interference cancellation technique utilizing convolutional codes and orthogonal multicarrier modulation for wireless indoor communications. *IEEE Journal on Selected Areas in Communications*, **14**(8), 1500–9, October.
- [69] Atarashi, H. and Nakagawa, M. (1998) A computational cost reduction scheme for a post distortion type nonlinear distortion compensator of OFDM. *IEICE Transactions on Communications*, **E81-B**(12), 2334–42, December.
- [70] Hanzo, L., Munster, M., Choi, B. J. and Keller, T. (2003) *OFDM and MC-CDMA for Broadband Multi-user Communications, WLANs and Broadcasting*. IEEE Press and John Wiley & Sons: London, UK.
- [71] Hanzo, L., Yang, L.-L., Kuan, E.-L. and Yen, K. (2003) *Single- and Multi-Carrier DS-CDMA – Multiuser Detection, Space-Time Spreading, Synchronisation and Standards*. John Wiley & Sons, IEEE Press.
- [72] Jeon, W. G., Chang, K. H. and Cho, Y. S. (1997) An adaptive data predistorter for compensation of nonlinear distortion in OFDM systems. *IEEE Transactions on Communications*, **45**(10), 1167–71, October.
- [73] Jong, J.-H. and Stark, W. E. (1999) *Power-controlled MC-CDMA in the Presence of Nonlinearities. I. System Analysis*. Proceedings of IEEE VTC'1999-Fall, **1**, 238–42.
- [74] Jong, J.-H. and Stark, W. E. (1999) *Power-controlled MC-CDMA in the Presence of Nonlinearities. II. Coded System Performance*. Proceedings of IEEE MILCOM'1999, **1**, 172–6.
- [75] Kang, H. W., Cho, Y. S. and Youn, D. H. (1999) On compensating nonlinear distortions of an OFDM system using an efficient adaptive predistorter. *IEEE Transactions on Communications*, **47**(4), 522–6, April.
- [76] Ohkawa, M., Wakana, H. and Kohno, R. (1999) Performance of orthogonal multi-carrier FH-CDMA system in the presence of selective fading and nonlinear amplification. *IEICE Transactions on Fundamentals*, **E82-A**(12), 2649–59, December.
- [77] Ochiai, H. and Imai, H. (1998) *OFDM-CDMA with Peak Power Reduction Based on the Spreading Sequences*. Proceedings of IEEE ICC'1998, Vol. 3, pp. 1299–303.
- [78] Ohkubo, N. and Ohtsuki, T. (2002) *A Peak to Average Power Ratio Reduction of Multicarrier CDMA Using Selected Mapping*. Proceedings of IEEE VTC'2002-Fall, Vol. 4, pp. 2086–90.
- [79] Shepherd, S., Orriss, J. and Barton, S. (1998) Asymptotic limits in peak envelope power reduction by redundant coding in orthogonal frequency-division multiplex modulation. *IEEE Transactions on Communications*, **46**(1), 5–10, January.
- [80] Wulich, D. and Goldfeld, L. (1999) Reduction of peak factor in orthogonal multicarrier modulation by amplitude limiting and coding. *IEEE Transactions on Communications*, **47**(1), 18–21, January.
- [81] Yamasaki, S. and Tanaka, H. (1998) A nonlinear distortion compensation on layered multicarrier modulation using iterative restoration. *IEICE Transactions on Fundamentals*, **E81-A**(10), 2109–16, October.
- [82] Pursley, M. B. (1977) Performance evaluation for phase-coded spread-spectrum multiple-access communications – Part I: System analysis. *IEEE Transactions on Communications*, **25**(7), 795–9, August.
- [83] Yang, L. L. and Hanzo, L. (2003) Performance of generalized multicarrier DS-CDMA using various chip waveforms. *IEEE Transactions on Communications*, **51**(5), 748–52, May.
- [84] Yang, L. L. and Hanzo, L. (2001) *A Unified Approach to the Analysis of Multicarrier DS-CDMA over Nakagami-m Fading Channels*. Proceedings of IEEE Globecom 2001 Conference, San Antonio, Texas, USA, pp. 3429–33, November.
- [85] Yang, L. L. and Hanzo, L. (2003) *Generalized Multicarrier DS-CDMA using Various Chip Waveforms*. Proceedings of the IEEE WCNC'2003, New Orleans, Louisiana, USA, 16–20 March.

- [86] Fiebig, U.-C. G. (1996) Iterative interference cancellation for FFH/MFSK MA systems. *IEE Proceedings Communications*, **143**, 380–8, December.
- [87] Halford, K. W. and Brandt-Pearce, M. (2000) Multistage multiuser detection for FHMA. *IEEE Transactions on Communications*, **48**(9), 1550–62, September.
- [88] Verdu, S. (1998) *Multiuser Detection*, Cambridge University Press: Cambridge, U.K.
- [89] Trees, H. L. V. (2002) *Optimum Array Processing: Part V of Detection, Estimation, and Modulation Theory*, John Wiley & Sons: New York.
- [90] Wang, X. and Poor, H. V. (2003) *Wireless Communication Systems – Advanced Techniques for Signal Reception*, Prentice-Hall.
- [91] Simon, M. K., Hinedi, S. M. and Lindsey, W. C. (1995) *Digital Communication Techniques – Signal Design and Detection*, Prentice-Hall: New Jersey, USA.
- [92] Yang, L. L. and Hanzo, L. (2002) *Broadband MC DS-CDMA using Space-time and Frequency-domain Spreading*. Proceedings of IEEE VTC'2002, Fall, Vancouver, British Columbia, Canada, pp. 1632–6, September.
- [93] Morrow, R. K. and Lehnert, J. S. (1989) Bit-to-bit error dependence in slotted DS/SSMA packet system with random signature sequences. *IEEE Transactions on Communications*, **COM-37**(10), 1052–61, October.
- [94] Rappaport, T. S. (1996) *Wireless Communications Principles and Practice*, Prentice-Hall: New York, USA.
- [95] Holtzman, J. M. (1992) A simple, accurate method to calculate spread-spectrum multiple-access error probabilities. *IEEE Transactions on Communications*, **40**(3), 461–4, March.
- [96] Walzman, T. and Schwartz, M. (1973) Automatic equalization using the discrete Fourier domain. *IEEE Transactions on Information Theory*, **19**, 59–68, January.
- [97] Sari, H., Karam, G. and Jeanclaude, I. (1995) Transmission techniques for digital terrestrial TV broadcasting. *IEEE Communications Magazine*, 100–9, February.
- [98] Adachi, F., Garg, D., Takaoka, S. and Takeda, K. (2005) Broadband CDMA techniques. *IEEE Wireless Communications*, 8–18, April.
- [99] Adachi, F., Sao, T. and Itagaki, T. (2003) Performance of multicode DS-CDMA using frequency domain equalization in frequency selective fading channel. *Electronics Letters*, **39**(2), 239–41, January.
- [100] Falconer, D. *et al.* Frequency domain equalization for single-carrier broadband wireless systems. *IEEE Communications Magazine*, 58–66, April.
- [101] Garg, D. and Adachi, F. (2006) Packet access using DS-CDMA with frequency-domain equalization. *IEEE Journal on Selected Areas in Communications*, **24**(1), 161–70, January.
- [102] Liu, L. and Adachi, F. (2006) Joint frequency-domain differential detection and equalization for DS-CDMA signal transmissions in a frequency-selective fading channel. *IEEE Journal on Selected Areas in Communications*, **24**(3), 649–58, March.
- [103] Takeda, K. and Adachi, F. (2007) Frequency-domain interchip interference cancellation for DS-CDMA downlink transmission. *IEEE Transactions on Vehicular Technology*, **56**(3), 1286–94, May.
- [104] Wang, Y. and Dong, X. (2006) A time-division multiple-access SC-FDE system with IBI suppression for UWB communications. *IEEE Journal on Selected Areas in Communications*, **24**(4), 920–6, April.
- [105] Wang, Y., Dong, X., Wittke, P. H. and Mo, S. (2006) Cyclic prefixed single carrier transmission in ultra-wideband communications. *IEEE Transactions on Wireless Communications*, **5**(8), 2017–21, August.
- [106] Zhu, Y. and Letaief, K. B. (2006) Single carrier frequency domain equalization with time domain noise prediction for wideband wireless communications. *IEEE Transactions on Wireless Communications*, **5**(12), 3548–57, December.
- [107] Alouini, M.-S. and Goldsmith, A. J. (1999) A unified approach for calculating error rates of linearly modulated signals over generalized fading channels. *IEEE Transactions on Communications*, **47**, 1324–34, September.
- [108] Nakagami, N. (1960) The m -distribution, a general formula for intensity distribution of rapid fading, in *Statistical Methods in Radio Wave Propagation*, ed. W. G. Hoffman, Oxford, England: Pergamon.

- [109] Simon, M. K. and Alouini, M.-S. (2000) *Digital communication over Fading Channels: A Unified Approach to Performance Analysis*, John Wiley & Sons: New York, USA.
- [110] Aalo, V., Ugweje, O. and Sudhakar, R. (1998) Performance analysis of a DS/CDMA system with noncoherent M -ary orthogonal modulation in Nakagami fading. *IEEE Transactions on Veh. Tech.*, **47**, 20–29, February.
- [111] Alouini, M.-S. and Simon, M. K. (1999) Application of the Dirichlet transformation to the performance evaluation of generalized selection combining over Nakagami- m fading channels. *Journal of Communications and Networks*, **47**, 5–13, March.
- [112] Alouini, M.-S. and Simon, M. K. (1999) Performance of coherent receivers with hybrid SC/MRC over Nakagami- m fading channels. *IEEE Transactions on Veh. Tech.*, **48**, 1155–64, July.
- [113] Annamalai, A. (1999) Microdiversity reception of spread-spectrum signals on Nakagami fading channels. *IEEE Transactions on Communications*, **47**, 1747–56, November.
- [114] Efthymoglou, G. P., Aalo, V. A. and Helmken, H. (1997) Performance analysis of coherent DS-CDMA system in a Nakagami fading channel with arbitrary parameters. *IEEE Transactions on Veh. Tech.*, **46**, 289–96, May.
- [115] Eng, T. and Milstein, L. B. (1995) Coherent DS-CDMA performance in Nakagami multipath fading. *IEEE Transactions on Communications*, **43**, 1134–43, Febuary/March/April.
- [116] Goldfeld, L. and Lyandres, V. (2000) Capacity of the multicarrier channel with frequency-selective Nakagami fading. *IEICE Transactions on Communications*, **E83-B**(3), 697–702, March.
- [117] Goldfeld, L. and Wulich, D. (1997) Multicarrier modulation system with erasure-correcting decoding for Nakagami fading channels. *European Transactions on Telecommunications*, **8**, 591–5, November–December.
- [118] Kim, J. Y. and Lee, J. H. (1998) *Performance of a Multicarrier DS/CDMA System with Adaptive Antenna Array in a Nakagami Fading Channel*. Proceedings of IEEE PIMRC'1998, Vol. 2, pp. 759–63.
- [119] Kim, S. W. and Lee, Y. H. (2000) Combined rate and power adaption in DS/CDMA communications over Nakagami fading channels. *IEEE Transactions on Communications*, **48**, 162–8, January.
- [120] Li, Z. and Latva-aho, M. (2002) *Error Probability for MC-CDMA in Nakagami- m Fading Channels Using Equal Gain Combining*. Proceedings of IEEE ICC'2002, Vol. 1, pp. 227–31.
- [121] Simon, M. K. and Alouini, M.-S. (1999) *BER Performance of Multicarrier DS-CDMA Systems over Generalized Fading Channels*. Proceedings of Communication Theory Mini-Conference, 1999, pp. 72–7.
- [122] Simon, M. K. and Alouini, M.-S. (1999) A unified performance analysis of digital communication with dual selective combining diversity over correlated Rayleigh and Nakagami- m fading channels. *IEEE Transactions on Communications*, **47**, 33–43, January.
- [123] Simon, M. K. and Alouini, M.-S. (1998) A unified approach to the probability of error for noncoherent and differentially coherent modulation over generalized fading channels. *IEEE Transactions on Communications*, **46**, 1625–38, December.
- [124] Simon, M. K. and Alouini, M.-S. (1998) *A Unified Approach to the Performance Analysis of Digital Communication over Generalized Fading Channels*. Proceedings of the IEEE, Vol. 86, pp. 1860–77, September.
- [125] Xiang, H. (1985) Binary code-division multiple-access systems operating in multipath fading, noise channels. *IEEE Transactions on Communications*, **33**, 775–84, August.
- [126] Yang, L.-L. and Hanzo, L. (2000) *Parallel Code-acquisition for Multicarrier DS-CDMA Systems Communicating over Multipath Nakagami Fading Channels*. Proceedings of IEEE GLOBECOM'2000, **2**, 890–4.
- [127] Yang, L. L. and Hanzo, L. (2001) *Acquisition Performance Study of Single- and Multi-carrier DS-CDMA over Nakagami- m Fading Channels*. Proceedings of IEEE VTC'2001-Spring, Vol. 4, pp. 2460–4.
- [128] Yang, L. L. and Hanzo, L. (2001) *A Unified Approach to the Analysis of Multicarrier DS-CDMA over Nakagami- m Fading Channels*. Proceeding of IEEE GLOBECOM'2001, Vol. 6, pp. 3429–33.
- [129] Yang, L. L. and Hanzo, L. (2002) Serial acquisition performance of single-carrier and multicarrier DS-CDMA over Nakagami- m fading channels. *IEEE Transactions on Wireless Communications*, **1**(4), 692–702, October.
- [130] Zhang, Q. T. (1998) Exact analysis of postdetection combining for DPSK and NKSF systems over arbitrarily correlated Nakagami channels. *IEEE Transactions on Communications*, **46**, 1459–67, November.

- [131] Stuber, G. L., ed. (2000) *Principles of Mobile Communication*, 2nd edn, Kluwer Academic Publishers.
- [132] Giannakis, G. B., Anghel, P. A. and Wang Z. (2000) *Wideband Generalized Multicarrier CDMA over Frequency-selective Wireless Channels*. Proceedings of IEEE ICASSP'2000, Vol. 5, pp. 2501–4.
- [133] Giannakis, G. B. and Wang, Z. (1999) *AMOUR-generalized Multicarrier CDMA Irrespective of Multipath*. Proceedings of IEEE GLOBECOM'99, **1B**, 965–9.
- [134] Giannakis, G. B. and Wang, Z. (1999) *Mutually Orthogonal Transceivers for Blind Uplink CDMA Irrespective of Multipath Channel Nulls*. Proceedings of ICASSP'99, **5**, 2741–4.
- [135] Giannakis, G. B., Wang, Z. et al. (2000) AMOUR-generalized multicarrier transceivers for blind CDMA regardless of multipath. *IEEE Transactions on Communications*, **48**(12), 2064–76, December.
- [136] McCormick, A. C., Grant, P. M. and Povey, G. J. R. (2000) A differential phase-shift keying multicarrier code division multiple access system with an equal gain combining receiver. *IEEE Transactions on Vehicular Technology*, **49**(5), 1907–17, September.
- [137] Muquet, B. et al. (2002) Cyclic prefixing or zero padding for wireless multicarrier transmissions? *IEEE Transactions on Communications*, **50**(12), 2136–48, December.
- [138] Wang, Z. and Giannakis, G. B. (2000) *Block Spreading for MUI/ISI-resilient Generalized Multi-carrier CDMA with Multirate Capabilities*. Proceedings of IEEE ICC'2000, Vol. 3, pp. 1477–81.
- [139] Wang, Z. and Giannakis, G. B. (2000) Wireless multicarrier communications – where Fourier meets Shannon. *IEEE Signal Processing Magazine*, 29–48, May.
- [140] Wang, Z. and Giannakis, G. B. (2001) Block precoding for MUI/ISI-resilient generalized multicarrier CDMA with multirate capabilities. *IEEE Transactions on Communications*, **49**(11), 2016–27, November.
- [141] Zhou, S. and Giannakis, G. B. (2001) Finite-alphabet based channel estimation for OFDM and related multicarrier systems. *IEEE Transactions on Communications*, **49**(8), 1402–14, August.
- [142] Zhou, W., Xia, P. and Zhu, J. (2000) *M-ary MC-CDMA using Quadrature Spreading Codes for Wireless Communications System*. Proceedings of IEEE VTC'2000-Spring, Vol. 1, pp. 249–53.
- [143] Kafle, P. L. and Sesay, A. B. (2001) *Performance of Multicarrier CDMA Uplink with Serial Concatenated Convolutional Coding and Successive Interference Cancellation*. Proceedings of IEEE MILCOM'2001, Vol. 2, pp. 1114–8.
- [144] Kafle, P. L. and Sesay, A. B. (2003) Iterative Semi-Blind Multiuser Detection for Coded MC-CDMA Uplink System. *IEEE Transactions on Communications*, **51**(7), 1034–9, July.
- [145] Krishnaiah, P. R. and Rao, M. M. (1961) Remarks on a multivariate gamma distribution. *American Mathematics Monthly*, **68**, 342–6, April.
- [146] Haykin, S. (1996) *Adaptive Filter Theory*, 3rd edn, Prentice-Hall: New Jersey, USA.
- [147] Li, Y., Seshadri, N. and Ariyavisitakul, S. (1999) Channel estimation for OFDM systems with transmitter diversity in mobile wireless channels. *IEEE Journal on Selected Areas in Communications*, **17**(3), 461–71, March.
- [148] Ghareeb, I. and Abu-Sbeih, M. (2004) Performance of MFSK signals with postdetection square-law diversity combining in arbitrarily correlated Nakagami-m fading channels. *IEEE Communications Letters*, **8**(2), 108–10, February.
- [149] Naguib, A. F. and Paulraj, A. (1996) Performance of wireless CDMA with M-ary orthogonal modulation and cell site antenna arrays. *IEEE Journal on Selected Areas in Communications*, **14**(9), 1770–83, December.
- [150] Yang, L.-L., Yen, K. and Hanzo, L. (2000), A Reed-Solomon coded DS-CDMA system using noncoherent M-ary orthogonal modulation over multipath fading channels. *IEEE Journal on Selected Areas in Communications*, **18**(11), 2240–51, November.
- [151] Yang L.-L. and Hanzo, L. (2001), Performance analysis of coded M-ary orthogonal signaling using errors-and-erasures decoding over frequency-selective fading channels. *IEEE Journal on Selected Areas in Communications*, **19**(2), 211–21, February.
- [152] Gradshteyn, I. S. and Ryzhik, I. M. (1980) *Table of Integrals, Series, and Products*, Academic Press, Inc., New York, London.
- [153] Abramowitz, M. and Stegun, I. A. (eds) (1972) *Handbook of Mathematical Functions – with Formulas, Graphs, and Mathematical Tables*, Dover Publications, INC., New York.

- [154] Pierce, J. N. and Stein, S. (1959) *Multiple Diversity with Nonindependent Fading*. Proceedings of the IRE, pp. 89–104, January.
- [155] Verdu, S. (1983) Minimum Probability of Error for Asynchronous Multiple Access Communication Systems. *IEEE Military Communications Conference*, 213–9, October.
- [156] Lutkepohl, H. (1988). *Handbook of Matrices*, John Wiley & Sons: New York, USA.
- [157] Cheng, Y.-P., Zhang, K.-Y. and Xu, Z. (2002) *Matrix Theory*, 2nd ed. Northwestern Polytechnical University Press, Xi'an, P.R. China.
- [158] Madhow, U. and Honig, M. L. (1994) MMSE interference suppression for direct-sequence spread-spectrum CDMA. *IEEE Transactions on Communications*, **42**, 3178–88, December.
- [159] Goldstein J. S. and Reed, I. S. (1997) Subspace selection for partially adaptive sensor array processing. *IEEE Transactions on Aerospace and Electronic Systems*, **33**, 539–44, April.
- [160] Goldstein, J. S., Reed, I. S. and Scharf, L. L. (1998) A multistage representation of the Wiener filter based on orthogonal projections. *IEEE Transactions on Information Theory*, **44**, 1943–2959, November.
- [161] Honig, M. L. and Xiao, W. (2001) Performance of reduced-rank linear interference suppression. *IEEE Transactions on Information Theory*, **47**, 1928–46, July.
- [162] Muller, R. R. and Verdu, S. (2001) Design and analysis of low-complexity interference mitigation on vector channels. *IEEE Journal on Selected Areas in Communications*, **19**, 1429–41, August.
- [163] Moshavi, S., Kanterakis, E. G. and Schilling, D. L. (1996) Multistage linear receivers for DS-CDMA systems. *International Journal of Wireless Information Networks*, **3**, 1–17, January.
- [164] Chen, W., Mitra, U. and Schniter, P. (2002) On the equivalence of three reduced rank linear estimators with applications to DS-CDMA. *IEEE Transactions on Information Theory*, **48**, 2609–14, September.
- [165] Varanasi, M. K. and Aazhang, B. (1991) Near-optimum detection in synchronous code-division multiple-access systems. *IEEE Transactions on Communications*, **39**(5), 725–36, May.
- [166] Divsalar, D., Simon, M. K. and Raphaeli, D. (1998) Improved parallel interference cancellation for CDMA. *IEEE Transactions on Communications*, **46**(2), 258–68, May.
- [167] Duel-Hallen, A. (1993) Decorrelating decision-feedback multiuser detector for synchronous code-division multiple-access channel. *IEEE Transactions on Communications*, **41**(2), 285–90, February.
- [168] Woodward, G. *et al.* (2002) Minimum mean-square error multiuser decision-feedback detectors for DS-CDMA. *IEEE Transactions on Communications*, **50**(12), 2104–12, December.
- [169] Poor, H. V. (2004) Iterative multiuser detection. *IEEE Signal Processing Magazine*, 81–8, January.
- [170] Wang, X., Lu, W.-S. and Antoniou, A. (2000) Constraint minimum-BER multiuser detection. *IEEE Transactions on Signal Processing*, **48**(10), 2903–9, October.
- [171] Chen, S., Samigan, A. K., Mulgrew, B. and Hanzo, L. (2001) Adaptive minimum-BER linear multiuser detection for DS-CDMA signals in multipath channels. *IEEE Transactions on Signal Processing*, **49**(6), 1240–7, June.
- [172] Yang, L.-L. and Chen, H.-H. (2007) Error probability of digital communications using relay diversity over Nakagami- m fading channel. To appear in *IEEE Transactions on Wireless Communications*.
- [173] Brandwood, D. H. (1983) A complex gradient operator and its application in adaptive array theory. *IEE Proceedings, Parts F and H*, **130**(1), 11–6, February.
- [174] Hjorungnes, A. and Gesbert, D. (2006) Complex-valued matrix differentiation: Techniques and key results. submitted for publication, <http://www.eurecom.fr/~gesbert/papers/matrixdiff.pdf>.
- [175] Kay, S. M. (1993) *Fundamentals of Statistical Signal Processing: Estimation Theory*, Prentice-Hall PTR: New Jersey, USA.
- [176] Chin, W. H. (2005) *QRD Based Tree Search Data Detection for MIMO Communication Systems*. Proceedings of IEEE Vehicular Technology Conference, **3**(3), 1624–7, May–June.
- [177] AlRustamani, A. (2002) A new approach to greedy multiuser detection. *IEEE Transactions on Communications*, **50**, 1326–36, August.
- [178] Dai, Y., Sun, S. and Lei, Z. (2005) *A comparative study of QRD-M detection and sphere decoding for MIMO-OFDM systems*. IEEE PIMRC'2005, 186–90.

- [179] Luo, J. *et al.* (2000) *A Class of Coordinate Descent Algorithms for Multiuser Detection*. Proceedings of International Conference on Acoustics, Speech, Signal Processing, Vol. 5, pp. 2853–6, June.
- [180] Lim, H. S. *et al.* (2003) Multiuser detection for DS-CDMA systems using evolutionary programming. *IEEE Communications Letters*, **7**(3), 101–3, March.
- [181] Ergun, C. and Hacioglu, K. (2000) Multiuser detection using a genetic algorithm in CDMA communications systems. *IEEE Transactions on Communications*, **48**(8), 1374–83, August.
- [182] Dorigo, M. and Gambardella, L. M. (1997) Ant colony system: a cooperative learning approach to the traveling salesman problem. *IEEE Transactions on Evolutionary Computation*, **1**(1), 53–66, April.
- [183] Hijazi, S. L. and Natarajan, B. (2004) Novel low-complexity DS-CDMA multiuser detector based on ant colony optimization. *IEEE Vehicular Technology Conference, VTC2004-Fall*, **3**, 1939–43.
- [184] Borran, M. J. and Nasiri-Kenari, M. (2000) An efficient detection technique for synchronous CDMA communication systems based on the expectation maximization algorithm. *IEEE Transactions on Vehicular Technology*, **49**(5), 1663–8, September.
- [185] Nelson, L. B. and Poor, H. V. (1996) Iterative multiuser receivers for CDMA channels: An EM-based approach. *IEEE Transactions on Communications*, **44**(12), 1700–10, December.
- [186] Luo, J. *et al.* (2001) Near-optimal multiuser detection in synchronous CDMA using probabilistic data association. *IEEE Communications Letters*, **5**(9), 361–3, September.
- [187] Rendl, F. (1999) Semidefinite programming and combinatorial optimization. *Applied Numerical Mathematics*, **29**, 255–81.
- [188] Abdi, M. *et al.* (2002) Semidefinite positive relaxation of the maximum-likelihood criterion applied to multiuser detection in a CDMA context. *IEEE Signal Processing Letters*, **9**(6), 165–7, June.
- [189] Liu, H., Wang, X. and Liu, S. (2004) The application of nonlinear programming for multiuser detection in CDMA. *IEEE Transactions on Wireless Communications*, **3**(1), 8–11, January.
- [190] Tan, P. H. and Rasmussen, L. K. (2001) The application of semidefinite programming for detection. *IEEE Journal on Selected Areas in Communications*, **19**, 1442–9, August.
- [191] Einarsson, G. (1980) Address assignment for a time-frequency-coded, spread-spectrum system. *Bell System Technical Journal*, **59**(7), 1241–55, September.
- [192] Das, D. and Varanasi, M. K. (2004) Optimum noncoherent multiuser decision feedback detection. *IEEE Transactions on Information Theory*, **50**(9), 1974–88.
- [193] Hegarty, C. J. and Vojcic, B. (1996) *Noncoherent Multiuser Detection of M-ary Orthogonal Signals using a Decorrelator*. Proceedings of MILCOM'96, Mclean VA, Vol. 3, pp. 903–7, October.
- [194] Hegarty, C. J. and Vojcic, B. (1997) *Noncoherent Multistage Multiuser Detection of M-ary Orthogonal Signals*. Proceedings of ICC'97, **2**, 595–9.
- [195] Kapur, A., Varanasi, M. K. and Das, D. (2002) Noncoherent MMSE multiuser receivers and their blind adaptive implementations. *IEEE Transactions on Communications*, **50**(3), 503–13, March.
- [196] Russ, A. and Varanasi, M. K. (2001) Noncoherent multiuser detection for nonlinear modulation over the Rayleigh-fading channel. *IEEE Transactions on Information Theory*, **47**(1), 295–305, January.
- [197] Sinha, R., Yener, A. and Yates, R. D. (2002) Noncoherent multiuser communications: Multistage detection and selective filtering. *EURASIP Journal on Applied Signal Processing*, **2002**(12), 1415–26.
- [198] Varanasi, M. K. and Das, D. (2000) Noncoherent decision-feedback multiuser detection. *IEEE Transactions on Communications*, **48**(2), 259–69, February.
- [199] Varanasi, M. K. and Russ, A. (1998) Noncoherent decorrelative detection for nonorthogonal multipulse modulation over the multiuser Gaussian channels. *IEEE Transactions on Communications*, **46**(12), 1675–84, December.
- [200] Fiebig, U.-C. G. and Robertson, P. (1999) Soft-decision and erasure decoding in fast frequency-hopping systems with convolutional, turbo, and Reed-Solomon Codes. *IEEE Transactions on Communications*, **47**(11), 1646–54, November.
- [201] Kozick, R. J. and Sadler, B. M. (2000) *Maximum Likelihood Multi-user Detection for Fast Frequency-hopping/multiple Frequency Shift Keying Systems*. IEEE Wireless Communications and Networking Conference, Vol. 1, pp. 67–72.

- [202] Lin S.-Y., Yang G.-C., Tseng S.-C. and Hong C.-F. (1999) Improve cochannel interference cancellation for MFSK/FH-SSMA systems. *IEEE Journal on Selected Areas in Communications*, **17**(11), 1940–52, November.
- [203] Mabuchi, T., Kohno, R. and Imai, H. (1994) Multiuser detection scheme based on canceling cochannel interference for MFSK/FH-SSMA system. *IEEE Journal on Selected Areas in Communications*, **12**(4), 593–604, May.
- [204] Su, Y. T., Shen, Y.-S. and Hsiao, C.-Y. (2001) On the detection of a class of fast frequency-hopped multiple-access signals. *IEEE Journal on Selected Areas in Communications*, **19**(11), 2151–64, November.
- [205] Skoglund, M. and Hedelin, P. (1999) Hadamard-based soft decoding for vector quantization over noisy channels. *IEEE Transactions on Information Theory*, **45**(2), 515–32, March.
- [206] Kay, S. M. (1998) *Fundamentals of Statistical Signal Processing: Detection Theory*, Prentice-Hall PTR: New Jersey, USA.
- [207] Golub, G. H. and Loan, C. F. V. (1996) *Matrix Computations*, 3rd edn, The Johns Hopkins University Press, Baltimore, London.
- [208] Timor, U. (1980) Improved decoding scheme for frequency-hopped multilevel FSK system. *The Bell System Technical Journal*, **59**(10), 1839–55, December.
- [209] Yue, O.-C. (1982) Maximum likelihood combining for noncoherent and differentially coherent frequency-hopping multiple-access systems. *IEEE Transactions on Information Theory*, **28**(4), 631–9, July.
- [210] Lee, J. S., French, R. H. and Miller, L. E. (1984) Probability of error analysis of a BFSK frequency-hopping system with diversity under partial-band jamming interference – Part I: performance of square-law linear combining soft-decision receiver. *IEEE Transactions on Communications*, **COM-32**(6), 645–53, June.
- [211] Teh, K. C., Kot, A. C. and Li, K. H. (1997) Partial-band jamming rejection of FFH/BFSK with product combining receiver over a Rayleigh-fading channel. *IEEE Communications Letters*, **1**(3), 64–6, May.
- [212] Lee, J. S., Miller, L. E. and Kim, Y. K. (1984) Probability of error analysis of a BFSK frequency-hopping system with diversity under partial-band jamming interference – Part II: performance of square-law nonlinear combining soft-decision receivers. *IEEE Transactions on Communications*, **COM-32**(6), 1243–50, December.
- [213] Robertson, R. C. and Ha, T.-T. (1992) Error probabilities of fast frequency-hopped MFSK with noise-normalization combining in a fading channel with partial-band interference. *IEEE Transactions on Communications*, **40**(2), 404–12, February.
- [214] Robertson, R. C. and Lee, K. Y. (1992) Performance of fast frequency-hopped MFSK receivers with linear and self-normalization combining in a Raician channel with partial-band interference. *IEEE Journal on Selected Areas in Communications*, **10**(4), 731–41, May.
- [215] Teh, K. C., Kot, A. C. and Li, K. H. (1998) Multitone jamming rejection of FFH/BFSK spread-spectrum system over fading channels. *IEEE Transactions on Communications*, **46**(8), 1050–7, August.
- [216] Hung, C. P. and Su, Y. T. (1995) Diversity combining consideration for incoherent frequency hopping multiple access systems. *IEEE Journal on Selected Areas in Communications*, **13**(2), 333–44, February.
- [217] Teh, K. C., Kot, A. C. and Li, K. H. (1999) Performance study of a maximum-likelihood receiver for FFH/BFSK systems with multitone jamming. *IEEE Transactions on Communications*, **47**(5), 766–72, May.
- [218] Choi, J. (2002) Interference mitigation using transmitter filters in CDMA systems. *IEEE Transactions on Vehicular Technology*, **51**(4), 657–66, July.
- [219] Choi, R. L.-U., Letaief, K. B. and Murch, R. D. (2001) MISO CDMA transmission with simplified receiver for wireless communication handsets. *IEEE Transactions on Communications*, **49**(5), 888–98, May.
- [220] Esmailzadeh, R., Sourour, E. and Nakagawa, M. (1999) Prerake diversity combining in time-division duplex CDMA mobile communications. *IEEE Transactions on Vehicular Technology*, **48**(3), 795–801, May.
- [221] Lebrun, G., Gao, J. and Faulkner, M. (2005) MIMO transmission over a time-varying channel using SVD. *IEEE Transactions on Wireless Communications*, **4**(2), 757–64, March.
- [222] Sampath, H., Stoica, P. and Paulraj, A. (2001) Generalized linear precoder and decoder design for MIMO channels using the weighted MMSE criterion. *IEEE Transactions on Communications*, **49**(12), 2198–206, December.

- [223] Tang, Z. and Cheng, S. (1994) *Interference Cancellation for DS-CDMA Systems over Flat Fading Channels through Pre-decorrelating*. PIMRC, The Hague, The Netherlands.
- [224] Vojcic, B. R. (1994) *Transmitter Precoding in Synchronous Multiuser Communications*. Symposium on Mobility Management, George Mason University, Fairfax, VA, USA.
- [225] Vojcic, B. R. and Jang, W. M. (1998) Transmitter precoding in synchronous multiuser communications. *IEEE Transactions on Communications*, **46**(10), 1346–55, October.
- [226] Choi, R. L.-U. and Murch, R. D. (2003) New transmit schemes and simplified receivers for MIMO wireless communications systems. *IEEE Transactions on Wireless Communications*, **2**(6), 1217–30, November.
- [227] Choi, R. L.-U. and Murch, R. D. (2004) A transmit MIMO scheme with frequency domain pre-equalization for wireless frequency selective channels. *IEEE Transactions on Wireless Communications*, **3**(3), 929–38, May.
- [228] Morelli, M. and Sanguinetti, L. (2005) A novel prefiltering technique for downlink transmissions in TDD MC-CDMA systems. *IEEE Transactions on Wireless Communications*, **4**(5), 2064–9, September.
- [229] Yang, L.-L. (2007) Design Linear Multiuser Transmitters from Linear Multiuser Receivers. Presented at the IEEE ICC 2007, Glasgow, Scotland, 24–28 June.
- [230] Choi, L.-U. and Murch, R. D. (2004) A transmit preprocessing techniques for multiuser MIMO systems using a decomposition approach. *IEEE Transactions on Wireless Communications*, **3**(1), 20–4, January.
- [231] Ding, Y. et al. (2003) Minimum BER block precoders for zero-forcing equalization. *IEEE Transactions on Signal Processing*, **51**(9), 2410–22, September.
- [232] Hjorungnes, A. and Diniz, P. S. R. (2005) Minimum BER prefilter transform for communications systems with binary signaling and known FIR MIMO channel. *IEEE Signal Processing Letters*, **12**(3), 234–7, March.
- [233] Cover, T. M. and Thomas, J. A. (1991) *Elements of Information Theory*, John Wiley & Sons, Inc: New York, USA.
- [234] Telatar, I. E. (1999) Capacity of multiantenna Gaussian channels. *European Transactions on Telecommunications*, **10**(6), 585–95, November/December.
- [235] Cosovic, I., Sand, S and Raulefs, R. (2005) *A Non-Linear Precoding Technique for Downlink MC-CDMA Systems*. IEEE Vehicular Technology Conference (VTC'05-Spring), Stockholm, Sweden, May 2005.
- [236] Tomlinson, M. (1971) New automatic equalizer employing modulo arithmetic. *Electronics Letters*, **7**(5), 138–9.
- [237] Special issue on MIMO systems and applications, *IEEE Journal on Selected Areas in Communications*, **21**, April 2003.
- [238] Special issue on MIMO systems and applications, *IEEE Journal on Selected Areas in Communications*, **21**, May 2003.
- [239] Special issue on MIMO wireless communications, *IEEE Transactions on Signal Processing*, **51**, November 2003.
- [240] Holter, B. (2001) *On the Capacity of MIMO Channels: A Tutorial Introduction*. Proceedings IEEE Norwegian Symposium on Signal Processing, Trondheim, Norway, 167–72, October.
- [241] Popescu, O., Rose, C. and Popescu, D. C. (2004) Maximizing the determinant for a special class of block-partitioned matrices. *Mathematical Problems in Engineering 2004*, **2004**(1), 49–61.
- [242] Stoica, P., Jiang, Y. and Li, J. (2005) On MIMO channel capacity: An intuitive discussion. *IEEE Signal Processing Magazine*, **22**(3), 83–4, May.
- [243] Alamouti, S. M. (1998) A simple transmit diversity technique for wireless communications. *IEEE Journal on Selected Areas in Communications*, **16**(8), 1451–8, October.
- [244] Soni, R. A., Buehrer R. M. and Benning, R. D. (2002) Intelligent Antenna System for cdma2000. *IEEE Signal Processing Magazine*, **19**(4), 54–67, July.
- [245] Tarokh, V., Jafarkhani, H. and Calderbank, A. R. (1999) Space-time block coding for wireless communications: performance results. *IEEE Journal on Selected Areas in Communications*, **17**, 451–60, March.

- [246] Tarokh, V., Seshadri, N. and Calderbank, A. R. (1998) Space-time codes for high data rate wireless communications: performance criterion and code construction. *IEEE Transactions on Information Theory*, **44**(2), 744–65, March.
- [247] Smida, B., Dspins, C. L. and Delisle, G. Y. (2001) MC-CDMA performance evaluation over a multipath fading channel using the characteristic function method. *IEEE Transactions on Communications*, **49**(8), 1325–8, August.
- [248] Soni, R. A. and Buehrer R. M. (2004) On the performance of open-loop transmit diversity techniques for IS-2000 systems: A comparative study. *IEEE Transactions on Wireless Communications*, **3**(5), 1602–15, September.
- [249] Aufftay, J. M. and Helard, J. F. (2002) Performance of multicarrier CDMA technique combined with space-time block coding over Rayleigh channel. *IEEE Seventh International Symposium on Spread Spectrum Techniques and Applications*, **2**, 348–52.
- [250] Cai, X. and Akansu, A. N. (2000) *Multicarrier CDMA Systems with Transmit Diversity*. Proceedings of IEEE VTC'2000, **6**, 2817–21.
- [251] Tarokh, V., Jafarkhani, H. and Calderbank, A. R. (1999) Space-time block codes from orthogonal designs. *IEEE Transactions on Information Theory*, **45**, 1456–67, July.
- [252] Yang, Z. and Lu, B. and Wang, X. (2001) Bayesian Monte Carlo multiuser receiver for space-time coded multicarrier CDMA systems. *IEEE Journal on Selected Areas in Communications*, **19**(8), 1625–37, August.
- [253] Ganesan, G. and Stoica, P. (2001) Space-time block codes: A maximum SNR approach. *IEEE Transactions on Information Theory*, **47**(4), 1650–6, May.
- [254] Dalton, L. A. and Georghiades, C. N. (2005) A full-rate, full-diversity four-antenna quasi-orthogonal space-time block codes. *IEEE Transactions on Wireless Communications*, **4**(2), 363–6, March.
- [255] Celebi, M. E., Sahin, S. and Aygolu, U. (2007) Full rate full diversity space-time block code selection for more than two transmit antennas *IEEE Transactions on Wireless Communications*, **6**(1), 16–9, January.
- [256] Hochwald, B., Marzetta, T. L. and Papadias, C. B. (2001) A transmitter diversity scheme for wideband CDMA systems based on space-time spreading. *IEEE Journal on Selected Areas in Communications*, **19**, 48–60, January.
- [257] Yang, L.-L. and Hanzo, L. (2005) Adaptive space-time-spreading-assisted wideband CDMA systems communicating over dispersive Nakagami- m fading channels. *EURASIP Journal on Wireless Communications and Networking*, 216–30, April.
- [258] Yang, L.-L. and Hanzo, L. (2005) Performance of broadband multicarrier DS-CDMA using space-time spreading-assisted transmit diversity. *IEEE Transactions on Wireless Communications*, **4**, 885–94, May.
- [259] Yang, L.-L. (2006) MIMO assisted space-code-division multiple-access: Linear detectors and performance over multipath fading channels. *IEEE Journal on Selected Areas in Communications – Special Issue on The Next Generation CDMA Techniques*, **24**(1), 121–31, January.
- [260] Yang, L.-L. and Hanzo, L. (2005) Performance of fractionally spread multicarrier CDMA in AWGN as well as slow and fast Nakagami- m fading channels. *IEEE Transactions on Vehicular Technology*, **54**(5), 1817–27, September.
- [261] Adachi, F., Sawahashi, M. and Okawa, K. (1997) Tree-structured generation of orthogonal spreading codes with different lengths for forward link of DS-CDMA mobile radio. *Electronics Letters*, **33**, 27–8, January.
- [262] Sayeed, A. M. and Aazhang, B. (1999) Joint multipath-Doppler diversity in mobile wireless communications. *IEEE Transactions on Communications*, **47**(1), 123–32, January. April.

Further Reading

- [263] Cances, J. P. and Meghdadi, V. (2002) Blind adaptive receiver for coded multicarrier DS-CDMA systems in multipath fading channels. *IEE Proceedings-Communications*, **149**(3), 171–8, June.
- [264] Canchi, R. and Akaiwa, Y. (1999) Threshold-free erasure decoded multicarrier local transmission over multipath channels. *IEICE Transactions on Communications*, **E82-B**(1), 129–35, January.

- [265] Cariolaro, G. and Vagliani, F. C. (1995) An OFDM scheme with a half complexity. *IEEE Journal on Selected Areas in Communications*, **13**(9), 1586–99, December.
- [266] Chang, R. W. and Gibby, R. A. (1968) A theoretical study of performance of an orthogonal multiplexing data transmission scheme. *IEEE Transactions on Communication Technology*, **COM-16**(4), 529–40, August.
- [267] Chen, H.-H., Yeh, J.-F. and Suehiro, N. (2001) A multicarrier CDMA architecture based on orthogonal complementary codes for new generations of wideband wireless communications. *IEEE Communications Magazine*, **39**(10), 126–35, October.
- [268] Chen, K.-H. and Wu, S.-T. (1999) A programmable architecture for OFDM-CDMA. *IEEE Communications Magazine*, **37**(11), 76–82, November.
- [269] Cook, C. E., Ellersick, F. W., Milstein, L. B. and Schilling, D. L. (1983) *Spread-Spectrum Communications*, IEEE Press: New York.
- [270] Diggavi, S. N. (2001) On achievable performance of spatial diversity fading channels. *IEEE Transactions on Information Theory*, **47**(1), 308–25, January.
- [271] Dillard, R. A. and Dillard, G. M. (1989) *Detectability of Spread-Spectrum Signals*, Artech House: Maryland, USA.
- [272] Douillard, C. *et al.* (1995) Iterative correction of intersymbol interference: turbo-equalization. *European Transactions on Telecommunications*, **6**(5), 507–11, September–October.
- [273] Elnoubi, S. M. and El-Beheiry, A. (2001) Effect of overlapping between successive carriers of multicarrier CDMA on the performance in a multipath fading channel. *IEEE Transactions on Communications*, **49**(5), 769–73, May.
- [274] Elnoubi, S. M., Sourour, E. and Elshamly, A. (2002) Performance of multicarrier CDMA with DPSK modulation and differential detection in fading multipath channels. *IEEE Transactions on Vehicular Technology*, **51**(3), 526–36, May.
- [275] Fang, L. and Milstein, L. B. (2000) Successive interference cancellation in multicarrier DS/CDMA. *IEEE Transactions on Communications*, **48**(9), 1530–40, September.
- [276] Fang, L. and Milstein, L. B. (2001) Performance of successive interference cancellation in convolutionally coded multicarrier DS/CDMA systems. *IEEE Transactions on Communications*, **49**(12), 2062–7, December.
- [277] Foschini, G. J. (1996) Layered space–time architecture for wireless communication in a fading environment when using multi-element antennas. *Bell Labs Technical Journal*, 41–59, Autumn.
- [278] Fuji, M., Itami, M. and Itoh, K. (2000) Performance of frequency-division CDMA systems for channels with frequency selective fading. *IEICE Transactions on Fundamentals*, **E83-A**(11), 2003–101, November.
- [279] Glavieux, A., Cochet, P. Y. and Picart, A. (1994) Orthogonal frequency division multiplexing with BFSK modulation in frequency selective Rayleigh and Rician fading channels. *IEEE Transactions on Communications*, **42**(2/3/4), 1919–28, February/March/April.
- [280] Goeckel, D. L. and Stark, W. E. (1999) Optimal diversity allocation in multiuser communication systems – Part I: System model. *IEEE Transactions on Communications*, **47**(12), 1828–36, December.
- [281] Goeckel, D. L. and Stark, W. E. (2000) Optimal diversity allocation in multiuser communication systems – Part II: Optimization. *IEEE Transactions on Communications*, **48**(1), 45–52, January.
- [282] Goldsmith, A., Jafar, S. A., Jindal, N. and Vishwanath, S. (2003) Capacity limits of MIMO channels. *IEEE Journal on Selected Areas in Communications*, **21**(5), 684–702, 2003.
- [283] Guimaraes, D. A. and Portugheis, J. (1998) Channel coding scheme for orthogonal multicarrier DS-CDMA system. *Electronics Letters*, **34**(24), 2308–9, November.
- [284] Hamaguchi, K. and Moriyama, E. (1998) Performance of multicarrier/QAM-level-controlled adaptive modulation for land mobile communication systems. *IEICE Transactions on Communications*, **E81-B**(4), 770–6, April.
- [285] Hara, S. and Prasad, R. (1999) Design and performance of multicarrier CDMA system in frequency-selective Rayleigh fading channels. *IEEE Transactions on Vehicular Technology*, **48**(5), 1584–95, September.
- [286] Helard, J. F., Baudais, J. Y. and Citerne J. Linear MMSE detection technique for MC-CDMA. *Electronics Letters*, **36**(7), 665–6, March.

- [287] Holmes, J. K. (1982) *Coherent Spread Spectrum Systems*, John Wiley & Sons: New York, USA.
- [288] Hong, C.-F. and Yang, G.-C. (2000) Multicarrier FH codes for multicarrier FH-CDMA wireless systems. *IEEE Transactions on Communications*, **48**(10), 1626–30, October.
- [289] Ikonomou, D. and Vandendorpe, L. (1999) A fractionally spaced decision feedback joint detection proposal for multi carrier CDMA. *European Transactions on Telecommunications*, **10**(4), 407–16, July–August.
- [290] Isson, O., Brossier, J.-M. and Mestdagh, D. (2002) Multi-carrier bit-rate improvement by carrier merging. *Electronics Letters*, **38**(19), 1134–1135, September.
- [291] Jeong, I. and Nakagawa, M. (1999) A time division duplex CDMA system using asymmetric modulation scheme in duplex channel. *IEICE Transactions on Communications*, **E82-B**(12), 1956–63, December.
- [292] Johnson, S. M. (1962) A new upper-bound for error-correcting codes. *IRE Transactions on Information Theory*, **8**(2), 203–7.
- [293] Jung, P., Berens, F. and Plechinger, J. (1996) *Joint Detection for Multicarrier CDMA Mobile Radio Systems. I. System Model*. IEEE International Symposium on Spread Spectrum Techniques and Applications, **3**, 991–5.
- [294] Jung, P., Berens, F. and Plochinger, J. (1996) *Joint Detection for Multicarrier CDMA Mobile Radio Systems. II. Detection Techniques*. IEEE International Symposium on Spread Spectrum Techniques and Applications, **3**, 996–1000.
- [295] Jung, P., Berens, P. and Plechinger, J. (1997) Uplink spectral efficiency of multicarrier joint detection code division multiple access based cellular radio systems. *Electronics Letters*, **33**(8), 664–5, April.
- [296] Jung, P., Berens, F. and Plechinger, J. (1997) Coverage of MC/JD-CDMA based macrocellular radio systems. *Electronics Letters*, **33**(8), 656–7, April.
- [297] Jung, P., Berens, F. and Plechinger, J. (1997) A generalized view on multicarrier CDMA mobile radio systems with joint detection (Part I). *Frequenze*, **5**, 174–85, July–August.
- [298] Kim, C. K. and Cho, Y. S. (2000) Performance of a wireless MC-CDMA system with an antenna array in a fading channel: Reverse link. *IEEE Transactions on Communications*, **48**(8), 1257–61, August.
- [299] Kim, D. K. and Hwang, S. H. (2002) Capacity analysis of an uplink synchronized multicarrier DS-CDMA system. *IEEE Communications Letters*, **6**(3), 99–101, March.
- [300] Kim, I. G. and Kim, D. (1999) Spectral overlay of multicarrier CDMA on existing CDMA mobile systems. *IEEE Communications Letters*, **3**(1), 15–17, January.
- [301] Kumar, P. V. (1988) Frequency-hopping code sequence designs having large linear span. *IEEE Transactions on Information Theory*, **34**, 146–51, January.
- [302] Laot, C., Glavieux, A. and Labat, J. (2001) Turbo equalization: adaptive equalization and channel decoding jointly optimized. *IEEE Journal on Selected Areas in Communications*, **19**(9), 1744–52, September.
- [303] Macwilliams, F. J. and Sloane, N. J. A. (1977). *The Theory of Error-Correcting Codes*, North-Holland, Netherlands.
- [304] Marie, S. V. and Titlebaum, E. L. (1992) A class of frequency hop codes with nearly ideal characteristics for use in multiple-access spread-spectrum communications and radar and sonar systems. *IEEE Transactions on Communications*, **40**(9), 1442–7, September.
- [305] Ojanpera, T. and Prasad, P. (1998) An overview of air interface multiple access for IMT-2000/UMTS. *IEEE Communications Magazine*, **36**, 82–95.
- [306] Progler, M., Evcı, C and Umehira, M. (1999) Air interface access schemes for broadband mobile wireless communications. *IEEE Communications Magazine* (9), 106–15, September.
- [307] Pu, Z., You, X. et al. (1999) *Transmission and Reception of TDD Multicarrier CDMA Signals in Mobile Communications System*. Proceedings of IEEE VTC'1999, **3**, 2134–8.
- [308] Rainbolt, B. J. and Miller, S. L. (1999) Multicarrier CDMA for cellular overlay systems. *IEEE Journal on Selected Areas in Communications*, **17**(10), 1807–14, October.
- [309] Rowitch, D. N. and Milstein, L. B. (1996) *Coded Multicarrier DS-CDMA in the Presence of Partial Band Interference*. Proceedings of IEEE MILCOM'1996, Vol. 1, pp. 204–9.
- [310] Rowitch, D. N. and Milstein, L. B. (1999) Convolutionally coded multicarrier DS-CDMA systems in a multipath fading channel. I. Performance analysis. *IEEE Transactions on Communications*, **47**(10), 1570–82, October.

- [311] Rowitch, D. N. and Milstein, L. B. (1999) Convolutionally coded multicarrier DS-CDMA systems in a multipath fading channel. II. Narrow-band interference suppression. *IEEE Transactions on Communications*, **47**(11), 1729–36, November.
- [312] Sabharwal, A., Mitra, U. and Moses, R. (2001) MMSE receivers for multirate DS-CDMA systems. *IEEE Transactions on Communications*, **49**(12), 2184–97, December.
- [313] Saltzberg, B. R. (1967) Performance of an efficient parallel data transmission system. *IEEE Transactions on Communications Technology*, **COM-15**(6), 805–11, December.
- [314] Salzer, T., Mottier, D. and Brunel, L. (2001) *Influence of System Load on Channel Estimation in MC-CDMA Mobile Radio Communication Systems*. Proceedings of IEEE VTC'2001-Spring, Vol. 1, pp. 522–6.
- [315] Sanada, Y. and Nakagawa, M. (1997) *An Initial Sequence Acquisition Technique for Multicarrier Time Division Duplex CDMA Systems on a Rayleigh Fading Channel*. Proceedings of IEEE PIMRC'1997, **2**, 342–6.
- [316] Sanada, Y., Takada, I. and Araki, K. (1998) A novel cumulant based MUSIC like DOA estimation algorithm with multicarrier modulation. *IEICE Transactions on Communications*, **E81-B**(12), 2318–25, December.
- [317] Sanada, Y., Padilla, M. and Araki, K. (1998) Performance of adaptive array antennas with multicarrier DS/CDMA in a mobile fading environment. *IEICE Transactions on Communications*, **E81-B**(7), 1392–400, July.
- [318] Sandberg, S. D. and Tzannes, M. A. (1995) Overlapped discrete multitone modulation for high speed copper wire communications. *IEEE Journal on Selected Areas in Communications*, **13**(9), 1571–85, December.
- [319] Sandouk, A. *et al.* (2001) BER analysis for multi-carrier DS CDMA with multi-rate traffic. *IEICE Transactions on Fundamentals*, **E84-A**(7), 1723–31, July.
- [320] Sanzi, F., Slama, A. and Speidel, J. (2001) *Multicarrier Code Division Multiplex with Iterative MAP Symbol-by-symbol Estimation*. Proceeding of IEEE GLOBECOM'2001, **2**, 886–90.
- [321] Sayeed, A. M. and Aazhang, B. (1997) Communication over multipath fading channels: A time-frequency perspective, in *Wireless Communication-TDMA versus CDMA* (eds S. G. Glisic and P. L. Leppanen), Kluwer Academic Publishers, pp. 73–98.
- [322] Sayeed, A. M., Sendonaris, A. and Aazhang, B. (1998) Multiuser detection in fast-fading multipath environments. *IEEE Journal on Selected Areas in Communications*, **16**, 1691–701, December.
- [323] Bhashyam, S., Sayeed, A. M. and Aazhang, B. (2000) Time-selective signaling and reception for communication over multipath fading channels. *IEEE Transactions on Communications*, **48**(1), 83–94, January.
- [324] Scaglione, A., Giannakis, G. B. and Barbarossa, S. (1999) Redundant filterbank precoders and equalizers. I. Unification and optimal designs. *IEEE Transactions on Signal Processing*, **47**(7), 1988–2006, July.
- [325] Scaglione, A., Giannakis, G. B. and Barbarossa, S. (1999) Redundant filterbank precoders and equalizers. II. Blind channel estimation, synchronization, and direct equalization. *IEEE Transactions on Signal Processing*, **47**(7), 2007–22, July.
- [326] Shamain, P. K. and Milstein, L. B. (2001) Acquisition of direct sequence spread spectrum signals with correlated fading. *IEEE Journal on Selected Areas in Communications*, **19**(12), 2406–19, December.
- [327] Sheen, W.-H., Chang, M.-J. *et al.* (1998) *Performance of Multiple-dwell Code Acquisition with Diversity for Multicarrier DS-CDMA Systems on Multipath Fading Channels*. IEEE International Symposium on Spread Spectrum Techniques and Applications, Vol. 2, pp. 489–93.
- [328] Shi, Q. and Latva-aho, M. (2002) An exact error floor for downlink MC-CDMA in correlated Rayleigh fading channels. *IEEE Communications Letters*, **6**(5), 196–8, May.
- [329] Shi, Q. and Latva-aho, M. (2002) Simple spreading code allocation scheme for downlink MC-CDMA. *Electronics Letters*, **38**(15), 807–9, July.
- [330] Shi, Q. and Latva-aho, M. (2002) Exact bit error rate calculations for synchronous MC-CDMA over a Rayleigh fading channel. *IEEE Communications Letters*, **6**(7), 276–8, July.
- [331] Siaud, I., Le Gouable, R. and Helard, M. (2001) *On Multicarrier Transmission Techniques over Recorded Indoor Propagation Channel Models for Future Broadband RLANs at 60 GHz*. IEEE International Symposium on PIMRC'2001, Vol. 2, pp. F-53–F-58.

- [332] Sigdel, S., Ahmed, K. M. and Rajatheva, R. M. A. P. (2002) *Performance Evaluation of Multicarrier CDMA Uplink System with Antenna Array and Multiuser Detection over Correlated Multipath Channel*. Proceedings of IEEE VTC'2002-Fall, Vol. 4, pp. 1958–62.
- [333] Slimane, S. B. (1998) MC-CDMA with quadrature spreading for wireless communication systems. *European Transactions on Telecommunications*, **9**(4), 371–78, July–August.
- [334] Soujeri, E. and Bilgekul, H. (2000) *Hopfield Neural Network and Viterbi Decoding for Asynchronous MC-CDMA Communication Systems*. Proceedings of the International Conference on Microelectronics, pp. 215–8.
- [335] Soujeri, E. and Bilgekul, H. (2002) Hopfield multiuser detection of asynchronous MC-CDMA signals in multipath fading channels. *IEEE Communications Letters*, **6**(4), 147–9, April.
- [336] Sourour, E. (2001) *Effect of Carrier Separation with Bandwidth Limitation on the Performance of Multi-carrier DS-CDMA Systems in Multipath Fading Channels*. IEEE International Symposium on PIMRC'2001, Vol. 2, pp. G-17–G-21.
- [337] Sourour, E. A. (1996) *The Effect of Non-linearity on the Performance of the Multi-carrier CDMA System*. Proceedings of IEEE VTC'1996, **3**, 1853–7.
- [338] Spencer, Q. H. and Swindlehurst, A. L. (2001) *On the Performance of Multicarrier CDMA using Multiple Transmitters*. Proceeding of IEEE International Conference on Acoustics, Speech, and Signal Processing, Vol. 4, pp. 2397–400.
- [339] Steendam, H. and Moeneclaey, M. (1999) The effect of carrier phase jitter on MC-CDMA performance. *IEEE Transactions on Communications*, **47**(2), 195–8, February.
- [340] Steendam, H. and Moeneclaey, M. E. (2001) The sensitivity of downlink MC-DS-CDMA to carrier frequency offsets. *IEEE Communications Letters*, **5**(5), 215–7, May.
- [341] Steendam, H. and Moeneclaey, M. (2001) *The Effect of Carrier Phase Jitter on MC-DS-CDMA*. Proceedings of IEEE ICC'2001, **6**, 1881–4.
- [342] Steendam, H. and Moeneclaey, M. (2001) The effect of carrier frequency offsets on downlink and uplink MC-DS-CDMA. *IEEE Journal on Selected Areas in Communications*, **19**(12), 2528–36, December.
- [343] Steiner, B. (1999) *Performance Aspects of an MC/JD-CDMA Mobile Radio System Employing Non-contiguous Frequency Bands*. Proceedings of IEEE VTC'1999, Vol. 1, pp. 30–4.
- [344] Sun, W. and Li, H. (2002) *Blind Channel Identification for Multicarrier CDMA Systems with Transmit Diversity*. Proceedings of IEEE ICC'2002, Vol. 2, pp. 727–31.
- [345] Sun, X., Jiao, Y., Chang, H. and Zhou, Z. (2001) *A Synchronization Scheme with Less Complexity on MC-CDMA Systems*. Proceedings of IEEE VTC'2001-Fall, Vol. 1, pp. 57–61.
- [346] Suwa, S., Atarashi, H., Abeta, S. and Sawahashi, M. (2001) Optimum bandwidth per sub-carrier of multicarrier/DS-CDMA for broadband packet wireless access in reverse link. IEEE International Symposium on PIMRC'2001, Vol. 2, pp. G-22–G-26.
- [347] Teich, W. G., Bury, A. et al. (1998) *Iterative Detection Algorithms for Extended MC-CDMA*. IEEE International Symposium on Spread Spectrum Techniques and Applications, Vol. 1, pp. 184–8.
- [348] Tomba, L. and Krzymien, W. A. (1998) *On the Use of Chip-level Differential Encoding for the Uplink of MC-CDMA Systems*. Proceedings of IEEE VTC'1998, Vol. 2, pp. 958–62.
- [349] Tomba, L. and Krzymien, W. A. (1999) Sensitivity of the MC-CDMA access scheme to carrier phase noise and frequency offset. *IEEE Transactions on Vehicular Technology*, **48**(5), 1657–65, September.
- [350] Tomba, L. and Krzymien, W. A. (1999) An analysis of the effect of chip timing jitter in MC-CDMA systems. *IEEE Transactions on Vehicular Technology*, **48**(6), 1889–98, November.
- [351] Tseng, S. M. and Bell, M. R. (2000) Asynchronous multicarrier DS-CDMA using mutually orthogonal complementary sets of sequences. *IEEE Transactions on Communications*, **48**(1), 53–9, January.
- [352] Tsumura, S. and Hara, S. (2001) *Design and Performance of Quasi-synchronous Multi-carrier CDMA System*. Proceedings of IEEE VTC'2001-Fall, Vol. 2, pp. 843–7.
- [353] Tuchler, M., Koetter, R. and Singer, A. C. (2002) Turbo equalization: Principles and new results. *IEEE Transactions on Communications*, **50**(5), 754–67, May.
- [354] Tureli, U., Kivanc, D. and Liu, H. (2000) *Channel Estimation for Multicarrier CDMA*. Proceedings of IEEE ICASSP'2000, Vol. 5, pp. 2909–12.

- [355] Vankka, J., Kosunen, M. and Halonen, K. (1999) *Multicarrier QAM Modulator*. Proceedings of IEEE International Symposium on Circuits and Systems, Vol. 4, pp. 415–8.
- [356] Vishwanath, S., Jafar, S. A. and Goldsmith, A. (2001) *Adaptive Resource Allocation in Composite Fading Environments*. Proceeding of IEEE GLOBECOM'2001, Vol. 2, pp. 1312–16.
- [357] Viterbi, A. J. and Omura, K. K. (1979) *Principles of Digital Communication and Coding*, McGraw-Hill Book Company: New York, USA.
- [358] Wang, J. and Huang, H. (2002) MC DS/SFH-CDMA systems for overlay systems. *IEEE Transactions on Wireless Communications*, **1**(3), 448–55, July.
- [359] Wang, J. and Huang, H. (2002) Multicarrier DS/SFH-CDMA systems. *IEEE Transactions on Vehicular Technology*, **51**(5), 867–76, September.
- [360] Wang, R., Cheng, S. and Wei, J. (2000) *Wavelet Packet Functions Based Coded MC-CDMA System and its Performance*. Proceedings of IEEE VTC'2000-Spring, Vol. 3, pp. 1933–7.
- [361] Wang, Y. et al. (2002) *Time-frequency Code for Multicarrier DS-CDMA Systems*. Proceedings on IEEE VTC'2002-Spring, Vol. 3, pp. 1224–7.
- [362] Welch, T. B. and Ziemer, R. E. (1998) *Analysis of MC-DS-CDMA Systems in Doubly Spread Channels*. Proceedings of IEEE MILCOM'98, Vol. 3, pp. 757–61.
- [363] Welch, T. B. (1999) *The Spaced-time Correlation Function and its Effect on the Efficient Simulation of Multicarrier Systems*. Proceedings of IEEE VTC'1999, Vol. 3, pp. 1984–8.
- [364] Welch, T. B. and Ziemer, R. E. (1999) Efficient simulation of coded MC-DS-CDMA systems. *IEEE Transactions on Microwave Theory and Techniques*, **47**(6), 675–80, June.
- [365] Wornell, G. W. (1996) *Emerging Applications of Multirate Signal Processing and Wavelets in Digital Communications*. Proceedings of the IEEE, Vol. 84(4), pp. 586–603, April.
- [366] Wu, J., Wang, Y. and Cheng, K. K. M. (2001) *Blind Channel Estimation based on Subspace for Multicarrier CDMA*. Proceedings of IEEE VTC'2001-Spring, Vol. 4, pp. 2374–8.
- [367] Wu, S. T. and Chen, K. C. (1999) *Orthogonal Frequency CDMA for Broadband Communications*. Proceedings of IEEE VTC'1999-Fall, Vol. 5, pp. 2890–4.
- [368] Wu, X., Jiang, B. and Yin, Q. (2001) *Software-defined Radio based Baseband Discrete Model for Orthogonal Frequency Division Multiplexing CDMA Systems*. Proceedings of IEEE VTC'2001-Spring, Vol. 2, pp. 771–5.
- [369] Wu, X., Zhao, Z. and Yin, Q. (2001) *General Baseband Digital Model and Matrix Representation for Different Orthogonal Frequency Division Multiplexing CDMA Schemes*. Proceedings of IEEE ICC'2001, Vol. 2, pp. 427–30.
- [370] Xu, W. and Milstein, L. B. (1998) *MMSE Interference Suppression for Multicarrier DS-CDMA in Frequency Selective Channels*. Proceedings of IEEE GLOBECOM'98, Vol. 1, pp. 259–64.
- [371] Xu, W and Milstein, L. B. (2001) On the use of interference suppression to reduce intermodulation distortion in multicarrier CDMA systems. *IEEE Transactions on Communications*, **49**(1), 130–41, January.
- [372] Xu, W. and Milstein, L. B. (2001) On the performance of multicarrier RAKE system. *IEEE Transactions on Communications*, **49**(10), 1812–23, October.
- [373] Wu, X. et al. (2001) *Equivalently Blind Time-domain Channel Estimation for MC-CDMA System over Frequency-selective Fading Channels in Multiuser Scenario*. Proceeding of IEEE VTC'2001-Fall, Vol. 4, pp. 2687–91.
- [374] Wu, X., Feng, A. and Yin, Q. (2001) *Blind Space-frequency Channel Estimator for MC-CDMA Systems with Antenna Arrays in Frequency-selective Fading Environment*. Proceeding of IEEE VTC'2001-Fall, Vol. 4, pp. 2173–7.
- [375] Xiao, L. and Liang, Q. (2000) *A Novel MC-2D-CDMA Communication Systems and its Detection Methods*. Proceedings of IEEE ICC'2000, Vol. 3, pp. 1223–7.
- [376] Xu, W. and Milstein, L. B. (1997) *Performance of Multicarrier DS CDMA Systems in the Presence of Correlated Fading*. Proceedings of IEEE VTC'1997, Vol. 3, pp. 2050–4.
- [377] Xu, W. and Milstein, L. B. (1999) *MMSE Interference Suppression for Coded Multicarrier DS-CDMA in the Presence of Intermodulation*. Proceedings of IEEE WCNC'1999, Vol. 1, pp. 85–9.

- [378] Yang, L. L. and Hanzo, L. (2000) *Performance of Parallel Code Acquisition Schemes for Multicarrier CDMA over Frequency-selective Rayleigh Fading Channels*. Proceeding of IEEE PIMRC'2000, Vol. 1, pp. 119–23.
- [379] Yang, L. L. and Hanzo, L. (2002) Software-defined-radio-assisted adaptive broadband frequency hopping multicarrier DS-CDMA. *IEEE Communications Magazine*, **40**(3), 174–83, March.
- [380] Yang, L. L. and Hanzo, L. (2003) Low complexity erasure insertion in RS-coded SFH spread-spectrum communications with partial-band interference and Nakagami- m fading. *IEEE Transactions on Communications*, **51**(5), 914–25, May.
- [381] Yang, L. L. and Hanzo, L. (2003) *Fractionally Spread Multicarrier CDMA: A Multiple-access Scheme for Various Wireless Channels*. Proceedings of IEEE PIMRC'2003, Beijing, China, 7–10 September.
- [382] Yin, H. and Liu, H. (1999) *Receiver Design in Multicarrier DS CDMA Communications*. Proceedings of IEEE ICC'99, Vol. 2, pp. 922–6.
- [383] Yip, K.-W. and Ng, T.-S. (1998) Tight error bounds for asynchronous multicarrier CDMA and their application. *IEEE Communications Letters*, **2**(11), 295–7, November.
- [384] Yip, K.-W. and Ng, T.-S. (1999) Effects of carrier frequency accuracy on quasi-synchronous, multicarrier DS-CDMA communications using optimized sequences. *IEEE Journal on Selected Areas in Communications*, **17**(11), 1915–23, November.
- [385] Zhang, H., Howard, H. and Lindsey, F. A. (2002) *Wavelet Packet Waveforms for Multicarrier CDMA Communications*. IEEE International Conference on Acoustics, Speech, and Signal Processing, Vol. 3, pp. 2557–60.
- [386] Zhang, Y. and Dill, J. (1999) *Comparison of Equalization Techniques in a Wavelet Packets based Multicarrier Modulation DS-CDMA System*. Proceedings of IEEE GLOBECOM'99, Vol. 4, pp. 2152–6.
- [387] Zhao, Y., Dong, M. and Wu, W. (2002) *An Adaptive Modulation Algorithm for Multicarrier DS/CDMA Systems*. Proceedings on IEEE VTC'2002-Spring, Vol. 4, pp. 1873–6.
- [388] Zhou, S. and Giannakis, G. B. (2000) *Generalized Frequency Hopping OFDMA through Unknown Frequency-selective Multipath Channels*. Proceeding of IEEE WCNC'2000, Vol. 1, pp. 56–60.
- [389] Zhou, S., Giannakis, G. B. and Swami, A. (2000) *Frequency-hopped Generalized MC-CDMA for Multipath and Interference Suppression*. Proceedings of IEEE MILCOM'2000, Vol. 2, pp. 937–41.
- [390] Zhou, S., Giannakis, G. B. and Scaglione, A. (2001) Long codes for generalized FH-OFDMA through unknown multipath channels. *IEEE Transactions on Communications*, **49**(4), 721–33, April.
- [391] Zhu, Y. and Gunawan, E. (2000) Performance of MC-CDMA system using controlled MRC with power control in Rayleigh fading channel. *Electronics Letters*, **36**(8), 752–3, April.
- [392] Zong, P., Wang, K. and Bar-Ness, Y. (2001) *A Novel Partial Sampling MMSE Receiver for Uplink Multicarrier CDMA*. Proceedings of IEEE VTC'2001-Spring, Vol. 1, pp. 741–5.
- [393] Zong, P., Wang, K. and Bar-Ness, Y. (2001) Partial sampling MMSE interference suppression in asynchronous multicarrier CDMA system. *IEEE Journal on Selected Areas in Communications*, **19**(8), 1605–13, August.

Index

- A priori* knowledge, 30
- Additive white Gaussian noise (AWGN), 15, 111, 153
- Altruistic-optimization, 549
- Altruistic-optimum, 549
- Anti-detection, 1
- Anti-jamming, 1
- Autocorrelation, 27, 571
- Autocorrelation coefficient, 571
- Autocorrelation function, 571
- Autocorrelation matrix, 288, 529, 530, 576, 577
- AWGN, 15, 17, 153, 161, 173, 288
- AWGN channel, 154, 155, 157, 158, 160, 168, 173, 176, 177, 181, 192, 195, 198, 275, 336, 337, 340, 406
- Band-pass filter, 32, 47, 102
- Base-station (BS), 475, 636
- Bayes rule, 322
- BER, 16
- Bessel function
- 0th order, 571
 - modified 0th-order, 421
- Bit-error rate (BER), 15
- Broadband, 1, 7, 10
- Capacity, 581, 584, 590
- multiple-input single-output (MISO), 588
 - single-input multiple-output (SIMO), 587
 - upper-bounds, 587
- Capacity of
- MIMO channel, 581, 582, 586
 - MIMO system, 583–590, 592, 595, 655
- Carrier synchronization, 25
- Cauchy–Schwarz inequality, 293
- CDMA, 8–11, 275, 276, 299, 303, 306, 308, 311, 340, 403
- multicarrier, 276, 277
- Cellular wireless communication, 14
- Cellular wireless system, 11
- Channel
- estimation, 14, 562, 572–578
 - prediction, 14, 562, 572–578
- Channel capacity, 298
- Channel distribution information (CDI), 581, 584
- Channel envelope, 639
- Channel impulse response (CIR), 11, 278, 346, 349, 355, 376, 378, 389, 411, 483, 561, 563, 568, 573, 578
- Channel state information (CSI), 581, 584
- Characteristic function, 271
- Chip, 2, 24
- Chip waveform, 24, 25
- rectangular, 25
 - time-limited, 135
- Choleski decomposition, 314
- Cholesky factorization, 541
- CIR, 207, 215
- Circulant matrix, 212
- Circularly symmetric complex Gaussian, 584, 586
- Co-channel interference, 115, 430
- Code-division multiple-access (CDMA), 6, 21, 33, 34, 38, 39, 68, 96, 275
- Coding
- gain, 601
- Coherence bandwidth, 17, 203
- Coherence time, 18
- Combiner
- hard-limiting, 430
 - linear, 430
 - optimum, 430
 - soft-limiting, 430
- Combining
- optimum, 430
- Complex
- matrix, 383
 - vector, 383
- Conditional capacity, 586
- Confluent hypergeometric function, 247

- Convex programming, 335
 Correlation
 detector, 112
 function, 170
 receiver, 111, 125, 131, 138
 Correlation coefficient, 275, 571, 647
 envelope, 204
 squared envelope, 204
 Correlation detection, 25
 Correlation factor, 639
 Cross-correlation, 9, 14
 matrix, 412, 423, 425, 426, 428
 Cross-correlation function, 577
 chip-partial, 113
 partial, 127, 133, 139
 Cross-correlation matrix, 289, 539, 541, 576
 Cyclic prefix (CP), 117, 618
 Cyclic-prefixing (CP), 211–214, 216, 226, 231, 267, 569
- Decorrelating, 277
 Degrees-of-freedom, 15, 16
 Delay spread, 11, 14, 204, 211, 264, 266
 Detection
 correlation, 238, 615
 matched filter (MF), 238
 Minimum mean-square error (MMSE), 615
 single-user, 185
 square-law, 405
 zero-forcing (ZF), 615
 Differential entropy, 584
 Digital modulation, 2
 Dirac delta function, 16
 Direct-sequence spread-spectrum
 frequency-domain, 114
 Distribution
 χ^2 , 246
 exponential, 204, 220, 222, 261, 624
 gamma, 203, 216, 219, 623, 646
 Gaussian, 220, 261, 271
 multivariate Gaussian, 231, 332
 Nakagami- m , 204, 259, 271
 Rayleigh, 15, 270
 uniform, 204, 221, 222, 261, 264, 624, 635
 Diversity, 14
 combining, 620
 frequency, 6, 17, 122, 136, 222, 267, 618, 621, 624, 625, 635, 637, 654
 frequency-domain, 424
 frequency-selective, 129
 gain, 136, 597, 600, 601, 612, 625, 651, 652, 654, 656
 MIMO, 581, 597, 613–614
 order, 16, 581, 597–599, 602, 611, 613, 614, 621, 624, 634, 646, 648, 649
 receive, 581, 597–598
 scheme, 597
 spatial, 17, 18, 581, 582, 597–614, 624, 625, 636
 technique, 581
 time, 17, 18, 637, 641, 654
 transmit, 581, 597–614
 Doppler frequency shift, 215, 570
 Downlink, 11, 13, 99, 115, 476, 562
 DS-CDMA, 33, 34, 68
 Duplex, 11
 code-division, 11, 14
 frequency-division, 11, 12, 476, 561, 563–564
 multicarrier-division, 11, 13, 476, 561, 564–578
 time-division, 11, 476, 561–563
 Duty factor, 31
- Eigen-analysis, 546, 552
 Eigen-decomposition, 300, 303, 304, 506, 585
 Eigen-representation, 549, 552
 Equal gain combining (EGC), 112, 139, 246, 412, 413, 421, 427, 449, 450, 471
 Equalization, 7, 214, 228, 267
 frequency-domain, 227, 228, 232, 267, 269
 Ergodic capacity, 586
 Ergodic channel capacity, 517, 520
 Ergodic mutual information, 552
 Euclidean distance, 601
 Excess delay spread, 204, 220, 222, 261, 624, 635
- F-preprocessing, 535
 Fading
 correlated Nakagami- m , 270–272
 flat, 203, 207
 flat Nakagami- m , 203
 frequency non-selective, 138, 207
 frequency selective, 6, 14, 205–211, 215, 256, 266–268, 582, 636
 Nakagami- m , 623, 638, 646
 one-side Gaussian, 204
 Rayleigh, 204, 247
 time-selective, 14, 582, 636
 Fading channels
 fast time-varying, 635
 flat, 345
 frequency non-selective, 125
 frequency selective, 125, 129, 203, 205, 226, 231, 232, 234, 245, 262, 266, 277, 278, 287, 292, 328, 330, 362, 370, 637
 frequency-selective Nakagami, 253, 267
 frequency-selective Nakagami- m , 204, 215, 216, 218, 222, 225, 232, 253, 264
 frequency-selective Rayleigh, 222, 232, 264, 283, 284, 287, 292, 313, 356, 361, 376
 frequency-selective slow, 211
 multipath Rayleigh, 17
 Nakagami- m , 406
 Rayleigh, 15
 Fading rate, 349

- Fast Fourier transform (FFT), 7
FDMA, 8
 interleaved, 116–122, 225–228
 localized, 116–122, 225–228
FFH, 44, 45, 47–50, 53, 56, 60, 65, 70
FFT, 7, 8, 635
FH, 22, 47, 51, 56, 67, 73
 address, 54
 address code, 49
 band, 48
 chip, 49
 code, 53
 dwell time, 43, 44, 46, 48
 interval, 44, 48
 pattern, 42, 44, 46–48, 51–53
 period, 51
 rate, 46
 slot, 43, 51, 52
FH pattern, 4, 5
FHMA, 51, 53, 54, 68, 71
Forward error control (FEC), 128
Frequency domain, 9, 12, 17
Frequency nonselective fading, 222
Frequency offset, 8, 14
Frequency selective, 17, 203
Frequency selectivity, 214, 257, 264, 656
Frequency-division multiplexing (FDM), 6
Frequency-hopping, 2, 40
 fast, 4, 5, 44–51, 405, 430, 467
 patterns, 40
 slow, 4, 5, 42–44
Frequency-selective fading channels, 568
 channel impulse response (CIR), 206
Frequency-time (FT) element, 413, 446
Frequency-time (FT) matrix, 145, 413, 431–434,
 436, 437, 439–443, 445, 446, 457, 469
Gamma function, 623
Gaussian Q -function, 16, 511
Gaussian channels, 565
Gaussian distribution, 15
Generalized MRC/SC, 598
Generalized space-time coding, 656
Guard-band, 12
Guard-time, 11
Hadamard product, 348
Hadamard transform, 408
Hadamard's inequality, 516
Hamming distance, 450
Hermitian matrix, 284, 387, 388
 autocorrelation, 300
Hopping pattern, 467
Hybrid
 direct-sequence/fast frequency-hopping, 78
 direct-sequence/fast time-hopping, 90
 direct-sequence/slow frequency-hopping, 75
 direct-sequence/slow time-hopping, 87
Hybrid DS/FFH, 78–86
Hybrid DS/SFH, 73–78
Hybrid spread-spectrum
 direct-sequence/frequency-hopping, 73–86
 direct-sequence/time-hopping, 86–96
Hypergeometric function, 217, 270
Improved Gaussian approximation, 192
Inter-cell, 12
Interbit interference, 241
Intercarrier interference, 14, 241, 345, 620, 631
Intercell, 13
Interference
 multiple access, 134
 multiuser, 139
Interference cancellation, 276, 306, 351
 multistage, 308
 parallel, 312
 successive, 308
Intersymbol interference (ISI), 7, 117, 205,
 211–214, 266, 562
Intracell, 12, 13
ISI, 11, 209, 211, 226, 231, 267
Jamming, 30
 multitone, 32
 partial-band, 30–32
 power, 31
 pulse, 32
Jensen's inequality, 515, 587
Khatri–Rao product, 346
Kronecker product, 640
Lagrange multiplier, 285, 501
Large area synchronous (LAS) code, 14
LDL-decomposition, 513, 529
Lognormal distributions, 204
Low-pass filter, 76
Majority logic decision, 413
Matched filter (MF), 27, 29, 227, 228, 232, 244,
 255, 630
Matched filtering (MF), 227
Matrix inverse, 386
Matrix inverse lemma, 289, 355, 375, 386, 402,
 505, 542, 549, 589
Maximal ratio combining (MRC), 112, 139, 150,
 219, 238, 347, 479, 485, 598
Maximum delay spread, 204, 206, 264
Maximum likelihood decoding, 608
Maximum-likelihood, 601
Maximum-likelihood sequence estimation (MLSE),
 382
MC-CDMA, 38, 39, 68
Mean-square error (MSE), 495
Minimum mean-square error (MMSE), 227, 228
MMSE, 589

- Modulation
M-ary amplitude modulation (M-AM), 338, 622
M-ary frequency-shift keying (MFSK), 40–42, 44–51, 56, 60, 78–80, 86, 87, 406, 430, 467
M-ary orthogonal signalling, 78–79, 82, 83, 90, 92, 93, 96
M-ary pulse-position modulation (MPPM), 56, 59, 61, 68, 87, 90, 140, 268, 405, 406, 411, 424, 443, 472
M-ary quadrature amplitude modulation (MQAM), 337, 530, 622
M-ary time-shift keying (MTSK), 56
binary frequency-shift keying (BFSK), 337, 622
binary phase-shift keying (BPSK), 17, 22–25, 27, 31, 33, 35–37, 74, 337, 492, 510, 622, 636
multiple phase-shift keying (MPSK), 337, 622
nonorthogonal multipulse, 423
time-shift keying (TSK), 73
- Moore–Penrose generalized inverse, 419, 488
- Multicarrier
demodulation, 7, 8, 214, 267–269
modulation, 6–8, 214, 267–269
- Multicarrier CDMA
frequency-domain, 381
frequency-domain spread, 108–114, 158–159, 206, 218–225, 277–344, 363, 475, 479–530, 582, 616–627, 634
time-hopping, 140–145, 245–251, 405–473
- Multicarrier demodulation, 103–108
- Multicarrier DS-CDMA, 159–168, 234–245, 343–362, 381, 531
generalized, 134–140, 206
multitone, 128–135, 206
orthogonal, 122–128, 134, 135, 206
space–time, 635–654
time-frequency-domain spread, 145–150, 177–193, 251–266, 362–381, 475, 530–557, 582
space–time, 627–635
- Multicarrier modulation, 99, 103–108
- Multipath delay profile (MDP), 278, 571
- Multiple access, 8–11
CDMA, 8
communication, 6, 8
direct-sequence code-division, 33
FDMA, 8
frequency-hopping, 51
fast, 53
slow, 51
multicarrier code-division, 38
SDMA, 8, 581, 614–615
TDMA, 8
time-hopping, 67
- time-hopping multicarrier, 140
- Multiple access interference (MAI), 275
- Multiple-input multiple-output (MIMO), 277, 389, 581–596, 604, 655
channel, 581
equation, 606, 608, 614, 615
system, 581, 613, 614, 655
- Multistage Wiener filter, 304
- Multiuser communications, 21
- Multiuser detection (MUD), 275
Decision feedback, 277, 306–318
matched filter, 308–314
Minimum mean-square error, 317–318
zero-forcing, 314–317
- Decorrelating or zero-forcing (ZF), 277, 280–285, 346–352, 365–371
- hybrid time-frequency-domain, 377–380
MMSE/ZF, 377
ZF/MMSE, 377
- Maximum *a posteriori* probability (MAP), 277, 318–329, 382
- Maximum likelihood decision (MLD), 277, 299, 329–331, 358–362, 380–381, 388
- Maximum signal-to-interference-plus-noise ratio (MSINR), 277, 292–294
- Minimum error-probability linear, 331–343
- Minimum mean-square error (MMSE), 277, 287–292, 353–358, 371–377
reduced-rank, 298
- minimum mean-square error (MMSE), 636, 644, 649
- Minimum power distortionless response (MPDR), 277, 294–296
- Minimum symbol-error-rate (MSER), 277
- Minimum variance distortionless response (MVDR), 277, 285–287
- optimum, 627
- Multiuser interference (MUI), 275, 405, 406, 411–413, 415, 418, 424, 426, 427, 429, 430, 438, 450, 457, 458, 461, 464, 465, 467, 471, 475, 531, 636
- Multiuser transmission, 475
- Multiuser transmitter preprocessing (MUTP), 475
eigenspace, 476, 506–510
interference cancellation, 476, 523–530
maximum mutual information (MMI), 476, 515–523, 551–554
joint, 515–518, 551
zero-forcing (ZF), 515, 518–520, 551
- maximum signal-to-interference-plus-noise ratio (MSINR), 476, 499–501
- minimum bit-error rate (MBER), 476, 510–515
- minimum mean-square error (MMSE), 476, 495–499, 508–510, 529, 540–542, 546–550
- minimum power distortionless response (MPDR), 476, 504–505

- minimum variance distortionless response (MVDR), 476, 501–503
- multiuser interference suppression, 475
- zero-forcing (ZF), 488–495, 497, 506–507, 542, 545–546, 556–557
- zero-forcing (ZF), 476
- Mutual information, 298, 515
- Nakagami- m distribution, 204, 270
- Narrow-band communication, 5
- Near-far problem, 276
- Noise-suppression factor, 496, 561
- Noncentrality parameter, 246
- Noncoherent detection
 - posterior
 - single-user, 443–450
- Noncoherent diversity combining, 469–471
 - clipping combining, 470
 - equal gain combining (EGC), 469
 - majority logic decision, 469
 - majority vote, 469
 - noise-normalization combining (NNC), 470
 - optimum diversity combining (ODC), 470
 - product combining (PC), 470
 - selection combining (SC), 469
 - self-normalization combining (SNC), 470
 - soft-limiting combining (SLC), 470
- Noncoherent multiuser detection (MUD), 405–473
 - interference cancellation, 430
 - iterative, 455–461
 - minimum-distance decoding, 450–455
 - multistage, 461–467
 - Maximum *a posteriori* probability (MAP), 415, 433, 434, 437
 - Maximum likelihood decision (MLD), 415, 433, 435, 437
 - multistage interference cancellation, 430
 - optimum, 415–418
 - posterior, 405
 - interference cancellation, 443–467
 - optimum, 429–439
 - prior, 405
 - decorrelating, 418–423
 - minimum mean-square error (MMSE), 423–429
 - suboptimum, 439–443
- Noncoherent processing, 405
- Nonlinear distortion, 100, 115
- Nonsearch algorithm, 398
 - expectation maximization, 398–400
 - probabilistic data associated, 400–403
 - semidefinite programming, 403–404
- OFDM, 6–8, 97, 99–108, 154–158, 205, 206, 211, 214–217, 228, 267–269, 522, 582, 590, 614, 616, 618, 625, 656
 - space–time, 621, 624, 625
- One-sided bandwidth, 23
- Orthogonal, 35
 - codes, 257
- Orthogonal variable spreading factor (OVSF), 636
 - codes, 257, 636, 637, 640, 653
 - codewords, 640
- Orthogonality, 37
- Overall-optimum, 549
- PDF, 203, 204, 216, 219–221, 240, 246, 247, 253, 271
- Peak-to-average power ratio (PAPR), 7, 98, 115, 119, 228, 234, 267, 268
 - reduction, 119
- PN sequence, 3
- PN sequence waveform, 27
- Post-processing matrix, 558
- Post-processing vector, 558
- Power spectral density, 2, 23, 25, 169–173, 179–181
- Power-efficiency, 475
- Prefiltering, 475
- Preprocessing matrix, 478, 480, 481, 483–485, 488, 489, 491, 492, 495, 496, 501, 503, 505–509, 512, 513, 515, 516, 518, 527–529, 541, 542, 548, 549, 552, 553, 555, 556, 559–561
- Probability density function, 321
 - χ^2 -distribution, 434
 - central, 175, 246, 271
 - noncentral, 175, 246
 - exponential distribution, 434
 - gamma, 203, 216
 - Gaussian, 154
 - multivariate Gaussian, 359, 415
 - Nakagami- m , 203
 - Rayleigh, 15, 270
- Processing gain, 131
- Pseudo-noise (PN) sequence, 1
- QR-decomposition, 299, 306, 307, 389, 391, 523, 528, 529, 544
- RAKE receiver, 129, 131
- Random variable
 - independent, 128
- Receive diversity, 613, 654
- Reduced-DFT (RDFT), 566
- Reduced-IDFT (RIDFT), 566
- Resolvable multipath, 215, 231
- Resolvable path, 207, 215, 226, 228, 277, 278, 283, 287, 292, 313, 328, 330, 331, 370, 376
- Rician distribution, 204
- SC/EGC, 449, 450
- SDMA, 11
- Search algorithm, 388
 - ant-colony-inspired, 396–398
 - coordinate decent, 392–393
 - evolutionary programming (EP), 393–394

- genetic, 394–396
- greedy search, 390–391
- QRD-M tree-search, 389–390
- sphere-decoding, 391–392
- Selection combining (SC), 449, 450, 470, 598
- Sequence
 - M -ary orthogonal, 82
 - pseudo-noise (PN), 24
 - random, 258
- Serial-to-parallel conversion, 7
- SFH, 45, 47, 48, 51
- Signal-to-interference-plus-noise ratio (SINR), 10
- Signal-to-noise ratio (SNR), 276, 283, 292, 294, 304, 305, 307, 308, 310, 313, 318, 330, 337, 338, 352, 356, 370, 379
- Signature
 - code, 561
 - spatial, 561, 615
- Signature code, 9
- Simplified improved Gaussian approximation, 153, 192, 259, 262–264
- Single-carrier DS-CDMA, 195–198, 228–234, 531
- Single-carrier frequency-division multiple-access, 115–122, 225–228
- Single-input multiple-output (SIMO), 597
- Single-input single-output (SISO), 581
- Single-user detector (SUD), 405
 - correlation, 636
- Single-user transmitter preprocessing (SUTP), 475
 - matched filter (MF), 542–545
 - pre-RAKE, 476
 - transmitter matched filter (TMF), 476, 479, 483–486, 497
- Singular-value-decomposition (SVD), 282, 299, 506, 516, 518, 553
- Soft-input soft-output, 382, 418
- Space domain, 17
- Space-time, 581
 - block, 619
 - combining, 614
 - F-domain spread MC-CDMA, 621
 - matrix, 630
 - MC-CDMA, 616, 623–625, 627
 - processing, 615, 655, 656
 - scheme, 614
 - signal, 637, 654
 - system, 599, 600, 609–611, 625
 - transmission scheme, 582
- Space-time code (STC), 601
 - block (STBC), 601
 - Alamouti, 602
 - complex signal constellation, 604–610
 - orthogonal, 605, 633
 - real signal constellation, 603–604
 - trellis (STTC), 601
- Space-time coding (STC), 581, 656
- Space-time spreading (STS), 581, 656
- Space-domain, 14
- Spatial-code-division multiple-access (SCDMA), 11
- Spatial-selective, 18
- Spectral-efficiency, 6, 581
- Spread-spectrum, 1, 21
 - communication, 5
 - direct-sequence, 2, 3, 21–34
 - frequency-domain direct-sequence, 21
 - frequency-hopping, 2, 4, 5, 21, 40–54
 - hybrid DS/FH, 21
 - hybrid DS/TH, 21
 - multicarrier, 2, 4, 21, 34–40
 - signal, 6
 - technique, 1, 21
 - time-domain direct-sequence, 21
 - time-hopping, 2, 5, 21, 54–73, 268
 - fast, 60–61, 64–67
 - slow, 56–64
 - transmission, 21
- Spread-spectrum multiple-access (SSMA), 6
- Spreading
 - code, 134
 - time-domain, 136
 - DFT, 115
 - factor, 124, 130, 134, 138
 - frequency domain, 114, 256, 259, 267, 268, 363, 630
 - code, 365, 367, 374, 376
 - factor, 277, 296
 - matrix, 367
 - sequence, 256–259, 284, 363, 365, 370, 372, 378, 379
 - gain, 124
 - matrix, 479
 - time domain, 114, 214, 259, 362
 - code, 122, 365, 367, 368, 373, 374, 376, 378
 - factor, 362, 376
 - sequence, 258, 259, 362, 365, 367, 370, 379, 381
- Spreading code, 10
- Spreading codes
 - frequency-domain, 479
- Spreading factor, 3, 24
- Spreading gain, 24
- Squared channel envelope, 639
- Standard Gaussian approximation, 153, 190, 199–201, 259, 260
- STBC, 601–605, 608–611, 613, 616, 617, 619, 621, 624, 627, 631, 633
 - Alamouti, 604, 605, 613
 - decoding, 618, 620
 - for complex signal constellations, 605
 - from orthogonal design, 603
 - full-diversity orthogonal, 620
 - full-rate full-diversity, 607–609
 - orthogonal, 607, 608
 - quasi-orthogonal, 607
 - real-domain, 602

- Steepest-descent gradient, 513
 - algorithm, 336
 - approach, 335
- STS, 581, 582, 610, 611, 614, 627–630, 633, 634, 636, 637, 653
 - code, 637, 641, 645
 - codeword, 640
 - full-rate, 611
 - matrix, 629
 - MC DS-CDMA, 627–630, 633, 634
 - time-frequency-domain, 628
 - orthogonal code, 636
 - scheme, 611, 612, 637, 642
 - signal, 612, 637
 - spreading code, 636
 - spreading sequence, 637
 - symbol, 629
 - system, 611
- STTC, 601, 611, 613
 - Subcarrier
 - spacing, 135
- Subspace, 296–304
 - detection, 297, 298, 300, 304
 - interference, 281, 282
 - noise, 299
 - null, 282
 - reduced-rank, 297
 - cross-spectral metric, 301–302, 304
 - principal components, 300–301, 304
 - Taylor polynomial approximation, 303–304
 - signal, 298–302, 304
- Sylvester-type Hadamard matrix, 408
 - Synchronization, 8
- TDMA, 8
 - TF-preprocessing, 535
- TH pattern, 5, 405, 413, 438, 439, 442, 453, 455, 464
 - TH-matrix, 412
 - THMA, 68, 70, 71, 73
 - Time dehopping, 246, 411
 - Time domain, 9, 11, 17
 - Time frequency, 2
 - Time-frequency matrix, 50
 - Time offset, 8
 - Time-hopping, 2, 406
 - fast, 5
 - multicarrier CDMA, 169–177
- patterns, 55
 - slow, 5
- Time-selective, 18
 - Time-selectivity, 656
- Time slot, 5, 11
 - Tomlinson–Harashima precoding, 530
- Transform
 - DFT, 103–108, 205, 209, 211, 212, 214–216, 218, 225, 226, 231, 279
 - FFT, 103–108, 267–269
 - matrix, 116
 - IDFT, 103–108, 205, 208, 211, 212, 214, 218, 226, 227, 232
 - IFFT, 103–108, 267
- Transmission power-allocation, 555–557
 - individual, 556
 - joint, 555
 - maximum signal-to-noise ratio, 556
- Transmit diversity, 610, 616, 627, 628, 636, 654
 - closed-loop, 598, 655
 - switched, 598
 - transmitter MRC, 598–599
 - open-loop, 598, 655
 - orthogonal, 598–600
 - space-time coding (STC), 598, 600–610
 - space-time spreading (STS), 598, 610–613
 - space-time spreading (STS), 636
- Transmitter multiuser detection, 475
 - Transmitter preprocessing, 13, 475
 - algorithm, 475
- Triangular matrix
 - lower, 300, 306, 314, 315, 387, 389
 - upper, 387, 389
- Ultrawide bandwidth (UWB), 1, 7, 22, 406
 - Uplink, 11, 13, 99, 115, 476, 562
 - UWB, 7, 10
- Viterbi algorithm, 601
 - Walsh–Hadamard code, 534, 637
 - Wideband, 1, 10
 - Wiener filter, 573, 575
- Zero-forcing (ZF), 227, 277
 - Zero-padding (ZP), 211–214, 216, 226, 231, 267, 569